University of Bradford

College of Computer Science

Elzein Salah Elzein

22/12/2021

1. Introduction



From MRAC to Learning-BasedMPC

The Emerging Importance of Machine Learning for Control of Robot Manipulators

*K. Soltani Naveh** and *P. R. McAree*

ABSTRACT

The increasing importance of machine learning in manipulator control is reviewed from two main perspectives: modeling and learning control. The chapter starts with an introduction to history and theory of Model Reference Adaptive Control (MRAC) and its application to manipulator control. Least Square Minimization (LSM) regression is highlighted as the machine learning element in indirect MRAC that seeks to find unknown parameters from a number of data points. The limitations of indirect and direct MRAC are identified. Specifically, indirect MRAC is limited by the need for persistent excitation and the use of simple modeling assumptions that lead to undesirable control performance. Direct MRAC is limited by reference model mismatch, adaptation rate, choice of control law, and relying on error feedback correction with the

frequent consequence of stability and adaptation problems. Moreover, neither direct nor indirect MRAC can handle state and input constraints which are important in the control of robotic manipulators. Machine learning techniques offer the promise of overcoming these limitations. Recent developments include Concurrent-MRAC which is able to alleviate the persistent excitation requirement for LTI systems and may have application to the control of robotic manipulators. The chapter covers the broader contributions of machine learning

School of Mechanical and Mining Engineering, University of Queensland, St. Lucia, Queensland,
Australia.
E-mail: p.mcaree@uq.edu.au
* Corresponding author: k.soltaninaveh@uq.edu.au

to recent developments in manipulator control that combine learning and adaptation. This includes: (i) the use of advanced modeling methods such as Mixture Models and Neural Networks and (ii) learning control methods such as Iterative Learning Control and modern Reinforcement Learning and their relation to adaptive control. State and input constraints are identified to be one of the significant remaining challenges in manipulator control. Model Predictive Control (MPC) is introduced as the control method that can handle state and input constraints in its formulation. A number of recent attempts to incorporate learning capabilities in MPC are discussed.

Keywords: Machine learning, learning control, neural networks, model predictive control

INTRODUCTION

Model Reference Adaptive Control (MRAC) was first employed for robot manipulator control in 1980s as researchers explored direct drive technology to eliminate gearboxes with the aim of faster more accurate manipulation. Before that, manipulators were generally controlled using PD controllers at each joint. Although manipulator dynamics is nonlinear, this approach worked in practice due to large gear ratios that made nonlinear inertia effects negligible from the view of the control system. In this case, it has been proven that PD controllers successfully accomplish trajectory tracking (Slotine and Li 1991). Once direct drive technology was adopted and gearboxes were eliminated faster operations became possible and undesirable gear effects such as deadzone and backlash were eliminated. However, nonlinear rigid body effects became no longer negligible and the conventional joint based PD controllers were unable to deliver required levels of performance. A MIMO control design approach that took into account the coupling and nonlinear effects was required.

Early interest in the application of MRAC to manipulator control was also motivated by model mismatch or model uncertainty. The emergence of direct drive manipulators and

the push for faster operation speed, led to the development of the so-called 'computed torque' control method, which uses a rigid body model of the manipulator to compute feedforward terms which are typically applied in conjunction with a feedback strategy. Modeling errors were, however, found to be significant enough to impact on trajectory tracking. This necessitated the development of control systems that were able to estimate the unknown model parameters and compute the inputs according to the estimated plant model.

As robot manipulators were increasingly applied to problems that required interaction with changing environment, manipulator controllers had to adapt to those changes in order to maintain acceptable performance. These applications involve changing loads, varying compliance and geometry.

MRAC was introduced as a control methodology in 1961 (Astrom and Wittenmark 2013, Osburn et al. 1961). It was proposed for manipulator control in 1979 by Dubowsky (Dubowsky and Deforges 1979). The adaptation mechanism in MRAC, in principle, allows the control system to maintain a desired response robust to model mismatch and changes to the plant. One way to specify the desired behavior is through defining a reference model. This is the basis for so-called ***direct MRAC***.

Alternatively, a desired behavior can be achieved by estimating the unknown or changing parameters of the system and adapting the control input based on those

estimations. This approach is known as ***indirect MRAC*** and it is the main focus of this chapter.

Indirect MRAC uses data to "learn" unknown parameters and this places it as essentially a machine learning algorithm. Machine learning is a well-studied and established area that focuses on algorithms that enable machines to adapt and change without the need to be reprogrammed. The advances that have been made in machine learning over the last 30 years offer the prospect for superior modeling approaches than classic adaptive control methods. For instance modern machine learning approaches now allow modeling a particular task such as playing table tennis (Muelling et al. 2010) while classic control approaches only work with plant models.

While MRAC was able to address most of the challenges arising from nonlinear effects, model mismatch and parameter variations, some other issues remained. As gearboxes were removed and direct drive technology replaced them, another issue appeared. The actuators would saturate when high performance was desired and this would lead to poor performance. In order to avoid constraint violation in systems, it is necessary to be able to predict or know in advance the response of the system to an input. This is the fundamental idea behind Model Predictive Control (Maciejowski 2001) which is capable of handling state and input constraints while optimizing the performance with respect to a defined metric. With the increase in computational power MPC is now applied to many systems including robotic manipulators for trajectory tracking applications (Verscheure et al. 2009). The success of MPC predominantly relies on the extent to which an analytical and linear model represents the behavior of the plant and allows predictions to be made. If the response of the plant includes unknown elements or elements that are very difficult to represent analytically or are highly nonlinear then predictions will be inaccurate or even impossible.

Just as machine learning allowed indirect MRAC to model a system with unknown parameters, it seems plausible it can help obtain better models for MPC. The composition of such models based on classical methods and modern machine learning methods will dominate part of the discussion in this chapter.

The structure of this chapter is as follows. The underlying theory of MRAC and its capabilities and limitations are explained as background to the work. Then we look at adaptation from a machine learning perspective and discuss how machine learning has the potential to improve control capabilities, especially for nonlinear systems. Following that we give a number of machine learning methods and include examples of their robotic applications. Then learning control is briefly introduced and compared to adaptive control. Finally we present MPC as the method of choice for optimal control of constrained systems and how machine learning methods are being used to combine MPC with learning and adaptive control.

FOUNDATIONS OF MRAC

Adaptive control is centered around the notion that it is necessary to adjust the parameters of a control law when faced with uncertainties that change the dynamic of a process. This uncertainty could be in the form of operational variations or structural unknowns. One particularly important application for adaptive control is in manipulator robots. For example, in manipulator control end-effector load variations can be significant. The load variations arise from interacting with a changing environment or time varying dynamics.

MRAC has been one of the well-known adaptive control methods for handling such problems. Direct MRAC allows for a desired system behavior to be specified as a reference model. This is particularly useful for MIMO systems such as robotic manipulators. Direct MRAC attempts to drive the plant response to reference model response by parametrizing the controller and estimating the "controller" parameters online. Indirect MRAC has as its objective obtaining the best estimates of "plant" parameters first and then using them to produce a suitable control input. This is why the adaptation process occurs indirectly. Common parameter estimation methods are based around Recursive Least Square (RLS) (Astrom and Wittenmark 2013), which can also be interpreted as Kalman filtering and Lyapunov based estimation (P. and Sun 1996, Slotine and Li 1987).

Direct MRAC

Direct MRAC is commonly formulated using Lyapunov methods (Astrom and Wittenmark 2013) with the advantage that such formulations are based in considerations of stability. However this approach requires identification of an appropriate Lyapunov function.

By way of introduction to the approach, consider the following first order system based off an example given in (Astrom and Wittenmark 2013):

$$\frac{dy_m}{dt} = -a_m y_m + b_m u_c$$

where $a_m > 0$ and the reference signal is bounded. Assume that the plant is described by

$$\frac{dy}{dt} = -ay + bu,$$

and the control law is defined as

$$u = u_1 + u_2 = -y.$$

The error is then

$$e = y - y_m$$

$$\frac{de}{dt} = -ay + b(u - y) = -a_m y$$

$$\frac{de}{dt} = (b - b_m)u - (a - a_m)y$$

$$\frac{de}{dt} = -a_m e + (b - b_m)u - (a - a_m)y$$

Knowing the error dynamics helps in creating the Lyapunov function. Since the aim is to drive the error to zero a good candidate Lyapunov function is

$$V(e, a, b) = \frac{1}{2}e^2 + \frac{1}{2\gamma}(b - b_m)^2 + \frac{1}{2b}(a - a_m)^2 .$$

This function adapts the control law while driving the error to zero.

Now evaluating $\frac{dV}{dt}$ and enforcing it to be negative definite would lead to the adaptation equations as demonstrated below:

$$\frac{dV}{dt} = e\dot{e} + \frac{1}{\gamma}(b_1 - \dot{b}_1)b_1 + \frac{1}{\gamma}(b_2 - \dot{b}_2)b_2,$$

$$\frac{dV}{dt} = e(a_m e + (b_1 - b_1)u + (a_1 - b_1 k_x)y) + \frac{1}{\gamma}(b_1 - \dot{b}_1)b_1 + \frac{1}{\gamma}(b_2 - \dot{b}_2)b_2,$$

$$\frac{dV}{dt} = a_m e^2 + (b_1 - \dot{b}_1)\left(\frac{1}{\gamma}\dot{b}_1 + ue\right) + (b_2 - \dot{b}_2)\left(\frac{1}{\gamma}\dot{b}_2 - ye\right),$$

To ensure that $V <= 0$ we need to set $\dot{\theta}_1 = \frac{1}{\gamma}\dot{\theta}_1 + u_c e$ and $\dot{\theta}_2 = \frac{1}{\gamma}\dot{\theta}_2 - ye$ to zero leading us to the following adaptation equations:

$$\dot{\theta}_1 = -\gamma u_c e$$

$$\dot{\theta}_2 = \gamma y e.$$

This approach extends to general linear dynamic systems. Choosing a notation similar to that of Chowdhary et al. (Chowdhary et al. 2013), consider a linear system with state $x \in R^n$ and input $u \in R^m$:

$$\dot{x}(t) = Ax(t) + Bu(t).$$

Assume that the reference model that represents the desired close loop response is:

$$\dot{x}_{rm}(t) = A_{rm}x_{rm} + B_{rm}r(t)$$

where A_{rm} is Hurwitz. A control law can be defined as a combination of feedforward and feedback terms:

$$u(t) = K_x^T(t)x(t) + K_r^T(t)r(t).$$

Substituting the control law into the state space equation of the system gives:

$$\dot{x}(t) = (A + BK_x^T(t))x(t) + BK_r^T(t)r(t).$$

If it is assumed that K_x^* and K_r^* exist such that:

$$A + BK_x^{*T} = A_{rm}$$

$BK_r^{*T} = B_{rm}$

then the tracking error dynamics is:

$\dot{e}(t) = \dot{x}(t) - \dot{x}^*(t) = [(A + BK_x^T(t))x(t) + BK_r^T(t)r(t)] - [(A + BK_{rm}^T)x + BK_{rm}^T r(t)]$.

Defining $\tilde{K} = K - K^*$ the equation can be reduced to

$\dot{e}(t) = A_{rm} e(t) + B\tilde{K}_x^T(t)\, x(t) + B\tilde{K}_r^T(t)r(t)$

Using Lyapunov theory it is possible to find the update law for gains K_x and K_r such that error converges to zero. To do that the well known Lyapunov equation for

linear systems is used to find the positive definite matrix $\dot{P} \in R^{n\times n}$ such that $\dot{V}(t) \leq 0$ for Lyapunov function $V(t) = \frac{1}{2} e^T(t)Pe(t)$:

$$A_{rm}^T P + PA_{rm} + Q = 0.$$

This leads to the following update equations:

$$\dot{K}_x(t) = -\Gamma_x e(t)e^T(t)PB$$
$$\dot{K}_r(t) = -\Gamma_r r(t)e^T(t)PB.$$

In general, the procedure involves:

1. Coming up with a controller structure.
2. Deriving the error dynamics equation based on the chosen controller.
3. Finding a Lyapunov equation and then using it to find the adaptation equations necessary to drive the error to zero.

An interesting property of the Lyapunov method is that the system response converges although the parameters are not guaranteed to converge. The fact that parameters can grow unboundedly can be problematic. This will be discussed later in the chapter.

Indirect MRAC

Indirect MRAC relies on estimating unknown system parameters to adapt control input accordingly. The well-known Least Square Minimization (LSM) forms the foundations of Indirect MRAC and it is where MRAC displays its machine learning features. LSM is sometimes implemented through a Kalman filter.

LSM has appeared in many areas of mathematics and engineering. It is simply defined as:

$$\text{minimize } ||Y - \Phi\Theta||^2$$

There are different ways to interpret LSM depending on how it is written. Assume that $R(\Phi)$ is the range of matrix Φ that is the vector space formed by the columns of matrix Φ. Then $\Phi\Theta$ is a point in the space defined by $R(\Phi)$. The above definition seeks the value of Θ for which $\Phi\Theta \in R(\Phi)$ is the

closest point to *Y*. If *Y* is a point somewhere in the space and ΦΘ is a hyperplane, the solution projects *Y* on to *R*(Φ).

A well-known applications of LSM is in regression and model fitting. The aim of regression is to fit a parametric model, usually termed a hypothesis in the machine learning literature to data points. Given data points $y \in R$ a function:

$$y(x) = \sum_{j=1}^{N} \theta_j \phi_j(x) = \Phi^T(x)\Theta$$

is sought where $\phi_i(x)$ are basis functions and θ_i are the model parameters that combine these basis functions so that the model best fits the data. This means that the model parameters have to be obtained through some optimization process and LSM is commonly used for this, i.e.,

$$\text{minimize} \sum_{i=1}^{N} (y_i - \phi^T(x_i)\Theta)^2$$

This can be expressed in matrix form as

$$\begin{bmatrix} y_1^T \\ y_2^T \\ \vdots \\ y_M^T \end{bmatrix} = \begin{bmatrix} \phi_1(x_1) & \phi_2(x_1) & \cdots & \phi_N(x_1) \\ \phi_1(x_2) & \phi_2(x_2) & \cdots & \phi_N(x_2) \\ \vdots & \vdots & \ddots & \vdots \\ \phi_1(x_M) & \phi_2(x_M) & \cdots & \phi_N(x_M) \end{bmatrix} + \begin{bmatrix} \varepsilon_1^T \\ \varepsilon_2^T \\ \vdots \\ \varepsilon_M^T \end{bmatrix}$$

$$\min_W \sum_{i=1}^{M} \|y_i - W^T \phi(x_i)\|_2^2 = \min_W \|Y - \Phi W\|_2^2$$

Here the Φ matrix is the regression matrix. If $\phi_j(x) = x^{(j)}$ where $x^{(j)}$ is the j-th element of x then the above expression reduces to the linear regression problem.

The above regression equation is sometimes called parametric estimation. The use of the regression equation is common in adaptive control whenever varying components of the system are modeled as a linear function of the unknown parameters. Recursive implementations also exist that are computational efficiency.

When using least square for parameter estimation, the Φ matrix often contains the **observations** either in its rows or columns depending on the problem description. For a good estimation, one would require that the observations provide as many independent information as possible in other words one would expect Φ to have complete rank. If some of these observations are not providing new information, i.e., the columns or rows are not independent the parameter

estimation would be poor and in some cases impossible. This leads to a concept called **persistent excitation** and it will be discussed later.

Applications of MRAC to Manipulator Control

Both direct and indirect MRAC have been applied to manipulator control in order to deal with the varying load or unknown parameters (Craig et al. 1987, Maliotis 1991, Ham 1993, Dubowsky and Deforges 1979, Slotine and Li 1987, Hsia 1984, Tung et al. 2000). In both approaches, the known part of the model is used in a direct torque control or feedforward framework and only the unknown or varying part is handled by an adaptive controller. In case of direct MRAC, the adaptive controller can be a PD controller with adaptive K_p and K_d gains (Maliotis 1991) while in the case of indirect MRAC it usually takes the form of a computed torque control based on estimated parameters (Craig et al. 1987, Slotine and Li 1987). In both approaches, MRAC design is predominantly based on Lyapunov method.

The common approach in applying direct MRAC to manipulators is to combine feedforward and feedback as shown by (Maliotis 1991), who shows, in this approach the feedforward component makes use of the known portion parameters of the plant such as inertia to calculate the likely input. The adaptive feedback aims to compensate for the varying nonlinear effects by using n linear decoupled second order systems as the reference model. The feedforward component could also be interpreted as the result of feedback linearization of the plant.

To make this explicit, assume that the dynamics of a robotic manipulator is expressed by

$$M(q)\ddot{q} + C(\dot{q}, q)\dot{q} + G(q)q = \tau$$

where the inertia matrix M, Coriolis and gravity terms C and G are all assumed to be composed of known and unknown parts as defined below.

$$M = M_k + M_u = M_k - I + M_u^* + I = M - I + M$$

$$C = C_k + C_u$$

$$G = G_k + G_u$$

The subscripts k and u define the known and unknown components. Note that M has been decomposed to known and unknown parts in a way that supports the construction of invertible matrices that are positive definite. When the above equations are substituted in the dynamic equations the following is obtained:

$$(M_k - I - M_u)\ddot{q} - u = (C_k - C_u)\dot{q} - (G_k - G_u)q - \tau,$$

$$M_u\ddot{q} - u = -C_u\dot{q} - G_u q - \tau_k - (M_k - I)\ddot{q} - C_k\dot{q} - G_k q + u,$$

$$-\tau_k - (M_k - I)\ddot{q} - C_k\dot{q} - G_k q.$$

And, if all parameters are known then $M_u = I$, $G_u = 0$, $C_u = 0$ and therefore $u = q$ and τ will only include the feedforward terms. However if there are unknown parameters, given a reference model then u can be calculated using adaptive terms in order to make the system behave like the reference model.

The reference model is chosen as:

$$\dot{x} = A x + B v \qquad \begin{bmatrix} I \\ 0 \end{bmatrix} x + \begin{bmatrix} 0 \\ I \end{bmatrix} v,$$

$$\begin{bmatrix} d \\ m \end{bmatrix} = \begin{bmatrix} d \\ p \end{bmatrix} v$$

$$\begin{bmatrix} K \\ T \end{bmatrix} \quad -K \quad I$$

.

where $x_d = [q_d \; \dot{q}_d]$. This model essentially forces the manipulator to behave like a number of uncoupled second order systems. The input u is chosen to be:

$$u = u_a + u_k,$$

$$u_k = -[K_p \; K_v]\, x + v$$

$$u_a = -[\Delta_1 \; \Delta_2]\, x + \Delta_v v$$

The first term is a state feedback and feedforward and the second term is the adaptive input that deals with the unknown variations. Using the above control law, the adaptation law can be derived using Lyapunov method:

$$\dot{\Delta}_1 = -a\omega q^T$$

$$\dot{\Delta}_2 = -a\omega \dot{q}$$

$$\dot{\Delta}_v = b\omega v^T$$

where a and b are positive scalar gains.

Computed torque control is also used in indirect MRAC where adaptation occurs through estimation of unknown parameters (Craig et al. 1987, Slotine and Li 1987).

The parameter estimation law is derived using Lyapunov method. The process is shown below:

$$\tau = M(q)\ddot{q} + C(q,\dot{q})\dot{q} + G(q)q.$$

The control law is then defined as;

$$\tau = \hat{M}\ddot{q}_d + \hat{C}(q,\dot{q})\dot{q}_d + \hat{G}(q) + K_p\tilde{q} + K_d\dot{\tilde{q}},$$

where $\hat{(.)}$ indicates associated quantity is an estimate, and:

$$\tilde{q} = q - q_d$$
$$\dot{\tilde{q}} = \dot{q} - \dot{q}_d.$$

A Lyapunov function is defined as $V = \frac{1}{2}(\dot{\tilde{q}}^T M(q)\dot{\tilde{q}} + \tilde{a}^T\Gamma\tilde{a} + \tilde{q}^T K_p\tilde{q})$ where a is the vector of unknown parameters and $\tilde{a} = \hat{a} - a$ is the estimation error. In order to make sure that $\dot{V} \leq 0$ the estimation law is chosen as:

$$\dot{\hat{a}} = -\Gamma^{-1}Y_d^T(q,\dot{q},\dot{q}_r,\ddot{q}_r)\dot{\tilde{q}}$$

with Y coming from

$$M_d\ddot{q}_r + C_d(q,\dot{q})\dot{q}_r + G_d(q) = Y\hat{a}.$$

This process is more or less followed in all Lyapunov-based indirect MRAC applications in manipulator control. See for example (Tsai and Tomizuka 1989, Rong 2012, Mohan and Kim 2012).

Researchers have also used indirect MRAC in combination with direct MRAC for manipulator control. This method utilizes both tracking error and prediction error for better adaptation (Yu et al. 1993, Ciliz and Cezayirli 2004).

Limitations of MRAC and the Adoption of Machine Learning

Traditional MRAC as presented in the previous section has limitations that arise from the assumptions, control architecture and the computational method. Direct and indirect MRAC have different limitations.

In traditional MRAC, it is assumed that the unknown parameters are either constant or change very slowly (Astrom and Wittenmark 2013, Slotine and Li 1987). This assumption is true in some circumstances but not in all and it is arguably

predicated on mathematical convenience rather than its appropriateness for manipulators and other high performing mechanical systems. Because of the improvements in actuator technology direct drive manipulators are capable of performing high speed high torque motions which means that variations and nonlinearities can occur at a faster rate. Therefore there is a need to account for such abrupt variations that do not fit in the classic MRAC framework.

Both direct and indirect MRAC are reliant on the so-called *persistent excitation* condition in order to guarantee stability and convergence for states and parameters (Narendra and Annaswamy 1987, Chowdhary et al. 2013). This requirement ensures that the input to the system meets the conditions for parameters to be bounded. If persistent excitation is not satisfied it can lead to robustness and stability problems due

to unbounded growth of parameters. The drift in parameters often occurs abruptly and, leads to the phenomenon known as bursting. This requirement is formally defined below.

Definition

A signal u is persistently exciting (PE) of order n if the following holds (Astrom and Wittenmark 2013):

$$\rho_1 I > \sum_{k=t}^{t+m} \phi(k)\phi^T(k) \geq \rho_2 I$$

where $\rho_1, \rho_2 > 0$ and

$$\phi(t) = \begin{bmatrix} u(t-1) \\ u(t-2) \\ \vdots \\ u(t-n) \end{bmatrix}$$

This definition shows that the essence of PE is that there is enough variance in input so that all adaptation parameters can be evaluated based on system measurements. However requiring PE can compromise performance when smooth or high precision performance is required. In order to prevent the unbounded growth of parameters, methods such as σ modification (Ioannou and Kokotovic 1983) and e modification (Narendra and Annaswamy 1986) were proposed.

In σ modification, the update equations are of the following form:

$$\dot{K}(t) = \gamma(x(t)e^T(t)PB - \sigma(K(t) - K))$$

where $\sigma > 0$ is the modification gain and K is a preselected value about which the parameter K is to be bounded. If $\Delta K = K - K^*$, $K = K - K^*$, $K = K$ then the parameter dynamics can be rewritten as below.

$$\dot{K}(t) = -\gamma(x(t)e^T(t)PB + \sigma K)$$

In this equation the parameter error dynamics is a linear dynamical system driven by the state error e. If the state error does not grow unbounded, this system is bounded input bounded output stable and therefore unbounded growth of parameters is prevented. Recently it has been shown that by using data collected over a finite period of time, it is possible

to achieve stability and exponential convergence in uncertain linear dynamical systems without PE as long as the system is excited over a sufficiently *finite* period of time (Chowdhary et al. 2013). In this approach the parameter update equations are augmented in the following manner. First a set of p state-input pairs
(x_j, r_j) are collected. Then the following errors are defined

$$K_{rj} = K_r^T(t) r_j - (B^T B)^{-1} B^T B r_j$$

$$x_j - B r_j = B K_{rj} - B (B^T B)^{-1} B^T (x_j - A_{rm}(t)).$$

$(B^T B)^{-1} B^T$ is the psudo-inverse of B and earlier we had $BK^{*T} = B$ therefore the above
equations can be rewritten as below.

$$K^{*T}_{r}(K^{T}(t) \quad K \quad r$$

$$K \quad r \quad j \quad r\,j$$

$$B)^{-1}B^{T}(B^{T} - A \quad x \quad B \quad r \quad BK^{T}(t)r)$$

$$K \quad {}_{j} \quad rm \quad j \quad rm \quad j \quad r \quad j$$

$$x$$

$$j$$

$$(B^{T}B)^{-1}{}_{x}B^{T}_{j}BK^{T}(t)x$$

$$K^{T}_{j}(t)x$$

These error variables are used as feedback for update equations giving:

$$K_{x} \quad (t)_{x} \quad \sum_{j=1}^{p} \quad (x(t)e^{T}_{j}K_{x_j}(t)),$$

$$(t)PB \quad x^{T}$$

$$K_{r} \quad (t)_{r} \quad \sum_{j=1}^{p} \quad (r(t)e^{T}_{j}K_{r_j}(t)).$$

$$(t)PB \quad r^{T}$$

This approach is called Concurrent-MRAC. Chowdhary et al. (2013) have demonstrated that by relying on a richer data set from past and present performance and leveraging machine learning, significant improvements on stability and convergance can be made.

Another limitation that is encountered in indirect MRAC arises from the choice of simple parametric models. Parametric models have been used in adaptive control because they facilitate the formulation of control laws and rigorous stability analysis. However these models can be too simplistic for complex robotic systems and they can fail to capture unknown nonlinear effects (Nguyen-Tuong and Peters 2011). Especially for manipulators, different tasks have different input-output profiles and features which may not be captured by a simple parametric model and using least square fitting. Parametric models are prone to underfitting and overfitting

which lead to erroneous estimations. Indirect MRAC is unable to cope with the great variety of motions that may be necessary for abstract tasks such as playing table tennis. As we shall see later, the developments in machine learning have allowed a task based control design based on collected motion data. In these methods, data from motions associated with a particular task such as playing golf (Khansari-Zadeh and Billard 2011) or playing table tennis (Muelling et al. 2010) have been used to design control systems that continuously adapt to changes in environment and even improve their performance as more observations are made.

Direct MRAC also has a number of limitations. One of the fundamental limitations lies at the core of direct MRAC and that is the choice of reference model and the control law. If the reference model has significant mismatch with the plant to the extent that it becomes unrealizable by the system then robustness and stability problems can materialize. This can be particularly problematic for a nonlinear plant like an airplane, as the use of LTI reference models cannot always capture the dynamic behavior of these systems (Crespo et al. 2010). The authors in (Krause and Stein 1987) also demonstrate that for a given combination of model mismatch and parameter uncertainty, MRAC cannot provide a solution. Similarly, the choice of control law and its parametrization can limit the adaptation capability of the controller. Control policies that are more sophisticated than linear feedback-feedforward can perform better in the face of variations. We did not identify any work that addresses the choice of control policy in direct MRAC.

Direct MRAC works based on feedback, which means its adaptation is based on local information only. This is a limiting approach especially for nonlinear systems with

rich dynamic behavior. It is expected that using a global approach where adaptation is not only based on local measurements but also past measurements can lead to better performance.

Adaptation rate is a structural element in direct MRAC that has been identified as a potential source of problem. While based on LTI theory high adaptation rates improve controller performance, it is not always true when the plant is nonlinear or delays are present. High adaptation rates can lead to oscillatory behavior and even instability in such scenarios. Therefore some trade-off is inevitable in order to ensure reasonable compensation of parametric uncertainties while avoiding the undesirable effects arising from nonlinearities and delays (Crespo et al. 2010).

In addition to the structural issues and limiting assumptions in MRAC, state and input constraints are also where adaptive control provides no solution. Ignoring these constraints can lead to saturation and instability. From a practical point, this is a problem that is increasingly encountered as industry moves towards high performance systems that often need to operate close to the extreme limits. While classic control approaches fail to provide a solution to this, Model Predictive Control (MPC) is not only able to accommodate complex state and input constraints but also is able to optimize system performance with regards to a given cost function. Therefore there has been an effort to integrate MPC and adaptive control through learning methods.

Machine Learning for Control

Models are an inseparable part of control design. In fact they are central to the control engineering design process. This is true for the very classical control design approaches like linear feedback control to modern approaches such as MPC. Models are needed for compensation, prediction and adaptation.

We begin with a few definitions based on (Nguyen-Tuong and Peters 2011) who distinguish the following types of models:

1. *Forward models*: Forward models are used to predict the next state of a system given the current state and input. This is the most common model that is used in control and can be generally represented as a first order ordinary differential equation $\dot{x} = f(x, u)$.
2. *Inverse models*: Inverse models calculate an input given an initial state and a desired state. These models are used generally for feedforward calculation. A well-known example of these models is the feedforward term for serial manipulators $\tau = M\ddot{\theta} + C(\theta,\dot{\theta})$. When the mapping from state to input is not unique, the inverse model can results in poor performance of a learning algorithm. Inverse kinematics is a well-know: for each pose in the workspace there may exist multiple configurations in joint space and this ambiguity can drive poor learning outcomes.
3. *Mixed models*: These are a combination of forward and inverse models. The combination of the forward and inverse models allows to compute the inverse model for systems which suffer from non-uniqueness. In this approach the forward model guides the computation of inverse model and prevents the ill-conditions arising from non-uniqueness.

Models for many systems can be obtained from the first principles and for a long time this was how models were obtained. However there are some limitations with

deriving models in this manner. First, the theoretical modeling often makes simplifying assumptions such as ignoring friction, backlash and deadzones. This is often because if we were to model the system without those assumptions then unknown parameters or very complex mathematical functions would have to be included. The resulting complexities influence the capacity to handle them within allowable control design frameworks. Second, theoretical modeling does not produce models that are fit-for- control-system purpose for complex systems such as robots with flexible structure or complex mechanical characteristics. Third, there are systems or tasks for which analytical models cannot be easily or effectively produced. An example of such a task is cutting different foods using robotic manipulators (Lenz et al. 2015). It is difficult to model the dynamics of cutting for all foods which can range from soft texture like cheese to hard texture like carrot. Insisting on theoretical modeling in the face of these limitations would only limit our ability to achieve better performance. For these reasons, data driven modeling has received an increasing level of attention.

However, the idea of using data to handle uncertainties and unknown parameters is not new. These ideas can be traced back to self-tuning controllers and in general classic adaptive control. In direct MRAC, for instance, the error signal between the plant and the desired forward model allows the system to learn the inverse model of the plant. Similarly in indirect MRAC, the inverse model of the plant is learned through parameter estimation.

Data driven modeling has the benefit of being able to encapsulate complex behaviors and nonlinear effects that are often ignored in theoretical modeling or which give rise to complex analytical expressions that are too difficult to work with. Perhaps more importantly, though, data driven modeling allows the system to cope with uncertainties and adapt to changing conditions as they occur instead of manually reprogramming the control system again and again.

Machine learning has witnessed significant development in the past thirty-five years. There are many different machine learning methods but they can be classified based on their

modeling, training and operation into:

1. parametric and non-parametric algorithms
2. supervised and unsupervised learning algorithms
3. local and global learning algorithms

Parametric models have a fixed number of parameters that have to be learned from data. In contrast, non-parametric models are not constained by having a fixed number of parameters and they rely directly on data for modeling, and the number of parameters can be chosen to best meet requirements in real time. The standard linear regression is an example of parametric learning algorithm while a locally weighted linear regression is an example of non-parametric learning algorithm.

Supervised learning refers to the training process where the “right” answers are provided to the machine learning algorithm and then the algorithm learns the model based on the training data. Neural Networks, logistic regression and linear regression are all examples of supervised learning. On the other hand, in unsupervised learning, only raw data is provided and the machine learning algorithm learns a model purely based on that. Clustering algorithms and Gaussian Mixture Models are among the well-known unsupervised learning algorithms.

Local learning algorithms construct models in a local neighborhood around a query point. The model then allows the prediction of the value for that query point. On the other hand, global learning algorithms fit one model to all of the data points. Global learning algorithms may involve a mixture of models in order to capture a wider range of behaviors that may be present in the data.

Earlier linear regression otherwise known as least square estimation was presented. Linear regression is one of the oldest and most common learning methods in control. Below we provide a short study of some of the other machine learning algorithms that are common in control.

NEURAL NETWORKS AND BEYOND

Neural Network is a parametric learning method which has been one of the most active research areas in machine learning. With the increase in computational power and algorithmic improvements, they are finding applications in a wide range of areas such as facial recognition, text recognition, signal processing, control and artificial intelligence. In control, neural networks have been used for learning both forward and inverse dynamic models. Neural networks are superior to other parametric learning methods because of the greater degree of freedom in their parameters (Nguyen-Tuong and Peters 2011). However the use of neural networks is not limited to learning models. They have also been used to solve optimization problems and learn control policies (Xia and Wang 2004, Yan and Wang 2014).

Neural networks were created as an attempt to mimic the learning ability in human brain where network of neurons are able to learn a great variety of tasks. In general neural networks consist of neurons that are arranged in three stages: (i) input layer (ii) hidden layers (iii) output layer. A typical neural network is shown in Fig. 1. Each neuron is a sigmoid function that receives a linear combination of the outputs from the nodes in the previous layer. Sigmoid function has the following form.

$$g(z) \square \frac{1}{}$$

$$\frac{1}{1+e^{-z}}$$

The output of sigmoid functions allow the neural network to construct features from input data in the hidden layers and then at the output layer those features are

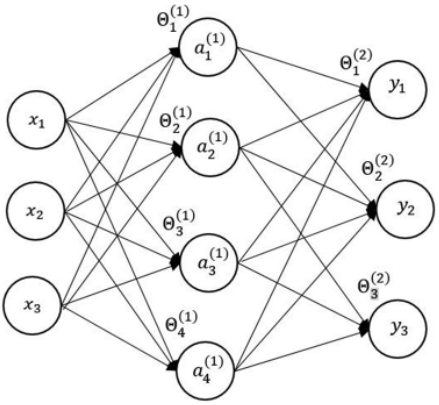


Figure 1. The representation of a typical neural network with one hidden layer.

combined to fit the data as closely as possible. Based on this description, the relation between layers is defined as

$$a^{(l+1)} = g(z^{(l)}) \quad g(\Theta^{(1)T} a^{(l)}) = \frac{1}{1 + e^{-(\Theta^{(1)T} a^{(l)})}}$$

where $a^{(l)}$ is the output from current layer, $\Theta^{(1)}$ is the vector of weights associated with the i th neuron in the layer $l + 1$. The weights in each layer are the parameters that most be computed in order to fit the training data. As the influence of each weight on the output, especially input layer weights, are complicated an algorithm repeatedly evaluates the gradient of the fitting error and adjusts the weights so that the fitting error is minimized. One such algorithm is called backpropagation algorithm.

One drawback in using neural networks for modeling is the long training time. A variant of neural networks called Extreme Learning Machines (ELM) have been developed that have much faster training. ELM is a neural network with one hidden layer whose input layer weights are chosen randomly while its hidden layer weights are calculated analytically using least squares. This method is much faster than the backpropagation algorithm used for ordinary neural networks.

For more complex tasks, often sequence of states and observations are important. Therefore the algorithm needs to learn features arising from data sequences which could represent temporal or spatial features. This arises in a number of applications such as speech and text recognition. In control this becomes particularly useful when we are dealing with dynamics that have temporal or structural variations such as the food cutting task in (Lenz et al. 2015). In order to introduce such learning capabilities Recurrent Neural Networks (RNN) have been developed where hidden layers not only work with the inputs coming from the previous layer but also use their previous outputs as well in order to identify features that may exist in the sequence of data. A simple representation of RNN

is shown in Fig. 2.

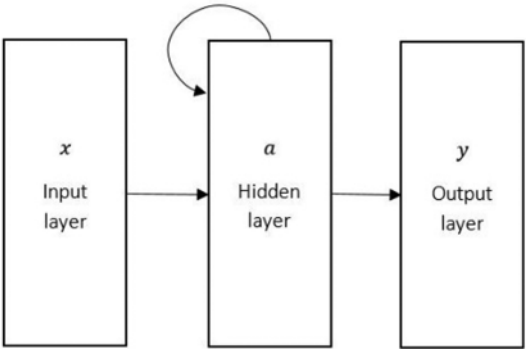


Figure 2. An abstract view of a Recurrent Neural Network.

MIXTURE MODELS

Mixture models are another group of machine learning methods that aim to model a set of data as a mixture of kernels such as Gaussians. This modeling approach has become popular in some of the recent work on manipulator control that aims to mimic the motor skills in humans. There are different theories on motor control and learning

in kinesiology however among these theories Generalized Motor Programs (GMP) have been supported by many lab experiments (Schmidt and Lee 2011). Based on this theory, all motions that are performed by humans are a mixture of general motor programs. By mixing these general motor programs with different force and temporal parameterization it is possible to produce a great variety of motions. Moreover these motor programs can be executed by a different set of muscles if desired. In other words there is a decoupling between the motor programs and the execution mechanisms. Learning how to construct and improve these mixtures can serve as a source of inspiration for achieving optimized control of nonlinear systems.

Schaal et al. (Schaal et al. 2007) layed the mathematical foundation for Dynamic Motor Primitives (DMPs), which can be viewed as an attempt to formulate GMP for manipulator control. In this approach, the motion of each degree of freedom is modeled as a stable autonomous nonlinear dynamical system like:

$$\dot{x} = f(x, z)$$

The model proposed by Schaal et al. is:

$$\dot{x}_2 = \alpha_x(\beta_x(x_g - x_1) - x_2) + \boldsymbol{A}\boldsymbol{h}(z)$$

$$\dot{x}_1 = \gamma x_2$$

where $x = [q_d, \dot{q}_d]^T$ contains position and velocity for the degree of freedom, $x_g = [q_{final}, \dot{q}_{final}]^T$ contains the goal state, $\boldsymbol{A} = diag(a_1, a_2, ..., a_n)$ is the amplitude matrix used to adjust relative amplitudes between the n degrees of freedom, $\boldsymbol{h}(z)$ is a transformation function acting as a nonlinear input and z is a phase variable that acts like an internal clock so
that the state does not depend on time directly. The phase variable z is defined as:

$$\dot{z} = -\gamma\alpha_z z$$

where γ and α_z are constants that are chosen through a parameter selection process. The function $\boldsymbol{h}(z)$ is the key element of this equation as it drives the nonlinear system. The values generated by $\boldsymbol{h}(z)$ dictate the sort of trajectoris that will be generated, therefore in order to produce a particular motion $\boldsymbol{h}(z)$ has to be evaluated using supervised learning. In doing so

$\boldsymbol{h}(z)$ is represented as:

$$\boldsymbol{h}(z) = \sum_{i=1}^{N} \psi_i(z)\boldsymbol{w}_i z$$

where $\boldsymbol{w}_i$ is the i-th adjustable parameter of all degrees of freedom. These parameters must be learned from motion data using supervised learning in order to produce the desired motions. N is the number of parameters per degree of freedom, and $\psi_i(z)$ are the corresponding weighting functions. The weighting functions are often chosen to be Normalized Gaussian kernels with centers c_i and widths h_i:

$$\psi_i(z) = \frac{\exp(-h_i (z - c_i)^2)}{\sum_{j=1}^{N} \exp(-h_j (z - c_j)^2)}$$

The attractive node of this autonomous system is the desired final state, meaning $x_g = [q_{final}, \dot{q}_{final}]^T$. The net result of this formulation is that the nonlinear autonomous system generates the desired position and velocity at each instant. If the system is perturbed the state x would follow a new path to the attractive node.

By inspecting the above system as z converges to zero with time, state x is driven to x_g, making the system behave like a nonlinear spring-damper (Schaal et al. 2007).

Note that DMP acts as a reference generator only and the generated reference has to be passed to a lower level feedforward-feedback controller for execution.

The DMP equations shown above are only useful for representing motions with a zero final velocity. The formulation was further generalized by Kober (Kober 2012) to also include non-zero final velocity in order to allow modeling motions such as forehand and backhand in table tennis. A mixture of motor primitives has been used to generalize between DMPs to construct more complex motions that for example can allow a robot arm play table tennis (Muelling et al. 2010).

Another example of application of mixture models in manipulator control is the work of Khansari-Zadeh and Billard where instead of using a mixture of motor primitives as defined above, a mixture of Gaussians is used to model the nonlinear dynamical system representing a task (Khansari-Zadeh and Billard 2011). The nonlinear model is autonomous and stable and is of the following form:

$$\dot{x} = f(x),$$

where $x \in R^d$ can be reference joint positions or Cartesian positions. Similar to DMP because of the stable node the reference trajectory always reaches the desired state even in the presence of perturbation.

The machine learning algorithm has to learn $f(x)$. GMM is considered an unsupervised learning approach as the algorithm has to find out: (i) which Gaussian each sample belongs to (ii) and what are the parameters (mean, covariance, etc.) that result in maximum likelihood of the samples. Therefore GMM is often solved using Expectation-Maximization (EM) algorithm that iteratively estimates the likelihood of each sample belonging to a particular Gaussian and then uses those results to solve for the parameters (mean, covariance, etc.) that maximize sample likelihood. The

algorithm eventually finds the best mixture of Gaussians that fits the data. However using EM to find GMM does not guarantee the stability of the resulting model. For this reason, Khansari-Zadeh and Billard proposed a constrained nonlinear optimization approach to obtain only the GMM that satisfies stability requirements.

Both in GMM and DMP, the demonstration data associated with the desired task is collected and the best model is fit to the data. However, the model will be only as good as the demonstration data. This can be problematic especially certain parts of the task are difficult to reproduce by an operator. In this case it is desirable that the system explore the operation space and use the resulting information to improve its performance. This leads us to the subject of learning control.

LEARNING AND ADAPTATION IN CONTROL

Learning and adaptation are closely related concepts. In order for a system to adapt it must learn about the changes in the plant through estimation or through learning the inverse model of the plant as changes occur. This is the basis of MRAC as discussed earlier. Therefore adaptation relies on learning and adaptive control has tried to use learning to adjust *controllers* in order to match the variations in the plant. However, learning can be used to make modifications at abstract levels. This allows systems to use previous performance data to find better “strategies” or better *control inputs* instead

of being tied to a particular controller structure. These capabilities impart a higher level intelligence that is able to learn from mistakes or shortcomings and improve upon them. This is the subject of learning control. Learning control has the potential to address some of the challenging problems such as optimal or near optimal control of constrained nonlinear systems. This is because the learning process could allow nonlinear systems achieve optimal performance as time goes on instead of attempting to solve a nonlinear optimization problem from instant to instant.

One of the earliest attempts to implement learning control is attributed to Uchiyama (Uchiyama 1978) and Arimoto (Arimoto et al. 1984) for their work on Iterative Learning Control (ILC). There are different definitions for ILC that can be found in (Ahn et al. 2007). While each definition emphasizes on a particular feature of ILC the following definitions are important from our point of view:

1. The learning control concept stands for the **repeatability** of operating a given objective system and the possibility of improving the control input on the basis of **previous actual operation data** (Arimoto et al. 1986).
2. ILC is to utilize the system repetitions as **experience** to **improve** the system control performance even under **incomplete knowledge** of the system to be controlled (Chen and Wen 1999).

As highlighted in the definitions, ILC can be considered as a feedforward control design that uses the experience obtained from previous operation data to improve control input. Figure 3 shows the general architecture of ILC. However, it is based on the assumption that a particular motion is repeated in trials as for industrial robotic manipulators. Instead it is desirable to have a control system that can learn even if the motions are not repeated exactly and are only **similar**. Despite the limitation of repeatability assumption, ILC is an inspiring control design method for us.

Before looking at ILC formulation it is helpful to clarify how ILC and in general learning control are different from adaptive control. In adaptive control, the *controller*, which is

a system, is modified while in ILC the *control input*, which is a signal, is modified. Furthermore, adaptive control methods do not take advantage of the information contained in the similarity of tasks, while ILC, and learning control in general, exploits this information for improving performance (Bristow et al. 2006). It must be emphasized that ILC is a feedforward control and it is only able to cope with repeatable disturbances if designed well. In practice ILC is implemented

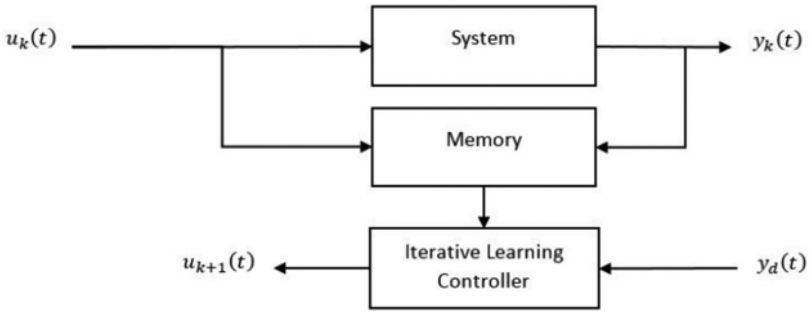


Figure 3. A representation of Iterative Learning Control architecture.

in conjunction with feedback control so that uncertain disturbances are compensated appropriately.

The formulation of ILC uses the tracking error from previous trials to adjust control input by feedforward compensation. One of the simplest ILC algorithms is the PD-type learning control. Assuming that the system needs to track a desired trajectory y_d and that $u_k(t)$ and $u_{k+1}(t)$ are the inputs at time t from trial k and $k + 1$ respectively and the tracking error is $e_k(t) = y_d(t) – y_k(t)$ the PD-type learning algorithm can be defined as:

$$u_{k+1}(t) = u_k(t) + (\Gamma_k + \Phi_k \frac{d}{dt})e_k(t)$$

$$u_{k+1}(t) = u_k(t) + (\Gamma_k + \Phi_k dt + \Psi_k)e_k(t)$$

PID-type learning algorithm can be formulated in similar manner. These formulations only use the information from one previous trial. Higher Order ILC (HOILC) makes use of the information from more than one previous trial in the update equation (Ahn et al. 2007). For example if N previous trials are used in the learning equation we would have:

$$u_{k+1} = (1-\Lambda)P_k u_k + \Lambda u_0 + (\Gamma_k e_{i,k+1} + \Phi_k e_{i,k+1} + \Psi_k e_{i,k+1})dt$$

where $\Lambda P_k u_k$ and $(1 – \Lambda)u_0$ are used to obtain the weighted average of the previous inputs. Another design approach in ILC is based on solving an optimization, usually a Quadratic Programming optimization, iteratively (Bristow et al. 2006). In this method, first state and input are written in lifted space:

$$\mathbf{u}_k = \begin{bmatrix} u_k(0) \\ u_k(1) \\ \vdots \\ u_k(N-1) \end{bmatrix}$$

□ *k* □

□ x_k (0)
□
x □ □
□
k □ x_k (1)
□
□□ □
x (N □1) □
□ *k* □

$$\mathbf{e}_k = \mathbf{x}_d - \mathbf{x}_k$$

Then an appropriate cost function is defined. For example:

$J(\mathbf{x}, \mathbf{u}) \; \mathbf{e}^T + \mathbf{u}^T R\mathbf{u}$ $Q\mathbf{e}$

k □1 *k* *k* *k* *k* *k* □1
k □1 □ □ □ □
1 1 1 1

By solving this optimization problem the optimal update equation for control input can be obtained. If the system has any constraints then these constraints can be incorporated in the optimization. In this case, constrained optimization techniques such as active set method and interior point method have been used to find optimal control inputs by mimicking optimization steps of these algorithms at each trial (Mishra et al. 2011). The advantage of using the optimization method is that the input and state trajectory eventually converge towards their optimal values.

Learning has also been studied in other areas such as psychology, aritificial intelligence and kinesiology. Robot Reinforcement Learning (RL) is one of the learning theories that has stemmed from psychology but developed in AI and has been applied to motion control problems in the recent years. Based on reinforcement learning theory, agents learn by exploration and exploitation. Agents explore by trying different actions and observing the outcomes and then use the obtained knowledge to improve performance through exploitation. This process allows the agent to find the optimal control policy that tells what the best action is given any state.

The formulation of reinforcement learning is very similar to Markov Decision Processes (MDPs) and relies on defining a set of states and actions.

The components of a MDP problem are:

1. Set of states $s \in S$
2. Set of inputs $u \in U$
3. Transition function $T(s, a, s') = P(s'|s, a)$
4. Reward function $R(s, a, s')$
5. Initial state s_0
6. Possibly a desired final state s_{final}
7. Policy $\pi^*(s) = a^*$ that must be computed

Here states and actions are discrete. It is possible to find an optimal policy $\pi^*(s)$ by solving the MDP offline using the above information. States and actions show what states the system can be in and what actions can be taken. Transition function provides information on how a system changes its state in response to an action a taken in state s. The reward function indicates what is good and what is bad. Based on these, an optimal policy that is a mapping from states to actions can be obtained by solving the value function:

$$V(s) \leftarrow \max_{a \in U} \sum_{s'} T(s, a, s')(R(s, a, s') + \gamma V(s')),$$

where γ is the discount factor and reflects the greater significance of earlier rewards.

The optimal policy indicates what is the best control input

to apply in a given state if the goal is to maximize utility. While in the case of MDP this can be done by well-known value iteration and policy iteration algorithms, in RL this is not possible. This is because the transition function and reward function are unknown. In this case, the agent has to learn what the optimal policy is by taking actions and observing the outcome. This is why RL is so much harder than MDP.

Like MDPs, RL can be solved by value function methods or policy methods. In value function methods, the policy is obtained by first approximating the value function $V(s)$ or Q-values, $Q(s, a)$. Q-values are defined as:

$$Q(s, a) = \sum_{s'} T(s, a, s')(R(s, a, s') + \gamma V(s'))$$

therefore it can be seen that:

$$V(s) = \max_{a \in U} Q(s, a).$$

Q-values are very useful in that they provides a measure of utility for a state action pair (*s*, *a*) also known as q-state. This measure shows what values can be obtained if an action *a* is taken in state *s* and from then on optimal actions are taken. In other words, Q-values can indicate the quality of actions taken in a state and for this reason they form the foundation of one of the early RL methods such as Q-Learning and a variant of it known as State Action Reward State Action (SARSA) (Russell and Norvig 2010).

According to the survey in (Kober 2012), the value function methods can be divided in three categories:

1. Dynamic programming-based optimal control approaches such as policy iteration or value iteration.
2. Rollout-based Monte Carlo methods.
3. Temporal difference methods such as TD, Q-learning and SARSA.

The value function methods become intractable for high dimensional problems, however they have been successfully applied to many different robotics problems (Kober 2012).

Policy search is another approach for solving RL where an initial control policy is locally optimized to produce better controllers. Policy methods have three clear advantages in comparison to value function methods. First, policies often have fewer unknown parameters than value functions. Second, policy methods can be extended to continuous state and action space straight forwardly. Third, it is possible to incorporate expert knowledge of the system through an initial policy. This is why policy search methods have been found more suitable for high dimensional problems. There are three categories of policy methods in RL (Kober 2012):

1. Policy gradient approach based on likelihood-ratio estimation.
2. Policy update based on Expectation Maximization: a well known optimization method that consists of repeatedly estimating the expected utility (E-step) and maximizing it (M-step) until convergence.
3. Path integral methods.

According to (Kober 2012), some of the common challenges encountered in RL are:

1. *Large state space*: For high dimensional problems RL has to search in a very large state-action space for the optimal policy. This can be intractable in practice.
2. *Wear and tear*: It is possible that the system under operation experiences tear and wear due to repeated undesirable motions.
3. *Change in operating condition and erroneous data*: If the environment changes, the optimal policy also needs to change. If this change is faster than the learning rate of the system, the optimal policy will never be found.

The first two problems have been addressed mostly by using simulation environment. Using a model of the system, RL can run in simulation and come up with a policy that is optimal. However, as model mismatch is inevitable often the computed policy needs to be tweaked to work on the real system.

In order to help RL find the optimal policy in the high dimensional space demonstration data has also been used to guide policy learning. In this approach which is called imitation learning or learning from demonstration first the desired task is

demonstrated by an operator and the data corresponding to that is collected to extract the initial control policy. Then the policy obtained from data can be deployed on the system and RL can be used to further improve that policy through more operations. This shows the sort of powerful control methods that can be synthesized using machine learning and learning control.

As mentioned earlier in the chapter, state and input constraints are some of the important challenges encountered in manipulator control and robotics in general. Some work on applying RL and ILC to constrained systems has been done (Andersson et al. 2015, He et al. 2007, Mishra et al. 2011). One promising approach has been to use constrained optimization formulations. This approach shares some resemblance with Nonlinear MPC (NMPC). However we believe there is still more work to be done to incorporate state and input constraints in the formulation of learning control so that effective exploration and exploitation can occur without constraint violation. In fact if the formulation incorporates the constraints, the search space for optimal actions will become smaller and the convergence rate could potentially be improved.

The needs for adaptation, learning and constraint handling has led to recent efforts to combine learning methods with MPC. This is discussed next.

LEARNING METHODS IN MPC

The presence of state and input constraints have posed a serious challenge at control design for a long time. This is particularly a problem as we aim to achieve high performance which would require operating systems close to their limits. In order to avoid constraint violation and saturation, one needs to make sure in advance that the input signal that is to be applied to the system over a period of T is not going to exceed the limits. One way is to rely on the experience obtained from operating the system. This can be captured by a learned inverse model of the system or a control policy obtained through learning control methods. Another way is to use

predictions based on a model of the system.

Predictions rely on the model and for a prediction to be representative of the actual behavior of the system, the model mismatch has to be as small as possible. Any uncertainty or unknown variations not accounted for in the model would undermine the validity of predictions.

Model Predictive Control (MPC) is widely considered an effective method for controlling constrained MIMO systems. MPC has had successful applications in chemical process control for its ability to handle constraints (Morari 1989). One of the earliest industrial MPC technologies was developed by engineers in Shell Oil in early 1970s (Qin and Badgwell 2003). With increasing computational power and the rise of more efficient numerical algorithms MPC is increasingly adopted for control of many other systems such as autonomous vehicles, trajectory control, HVAC and so on. In the following section a brief introduction to MPC is presented.

MODEL PREDICTIVE CONTROL

The idea of receding horizon MPC is simple and elegant. In this approach, at time t_0 and for a prediction horizon of N_p, the controller uses the current state of the system $\mathbf{x}_0 = \mathbf{x}(\mathbf{k} \mid \mathbf{k})$ to calculate the input $\mathbf{u} = [u(k \mid k), u(k+1 \mid k), u(k+2 \mid k),..., u(k+N_p \mid k)]$

that would drive the system to the desired state $\mathbf{x}_1$ such that a cost function $J = g(x(k + N_p|k)) + \sum_{i=0}^{i=N_p-1} l(x(k + i|k), u(k+i|k))$ is minimized and operational constraints are not violated. Then the controller applies the first element of the input to the system. In the next step, the controller takes the new state measurement/estimation and repeats the same calculations for a prediction horizon of N_p, and applies only the first element of the resulting input **u**. Provided that the calculations are fast and the system models are accurate this control system will achieve optimal performance. The advantage of MPC in comparison to the classic optimal control theory methods is its ability to handle constraints by defining the control problem as a constrained optimization problem. This is invaluable in practical scenarios such as the manipulator control as actuator constraints are present. In addition, because the controller computes the input at every step based on the observed state, a feedback action is also present.

MPC computes input and state trajectories by solving an optimization problem such as:

Minimize $\boldsymbol{J_{x,u}}$

subject to

$\mathbf{x}(k + i + 1 \mid k) = f(\mathbf{x}(k + i \mid k), u(k + i \mid k))$ $i =$

$0,1,2,3,..., N_p-1$ $u_{lower} \leq u(k + i \mid k) \leq u_{upper}$ i

$= 0,1,2,3,..., N_p-1$

$\mathbf{x}_{lower} \leq \mathbf{x}(k + i \mid k) \leq \mathbf{x}_{upper} \qquad i = 0,1,2,3,..., N_p-1$

$\mathbf{x}(k \mid k) = \mathbf{x}_0$

The forward model of the system is at the heart of MPC and is used for making predictions about the state trajectory. When the model is linear, i.e., $\mathbf{x}(k + i + 1|k) = A\mathbf{x}(k + i \mid k) + Bu(k + i \mid k)$ and the system is subject to linear semi-algebraic constaints. MPC can be solved easily and efficiently. The reason for this is that the optimization problem can be solved

by convex mathematical programming techniques (Boyd and Vandenberghe 2004). However, if the model is nonlinear, as in the case of manipulators, solving the optimization problem is very difficult. This is somewhat expected for nonlinear systems. The complexities introduced by nonlinearities make it difficult to even simulate such systems given an input trajectory **u**, let alone solving for both input and state trajectory. This can also be explained from a geometric point of view. Linear systems have a state manifold which has zero curvature and state gradient has a linear relation with the input. This means the state of the system evolves on the same hyperplane which leads to a set of linear algebraic equations. In contrast, the state manifold of nonlinear systems has varying curvature and the input does not have a linear relation with a state gradient. It is this curvature variation that prevents us from solving predictive problems using such models.

Prediction for Nonlinear Systems

Model predictions for nonlinear systems is one of the most difficult problems in MPC. For this reason, nonlinear systems are often linearized about an initial trajectory and the optimization problem is solved to obtain a new trajectory. Then the model is linearized

about the new trajectory and the process is repeated until convergence is achieved. Sequential Quadratic Programming (SQP) and Sequential Convex Programming (SCP) are two optimization methods that operate in this manner and they are commonly used for Nonlinear MPC (NMPC) problems. However both methods are largely dependent on a “good” starting trajectory and may not converge to the global optimal solution.

In many problems the nonlinearities of the system are not theoretically modeled. However, their influence on model predictions cannot be ignored. In this scenario, the only option is to rely on data driven modeling to incorporate these nonlinearities into model predictions.

These issues have been recognized in the most recent research on MPC. Researchers have tried to account for the sort of nonlinear dynamics that is difficult or even impossible to model analytically. One of the first prominent works in this areas is Learning Based MPC presented by Aswani et al. (Aswani et al. 2013). The paper proposes a robust adaptive MPC that guarantees robustness and achieves performance improvement. In this approach two linear models are used in MPC. One model consists of the nominal linear model with state $\bar{x}$ and uncertainties d due to nonlinear effects. This is of the form:

$$\bar{x}_{n+1} = A_n \bar{x}_n + B_n \bar{u}_n + d$$

The robustness conditions are then established by introducing an invariant set for the terminal state and using tube MPC one of the common methods in robust MPC. Tube MPC uses the nominal model $\bar{x}_{n+1} = A_n \bar{x}_n + B_n \bar{u}_n$ for predictions while it accounts for the effect of disturbance d by shrinking the state constraints by some value given by set Ω.

The other model is linearized with state x but contains some unknown nonlinear component $\Phi_n(x_n, u_n)$ and is of the following form:

$$x_{n+1} = A_n x_n + B_n u_n + \Phi_n(x_n, u_n).$$

$\Phi_n(x_n, u_n)$ can be “learned” as an “oracle” which returns the value of nonlinear component and its gradient as a function of current state and

input. Using both models in the optimization problem formulated for MPC would satisfy robustness conditions while optimizing and system performance. The learning process has been shown to improve the performance of MPC by making better dynamic predictions. Indeed, it has been shown that given sufficient excitation the MPC would converge to a performance that would be achieved if the exact model of the plant was known (Aswani et al. 2013). Yan and Wang (Yan and Wang 2014) have also carried out a similar strategy to solve robust model predictive control for nonlinear systems by adopting neural networks not only for model learning but also for solving the optimization problem. In their approach, the nonlinear system is represented as:

$$x(k+1) = f(x(k), u(k)) + w(x(x), u(k)) + v(k)$$

where $x \in \mathbb{R}^n$ is the state vector, $u \in \mathbb{R}^m$ is the input vector, $w \in \mathbb{R}^n$ represents unmodeled dynamics, $v \in \mathbb{R}^n$ is the additive bounded uncertainties and $f(.)$ is a nonlinear function representing the modeled dynamics.

This model is then linearized about the operating point (x_0, u_0) similar to the previous case:

$$\Delta x(k+1) \approx \frac{\partial f(x_0, u_0)}{\partial x} \Delta x(k) + \frac{\partial f(x_0, u_0)}{\partial u} \Delta u(k) + d(k) + v(k)$$

$$\Delta x(k+1) = A(k)\Delta x(k) + B(k)\Delta u(k) + d(k) + v(k)$$

where $d(k)$ represents the nonlinearities and unmodeled dynamics.

In order to achieve robustness the authors employ a minimax approach where the control cost is minimized for the worst uncertainty scenario:

$$\min_{\delta \boldsymbol{u}} \max_{\boldsymbol{v}} \boldsymbol{J}(\boldsymbol{x}, \Delta \boldsymbol{u}, \boldsymbol{v})$$

subject to:

$$\Delta x(k+i+1|k) = A\Delta x(k+i|k) + B[\Delta u(k+i+1|k) + \Delta u(k+i|k)] +$$

$$d(k+i|k) + v(k+i|k)$$

$$v_{min} \le v(k+i|k) \le v_{max}$$

$$x_{min} \le x(k+i|k) \le x_{max}$$

$$u_{min} \le u(k+i+1|k) \le u_{max} \quad i = 1, 2, \ldots, N$$

In order to learn the nonlinearities and unmodeled effects, an **Extreme Learning Machine (ELM)** is used. In the next step, the minimax optimization is transformed to a nonlinear convex optimization problem that is solved using a **Recurrent Neural Network (RNN)** based on the work in (Xia and Wang 2004).

Learning based MPC has been applied to trajectory tracking in robotic manipulators as well. In (Lehnert and Wyeth 2013), the authors use local weighted regression to construct m different local linear models based on observed input-output data. The learned models, which are constantly updated during operation, are then used to solve m linear MPC problems to obtain m candidate inputs to be applied to the system. These inputs are then mixed using a kernel that weighs each input according to the distance between the center of each local linear model and the current state of the system. Gaussian kernel is commonly used for calculating weights w_i.

$$w_i(z) = e^{-\frac{1}{2}(z-c_i)^T D_i (z-c_i)}$$

Where c_i is the center of the kernel and D_i controls the shape

of the kernel function. Using these weights, the inputs calculated from each MPC can be mixed according to the following equations

$$u_{k+1} = \frac{1}{W} \sum_{i=1}^{m} w_i(x_k, u_k) u_{k+1}$$

$$W = \sum_{i=1}^{m} w_i(x_k, u_k).$$

Here u_k is the current input, u_{k+1} is the next input to be applied and u^i_{k+1} is the next input as calculated using MPC from the ith local linear model.

Although this work solves an unconstrained MPC and does not address the issues related to constraint handling, it demonstrates that manipulators can be modeled using observed input-output data. Furthermore experimental results have shown that the learning process indeed improves the tracking performance of the MPC over time.

More recently deep learning and MPC have been combined to compute the forces required for a robotic manipulator to cut a variety of foods (Lenz et al. 2015). The dynamic model of a cutting process which has position of the knife as its states and knife forces as its inputs cannot be dynamically modeled due to a great variety of food properties and complex interaction between the robot and the food. Therefore the task represents a challenging combination of time variance, nonlinearity and structural variations such as food stiffness and geometry. The deep learning architecture proposed in (Lenz et al. 2015) is able to use learned recurrent features to integrate long term information such as material properties into the model. Therefore this modeling approach is able to combine local information with global knowledge obtained from previous observations. DeepMPC is able to produce state predictions from a trajectory that is chosen based on past observations. The algorithm then evaluates MPC cost function and its gradient. After that the input is adjusted using gradient descent and the process is repeated until convergence.

CONCLUSION

In this chapter we first presented a review of MRAC and identified to the role of machine learning in traditional MRAC. We then discussed the limitations of MRAC and explained how more advanced machine learning methods have shown promise in offering more in terms of modeling more complex dynamics, removing requirements such as persistent excitation and look poised to move adaptive control methods forward significantly over what has been possible to date. The role of machine learning in control was discussed here from a modeling perspective and some of the most common machine learning models such as NN and mixture models were presented. Particularly, the idea of motor primitives was introduced as a biologically inspired method for motion representation and learning. In addition learning control and its connection with adaptive control were discussed and methods such as ILC and RL were introduced. Handling state and input

constraints was identified as one of the challenges that still needs further work. We gave an introduction to MPC for its constraint handling capability and reviewed some of the recent work that have aimed to incorporate learning methods in MPC framework. While data driven modeling and policy synthesis has demonstrated its benefits,
it does not mean that analytical modeling and control approaches should be deserted altogether. Instead machine learning should play a complementary role to analytical approaches. This is an idea that has appeared in some of the literature in MRAC for manipulators where adaptation was only introduced on the unknown portion of the dynamics of the system (Maliotis 1991, Craig et al. 1987). We nevertheless see a bright future for the formulation and application of machine learning methods in control engineering.

REFERENCES

Ahn, H. -S., Y. Q. Chen and K. L. Moore. 2007. Iterative learning control: Brief survey and categorization. Systems, Man, and Cybernetics, Part C: Applications and Reviews, IEEE Transactions on, 37(6): 1099–1121.

Andersson, O., F. Heintz and P. Doherty. 2015. Model-based reinforcement learning in continuous environments using real-time constrained optimization. AAAI Conference on Artificial Intelligence.

Arimoto, S., S. Kawamura and F. Miyazaki. 1984. Bettering operation of robots by learning. Journal of Robotic Systems, 1(2): 123–140.

Arimoto, S., S. Kawamura and F. Miyazaki. 1986. Convergence, stability and robustness of learning control schemes for robot manipulators. Proceedings of the International Symposium on Robot Manipulators on Recent Trends in Robotics: Modelling, Control and Education, pp. 307–316.

Astrom, K. J. and B. Wittenmark. 2013. Adaptive Control: Second Edition, Dover Publications, Inc.

Aswani, A., H. Gonzalez, S. S. Sastry and C. Tomlin. 2013. Provably safe and robust learning-based model predictive control. Automatica, 49(5): 1216–1226.

Boyd, S. P. and L. Vandenberghe. 2004. Convex Optimization, Cambridge University Press.

Bristow, D. A., M. Tharayil and A. G. Alleyne. 2006. A survey of iterative learning control. Control Systems, IEEE, 26(3): 96–114.

Chen, Y. and C. Wen. 1999. Iterative learning control: Convergence, robustness and applications.

Chowdhary, G., T. Yucelen, M. Muhlegg and E. N. Johnson. 2013. Concurrent learning adaptive control of linear systems with exponentially convergent bounds. International Journal of Adaptive Control and Signal Processing, 27(4): 280–301.

Ciliz, K. and A. Cezayirli. 2004. Combined direct and indirect adaptive control of robot manipulators using multiple models. Robotics, Automation and Mechatronics, 2004 IEEE Conference on, 1: 525–529.

Craig, J. J., P. Hsu and S. S. Sastry. 1987. Adaptive control of mechanical manipulators. The International Journal of Robotics Research, 6(2): 16–28.

Crespo, L. G., M. Matsutani and A. M. Annaswamy. 2010. Design of a model reference adaptive controller for an unmanned air vehicle. American Institute of Aeronautics and Astronautics.

Dubowsky, S. and D. T. Deforges. 1979. The application of model reference adaptive control to robotic manipulators.

International Journal of Adaptive Control and Signal Processing, 101(3): 193–200.

Ham, W. 1993. Adaptive control based on explicit model of robot manipulator. Automatic Control, IEEE Transactions on, 38(4): 654–658.

He, P., M. Rolla and S. Jagannathan. 2007. Reinforcement learning neural-network-based controller for nonlinear discrete-time systems with input constraints. Systems, Man, and Cybernetics, Part B: Cybernetics, IEEE Transactions on, 37(2): 425–436.

Hsia, T. C. 1984. Adaptive control of robot manipulators—A review. Robotics and Automation.

Proceedings, 1986 IEEE International Conference on.

Ioannou, P. and P. Kokotovic. 1983. Adaptive Systems with Reduced Models, Springer Verlag: Secaucus.

Khansari-Zadeh, S. M. and A. Billard. 2011. Learning stable nonlinear dynamical systems with Gaussian mixture models. Robotics, IEEE Transactions on, 27(5): 943–957.

Kober, J. 2012. Learning Motor Skills: From Algorithms to Robot Experiments, Technische Universitat Darmstadt.

Krause, J. and G. Stein. 1987. Structural limitations of model reference adaptive controllers. American Control Conference, 1987.

Lehnert, C. and G. Wyeth. 2013. Locally weighted learning model predictive control for nonlinear and time varying dynamics. Robotics and Automation (ICRA), 2013 IEEE International Conference on. Lenz, I., R. Knepper and A. Saxena. 2015. DeepMPC: Learning Deep Latent Features for Model

Predictive Control. Robotics Science and Systems (RSS).

Maciejowski, J. M. 2001. Predictive Control with Constraints, Pearson Education (US).

Maliotis, G. 1991. A hybrid model reference adaptive control/computed torque control scheme for robotic manipulators. Proceedings of the Institution of Mechanical Engineers, Part I: Journal of Systems and Control Engineering.

Mishra, S., U. Topcu and M. Tomizuka. 2011. Optimization-based constrained iterative learning control. Control Systems Technology, IEEE Transactions on, 19(6): 1613–1621.

Mohan, S. and J. Kim. 2012. Indirect adaptive control of an autonomous underwater vehicle- manipulator system for underwater manipulation tasks. Ocean Engineering, 54: 233–243.

Morari, M. a. Z. E. 1989. Robust Process Control, Prentice-Hall.

Muelling, K., J. Kober and J. Peters. 2010. Learning Table Tennis with a Mixture of Motor Primitives. Humanoid Robots (Humanoids), (2010) 10th IEEE-RAS International Conference on.

Narendra, K. and A. Annaswamy. 1986. Robust adaptive control in the presence of bounded disturbances. IEEE Transactions on Automatic Control, 31(4): 306–315.

Narendra, K. S. and A. M. Annaswamy. 1987. Persistent excitation in adaptive systems. International Journal of Control, 45(1): 127–160.

Nguyen-Tuong, D. and J. Peters. 2011. Model learning for robot control: A survey. Cognitive Processing, 12(4): 319–340.

Osburn, P. V., H. P. Whitaker and A. Kezer. 1961. New developments in the design of adaptive control systems. Institute of Aeronautical Sciences.

P., I. and J. Sun. 1996. Robust Adaptive Control, Prentice Hall, Inc.

Qin, S. J. and T. A. Badgwell. 2003. A survey of industrial model predictive control technology.
Control Engineering Practice, 11(7): 733–764.

Rong, H. -J. 2012. Indirect adaptive fuzzy-neural control of robot manipulator. High Performance Computing and Communication 2012 IEEE 9th International Conference on Embedded Software and Systems (HPCC-ICESS), 2012 IEEE 14th International Conference on, pp. 1776–1781.

Russell, S. and P. Norvig. 2010. Artificial Intelligence: A Modern Approach, Prentice Hall.

Schaal, S., P. Mohajerian and A. Ijspeert. 2007. Dynamics systems vs. Optimal control—A unifying view. *In*: P. Cisek, T. Drew and J. F. Kalaska. Computational Neuroscience: Theoretical Insights into Brain Function. Elsevier, 165: 425–445.

Schmidt, R. A. and T. D. Lee. 2011. Motor Control and Learning: A Behavioral Emphasis, Human Kinetics.

Slotine, J. -J. E. and W. Li. 1987. On the adaptive control of robot manipulators. The International Journal of Robotics Research, 6(3): 49–59.

Slotine, J. -J. E. and W. Li. 1991. Applied Nonlinear Control, Prentice-Hall International, Inc.

Tsai, M. C. and M. Tomizuka. 1989. Model reference adaptive control and repetitive control for robot manipulators. Robotics and Automation, 1989. Proceedings, 1989 IEEE International Conference on, 3: 1650–1655.

Tung, P. -C., S. -R. Wang and F. -Y. Hong. 2000. Application of MRAC theory for adaptive control of a constrained robot

manipulator. International Journal of Machine Tools and Manufacture, 40(14): 2083–2097.

Uchiyama, M. 1978. Formation of High-Speed Motion Pattern of a Mechanical Arm by Trial (Japanese Title: 試行による人工の手の高速運動パターンの形成). Transactions of the Society of Instrument and Control Engineers, 14: 706–712.

Verscheure, D., B. Demeulenaere, J. Swevers, J. De Schutter and M. Diehl. 2009. Time-optimal path tracking for robots: A convex optimization approach. Automatic Control, IEEE Transactions on, 54(10): 2318–2327.

Xia, Y. and J. Wang. 2004. A recurrent neural network for nonlinear convex optimization subject to nonlinear inequality constraints. Circuits and Systems I: Regular Papers, IEEE Transactions on, 51(7): 1385–1394.

Yan, Z. and J. Wang. 2014. Robust model predictive control of nonlinear systems with unmodelled dynamics and bounded uncertainties based on neural networks. Neural Networks and Learning Systems, IEEE Transactions on, 25(3): 457–469.

Yu, H., L. D. Seneviratne and S. W. E. Earles. 1993. Combined adaptive control of constrained robot manipulators. Intelligent Robots and Systems '93, IROS '93. Proceedings of the 1993 IEEE/RSJ International Conference on, 2: 740–745.

2

Discussion on Model Reference Adaptive Control of Robotic Manipulators

Dan Zhang[1] and *Bin Wei*[2,*]

ABSTRACT

Motion control accuracy of robotic manipulators affects the overall robotic system performance. When the end-effector grabs different payloads, the joint motion of robotic manipulators will vary depending on the different payload masses. Traditional controllers have the problem of not being able to compensate the payload variation effect. Model reference adaptive control has been proposed to address the above problem. This paper discusses the model reference adaptive control of robotic manipulators initially raised by the scholar Roberto Horowitz and its associated development by other authors. Some issues of model reference adaptive control (MRAC) for robotic manipulators are presented. Very few recent papers can be found in the area of model reference adaptive control of robotic manipulators, and this paper will provide a guideline for future research in the direction of model reference adaptive control for robotic arms.

Keywords: Adaptive control, robotic manipulator, model reference approach

1 Department of Mechanical Engineering, York University, Toronto, Ontario, M3J 1P3, Canada.
E-mail: dzhang99@yorku.ca

2 Faculty of Engineering and Applied Science, University of Ontario Institute of Technology, 2000 Simcoe Street North, Oshawa, Ontario, Canada.
E-mail: Bin.Wei@uoit.ca

* Corresponding author

INTRODUCTION

The robotic manipulator control problem is generally formulated as follows, given a desired trajectory, a mathematical model of the manipulator and its interactions with the environment, find the control algorithm which sends torque commands to the actuators so that the robotic manipulator can achieve expected motion. The control design for a serial robotic manipulator involves two steps. Firstly, an end-effector motion trajectory has been given, i.e., say one wants to move the end-effector from point A to point B. From this end-effector motion trajectory, and by using the inverse kinematics, the joint motion can be determined so as to produce this desired end-effector motion trajectory. The second step is to determine the joint torque, how much torque does one have to apply to the joint so that the joint will have the desired motion? The joint torque can be determined by solving the inverse dynamic equation.

Control the robot to perform in a certain way is one of the most challenging problems because the robotic manipulator mechanism is highly nonlinear. For the robotic manipulators, the coefficients of the dynamic equations are functions of joint variables and also the function of payload mass which may be unknown or change throughout the task. When the manipulator moves, the joint variables are changing, which will cause the robotic manipulator's dynamic equation to change throughout a given task. In order to obtain a high degree of accuracy and repeatability in the manipulator performance, it is necessary to use a control system (e.g., MRAC) that will account for the changes in the dynamic characteristic of the manipulator. Conventional control methods model the manipulator as uncoupled linear subsystems, these methods can produce satisfactory performances at low speeds, but it is not efficient anymore when used for high speed and high accuracy operations. The use of the PID controller for control does not guarantee optimal control of the system or system stability (https://en.wikipedia.org/ wiki/PID_controller). In order to address the above problem, adaptive control can be applied.

Model reference adaptive approach is most popular and established technique. Adaptive control adapts to a controlled system with parameters which vary, or are initially uncertain. For non-adaptive controller, the controller is designed based on the priori information of the system, i.e., one knows the system and designs the controller (e.g., PID controller) gears to that system and assume there is no change in the system. Whereas for the adaptive controller, the controller does not necessary need to depend on previous information of the system, and if there is sudden change in environment, the controller can cope with it to adapt to the changed conditions. If one considers a system that its transfer function is known, one designs a fixed classical controller, the controller will remain fixed parameters as long as it applies to the system, so one can say that this controller depends on its structure and designed on a-priori information, this is non-adaptive controller. However, if the controller is depending on posteriori information, for example, if one is changing the parameters of the controller, because of the changes of the parameters of the system or because of the disturbances coming from the environment, this controller is called adaptive. If the system is subject to unknown disturbances, or the system is expected to undergo changes in its parameters in a way which is not pre-determined from the beginning, in that case one uses adaptive control. However, in some cases one knows how the system operating condition will change, for example, for an aircraft, one knows that the aircraft controller is determined by its altitude and speed, and one expects that aircraft to fly at specific value for altitude and

speed, in that case one can design a controller for each expected operating point and switch between the different controllers, this is called gain-scheduling. In other cases one knows that the parameters of the system change, but one also knows a range for the change of every parameter, in that case it is possible to design a fixed controller that can cope with different changes of the parameters, and guarantee the stability and performance, this kind of controller is robust controller.

For non-adaptive control, say fixed-gain control, according to Fig. 1, one can see that firstly when one needs to improve the performance error, the modelling accuracy will also be increased, secondly it cannot improve itself, and thirdly it is assumed that future will be much like present, ignoring environment changes, change in dynamics and structure damage.

For the adaptive control, it achieves a given system performance asymptotically, it does not trade performance for modelling accuracy, as shown in Fig. 2, and more importantly, it improves itself under unforeseen and adverse conditions.

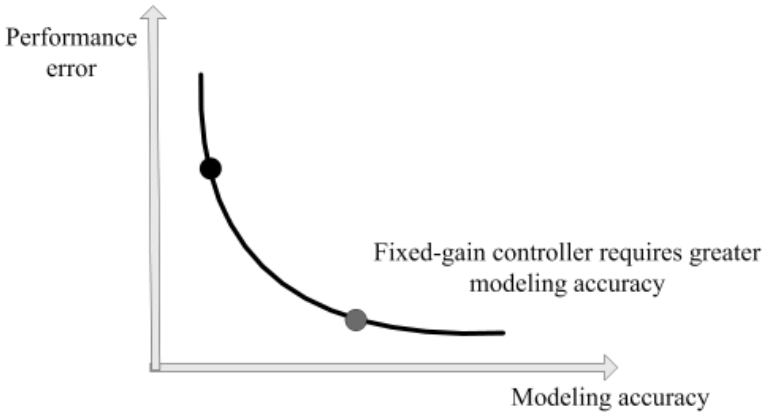


Figure 1. Non-adaptive control.

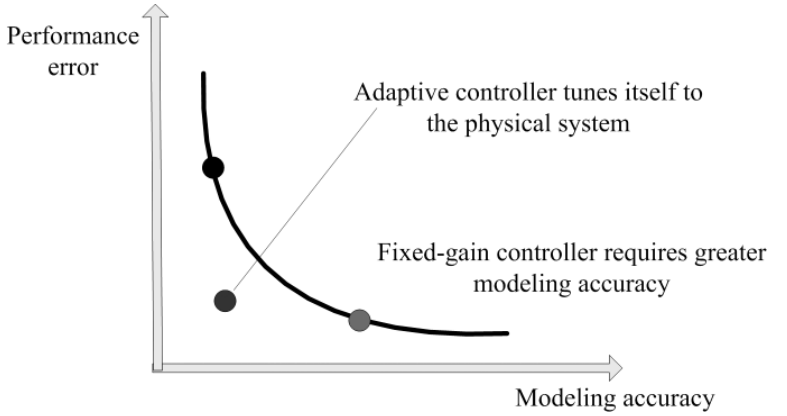


Figure 2. Adaptive control.

The adaptive control can be categorized into the following, model reference adaptive control, self-tuning adaptive control and gain-scheduled control, as shown in Fig. 3. Here we will mainly consider the model-reference approach.

For the model-reference adaptive control, the set value is used as an input to both the actual and the model systems, and difference between the actual output and the output from the model is compared. The difference in these signals is then used to adjust the parameters of the controller to minimize the difference. Figure 4 shows such control system.

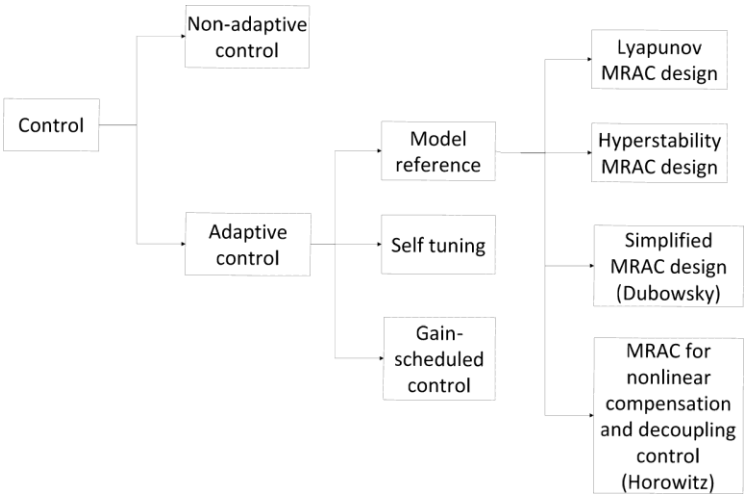


Figure 3. Adaptive control categorization.

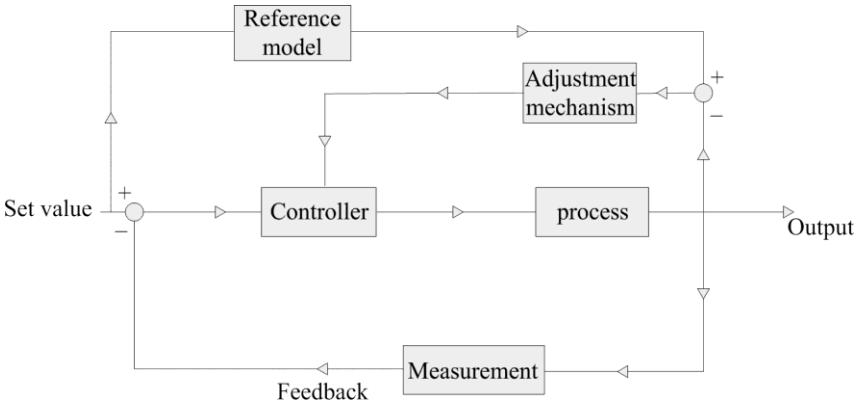


Figure 4. Model reference adaptive control.

Compared to other control methods, adaptive control is possible to achieve good performance over a wide range of motions and payloads. The advantage of the model reference adaptive control is that the plant parameters need not be fully known, instead, estimates of the plant parameters are used and the adaptive controller utilizes past input/ output information to improve these estimates. However there are two drawbacks to

MRAC. Stability analysis of the system is critical as it is not easy to design a stable adaptive law. The other problem is that MRAC relies on cancellation of the non-linear terms by the reference model (Sutherland 1987). In reality, exact cancellation cannot be expected, but the non-linear terms may be made so small so as to be negligible. Model reference adaptive control method was initially introduced in (Whitaker et al. 1958), when they considered adaptive aircraft flight control systems, using a reference model to obtain error signals between the actual and desired behavior. These error signals were used to modify the controller parameters to attain ideal behavior in spite of uncertainties and varying system dynamics. The goal of an adaptive control system is to achieve and maintain an acceptable level in the performance of the control system in the presence of plant parameter variations. Whereas a conventional feedback control system is mainly dedicated to the elimination of the effect of disturbances upon the controlled variables, also known as manipulated variables. An adaptive control system is mainly dedicated to the elimination of the effect of parameter disturbances/variations upon the performance of the control system.

ADAPTIVE CONTROL OF ROBOTIC MANIPULATORS

General Adaptive Control

In traditional control system, feedback is used to reject the disturbance effect that are acting on the controlled variables in order to bring the controlled variables back to their desired value. To do that, the variables are measured and compared to the desired values and the difference is fed into the controller. In these feedback systems, the designer adjusts the parameters of the controller so that a desired control performance is achieved. This is done by having a priori knowledge of the plant dynamics. When the parameters of the plant dynamic models change with time due to disturbances, the conventional control cannot deal with it anymore as the control performance will be degraded. At this time, one needs to resort to the adaptive control. A structured approach for the design of distributed and reconfigurable control system is

presented in (Valente et al. 2011). Distributed architectures are conceived as interconnected independent modules with standard interfaces which can be modified and reused without affecting the overall control structure. Whereas for the centralized control architectures, any change of the machine structure requires an extensive replacement of the control system. In RMS, modular and distributed architecture is essential to guarantee the capability of each single module or portions of the control to be adapted when a hardware reconfiguration occurs. In (Bi et al. 2015), the sustainable manufacturing by reconfiguration of robots through using robot modules was presented. The customized modules are end-effector, suction pump and adapters, modular frame, steering guide, PLC and robot controller, sensors, power supply and indicators, and touch screen. In terms of control, there are two separate controllers to operate. One controller is used to control the robot arm and the other is programmable logic controller (PLC) that will handle user inputs and sensor data in order to inform the robot arm controller which program to run. When the robot is reconfigured, the control system needs to be reconfigured as well, i.e., the software system should be reconfigured to support the communication and interactions among
system components. This is called software reconfiguration.

In (Wilson and Rock 1995), the neural networks is used for the control reconfiguration design for a space robot. The traditional controller was presented, and by using the neural networks, the traditional controller is updated to a reconfigurable controller. Two neural-network-control were developed to achieve quick adaptation controller. Firstly, a fully-connected architecture was used that has the ability to incorporate an a priori approximate linear solution instantly, this permits quick stabilization by an approximate linear controller. Secondly, a back-propagation learning method was used that allows back-propagation with discrete-valued functions. It presents a new reconfigurable neural-network-based adaptive control system for the space robot. In (Jung et al. 2005), it studied an adaptive reconfigurable flight control system using the mode switching of multiple models. The basic idea is to use the on-line estimates of the aircraft parameters to decide which controller to choose in a particular flight condition. It is related to the multi-mode adaptive control. In (Landau et al. 2011), the basic concept of adaptive control and several kinds of categories were introduced, i.e., open-loop adaptive control, direct adaptive control, indirect adaptive control, robust control, and conventional control, etc. The adaptive control can be seen as a conventional feedback control system but where the controlled variable is the performance index.

So there are two loops for the adaptive control, one is the conventional feedback loop and the other is the adaptation loop.

A control development approach is proposed in (Valentea et al. 2015) which consists of three steps: control conceptual design, application development and evaluation of solution robustness. The control system should be conceived as a set of independent and distributed control modules, capable of nesting one to each other. The structuring of control logics is the basis of the entire control development process. In order to enable the control system reconfiguration, an essential feature of the control architecture is the modularity and distribution of the control decisions across the various entities.

Adaptive Control for Robotic Manipulators

Non-adaptive controller designs often ignores the nonlinearities and dynamic couplings between joint motions, when robot motions require high speed and accelerations, it greatly deteriorate its control performance. Furthermore, non-adaptive controller designs requires the exact knowledge and explicit use of the complex system dynamics and system parameters. Uncertainties will cause dynamic performance degradation and system instability. There are many uncertainties in all robot dynamic models, model parameters such as link length, mass and inertia, variable payloads, elasticities and backlashes of gear trains are either impossible to know precisely or varying unpredictably. That is why adaptive control is needed to address the above problem.

Model reference adaptive control and its usage to robotic arms were introduced in (Neuman and Stone 1983) and (Amerongen 1981). Some design problems in adaptive robot control are briefly stated. S. Dubowsky (Dubowsky and Desforges 1979) is the first one that applies the model reference adaptive control in the robotic manipulator. The approach follows the method in (Donalson and Leondes 1963). A linear, second-order, time-invariant differential equation was used as the reference model for each degree of freedom of the manipulator arm. The manipulator was controlled by adjusting the position and velocity feedback gains to follow the model. A steepest-descent method was

used for updating the feedback gains. Firstly the reference model dynamics was written, subsequently the nonlinear manipulator (plant) dynamic equation was written, but how this equation is related to the Lagrange equation is not clear, thirdly an error function was written and it follows the method of steepest descent and a set of equations was derived for the parameter adjustment mechanism, which will minimize the difference between the actual closed-loop system response and the reference model response.

An adaptive algorithm was developed in (Horowitz and Tomizuka 1986) for serial robotic arm for the purpose of compensating nonlinear term in dynamic equations and decoupling the dynamic interaction among the joints. The adaptive method proposed in this paper is different from Dubowsky's approach (Dubowsky and Desforges 1979). Three main differences are concluded as follows: firstly, in Horowitz's method, the overall control system has an inner loop model reference adaptive system controller and an outer loop PID controller, whereas the control system in Dubowsky's method is entirely based on the model reference adaptive controller; secondly, in Dubowsky's paper, the coupling among joints and nonlinear terms in the manipulator equations are ignored whereas this is considered in Horowitz's method; thirdly, in Horowitz's paper, the design method is based on the hyper-stability method whereas the adaptive algorithm design in (Dubowsky and Desforges 1979) is based on the steepest descent method. Also in (Horowitz and Tomizuka 1986), there are some issues as follows. (1) The authors stated in (Horowitz and Tomizuka 1986) that "The overall control system will have an inner loop MRAS controller and an outer loop PID action controller with fixed gains". The above statement is not consistent with the Figs. 4 and 5 in (Horowitz and Tomizuka 1986). According to Figs. 4 and 5 in (Horowitz and Tomizuka 1986), the control system has an inner loop MRAS controller, but it does not have an outer loop PID action controller. The PID controller is in the form of $K_p e \square K_i \int e dt \square K_d \dot{e}$, but in the paper (Horowitz and Tomizuka 1986), the outer loop controller is in the form of $K_i \int e \square K_p x_p \square K_d x_v$, which is absolutely not a PID

controller. (2) For the Figs. 4 and 5 in (Horowitz and Tomizuka 1986), the outer loop controller is in the form of $K_i \int e - K_p x_p - K_d x_v$, but in the similar paper (Horowitz et al. 1987) by the same authors,
the outer loop controller is in the form of $K_i \int e - K_p x_p - K_d x_v$. It is not consistent.
(3) For the Equation (13) in (Horowitz and Tomizuka 1986), the adaptive algorithm
are all positive, but in (Horowitz 1983) (note that (Horowitz and Tomizuka 1986) is part of the dissertation (Horowitz 1983)), the adaptive algorithms are all negative, it is also not consistent.

Model reference adaptive control, self-tuning adaptive control and linear perturbation adaptive control are briefly reviewed in (Hsia 1986). For the model reference adaptive control, the main idea is to synthesize/design a control signal to the robot dynamic equation, which will force the robot to behave in a certain manner specified by the reference model, and the adaptive algorithm is designed based on the Lyapunov stability criterion. The MRAC methods presented in (Srinivasan 1987) is based on the theory of partitioning control, which makes them capable of compensating for non-linear terms in the dynamic equations and also to decouple the dynamic interactions between the links. It followed and used the method in (Horowitz 1983). Future research would focus on further simplification of MRAC schemes since the implementation of MRAC methods for the real time control of manipulators has proven to be a challenging task.

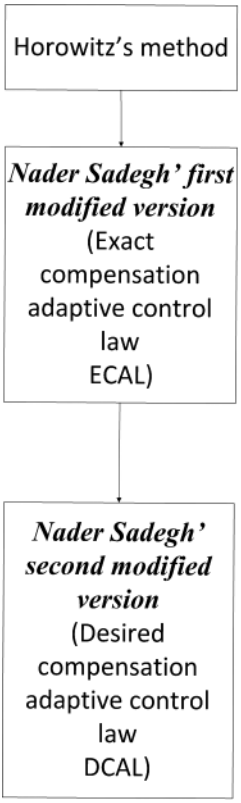


Figure 5. Modification process.

A MRAC system of 3-DOF serial robotic manipulator was presented in (Horowitz 1983). It was concerned with the application of MRAC to mechanical manipulators. Due to the dynamic equations of mechanical manipulators are highly nonlinear and complex, and also the payload sometimes varies or unknown, the MRAC was applied to the mechanical manipulators. An adaptive algorithm was developed for compensating nonlinear terms in the dynamic equations and for decoupling the dynamic interactions. Finally a 3-DOF serial manipulator was used as computer simulation and the results show that the adaptive control scheme is effective in reducing the sensitivity of the manipulator performance to configuration and payload variations. The core content of the method in (Horowitz 1983) can be concluded as four steps: first step, deterministic nonlinearity compensation and decoupling

control. Because one needs to calculate the inertia matrix and nonlinear term, the second step is therefore proposed, i.e., adaptive nonlinearity compensation and decoupling control, which is to adaptively adjust the inertia matrix and nonlinear term instead of calculating them, and the adaptive algorithm was developed; final step, complete the overall control system by adding the feedback gain. In (Horowitz 1983), it did not entirely use the Landau's hyperstability design (Landau 1979), the authors used some part of it, and they themselves developed the adaptive algorithm. Because according to (Hsia 1986), Horowitz's method was separated from the Landau's hyperstability design. And also from (Sutherland 1987), it is stated

that “While Landau’s method replied on a pre-specified parameter matrix for a model and continuous adaptation of the plant parameters, it will be seen later that it is possible to estimate the model parameters and adapt them continuously”, from this statement, it is clearly that Horowitz has his own theory to derive the adaptive algorithm, he did not use Landau’s method to derive the adaptive algorithm, but how the adaptive algorithm was derived was not explicitly addressed. In (Sutherland 1987), it used the same approach with Horowitz’s (Horowitz 1983) to a 2-DOF serial robotic manipulator and a flexible manipulator.

In (Tomizuka et al. 1986, Tomizuka and Horowitz 1988), the experiment on the continuous time and discrete time adaptive control on 1-DOF test stand robot arm and Toshiba TSR-500V robot were briefly conducted. The theory of Horowitz et al. (1987) is the continuation of the theory of Tomizuka et al. (1986) on a single axis direct drive robotic arm. It applies to a two axis direct drive robotic arm. In (Tomizuka et al. 1985), it presented the experiment evaluation of model reference adaptive controller and robust controller for positioning of a robotic arm under variation of payload. The results show that both method can be insensitive of the payload variation. Four adaptive control methods for the robotic arm were summarized in (Hamadi 1989), i.e., computed torque technique, variable structure systems, adaptive linear model following control, and adaptive perturbation control, and the adaptive nonlinear model following control was proposed subsequently, which combines the self-tuning regulator and the model reference adaptive control.

A modified version of the method in (Horowitz 1983) was proposed in (Sadegh and Horowitz 1987). The assumption that inertia matrix and nonlinear term are constant during adaptation can be removed by modifying the control law and parameter adaptation law. It is demonstrated that by modifying the control law (i.e., making the Coriolis and centripetal acceleration compensation controller a bilinear function of the joint and model reference velocities instead of a quadratic function of the joint velocities) and by modifying the parameter adaptation law (i.e., decomposing the nonlinear parameters in the

manipulator dynamic equations into the product of two quantities: one constant unknown quantity, which includes the numerical values of the masses, moments of inertia of the links, payload and link dimensions, and the other a known nonlinear function of the manipulator structural dynamics. The nonlinear functions are assumed to be known and calculable), the assumption that the inertia matrix and nonlinear term are constant during adaptation is removed. Finally the stability of the above adaptive control law is proved. The above called "exact compensation adaptive control law (ECAL)". In the conclusion, it was found that this procedure is excessively time consuming since it involves computations of highly nonlinear functions of joint position and velocities, to overcome this difficulty, later in (Sadegh and Horowitz 1990) and (Sadegh 1987), further modified version was proposed. The modification consists in utilizing the desired joint positions and velocities in the computation of the nonlinearity compensation controller and the parameter adaptation law instead of the actual quantities, this is known as "desired compensation adaptive control law (DCAL)". The above whole modification process is shown in Fig. 5.

S. Nader applied Craig's method (Craig et al. 1986) to the Horowitz's method, so the condition inertia matrix and nonlinear term assume constant during adaptation can be removed. Craig's method is re-parametrization, i.e., decompose the manipulator dynamic equation's nonlinear parameters into the product of two quantities: one constant unknown quantity, which includes the numerical values of the masses, moments of

inertia of the links, payload and link dimensions, and a known nonlinear function of the manipulator structural dynamics. The parameter adaptation law is only used to estimate the unknown constant quantities. One method of reparametrizing the manipulator's dynamic equations consists in decomposing each element of inertia matrix, nonlinear term and gravity term into products of unknown constant terms and known functions of the joint displacement vector. Or a second method consists in the re-parametrization of dynamic equation into the product of unknown constant vector, and a matrix formed by known functions of joint position.

CONCLUSION

This paper discusses the model reference adaptive control of robotic manipulators initially raised by the scholar Roberto Horowitz and its associated development by other authors. Some issues of model reference adaptive control for robotic manipulators are also presented. Very few recent papers can be found in the area of model reference adaptive control of robotic manipulators, and this paper will provide a guideline for future research in the direction of model reference adaptive control for robotic arms.

ACKNOWLEDGMENT

The authors would like to thank the financial support from the Natural Sciences and Engineering Research Council of Canada (NSERC) and Canada Research Chairs program.

REFERENCES

Amerongen, J. 1981. MRAS: Model Reference Adaptive Systems. Journal A, 22(4): 192–198.

Bi, Z. M., Y. Liu and B. Baumgartner, etc. 2015. Reusing industrial robots to achieve sustainability in small and medium-sized enterprises (SMEs). Industrial Robot: An International Journal, 42(3): 264–273.

Craig, J. J., P. Hsu and S. S. Sastry. 1986. Adaptive control of mechanical manipulators. Proceedings of the 1986

IEEE International Conference on Robotics and Automation, San Francisco, April, 1986.

Donalson, D. and T. Leondes. 1963. A model referenced parameter tracking technique for adaptive control systems. IEEE Transactions on Applications and Industry, 82(68): 241–252.

Dubowsky, S. and D. Desforges. 1979. The application of model-referenced adaptive control to robotic manipulators. Journal of Dynamic Systems Measurement and Control, 101: 193–200.

Hamadi, J. 1989. Adaptive Control Methods for Mechanical Manipulators: A Comparative Study, Master Thesis, Naval Postgraduate School.

Horowitz, R. 1983. Model Reference Adaptive Control of Mechanical Manipulators, Ph.D. Thesis, University of California.

Horowitz, R. and M. Tomizuka. 1986. An adaptive control scheme for mechanical manipulators— compensation of nonlinearity and decoupling control. Journal of Dynamic Systems, Measurement, and Control, 108(2): 1–9.

Horowitz, R., M. C. Tsai, G. Anwar and M. Tomizuka. 1987. Model reference adaptive control of a two axis direct drive manipulator arm. Proceedings of 1987 IEEE International Conference on Robotics and Automation, pp. 1216–1222.

Hsia, T. 1986. Adaptive control of robot manipulators—A review. Proceedings of 1986 IEEE International Conference on Robotics and Automation, pp. 183–189.

https://en.wikipedia.org/wiki/PID_controller.

Jung, B., S. Jeong, D. Lee and Y. Kim. 2005. Adaptive reconfigurable flight control system using multiple model mode switching. Proceedings of the 16th IFAC World Congress, Vol. 16, Part 1.

Landau, Y. 1979. Adaptive control—the model reference approach. CRC Press.

Landau, I. D. et al. 2011. Introduction to adaptive control. *In*: Adaptive Control, Communications and Control Engineering, Springer-Verlag London Limited.

Neuman, C. P. and H. W. Stone. 1983. MRAC control of robotic manipulators. pp. 203–210. *In*: K. S. Narendra (ed.). 3rd Yale Workshop on Applications of Adaptive Systems Theory. Yale Univ., New Haven, CT.

Sadegh, N. 1987. Adaptive control of mechanical manipulators: Stability and robustness analysis, Ph.D. Thesis, University of California.

Sadegh, N. and R. Horowitz. 1987. Stability analysis of an adaptive controller for robotic manipulators. Proceedings of 1987 IEEE International Conference on Robotics and Automation, pp. 1223–1229.

Sadegh, N. and R. Horowitz. 1990. Stability and robustness analysis of a class of adaptive controllers for robotic manipulators. International Journal of Robotics Research, 9(3): 74–92.

Srinivasan, R. 1987. Adaptive control for robotic manipulators, Master Thesis, Carleton University. Sutherland, J. 1987. Model reference adaptive control of a two link manipulator, Master Thesis,
Carleton University.

Tomizuka, M., R. Horowitz and G. Anwar. 1986. Adaptive techniques for motion controls of robotic manipulators. *In*: Japan—USA Symposium on Flexible Automation, July 1986, Osaka, Japan.

Tomizuka, M. and R. Horowitz. 1988. Implementation of adaptive techniques for motion control of robotic manipulators. J. Dyn. Sys., Meas., Control, 110(1): 62–69.

Tomizuka, M., R. Horowitz and G. Anwar. 1986. Adaptive techniques for motion controls of robotic manipulators. pp. 117–224. *In*: Japan—USA Symposium on Flexible

Automation, Japan.

Tomizuka, M., R. Horowitz and C. L. Teo. 1985. Model reference adaptive controller and robust controller for positioning of varying inertia. pp. 191–196. *In*: Proceedings of Conference on Applied Motion Control, University of Minnesota.

Valente, A., E. Carpanzano and M. Brusaferri. 2011. Design and implementation of distributed and adaptive control solutions for reconfigurable manufacturing systems. *In*: CIRP Sponsored ICMS. International Conference on Manufacturing Systems.

Valentea, A., M. Mazzolinib and E. Carpanzanoa. 2015. An approach to design and develop reconfigurable control software for highly automated production systems. International Journal of Computer Integrated Manufacturing, 28(3): 321–336.

Whitaker, H. P., J. Yamron and A. Kezer. 1958. Design of Model Reference Adaptive Control Systems for Aircraft. Report R-164, Instrumentation Laboratory. M. I. T. Press, Cambridge, Massachusetts.

Wilson, E. and S. Rock. 1995. Reconfigurable control of a free-flying space robot using neural networks. Proceedings of the 1995 American Control Conference, 2: 1355–1359.

3

Data-Based Learning for Uncertain Robotic Systems

Anup Parikh,[1,*] *Rushikesh Kamalapurkar*[2] and *Warren E. Dixon*[1]

ABSTRACT

An adaptive controller based on the concurrent learning method is developed for uncertain Euler-Lagrange systems. Using a Lyapunov-based analysis, it is shown that this design achieves the tracking objective, as well as identifies the uncertain parameters, without requiring the well-known and restrictive persistence of excitation condition. Simulation results are provided to demonstrate faster convergence compared to gradient based adaptive controllers without concurrent learning.

Keywords: Robotic systems, concurrent learning method, adaptive controller

INTRODUCTION

Robot manipulators have been used for a variety of motion control applications, and therefore high precision control of robot manipulators has been of interest in the control community for a number of decades. The general equations of motion for robot manipulators (i.e., Euler-Lagrange system) can be used to describe the dynamics for a variety of electromechanical systems, and therefore have become a benchmark system for novel control design techniques, e.g.,

adaptive control, robust control, output feedback, and control with limited actuation (Lewis et al. 2003, Behal et al. 2009). Adaptive control refers to a number of techniques for achieving a tracking or regulation

---

[1] Department of Mechanical and Aerospace Engineering, University of Florida, Gainesville FL 32611-6250.

[2] School of Mechanical and Aerospace Engineering, Oklahoma State University, Stillwater OK 74078.

* Corresponding author

control objective while compensating for uncertainties in the model by estimating the uncertain parameters online. It is well known that least-squares or gradient based adaptation laws rely on persistence of excitation (PE) to ensure parameter convergence (Ioannou and Sun 1996, Narendra and Annaswamy 1989, Sastry and Bodson 1989), a condition which cannot be guaranteed *a priori* for nonlinear systems, and is difficult to check online, in general.

Motivated by the desire to learn the true parameters, or at least to gain the increased robustness (i.e., bounded solutions in the presence of disturbances) and improved transient performance (i.e., exponential tracking versus asymptotic tracking of many adaptive controllers) that parameter convergence provides, a new adaptive update scheme known as concurrent learning (CL) was recently developed in the pioneering work of (Chowdhary and Johnson 2011, Chowdhary 2010, Chowdhary et al. 2013). The principle idea of CL is to use recorded input and output data of the system dynamics to apply batch-like updates to the parameter estimate dynamics. These updates yield a negative definite, parameter estimation error term in the stability analysis, which allows parameter convergence to be established provided a finite excitation condition is satisfied. The finite excitation condition is a weaker condition than persistent excitation (since excitation is only required for a finite amount of time), and can be checked online by verifying the positivity of the minimum singular value of a function of the regressor matrix.

In this chapter, a concurrent learning based adaptation law for general Euler- Lagrange systems is developed. We also demonstrate faster tracking error and parameter estimation error convergence compared to a gradient based adaptation law through a simulation.

CONTROL DEVELOPMENT

Consider robot manipulator equations of motion of the form (Lewis et al. 2003, Spong and Vidyasagar 1980)

$$M(q)\ddot{q} + V_m(q, \dot{q})\dot{q} + F\dot{q} + G(q) = \tau \qquad (1)$$

where $q(t)$, $\dot{q}(t)$, $\ddot{q}(t) \in \mathbb{R}^n$ represent the measurable link position, velocity and acceleration vectors, respectively, $M : \mathbb{R}^n \to \mathbb{R}^{n\times n}$ represents the inertial matrix, $V_m : \mathbb{R}^n \times \mathbb{R}^n \to \mathbb{R}^{n\times n}$ represents centripetal-Coriolis effects, $F_d \in \mathbb{R}^{n\times n}$ represents frictional effects, $G : \mathbb{R}^n \to \mathbb{R}^n$ represents gravitational effects and $\tau(t) \in \mathbb{R}^n$ denotes the control input. The system in (1) has the following properties (See Lewis et al. 2003).

Property 1. The system in (1) can be linearly parameterized, i.e., (1) can be rewritten as

$$Y_1(q, \dot{q}, \ddot{q})\,\theta = M(q)\,\ddot{q} + V_m(q, \dot{q})\,\dot{q} + F_d\,\dot{q} + G(q) = \tau$$

where $Y_1 : \mathbb{R}^n \times \mathbb{R}^n \times \mathbb{R}^n \to \mathbb{R}^{n\times m}$ denotes the regression matrix, and $\theta \in \mathbb{R}^m$ is a vector of uncertain parameters.

Property 2. The inertia matrix is symmetric and positive definite, and satisfies the following inequalities

$$m_1 \|\xi\|^2 \le \xi^T M(q)\,\xi \le m_2 \|\xi\|^2, \ \forall \xi \in \mathbb{R}^n$$

where m_1 and m_2 are known positive scalar constants, and $\|\cdot\|$ represents the Euclidean norm.

Property 3. The inertia and centripetal-Coriolis matrices satisfy the following skew symmetric relation

$$\xi^T \left(\frac{1}{2}\dot{M}(q) - V_m(q, \dot{q}) \right) \xi = 0, \; \forall \xi \in \mathbb{R}^n$$

where $\dot{M}(q)$ is the time derivative of the inertial matrix.

To quantify the tracking objective, the link position tracking error, $e(t) \in \mathbb{R}^n$, and the filtered tracking error, $r(t) \in \mathbb{R}^n$, are defined as

$$e = q_d - q \tag{2}$$

$$r = \dot{e} + \alpha e \tag{3}$$

where $q_d(t) \in \mathbb{R}^n$ represents the desired trajectory, whose first and second time derivatives exist and are continuous (i.e., $q_d \in C^2$). To quantify the parameter identification objective, the parameter estimation error, $\tilde{\theta}(t) \in \mathbb{R}^m$, is defined as

$$\tilde{\theta} = \theta - \hat{\theta} \tag{4}$$

where $\hat{\theta}(t) \in \mathbb{R}^m$ represents the parameter estimate.

Taking the time derivative of (3), premultiplying by $M(q)$, substituting in from (1), and adding and subtracting $V(q, \dot{q})\, r$ results in the following open loop error dynamics

$$M(q)\, \dot{r} = Y_d(q_d, \dot{q}_d, q, \dot{q}, \ddot{q})\, \theta - V(q, \dot{q})\, r - \tau \tag{5}$$

where $Y : \mathbb{R}^n \times \mathbb{R}^n \times \mathbb{R}^n \times \mathbb{R}^n \times \mathbb{R}^n \to \mathbb{R}^{n \times m}$ is defined based on the relation

$$Y_2(q, \dot{q}, q_d, \dot{q}_d, \ddot{q})\, \theta \triangleq M(q)\, \ddot{q}_d + V_m(q, \dot{q})\, (\dot{q}_d + \alpha e) + F_d \dot{q} + G(q) + \alpha M(q)\, \dot{e}.$$

To achieve the tracking objective, the controller is designed as

$$\tau(t) = Y \hat{\theta} + e + k\, r \tag{6}$$

where $k_1 \in \mathbb{R}$ is a positive constant. To achieve the parameter identification objective,
the parameter estimate update law is designed as

$$\dot{\hat{\theta}} = \Gamma Y_2^T r + k_2 \Gamma \sum_{i=1}^{N} Y_{1i}^T (\tau_i - Y_{1i} \hat{\theta}) \tag{7}$$

where $k \in \mathbb{R}$ and $\Gamma \in \mathbb{R}^{m \times m}$ are constant positive definite and symmetric control gains, $Y_{1i} \in Y_1(q(t_i), \dot{q}(t_i), \ddot{q}(t_i))$, $\tau_i \in \tau(t_i)$, $^0 t_i$ represent past time points, i.e., $t_i \in [0, t]$, and $N \in \mathbb{N}$.
Using (1), (7) can be rewritten as

$$\dot{\hat{\theta}} = \Gamma Y_2^T r + k_2 \Gamma \sum_{i=1}^{N} Y_{1i}^T (Y_{1i} \theta - Y_{1i} \hat{\theta})$$

$$= \Gamma Y_2^T r + k_2 \Gamma \left[\sum_{i=1}^{N} Y_{1i}^T Y_{1i} \right] \tilde{\theta}. \tag{8}$$

The principal idea behind this design is to use recorded input and trajectory data to identify the uncertain parameter vector θ. The time points t_i and the corresponding τ_i and Y_{1i} used in the summation in (7) are referred to as the history stack. As shown in the subsequent stability analysis, the parameter estimate learning rate is related to the minimum eigenvalue of $\sum_{i=1}^{N} Y_{1i}^T Y_{1i}$, motivating the use of the singular value maximization algorithm in (Chowdhary 2010) for adding data to the history stack. It is also important to note that although this design uses higher state derivatives which are typically not measured (i.e., $\ddot{q}$), this data is only required for time points in the past, and therefore smoothing techniques can be utilized to minimize noise without inducing a phase shift, e.g., (Mühlegg et al. 2012).

Substituting the controller from (6) into the error dynamics in (5) results in the following closed-loop tracking error dynamics

$$M(q)\dot{r} = Y(q, \dot{q}, \ddot{q}, \dot{q}_d, \ddot{q}_d)\tilde{\theta} - e_1 - V_m(q, \dot{q})r - k_r r. \qquad (9)$$

Similarly, taking the time derivative of (4) and substituting the parameter estimate update law from (8) results in the following closed-loop parameter estimation error dynamics

$$\dot{\tilde{\theta}} = -k_\Gamma \Gamma Y_r^T \left[\sum_{i=1}^{N} Y_{1i}^T Y_{1i}\right]\tilde{\theta}. \qquad (10)$$

STABILITY ANALYSIS

To analyze the stability of the closed loop system, two periods of time are considered. During the initial phase, insufficient data has been collected to satisfy a richness condition on the history stack. In Theorem 1 it is shown that the designed controller and adaptive update law are still sufficient for the system to remain bounded for all time despite the lack of data. After a finite period of time, the system transitions to the second phase, where the history stack is sufficiently rich and

the controller and adaptive update law are shown, in Theorem 2, to bound the system by an exponentially decaying envelope, therefore achieving the tracking and identification objectives. To guarantee that the transition to the second phase happens in finite time, and therefore the overall system trajectories can be bounded by an exponentially decaying envelope, we require the history stack be sufficiently rich after a finite period of time, i.e.,

$$\exists \lambda, T > 0 : \forall t \geq T, \lambda \min \left\{ \sum_{i=1}^{N} Y_{1i}^T Y_{1i} \right\} \geq \lambda. \tag{11}$$

The condition in (11) requires that the system be sufficiently excited, though is weaker than the persistence of excitation condition since excitation is unnecessary once $\sum_{i=1}^{N} Y_{1i}^T Y_{1i}$ is full rank.

Theorem 1. *For the system defined in (1), the controller and adaptive update law defined in (6) and (7) ensure bounded tracking and parameter estimation errors.*

Proof: Let $V : \mathbb{R}^{2n+m} \to \mathbb{R}$ be a candidate Lyapunov function defined as

$$V(\eta) = \frac{1}{2} e^T e + \frac{1}{2} r^T M(q) r + \frac{1}{2} \tilde{\theta}^T \Gamma^{-1} \tilde{\theta} \quad (12)$$

where $\eta \triangleq [e^T \; r^T \; \tilde{\theta}^T]^T \in \mathbb{R}^{2n+m}$ is a composite state vector. Taking the time derivative of (12) and substituting (3), (9), and (10) yields

$$\dot{V} = e^T(r - \alpha e) + r^T\left(-\frac{1}{2}\dot{M}(q)r + Y(q, \dot{q}, \dot{q}_r, \ddot{q}_r)\tilde{\theta} - e - (K_D + K_N)r\right) - \tilde{\theta}^T\Gamma^{-1}\dot{\hat{\theta}}.$$

Simplifying and noting that $\dot{M}(q, \dot{q}) - 2V_m(q, \dot{q})$ is always positive semi-definite, $\dot{V}$ can be upper bounded as

$$\dot{V} \leq -\alpha e^T e - k_1 r^T r - k_2 r^T \sum_{i=1}^{N} Y_{1i} Y_{1i}^T r + \tilde{\theta}^T Y^T r - \tilde{\theta}^T \Gamma^{-1} \dot{\hat{\theta}}.$$

Therefore, η is bounded based on (Khalil 2002). Furthermore, since $\dot{V} \leq 0$, $V(\eta(T)) \leq V(\eta(0))$ and therefore $\|\eta(T)\| \leq \sqrt{\frac{b_2}{b_1}} \|\eta(0)\|$, where $\beta \triangleq \frac{1}{2} \min\{1, m, \lambda_1\} \sqrt{\frac{1}{b_2}}$ and $\Delta \triangleq 2 \max\{1, m, \lambda_2\}$. ■

Theorem 2. *For the system defined in (1), the controller and adaptive update law defined in (6) and (7) ensure globally exponential tracking in the sense that*

$$\|\eta(t)\| \leq \left(\frac{\beta_2}{\beta_1}\right) \exp(\lambda_1 T) \|\eta(0)\| \exp(-\lambda_1 t), \quad \forall t \in [0, \infty) \quad (13)$$

where $\lambda_1 \triangleq \frac{1}{2}\beta \min\{\alpha, k_1, k_2\lambda_2\}$.

Proof: Let $V : \mathbb{R}^{2n+m} \to \mathbb{R}$ be a candidate Lyapunov function defined as in (12). Taking the time derivative of (12), substituting (3), (9), (10) and simplifying yields

$$\dot{V} = -\alpha e^T e - k_r r^T \left[r - k_\theta \tilde{\theta} \right]. \quad (14)$$

From the finite excitation condition, $\lambda_{\min}\{\sum_{i=1}^{N} Y_{1i}^T Y_{1i}\} > 0$, $\forall t \in [T, \infty)$, which implies that $\sum_{i=1}^{N} Y_{1i}^T Y_{1i}$ is positive definite, and therefore $\dot{V}$ can be upper bounded as

$$\dot{V} \leq -\alpha e^T e - k_r r^T r - k_\theta \underline{\lambda} \|\tilde{\theta}\|^2, \quad \forall t \in [T, \infty).$$

Invoking (Khalil 2002), η is globally exponentially stable, i.e., $\forall t \in [T, \infty)$,

$$\|\eta(t)\| \leq \sqrt{\frac{b_2}{b_1}} \|\eta(T)\| \exp(-\lambda_1 (t - T)).$$

The composite state vector can be further upper bounded using the results of Theorem 1, yielding (13).

□

Remark 1. Although the analysis only explicitly considers two periods, i.e., before and after the history stack is sufficiently rich, additional data may be added into the history stack after T as long as the data increases the minimum eigenvalue of $\sum_{i=1}^{N} Y_{1i}^T Y_{1i}$.

By using the data selection algorithm in (Chowdhary 2010), the minimum eigenvalue of $\sum_{i=1}^{N} Y_{1i}^T Y_{1i}$ is always increasing, and therefore the Lyapunov function derivative upper bound in (14), is valid for all time after T. Hence (12) is a common Lyapunov function (Liberzon 2003).

SIMULATION

A simulation of this control design applied to a two-link planar robot was performed. The dynamics of the two-link robot are given as

$$\begin{bmatrix} p_1 + 2p_3 c_2 & p_2 + p_3 c_2 \\ p_2 + p_3 c_2 & p_2 \end{bmatrix} \begin{bmatrix} \ddot{q}_1 \\ \ddot{q}_2 \end{bmatrix} + \begin{bmatrix} -p_3 s_2 \dot{q}_2 & -p_3 s_2 (\dot{q}_1 + \dot{q}_2) \\ p_3 s_2 \dot{q}_1 & 0 \end{bmatrix} \begin{bmatrix} \dot{q}_1 \\ \dot{q}_2 \end{bmatrix} + \begin{bmatrix} f_{d1} & 0 \\ 0 & f_{d2} \end{bmatrix} \begin{bmatrix} \dot{q}_1 \\ \dot{q}_2 \end{bmatrix} = \begin{bmatrix} \tau_1 \\ \tau_2 \end{bmatrix}$$

$M(q)$ $V_m(q, \dot{q})$ F_d

where c_2 denotes cos (q_2) and s_2 denotes sin (q_2). The nominal parameters are given by

$p_1 = 3.473 \quad f_{d1} = 5.3$

$p_2 = 0.196 \quad f_{d2} = 1.1$

$p_3 = 0.242$

and the controller gains were selected as

$\alpha = 1.0 \qquad \Gamma = 0.1 I_5$

$k_1 = 0.1 \qquad k_2 = 0.1.$

The desired trajectory was selected as

$q_{d1} = (1 + 10 \exp(-2t)) \sin(t)$,

$q_{d2} = (1 + 10 \exp(-t)) \cos(3t)$,

and a history stack of up to 20 data points was used in the adaptive update. The tracking and parameter estimation error trajectories are show in Figs. 1 and 2. From Fig. 2, it is clear that the system parameters have been identified. A comparison simulation was also performed without concurrent learning (i.e., setting $k_2 = 0$), representing a typical control design that asymptotically tracks the desired trajectory based on Theorem 1, with error trajectories shown in Figs. 3 and 4. In comparison to a typical gradient based adaptive controller that yields the trajectories in Figs. 3 and 4, the contribution of the concurrent learning method is evident by the exponential trajectories in Figs. 1 and 2. It is also important to note that a number techniques have been developed for improving transient performance of adaptive control architectures such as the gradient based adaptive update law simulated here (e.g. (Duarte and Narendra 1989, Krstić et al. 1993, Yucelen and Haddad 2013, Pappu et al. 2014, Yucelen et al. 2014)),

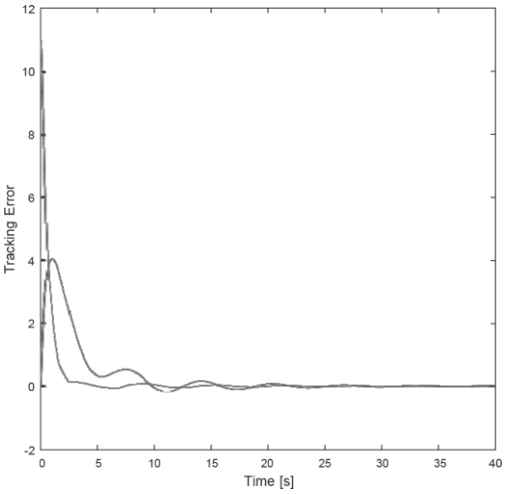


Figure 1. Tracking error trajectory using concurrent learning based control design.

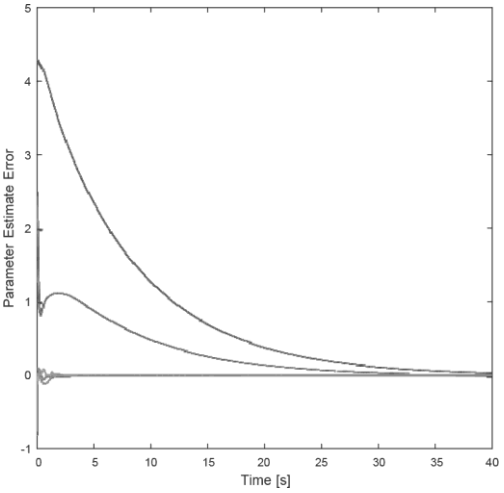


Figure 2. Parameter estimation error trajectory using concurrent learning based control design.

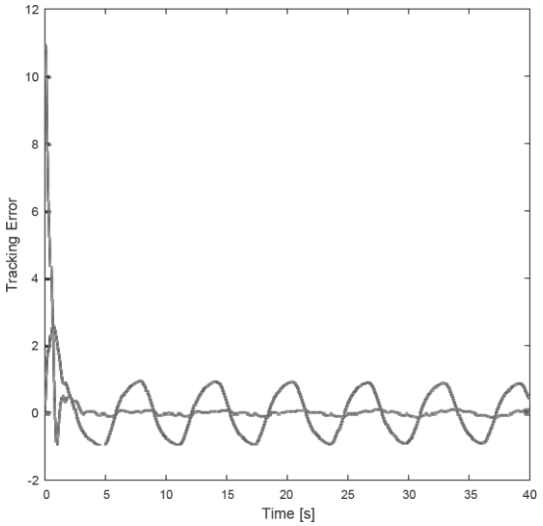


Figure 3. Tracking error trajectory using traditional gradient based control design.

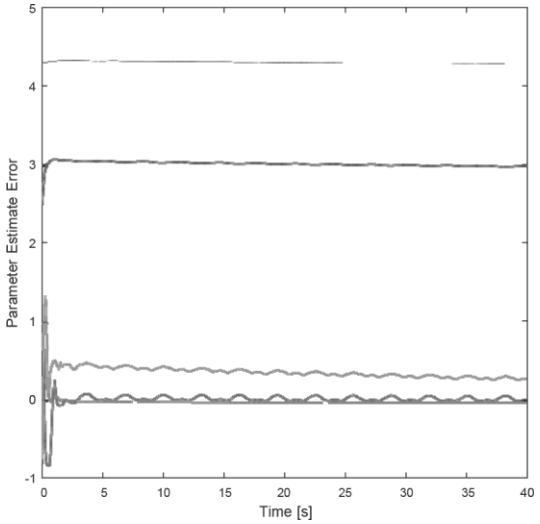


Figure 4. Parameter estimation error trajectory using traditional gradient based control design.

though cannot guarantee parameter identification, and hence exponential trajectories, without persistence of excitation.

CONCLUSION

In this chapter a novel adaptive controller is developed for Euler-Lagrange systems. The concurrent learning based design incorporates recorded data into the adaptive update law, resulting in exponential convergence of the tracking and parameter estimation

errors. The excitation condition required for convergence is weaker than persistent excitation, and is easier to check online. The provided simulation results demonstrate the increased convergence rate of this design compared to traditional adaptive controllers with gradient based update laws.

REFERENCES

Behal, A., W. E. Dixon, B. Xian and D. M. Dawson. 2009. Lyapunov-Based Control of Robotic Systems. Taylor and Francis.

Chowdhary, G. V. and E. N. Johnson. 2011. Theory and flight-test validation of a concurrent-learning adaptive controller. J. Guid. Control Dynam., 34(2): 592–607, March.

Chowdhary, G. 2010. Concurrent learning for convergence in adaptive control without persistency of excitation, Ph.D. dissertation, Georgia Institute of Technology, December.

Chowdhary, G., T. Yucelen, M. Mühlegg and E. N. Johnson. 2013. Concurrent learning adaptive control of linear systems with exponentially convergent bounds. Int. J. Adapt. Control Signal Process., 27(4): 280–301.

Duarte, M. A. and K. Narendra. 1989. Combined direct and indirect approach to adaptive control.
IEEE Trans. Autom. Control, 34(10): 1071–1075, October.

Ioannou, P. and J. Sun. 1996. Robust Adaptive Control. Prentice Hall.

Khalil, H. K. 2002. Nonlinear Systems, 3rd ed. Upper Saddle River, NJ: Prentice Hall.

Krstic´, M., P. V. Kokotovic´ and I. Kanellakopoulos. 1993. Transient-performance improvement with a new class of adaptive controllers. Syst. Control Lett., 21(6): 451–461. [Online]. Available: http://www.sciencedirect.com/science/article/pii/016769119390050G.

Lewis, F. L., D. M. Dawson and C. Abdallah. 2003. Robot Manipulator Control Theory and Practice.
CRC.

Liberzon, D. 2003. Switching in Systems and Control. Birkhauser.

Mühlegg, M., G. Chowdhary and E. Johnson. 2012.

Concurrent learning adaptive control of linear systems with noisy measurements. *In*: Proc. AIAA Guid. Navig. Control Conf.

Narendra, K. and A. Annaswamy. 1989. Stable Adaptive Systems. Prentice-Hall, Inc.

Pappu, V. S. R., J. E. Steck, K. Rajagopal and S. N. Balakrishnan. 2014. Modified state observer based adaptation of a general aviation aircraft—simulation and flight test. *In*: Proc. AIAA Guid. Navig. Control Conf., National Harbor, MD, January.

Sastry, S. and M. Bodson. 1989. Adaptive Control: Stability, Convergence, and Robustness. Upper Saddle River, NJ: Prentice-Hall.

Spong, M. and M. Vidyasagar. 1980. Robot Dynamics and Control. New York: John Wiley & Sons Inc.

Yucelen, T. and W. M. Haddad. 2013. Low-frequency learning and fast adaptation in model reference adaptive control. IEEE Trans. Autom. Control, 58(4): 1080–1085.

Yucelen, T., G. D. L. Torre and E. N. Johnson. 2014. Improving transient performance of adaptive control architectures using frequency-limited system error dynamics. Int. J. Control, 87(11): 2383–2397.



Reinforcement Learning of Robotic Manipulators

*Kei Senda** and *Yurika Tani*

ABSTRACT

This chapter discusses an autonomous space robot for a truss structure assembly using some reinforcement learning. It is difficult for a space robot to complete contact tasks within a real environment, e.g., a peg-in-hole task, because of the potential discrepancy between the real environment and the controller model. In order to solve problems, we propose an autonomous space robot able to obtain proficient and robust skills by overcoming error prospects in completing a task. The proposed approach develops skills by reinforcement learning that considers plant variation, i.e., modeling error. Numerical simulations and experiments show the proposed method is useful in real environments.

Keywords: Reinforcement learning, Robust skills, Plant variation/modeling error, Contact tasks

INTRODUCTION

This chapter discusses an unresolved robotics issue, i.e., how to make a robot autonomous. A robot with manipulative skills capable of flexibly achieving tasks, like a human being,

is desirable. Autonomy is defined as “automation to achieve a task robustly”. Skills can be considered to be solutions to achieve autonomy. Another aspect of a skill is including a solution method. Most human skill proficiency is acquired by experience. Since the way to realize autonomy is not clear, skill development must

Department of Aeronautics and Astronautics, Kyoto University, Japan.
* Corresponding author

include solution methods for unknown situations. Our problem is how to acquire skills autonomously, i.e., how to robustly and automatically complete a task when the solution is unknown.

Reinforcement learning (Sutton and Barto 1998) is a promising solution, whereas direct applications of existing methods with reinforcement learning do not robustly complete tasks. Reinforcement learning is a framework in which a robot learns a policy or a control that optimizes an evaluation through trial and error. It is teacherless learning. By means of reinforcement learning, a robot develops an appropriate policy as mapping from state to action when an evaluation is given. The task objective is prescribed, but no specific action is taught. Reinforcement learning often needs many samples. The large number of samples is due to the large number of states and actions. Online learning in a real environment is usually impractical. Most learning algorithms consist of two processes (Bertsekas and Tsitsiklis 1996): (1) online identification by trial and error sampling and (2) finding the optimal policy for the identified model. These two processes are not separated in typical learning algorithms such as Q-learning (Fujii et al. 2006). Reinforcement learning is said to be adaptive because it uses online identification and on-site optimal control design. Robustness attained using this adaptability is often impractical. It takes a very long time for online identification by means of trial and error. Real-world samples are expensive in terms of time, labor, and finances, and is referred to as a curse of real-world samples (Kober and Peters 2012). They also state that it is often more important to limit the real-world interaction time instead of limiting memory consumption or computational complexity.

In our approach, by following a robust policy rather than by online identification, reinforcement learning is used to achieve a solution to an unknown task. Such reinforcement learning to obtain a robust policy against model uncertainty is a recent research topic.

This chapter addresses an autonomous space robot for a truss structure assembly. For a space robot, it is difficult to achieve a task contacting with a real environment, e.g., peg-in-hole task, because there is the error between the real

environment and the controller model. A space robot must autonomously obtain proficiency and robust skills in order to counter the error in the model. Using the proposed approach, reinforcement learning can achieve a policy that is robust in the face of plant variation, i.e., the modeling error. Numerical simulations and experiments show that a robust policy is effective in a real environment and the proposed method is used.

NEED FOR AUTONOMY AND APPROACH

Need for Autonomy

Autonomy is needed wherever robots work. Below, we discuss why and what kind of autonomy is required (Senda 2001, Senda et al. 2002) for space robots.

Space robots are required to complete tasks in the place of extra vehicular activity by an astronaut. Studies of autonomous systems are needed to realize space robots that can achieve missions under human-operator command. There are many applications for the autonomous space robots (Skaar and Ruoff 1995).

We developed ground experiments to simulate a free-flying space robot under orbital microgravity conditions (Fig. 1). Using this apparatus, we have studied robot autonomy. Targeting control-based autonomy, we developed an automatic truss structure

assembly, etc. However, it has been hard to achieve perfect robot automation because of various factors. To make a robot autonomous in the face of the following challenges, we must:

(a) solve problems in the actual robot-environment;
(b) operate robustly in the face of uncertainties and variations;
(c) overcome the difficulty of comprehensively predicting a wide variety of states;
(d) identify tasks and find unknown solutions to realize robust robot autonomy.

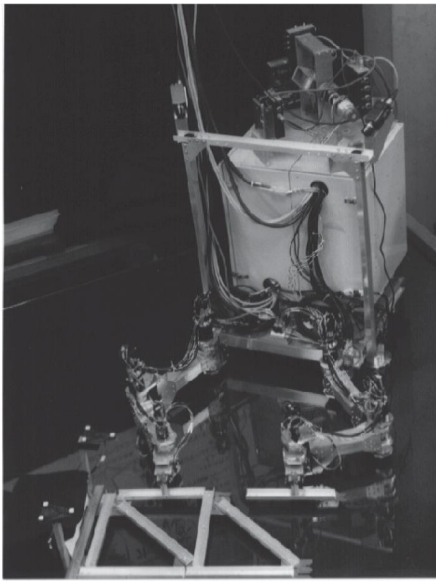


Figure 1. Photograph of space robot model and truss.

Approach to Autonomy Based on Reinforcement Learning

Human beings achieve tasks regardless of the above complicating factors, but robots cannot. Many discussions have rationalized the difficulties as originating in the nature of human skills. We have not established a means by which we can realize such skills. This chapter takes the following approach to this problem.

The fourth section approaches to factors (a) and (b) in part by way of control-based automation taking account of the

robustness of controls. The autonomous level of this approach is low because only small variations are allowable.

The fifth section considers how to surmount factors (a), (b), and (c) by learning. Using a predicted model and transferring the learned results to the actual system (Asada 1999) is studied. This model is identified online and relearned. This procedure is applied where adaptability or policy modification is needed to thwart variations in the real environment. In some cases, the robot completes the targeted tasks autonomously. Learning is completed within an acceptable calculation time.

The sixth section considers factors (a), (b), (c), and (d). A peg-in-hole task has higher failure rates using the same approach as used in the fifth section. Because of small differences between the model and the real environment, failure rates are excessive.

The robot thus must gain skills autonomously. Skills similar to those of human beings must be generated autonomously. These skills are developed by reinforcement learning and additional procedures.

The seventh evaluates approach robustness and control performance of the newly acquired skills. The skills obtained in the sixth section are better than those in the fifth section.

EXPERIMENTAL SYSTEM AND TASKS

Outline of Experimental System

Our experimental system (Figs. 1 and 2) simulates a free-flying space robot in orbit. Robot model movement is restricted to a two-dimensional plane (Senda et al. 2002).

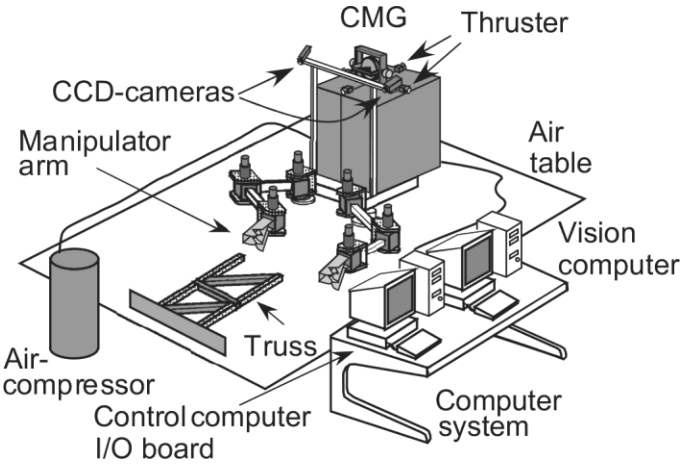


Figure 2. Schematic diagram of experimental system.

The robot model consists of a satellite vehicle and dual three-degrees-of-freedom (3-DOF) rigid SCARA manipulators. The satellite vehicle has CCD cameras for stereovision and a position/attitude control system. Each joint has a torque sensor and a servo controller for fine torque control of the output axis. Applied force and torque at the end-

effector are calculated using measured joint torque. Air-pads are used to support the space robot model on a friction-less planar table and to simulate the space environment. RTLinux is installed on a control computer to control the space robot model in real time. Stereo images from the two CCD cameras are captured by a video board and sent into an image-processing computer with a Windows OS. The image-processing computer measures the position and orientation of target objects in the worksite by triangulation. Visual information is sent to the control computer via Ethernet.

The position and orientation measured by the stereo vision system involves errors caused by quantized images, lighting conditions at the worksite, etc. Time-averaged errors are almost constant in each measurement. Evaluated errors in the peg-in-hole experiments are modelled as described below. Hole position errors are modeled as a

normal probability distribution, where the mean is $m = 0$ [mm], and standard deviation is $\sigma = 0.75$ [mm]. Hole orientation errors are modeled as a normal probability distribution, where the mean is $m = 0$ [rad], and standard deviation is $\sigma = 0.5\pi/180$ [rad].

We accomplish a hand-eye calibration to achieve tasks in following sections. An end-effector, a manipulator hand, grasps a marker with a light-emitting diode (LED). The arm directs the marker to various locations. The robot calculates the marker location by using sensors mounted at the joints of the manipulator arm. The vision system also measures the marker location by using the stereo image by triangulation. Measurements using these joint-angle sensors have more precise resolution and accuracy. Hence, we calibrate the visual measurements based on measurements using the joint angle sensors. We consider the joint angle sensor measurement data to be the true value.

Tasks

Truss Assembly Task

Figure 3 illustrates the truss structure assembly sequence. Manipulating a truss component and connecting it to a node proceeds the assembly process. Later this task is achieved by controls based upon mechanics understanding (Senda et al. 2002). The truss design is robot friendly for easy assembling.

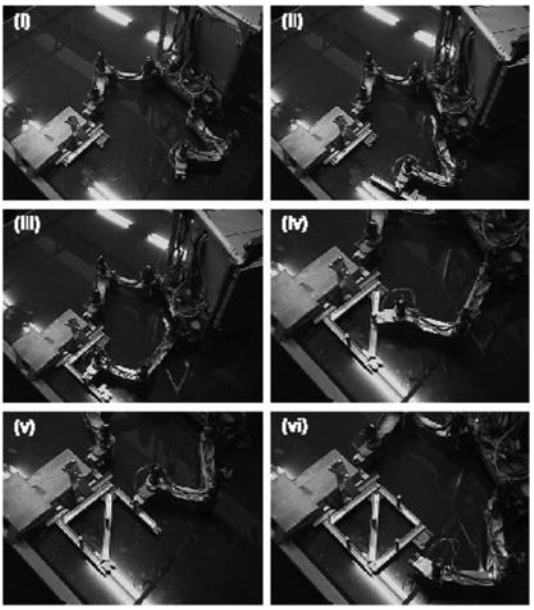


Figure 3. Sequence of truss structure assembly.

Peg-in-hole Task

The peg-in-hole task is an example that is intrinsic to the nature of assembly. The peg-in-hole task involves interaction within the environment that is easily affected by

uncertainties and variations, e.g., errors in force applied by the robot, manufacturing accuracy, friction at contact points, etc. The peg easily transits to a state in which it can no longer move, e.g., wedging or jamming (Whitney 1982). Such variations cannot be modeled with required accuracy.

To complete a task in a given environment, a proposed method analyzes the human working process and applies the results to a robot (Sato and Uchiyama 2007). Even if the human skill for a task can be analyzed, the results are not guaranteed to be applicable to a robot. Another method uses parameters in a force control designed by means of a simulation (Yamanobe et al. 2006) but was not found to be effective in an environment with uncertainty. In yet another method (Fukuda et al. 2000), the task achievement ratios evaluated several predesigned paths in an environment with uncertainty. An optimal path is determined among the predesigned paths. There was the possibility a feasible solution did not exist among predesigned paths.

In the peg-in-hole experiment (Fig. 4), the position and orientation of the hole is measured using a stereo camera. The robot manipulator inserts a square peg into a similar sized hole. This experiment is a two-dimensional plane problem (Fig. 5). The space robot model coordinate system is defined as Σ_0, the end-effector coordinate system as Σ_E, and the hole coordinate system as Σ_{hl}. While the space robot completes its task, the robot grasps the structural site with other manipulator, the relative relation between Σ_0 and Σ_{hl} is fixed. State variables are defined as $[y_X, y_Y, y_\theta, f_X, f_Y, f_\theta]$, where (y_X, y_Y) is the position of Σ_E in Σ_0, y_θ is the orientation about $\boldsymbol{k}_0$-axis, (f_X, f_Y) and f_θ are the forces and torque in Σ_0 that end-effector applies to the environment.

The peg width is 74.0 [mm] and the hole width is 74.25 [mm]. The hole is only 0.25 [mm] wider than the peg. The positioning error is composed of the measurement error and the control error. The robot cannot insert the peg in the hole by position control if the positioning error is beyond ±0.125 [mm]. Just a single measurement error by stereo vision often moves the peg outside of the acceptable region.

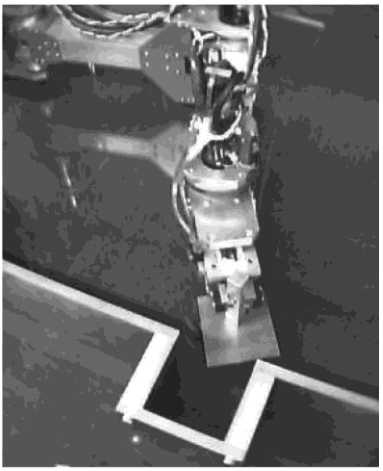


Figure 4. Photograph of peg-in-hole experiment setup.

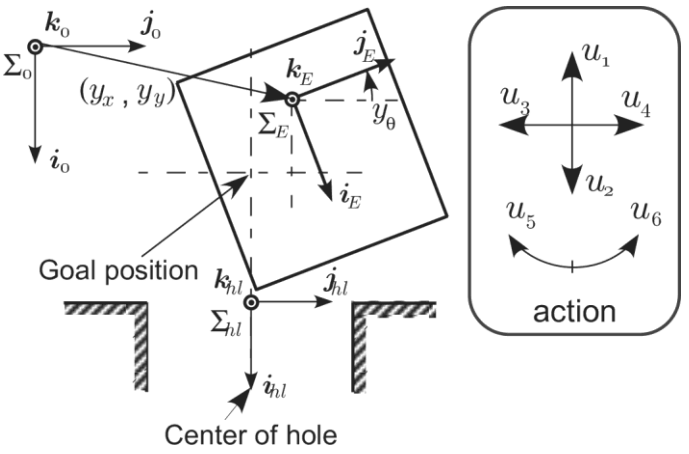


Figure 5. Definition of peg-in-hole task.

CONTROL-BASED AUTOMATION

Truss Assembly Task

Automatic truss assembly was studied via controls-based automation with mechanics understanding. The robot achieved an automatic truss structure assembly (Senda et al. 2002) by developing basic techniques and integrating them within the experimental system.

The following sensory feedback control (Miyazaki and Arimoto 1985) is used for controlling manipulators:

$$\boldsymbol{\tau} = -\boldsymbol{J}^T \boldsymbol{K}_P (\boldsymbol{y} - \boldsymbol{y}_d) - \boldsymbol{K}_D \dot{\boldsymbol{q}} \quad (1)$$

where $\boldsymbol{\tau}$ is the control input to the manipulator, $\boldsymbol{J}$ is the Jacobean matrix. The $\boldsymbol{y}$ is the manipulation variable whose elements are the hand position/orientation $[y_X, y_Y, y_\theta]$, $\boldsymbol{y}_d$ is the reference value of $\boldsymbol{y}$, $\boldsymbol{q}$ is the joint angle vector, and $\boldsymbol{K}_P$ and $\boldsymbol{K}_D$ are feedback gains. When the end-effector contacts the environment and manipulation variable $\boldsymbol{y}$ is stationary under constraint, the end-effector applies force and torque to the environment:

$$\boldsymbol{f} = -\boldsymbol{K}_P\ (\boldsymbol{y} - \boldsymbol{y}_d) \tag{2}$$

The force and torque can be controlled by $\boldsymbol{y}_d$. This is a compliant control.

Figure 3 is a series of photographs of the experimental assembly sequence. As shown in panel (i), the robot holds on to the worksite with its right arm to compensate for any reaction force during the assembly. The robot installs the first component, member 1, during panels (ii) and (iii). The robot installs other members successively and assembles one truss unit, panels (iv)–(vi).

Control procedures for the assembly sequence are as follows. There are target markers in the experiment environment as shown in Figs. 1 and 3. Target markers are located at the base of the truss structure and at the storage site for structural parts. Each

target marker has three LEDs at triangular vertices. The vision system measures the marker position and orientation simultaneously. The robot recognizes the position of a part relative to the target marker before assembly. The robot places the end-effector position at the pick-up point, which is calculated from the target marker position as measured by the stereo vision system. At the pick-up point, the end-effector grasps a handgrip attached to the targeted part. The position and orientation of the part to the end-effector is settled uniquely when the end-effector grasps the handgrip. The robot plans the path of the arm and part to avoid collision with any other object in the work environment. It controls the arm to track along the planned path. The robot plans a path from the pick-up point to the placement point, avoiding obstacles by means of an artificial potential method (Connolly et al. 1990). Objects in the environment, e.g., the truss under assembly, are regarded as obstacles. The arm is then directed along a planned trajectory by the sensory feedback control, Eq. (1). The end-effector only makes contact with the environment when it picks-up or places the part. Hence, feedback gains in Eq. (1) are chosen to make it a compliant control.

Consequently, the truss assembly task is successfully completed by controls- based automation. However, measurement error in the vision system sensors, etc. prevents assembly from being guaranteed. Irrespective of uncertainties and variations at the worksite, the space robot model requires autonomy to complete the task goal.

Peg-in-hole Task

The positioning control of Eq. (1) tries to complete the peg-in-hole task. The peg first is positioned at $y_\theta = 0$ [rad], it transits to the central axis of the hole, and it moves in a positive direction, toward $\boldsymbol{i}_0$. The peg does not contact the environment during transition from the initial state to the goal. Insertion is successful if the position control of the peg relative to the hole is free from error. Unfortunately, the peg-in-hole task is often unsuccessful because of the existing error. The robot cannot insert the peg in the hole by position control if the positioning error is greater than ±0.125 [mm]. So, single measurement error using stereo vision is often beyond the acceptable error. The manner

in which the task fails is almost the same as shown in Fig. 8 in the next section.

EXISTING METHOD FOR AUTONOMY WITH REINFORCEMENT LEARNING

Outline of Existing Method with Reinforcement Learning

Reinforcement learning (Sutton and Barto 1998) is used to generate autonomous robot action.

In "standard" learning (Fig. 6 (a)), controller $\boldsymbol{K}_Q$ is designed in advance by learning the nominal plant model $\boldsymbol{P}_N$, and it is applied to real plant $\boldsymbol{P}$. We use a policy called controller $\boldsymbol{K}_Q$, which is designed with reinforcement learning methods. When variations exist, e.g., measurement error in the vision system, unexpected obstacles appear in the environment, etc., $\boldsymbol{K}_Q$ cannot complete tasks due to poor robustness and adaptability.

As shown in Fig. 6 (b), new plant model $\boldsymbol{P}'_N$ is reconstructed using visual measurement. Controller $\boldsymbol{K}'_Q$ is designed for the reconstructed model $\boldsymbol{P}'_N$. Controller $\boldsymbol{K}'_Q$

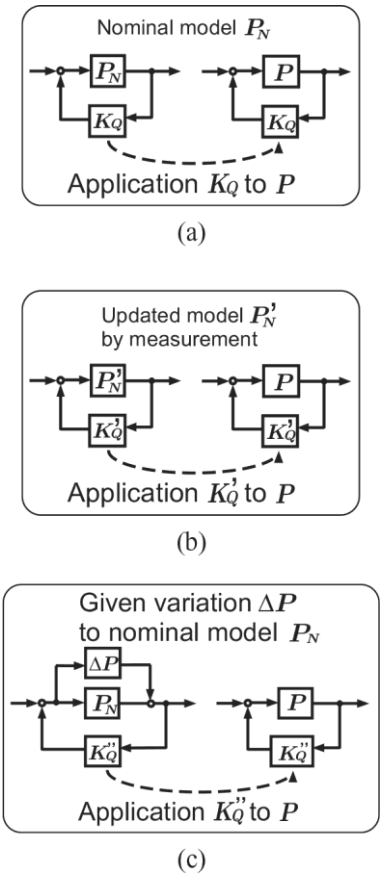


Figure 6. Learning using: (a) nominal plant model, (b) updated plant model and (c) plant model with variation.

is then applied to real plant ***P***. Learning converges within a practical calculation time and the new policy is applicable to the truss structure assembly (Senda et al. 2002). This method works well because it treats the kinematic problem without force interaction between the robot and the environment. The plant model for learning is reconstructed by visual measurement within a short time. This method has adaptability only if the model can be reconstructed accurately within a short time.

If the robot cannot complete the task with the controller due to error between the model and the real plant, the robot switches to online learning. Adaptability is realized by online

identification and learning. However, this cannot be used for peg-in-hole task, because online identification requires too much time. In the next section, a reinforcement learning problem for a peg-in-hole task requires several tens of thousands of state-action pairs. It requires tens of days for online identification if a hundred samples are selected for each state-action pair and each sampling takes one second.

Existing Method with Reinforcement Learning

Problem Definition

Following general dynamic programming (DP) formulations, this chapter treats a discrete-time dynamic system in a reinforcement learning problem. A state s_i and an action u_k are the discrete variables and the elements of finite sets $\Box$ and $\Box$, respectively. The state set $\Box$ is composed of N_S states denoted by $s_1, s_2, \cdots, s_{NS}$, and an additional termination state s_0. The action set $\Box$ is composed of K actions denoted by $u_1, u_2, \cdots, u_K$. If an agent is in state s_i and chooses action u_k, it will move to state s_j and incur a one-step cost $g(s_i, u_k, s_j)$ within state transition probability $p_{ij}(u_k)$. This transition is denoted by (s_i, u_k, s_j). There is a cost-free termination state s_0 where $p_{00}(u_k) = 1, g(s_0, u_k, s_0) = 0, Q(s_0, u_k) = 0, \forall u_k$. We assume that the state transition probability $p_{ij}(u_k)$ is dependent on only current state s_i and action u_k. This is called a discrete-time finite Markov Decision Process (MDP). The system does not explicitly depend on time. Stationary policy μ is a function mapping states into actions with $\mu(s_i) = u_k \in \Box$, and μ is given by the corresponding time-independent action selection probability $\pi(s_i, u_k)$. In this chapter, we deal with an infinite horizon problem where the cost accumulates indefinitely. The expected total cost starting from an initial state $s^0 = s$ at time $t = 0$,

and using a stationary policy μ is

$$J^{\mu}(s) = \lim_{N \to \infty} E_{s_t, t=0} \left\{ \sum_{t=0}^{N} g(s_t, \mu(s_t), s_{t+1}) \,\middle|\, s^0 = s_i \right\} \tag{3}$$

where $E_X[\cdot]$ denotes an expected value, and this cost is called J-factor. Because of the Markov property, a J-factor of a policy μ satisfies

$$J^{\mu}(s_i) = \sum_{k=1}^{K} p_{ij}(u_k) \sum_{j=0}^{N_S} p_{ij}(u_k) \{ g(s_i, u_k, s_j) + J^{\mu}(s_j) \}, \tag{4}$$

A policy μ is said to be proper if μ satisfies $J^{\mu}(s) < \infty, \forall s$.

We regard the J-factor of every state as an evaluation value, and the optimal policy μ^* is defined as the policy that minimizes the J-factor:

$$\mu^*(s_i) = \arg\min_{\mu} J^{\mu}(s_i), \quad \forall s_i \in S \tag{5}$$

The J-factor of the optimal policy is defined as the optimal J-factor. It is denoted by $J^*(s_i)$.

The optimal policy defined by (5) satisfies Bellman's principle of optimality. Then, the optimal policy is stationary and deterministic. The optimal policy can be solved by minimizing the J-factor of each state independently. Hence, the optimal J-factors satisfy the following Bellman equation, and the optimal policy is derived from the optimal J-factors:

$$J^*(s_i) = \min_{u_k} \sum_{j=1}^{N_S} p_{ij}(u_k)\{g(s_i, u_k, s_j) + J^*(s_j)\}, \tag{6}$$

$$m^*(s_i) = \arg\min_{u_k} \sum_{j=0}^{N_s} p_{ij}(u_k)\{g(s_i, u_k, s_j) + J^*(s_j)\}. \quad (7)$$

Solutions

The existing type of reinforcement learning problem is solved as "standard" learning in Fig. 6 (a). It obtains the optimal policy μ^*_{nom}, which minimizes the J-factors of Eq. (7) for the nominal plant. It corresponds to controller $\boldsymbol{K}_Q$ in Fig. 6 (a). The optimal J-factor J^*_{nom} of μ^*_{nom} can be obtained by the DP-based solutions. The solutions are mentioned in reference (Sutton and Barto 1998, Bertsekas and Tsitsiklis 1996), but they are omitted here.

Learning Skill for Peg-in-hole by Existing Method

Problem Definition of Peg-in-hole

Here, the peg-in-hole task defined in subsection "Peg-in-hole task" is redefined as a reinforcement learning problem.

State variables [y_X, y_Y, y_θ, f_X, f_Y, f_θ] in subsection "Peg-in-hole task" are continuous but discretized into 1.0 [mm], 1.0 [mm], $0.5\pi/180$ [rad], 2.0 [N], 1.0 [N], and 0.6 [Nm] in the model for reinforcement learning. The discrete state space has 4,500 discrete states, where the number of each state variable is [5, 5, 5, 4, 3, 3]. Robot action at the end-effector is u_1, u_2, u_3, u_4, at each of the end-effector states transiting by ±1 in the direction of the $\boldsymbol{i}_0$-axis or $\boldsymbol{j}_0$-axis, u_5 and u_6, at each of the end-effector states transiting by ±1 about the $\boldsymbol{k}_0$-axis of rotation. State-action space is described in the space robot model coordinate system Σ_0. The hole is 0.25 [mm] wider than the peg, and (y_X, y_Y) are quantized larger than this difference.

Control in Eq. (1) is used to transit from present state s_i to the next state s_j by action $u(s_i) = u_k$. The reference manipulation variable to make the transition to s is given by $\boldsymbol{y}^d_k(s_i) = \boldsymbol{y}^d(s_i) + \delta\boldsymbol{y}^d_k(s_i)$ during transition. When $\delta\boldsymbol{y}^d_k(s_i)$ (k = 1, 2, · · · , 6), where $\delta\boldsymbol{y}^d_j(s_i) = \boldsymbol{y}^d_d - \boldsymbol{y}^d_d$ is kept constant

the end-effector contacts the environment and manipulation variable $\boldsymbol{y}$ is stationary under constraint, the end-effector applies force and torque to the environment $\boldsymbol{f} = -\boldsymbol{K}_P(\boldsymbol{y} - \boldsymbol{y}_d)$ as Eq. (2) where $\boldsymbol{y}_d$ is the reference manipulation variable. Force and torque are controlled by $\boldsymbol{y}_d$, which is changed by an action. This is a compliant control, a force control. Tasks in which the end-effector contacts the environment, e.g., peg-in-hole, demand a control with compliance. Therefore, a compliant control is essential as a basic control.

The robot takes the next action after Eq. (1) control settles and the peg becomes stationary. Regardless of whether the peg is in contact with the environment, the robot waits for settling and proceeds to the next action. For this reason, state variables do not include velocity.

The goal is to achieve states with the largest y_X, the peg position in $\boldsymbol{i}_0$-direction, in the state space. The one step cost is $g(s_i, u_k, s_j) = 1$ for all states other than the goal state. Hence, the J-factor is the expected step number from s_i to the goal.

Learning Method

State transition probabilities for the state-action space in the previous section are calculated with sample data. Sample data are calculated with a dynamic simulator in a spatially continuous state space. The dynamic simulator is constructed with an open- source library, the Open Dynamics Engine (ODE) developed by Russell Smith. The numerical model of this simulator has continuous space, force and time in contrast to the discretized models for reinforcement learning in subsection “Problem definition”. This discretized state transition model is regarded as plant P_N, and the method in Fig. 6
(a) is applied. The optimal policy μ^*_{nom}, i.e., controller $\boldsymbol{K}_Q$, is derived from the solution
in subsection “Solutions”. The optimal policy μ^*_{nom} is applied to the dynamic simulator with a continuous state-action space or the hardware experimental setup, the real plant $\boldsymbol{P}$ in Fig. 6 (a). This chapter does not deal with the online learning.

Learning Result

The result of a numerical simulation in which controller $\boldsymbol{K}_Q$ is applied to the environment with no position/orientation error is shown. The peg moves and arrives at the goal as shown in Fig. 7. Peg positioning is first changed to y_θ = 0 [rad]. After the peg transits to the hole central axis, it is moved in a positive direction, toward $\boldsymbol{i}_0$. Then the peg is inserted into the hole. During the transition from the initial state to the goal, the peg does not make contact with the environment, and the end-effector applies force and torque, $[f_X, f_Y, f_\theta]$ = [0, 0, 0].
In an environment with the hole position error of −0.5 [mm] in $\boldsymbol{j}_0$ direction, the peg
does not arrived at the goal with controller $\boldsymbol{K}_Q$, see Fig. 8. The task is not completed using $\boldsymbol{K}_Q$ due to small errors caused by visual measurement, etc.

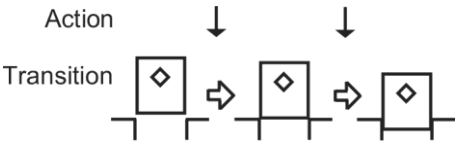


Figure 7. Trajectory of controller $\boldsymbol{K}_Q$ in a simulation without any hole position error.

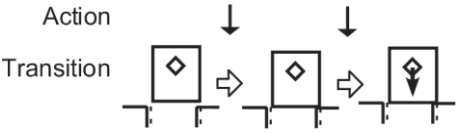


Figure 8. Trajectory of controller $\boldsymbol{K}_Q$ in a simulation with hole position error −0.5 [mm] in $\boldsymbol{j}_0$.

Discussion of Existing Reinforcement Learning Methods

If the robot cannot complete the task due to the errors, the robot switches to on-line learning. Reinforcement learning is said to be adaptive because of the online learning that uses online identification and on-site optimal control design. As mentioned before, the online learning cannot be used for peg-in-hole task, because it takes too long time

for online learning by means of trial and error. Kober and Peters referred this as curse of real-world samples and mentioned it is more important to limit the real-world interaction time instead of limiting memory consumption or computational complexity (Kober and Peters 2012). Therefore, this study takes an approach different from the online learning. On the other hand, the state and the action constitute continuous spaces in robot reinforcement learning. For such case, function approximation methods to approximate the state transition probability model, the value functions, and the policy are proposed (Bertsekas and Tsitsiklis 1996, Szepesvari 2010, Powell 2007, Lagoudakis and Parr 2003, Xu et al. 2007, Boyan 2002). The methods have some advantages, e.g., continuous action, memory saving, and so on. But, the function approximation framework also yields situations, e.g., DP solutions are no longer applicable, theoretical guarantees of convergence no longer hold, learning processes often prove unstable (Boyan and Moore 1995, Kakade and Langford 2002, Bagnell et al. 2003), and so on. Therefore,
this study does not use function approximation methods.

AUTONOMOUS ACQUISITION OF SKILL BY LEARNING

Autonomous Acquisition of Skill for Peg-in-hole

A robot can achieve peg positioning or movement with contact force, and it must have basic control functions the same as a human being. Human vision measurement and positioning control are not accurate enough. However, the rate of a human failure in the same task is not as high as that of a robot. One reason for this may be skills human being brings to the task.

A human being conducting peg-in-hole task uses a typical sequence of actions (Fig. 9). First, the human being puts a corner of the peg inside the hole. The peg orientation is inclined. The peg is in contact with the environment. Two points of the peg, the bottom and a side, are in contact with the environment, as shown in the close-up, Fig. 9. The human then rotates the peg and pushes it against the hole and maintains the two contact points. The two corners are then inserted into

the hole. Finally, the human inserts the peg into the hole and completes the task.

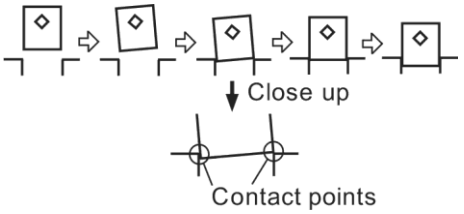


Figure 9. Human skill.

Human vision measurement accuracy and positioning control accuracy are not high. A human presumably develops skill while manipulating this situation. We conducted an experiment to check whether robot learning in the same situation could achieve the task as well as a human.

This situation conceptually corresponds to Fig. 6 (c). Plant $\boldsymbol{P}_N + \Delta\boldsymbol{P}$ denotes a variation plant with error caused by visual measurement, etc. Variation plant set $\{\boldsymbol{P}_N +$

$\Delta \boldsymbol{P}\}$ is composed of all the variation plants that can exist. Real plant $\boldsymbol{P}$ is supposed to be a member of variation plant set $\{\boldsymbol{P}_N + \Delta \boldsymbol{P}\}$. The learning robot obtains controller $\boldsymbol{K}_Q$''. The controller is able to complete the task for all of the variation plants in $\{\boldsymbol{P}_N + \Delta \boldsymbol{P}\}$.

Such reinforcement learning to obtain a policy robust to model uncertainty is a research topic currently. It was found that artificially adding a little noise would smooth model errors and avoid policy over-fitting (Jakobi et al. 1995, Atkeson 1998). Evaluations in the model were exploited to ensure that control was robust to model uncertainty (Schneider 1996, Bagnell and Schneider 2001). Then, it was established that a robust policy would be obtained by learning for a variation plant set (Senda 2008). But, its theoretical background was unclear. The following method in this study efficiently obtains a policy robust to model uncertainty and is theoretically clear.

Problem Definition for Reinforcement Learning with Variation

We assume there are N variation plants around the estimated plant (the nominal plant). We use a set composed of N variation plants for learning.

We consider difference w_l between a variation plant and the nominal plant in each state, which is a discrete variable and the element of finite set □. Finite set □ is composed of L differences denoted by $w_0, w_1, \cdots, w_{L-1}$. Difference w_0 indicates no difference. If an agent is in state s_i with difference w_l and chooses action u_k, it will move to s_j within a state transition probability $p_{ij}(u_k ; w_l)$ and incur a one-step cost $g(s_i, u_k, s_j; w_l)$. This transition is denoted by $(s_i, u_k, s_j; w_l)$. Difference w_l can be considered as the disturbance that causes state transition probability $p_{ij}(u_k; w_0)$ to vary to $p_{ij}(u_k; w_l)$. We assume that the $p_{ij}(u_k; w_l)$ and $g(s_i, u_k, s_j; w_l)$ are given.

Difference w_l at each state is determined by a variation plant. Variation η is a function mapping states into difference with $\eta(s_i) = w_l \in$ □. The nominal plant is defined by $\eta_0(s_i) = w_0$ for all states s_i. The plant does not explicitly depend on time, so variation η is time-

invariant. We assume that $\eta(s_i) = w_I$ is given.

A plant set composed of N plants used for learning is represented by $\Omega = \{\eta_0, \eta_1, \cdots, \eta_{N-1}\}$. Set Ω corresponds to $\{\boldsymbol{P}_N + \Delta\boldsymbol{P}\}$. Let $\rho(\eta_n)$ denote the probability that the plant variation is η_n. We call this the existing probability of variation plant η_n. We assume that $\rho(\eta)$ is given at time $t = 0$.

For set Ω, the expected cost of a policy μ starting from an initial state $s\,0 = s_i$ at $t = 0$ is

$$J^{\mu}(s_i) = E\left\{\sum_{t=0}^{\infty} g(s_t, h(s_t)) \,\middle|\, s\,0 = s_i\right\} \tag{8}$$

which is the J-factor of this problem. This J-factor formula using the plant existing probability is

$$\bar{J}^{\mu}(s_i) = \sum_{n=0}^{N-1} \rho(\eta_n) J^{\mu,\eta_n}(s_i), \tag{9}$$

where $J^{\mu,\eta_n}(s_i)$ denotes the expected cost using the policy μ on a plant η_n starting from an initial state s_i. It satisfies

$$J^{\mu}(s_i) = \sum_{k=1}^{K} p(s_i, \mu(s_i), s_k) \left[g(s_i, \mu(s_i), s_k) + \sum_{j=0}^{N_S} p(\mu(s_i), s_k, s_j) J^{\mu}(s_j) \right] \quad (10)$$

We define the optimal policy as

$$\mu^*(s_i) \equiv \arg\min_{\mu} J^{\mu}(s_i), \quad (11)$$

that minimizes the J-factor of every state. The J-factor of the optimal policy μ^* is defined as the optimal J-factor, represented by $J^*(s_i)$. The objective is to obtain the optimal policy. We assume that there is at least one policy μ satisfying $J^{\mu}(s_i) < \infty$, $\forall s_i$ in this problem. Henceforth, we will call this problem the original problem.

The variation plant in the original problem correlates with differences between any two states. Due to this correlation, the optimal policy does not satisfy Bellman's principle of optimality (Senda and Tani 2011). Therefore the optimal policy and the optimal J-factor in this problem do not satisfy Eqs. (6) and (7). In general, the optimal policy is not stationary. If policies are limited to stationary, the optimal policy is stochastic.

Therefore, another problem definition or another solution method is needed.

Solutions for a Relaxed Problem of Reinforcement Learning with Variation

We relax the original problem to recover the principle of optimality. Then, we can find the optimal J-factor efficiently by applying DP algorithms to the relaxed problem. We treat a reinforcement learning problem based on a two-player zero-sum game.

We assume that differences, w_0, w_1, $\cdots$, w_L, exist

independently in each state s_i. Then the original problem is relaxed to a reinforcement learning problem (Littman 1994, Morimoto and Doya 2005, Al-Tamimi et al. 2007) based on a two-player zero-sum
game (Basar and Bernhard 1995) whose objective is to obtain the optimal policy for the worst variation maximizing the expected cost. Since the correlations of differences in a variation plant are ignored, the principle of optimality is recovered.

The Ω_{2pzs} is defined as the set of variation plants consisting of all possible combinations of any differences. Since each state has L types of differences, the number of variation plants in Ω_{2pzs} is L^{N_s}. We define the optimal policy μ^* as the policy minimizing the expected cost against the worst variation $\eta^* \in \Omega_{2pzs}$ maximizing the expected cost

$$(\mu^*, \eta^*) = \arg\min_{\mu} \max_{\eta \in \Omega_{2pzs}} \sum_{i=1}^{N_s} J^{\mu,\eta}(s_i), \tag{12}$$

and the optimal J-factor $J^*_{2pzs}(s_i)$ is defined as the J-factor of the optimal policy and the worst variation.

Since the principle of optimality is recovered, the optimal J-factor satisfies the following Bellman equation.

$$J_{2pzs}^{*}(s) = \min_{u_k} \max_{w_l} \sum_{j=0}^{N_S} p(u_k; w_l)\{g(s, u_k, s'; w_l) + J_{2pzs}^{*}(s')\}. \quad (13)$$

Therefore the optimal J-factor can be obtained by a DP algorithm. Using the optimal J-factor, the optimal policy and the worst variation are obtained by

$$(m_{2pzs}^{*}(s), n_{2pzs}^{*}(s)) = \arg\min_{u_k} \max_{w_l} \sum_{j=0}^{N_S} p(u_k; w_l)\{g(s, u_k, s'; w_l) + J_{2pzs}^{*}(s')\}. \quad (14)$$

The optimal policy μ_{2pzs}^{*} is applicable to all L^{N_S} variation plants in Ω_{2pzs}. The optimal policy μ_{2pzs}^{*} is proper for all plants in Ω of subsection "Problem definition for reinforcement learning with variation" because $\Omega \subseteq \Omega_{2pzs}$ holds. However, the actual number of plants to which the policy should be applied is only N and $N \ll L^{N_S}$. Hence,

the optimal policy of the reinforcement learning problem based on the two-player zero-sum game is often conservative and yields poor performance because the problem does not consider the existence of variation plants. We cannot solve this problem if

there is no policy satisfying $J^{\mu,\eta}(s) < \infty$, $\forall s, \forall \eta \in \Omega_{2pzs}$ even though there policy μ exists and satisfies $\sum_{i} J^{\mu,\eta_i}(s) < \infty$, $\forall \eta \in \Omega$. Hence, a solution method to solve the original problem is desired.

Learning of Peg-in-hole Task with Variation

Problem Definition of Peg-in-hole Task with Variations

This section uses the same problem definition for peg-in-hole as subsection “Problem definition of peg-in-hole”. The following is added to take variations into account.

The hole position and orientation is measured by the stereo vision system. These measurements involve errors caused by quantized images, lighting conditions at a worksite, etc. Time-averaged errors are almost constant while the space robot performs the task, unlike white noise whose time-averaged error is zero. Error evaluations are modeled as described below. Hole position errors are modeled as normal probability distributions, where the mean is $m = 0$ [mm], and standard deviation is $\sigma = 0.75$ [mm]. Hole orientation errors are modeled as normal probability distributions, where the mean is $m = 0$ [rad], and standard deviation is $\sigma = 0.5\pi/180$ [rad]. If the error’s statistical values gradually vary, we have to estimate them on-line. The relative position and orientation between Σ_0 and Σ_{hl} are fixed during the task. The plant variations are modeled as hole
position and orientation measurement errors.

Consider these errors as variations $\Delta \boldsymbol{P}$ added to nominal model $\boldsymbol{P}_N$ (Fig. 6(c)). We constructed 9 plants $\eta_0 \sim \eta_8$ for learning as listed in Table 1, where each plant has a combination of errors among [−1.0, 0.0, 1.0] [mm] in $\boldsymbol{j}_0$-axis direction and [−(0.5/180)π, 0.0, (0.5/180)π] [rad] in $\boldsymbol{k}_0$-axis rotation. Plant η_0 with no error both in $\boldsymbol{j}_0$-axis direction and $\boldsymbol{k}_0$-axis rotation is the nominal plant. The plant existing probabilities followed the above-mentioned normal probability distributions.

Table 1. Hole position of variation plant η_n from the nominal plant.

Plants	Variations: Position in $\boldsymbol{j}_0$ [mm]	Rotation about $\boldsymbol{k}_0$ [rad]
η_0	0.0	0.0
η_1	0.0	$-(0.5/180)\pi$
η_2	-1.0	0.0
η_3	-1.0	$-(0.5/180)\pi$
η_4	-1.0	$(0.5/180)\pi$
η_5	0.0	$(0.5/180)\pi$
η_6	1.0	0.0
η_7	1.0	$(0.5/180)\pi$
η_8	1.0	$-(0.5/180)\pi$

In the original problem, plant η_n determines the state transition probability as $p_{ij}(u_k; \eta_n)$ for all state transitions (s_i, u_k, s_j) simultaneously. The state transition probability is represented by $p_{ij}(u_k; w_n(s_i))$ where $\Box(s_i) = \{w_0(s_i), \ldots, w_{N-1}(s_i)\}$ and $w_n(s_i) = \eta_n(s_i)$. On the other hand, the two-player zero-sum game allows difference w_l at state s_i to be chosen arbitrary from $\Box(s_i)$. The one step cost is $g(s_i, u_k, s_j; w_l) = 1$.

In the later simulations and experiments to evaluate the learned results, the hole position and orientation are derived from the above normal probability distribution. In the simulations, a variation in the hole position and attitude is chosen for each episode, but the variation is invariant during the episode.

Learning Method

Under the conditions of the above problem definition, a policy is obtained by the solution in subsection “Solutions for a relaxed problem of reinforcement learning with variation”. It is the optimal policy μ^*_{2pzs} of the two-player zero-sum game, i.e., $\boldsymbol{K}_Q'$ in Fig. 6 (c). The optimal policy μ^*_{2pzs} is applied to the dynamic simulator with a continuous state-action space or the experimental hardware setup, which is a real plant $\boldsymbol{P}$ in Fig. 6 (c). No on-line learning is needed.

There is no proper policy for all plants in $\Box_{2pzs}$ if the variations in Table 1 are too large. In this case, there is no policy satisfying the reinforcement learning problem based on the two-player zero-sum game. A typical approach for this situation is to make the variations smaller, to reconstruct $\Box_{2pzs}$, and to solve the two-player zero-sum game again. This

approach is repeated if we cannot obtain any solutions. This approach reduces the robustness of solutions.

Control Results

In results for numerical simulation (Fig. 10), where the peg arrives at the goal using controller $\boldsymbol{K}'_{Q'}$ in the environment without hole position/orientation error. Peg positioning is firstly inclined, and the peg moves in the positive direction, toward $\boldsymbol{i}_0$. Then, the peg's corner is inserted in the hole. The peg makes contact with a corner of the hole. The peg transits in a positive direction, toward $\boldsymbol{j}_0$, while maintaining contact. Another corner of the peg is put inside the hole when the action in the direction of $\boldsymbol{i}_0$ and $\boldsymbol{j}_0$ is repeated. Peg positioning is changed to $y\theta = 0$ [rad], and the peg slips into the hole. The task is completed. The learned result is similar to human skill for the peg-in-hole task in Fig. 9.

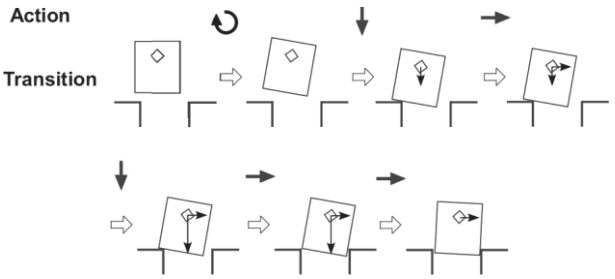


Figure 10. Trajectory of controller $\boldsymbol{KQ}'$ in a simulation using nominal plant η_0 without any hole position error.

The peg has arrived at the goal using controller $\boldsymbol{KQ}'$ for variation plants $\eta_1 - \eta_8$. The numerical results for $\eta_1 - \eta_4$ are shown in Figs. 11–14. Each transition is similar to the case of η_0, and the peg is inserted into the hole.

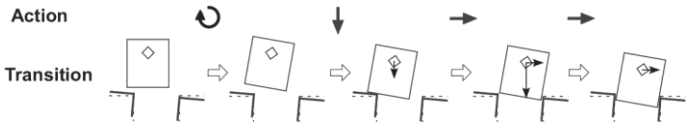


Figure 11. Trajectory of controller $\boldsymbol{K'Q}'$ in a simulation using plant η_1.

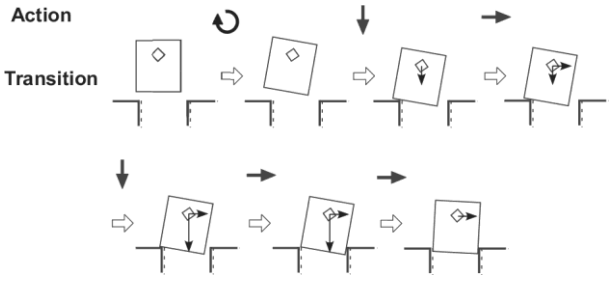


Figure 12. Trajectory of controller $\boldsymbol{K'Q}'$ in a simulation using plant η_2.

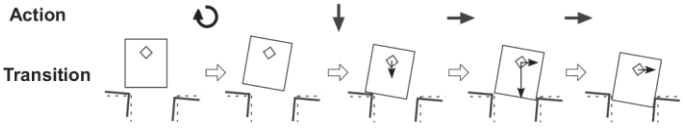


Figure 13. Trajectory of controller $\boldsymbol{K'Q'}$ in a simulation using plant η_3.

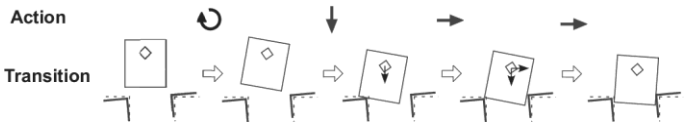


Figure 14. Trajectory of controller $\boldsymbol{K'Q'}$ in a simulation using plant η_4.

The task is achieved with controller $\boldsymbol{K}_{Q'}$ in the same environment with error, where $\boldsymbol{K}_{Q}$ previously did not work at all. This means that the action generated by controller $\boldsymbol{K}_{Q'}$ is robust against variations as well as human skill. We judge the robot, i.e., controller
$\boldsymbol{K}_{Q'}$, to have obtained a skill, the ability to complete a task when the vision measurement accuracy is low.

EVALUATION OF OBTAINED SKILL

Results of Hardware Experiments

Example results in the hardware experiment using controllers $\boldsymbol{K}_{Q}$ and $\boldsymbol{K}_{Q'}$ are shown in Fig. 15. The following variations are used +0.3 [mm] in $\boldsymbol{i}_0$, +1.2 [mm] in $\boldsymbol{j}_0$ and
+0. 5π/180 [rad] rotation about the $\boldsymbol{k}_0$-axis. Controller $\boldsymbol{K}_{Q}$ cannot complete the task due to environmental variations, but controller $\boldsymbol{K}_{Q'}$ can.

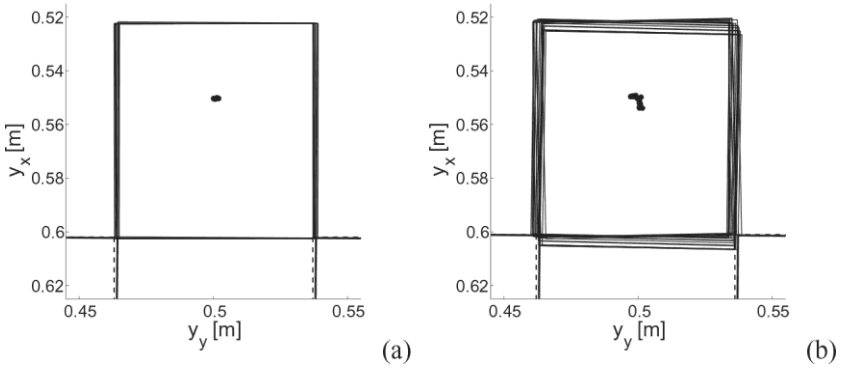


Figure 15. Experimental trajectories using two controllers in an environment with error: (a) controller
$\boldsymbol{K}_{Q}$ and (b) controller $\boldsymbol{K}'_{Q'}$.

Evaluation of Robustness and Control Performance

Robustness and control performance of controllers $\boldsymbol{K}_{Q}$ and $\boldsymbol{K}'_{Q'}$ are evaluated by simulations and hardware experiments, the peg-in-hole task.

Variation plants, i.e., error in hole position and orientation, are derived from the normal probability distribution in section

"Learning of peg-in-hole task with variation". The robustness and the control performance are evaluated respectively by the task achievement ratio and the average step number to the goal. The achievement ratio equals the number of successes divided by the number of trials. Table 2 shows the achievement ratios and the average step number of $\boldsymbol{K}_Q$ and $\boldsymbol{K}_Q''$ as evaluated by simulations and hardware experiments. The simulations and the experiments are executed 10,000 times and 50 times, respectively. The achievement ratios of $\boldsymbol{K}_Q$ are 59 percent and 64 percent in simulation and hardware experiments. Those of $\boldsymbol{K}_Q''$ dramatically increase to 99 percent in numerical simulation and 96 percent in hardware experiments. These results show the robot autonomously generates robust skill using the proposed learning method. The difference in step numbers between hardware experiments and simulations, an

increase in hardware steps, may be due to variations, e.g., irregular friction in the environment, joint flexibility, etc. Such variables are not considered in the numerical simulation.

Robust skills are thus autonomously generated by learning in this situation, where variations make a task achievement difficult.

Table 2. Achievement ratios and averaged step numbers of peg-in-hole task with controllers $\boldsymbol{K}_Q$ and $\boldsymbol{K}_{Q''}$.

Controller	Simulation Ratio	Simulation Step no.	Experiment Ratio	Experiment Step no.
$\boldsymbol{K}_Q$	58.7%	19.3	64%	21
$\boldsymbol{K}_{Q''}$	98.7%	9.83	96%	17

CONCLUSIONS

We have applied reinforcement learning to obtain successful completion of a given task when a robot normally cannot complete the task using controller designed in advance. Peg-in-hole achievement ratios are usually low when we use conventional learning without consideration of plant variations. In the proposed method, using variation consideration, the robot autonomously obtain robust skills which enabled the robot to achieve the task. Simulation and hardware experiments have confirmed the effectiveness of our proposal. Our proposal also ensures robust control by conducting learning stages for a set of plant variations.

REFERENCES

Al-Tamimi, A., F. L. Lewosa and M. Abu-Khalaf. 2007. Model-free Q-learning designs for linear discrete time zero-sum games with application to H-infinity control. Automatica, 43(3): 473– 481.

Asada, M. 1999. Issues in applying robot learning and evolutionary methods to real environments.
Journal of the Society of Instrument and Control Engineers, 38(10): 650–653 (in Japanese).

Atkeson, C. G. 1998. Nonparametric model-based reinforcement learning. Advances in Neural Information

Processing Systems (NIPS).

Bagnell, J. A. and J. C. Schneider. 2001. Autonomous helicopter control using reinforcement learning policy search methods. IEEE International Conference on Robotics and Automation.

Bagnell, J. A., A. Y. Ng, S. Kakade and J. Schneider. 2003. Policy search by dynamic programming.
Advances in Neural Information Processing Systems (NIPS).

Bas¸ar, T. and P. Bernhard. 1995. H∞-Optimal Control and Related Minimax Design Problems.
Birkhäuser, Boston.

Bertsekas, D. P. and J. N. Tsitsiklis. 1996. Neuro-Dynamic Programming. Athena Scientific, Belmont, MA.

Boyan, J. 2002. Technical update: Least-squares temporal difference learning. Machine Learning, Special Issue on Reinforcement Learning, 49(2–3): 233–246.

Boyan, J. A. and A. W. Moore. 1995. Generalization in reinforcement learning: Safely approximating the value function. Advances in Neural Information Processing Systems (NIPS).

Connolly, C. I., J. B. Burns and R. Weiss. 1990. Path planning using Laplace's equation. IEEE International Conference on Robotics and Automation, pp. 2102–2106.

Fujii, S., K. Senda and S. Mano. 2006. Acceleration of reinforcement learning by estimating state transition probability model. Transactions of the Society of Instrument and Control Engineers, 42(1): 47–53 (in Japanese).

Fukuda, T., W. Srituravanich, T. Ueyama and Y. Hasegawa. 2000. A study on skill acquisition based on environment information (Task Path Planning for Assembly Task Considering Uncertainty). Transactions of the Japan Society of Mechanical Engineers, 66(645): 1597–1604 (in Japanese).

Jakobi, N., P. Husbands and I. Harvey. 1995. Noise and the reality gap: The use of simulation in evolutionary robotics. The 3rd European Conference on Artificial Life.

Kakade, S. and J. Langford. 2002. Approximately optimal approximate reinforcement learning. International Conference on Machine Learning (ICML).

Kober, J. and J. Peters. 2012. Reinforcement learning in robotics: A survey. pp. 579–610. *In*: M. Wiering and M. van Otterlo (eds.). Reinforcement Learning: State-of-the-Art. Springer, Heidelberg.

Lagoudakis, M. G. and R. Parr. 2003. Least-squares policy iteration. Journal of Machine Learning Research, 4: 1107–1149.

Littman, M. L. 1994. Markov games as a framework for multi-agent reinforcement learning. International Conference on Machine Learning (ICML), pp. 157–163.

Mahadevan, S. and M. Maggioni. 2007. Proto-value functions: A Laplacian framework for learning representation and control in Markov decision processes. Journal of Machine Learning Research, 8: 2169–2231.

Miyazaki, F. and S. Arimoto. 1985. Sensory feedback for robot manipulators. Journal of Robotic Systems, 2(1): 53–71.

Morimoto, J. and K. Doya. 2005. Robust reinforcement learning. Neural Computation, 17(2): 335– 359.

Powell, W. B. 2007. Approximate Dynamic Programming: Solving the Curses of Dimensionality. Wiley, Hoboken, NJ.

Sato, D. and M. Uchiyama. 2007. Peg-in-hole task by a robot. Journal of the Japan Society of Mechanical Engineers, 110(1066): 678–679 (in Japanese).

Schneider, J. G. 1996. Exploiting model uncertainty estimates for safe dynamic control learning. Advances in Neural Information Processing Systems (NIPS).

Senda, K. 2001. An approach to autonomous space robots. Systems. Control and Information, 45(10): 593–599 (in Japanese).

Senda, K. and Y. Tani. 2011. Optimality principle broken by considering structured plant variation and relevant robust

reinforcement learning. IEEE International Conference on Systems, Man, and Cybernetics, pp. 477–483.

Senda, K., T. Kondo, Y. Iwasaki, S. Fujii, N. Fujiwara and N. Suganuma. 2008. Hardware and numerical experiments of autonomous robust skill generation using reinforcement learning. Journal of Robotics and Mechatronics, 20(3): 350–357.

Senda, K., Y. Murotsu, A. Mitsuya, H. Adachi, S. Ito, J. Shitakubo and T. Matsumoto. 2002. Hardware experiments of a truss assembly by an autonomous space learning robot. AIAA Journal of Spacecraft and Rockets, 39(2): 267–273.

Skaar, S. B. and C. F. Ruoff (eds.). 1995. Teleoperation and Robotics in Space. AIAA, Washington, DC.

Sutton, R. S. and A. G. Barto. 1998. Reinforcement Learning: An Introduction. MIT Press, Cambridge, MA.

Szepesva´ri, Cs. 2010. Algorithms for Reinforcement Learning. Morgan and Claypool, San Rafael, CA.

Whitney, D. E. 1982. Quasi-static assembly of compliantly supported rigid parts. Transactions of ASME, Journal of Dynamic Systems, Measurement, and Control, 104: 65–77.

Xu, X., D. Hu and X. Lu. 2007. Kernel based least squares policy iteration for reinforcement learning.

IEEE Transactions on Neural Networks, 18(4): 973–992.

Yamanobe, N., Y. Maeda, T. Arai, A. Watanabe, T. Kato, T. Sato and K. Hatanaka. 2006. Design of force control parameters considering cycle time. Journal of the Robotics Society of Japan, 24(4): 554–562 (in Japanese).

5

Adaptive Control for Multi-Fingered Robot Hands

Satoshi Ueki[1,*] and *Haruhisa Kawasaki*[2]

ABSTRACT

This chapter discusses adaptive control for object manipulation according to the contact condition. When a robot grasps an object, its fingers come into contact with the surface of the object and constrained its hand motion by that contact. Robotic hands are mechanical non-linear systems. In general, treat adaptive control systems as time-varying systems. For dexterous manipulation, the control objective is to control the object position and velocity; that is, to coordinately-control the force at the contact point that occurs for multiple robotic fingers. This is one of the challenging problems in robotics. In the controller presented here, the shapes of the object and positions of the contact points are already known. In fact, position of the contact point could be calculated using the force sensor variable. However, the accuracy is insufficient. Thus, need study of adaptive controls with fewer restrictions.

Keywords: Adaptive control, robot hand, coordinate,

manipulation, force control

INTRODUCTION

Multi-fingered robot hands are expected to replace human hands in tasks requiring dexterous manipulation of objects. When a robot grasps an object, its fingers come

1 Department of Mechanical Engineering, National Institute of Technology, Toyota College, Toyota, Japan.
E-mail: s_ueki@toyota-ct.ac.jp

2 Department of Mechanical Engineering, Gifu University, Gifu, Japan. E-mail: h_kawasa@gifu-u.ac.jp

* Corresponding author

into contact with the surface of the object, and its hand motion is constrained by that contact. For dexterous manipulation, a basic understanding of the contact model between a finger and an object, the motion constraint during contact, and the dynamics of these constraints is important. Furthermore, the dynamics of robot hands are non-linear, and require control methods that take constraints into consideration.

When a robot hand grasps and manipulates an object, contact models are important for the analysis of object constraint conditions and robotic hand control. Since contact conditions vary according to point, line, and surface contact, as well as whether or not friction exists at the contact point, the object is affected by diverse constraint conditions. Moreover, kinematic constraints occur according to contact conditions between the robotic finger and the object. Therefore, relative translational velocity and relative angular velocity should be taken into account for robotic hand control.

The cooperative control of multiple fingers on a robotic hand used to perform an orientation by grasping a target object is a basic technique of dexterous manipulation. For many cooperative controls, widely used control laws are based on compliance control (Cutkosky and Kao 1989), impedance control (Kosuge et al. 1995), control of under-actuated fingers (Birglen et al. 2010), dynamic control (Zheng et al. 2000), together with position and force laws grounded in hybrid control (Hayati 1986), the hybrid system approach (Schlegl et al. 2003), and model predictive control (Yingjie and Hosoe 2005). In these control laws, it is assumed that the dynamics of the system control are known. However, it is often difficult to determine the exact dynamics of a system. In addition, the dynamic parameters of the system will vary depending on the object being manipulated. Several approaches have been proposed to accommodate cases where the model parameters of the system are either unknown or fluctuating, including cooperative control using a neural network (Hwang and Toda 1994), learning control (Naniwa and Arimoto 1995), control without object sensing (Ozawa et al. 2005), adaptive sliding control (Su and Stepanenco 1995, Ueki et al. 2006), and adaptive coordinated

control (Kawasaki et al. 2006). Adaptive compliant grasp (Zhaopeng et al. 2015), adaptive force control with estimation of environmental stiffness (Wakamatsu et al. 2010), and others have also been proposed.

This chapter describes adaptive control for object manipulation. First, we review the mathematical models and basic theory for stability analysis. In the mathematical models, we explore the equations of motion at the contact point for relative motion between the robotic finger and the object, the dynamic model of a rigid body, and the dynamic model of a robotic hand. We then describe adaptive controllers for object manipulation. We present experimental verification result to demonstrate the effectiveness of the proposed adaptive controller. Finally, conclusions are given.

In general, force sensors are expensive and susceptible to noise. An adaptive control for object manipulation without a force sensor under a condition of rolling-contact can thus prevent a control system from being highly reliable. If a stable controller is configurable without a force sensor, the control law increases the usefulness of the control system. On the other hand, humans use hands to grasp and manipulate objects dexterously using force sensation. To realize dexterous manipulation like that of the human hand, it is necessary to study adaptive control using a force sensor. Moreover, dexterous object manipulation is possible if the finger slides on the object surface. For these reasons, we describe an adaptive control for object manipulation without a force sensor under a condition of rolling-contact, an adaptive control for object manipulation

using a force sensor under a condition of rolling-contact, and an adaptive control for object manipulation using a force sensor under a condition of sliding-contact. An introduction to robot hand control and the details of contact models may be found in the references (Mason and Salisbury 1985, Mason 1998, Murray et al. 1993, Kawasaki 2015).

MATHEMATICAL MODELS OF MULTI-FINGERED HANDS

When a robotic hand with k fingers, each with three DOFs (degree of freedom), grasps and manipulates a rigid body (as shown in Fig. 1), in which the i-th robotic finger contacts the object at point C_i, the coordinate systems are defined as follows: Σ_P is the task coordinate system, Σ_O is the object coordinate system fixed on the object, and Σ_{Fi} is the i-th fingertip coordinate system fixed on the i-th fingertip.

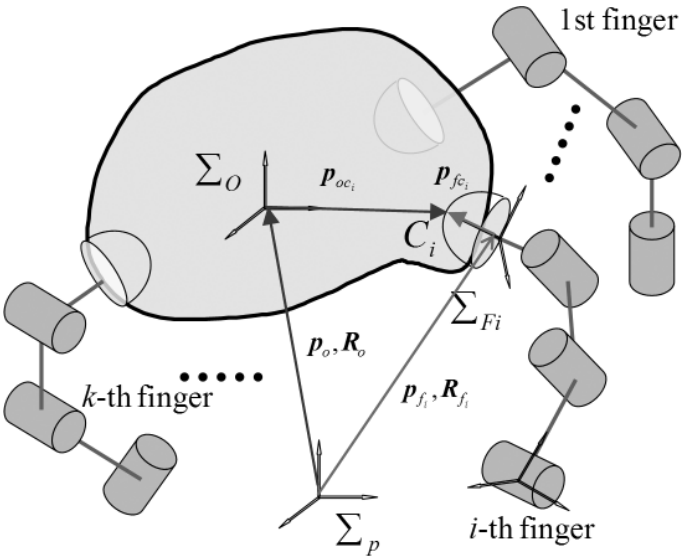


Figure 1. Grasped object and multi-fingered hand coordinate system.

To facilitate the dynamic formulation, we make the following assumptions.

(A1) All the fingertips contact the common object; the grasp is a force closure and manipulable grasp.

(A2) The Jacobian matrix is a non-sigular matrix. That is, the DOF of the finger is not redundant, and there is sufficient DOF to manipulate the object.

(A3) The contact force is all in the friction cone. This indicates that there is no slippage at the contact point, and the contact force has three elements.

(A4) The object and fingertip surfaces are described by twice continuously differentiable hyper surfaces.

The constraint at each contact point is described by the rolling contact. The force generated by the constraint does not work on the system (d'Alembert's principle).

Equation of Motion at the Contact Point

To perform system modeling, it is necessary to describe a contact condition that takes into account the relative motion between the object motion and that of the robot fingertip.

When the *i*-th robot finger manipulates the object, the position vector of the contact point is expressed as

$$\boldsymbol{p}_{OCi} = \boldsymbol{R}_{O} \boldsymbol{p}_{FiCi} + \boldsymbol{p}_{Fi} - \boldsymbol{p}_{O} \quad . \tag{1}$$

Let $\mathbb{R}$ denote the set of all real numbers. Then, $\boldsymbol{p}_O \in \mathbb{R}^3$ is a position vector of the origin of the object coordinate system Σ_O, with respect to Σ, $\boldsymbol{R}_O \in \mathbb{R}^{3\times 3}$ is a rotation matrix from Σ to Σ_O, $\boldsymbol{p}_{OCi} \in \mathbb{R}^3$ is a position vector from Σ to the contact point C_i with respect to Σ, $\boldsymbol{p}_{FiCi} \in \mathbb{R}^3$ is a position vector of the origin of the *i*-th fingertip coordinate system Σ_{Fi} with respect to Σ, $\boldsymbol{R}_{Fi} \in \mathbb{R}^{3\times 3}$ is a rotation matrix from Σ to Σ_{Fi}, and $\boldsymbol{p}_{Fi} \in \mathbb{R}^3$ is a position vector from Σ to the contact point C_i with respect to Σ_{Fi}. The first-order time differentials of Eq. (1) are expressed as

$$\dot{\boldsymbol{p}}_{OCi} = \boldsymbol{\omega}_O \times \boldsymbol{R}_O \boldsymbol{p}_{FiCi} + \dot{\boldsymbol{p}}_{Fi} - \dot{\boldsymbol{p}}_O + \boldsymbol{R}_O \dot{\boldsymbol{p}}_{FiCi} \quad , \tag{2}$$

where $\boldsymbol{\omega}_O \in \mathbb{R}^3$ is an angle velocity of the object, and $\boldsymbol{\omega}_{Fi} \in \mathbb{R}^3$ is an angle velocity of the *i*-th robot fingertip.

Moreover, consider two coordinate systems at the contact point, as shown in Fig. 2. Σ_{COi} is the contact point of the C_i coordinate system on the object with the *z* axis outward and normal to the object surface, and Σ_{CFi} is the contact point of the C_i coordinate system on the robot fingertip with the *z* axis outward and normal to the robot fingertip surface. The rotation matrix at the contact point is expressed as

$$\boldsymbol{R}_{C_{Oi}}^{O} = \boldsymbol{R}_{C_{Fi}}^{O} \boldsymbol{R}_{C_{Fi}}^{T}, \tag{3}$$

where $\boldsymbol{R}_{C_{Oi}}^{O} \in \mathbb{R}^{3\times 3}$ is a rotation matrix from $\Sigma_{C_{Oi}}$ to Σ_O, $\boldsymbol{R}_{C_{Fi}}^{O} \in \mathbb{R}^{3\times 3}$ is a rotation matrix from $\Sigma_{C_{Fi}}$ to Σ_O and $\boldsymbol{R}_{C_{Fi}}^{C_{Oi}} \in \mathbb{R}^{3\times 3}$ is a rotation matrix from $\Sigma_{C_{Fi}}$ to $\Sigma_{C_{Oi}}$. The first-order time differentials of Eq. (3) are expressed as

$$\omega_O \times \boldsymbol{R}_{C_{Oi}}^{O} = \dot{\boldsymbol{R}}_{C_{Oi}}^{O} = \dot{\boldsymbol{R}}_{C_{Fi}}^{O} \boldsymbol{R}_{C_{Fi}}^{T} + \boldsymbol{R}_{C_{Fi}}^{O} \dot{\boldsymbol{R}}_{C_{Fi}}^{T} = \omega_O \times \boldsymbol{R}_{C_{Fi}}^{O} \boldsymbol{R}_{C_{Fi}}^{T} + \boldsymbol{R}_{C_{Fi}}^{O} \dot{\boldsymbol{R}}_{C_{Fi}}^{T}. \tag{4}$$

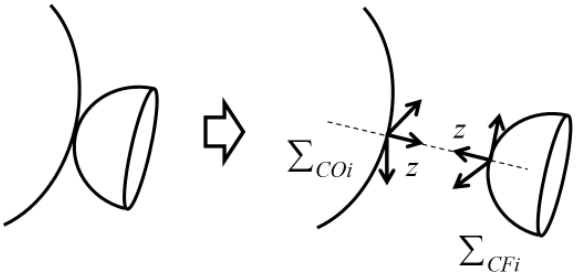


Figure 2. Contact coordinate systems at the contact point.

To consider the details of the relative motion between the object motion and that of the robot fingertip, consider the motion representation by curved surface coordinates. Using the mapping $\boldsymbol{c} : \mathbb{R}^2 \rightarrow \mathbb{R}^3$ from 2D to 3D, as shown in Fig. 3, a point on the 2D surface $\boldsymbol{\alpha} = [u\ v]^T$ is mapped to a point on the object's 3D surface, $\boldsymbol{p}$, as

$$\boldsymbol{p} = \boldsymbol{c}(\boldsymbol{\alpha}), \tag{5}$$

where it is assumed that mapping $\boldsymbol{c}$ is a diffeomorphic mapping, and that the coordinate system on the 2D surface is orthogonal for the sake of simplicity. In this case, the tangent plane of the object is a space spanned by two vectors, $\frac{\partial \boldsymbol{c}}{\partial u}$ and $\frac{\partial \boldsymbol{c}}{\partial v}$.

The contact coordinate system $\Sigma_{Ci} = [\boldsymbol{x}\ \boldsymbol{y}\ \boldsymbol{z}]$ that consists of the two axes on the tangent plane and the outward normal orthogonal line is represented by

$$[\ \boldsymbol{x}\ \ \boldsymbol{y}\ \ \boldsymbol{z}] = \begin{bmatrix} \frac{\boldsymbol{c}_u}{\|\boldsymbol{c}_u\|} & \frac{\boldsymbol{c}_v}{\|\boldsymbol{c}_v\|} & \frac{\boldsymbol{c}_u \times \boldsymbol{c}_v}{\|\boldsymbol{c}_u \times \boldsymbol{c}_v\|} \end{bmatrix}. \tag{6}$$

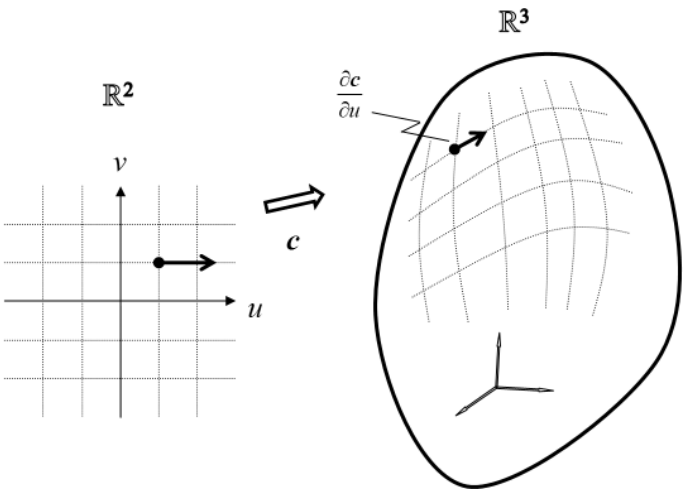


Figure 3. Mapping ***c.***

This is called a normalized Gauss frame. Here, the metric tensor $\boldsymbol{M}_C$ on the curved surface is given as

$$\boldsymbol{M}_C = \begin{bmatrix} \|\boldsymbol{c}_u\|^2 & 0 \\ 0 & \|\boldsymbol{c}_v\|^2 \end{bmatrix}. \tag{7}$$

In addition, the curvature tensor $\boldsymbol{K}_C$ on the curved surface is given as

$$\boldsymbol{K}_C = \begin{bmatrix} \boldsymbol{x}_{uu}^T \dfrac{\boldsymbol{c}_u \times \boldsymbol{c}_v}{\|\boldsymbol{c}_u \times \boldsymbol{c}_v\|} & \boldsymbol{x}_{uv}^T \dfrac{\boldsymbol{c}_u \times \boldsymbol{c}_v}{\|\boldsymbol{c}_u \times \boldsymbol{c}_v\|} \\ \boldsymbol{y}_{uv}^T \dfrac{\boldsymbol{c}_u \times \boldsymbol{c}_v}{\|\boldsymbol{c}_u \times \boldsymbol{c}_v\|} & \boldsymbol{y}_{vv}^T \dfrac{\boldsymbol{c}_u \times \boldsymbol{c}_v}{\|\boldsymbol{c}_u \times \boldsymbol{c}_v\|} \end{bmatrix}, \tag{8}$$

where $\boldsymbol{z}_u = \frac{\partial \boldsymbol{z}}{\partial u}$ and $\boldsymbol{z}_v = \frac{\partial \boldsymbol{z}}{\partial v}$. This curvature tensor is considered to be the magnitude

of the fluctuation of the unit normal to the tangent plane. Twist on the curved surface is defined as the change rate of the curvature along the curved surface, and is represented by

$$\boldsymbol{T}_C = \begin{bmatrix} \boldsymbol{x}_U^T \frac{\boldsymbol{c}_u}{\|\boldsymbol{c}_u\|} & \boldsymbol{x}_V^T \frac{\boldsymbol{c}_v}{\|\boldsymbol{c}_v\|} \end{bmatrix}, \tag{9}$$

where $\boldsymbol{x}_u = \frac{\partial \boldsymbol{x}}{\partial u}$ and $\boldsymbol{x}_v = \frac{\partial \boldsymbol{x}}{\partial v}$. These are collectively referred to as the geometric

parameters of the surface. When the object surface is a plane, then $\boldsymbol{z}_U = \boldsymbol{z}_V = \boldsymbol{x}_U = \boldsymbol{x}_V = \boldsymbol{0}$, and the following are obtained: $\boldsymbol{K}_C = \boldsymbol{0}$ and $\boldsymbol{T}_C = \boldsymbol{0}$.

Using the details of relative motion between the motion of the object and that of the robot fingertip, consider the motion of a rigid finger and a rigid object, both with a smooth curved surface, while a point of contact is maintained between them. Using the mapping $\boldsymbol{c}_{Fi}: \mathbb{R}^2 \to \mathbb{R}^3$ and $\boldsymbol{c}_{Oi}: \mathbb{R}^2 \to \mathbb{R}^3$ to represent the surface shapes of the object and the finger, and the 2D orthogonal surface coordinates $\boldsymbol{\alpha}_{Fi} = [u_{Fi}\ v_{Fi}]^T$ and $\boldsymbol{\alpha}_{Oi} = [u_{Oi}\ v_{Oi}]^T$, a point of the fingertip surface can be expressed by the finger coordinates and a point of the object surface by the object coordinates as

$$\boldsymbol{p}_{Fi} = \boldsymbol{c}_{Fi}(\boldsymbol{\alpha}_{Fi}), \quad \boldsymbol{p}_{Oi} = \boldsymbol{c}_{Oi}(\boldsymbol{\alpha}_{Oi}). \tag{10}$$

The deviation of relative attitude between the contact coordinate system on the finger side $\Sigma_{CFi} = [\boldsymbol{x}_{CFi}\ \boldsymbol{y}_{CFi}\ \boldsymbol{z}_{CFi}]$ and that on the object side $\Sigma_{COi} = [\boldsymbol{x}_{COi}\ \boldsymbol{y}_{COi}\ \boldsymbol{z}_{COi}]$ is represented with the angle ϕ_i from $\boldsymbol{x}_{CFi}$ to $\boldsymbol{x}_{COi}$, which is called the angle of contact. Note that the z-axis in each coordinate is in the outward normal direction. Let us denote

the relative translational velocity and relative angular velocity of the finger contact point when referring to the object contact point as

$$\begin{bmatrix} {}^{C_{Fi}}\boldsymbol{v} \\ {}^{C_{Fi}}\boldsymbol{\omega} \end{bmatrix} = \begin{bmatrix} {}^{C_{Si}}\boldsymbol{R}_{C_{Fi}} & {}^{C_{Si}}\boldsymbol{S}({}^{C_{Si}}\boldsymbol{p}_{C_{Fi}}) \\ \boldsymbol{O} & {}^{C_{Si}}\boldsymbol{R}_{C_{Fi}} \end{bmatrix}^{T} \begin{bmatrix} {}^{C_{Fi}}\boldsymbol{R}_{O_i} & {}^{C_{Fi}}\boldsymbol{S}({}^{C_{Fi}}\boldsymbol{p}_{O_i}) {}^{C_{Fi}}\boldsymbol{R}_{O_i} \\ \boldsymbol{O} & {}^{C_{Fi}}\boldsymbol{R}_{O_i} \end{bmatrix}^{T} \begin{bmatrix} {}^{O_i}\boldsymbol{v} \\ {}^{O_i}\boldsymbol{\omega} \end{bmatrix} \tag{11}$$

and

$${}^{C_{Fi}}\boldsymbol{\omega} = {}^{C_{Si}}\boldsymbol{R}_{C_{Fi}}{}^{T}({}^{C_{Fi}}\boldsymbol{\omega} - {}^{C_{Fi}}\boldsymbol{\omega}_{O}), \tag{12}$$

respectively. Then, $\boldsymbol{q}_{Ci} = [\boldsymbol{\alpha}^T \; \boldsymbol{\alpha}^T \; \phi_i]^T \in \mathbb{R}^5$ is the contact coordinates on the two-object surface. Using Eqs. (7)–(9), the geometrical parameters for the contact coordinates of the object side and finger side are represented as ($\boldsymbol{M}_{CFi}$, $\boldsymbol{K}_{CFi}$, $\boldsymbol{T}_{CFi}$) and ($\boldsymbol{M}_{COi}$, $\boldsymbol{K}_{COi}$, $\boldsymbol{T}_{COi}$), respectively. From Eq. (2) and Eq. (4), the following theorem is verified (Montana 1988).

Theorem 1. (Equation of motion at the contact point)

The motion of contact coordinates are described as

$$\approx \quad 1 \quad CFi \qquad \left(M \right. \qquad CF \; i \; v$$

$$1 \quad CFi \qquad C \quad COi \quad K \quad Siy \quad K \quad COi \quad Six \quad F \quad i \quad CF \quad K \quad Six \quad Siy \quad i \quad CFi \quad v$$

$$q \quad M \quad 1 \quad \sim \quad 1 \quad Siy \quad CF \quad Six \qquad (13)$$
$$R \quad K \quad K \quad CFi \quad K \quad I_{Oi} \quad v$$
$$+ \quad \omega \quad {}^{Fi}$$

$$Ci \quad CO \quad C \quad C \quad CFi \quad Si \quad C \quad Siy \quad i \quad i \quad Fi \quad O \quad x \quad \alpha_{Oi} \quad i \quad \dot{\alpha}_{Fi} \quad C \quad Fi \quad v$$

$$Fi \quad C \quad S \quad C \quad M \; T \quad M \; CO_i \quad i \quad Fi \quad CF \quad C \quad z \quad i \quad Oi$$

$$CFi = 0$$
$$Siz$$

where $\boldsymbol{R} \in \mathbb{R}^{2\times 2}$ *is a rotation matrix that represents the orientation of the finger contact coordinate system* Σ_{CFi} *in reference to the object contact point coordinate system* Σ_{COi}*, and given by*

$$\boldsymbol{R} = \begin{bmatrix} \cos\phi_i & \sin\phi_i \\ -\sin\phi_i & \cos\phi_i \end{bmatrix}, \qquad (14)$$

and $\tilde{\boldsymbol{K}}_{C_{Oi}} = \boldsymbol{R}_{\phi i} \boldsymbol{K}_{C_{Oi}} \boldsymbol{R}_{\phi i}^{T}$.

Equation of Motion of a Rigid Body

According to the Newton-Euler equation and Euler equations, the motion of a rigid body on which gravity acts in 3D space can be written as

$$\boldsymbol{f} = m_O \ddot{\boldsymbol{p}}_{Co} - m_O \tilde{\boldsymbol{g}}, \tag{15}$$

$$\boldsymbol{n} = \frac{d}{dt}\left(\tilde{\boldsymbol{I}}_O \boldsymbol{\omega}_O\right) = \tilde{\boldsymbol{I}}_O \dot{\boldsymbol{\omega}}_O + \boldsymbol{\omega}_O \times \tilde{\boldsymbol{I}}_O \boldsymbol{\omega}_O, \tag{16}$$

where $\boldsymbol{p}_{Co} \in \mathbb{R}^3$ is a position vector at the center of mass, $\boldsymbol{f} \in \mathbb{R}^3$ is a force applied to the object's center of mass, $\boldsymbol{n} \in \mathbb{R}^3$ is an applied moment to the object's center of mass, $\boldsymbol{\omega}_O \in \mathbb{R}^3$ is the angle velocity of the object, $\tilde{\boldsymbol{g}} \in \mathbb{R}^3$ is the gravitational acceleration, m_O is the mass of the object, and $\tilde{\boldsymbol{I}}_O \in \mathbb{R}^{3\times 3}$ is an inertia tensor around the object's center of mass. These are denoted within the reference coordinate system. It is not convenient to deal with the inertia tensor $\tilde{\boldsymbol{I}}_O$, since its value alters with changes in the orientation of the object. Consider the object coordinate system Σ_{Co}, which is attached to the center of mass. The inertia tensor of the rigid body referred to in the object coordinate system ${}^{Co}\tilde{\boldsymbol{I}}_O$ is represented by

$${}^{Co}\tilde{\boldsymbol{I}}_O = \boldsymbol{R}_{Co}^{T} \tilde{\boldsymbol{I}}_O \boldsymbol{R}_{Co}, \tag{17}$$

where $\boldsymbol{R}_{Co} \in \mathbb{R}^{3\times 3}$ is a rotation matrix that represents the transformational matrix of vector coordinates in the object coordinate system Σ_{Co} into the coordinates of the same vector in the reference coordinate system. The dynamic equation of the object using ${}^{Co}\tilde{\boldsymbol{I}}_O$ is easily handled, because ${}^{Co}\tilde{\boldsymbol{I}}_O$ is the constant. The relation $\tilde{\boldsymbol{I}}_O = \boldsymbol{R}_{Co}\, {}^{Co}\tilde{\boldsymbol{I}}_O \boldsymbol{R}_{Co}^{T}$ is derived from Eq. (17). By substituting this into Eq. (16), and then putting it together with Eq. (15), it is expressed as

$$\begin{bmatrix} \boldsymbol{f} \\ \boldsymbol{n} \end{bmatrix} = \begin{bmatrix} m_O \boldsymbol{I}_{3\times 3} & \boldsymbol{0} \\ \boldsymbol{0} & {}^{O}\boldsymbol{I}_{O} \end{bmatrix} \begin{bmatrix} \dot{\boldsymbol{v}}_O \\ \dot{\boldsymbol{\omega}}_O \end{bmatrix} + \begin{bmatrix} \boldsymbol{0} \\ \tilde{\boldsymbol{\omega}}_O {}^{O}\boldsymbol{I}_{O} \boldsymbol{\omega}_O \end{bmatrix} - \begin{bmatrix} m_O \boldsymbol{g} \\ \boldsymbol{0} \end{bmatrix} \quad (18)$$

Next, we set a new object coordinate system, Σ_O, that is transferred to a position different from the center of mass of the object, as shown in Fig. 4. Using the origin of the new object coordinate system as a position vector, $\boldsymbol{p}_O$, and an inertia tensor ${}^{O}\boldsymbol{I}_{O}$ of the object around the origin of new object coordinate system, Σ_O, we can derive the equation of object motion using ${}^{O}\boldsymbol{I}_{O}$. The position of the origin of Σ_O to the center of mass is expressed as

$$\boldsymbol{p} = \boldsymbol{p}_O + \boldsymbol{R}_O {}^{O}\boldsymbol{s}_{OCo}, \quad (19)$$

where ${}^{O}\boldsymbol{s}_{OCo}$ is a position vector from the origin of Σ_O to with respect to Σ_O and $\boldsymbol{R}_O \in \mathbb{R}^{3\times 3}$ is a rotation matrix from Σ_O to Σ_O. Since ${}^{O}\boldsymbol{s}_{OCo}$ is a constant vector, the first- and second-order time differentials of Eq. (19) are expressed as

$$\dot{\boldsymbol{p}} = \dot{\boldsymbol{p}}_O + \boldsymbol{\omega}_O \times \boldsymbol{R}_O {}^{O}\boldsymbol{s}_{OCo}, \quad (20)$$

$$\ddot{\boldsymbol{p}} = \ddot{\boldsymbol{p}}_O + \dot{\boldsymbol{\omega}}_O \times \boldsymbol{R}_O {}^{O}\boldsymbol{s}_{OCo} + \boldsymbol{\omega}_O \times (\boldsymbol{\omega}_O \times \boldsymbol{R}_O {}^{O}\boldsymbol{s}_{OCo}). \quad (21)$$

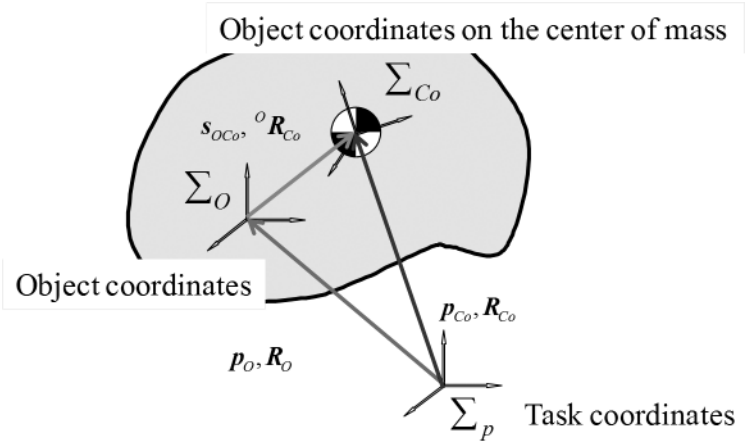


Figure 4. Coordinate system to be set for the target object.

The relationships between force and moment acting on the center of mass, and the equivalent force $\boldsymbol{f}_O$ and moment $\boldsymbol{n}_O$ acting on the origin of the coordinate system Σ_O are given by

$$\boldsymbol{f}_O = \boldsymbol{f}, \tag{22}$$

$$\boldsymbol{n}_O = \boldsymbol{n} + \boldsymbol{s}_{OCo} \times \boldsymbol{f}. \tag{23}$$

Moreover, according to the parallel axis theorem regarding the inertia tensor, there is a relationship as follows

$$\dot{\boldsymbol{I}}_O = \dot{\boldsymbol{C}}_O \boldsymbol{I}_O \boldsymbol{C}_O^T + \boldsymbol{C}_O \dot{\boldsymbol{I}}_O \boldsymbol{C}_O^T + \boldsymbol{C}_O \boldsymbol{I}_O \dot{\boldsymbol{C}}_O^T + m \left(\dot{\boldsymbol{C}}_O \boldsymbol{S}_O \boldsymbol{C}_O^T + \boldsymbol{C}_O \dot{\boldsymbol{S}}_O \boldsymbol{C}_O^T + \boldsymbol{C}_O \boldsymbol{S}_O \dot{\boldsymbol{C}}_O^T \right). \tag{24}$$

By substituting Eqs. (20)–(24) into Eq. (18), it is expressed as

$$\boldsymbol{F}_O = \boldsymbol{M}_O \dot{\boldsymbol{v}}_O + \boldsymbol{C}_O \boldsymbol{v}_O + \boldsymbol{g}_O, \tag{25}$$

where

$$\boldsymbol{M}_O = \begin{bmatrix} m\boldsymbol{I} & -m\boldsymbol{S}_O \\ m\boldsymbol{S}_O & \boldsymbol{I}_O - m\boldsymbol{S}_O^2 \end{bmatrix}, \quad \boldsymbol{C}_O = \begin{bmatrix} \boldsymbol{0} & -m\boldsymbol{R}_O \dot{\boldsymbol{S}}_O \boldsymbol{R}_O^T \\ m\boldsymbol{R}_O \dot{\boldsymbol{S}}_O \boldsymbol{R}_O^T & \boldsymbol{I}_O \boldsymbol{R}_O^T \boldsymbol{\omega}_O \end{bmatrix}, \quad \boldsymbol{g}_O = \begin{bmatrix} -m\boldsymbol{g} \\ m\boldsymbol{R}_O \boldsymbol{S}_O \boldsymbol{R}_O^T \boldsymbol{g} \end{bmatrix}, \quad \boldsymbol{F}_O = \begin{bmatrix} \boldsymbol{f} \\ \boldsymbol{n} \end{bmatrix}.$$

Equation (25) is the equation of object motion established by the force and moment acting on the origin of the coordinate system Σ_O. When the orientation of the object is represented by the zyz-Euler angle $\boldsymbol{\eta} = [\phi\ \theta\ \varphi]^T$, the position and orientation is expressed as $\boldsymbol{r}_O = [\boldsymbol{p}_O^T\ \boldsymbol{\eta}_O^T]^T$, and its time derivative is expressed by $\dot{\boldsymbol{r}}_O = [\dot{\boldsymbol{p}}_O^T\ \dot{\boldsymbol{\eta}}_O^T]^T$. On the other hand, the object velocity can be expressed by $\boldsymbol{v}_O = [\dot{\boldsymbol{p}}_O^T\ \boldsymbol{\omega}_O^T]^T$ when the object angular velocity $\boldsymbol{\omega}_O$ is used. Both have a relation of

$$\boldsymbol{v}_O = \boldsymbol{T}_O \dot{\boldsymbol{r}}_O, \tag{26}$$

where

$$\boldsymbol{T}_O = \begin{bmatrix} \boldsymbol{I}_3 & \boldsymbol{0} \\ \boldsymbol{0} & \boldsymbol{\Pi}_O \end{bmatrix} \in \mathbb{R}^{6\times 6}, \quad \boldsymbol{\Pi}_O = \begin{bmatrix} 0 & -\sin\phi \\ 0 & \cos\phi \end{bmatrix}$$

cos□
sin□ □
sin□ (27)
sin□ □
.

□ □ □□1 cos□ □□
0

The dynamic Eq. (25) are characterized by the following structural properties, which are utilized in our controller design.

(P1) $\boldsymbol{M}_O$ is symmetric positive definite.

(P2) The suitable definition of $\boldsymbol{C}_O$ makes matrix $\dot{\boldsymbol{M}}_O - 2\boldsymbol{C}_O$ skew-symmetric.

(P3) The dynamic equation is linear with respect to the dynamic parameter vector, as follows:

$$\boldsymbol{M}_O \dot{\boldsymbol{v}}_{Or} + \boldsymbol{C}_O \boldsymbol{v}_{Or} + \boldsymbol{g}_O = \boldsymbol{Y}_O(\boldsymbol{r}_O, \dot{\boldsymbol{r}}_O, \boldsymbol{v}_{Or}, \dot{\boldsymbol{v}}_{Or})\boldsymbol{\sigma}_O, \quad (28)$$

where □ ρ . . □ □6×ρo

$_O$ is a dynamic parameter vector of the object, $\boldsymbol{Y}_O(\boldsymbol{r}_O, \dot{\boldsymbol{r}}_O, \boldsymbol{v}_{Or}, \dot{\boldsymbol{v}}_{Or})$ is a regressor with respect to the dynamic parameters $\boldsymbol{\sigma}_O$, and ρ_O is the number of the object dynamics parameter. The ρ_O is 10 if Eq. (25) is used, and 7 if Eq. (18) is used.

Equation of Motion of both Robot Fingers and Grasped Object

When a robotic hand with k fingers manipulates an object under a condition of rolling contact without slip ("without slip" means $S_{CFi_V} = S_{x\,CFi\,V} = 0$ in Eq. [11]), the following relation on the rolling velocities of the contact position on both surfaces with respect to Σ_P, is obtained:

$$\boldsymbol{R}_{O}\,\boldsymbol{p}_{Fi} \quad . \tag{29}$$
$$\boldsymbol{R}\,\boldsymbol{p}$$

$$O \quad OCi \quad Fi \quad FiCi$$

Therefore, the relation between the object velocity and angular velocity of the *i*-th robot finger is expressed as

$$w_{Ci} = \boldsymbol{J}_{Ci}\begin{bmatrix}\boldsymbol{q}_{Fi}\\ \end{bmatrix}, \tag{30}$$
$$O$$

where $\boldsymbol{W}_{Ci} = \begin{bmatrix} I_{3\times3} \\ \hat{O} \end{bmatrix}_{p}[R \quad \times]] \in \Re^{6\times3}$ is a grasp form matrix, and $\boldsymbol{J}_{O\ OCi} \in \Re^{3\times3}$ is a Jacobian matrix at the contact point. For all fingers, Eq. (30) is represented as follows:

$$\begin{bmatrix}\boldsymbol{W}_{C}^{T}\\ \boldsymbol{v}\end{bmatrix} = \boldsymbol{J}_{C}\,\boldsymbol{q}_{F}, \tag{31}$$

where $[\boldsymbol{W}_{C1} \quad \boldsymbol{W}_{Ck}] \in \Re^{6\times3k}$, $\boldsymbol{J}_{C} = diag[\boldsymbol{J}_{C1} \quad \cdots \quad \boldsymbol{J}_{Ck}] \in \Re^{3k\times3k}$, and $\boldsymbol{q}_{F} = [\boldsymbol{q}_{F1}^{T} \quad \cdots \quad \boldsymbol{q}_{Fk}^{T}]^{T} \in \Re^{3k}$. Furthermore, by defining $\boldsymbol{x} = [\boldsymbol{v}^{T} \quad \boldsymbol{q}^{T}]^{T}$ and $G = [\boldsymbol{W}^{T} \quad -\boldsymbol{J}_{C}^{T}]^{T}$, Eq. (31) can be represented in a more compact form as follows:

$$\boldsymbol{G}\dot{\boldsymbol{x}} = \boldsymbol{0}. \tag{32}$$

The Lagrangian of the target system is given by L. Using the Lagrange multipliers, the Lagrange's equation of motion is derived by applying the variational principle in such a way that

$$\int_{t1}^{t2} \delta L + \boldsymbol{u}_{c}^{T}\delta\boldsymbol{x} + \boldsymbol{f}\boldsymbol{G}\delta\boldsymbol{x}\,dt = 0, \tag{33}$$

where $\boldsymbol{f}_{C} = [\boldsymbol{f}_{C1} \quad \cdots \quad \boldsymbol{f}_{Ck}] \in \Re^{3k}$ are the Lagrange multipliers corresponding to the contact force, and $\boldsymbol{u}$ is a non-conservative and external force. Let us define $\boldsymbol{u}$ as $[\boldsymbol{0}^{T} \quad \boldsymbol{\tau}^{T}]^{T}$, where

$\boldsymbol{\tau}_F \in \mathbb{R}^{3k}$ is the input joint torque. The dynamic equation of motion for both the object

and the robot hand are given by

$$\boldsymbol{M}_O \dot{\boldsymbol{v}}_O + \boldsymbol{C}_O \boldsymbol{v}_O + \boldsymbol{g}_O = \boldsymbol{W}_C \boldsymbol{f}_C, \tag{34}$$

$$\boldsymbol{M}_F(\boldsymbol{q}_F)\ddot{\boldsymbol{q}}_F + (\boldsymbol{C}_F(\boldsymbol{q}_F, \dot{\boldsymbol{q}}_F) + \dot{\boldsymbol{C}}_F)\dot{\boldsymbol{q}}_F + \boldsymbol{g}_F(\boldsymbol{q}_F) = \boldsymbol{J}_F^T \boldsymbol{f}_C + \boldsymbol{\tau}_F, \tag{35}$$

where $\boldsymbol{M}_F \in \mathbb{R}^{3k \times 3k}$ is the inertia matrix, $\boldsymbol{C}_F \dot{\boldsymbol{q}}_F \in \mathbb{R}^{3k}$ is the velocity square term consisting

of centrifugal and Coriolis force, and $\boldsymbol{g}_F$ is the gravitational term. The left side of Eq. (34) is the same structure as right side of Eq. (25). In addition to (P1) – (P3), the dynamic equations (35) are characterized by the following structural properties, which are utilized in our controller design.

(P4) $\boldsymbol{M}_F$ is symmetric positive definite.

(P5) A suitable definition of $\boldsymbol{C}_F$ makes matrix $\dot{\boldsymbol{M}}_F - 2\boldsymbol{C}_F$ skew-symmetric.

(P6) The dynamic equation is linear with respect to the dynamic parameter vector, as follows:

$$\boldsymbol{M}_F \ddot{\boldsymbol{q}}_{Fr} + \boldsymbol{C}_F \dot{\boldsymbol{q}}_{Fr} + \boldsymbol{g}_F = \boldsymbol{Y}_F(\boldsymbol{q}_F, \dot{\boldsymbol{q}}_F, \dot{\boldsymbol{q}}_{Fr}, \ddot{\boldsymbol{q}}_{Fr})\boldsymbol{\sigma}_F, \tag{36}$$

where $\boldsymbol{\sigma}_F \in \mathbb{R}^{\rho_F}$ is a dynamic parameter vector of the robot hand, $Y_F(\boldsymbol{q}_F, \dot{\boldsymbol{q}}_F, \dot{\boldsymbol{q}}_{Fr}, \ddot{\boldsymbol{q}}_{Fr}) \in \mathbb{R}^{3k\times\rho_F}$ is a regressor with respect to the dynamic parameters $\boldsymbol{\sigma}_F$, and ρ_F is the number of robot hand dynamic parameters.

ADAPTIVE CONTROL

Adaptive Control without a Force Sensor

The dynamic equations of the object and robot fingers contain dynamic parameters such as the mass and inertia tensor of the link between object and fingers. When these dynamic parameters are unknown, it is very difficult to precisely control the motion of the object. The purpose of control here is to find a control law such that the object motion follows the desired trajectory asymptotically. The adaptive control is designed in three steps:

(1) Calculate the desired external force, $\boldsymbol{F}^d$, to be applied to the object using an estimated reference model of the object, which is generated by the desired trajectories of the object, $\boldsymbol{r}_O^d$, $\dot{\boldsymbol{r}}_O^d$, and $\ddot{\boldsymbol{r}}_O^d$. It is assumed that the desired values are bounded and continuous.

(2) Compute the desired contact force $\boldsymbol{f}^d$ at the contact point using the desired external force.

(3) Compute an adaptive control law of the i-th robot finger using an estimated reference model of the robot finger.

The proposed adaptive coordinated control does not need the measurement of the force at the contact point. It only needs the measurements of position and velocity of the object and all robot fingers.

First, the reference velocity of the object $\boldsymbol{v}_{Or} \in \mathbb{R}^6$ is defined as

$$\boldsymbol{v}_{Or} = \dot{\boldsymbol{r}}_O^d + \boldsymbol{T}_O(\boldsymbol{r}_O - \boldsymbol{r}_O^d + \boldsymbol{\Lambda}\boldsymbol{e}_O), \tag{37}$$

where $\boldsymbol{e}_O = \begin{bmatrix} \boldsymbol{r}_O - \boldsymbol{r}_O^d \\ \boldsymbol{\varepsilon}_O - \boldsymbol{\varepsilon}_O^d \end{bmatrix}$ is the position and orientation error vector of the object, $\boldsymbol{T}_O \in \mathbb{R}^{6\times 6}$

is the matrix that converts the velocity of the Euler angles into angular velocity, and $\boldsymbol{\Lambda}_O \in \mathbb{R}^{6\times 6}$ is a weighting matrix that is positive and diagonal. Moreover, the residual velocity of the object, $\boldsymbol{s}_O \in \mathbb{R}^6$, is defined as

$$\boldsymbol{s}_O = \boldsymbol{v}_O - \boldsymbol{v}_{Or}. \tag{38}$$

Then, the relation of $\boldsymbol{s}_O = -\boldsymbol{T}_O(\boldsymbol{e}_O + \boldsymbol{\Lambda}\boldsymbol{e}_O)$ is obtained. The desired external force to be applied to the object, $\boldsymbol{F}_O^d$, is generated from the reference model of the object using the following equation:

$$\boldsymbol{F}_O^d = \hat{\boldsymbol{M}}_O(\boldsymbol{r}_O)\dot{\boldsymbol{v}}_{Or} + \hat{\boldsymbol{C}}_O(\boldsymbol{r}_O, \dot{\boldsymbol{r}}_O)\boldsymbol{v}_{Or} + \hat{\boldsymbol{g}}_O(\boldsymbol{r}_O) - \boldsymbol{Y}_O(\boldsymbol{r}_O, \dot{\boldsymbol{r}}_O, \boldsymbol{v}_{Or}, \dot{\boldsymbol{v}}_{Or})\hat{\boldsymbol{\sigma}}_O, \tag{39}$$

where $\hat{\boldsymbol{M}}_O$, $\hat{\boldsymbol{C}}_O$ and $\hat{\boldsymbol{g}}_O$ are the estimates of $\boldsymbol{M}_O$, $\boldsymbol{C}_O$, and $\boldsymbol{g}_O$ using $\hat{\boldsymbol{\sigma}}_O$. Now, an estimated law of the dynamic parameter vector of the object is given by

$$\hat{\boldsymbol{\sigma}}_O = \boldsymbol{\Gamma}_O \boldsymbol{Y}_O^T (\dot{\boldsymbol{r}}_{Or}, \boldsymbol{r}_{Or}, \boldsymbol{s}), \tag{40}$$

where, $\boldsymbol{\Gamma}_O > 0$ is an adaptive gain matrix that is symmetric. The desired external force of the object is sequentially updated based on the estimation of the dynamic parameters of the object. Also, the reference acceleration of the object $\boldsymbol{v}_{Or}$ is given by

$$\dot{\boldsymbol{v}}_{Or} = \boldsymbol{T}_O (\ddot{\boldsymbol{r}}_O^d + \boldsymbol{\Lambda}\dot{\boldsymbol{e}}_O) + \dot{\boldsymbol{T}}_O (\dot{\boldsymbol{r}}_O^d + \boldsymbol{\Lambda}\boldsymbol{e}_O). \tag{41}$$

Forces and moments at the contact points are in equilibrium with the external force. Therefore, the desired force at the contact point $\boldsymbol{f}^d$ is provided by the following equation:

$$\boldsymbol{f}^d = \boldsymbol{W}_C^{\#} \boldsymbol{F}_O^d + (\boldsymbol{I} - \boldsymbol{W}_C^{\#} \boldsymbol{W}_C) \boldsymbol{f}_0^d. \tag{42}$$

The first term of Eq. (42) is the external force that has an effect on the object motion, and the second term is the internal force that does not have such an effect. The internal force that is bounded and uniformly continuous is a vector in the null space of $\boldsymbol{W}_C$. Therefore, as long as it meets the contact conditions, the way of setting is unlimited.

The following relationship is established in the joint velocity of the *i*-th robot finger and the object velocity, as was seen in Eq. (30):

$$\dot{\boldsymbol{q}}_{Fi} = (\boldsymbol{J}_{Ci} \boldsymbol{G}_{Ci}^{-1} \boldsymbol{W}_C^T)^{\#} \boldsymbol{v}_O. \tag{43}$$

From this relationship, the reference joint velocity of the *i*-th robot finger $\boldsymbol{q}_{Fri}$ is given by

$$\dot{\boldsymbol{q}}_{Fri} = (\boldsymbol{J}_{Ci} \boldsymbol{G}_{Ci}^{-1} \boldsymbol{W}_C^T)^{\#} \boldsymbol{v}_{Or}. \tag{44}$$

Using the estimate $\hat{\boldsymbol{\sigma}}_{Fi}$ of the dynamic parameter vector of the *i*-th robot finger $\boldsymbol{\sigma}_{Fi}$,

Fi
the reference model of the *i*-th robot finger is given by

$$\hat{\boldsymbol{M}}_{Fi}(\boldsymbol{q}_{Fi})\dot{\boldsymbol{q}}_{Fri} + \hat{\boldsymbol{C}}_{Fi}(\boldsymbol{q}_{Fi},\dot{\boldsymbol{q}}_{Fi})\dot{\boldsymbol{q}}_{Fri} + \hat{\boldsymbol{g}}_{Fi}(\boldsymbol{q}_{Fi}) + \boldsymbol{Y}_{Fi}(\boldsymbol{q}_{Fi},\dot{\boldsymbol{q}}_{Fi},\dot{\boldsymbol{q}}_{Fri},\ddot{\boldsymbol{q}}_{Fri})\hat{\boldsymbol{\sigma}}_{Fi}, \quad (45)$$

where , $\hat{\boldsymbol{C}}$, and $\hat{\boldsymbol{g}}$ are the estimates of $\boldsymbol{M}$, $\boldsymbol{C}$, . The control law
$\boldsymbol{M}$ and $\boldsymbol{g}$ using $\hat{\boldsymbol{\sigma}}$

Fi Fi Fi Fi Fi Fi Fi
of the *i*-th robot finger is given by

$$\boldsymbol{\tau}_{Fi} = \boldsymbol{Y}_{Fi}(\boldsymbol{q}_{Fi},\dot{\boldsymbol{q}}_{Fi},\dot{\boldsymbol{q}}_{Fri},\ddot{\boldsymbol{q}}_{Fri})\hat{\boldsymbol{\sigma}}_{Fi} - \boldsymbol{f}_{Fi}^{d} - \boldsymbol{K}_{Ci}\boldsymbol{J}_{Ci}^{T}\boldsymbol{s}_{Fi}, \quad (46)$$

where $\boldsymbol{K}_{Fi} > 0$ is a feedback gain matrix, and $\boldsymbol{s}_{Fi}$ is the residual between the actual
velocity and the reference velocity defined by

$$\boldsymbol{s}_{Fi} = \dot{\boldsymbol{q}}_{Fi} - \dot{\boldsymbol{q}}_{Fri}; \quad (47)$$

it is represented by

$$\boldsymbol{s}_{Fi} = \boldsymbol{J}_{Ci}^{-1}\boldsymbol{W}_{Ci}^{T}\boldsymbol{s}_{O} . \quad (48)$$

The adaptive law of the parameter estimate of the *i*-th robot finger is given by

$$\dot{\hat{\boldsymbol{\sigma}}}_{Fi} = -\boldsymbol{\Gamma}_{Fi}\boldsymbol{Y}_{Fi}^{T}(\boldsymbol{q}_{Fi},\dot{\boldsymbol{q}}_{Fi},\dot{\boldsymbol{q}}_{Fri},\ddot{\boldsymbol{q}}_{Fri})\boldsymbol{s}_{Fi} , \quad (49)$$

where $\boldsymbol{\Gamma}_{Fi} > 0$ is an adaptive gain matrix that is symmetric. On the right-hand side of Eq. (46), the first term is a feed-forward input term based on the estimated reference model,

the second term is a feed-forward input term corresponding to the desired force at the contact point, and the third term is a feedback input term based on the object trajectory errors. It should be noted that the adaptive control does not require measurements of forces and moments at each contact point. The integrated control law and adaptive law can be written as follows:

$$\tau = Y(q, \dot{q}, \dot{q}_r, \ddot{q}_r)\hat{\sigma}_F - J_C^T f_d - K_s s_F \tag{50}$$

$$\dot{\hat{\sigma}}_F = -\Gamma_F Y_{Fr}^T(q, \dot{q}, \dot{q}_{Fr}, \ddot{q}_{Fr}) s_F \tag{51}$$

where $\hat{\sigma}_F = [\hat{\sigma}_{F1}^T \ \cdots \ \hat{\sigma}_{Fk}^T]^T$ and $\Gamma_F = diag[\Gamma_{F1} \ \cdots \ \Gamma_{Fk}]$. If the grasping conditions (A1)–(A4) are assumed, the following theorem is proved for adaptive control without use of a force sensor.

Theorem 2. *Consider a rigid body that is grasped by k robot fingers, each with three DOFs. For the system in Eqs. (34), (35), and (31), given that Eq. (40) is the parameter estimation law of the object, Eq. (39) is the desired external force of the object, Eq. (42) is the desired force at the contact point, Eq. (48) is the residual, Eq. (51) is the parameter estimate law of the robotic fingers, and Eq. (50) is the control law, the closed-loop system is then asymptotic stable in the following sense:*

(1) $r_O \to r_O^d$ *and* $\dot{r}_O \to \dot{r}_O^d$ *as* $t \to \infty$ *is bounded.*

(2) *The force error at the contact point* $f^d - f$

The error dynamics of the object is given by

$$F_O = \hat{M}_O(r_O)\dot{v}_{Or} + \hat{C}_O(r_O, \dot{r}_O)v_{Or} + \hat{g}_O(r_O) - M_O(r_O)\dot{v}_O - C_O(r_O, \dot{r}_O)v_O - g_O(r_O)$$

$$= \hat{M}_O(r_O)\dot{v}_{Or} + \hat{C}_O(r_O, \dot{r}_O)v_{Or} + \hat{g}_O(r_O) - M_O$$

$$
\begin{aligned}
&(\boldsymbol{r}_O)(\dot{\boldsymbol{s}}_O - \boldsymbol{v}_{Or}) \\
&+\boldsymbol{C}_O(\boldsymbol{r}_O, \dot{\boldsymbol{r}}_O)(\boldsymbol{s}_O - \boldsymbol{v}_{Or}) - \boldsymbol{g}_O(\boldsymbol{r}_O) \\
&- \boldsymbol{Y}(\boldsymbol{r}_O, \dot{\boldsymbol{r}}_O, \boldsymbol{v}_{Or}, \dot{\boldsymbol{v}}_{Or})(\hat{\boldsymbol{\sigma}}_O - \boldsymbol{\sigma}_O) - \\
&\boldsymbol{M}_O(\boldsymbol{r}_O)\dot{\boldsymbol{s}}_O - \boldsymbol{C}_O(\boldsymbol{r}_O, \dot{\boldsymbol{r}}_O)\boldsymbol{s}_O,
\end{aligned}
\tag{52}
$$

where $\Delta \boldsymbol{F} = \boldsymbol{F}^d - \boldsymbol{f}^d = \boldsymbol{W}\boldsymbol{f} = \boldsymbol{W}\Delta\boldsymbol{f}$. The error dynamics of the robot fingers is given by

$$
\begin{bmatrix} \boldsymbol{0} \\ \boldsymbol{M}_F \dot{\boldsymbol{s}}_F \end{bmatrix} = \begin{bmatrix} -\boldsymbol{C}_F \boldsymbol{s}_F \\ \boldsymbol{Y}_F(\hat{\boldsymbol{\sigma}}_F - \boldsymbol{\sigma}_F) \end{bmatrix} - \begin{bmatrix} \boldsymbol{K}_F \boldsymbol{s}_F \\ \boldsymbol{0} \end{bmatrix} + \boldsymbol{J}_F^T(\boldsymbol{f}^d). \tag{53}
$$

Theorem 2 can be proved using a candidate Lyapunov function given by

$$
V = \frac{1}{2}(\boldsymbol{s}_F^T \boldsymbol{M}_F \boldsymbol{s}_F + \Delta\boldsymbol{\sigma}_F^T \boldsymbol{\Gamma}^{-1} \Delta\boldsymbol{\sigma}_F + \Delta\boldsymbol{\sigma}_O^T \boldsymbol{\Gamma}^{-1} \Delta\boldsymbol{\sigma}_O), \tag{54}
$$

where $\Delta\boldsymbol{\sigma}_O = \hat{\boldsymbol{\sigma}}_O - \boldsymbol{\sigma}_O$ and $\Delta\boldsymbol{\sigma} = \hat{\boldsymbol{\sigma}}_F - \boldsymbol{\sigma}_F$. A time derivative along the solution of the error equation gives as the following equation:

$$
\begin{aligned}
\dot{V} = &\left(\frac{1}{2}\boldsymbol{s}_O^T \dot{\boldsymbol{M}}_O \boldsymbol{s}_O + \boldsymbol{s}_O^T \boldsymbol{M}_O \dot{\boldsymbol{s}}_O\right) + \left(\frac{1}{2}\boldsymbol{s}_F^T \dot{\boldsymbol{M}}_F \boldsymbol{s}_F + \boldsymbol{s}_F^T \boldsymbol{M}_F \dot{\boldsymbol{s}}_F\right) + \Delta\dot{\boldsymbol{\sigma}}_O^T \boldsymbol{\Gamma}^{-1} \Delta\boldsymbol{\sigma}_O \\
&+ \Delta\dot{\boldsymbol{\sigma}}_F^T \boldsymbol{\Gamma}^{-1} \Delta\boldsymbol{\sigma}_F.
\end{aligned}
\tag{55}
$$

Substituting Eqs. (52), (53), (40), and (51) into (55), and using (P2) and (P5),

$$\dot{V} = \begin{bmatrix} \boldsymbol{s}_O^T & \boldsymbol{s}_F^T \end{bmatrix} \begin{bmatrix} \boldsymbol{Y}_O^T \boldsymbol{s}_O + \boldsymbol{s}_F^T \boldsymbol{Y}_F - \boldsymbol{K}_O \boldsymbol{s}_O - \boldsymbol{J}_C^T \boldsymbol{f}_C \\ \boldsymbol{\Gamma}_F \dot{\boldsymbol{\sigma}}_F \end{bmatrix} + \begin{bmatrix} \boldsymbol{s}_O^T & \boldsymbol{s}_F^T \end{bmatrix} \begin{bmatrix} \boldsymbol{O} & \boldsymbol{O} \\ \boldsymbol{O} & \boldsymbol{\Gamma}_F \end{bmatrix} \begin{bmatrix} \boldsymbol{\Gamma}_O^{-1} \Delta\dot{\boldsymbol{\sigma}}_O \\ \Delta\dot{\boldsymbol{\sigma}}_F \end{bmatrix}$$

$$+ \begin{bmatrix} \boldsymbol{s}_O^T & \boldsymbol{s}_F^T \end{bmatrix} \begin{bmatrix} \boldsymbol{O} & \boldsymbol{O} \\ \boldsymbol{Y}_F^T & \boldsymbol{O} \end{bmatrix} \begin{bmatrix} \boldsymbol{\Gamma}_O \Delta\boldsymbol{\sigma}_O \\ \boldsymbol{\Gamma}_F \Delta\boldsymbol{\sigma}_F \end{bmatrix} - \boldsymbol{s}_F^T \boldsymbol{K}_F \boldsymbol{s}_F - \boldsymbol{s}_F^T \boldsymbol{J}_C^T \boldsymbol{f}_C . \quad (56)$$

From the relationship in Eq. (48),

$$\dot{V} = -\boldsymbol{s}_F^T \boldsymbol{K}_F \boldsymbol{s}_F \leq 0. \quad (57)$$

This shows that Eq. (54) is the Lyapunov function; hence, $\boldsymbol{s}_O$, $\boldsymbol{s}_F$, $\Delta\boldsymbol{\sigma}_O$, and $\Delta\boldsymbol{\sigma}_F$ are bounded. To prove asymptotic convergence using a Lyapunov-like lemma, it is necessary to show the uniform continuity of V. The second-order time differentials of Eq. (54) is given by

$$\ddot{V} = -2\boldsymbol{s}_F^T \boldsymbol{K}_F \dot{\boldsymbol{s}}_F . \quad (58)$$

Therefore, it is necessary to show the boundedness of $\dot{\boldsymbol{s}}_F$. Because $\boldsymbol{\sigma}_O$ and $\boldsymbol{\sigma}_F$ are bounded and $\dot{\boldsymbol{\sigma}}_O$ and $\dot{\boldsymbol{\sigma}}_F$ are constant, the boundedness of $\boldsymbol{T}_O$ leads to the boundness of $\boldsymbol{e}_O$ and $\dot{\boldsymbol{e}}_O$ by the following equation:

$$\boldsymbol{e}_O(t) = e^{-At}\boldsymbol{e}_O(t) + \int_0^t e^{-A(t-\tau)}\boldsymbol{T}_O^{-1}(\tau)d\tau . \quad (59)$$

These results yield the boundedness of $\boldsymbol{r}_O$, $\dot{\boldsymbol{r}}_O$, and $\boldsymbol{v}_{Or}$ because of the desired trajectory. $\boldsymbol{T}_O$ is bounded from the boundedness of $\boldsymbol{r}_O$. Hence, $\dot{\boldsymbol{v}}_{Or}$ is bounded. These results yield $\boldsymbol{Y}_O(\boldsymbol{r}_O^d, \dot{\boldsymbol{r}}_O, \boldsymbol{v}_{Or}, \dot{\boldsymbol{v}}_{Or}^d)$, and $\boldsymbol{F}_O$ are bounded from Eq. (44); $\boldsymbol{f}_C$ is bounded from the boundedness of $\boldsymbol{F}_O$ and the second term of Eq. (42); $\boldsymbol{q}_{Fr}$ is bounded. $\dot{\boldsymbol{q}}_F$ is bounded from Eq. (47); and $\boldsymbol{J}_C$ and $\dot{\boldsymbol{W}}_C$ are bounded from

the boundedness of $\boldsymbol{q}_F$, $\dot{\boldsymbol{q}}_F$, $\ddot{\boldsymbol{q}}_F$ and $\boldsymbol{v}_O$. These results yield a $\boldsymbol{q}_{Fri}$ that is bounded. Then, $\boldsymbol{Y}_F(\boldsymbol{q}_F, \dot{\boldsymbol{q}}_F, \ddot{\boldsymbol{q}}_{Fr}, \dot{\boldsymbol{q}}_{Fr})$ is bounded.

Using the relationship $\Delta \boldsymbol{F}_O = \boldsymbol{W}_C \Delta \boldsymbol{f}_C$, from Eqs. (52) and (53), the following equation is derived.

$$\begin{bmatrix} \boldsymbol{W}_C \boldsymbol{J}_C^{T} \boldsymbol{s}_F \\ \boldsymbol{M}_F \boldsymbol{s}_F \end{bmatrix} \Delta\boldsymbol{\sigma}_F + \begin{bmatrix} \boldsymbol{C}_F \boldsymbol{s}_F \\ \boldsymbol{Y}_F \end{bmatrix} \Delta\boldsymbol{\sigma}_F + \begin{bmatrix} \boldsymbol{K}_O \boldsymbol{s}_O \\ \boldsymbol{M}_O \boldsymbol{s}_O \end{bmatrix} \Delta\boldsymbol{\sigma}_O + \begin{bmatrix} \boldsymbol{C}_O \boldsymbol{s}_O \\ 0 \end{bmatrix}. \quad (60)$$

Moreover, the time derivative of Eq. (48) for all fingers is given by

$$\dot{\boldsymbol{s}} = \dot{\boldsymbol{J}}_C \boldsymbol{J}_C^{-1} \boldsymbol{s} + \boldsymbol{J}_C^{-T} \boldsymbol{W}_C^{T} \dot{\boldsymbol{s}}. \quad (61)$$

Substituting the equation above into Eq. (60),

$$\begin{bmatrix} \boldsymbol{M}_F \boldsymbol{W}_C^{T} \boldsymbol{J}_C^{-T} \\ \boldsymbol{Y}_F \end{bmatrix} \dot{\boldsymbol{s}} + \begin{bmatrix} \boldsymbol{W}_C \boldsymbol{J}_C^{T} \Delta\tilde{\boldsymbol{A}}_O \\ \Delta\tilde{\boldsymbol{A}}_F \end{bmatrix} \boldsymbol{Y} = \begin{bmatrix} \boldsymbol{W}_C \boldsymbol{J}_C^{T} \boldsymbol{M}_O \dot{\boldsymbol{J}}_C \boldsymbol{J}_C^{-1} \boldsymbol{W}_C^{T} \Delta\boldsymbol{\sigma}_O \\ \boldsymbol{K}_F \boldsymbol{s}_F \end{bmatrix} + \begin{bmatrix} \boldsymbol{W}_C \boldsymbol{J}_C^{T} \boldsymbol{C}_O \boldsymbol{s}_O \\ \boldsymbol{M}_F \dot{\boldsymbol{J}}_C \boldsymbol{J}_C^{-1} \boldsymbol{J}_C^{-T} \boldsymbol{C}_F \boldsymbol{s}_F \end{bmatrix} \Delta\boldsymbol{\sigma}_F. \quad (62)$$

From $\boldsymbol{M}_F > 0$, $\boldsymbol{M}_O > 0$, and $\boldsymbol{W}_C \boldsymbol{J}_C^{-T} \boldsymbol{M}_O \boldsymbol{J}_C^{-1} \boldsymbol{W}_C^{T} > 0$,

$$\begin{bmatrix} \boldsymbol{M}_O \boldsymbol{W}_C \boldsymbol{J}_C^{-T} \\ \boldsymbol{M}_F \end{bmatrix} \boldsymbol{J}_C^{-1} \boldsymbol{W}_C^{T} > 0. \quad (63)$$

Therefore, $\dot{\boldsymbol{s}}_O$ is bounded because of the boundedness of right-hand side of Eq. (62). This result yield an $\boldsymbol{s}_F$ that is bounded. The $\dot{\boldsymbol{s}}_F$ yields a bounded ness of bounded $\boldsymbol{f}_C^d - \boldsymbol{f}_C$, and $\boldsymbol{V}$ is uniformly continuous. It is shown that $\boldsymbol{V} \to 0$ as $t \to \infty$ from the Lyapunov-like Lemma. This implies that $\boldsymbol{s}_F \to 0$ as $t \to \infty$. Using Eq. (48), $\boldsymbol{s}_O \to 0$ as $t \to \infty$. This result yields $\dot{\boldsymbol{r}}_O \to \dot{\boldsymbol{r}}_O^d$ and $\boldsymbol{r}_O \to \boldsymbol{r}_O^d$ as $t \to \infty$. These results yield $\boldsymbol{e}_O \to \boldsymbol{0}$ and $\dot{\boldsymbol{e}}_O \to \boldsymbol{0}$ as $t \to \infty$.

The convergence to the desired trajectory does not guarantee that the estimated parameter $\hat{\boldsymbol{\sigma}}(t)$ will converge to the true parameter $\boldsymbol{\sigma}$, but the estimated parameter converges to a constant $\boldsymbol{\sigma}(\infty)$ asymptotically. If $\boldsymbol{Y}$ satisfies the *persistently exciting condition* and is uniformly continuous, the estimate parameter will converge to the true value asymptotically (Anderson 1977). By a *persistently exciting condition* on $\boldsymbol{Y}$, we mean that there exist strictly positive constants α and T such that for any $t > 0$,

$$\int_t^{t+T} \boldsymbol{Y}^T \boldsymbol{Y} d\tau \geq \alpha \boldsymbol{I}. \tag{64}$$

From Eq. (62), it can be shown that $\boldsymbol{s}_O$ is uniformly continuous. Hence, $\dot{\boldsymbol{s}}_F$ is uniformly continuous also. Using Barbalat's lemma, $\boldsymbol{s}_O \to 0$ and $\boldsymbol{s}_F \to 0$ as $t \to \infty$. If $\boldsymbol{s}_O \to 0$, $\boldsymbol{s}_F \to 0$, $\dot{\boldsymbol{s}}_O \to 0$, and $\dot{\boldsymbol{s}}_F \to 0$, then Eq. (60) is represented as

$$\tilde{\boldsymbol{Y}} \Delta\tilde{\boldsymbol{\sigma}} = \boldsymbol{0}, \tag{65}$$

where $\tilde{\boldsymbol{Y}} = [\boldsymbol{Y}_O \quad \boldsymbol{W}_C \quad \boldsymbol{J}_C^{-T} \boldsymbol{Y}_F]$ and $\Delta\tilde{\boldsymbol{\sigma}} = [\Delta\boldsymbol{\sigma}^T \quad \Delta\boldsymbol{\sigma}^T]^T$. Now, $\tilde{\boldsymbol{Y}}$ is also uniformly continuous, and $\Delta\tilde{\boldsymbol{\sigma}}$ is constant because $\dot{\boldsymbol{s}}_O \to 0$ and $\dot{\boldsymbol{s}}_F \to 0$. By multiplying $\tilde{\boldsymbol{Y}}^T$ from the left-hand side of Eq. (65) and integrating the equation for a period of time T, we get:

$$\int_t^{t+T} \tilde{\boldsymbol{Y}}^T \tilde{\boldsymbol{Y}} d\tau \, \Delta\tilde{\boldsymbol{\sigma}} = \boldsymbol{0}. \tag{66}$$

If Eq. (64) is satisfied, then $\Delta\tilde{\boldsymbol{\sigma}} \to \boldsymbol{0}$ as $t \to \infty$, and $\hat{\boldsymbol{\sigma}}_F \to \boldsymbol{\sigma}$ and $\hat{\boldsymbol{\sigma}}_O \to \boldsymbol{\sigma}$ as $t \to \infty$. Moreover, these results yield $\Delta\boldsymbol{F}_O \to \boldsymbol{0}$ and $\Delta\boldsymbol{f}_C \to \boldsymbol{0}$ as $t \to \infty$.

Adaptive Control using a Force Sensor

Consider an adaptive control law that uses a force sensor in which the contact force converges to the desired contact force asymptotically. The definition of the reference velocity, $\boldsymbol{v}_{Or}$,

and the residual velocity, $\boldsymbol{s}_O$, of the object are used for Eq. (37) and Eq. (38), respectively. The vector of contact force error,

$$\Delta \boldsymbol{f}_{Ci} = \boldsymbol{f}_{Ci} - \boldsymbol{f}_{Ci}^{d}, \tag{67}$$

is passed through a low-pass filter given by

$$\dot{\boldsymbol{v}}_{Ci} + \alpha_C \boldsymbol{v}_{Ci} = \alpha_C \Delta \boldsymbol{f}_{Ci}, \tag{68}$$

where $\alpha_C > 0$ is a design parameter of the filter, $\boldsymbol{v}_{Ci}$ is an output signal passed through the filter, and its continuity is guaranteed. The reference model of the object is given as follows on behalf of Eq. (39):

$$\boldsymbol{F}_O^{d} = \hat{\boldsymbol{M}}_O(\boldsymbol{r}_O)\dot{\boldsymbol{v}}_{Or} + \hat{\boldsymbol{C}}_O(\boldsymbol{r}_O, \dot{\boldsymbol{r}}_O)\boldsymbol{v}_{Or} + \hat{\boldsymbol{g}}_O(\boldsymbol{r}_O) - \boldsymbol{K}_O \boldsymbol{s}_O$$

$$= \boldsymbol{Y}_O(\boldsymbol{r}_O, \dot{\boldsymbol{r}}_O, \boldsymbol{v}_{Or}, \dot{\boldsymbol{v}}_{Or})\hat{\boldsymbol{\sigma}}_O - \boldsymbol{K}_O \boldsymbol{s}_O, \tag{69}$$

where $\boldsymbol{K}_r > 0$ is a symmetric feedback gain matrix. Furthermore, the reference angular velocity of the *i*-th robot finger, $\boldsymbol{q}_{Fri}$, is defined as the following formula, instead of Eq. (44), and the feedback terms of the force error and integral force errors are added.

$$\boldsymbol{q}_{Fri} = \boldsymbol{J}_{Ci}^{-1}\left(\boldsymbol{W}_{Ci}^{T}\boldsymbol{v}_{Or} + \boldsymbol{\Omega}_{Fi}\boldsymbol{s}_{Fi} + \boldsymbol{\Psi}_{Fi}\boldsymbol{\eta}_{Ci}\right), \tag{70}$$

where $\boldsymbol{\eta}_{Ci}$ is an integral of the contact force error defined by

$$\boldsymbol{\eta}_{Ci} = \int_0^t \Delta \boldsymbol{f}_{Ci}\, dt. \tag{71}$$

In addition, $\boldsymbol{\Omega}_{Fi} > 0$ and $\boldsymbol{\Psi}_{Fi} > 0$ are the symmetric feedback gain matrices of force error and integral force error, respectively. Then, the residuals defined by Eq. (47) are represented as

$$\boldsymbol{s}_{Fi} = \boldsymbol{J}_{Ci}^{-1}\left(\boldsymbol{W}_{Ci}^{T}\boldsymbol{s}_{Or} - \boldsymbol{\Omega}_{Fi}\boldsymbol{v}_{Ci} - \boldsymbol{\Psi}_{Fi}\boldsymbol{\eta}_{Ci}\right). \tag{72}$$

The control law of the *i*-th robot finger is given as follows on behalf of Eq. (46):

$$\boldsymbol{\tau}_{Fi} = \boldsymbol{Y}_{Fi}(\boldsymbol{q}_{Fi}, \dot{\boldsymbol{q}}_{Fi}, \dot{\boldsymbol{q}}_{Fri}, \ddot{\boldsymbol{q}}_{Fri})\hat{\boldsymbol{\sigma}}_{Fi} - \boldsymbol{K}_{Fi}\boldsymbol{s}_{Fi} - \boldsymbol{J}_{Ci}^{T}\boldsymbol{f}_{Ci}^{d} - \boldsymbol{J}_{Ci}^{T}\boldsymbol{f}_{Ci} \tag{73}$$

It is noted that $\boldsymbol{s}_{Fi}$ contains a feedback term of the contact force error.

The control law and estimation law that are integrated from the *i*-th finger to the *k*-th finger are represented as

$$\boldsymbol{\tau}_{F} = \boldsymbol{Y}_{F}(\boldsymbol{q}_{F}, \dot{\boldsymbol{q}}_{F}, \dot{\boldsymbol{q}}_{Fr}, \ddot{\boldsymbol{q}}_{Fr})\hat{\boldsymbol{\sigma}}_{F} - \boldsymbol{J}_{C}^{T}\boldsymbol{f}_{C}^{d} - \boldsymbol{K}_{F}\boldsymbol{s}_{F}, \tag{74}$$

$$\dot{\hat{\boldsymbol{\sigma}}}_{F} = -\boldsymbol{\Gamma}_{F}\boldsymbol{Y}_{F}^{T}(\boldsymbol{q}_{F}, \dot{\boldsymbol{q}}_{F}, \dot{\boldsymbol{q}}_{Fr}, \ddot{\boldsymbol{q}}_{Fr})\boldsymbol{s}_{F}. \tag{75}$$

$F \quad F \quad F\ F \quad Fr \quad Fr\ F$
F

The following theorem is established if the grasping conditions (A1)–(A4) are assumed (Ueki et al. 2009).

Theorem 3. *Consider a rigid body that is grasped by k robot fingers, each with three DOFs. For the system in Eqs. (34), (35), and (31), given that Eq. (40) is the parameter estimation law of the object, Eq. (69) is the desired external force of the object, Eq. (42) is the desired force at the contact point, Eq. (61) is the residual, Eq. (75) is the parameter estimate law of the robotic fingers, and Eq. (74) is the control law, β is sufficiently large. The closed-loop system is then asymptotic stable in the following sense:*

(1) $\boldsymbol{r}_O \to \boldsymbol{r}_O^d$ *and* $\dot{\boldsymbol{r}}_O \to \dot{\boldsymbol{r}}_O^d$ *as* $t \to \infty$

(2) $\boldsymbol{f}_C \to \boldsymbol{f}_C^d$ *as* $t \to \infty$.

The error dynamics of the object is given by

$$\Box \boldsymbol{F}_O \quad \Box \boldsymbol{Y}(\boldsymbol{r}_O, \dot{\boldsymbol{r}}\Box_O, \boldsymbol{v}_{Or}, \dot{\boldsymbol{v}}\Box_{Or})\Delta\boldsymbol{\sigma}_O \quad \Box \boldsymbol{K}_O \boldsymbol{s}_O \quad \Box \boldsymbol{M}_O(\boldsymbol{r}_O)\dot{\boldsymbol{s}}\Box_O \quad \Box \underset{(\hat{\boldsymbol{\sigma}}_F - \boldsymbol{\sigma}_F)}{\boldsymbol{C}_O}(\boldsymbol{r}_O, \dot{\boldsymbol{r}}\Box_O)\boldsymbol{s}_O . \tag{76}$$

The error dynamics of the robot fingers is given by

$$\boldsymbol{0} \Box \Box \boldsymbol{M}\dot{\boldsymbol{s}}\Box \Box \boldsymbol{C}\boldsymbol{s} \quad \Box \boldsymbol{K}\boldsymbol{s} \quad \Box \Box \boldsymbol{J}^T \Box \boldsymbol{f} . \tag{77}$$
$\Box \boldsymbol{Y}$

$F \quad F\ F \quad F \quad F \quad F \quad F \Box 1 \quad C\ C$
F

where $\beta_{+1} = \beta + 1$. Theorem 3 can be proved using a candidate Lyapunov function given by

$$V = \frac{1}{2}\left[\Delta\tilde{\sigma}_O^T \Gamma_O^{-1}\Delta\tilde{\sigma}_O + \eta^T \Psi_C \eta_C + \Delta\sigma_F^T \Gamma_F^{-1}\Delta\sigma_F + s_O^T M_O s_O + s_F^T M_F s_F + v_C^T \Omega_F^T \Omega_F v_C\right] + C \quad (78)$$

A time derivative along the solution of the error equation gives as the following equation:

$$\dot{V} = -s_O^T K_O s_O - s_F^T K_F s_F - v_C^T \Omega_F^T K_C \Omega_F v_C \le 0. \quad (79)$$

This shows that Eq. (78) is the Lyapunov function; hence, s_O, s_F, $\Delta\sigma_O$, $\Delta\sigma_F$, η_C, and v_C are bounded. Therefore, by an analysis similar to that of the case without a force sensor, σ_O, σ_F, e_O, $\dot{e}_O$, r_O, $\dot{r}_O$, v_{Or}, T_O, $\dot{v}_{Or}$, $Y_O(r_O, \dot{r}_O, v_{Or}, \dot{v}_{Or})$, F_O, f_C, q_{Fr}, $\dot{q}_F$, J_C, and W_C are bounded. In using the force sensor, q_{Fr} contains Δf_C. Therefore, the proof from here is different from that of the case of without a force sensor.

The time derivative of Eq. (72) for all fingers is given by

$$\dot{s} = J W^T \left[\ddot{\Theta}_F + \dot{E}_F \left(f - J^T s\right)\right] - \dot{J} W^T s. \quad (80)$$

Equation (76) is represented as

$$\dot{s} = M^{-1}\left[Y\dot{\Delta\sigma} - W\dot{f} - K_s s - C s\right]. \quad (81)$$

The time derivative of Eq. (70) is represented as

$$\dot{q}_{Fr} = a_F^{-1}\left[J\dot{\Omega}_F + \dot{\Psi}_F - f_C\right], \quad (82)$$

wher e $\boldsymbol{a} = \dot{\boldsymbol{v}}_{Or} + \dot{\boldsymbol{\omega}}_C \times \boldsymbol{r}_{OrC} + \boldsymbol{\omega}_C \times (\boldsymbol{\omega}_C \times \boldsymbol{r}_{OrC}) - \dot{\boldsymbol{J}}_C \dot{\boldsymbol{q}}_{Fr}$ and

(82) into Eq. (77),

$$\boldsymbol{Y}_F(\boldsymbol{q}_F, \dot{\boldsymbol{q}}_{Fr}, \boldsymbol{a}_F, \Delta\boldsymbol{\sigma}_F)\boldsymbol{\pi}_F = \boldsymbol{J}_C^{-T}\left(\boldsymbol{M}_F\begin{bmatrix}\boldsymbol{J}_C^{-1}(\dot{\boldsymbol{\omega}}_F + \boldsymbol{\psi}_F) \\ \boldsymbol{f}_C\end{bmatrix} - \boldsymbol{K}_F\boldsymbol{s}_F - \boldsymbol{J}_C^T\boldsymbol{f}_F\right)$$

$$\boldsymbol{M}_O\boldsymbol{J}_O^{-1}\boldsymbol{W}^T\boldsymbol{M}_O^{-1}\boldsymbol{Y}_O\boldsymbol{\pi}_O + \boldsymbol{W}\boldsymbol{f}_C + \boldsymbol{K}_O\boldsymbol{s}_O + \boldsymbol{M}_O\boldsymbol{J}_O^{-1}\dot{\boldsymbol{J}}_C\boldsymbol{\omega}_F\boldsymbol{v}_C + \boldsymbol{M}_O\boldsymbol{J}_O^{-1}\dot{\boldsymbol{f}}_F - \boldsymbol{J}_O^{-T}\dot{\boldsymbol{s}}_C \quad (83)$$

$$\boldsymbol{J}_C\boldsymbol{\omega}_F + \boldsymbol{\psi}_F \quad \boldsymbol{f}_C \quad \boldsymbol{s}_F \quad \boldsymbol{f}_F$$

By multiplying $\boldsymbol{M}_O^{-1}$ from the left-hand side of Eq. (83), we get:

$\boldsymbol{J}_C$

$$\boldsymbol{A}\Delta\boldsymbol{f}_C = \boldsymbol{b}, \quad (84)$$

where

$$\boldsymbol{A} = \boldsymbol{M}_O^{-1}\boldsymbol{M}_O\boldsymbol{J}_O^{-1}\begin{bmatrix}\boldsymbol{I} \\ \boldsymbol{J}_C\end{bmatrix}, \quad \boldsymbol{b} = \boldsymbol{M}_O^{-1}\begin{bmatrix}\dot{\boldsymbol{\omega}}_F + \boldsymbol{\psi}_F \\ \dot{\boldsymbol{J}}_C\boldsymbol{\omega}_F\boldsymbol{v}_C\end{bmatrix} - \boldsymbol{M}_O^{-1}\boldsymbol{W}^T\boldsymbol{J}_O^{-T}\boldsymbol{\tau}_O \quad (85)$$

$$\boldsymbol{J}_C \quad \boldsymbol{f}_C \quad \boldsymbol{s}_F \quad \boldsymbol{C}$$

$$\boldsymbol{b} = \boldsymbol{M}_O^{-1}\boldsymbol{Y}_O(\boldsymbol{q}_F, \dot{\boldsymbol{q}}_{Fr}, \boldsymbol{a}_F, \Delta\boldsymbol{\sigma}_F)\boldsymbol{\pi}_F - \boldsymbol{K}_F\boldsymbol{s}_F - \boldsymbol{J}_C^{-T}\dot{\boldsymbol{J}}_C\boldsymbol{\omega}_F\boldsymbol{v}_C$$

$$\dot{\boldsymbol{W}}_{F}^{T}\boldsymbol{M}_{F}\dot{\boldsymbol{Y}}_{1}-\boldsymbol{K}_{s}\boldsymbol{J}_{s}^{T}\boldsymbol{W}_{F}\boldsymbol{C}_{s}. \tag{86}$$

$$C\ 8\ \Delta\sigma_{O}\quad 8\ O\quad O\quad O\quad C\ C\ F$$

When β_{+1} is sufficiently large and ($\alpha_C \boldsymbol{\Omega}_F + \boldsymbol{\Psi}_F$) is sufficiently small, the matrix $\boldsymbol{A}$ approaches $\beta_{+1} \boldsymbol{J}_C^T \boldsymbol{M}^{-1} \boldsymbol{J}_C + \boldsymbol{W}^T \boldsymbol{M}^{-1} \boldsymbol{W}$, which is nonsingular. In this time, $\Delta \boldsymbol{f}_C$ is bounded because of the boundedness of $\boldsymbol{b}$. This result yields $\boldsymbol{f}_C$, $\Delta \boldsymbol{F}_O$, $\boldsymbol{s}_O$, $\boldsymbol{v}_O$, $\boldsymbol{v}_C$, $\boldsymbol{q}_{Fr}$, and $\boldsymbol{s}_F$ that are bounded, sequentially.

Differentiating Eq. (79) with respect to time is given as

$$\dot{V} = \boldsymbol{s}_O^T \boldsymbol{K}_O \dot{\boldsymbol{v}}_O + \boldsymbol{\Omega}_O \boldsymbol{v}_O \boldsymbol{s}_O + 2\boldsymbol{s}_F^T \boldsymbol{K}_F \dot{\boldsymbol{v}}_C - \boldsymbol{\Omega}_F \boldsymbol{v}_C \boldsymbol{s}_F . \quad (87)$$

$\dot{V}$ is bounded because of the boundedness of $\dot{\boldsymbol{s}}_O$, $\boldsymbol{s}_O$, $\dot{\boldsymbol{v}}_C$, $\boldsymbol{v}_C$, $\dot{\boldsymbol{s}}_F$, and $\boldsymbol{s}_F$. This means that $\dot{V}$ is uniformly continuous. It is shown that $V \to 0$ as $t \to \infty$ from the Lyapunov-like Lemma. This implies that $\boldsymbol{s}_O \to \boldsymbol{0}$, $\boldsymbol{v}_C \to \boldsymbol{0}$, and $\boldsymbol{s}_F \to \boldsymbol{0}$ as $t \to \infty$. These results yield $\dot{\boldsymbol{e}}_O \to \boldsymbol{0}$ and $\boldsymbol{e}_O \to \boldsymbol{0}$ as $t \to \infty$. These results in turn yield $\boldsymbol{r}_O \to \boldsymbol{r}_O^d$ and $\dot{\boldsymbol{r}}_O \to \dot{\boldsymbol{r}}_O^d$ as $t \to \infty$.

Moreover, these result can lead to the uniform continuity of $\boldsymbol{A}$ and $\boldsymbol{b}$. Therefore, $\Delta \dot{\boldsymbol{f}}_C$ is uniformly continuous, and $\boldsymbol{s}_O$, $\boldsymbol{s}_F$, and $\boldsymbol{v}_C$ are uniformly continuous because of the uniform continuity of $\Delta \boldsymbol{f}_C$. Using Barbalat's lemma, $\dot{\boldsymbol{s}}_O \to \boldsymbol{0}$, $\dot{\boldsymbol{s}}_F \to \boldsymbol{0}$, and $\dot{\boldsymbol{v}}_C \to \boldsymbol{0}$ as $t \to \infty$. As a result, $\Delta \boldsymbol{f}_C \to \boldsymbol{0}$ as $t \to \infty$.

The asymptotic stability can be shown by the Lyapunov-like lemma. However, the estimated parameter convergence to the true value is not guaranteed. If $\boldsymbol{Y}_i$ ($i = O, F$) satisfy the persistently exciting condition, that is, there exists strictly positive constants $\alpha > 0$ and T such that for any $t > 0$,

$$\int_t^{t+T} \boldsymbol{Y}_i^T \boldsymbol{Y}_i \, dt \geq \alpha \boldsymbol{I}_i \quad (i = O, F), \quad (88)$$

where $\boldsymbol{I}_i$ ($i = O, F$) is the identity matrix of appropriate size, then the parameter error $\Delta \boldsymbol{\sigma}_i$ ($i = O, F$) will converge to zero exponentially.

Adaptive Control at a Sliding Contact

Consider control when the robot fingers are in point contact with an object; some fingers are in slide-rolling contact on the object surface, while the rest are in twist- rolling contact. In the following, given k robot fingers, the number of fingers in sliding

contact is *s*; it is assumed that the each finger is has three DOF, where the conditions $m = 3k\text{-}2s > 6$ and the grasping conditions (A1)–(A4) are satisfied. Consider that the control of the finger without sliding contact is the same as that with adaptive control using a force sensor in Sec. 3.2, and that control of the finger(s) with sliding contact is such that the desired velocity and position of the finger(s) are expressed with the curved surface coordinates.

First, consider the relationship between the sliding velocity and the velocity with the surface coordinate variable. The motion of contact coordinates Eq. (13) are represented in another form as follows:

$$\boldsymbol{M} \quad CFi \; Six \quad \boldsymbol{M} \quad \dot{\alpha}_{Fi}, \tag{89}$$

$$\dot{\alpha}_{Oi}$$

$$i \quad Oi \; C \qquad CFi \qquad \dot{\alpha}_{Oi}.$$

$$CFi \qquad \dot{\alpha}_{Oi} \; y$$

$$-\boldsymbol{R} \quad \boldsymbol{M}_C \qquad CFi \quad Siy \quad \boldsymbol{M}_C \tag{90}$$

$$i \; \boldsymbol{K} \qquad Oi \qquad = - \quad CFi \quad \boldsymbol{K} \quad Fi$$

$$\delta \qquad \delta$$

$$p \qquad f$$

$$Six$$

Also, Eq. (11) is represented in another form, taking $v_{Siz} = 0$ as into account follows:

$$\dot{\boldsymbol{p}}_{Si} = \boldsymbol{D}\boldsymbol{J}_{Six}\dot{\boldsymbol{q}} + \boldsymbol{D}\boldsymbol{W}^{T}\boldsymbol{v}_{CFi}, \tag{91}$$

where $\boldsymbol{D} = \begin{bmatrix} \boldsymbol{R}_{CFi} & \boldsymbol{0} \\ \boldsymbol{0} & \boldsymbol{R}_{CFi} \end{bmatrix}$, $\boldsymbol{R}_{CFi}$ is a rotation matrix from Σ_P to Σ_{CFi}, and $\boldsymbol{p}_{Si}$ is a sliding velocity with respect to Σ_P. The rolling angular velocity can be represented by

$$\boldsymbol{\omega}_{CFi} = \boldsymbol{C}_{CFi}^{T}\boldsymbol{J}_{Siy}\dot{\boldsymbol{q}} + \boldsymbol{\omega}_{CFi}, \tag{92}$$

where $\boldsymbol{J}_{Six} \in \mathbb{R}^{3\times 3}$ is a Jacobian matrix for angular velocity, $\boldsymbol{C}_{CFi} = \boldsymbol{R}_{CFi}\begin{bmatrix} 0 & 1 \\ -1 & 0 \end{bmatrix}$. Obtaining $\dot{\boldsymbol{q}}$ from Eq. (91), and substituting it with $\boldsymbol{v} = [\boldsymbol{p}^{T}\ \boldsymbol{\omega}^{T}]^{T}$ into Eq. (92), it can be expressed by

$$\begin{bmatrix} \dot{\boldsymbol{p}}_{CFi} \\ \boldsymbol{\omega}_{CFi} \end{bmatrix} = \begin{bmatrix} \boldsymbol{D}\boldsymbol{J}_{Six}\boldsymbol{J}^{-1}\boldsymbol{D}^{-1} & \boldsymbol{0} \\ \boldsymbol{C}_{CFi}^{T}\boldsymbol{J}_{Siy}\boldsymbol{J}^{-1}\boldsymbol{D}^{-1} & \boldsymbol{I} \end{bmatrix}\boldsymbol{v}_{CFi}. \tag{93}$$

By substituting Eqs. (89) and (92) into Eq. (90), the following

equation is obtained:

$$\dot{\boldsymbol{p}}_{Si} = \boldsymbol{A}_i \dot{\boldsymbol{q}}_{Oi} + \boldsymbol{B}_i \boldsymbol{v}_O, \tag{94}$$

where

$$\boldsymbol{A}_i = \boldsymbol{D}_{Ci}^T \boldsymbol{J}_{Ci} \boldsymbol{K}_i^{-1} \boldsymbol{D}_i \left(\boldsymbol{K}_i - \boldsymbol{R}_i \boldsymbol{K}_i \boldsymbol{R}_i^T \right)^{-1} \boldsymbol{R}_i \boldsymbol{M}_i, \tag{95}$$

$$\boldsymbol{B}_i = \boldsymbol{D}_{Ci}^T \boldsymbol{J}_{Ci} \boldsymbol{K}_i^{-1} \boldsymbol{D}_i \left(\boldsymbol{K}_i - \boldsymbol{R}_i \boldsymbol{K}_i \boldsymbol{R}_i^T \right)^{-1} \boldsymbol{R}_i \boldsymbol{J}_{Ci} \boldsymbol{J}_{Oi}^{-1} \boldsymbol{W}_i^T. \tag{96}$$

Equation (94) represents the relationship between the sliding velocity, the velocity of the surface coordinate variables, and the object velocity.

Next, consider the friction force on the tangent plane at the contact point. Let us assume that the i-th robot finger is sliding on the object surface at contact point C_i. At this time, the contact force $\boldsymbol{f}_{Ci}$ can be decomposed into a component of the normal direction, $\boldsymbol{f}_{ni}$, and a dynamic friction force on the tangent plane, $\boldsymbol{f}_{ti}$, as follows:

$$\boldsymbol{f}_{Ci} = \boldsymbol{f}_{ni} + \boldsymbol{f}_{ti}. \tag{97}$$

When the unit normal vector at the contact point C_i is expressed by $\boldsymbol{n}_i$, then $\boldsymbol{f}_{ni} = \boldsymbol{n}_i \boldsymbol{n}_i^T \boldsymbol{f}_{Ci}$. It is assumed that the dynamic friction force is represented by

$$\boldsymbol{f}_{ti} = -\boldsymbol{n}_i f_{Ci} \frac{\dot{\boldsymbol{p}}_{Si}}{\left\| \dot{\boldsymbol{p}}_{Si} \right\|} - D_i \dot{\boldsymbol{p}}_{Si}$$

$\boldsymbol{p}_{Si}$,

(98)

where μ_{Ci} is the Coulomb dynamic friction coefficient, and μ_{Di} is a viscous friction coefficient. Equation (98) is linear regarding the friction parameters μ_{Ci} and μ_{Di}; therefore, it can be represented as

$$\boldsymbol{f}_{ti} = \boldsymbol{Y}_{ti}(\boldsymbol{p}_{Si}, \boldsymbol{n}_i, \boldsymbol{f}_{Ci})\boldsymbol{\mu}_i, \tag{99}$$

where $\boldsymbol{\mu}_i = [\mu_{Ci} \; \mu_{Di}]^T$.

In order to compensate for the friction force at the sliding fingers, let us generate the desired friction force on the tangent plane based on an estimate of the friction parameter. First, we define a reference velocity of sliding motion by

$$\boldsymbol{v}_{Si} = \boldsymbol{A}_S \dot{\boldsymbol{x}}_{Oi}^d + \boldsymbol{B}_S(\boldsymbol{x}_{Oi} - \boldsymbol{x}_{Oi}^d), \tag{100}$$

and a residual of the sliding velocity is given by

$$\boldsymbol{s}_{Si} = \boldsymbol{v}_{Si} - \boldsymbol{v}_{Sri}, \tag{101}$$

where $\boldsymbol{x}_{Oi}^d$ is a smooth desired position of the fingertip on the curved surface coordinates, $\boldsymbol{\Lambda}_S > 0$ is a diagonal weight matrix, and $\boldsymbol{v}_{Si}^T = \boldsymbol{p}_{Si}^T = \boldsymbol{J}_{Ci}\dot{\boldsymbol{q}}_{Fi} - \boldsymbol{W}_{Ci}\dot{\boldsymbol{v}}_O$ is the sliding velocity. Then, a desired friction force and estimation law of the friction parameters can be given by

$$\boldsymbol{f}_{ti}^d = \boldsymbol{Y}_{ti}(\boldsymbol{p}_{Si}, \boldsymbol{n}_i, \boldsymbol{f}_{Ci})\hat{\boldsymbol{\mu}}_i, \tag{102}$$

$$\dot{\hat{\boldsymbol{\mu}}}_i = -\boldsymbol{\Gamma}_i \boldsymbol{Y}_{ti}^T(\boldsymbol{p}_{Si}, \boldsymbol{n}_i, \boldsymbol{f}_{Ci})\boldsymbol{s}_{ti}, \tag{103}$$

where $\hat{\boldsymbol{\mu}}_i$ is an estimation of $\boldsymbol{\mu}_i$, and $\boldsymbol{\Gamma}_i > 0$ is a symmetrically adaptive gain matrix. It is noted that the desired friction force at the rolling contact is $\boldsymbol{f}_{ti}^d = \boldsymbol{0}$.

Next, consider the desired contact force of the robot finger. The desired external force of the object is provided by Eq. (69) in the same way as adaptive control using a force sensor in Sec. 3.2; that is,

$$\boldsymbol{F}_{O}^{d} = \begin{pmatrix} \boldsymbol{r}_{O} & \boldsymbol{r}_{O} \\ \boldsymbol{v}_{O} & \boldsymbol{v}_{O} \end{pmatrix} \begin{pmatrix} \boldsymbol{Y}_{O}^{d} \\ \boldsymbol{K}_{O} \boldsymbol{s}_{O} \end{pmatrix}. \tag{104}$$

The desired contact force to balance the desired external force should satisfy the following relation:

$$\boldsymbol{F}_{O}^{d} = \boldsymbol{W}_{C} \boldsymbol{f}_{C}^{d}. \tag{105}$$

The desired contact force $\boldsymbol{f}_{Ci}^{d}$ at the contact point C_i is then decomposed into the normal direction and force on the tangent plane, which is represented by

$$\boldsymbol{f}_{Ci}^{d} = f_{ni}^{d} \boldsymbol{n}_{i} + \boldsymbol{f}_{ti}^{d}, \tag{106}$$

where f_{ni}^{d} is the size of the desired contact force in the normal direction, and $\boldsymbol{f}_{ti}^{d}$ is the desired force on the tangent plane. For the sliding contact fingers, the desired external force is in the normal direction, and the desired friction force is in the direction of the tangent. For the rolling-contact fingers, such decomposition is not performed. Then, the desired external force satisfies:

$$\boldsymbol{F}_{O}^{d} = \boldsymbol{G}_{C} \boldsymbol{f}_{Cn}^{d} + \boldsymbol{W}_{Ct} \boldsymbol{f}_{t}^{d}, \tag{107}$$

where $\boldsymbol{f}_{Cn}^{d} \in \mathbb{R}^{3k-2s}$ is a vector that is the summation of the desired contact force of the robot fingers with rolling contact, $\boldsymbol{G}_C \in \mathbb{R}^{6k\times(3k-2s)}$ is a matrix with a list of $\boldsymbol{W}_C$ corresponding to $\boldsymbol{f}_{Cn}^{d}$, and $\boldsymbol{f}_t^{d} = [(\boldsymbol{f}_{t1}^{d})^T \ldots (\boldsymbol{f}_{tk}^{d})^T]^T$. The contact force generates the internal forces that do not affect motion of the object. Therefore, the general solution for $\boldsymbol{f}_{Cn}^{d}$ is provided by

$$\boldsymbol{f}_{Cn}^{d} = \boldsymbol{G}_C^{+}\boldsymbol{F}_O^{d} + \boldsymbol{W}_C\left(\boldsymbol{I} - \boldsymbol{G}_C^{+}\boldsymbol{G}_C\right)\boldsymbol{f}_{Cint}^{d}, \tag{108}$$

where $\boldsymbol{G}_C^{+}$ $(= \boldsymbol{G}_C^T(\boldsymbol{G}_C\boldsymbol{G}_C^T)^{-1})$ is a generalized inverse matrix of $\boldsymbol{G}_C$, and $\boldsymbol{f}_{Cint}^{d}$ is an arbitrary force vector that generates the internal force, which is continuous and bounded.

Finally, consider the control of the robot fingers. The reference velocity of the i-th robot finger is defined by

$$\boldsymbol{q}_{Fir} = \boldsymbol{J}_{Ci}^{-1}\boldsymbol{W}_{Ci}^{T}\left(\boldsymbol{\Omega}_{Fi}\boldsymbol{v}_{Ci} + \boldsymbol{\Psi}_{Fi}\boldsymbol{\eta}_{Ci}\right) + \boldsymbol{v}_{Sri}. \tag{109}$$

It is given that $\boldsymbol{v}_{Ci} = \boldsymbol{f}_{Ci}^{0} - \boldsymbol{f}_{Ci}$, as in Eq. (68), and $\boldsymbol{\eta}_{Ci}$ is the integration of a normal component of contact force errors $\Delta\boldsymbol{f}_{Ci}$, which is represented by

$$\boldsymbol{\eta}_{Ci} = \boldsymbol{\Gamma}_{Ci}\boldsymbol{n}_i, \tag{110}$$

$$\boldsymbol{\Gamma}_{Ci} = \int_0^t \boldsymbol{n}_i^T\Delta\boldsymbol{f}_{Ci}\,dt. \tag{111}$$

Using the residual of the i-th robot finger variable, $\boldsymbol{s}_{Fi} = \boldsymbol{q}_{Fi} - \boldsymbol{q}_{Fir}$, the control law and the estimation law of the dynamic parameters of the i-th robot finger are given by

$$\boldsymbol{\tau}_{Fi} = \boldsymbol{Y}_{Fi}(\boldsymbol{q}_{Fi}, \dot{\boldsymbol{q}}_{Fi}, \dot{\boldsymbol{q}}_{Fir}, \ddot{\boldsymbol{q}}_{Fir})\hat{\boldsymbol{\sigma}}_{Fi} + \boldsymbol{J}_{Ci}^T\boldsymbol{f}_{Ci}^{d} - \boldsymbol{K}_{Fi}\boldsymbol{s}_{Fi} + \boldsymbol{J}_{Ci}^T\Delta\boldsymbol{f}_{Ci}, \tag{112}$$

$$\boldsymbol{\varphi}_{Ci}(\bar{\boldsymbol{q}}_{Ci} - \boldsymbol{\Gamma}_{Ci}\boldsymbol{Y}_{Fi}(\boldsymbol{q}_{Fi}, \dot{\boldsymbol{q}}_{Fi}, \dot{\boldsymbol{q}}_{ri}, \dot{\boldsymbol{q}}_{Fi})\boldsymbol{s}_{Fi} \quad . \tag{113}$$

At this time, the control law and estimation law integrating the 1st to the *k*-th finger are expressed by

$$\boldsymbol{\tau}_{F} = \boldsymbol{Y}_{F}(\boldsymbol{q}_{F}, \dot{\boldsymbol{q}}_{F}, \dot{\boldsymbol{q}}_{Fr}, \dot{\boldsymbol{q}}_{F})\hat{\boldsymbol{\sigma}}_{F} + \boldsymbol{J}_{C}^{T}\boldsymbol{f}_{C}^{d} - \boldsymbol{K}_{F}\boldsymbol{s}_{F} + \beta\boldsymbol{J}_{C}^{T}\Delta\boldsymbol{f}_{C} \tag{114}$$

$$\dot{\hat{\boldsymbol{\sigma}}}_{F} = -\boldsymbol{\Gamma}_{F}\boldsymbol{Y}_{F}^{T}(\boldsymbol{q}_{F}, \dot{\boldsymbol{q}}_{F}, \dot{\boldsymbol{q}}_{Fr}, \dot{\boldsymbol{q}}_{F})\boldsymbol{s}_{F} \quad . \tag{115}$$

The difference of the control at the rolling contact is that the desired contact force is given based on the estimation of the friction parameters. Other configurations are almost the same as the estimation law and control law in Sec. 3.2. The following theorem is then provided by this control (Ueki et al. 2006).

Theorem 4. *Consider a rigid body that is grasped by k robot fingers, each with three DOFs. For the system in Eqs. (34), (35), and (31), given that Eq. (40) is the parameter estimation law of the object, the estimation law of friction parameters with sliding fingers at the contact point is Eq. (103), Eq. (69) is the desired external force of the object, Eq. (108) is the desired force at the contact point, Eq. (115) is the parameter estimate law of the robotic fingers, and Eq. (114) is the control law, then β is sufficiently large, and the closed-loop system is asymptotic stable in the following sense:*

(1) $r_O \to r_O^d$ and $\dot{r}_O \to \dot{r}_O^d$ as $t \to \infty$.
(2) $f \to f^d$ as $t \to \infty$.
(3) $\alpha_{Oi}^C \to \alpha_{Oi}^d$ and $\alpha_{Oi}^C \to \alpha_{Oi}^d$ as $t \to \infty$.

Outline of proof. To prove this theorem, a candidate Lyapunov function is given by

$$V = \frac{1}{2} s_O^T M_O s_O + \frac{1}{2} \Delta\tilde{\sigma}_O^T \Gamma_O^{-1} \Delta\tilde{\sigma}_O + \eta^T \Psi_{CF}^C \eta + \frac{1}{2} v_{CF}^C \Omega^C v_{CF}^C + \frac{1}{2} s^T M s + \frac{1}{2} \Delta\sigma_F^T \Gamma_F^{-1} \Delta\sigma_F + \frac{1}{2} \Delta\mu^T \Gamma_F^{-1} \Delta\mu, \quad (116)$$

where $\Delta\mu = \hat{\mu} - \mu$. Its time derivative is represented by

$$\dot{V} = s^T K s + v_{CF}^C \Omega^C \dot{v}_{CF}^C + s^T \dot{M} s \le 0. \quad (117)$$

$K s$

$$\dot{V} = s_O^T K_O s_O + s_F^T K_F s_F \le 0$$

Using a Lyapunov-like lemma, the asymptotic stability can be demonstrated in a procedure similar to the case of Theorem 3.

It should be noted that although this control is complicated, even more dexterous object manipulation is possible if the finger slides on the object surface.

EXPERIMENTAL VERIFICATIONS OF ADAPTIVE CONTROL USING A FORCE SENSOR

Experimental Setup

Experiment of a ball handing by the human-type robot hand named Gifu-Hand III (Mouri et al. 2002) was performed to show the effectiveness of the adaptive control using a force sensor, by comparison of with adaptive law and without adaptive law. In the experiment, as shown in Fig. 5, three

fingers grasp the ball of radius of 0.0625 m and mass of 0.05 kg. The joint angle of robot hand is measured by rotary encoder, and the contact force is measured by 6-axis force sensor (NANO sensor, BL AUTOTEC, LTD.). The position and orientation of the object is measured by 3-D position measurement device (OPTRAK, Northern Digital Co.). The resolution of this device is 0.1 mm and sampling frequency is 500 Hz. The orientation vector of the object is represented by the ZYZ-Euler angles. The object coordinate system Σ_O is set in consideration of singular point of To. The contact position ${}^{Fi}\boldsymbol{p}_{FiCi}$ is calculated using contact force by reference (Bicchi et al. 1993). The joint angle velocity, object velocity, object angular velocity, and contact point velocity are calculated using measured value by differential filter. The control sampling is 1000 Hz. The experiment conditions are as follows: the initial values of the unknown dynamic parameters are set to zero, that is $\hat{\boldsymbol{\sigma}}_O = \boldsymbol{0}$ and $\hat{\boldsymbol{\sigma}}_F = \boldsymbol{0}$.

The unknown dynamic parameters of the object is mass, center of mass, and inertia tensor. Those of the robot are inertia sensor of link, first moment of link, inertia of motor, and viscosity friction coefficient of motor. The desired trajectory of the ball is given repeatedly by 5 order polynomial in time with initial $\boldsymbol{r}_O^d(0) = \boldsymbol{r}_O(0)$ and $\boldsymbol{r}_O^d(1.5) = \boldsymbol{r}_O(0) + [0.03\ 0\ 0\ 0\ -\pi/9\ 0]^T$. $\boldsymbol{f}_{int}^d$ is given as follows:

$$T_{f_d} = -1.5\left[\frac{\partial \|p_1 - C_1\|}{\partial p}^T \quad \frac{\partial \|p_2 - C_2\|}{\partial p}^T \quad \frac{\partial \|p_3 - C_3\|}{\partial p}^T\right] \cdot \begin{bmatrix} F_1 - C_1 \\ F_2 - C_2 \\ F_3 - C_3 \end{bmatrix}$$

The controller gains were selected to be:
$\boldsymbol{\Gamma}_O$ = *diag*[0.02 0.0001 ... 0.0001], $\boldsymbol{K}_O$ = *diag*[0.04 ... 0.04 0.005 ..... 0.005], $\boldsymbol{\Lambda}_O$ = *diag*[40 ... 40 30 ... 30], $\boldsymbol{\Gamma}_F$ = *diag*[0.0003 ... 0.0003], $\boldsymbol{K}_{Fi}$ = *diag*[0.4 0.4 0.04], $\boldsymbol{\Omega}_F$ = *diag*[0.4 ... 0.4], $\boldsymbol{\Psi}_F$ = *diag*[0.04 ... 0.04], $\alpha_C = 0.05/\pi$, and $\beta = 1.2$. In the case of without adaptive law, the experimental conditions are same excluding adaptive gains. The adaptive gains were changed to zero, i.e., $\boldsymbol{\Gamma}_O = \boldsymbol{0}$ and $\boldsymbol{\Gamma}_F = \boldsymbol{0}$.

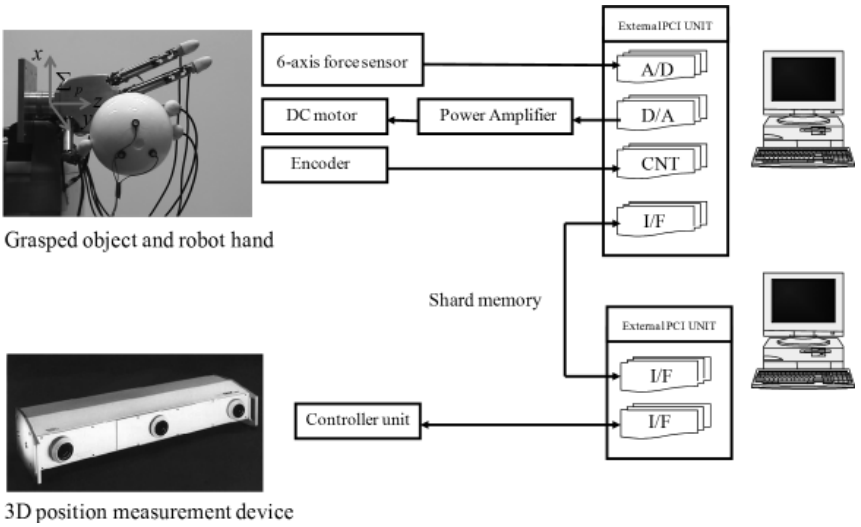
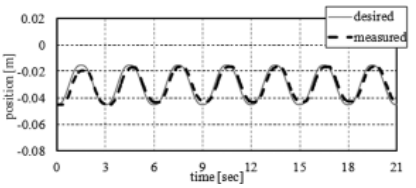


Figure 5. Experiment system consisting of robot hand and 3-D position measurement device.

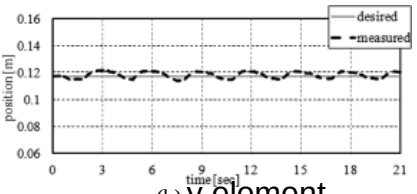
Experimental Results

Figure 6 shows the desired object position $\boldsymbol{p}^d$ and measured object position $\boldsymbol{p}_O$ in case of with adaptive law. Figure 7 shows the norm of object position error $\|\boldsymbol{p}^d - \boldsymbol{p}_O\|$. In case of with adaptive law, the object position error decreased by repetition of motion. On the other hand, in case of without adaptive law, the object position error increased by repetition of motion. The contact constraint of rolling contact is nonholonomic constraint, this means nonintegrable. Therefore, the desired motion is not a repetitive motion. Nevertheless, the object position error shows that the adaptation was working successfully.

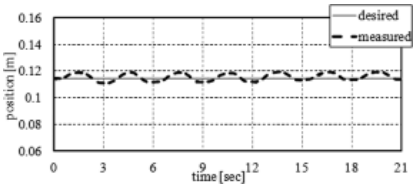
Figure 8 shows the desired object orientation $\boldsymbol{\eta}^d$ and measured object orientation $\boldsymbol{\eta}_O$ in case of with adaptive law. Figure 9 shows the norm of object orientation error $\|\boldsymbol{\eta}^d - \boldsymbol{\eta}_O\|$. In case of with adaptive law, the object orientation error decreased by repetition of motion. On the other hand, in case of without adaptive law, the object orientation error increased by repetition of motion. For position and orientation in case of with adaptive law, capabilities of both response and tracking are better compared with case of without adaptive law.



(a) x element



(b) y element



(c) z element

Figure 6. Trajectory of object position with adaptive law.

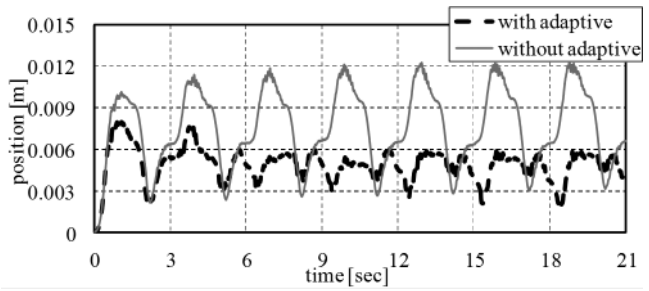
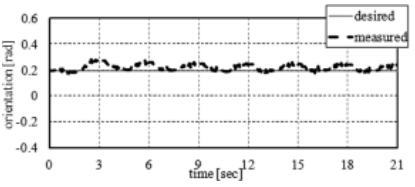
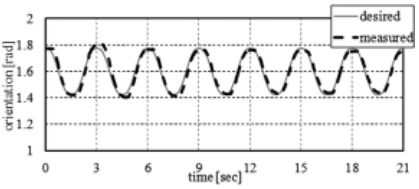
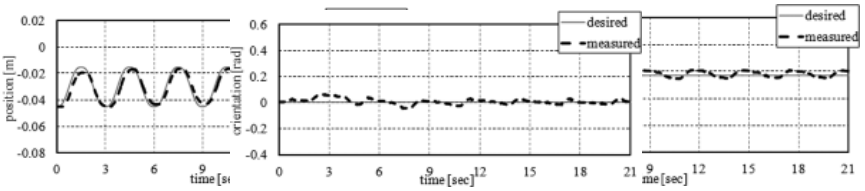


Figure 7. The norm of $\boldsymbol{p}^d - \boldsymbol{p}$. object position error





(a) 1st element (b) 2nd element



(c) 3rd element

Figure 8. Trajectory of object orientation with adaptive law.

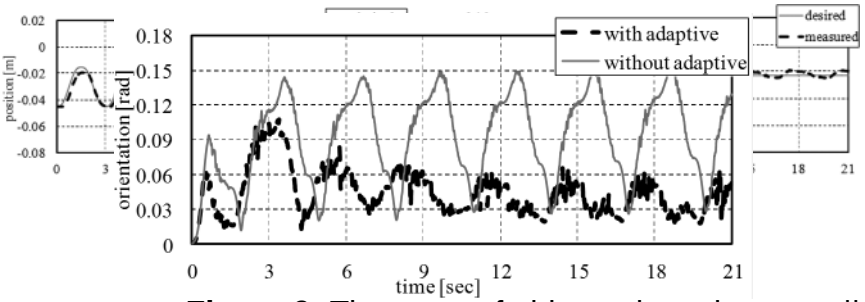
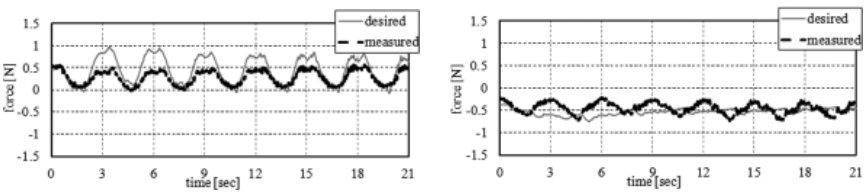
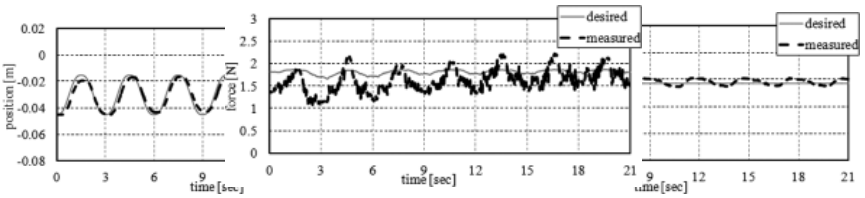


Figure 9. The norm of object orientation error $||\boldsymbol{\eta}^d - \boldsymbol{\eta}_O||$.

Figures 10–12 show the desired contact force $\boldsymbol{f}_C^d$ and measured contact force $\boldsymbol{f}_C$ of the 1st finger, 2nd finger, and 3rd finger in case of with adaptive law. Figure 13 shows the norm of contact force error $||\boldsymbol{f}_C^d - \boldsymbol{f}_C||$. These show that the x and y elements of measured contact force track the desired contact force well, and contact force error decreased by repetition of motion in both cases. The contact force error decrease by the integral of the contact force error $\boldsymbol{\eta}_{Ci}$ in case of without adaptive law differing from the results of position and orientation. Figure 13 shows that the decrease speed of contact force error in case of with adaptive law is faster than it in case of without adaptive law. However, though measured z element of contact force converges to desired contact force, tracking capability is not sufficient. The z element of contact force correspond to the internal force, and there are several reasons the tracking capability of z element of contact force is not sufficient: the dynamics of the mechanism such as the flexibility of the joint is not modeled; the controller is not a continuous-time control system but a discrete-time control system whose accuracy of trajectory depends on the sampling cycle (Kawasaki and Li 2004); the difference in response occur by the difference in property of individual finger.

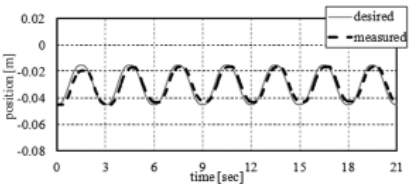


(a) x element (b) y element

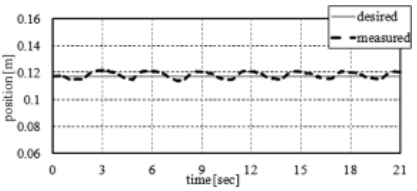


(c) z element

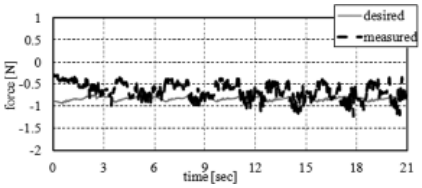
Figure 10. Contact force of 1st finger with adaptive law.



(a) x element

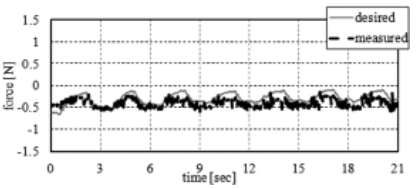


(b) y element

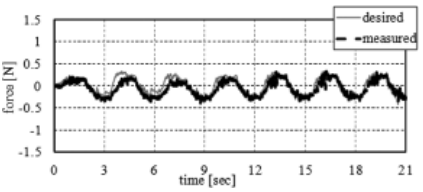


(c) z element

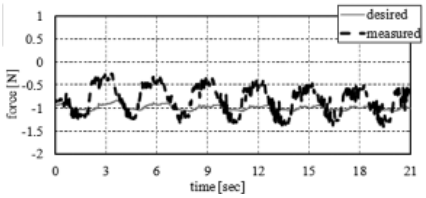
Figure 11. Contact force of 2nd finger with adaptive law.



(a) x element



(b) y element



(c) z element

Figure 12. Contact force of 3rd finger with adaptive law.

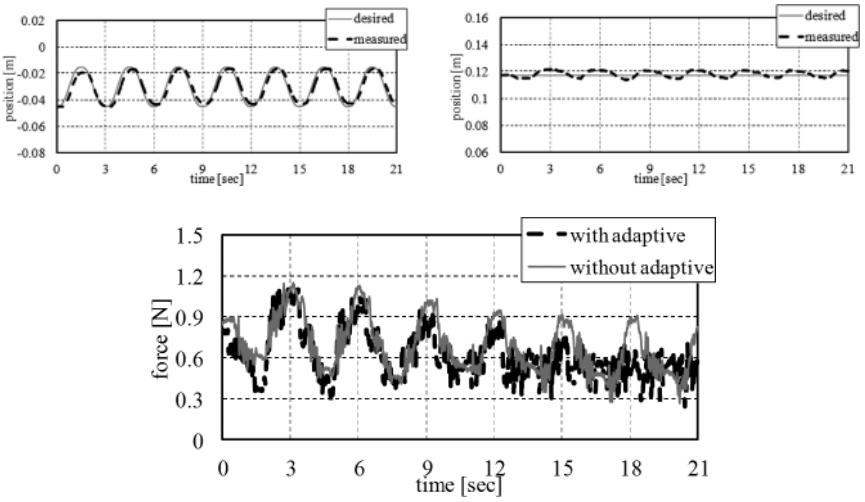
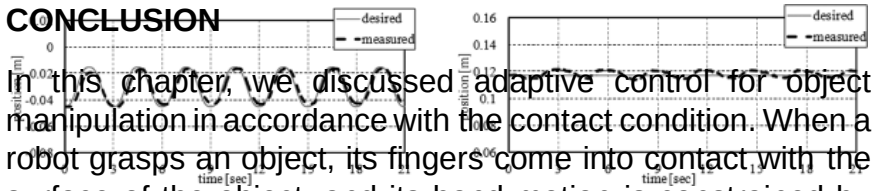


Figure 13. The norm of contact force error $\| \boldsymbol{f}_c^d - \boldsymbol{f}_c \|$.



CONCLUSION

In this chapter, we discussed adaptive control for object manipulation in accordance with the contact condition. When a robot grasps an object, its fingers come into contact with the surface of the object, and its hand motion is constrained by that contact. Robotic hands are mechanical non-linear systems. In general, adaptive control systems are treated as time-varying systems. For dexterous manipulation, the control objective is to control the object position and velocity; that is, to coordinately-control the force at the contact point that occurs for multiple robotic fingers. This is one of the challenging problems in robotics. In the controller presented here, the shapes of the object and positions of the contact points are already known. In fact, the position of the contact point can be calculated using the force sensor variable. However, the accuracy is insufficient. Thus, study of adaptive controls with fewer restrictions is needed. In addition, dynamic control by soft fingers will be an upcoming challenge.

REFERENCES

Anderson, B. O. D. 1977. Exponential stability of linear system arising from adaptive identification.
IEEE Transactions on Automatic Control, 22(2): 83–88.

Bicchi, A., J. K. Salisbury and D. L. Brock. 1993. Contact sensing from force measurements.
International Journal of Robotics Research, 12(3): 249–262.

Birglen, L., T. Lalibert and C. M. Gosselin. 2010. Under-actuated Robotic Hands. New York: Springer Verlag.

Cutkosky, M. R. and I. Kao. 1989. Computing and controlling the compliance of a robot hand. IEEE Transactions on Robotics and Automation, 5(2): 151–165.

Hayati, S. 1986. Hybrid position/force control of multi-arm cooperating robots. Proceedings of IEEE International Conference on Robotics and Automation, San Francisco, CA, USA, pp. 82–89.

Hwang, Y. Y. and I. Toda. 1994. Coordinated control of two direct-drive robots using neural networks.
JSME International Journal Series C, Mechanical Systems, 37:

335–341.

Kawasaki, H. 2015. Robot hands and multi-fingered haptic interfaces. Fundamentals and Applications, World Scientific.

Kawasaki, H. and G. Li. 2004. Expert skill-based gain tuning in discrete-time adaptive control for robots. The Journal of Robotics and Mechatronics, 16(1): 54–60.

Kawasaki, H., S. Ueki and S. Ito. 2006. Decentralized adaptive coordinated control of multiple robot arm without using force sensor. Automatica, 42(3): 481–488.

Kosuge, K., H. Yoshida, T. Fukuda, K. Kanitani, M. Sakai and K. Hariki. 1995. Coordinated motion control of manipulation based on impedance control. Journal of the Robotics Society of Japan, 13(3): 404–410 (in Japanese).

Mason, M. T. and J. K. Salisbury. 1985. Robot Hands and Mechanics of Manipulation. Cambridge, MA, USA: The MIT Press.

Mason, M. T. 1998. Mechanics of Robotic Manipulation. Cambridge, MA, USA: The MIT Press. Montana, D. J. 1988. The kinematics of contact and grasp. The International Journal of Robotics

Research, 7(3): 17–32.

Mouri, T., H. Kawasaki, K. Yoshikawa, J. Takai and S. Ito. 2002. Anthropomorphic robot hand: Gifu Hand III. Proceedings of International Conference on Control, Automation and Systems, pp. 1288–1293, Jeonbuk, Korea.

Murray, R. M., Z. Li and S. S. Sastry. 1993. A Mathematical Introduction to Robotic Manipulation, Boca Raton, Florida: CRC Press.

Naniwa, T. and S. Arimoto. 1995. Learning control for robot task under geometric endpoint constraints.

IEEE Transactions on Robotics and Automation, 2(3): 432–441.

Ozawa, R., S. Arimoto, S. Nakamura and J. Bae. 2005. Control of an object with parallel surface by a pair of finger robots without object sensing. IEEE Transactions on Robotics and Automation, 21(5): 965–976.

Schlegl, T., M. Buss and G. Schmidt. 2003. A hybrid system approach toward modeling and dynamical simulation of dextrous manipulation. IEEE/ASME Transactions on Mechatronics, 8(3): 352– 361.

Su, Y. and Y. Stepanenco. 1995. Adaptive sliding mode coordinated control of multiple robot arms attached to a constrained object. IEEE Transactions on Systems, Man, and Cybernetics, 25: 871–877.

Ueki, S., H. Kawasaki and T. Mouri. 2006. Adaptive coordinated control of multi-fingered hands with sliding contact. Proceedings of SICE-ICASE International Joint Conference, pp. 5893–5898, Busan, South Korea.

Ueki, S., H. Kawasaki and T. Mouri. 2009. Adaptive coordinated control of multi-fingered robot hand.
Journal of Robotics and Mechatronics, 21(1): 36–43.

Wakamatsu, H., M. Yamanoi and K. Tatsuno. 2010. Adaptive force control of robot arm with estimation of environmental stiffness. Proceedings of International Symposium on Micro- NanoMechatronics and Human Science, pp. 226–231, Nagoya, Japan.

Yingjie, Y. and S. Hosoe. 2005. MLD modeling and optimal control of hand manipulation. Proceedings of IEEE/RSJ International Conference on Intelligent Robotics and Systems, pp. 838–843, Alberta, Canada.

Zhaopeng, C., T. Wimbock, M. A. Roa, B. Pleintinger, M. Neves, C. Ott, C. Borst and N. Y. Lii. 2015. An adaptive compliant multi-finger approach-to-grasp strategy for objects with position uncertainties. Proceedings of IEEE International Conference on Robotics and Automation, pp. 4911–4918, Seattle, WA.

Zheng, X., R. Nakashima and T. Yoshikawa. 2000. On dynamic control finger sliding and object motion in manipulation with multi-fingered hands. IEEE Transactions on Robotics and Automation, 16(5): 469–481.

6

Output Feedback Adaptive Control of Uncertain Dynamical Systems with Event-Triggering

Ali Albattat,[1] *Benjamin Gruenwald*[2] and *Tansel Yucelen*[2,*]

ABSTRACT

Networked control for a class of uncertain dynamical systems is studied, where the control signals are computed via processors that are not attached to the dynamical systems and the feedback loops are closed over wireless networks. Since a critical task in the design and implementation of networked control systems is to reduce wireless network utilization while guaranteeing system stability in the presence of system uncertainties, an event-triggered adaptive control architecture is presented in an output feedback setting to schedule the data exchange dependent upon errors exceeding user-defined thresholds. Specifically, using tools and methods from nonlinear systems theory and Lyapunov stability in particular, it is shown that the proposed approach guarantees system stability in the presence of system uncertainties and does not yield to a Zeno behavior. In addition, the effect of user-defined thresholds and output feedback adaptive controller design parameters to the system performance is rigorously characterized and discussed. The efficacy of the proposed event-triggered output feedback adaptive control approach is demonstrated in an illustrative numerical example.

Keywords: Networked control systems, output

feedback adaptive control, event- triggering control, system uncertainties, system stability, system performance

[1] Department of Mechanical and Aerospace Engineering, Missouri University of Science and Technology.

[2] Department of Mechanical Engineering, University of South Florida.

* Corresponding author: tyucelen@gmail.com

INTRODUCTION

Networked control of dynamical systems is an appealing methodology in reducing cost for the development and implementation of control systems (Zhang et al. 1993, Walsh and Ye 2001, Tipsuwan and Chow 2003, Zhang and Hristu-Varsakelis 2006, Hespanha et al. 2007, Alur et al. 2007, Wang and Liu 2008, Bemporad et al. 2010). These systems allow the computation of control signals via processors that are not attached to the dynamical systems and the feedback loops are closed over wireless networks. In a networked control setting, since the processors computing control signals are separated from the dynamical systems, not only the feedback control algorithms can be easily modified as necessary but also this setting allows to develop small-size physical systems for low-cost control theory applications.

Motivation and Literature Review

A challenge in the design and implementation of networked control systems is to reduce wireless network utilization. To this end, the last decade has witnessed an increased interest in event-triggering control theory (Tabuada 2007, Mazo, Jr. and Tabuada 2008, Mazo, Jr. et al. 2009, Lunze and Lehmann 2010, Postoyan et al. 2011, Heemels et al. 2012), where it relaxes periodic data exchange demand of the feedback loops closed over wireless networks. Specifically, this theory allows aperiodic data exchange between the processors computing control signals and the dynamical systems, and hence, asynchronous data can be exchanged only when needed.

In networked control systems, another challenge is to guarantee system stability in the presence of system uncertainties. Often when designing feedback controllers for dynamical systems, idealized assumptions, linearization, model-order reduction, exogenous disturbances, and unexpected system changes lead to modeling inaccuracies. If not mitigated, the uncertainties present in the system model can result in poor system performance and system instability (Slotine and Li 1987, Krstic et al. 1995, Zhou et al. 1996, Zhou

and Doyle 1998, Narendra and Annaswamy 2012, Ioannou and Sun 2012, Lavretsky and Wise 2012, Astrom and Wittenmark 2013). Therefore, it is essential in the feedback control design process to achieve robust stability and a desired level of system performance when dealing with dynamical systems subject to system uncertainties.

Motivated by these two challenges of networked control systems, this chapter studies control of uncertain dynamical systems over wireless networks with event-triggering. To this end, we consider an adaptive control approach rather than a robust control approach, since the former approach requires less system modeling information than the latter and can address system uncertainties and failures effectively in response to system variations. Notable contributors that utilize event-triggered adaptive control approaches include (Sahoo et al. 2013, Sahoo et al. 2014, Wang and Hovakimyan 2010, Wang et al. 2015, Albattat et al. 2015).

In particular (Sahoo et al. 2013, Sahoo et al. 2014) develop neural networks- based adaptive control approaches to guarantee system stability in the presence of system uncertainties, where these results only consider one-way data transmission from a dynamical system to the controller. Two-way data transmission over a wireless network; that is, from a dynamical system to the controller and from the controller to this dynamical system, is considered in (Wang and Hovakimyan 2010, Wang et al. 2015, Albattat et al. 2015) to guarantee system stability under system uncertainties.

The major difference between the results in (Wang and Hovakimyan 2010, Wang et al. 2015, Albattat et al. 2015) is that the latter does not require the knowledge of a conservative upper bound on the unknown constant gain resulting from the system uncertainty parameterization. Finally, it should be noted that all these approaches documented in (Sahoo et al. 2013, Sahoo et al. 2014, Wang and Hovakimyan 2010, Wang et al. 2015, Albattat et al. 2015) consider an event-triggered state feedback adaptive control approach. Yet, output feedback is required for most applications that involve high-dimensional models such as active noise suppression, active control of flexible structures, fluid flow control systems, and combustion control processes (Khalil 1996, Calise et al. 2001, Hovakimyan et al. 2002, Volyanskyy et al. 2009, Yucelen and Haddad 2012, Lavretsky 2012, Gibson et al. 2014, Lavretsky 2015).

Contribution

In this chapter, networked control for a class of uncertain dynamical systems is studied. Since a critical task in the design and implementation of networked control systems is to reduce wireless network utilization while guaranteeing system stability in the presence of system uncertainties, an event-triggered adaptive control architecture is presented in an output feedback setting to schedule two-way data exchange dependent upon errors exceeding user-defined thresholds. Specifically, we consider the output feedback adaptive control architecture predicated on the asymptotic properties of LQG/LTR controllers (Lavretsky and Wise 2012, Lavretsky 2012, Gibson et al. 2014, Lavretsky 2015), since this framework has the capability to achieve stringent performance specifications without causing high-frequency oscillations in the controller response, asymptotically satisfies a strictly positive real condition for the closed-loop dynamical system, and is less complex than other approaches to output feedback adaptive control (see, for example (Calise et al. 2001, Hovakimyan et al. 2002, Volyanskyy et al. 2009)). Building on this output feedback adaptive control architecture as well as our previous event-

triggered state feedback adaptive control methodology (Albattat et al. 2015), it is shown using tools and methods from nonlinear systems theory and Lyapunov stability in particular that the proposed feedback control approach guarantees system stability in the presence of system uncertainties. In addition, the effect of user-defined thresholds and output feedback adaptive controller design parameters to the system performance is rigorously characterized and discussed. Moreover, we show that the proposed event- triggered output feedback adaptive control methodology does not yield to a Zeno behavior, which implies that it does not require a continuous two-way data exchange and reduces wireless network utilization. Similar to the state feedback case (Albattat et al. 2015), we also show that the resulting closed-loop dynamical system performance is more sensitive to the changes in the data transmission threshold from the physical system to the adaptive controller (sensing threshold) than the data transmission threshold from the adaptive controller to the physical system (actuation threshold), which implies that the actuation threshold can be chosen large enough to reduce wireless network utilization between the physical system and the adaptive controller without sacrificing closed-loop dynamical system performance. The efficacy of the proposed event-triggered output feedback adaptive control approach is demonstrated in an illustrative numerical example. Although this chapter considers a particular output feedback adaptive control formulation to present its main contributions, the proposed approach can be used in a

complimentary way with many other approaches to output feedback adaptive control concerning robotic manipulators (see, for example (Kaneko and Horowitz 1997, Burg et al. 1997, Zergeroglu et al. 1999, Zhang et al. 2000)).

Notation

The notation used in this chapter is fairly standard. Specifically, $\mathbb{R}$ denotes the set of real numbers, $\mathbb{R}^n$ denotes the set of $n \times 1$ real column vectors, $\mathbb{R}^{n\times m}$ denotes the set of $n \times m$ real matrices, $\mathbb{R}_+$ denotes the set of positive real numbers, $\mathbb{R}^{n\times n}_+$ denotes the set of $n \times n$ positive-definite real matrices, $\mathbb{R}^{n\times n}$ denotes the set of $n \times n$ symmetric real matrices, $\mathbb{R}^{n\times n}$ denotes the set of $n \times n$ real matrices with diagonal scalar entries, $(\cdot)^{\mathrm{T}}$ denotes transpose, $(\cdot)^{-1}$ denotes inverse, tr$(\cdot)$ denotes the trace operator and ‘$\triangleq$’ denotes equality by definition. In addition, we write $\lambda_{\min}(A)$ (respectively, $\lambda_{\max}(A)$) for the minimum and respectively maximum eigenvalue of the Hermitian matrix A, $\|\cdot\|$ for the Euclidean norm, and $\|\cdot\|_{\mathrm{F}}$ for the Frobenius matrix norm. Furthermore, we use “v” for the “or” logic operator and “$\neg(\cdot)$” for the “not” logic operator.

OUTPUT FEEDBACK ADAPTIVE CONTROL OVERVIEW

In this section, we overview the output feedback adaptive control architecture predicated on the asymptotic properties of LQG/LTR controllers (Lavretsky and Wise 2012, Lavretsky 2012, Gibson et al. 2014, Lavretsky 2015), which are needed for the main results of this chapter. For this purpose, consider the uncertain dynamical system given by

$$\dot{x}_{\mathrm{p}}(t) = A_{\mathrm{p}}x_{\mathrm{p}}(t) + B_{\mathrm{p}}\Lambda\,[u(t) + \Delta\,(x_{\mathrm{p}}(t))], \quad x_{\mathrm{p}}(0) = x_{\mathrm{p}0}, \tag{1}$$

$$y_{\mathrm{reg}}(t) = C_{\mathrm{reg}}\,x_{\mathrm{p}}(t), \tag{2}$$

where $A_{\mathrm{p}} \in \mathbb{R}^{n_{\mathrm{p}}\times n_{\mathrm{p}}}$, $B_{\mathrm{p}} \in \mathbb{R}^{n_{\mathrm{p}}\times m}$, and $C_{\mathrm{reg}} \in \mathbb{R}^{m\times n_{\mathrm{p}}}$ are known system matrices, $x_{\mathrm{p}}(t) \in \mathbb{R}^{n_{\mathrm{p}}}$ is the state vector, which is not available for state feedback design, $u(t) \in \mathbb{R}^m$ is the control input, $\Lambda \in \mathbb{R}^{m\times m}$ is an unknown control effectiveness matrix, $\Delta : \mathbb{R}^n \to \mathbb{R}^m$ is

a system uncertainty, and $y_{reg}(t) \in \mathbb{R}^{m}$ is the regulated output vector. In addition, we assume that the uncertain dynamical system given by (1) and (2) has a measured output vector

$$y_p(t) = C_p x_p(t), \tag{3}$$

where $y_p(t) \in \mathbb{R}^{l_p}$, $C_p \in \mathbb{R}^{l_p \times n_p}$, and $l_p \geq m$ such that the elements of $y_{reg}(t)$ are a subset of the elements of $y_p(t)$. Throughout this chapter, we assume that the triple (A_p, B_p, C_p) is minimal, the system uncertainty in (1) can be linearly parameterized as

$$\Delta(x_p(t)) = W_p^{T} \sigma_p(x_p(t)), \tag{4}$$

where $W_p \in \mathbb{R}^{s \times m}$ is an unknown weight matrix satisfying $\|W_p\|_F \leq \omega_p^*$, $\omega_p^* \in \mathbb{R}_+$, and $\sigma_p(x_p(t))$ is a known Lipschitz continuous basis vector satisfying

$$\|\sigma_p(x_p) - \sigma_p(\hat{x}_p)\| \leq L_{\sigma_p} \|x_p - \hat{x}_p\|, \tag{5}$$

with $L_{\sigma_p} \in \mathbb{R}_+$. These assumptions are standard in the output feedback adaptive control literature (see, for example (Lavretsky and Wise 2012, Lavretsky 2012, Gibson et al. 2014, Lavretsky 2015, Kim et al. 2011a, Kim et al. 2011b). For the case when the system

uncertainty given by (4) cannot be perfectly parameterized and/or the basis vector does not satisfy (5), note that universal approximation tools such as neural networks can be used in the basis vector on a compact subset of the state space (see, for example (Yesildirek and Lewis 1995, Kim and Lewis 1999)).

Similar to the approaches documented in (Lavretsky 2012, Kim et al. 2011, Kim et al. 2011), we consider a state observer-based nominal control architecture to achieve command following, where control of the regulated outputs that are commanded include integral action and the regulated outputs that are not commanded are subject to proportional control. For this purpose, let

$$y_{\text{reg}}(t) = \begin{bmatrix} y_{\text{reg1}}(t) \\ y_{\text{reg2}}(t) \end{bmatrix} = \begin{bmatrix} C_{\text{reg1}} \\ C_{\text{reg2}} \end{bmatrix} x_{\text{p}}(t), \tag{6}$$

where $y_{\text{reg1}}(t) \in \mathbb{R}^r$, $r \le m$, is regulated with proportional and integral control to track a given command vector $r(t) \in \mathbb{R}^r$, $y_{\text{reg2}}(t) \in \mathbb{R}^{m-r}$ is regulated with proportional control, $C_{\text{reg1}} \in \mathbb{R}^{r \times n_{\text{p}}}$, $C_{\text{reg2}} \in \mathbb{R}^{(m-r) \times n_{\text{p}}}$. Now, we define the integrator dynamics as

$$\dot{x}_{\text{int}}(t) = y_{\text{reg1}}(t) + r(t) = C_r x_{\text{p}}(t) + r(t), \tag{7}$$

where $x_{\text{int}}(t) \in \mathbb{R}^r$ is the integral state vector. Utilizing (1), (2), and (7), the augmented system dynamics are now given by

$$\dot{x}(t) = \underbrace{\begin{bmatrix} A_{\text{p}} & 0 \\ -C_r & 0 \end{bmatrix}}_{A} x(t) + \begin{bmatrix} B_{\text{p}} \\ 0 \end{bmatrix} \Lambda [u(t) + \Theta^{\text{T}} \sigma(x_{\text{p}}(t))] + \begin{bmatrix} 0 \\ I \end{bmatrix} r(t), \tag{8}$$

$$\dot{x}_{reg}(t) = A_{reg}x(t), \quad y_{reg}(t) = C_{reg}x(t), \tag{9}$$

where $x(t) = [x_p(t)^T \; x_{int}(t)^T]^T \in \mathbb{R}^n$, $A \in \mathbb{R}^{n\times n}$, $B \in \mathbb{R}^{n\times m}$, $C \in \mathbb{R}^{l\times n}$, and $n = n_p + r$. In addition, the augmented measured output vector becomes

$$y(t) = \begin{bmatrix} y_p(t) \\ x_{int}(t) \end{bmatrix} = \begin{bmatrix} C_p & 0 \\ 0 & I_r \end{bmatrix} \begin{bmatrix} x_p(t) \\ x_{int}(t) \end{bmatrix} = Cx(t), \tag{10}$$

where $y(t) \in \mathbb{R}^l$, $C \in \mathbb{R}^{l\times n}$, and $l = l_p + r$.

Next, we define the feedback control law as

$$u(t) = u_n(t) + u_a(t), \tag{11}$$

where $u_n(t)$ is a nominal control law and $u_a(t)$ is an adaptive control law. Using the output feedback adaptive control architecture documented in (Lavretsky and Wise 2012, Lavretsky 2012, Gibson et al. 2014, Lavretsky 2015), we consider the nominal controller given by

$$u_n(t) = -K_x \hat{x}(t), \tag{12}$$

where $K \in \mathbb{R}^{m \times n}$ is a feedback matrix and $\hat{x}(t)$ is an estimate of the augmented system state vector $x(t)$ through a state observer to be defined later in this section. In order to determine the structure of the adaptive controller, we rewrite the augmented system dynamics given by (8) and (9) as

$$\dot{x}(t) = Ax(t) + Bu(t) + B\Lambda(u(t) + W^{\mathrm{T}}\sigma(x(t), u(t))) + B\,\mathrm{r}(t), \quad (13)$$

where $W \triangleq [W_{m} - \Lambda^{-1}]^{\mathrm{T}} \in \mathbb{R}^{(n+m)\times m}$ and $\sigma(x(t), u(t)) \triangleq [\sigma(x(t))^{\mathrm{T}}, u^{\mathrm{T}}(t)]^{\mathrm{T}} \in \mathbb{R}^{n+m}$.

Motivating from the structure of the system uncertainties appearing in (13), consider the adaptive controller given by

$$u(t) = -\hat{W}^{\mathrm{T}}\sigma(\hat{x}(t), u(t)), \quad (14)$$

where $\sigma(\hat{x}(t), u(t)) \triangleq [\sigma(\hat{x}(t))^{\mathrm{T}}, u^{\mathrm{T}}(t)]^{\mathrm{T}} \in \mathbb{R}^{n+m}$ and $\hat{W}(t) \in \mathbb{R}^{(n+m)\times m}$ is the estimate of the unknown weight matrix W through the weight update law

$$\dot{\hat{W}}(t) = \Gamma\,\mathrm{Proj}_{m}[\hat{W}(t), -\sigma(\hat{x}(t), u(t))\,\tilde{y}^{\mathrm{T}}(t)\,R^{2}\,ZS^{\mathrm{T}}], \quad (15)$$

where Proj_{m} denotes the projection operator defined for matrices (Lavretsky and Wise 2012, Albattat et al. 2015, Pomet and Praly 1992, Lavretsky et al. 2011), $\Gamma \in \mathbb{R}^{(s+m)\times(s+m)} \cap \mathbb{R}^{(s+m)\times(s+m)}$ is a learning rate matrix, $\tilde{y}(t) \in \mathbb{R}^{l}$ given by

$$\tilde{y} \triangleq \hat{y}(t) - y(t) = C(\hat{x}(t) - x(t)), \quad (16)$$

is the measured output error, and $\hat{x}(t) \in \mathbb{R}^{n}$ is the estimated augmented system state obtained through the state observer given by

$$\dot{\hat{x}}(t) = A\hat{x}(t) + Bu(t) + L(y(t) - \hat{y}(t)) + B\,\mathrm{r}(t), \quad (17)$$

$$\hat{y}(t) = C\hat{x}(t), \quad (18)$$

with $L \in \mathbb{R}^{n\times l}$ being the state observer gain matrix.

Following (Lavretsky and Wise 2012, Lavretsky 2012), the state observer gain matrix is given by

$$L_{V} = PC_{V}^{\mathrm{T}}R^{-1}, \quad (19)$$

with $P \in \mathbb{R}^{n\times n}$ being the unique solution to the algebraic Riccati

equation

$$0 = P_v(A + \eta_v I_n)^{\mathrm{T}} + (A + \eta_v I_n)P_v - P_v C^{\mathrm{T}} R_v^{-1} C P_v + Q_v, \ \eta_v \in \mathbb{R}, \tag{20}$$

$$Q_v = Q_0 + \left(\frac{v+1}{v}\right) B_s B_s^{\mathrm{T}}, \ Q_0 \in \mathbb{P}^{n\times n}, \ v \in \mathbb{P}, \tag{21}$$

$$R_v = \left(\frac{v}{v+1}\right) R_0, \ R_0 \in \mathbb{R}^{l\times l}. \tag{22}$$

In (21), $B_s = [B, B_2]$, where $B \in \mathbb{R}^{n\times(l-m)}$ is a matrix such that $\det(CB_s) \neq 0$ and $C(sI_n - A)^{-1}B_2$ is minimum phase. Note that $l > m$ is assumed in the above construction,

where if $l = m$ then $B_2 = 0$. In addition, the observer closed-loop matrix given by

$$A_v = A - L_v C = A - P_v C^{\mathrm{T}} R_v^{-1} C \tag{23}$$

is Hurwitz for all $v \in \square$. Moreover, let $\tilde{P}_v = P_v - \begin{bmatrix} P_{v0} & 0 \\ 0 & 0 \end{bmatrix}$ and $S = [I_m \quad 0_{m\times(l-m)}]^T$ to note (Lavretsky and Wise 2012, Lavretsky 2012)

$$\tilde{P}_v B = C_0^T R_v^{-1} Z S^T + O(v), \tag{24}$$

and

$$A_v^T \tilde{P}_v + \tilde{P}_v A_v = -C_v^T R_v^{-1} C_v - \tilde{P}_v Q_v \tilde{P}_v - 2\eta \tilde{P}_v < 0. \tag{25}$$

In (15) and (24), $Z = (UV)^T$, where two unitary matrices U and V result from the singular value decomposition $B^T C^T R^{-1/2} = U \Sigma V$ and Σ is the diagonal matrix of the corresponding singular values. In (24), "$O(\cdot)$" denotes the Bachmann-Landau asymptotic order notation (Kevorkian and Cole 1996, Murray 1984). For additional details on the output feedback adaptive control architecture overviewed in this section, we refer to (Lavretsky and Wise 2012, Lavretsky 2012) as well as (Gibson et al. 2014, Lavretsky 2015). To summarize, as previously discussed, the considered architecture has the capability to achieve stringent performance specifications without causing high-frequency oscillations in the controller response, asymptotically satisfies a strictly positive real condition for the closed-loop dynamical system, and is less complex than other approaches to output feedback adaptive control.

Finally, for analysis purposes later in this chapter, we define the reference model capturing the ideal closed-loop dynamical system performance given by

$$\dot{x}_m = A_m x_m(t) + B_m r(t), \quad x_m(0) = x_{m0}, \tag{26}$$

$$y_m = C_{Reg} x_m, \tag{27}$$

where $x_m(t) \in \square^n$ is the reference model state, $A_m = A - BK_x$ is Hurwitz, and $B_m = B_r$. In addition, let

$$\tilde{x}(t) \triangleq \hat{x}(t) - x(t), \tag{28}$$

$$\hat{e}(t) \triangleq \hat{x}(t) - x_m(t), \tag{29}$$

$$\tilde{W}(t) \triangleq \hat{W}(t) - W. \tag{30}$$

be the state estimation error, the state tracking error, and the weight estimation error, respectively. Now, we can write

$$\dot{\hat{e}}(t) = A_m \hat{e}(t) + L_v (y(t) - \hat{y}(t)), \tag{31}$$

using (17) and (26), and write

$$\begin{aligned}\dot{\tilde{x}}(t) &= (A - L_v C)\tilde{x}(t) + B\Lambda(\hat{W}_p^T(t)\,\sigma(\hat{x}_p(t), u_n(t)) - W_p^T\,\sigma(x_p(t), u_n(t))) \\ &= A_v\tilde{x}(t) + B\Lambda(\tilde{W}_p^T(t)\,\sigma(\hat{x}_p(t), u_n(t)) - g(\cdot)),\end{aligned} \tag{32}$$

using (13) and (17), where $g(\cdot) \triangleq W_p^T(\sigma(\hat{x}_p(t), u_n(t)) - \sigma(x_p(t), u_n(t)))$.

EVENT-TRIGGERED OUTPUT FEEDBACK ADAPTIVE CONTROL

In this section, we present the proposed event-triggered output feedback adaptive control architecture, which allows a desirable command following performance while the proposed controller exchanges data with the uncertain dynamical system through a wireless network. Mathematically speaking, the uncertain dynamical system sends its output signal to the adaptive controller only when a predefined event occurs. The *k*th time instants of the output transmission is represented by the monotonic sequence $\{s_k\}_{k=1}^{\infty}$, where $s_k \in \mathbb{R}_+$. The controller then uses this triggered system output signal to compute the control signal using the output feedback control architecture. Likewise, the updated feedback control input is transmitted to the uncertain dynamical system only when another predefined event occurs. The *j*th time instants of the feedback control transmission is then represented by the monotonic sequence $\{r_j\}_{j=1}^{\infty}$, where $r_j \in \mathbb{R}_+$. As depicted in Fig. 1, each system output signal and control input is held by a zero-order- hold operator (ZOH) until the next triggering event for that signal takes place. In this chapter, we do not consider delay in sampling, data transmission, and computation.

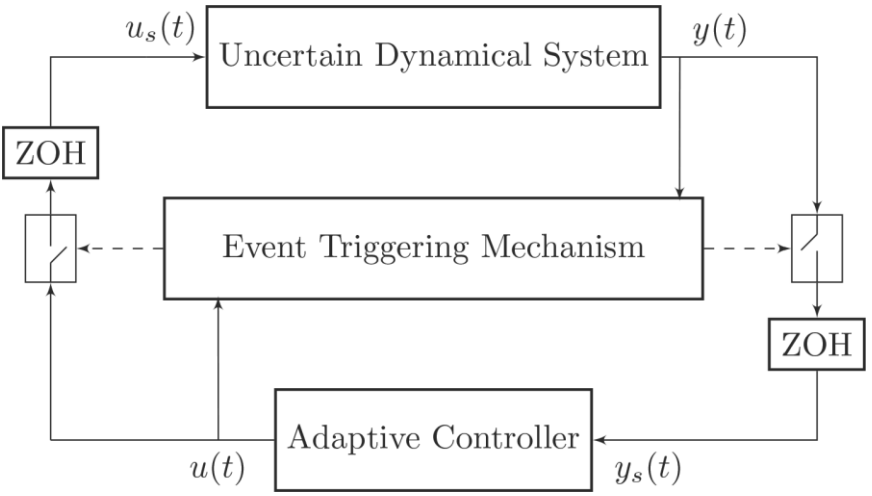


Figure 1. Event-triggered adaptive control system.

Proposed Event-Triggered Adaptive Control Algorithm

Based on the two-way data exchange structure depicted in Fig. 1, consider the augmented uncertain dynamical system given by

$$\dot{x}(t) = Ax(t) + B\Lambda[u_S(t) + \Delta(x_p(t))] + B_r r(t), \quad (33)$$

$$y_{reg}(t) = C_{Reg}x(t), \quad y(t) = Cx(t), \quad (34)$$

where $u(t) \in \mathbb{R}^m$ is the sampled control input vector. Under the assumptions stated in Section (**Output Feedback Adaptive Control Overview**) and considering the feedback control law given by (11) subject to the nominal controller given by (12) and the adaptive

controller given by (14), the augmented uncertain dynamical system given by (33) and
(34) can be equivalently written as

$$\dot{x}(t) = Ax(t) + Bu_n + B\Lambda(u_a(t) + W^{\mathrm{T}}\sigma(x(t), u(t))) + B\Lambda(u(t) - u(t)) + B\,\mathrm{r}(t), \quad (35)$$

$$y_{\mathrm{reg}}(t) = C_{\mathrm{Reg}}\,x(t), \quad y(t) = Cx(t). \quad (36)$$

In addition, we consider

$$\dot{\hat{W}}(t) = \mathrm{Proj}[\Gamma\,\sigma(\hat{x}(t), u(t))(\hat{y}(t) - y(t))^{\mathrm{T}} R^{2} Z S^{\mathrm{T}}], \quad (37)$$

for the estimated weight matrix $\hat{W}(t)$ in (14) and

$$\dot{\hat{x}}(t) = A\hat{x}(t) + Bu(t) + L(y(t) - \hat{y}(t)) + B\,\mathrm{r}(t)$$
$$= A_{\mathrm{m}}\hat{x}(t) + L(y(t) - \hat{y}(t)) + B\,\mathrm{r}(t), \quad (38)$$

$$\hat{y}(t) = C\hat{x}(t), \quad (39)$$

for the state observer, where $y(t) \in \mathbb{R}^{l}$ in (37) and (38) denotes the sampled augmented
measured output vector.

The proposed event-triggered output feedback adaptive control algorithm is summarized in Table 1. Specifically, based on the two-way data exchange structure depicted in Fig. 1, the controller generates $u(t)$ and the uncertain dynamical system is driven by the sampled version of this control signal $u_S(t)$ depending on an event-
triggering mechanism. Similarly, the controller utilizes $y_S(t)$ that represents the sampled
version of the uncertain dynamical system measured output $y(t)$ depending on an event-
triggering mechanism. These event-triggering mechanisms are stated next.

Scheduling Two-Way Data Exchange

Let $\varepsilon_y \in \mathbb{R}_+$ be a given, user-defined sensing threshold to allow for data transmission
from the uncertain dynamical system to the controller. In addition, let

$u \in \mathbb{R}^{m}$ be a given, userdefined actuation threshold to allow for data transmission from the controller to the uncertain dynamical system. Similar in fashion to (Wang and Hovakimyan 2010, Albattat et al. 2015), we now define three logic rules for scheduling the two-way data exchange

Table 1. Event-triggered output feedback adaptive control algorithm.

Augmented unc. dyn. sys.	$\dot{x}(t) = Ax(t) + B\Lambda [u_s(t) + \Delta(x_p(t))] + B_r r(t)$, $y_{reg}(t) = C_{Reg}x(t)$, $y(t) = Cx(t)$
Feedback control law	$u(t) = u_n(t) + u_a(t)$
Nominal control law	$u_n(t) = -K_x\hat{x}(t)$
Adaptive control law	$u(t) = -\hat{W}^T\sigma(\hat{x}(t), u(t))$, $\dot{\hat{W}}(t) = \Gamma \mathrm{Proj}[\hat{W}(t), -\sigma(\hat{x}(t), u(t))(\hat{y}(t) - y(t))^T R_m]$, $\hat{y}(t) = C\hat{x}(t)$
State observer	$\dot{\hat{x}}(t) = A\hat{x}(t) + L(y(t) - \hat{y}(t)) + Br(t)$,

$$E_1 : \|y_S(t) - y(t)\| \leq \varepsilon_y, \tag{40}$$

$$E_2 : \|u_S(t) - u(t)\| \leq \varepsilon_u, \tag{41}$$

$$E_3 : \text{The controller receives } y_S(t). \tag{42}$$

Specifically, when the inequality (40) is violated at the s_k moment of the kth time instant, the uncertain dynamical system triggers the measured output signal information such that $y_S(t)$ is sent to the controller. Likewise, when (41) is violated or the controller receives a new transmitted system output from the uncertain dynamical system (i.e., when $E_2 \vee E_3$ is true), then the feedback controller sends a new control input $u_S(t)$ to the uncertain dynamical system at the r_j moment of the j th time instant. Finally, using the definitions given by (28), (29), and (30), we write

$$\dot{\hat{e}}(t) = A_m \hat{e}(t) + L_s(y(t) - \hat{y}(t)), \hat{e}(0) = \hat{e}_0, \tag{43}$$

$$\dot{\tilde{x}}(t) = A_v \tilde{x}(t) + L_s(y(t) - y(t)) + B\Lambda(\tilde{W}^{\mathrm{T}}\sigma(\hat{x}(t), u(t)) + g(\cdot)) - B\Lambda(u(t) - u(t)),$$

$$\tilde{x}(0) = \tilde{x}_0. \tag{44}$$

In the next section, we analyze the stability and performance of the proposed event-triggered output feedback adaptive control algorithm introduced in this section (see Table 1) using the error dynamics given by (43) and (44) well as the data exchange rules E_1, E_2, and E_3 respectively given by (40), (41), and (42).

STABILITY AND PERFORMANCE ANALYSIS

For organizational purposes, this section is divided into three subsections. Specifically, we analyze the uniform ultimate boundedness of the resulting closed-loop dynamical system in Section (Uniform Ultimate Boundedness Analysis), compute the ultimate bound and highlight the effect of user-defined thresholds and the adaptive controller design parameters to this ultimate bound in Section (Ultimate Bound Computation), and show that the proposed architecture does not yield to a Zeno behavior in Section (Zeno Behavior Analysis).

Uniform Ultimate Boundedness Analysis

The following theorem presents the first result of this chapter.

Theorem 1. *Consider the uncertain dynamical system given by (33) and (34), the reference model given by (26) and (27), the state observer given by (38) and (39) with the state observer gain matrix in (19) along with (20), (21), and (22), and the feedback control law given by (11), (12), (14), and (37). In addition, let the data transmission from the uncertain dynamical system to the controller occur when* E_1 *is true and the data transmission from the controller to the uncertain dynamical system occur when* $E_2 \vee E_3$ *is true. Then, the closed-loop solution* $(\tilde{x}(t), \tilde{W}(t), \hat{e}(t))$ *is uniformly ultimately bounded for all initial conditions.*

Proof. Since the data transmission from the uncertain dynamical system to the controller and from the controller to the uncertain dynamical system occur when E_1 and $E_2 \vee E_3$ are true, respectively, note that $\|y_S(t) - y(t)\| \leq \varepsilon_y$ and $\|u_S(t) - u(t)\| \leq \varepsilon_u$ hold.

Consider the Lyapunov-like function given by

$$\mathcal{V}(\tilde{x}, \tilde{W}, \hat{e}) = \tilde{x}^{\mathrm{T}}\tilde{P}\,\tilde{x} + \mathrm{tr}\,(\tilde{W}\Lambda^2)^{\mathrm{T}}\Gamma^{-1}(\tilde{W}\Lambda^2) + \beta\hat{e}^{\mathrm{T}}P\hat{e}, \quad (45)$$

where $\tilde{P} \in \mathbb{R}^{n\times n}$ is a solution to (25) with $R \in \mathbb{R}^{l\times l}$ and $Q \in \mathbb{R}^{n\times n}$, $\nu > 0$, $\eta \in \mathbb{R}$, $\beta > 0$, and $P \in \mathbb{R}^{n\times n} \cap \mathbb{R}^{n\times n}_{+}$ is a solution to

$$0 = A^{\mathrm{T}}P + PA - PBR^{-1}B^{\mathrm{T}}P + Q, \quad (46)$$

with $R \in \mathbb{R}^{m\times m}_{+}$ and $Q \in \mathbb{R}^{n\times n}_{+}$. Note that $\mathcal{V}(0, 0, 0) = 0$ and $\mathcal{V}(\tilde{x}, W, \hat{e}) > 0$ for all $(\tilde{x}, W, \hat{e}) \neq (0, 0, 0)$.

The time-derivative of (45) is given by

$$\begin{aligned}
&\dot{\mathcal{V}}(\tilde{x}(t), \tilde{W}(t), \hat{e}(t)) \\
&= 2\tilde{x}^{\mathrm{T}}\tilde{P}\,\dot{\tilde{x}} + 2\mathrm{tr}(\tilde{W}^{\mathrm{T}}(t)\Gamma^{-1}\dot{\tilde{W}}(t)\Lambda) + 2\beta\,\hat{e}^{\mathrm{T}}P\,\dot{\hat{e}} \\
&= 2\tilde{x}^{\mathrm{T}}\tilde{P}\,(A_{\nu}\tilde{x}(t) + L_{\nu}(y(t) - y(t)) + B\Lambda(\tilde{W}^{\mathrm{T}}\sigma(\hat{x}(t), u(t)) + g(\cdot)) \\
&\quad - B\Lambda(u(t) - u(t))) + 2\mathrm{tr}(\tilde{W}^{\mathrm{T}}(t)\Gamma^{-1}\dot{\tilde{W}}(t)\Lambda) + 2\beta\,\hat{e}^{\mathrm{T}}P\,\dot{\hat{e}} \\
&= -\tilde{x}^{\mathrm{T}}(C^{\mathrm{T}}R^{-1}C + \tilde{P}\,Q\,\tilde{P} + 2\eta\tilde{P})\,\tilde{x} + 2\tilde{x}^{\mathrm{T}}\tilde{P}\,L_{\nu}(y(t) - y(t)) + 2\tilde{x}^{\mathrm{T}}\tilde{P}\,B\Lambda\,\tilde{W}^{\mathrm{T}}\sigma(\hat{x}(t), u(t)) \\
&\quad + 2\tilde{x}^{\mathrm{T}}\tilde{P}\,B\Lambda g(\cdot) - 2\tilde{x}^{\mathrm{T}}\tilde{P}\,B\Lambda(u(t) - u(t)) + 2\mathrm{tr}(\tilde{W}^{\mathrm{T}}(t)\Gamma^{-1}\dot{\tilde{W}}(t)\Lambda) + 2\beta\,\hat{e}^{\mathrm{T}}P\,\dot{\hat{e}} \\
&= -\left(1 + \frac{1}{\nu}\right)\tilde{x}^{\mathrm{T}}C^{\mathrm{T}}R^{-1}C\,\tilde{x} - \tilde{x}^{\mathrm{T}}\tilde{P}\,Q\,\tilde{P}\,\tilde{x} - \left(1 + \frac{1}{\nu}\right)\tilde{x}^{\mathrm{T}}\tilde{P}\,B\,B^{\mathrm{T}}\tilde{P}\,\tilde{x} - 2\eta\tilde{x}^{\mathrm{T}}\tilde{P}\,\tilde{x} \\
&\quad + 2\tilde{x}^{\mathrm{T}}\left(C^{\mathrm{T}}R^{-1}ZS^{\mathrm{T}} + O(\nu)\Lambda\tilde{W}^{\mathrm{T}}\sigma(\hat{x}(t), u(t)) + 2\tilde{x}^{\mathrm{T}}\tilde{P}\,B\Lambda g(\cdot)\right. \\
&\quad + 2\tilde{x}^{\mathrm{T}}\tilde{P}\,L_{\nu}(y(t) - y(t)) - 2\tilde{x}^{\mathrm{T}}\tilde{P}\,B\Lambda(u(t) - u(t)) + 2\mathrm{tr}(\tilde{W}^{\mathrm{T}}(t)\Gamma^{-1}\dot{\tilde{W}}(t)\Lambda) + 2\beta\,\hat{e}^{\mathrm{T}}P\,\dot{\hat{e}} \\
&= -\left(1 + \frac{1}{\nu}\right)\tilde{x}^{\mathrm{T}}C^{\mathrm{T}}R^{-1}C\,\tilde{x} - \tilde{x}^{\mathrm{T}}\tilde{P}\,Q\,\tilde{P}\,\tilde{x} - \left(1 + \frac{1}{\nu}\right)\tilde{x}^{\mathrm{T}}\tilde{P}\,B\,B^{\mathrm{T}}\tilde{P}\,\tilde{x} - 2\eta\tilde{x}^{\mathrm{T}}\tilde{P}\,\tilde{x} \\
&\quad + 2\tilde{x}^{\mathrm{T}}O(\nu)\Lambda\tilde{W}^{\mathrm{T}}\sigma(\hat{x}(t), u(t)) + 2\tilde{x}^{\mathrm{T}}\tilde{P}\,B\Lambda g(\cdot) + 2\tilde{x}^{\mathrm{T}}\tilde{P}\,L_{\nu}(y(t) - y(t)) \\
&\quad - 2\tilde{x}^{\mathrm{T}}\tilde{P}\,B\Lambda(u(t) - u(t)) + 2\mathrm{tr}(\tilde{W}^{\mathrm{T}}(t)(\Gamma^{-1}\dot{\tilde{W}}(t) + \sigma(\hat{x}(t), u(t))\tilde{y}^{\mathrm{T}}R^{-1}ZS^{\mathrm{T}})\Lambda) \\
&\quad + 2\beta\,\hat{e}^{\mathrm{T}}P(A\,\hat{e}(t) + L(y(t) - \hat{y}(t))). \quad (47)
\end{aligned}$$

Now, noting $||O(v)|| \leq vK$, $K \in \mathbb{R}$, and using (37) in (47) yields

$$\begin{aligned}
&\dot{\mathcal{V}}(\tilde{x}(t), \tilde{W}(t), \hat{e}(t)) \\
&\leq -\left(1 + \frac{1}{\nu}\right)\tilde{x}^{\mathrm{T}} C^{\mathrm{T}} R^{-1} C\tilde{x} - \tilde{x}^{\mathrm{T}}\tilde{P}\, Q\, \tilde{P}\, \tilde{x} - \left(1 + \frac{1}{\nu}\right)\tilde{x}^{\mathrm{T}}\tilde{P}\, B\, B^{\mathrm{T}}\tilde{P}\, \tilde{x} - 2\eta\tilde{x}^{\mathrm{T}}\tilde{P}\, \tilde{x} \\
&\quad + 2\tilde{x}^{\mathrm{T}} O(\nu)\Lambda\tilde{W}^{\mathrm{T}}\sigma(\hat{x}(t), u(t)) + 2\tilde{x}^{\mathrm{T}}\tilde{P}\, B\Lambda g(\cdot) + 2\tilde{x}^{\mathrm{T}}\tilde{P}\, L(y(t) - y(t)) \\
&\quad - 2\tilde{x}^{\mathrm{T}}\tilde{P}\, B\Lambda(u(t) - u(t)) + 2(y(t) - y(t))^{\mathrm{T}} R^{2} Z S^{\mathrm{T}}\Lambda\tilde{W}^{\mathrm{T}}(t)\, \sigma(\hat{x}(t), \\
&\quad - \beta\hat{e}^{\mathrm{T}}(t)(-PBR^{-1}\mathrm{B}^{\mathrm{T}} P + Q)\hat{e}(t) - 2\beta\hat{e}^{\mathrm{T}}(t)PL\, C\tilde{x}(t) + 2\beta\hat{e}^{\mathrm{T}}(t)PL \\
&\quad (y(t) - y(t)) \\
&\leq -\left(1 + \frac{1}{\nu}\right)\lambda(R^{-1})\, ||C||^{2}\, (Q)\, \lambda^{2} (\tilde{P})||\tilde{x}(t)||^{2}\, (\tilde{P}) \\
&\quad ||\tilde{x}(t)||^{2} - \lambda - \left(1 + \frac{1}{\nu}\right)\lambda^{2}
\end{aligned}$$

$$\nu \min_{\mathrm{F}} \min \quad \min \quad \nu \min \nu$$

$$\dot{V}(t) \le -\eta \lambda_{\min}(\tilde{P}) \|\tilde{x}(t)\|^2 - 2K_v \|\Lambda\| \|\tilde{W}\| \|\sigma(\hat{x}(t), u(t))\| \|\tilde{x}(t)\| + 2\|\tilde{x}\| \|\tilde{P}B\| \|\Lambda\| \|g(\cdot)\| + 2\|\tilde{x}\| \|\tilde{P}B\| \|\Lambda\| \|L_\sigma\| \|\tilde{x}\| + 2\|\tilde{x}\| \|\tilde{P}B\| \|\Lambda\| \|\tilde{W}(t)\| \|\sigma(\hat{x}(t), u(t))\| - \beta(\lambda_{\min}(Q) - \lambda_{\max}(R^{-1}) \|\tilde{P}\|^2) \|\tilde{x}(t)\|^2 + 2\beta \|\hat{e}(t)\| \|PL_C\| \|\tilde{x}(t)\| + 2\beta \|\hat{e}(t)\| \|PB\| \|\Lambda\| \|\tilde{W}(t)\| \|\sigma(\hat{x}(t), u(t))\| + 2\beta \|\hat{e}(t)\| \|PB\| \|\Lambda\| \|L_\sigma\| \|\tilde{x}(t)\| + 2\beta \|\hat{e}(t)\| \|PB\| \|\Lambda\| \|W\| \|\sigma(\hat{x}(t), u(t))\| + 2\beta \|\hat{e}(t)\| \|PB\| \|\Lambda\| \|g(\cdot)\| \tag{48}$$

Next, using (5), an upper bound for $\|g(\cdot)\|$ in (48) is given by

$$\begin{aligned} \|g(\cdot)\| &= \|W_p^T(\sigma(\hat{x}_p(t), u_p(t)) - \sigma(x_p(t), u_p(t))\| \\ &\le W_{\max} L_\sigma \|\hat{x}_p(t) - x_p(t)\| \\ &\le K_g \|\tilde{x}(t)\|, \end{aligned} \tag{49}$$

where $K_g = W_{\max} L_\sigma$ and $\|W_p\| \le W_{\max}$. In addition, noting $\|\hat{x}_p(t)\| \le \|\hat{x}(t)\|$ and using (5), one can compute an upper bound for $\|\sigma(\hat{x}_p(t), u_p(t))\|$ in (48) as

$$\begin{aligned} \|\sigma(\hat{x}_p(t), u_p(t))\| &= \|\sigma(\hat{x}_p(t), u_p(t)) + \sigma(0) - \sigma(0)\| \\ &\le \|\sigma(0)\| + \|\sigma(\hat{x}_p(t), u_p(t)) - \sigma(0)\| \\ &\le b_\sigma + L_\sigma \|\hat{x}_p(t) - 0\| \\ &\le b_\sigma + L_\sigma \sqrt{\|\hat{x}_p(t) - s(0)\|^2 + \|K_x\|^2 \|\hat{x}(t)\|^2} \\ &\le b_\sigma + \sqrt{L_\sigma^2 \|\hat{x}(t)\|^2 + \|K_x\|^2 \|\hat{x}(t)\|^2} \\ &\le b_\sigma + \sqrt{L_\sigma^2 + \|K_x\|^2} \|\hat{x}(t)\|. \end{aligned} \tag{50}$$

Furthermore, since A_m is Hurwitz and $r(t)$ is bounded in (38), there exist constants ζ_1 and ζ_2 such that $\|\hat{x}(t)\| \le \zeta_1 + \zeta_2 \|y_s(t) - \hat{y}(t)\|$ holds (Lavretsky 2010), where this yields

$$\| \hat{x}(t) \| \leq \frac{1}{2\gamma_y} \| C \| \, \| \tilde{x}(t) \| . \tag{51}$$

Finally, using (51) in (50) gives

$$\begin{aligned} \| \sigma(\hat{x}(t), u(t)) \| &\leq b + \sqrt{L_\sigma^2 \| K \|^2 (\zeta_x + \zeta_y \| C \|)^2} \, \| \tilde{x}(t) \| \\ &= b_0 + b_1 \| \tilde{x}(t) \|, \end{aligned} \tag{52}$$

where $b_0 = b_\sigma + \sqrt{L_\sigma^2 \| K \|^2} \, \zeta_x \| K \|$, $b_1 = \sqrt{L_\sigma^2 \| K \|^2} \, \zeta_y \| C \|$, and $b = \sqrt{\zeta_x^2 + \zeta_y^2 \| C \|^2} \, \| K \|$.

Noting that $\lambda_{\min}(P) \geq \lambda_{\min}(P) > 0$ (Lavretsky and Wise 2012) and using the bounds given by (49) and (52) in (48), one can write

$$\begin{aligned} \dot{V}(\tilde{x}(t), \tilde{W}(t), \hat{e}(t)) &\leq -\left(1 + \frac{1}{\gamma_y}\right) \lambda_{\min}(R^{-1}) \, \lambda_{\min}(Q) \, \| \tilde{x}(t) \|^2 - \left(1 - \lambda_{\max}(P)\right) \\ &\quad \| C \|^2 \, \| \tilde{x}(t) \|^2 - \lambda_{\min}(P) \left(\frac{1}{\gamma_y}\right) \| B \|^2 \end{aligned}$$

$$\dot{V} \le -\|\tilde{x}(t)\|^2 \underline{\sigma}(Q) + 2\eta\lambda_{\max}(\tilde{P})\|\tilde{x}(t)\|^2 + 2K_2 v\|\Lambda\|\,\|\tilde{W}\|(b_0 + b_1\|\tilde{x}(t)\|)\,\|\tilde{x}(t)\|$$

$$+ 2\|\tilde{P}B\|\|\Lambda\|K\|\tilde{x}(t)\|^2 + 2\|\tilde{P}\|\|L\|\|\tilde{x}\| + 2\|\tilde{P}B\|\|\Lambda\|\|\tilde{x}\|$$

$$\pm 2\lambda_{\max}(R^{-1})\|ZS^{\mathrm{T}}\|\,\|\Lambda\|\,\|\tilde{W}\|(b_0 + b_1\|\tilde{x}(t)\|) - \beta(\lambda_{\min}(Q) - \lambda_{\max}(R^{-1})\|PB\|^2)\|\hat{e}^{\mathrm{T}}(t)\|^2 + 2\beta\|\hat{e}(t)\|\,\|PLC\|\,\|\tilde{x}(t)\| + 2\beta\|P\|\,\|L\|\,\|\hat{e}(t)\|$$

$$= -\left(1 + \frac{1}{2\eta\lambda_{\min}(\tilde{P})}\right)\lambda_{\min}(Q)\|\tilde{x}(t)\|^2 - \left(\frac{1}{2\eta\lambda_{\min}(\tilde{P})} - 1\right)\|C\|^2 + \lambda_{\max}(R)\|B\|^2\lambda_{\max}(\tilde{P})\left(1 + \frac{1}{2\eta\lambda_{\min}(\tilde{P})}\right) + \lambda_{\max}(\tilde{P})$$

$$- 2K_2 v\|\Lambda\|\,\|\tilde{W}\|\left(b_0 - 2\|\tilde{P}B\|\|\Lambda\|K\|\tilde{x}(t)\|^2 - b_1\right)$$

$$+ \left[2K_2 v\|\Lambda\|\,\|\tilde{W}\|(b_0 + 2\|\tilde{P}\|\|L\| + 2\|\tilde{P}B\|\|\Lambda\| + 2\lambda_{\max}(R^{-1})\|ZS^{\mathrm{T}}\|\,\|\Lambda\|\,\|\tilde{W}(t)\|\right]b_1\|\tilde{x}(t)\|$$

$$\le -\underline{\sigma}(Q)\|\tilde{x}(t)\|^2 - (R^{-1})\|PB\|^2)\|\hat{e}(t)\|^2 + 2\beta\|\hat{e}(t)\|\,\|PLC\|\,\|\tilde{x}(t)\|$$

$$+ 2\beta\|P\|\,\|L\|\,\|\hat{e}(t)\| + 2\lambda_{\max}(R^{-1})\|ZS^{\mathrm{T}}\|\,(b_0 + b_1\|\tilde{x}(t)\|)\,\|\Lambda\|\,\|\tilde{W}(t)\|. \quad (53)$$

Moreover, consider $2xy \le \alpha x^2 + \frac{1}{\alpha}y^2$ that follows from Young's inequality (Bernstein 2009) applied to scalars in $x \in \mathbb{R}$ and $y \in \mathbb{R}$, where $\alpha \in \mathbb{R}$. Using this inequality for the $2\beta\|\hat{e}(t)\|\,\|PLC\|\,\|\tilde{x}(t)\|$ term in (53) yields

$$\dot{\Box}(\tilde{x}(t), \tilde{W}(t), \hat{e}(t))$$

$$\leq -\left[\left(1+\frac{1}{\quad}\right)\lambda \quad (R - (Q)\lambda^2 \quad (\tilde{P}) + \left(1+(\tilde{P})\right) + (\tilde{P})\right.$$
$$\left.1)\,\|C\|^2 + \lambda \quad \frac{1}{\quad})\|B\|^2 \lambda^2 \quad 2\eta\lambda\right.$$

$$v \;\min \quad \text{F} \quad 0 \;\min \quad \text{F} \quad s \quad \min \quad \min 0$$
$$0 \qquad\qquad 0 \qquad\qquad\quad 0$$
$$\min$$

$$-2K\,v\|\Lambda\|\,\|\tilde{W}\|\,b_v - 2\,\|\tilde{P}_g\,B\|\,\|\Lambda\|\,K\,\left]\|\tilde{x}(t)\|^2 + b_y\Box\right)$$
$$+\left[2K\,v\|\Lambda\|\,\|\tilde{W}\|\,(b\right.$$
$$+ 2\|\tilde{P}\|\,\|L\|\,\Box + 2\,\|\tilde{P}B\|\,\|\quad (R_1^{-2})\,\|ZS^{\mathrm{T}}\|\,\|\Lambda\|\,\|\tilde{W}(t)\|\;b\,\left]\tilde{}\right.$$
$$\Lambda\|\,\Box + 2\Box\lambda \qquad\qquad\qquad\qquad\qquad\qquad\qquad\qquad\qquad\qquad \|\tilde{x}(t)\|$$

$$v\,\text{F}\;v\,\text{F} \quad v \quad \text{F} \quad \min \quad \text{F} \quad \text{F} \quad \text{F}\;3$$
$$y \qquad\qquad\quad \text{F} \quad 0 \qquad\qquad\quad \beta^2$$
$$u$$

$$\bar{\beta}(\lambda \quad (Q) - \quad (R^{-1})\|PB\|^2\,)\|\quad \hat{e}(t)\|^2 \quad + \quad \|\hat{e}(t)\|^2$$
$$\min \qquad \max \qquad\qquad \text{F} \quad 2_1 \quad v\;\text{F} \quad 2\;\alpha \quad 2$$
$$\hat{e}(t)\|^2 + 2\Box\lambda \qquad\qquad\qquad\qquad\qquad\qquad \|\tilde{W}(t)\|$$
$$+ 2\beta\|P\|\,\|L\|\,\Box\,\|\quad (R^{-2})\|ZS^{\mathrm{T}}\|\,\|\Lambda\|\,(b + b\,\Box)$$
$$\text{F}\;v\,\text{F} \qquad 0 \qquad\qquad\quad \text{F} \quad \text{F} \quad \text{F}\;1 \quad 2\;y$$
$$y \qquad\qquad\quad \min$$

$$= -\left[\left(1+\frac{1}{\quad}\right)\lambda \quad (R - (Q)\lambda^2 \quad (\tilde{P}) + \left(1+(\tilde{P})\right) + (\tilde{P})\right.$$
$$\left.1)\,\|C\|^2 + \lambda \quad \frac{1}{\quad})\|B\|^2 \lambda^2 \quad 2\eta\lambda\right.$$

$$v \;\min \quad \text{F} \quad 0 \;\min \quad \text{F} \quad s \quad \min \quad \min 0$$
$$0 \qquad\qquad 0 \qquad\qquad\quad 0$$
$$\min$$

$$-2K\,v\|\Lambda\|\,\|\tilde{W}\|\,b_v - 2\,\|\tilde{P}_g\,B\|\,\|\Lambda\|_v K - \alpha\|PL\,C\|_{\text{F}}^2\,\left]\|\tilde{x}(t)\|_{\text{F}}^2 + \left[2K\right.\right.$$
$$v\|\Lambda\|\,\|\tilde{W}\|\,(b \qquad\qquad\qquad\qquad\qquad\qquad\qquad\qquad\qquad\

$$\dot{V} \le -\left(\lambda_{\min}(Q) - \frac{1}{\beta}\lambda_{\max}(R^{-1})\|PB\|^2\right)\|\tilde{x}(t)\|^2 - \left(\beta\lambda_{\min}(R) - \frac{\beta^2}{\alpha}\right)\|\hat{e}(t)\|^2 + 2\beta\|P\|\,\|L\|\,\|\tilde{x}(t)\|\,\|\hat{e}(t)\| + 2\|\Lambda\|\,\|Z S^{T}\|\,\|\tilde{W}(t)\|\,(b_M + b_0)$$

$$\le -d_1\|\tilde{x}(t)\|^2 - d_2\|\hat{e}(t)\|^2 + d_3\|\tilde{x}(t)\|\,\|\hat{e}(t)\| + d_4\|\tilde{x}(t)\| + d_5\|\hat{e}(t)\| + d_6 \qquad (54)$$

where $d_1 = \left(1 - \frac{1}{\eta}\right)\lambda_{\min}(Q) - \lambda^2\|C\|^2 - \lambda^{-1}\|B\|^2\lambda_{\max}(\tilde{P}) - \left(1 - \frac{1}{\eta}\right)\lambda_{\min}(\tilde{P}) - 2\eta\lambda$

$$d_2 = \beta\lambda_{\min}(R) - \frac{\beta^2}{\alpha} - \frac{1}{\beta}\lambda_{\max}(R^{-1})\|PB\|^2 - \alpha\|PL\,C\|^2 \in \mathbb{R},\ d_3 = 2K_v\|\Lambda\| + 2\|\tilde{P}B\|\,\|L\| + 2\|\tilde{P}B\|\,\|\Lambda\|K_v,$$

$$d_4 = 2\|\tilde{P}B\|\,\|\Lambda\|\,\|\tilde{w}^*\|(b_M + b_0) + 2\|\tilde{P}B\|\,\|\Lambda\|\,b_0,\ d_5 = 2\|\tilde{P}B\|\,\|\Lambda\|\,\|\tilde{w}^*\|(b_M + b_0),$$

$$d_6 = 2\|\tilde{P}B\|\,\|\Lambda\|\,\|\tilde{w}^*\|b_0 + \frac{\beta^2}{4\alpha}\|\tilde{P}B\|^2\|\Lambda\|^2\|\tilde{w}^*\|^2(b_M + b_0)^2 + \frac{\beta^2}{4\alpha}\|\tilde{P}B\|^2\|\Lambda\|^2\|\tilde{w}^*\|^2 b_0^2 + \frac{\beta}{4}\|\tilde{P}B\|^2\|\Lambda\|^2\|\tilde{w}^*\|^2 b_0^2 + \frac{\beta}{4}\|\tilde{P}B\|^2\|\Lambda\|^2\|\tilde{w}^*\|^2(b_M + b_0)

$2\lambda_{\min}(R^{-\frac{1}{2}})\|ZS^{\mathrm{T}}\|\|\Lambda\|$, $\bar{d}_2 = 2\beta\|P\|\|L\|$, and $(R^{-\frac{1}{2}})\|ZS^{\mathrm{T}}\|\|\Lambda\|$ $\|\tilde{W}^*\| + b$) with $\|\tilde{W}^*\| \le \|W(t)\|$ due to utilizing the projection operator in the weight update law given by (37).

Finally, we rearrange (54) as

$$\dot{V}(\tilde{x}(t), \tilde{W}(t), \hat{e}(t)) \le -\left(\sqrt{d_1}\|\tilde{x}(t)\| - \frac{\bar{d}_1}{\sqrt{d_1}}\right)^2 - \sqrt{d_2}\left\|\hat{e}(t) - \frac{\bar{d}_2}{\sqrt{d_2}}\right\|^2 + \frac{\bar{d}_1^2}{4d_1} + \frac{\bar{d}_2^2}{4d_2} \tag{55}$$

which shows that $\dot{V}(x(t), W(t), e(t)) \le 0$ when $\|x(t)\| \ge \psi_1$ and $\|\hat{e}(t)\| \ge \psi_2$, where

$$\psi_1 = \frac{\frac{\bar{d}_3}{2\sqrt{d_1}} + \sqrt{\frac{\bar{d}_3^2}{4d_1} + \frac{\bar{d}_4^2}{4d_2}}}{\sqrt{d_1}} \tag{56}$$

$$\psi_2 = \frac{\frac{\bar{d}_4}{2\sqrt{d_2}} + \sqrt{\frac{\bar{d}_3^2}{4d_1} + \frac{\bar{d}_4^2}{4d_2}}}{\sqrt{d_2}} \tag{57}$$

This argument proves uniform ultimate boundedness of the closed-loop solution $(\tilde{x}(t), \tilde{W}(t), \hat{e}(t))$ for all initial conditions (Lavretsky and Wise 2012, Khalil 1996).

□

In the proof of Theorem 1, it is implicitly assumed that $d_1 \in \square_+$ and $d_2 \in \square$, which can be satisfied by suitable selection of the event-triggered output feedback adaptive controller design parameters. Although this theorem shows uniform ultimate boundedness of the closed-loop solution $(\tilde{x}(t), \tilde{W}(t), \hat{e}(t))$ for all initial conditions, it is of practical importance to compute the ultimate bound, which is given next.

Ultimate Bound Computation

For revealing the effect of user-defined thresholds and the event-triggered output feedback adaptive controller design parameters to the system performance, the next corollary presents a computation of the ultimate bound, which presents the second result of this chapter.

Corollary 1. Consider the uncertain dynamical system given by (33) and (34), the reference model given by (26) and (27), the state observer given by (38) and (39) with the state observer gain matrix in (19) along with (20), (21), and (22), and the feedback control law given by (11), (12), (14), and (37). In addition, let the data transmission from the uncertain dynamical system to the controller occur when $\bar{E}_1$ is true and the data transmission from the controller to the uncertain dynamical system occur when $E_2 \vee E_3$ is true. Then, the ultimate bound of the system error between the uncertain dynamical system and the reference model is given by

$$\|e(t)\| = \|x(t) - x(t)\| \leq \Phi \left[\lambda_{\min}^{-1}(\tilde{P}) + \beta^{-1}\lambda_{\min}^{-1}(P)\right]^{\frac{1}{2}}, \quad t \geq T, \tag{58}$$

where $\Phi = \left[\lambda_{\max}(\tilde{P})\psi_1^2 + \beta\lambda_{\max}(P)\psi_2^2 + \Gamma^{-1}\|\tilde{W}^*\|_F^2\,\|\Lambda\|\right]^{\frac{1}{2}}$.

Proof. It follows from the proof of Theorem 1 that $\dot{\mathcal{V}}(\tilde{x}(t), \tilde{W}(t), \hat{e}(t)) \leq 0$ outside the compact set given by $\mathcal{D} = \{(\tilde{x}(t), \hat{e}(t)) : \|\tilde{x}(t)\| \leq \psi_1\} \cap \{(\tilde{x}(t), \hat{e}(t)) : \|\hat{e}(t)\| \leq \psi_2\}$. That is, since $\mathcal{V}(\tilde{x}(t), \tilde{W}(t), \hat{e}(t))$ cannot grow outside $\mathcal{D}$, the evolution of $\mathcal{V}(\tilde{x}(t), \tilde{W}(t), \hat{e}(t))$ is upper bounded by

$$\begin{aligned}\mathcal{V}(\tilde{x}(t), \tilde{W}(t), \hat{e}(t)) &\leq \max_{(\tilde{x}(t),\hat{e}(t)) \in \mathcal{D}} \mathcal{V}(\tilde{x}(t), \tilde{W}(t), \hat{e}(t)) \\ &= \lambda_{\max}(\tilde{P})\psi_1^2 + \beta\lambda_{\max}(P)\psi_2^2 + \Gamma^{-1}\|\tilde{W}^*\|_F^2\,\|\Lambda\| \\ &= \Phi^2. \end{aligned} \tag{59}$$

It follows from $\tilde{x}^{\mathrm{T}}\tilde{P}\tilde{x} \leq \mathcal{V}(\tilde{x}, \tilde{W}, \hat{e})$ and $\beta\hat{e}^{\mathrm{T}}P\hat{e} \leq \mathcal{V}(\tilde{x}, \tilde{W}, \hat{e})$ that $\|\tilde{x}(t)\|^2 \leq \frac{\Phi^2}{\lambda_{\min}(\tilde{P})}$ and $\|\hat{e}(t)\|^2 \leq \frac{\Phi^2}{\beta\lambda_{\min}(P)}$. Finally, since $e(t) = x(t) - \hat{x}(t) + \hat{x}(t) - x(t)$, and hence, $\|e(t)\| \leq \|x(t) - \hat{x}(t)\| + \|\hat{x}(t) - x(t)\| = \|\tilde{x}\| + \|\hat{e}(t)\|$, the bound given by (58) follows.

To elucidate the effect of the user-defined thresholds and the event-triggered output feedback adaptive controller design parameters to the ultimate bound given by (58), let $A_r = -5$, $B = 1$, $C = 1$, $W = 1$, $R_0 = 1$, $R = 1$, $Q_0 = 1$, $Q = 1$, $\Lambda = 1$, $\alpha = 0.5$, and $\beta = 0.25$. In this case, Fig. 2 shows the effect of the variation in v and Γ on the system error bound for $\eta = 5$, $\mathcal{D}_y = 0.1$ and $\mathcal{D}_u = 0.1$. Specifically, one can conclude from this

figure that increasing Γ reduces the ultimate bound and the minimum value of this bound is obtained for $v = 0.35$. Figure 3 shows the effect of the variation in v and η on the system error bound for Γ = 100 and the same previously defined parameters. It is

evident from the figure, that increasing η increases the ultimate bound.

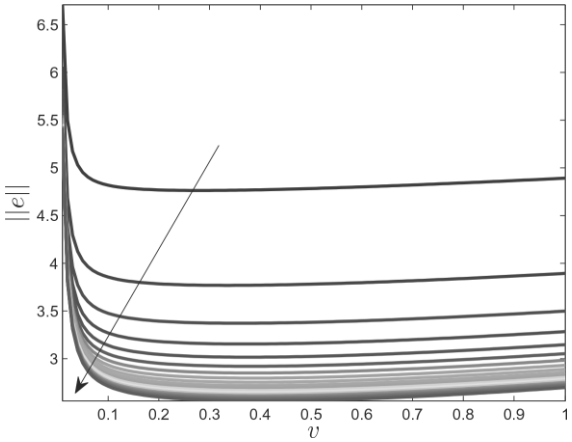


Figure 2. Effect of Γ □ [5,100] and v □ [0.01,1] to the ultimate bound y (58) for η = 5, □ = 0.1 and □ = 0.1, where the arrow indicates the increase in Γ (dashed line denotes the case with Γ = 100).

This figure also shows that there exists an optimum value of v for each η value, which allows the selection of the best value of v to avoid increasing the ultimate bound. Figures 4 and 5 show the effect of the variations in Δ_y and Δ_u, respectively. In particular, these figures show that the system error bound is more sensitive to the changes in the data transmission threshold from the physical system to the adaptive
controller (sensing threshold, Δ_y) than the data transmission threshold from the adaptive controller to the physical system (actuation threshold, Δ_u), which implies that the actuation threshold can be chosen large enough to reduce wireless network utilization between the physical system and the adaptive controller without sacrificing closed-loop dynamical system performance.

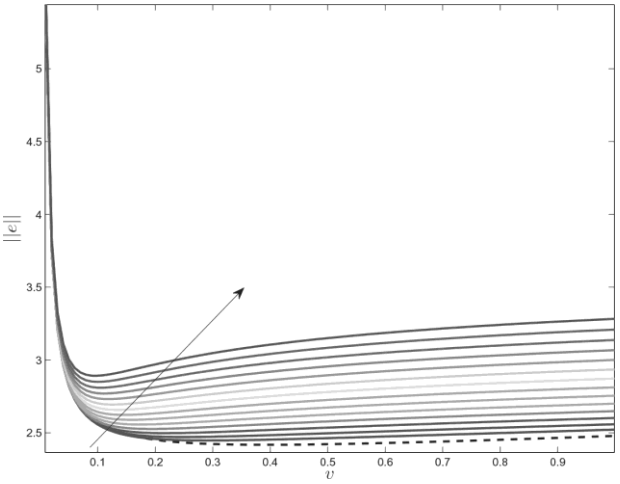


Figure 3. Effect of $\eta \in [5, 20]$ to the ultimate bound (58) for $\Delta = 0.1$, $\Delta = 0.1$, $v \in [0.0, 1]$ and $r = 100$, where the arrow indicates the increase in η (dashed line denotes the case with $\eta = 5$).

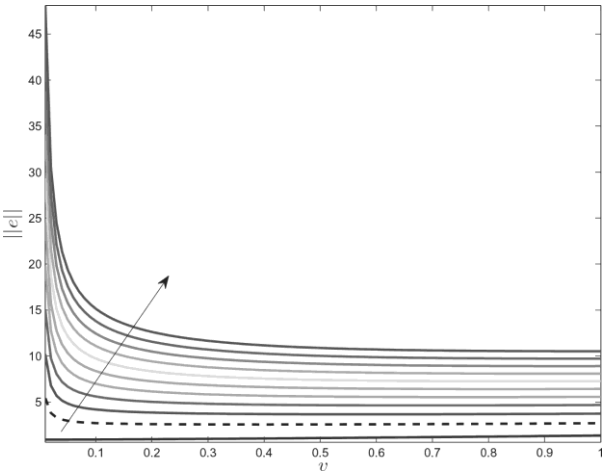


Figure 4. Effect of $\gamma_u \in [0, 1]$ to the ultimate bound (58) for $\eta = 5$, $\gamma_y = 0.1$, $v \in [0.01, 1]$, and $F = 100$, where the arrow indicates the increase in γ_y (dashed line denotes the case with $\gamma_y = 0.1$ and blue bottom line denotes the case with $\gamma_y = 0$).

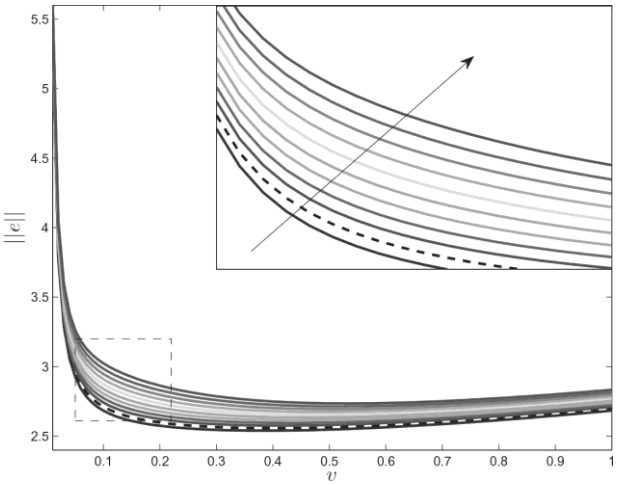


Figure 5. Effect of $\nu_u \in [0.1, 1]$ to the ultimate bound (58) for $\eta = 5$, $\nu = 0.1$, $v \in [0.01, 1]$, and $\Gamma = 100$, where the arrow indicates the increase in ν_u (dashed line denotes the case with $\nu_u = 0.1$).

Zeno Behavior Analysis

We now show that the proposed event-triggered output feedback adaptive control architecture does not yield to a Zeno behavior, which implies that it does not require a continuous two-way data exchange and reduces wireless network utilization. For the following corollary presenting the third result of this chapter, we consider $r^k \in (s_k, s_{k+1})$ to be the jth time instant when E_2 is violated over (s_k, s_{k+1}), and since $\{s_k\}_{k=1}^{\infty}$ is a subsequence of $\{r_j\}_{j=1}^{\infty}$, it follows that $\{r_j\}_{j=1}^{\infty} = \{s_k\}_{k=1}^{\infty} \cup \{r^k\}_{k=1}^{\infty}$, m_k, where $m \in \mathbb{N}$ is the number of violation times of E_2 over (s_k, s_{k+1}).

Corollary 2. Consider the uncertain dynamical system given by (33) and (34), the reference model given by (26) and (27), the state observer given by (38) and (39) with the state observer gain matrix in (19) along with (20), (21), and (22), and the feedback control law given by (11), (12), (14), and (37). In addition, let the data transmission from the uncertain dynamical system to the controller occur when E_1 is true and the

data transmission from the controller to the uncertain dynamical system occur when $E_2 \vee E_3$ is true. Then,

$$s_{k+1} - s_k > 0, \quad \forall k \in \mathbb{N}, \tag{60}$$

$$r^k_{i+1} - r^k_i > 0, \quad \forall i \in \{0, \ldots, m\}, \quad \forall k \in \mathbb{N}, \tag{61}$$

holds.

Proof. The time derivative of $\|x_S(t) - x(t)\|$ over $t \in (s_k, s_{k+1})$, $\forall k \in \mathbb{N}$, is given by

$$\begin{aligned}\frac{d}{dt}\|y_S(t) - y(t)\| \leq \|\dot{y}_S(t) - \dot{y}(t)\| &= \|C\dot{x}(t)\| \leq \|C\|_F \|x(t)\| \\ &\leq \|C\|_F \left[\|A\|_F \|x(t)\| + \|B\|_F \|\Lambda\|_F \|u_S(t)\| + \|B\|_F \|\Lambda\|_F \right. \\ &\quad \|W\|_F \|\sigma(x_p(t))\| \\ &\quad \left. + \|B_r\|_F \|r(t)\|\right].\end{aligned} \tag{62}$$

Now, we determine an upper bound for $||x(t)||$ in (62) as

$$||x(t)|| = ||\tilde{x}(t) + \hat{x}(t)|| \leq ||\tilde{x}(t)|| + ||\hat{x}(t)||$$
$$= \zeta_1 + \zeta_2 \zeta_3 + (1 + \zeta_4 ||C||)||\tilde{x}(t)||. \quad (63)$$

In addition, we determine an upper bound for $||\sigma(x_p(t))||$ in (62) as

$$||\sigma(x_p(t))|| = ||\sigma(x_p(t)) - \sigma(\hat{x}_p(t)) + \sigma(\hat{x}_p(t))||$$
$$\leq L_\sigma ||\tilde{x}_p(t)|| + ||\sigma(\hat{x}_p(t))||$$
$$\leq L_\sigma ||\tilde{x}_p(t)|| + ||\sigma(\hat{x}_p(t)) - \sigma(0)|| + ||\sigma(0)||$$
$$\leq L_\sigma ||\tilde{x}_p(t)|| + L_\sigma ||\hat{x}_p(t)|| + b$$
$$\leq L_\sigma ||\tilde{x}(t)|| + L_\sigma ||\hat{x}(t)|| + b$$
$$\leq L_\sigma ||\tilde{x}(t)|| + L_\sigma (\zeta_1 + \zeta_2 \zeta_3 + \zeta_4 ||C||_F ||\tilde{x}(t)||) + b$$
$$= L_\sigma (1 + \zeta_4 ||C||_F)||\tilde{x}(t)|| + L_\sigma (\zeta_1 + \zeta_2 \zeta_3) + b. \quad (64)$$

Substituting (63) and (64) into (62), gives

$$\frac{d}{dt}||y_s(t) - y(t)|| \leq ||C||_F \zeta_2 \zeta_3 + (1 + \zeta_4 ||C||_F)||\tilde{x}(t)|| + ||C||_F ||B||_F ||\Lambda||_{max} ||u_s(t)||$$
$$+ ||C||_F ||B||_F ||\Lambda||_{max} W [L_\sigma (1 + \zeta_4 ||C||_F)||\tilde{x}(t)|| + L_\sigma (\zeta_1 + \zeta_2 \zeta_3) + b]$$
$$+ ||C||_F ||B_r||_F ||r(t)||. \quad (65)$$

Since the closed-loop dynamical system is uniformly ultimately bounded by Theorem 1, there exists an upper bound to (65). Letting Φ_1 denote this upper bound and with the initial condition satisfying $\lim_{t \to s_k^+} ||y_s(t) - y(t)|| = 0$, it follows from (65) that

$$||y_s(t) - y(t)|| \leq \Phi_1 (t - s_k), \forall t \in (s_k, s_{k+1}). \quad (66)$$

Therefore, when E_1 is true, then $\lim_{t \to s_{k+1}^-} ||y_s(t) - y(t)|| = \delta_y$ and it then follows from (66) that $s_{k+1} - s_k \geq \Phi_1^{-1}(\delta_y)$.

Similarly, the time derivative of $||u_i(t) - u(t)||$ over $t \in (r^k, r^{k+1})$, $\forall i \in \mathbb{N}$, is given by

s d . . . . . i $i+1$

$$\frac{}{dt}\|u_S(t) - u(t)\| \le \|u_S(t) - u(t)\| = \|u(t)\| \le \|u_n(t)\| + \|u_a(t)\|. \quad (67)$$

Now, we determine an upper bound for $\|\dot{u}_n(t)\|$ in (67) as

$$\|u_n(t)\| = \int_x \|K\hat{x}(t)\|$$

$$\le \|K_x\|_F \dot{} \|\hat{x}(t)\|$$

$$\le \|K_X\|_F[\|A\|_F\|\hat{x}(t)\| + \|B\|_F\|u_n(t)\| + \|L_V\|_F\|y_S(t) - \hat{y}(t)\| + \|B_r\|_F\|r(t)\|]$$

$$\le \|K_X\|_F[\|A\|_F[\zeta_1 + \zeta_2 \square_y + \zeta_2\|C\|_F\|\tilde{x}(t)\|] + \|B\|_F\|u_n(t)\| + \|L_V\|_F\|C\|_F\|\tilde{x}(t)\|$$

$$+ \|L_V\|_F \square_y + \|B_r\|_F\|r(t)\|]. \quad (68)$$

Letting β_1 to denote the upper bound of $\|\dot{u}_n(t)\|$, we determine the upper bound of $\|\dot{u}_a(t)\|$ in (67) as

$$\begin{aligned}\|\dot{u}_a(t)\| &= \|\dot{\hat{W}}_p^T(t)\,\sigma(\hat{x}(t), u(t))_n + \hat{W}_p^T(t)\dot{\sigma}(\hat{x}(t), u(t))_n\| \\ &\le \|SZ^{-1}R^{-1}(\hat{y}(t) - y(t))_s\sigma_p^T(\hat{x}(t), u(t))_n\,\Gamma\sigma(\hat{x}(t), u(t))\| \\ &\quad + \|\hat{W}(t)\|_F[\|\dot{\sigma}(\hat{x}(t))\| + \|\dot{u}(t)\|] \\ &\le \lambda_{\max}(\Gamma)\|SZ^{-1}R^{-1}\|\,\|\sigma(\hat{x}(t), u(t))\|^2\Phi_0 + \|\hat{W}(t)\|_F[\sigma^* + \beta_1], \end{aligned} \tag{69}$$

where $\|\dot{\sigma}(\hat{x}(t))\| \le \sigma^*$. Substituting (68) and (69) into (67), gives

$$\frac{d}{dt}\|u_s(t) - u(t)\| \le \lambda_{\max}(\Gamma)\|SZ^{-1}R^{-1}\|\,\|\sigma(\hat{x}(t), u(t))\|^2\Phi_0 + \|\hat{W}(t)\|_F[\sigma^* + \beta_1] + \beta_1 \tag{70}$$

Once again, since the closed-loop dynamical system is uniformly ultimately bounded by Theorem 1, there exists an upper bound to (70). Letting Φ_2 denote this upper bound and with the initial condition satisfying $\lim_{t\to r_i^{k+}}\|u_s(t) - u(t)\| = 0$, it follows from (70) that

$$\|u_s(t) - u(t)\| \le \Phi_2(t - r_i^k), \quad \forall t \in [r_i^k, r_{i+1}^k). \tag{71}$$

Therefore, when $E_2 \vee E_3$ is true, then $\lim_{t\to r_{i+1}^{k-}}\|u_s(t) - u(t)\| = \varepsilon_u$ and it then follows from (71) that $r_{i+1}^k - r_i^k \ge \frac{\varepsilon_u}{\Phi_2}$.

Corollary 2 shows that the intersample times for the system output vector and feedback control vector are bounded away from zero, and hence, the proposed event-triggered adaptive control approach does not yield to a Zeno behavior.

ILLUSTRATIVE NUMERICAL EXAMPLE

In this section, the efficacy of the proposed event-triggered output feedback adaptive control approach is demonstrated in an illustrative numerical example. For this purpose, we consider the uncertain dynamical system given by

$$\begin{bmatrix} \dot{x}_{p1}(t) \\ \dot{x}_{p2}(t) \end{bmatrix} = \begin{bmatrix} 0 & 1 \\ 0 & 0 \end{bmatrix} \begin{bmatrix} x_{p1}(t) \\ x_{p2}(t) \end{bmatrix} + \begin{bmatrix} 0 \\ 1 \end{bmatrix} \Lambda [u(t) + \Delta(x(t))], \quad (72)$$

$$y_p(t) = \begin{bmatrix} 0.5 & 0 \end{bmatrix} \begin{bmatrix} x_{p1}(t) \\ x_{p2}(t) \end{bmatrix}, \; y_{reg}(t) = x_{p1}(t).$$

For this study, let the uncertain parameters be $\Lambda = 0.5$ and $W = [-2, 3]^T$, and we choose $\sigma(x_p(t)) = x_p(t)$ as the basis function.

For the nominal control design, we note

$$A = \begin{bmatrix} 0 & 1 \\ 0 & 0 \end{bmatrix}, \; B = \begin{bmatrix} 0 \\ 1 \end{bmatrix}, \; B_r = \begin{bmatrix} 0 \\ 1 \end{bmatrix},$$

$$= \begin{bmatrix} \\ -1 & 0 \end{bmatrix}$$

$$C = \begin{bmatrix} 1 & 0 & 0 \\ 0.5 & 0.5 & 0 \\ 0 & 0 & 1 \end{bmatrix}, C_{\text{Reg}} = [1\ 0\ 0]. \tag{73}$$

for (33) and (34). In particular, a linear quadratic regulator formulation is used to choose K_x of the nominal controller as

$$K_x = R_{\text{lqr}}^{-1} B^{\mathrm{T}} P, \tag{74}$$

$$0 = (A + \eta_{\text{lqr}} I_{n\times n})^{\mathrm{T}} P + P (A + \eta_{\text{lqr}} I_{n\times n}) - P B R_{\text{lqr}}^{-1} B^{\mathrm{T}} P + Q_{\text{lqr}}, \tag{75}$$

where $Q_{\text{lqr}} = \text{diag}([20, 3, 1])$, $R_{\text{lqr}} = 0.5$, and $\eta_{\text{lqr}} = 0.2$ is considered, which yields $K_x = [9.6, 5.2 -3.6]$. Next, for the adaptive control design, we choose

$$B_2 = \begin{bmatrix} 1 & 0 \\ 0 & 1 \\ 1 & 0 \end{bmatrix}, \tag{76}$$

to square up the dynamical system [21], which results in

$$B_{\text{s}} = \begin{bmatrix} 1 & 1 & 0 \\ 0 & 0 & 1 \end{bmatrix}. \tag{77}$$

In particular, with (77), $\det(CB_{\text{s}})$ is nonzero and $G(s) = C(sI_{n\times n} - A)^{-1} B$ is minimum phase. To calculate the observer gain L_V given by (19), we set $Q_0 = I$, $R_0 = 30I$, $\eta = 10$, and $v = 0.1$ for (20), (21), and (22), which yields

$$L_v = \begin{bmatrix} 0.72 & 39.84 & -0.48 \\ 20.24 & -18.79 & -0.97 \\ -0.97 & 0.01 & 20.16 \end{bmatrix} \quad (78)$$

Finally, note that $d_1 \in \mathbb{R}_+$ and $d_2 \in \mathbb{R}_+$ for $\alpha = 1$ and $\beta = 1$.

Figure 6 presents the results with the proposed event-triggered output feedback adaptive control approach when $\mu_y = 0.3$, and $\mu_u = 0.3$ are chosen, where the output of the uncertain dynamical system achieves a good command following performance. In Figs. 7 and 8, we fix μ_y to 0.3 and change μ_u to 0.1 and 0.5, respectively. As expected from the proposed theory, the variation on μ_u does not alter the command following performance significantly. In addition, in Figs. 9 and 10, we fix μ_u to 0.3 and change μ_y to 0.1 and 0.5, respectively, where it can be seen that the variation on μ_y alters the command following performance more than the variation in μ_u, as discussed earlier in this chapter. Finally, output and control event triggers for the cases in Figs. 6–10 are given in Fig. 11, where it can be seen that increasing μ_y (respectively, μ_u) yields less output event triggers when μ_u (respectively, less control event triggers when μ_y) is fixed, which reduces network utilization.

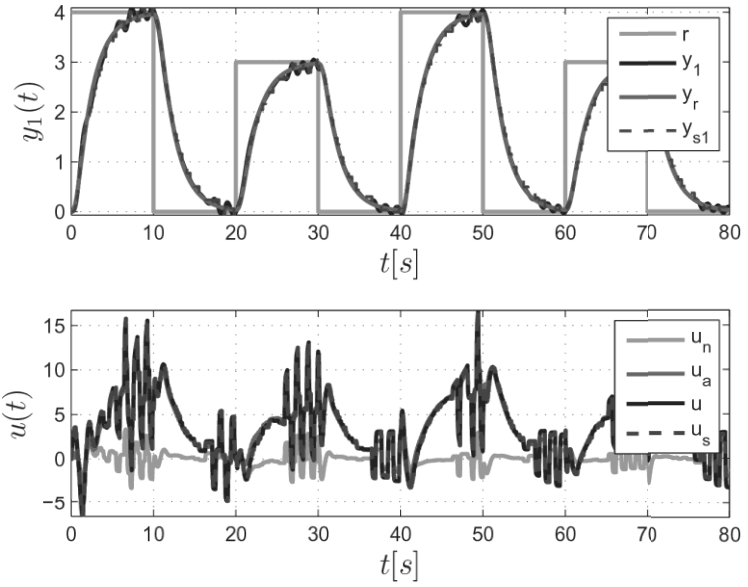


Figure 6. Command following performance for the proposed event-triggered output feedback adaptive control approach with $\Gamma = 50I$, $\square_y = 0.3$, and $\square_u = 0.3$.

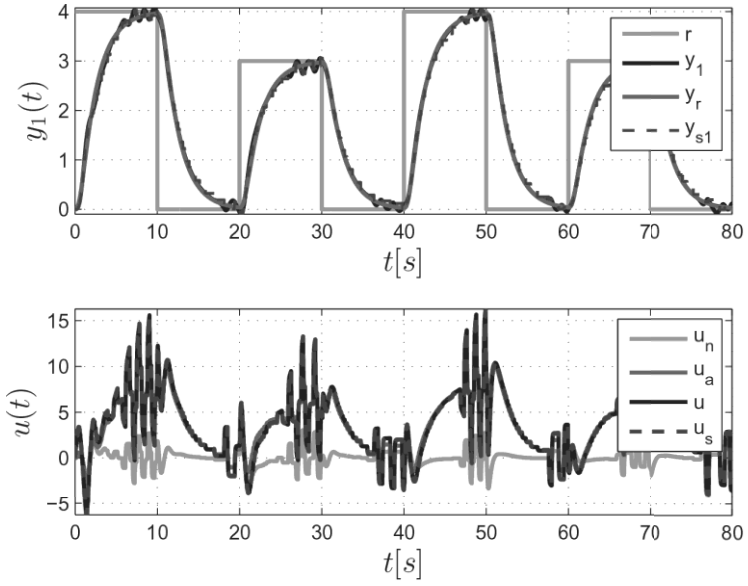


Figure 7. Command following performance for the proposed event-triggered output feedback adaptive control approach with $\Gamma = 50I$, $\sigma_y = 0.3$, and $\sigma_u = 0.1$.

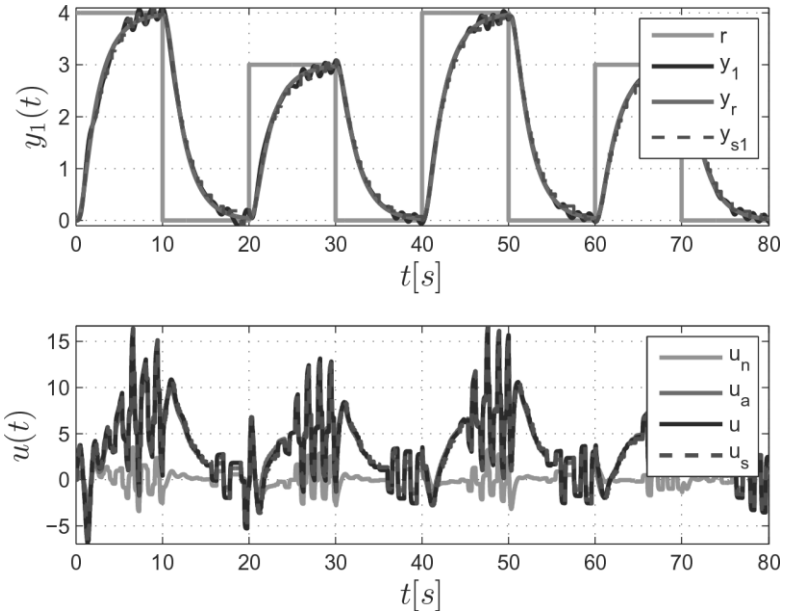


Figure 8. Command following performance for the proposed event-triggered output feedback adaptive control approach with Γ = 50*1,* $\square_y$ = 0.3, and $\square_u$ = 0.5.

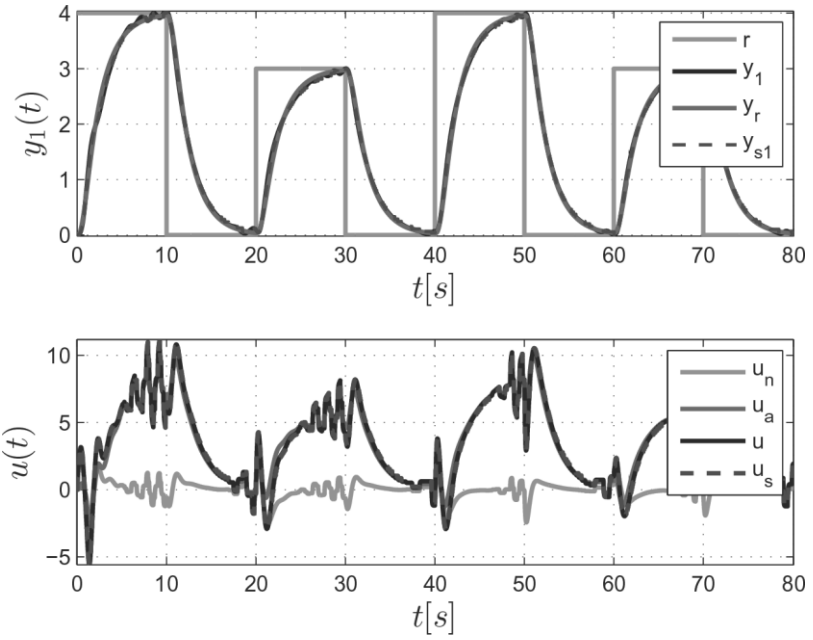


Figure 9. Command following performance for the proposed event-triggered output feedback adaptive control approach with Γ = 50*1,* $\square_y$ = 0.1, and $\square_u$ = 0.3.

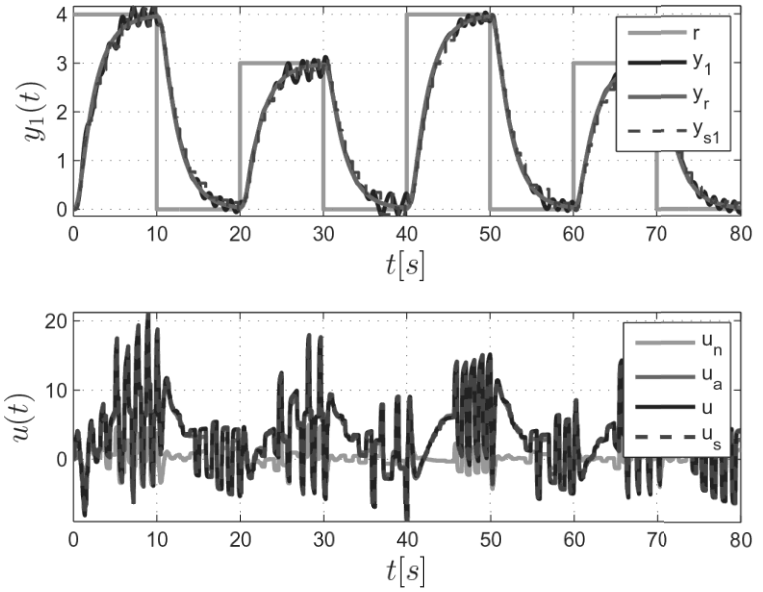


Figure 10. Command following performance for the proposed event-triggered output feedback adaptive control approach with $\Gamma = 50I$, $\varepsilon_y = 0.5$, and $\varepsilon_u = 0.3$.

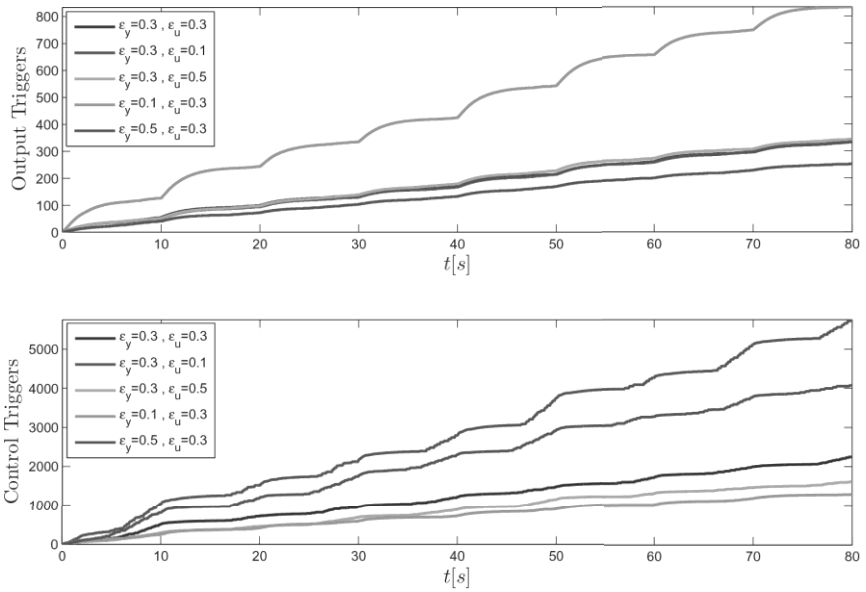


Figure 11. Output and control event triggers for the cases in Figs.

7–10.

CONCLUSION

A critical task in the design and implementation of networked control systems is to guarantee system stability while reducing wireless network utilization and achieving a given system performance in the presence of system uncertainties. Motivating from this standpoint, design and analysis of an event-triggered output feedback adaptive control methodology was presented for a class of uncertain dynamical systems in the presence of two-way data exchange between the physical system and the proposed controller over a wireless network. Specifically, we showed using tools and methods from nonlinear systems theory and Lyapunov stability in particular that the proposed feedback control approach guarantees system stability in the presence of system uncertainties. In addition, we characterized and discussed the effect of user-defined thresholds and output feedback adaptive controller design parameters to the system performance and showed that the proposed methodology does not yield to a Zeno behavior. Finally, we illustrated the efficacy of the proposed adaptive control approach in a numerical example.

REFERENCES

Albattat, A., B. C. Gruenwald and T. Yucelen. 2015. Event-triggered adaptive control, in ASME 2015 Dynamic Systems and Control Conference. American Society of Mechanical Engineers.

Alur, R., K. -E. Arzen, J. Baillieul, T. Henzinger, D. Hristu-Varsakelis and W. S. Levine. 2007. Hand- book of networked and embedded control systems. Springer Science & Business.

Astrom, K. J. and B. Wittenmark. 2013. Adaptive Control. Courier Corporation.

Bemporad, A., M. Heemels and M. Johansson. 2010. Networked Control Systems. Springer. Bernstein, D. S. 2009. Matrix mathematics: Theory, Facts, and Formulas. Princeton University Press.

Burg, T., D. Dawson and P. Vedagarbha. 1997. A redesigned dcal controller without velocity measurements: theory and

demonstration. Robotica, 15(03): 337–346.

Calise, A. J., N. Hovakimyan and M. Idan. 2001. Adaptive output feedback control of nonlinear systems using neural networks. Automatica, 37(8): 1201–1211.

Gibson, T. E., Z. Qu, A. M. Annaswamy and E. Lavretsky. 2014. Adaptive output feedback based on closed-loop reference models. arXiv preprint arXiv: 1410.1944.

Heemels, W., K. H. Johansson and P. Tabuada. 2012. An introduction to event-triggered and self- triggered control. pp. 3270–3285. *In*: Decision and Control (CDC), 2012 IEEE 51st Annual Conference on. IEEE.

Hespanha, J. P., P. Naghshtabrizi and Y. Xu. 2007. A survey of recent results in networked control systems. Proceedings of the IEEE, 95(1): 138–162.

Hovakimyan, N., F. Nardi, A. Calise and N. Kim. 2002. Adaptive output feedback control of uncertain nonlinear systems using single-hidden-layer neural networks. Neural Networks, IEEE Transactions on, 13(6): 1420–1431.

Ioannou, P. A. and J. Sun. 2012. Robust adaptive control. Courier Corporation.

Kaneko, K. and R. Horowitz. 1997. Repetitive and adaptive control of robot manipulators with velocity estimation. Robotics and Automation, IEEE Transactions on, 13(2): 204–217.

Kevorkian, J. and J. D. Cole. 1996. Multiple Scale and Singular Perturbation Methods. Springer- Verlag New York.

Khalil, H. K. 1996. Adaptive output feedback control of nonlinear systems represented by input-output models. Automatic Control, IEEE Transactions on, 41(2): 177–188.

Khalil, H. K. 1996. Nonlinear Systems. Upper Saddle River, NJ: Prentice Hall.

Kim, K., A. J. Calise, T. Yucelen and N. Nguyen. 2011a. Adaptive output feedback control for an aeroelastic generic transport model: A parameter dependent Riccati equation approach, in AIAA Guidance. Navigation and Control Conference.

Kim, K., T. Yucelen and A. J. Calise. 2011b. A parameter dependent Riccati equation approach to output feedback adaptive control. *In*: AIAA Guidance, Navigation and Control Conference.

Kim, Y. H. and F. L. Lewis. 1999. Neural network output feedback control of robot manipulators.
Robotics and Automation, IEEE Transactions on,
15(2): 301–309.

Krstic, M., P. V. Kokotovic and I. Kanellakopoulos. 1995. Nonlinear and Adaptive Control Design.
John Wiley & Sons, Inc.
Lavretsky, E. and K. Wise. 2012. Robust and Adaptive Control: With Aerospace Applications.
Springer.
Lavretsky, E. 2010. Adaptive output feedback design using asymptotic properties of lqg/ltr controllers.
AIAA Guidance, Navigation, and Control Conference.
Lavretsky, E. 2012. Adaptive output feedback design using asymptotic properties of LQG/LT controllers. Automatic Control, IEEE Transactions on, 57(6): 1587–1591.
Lavretsky, E. 2015. Transients in output feedback adaptive systems with observer-like reference models. International Journal of Adaptive Control and Signal Processing, 29(12): 1515–1525.
Lavretsky, E., T. E. Gibson and A. M. Annaswamy. 2011. Projection operator in adaptive systems. Lunze, J. and D. Lehmann. 2010. A state-feedback approach to event-based control. Automatica,
46(1): 211–215.
Mazo, Jr. M. and P. Tabuada. 2008. On event-triggered and self-triggered control over sensor/actuator networks. pp. 435–440. *In*: Decision and Control, 2008. CDC 2008. 47th IEEE Conference on. IEEE.
Mazo, Jr. M., A. Anta and P. Tabuada. 2009. On self-triggered control for linear systems: Guarantees and complexity. pp. 3767–3772. *In*: Control Conference (ECC), 2009 European. IEEE.
Murray, J. D. 1984. Asymptotic Analysis. Springer-Verlag New York.
Narendra, K. S. and A. M. Annaswamy. 2012. Stable Adaptive Systems. Courier Corporation.
Pomet, J. -B. and L. Praly. 1992. Adaptive nonlinear regulation: estimation from the Lyapunov equation. IEEE Transactions on Automatic Control, 37(6): 729–740.
Postoyan, R., A. Anta, D. Nesic and P. Tabuada. 2011. A unifying lyapunov-based framework for the event-triggered control of nonlinear systems. pp. 2559–2564. *In*: Decision and Control and European Control Conference

(CDC-ECC), 2011 50th IEEE Conference on. IEEE.
Sahoo, A., H. Xu and S. Jagannathan. 2013. Neural network-based adaptive event-triggered control of nonlinear continuous-time systems. IEEE International Symposium on Intelligent Control, pp. 35–40.
Sahoo, A. H. Xu and S. Jagannathan. 2014. Neural network approximation-based event-triggered control of uncertain MIMO nonlinear discrete time systems. IEEE American Control Conference, pp. 2017–2022.
Slotine, J. -J. E. and W. Li. 1987. On the adaptive control of robot manipulators. The International Journal of Robotics Research, 6(3): 49–59.
Tabuada, P. 2007. Event-triggered real-time scheduling of stabilizing control tasks. Automatic Control, IEEE Transactions on, 52(9): 1680–1685.
Tipsuwan, Y. and M. -Y. Chow. 2003. Control methodologies in networked control systems. Control Engineering Practice, 11(10): 1099–1111.
Volyanskyy, K. Y., W. M. Haddad and A. J. Calise. 2009. A new neuroadaptive control architecture for nonlinear uncertain dynamical systems: Beyond-and-modifications. IEEE Transactions on Neural Networks, 20(11): 1707–1723.
Walsh, G. C. and H. Ye. 2001. Scheduling of networked control systems. Control Systems, IEEE, 21(1): 57–65.
Wang, F. -Y. and D. Liu. 2008. Networked control systems. Springer.
Wang, X. and N. Hovakimyan. 2010. *L*1 adaptive control of event-triggered networked systems. IEEE American Control Conference, pp. 2458–2463.
Wang, X., E. Kharisov and N. Hovakimyan. 2015. Real-time *L*1 adaptive control for uncertain networked control systems. IEEE Transactions on Automatic Control, 60(9): 2500–2505.
Yesildirek, A. and F. L. Lewis. 1995. Feedback linearization using neural networks. Automatica, 31(11): 1659–1664.
Yucelen, T. and W. M. Haddad. 2012. Output feedback adaptive stabilization and command following for minimum phase dynamical systems with unmatched uncertainties and disturbances. International Journal of Control, 85(6): 706–721.

Zergeroglu, E., W. Dixon, D. Haste and D. Dawson. 1999. A composite adaptive output feedback tracking controller for robotic manipulators. Robotica, 17(06): 591–600.

Zhang, L. and D. Hristu-Varsakelis. 2006. Communication and control co-design for networked control systems. Automatica, 42(6): 953–958.

Zhang, F., D. M. Dawson, M. S. de Queiroz, W. E. Dixon et al. 2000. Global adaptive output feedback tracking control of robot manipulators. IEEE Transactions on Automatic Control, 45(6): 1203–1208.

Zhang, W., M. S. Branicky and S. M. Phillips. 1993. Stability of networked control systems. Control Systems, IEEE, 21(1): 84–99.

Zhou, K. and J. C. Doyle. 1998. Essentials of robust control. Prentice hall Upper Saddle River, NJ, Vol. 180.

Zhou, K., J. C. Doyle and K. Glover. 1996. Robust and optimal control. Prentice hall New Jersey, Vol. 40.

7

Event Sampled Adaptive Control of Robot Manipulators and Mobile Robot Formations

N. Vignesh, H. M. Guzey* and *S. Jagannathan*

ABSTRACT

In this chapter, the design of adaptive control of both robot manipulator and consensus-based formation of networked mobile robots in the presence of uncertain robot dynamics and with event-based feedback is presented. The linearity in the unknown parameter (LIP) property is utilized to represent the uncertain nonlinear dynamics of the robotic manipulator which is subsequently employed to generate the control torque with event-sampled measurement update. For the case of consensus-based formation control of mobile robots, by utilizing the LIP based representation of the robot dynamics, an adaptive back-stepping based controller with event-sampled feedback is designed. The networked robots communicate their location and velocity information with their neighbors which is ultimately utilized to derive the desired velocities to move the robots to a required consensus-based formation. The control torque is designed to minimize the velocity tracking error by explicitly taking into account the dynamics of the individual robot and by

relaxing the perfect velocity tracking assumption. The Lyapunov stability method is utilized in both the applications to develop an event-sampling condition and to demonstrate the tracking performance of the robot manipulator and consensus of the overall formation of the networked

Department of Electrical and Computer Engineering, Missouri University of Science and Technology,
Rolla, Missouri,
USA.
E-mail: vnxv4; hmgb79; sarangap@mst.edu
* Corresponding author

mobile robots. Finally, simulation results are presented to verify theoretical claims and to demonstrate the reduction in the computations with event-sampled control execution.

Keywords: Event-sampled control, adaptive consensus, mobile robot formations, LIP

INTRODUCTION

Traditional feedback control systems rely on the periodic sampling of the sensors and use this measurement to compute appropriate control input. However, such controllers may be computationally inefficient as the sampling instants are not based on the actual system state and are based on the worst-case analysis. Therefore, in the recent years, event-based sampling has become popular (Tabuada 2007, Sahoo et al. 2015, Zhong et al. 2014, Guinaldo et al. 2012, Wang and Lemmon 2012) wherein the execution time of the control inputs is based on the real-time operation of the system. In the event- sampled framework (Tabuada 2007, Sahoo et al. 2015, Zhong et al. 2014, Guinaldo et al. 2012, Wang and Lemmon 2012), the measured state vector is sampled based on certain state dependent criteria referred to as event-triggering condition and the controller is executed at these aperiodic sampling instants. The event-triggering condition is designed by taking into account the stability and closed-loop performance, and, hence, proven to be advantageous over its periodic counterpart.

Initially, the event-triggered techniques from the literature (Tabuada 2007, Guinaldo et al. 2012, Wang and Lemmon 2012) were designed for ensuring stable operation of the closed-loop system by assuming that a stabilizing controller exists for the system under consideration. Developing an event-triggering condition and establishing the existence of positive inter-event time with the proposed event-sampling condition was the main focus in these works (Tabuada 2007, Guinaldo et al. 2012, Wang and Lemmon 2012). The traditional optimal control problem under the event-sampled framework is studied in Molin and Hirche 2013 while in Sahoo et al.

2015, the event-sampled adaptive controller design was presented for physical systems with uncertain dynamics. In this chapter, an event-based adaptive controller design is covered for uncertain robotic systems–tracking control of robotic manipulator and adaptive consensus based formation control of mobile robots. The controller design for the robotic manipulators has been studied by several researchers (Lewis et al. 2003) over the past decade by using the traditional periodic feedback approach. The computed torque based controllers were originally popular as they converted the nonlinear dynamics of the robotic manipulator into linear dynamics. The filtered tracking error (Narendra and Annaswamy 2012) was defined to augment the tracking error and the linear controller was designed to stabilize the dynamics of this filtered tracking error. However, this controller required the complete knowledge of the manipulator dynamics. Later, adaptive controller which uses estimated values of the uncertain robot dynamics was presented. The uncertainties were assumed to satisfy linearity-in-the-unknown parameters (LIP) property and the uncertain parameters are adaptively estimated. With the parameter adaptation, the adaptive controllers are computationally intensive when compared to the traditional
PID controllers.

Due to the application in the manufacturing and process industry, the control problem for the robotic manipulators is still actively pursued (Cheah et al. 2015, He 2015a, He 2015b, Galicki 2015). The controllers use continuous feedback

information of the manipulator to generate the control torque, which are computationally inefficient. Especially, for the application in the manufacturing and process industry, the robot manipulators in large-numbers are used, which do not require periodic update in the control. Event-sampled implementation of the control of these robotic manipulators will significantly reduce the computational costs.

Therefore, in this chapter, an event-sampled adaptive control of robotic manipulator is presented. The uncertain dynamics of the robot manipulator are represented by utilizing the LIP property and the control torque is generated by using the event-sampled feedback information. The tracking performance of the robot manipulator is studied under the event-sampled implementation using Lyapunov stability theory.

Next, the event-based adaptive control of robotic manipulator is extended to the formation control of mobile robots which has been examined in several works by using various approaches including leader-follower control (Fierro and Lewis 1998, Hong et al. 2006), virtual structure (Low 2011) or behavior-based approaches (Balch and Arkin 1998), to name a few. Of all these approaches, consensus-based formation control (Ren et al. 2005b, Min et al. 2011, Semsar-Kazerooni and Khorasani 2009, Bauso et al. 2009, Tian and Liu 2008, Olfati-Saber and Murray 2004) is considered to be more robust and reliable due to scalability and its inherent properties that enable the robots to maintain their formation even if one of the robots experiences a failure.

In earlier works (Ren and Beard 2005a, Olfati-Saber and Murray 2004, Qu 2009, Bauso et al. 2009, Tian and Liu 2008, Sheng et al. 2012), consensus-based schemes have been studied for generalized linear systems with known system dynamics and applied to systems with time varying communication graphs (Ren and Beard 2005a), bounded disturbances (Bauso et al. 2009), and communication delays during state information sharing (Olfati-Saber and Murray 2004, Tian and Liu 2008). Further, the consensus- based optimal formation control scheme was also presented in Semsar-Kazerooni and Khorasani 2008.

Traditionally, adaptive controllers require more computations when compared to the PID controllers. Moreover, since the mobile robots use their neighbor information to reach consensus, they share information among each other through a communication network. Therefore, utilizing the communication network continuously will lead to higher communication cost and inefficient use of the communication resource. It may also lead to network congestion and undesired performance of the controller. Therefore, event-sampled execution of the controller in this case not only reduces computations, but also reduces the overhead in communication cost.

Motivated by the aforementioned challenges, an event-sampled adaptive consensus based formation control is proposed for mobile robots. The robots communicate their location and the velocity information with the neighborhood robots, which are used to obtain the consensus based formation errors. The formation errors are used to obtain the desired velocities for each robot which would drive the robots to a desired formation. These velocities are required to be tracked by each mobile robot. However, due to the robot dynamics, a velocity tracking error exists. Using the LIP-based representation of the mobile robot dynamics, the control inputs are obtained to minimize this velocity tracking error with event-sampled feedback. It is worth mentioning that the velocity tracking errors at each robot acts as a virtual controller for the formation error system. Thus using the back-stepping controller design, if the velocity tracking error is reduced, the formation error reduces and the robots reach a desired formation. It should to noted that, in contrast to the existing consensus based formation control approaches (Ren and

Beard 2005a, Olfati-Saber and Murray 2004, Qu 2009, Bauso et al. 2009, Tian and Liu 2008, Sheng et al. 2012), the dynamics of the mobile robot is explicitly taken into account, relaxing the perfect velocity tracking assumption.

For both the robotic systems, an adaptive event-sampling condition is required to determine the sampling instants to generate the feedback information in order to update the controllers. Since the unknown parameters are tuned at the event sampled instants, the computations are reduced when compared to traditional adaptive control schemes, but it introduces aperiodic parameter updates. Therefore, an event-sampling condition is derived using the stability conditions directly to ensure that the performance of the adaptive controller is not deteriorated due to the intermittent feedback. Finally, the extension of Lyapunov direct method is used to prove the local uniform ultimate boundedness (UUB) of the tracking errors and the parameter estimation error in each application with event-sampled feedback.

The contributions of this chapter include—(a) the design of novel event-based adaptive control of robotic manipulator and adaptive consensus based formation control of mobile robots; (b) development of novel event-sampling condition to determine the sampling instants and generate feedback signals for the controller; and (c) demonstration of stability of the robotic systems with the proposed event-sampled controller using Lyapunov stability theory.

In this chapter, R^n is used to denote n dimensional Euclidean space. Euclidean-norm is used for vectors and for matrices, Frobenius norm is used.

BACKGROUND AND PROBLEM FORMULATION

In this section, a brief background on the event-sampled control implementation is provided first. Later, the dynamics of the robotic systems are introduced and the event- based tracking control problem for the robotic manipulator is formulated. Finally, the adaptive consensus based formation control problem, with event-sampled feedback, for mobile robots is presented. Here the state vector is considered measurable for both the robot manipulator and mobile robot.

Event-sampled Control

The traditional periodic/continuous feedback based control problem is well-established in the literature and several techniques are available to analyze the performance of these controllers. However, the event sampled controller implementation is relatively new and involves many challenges. Here, the event-based control problem is introduced by highlighting the challenges involved in the design with respect to controller adaptation and system stability.

In an event sampled framework, the system state vector is sensed continuously and released to the controller only at the event sampled instants. To denote the sampling instants we define an increasing sequence of time instants $\{t_k\}_{k=1}^{\infty}$, referred to as event sampling instants $t_k \geq t_{k-1}$, $k = 1,2,\ldots$, and $t_0 = 0$, the initial sampling instant.

The sampled state $x(t_k)$, is released to the controller and the last sampled state at the controller denoted by $x(t)$ is updated. Then it is held by using a zero order hold (ZOH) at the controller until the next update and it is denoted as

$$\hat{x}(t) = x(t_k), t_k \le t < t_{k+1}, k = 1, 2, \ldots. \quad (1)$$

The error, $e_{ET}(t)$, introduced due to the event sampled state can be written as

$$e_{ET}(t) = \hat{x}(t) - x(t) = -x(t), \quad t_k \le t < t_{k+1}, \; k = 1, 2, \ldots, \quad (2)$$

where $e_{ET}(t)$ is referred to as event sampling error. Thus, the event sampling error is reset to zero with sampling and update in the state, that is, $e_{ET} = 0$, $t = t_k$, $k = 1,2,\cdots$.

For the event-triggered controllers, an event-sampling mechanism/condition is required to determine the sampling instants, without jeopardizing the system stability. Also, if the controller parameters are adaptive and learn from the feedback information, the parameter adaptation process is also dependent on the event-based sampling instants. Therefore, the event-sampling mechanism should be carefully designed so that event- based feedback does not impede the adaptation process of the controller as well.

Remark 1. In the inter-event period, the control input is held by a ZOH and hence the control policy is piecewise continuous. It can also be viewed as continuously updated signal driven by the event-sampled measurement errors given by (2).

Next, the dynamics of the robotic system will be presented first followed by the control problem formulation with event-sampled feedback.

Robot Manipulator Dynamics

The dynamics of an n-link robot manipulator can be expressed as (Lewis et al. 2003)

$$M(q)\ddot{q} + V_m(q, \dot{q})\dot{q} + G(q) + F(\dot{q}) = \tau_d(t) - \tau(t), \quad (3)$$

with $q(t) \in R^n$

. the joint variable vector, $M(q)$ the inertia matrix, $V(q,q)$ the Coriolis/centripetal matrix, $G(q)$ the gravity vector, and $F(q)$ the friction, $\tau_d(t)$ represents the unknown bounded disturbance, and $\tau(t)$ is the control torque, with appropriate dimensions. It should be noted that the robot manipulators of the form given by (3), satisfy certain properties. With the following assumptions, the tracking control problem is formulated next.

Assumption 1 (Lewis et al. 2003). The mass matrix $M(q)$ is a positive definite matrix and satisfies $B_m I \le M(q) \le B_M I$, with B_m , B_M being known positive constants, and Coriolis matrix $V_m(q, q)$ is bounded by $V_b \|q\|$ such that V_b is a constant. The gravity vector is bounded by $g_B > 0$ and the bound on the friction term is assumed to be of the form $B_F \|q\| + B_f$, such that B_F , B_f are positive constants. The matrix $M - 2V_m$ is skewsymmetric. The disturbance vector τ_d is bounded such that $\|\tau_d\| \le \tau_{dM}$, with τ_{dM} a known positive constant.

A nonlinear state space representation of the robot manipulator, which can be obtained with the joint angle and its velocity as state variables, is given by

$$\dot{q} = \begin{bmatrix} 0 & I \\ 0 & 0 \end{bmatrix} \begin{bmatrix} q \\ \dot{q} \end{bmatrix} + \begin{bmatrix} 0 \\ M^{-1}(q) \end{bmatrix} \tau(t) + \begin{bmatrix} 0 \\ M^{-1}(q) \end{bmatrix} d \tag{4}$$

$$\dot{q} = -M^{-1}(q)(V_m(q,\dot{q})\dot{q} + F(\dot{q}) + G(q)) + M^{-1}(q)\tau(t) + M^{-1}(q)\tau_d(t)$$

m

Assumption 2. The desired motion trajectory for the robotic manipulator $q_d(t) \in R^n$ is prescribed such that $||Q_d|| \leq q_B$, where $Q_d(t) = [q_d(t)\ \dot{q}_d(t)\ \ddot{q}_d(t)]^T$ and q_B is a known scalar bound.

Now, we can define the tracking error as

$$e(t) = q_d(t) - q(t) \tag{5}$$

and the filtered tracking error as (Lewis et al. 2003)

$$r(t) = \dot{e}(t) + \lambda e(t) \tag{6}$$

where λ is a symmetric, positive definite matrix of appropriate dimension.

Remark 2. It can be seen that choosing λ as a diagonal matrix with positive entries ensures that the $e(t)$ will be stable and $e(t)$ will remain bounded as long as the designed control torque $\tau(t)$ ensures that the filtered tracking error remain bounded.

On differentiating (6), the dynamics of the filtered tracking error can be obtained as $\dot{r}(t) = \ddot{e}(t) + \lambda \dot{e}(t)$. Using the robot manipulator dynamics (4) and the definition of the tracking error (5), we get the following filtered error dynamics (Lewis et al. 2003)

$$M\dot{r} = -V_m r - \tau + f(x) + \tau_d \tag{7}$$

where $f(x) = M(q)(\ddot{q}_d + \lambda \dot{e}) + V_m(q, \dot{q})(\dot{q}_d + \lambda e) + F(q) + G(q)$ and x is a vector that includes all the signals required to compute $f(.)$ and it is defined as $x = [e^T\ \dot{e}^T\ q_d^T\ \dot{q}_d^T\ \ddot{q}_d^T]^T$.

If the function $f(x)$ is known, it is straight-forward to generate a control torque such that the filtered tracking error dynamics in (7) are stable. However, it is important to note that the parameters in $f(x)$ are uncertain and tend to vary with time. This calls for the design of adaptive controllers, which are based on representing the uncertain function $f(x)$ using LIP property.

Assumption 3. The mass of each link, denoted by m_i, is considered unknown and the friction are considered negligible. The nonlinearity $f(x)$, is Lipschitz continuous function on a compact set, such that $||f(x) - f(y)|| \leq L_f ||x - y||$ and satisfies LIP (Khalil and Grizzle 1996).

Let us consider the dynamics of the two-link robot manipulator (Lewis et al. 2003) with

$$(m_1 + m_2)l_1^2 + m_2 l_2^2 + 2m_2 l_1 l_2 \cos q_2 \quad m_2 l_2^2 + m_2 l_1 l_2 \cos q_2$$

the following matrices, $M(q) = \begin{bmatrix} m_1 l_1^2 + m_2(l_1^2 + l_2^2 + 2l_1 l_2 \cos q_2) & m_2(l_2^2 + l_1 l_2 \cos q_2) \\ m_2(l_2^2 + l_1 l_2 \cos q_2) & m_2 l_2^2 \end{bmatrix}$,

with m_i being the mass of each robot link, l_i being the length of each link. $V(q, \dot{q}) = \begin{bmatrix} -m_2 l_1 l_2 (2\dot{q}_1 \dot{q}_2 + \dot{q}_2^2)\sin q_2 \\ m_2 l_1 l_2 \dot{q}_1^2 \sin q_2 \end{bmatrix}$ and $G(q) = \begin{bmatrix} (m_1 + m_2) g l_1 \cos q_1 + m_2 g l_2 \cos(q_1 + q_2) \\ m_2 g l_2 \cos(q_1 + q_2) \end{bmatrix}$ with g representing the acceleration due to gravity. With the dynamics in (3), the nonlinear function $f(x)$, with the masses m_1, m_2 considered uncertain, can be represented in the LIP form, such that (Lewis et al. 2003), $f(x) = \theta^T \phi(x)$, with $\theta = [m_1 \; m_2]^T$, being the uncertain parameters and the corresponding regression function $\phi(x) = \begin{bmatrix} \phi_1 & \phi_2 \\ \phi_3 & \phi_4 \end{bmatrix}$, where $\phi_1 = l_1^2 \ddot{q}_1 + l_1 g c_1$, $\phi_2 = 0$, $\phi_3 = l_1 l_2 c_{12}(\ddot{q}_1 + \ddot{q}_2) + l_1 l_2 s_{12}\dot{q}_1^2 + l_1 g c_{12} + l_1 g c_1$, and $\phi_4 = l_1 l_2 (\ddot{q}_1 + \ddot{q}_2) + l_1 l_2 s_2 \dot{q}_1^2 + l_2 g c_{12}$, s_1 represent $s_{12} = \sin(q_1 + q_2)$, c_1, s_2 cosine and sine functions of the parameter q_i, $c_{12} = \cos(q_1 + q_2)$.

Remark 3. For the robotic manipulator, the mass matrix changes with the object carried by the manipulator and it depends on the application.

For the robot manipulator, using the event-sampled state estimate $f(x)$, of the function $f(x)$, an adaptive control torque input can be generated as

$$\tau = \hat{f}(x_k, v_r) - K_v r_k, \quad t_k \le t < t_{k+1} \tag{8}$$

where K_v is a positive definite design matrix and $r(t) = \dot{e}_v(t) + \Lambda e_v(t)$, $t \in [t_k, t_{k+1})$. With the adaptive control (8), the filtered tracking-error dynamics become

$$M\dot{r} = -(V_m + K_v)r + \tilde{f}(x_k, v_r) + \varepsilon_{ET}(t), \quad t_k \le t < t_{k+1} \tag{9}$$

Defining the function estimation error as $\tilde{f}(x_k) = f(x_k) - \hat{f}(x_k)$, we get the filtered tracking error dynamics

$$M\dot{r} = -(V_m + K_v)r + \tilde{f}(x_k) + f(x) - f(x_k) + \varepsilon_{ET}(t), \quad t_k \le t < t_{k+1} \tag{10}$$

Here the filtered tracking error dynamics are driven by the function estimation and the event sampled measurement errors. The LIP property of the robotic manipulator dynamics can be exploited to estimate the function $\hat{f}(x_k)$, which can be utilized to obtain the adaptive control torque input (8). If the parameter adaptation is accurate, the estimation error will become zero and the filtered tracking error will remain bounded due to the disturbance torque.

Therefore, the objective is to design an adaptive control torque input such that the filtered tracking error dynamics are stable. In order to minimize the event sampling error, which is

a part of estimation error, a suitable event trigger condition needs to be designed while ensuring stability. Next, the background on the formation control for the mobile robot will be presented and adaptive control problem with event-sampled feedback will be formulated.

Mobile Robot Dynamics

Consider the non-holonomic robot shown in Fig. 1, where x_r, y_r denote Cartesian positions with respect to the robot frame, d is the distance between the rear-axis and the center of mass of the robot, r, R are the radius of the rear wheels, and half of the robot width, respectively.

The equations of motion about the center of mass, C, for the i^{th} robot in a networked robot formation are written as

$$\begin{bmatrix} \dot{x}_{ci} \\ \dot{y}_{ci} \\ \dot{\theta}_i \end{bmatrix} = \begin{bmatrix} \cos\theta_i & -d_i \sin\theta_i \\ \sin\theta_i & d_i \cos\theta_i \\ 0 & 1 \end{bmatrix} \begin{bmatrix} v_i \\ \omega_i \end{bmatrix}, \quad \dot{q}_i = S(q_i)v_i, \tag{11}$$

where d_i is the distance from the rear axle to the robot's center of mass; $q_i = [x_{ci} \; y_{ci} \; \theta_i]^T$ denotes the Cartesian position of the center of mass and orientation of the i^{th} robot; v_i, and ω_i represent linear and angular velocities, respectively, and $v_i = [v_i \; \omega_i]^T$ for the i^{th} robot.

Mobile robotic systems, in general, can be characterized as having an n-dimensional configuration space $\mathcal{Q}$ with generalized coordinates $(q_1, \ldots q_n)$ subject to ℓ constraints

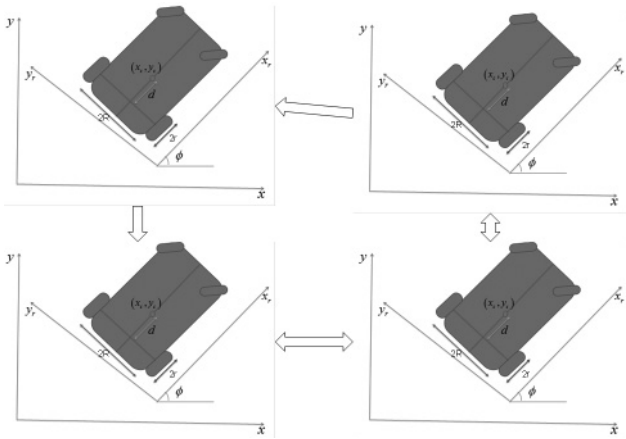


Figure 1. Differentially driven mobile robot.

(Fierro and Lewis 1998). Applying the transformation, the dynamics of the mobile robot are given by

$$M_i \dot{v}_i - \bar{m}_i V_m(q_i, \dot{q}_i) v_i + F_i(v_i) + \tau_{di} = \tau_i, \qquad (12)$$

where $M_i \in R^{\rho x \rho}$ is a constant positive definite inertia matrix, $V_{mi} \in R^{\rho x \rho}$ is the bounded centripetal and Coriolis matrix, $F_i \in R^{\rho}$ is the friction vector, $\tau_{di} \in R^{\rho}$ represents unknown bounded disturbances such that $\|\tau_{di}\| \le d_M$ for a known constant d_M, $B_i \in R^{\rho x \rho}$ is a constant, nonsingular input transformation matrix, $\tau_i = B_i \tau_i \in R^{\rho}$ is the input vector, and $\tau_i \in R^{\rho}$ is the control torque vector. For complete details on (12) and the parameters, refer to (Fierro and Lewis 1998).

Assumption 4. The robotic system (12) satisfies the following properties: M_i is a known positive definite matrix and it is bounded by $B_{im}^{-1} < \|M_i^{-1}\| < B_{iM}$ and $0 < \|V_{mi}\| < \bar{V}_{mi}$, the norm of V_{mi} and $\|\tau_{di}\| \le d_M$ are all bounded. The matrix $\dot{M}_i - 2V_{mi}$ is the skew-symmetric (Fierro and Lewis 1998).

Remark 4. In (Ren et al. 2005b), a controller was designed to ensure that all regulation errors for the linear systems achieved a common value. Due to the nonholonomic constraints considered in this paper, the formation consensus

error is defined as the difference between the robot's own regulation error and the regulation error of one of its neighbor, referred to as robot *j*. The benefit of such consensus based formation controller is that the i^{th} robot will be able to reach consensus with another neighbor when the communication is not available with the j^{th} robot anymore. As shown in (Ren et al. 2005b), average consensus is achieved if the information exchange topology is both strongly connected and balanced. In the case that the information exchange topology has a spanning tree, the final consensus value is equal to the weighted average of initial conditions of those agents that have a directed path to all the other agents (Ren et al. 2005b). In this work, we will assume that the information exchange topology forms a spanning tree.

The main focus of this section is to formulate the back-stepping control problem for the mobile robots to minimize the consensus based formation error. For this, the

consensus based formation error is obtained from the robot kinematics and it is utilized to derive the velocities at which the robots should move in-order to achieve the desired consensus. Due to the dynamics of the individual robot, perfect velocity tracking assumption (Fierro and Lewis 1998) becomes undesired. Therefore, explicitly taking into account the dynamics of each robot, controllers are designed to minimize the velocity tracking error which in turn acts as a virtual controller to the formation error dynamics and helps the robots reach consensus.

In order to develop such controller, we first define the regulation errors for each robot on positions and velocities as $\tilde{x}_i = x_{ci} - x_i^r$, $\tilde{y}_i = y_{ci} - y_i^r$, $\tilde{\theta}_i = \theta_{ci} - \theta_i^r$ with x_i^r, y_i^r, θ_i^r being the reference positions and bearing angles which forms a desired formation shape for the group of robots. Now, the consensus errors between the i^{th} robot and j^{th} robot are defined as $\delta_{xi} = \tilde{x}_i - \tilde{x}_j$, $\delta_{yi} = \tilde{y}_i - \tilde{y}_j$ and $\delta_{\theta i} = \tilde{\theta}_i - \tilde{\theta}_j$, for x and y directions and the bearing angle, respectively. In this work, it will be assumed that the desired heading angles, θ^r, are common for each robot in the formation so that each robot is oriented in the same direction, which yields $\delta_{\theta i} = \theta_i - \theta_j$.

Next, the consensus formation error is transformed into the reference frame attached to the mobile robot using the transformation

$$\begin{bmatrix} e_{i1} \\ e_{i2} \\ e_{i3} \end{bmatrix} = \begin{bmatrix} \cos\theta_i & \sin\theta_i & 0 \\ -\sin\theta_i & \cos\theta_i & 0 \\ 0 & 0 & 1 \end{bmatrix} \begin{bmatrix} \delta_{xi} \\ \delta_{yi} \\ \delta_{\theta i} \end{bmatrix}. \tag{13}$$

Taking the derivative of (13) reveals

$$\dot{e}_{iF} = \begin{bmatrix} -\sin\theta_i\dot{\theta}_i x_{Fi} + \cos\theta_i \dot{x}_{Fi} - \cos\theta_i\dot{\theta}_i y_{Fi} - \sin\theta_i \dot{y}_{Fi} \\ \cos\theta_i\dot{\theta}_i x_{Fi} + \sin\theta_i \dot{x}_{Fi} - \sin\theta_i\dot{\theta}_i y_{Fi} + \cos\theta_i \dot{y}_{Fi} \\ \dot{\theta}_i \end{bmatrix} \quad (14)$$

Using the expression (11) in (14) gives

$$\dot{e}_{iF} = \begin{bmatrix} -\sin\theta_i\dot{\theta}_i x_{Fi} + \cos\theta_i \left(\cos\theta_i v_i - d_i \sin\theta_i \dot{\theta}_i - \cos\theta_j v_j + d_j \sin\theta_j \dot{\theta}_j\right) \\ \cos\theta_i\dot{\theta}_i y_{Fi} + \sin\theta_i \left(\sin\theta_i v_i + d_i \cos\theta_i \dot{\theta}_i - \sin\theta_j v_j + d_j \cos\theta_j \dot{\theta}_j\right) \\ \dot{\theta}_i - \dot{\theta}_j \end{bmatrix}$$

$$\dot{e}_{iF} = \begin{bmatrix} -\sin\theta_i \dot{\theta}_i x_{Fi} + \cos\theta_i \cos\theta_i v_i + d_i \sin\theta_i \dot{\theta}_i - \cos\theta_j v_j + d_j \sin\theta_j \dot{\theta}_j \\ \cos\theta_i \dot{\theta}_i y_{Fi} + \sin\theta_i \cos\theta_i v_i + d_i \cos\theta_i \dot{\theta}_i - \sin\theta_j v_j + d_j \cos\theta_j \dot{\theta}_j \\ \dot{\theta}_i - \dot{\theta}_j \end{bmatrix} \quad (15)$$

$$\dot{e}_{iF} = \begin{bmatrix} -\sin\theta_i \dot{\theta}_i x_{Fi} + \cos\theta_i \cos\theta_i v_i + \sin\theta_i d_i \dot{\theta}_i - \cos\theta_j v_j + d_j \sin\theta_j \dot{\theta}_j \\ \cos\theta_i \dot{\theta}_i y_{Fi} + \sin\theta_i \cos\theta_i v_i - d_i \cos\theta_i \dot{\theta}_i - \sin\theta_j v_j + d_j \cos\theta_j \dot{\theta}_j \\ \dot{\theta}_i - \dot{\theta}_j \end{bmatrix}$$

On simplification using the trigonometric identities and using (13), yields the formation error dynamics as

$$\dot{e}_{i1} = e_{i2} - v_i + v_j \cos(\theta_i - \theta_j)$$
$$\dot{e}_{i2} = -v_j \sin(\theta_i - \theta_j), \quad i = 1, 2, \quad j = i + 1 \bmod 3 \tag{16}$$

Remark 5. It can be observed that (16) resembles the trajectory tracking error system from a single robot control architecture tracking a virtual reference cart. In this work, instead of tracking a virtual cart, the mobile robots attempt to reach consensus with their neighbors to a desired formation, and each $e_{i(-)}$ represents the consensus error instead of the trajectory tracking error (Fierro and Lewis 1998).

Under the perfect velocity tracking assumption, the consensus-based formation control velocity is given by

$$v_{id}^F = k_1 e_{i1} - v_j \cos(\theta_i - \theta_j)$$
$$\omega_{id}^F = k_2 v_j e_{i2} + k_3 \sin(\theta_{ij}) \tag{17}$$

with $k_1, k_2, k_3 > 0$, being the design constants. Next, the back-stepping technique is utilized, wherein the desired velocity (17) is utilized in (16) to drive the consensus error dynamics. We denote the velocity tracking error as e_{iv}^F, for formation control and defining $e_{iv} = v_i - v_{id}$ reveals $v_i = v_{id} + e_{iv}$, and the consensus error system (16) becomes

$$\dot{e}_{i1} = e_{i2} - k_1 e_{i1} + e_{iv} - v_j \cos(\theta_i - \theta_j)$$
$$\dot{e}_{i2} = -k_2 v_j e_{i1} - k_3 \sin(\theta_{ij}) + v_j \cos(\theta_i - \theta_j)$$
$$\dot{e}_{iv} = \dot{v}_i - \dot{v}_{id}^F, \quad i = 1, 2, \quad j = i + 1 \bmod 3 \tag{18}$$

$$v_e = k \sum_{j=1}^{3} \sin(\theta_i - \theta_j) + \sum_{j=1}^{3} (\theta_i - \theta_j)$$

Simplifying the expression in (18), leads to the consensus error dynamics as

$$\begin{aligned} \dot{e}_{i1} &= e_{i2} - k e_{i1} - e^F_{i1} \\ \dot{e}_{i2} &= -k e_{i2} - v_{i1} \sin(\theta_{i1}) \end{aligned} \tag{19}$$

$$\dot{e}_{i3} = -k \sin(\theta_{i1}) - e^F_{iv1}$$

Using (12) and the definition of the velocity tracking error, its dynamics are obtained as

$$\bar{M}_i \dot{e}^F_{iv} = \bar{F}_{di} - \bar{M}_i \dot{v}_{id} - \bar{V}_{mi}(q_i, \dot{q}_i) v_{id} - \bar{F}_i(v_i) \tag{20}$$

Defining $f(z_i) = \bar{V}_{mi}(q_i, \dot{q}_i)(v_{id} + e_{iv}) + \bar{F}_i(v_i)$ and using (20)

$$\bar{M}_i \dot{e}^F_{iv} = \bar{F}_{di} - \bar{M}_i \dot{v}_{id} - f(z_i) \tag{21}$$

where $z_i = [e^F_{iv1} \; e^F_{iv2} \; v_i \; \omega_i]$ is the set of signals required to construct the uncertain function $f(z_i)$ (Fierro and Lewis 1998) as

$$f(z_i) = \begin{bmatrix} 0 \\ 2mW_i v_i \end{bmatrix} + \begin{bmatrix} d_i \dot{\theta}_i + m_i \\ d_i + 2mW_i \end{bmatrix} + \begin{bmatrix} e^F_{iv1} \\ e^F_{iv2} \end{bmatrix} + \begin{bmatrix} F_{vv_i} v_i + F_{dsign}(v_i) \\ F_{v\dot{\theta}_i} \dot{\theta}_i + F_{dsign}(\dot{\theta}_i) \end{bmatrix}, \tag{22}$$

with $e^F_{iv} = [e^F_{iv1}\ e^F_{iv2}]$, F_v, F_d being the unknown friction coefficients, m_i, mW_i being the total mass of the robot and the mass of a wheel respectively. Defining $\ell_i = d_i(m_i - 2mW_i)$, we get the uncertain nonlinear function as

$$f_i(z_i) = \begin{bmatrix} \ell_i \dot{v}_{id} - \ell_i e^F_{iv2} - F_{vi} v_{id} - F_d sign(v_{id}) \\ \dot{v}_{id} - e^F_{iv1} - F_{vi} v_{id} - F_d sign(v_{id}) \end{bmatrix}. \quad (23)$$

Finally, recalling the velocity tracking error dynamics (21), define the control torque such that the robot tracks its desired velocity as

$$\tau_i = -M_i \dot{v}_{id} + F_i + K_i e^F_{iv} - \hat{f}_i(z_i) - \gamma(e_{i1}, e_{i2}, e_{i3}), \quad (24)$$

where $\gamma(e_{i1}, e_{i2}, e_{i3})$ is a function of the consensus error states (19) required for the purpose of stability, and $\hat{f}_i(z_i)$ is the estimated unknown dynamics which will be parametrized next.

Assumption 5. The nonlinearity $f_i(z_i)$, is Lipschitz continuous function on a compact set, such that $\|f_i(x_i) - f_i(y_i)\| \le L_\phi \|x_i - y_i\|$ and satisfies LIP. Also, the derivative of the desired velocities $\dot{v}_{id}(x)$ satisfy Lipschitz continuity such that $\|\dot{v}_{id}(x) - \dot{v}_{id}(y)\| \le L_v \|x - y\|$.

Substituting (24) into (21) reveals the closed loop velocity tracking error dynamics

$$M_i \dot{e}^F_{iv} = -K_i e^F_{iv} + \gamma(e_{i1}, e_{i2}, e_{i3}) + \tilde{f}_i(z_i). \quad (25)$$

where the function estimation error is given by $\tilde{f}_i(.) = \hat{f}_i(.) - f_i(.)$.

Remark 6. For the case of mobile robots, the friction coefficients and the Coriolis matrices are assumed to be

uncertain. Using the event-sampled feedback of the sensor measurements, and the LIP based representation of the uncertain nonlinearity these quantities are adaptively tuned to generate the desired control torque.

In the next section, the event-sampling mechanism will be designed first to determine the event-based sampling instants and then the controller design for the tracking control of the robotic manipulator followed by the formation control of the mobile robots will be presented.

CONTROLLER DESIGN

In this section the adaptive controller design, with event-sampled feedback, for the robotic systems will be presented and the parameter adaptation laws will be derived from the Lyapunov stability analysis.

Robot Manipulator

For the controller design, the event-sampling mechanism which decides the feedback instants is crucial and is usually designed based on the closed-loop stability analysis. The event-sampling mechanism is designed such that the measurement error (2) satisfy a state-dependent threshold for every inter-event period, which is of the form

$$\|e(t)\|^2 \le \|r(t)\|^2, \quad t_k \le t < t_{k+1}, \quad k = 1,2,3.. \tag{26}$$

t_k ET k k $k-1$

with $0 < \sigma < 1$, and μ_K is a positive design parameter. Due to the parameter adaptation at periodic sampling instants, the adaptive controllers involve more computations when compared to traditional controllers. However by using the event-sampled feedback, the objective is to reduce these computations without compromising the stability while ensuring acceptable tracking performance.

Using the results of Assumption 2, the unknown dynamics of the robot manipulator can be represented by using standard LIP formulation. The resulting dynamics can be used to design the feedback-linearizing controller to achieve satisfactory tracking performance of the robot manipulator.

Consider the uncertain robot manipulator dynamics in (4), using Assumption 2,

the unknown nonlinear dynamics can be represented as $f(x) = \theta^T \phi(x)$, with θ being the unknown masses in the robot manipulator dynamics and $\phi(x)$ is the regression vector obtained from the system dynamics (7). The estimated dynamics with event-sampled states is given as

$$\hat{f}(x_k, \hat{\theta}_k) = \hat{\theta}_k^T \phi(x_k), \quad t_k \le t < t_{k+1} \tag{27}$$

where $\hat{\theta}$ is the estimate of the unknown parameter matrix in the manipulator dynamics.

Defining the parameter estimation error $\tilde{\theta}_R = \theta_R - \hat{\theta}_R$ and using filtered tracking error dynamics in (10) and the estimation of the unknown parameters, we have

$$M\dot{r} = -(V_m + K_v)r + \tilde{\theta}_R^T \phi(x) + K_x e(t_k), \quad t_k \le t < t_{k+1} \tag{28}$$

The filtered error dynamics can be rewritten as

$$M\dot{r} = -(V_m + K_v)r + \tilde{\theta}_R^T [\phi(x) - \phi(x(t_k))] + K_x e(t_k), \quad t_k \le t < t_{k+1}. \tag{29}$$

For the stability analysis of the event-sampled controller,

the closed-loop system with event-sampled measurement error is analyzed in the following theorem, and the adaptation rule for tuning the unknown parameters (27) with event-sampled states is presented.

With the following definition on input-to-state stability (ISS), it will be shown in Theorem 1 that the closed-loop system admits an ISS Lyapunov function in the presence of bounded measurement error. Later, the assumption on the boundedness of the measurement error introduced by the event-sampled feedback will be relaxed in the subsequent theorem. The ISS result will be used only to establish the existence of positive inter event time, which is required to demonstrate that the event-sampling mechanism does not exhibit zeno-behavior (Tabuada 2007).

Definition 1. (Khalil and Grizzle 1996) Let $L(t, Z)$ be a continuously differentiable function such that

$$\underline{L}(\|Z\|) \le L(t, Z) \le \bar{L}(\|Z\|) \tag{30}$$

$$L(t, Z, e) \ge \gamma(\|e\|) > 0, \quad \forall \|Z\| \ge \Phi(e) > 0 \tag{31}$$

where $\underline{L}$, $\bar{L}$ are class κ_∞ functions, e is a bounded measurement error and γ is a class κ function and $\Phi(Z)$ is a continuous positive definite function on R^n. Then the system $\dot{Z} = f(t, Z, e)$, $Z(0) \in A$ is input-to-state stable.

Theorem 1 (Input-to-state stability). *Consider the filtered tracking error dynamics of the robotic manipulator given in (29) with τ_d being the disturbance torque. Let the Assumptions 1–3 hold. Using the LIP representation of the uncertain robot manipulator dynamics given in (27), generate the control torque from (8). Let the parameters be tuned using the following adaptation rule*

$$\dot{\hat{\theta}} = \Gamma \phi(x) r^T - \kappa \Gamma \left\| I + k_v \right\| \hat{\theta} \tag{32}$$

where $\Gamma > 0$, $\kappa > 0$, $k_v > \frac{1}{2}$. Let B_{ETM} be the bound on the measurement error e_{ET} which is allowed to satisfy the condition $\|e_{ET}\| \leq \mu \|r\|$, such that $0 < \mu < 1$, $\forall k$, and let θ_M be the bound on the unknown mass matrix. The tracking and the parameter estimation errors are bounded and the closed-loop system is input to state stable, with the input being a function of the measurement error e_{ET}.

Proof. Consider the Lyapunov candidate function of the form, $L(r, \tilde{\theta}) = \frac{1}{2} r^T M r + \frac{1}{2} tr(\tilde{\theta}^T \Gamma^{-1} \tilde{\theta})$, the first derivative using the filtered tracking error dynamics (29) and the parameter update rule (32) is given by

$$\dot{L}(r, \tilde{\theta}) = r^T (V_m \dot{x} + \tau_d - \tau) + \frac{1}{2} r^T \dot{M} r - r^T \left[\hat{\theta}^T \phi(x) \dot{x} + \frac{1}{2} \hat{\theta}^T \dot{\phi}(x) \dot{x} + k_v e_{ET} \right] - tr(\tilde{\theta}^T \Gamma^{-1} \dot{\hat{\theta}}) \tag{33}$$

With the skew-symmetry property in Assumption 1 and the Lipschitz continuity of the regression function, we obtain

$$\dot{L}(r, \tilde{\theta}) \leq \|r\| \|\tilde{\theta}\| \|\phi(x)\| \|\dot{x}\| + \|r\| \|\tau_d\| + k_v \|r\| \|e_{ET}\| - k_v \|e_{ET}\|^2 + \kappa \|\tilde{\theta}\| \|\hat{\theta}\| \tag{34}$$

Applying norm operator and using the bounds on the disturbance torque from Assumption 1, we obtain

$$\dot{L}(r, \tilde{\theta}) \leq \|r\| \|\tilde{\theta}\| \|\phi(x)\| \|\dot{x}\| + \|r\| (B_d + \mu k_v \|r\|) - k_v \|e_{ET}\|^2 + \kappa \|\tilde{\theta}\| \|\hat{\theta}\| \tag{35}$$

$$v \quad R \quad ET \quad RM \| r \quad R \| r \| \quad 1 \; ETM$$

where, $\zeta_1(B_{ETM}) = \theta_{RM} L_\phi B_{ETM} + k_v B_{ETM} + \tau_{dM}$.

Using the Young's inequality and the relation $\|e_{ET}\| \leq \mu \|r\|$, we obtain

$$(k \quad \frac{1}{2}) \quad r \quad \frac{2}{2} \quad r \quad \frac{2}{2} \quad e \quad e \qquad (36)$$

$$v \quad R \quad R \quad ET \quad 1 \quad R \quad x \quad R \quad ET \quad B$$

where $\quad 1 \quad \frac{\|\zeta_1(B_{ETM})\|^2}{2}$. From the Lipschitz continuity of the regression $(2 \quad RM)$, B

vector, we have

$$(k \quad \frac{1}{2}) \quad r \quad \frac{2}{2} \quad r \quad \frac{2}{2} \quad r \quad L r \quad B$$

$$v \quad R \quad R \quad k \quad 1 \quad R \; ETM$$

$$R$$

$$r \quad L \quad B \qquad (37)$$

$$R \quad k \quad ETM \quad B$$

Grouping similar terms, with $\bar{\alpha}_1 = (\alpha - \bar{R}_M) > L_B > B_{ETM} > L_B > B_{ETM}$, we get

$$\dot{V} \le -k_v \|r\|^2 + \frac{1}{2}\|r\|^2 + \frac{1}{2}\|r\|^2 + \frac{1}{2}\|r\|^2 + \frac{1}{2}\|R\|^2\|B\|^2 \tag{38}$$

On simplifying (38), using the notations $\kappa = \kappa(1 - \mu_k)$, $k_V = k_V - \frac{1}{2}$, we arrive at

$$\dot{V} \le -k_v \|r\|^2 + \frac{1}{2}\|R\|^2\|B\|^2 \tag{39}$$

By completing the squares, we get the Lyapunov first derivative as

$$\dot{V} \le -\left(k_v - \frac{1}{2}\right)\|r\|^2 + \frac{1}{4\alpha}\|R\|^2\|B\|^2 \tag{40}$$

The Lyapunov function derivative in (40) is less than zero as long as r, W are outside their respective ultimate bounds. The ultimate bounds are a function of η_B, δ_1, which in turn are obtained as a function of the measurement error and disturbance torque input. Hence, (40) is in a form similar to the input-to-state stability characterization given by (30) and (31).

Remark 7. The result in Theorem 1 shows that the closed-loop system in the presence of a bounded measurement error is locally ISS. That is, the continuous closed-loop system admits an ISS Lyapunov function. However, for the event-sampled implementation of the controller, the boundedness of the event-sampled measurement error is required to be proven. In the following theorem, the closed-loop signals are indeed shown to be bounded using which the measurement error and the existence of $0 < \mu < 1$, satisfying the event trigger condition $\|e_k\| \le \mu \|r\|$ will be demonstrated.

In the following theorem, the event-sampling mechanism is designed and stability of the robotic manipulator is analyzed by using the Lyapunov stability theory, in the ideal case,

where the sensor signal is noise free, the epsilon modification term in (41) is not used and there is no disturbance torque input.

Theorem 2. *(Ideal case) Consider the filtered tracking error dynamics of the robotic manipulator given in (29) with* $\tau_d = 0$. *Let the Assumptions 1 and 3 hold. Apply the LIP representation of the uncertain robot manipulator dynamics given in (27), and use the estimated values of the unknown parameter to generate the control torque (8). Let the condition (26) be utilized to determine the event-sampling instants and (41) be used to tune the unknown parameters at the event-sampling instants with* $\kappa = 0$, $\Gamma > 0$. *Let* θ_{RM} *be the bound on the unknown mass matrix,* L_ϕ, *is the Lipschitz constant for the regression vector. The tracking and the parameter estimation errors are locally UUB, both at the event-sampling instants and during the inter-event period.*

Proof. Case 1. At the event-sampling instants $t = t_k$, $\forall k$, the event-sampling error $e = 0$, and the tracking error and regression function in (29) becomes $r = r$, $\phi(x) = \phi(x)$.

The adaptation law becomes

$$\dot{\hat{\theta}}_R = \Gamma \phi(x) r^T \tag{41}$$

Consider the following Lyapunov candidate function $L(r, \tilde{\theta}_R^T) = L(r) + L(\tilde{\theta}_R)$, such that

$$L(r, \tilde{\theta}_R^T) = \frac{1}{2} r^T M r + \frac{1}{2} tr(\tilde{\theta}_R^T \Gamma^{-1} \tilde{\theta}_R) \tag{42}$$

Taking the first derivative of (42), we get

$$\dot{L}(r,\hat{\theta}^T) = r^T M\dot{r} + \frac{1}{2}r^T\dot{M}r - tr(\tilde{\theta}^T\Gamma^{-1}\dot{\hat{\theta}}) = r^T M\dot{r} + \frac{1}{2}r^T\dot{M}r \tag{43}$$

$$R \qquad R \quad R_2$$

Using the filtered tracking error dynamics in (29), we have

$$\dot{L}(r,\hat{\theta}^T) = r^T(-V_m - k_v)r + r^T\tilde{\theta}^T Y(x) + tr(\tilde{\theta}^T\Gamma^{-1}\dot{\hat{\theta}}) = r^T M\dot{r} + \frac{1}{2}r^T\dot{M}r \tag{44}$$

$$R \qquad m \quad v \qquad R \qquad R \quad R_2$$

Utilizing the skew-symmetry property mentioned in Assumption 1, we obtain

$$\dot{L}(r,\hat{\theta}^T) = -r^T k_v r + tr(\tilde{\theta}^T\Gamma^{-1}\dot{\hat{\theta}} - r^T\tilde{\theta}^T Y(x)) \tag{45}$$

$$R \qquad v \qquad R \quad R \quad R$$

Using the property of trace of a matrix and with $\hat{\theta} = \hat{\theta}$, we obtain the definition

$$R \quad R \quad R$$

$$\dot{L}(r_R,\hat{\theta}^T)_v = -r_R^T k_v r + tr(\tilde{\theta}_R^T(Y(x)r^T\hat{\theta}\Gamma^{-1}\dot{\hat{\theta}})) \tag{46}$$

Utilizing the parameter update rule in (41), we get the first derivative of the Lyapunov function as

$$\dot{L}(r,\hat{\theta}^T)_v = -r^T k_v r \tag{47}$$

It can be concluded from (47), that the filtered tracking and the parameter estimation errors are bounded when $e_{ET} = 0$. It can be observed from (47), $\dot{L} \leq 0$, negative semi-definite when $e_{ET} = 0$, during the event-sampling instants. Taking the second derivative of the Lyapunov function using (47), we get the expression $\ddot{L} \leq -2r^T k_v\dot{r}$, r bounded, $\dot{r}$ bounded, therefore $\dot{L}$ is uniformly continuous and from Barbalat's Lemma, $r \to 0$ as the event-sampling instants $t_k \to \infty$.

Case 2: In the inter-event period $t_k \leq t < t_{k+1}$, the measurement error due to event-sampled feedback is non-zero, $e_{ET} \neq 0$.

The parameters are not updated during this period and therefore $\dot{\hat{\theta}}_R = 0$. Using the Lyapunov candidate function (42), the first derivative is obtained as

$$L(r, \hat{\theta}_R^T) = r^T M r + tr(\hat{\theta}_R^T \Gamma_R^{-1} \hat{\theta}_R) = \frac{1}{2} r^T M_R r \quad (48)$$

Substituting the filtered tracking error dynamics (29), with $\tau_d = 0$, $e_{ET} \neq 0$, and since $\dot{\hat{\theta}}_R = 0$, we have

$$L(r, \hat{\theta}_R^T) = r^T (V_m(x) + k_v) r - r^T [\hat{\theta}_R^T Y_R(x, \dot{x}) + k_x(x) e_{ET}] + \frac{1}{2} r^T M_R r \quad (49)$$

Utilizing the skew-symmetry property mentioned in Assumption 1, we obtain

$$L(r, \hat{\theta}_R^T) = -r^T k_v r - r^T \hat{\theta}_R^T Y_R(x, \dot{x}) + r^T k_x(x) e_{ET} \quad (50)$$

Utilizing the definition of the parameter estimation error, we have

$$L(r, \hat{\theta}_R^T) = -r^T k_v r - r^T \tilde{\theta}_R^T Y_R(x, \dot{x}) + r^T k_x(x) e_{ET} \quad (51)$$

On grouping the estimated parameters together, we obtain

$$L(r, \Box^T) \Box \Box r^T k_r r \Box r^T \hat{\Box}^T [\Box(x) \Box \Box \quad (52)$$

$$\Box r^T \Box^T \Box(x) \Box r^T k_r e$$

$$x \qquad R \qquad v \; ET$$

$$R \qquad v$$

$$R$$

Using the Assumption on the regression vector and applying the norm operator, we obtain

$$L(r, \Box^T) \Box \Box k_r \| r \|^2 \Box \| r^T \| \| \hat{\Box}^T \| \| e \| \Box k_r \| r \|^2 + \| r^T \| \| \Box^T \| \| \Box(x) \| \quad (53)$$

$$R \qquad v \qquad R \qquad v \; ET \qquad R$$

Adding and subtracting $\| r^T \| \| \theta^T \| \| \phi(\bar{x}) \|$ to get

$$L(r, \Box^T) \Box \Box k_r \| r \|^2 \Box \| r^T \| \| \hat{\Box}^T \| \| e \| \Box k_r \| r \|^2 + \| r^T \| \| \Box^T \| \| \Box(x) \| \Box \| r^T \| \| \Box^T \| \| \phi(\bar{x}) \| \quad (54)$$

$$v \qquad R \qquad v \; R \; T \qquad x \qquad R \qquad x$$

Using the Lipschitz assumption on the regression function, we get

$$L \Box \Box k_r \| r \|^2 \Box \| r^T \| \| \hat{\Box}^T \| \| e \| + \| r^T \| \| \Box^T \| L_\phi \| e \| \quad (55)$$

$$v \qquad R \qquad v \; R \qquad ET \qquad R \qquad x$$

Applying the definition of the parameter estimation error and triangle inequality to get

$$L(r, \Box^T) \Box \Box k_r \| r \|^2 \Box \| r^T \| \| \Box^T \| \| e \| \Box \| r^T \| \| \phi \| \quad (56)$$

$$R \qquad v \qquad R \qquad v \; RM \qquad ET \; R \qquad x$$

Using Young's inequality, $2ab \le a^2 + b^2$, $\Box a,b > 0$, we have the relation

$$L(r, \Box^T) \Box \Box \frac{k_r}{2} \| r \|^2 \Box \frac{(\theta_{RM}^2 L_\phi^2 + k_r^2 + 4 \| \hat{\theta}_R^T \|^2 L_\phi^2) \| e_{ET} \|^2}{2} \Box \frac{\| \tilde{\theta}_R^T \|^2 \| \phi(\bar{x}) \|^2}{2} \Box \frac{\| r \|^2}{2} \Box$$

$$R \qquad v$$

(57)

By grouping the similar terms in (57), we arrive at

$$L(r,\Box T) \Box \Box(k \Box 2)\, r^{2} \Box 2(\Box \| \| \frac{2L}{2} \| \| k\frac{\|\tilde{\theta}_R{}^T\|^2 \|\phi(\bar{x})\|^2}{)} \qquad (58)$$

$$\Box$$

$$R \quad v \quad RM \quad v \quad R \Box \quad 2 \quad 2$$

$$\Box$$

Using the event-sampling condition (26), we have

$$L(r,\Box T) \Box \Box(k \Box 2)\, r^{2} \Box (\Box \| \| \frac{2L}{2} \| \| k\frac{\|\tilde{\theta}_R{}^T\|^2 \|\phi(\bar{x})\|^2}{} \qquad (59)$$

$$\Box 4 \Box \hat{} T \quad 2 \| \| L \quad 2) \Box k \quad r \quad \Box \| \|$$

$$R \quad v \quad RM \quad \Box \quad v \quad R \Box \quad 2 \quad 2$$

Choosing $\Box \Box \frac{2}{\quad}$, for each inter event period, the

$$k \quad (\Box^{2} L^{2} \Box k^{2} \Box 4 \Box \hat{} T^{2} L^{2})$$

$$RM \quad \Box \quad v \| \quad R \quad \Box$$

Lyapunov first derivative can be obtained as

$$L(r_k, \Box T \quad \Box \Box T^{2} \| \quad \Box (^{2} \quad (60)$$

$$) \Box \Box(k \quad {}_{v} \Box 3) \| \, r^{2} \frac{\| \, t}{R} \Box \Box) \quad .$$

$$2 \; x$$

With $k > 3$, and using the fact that $\tilde{\theta}(t) = \tilde{\theta}(t)$, $\phi(\bar{x}(t)) = \phi(t)$, $\Box t \Box [t, t)$, it

$$R \quad R \quad k \quad k \quad k\,k+1$$

can be concluded that the filtered tracking error and the parameter estimation error are bounded during the inter-event period since the regression function with previously sampled state vector is proven to be bounded.

Remark 8. It should be noted that the filtered tracking and the parameter estimation errors are bounded both at the event-sampling instants and during the inter-event period. However, in order to avoid the parameter drift and to relax PE condition, additional terms are included in the parameter update rule (Narendra and Annaswamy 2012).

Remark 9. It should be noted that the bounds obtained for the filtered tracking error from Theorem 2 for both the cases are independent of the measurement error demonstrating that the closed-loop system is bounded.

Remark 10. Since the target parameters are constant and the estimated parameters are not tuned during the inter-event period, the parameter estimation error dynamics are zero during this period. From Theorem 2, it can be concluded that if the parameters are tuned using the proposed adaptation rule at the event-sampling instants, the parameter estimation error converges to its ultimate bounds as the number of event sampled instants increase. However, for the analysis of the tracking error of the robotic manipulator with event-sampled implementation, it is required to show that the tracking error is bounded during the inter-event period and the event-sampling instants.

In the following theorem, the evolution of the tracking error with event-sampled implementation of the controller is presented with the adaptation rule (32) with the additional term to relax the PE condition and to ensure that the parameter estimation errors are bounded.

Theorem 3. *Consider the filtered tracking error dynamics of the robotic manipulator given in (29) with* τ_d *being the disturbance torque. Let the Assumptions 1-3 hold. Using the LIP based representation of the uncertain robot manipulator dynamics (27), generate the control torque (8). Let the unknown parameters be tuned at the event-sampling instants using (32), where* $\Gamma > 0$, $\kappa > 0$, $k_V \geq 3$. *Let the measurement error satisfy the condition in (26), with* $0 < \mu_k < 1$, *for each inter-event period and* $0 < \sigma < 1$. *The tracking and the parameter estimation errors are locally UUB both at the event-sampling instants and during the inter-event period. In addition the measurement error introduced (2) due to the event-sampled feedback is bounded during the time interval* $[t_k, t_{k+1})$ *for all*

k. Moreover, the bounds for the filtered tracking error and the parameter estimation error are obtained independent of the measurement error.

Proof. Case 1. At the event-sampling instants $t = t_k$, the event-sampling error $e = 0$, and the tracking error and regression function in (29) becomes $r = r, \hat{f}(x) = f(x)$. Consider the Lyapunov candidate function (42). Its first derivative using the filtered tracking error dynamics and the parameter update law, is obtained as

$$L(r, \hat{W}) = -r^T k_v r + r^T \varepsilon + \tilde{W}^T \hat{\phi}(x) - r^T \{\varepsilon_N\} - tr(\tilde{W}^T (\hat{\phi}(x) r^T + \kappa \|r\| \hat{W})) \quad (61)$$

with $\zeta_1 = \tau_d$. Using the property of trace operator, we get

$$L(r, \hat{W}) = -r^T k_v r + r^T \varepsilon + \tilde{W}^T \hat{\phi}(x) - r^T \varepsilon_N - tr(\kappa \|r\| \tilde{W}^T \hat{W} - \hat{\phi}(x) r^T + \kappa \|r\| \tilde{W}^T W) \quad (62)$$

Applying the norm operator and using the bounds on the target parameter, we obtain

$$L(r, \hat{W}) \le -k_v \|r\|^2 + \|r\| \varepsilon_N + \kappa \|r\| \|\tilde{W}\| \|W\| - \|r\| \varepsilon_N \quad (63)$$

On completing the squares, we get

$$\dot{r} \leq \|r\|\left(k_v - \frac{\rho_{RM}^2}{2} - \frac{\rho_{RM}^2}{4}\right) + \frac{1}{2} \tag{64}$$

Using the Lyapunov first derivative in (64), the bounds on the tracking and the parameter estimation errors are obtained as

$$\|r\| \geq \frac{\rho_{RM}}{2}, \quad \|\tilde{\theta}_R\| \geq \sqrt{\frac{\kappa\theta_{RM}^2 + 4}{4\kappa}} \quad \text{or, } 4k_v$$

Case 2: In the inter-event period $t_k \leq t < t_{k+1}$, the measurement error due to event- sampled feedback is non-zero, $e_{ET} \neq 0$. The adaptive parameters are not updated during this period and therefore $\dot{\hat{\theta}}_R = 0$. Using the Lyapunov candidate function (42), the first derivative is obtained as

$$\dot{L}(r, \tilde{\theta}_R^T) = r^T M\dot{r} + \frac{1}{2} r^T \dot{M} r - tr(\tilde{\theta}_R^T \kappa^{-1} \dot{\hat{\theta}}_R) \tag{65}$$

Using the filtered tracking error dynamics and the skew-symmetry property in Assumption 1, we have

$$\dot{L}(r, \tilde{\theta}_R^T) = r^T k_v r - r^T \tilde{\theta}_R^T \phi(x) - r^T \tilde{\theta}_R^T \phi(x) e_{ET} + r^T \varepsilon_d - tr(\tilde{\theta}_R^T \kappa^{-1} \dot{\hat{\theta}}_R) \tag{66}$$

Since the parameter adaptation is not carried out during the inter-event period, the parameter error dynamics are zero. Now, applying the norm operator, we get

$$\dot{L}(r, \tilde{\theta}_R^T) \leq -k_v \|r\|^2 + \|r^T\| \|\tilde{\theta}_R^T\| \|\phi(x)\| \|e_{ET}\| + \|r^T\| \|\varepsilon_d\| \tag{67}$$

Adding and subtracting $\|r^T\| \|\tilde{\theta}_R^T\| \|\phi(\bar{x})\|$ and using the Lipschitz inequality to get

$$\dot{L} \leq -k_v \|r\|^2 + \|r^T\| \|\tilde{\theta}_R^T\| (\|\phi(\bar{x})\| + \|\tilde{\theta}_R^T\| L_\phi) \|e_{ET}\| + \|r^T\| \varepsilon_d$$

$$\| \square \| \quad v \qquad R \qquad v \| R \| \qquad ET \| \quad \| R \| \quad x \quad \| \quad \| dM \tag{68}$$

Applying the definition of parameter estimation error and using triangle inequality, we get

$$\square k r \quad r^T (2 \square \hat{} \; ^T L \quad L \;) e \; (\;) \square r^T r \square \phi \sim \square \square \; _T \; T \tag{69}$$

$$v \qquad R \qquad v \quad RM \quad \square \quad \| \quad \| \| \quad ET \| \quad R \quad \| \quad \| \quad x \quad dM$$

Using the Lipschitz continuity of the regression vector and applying Young's inequality, we get

$$\square \; k r \; 2 \; \square \; ((4 \; \square \hat{} \; T \; 2 \; \square \; \square \frac{\| e_{ET} \|^2}{2} dM \frac{\| r^T \|^2}{2} \square \frac{\| \tilde{\theta}_R^{\;T} \|^2 \| \phi(\tilde{x}) \|^2}{2} \square 2 \| r^T \|^2 \frac{\tau \square}{2}$$

$$2 \;)L \; 4 \; \square \; k \; 2 \;) \; \| \; v \qquad R \qquad RM \qquad v \tag{70}$$

On simplifying the expression, we arrive at

$$2 \qquad \square \quad 2) \| \; r \; 2 \frac{(4 \| \hat{\theta}_R^{\;T} \|^2 + \theta_{RM}^2) L_\phi^{\;2} + k_v^3 \| e_{ET} \|^2}{2} \square \frac{\| \tilde{\theta}_R^{\;T} \|^2 \| \phi(\tilde{x}) \|^2}{2} \square \frac{\square}{2} \tag{71}$$

$$\square (k \quad dM$$

$$v$$

Using the event-sampling condition, $\|e\|^2 \leq \sigma\mu \|r\|^2$, we get

$$\dot{L}(r, \tilde{\theta}_R^T) \leq -(k_v - 2)\|r\|^2 + (2\hat{\theta}_R^T L^2 \|H\| + \frac{\|\tilde{\theta}_R^T\|^2 L^2 \|\phi(\tilde{x})\|^2}{2} + k_v^2 \frac{\mu_k}{dM}) \|r\|^2 \quad (72)$$

By choosing μ_k, as in (59), for each inter-event period, we have the Lyapunov first derivative as

$$\dot{L}(r, \tilde{\theta}_R^T) \leq -(k_v - 3)\|r\|^2 + \frac{\|\tilde{\theta}_R^T\|^2 \|\phi(\tilde{x})\|^2}{2} + \tau \quad (73)$$

From (73), it can be seen that the filtered tracking error is bounded during the inter-event period as long as $k_v > 3$, and since the unknown parameters are not updated, they remain bounded during the inter-event period such that

$$\|\tilde{\theta}_R^T(t)\| \leq \|\tilde{\theta}_R^T(t_k)\|, \quad t \in [t_k, t_{k+1}). \quad (74)$$

Therefore, from Case (i) and Case (ii), it can be concluded that the filtered-tracking error and the parameter estimation error remain bounded during the inter-event period. Due to the event-sampling condition, the measurement error introduced by the event- sampled feedback is also bounded during the inter-event period.

Remark 11. Notice that the value of μ_k obtained from (71) requires the information regarding the estimated parameters to determine the event-based sampling instants and also the bounds on the unknown mass matrix. This requires an additional adaptive estimator at the event-sampling mechanism that runs in parallel with the estimator at the controller. Also, it can be seen from the value of μ_k, that as the bounds on the mass matrix is increased, the event-sampling threshold is decreased causing frequent events.

Remark 12. From the results in Theorem 3, it can be seen that

the measurement error is bounded for all the inter-event period due to the event-sampling condition (26) with the value of μ_k obtained from (72). By choosing the k_V as required in the Lyapunov conditions in (73), we obtain $0 < \mu < 1$, $\forall k$. With the states of the closed-loop system defined as $Z = [r \; \theta_R]$, and using the Theorems 1 and 3, we have the ISS characterization in (30) and (31). Thus combining the results from Theorem 1, 3, the existence of a positive minimum inter event time can be established (Tabuada 2007).

Remark 13. The ultimate bound obtained in (64) can be made arbitrarily small by adjusting the controller gains K_V, κ. An increase in the disturbance input will increase the bounds on the tracking and parameter estimation errors.

Remark 14. Once the tracking error converges to a small value, a dead-zone operator can be used to minimize the events. This way the feedback information is not utilized frequently and computations can be reduced further. This is the trade-off between the tracking accuracy and computational cost, due to the event-sampled feedback.

Remark 15. With the event-sampling condition of the form (26), one can conclude that the tracking error is bounded during the inter-event period. By choosing a suitable Lyapunov function for the tracking error and by selecting the event-sampling condition such that the inequality $||r(t)||^2 \leq (1 - \tau_S)\alpha||r(t_k)||^2$, $t_k \leq t < t_{k+1}$, is satisfied during the

inter-event period, the tracking error can be made to decrease both during the event- sampling period and the inter event period (Wang and Lemmon 2011).

Next, the adaptive control design of the mobile robot is presented.

Mobile Robots

For the controller design of mobile robots, the event-sampling mechanism which decides the event-based feedback instants is crucial and is usually designed based on the closed-loop stability analysis. The event-sampling mechanism is designed such that the event-sampling error (2) satisfy a state-dependent threshold for every inter-event period for each robot, which is of the form

$$\|\square_i \;\square\; \square\; i\;\square_{ik} \quad t_k \square t \square t_k \square 1,\; k \;\square\; 1,\; 2,3.. \tag{75}$$

with $0 < \sigma_i < 1$, and μ_{ik} is a positive design parameter and E_{iET}, E_i are functions of event- sampling error and the formation, and velocity tracking errors respectively.

Using the results of Assumption 4, the unknown dynamics of the mobile robot can be represented by using standard LIP formulation. The unknown dynamics (23) is parametrized as

$$f(z) \;\square\; \square_{i\,i\,i}\square^{T}\square \tag{76}$$

where $\square$ is the unknown coefficients matrix with $\Theta = [-\ell\, Fv$

$\square_i \quad \square \quad \square_0$

$1i \quad i$

$\square\; 1\square 3 \quad 2i\;\square$

$Fd]$, $_{2i} = [\ell\, Fv\; Fd]$ with $\|\Theta_{iM}$ and $\square \quad \square \quad e \quad F$

$\Theta \quad \| \le \Theta \quad \square \quad \square_{\square} \quad \square \quad v \quad sign\square v \square \square v \square e^{F} \square$

$\square\square$

$\square$ $sign\square\square\square\square^{T}$ is the regression vector. The unknown parameters can be estimated as

$\hat{\Theta}_i$ and estimation of the unknown dynamics (76) with event sampled feedback can be given as

$$\hat{f}(z) \square \square \hat{T}\square \quad (77)$$

with $z_i \square e_i$ being the event-sampled signals at the i^{th} mobile robot. The unknown parameter estimation error is defined as $\square_i \square \square_i \square \hat{\square}_i$ and the estimation error dynamics can be given as

$$\square \quad \square \quad \square \quad \

with $\tilde{F}_{id} = F_{id} - F_{id}$ and $\tilde{v}_{id}$ is the stabilizing term with measurement error due to event-sampled mechanism. Substituting (78) into (21) reveals the closed-loop velocity tracking error dynamics

$$M_i \dot{e}_{iv} = -\left[e_{i1}, e_{i2}, e_{i3}\right] f(z_i) - K_v e_{iET} - \left[f(z_i) - f(z_i)\right] M_i \left[\dot{v}_{id} - \dot{\tilde{v}}_{id}\right] - K_v e_{iv}, \quad t_k \le t < t_{k+1}. \tag{79}$$

where $f(z_i) = \dot{\theta}_i \dot{\theta}_i z_i$.

Now, to define the formation error dynamics with event-sampled measurement error, consider (17), during the k^{th} inter-event period, the desired virtual control equations are obtained as

$$\begin{aligned} \dot{F}_{id} &= k_1 e_{i1} - \omega_i + \omega_j \\ \dot{v}_{id} &= \dot{F}_{id} - k_2 v_j e_{i2} - \beta_3 \sin(\theta_i - \theta_j) \end{aligned}, \quad t_k \le t < t_{k+1}. \tag{80}$$

where $e_{i1}, e_{i2}, v_j, \omega_i, \omega_j, \dot{\omega}_j$ are event-sampled formation error along x_{ci}, y_{ci}, event-sampled linear velocity of the j^{th} robot, event-sampled bearing angle of the i^{th}, j^{th} robot and the angular velocity of the j^{th} robot, respectively. Defining the event-sampled signals $\dot{\tilde{F}}_{id}(t) = \dot{F}_{id}(t_k)$, $\dot{\tilde{v}}_{id}(t) = \dot{v}_{id}(t_k)$, $t \in [t_k, t_{k+1})$, (80) can be rewritten with the measurement error as

$$\begin{aligned} \dot{\tilde{F}}_{id} &= k_1 e_{i1} - v_j \cos(\theta_i - \theta_j) \omega_i + v_j \omega_j \\ \dot{\tilde{v}}_{id} &= \dot{\tilde{F}}_{id} - k_2 v_j e_{i2} - \beta_3 \sin(\theta_i - \theta_j) \end{aligned}, \quad t_k \le t < t_{k+1}. \tag{81}$$

$$id \quad 2\ j\ i\ 2 \quad i \quad j \quad i \square$$
$$3 \qquad \square\ \square$$
$$j$$

where $v_{i\varepsilon}$, $\omega_{i\varepsilon}$ are given by $v_{i\varepsilon} = k_3[\sin(\theta_i - \theta_j) - \sin(\square_i \square \square_j)] + \varepsilon_{\omega j} - k_2 v_j \varepsilon_{i2} - k_2 \varepsilon_{vj} e_{i2} - k_2 \varepsilon_{vj} \varepsilon_{i2}$, and $\omega_{i\varepsilon} = - v_j [\cos(\theta_i - \theta_j) - \cos(\square_i \square \square_j)] + \varepsilon_{Vj} \cos(\square_i \square \square_j) - k_1 \varepsilon_{i1}$. To get the closed-loop formation error dynamics in the presence of measurement error, use (81) in (16) to get

$$\begin{aligned} e_{\square} \quad & e_{\square} \square \quad ke \ - e^F \quad \square \\ \square\ i1 \square \quad & i\,2 \quad i \quad 1 \ i1 \quad i \square \quad iv1 \quad \square \\ \square e \square \quad & \square e \square \square v \ \sin \square \square \square \square \quad (82) \\ \square \quad & \square \\ \square \quad & \square \\ \square\ i \ 2 \quad & \\ \square \quad & i1 \quad ij \quad i \quad j \\ \square e \square i3 \ \square_{2\ \square i\,2} \quad & \square_{3} \square k_i v \ e_j \quad \square_{i\varepsilon} \square_{iv\,2} \quad e^F \ \square \square \\ k \ \sin(\square \ \square \ \square) \ \square \ \square & \end{aligned}$$

The following theorem provides the stability analysis for the control law that does not require the perfect velocity tracking assumption. As noted before, the theorem does not assume that complete knowledge of the robot dynamics is available to compute the control law (24), and the controller is updated only during the event-based sampling instants. Similar to the case of the robot manipulator, it can also be shown that the mobile robot closed-loop dynamics is input-to-state stable, the proof of which is not included due to space consideration.

Theorem 4. *(Ideal case) Given the consensus error dynamics (79) for the i^{th} robot in the network with the disturbance torque $\bar{\tau}_d = 0$, let the consensus-based formation controller (78) be applied to the i^{th} robot. Let the control torque be defined by (78) with*

$$\square \quad \square \qquad \square e_{i1} \qquad \underline{1}$$
$$\square \square e_{i1}, e_{i\,2}, e_{i3} \qquad \square \qquad \square$$
$$\square \square M_i \qquad \lrcorner$$

(83)

$$\square\square \quad \sin e_{i3} \square$$
$$\square\square\ k_2$$

and the event-sampling condition (75) is used to determine the sampling instants. Further, when the unknown parameters are tuned at the sampling instants using the parameter adaptation rule

$$\dot{\hat{\theta}}_i = T_i \left(\frac{z_i}{e_{iv}} \right) F_i \qquad (84)$$

where $\Lambda_i = B_{im}^{-1} \Lambda_{im}$, $B_{im}, \Lambda_{im} > 0$, and $\kappa = 0$. *The velocity tracking error system (79) and consensus error system (19) remain bounded and the* i^{th} *robot tracks its desired velocity and reaches consensus with its neighbor robot j when the gains are chosen such that*

$$k_1 > \frac{k_2}{2} + \frac{5}{2}, \; k_2 > \frac{3}{2}, \; B_{im} K_{Vi} > 3, \; \Lambda_{im} > 0.$$

Proof. Case 1. With the event-sampled measurement error, $e_i = 0$, $\forall i$, $\kappa = 0$. The adaptation rule (84) is rewritten as

$$\dot{\hat{\theta}}_i = F_i T_i \left(\frac{z_i}{e_{iv}} \right) \qquad (85)$$

Consider the following Lyapunov candidate

$$L = \frac{1}{2} e_{i2}^2 + \frac{1}{2} e_{iv}^2 + \frac{1}{2} \tilde{\theta}_i^T F_i^{-1} \tilde{\theta}_i + \frac{1}{k_2} (1 - \cos e_{i3}) + \frac{1}{2} tr\{ \tilde{\theta}_i^T T_i^{-1} \tilde{\theta}_i \}. \qquad (86)$$

Taking the derivative of (86), we get

$$\dot{L} = e_{i2} \dot{e}_{i2} + e_{iv} \dot{e}_{iv} + \frac{1}{k_2} \dot{e}_{i3} \sin e_{i3} + \tilde{\theta}_i^T F_i^{-1} \dot{\tilde{\theta}}_i + tr\{ \tilde{\theta}_i^T T_i^{-1} \dot{\tilde{\theta}}_i \} \qquad (87)$$

$$2 \qquad \begin{matrix} iv \\ i \\ i \end{matrix} \qquad iv$$

Substituting the consensus error system (19) and velocity tracking error dynamics

(79) keeping the measurement error and the disturbance torque zero, reveals

$$L_i \square \square e_{i2} \square e \square \square e^F \square \square e \square \square v \sin \square \square \square \square \square \square \square \square k e \square \square e$$

$$\frac{1}{k_2} \square \square k v e \square k \sin \square \square \square \square \square \square e^F \square \sin e \qquad (88)$$

$$\square e^F T \square \square M \square 1 K e^F \square \square \square M \square 1 \square T \square \square z \square \square M \square 1 \gamma \square e ,e ,e \square tr \square \square T \square \square \square \square$$

Using the definition of e_{i3} in (88), we obtain the first derivative as

$$L_j \square \square k_1 e_{i1} \square e_{i1} e_{iv1} \square e_i \, 2v \, j \sin e_{i3} \qquad (89)$$

$$e_{i3} \square v \, j e_i \, 2 \sin e_{i3} \square \frac{3}{k_2} \sin \square \square \square i3 \; iv \; 2 \; k_2$$

$$\square e^F T \square \square M \square 1 K e^F \square \square \square M \square 1 \square T \square \square z \square \square tr \square \square T \square \square \square M \square 1 \gamma \square e ,e ,e$$

Utilizing the stabilizing term (83) in the control torque, we get

$$L \square \square \square k_3 e^2 \square e \, e^F \; \sin e \; e^F \; iv \; 2 \square \square \square ei1 \square \square \square k_3 \sin^2 e \; M \; K \; F \; 2 \; 1 \; F \; T \square \square$$

$$i \quad 1 \quad i1 \; iv1 \quad i3 \quad k \quad i \quad v \quad iviv \quad \sin e \square \square \quad k$$

$$i1 \quad k \quad 2 \quad 2 \quad \square \square^2$$

$i3$ □□

$$tr\{e_{iv}^{F} T_i M_i \tau_i T_i z_i\} \quad (90)$$

Using the bound on the mass matrix from Assumption 4 and trace property, we get

$$L_i \le -k_1 e_{i1}^2 - \frac{k_3}{2}\sin^2 e_{i3} + \frac{1}{k_2}\left(\frac{\|e_{i3}\|\|e_{iv}\|K_V}{2} + \frac{\|e_{iv}\|^2}{2}\sin^2 e_{i3}\right) + \frac{k_2}{2}\|e_{i1}\|^2\|e_{iv}\|^2 - e_{i1}^T e_{iv}^F + \frac{1}{k_2}\|e_{iv}\|\|e_{iv}^F\| + \frac{1}{k_2}\|e_{iv}\|\|e_{iv}^F\|^2$$

$$tr\{e_{iv}^{F} \tau_{im} T_i z_i T_i\} \le \|T_B\| \|e_{iv}^F\| \quad (91)$$

Using the parameter adaptation rule defined in (85) to get

$$\dot{L}_i \le -k_1 e_{i1}^2 - \frac{k_3}{2}\sin^2 e_{i3} + \frac{K_V}{k_2}\|e_{iv}^F\|^2 + \frac{1}{k_2}\|e_{iv}\|\|e_{iv}^F\| + \frac{1}{k_2}\|e_{iv}\|\|e_{iv}^F\|^2 \quad (92)$$

Since (92) is not a function of e_{i2} and the parameter estimation error, L_i is negative semi-definite, and the consensus errors and velocity tracking error are bounded. Therefore, Barbalat's Lemma can be used to show that the formation errors and the velocity tracking errors approach zero.

First, take the derivative of (92) while using (16) and (79), and observing the boundedness of all signals reveals that $\dot{L}_i$ is also bounded. Therefore, L_i converges to zero and thus $e_{i1}, e_{i3}, e_{iv}, \|e_{iv}^F\|$, and $\|e_{iv}^F\|$ all converge to zero as well. Finally, examining the definition in (16) while noting that $e_{i3} \to 0$ reveals that e_{i2} must also converge to zero. Therefore, the velocity tracking error system (79) and consensus error system (19) converge to the origin asymptotically, and the i^{th} robot

tracks its desired velocity and reaches consensus with its neighbor robot *j*.

Case 2: When the measurement error, $e_{i3} = 0, \forall t \in [t_k, t_{k+1}), \forall i \in T$, therefore, using the Lyapunov candidate function (86) and the first derivative is obtained as

$$\dot{L} = e_{i1}^T e_{i2} + e_{i2}^T \dot{e}_{i2} + e_{i3}^T \dot{e}_{i3} + \frac{1}{2} e_{i2}^T F_i^T e_{i2} F_i + \frac{1}{2} tr\{F_i^T \dot{F}_i\} \tag{93}$$

Utilizing the consensus error dynamics and the velocity tracking error dynamics with event-sampled measurement error from (82) and (79), we get

$$\dot{L} = e_{i1}^T e_{i2} + e_{i2}^T \dot{e}_{i2} + e_{i3}^T \dot{e}_{i3} + e_{i2}^T F_i \sin(e_{i3}) + e_{i2}^T F_i \sin(e_{i3}) - k_v e_{i2}^T e_{i3} - k_v e_{i3}^T e_{i3} + e_{i3}^T F_i \sin(e_{i3}) + e_{i3}^T F_i \sin(e_{i3}) + \frac{1}{2} F_i^T \dot{F}_i - \frac{1}{2} F_i^T \dot{F}_i$$

$$\dot{L} = e_{i1}^T e_{i2} + e_{i2}^T \dot{e}_{i2} + e_{i3}^T \dot{e}_{i3} + e_{i2}^T F_i \sin(e_{i3}) + e_{i3}^T F_i \sin(e_{i3}) - k_v e_{i2}^T e_{i3} - k_v e_{i3}^T e_{i3} + \frac{1}{2} F_i^T \dot{F}_i$$

$$\dot{e}_{iv} = K_v e_{iv} + \gamma e_i + f z_i + K_v e_{iET} - \frac{M_i}{e_{iv} M_i} e_{iv} - \frac{M_i}{e_{iv} M_i} e_{iv}$$

$$\dot{e}_{iv} = K_v e_{iv} + \gamma e_i + f z_i + K_v e_{iET} - \frac{M_i}{e_{iv} M_i} e_{iv} - \frac{M_i}{e_{iv} M_i} e_{iv}$$

$$\dot{e}_{iv} = K_v e_{iv} + \gamma e_i + f z_i + K_v e_{iET} - \frac{M_i}{e_{iv} M_i} e_{iv} - \frac{M_i}{e_{iv} M_i} e_{iv} \tag{94}$$

Using the definition of e_{i3} and expanding the expression, we obtain

$$\dot{e}_{i3} = \dot{e}_{iv} + k_{i2} e_{iv} + \frac{k_{i2}}{k_{i1}} \dot{e}_{i1} + k_{i1} e_{i1} + \frac{k_{i2}}{k_{i1}} \left(\frac{k_{i3}}{2} \sin^2(e_{i1}) + \frac{1}{2} \right) \dot{e}_{i1} + \frac{k_{i2}}{k_{i1}} \left(\frac{k_{i3}}{2} \sin^2(e_{i1}) + \frac{1}{2} \right) k_{i1} e_{i1}$$

$$+ \frac{k_{i2}}{k_{i1}} \left(\frac{k_{i3}}{2} \sin^2(e_{i1}) + \frac{1}{2} \right) \left(\frac{k_{i3}}{2} \sin^2(e_{i1}) + \frac{1}{2} \right) \dot{e}_{i1} + \frac{k_{i2}}{k_{i1}} \left(\frac{k_{i3}}{2} \sin^2(e_{i1}) + \frac{1}{2} \right) \left(\frac{k_{i3}}{2} \sin^2(e_{i1}) + \frac{1}{2} \right) k_{i1} e_{i1}$$

$$+ \frac{k_{i2}}{k_{i1}} \left(\frac{k_{i3}}{2} \sin^2(e_{i1}) + \frac{1}{2} \right) \left(\frac{k_{i3}}{2} \sin^2(e_{i1}) + \frac{1}{2} \right) \left(\frac{k_{i3}}{2} \sin^2(e_{i1}) + \frac{1}{2} \right) \dot{e}_{i1} + \frac{k_{i2}}{k_{i1}} \left(\frac{k_{i3}}{2} \sin^2(e_{i1}) + \frac{1}{2} \right) \left(\frac{k_{i3}}{2} \sin^2(e_{i1}) + \frac{1}{2} \right) \left(\frac{k_{i3}}{2} \sin^2(e_{i1}) + \frac{1}{2} \right) k_{i1} e_{i1}$$

$$+ \frac{k_{i2}}{k_{i1}} \left(\frac{k_{i3}}{2} \sin^2(e_{i1}) + \frac{1}{2} \right) \left(\frac{k_{i3}}{2} \sin^2(e_{i1}) + \frac{1}{2} \right) \left(\frac{k_{i3}}{2} \sin^2(e_{i1}) + \frac{1}{2} \right) \left(\frac{k_{i3}}{2} \sin^2(e_{i1}) + \frac{1}{2} \right) \dot{e}_{i1}$$

$$+ \frac{k_{i2}}{k_{i1}} \left(\frac{k_{i3}}{2} \sin^2(e_{i1}) + \frac{1}{2} \right) \left(\frac{k_{i3}}{2} \sin^2(e_{i1}) + \frac{1}{2} \right) \left(\frac{k_{i3}}{2} \sin^2(e_{i1}) + \frac{1}{2} \right) \left(\frac{k_{i3}}{2} \sin^2(e_{i1}) + \frac{1}{2} \right) k_{i1} e_{i1}$$

$$+ \frac{k_{i2}}{k_{i1}} \left(\frac{k_{i3}}{2} \sin^2(e_{i1}) + \frac{1}{2} \right) \left(\frac{k_{i3}}{2} \sin^2(e_{i1}) + \frac{1}{2} \right) \left(\frac{k_{i3}}{2} \sin^2(e_{i1}) + \frac{1}{2} \right) \left(\frac{k_{i3}}{2} \sin^2(e_{i1}) + \frac{1}{2} \right) \left(\frac{k_{i3}}{2} \sin^2(e_{i1}) + \frac{1}{2} \right) \dot{e}_{i1}$$

$$+ \frac{k_{i2}}{k_{i1}} \left(\frac{k_{i3}}{2} \sin^2(e_{i1}) + \frac{1}{2} \right) \left(\frac{k_{i3}}{2} \sin^2(e_{i1}) + \frac{1}{2} \right) \left(\frac{k_{i3}}{2} \sin^2(e_{i1}) + \frac{1}{2} \right) \left(\frac{k_{i3}}{2} \sin^2(e_{i1}) + \frac{1}{2} \right) \left(\frac{k_{i3}}{2} \sin^2(e_{i1}) + \frac{1}{2} \right) k_{i1} e_{i1}$$

$$+ \frac{k_{i2}}{k_{i1}} \left(\frac{k_{i3}}{2} \sin^2(e_{i1}) + \frac{1}{2} \right) \left(\frac{k_{i3}}{2} \sin^2(e_{i1}) + \frac{1}{2} \right) \left(\frac{k_{i3}}{2} \sin^2(e_{i1}) + \frac{1}{2} \right) \left(\frac{k_{i3}}{2} \sin^2(e_{i1}) + \frac{1}{2} \right) \left(\frac{k_{i3}}{2} \sin^2(e_{i1}) + \frac{1}{2} \right) \left(\frac{k_{i3}}{2} \sin^2(e_{i1}) + \frac{1}{2} \right) \dot{e}_{i1}$$

$$+ \frac{k_{i2}}{k_{i1}} \left(\frac{k_{i3}}{2} \sin^2(e_{i1}) + \frac{1}{2} \right) \left(\frac{k_{i3}}{2} \sin^2(e_{i1}) + \frac{1}{2} \right) \left(\frac{k_{i3}}{2} \sin^2(e_{i1}) + \frac{1}{2} \right) \left(\frac{k_{i3}}{2} \sin^2(e_{i1}) + \frac{1}{2} \right) \left(\frac{k_{i3}}{2} \sin^2(e_{i1}) + \frac{1}{2} \right) \left(\frac{k_{i3}}{2} \sin^2(e_{i1}) + \frac{1}{2} \right) k_{i1} e_{i1}$$

$$+ \frac{k_{i2}}{k_{i1}} \left(\frac{k_{i3}}{2} \sin^2(e_{i1}) + \frac{1}{2} \right)

$$iv1\ \ i2i\ \ iv\ i\ \ i\ \ _{iv}\ \ i\square\ \ _{v}\ \ iE\ \ iv1\ i1\ \ i3\ \ i1\ \ iv1\ v\ i$$
$$2$$

with $\varepsilon_i = [\varepsilon_{i1}\ \varepsilon_{i2}]$. Utilizing the definition of the event-sampled formation errors, we get

$$L\square 1K\ e^{F}k\ 2e\ \square\ 1\ k3\sin^{2}(e\ )\square M\ \square e^{F}\ [\sin\ \ \sin\square]\square e\ k\ \square\ \ e\ k\square e$$
$$\|\ \|\qquad\qquad e$$

$$i\ \ 1\ \ i1\ \ \ i3\ \ i\ \ v\ \ \ iv\ \ \ k\ \ \ iv\ \ 2\ \ e\ \ i1\ 2\ j\ \ i1\ 2\ vj\ i\ 2$$
$$k\qquad\qquad 3\qquad f\qquad 3\qquad i2$$
$$i3\ k$$

$$\square e^{F}T\ \ M^{2}\square 1\ \square\ T\ \ 1\ \square)e\ \ K\square\ \ e^{2}k\ [\sin\ \ \sin\ ]\ \square\ \square\ \ e\ k\square\ \square$$
$$(L\qquad\qquad e\qquad\qquad e$$
$$iv\ i\ \ i\ \ z_i\ \ iv\ i\qquad\qquad\qquad e_{i3}\ i1$$
$$i\square\qquad\qquad v\ \ \ iv\ \ \ i1\ \ \ 3\qquad\square j\qquad i1\ 2\ vj\ i\ 2$$
$$iE\qquad 1\qquad\qquad i$$
$$T\qquad i1\ \ 3$$

$$\square\ \ \frac{1}{}\ \sin\ \cos\qquad\sin\square\ \cos\ \square\ \ \frac{1}{}\ \square\ .L\qquad\qquad (96)$$
$$e\ v\ [\cos e\qquad e\square\qquad\qquad\sin e\ k\ \square$$
$$k\qquad i3\ \ j\ \ i3\qquad e_{i3}\ \frac{1}{k}\qquad i3\qquad vj$$
$$e_{i3}\ k\qquad\qquad\qquad\qquad i3\ \ 1\ \ i1\ \ v\ i$$
$$2\qquad\qquad\qquad 2\qquad\qquad 2$$

Using the definition of $\breve{y}$ in (96) to obtain

$$\square\qquad 2\ k\qquad\qquad\square 1\ \ F\ \ 2\qquad e^{F}\qquad\square\qquad\square$$
$$2$$
$$L_j\ \square\ \square k_1 e_{i1}\ \square\ \frac{3}{}\ K\|\ \|\ \square\ \ \frac{iv\ 2}{}\ [\sin e_{i3}\square\sin e_{i3}\ ]\square e_{i1}k_2\ (v_j$$
$$\sin\ (e_{i3})\square M_i\qquad e_{iv}\qquad\qquad k_2\qquad\qquad vj\ )\square i\ 2\ \square\ e_{i1}k_2\square vje_{i\ 2}$$
$$k_2$$
$$\square e^{F}T\ \ M^{2}\square 1\ \square\ T\qquad\qquad e_{i3}\ i1$$
$$\square\ \ e\qquad M\ \ 1\ \square\ \ \square)e\ \ K\square F\ \ e_k\ [\sin\ \ \sin\ ]\ \square\ \square\ \ e\ k\square\ \square$$
$$iv\ i\ \ i\ \ z_i\ \ iv\ i\qquad\qquad\qquad e$$
$$i\square\qquad\qquad v\ \ \ iv\ \ \ i1\ \ \ 3\qquad\square j\qquad i1\ 2\ vj\ i\ 2$$
$$iE\qquad 1\qquad\qquad i$$
$$T\qquad i1\ \ 3$$

$$\square\ \frac{1}{}\ \sin\ e\ (\ )[\cos e\ \cos\qquad\qquad\square\ \ \frac{1}{}\ \sin\ e\ k\ \square$$
$$\sin e\ \square\ ]\ \square\qquad\square\ \ L\ \square\ .\qquad\qquad (97)$$
$$k\qquad i3\ \ v\ j\qquad\qquad i3\qquad e_{i3}\qquad\qquad i3\qquad vj\ \cos e_{i3}\qquad k$$
$$i3\ \ 1\ \ i1\ \ v\ i\qquad\qquad k$$
$$2\qquad\qquad\qquad 2\qquad\qquad 2$$

Applying the norm operator, we obtain the inequality as

$$L \le -\frac{1}{2}k_2 e_{i1}^2 - \frac{1}{2}k_3 \sin^2(e_{i3}) + M_F \left[\sin\left(\frac{k_1\|\varepsilon_{i1}\|}{k_2}\right)\right] \|e_{i3}\| + \|e_{i1}\| k \|e_{i2}\| + \|e_{i2}\| k \|e_{i3}\| + \|e_{i1}\| k \|e_{i3}\| + \|e_{i3}\| k \|e_{i3}\| + \|e_{i3}\| k \|e_{i3}\| + \|e_{i3

$$\frac{1}{2}M_{i\phi}(L_{i\phi}+K_{i\phi}\|e_i\|^2)\|e_i\|^2+\frac{1}{2}\left(\frac{1}{\gamma_{i1}}+k_{i1}\right)\|v_i\|^2+\frac{1}{2}k_{i2}\|v_i\|^2+\frac{1}{2}\left(\frac{1}{\gamma_{i2}}+k_{i2}\right)\|v_j\|^2+\frac{1}{2}\|e_i\|^2+\frac{1}{2}\|e_i\|^2+\frac{1}{2}\left(\frac{1}{\gamma_{i2}}+k_{i2}\right)\|v_j\|^2+\frac{1}{2}\left(\frac{1}{\gamma_{i1}}+k_{i1}\right)\|v_i\|^2+B_i.$$

$$\frac{1}{2}\|e_i\|^2+\frac{1}{2}\left(\frac{1}{\gamma_{i1}}+k_{i1}\right)\|v_i\|^2+\frac{1}{2}\left(\frac{1}{\gamma_{i2}}+k_{i2}\right)\|v_j\|^2+\frac{1}{2}\|e_i\|^2+\frac{1}{2}\|e_i\|^2+\frac{1}{2}\left(\frac{1}{\gamma_{i2}}+k_{i2}\right)\|v_j\|^2+\frac{1}{2}\left(\frac{1}{\gamma_{i1}}+k_{i1}\right)\|v_i\|^2+B_i.$$

with the bounding term $B_i=\frac{1}{2}k_{i3}^2+\frac{1}{2}\|e_i\|^2+\frac{1}{2}\|\tilde{v}_i\|

$i3 \| iv \| \quad i \quad 1 \quad 2 \quad ET \| iET \quad i1$

$\| \square i \|^2 \quad \square i \quad i$

$2 \quad 1 \square \quad 1 \; 2 \;]T$,

$i \, 2$

we get

$$L \le \frac{1}{M}\left(L - \left[\frac{1}{2} - K\right)\left(k_1 - \frac{k_2 v_i^2}{2}\right) - \frac{1}{2}\left(\frac{1}{k_2} + \frac{1}{2}\right)\left\|\varepsilon_{i1}\right\|^2 + \frac{1}{2}\left\|\varepsilon_{iET}\right\|^2\right] + \frac{1}{2}\left\|\varepsilon_{i2}\right\|^2 + \frac{1}{2}\left(\frac{1}{2} - \frac{k_2 v_i^2}{2}\right)\left\|e_{i1}\right\|^2 + \frac{5}{2}\left\|\varepsilon_{iET}\right\|^2 + \frac{1}{2}\left\|\varepsilon_{i2

From (103), it can be seen that the formation and velocity tracking errors are

bounded during the inter-event period $[t_k, t_{k+1})$, provided $k_1 > \frac{k_2 \|B\|^2 \|K\|^2}{\lambda_{min}(Q)}$

and since the unknown parameters are not updated, they remain bounded during the inter-event period such that

$$\|\tilde{\theta}_i(t)\| \leq \|\tilde{\theta}_i(t_k)\|, \quad t \in [t_k, t_{k+1}). \tag{104}$$

Therefore, from Case (i) and Case (ii), it can be concluded that the velocity-tracking errors, formation and the parameter estimation errors remain bounded during the inter- event period. Due to the event-sampling condition, the measurement error introduced by the event-sampled feedback is also bounded during the inter-event period.

Remark 17. The evolution of the velocity tracking error and the formation error with event-sampled implementation of the controller is presented with the adaptation law (84) with an additional term to relax the PE condition and to ensure that the parameter estimation errors are bounded. Similar to the ideal case, analytical results can be obtained for $\tau_d, \kappa \neq 0$. The bounds on the closed loop signals for this case will be obtained as a function of the τ_d and the epsilon modification (Narendra and Annaswamy 2012) term in the adaptation rule.

Remark 18. From the results in Theorem 4, it can be seen that the measurement error is bounded for all the inter-event period due to the event-sampling condition (75) with the value of μ_k obtained from (102). Similar to the case of robot manipulator, with the states of the closed-loop system defined as $Z = [e\ e^F\ \Theta]^T$, the ISS characterization can be obtained. With the ISS characterization and the Assumption 5 on Lipschitz continuity of the error dynamics, the existence of a positive minimum inter event time can be established (Tabuada 2007).

Remark 19. Notice that the value of μ_k obtained from (102) requires the information regarding the last updated information of the j^{th} robot to determine the event-based sampling instants. Also, for the event-sampling condition, the formation errors and the measurement errors for the i^{th} robot can be calculated with the previously obtained information from the j^{th} robot, the details of which are not included in this chapter. This makes the event-sampling mechanism decentralized.

Remark 20. From the results in Theorem 4, it can be seen that the measurement error is bounded for all the inter-event period due to the event-sampling condition (75) with the value of μ_k obtained from (102). By choosing the gains as required in the Lyapunov conditions in (103), we obtain $0 < \mu < 1$, $\forall k$.

Remark 21. Once the velocity tracking and the formation errors converge to a small value, a dead-zone operator can be used to minimize the events. This way the feedback information is not utilized frequently and computations, communication can be reduced further.

Next, the simulation results are presented to verify the proposed event-sampled controller design for the robotic systems.

RESULTS AND DISCUSSIONS

In this section, the simulation results for the event-sampled control of a 2-link robotic manipulator are presented first, followed by the results of event-sampled formation control to illustrate the effectiveness of the proposed analytical design.

Example 1. Consider the dynamical equation of the robotic

manipulator with two-joint angles q_1, q_2. The following parameters are used in the simulation results presented here. $m_1 = 1$, $m = 2.3$, $L_1 = 1$, $L_2 = 1$, $g = 9.8$. The following parameters are used in the controller $k_V = 30I$; $\lambda = 0.5I$, $\kappa = 0.1$ and the event-sampling mechanism with $\sigma = 0.05$, $L_\phi = 5$, $\theta_{RM} = 5$. The initial joint angles and the unknown parameters were chosen randomly in the interval [0,1]. For the desired trajectory, $\sin(\omega t)$, $\cos(\omega t)$ were chosen with $\omega = 0.4$, $\tau = [0.8 \sin(2\omega t)\ 0.7 \cos(4\omega t)]^T$. It should be noted from the event-sampling condition (59) that as the bounds on the mass matrix is increased, the event-sampling threshold is decreased causing frequent events.

The performance of the adaptive controllers with continuous feedback is presented first Figs. 2 and 3. This will be used to analyze the performance of the event-sampled controllers. Due to the continuous feedback, the tracking error and the parameter estimation error converges to their respective ultimate bounds very quickly. In order to compare the performance of the event-sampled controllers, simulations are carried out without changing any controller parameters and initial conditions.

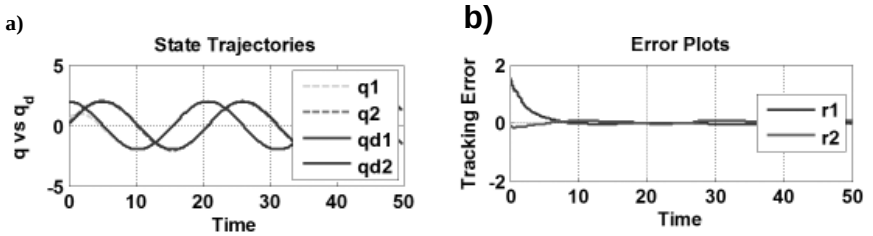


Figure 2(a). Joint angle trajectories. **(b)** Tracking errors (Continuous feedback).

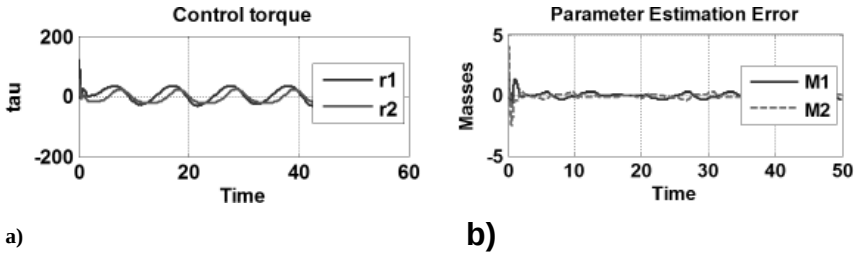


Figure 3(a). Control torque. **(b)** Estimation error (Continuous feedback).

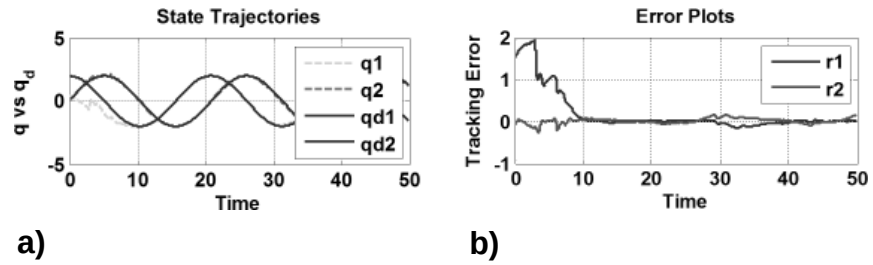


Figure 4(a). Joint angle trajectories. **(b)** Tracking errors (Event-sampled feedback).

The designed event-sampled controllers were able to stabilize the robotic manipulator and the parameter tuning rule was able to learn the uncertain dynamics of the robotic manipulator. The desired and actual joint angles are plotted together in Fig. 4a while the tracking error trajectory is plotted in Fig. 4b. The ultimate bounds of the tracking error were slightly larger when compared to the continuous feedback

case (Figs. 2a and 2b).

The control torque and parameter estimation error with event-sampled feedback is shown in Figs. 5a and 5b. It can be observed that with the event-sampled feedback, the bound on parameter estimation error is slightly higher compared to continuous feedback (Figs. 3a and 3b). This is due to intermittent feedback based on the event- sampling instants.

Figure 6 depicts the performance of the event-sampling mechanism. It can be seen that the computations, for a single robotic manipulator operated for 50 seconds, are reduced by approximately 33%. During this adaptation period, out of the 5000 sensor samples 3365 samples are utilized to generate the control torque, without compromising the tracking performance. If the bound on the unknown mass matrix is increased, the event-sampling threshold is reduced creating more events.

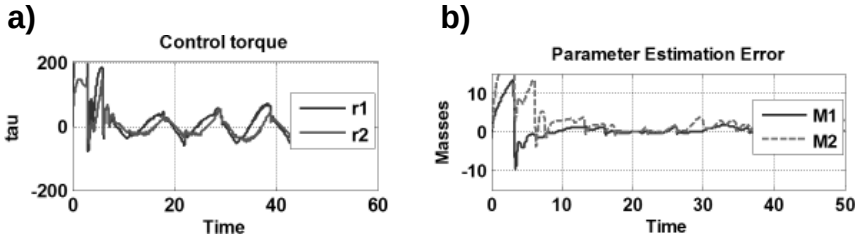


Figure 5(a). Control torque. **(b)** Estimation error (Event-sampled feedback).

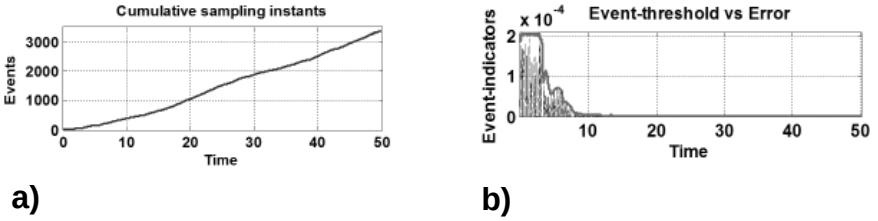


Figure 6. Event-sampling mechanism **(a).** Total events, and **(b)** Measurement error vs. Threshold.

Table 1. Number of sampling instants with different threshold parameter σ.

σ	Total Sensor Samples	Event-based Samples	Percentage Reduction
0.03	5000	3739	25.22
0.04	5000	3647	27.06
0.05	5000	3365	32.7

The design parameter σ in the event-sampling mechanism can be used to change the threshold on the measurement error during the inter-event period. When the threshold is large, the measurement error is allowed to increase to a larger value and therefore, the events are spaced out. This reduces the computations, while the tracking error and the parameter estimation errors remain bounded. The Table 1, lists the variation in the event-based sampling instants as the design parameter σ is increased. It can be seen that as the threshold is increased the event-based sampling instants are reduced

considerably. The simulation figures presented before are obtained with $\sigma = 0.05$, where all the signals are very close to those obtained with continuous feedback. This indicates the efficiency of using the event-based feedback. It should also be noted that increasing σ further, reduced the event-based sampling instants. However, the tracking performance is still achieved at the expense of more control effort.

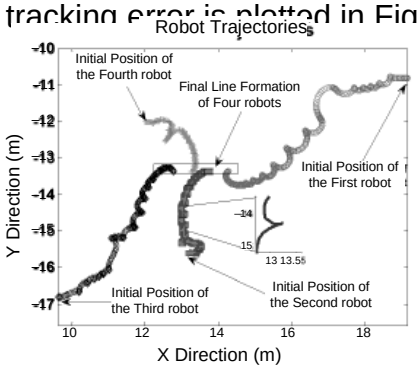
Example 2. To illustrate the effectiveness of the proposed event-based adaptive controller, a group of four non-holonomic mobile robots is considered. The robots are initiated from an arbitrary position and move to a desired shape of a square. The desired and initial positions, initial bearing angles and the initial velocities of the non- holonomic mobile robots are given by

$x_1(t_0) = 15.6$, $x_2(t_0) = 13.1$, $x_3(t_0) = 9.6$, $x_4(t_0) = 12$, $x_1^d = .5$, $x_2^d = .5$, $x_3^d = -.5$, $x_4^d = -.5$, $y_1^d = .5$, $y_2^d = -.5$, $y_3^d = -.5$, $y_4^d = .5$, $y_1(t_0) = -10.8$, $y_2(t_0) = -15.6$, $y_3(t_0) = -16.8$, $y_4(t_0) = -12$, $\theta_1(t_0) = 0$, $\theta_2(t_0) = 0$, $\theta_3(t_0) = 0$, $\theta_4(t_0) = 0$, $\theta_1^d = \pi$, $\theta_2^d = \pi$, $\theta_3^d = \pi$, $\theta_4^d = \pi$

The controller gains are selected as $K_V = 80$, $k_1 = 2$, $k_2 = 1$, $k_3 = 0.5$. The parameters for the robot dynamics are selected as $m = 5$ kg, $I = 3$ kg^2, $R = 0.15$ m, r = 0.08 m, d = 0.1 m for each robot and the mass matrix is calculated as $M = \begin{bmatrix} 810 & 0 \\ 0 & 133.02 \end{bmatrix}$, and $||M^{-1}|| = 0.0075$. Figure 7 depicts the motion of four independent non-holonomic mobile robots with continuous feedback. They are initiated in a non-square shape which can be seen on the plot.

Given their desired locations, they form a square shape by minimizing the consensus error along x, y, θ in the first case and in the second case the robots align along a straight line. The friction coefficients and the Coriolis matrix are considered uncertain as described in the problem formulation. The initial movements of the robots are oscillatory because of the unknown dynamics. With the parameter adaptation using $\Lambda = 40$, $\kappa_i = 50$, the controllers of each robot learns the unknown parameters. Once the uncertain parameters are tuned, the robots reach consensus.

The robots reach consensus around 30th second as it can be viewed in Figs. 8 and 9. The difference between the virtual controller (which is the desired linear and angular velocities to reach consensus) and the actual linear and angular velocities which is the velocity tracking error is plotted in Fig. 9.



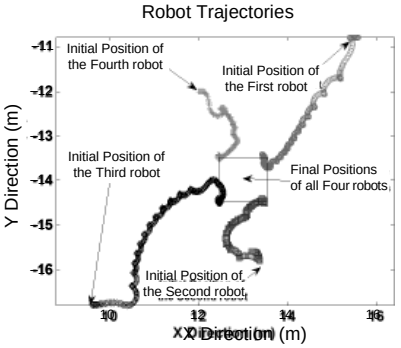


Figure 7. Mobile robots moving to their desired formation.

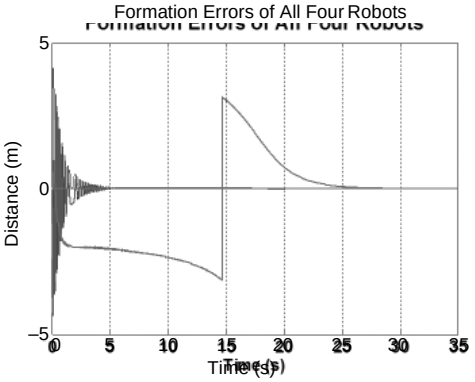


Figure 8. Formation errors on bot x and y directions.

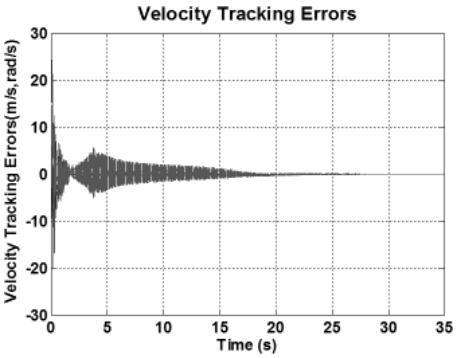


Figure 9. Velocity tracking errors.

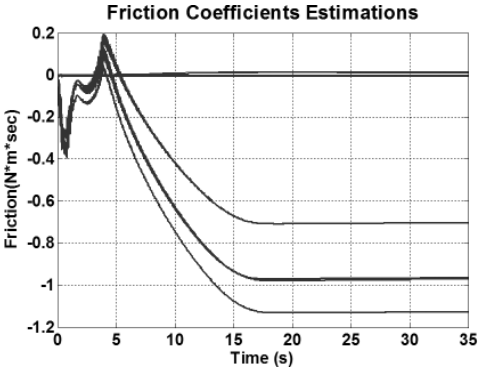


Figure 10. Frictions parameters estimates their desired formation.

The viscous and Coulomb frictions coefficients of each robot converge to a steady state value as shown in Fig. 10. Since the robots may move in different terrain, the friction terms may change over time. Therefore, adaptation by the controller is valuable and is achieved with the designed controller.

The event-sampling mechanism was designed with k_1, k_2, k_3, k_V as selected in the controller and $\sigma = 0.5$, $N_i = 1$, $L_{\phi i} = 5$, $B_{im} = 0.075$. To compare with the controller with continuous feedback, all the controller gains and initial values of the parameters and
the initial conditions of the robots were unchanged. With the

proposed event-sampled feedback, the mobile robots were able to reach the desired consensus as seen in Fig. 11. The formation errors remain bounded in Fig. 12 and the velocity tracking error remains bounded as in Fig. 13. However, due to the aperiodic feedback, these bounds are slightly larger compared to their continuous counterpart.

The parameter adaptation with aperiodic event-based updates resulted in a bounded parameter estimation error as depicted in Fig. 14. Clearly, the bounds on these errors were higher compared to the continuously updated case. Due to the designed event- sampling mechanism at each robot, the total number of parameter updates and the communication instants are considerably reduced as seen in Fig. 15.

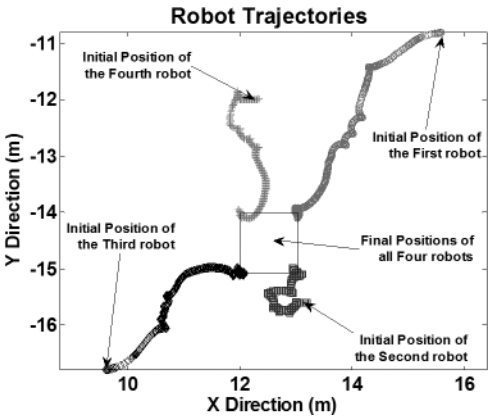


Figure 11. Mobile robots moving to their desired formation.

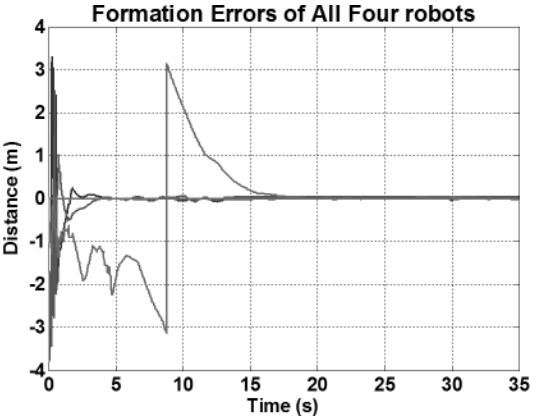


Figure 12. Formation errors on bot x and y directions.

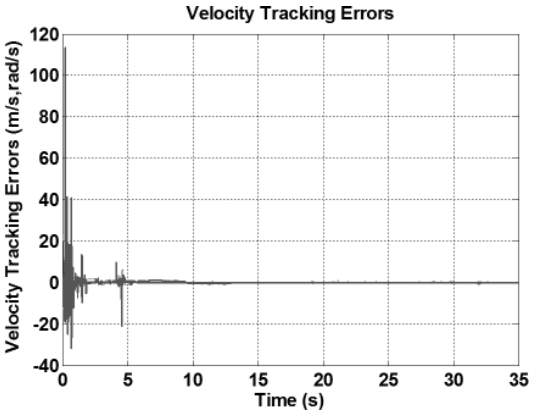


Figure 13. Velocity tracking errors.

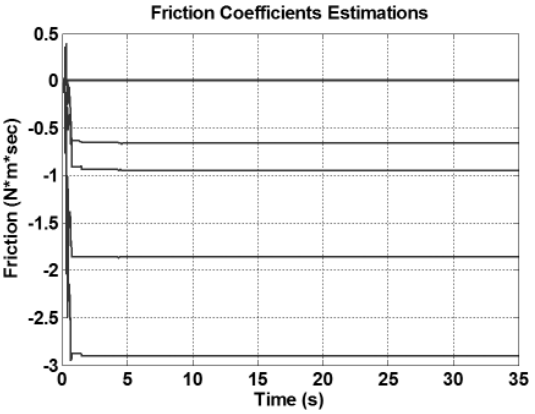


Figure 14. Friction coefficient estimates.

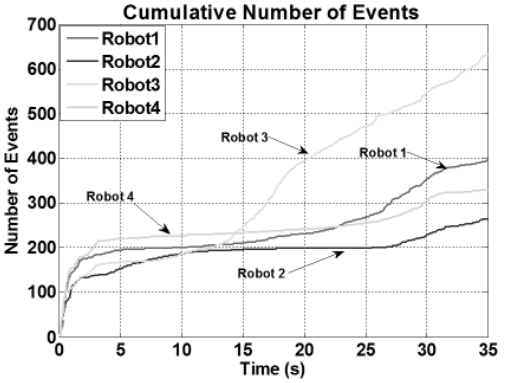


Figure 15. Cumulative number of events of each robot.

Table 2. Number of sampling instants (average of four robots) with different threshold parameter σ.

σ	Total Sensor Samples	Event-based Samples	Percentage Reduction
0.4	5237	690	86.82
0.2	5357	806	84.96
0.1	5517	1138	79.37

In the event-sampling condition, when the design parameter σ_i was varied, the threshold on the event-sampled measurement error changed. This resulted in the reduction of

events with an increase in σ_i whereas the bounds on the closed-loop error signals go up.

CONCLUSIONS

In this chapter, the event-based control implementations for the robotic systems were presented. The adaptive event-sampled torque control for the robotic manipulator was able to drive the joint angles to track the desired trajectories with bounded error due to

event sampled measurement errors. The bounds are also found to be a function of the disturbance bounds. The event-sampling mechanism was able to generate additional events so that the tracking error remains bounded in the presence of disturbance.

Next the event-sampled adaptive control of mobile robot formation was derived. The uncertain friction and Coriolis terms are represented in the LIP form and are adaptively tuned by the controller at event-sampled instants. Using the dynamics as well as the kinematics of the mobile robot, the consensus error and the velocity tracking errors were controlled. The event-sampling condition at each robot and the parameter adaptation rules were derived using the Lyapunov stability analysis. The analytical results were verified using the simulation examples and the efficiency of the event- sampled controller execution was demonstrated.

REFERENCES

Balch, T. and R. C. Arkin. 1998. Behaviour-based formation control for multi-robot teams. Robotics and Automation, IEEE Transactions on, 14(6): 926–939.

Bauso, D., L. Giarré and R. Pesenti. 2009. Consensus for networks with unknown but bounded disturbances. SIAM Journal on Control and Optimization, 48(3): 1756–1770.

Cheah, C. C., X. Li, X. Yan and D. Sun. 2015. Simple PD control scheme for robotic manipulation of biological cell. Automatic Control, IEEE Transactions on, 60(5): 1427–1432.

Fierro, R. and F. L. Lewis. 1998. Control of a non-holonomic mobile robot using neural networks.

Neural Networks, IEEE Transactions on, 9(4): 589–600.

Galicki, M. 2015. Finite-time control of robotic manipulators. Automatica, 51: 49–54.

Guinaldo, M., D. Lehmann, J. Sanchez, S. Dormido and K. H. Johansson. 2012. December. Distributed event-triggered control with network delays and packet losses. pp. 1–6. *In*: Decision and Control (CDC), 2012 IEEE 51st Annual Conference on, IEEE.

He, W., A. O. David, Z. Yin and C. Sun. 2015a. Neural network

control of a robotic manipulator with input deadzone and output constraint. Systems, Man and Cybernetics: Systems, IEEE Transactions on (In Press).

He, W., Y. Dong and C. Sun. 2015b. Adaptive neural impedance control of a robotic manipulator with input saturation. Systems, Man and Cybernetics: Systems, IEEE Transactions on (In Press).

Hong, Y., J. Hu and L. Gao. 2006. Tracking control for multi-agent consensus with an active leader and variable topology. Automatica, 42(7): 1177–1182.

Khalil, H. K. and J. W. Grizzle. 1996. Nonlinear systems (Vol. 3). New Jersey: Prentice hall.

Lewis, F. L., D. M. Dawson and C. T. Abdallah. 2003. Robot manipulator control: theory and practice.

CRC Press.

Low, C. B. 2011. December. A dynamic virtual structure formation control for fixed-wing UAVs. pp.

627–632. *In*: Control and Automation (ICCA), 2011 9th International Conference on, IEEE. Min, H. K., F. Sun, S. Wang and H. Li. 2011. Distributed adaptive consensus algorithm for networked

Euler-Lagrange systems. Control Theory & Applications, IET, 5(1): 145–154.

Molin, A. and S. Hirche. 2013. On the optimality of certainty equivalence for event-triggered control systems. Automatic Control, IEEE Transactions on, 58(2): 470–474.

Narendra, K. S. and A. M. Annaswamy. 2012. Stable adaptive systems. Courier Corporation.

Olfati-Saber, R. and R. M. Murray. 2004. Consensus problems in networks of agents with switching topology and time-delays. Automatic Control, IEEE Transactions on, 49(9): 1520–1533.

Qu, Z. 2009. Cooperative control of dynamical systems: applications to autonomous vehicles. Springer Science & Business Media.

Ren, W. and R. W. Beard. 2005a. Consensus seeking in multi-agent systems under dynamically changing interaction topologies. Automatic Control, IEEE Transactions on, 50(5): 655–661.

Ren, W., R. W. Beard and E. M. Atkins. 2005b. June. A survey of consensus problems in multi-agent coordination. pp.

1859–1864. *In*: American Control Conference, 2005. Proceedings of the 2005, IEEE.

Sahoo, A., H. Xu and S. Jagannathan. 2015. Near optimal event-triggered control of nonlinear discrete- time systems using neuro-dynamic programming. Neural Networks and Learning systems, IEEE Transactions on (In press).

Semsar-Kazerooni, E. and K. Khorasani. 2008. Optimal consensus algorithms for cooperative team of agents subject to partial information. Automatica, 44(11): 2766–2777.

Semsar-Kazerooni, E. and K. Khorasani. 2009. June. Analysis of actuator faults in a cooperative team consensus of unmanned systems. pp. 2618–2623. *In*: American Cont. Conf., 2009. ACC'09. IEEE.

Sheng, L., Y. J. Pan and X. Gong. 2012. Consensus formation control for a class of networked multiple mobile robot systems. Journal of Control Science and Engineering, pp. 1–12.

Tabuada, P. 2007. Event-triggered real-time scheduling of stabilizing control tasks. Automatic Control, IEEE Transactions on, 52(9): 1680–1685.

Tian, Y. P. and C. L. Liu. 2008. Consensus of multi-agent systems with diverse input and communication delays. Automatic Control, IEEE Transactions on, 53(9): 2122–2128.

Wang, X. and M. D. Lemmon. 2011. Event-triggering in distributed networked control systems.
Automatic Control, IEEE Transactions on, 56(3): 586–601.

Zhong, X., Z. Ni, H. He, X. Xu and D. Zhao. 2014. July. Event-triggered reinforcement learning approach for unknown nonlinear continuous-time system. pp. 3677–3684. *In*: Neural Networks (IJCNN), 2014 International Joint Conference on, IEEE.

8

Design, Integration and Analysisof a Hybrid Controller for MultiDegrees of Freedom Serial Mechanisms

Dan Zhang[1] and *Bin Wei*[2,*]

ABSTRACT

This paper proposes a hybrid controller by combining a PID controller and a model reference adaptive controller (MRAC), and also compares the convergence performance of the PID controller, model reference adaptive controller, and PID+MRAC hybrid controller. The results show that the convergence speed and its performance for the MRAC controller and PID+MRAC controller is better than that of the PID controller. The convergence performance for the hybrid control is better than that of the MRAC control.

Keywords: PID control, model reference adaptive control, hybrid control, convergence speed, robotic arm

INTRODUCTION

PID control is the widely used control method in many industries. For example, in many robotic arm used industries, PID control applies to each joint to control the whole robotic arm. By adjusting the PID gains of the PID controller, we can have the desired

1 Department of Mechanical Engineering, York University, Toronto, Ontario, M3J 1P3, Canada.
E-mail: dzhang99@yorku.ca

2 Faculty of Engineering and Applied Science, University of Ontario Institute of Technology, 2000 Simcoe Street North, Oshawa, Ontario, Canada.

E-mail: Bin.Wei@uoit.ca
* Corresponding author

output performance. Model reference adaptive control is another control method that was proposed early by Landau (Landau 1979) and it has been developed afterwards (Dubowsky and Desforges 1979, Cao and Hovakimyan 2008, Priyank Jain and Nigam 2013, Nhan T. Nguyen et al. 2008, Idan et al. 2002, Li and Cheah 2012, Rossomando et al. 2011, Sharifi et al. 2014, Ortega and Panteley 2014). The reason that one needs to apply adaptive control, especially the model reference adaptive control approach is that traditional controllers cannot compensate the payload variations, i.e., when the end-effector grasps different payload masses, the joint output will vary, which affects the positioning accuracy of the end-effector. However for the model reference adaptive control, the above problem can be effectively resolved and payload variation effect can be compensated. For example, the MRAC controller proposed by R. Horowitz and later associated developments by other authors (Horowitz and Tomizuka 1986, Horowitz 1983) contains an adaptive algorithm block and a position feedback loop which provides the difference between desired and actual position of the joints. This difference is acted upon by the integral portion of a seemingly PID control structure before feedback values of position and velocity are subtracted from it. In this chapter, by combining the PID controller and MRAC controller, a hybrid controller is proposed and designed. In Horowitz's MRAC controller (Horowitz 1983), it assumes that M and N are constant during adaptation. For the 1-DOF link, because its M and N matrices of the dynamic equation are constant (M is constant, N is 0), it can directly combine the PID and MRAC controllers to design the PID+MRAC controller. The convergence performance is compared among these three controllers. The results show that the convergence speed and its performance for MRAC controller and PID+MRAC controller is better than that of the PID controller. The convergence performance for the hybrid control is better than that of the MRAC control. For the MRAC, the joint output gradually goes towards to the desired position while for the PID+MRAC, it overshoots the desired position and then gradually comes back to the desired position. But for more than 1-DOF link, it is not applicable anymore because

the M and N matrices of the dynamic equation are not constant. For the PID control, we need to use the Lagrange dynamic model, but for the MRAC, we need to use the Gibbs-Appell dynamic formulation. Since they are not compatible, we cannot combine the PID and MRAC in this case. On the positive side, however, Sadegh proposed an improved MRAC that can remove the condition that the M and N matrices are constant (Sadegh and Horowitz 1987, Sadegh and Horowitz 1990), so that the Lagrange dynamic equation can be used. By using Sadegh's improved adaptive algorithm and structure, and by combining the PID and MRAC controllers, a hybrid controller is designed for the more than one-DOF link (e.g., 2-DOF and 3-DOF links) case. The results show that the convergence speed for the hybrid controller is faster than that of the MRAC controller. The hybrid controller and MRAC controller are both better than that of the PID controller.

PID CONTROLLER, MRAC CONTROLLER, AND PID+MRAC HYBRID CONTROLLER

PID Controller

The PID controller is illustrated in Fig. 1. The output of the plant will compare with the desired model rp and then will have an error. This error will go through the PID control

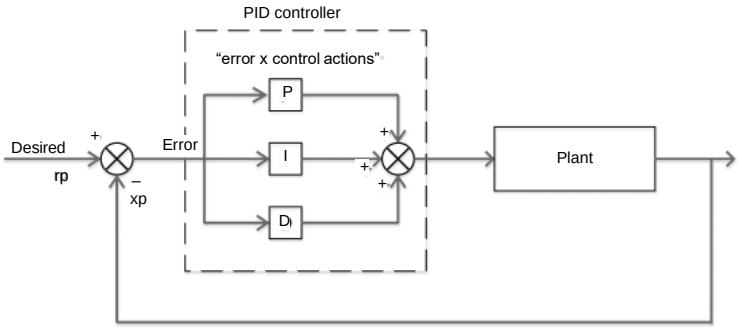


Figure 1. PID controller.

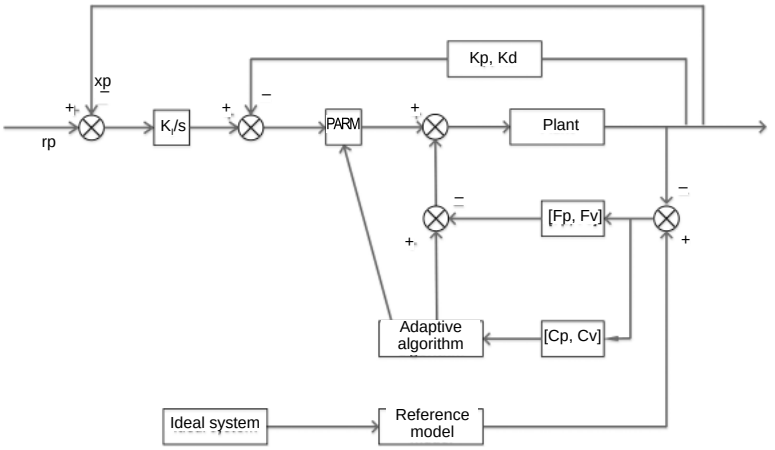


Figure 2. MRAC controller.

and through "error times control actions". The output of the PID controller will be the input to the plant model, and this circle will continue until the error between the actual output from the plant and the desired model converges to 0. This is the basic working principle of the PID control.

MRAC Controller

For the MRAC controller, the following Fig. 2 shows such a system.

One can see that this system does not contain any PID control. The output from the plant will compare with the reference model, which will produce an error. This error will be used by the adaptive algorithm block and then produce the input elements to the plant. In the meantime, the output of the

plant will compare with the desired model rp and will produce another error. This error will go through the integration action and then subtract the feedback processed position and velocity by the Kp and Kd elements. This process is very similar to the PID control, but it is not a PID control. The output from this process, times the elements from the adaptive algorithm, plus the elements from the adaptive algorithm, will be the input to the plant. This process will continue until the error between the output of the plant and the reference model converges to 0.

The ideal system is isolated from the plant, in the sense that feedback values of the plant variables are not used to process the input to the reference model. The reference model input is processed from its own output variables by the “similar PID controller”. The ideal system is completely unaffected by the plant performance. Sadegh’s improved MRAC is illustrated in Fig. 3:

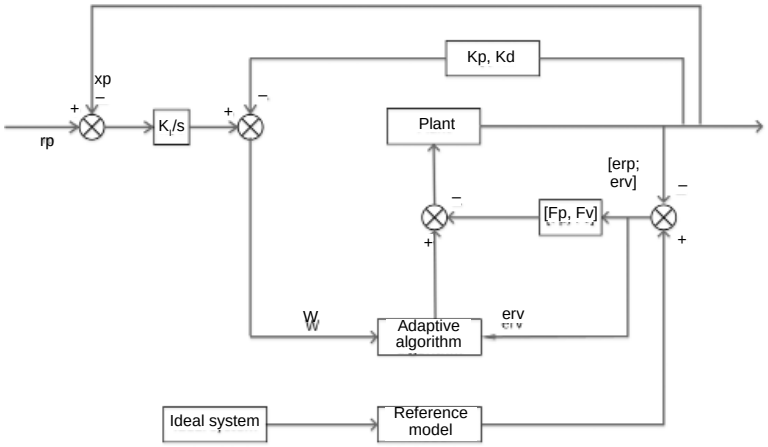


Figure 3. Improved MRAC controller.

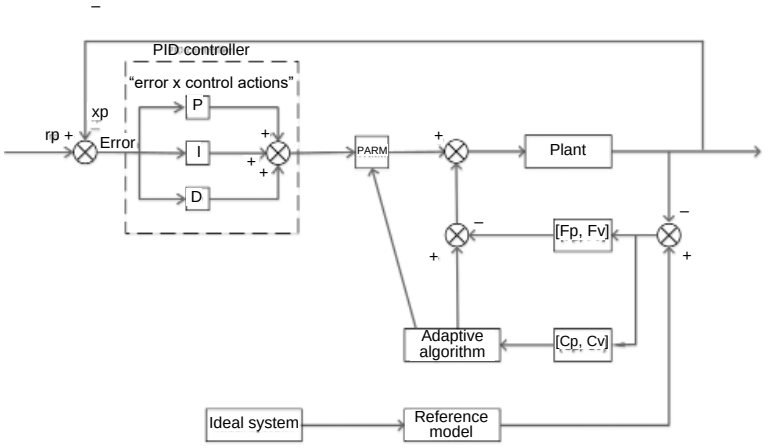


Figure 4. PID+MRAC hybrid controller for 1-DOF link.

PID+MRAC Hybrid Controller

By combining the PID controller and MRAC controller, the PID+MRAC hybrid controller is obtained as shown in Fig. 4.

Same with the MRAC, the only difference between this hybrid PID+MRAC and MRAC is that the output of the plant will compare with the desired model rp and will produce an error. This error will go through the PID controller. The output of the PID controller, times the elements from the adaptive algorithm, plus the elements from the adaptive algorithm, will be the input to the plant. For 2-DOF and 3-DOF link cases, the hybrid controller is shown in Fig. 5.

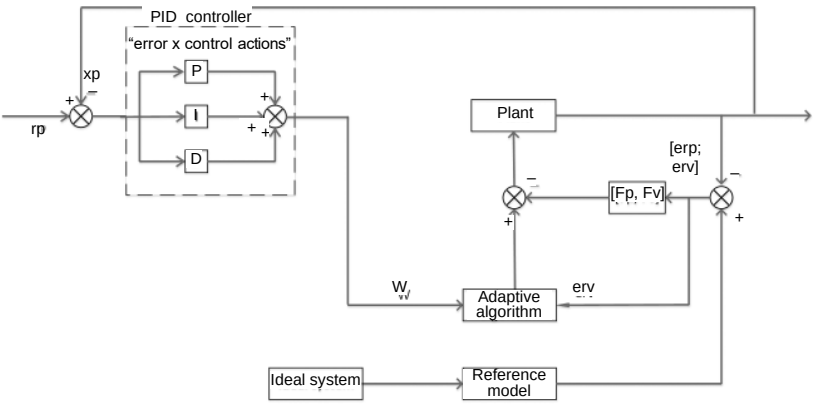


Figure 5. PID+MRAC hybrid controller for more than 1-DOF link.

CONVERGENCE PERFORMANCE COMPARISON BETWEEN PID, MRAC AND HYBRID CONTROLLER

One-DOF Link Case

Here the one link manipulator as shown in Fig. 6 will be used as an example. In order to implement PID control of the one link manipulator case, the dynamic equation has to be derived. By using the Lagrange method (John J. Craig 2005), the dynamic equation is presented as follows:

The kinetic and potential energy of this link are as follows:

$$K = \frac{1}{2} m (l \dot{\theta})^2 , P = m g (l \sin\theta) \quad (1)$$

The total kinetic and potential energy are:

$$K = K_1 + K_2 = \frac{1}{2} m (l \dot{\theta})^2 , P = P_1 + P_2 = m g (l \sin\theta) \quad (2)$$

According to the Lagrange method,

$$L = K - P = \frac{1}{2} m (l \dot{\theta})^2 - m g (l \sin\theta) \quad (3)$$

Thus the torque applied to the joint can be dete

rmined by:

$$\frac{d}{dt}\frac{\partial L}{\partial \dot{\theta}_1} - \frac{\partial L}{\partial \theta_1} \quad (4)$$

where $\frac{\partial L}{\partial \dot{\theta}_1} = ml^2\dot{\theta}_1$, $\frac{d}{dt}\frac{\partial L}{\partial \dot{\theta}_1} = ml^2\ddot{\theta}_1$, $\frac{\partial L}{\partial \theta_1} = -mgl\cos\theta_1$

Rewriting equation (4) results in:

$$(ml^2)\ddot{\theta}_1 + (ml\cos\theta_1)g = M_1\ddot{\theta}_1 + \ddot{\theta}_1 0 + (ml\cos\theta_1)g = M\ddot{\theta}_1 + 0 = Gg \quad (5)$$

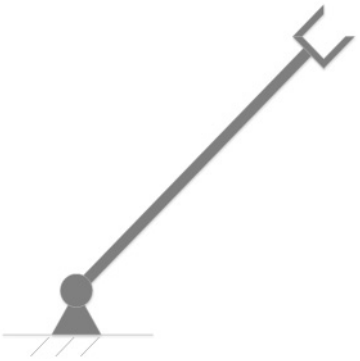


Figure 6. One link manipulator.

Through applying PID control, the controller output is the torque, i.e.,

$$K_p e + K_i \int e dt + K_d \dot{e} = \tau_1 \quad (6)$$

where error $e = r_p - x_p$

We know from the one-link manipulator M and N_1 matrices, $M = m_1 l_1^2$, $N = 0$, the output from the manipulator (i.e., acceleration of the joint) can be determined as follows:

$$\ddot{e} = \ddot{r}_p - \frac{1}{m_1 l_1^2}\left(K_p e + K_i \int e dt + K_d \dot{e}\right) \quad (7)$$

After deriving the acceleration of joint 1, take the integral with respect to time to obtain the velocity of joint 1 and take another integral to obtain the position of joint 1.

$$\ddot{\theta}_1 \rightarrow \int \ddot{\theta}_1 dt, \dot{\theta}_1 \rightarrow \int \dot{\theta}_1 dt \quad (8)$$

After the simulation, as shown in Fig. 5, the blue line represents the joint output under the PID control.

For the MRAC, as with the PID control, the output from the controller will be:

$$ControllerOut = M(u + V) + F_p e + F_V e \quad (9)$$

where $u = K_I \int (r_p - x_p) - K_p x_p - K_d x_V$

The manipulator dynamic equation is:

$$\tau_1 = (ml_1^2)\alpha_1 + (ml_1 \cos\theta)g + Ma + 0 + Gg \quad (10)$$

So the output from the manipulator (i.e., acceleration of the joint) is written as:

$$a = M^{-1}(u + V) + e + F_p e + F_V e \quad (11)$$

$$Mu = V_p + F_V e \qquad V = Mu - F_p - F_V e$$

After the simulation, as shown in Fig. 7, the red line represents the joint output under the MRAC control, and yellow line represents the hybrid control. From this

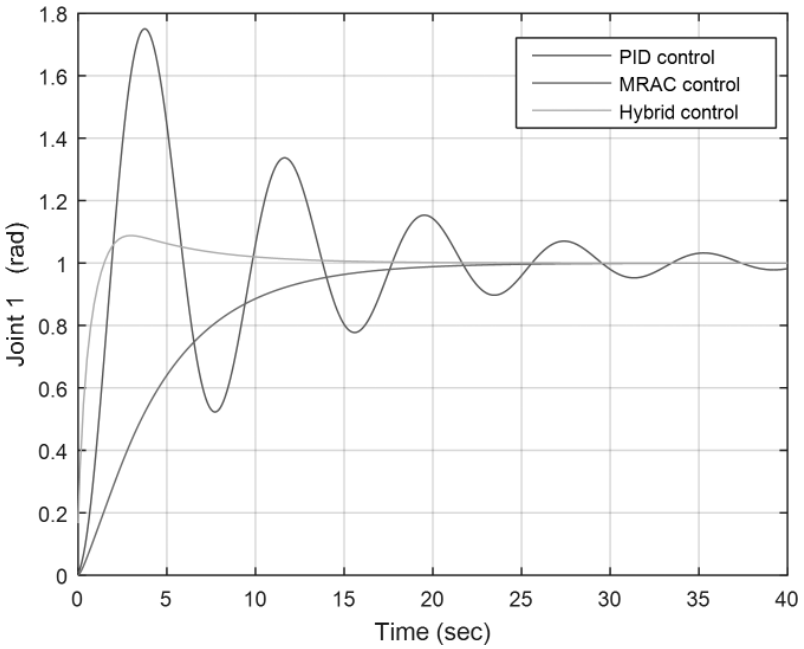


Figure 7. Joint output under PID, MRAC and hybrid control.

figure, one can see that for the PID control, it will take roughly 40 seconds to converge to 0, for the MRAC control, it will take about 20 seconds to converge to the desired position, which is half the time of the PID control. Finally for the hybrid control, it takes about 10 seconds to converge to the desired position, which halves the time of MRAC control. Furthermore, another difference between the MRAC and the hybrid control is that the MRAC control gradually converges to the desired position whereas for the hybrid control, it first overshoots the desired position very quickly and then gradually converges to the desired position. From above analysis, one can see that the convergence performance for the hybrid control is better than that of the MRAC control, and the MRAC control is better than the PID control.

Two-DOF Link Case

The two-link manipulator is shown in Fig. 8, based on the Lagrange method, the dynamic equation is derived as follows:

$$N = \begin{bmatrix} m_{11} & m_{12} \\ m_{21} & m_{22} \end{bmatrix} \begin{bmatrix} \ddot{\theta}_1 \\ \ddot{\theta}_2 \end{bmatrix} + \begin{bmatrix} n_{11} \\ n_{21} \end{bmatrix} \tag{12}$$

where

$m_{11} = (m_1 + m_2)l_1^2 + m_2 l_2^2 + 2m_2 l_1 l_2 \cos\theta_2$, $m_{12} = m_2 l_2^2 + m_2 l_1 l_2 \cos\theta_2$, $m_{21} = m_2 l_2^2 + m_2 l_1 l_2 \cos\theta_2$, $m_{22} = m_2 l_2^2$

$n_{11} = 2(-m_2 l_1 l_2 \sin\theta_2)\dot{\theta}_1\dot{\theta}_2 + (-m_2 l_1 l_2 \sin\theta_2)\dot{\theta}_2^2$, $n_{21} = m_2 l_1 l_2 \sin\theta_2 \dot{\theta}_1^2$

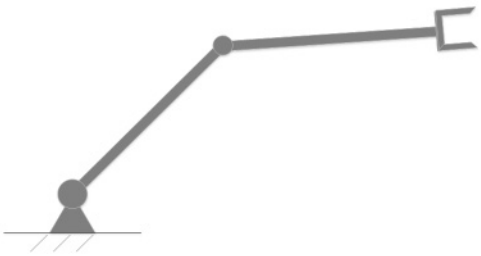


Figure 8. Two-link manipulator.

By re-parametrization of the above dynamic equation,

$$\begin{bmatrix} (m_1+m_2)l_2^2 + m_2 l_1^2 + 2m_2 l_1 l_2 \cos\theta_2 & m_2 l_2^2 + m_2 l_1 l_2 \cos\theta_2 \\ m_2 l_2^2 + m_2 l_1 l_2 \cos\theta_2 & m_2 l_2^2 \end{bmatrix} \begin{bmatrix} u_1 \\ u_2 \end{bmatrix} \quad (13)$$

$$+ \begin{bmatrix} -2(m_2 l_1 l_2 \sin\theta_2)\theta_1 \theta_2 - (m_2 l_1 l_2 \sin\theta_2)\theta_2^2 \\ m_2 l_1 l_2 \sin\theta_2 \theta_1^2 \end{bmatrix} + \begin{bmatrix} W_1 \\ W_2 \end{bmatrix}$$

By choosing $\alpha_1 = (m_1+m_2)l_2^2 + m_2 l_1^2$, $\alpha_2 = m_2 l_2^2$, $\alpha_3 = m_2 l_1 l_2$

$$\begin{bmatrix} u_1 \\ u_2 \end{bmatrix} = \begin{bmatrix} 2u_1 \cos\theta_2 - u_2 \cos\theta_2 & -u_2 \cos\theta_2 \\ -u_2 \cos\theta_2 & 0 \end{bmatrix} \begin{bmatrix} \alpha_1 \\ \alpha_2 \\ \alpha_3 \end{bmatrix} \quad (14)$$

$$+ \begin{bmatrix} 0 & u_1 \\ -u_2 & u_1 \cos\theta_2 \end{bmatrix} \begin{bmatrix} \theta_1 \theta_2 \\ \theta_2^2 \end{bmatrix} + \begin{bmatrix} W_1 \\ W_2 \end{bmatrix} - \begin{bmatrix} F_{v1} & 0 \\ 0 & F_{v2} \end{bmatrix} \begin{bmatrix} \theta_1 \\ \theta_2 \end{bmatrix} - \begin{bmatrix} F_{p1} \\ F_{p2} \end{bmatrix}$$

$$M \qquad 1 \qquad N \quad W \quad 2 \quad F_v \quad erv \quad F_p \quad erp \qquad (15)$$

$$3$$

$$1 \qquad (16)$$

$$(W \quad 2 \quad F_v \quad erv \quad F_p \quad erp \quad N) / M$$

$$3$$

After deriving the acceleration of joint, take the time integral to obtain the velocity of joint and take another integral to obtain the position of joint.

$$1 \quad 1 \quad dt, \quad 1 \qquad (17)$$

$$dt$$

$$\theta$$

$$2$$

$$2 \quad 2$$

$$2$$

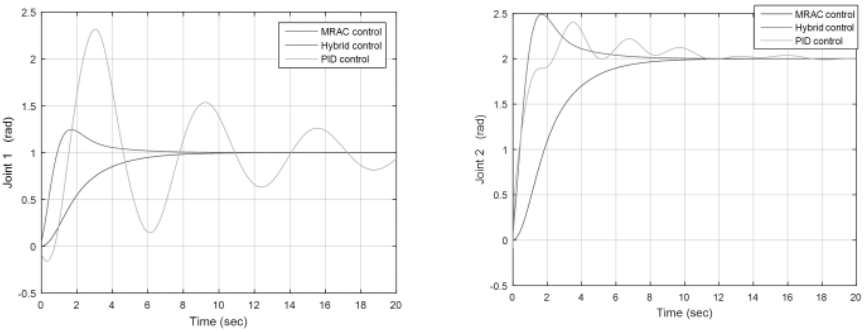


Figure 9. Joints 1 and 2 output under PID, MRAC and hybrid control.

As shown in Fig. 9, the results show that the convergence speed for the hybrid controller is faster than that of the MRAC controller. The hybrid controller and MRAC controller are both better than that of the PID controller. By using the same method, it can be extended to multi-DOF serial manipulators.

Three-DOF Link Case

The three-link manipulator is shown in Fig. 10, based on the Lagrange method, the dynamic equation is derived as follows:

$$\begin{bmatrix} \\ \\ \\ \end{bmatrix} \begin{bmatrix} \\ \\ \\ \end{bmatrix} \begin{bmatrix} m & m_{13} & n_{11} \\ m_{11} & m_1 & 1 \\ & 2 & \end{bmatrix} \begin{bmatrix} \\ \\ \\ \end{bmatrix} \begin{bmatrix} \\ \\ \\ \end{bmatrix} \begin{bmatrix} 1 \\ \\ \end{bmatrix}$$

$$\begin{bmatrix} m \\ \\ \end{bmatrix} \begin{bmatrix} \\ M \\ \end{bmatrix} \begin{bmatrix} \\ m \\ \end{bmatrix} \begin{bmatrix} \\ N \\ \end{bmatrix} \begin{bmatrix} \\ n \\ \end{bmatrix} \tag{18}$$

$$\begin{bmatrix} \\ 2 \\ \end{bmatrix} \begin{bmatrix} \\ \\ \end{bmatrix} \begin{bmatrix} 12 & 22 & 23 & 21 \\ & 2 & & \end{bmatrix} \begin{bmatrix} \\ \\ \end{bmatrix} \begin{bmatrix} \\ \\ \end{bmatrix}$$

$$\begin{bmatrix} \\ \\ \end{bmatrix} \begin{bmatrix} \\ \\ \end{bmatrix} \begin{bmatrix} m & m_{33} & n_{31} \\ m_{13} & m_2 & \\ & 3 & \end{bmatrix} \begin{bmatrix} \\ \\ \end{bmatrix} \begin{bmatrix} \\ \\ \end{bmatrix} \begin{bmatrix} \\ [\theta_3] \\ \end{bmatrix}$$

$$\begin{bmatrix} 3 \\ \\ \end{bmatrix}$$

whe
re

$$m_{11} = m_1 a^2 + m_2 r_1^2 + m_3 r_1^2, m_{12} = r_1 (m_2 b + m_3 r_2) \cos(\theta_2 - \theta_1), m_{13} = m_3 r_1 c \cos(\theta_3 - \theta_1),$$
$$m_{22} = m_2 b^2 + m_3 r_2^2, m_{23} = m_3 r_2 c \cos(\theta_3 - \theta_2), m_{33} = m_3 c^2$$

$$n_{11} = -r_1 (m_2 b + m_3 r_2) \sin(\theta_2 - \theta_1) \dot{\theta}_2^2 - m_3 r_1 c \sin(\theta_1 - \theta_3) \dot{\theta}_3^2$$

$$n_{21} = r_1 (m_2 b + m_3 r_2) \sin(\theta_2 - \theta_1) \dot{\theta}_1^2 - m_3 r_2 c \sin(\theta_2 - \theta_3) \dot{\theta}_3^2$$

$$n_{31} = m_3 r_1 c \sin(\theta_1 - \theta_3) \dot{\theta}_1^2 + m_3 r_2 c \sin(\theta_2 - \theta_3) \dot{\theta}_2^2$$

$$a = \frac{l_1}{2}, b = \frac{l_2}{2}, c = \frac{l_3}{2}, r_1 = l_1, r_2 = l_2, r_3 = l_3$$

By re-parametrization of the above dynamic equation,

$$\ddot{\theta}_1 = \frac{m_1 a^2 + m_2 r_1^2 + m_3 r_1^2}{m_3 r_1 c \cos(\theta_1 - \theta_3)} u_1 - \frac{r_1 (m_2 b + m_3 r_2) \cos(\theta_2 - \theta_1)}{m_3 r_1 c \cos(\theta_1 - \theta_3)} \ddot{\theta}_2 - \frac{m_3 r_1 c \cos(\theta_1 - \theta_3)}{m_3 r_1 c \cos(\theta_1 - \theta_3)} u_3$$

$$\ddot{\theta}_2 = \frac{r_1 (m_2 b + m_3 r_2) \cos(\theta_2 - \theta_1)}{m_2 b^2 + m_3 r_2^2} \ddot{\theta}_1 + \frac{m_3 r_2 c \cos(\theta_2 - \theta_3)}{m_2 b^2 + m_3 r_2^2} u_2 - \frac{m_3 r_2 c \cos(\theta_2 - \theta_3)}{m_2 b^2 + m_3 r_2^2} u_3$$



Figure 10. Three-link manipulator.

$$W = \begin{bmatrix} r_1(m_2 b + m_3 r_2)\sin(\theta_2 - \theta_1)\dot{\theta}_1^2 + m_3 r_2 c \sin(\theta_2 - \theta_3)\dot{\theta}_3^2 \\ -r_1(m_2 b + m_3 r_2)\sin(\theta_2 - \theta_1)\dot{\theta}_2^2 - m_3 r_2 c \sin(\theta_1 - \theta_3)\dot{\theta}_3^2 \\ m_3 r_2 c \sin(\theta_2 - \theta_3)\dot{\theta}_2^2 + m_3 r_1 c \sin(\theta_1 - \theta_3)\dot{\theta}_1^2 \end{bmatrix} \quad (19)$$

By choosing $\alpha_1 = m_2 a^2 + m_3 r_1^2 + m_2 r_2^2$, $\alpha_2 = m_3 r_2 (m_2 b + m_3 r_2)$, $\alpha_3 = m_3 r_2 c$, $\alpha_4 = m_2 b^2 + m_3 r_2^2$, $\alpha_5 = m_3 r_1 r_2$, $\alpha_6 = m_3 r_1 c$, $\alpha_7 = m_3 c^2$

$$\begin{bmatrix} u_1 \\ W = \sin(\theta_2 - \theta_1)\dot{\theta}_2^2 \\ 0 \end{bmatrix} \begin{bmatrix} u_2 \cos(\theta_2 - \theta_1)\dot{\theta}_2^2 + u_3 \cos(\theta_1 - \theta_3)\dot{\theta}_3^2 \\ \sin(\theta_1 - \theta_3)\dot{\theta}_3^2 \\ u_1 \cos(\theta_2 - \theta_1)\dot{\theta}_2^2 + 0 \\ \sin(\theta_2 - \theta_1)\dot{\theta}_1^2 \end{bmatrix}$$

$$\begin{bmatrix} 0 & 0 & u_1 \cos(\theta_1 - \theta_3)\dot{\theta}_3^2 + \sin(\theta_1 - \theta_3)\dot{\theta}_1^2 \\ 0 & 0 & 0 \end{bmatrix}$$

$$\begin{bmatrix} u_2 & u_3\cos(\theta_2-\theta_3)\dot{\theta}_3^2\sin(\theta_2-\theta_3)\dot{\theta}_3 & 0 \\ 0 & u_2\cos(\theta_2-\theta_3)\dot{\theta}_2^2\sin(u_2-\theta_3)\dot{\theta}_2 & 3 \end{bmatrix}$$

$$\begin{bmatrix} \theta_1 \\ \theta_2 \\ \theta_3 \end{bmatrix} \begin{bmatrix} W \\ F \\ V \end{bmatrix} \begin{bmatrix} erv \\ erp \\ p \end{bmatrix} \begin{bmatrix} \theta_4 \\ \theta_5 \\ \theta_6 \end{bmatrix} \quad (20)$$

$$M \cdot N \cdot W \cdot F_v \cdot erv \cdot F_p \cdot erp \tag{21}$$

$$(W \cdot F \cdot erv \cdot F \cdot erp) / M \cdot N \tag{22}$$

After deriving the acceleration of joint, take the time integral to obtain the velocity of joint and take another integral to obtain the position of joint.

$$\theta = \int \theta \, dt, \quad \theta = \int \theta \, dt \tag{23}$$

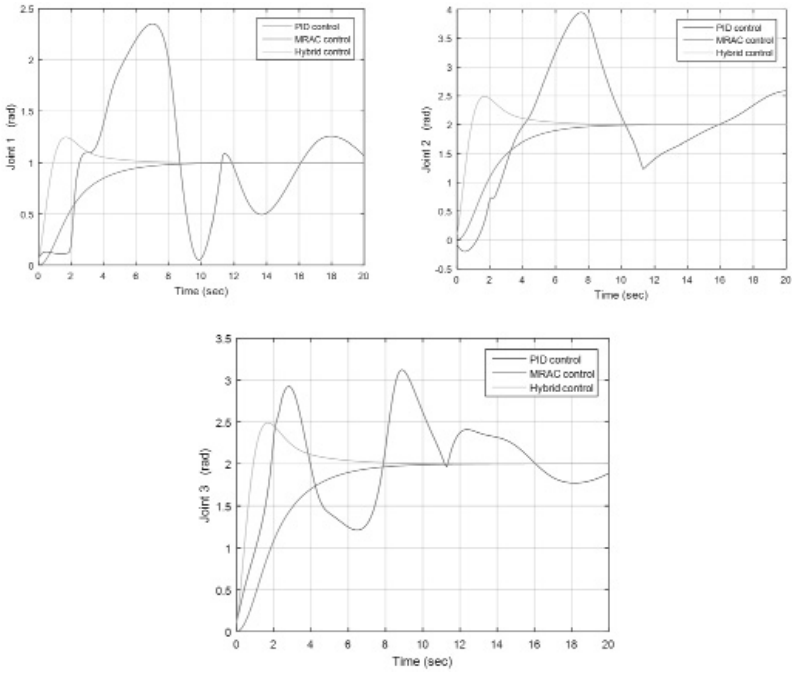


Figure 11. Joints 1, 2 and 3 output under PID, MRAC and hybrid control.

CONCLUSION

This paper proposes a hybrid controller by combining a PID controller and a MRAC controller, and also compares the convergence performance of PID, MRAC, and PID+MRAC hybrid controllers for one-DOF, two-DOF and three-DOF manipulators. For the one-DOF case, the results show that the convergence speed and its performance for MRAC controller and PID+MRAC controller is better than that of the PID controller. Whereas for the MRAC controller and PID+MRAC controller, the convergence performance for the hybrid control is better than that of the MRAC control. For the MRAC, the joint output gradually goes towards to the desired position while for the PID+MRAC, it overshoots the desired position and then gradually comes back to the desired position. For more than one-DOF case, the results show that the convergence speed for the hybrid controller is faster than that of the MRAC controller. The hybrid controller and MRAC controller are both better than that of the PID controller. This study will provide a guideline for future research in the direction of new controller designs for manipulators in terms of convergence speed and other performances.

ACKNOWLEDGMENT

The authors would like to thank the Natural Sciences and Engineering Research Council of Canada (NSERC) for the financial support. The authors gratefully acknowledge the financial support from Canada Research Chairs program.

REFERENCES

Cao, C. and N. Hovakimyan. 2008. Design and analysis of a Novel L1 adaptive control architecture with guaranteed transient performance. IEEE Transactions on Automatic Control, 53(2): 586–591.

Dubowsky, S. and D. Desforges. 1979. The application of model-referenced adaptive control to robotic manipulators. Journal of Dynamic Systems Measurement and Control, 101: 193–200.

Horowitz, R. 1983. Model reference adaptive control of mechanical manipulators, PhD Thesis, University of California.

Horowitz, R. and M. Tomizuka. 1986. An adaptive control scheme for mechanical manipulators— Compensation of nonlinearity and decoupling control. Journal of Dynamic Systems, Measurement and Control, 108(2): 1–9.

Idan, M., M. D. Johnson and A. J. Calise. 2002. A hierarchical approach to adaptive control for improved flight safety. AIAA Journal of Guidance, Control and Dynamics, 25(6): 1012–1020.

John J. Craig. 2005. Introduction to robotics: mechanics and control. 3rd ed., Pearson/Prentice Hall. John J. Craig, Ping Hsu and S. Shankar Sastry. 1986. Adaptive control of mechanical manipulators.

IEEE International Conference on Robotics and Automation, pp. 190–195.

Landau, Y. D. 1979. Adaptive control: the model reference approach. Marcel Dekker, New York.

Li, X. and C. C. Cheah. 2012. Adaptive regional feedback control of robotic manipulator with uncertain kinematics and depth information. pp. 5472–5477. *In*: Proceedings of the American Control Conference, Montr´eal, Canada.

Nhan T. Nguyen, Kalmanje Krishnakumar and Jovan Boskovic. 2008. An optimal control modification to model-reference adaptive control for fast adaptation. AIAA Guidance, Navigation and Control Conference and Exhibit, August, 2008, Honolulu, Hawaii, pp. 1–19.

Ortega, R. and E. Panteley. 2014. L1—Adaptive control always converges to a linear PI control and does not perform better than the PI. Proceedings of 19th IFAC World Congress, pp. 6926–6928. Priyank Jain and M. J. Nigam. 2013. Design of a model reference adaptive controller using modified MIT rule for a second order system. Advance in Electronic and Electric Engineering,

3(4): 477–484.

Rossomando, F. G., C. Soria, D. Patiño and R. Carelli. 2011. Model reference adaptive control for mobile robots in trajectory tracking using radial basis function neural networks. Latin American Applied Research, 41: 177–182.

Sadegh, N. and R. Horowitz. 1987. Stability analysis of an adaptive controller for robotic manipulators. Proceedings of 1987 IEEE International Conference on Robotics and Automation, pp. 1223–1229.

Sadegh, N. and R. Horowitz. 1990. Stability and robustness analysis of a class of adaptive controllers for robotic manipulators. International Journal of Robotics Research, 9(3): 74–92.

Sharifi, M., S. Behzadipour and G. R. Vossoughi. 2014. Model reference adaptive impedance control in Cartesian coordinates for physical human–robot interaction. Advanced Robotics, 28: 19, 1277–1290.

11

The Adaptive Control Algorithm for Manipulators with Joint Flexibility

*Krzysztof Kozłowski** and *Piotr Sauer*

ABSTRACT

Two control problems, present in this chapter are sent point and trajectory tracking control for robots with elastic joints. Firstly, discuss a simple non- adaptive case of the set point and illustrated by simulation results. Secondly, present a new adaptive tracking control scheme for robots with elastic joint. The proposed algorithm is the control algorithm extension proposed by Loria and Ortega. It assumes that link and motor positions are available for measurements and model of manipulator with elastic joints contain dynamic friction components on both link and motor sides. Construction of this algorithm is based on Lyapunov stability theory. In this chapter, shown is the proof of semiglobal asymptotic stability of the proposed system. The presented algorithm was tested and verified on experimental set-up. The experimental set-up consists of manipulator with two degree of freedom and control system based on card with signal processor DS1102. Two DC motors with harmonics gear were used as the actuators of manipulator. These gears are a source of flexibility in the joints. Software implementation of the proposed control algorithm is described using fast prototyping methodology in MATLAB and SIMULINK environment.

Keywords: Joint flexibility, set point control, trajectory control, adaptive control, feedback linearization, Lyapunov stability theory

Chair of Control and Systems Engineering, Poznań University of Technology, ul. Piotrowo 3a, 60-965 Poznań, Poland.
E-mail: piotr.sauer@put.poznan.pl
* Corresponding author: krzysztof.kozłowski@put.poznan.pl

INTRODUCTION

Many current manipulators are equipped with elastic motion transmission elements as harmonic drives, transmission belts and long shafts. These elements introduce elastic deformations at the joints. Such deformations are regarded as a source of problems, especially when accurate trajectory tracking of high sensitivity to end-effector forces is mandatory. It is shown that the joint elasticity should be taken into account in the modeling of a manipulator and designing of a control algorithm with the help of highly nonlinear equations. The modeling of flexible-joint robots is far more complex than that of rigid-joint robots. Two different models are used in the modeling of the flexible joint robots: complete and reduced models (De Luca and Tomei 1996). The reduced model was proposed by Spong (1987). It differs from the complete model in the assumption that the kinetic energy of the rotors is determined only by their own rotation (Ott 2008). One of the assumptions to build a complete model is that elasticity of a gear is modeled as a linear spring located between the rotor and the subsequent link (Ott 2008). Readman and Belanger (1990) presented a precise model based on Lagrange dynamics without simplifying assumptions. Very often a manipulator with flexible joints contains uncertain elements, i.e., elements which are not exactly known (for example system parameters which are difficult to measure with certainty, disturbance inputs which cannot be precisely predicted, nonlinear elements which are difficult to characterize exactly). If dynamic parameters are not exactly known, adaptive control laws must be designed to guarantee stabilization or tracking. Control of a system with uncertain elements has been discussed in the robotics literature (Barany and Colbaugh 1998, Corless 1989, Leitmann 1981). Spong proposed an adaptive controller for flexible-joint robots by using the singular perturbation formulation (Spong 1989, 1995). Khorasani proposed an adaptive controller using the concept of integral manifolds for n-link flexible-joint robots (Khorasani 1992). Madoński et al. (2014) presented an application of a special case of an Active Disturbance Rejection Controller

(ADRC) for controlling a flexible joint manipulator designed as a rehabilitation device. Using the ADRC approach, the modeling uncertainty in the system is partially decoupled from the system, which increases the robustness of the whole control framework against both internal and external disturbances. Sauer and Kozlowski (2007) presented an adaptive tracking controller for a manipulator with only a revolute joint in which link and motor positions are available for measurements.

In this chapter, a new adaptive tracking controller that is an extension of the one proposed by Loria and Ortega (1995) is presented. The construction of this controller is based on Lyapunov theory (Barany and Colbaugh 1998, Colbaugh et al. 1994, Corless 1990, Slotine and Li 1991). The algorithm presented assumes that link and motor positions are available for measurements and the model of the manipulator with elastic joints contain dynamic friction components on both link and motor sides. In this chapter, the proof of semiglobal asymptotic stability of the proposed system is shown. This proof shows that the domain of attraction can be arbitrarily enlarged by increasing the gain.

The chapter is organized as follows. In Section **Nonadaptive Set Point Control of a Two Link Robot** a simple non-adaptive case of the set point is discussed. A more general mathematical description of the robot model, control algorithm and the stability properties of the adaptive tracking controller are described in Section **Adaptive Control Algorithm**. It also describes an experimental set-up and implemetation of the control

algorithm. The experimental set-up consists of two links and a control system based on a card with signal processor DSP1102. Finally, concluding remarks are given.

NONADAPTIVE SET POINT CONTROL OF A TWO LINK ROBOT

In this section a simple example of one link robot with joint flexibility is considered assuming that all parameters of this mechanical structure are exactly known. This example is discussed in (Isidori 1995) and it is considered here because stabilization to equilibrium point discussed in reference (Isidori 1995) is not fully correct. The mechanical structure of the robot is depicted in Fig. 1.

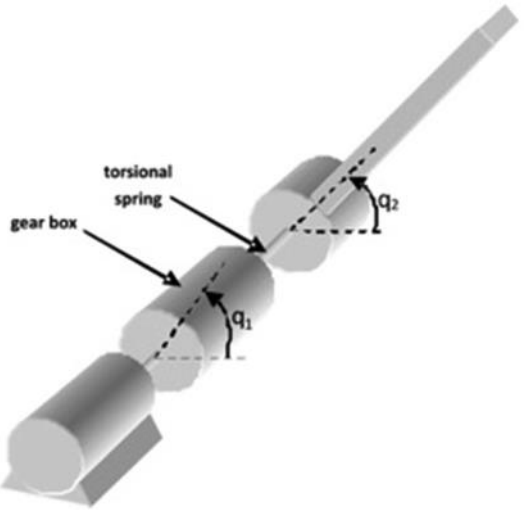


Figure 1. Mechanical structure of a simple one link robot with joint flexibility.

The system presented in Fig. 1 is described in terms of generalized coordinates, one variable q_1 represents angular position of the motor and is measured with respect to a fixed coordinate system shown in Fig. 1. It can be seen that the actuator shaft is connected directly to the gearbox that is linked via a torsional spring to the link. This is a simple one-link arm. Its joint variable is denoted by q_2 and stands for angular displacement of the arm measured again with respect to a fixed coordinate system. Elasticity constant of the spring

here represents elastic coupling between the gearbox and link, and it is
denoted by constant parameter K. Denoted by J_1 and F_1, inertia constant of the motor and viscous friction coefficient actuator equation can be written in the following form:

$$J_1\ddot{q}_1 + F_1\dot{q}_1 + \frac{K}{N}\left(\frac{q_1}{N} - q_2\right) = \tau \quad (1)$$

where τ represents torque generated by the motor. On the other hand, the link equation can be written as follows:

$$J_2\ddot{q}_2 + F_2\dot{q}_2 + K\left(q_2 - \frac{q_1}{N}\right) + mgd\cos q_2 = 0. \quad (2)$$

In the last equation J_2 and F_2 stand for inertia and velocity coefficient constants, respectively, m is the mass of the link, d represents the position of the center of gravity of the link, N stands for gear ratio and g is gravity constant. Note that Eq. (1) given here differs from the one presented in Isidori's book, namely the third term given in Eq.

(1) has a minus sign when compared to the one given in this reference book. It is due to the fact that we consider this term in comparison to Eq. (2) as being on a different side of the torsional spring. This reasoning comes from a physical interpretation of the mechanical system.

Consequently, we follow analysis discussed in reference (Isidori 1995) and apply an apparatus of the differential geometry. Following this analysis one can choose the state vector as $\boldsymbol{x} = [q_1, q_2, \dot{q}_1, \dot{q}_2]$ consisting of angular positions and their velocities.

Equations (1) and (2), taking into account the state vector with input $u = \tau$ can be written in the following form:

$$\dot{\mathbf{x}} = \mathbf{f}(\mathbf{x}) + \mathbf{g}(\mathbf{x})u$$

where

$$\mathbf{f}(\mathbf{x}) = \begin{bmatrix} x_3 \\ x_4 \\ -\frac{K}{J_1 N^2} x_1 + \frac{K}{J_1 N} x_2 - \frac{F_1}{J_1} x_3 \\ \frac{K}{J_2 N} x_1 - \frac{K}{J_2} x_2 + \frac{mgd}{J_2} \cos x_2 - \frac{F_2}{J_2} x_4 \end{bmatrix}, \quad \mathbf{g}(\mathbf{x}) = \begin{bmatrix} 0 \\ 0 \\ \frac{1}{J_1} \\ 0 \end{bmatrix}. \tag{3}$$

This system is under-actuated and has one control signal, namely the torque generated by the actuator. It is assumed that all parameters of the system given by Eq. (3) are known and one can apply one of the control algorithms originated in the differential geometry. It would be natural to select an output of the system as the angular position of the link q_2. Therefore one can write the output function as:

$$y = h(\mathbf{x}) = x_2. \tag{4}$$

Calculating the first Lie derivative of this output function results in

$$L_{\mathbf{f}} h(\mathbf{x}) = \frac{\partial h}{\partial \mathbf{x}} \mathbf{f}(\mathbf{x}) = [0\ 1\ 0\ 0]\mathbf{f}(\mathbf{x}) = \mathbf{g}(\mathbf{x})u = f_2(\mathbf{x}) = x_3$$

Here $\mathbf{f}(\mathbf{x})$ is represented as a vector $\mathbf{f}(\mathbf{x}) = [f_1(\mathbf{x})\ f_2(\mathbf{x})\ f_3(\mathbf{x})\ f_4(\mathbf{x})]^T$

Consequently, higher order Lie derivatives are:

$$L_{\mathbf{f}}^2 h(\mathbf{x}) = \frac{\partial}{\partial \mathbf{x}} [L_{\mathbf{f}} h(\mathbf{x})] \mathbf{f}(\mathbf{x}) = f_3(\mathbf{x})$$

$$L_{\mathbf{f}}^3 h(\mathbf{x}) = \frac{\partial f_3}{\partial x_1} f_1(\mathbf{x}) + \frac{\partial f_3}{\partial x_2} f_2(\mathbf{x}) + \frac{\partial f_3}{\partial x_4} f_4(\mathbf{x})$$

due to the fact that $f_4(\mathbf{x})$ does not depend on x_3. From the previous calculations it also follows that

$$L_{\mathbf{g}}h(\mathbf{x}) = L_{\mathbf{g}} L_{\mathbf{f}} h(\mathbf{x}) = L L^2 h(\mathbf{x}) = 0$$

and

$$L_{\mathbf{g}} L_{\mathbf{f}}^3 h(\mathbf{x}) = \frac{\partial}{\partial x_3}\left(\frac{\partial}{\partial x_1}\left(\frac{\partial f_1}{\partial x_4}\right)\right) = \frac{K}{J_1 J_2 N}.$$

The considered system has relative degree $r = 4 = n$ at each point x^0 in the state space, here the dimension of the system $n = 4$. Thus one can conclude that the system can be exactly linearized via state feedback and coordinate transformation around any point x^0 of state space. The linearizing coordinates are defined as follows:

$$z_1 = h(\mathbf{x}),\ z_2 = L_{\mathbf{f}} h(\mathbf{x}),\ z_3 = L_{\mathbf{f}}^2 h(\mathbf{x}),\ z_4 = L_{\mathbf{f}}^3 h(\mathbf{x}). \tag{5}$$

Taking into account Eq. (4), it is easy to notice that

$$y, \frac{dy}{dt} = L_{\mathbf{f}} h(\mathbf{x}),\ \frac{d^2 y}{dt^2} = L_{\mathbf{f}}^2 h(\mathbf{x}),\ \frac{d^3 y}{dt^3} = L_{\mathbf{f}}^3 h(\mathbf{x}).$$

Also note that output function and its time derivatives up to the third order have nice physical interpretation, namely they represent angular position, velocity, acceleration and jerk of the link with respect to the fixed coordinate frame.

The linearizing feedback is

$$u = \frac{-L_{\mathbf{f}}^4 h(\mathbf{x}) + v}{L_{\mathbf{g}} L_{\mathbf{f}}^3 h(\mathbf{x})} \tag{6}$$

and v has the following form:

$$v = c_0 h(\mathbf{x}) + c_1 L_{\mathbf{f}} h(\mathbf{x}) + c_2 L^2 h(\mathbf{x}) + c_3 L^3 h(\mathbf{x}).$$

Taking into account the previously defined linearizing coordinates, the linear system in *z* coordinates can be written as follows:

$$\begin{bmatrix} \dot{z}_1 \\ \dot{z}_2 \\ \dot{z}_3 \\ \dot{z}_4 \end{bmatrix} = \begin{bmatrix} 0 & 1 & 0 & 0 \\ 0 & 0 & 1 & 0 \\ 0 & 0 & 0 & 1 \\ c_0 & c_1 & c_2 & c_3 \end{bmatrix} \begin{bmatrix} z_1 \\ z_2 \\ z_3 \\ z_4 \end{bmatrix}.$$

Now it is easy to choose coefficients c_0, c_1, c_2, c_3 such as the constant matrix above has eigenvalues with negative values making the system asymptotically stable. As a consequence in view of the transformation given by Eq. (5) leads the original coordinates in *x* to be asymptotically stable to the desired value in *x* coordinates. The last equation can be written in a matrix form as:

$$\dot{\mathbf{z}} = \mathbf{A}\mathbf{z}. \tag{7}$$

Based on Eq. (7) one can calculate

$$\begin{bmatrix} s^2(s+c_3)+c_1+c_2 s & s(s+c_3)+c_2 & s+c_3 & 1 \\ 1 & 1 & 0 & 0 \\ s^2(s+c_3)+c_2 s & s(s+c_3) & c_3 & 0 \\ s^2 & s & 1 & 0 \end{bmatrix}$$

$$\begin{bmatrix} sc & c+cs & s^2(s+c)+s^2 & \\ c & s^2+c & cs+c & s^3 \\ 0 & 0 & 1 & 0 \end{bmatrix}$$

where Δ stands for the determinate of the characteristic equation and

$$\Delta = s^4 + c_3 s^3 + c_2 s^2 + c_1 s + c_0 .$$

Selecting proper coefficient c_0, c_1, c_2, c_3 as discussed above guarantees that the system (6) is asymptotically stable and in the steady state all variables z tend to zero. Taking into account Eq. (6) and assuming for the sake of simplicity that all mechanical parameters are unit elements the transformation (5) results in the following equations:

$$\begin{aligned} z_1 &= x_2 \\ z_2 &= -x_4 \\ z_3 &= -x_1 - x_2 - g\cos x_2 - x_4 \\ z_4 &= -x_3 - gx_4 \sin x_2 - x_1 - x_2 - g\cos x_2 \end{aligned} \quad \text{or } \mathbf{z} = \mathbf{\Phi}(\mathbf{x}). \tag{8}$$

Note that if x^0 is an equilibrium point of the original system (3) then $\mathbf{f}(\mathbf{x}^0) = \mathbf{0}$. However, it is immediately seen that a state of this type cannot be an equilibrium for the vector field $\mathbf{f}(\mathbf{x})$, because the constraints $\mathbf{f}(\mathbf{x}^0) = \mathbf{0}$ and $x_2^0 = 0$ are not compatible. Note that $x_2^0 = 0$ is equivalent by definition that the output function $h(\mathbf{x}^0) = x_2^0 = 0$.

Equating vector $\mathbf{f}(\mathbf{x})$ to zero with the assumption of unit elements of the mechanical elements results in

$$x_1^0 = -\frac{1}{2}, \; x_2^0 = -\frac{1}{2}, \; x_3^0 = 0, \; x_4^0 = 0.$$

Now making use of the control law given by Eq. (6) results in $x_4^0 = 0$, $x_1^0 = 0$, $x_2^0 =$

g, and $x^0 = 0$. Comparing both results it is evident that both conditions discussed above are not compatible. In this case, one may try to order a point of this type equilibrium by means of feedback. This condition can be established for some real number c such as the following condition is satisfied:

$$\mathbf{f}(\mathbf{x}^0) + \mathbf{g}(\mathbf{x}^0)c \neq \mathbf{0}. \quad (9)$$

Taking into account unit elements of the mechanical parameters Eq. (9) and assuming that $x^0 = 0$ results in:

$$x_3^0 = 0$$
$$x_4^0 = 0$$
$$x_1^0 + c = 0$$
$$x_1^0 - g = 0$$

that can be uniquely solved for c and x^c namely $x^0 = g$ and $c = -g$. The control law

proposed by Isidor is as follows:

$$u = \frac{-L_{\mathbf{f}}^4 h(\mathbf{x}) + v}{L_{\mathbf{g}} L_{\mathbf{f}}^3 h(\mathbf{x})} + c \qquad (10)$$

As a consequence, the linearized system will be defined around the point $\mathbf{z} = \mathbf{0}$. Adding constant c to the right side of Eq. (6) as proposed in Eq. (10) is not correct in general because it does not guarantee the linearization of the original system. This is due do the fact that because in the last equation of (7) the term $\frac{c}{L_{\mathbf{g}} L_{\mathbf{f}}^3 h(\mathbf{x})}$ will appear (in general it should be $\frac{c}{L_{\mathbf{g}} L_{\mathbf{f}}^n 1 h(\mathbf{x})}$ in case when the system has a relative degree equal to n). In this particular example $L_{\mathbf{g}} L_{\mathbf{f}}^3 h(\mathbf{x})$ is constant but in general it can be a nonlinear term, therefore this control law cannot linearize the system. The correct version of the control law should be written as follows

$$u = \frac{-L_{\mathbf{f}}^4 h(\mathbf{x}) + v + c}{L_{\mathbf{g}} L_{\mathbf{f}}^3 h(\mathbf{x})}. \qquad (11)$$

As a consequence in the last equation of the system (7) constant term appears as c. Taking into account the general solution the steady state of the system (7) with control law (11) can be calculated as follows

$$\lim_{s \to 0} \left| \begin{matrix} 1 & 1 \\ s & s^2 \end{matrix} \right| \cdot \frac{c}{s^3}.$$

Taking into account the analytical expression of the determinant in the considered case one can calculate that

$$\lim z_1(t) = \frac{c}{2}, \lim z_2(t) = 0, \lim z_3(t) = 0 \text{ and } \lim z_4(t) = 0.$$

t c_0 t t □□
□
□

$t\to\infty$

As can be seen, the steady state of the first variable z^0 can be changed and it is $\frac{c}{c_0}$ – 1 equal to . Now when this is taken into account, Eq. (8) takes the following form
in the steady state:

$$
\begin{aligned}
z_1^0 &= \frac{c}{c_0} x_2^0 \\
z_2^0 &= x_4^0 \\
z_3^0 &= x_1^0 - x_2^0 - g\cos x_1^0 - x_3^0 \\
z_4^0 &= x_3^0 - gx_2^0 \sin x_1^0 - x_2^0 - x_4^0 \\
&\quad - g\cos x_1^0.
\end{aligned}
\tag{12}
$$

From Eq. (12) it can be seen that the linearized system is not necessarily defined around the point $z^0 = 0$. In other words one cannot set up an arbitrary value to the angular displacement x^0 applying to the nonlinear system (3) control law defined by Eq. (11).

The theoretical considerations were verified by simulation but since only the steady state is of interest it can be calculated easily by hand as done here.

ADAPTIVE CONTROL ALGORITHM

Mathematical Description of an Adaptive Tracking Controller

In general the system considered here can be described by the following equations

$$\mathbf{M}_l(\mathbf{q}_l)\ddot{\mathbf{q}}_l + \mathbf{C}_l(\mathbf{q}_l, \dot{\mathbf{q}}_l)\dot{\mathbf{q}}_l + \mathbf{F}_l + \mathbf{G}_l(\mathbf{q}_l) = \mathbf{K}(\mathbf{N}^{-1}\mathbf{q}_m - \mathbf{q}_l) \tag{13}$$

$$\mathbf{J}_m\ddot{\mathbf{q}}_m + \mathbf{N}^{-1}\mathbf{K}(\mathbf{q}_m\mathbf{N}^{-1} - \mathbf{q}_l) + \mathbf{F}_m = \mathbf{u}, \tag{14}$$

where $\mathbf{M}_l(\mathbf{q}_l)$ is a $n \times n$ link inertia matrix, $\mathbf{C}_l(\mathbf{q}_l, \dot{\mathbf{q}}_l)$ is a $n \times n$ matrix containing the centripetal and Coriolis terms, $\mathbf{G}_l(\mathbf{q}_l)$ is a $n \times 1$ vector containing the gravity terms. Friction forces are represented by vectors $\mathbf{F}_l(n \times 1)$ for links and $\mathbf{F}_m(n \times 1)$ for actuators. Vector $\mathbf{q}_l$ $(n \times 1)$ represents the link displacements, and $\mathbf{q}_m$ is a $n \times 1$ vector of the actuator displacements. $\mathbf{J}_m$ is a $n \times n$ positive definite constant diagonal actuator inertia matrix. $\mathbf{N}$ is a positive–definite constant diagonal $n \times n$ matrix containing the gear ratios
for each harmonic drive and $\mathbf{K}$ is a $n \times n$ diagonal matrix of the torsional stiffness. Finally, $\mathbf{u}$ is a $n \times 1$ vector of input torque control. The system described by Eqs. (13), (14) follows the description given in reference (Tian and Goldenberg 1995) assuming that the joint torques can be measured. Note that Eqs. (13) and (14) are generalization of Eqs. (1) and (2) developed for non-adaptive case.

This model was defined assuming that:

- matrix $\mathbf{M}_l(\mathbf{q}_l)$ is positive definite, while matrix which has the form

$\mathbf{N} = \mathbf{M}_I(\mathbf{q}_I) - 2\mathbf{C}_I(\mathbf{q}_I, \mathbf{q}_I)$, is a skew-symmetric matrix,

- we can write $\mathbf{C}(\mathbf{x},\mathbf{y})\mathbf{z} = \mathbf{C}(\mathbf{x},\mathbf{z})\mathbf{y}$ for any vector $\mathbf{z} \in R^n$, and $\mathbf{C}(\mathbf{x},\mathbf{y})$ is bounded for the sake of $\mathbf{x}$ and linear in $\mathbf{y}$, and $\|\mathbf{C}(\mathbf{x},\mathbf{y})\| \le k_C \|\mathbf{y}\|$, $k_C > 0$, where $\|\cdot\|$ denotes Euclidean norm,
- the manipulator works in horizontal plane only (therefore gravity term can be neglected).

Consider a manipulator with two degrees of freedom presented in Fig. 2. In this particular example we have:

- Cartesian coordinates x_1, y_1, and x_2, y_2 are described as follows (compare Fig. 2):

$$x_1 = l_{C_1} sin(q_{I1}), \quad y_1 = l_{C_1} cos(q_{I1}), \tag{15}$$

$$x_2 = l_1 sin(q_{I1}) + l_{C_2} sin(q_{I1} + q_{I2}), \tag{16}$$

$$y_2 = l_1 cos(q_{I1}) + l_{C_2} cos(q_{I1} + q_{I2}). \tag{17}$$

(18)

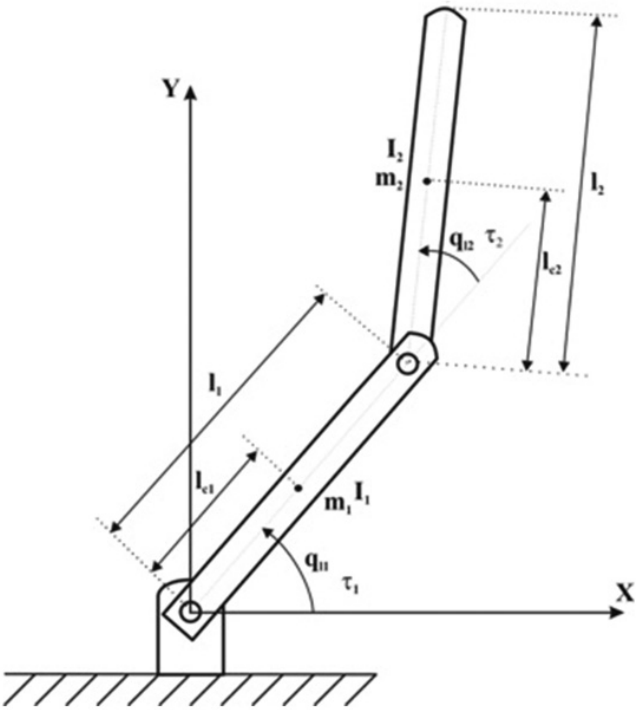


Figure 2. A scheme of a manipulator with two degrees of freedom.

- inertia matrix $\mathbf{M} = \begin{bmatrix} I_1 + m_1 l_{c1}^2 + I_2 + m_2 (l_1^2 + l_{c2}^2 + 2 l_1 l_{c2} \cos(q_{l2})) & I_2 + m_2 (l_{c2}^2 + l_1 l_{c2} \cos(q_{l2})) \\ I_2 + m_2 (l_{c2}^2 + l_1 l_{c2} \cos(q_{l2})) & I_2 + m_2 l_{c2}^2 \end{bmatrix}$ (19)

- matrix containing the centripetal and Coriolis terms $\mathbf{C}_l = \begin{bmatrix} -2 m_2 l_1 l_{c2} \sin(q_{l2}) \dot{q}_{l2} & -m_2 l_1 l_{c2} \sin(q_{l2}) \dot{q}_{l2} \\ m_2 l_1 l_{c2} \sin(q_{l2}) \dot{q}_{l1} & 0 \end{bmatrix}$

$$m \quad l \quad l \;)q \; \square\square 0 \qquad (20)$$
$$\sin(q$$

$$\square\square 2\ 1\ C_2\ l\ 2 \quad l1 \qquad \square\square$$

- matrix containing the gravity terms, which in our case is

$$\mathbf{G}_{\square 0\square_{,0}} = \qquad (21)$$
$$l \quad \square\ \square$$

- vector containing friction forces for links

$$\mathbf{F}_{\square} = \begin{matrix} \square\ F_{ld1}q\square l1 \ \square\ F_{ls1}sgn(q\square l1) \\ , \\ l \quad \square F_{ld\,2}q\square l\,2 \ \square\ F_{ls}2sgn(q\square l\,2\,)\square \end{matrix} \qquad (22)$$

- vector containing friction forces for actuators

$$\mathbf{F}_m = \begin{bmatrix} F_{md1}\dot{q}_{m1} \\ F_{md2}\dot{q}_{m2} + F_{ms2}\,sgn(\dot{q}_{m2}) \end{bmatrix}, \tag{23}$$

- stiffness matrix

$$\mathbf{K} = \begin{bmatrix} K_1 & 0 \\ 0 & K_2 \end{bmatrix}, \tag{24}$$

- gear ratio matrix

$$\mathbf{N} = \begin{bmatrix} N_1 & 0 \\ 0 & N_2 \end{bmatrix}, \tag{25}$$

- actuators inertia matrix

$$\mathbf{J}_m = \begin{bmatrix} J_{m1} & 0 \\ 0 & J_{m2} \end{bmatrix}. \tag{26}$$

Equations (13) and (14) can be rewritten in the following form

$$\mathbf{M}(\mathbf{q})\ddot{\mathbf{q}} + \mathbf{C}(\mathbf{q},\dot{\mathbf{q}}) + \mathbf{G}(\mathbf{q}) + \mathbf{F}(\dot{\mathbf{q}}) = \mathbf{K}(\mathbf{N}^{-1}\mathbf{q}_m - \mathbf{q}), \tag{27}$$

$$\mathbf{k}_m^{-1}\mathbf{J}_m\ddot{\mathbf{q}}_m + \mathbf{k}_m^{-1}\mathbf{F}(\dot{\mathbf{q}}_m) + \mathbf{k}_m^{-1}\mathbf{K}(\mathbf{N}^{-1}\mathbf{q}_m - \mathbf{q}) = \mathbf{i},$$

where $\mathbf{k}_m$ is a diagonal matrix (in our case (2 × 2)), which contains electromotive force constants (SEM), and $\mathbf{i}$ is a vector (in our case (2 × 1)) which contains currents. A set of

Eqs. (13) and (14) is similar to that presented in references (Loria and Ortega 1995, Tian and Goldenberg 1995) with the extensions described above. The tracking error is defined as:

$$\tilde{\mathbf{q}}_l = \mathbf{q}_l - \mathbf{q}_{md}, \quad \mathbf{q}_{ld}, \tag{28}$$

$$\tilde{\mathbf{q}}_m = \mathbf{q}_m \tag{29}$$

where $\mathbf{q}_{ld}$ and $\mathbf{q}_{md}$ denote $n \times 1$ vectors of the desired link and motor trajectories, respectively. It is also assumed that all $\mathbf{q}_{ld}$, $\dot{\mathbf{q}}_{ld}$, $\ddot{\mathbf{q}}_{ld} \in C$, and $\| \mathbf{q}_{ld} \|, \| \dot{\mathbf{q}}_{ld} \|, \| \ddot{\mathbf{q}}_{ld} \| \le B_d$.

The new adaptive version of the control law is derived from the Lyapunov stability theory (Kozłowski and Sauer 1998). The adaptation law for links can be described in the following form:

$$\dot{\tilde{\mathbf{a}}}_l = -\eta_l \hat{\mathbf{a}}_l + \varepsilon \boldsymbol{\Gamma}_l^{-1} \mathbf{Y}_l^T (\tilde{\mathbf{v}} + \tilde{\mathbf{q}}). \tag{30}$$

and the adaptation law for actuators:

$$\dot{\tilde{\mathbf{a}}}_m = -\eta_m \hat{\mathbf{a}}_m + \varepsilon \boldsymbol{\Gamma}_m^{-1} \mathbf{Y}_m^T (\tilde{\mathbf{v}}_m + \tilde{\mathbf{q}}), \tag{31}$$

where $\mathbf{Y}_l$ and $\mathbf{Y}_m$ are appropriate matrices (regressor factors) associated with links and motors, respectively. In Eqs. (30) and (31) ε is a small positive constant, $\mathbf{\Gamma}_l$, $\mathbf{\Gamma}_m$ are positive definite constant gain matrices and $\tilde{\mathbf{a}}$ ($\tilde{\mathbf{a}}_l$, $\tilde{\mathbf{a}}_m$) is an estimate error $\tilde{\mathbf{a}} = \mathbf{a} - \hat{\mathbf{a}}$ ($\tilde{\mathbf{a}}_l = \mathbf{a}_l - \hat{\mathbf{a}}_l$, $\tilde{\mathbf{a}}_m = \mathbf{a}_m - \hat{\mathbf{a}}_m$) between parameter $\mathbf{a}_l$ ($\mathbf{a}_m$) and its estimate $\hat{\mathbf{a}}_l$ ($\hat{\mathbf{a}}_m$). The adaptive version of control algorithms for the system given by Eqs. (13) and (14) can be written in the following form:

$$\mathbf{u} = \hat{\mathbf{J}}_m \dot{\mathbf{q}}_{md} - \hat{\mathbf{N}}^{-1}\hat{\mathbf{K}}(\hat{\mathbf{N}}^{-1}\mathbf{q}_{md} - \mathbf{q}_{ld}) - \hat{\mathbf{F}}_m(\dot{\mathbf{q}}_{md}) - \mathbf{K}_{pm}\dot{\mathbf{q}}_m - \mathbf{K}_{dm}\tilde{\mathbf{v}}_m \quad (32)$$

where $\mathbf{q}_{md}$ is calculated by performing the differentiation operation twice to the following equation:

$$\mathbf{q}_{md} = \hat{\mathbf{N}}\hat{\mathbf{K}}^{-1}\hat{\mathbf{M}}_l(\mathbf{q}_l)\ddot{\mathbf{q}}_{ld} - \hat{\mathbf{C}}_l(\mathbf{q}_l, \dot{\mathbf{q}}_{ld}) - \hat{\mathbf{G}}_l(\mathbf{q}_l) - \hat{\mathbf{F}}_l(\dot{\mathbf{q}}_{ld}) - \mathbf{K}_{pl}\dot{\mathbf{q}}_l - \mathbf{K}_{dl}\tilde{\mathbf{v}}_l - \hat{\mathbf{N}}\mathbf{q}_{ld} \quad (33)$$

where $\tilde{v}_j$ for $j = l, m$ is calculated from Eq. (34).

$$\tilde{\mathbf{v}}_{diag} = b_{ij}\, s_j \quad m = l, \quad \dot{\mathbf{q}}_j, \quad s_j = \dot{q}_j + a_{ij} q_j \quad (34)$$

where $\tilde{v}_m$ and $\tilde{v}_l$ denote vectors of the filtered position error for the link and actuator, respectively.

In (32) and (33) " ~ " denotes an appropriate estimate. Equations (32) and (33) can be presented in general form:

$$\mathbf{q}_{md} = \mathbf{Y}_l(\mathbf{q}_{ld}, \dot{\mathbf{q}}_{ld}, \ddot{\mathbf{q}}_{ld})\hat{\mathbf{a}}_l - \mathbf{K}_{pl}\dot{\mathbf{q}}_l - \mathbf{K}_d\tilde{\mathbf{v}}_l,$$

$$\mathbf{u} = \mathbf{Y}_m(\mathbf{q}_{md}, \dot{\mathbf{q}}_{md}, \ddot{\mathbf{q}}_{md})\hat{\mathbf{a}}_m - \mathbf{K}_{pm}\dot{\mathbf{q}}$$

$$m \; \square \; \mathbf{K}_{dm} \mathbf{v} \square \; m. \tag{35}$$

Adaptive gain coefficients for position control of the motor and current control for the first link and second link can be defined, respectively:

$$\mathbf{\Gamma}_{l} = diag \square \square_{M} \square \square_{N} \square \quad _{F} \tag{36}$$

$$\square \square l \qquad ls \quad ld \; \square \square$$

$$\mathbf{\Gamma}_{m} = diag \square \square_{J} \square \square_{K} \square \quad _{F} \tag{37}$$

$$\square \square \qquad m \;\; ms \;\; md \; \square \square$$

Matrices $_{m}\mathbf{Y}_{l\,m,l}\mathbf{Y}$, $\tilde{\mathbf{a}}$, $\tilde{\mathbf{a}}$ have the following form:

$$\mathbf{Y} \; (\mathbf{q} \; ; \mathbf{q} \qquad) \square = \quad \square \; \mathbf{q}_{md} \; \square \; (\mathbf{q} \quad sgn \quad) \quad \mathbf{q} \tag{38}$$

$$\mathbf{q} \qquad \qquad ,$$

$$m \qquad md \; md \quad md \quad \square \quad \hat{\mathbf{N}} \quad ld \qquad md \quad md \; \square$$

$$\mathbf{Y}_{l} \; (\mathbf{q}_{ld} \; , \mathbf{q} \; _{ld} \quad \mathbf{q}_{l} \quad sgn(\mathbf{q} \quad \mathbf{q} \; \square \; _{ld}) \quad _{ld} \tag{39}$$

$$, \mathbf{q} \; _{ld}) = \square \mathbf{q} \; \square _{ld} \qquad d \qquad \square \; ld \;) \qquad \square,$$

$$\mathbf{a}_{m}^{T} = _{m} \quad \mathbf{K} \; \square \quad _{ms} \quad \mathbf{F}_{md} \tag{40}$$

$$\square \; \mathbf{J} \; \square \qquad \mathbf{F} \qquad \square$$

$$\square \qquad \square,$$

$$\mathbf{a}_{l}^{T} = \quad \mathbf{N} \; \square \quad \mathbf{F} \tag{41}$$

$$\square \; \mathbf{M} \; \square \qquad \square \; \mathbf{F} \; \square.$$

$$l \; \square \quad l \quad ls \quad ld \; \square$$

The Stability Properties of the Adaptive Tracking Controller

The stability properties of the adaptive tracking controller, which was presented in Section Mathematical Description of an Adaptive Tracking Controller, can be derived using the following theorem (Corless 1990).

Theorem 1. Consider the dynamic system $\dot{x}_1 = f_1(x_1, x_2, t)$, $\dot{x}_2 = f_2(x_1, x_2, t)$. Let $V(x_1, x_2, t)$ be a Lyapunov function for the system with the properties:

$$\square_1 \| x_1 \|^2 \square\square_2 \| x_2 \|^2 \square V \square \square_3 \| x_1 \|^2 \square\square_4 \| x_2 \|^2$$
$$\dot{V}\square \square \square\square_5 \| x_1 \|^2 \square\square_6 \| x_2 \|^2 \square\square$$

where ε and μ_i are positive scalar constants. Define $\sigma_1 = max(\mu_3/\mu_5, \mu_4/\mu_6)$ and $r_i = (\sigma_1 \varepsilon/\mu_i)\mu_2$ for $i = 1,2$. Then for any initial state $x(0)$, $\dot{x}(0)$ the model will evolve so that $x_1(t)$, $x_2(t)$ are uniformly bounded and converge exponentially to the closed balls Br_1, Br_2, respectively, where

$$Br_1 = \{x_i : \| x_i \| \le r_i\}.$$

The control law given by Eq. (32) is semiglobally asymptotically stable because the domain of atraction can be arbitrarily enlarged by increasing the gain of the controller. First we consider the case in which we neglect flexibility ($K \to \infty$) (Loria and Ortega 1995, Nicosia and Tomei 1994). In this case the model given by Eqs. (13) and (14) is reduced to

$$\mathbf{D}_l(\mathbf{q}_l)\ddot{\mathbf{q}}\square\square_l \square \mathbf{C}_l(\mathbf{q}_l, \dot{\mathbf{q}}\square_l)\dot{\mathbf{q}}\square_l \square \mathbf{G}(q_l) \square \mathbf{F} = \mathbf{u} \qquad (42)$$

where $\mathbf{D}_l(\mathbf{q}_l) = \mathbf{M}_l(\mathbf{q}_l) + \mathbf{N}\,\mathbf{J}_m$ and $\mathbf{F} = \mathbf{F}_l(\dot{\mathbf{q}}_l) + \mathbf{N}\mathbf{F}_m(\dot{\mathbf{q}}_m)$.

It is assumed that $\mathbf{F}$ is a combined $n \times 1$ vector containing the dynamic friction terms associated with link bearings and actuators. For Eq. (42) the following adaptive control law will be proposed:

$$\mathbf{u} = \hat{\mathbf{D}}_l(\mathbf{q}_l)\ddot{\mathbf{q}}\square\square_{ld} \square \hat{\mathbf{C}}(\mathbf{q}_l, \dot{\mathbf{q}}\square_{ld})\dot{\mathbf{q}}\square_{ld} \square \hat{\mathbf{G}}(\mathbf{q}_l) \square \hat{\mathbf{F}}(\dot{\mathbf{q}}\square_{ld}$$

$$) \; \mathbf{K}_{pl}\tilde{\mathbf{q}}_l \; \mathbf{K}_{dl}\tilde{\mathbf{v}}_l . \tag{43}$$

First the following Lyapunov function candidate will be chosen:

$$V(\tilde{\mathbf{q}}, \tilde{\mathbf{q}}, \tilde{\mathbf{v}}, t) = \frac{1}{2}\tilde{\mathbf{q}}^T \mathbf{K}\tilde{\mathbf{q}} + \frac{1}{2}\mathbf{B}_v^{-1}\tilde{\mathbf{q}}^T \mathbf{D}\tilde{\mathbf{q}} + \frac{1}{2}\tilde{\mathbf{v}}^T \mathbf{D}\tilde{\mathbf{q}} + \frac{1}{2}\tilde{\mathbf{a}}^T \boldsymbol{\Gamma}\tilde{\mathbf{a}}$$

$$\frac{1}{2}\|\tilde{\mathbf{q}}_l\|^2 + \frac{1}{2}\|\tilde{\mathbf{q}}_l\|^2 + \frac{1}{2}\|\tilde{\mathbf{v}}_l\|^2 + \frac{1}{2}\|\tilde{\mathbf{a}}_l\|^2 \tag{44}$$

where $\boldsymbol{\Gamma}_l$ is a symmetric positive–definite matrix, ε is a constant value coefficient. The function $V(t)$ in (44) can be bounded in the following manner:

$$\frac{1}{2}\|\mathbf{z}\|^2 \le V(t) \le \frac{1}{2}\|\mathbf{z}\|^2 \tag{45}$$

where vector $\mathbf{z} = [\mathbf{q}^T, \dot{\mathbf{q}}^T, \mathbf{v}^T]^T$, and matrices $\mathbf{Q}_1$, $\mathbf{Q}_2$:

$$\mathbf{Q}_1 = \begin{bmatrix} \frac{1}{2}k_{plm} & 0 & -\frac{1}{2}d_{lm} \\ 0 & \frac{1}{2}d_{lm} & -\frac{1}{2}d_{lm} \\ -\frac{1}{2}d_{lm} & -\frac{1}{2}d_{lm} & \frac{1}{2}d_{lm}k_{lm}^{-1}b_m^{-1} \end{bmatrix},$$

$$\mathbf{Q}_2 = \begin{bmatrix} \frac{1}{2}k_{plM} & 0 & -\frac{1}{2}d_{lM} \\ 0 & \frac{1}{2}d_{lM} & -\frac{1}{2}d_{lM} \\ -\frac{1}{2}d_{lM} & -\frac{1}{2}d_{lM} & \frac{1}{2}d_{lM}k_{lm}^{-1}b_M^{-1} \end{bmatrix}.$$

The matrices $\mathbf{Q}_1$ and $\mathbf{Q}_2$ are positive definite, respectively, if

$$\begin{aligned} \varepsilon &< \min\left\{\sqrt{\frac{k_{plm}}{d_{lm}}}, \frac{k_{plm}k_{dlm}k_{lm}b_m^{-1}}{d_{lm}(k_{plm}+d_{lm}k_{lm}b_m^{-1})}\right\} \\ \varepsilon &< \min\left\{\sqrt{\frac{k_{plM}}{d_{lM}}}, \frac{k_{plM}k_{dlM}k_{lm}b_M^{-1}}{d_{lM}(k_{plM}+d_{lM}k_{lm}b_M^{-1})}\right\} \end{aligned} \tag{46}$$

As a consequence, the Lyapunov function (45) can be bounded as

$$\frac{1}{2}\lambda_1(\mathbf{Q}_1)\|\mathbf{z}\|^2 + \frac{1}{2}\|\mathbf{a}\|^2 \le V(t) \le \frac{1}{2}\lambda_2(\mathbf{Q}_2)\|\mathbf{z}\|^2 + \frac{1}{2}\|\mathbf{a}\|^2 \tag{47}$$

$$m \quad 1 \qquad 2 \quad lm \; l \qquad M \quad 2 \qquad \frac{1}{2} \mathbf{r}_{lM} \qquad l$$

where λ_m ($\mathbf{Q}_1$), λ_M ($\mathbf{Q}_2$) denote the smallest and the biggest eigenvalues of matrices $\mathbf{Q}_1$ and $\mathbf{Q}_2$, respectively.

Taking the first derivative of the Lyapunov function, one can get

$$V = \tilde{\mathbf{q}}^T \quad \mathbf{q} \quad \tilde{\mathbf{v}}^T \quad \mathbf{K} \quad \tilde{\mathbf{q}}^T \mathbf{D} \quad \tilde{\mathbf{q}} \quad \tilde{\mathbf{q}}^T \mathbf{D}\tilde{\mathbf{q}} = \tilde{\mathbf{q}}^T \quad \tilde{\mathbf{q}}^T \mathbf{K} \mathbf{B} \tilde{\mathbf{v}} \quad \tilde{\mathbf{q}} \mathbf{D}\tilde{\mathbf{q}}^T \quad \mathbf{D} \tilde{\mathbf{q}}$$

$$l \quad l \quad 2 \; l \quad l \quad l \quad pl \quad l \quad dl \qquad l \quad l \quad l \quad l \quad l \quad l$$

$$\tilde{\mathbf{v}}^T \mathbf{D}\tilde{\mathbf{q}} \quad \tilde{\mathbf{v}}^T \quad \tilde{\mathbf{v}}^T \quad \tilde{\mathbf{a}}^T \boldsymbol{\Gamma} \tilde{\mathbf{a}} . \qquad (48)$$

$$\mathbf{D}\tilde{\mathbf{q}} \quad \mathbf{D}\tilde{\mathbf{q}}$$

$$l \quad l \quad l \qquad l \quad l \quad l \; l \; l$$

Taking into account the skew symmetric property of the matrix $\mathbf{D}(\mathbf{q}_l) - 2\mathbf{C}(\mathbf{q}_l, \mathbf{q}_l)$ and Eqs. (34), (42) and (43) the last equation can be rewritten in the following form:

$$V = \mathbf{q}^T \mathbf{F}(\mathbf{q} \quad) \quad \mathbf{q}^T \mathbf{F}(\mathbf{q} \quad) \quad \mathbf{q}^T \mathbf{F}(\mathbf{q} \quad) \quad \mathbf{q}^T \mathbf{F}(\mathbf{q} \quad) \quad \mathbf{v}^T \mathbf{F}(\mathbf{q} \quad)$$

$$l \quad l \quad l \quad ld \quad l \quad l \quad l \quad ld \quad l \quad l \quad) \quad - \tilde{\mathbf{q}}^T \mathbf{Y} \tilde{\mathbf{a}} \quad \tilde{\mathbf{v}}^T \mathbf{Y} \tilde{\mathbf{a}} \quad \tilde{\mathbf{q}}^T \mathbf{Y} \tilde{\mathbf{a}}$$

$$\tilde{\mathbf{v}}^T \quad \tilde{\mathbf{a}}^T \quad \boldsymbol{\Gamma} \quad \mathbf{F}(\mathbf{q} \quad \tilde{\mathbf{a}}$$

$$l \quad ld \quad l \qquad l \; l \; l \qquad l \; l \; l \qquad l \; l \; l$$

$$\mathbf{v}^T \mathbf{K} - \mathbf{q}^T \mathbf{q} \mathbf{q}$$
$$\mathbf{B}^{-1}\mathbf{A}\mathbf{v} \quad \mathbf{C}\mathbf{q}\mathbf{q}^T \quad T\mathbf{C}^T\mathbf{C}$$
$$\mathbf{D}\mathbf{q}$$

$$\mathbf{q}^T \mathbf{C}^T - \mathbf{q}^T - \mathbf{q}^T \mathbf{K} \mathbf{v}$$
$$\mathbf{C}^T\mathbf{q} \quad \mathbf{K}\mathbf{q}$$

$$\mathbf{v}^T \quad \mathbf{v}^T\mathbf{C}^T \mathbf{C}^T\mathbf{q}$$
$$\mathbf{A}^T\mathbf{D}\mathbf{q} \quad \mathbf{q} \quad \mathbf{B}^T$$
$$\mathbf{D}\mathbf{q}$$

$$\mathbf{v}^T \quad \mathbf{C}^T \quad \mathbf{C} \quad \mathbf{q} - \mathbf{v}_{pl}^T - \mathbf{v}^T\mathbf{K} \quad (49)$$
$$\mathbf{K}\mathbf{q} \quad \mathbf{v} .$$

where $\mathbf{C}$, $\mathbf{C}_d$ denote $\mathbf{C}(\mathbf{q}_l, \mathbf{q}_l)$, $\mathbf{C}(\mathbf{q}_l, \mathbf{q}_l, \mathbf{q}_d)$, respectively.

Next, upper bounds for some expressions are calculated. First take $\varepsilon\mathbf{q}_l^T(\mathbf{C}^T - \mathbf{C}_d^T)\dot{\mathbf{q}}_l$, the following calculations can be obtained.

$$\mathbf{q}^T\mathbf{C}^T = \mathbf{q}^T\mathbf{C}^T(\mathbf{q},\mathbf{q})\mathbf{q} \quad \mathbf{q}^T\mathbf{C}^T(\mathbf{q},\mathbf{q})\mathbf{q} =$$
$$\mathbf{C}^T\mathbf{q}$$

$$= \mathbf{q}^T\mathbf{C}(\mathbf{q},\mathbf{q})\mathbf{q} \quad \mathbf{q}^T\mathbf{C}(\mathbf{q},\mathbf{q})\mathbf{q} = \mathbf{q}^T\mathbf{C}(\mathbf{q},\mathbf{q})\mathbf{q}$$
$$\mathbf{q}^T\mathbf{C}(\mathbf{q},\mathbf{q})\mathbf{q} = \mathbf{q}^T = \mathbf{q}^T\mathbf{C}(\mathbf{q},\mathbf{q})\mathbf{q} =$$
$$\mathbf{q}^T\mathbf{C}(\mathbf{q},\mathbf{q})\mathbf{q}$$

$$= \mathbf{q}^T\mathbf{C}(\mathbf{q},\mathbf{q})\mathbf{q} \quad \|\mathbf{q}\|^2\|\mathbf{q}\| \quad (50)$$
$$k\|\mathbf{q}\|^2\|\mathbf{q}\|$$

The upper bound for $\varepsilon\mathbf{v}_l(\mathbf{C} - \mathbf{C}_d)\dot{\mathbf{q}}_l$ can be evaluated similarly.

To perform further calculations for the sake of simplicity the following model of friction will be used:

$$\mathbf{F}(\dot{\mathbf{q}}_l) = \mathbf{F}_C sgn(\dot{\mathbf{q}}_l) + \mathbf{F}_V \dot{\mathbf{q}}_l$$

$$\mathbf{F}(\dot{\mathbf{q}}_{ld}) = \mathbf{F}_C sgn(\dot{\mathbf{q}}_{ld}) + \mathbf{F}_V \dot{\mathbf{q}}_{ld}. \quad (51)$$

where $\mathbf{F_V}$ denotes a diagonal matrix consisting of viscous friction coefficients associated with the links, and $\mathbf{F_C}$ denotes static friction. Next, the following bounds can be established for the terms associated with the friction coefficients which appear in Eq. (49) taking into account Eq. (51)

$$\dot{\mathbf{q}}_l^T \mathbf{F}(\dot{\mathbf{q}}_l) \geq \dot{\mathbf{q}}_l^T \mathbf{F}(\mathbf{0}) + F_{vm} \|\dot{\mathbf{q}}_l\|^2$$

$$\|\dot{\mathbf{q}}_l^T \mathbf{F}(\dot{\mathbf{q}}_l) - \dot{\mathbf{q}}_l^T \mathbf{F}(\dot{\mathbf{q}}_{ld})\| \leq 2F_{cM} \|\dot{\mathbf{q}}_l\| + F_{vM} \|\dot{\mathbf{q}}_l\| \|\dot{\mathbf{q}}_l - \dot{\mathbf{q}}_{ld}\|$$

$$\|\mathbf{v}_l^T \mathbf{F}(\dot{\mathbf{q}}_l) - \mathbf{v}_l^T \mathbf{F}(\dot{\mathbf{q}}_{ld})\| \leq 2F_{cM} \|\mathbf{v}_l\| + F_{vM} \|\mathbf{v}_l\| \|\dot{\mathbf{q}}_l - \dot{\mathbf{q}}_{ld}\|$$

where F_{vm} denotes the smallest eigenvalue of the matrix $\mathbf{F_V}$ and F_{cM} denotes the biggest eigenvalue of the matrix $\mathbf{F_C}$. By virtue of some properties we can establish the following bounds for the other terms in Eq. (49) which do not include elements with vector $\tilde{\mathbf{a}}$:

$$\mathbf{v}_l^T \mathbf{K}_1 \mathbf{B}^{-1} \mathbf{A} \mathbf{v}_l \leq \frac{k_b}{k_a} \|\mathbf{v}_l\|^2$$

$$\dot{\mathbf{q}}_l^T \mathbf{C}_l \dot{\mathbf{q}}_l \leq k_B \|\dot{\mathbf{q}}_l\|^2$$

$$\dot{\mathbf{q}}_l^T \mathbf{D} \dot{\mathbf{q}}_l \leq d \|\dot{\mathbf{q}}_l\|^2$$

$$\dot{\mathbf{q}}_l^T \mathbf{C}_d^T \mathbf{C}_l \dot{\mathbf{q}}_l - \dot{\mathbf{q}}_{ld}^T \mathbf{C}_c^T \mathbf{C}_l \dot{\mathbf{q}}_{ld} \leq 2k_B \|\dot{\mathbf{q}}_l\| \|\dot{\mathbf{q}}_l - \dot{\mathbf{q}}_{ld}\|$$

$$\dot{\mathbf{q}}_l^T \mathbf{C}_d^T \mathbf{C}_l \dot{\mathbf{q}}_l - \dot{\mathbf{q}}_{ld}^T \mathbf{C}_c^T \mathbf{C}_l \dot{\mathbf{q}}_{ld} \leq k \|\dot{\mathbf{q}}_l\|^2$$

$$\dot{\mathbf{q}}^T \mathbf{K}\, \mathbf{q} \le k \|\mathbf{q}\|^2$$

$$\dot{\mathbf{q}}_l^T \mathbf{K}_{dl} \mathbf{v}_l \le k_{dlM} \|\mathbf{q}_l\| \|\mathbf{v}_l\|$$

$$\mathbf{v}_l^T \mathbf{A}_l^T \mathbf{D}_{lM} \mathbf{q}_l \le a_{lM} \|\mathbf{v}_l\| \|\mathbf{q}_l\|$$

$$\dot{\mathbf{q}}_l^T \mathbf{B}_l^T \mathbf{D}_{lM} \mathbf{q}_l \le b_{lM} \|\mathbf{q}_l\|^2$$

$$\mathbf{v}_l^T \mathbf{C}_l^T \mathbf{C}_l^T \le \|\mathbf{v}_l\|^2 \|\mathbf{v}_l\|$$

$$\mathbf{q}_l \le k \|\mathbf{q}_l\|$$

$$\mathbf{v}_l^T \mathbf{C}_l \le 2k_{dl} \|\mathbf{v}_l\| \|\mathbf{q}_l\|$$

$$\mathbf{C}^T \mathbf{C} \le B \mathbf{v}$$

$$\mathbf{q}$$

$$\mathbf{v}_{pl}^T \mathbf{K}_{pl} \mathbf{q}_{plM} \le k \|\mathbf{v}_l\| \|\mathbf{q}_l\|$$

$$\mathbf{v}_{dl}^T \mathbf{K}_{dlM} \le k \|\mathbf{v}_l\|^2$$

. .

where $\mathbf{C}(\mathbf{q}, \dot{\mathbf{q}}) \le k_C \|\dot{\mathbf{q}}\|$ and $k_C > 0$. The above inequalities are useful in evaluating the upper bound of the time derivative of the Lyapunov function given by Eq. (49). All constants with index M denote the biggest eigenvalue of an appropriate matrix.

The elements of the matrices are denoted by corresponding small letters and are self- explanatory. Then the following adaptive law can be proposed:

$$\dot{\hat{\mathbf{a}}} = \Gamma^{-1} \mathbf{Y}^T (\tilde{\mathbf{v}} \; \tilde{\mathbf{q}}). \tag{52}$$

$$l \quad l \quad l \; l \; l \; l$$

When it and the previously evaluated upper bounds are taken into account, the time derivative of the proposed Lyapunov function can be evaluated as follows:

$$\dot{Q} \le \sum_{l} \underline{\quad} \|\dot{\mathbf{q}}\|^T$$

$$\frac{1}{2}k_{plm} \quad -k_{pl} \quad M \quad k_{dl} \quad M \quad I$$

$$V(t) \quad \left[2 \quad k_{plM} \quad k_{dlM} \right] \quad \frac{1}{a} \; k \; b^{1} \quad \left[\quad \tilde{\mathbf{q}} \quad \right] \quad \mathbf{v}$$

$$dlm \; lM \; lm \quad 2$$

$\mathbf{Q}_2$

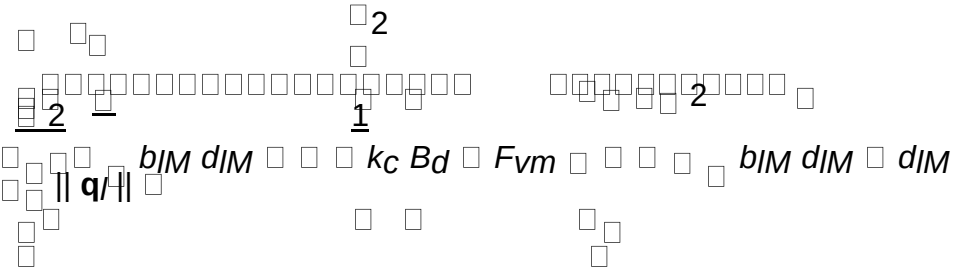
$$\frac{1}{} \; k \; dlm \; lM \quad 2k_c \; B_d \quad a_{lM} \quad d_{lM} \quad F_{vM} \quad \hat{\mathbf{v}} \quad I \quad 2 \quad 2 \quad 2k \; B \quad a \quad d \quad \frac{1}{} \; d \; b \quad \mathbf{q} \quad I \quad F$$

$$c \quad d \; lM \quad lM \quad lM \quad lM \quad vM$$

$\mathbf{Q}_3$

$$\frac{1}{} \; k_{pl} \quad 2k_c \quad B_d \quad F_{vM} \quad \mathbf{q} \quad I \quad 2 \quad 2k \quad B \quad \frac{1}{} \quad b \quad 2 \; k_c \; B_d \quad \mathbf{q} \quad I \quad F \quad d$$

$$c \quad d \quad lM \; lM \quad vM \quad 1$$



$$\dot{V} = -\frac{1}{3}k_{plm}\,b_{lm}\,\|\tilde{\mathbf{q}}\|^2 - k_{dlm}\,(\|\tilde{\mathbf{v}}\| - \|\tilde{\mathbf{q}}\|)\,\|\tilde{\mathbf{q}}\| - \|\tilde{\mathbf{v}}\|^2 -$$

$$-\frac{2\,d_{lm}}{l_{lM}} - \frac{d_{lm}}{l_{lm}}\,\|\tilde{\mathbf{q}}\|\,\|\tilde{\mathbf{v}}\| + \frac{l_{lm}\,c_{lm}}{l_{lM}}\,\|\tilde{\mathbf{q}}\|^2 + \frac{l_{lm}}{l_{lM}}\,\|\tilde{\mathbf{v}}\|^2 +$$

$$+\frac{l_{lm}}{2}\,\tilde{\mathbf{a}}^T\boldsymbol{\Gamma}\,\dot{\hat{\mathbf{a}}} - \tilde{\mathbf{q}}^T\,(\|\tilde{\mathbf{q}}\| - \|\tilde{\mathbf{v}}\|) - \frac{k_{plm}}{2}\,\|\tilde{\mathbf{q}}\|^2 - \frac{k_{dlm}}{2}\,\|\tilde{\mathbf{v}}\|^2 \qquad (53)$$

$$\mathbf{Y}\,\tilde{\mathbf{a}} = 2\,F_{vM}\,\|\tilde{\mathbf{v}}\| - \frac{l_{lm}\,c_{lM}}{l_{lM}}\,\|\tilde{\mathbf{q}}\|^2 - \frac{l_{lm}}{l_{lM}}\,\|\tilde{\mathbf{v}}\|^2 - \frac{k_{plm}}{2}\,\|\tilde{\mathbf{q}}\|^2 - \frac{k_{dlm}}{2}\,\|\tilde{\mathbf{v}}\|^2 .$$

where $\alpha + \gamma = 1$ and $\alpha, \gamma, \beta > 0$.

The condition for the positive definiteness of the matrix $\mathbf{Q}_1$ results in upper bound for ε (recall that $\varepsilon > 0$):

$$\varepsilon < \frac{k_{plm}\,k_{dlm}\,a_{lm}}{4\,b_{lM}\,(k_{plM} + k_{dlM})^2} \qquad (54)$$

For the matrix $\mathbf{Q}_2$ the positive definiteness condition can be written in the following form:

$$\varepsilon < \frac{k_{dlm}\,b_{lm}\,a_{lm}\,d_{lm}}{2\,(2k_c\,B_d + a_{lM}\,d_{lM} + F_{vM})^2} \qquad (55)$$

Then the positive definiteness of the matrix $\mathbf{Q}_3$ is guaranteed when two conditions are satisfied and derived from

$$\frac{1}{2}\,k_{plm}\,b_{lm}\,d_{lm} - (2k_c\,B_d + F_{vM})^2 + \frac{1}{2}\,k_{plm}\,a_{lm}\,d_{lm} > 0$$

$$2\,k_{plm}\,l_{lM}\,l_{lM} - c_{lm}\,d_{lm}\,l_{vM} - 2\,k_{plm}\,l_{lm} > 0$$

$$\frac{1}{2}\left[k_{plm}\ b_{lM}\ d_{lM}\right]\begin{bmatrix} 2k_c & -B_d \\ -B_d & F_{vM} \end{bmatrix}\begin{bmatrix} k_{plm} \\ b_{lM} \\ d_{lM} \end{bmatrix} = C > 0$$

$$k_{plm} > \frac{2\left(2k_c B_d\right)^2}{F_{vM}\left(2k_c - B_d\right)} \tag{56}$$

$$\gamma > \frac{k_{plm} k_c B_d}{C_2}. \tag{57}$$

Note that the positive definiteness of constant λ_1 imposes a lower bound on ε, i.e.,

$$\varepsilon < \frac{\left(F_{vm} - k_c B_d\right)\gamma}{2\, b_{lM}\, d_{lM}} \tag{58}$$

In the case when $F_{vm} - k_c B_d \gamma > 0$:

$$\varepsilon < \frac{F_{vm}}{k_c B_d} \tag{59}$$

λ_2 is positive under the following condition

$b_{lM} > 0$. (60)

Finally, λ_3 is always positive. Then define matrix **Q** as:

$$\mathbf{Q} = \begin{bmatrix} k_{pl} - \frac{1}{2} F_{vM} k_c B_d & -\frac{1}{2} F_{vM} k_c a_{lM} d_{lM} & -\frac{1}{2} k_{pl} d_{lM} \\ -\frac{1}{2} F_{vM} k_c a_{lM} d_{lM} & B_d - F_{vm} k_c B_d (a_{lm} + a_{lM}) d_{lM} d_{lm} b_{lm} & -\frac{1}{2} k_c B_d d_{lm} b_{lm} \\ -\frac{1}{2} k_{pl} d_{lM} & -\frac{1}{2} k_c B_d d_{lm} b_{lm} & \frac{1}{2} k_{pl} d_{lM} - \frac{1}{2} k_c F_{vM} a_{lM} d_{lM} b_{lM} \end{bmatrix} \quad (61)$$

and note that **Q** is positive-definite if conditions (54)–(60) are satisfied. Further evaluation of the time derivative of Lyapunov function (53) is as follows:

$$\dot{V}(t) = -\mathbf{z}^T \mathbf{Q} \mathbf{z} - k_c \|\tilde{\mathbf{v}}\|^2 \|\tilde{\mathbf{q}}\| - \tilde{\mathbf{q}}^T \mathbf{Y} \tilde{\mathbf{a}} - \frac{1}{2} k_c \|\tilde{\mathbf{v}}\|^2 \|\tilde{\mathbf{q}}\| - \tilde{\mathbf{a}} \Gamma^T \dot{\hat{\mathbf{a}}} - \frac{1}{2} k_{plm} \|\tilde{\mathbf{q}}\|^2$$

$$\square 2\square F_{CM}\ (\|\ \mathbf{q}\square_{I} \|\ \square\ \|\ \mathbf{v}\square_{I}\ \|). \qquad (62)$$

Introducing bounds of the regresion function $\mathbf{Y}_I$, the expression: $\mathbf{Ya}_I$ is a scalar function.

Due to the fact that the matrix $\mathbf{Y}$ is a rectangular matrix ($\mathbf{Y} \in \mathbf{R}^{m\times n}$), the Frobenius norm should be applied:

$$\|\mathbf{A}\|_F = \sqrt{\sum_{i=1}^{m}\sum_{j=1}^{n} |a_{ij}|^2}\ . \qquad (63)$$

As a consequence, all elements of regresion function $\mathbf{Y}_I(\mathbf{q}_I, \mathbf{q}_{Id}, \mathbf{q}_{Id})$ are bounded as

$$\|\ \mathbf{q}\square^{T}\mathbf{Y}\,\hat{\mathbf{a}}\ \square\|\ \mathbf{Y}\ \|= C\ \|\ \|\ \mathbf{q}\square\ \|\|\|\ \hat{\mathbf{a}}\ \ \mathbf{q}\square\ \|\|\|\ \hat{\mathbf{a}}\ \|! \qquad (64)$$

Taking into account Eq. (64), the upper bound of $-\mathbf{a}_I^T\mathbf{\Gamma}\eta\mathbf{a}_I - \mathbf{q}_I\mathbf{Y}\,\mathbf{a}_I$ can be calculated as follows:

$$\square\square\hat{\mathbf{a}}\square^{T}\mathbf{\Gamma}\,\hat{\mathbf{a}}\ \square\ \mathbf{q}\square^{T}\mathbf{Y}\,\hat{\mathbf{a}}\square\ =\ \square\square\ \mathbf{a}\square^{T}\mathbf{\Gamma}\,\mathbf{a}\square\ \square\ \|^2\ \square$$
$$\mathbf{a}\square^{T}\mathbf{\Gamma}\,\mathbf{a}\ \square\ \mathbf{q}\square^{T}\mathbf{Y}\,\hat{\mathbf{a}}\ \square\ \square\square\ \square\ \|\ \mathbf{a}\square$$

$$\| \mathbf{a} \| \| \mathbf{a} \| \| \mathbf{a} \| = \| \|^2 C \| \| C \| \mathbf{q} \| = \| \mathbf{a} \| \mathbf{q} \| \| \mathbf{a}$$

$$lM \; l \quad l \; 1 \; l \quad l \quad 2 \quad lm \quad 1 \; l \quad l$$

$$\sqrt{\eta\Gamma_{lm}} \quad 1 \; 2 \; 2 \quad 2 \; 1$$

$$2 \quad lM \| \mathbf{a}_l \| \quad lM \quad \| \mathbf{a}_l \| \quad \| \mathbf{a}_l \|$$

$$\sqrt{2\eta\Gamma_{lm}} \quad 2 \; lm \quad 2$$

$$C \quad 2 \quad C^2 \quad 2 \; 1 \quad 2 \; 1 \; 2 \quad 2$$

$$\sqrt{\eta\Gamma_{lm}} \| \mathbf{q} \| \quad 1 \quad \| \mathbf{a} \| \quad lM \quad \| \mathbf{a} \|$$

$$\| \mathbf{q} \| \; l \quad l \quad 4 \; lm \; l \quad 2 \quad l$$

$$C^2 \quad 2 \; 1 \quad lm \quad lm$$

$$l \quad 2$$

$$1 \quad \| \mathbf{q} \| \quad \| \mathbf{a}_l \| \; lm \; 1 \qquad (65)$$

$$m$$

Assuming that the parameter $\mathbf{a}$ is bounded ($\|\mathbf{a}\| \le \bar{a}$), one can write:

$$1 \quad 1 \; 2 \; 2$$

$$lM \| \mathbf{a}_l \| > 0.$$

$$2 \; lm$$

Next the upper bound of the time derivative of Lyapunov function can be calculated as:

$$V(t) \; \mathbf{z}^T \mathbf{Q} \mathbf{z} \; k_C \| \mathbf{q} \| \| \mathbf{q} \|^2 \; k_C \| \mathbf{v} \| \| \mathbf{q} \|^2$$

$$C^2 \quad 2 \; 1 \quad 2 \quad 2 \quad 2$$

$$\| \mathbf{q} \| \quad 1 \quad lm \| \mathbf{a}_l \| \; 1 \quad k_{plm} \; 2 \; k_{dlm} \| \mathbf{v}_l \|$$

$$lm \quad 4 \quad 2 \| \mathbf{q}_l \|$$

$$2 \; F_{cM}(\| \mathbf{q}_l \| \; \| \mathbf{v}_l \|). \qquad (66)$$

$$C^2 \quad 2$$

Including term $lm \; \frac{1}{l} \| \mathbf{q} \|$

in matrix **Q** one can define matrix **Q**' as:

$$\mathbf{Q}' = \begin{bmatrix} \frac{k}{m} & pl & -\frac{F}{2} & -\frac{k B}{vM\ c\ d} \\ -F_{vM} & F_{vm} - k_c B_d & \frac{1}{2}(\quad\quad) & 2\, d_{lM} - d_{lM} b_{lM} - \frac{1}{lm} \\ \frac{k}{k} & -\frac{k}{k} & -\frac{F}{k B} & -\frac{a\ d}{} \\ \frac{d}{l} & 2 & \frac{2}{d} & vM\ c \quad 2\, lM\ lM \\ 2 & pl_{M} & & \end{bmatrix}$$

$$\begin{bmatrix} -\frac{dl}{k\ M} & -\frac{pl_{M}}{2k} \\ 2 & \end{bmatrix}$$

$$\begin{bmatrix} -\frac{F}{k B} & a_{lM} \\ 2\ vM & \frac{c}{2}\ d_{lM} \end{bmatrix}. \qquad (67)$$

$$\begin{bmatrix} k & b^{-1} & -k \\ a & & \\ dlm & lM & lm \end{bmatrix} \quad dlm$$

Taking into account Eq. (67), the time derivative of the Lyapunov function is bounded as:

$$V(t) = \mathbf{z}^T \begin{bmatrix} \frac{1}{4}\mathbf{Q} & \mathbf{I} \\ \mathbf{I} & \mathbf{I} \end{bmatrix} \mathbf{z} + \frac{1}{2}\|\mathbf{a}\|^2 + \frac{1}{2}k_c\|\mathbf{q}\|^2 + \frac{1}{2}\|\mathbf{v}\|^2 + \frac{1}{2}k_c\|\mathbf{q}\|^2 +$$

$$+ \frac{1}{2}k_c\|\mathbf{q}\|^2 + \frac{1}{2}k_c\|\mathbf{v}\|^2 + (\|\mathbf{q}\| + \|\mathbf{v}\|)2F_{cM} \qquad (68)$$

The expression $2F_{cM}(\|\mathbf{q}\| + \|\mathbf{v}\|) + \frac{1}{2}k_{plm}\|\mathbf{q}\|^2 + \frac{1}{2}k_{dlm}\|\mathbf{v}\|^2$ can be recalculated as follows:

$$2F_{cM}(\|\mathbf{q}\| + \|\mathbf{v}\|) + \frac{1}{2}k_{plm}\|\mathbf{q}\|^2 + \frac{1}{2}k_{dlm}\|\mathbf{v}\|^2 =$$

$$= \frac{1}{2}k_{plm}\left\|\mathbf{q} + \frac{2F_{cM}}{k_{plm}}\right\|^2 + \frac{1}{2}k_{dlm}\left\|\mathbf{v} + \frac{2F_{cM}}{k_{dlm}}\right\|^2 =$$

$$= \frac{1}{2}k_{plm}\left\|\mathbf{q} + \frac{2F_{cM}}{k_{plm}}\right\|^2 + \frac{1}{2}k_{dlm}\left\|\mathbf{v} + \frac{2F_{cM}}{k_{dlm}}\right\|^2 +$$

$$+ \frac{2F_{cM}^2}{k_{dlm}} + 2\frac{2F_{cM}^2}{\sqrt{k_{plm}k_{dlm}}} \qquad (69)$$

As a result, the time derivative of the Lyapunov function can be bounded as:

$$\dot{V}(t) \le -\mathbf{z}^T \mathbf{Q}\mathbf{z} + k_{c1}\|\mathbf{v}\|\|\mathbf{q}\| + \|\mathbf{v}\|\|\mathbf{q}\| + \frac{1}{4}k_{lm1}\|\mathbf{a}\|^2 + \varepsilon_2, \quad (70)$$

where ε_2 was defined as:

$$\varepsilon_2 = 2F_{cM}^2 \frac{k_{dlm}k_{plm}}{k_{dlm}k_{plm}} \quad (71)$$

The second component of Eq. (71) can be estimated as follows:

$$k_{c1}\|\mathbf{v}_1\|\|\mathbf{q}_1\|\|\mathbf{q}_1\|^2 = k_{c1}\|\mathbf{v}_1\|\|\mathbf{q}_1\|\|\mathbf{q}_1\|\|\mathbf{q}_1\| = k_{c1}\sqrt{2}\|\mathbf{v}\|\|\mathbf{q}\|\|\mathbf{q}\| \cdot \frac{\sqrt{2}\|\mathbf{q}\|\|\mathbf{q}\|}{2} \le \frac{k_{c1}}{2}\|\mathbf{v}\|^2\|\mathbf{q}\|^2\|\mathbf{q}\|^2 + \frac{1}{2}k_{c1}\|\mathbf{q}\|^2\|\mathbf{z}\|^2. \quad (72)$$

Now consider the lower bound of the Lapunov function:

$$V(t) \ge \frac{1}{2}d\|\mathbf{q}\|^2 + \frac{1}{2}k_{l1}\|\mathbf{q}\|^2 + \frac{1}{2}k_{l1}k_{b1}\|\mathbf{v}\|^2\|\mathbf{q}\|^2 - \|\mathbf{q}\|\|d\mathbf{q}\|\|\mathbf{q}\|$$

$$\frac{2k_{lm1}}{k_{l1}}\frac{2k_{plm1}}{k_{l1}}2k_{dlm1}k_{lM1}k_{l1}k_{lm1}k_{l1}\|d\mathbf{q}\|\|\mathbf{v}\|\|\mathbf{q}\|$$

$$\| \quad \| \quad (73)$$
$$\frac{1}{\quad} \| \quad \|$$
$$\mathbf{a} \quad \|^2$$
$$\quad .$$
$$lM \; l \qquad 2 \; l \quad m$$

where

$$\|\mathbf{q}\|^2 \quad \|\mathbf{q}\|\|\mathbf{q}\| \quad \|\mathbf{q}\|\|\mathbf{q}\| \quad \|\mathbf{q}\|^2 \quad \|\mathbf{q}\|\|\mathbf{q}\|$$

$$\frac{1}{k} \quad \frac{1}{k}$$

$$\frac{2}{} \quad \frac{2}{k_{plm}} \quad \frac{d_{lm}}{k_{plm}}$$

$$= \frac{1}{\|\mathbf{q}\|^2} \quad \frac{d_{lm}}{k_{plm}} \tag{74}$$

$$\frac{2}{\|\mathbf{q}\|^2} \quad \frac{2d^2}{k_{pl}} \quad \frac{1}{m^2}$$

$$\frac{1}{\|\mathbf{v}\|^2} \quad \frac{2}{\|\mathbf{v}\|^2} \quad \frac{1}{kb} \quad \frac{2}{\|\mathbf{v}\|} \quad \|\mathbf{q}\|$$

$$\frac{1}{k_{dlm}} \quad \frac{1}{b_{lM}} \quad \frac{d}{k_{dlm}B_{lM}} \quad \frac{2}{\|\mathbf{v}\|} \quad \frac{lm}{\|\mathbf{q}\|}$$

$$\frac{2d_{lm}}{k_{dlm}b_{lM}} \quad \|\mathbf{q}\| \tag{75}$$

Consequently, the lower bound of the Lyapunov function (73) can be calculated as follows:

$$V(t) \quad \|\mathbf{q}\| \quad \|\mathbf{q}\| \quad \frac{k_{lm}}{} \quad \|\mathbf{q}\| \quad \|\mathbf{q}\| \quad \frac{lm}{} \quad \|\mathbf{q}\|$$

$$\dot{\mathbf{v}} = -\frac{1}{k_{dlm}b_{lM}}\left[k_{plm}\left(\mathbf{q}_l - \frac{d_{lm}}{k_{dlm}}\left\|\dot{\mathbf{q}}_l - \frac{k_{plm}}{d_{lm}}\left\|\mathbf{q}_l - \frac{d_{lm}^2 + k_{dlm}b_{lM}}{2k_{plm}}\dot{\mathbf{q}}_l\right\|\right\|\right) + \frac{d_{lm}^2 + k_{dlm}b_{lM}}{2k_{dlm}}\dot{\mathbf{q}}_l\right] \tag{76}$$

$$-\frac{d_{lm}}{2k_{plm}}\left\|\dot{\mathbf{q}}_l - \frac{k_{plm}}{d_{lm}}\left\|\mathbf{q}_l - \frac{d_{lm}^2 + k_{dlm}b_{lM}}{2k_{plm}}\dot{\mathbf{q}}_l\right\|\right\| - \frac{d_{lm}^2 + k_{dlm}b_{lM}}{2k_{dlm}}\dot{\mathbf{q}}_l - \frac{d_{lm}}{2k_{dlm}}\left\|\dot{\mathbf{q}}_l - \frac{k_{plm}}{d_{lm}}\left\|\mathbf{q}_l - \frac{d_{lm}^2 + k_{dlm}b_{lM}}{2k_{plm}}\dot{\mathbf{q}}_l\right\|\right\|\right\| .$$

Note that if the condition

$$2 < \frac{k_{plm}b_{lM}}{d_{lm}d_{lm}b_{lM}} \tag{77}$$

is true, the parameter ξ_1, which is defined as:

$$\xi_1 = k_{plm}b_{lM} - 2d_{lm}b_{lM} - 2d_{lM}, \tag{78}$$

is always positive. Therefore one can write:

$$\| \mathbf{q} \| \leq \frac{\sqrt{V}}{\sqrt{\xi_1}}. \qquad (79)$$

From (65), (69), (72), (79), and matrix $\mathbf{Q}'$,V can be bounded as follows:

$$\dot{V}(t) \leq -\frac{1}{2}\lambda_{\min}(\mathbf{Q}') \|\mathbf{z}\|^2 + k \frac{\sqrt{V}}{\sqrt{\xi}} \|\mathbf{a}\|^2 \qquad (80)$$

The time derivative of the Lyapunov function considered here is of the form at Theorem 1 assuming that:

$$\lambda_1 = \lambda_{\min}(\mathbf{Q}) = \frac{1}{2} k_{dlm} b_{lm}^{-1},$$

$$\lambda_2 = \frac{1}{2} k_{dlm},$$

$$\lambda_3 = \lambda_M(\mathbf{Q}_2),$$

$$\lambda_4 = \frac{1}{2} l_M,$$

$$\lambda_5 = \lambda_m(\mathbf{Q}) \frac{\sqrt{V}}{\sqrt{\xi}} + k_c,$$

$$\lambda_6 = \frac{1}{4} l_m,$$

$$\lambda_3 = \frac{1}{2} M \|\mathbf{a}_l\|^2 + \frac{1}{2} \frac{F_c^2}{l_m} + \frac{k_{dlm} k_{plm}}{2 l_m k_{dlm} k_{plm}} = \frac{4F_c^2 (k_{dlm} + k_{plm}) + c_M k_{dlm} k_{plm} \|\mathbf{a}\|^2}{2 l_m k_{dlm} k_{plm}}. \qquad (81)$$

One can set the parameter ε_3 to a small value, if parameters ε, and η are small. Assuming that:

$$k_{plm} = k,$$

$$k_{dlm} = \sigma k \tag{82}$$

the parameter ε_3 can be written in the following form:

$$\varepsilon_3 = \frac{4F^2 \cdot (1 + \eta) \cdot \sigma^2 k \, \|\mathbf{a}\|^2}{cM_{lm} \, \sigma \, lM_{mk} \, l} \tag{83}$$

.

where σ is a positive constant. As a consequence $V(t)$ and $\dot{V}(t)$ satisfy Theorem 1 under the following definitions:

$$\lambda_{max}(\mathbf{Q}_2) \geq \frac{\lambda_{min}(\mathbf{Q})}{2} \geq \frac{1}{k}\sqrt{\frac{\lambda_{min}(\mathbf{Q})}{m\, c}} \tag{84}$$

and radii

$$r_1 = \sqrt{\frac{2\,(16F_{cM}^2\,(1+\sigma)\,\lambda_{max}(I_M) + k\,\|\mathbf{a}\|^2)}{\lambda_{min}^2(I_M)\,\sigma k b \Gamma_{lm}}},$$

$$r_2 = \sqrt{\frac{2\sigma_1(16F_{cM}^2\Gamma_{lm}(1+\sigma)+\eta\sigma\Gamma_{lm}k_{1M}^2\|\mathbf{a}\|)^2}{\sigma\Gamma_{lm}^2 k}}. \tag{85}$$

Based on Theorem 1 $\mathbf{z}$ and $\mathbf{a}$ are uniformly bounded $\mathbf{q}_l$, $\dot{\mathbf{q}}_l$ (which implies that $\tilde{\mathbf{v}}$ and $\dot{\tilde{\mathbf{v}}}$ are uniformly bounded too) and converge exponentially to the closed balls B_{r_1}, B_{r_2}, respectively. The radius of the balls can be decreased by increasing coefficient k or increasing the parameter Γ_{lm}.

The adaptive version of the control algorithms for the system, given by Eqs. (13) and (14) is the same, assuming that Eq. (42) is written in the following form:

$$\mathbf{D}\ddot{\mathbf{q}} + [\mathbf{C} + \mathbf{C}']\dot{\mathbf{q}} + \mathbf{Y}(\mathbf{q}, \dot{\mathbf{q}}, \dot{\mathbf{q}}_{md}, \ddot{\mathbf{q}}_{md})\mathbf{a} + \mathbf{K}\tilde{\mathbf{q}} = 0 \tag{86}$$

$$\dot{\mathbf{q}} = \begin{bmatrix} \mathbf{d} & \mathbf{I} \\ A\mathbf{v} & B\mathbf{q} \end{bmatrix} \begin{bmatrix} \mathbf{q} - \mathbf{q}_{md} \\ \dot{\mathbf{q}} - \dot{\mathbf{q}}_{md} \end{bmatrix} + \begin{bmatrix} \mathbf{p} \\ \mathbf{d} \end{bmatrix} \tag{87}$$

where $\boldsymbol{D} = blockdiag[\mathbf{M}, \mathbf{J}]$, $\tilde{\mathbf{q}} = [\tilde{\mathbf{q}}^T, \tilde{\mathbf{q}}^T]^T$, $\tilde{\mathbf{v}} = [\tilde{\mathbf{v}}^T, \tilde{\mathbf{v}}^T]^T$, $\boldsymbol{K} = blockdiag[\mathbf{K}, \mathbf{K}]$,

$$\boldsymbol{l} \quad \boldsymbol{d} \quad \boldsymbol{l}_m \quad \boldsymbol{l} \quad \boldsymbol{m} \quad \boldsymbol{d} \quad dl \quad dm$$

and $\boldsymbol{C} = blockdiag\{\mathbf{B}, \mathbf{B}\} = \begin{bmatrix} \mathbf{C}(\boldsymbol{q_l}) & \mathbf{0} \\ \mathbf{0} & \boldsymbol{C_d} \end{bmatrix}$, $\boldsymbol{q} = \begin{bmatrix} \boldsymbol{q_l} \\ \boldsymbol{q_{ld}} \end{bmatrix}$,

$$1 \quad 2 \quad 1 \quad \mathbf{0} \quad \mathbf{0} \quad \boldsymbol{d} \quad \mathbf{0} \quad \mathbf{0}$$

$$\boldsymbol{K} = \begin{bmatrix} \mathbf{K}_{pl} & \mathbf{K} \\ \mathbf{K} & \end{bmatrix}, \quad \mathbf{Y} = \begin{bmatrix} \mathbf{Y}_l(\mathbf{q}_l, \mathbf{q}_{ld}, \mathbf{q}_{ld}) & \mathbf{0} \end{bmatrix}$$

$$\boldsymbol{p} \quad \begin{bmatrix} \mathbf{K} \\ \mathbf{K} \end{bmatrix} \quad \mathbf{K} \quad \begin{bmatrix} \mathbf{0} \\ \end{bmatrix} \quad \mathbf{Y} \quad (\mathbf{q}_{md}, \mathbf{q}_{md})$$

$$pm \quad 1 \quad m$$

where $\mathbf{Y}_l$ and $\mathbf{Y}_m$ are appropriate matrices associated with the links and motors, respectively.

Now, consider the Lyapunov function candidate

$$\boldsymbol{V}(t) = \frac{1}{2}\mathbf{q}^T\boldsymbol{D}\mathbf{q} + \frac{1}{2}\mathbf{q}^T\boldsymbol{K}_p\mathbf{q} + \frac{1}{2}\mathbf{v}^T\boldsymbol{K}\boldsymbol{B}^{-1}\mathbf{v} \qquad (88)$$

$$\mathbf{q}^T\boldsymbol{D}\mathbf{q} \quad \mathbf{v}^T\boldsymbol{D}\mathbf{q} \quad \frac{1}{2}\mathbf{a}^T\boldsymbol{\Gamma}\mathbf{a}$$

$$2 \quad 2 \quad p \quad 2 \quad d \quad 2$$

and note that (86) is similar to (42), as well as (88) is similar to (44). The main difference is that $\boldsymbol{K_p}$ is no longer diagonal but is positive–definite if $\mathbf{K}_{pl}$ and $\mathbf{K}_{pm}$ are positive–definite. Note also that the adaptation law for the motor parameters has the following form

$$\dot{\tilde{\mathbf{a}}} = -\boldsymbol{\Gamma}^{-1}\mathbf{Y}^T(\tilde{\mathbf{v}} + \tilde{\mathbf{q}}) \qquad (89)$$

$$m \quad m \quad m \quad m \quad m \quad m$$

where $\boldsymbol{\Gamma}_m$ is a positive–definite matrix.

Example—The Control System With A Signal Processor For A Manipulator With Two Degrees Of Freedom

The Control Scheme Of A Manipulator With Two Degrees

The experimental set-up (Fig. 3) was designed based on a manipulator with two links with a different cross-section and stiffness. It is a SCARA manipulator. The links of the manipulator were made of an alloy of light metals. Each link has a cross-section of a rectangular shape. The manipulator consists of

- two DC motors (PRM 76-05TR) with the following parameters: nominal torque:
  0.55 Nm, maximum torque: 2.6 Nm, maximum speed: 4000 rpm, maximum current: 19A, maximum voltage: 60V,
- two harmonic-drives (HDU C2) with the gear ratio 1:158,
- belt transmission with a gear ratio 1:1,
- encoders MOZ 30/500/5/K with a resolution 500 counts per revolution and voltage supply +5V,
- two tachometric generators with a constant voltage 3.3V/1000 revolutions,
- accelerometers,
- safety cut-off switch (TCST 2000).

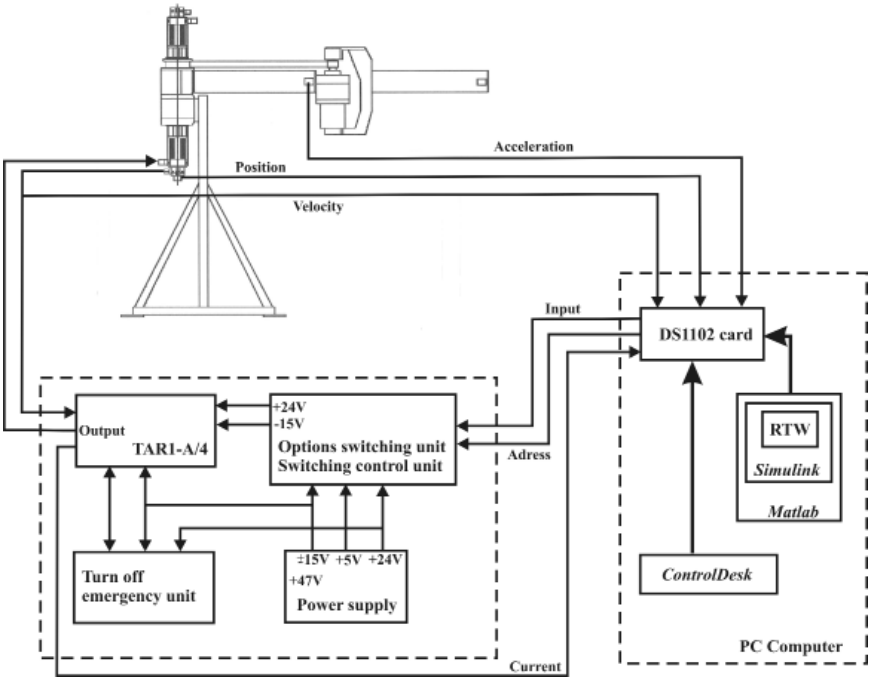


Figure 3. An experimental set-up.

The control system consists of the following elements:

- **Control unit TAR 1-A/4**. This is a power module which operates DC motor directly. The system TAR1-A/4 is a solid-state speed controller of DC motors with a maximum voltage of 50V and a maximum current of 15A. This module was used in control systems of the IRp6 robots. This control unit can be divided into the following functional blocks:
  - motor speed controller implemented in three operational amplifiers: the first amplifier protects the motor against the influence of the voltage drop at engine speed, the second amplifier compares the voltage proportional to motor speed with a predetermined voltage (speed setpoint), the third realizes a PI controller,
  - motor current PI controller, output signal from this controllers controls the modulator,
  - the tringular voltage generator—output signal is a tringular waveform voltage with a frequency of 4kHz,
  - modulator—converts the voltage signal from output of the current controller to pulse with adjustable filling,
  - class-D amplifier—amplifies the output pulses from the current controller to control the power transistors,
  - solid-state power amplifier—circuit of H-bridge,
  - overcurrent protection—motor overload protection.
- **Options switching unit**. This module was built in order to reconfigure the control unit. It allows performing the following functions:
  - unblocking the controller,
  - changing the voltage polarization,
  - switching the desired signal to the different loops of the controller, namely:
    - to the velocity controller loop,
    - to the current controller loop,
    - to the power amplifier loop.
- **A microprocessor controller unit**. This unit protects the

switching module from incorrect configuration set by the operator, and sets up control signals necessary to perform non-failure operation of the unit described in the previous point. The controller consists of the following blocks:

- block of manual dialing,
- block select options using a PC,
- executive module,
- blockade.

- **Supply system**, which consists of a power supply of control units and power supply. The power supply delivers unstabilized voltage (50V) to the TAR1-A/4 unit.
- **DS1102 signal processor card (dSPACE Company)**, it is the most important element of the control system. This card has been built on the basis of TMS320C31 digital signal processor from Texas Instruments. It is equipped with:

  - four analog-to-digital converters (ADC)—transducers which have a resolution of 12-bits and 16-bits,
  - four 16-bit digital-to-analog converters (DAC),
  - 16-bit input-output system,
  - two interfaces of rotary encoders.
- **Turn off emergency unit**, which protects the manipulator against unspecified behavior. When the manipulator reaches the end position or the user presses the RESET button then be shut off motor voltage.
- **Measurement module**. This unit consists of the following elements: rate generators, encoders and accelerometers. Accelerometers (mounted at the end of each link) are connected to DSP card directly. The converter does not work in RS422 standard but in TTL standard open collector therefore an appropriate interface for the encoders was designed.

Implementation of the proposed control algorithms (which are presented in Section Mathematical Description of an Adaptive Tracking Controller) are described using fast prototyping methodology. The algorithms were implemented with the help of MATLAB environment with SIMULINK. To use the program implemented in SIMULINK to control the device using the DSP card, the MATLAB RTI toolbox (Real Time Interface) was employed. The RTI toolbox enables the use of SIMULINK blocks that represent the DS1102 card. The implemented algorithm uses the following blocks of the RTI toolbox (Fig. 7):

- DS1102DAC—digital-to-analog converters,
- DS1102ENC_POS—a block for cooperation with encoders which enable the measurement position relative to the zero position,
- DS1102IN – represents a 16-bit input DSP card.

Initially, simulation results were carried out, which initially verified the proposed control algorithm (Fig. 4).

First, model of the manipulator with two links (in Fig. 4 the block titled Object) was implemented in SIMULINK and

subdivided into two subsystems:

- linear part of the system,
- non-linear part of the system added as feedback to the linear subsystem.

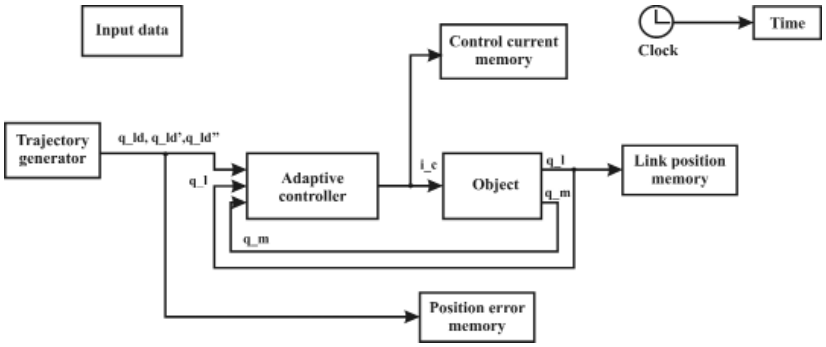


Figure 4. Scheme of adaptive control algorithm for simulation research.

The linear elements were described by the transfer function $G_l(s)$, with input signal as torque, and output signal as link position. The transfer function for the link is described by the following equations:

- first link

$$G_{l1}(s) = \frac{Q_{l1}(s)}{U_{1}(s)} = \frac{1}{I_1 s^2 + F_{d1} s + K_1}, \quad (90)$$

$$I_1 = m_1 d_1^2 + m_2 d_1^2 + m_2 l_1^2 + I_{m1}$$

- second link

$$G_{l2}(s) = \frac{Q_{l2}(s)}{U_{2}(s)} = \frac{1}{I_2 s^2 + F_{d2} s + K_2}, \quad (91)$$

$$I_2 = m_2 d_2^2 + I_{m2}$$

where K_1, K_2 are stiffness coefficients for the first and second link, respectively.

The transfer function of the motor has the following form (where input signal is the current i, and output signal is the motor position q_m):

$$G_{mj}(s) = \frac{Q_{mj}(s)}{I_{mj}(s)} = \frac{k_{mj}}{J_{mj} s + F_{mdj}}, \quad (92)$$

where $j = 1,2$.

Expressions $P_1,..., P_7$ describe nonlinear elements in the following form:

- inertia of the first link

$$P_1 = -2 d_1 d_2 m_2 \cos(q_{l2}) \ddot{q}_{l1} - d_2^2 m_2 \ddot{q}_{l2} - d_1 d_2 m_2 \cos(q_{l2}) \dot{q}_{l2}^2, \quad (93)$$

- inertia of the second link

$$P_2 = -d_2^2 m_2 \ddot{q}_{l1} - d_1 d_2 m_2 \cos(q_{l2}) \dot{q}_{l1}^2$$

$$d_1 d_2 m_2 \cos(q_1 - q_2)\ddot{q}_1, \qquad (94)$$

- centripetal and Coriolis terms of the first link

$$P_3 = m_2 d_1 d_2 \sin(q_1 - q_2)\dot{q}_2^2 - 2m_2 d_1 d_2 \sin(q_1 - q_2)\dot{q}_1\dot{q}_2, \qquad (95)$$

- centripetal and Coriolis terms of the second link

$$P_4 = -m_2 d_1 d_2 \sin(q_1 - q_2)\dot{q}_1^2, \qquad (96)$$

- static friction term of the first and second link, respectively

$$P_5 = F_{sj}\,\mathrm{sgn}(\dot{q}_j), \quad j = 1, 2, \qquad (97)$$

- static friction term of the first and second motor, respectively

$$P_6 = \frac{F_{sj}\,\mathrm{sgn}(\dot{q}_j)}{k_{mj}}, \quad j = 1, 2, \qquad (98)$$

- gear and stiffness terms of the first and second link, respectively

$$P_7 = \frac{K_j}{k_{mj} N_j} q_j \quad j = 1, 2. \tag{99}$$

The implementation scheme of the manipulator with two links is shown in Fig. 5 The first and second links are implemented similarly (compare Fig. 6).

Next the adaptive control algorithm for the manipulator with two degrees of freedom was implemented. The following block diagram of control scheme for a manipulator with joint flexibility is proposed, see Fig. 8.

Next, this simulation program was transformed into a program to control of the real manipulator. For this purpose, the RTW toolbox (Real Time Workshop) and RTI toolbox were used. In the implemented control algorithm (Fig. 4), a block representing the mathematical description of the manipulator (object model) was replaced by the respective blocks of the DSP card. These blocks allow cooperation of this program with the real device. In place of the block **Object** (Fig. 4) a block of digital-to-analog converters (block DS1102DAC which allows controlling motors) were introduced and a block for cooperation with encoders (block DS1102ENC_POS which enables measuring the position of the manipulator links). Figure 7 shows a block diagram of an adaptive control algorithm of the manipulator implemented in SIMULINK.

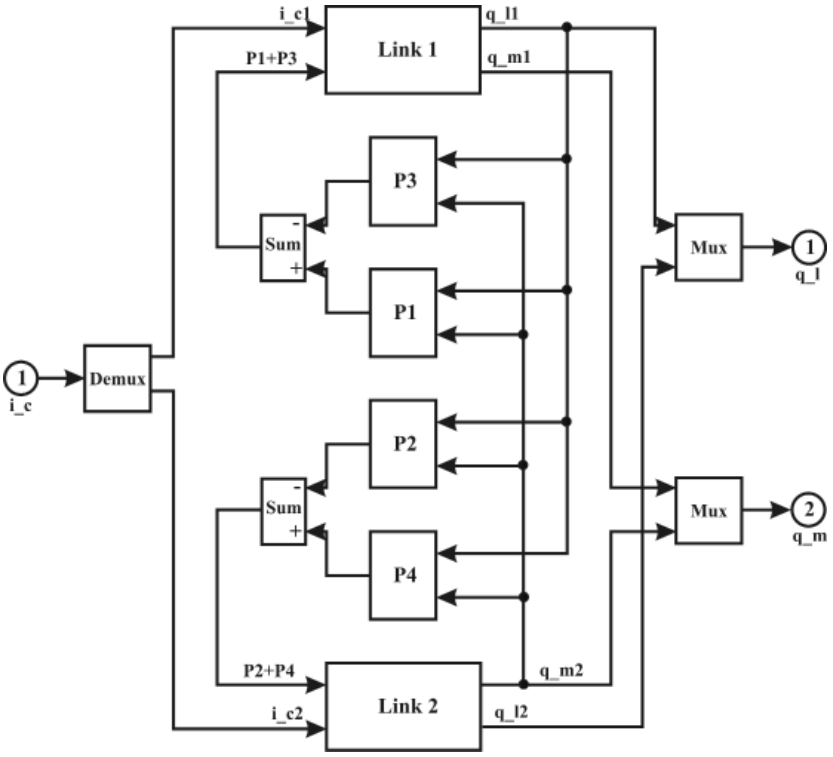


Figure 5. SIMULINK implementation of a two degrees of freedom manipulator with elastic joints (P1—Inertia of the link 1, P2—Inertia of the link 2, P3—Centripetal and Coriolis terms for link 1, P4—Centripetal and Coriolis terms for link 2).

The block named **Adaptive controller** includes implementation of the control algorithm which was described in Section Mathematical Description of an Adaptive Tracking Controller (Fig. 8). This block consists of the following elements:

- **Motor position controller—**estimates of link parameters: inertia, static and viscous friction are calculated.
- **Link position controller—**estimates of motor parameters are calculated.
- **Gear estimate**,
- **Stiffness estimate**,
- **Link (motor) position filter—**block performing differentiation operation on link (motor) error position.

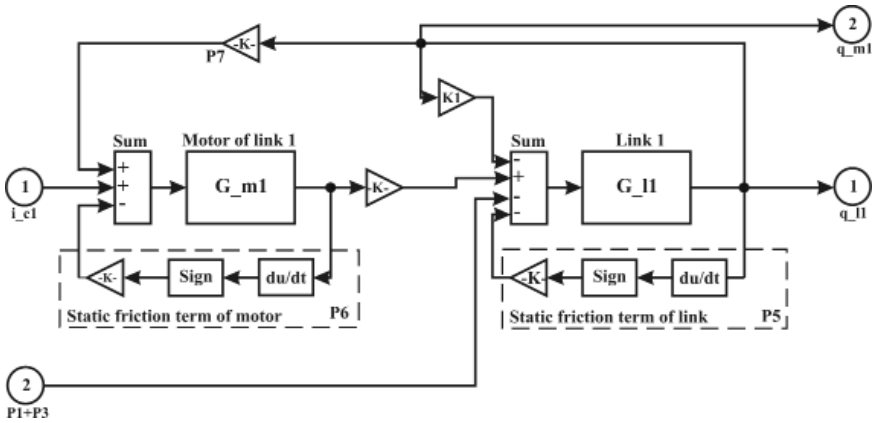


Figure 6. A block diagram for link 1 (P5—Static friction term of link 1, P6—Static friction term of motor 1, P7—Gear and stiffness term).

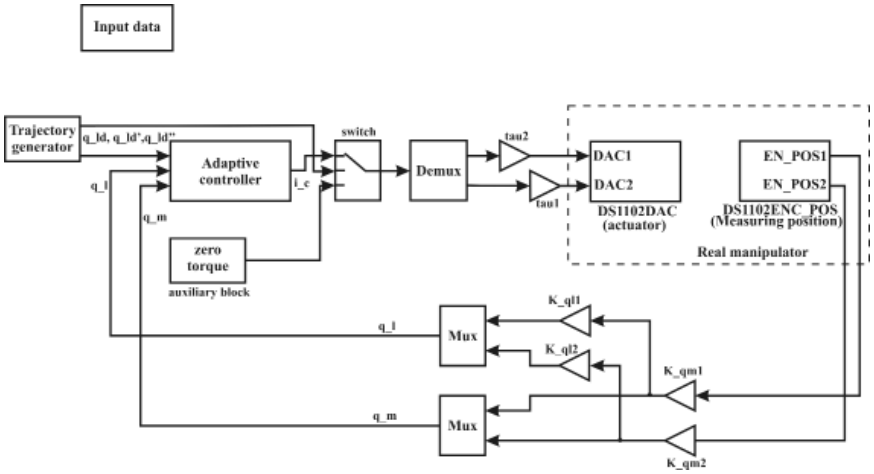


Figure 7. Scheme of the adaptive control algorithm for the real manipulator (tau1, tau2 adjust the control signals to the ranges of analog-to-digital converters, K_qm1, K_qm2—converting signals from the encoders to position signal in radians).

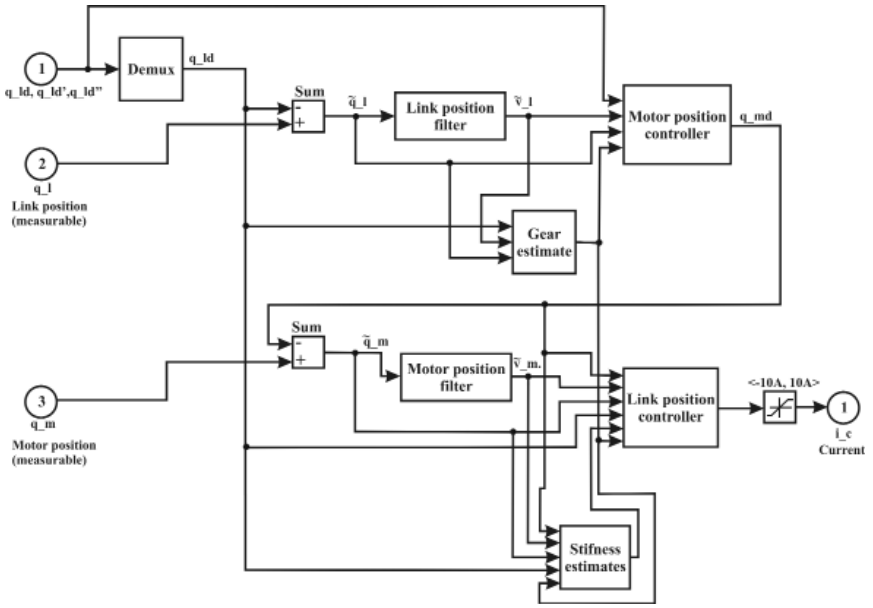


Figure 8. SIMULINK implementation of adaptive control algorithm.

The parameter estimates were calculated on the basis of the equation:

$$\hat{\mathbf{a}}_{m,l} = \Gamma_{m,l}^{-1} Y_{m,l}^{T}(\mathbf{v}_{m,l}, \mathbf{q}_{m,l}). \quad (100)$$

In Fig. 9, a block diagram of a trajectory generator is presented, which allows setting two trajectories. The reference trajectory is a trajectory of the sine at a set amplitude and frequency, and zero trajectory, which keeps the manipulator in the position in which the internal coordinates are equal to zero. Choosing the type of trajectory is done with the START button, which is connected to the input of the DSP card. DS1102IN_C16 block represents a 16 bit of input of the DSP card, which is connected to the START button.

The implemented program was compiled using an RTI package and as a result of this action, C program and its object code were obtained. The object code was automatically loaded into memory of the DSP card and executed. In order

to register date from experiments, Control Desk program (dSPACE Company) was used.

Experimental Results

The new adaptive control algorithm was tested carrying out simulations and experiments on a manipulator with two degrees of freedom. For the sake of simulation its mathematical model was implemented in SIMULINK. The desired trajectory was sinusoidal with amplitude $A_1 = \pi/4$, $A_2 = -\pi/4$ with full cycle during $T_1 = T_2 = 16s$. The following values of the parameters of manipulator were identified:

- links masses: $m_1 = m_2 = 3\,kg$,
- SEM: $k_{m1} = k_{m2} = 0.128 \quad \frac{Nm}{A}$,

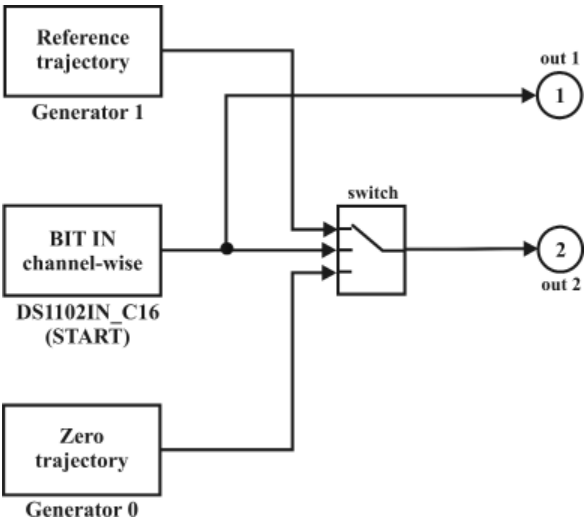


Figure 9. Scheme of a trajectory generator.

- joint stiffness: $K_1 = K_2 = 4000 \frac{Nm}{rad}$,
- motor inertias: $J_{m1} = J_{m2} = 6e-6\, kgm^2$,
- link inertias: $I_1 = I_2 = 0.27\, kgm^2$,
- distance of the load from the axis of rotation: $l_{c1} = l_{c2} = 0.31\, m$.

It was assumed that the purpose of control is achieved when the tracking trajectory error is smaller than 1%. On the basis of wide examinations carried out the following parameters of adaptive controllers were selected (the units are in SI and are omitted):

- PD controller

$$K_{pl1} = K_{dl1} = K_{pl2} = 0.75,\quad 0.75,\quad 0.2,$$
$$K_{dl2} = K_{pm1} = K_{dm1} = 0.2,\quad 0.75,\quad 0.2,$$
$$K_{pm2} = K_{dm2} = 0.2,\quad 0.2. \qquad (101)$$

- Filter parameters

$$a_{l1} = a_{m1} = 35, \quad a_{l2} = a_{m2} = 25, \quad b_{l1} = b_{m1} = 4, \quad b_{l2} = b_{m2} = 5, \tag{102}$$

- Initial value of the estimates

$$\hat{M}_{1a}(0) = 0.0045, \quad \hat{M}_{2a}(0) = 0.005, \quad \hat{M}_{1b}(0) = 0.0051, \quad \hat{M}_{2b}(0) = 0.005, \quad \hat{M}_{1c}(0) = 0.0046, \quad \hat{M}_{2c}(0) = 0.005, \quad \hat{M}_{1d}(0) = 0.0048, \quad \hat{C}_2(0) = 0.001, \tag{103}$$

$\hat{C}_{1a}(0) = 0.001, \hat{F}_{ld2}(0) = 6.3e\square$
$\hat{C}_{1b}(0) = 0.001, \hat{F}_{ls2}(0) = 3.3e\square$
$\hat{I}_{d1}(0) = 6.3e\square 3, \hat{J}_{m2}(0) = 6.4e\square$

$\hat{I}_{s1}(0) = 3.3e\square 2, \hat{I}_{mg2}(0) = 3.9e\square$

$\hat{J}_{m1}(0) = 6.4e\square 5, \hat{K}_2(0) = 3.1e\square$
$\hat{F}_{md1}(0) = 3.9e\square 3, \hat{K}_2(0) = 105,$
$\hat{F}_{ms1}(0) = 3.1e\square 2, \hat{N}_2(0) = 100,$
$\hat{K}_1(0) = 105, \quad \hat{N}_1(0) = 100.$

- Adaptive gain coefficient

$\square_{I1} = 0.5$
$\square_{I2} = 0.5$
$\square_{M1a} = 100,$
$\square_{M1b} = 6,$
$\square_{M1c} = 300,$
$\square_{M1d} = 400,$
$\square_{C1a} = 500,$
$\square_{C1b} = 100,$
$\square_{Fld1} = 500,$
$\square_{Fls1} = 1e4,$
$\square_{Jm1} = 5e8,$
$\square_{Fmd1} = 1e6,$
$\square_{Fms1} = 2e6,$
$\square_{I1} = 60,$

$\square_{m1} = 0.5$
$\square_{m2} = 0.5$
$\square_{M2a} = 50,$
$\square_{M2b} = 50,$
$\square_{M2c} = 50,$
$\square_{C2} = 100,$
$\square_{Fld2} = 5e6,$
$\square_{Fls2} = 1e2,$
$\square_{Jm2} = 3.5e7,$
$\square_{Fmd2} = 1.5e6,$
$\square_{Fms2} = 2e6,$
$\square_{K2} = 0.01,$

$\square_{I2} = 60,$

(104)

$\Gamma_{m1} = 800, \quad \Gamma_{m2} = 100,$

The experiment consists of tracking the desired link and motor trajectories. The large parameter values of $\Gamma_{Fls1}, \Gamma_{Fmd1}, \Gamma_{Fms1}, \Gamma_{Fld2}, \Gamma_{Fls2}, \Gamma_{Fmd2}, \Gamma_{Fms2}, \Gamma_{Jm1}, \Gamma_{Jm2}$ are questionable but they result from many experiments carried out and from the fact that the initial estimates of friction and moment of inertia were very small (Eq. (103)).

The stability analysis carried out in Section The Stability Properties of The Adaptive Tracking Controller, shows that $\tilde{\mathbf{q}}, \dot{\tilde{\mathbf{q}}}, \ddot{\tilde{\mathbf{q}}}, \tilde{\mathbf{v}}, \dot{\tilde{\mathbf{v}}}$ and $\tilde{\mathbf{a}}$ are uniformly bounded and converge exponentially to the closed balls B_{r1}, B_{r2}, respectively. The radii of these balls depend on gains of the PD controller $\mathbf{K_1}, \mathbf{K_m}$ and eigenvalues of matrices $\mathbf{F_C}, \mathbf{Q}, \boldsymbol{\Gamma}_1, \boldsymbol{\Gamma}_m$. When gains of the PD controller $\mathbf{K_1}, \mathbf{K_m}$ or parameters Γ_{lm}, Γ_{mm} are increased, the radii of the balls will decrease.

In the program ControlDesk one can observe changes of the generalized positions and output signals. In Figs. 10, 11, 12, experimental results are presented. Control of the manipulator went smoothly with soft undulation, which results from mechanism flexibility. The robot obtained the desired position in the defined time (3 sec) without

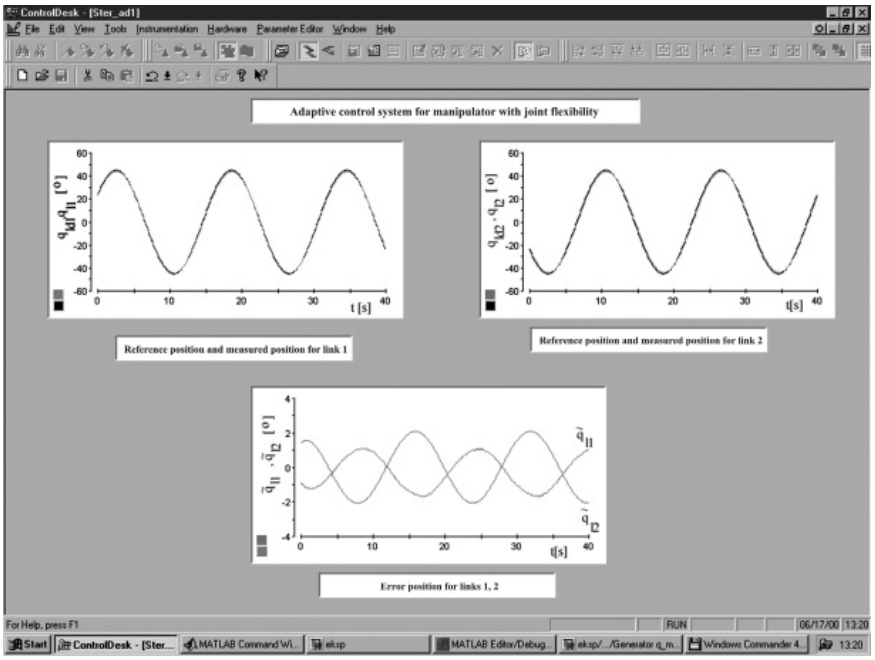


Figure 10. Position links and error link position for k_{pl1} = 0.75, k_{pm1} = 0.75, k_{pl2} = 0.2, k_{pm2} = 0.2.

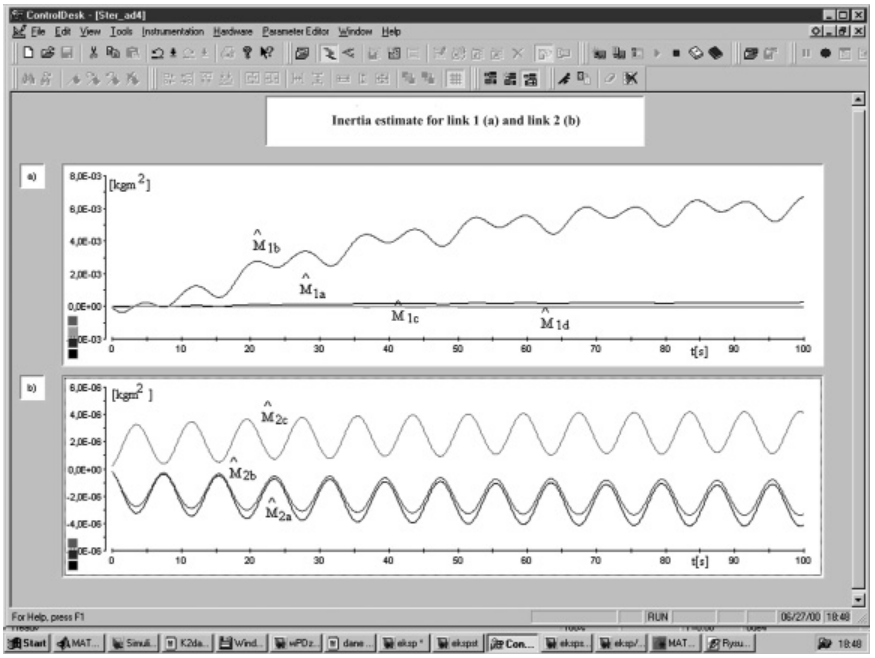


Figure 11. Inertia estimates for k_{pl1} = 1.1, k_{pm1} = 0.9, k_{pl2} = 1.1, k_{pm2} = 0.95.

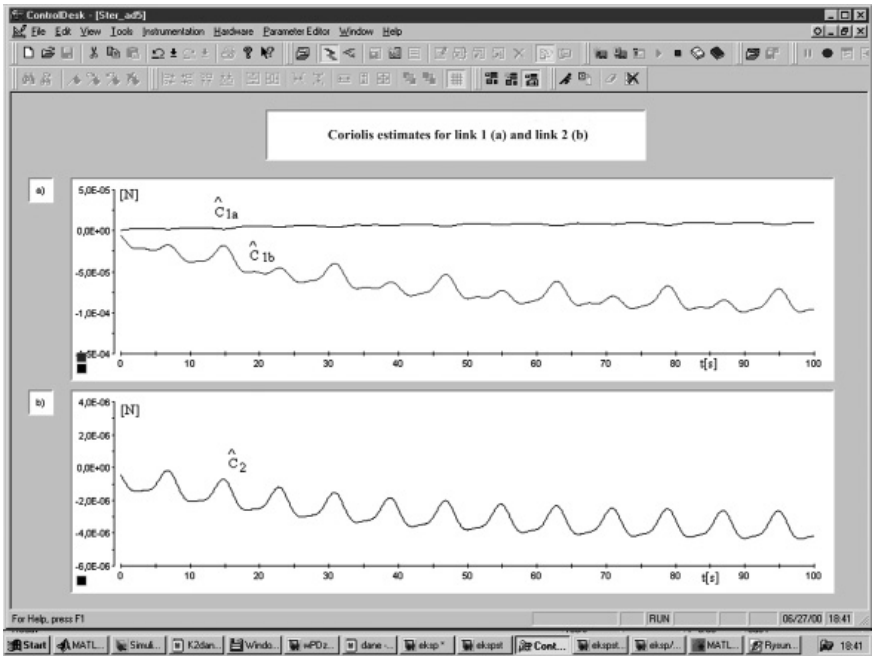


Figure 12. Coriolis estimates for $k_{p/1} = 0.75$, $k_{pm1} = 0.75$, $k_{p/2} = 0.2$, $k_{pm2} = 0.2$.

jerks. Peaks occurring in initial response resulted from static friction. In experiments we obtained error tracking trajectory in the steady state for the first link was about 0.5% and for the second link 0.2% (compare Fig. 10). Inertia estimates for two links are presented in Fig. 11. Coriolis estimates for two links are presented in Fig. 12. The trajectory tracking of the second link progressed almost perfectly. The current is not smooth and many peaks appear due to static friction.

CONCLUDING REMARKS

In this chapter two basic control problems, namely set point and trajectory following control, are discussed in application to rigid body manipulators with joint flexibility.

In the very beginning it is assumed that all kinematic and dynamic parameters of a simple one link robot with joint flexibility are known. It is a typical structure consisting of motor, gear box and torsional spring connected to one link robot. Set

point control is derived based on linearization of the system that is originated in differential geometry. Basic algorithm is borrowed from Isidori's book and it is shown that stabilization at an arbitrary point in the joint space according to his proposition does not work.

Next a more general structure of robot with joint flexibility is modelled assuming that not all dynamical parameters are known. The trajectory following algorithm was derived based on Lyapunov stability and discussed, thus it is the adaptive case. Both simulation and experimental results are presented. In all cases experiments are carried out on set-up built at the Chair of Control and Systems Engineering.

REFERENCES

Barany, E. and R. Colbaugh. 1998. Global stabilization of uncertain mechanical system with bounded controls. Proceedings of the American Control Conference. Philadelphia, Pensylvania, pp. 2212–2216.

Colbaugh, R., K. Glass and E. Barany. Adaptive output stabilization of manipulators. Proceedings of the 33rd Conference on Decision and Control, pp. 1296–1302.

Corless, M. 1989. Tracking controllers for uncertain systems: Application to a Manutec R3 robot. Journal of Dynamic Systems Measurement and Control, 111: 609–618.

Corless, M. 1990. Guarenteed rates of exponential convergence for uncertain systems. Journal of Optimization Theory and Applications, 64(3): 481–494.

De Luca, A. and P. Tomei. 1996. Elastic joints. pp. 179–218. *In*: C. C. de Wit, B. Siciliano and G. Bastin (eds.). Theory of Robot Control. Springer, London. Isidori, A.

1995. Nonlinear Control Systems, Springer Verlag.

Khorasani, K. 1992. Adaptive control of flexible-joint robots. IEEE Trans. on Robotics and Automation, 8(2): 250–267.

Kozłowski, K. and P. Sauer. 1998. On adaptive tracing control of rigid and flexible joint robots. Proceedings of the Fifth International Symposium on Methods and Models in Automation and Robotics, pp. 897–903.

Loria, A. and R. Ortega. 1995. On tracking control of rigid and flexible joint robots. Applied Mathematics and Computer Science, 5(2): 329–341.

Leitmann, G. 1981. On the efficacy of nonlinear control in uncertain linear systems. Journal of Dynamic Systems, Measurement and Control, 102: 95–102.

Madoński, R., M. Kordasz and P. Sauer. 2014. Application of a disturbance-rejection controller for robotic-enhanced limb rehabilitation trainings. ISA Transaction The Journal of Automation, 53: 899–908.

Nicosia, S. and P. Tomei. 1994. On the control of flexible joint robots by dynamic output feedback. Preprints of the Fourth IFAC Symposium on Robot Control, pp. 717–722.

Ott, Ch. 2008. Cartesian impedance control of redundant and flexible-joint robots. Springer Tracts in Advanced Robotics, Vol. 49, Springer-Verlag.

Readman, M. C. and P. R. Belanger. 1990. Analysis and control of a flexible joint robot. Proc., IEEE Conf. Decis. Contr. Honolulu. HI, USA, 4: 2551–2559.

Sauer, P. and K. Kozłowski. 2007. A new control algorithm for manipulators with joint flexibility, robot motion and control. Lecture Notes in Control and Information Sciences. Springer-Verlag London Limited 360: 119–136.

Slotine, J. and W. Li. 1991. Applied Nonlinear Control, Prentice Hall, Englewood Cliffs, NJ.

Spong, M. W. 1987. Modelling and control of elastic joint robots. Transactions of the ASME. Journal of Dynamic Systems, Measurement and Control, 109: 310–319.

Spong, M. W. 1989. Adaptive control of flexible-joint manipulators. Systems and Control Letters, 13: 15–21.

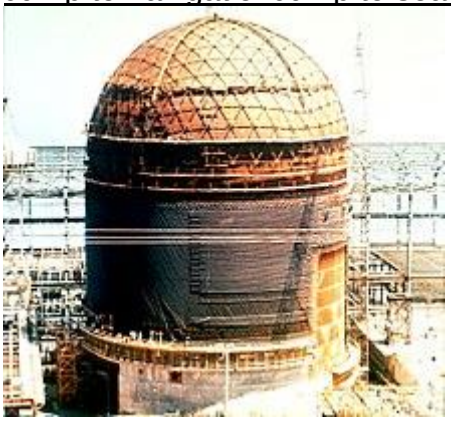
Spong, M. W. 1995. Adaptive control of flexible-joint manipulators: Comments on two papers. Automatica, 31(4): 585–590.

Tian, L. and A. A. Goldenberg. 1995. Robust adaptive control of flexible joint robots with joint torque feedback. Proceedings of the IEEE International Conference on Robotics and Automation, pp. 1229–1234.

3.Nuclear Decommissioning Applications

Nuclear decommissioning

From Wikipedia, the free encyclopedia
Jump to navigationJump to search



Example of decommissioning work underway.



The reactor pressure vessel being transported away from the site for burial.

Nuclear decommissioning is the process whereby a nuclear facility is dismantled to the point that it no longer requires measures for radiation protection. The presence of radioactive material necessitates processes that are potentially occupationally hazardous, expensive, time-intensive, and present environmental risks that must be addressed to ensure radioactive materials are either transported elsewhere for storage or stored on-site in a safe manner.[1] The challenge in nuclear decommissioning is not just technical, but also economical[2] and social.[3]

Decommissioning is an administrative and technical process. It includes clean-up of radioactive materials and progressive demolition of the facility. Once a facility is fully decommissioned, no radiological danger should persist. The costs of decommissioning are generally spread over the lifetime of a facility and saved in a decommissioning fund.[4] After a facility has been completely decommissioned, it is released from regulatory control and the plant licensee is no longer responsible for its nuclear safety. Decommissioning may proceed all the way to "greenfield" status.

Contents

- 1 Definition
- 2 Options
- 3 Legal aspects
- 4 Cost
  - 4.1 Decommissioning funds
- 5 International collaboration
- 6 Experience
  - 6.1 Ships, mobile reactors, military reactors
- 7 See also
- 8 References
- 9 External links

Definition

Nuclear decommissioning is the administrative and technical process whereby a nuclear facility such as a nuclear power plant (NPP), a research reactor, an isotope production plant, a particle accelerator, or uranium mine is dismantled to the point that it no longer requires measures for radiation protection. The progressive demolition of buildings and removal of radioactive material is potentially occupationally hazardous, expensive, time-intensive, and presents environmental risks that must be addressed to ensure radioactive materials are either transported elsewhere for storage or stored on-site in a safe manner.[1][*better source needed*] Decommissioning may proceed all the way to "greenfield status". Once a facility is decommissioned no radioactive danger persists and it can be released from regulatory control.[5]

Options

The International Atomic Energy Agency defines three options for decommissioning:

- *Immediate Dismantling* (Early Site Release/Decon in the United States) allows for the facility to be removed from regulatory control relatively soon after shutdown. Final dismantling or decontamination activities begin within a few months or years, and depending on the facility, it could take five years or more.[6] After being removed from regulatory control, the site becomes available for unrestricted use.[7]
- *Safe Enclosure* (or Safestor(e) Safstor) postpones the final decommissioning for a longer period, usually 40 to 60 years. The nuclear facility is placed into a safe storage configuration during this time.[8]
- *Entombment/Entomb* involves placing the facility in a condition that allows the remaining radioactive material to remain on-site indefinitely. The size of the area where the radioactive material is located is generally minimized and the facility is encased in a long-lived material such as concrete, with the aim of preventing a release of radioactive material.[9]

Legal aspects

The decommission of a nuclear reactor can only take place after the appropriate licence has been granted pursuant to the relevant legislation. As part of the licensing procedure, various documents, reports and expert opinions have to be written and delivered to the competent authority, e.g. safety report, technical documents and an environmental impact study (EIS).

In the European Union these documents are the basis for the environmental impact assessment (EIA) according to Council Directive 85/337/EEC. A precondition for granting such a licence is an opinion by the European Commission according to Article 37 of the Euratom Treaty. Article 37 obliges every Member

State of the European Union to communicate certain data relating to the release of radioactive substances to the Commission. This information must reveal whether and if so what radiological impacts decommissioning – planned disposal and accidental release – will have on the environment, i.e. water, soil or airspace, of the EU Member States.[10] On the basis of these general data, the Commission must be in a position to assess the exposure of reference groups of the population in the nearest neighbouring states.

Cost

This section **needs expansion**. You can help by adding to it. *(December 2017)*

This section **needs additional citations for verification**. Please help improve this article by adding citations to reliable sources. Unsourced material may be challenged and removed. *(December 2017) (Learn how and when to remove this template message)*

In the United States, the NRC recommends that the costs of decommissioning should be spread over the lifetime of a facility and saved in a decommissioning fund.[11] Repository delay seems to be effective in reducing NPP decommissioning costs.[12]

In France, decommissioning of Brennilis Nuclear Power Plant, a fairly small 70 MW power plant, already cost €480 million (20x the estimate costs) and is still pending after 20 years. Despite the huge investments in securing the dismantlement, radioactive elements such as plutonium, caesium-137 and cobalt-60 leaked out into the surrounding lake.[13][14]

In the UK, decommissioning of the Windscale Advanced gas cooled reactor (WAGR), a 32 MW prototype power plant, cost €117 million.[*citation needed*] A 2013 estimate by the United Kingdom's Nuclear Decommissioning Authority predicted costs of at least £100 billion to decommission the 19 existing United Kingdom nuclear sites.[15]

In Germany, decommissioning of Niederaichbach nuclear power plant, a 100 MW power plant, amounted to more than €143 million.[*citation needed*]

New methods for decommissioning have been developed in order to minimize the usual high decommissioning costs. One of these methods is in situ decommissioning (ISD), meaning that the reactor is entombed instead of dismantled. This method was implemented at the U.S. Department of Energy Savannah River Site in South Carolina for the closures of the P and R Reactors. With this tactic, the cost of decommissioning both reactors was $73 million. In comparison, the decommissioning of each reactor using traditional methods would have been an estimated $250 million. This results in a 71% decrease in cost by using ISD.[16]

In 2004, in a meeting in Vienna, the International Atomic Energy Agency estimated the total cost for the decommissioning of all nuclear facilities. Decommissioning of all nuclear power reactors in the world would require US$187 billion; US$71 billion for fuel cycle facilities; less than US$7 billion for all research reactors; and US$640 billion for dismantling all military reactors for the production of weapons-grade plutonium, research fuel facilities, nuclear reprocessing chemical separation facilities, etc. The total cost to decommission the nuclear fission industry in the World (from 2001 to 2050) was estimated at around US$1 trillion.[17]

Decommissioning funds

In Europe there is considerable concern over the funds necessary to finance final decommissioning. In many countries either the funds do not appear sufficient to cover decommissioning and in other countries decommissioning funds are used for other activities, putting decommissioning at risk, and distorting competition with parties who do not have such funds available.[18]

In 2016 the European Commission assessed that European Union's nuclear decommissioning liabilities were seriously underfunded by about 118 billion euros, with only 150 billion euros of earmarked assets to cover 268 billion euros of expected decommissioning costs covering both dismantling of nuclear plants and storage of radioactive parts and waste. France had the largest shortfall with only 23 billion euros of earmarked assets to cover 74 billion euros of expected costs.[19]

Similar concerns exist in the United States, where the U.S. Nuclear Regulatory Commission has located apparent decommissioning funding assurance shortfalls and requested 18 power plants to address that issue.[20] The decommissioning cost of Small modular reactors is expected to be twice as much respect to Large Reactors.[21]

International collaboration

Organizations that promote the international sharing of information, knowledge, and experiences related to nuclear decommissioning include the International Atomic Energy Agency, the Organization for Economic Co-operation and Development's Nuclear Energy Agency and the European Atomic Energy Community.[22] In addition, an online system called the Deactivation and Decommissioning Knowledge Management Information Tool was developed under the United States Department of Energy and made available to the international community to support the exchange of ideas and information. The goals of international collaboration in nuclear decommissioning are to reduce decommissioning costs and improve worker safety.[22]

Experience



The Pickering Nuclear Generating Station, viewed from the west. All eight reactors are visible; two units have been shut down.

A wide range of nuclear facilities have been decommissioned so far. The number of decommissioned nuclear reactors out of the List of nuclear reactors is small. As of 2016, 150 nuclear reactors were shut-off, in several early and intermediate stages (cold shut-down, defueling, SAFSTOR, internal demolition), but only 17 have been taken to fully "greenfield status".[23] Some of these sites still host spent nuclear fuel in the form of dry casks embedded in concrete filled steel drums.[24][25]

Several nuclear engineering and building demolition companies specialize in nuclear decommissioning, which has become a profitable business. More recently, construction and demolition companies in the UK have also begun to develop nuclear decommissioning services. Due to the radioactivity in the reactor structure (specially with high neutron-flux), decommissioning takes place in stages.[26] Plans for decommissioning reactors have a time frame of decades.[27] The long time frame makes reliable cost estimates difficult and cost overruns are common even for "quick" projects.[*citation needed*]

As of 2017, most nuclear plants operating in the United States were designed for a life of about 30–40 years[28] and are licensed to operate for 40 years by the US Nuclear Regulatory Commission.[29][30] The average age of these reactors is 32 years.[30] Many plants are coming to the end of their licensing period and if their licenses are not renewed, they must go through a decontamination and decommissioning process.[28][31][32]

decommissioning complete
decommissioning in progress
suffered partial or complete core meltdown

Dismantled or inactive civil nuclear reactors in the World[22][33][34]

Country	Location	Reactor type	Operative life	Decommissioning phase	Dismantling costs
Austria[35]	Zwentendorf	PWR 723 MWe	Never activated due to referendum in 1978[36]		
Belgium	SCK•CEN – BR3, located at Mol, Belgium	PWR (BR-3)	25 years (1962–1987)	Decon completed (2011)[37][38] European pilot project (underwater cutting and remote operated tools) [39][40]	
Bulgaria	Kozloduy Units 1, 2, 3, 4[41]	PWR VVER-440 (4 x 408 MWe)	Reactors 1,2 closed in 2003, reactors 3,4 closed in 2006	De-fuelling (Closing forced by European Union)	
Canada	Gentilly Unit 1 (Québec)	CANDU-BWR 250 MWe	180 days (between 1966 and 1973)	"Static state" since 1986[42][43][44]	stage two:[*clarification needed*] $25 million
Canada	Pickering NGS Units A2, A3 (Ontario)	CANDU-PWR 8 x 542 MWe	30 years (from 1974 to 2004)	Two units currently in "cold standby" Decommissioning to begin in 2020[45][46]	calculated:[*clarification needed*] $270–430/kWe[*citation needed*]
China[47]	Beijing (CIAE)	HWWR 10 MWe (multipurpose Heavy Water Experimental Reactor for the production of plutonium and tritium)	49 years (1958–2007)	SAFSTOR until 2027	proposed: $6 million for dismantling $5 million for fuel remotion
France[48]	Brennilis	HWGCR 70 MWe	12 years (1967–1979)	Phase 3 (fire during decommissioning in 2015) [49]	already spent €480 million (20 times the

					forecasted amount)[50][51]
France	Bugey Unit 1	UNGG Gas cooled, graphite moderator	1972–1994	postponed	
France	Chinon Units 1, 2, 3	Gas-graphite	(1973–1990)	postponed	
France	Chooz-A	PWR 300 MW	24 years (1967–1991)	Fully decommissioned – Greenfield[52][53][54] (Nuclear reactor was located inside a mountain cave)	
France	Saint-Laurent	Gas-graphite	1969–1992	Postponed	
France	Rapsodie at Cadarache	Experimental Fast breeder nuclear reactor (sodium-cooled) 40 MWe	15 years (1967–1983)	1983: Defuelling 1987: Remotion of neutron reflectors 1985–1989: Decontamination of sodium coolant Accident when cleaning residual sodium in vessel with ethyl carbitol (March 31° 1994)	The removed activity is estimated to around 4800 TBq. 600 TBq (^{60}Co) in 1990 still contained in 1ry vessel The dose burden from 1987 to 1994 was 224 mSv. RAPSODIE reached IAEA level 2 of decomm in 2005 STAGE 3 is planned in 2020[55]
France	Phénix at Marcoule	Experimental Fast breeder nuclear reactor (sodium-cooled) 233 MWe	36 years (1973–2009)[56]	1) Defuelled	estimated for the future: $4000/kWe[*citation needed*]
France	Superphénix at Creys-Malville	Fast breeder nuclear reactor (sodium-cooled)	11 years (1985–1996)[57]	1) Defuelled 2) Extraction of Sodium[58] Pipe cutting with a robot [59][60]	estimated for the future: $4000/kWe[*citation needed*]
East Germany	Greifswald Units 1, 2, 3, 4, 5, 6	VVER-440 5 x 408 MWe	Reactors 1–5 closed in 1989/1990, reactor 6: finished but never operated	Immediate dismantling (underwater cutting)	~ $330/kWe

East Germany	Rheinsberg Unit 1	VVER-210 70–80 MWe	24 years (1966–1990)	In dismantling since 1996 Safstor (underwater cutting)	~ $330/kWe
East Germany	Stendal Units 1, 2, 3, 4	VVER-1000 (4 x 1000 MWe)	Never activated (1st reactor 85% completed)	Not radioactive (Cooling towers demolished with explosives)	(Structure in exhibition inside an industrial park)
West Germany	Gundremmingen-A	BWR 250 MWe	11 years	Immediate dismantling pilot project (underwater cutting)	(~ $300–550/kWe)
India[61]	Rajasthan Atomic Power Station Unit 1 (Rajasthan)	PHWR 100 MWe (similar to CANDU)	44 years (1970–2014)		
Iraq	Osiraq/Tammuz Unit 1[62]	BWR 40 MWe Nuclear reactor with weapons-grade plutonium production capability	(Destroyed by Israeli Air Force in 1981)	Not radioactive: never supplied with uranium	
Italy[63]	Caorso	BWR 840 MWe[64][65]	3 years[*citation needed*] (1978 – Closed in 1987 after referendum in 1986)	SAFSTOR: 30 years (internal demolition)	€450 million (dismantling) + €300 million (fuel reprocessing)[66][67][68][69]
Italy	Garigliano (Caserta)	BWR 150 MWe[70]	Closed on March 1, 1982	SAFSTOR: 30 years (internal demolition)	
Italy	Latina (Foce Verde)	Magnox 210 MWe Gas-graphite[71]	24 years (1962 – Closed in 1986 after referendum)	SAFSTOR: 30 years (internal demolition)	
Italy	Trino Vercellese	PWR Westinghouse, 270 MWe[72]	(Closed in 1986 after referendum)	SAFSTOR: 30 years (internal demolition)	
Japan	Fukushima Dai-ichi Unit 1	BWR 439 MWe	November 17, 1970 - March 11, 2011	Since 2011 Tōhoku earthquake and tsunami of March 11 [73][74][75]	Estimated at ¥10 trillion (US$100 billion) for decontaminating Fukushima and dismantling all

				Hydrogen explosion (INES 7)[76][77]	reactors in Japan and considering long time damage to environment and economy, including agriculture, cattle breeding, fishery, water potabilization, tourism, lost of reputation in the world (without considering further health care spending and reduction of life expectancy).[78]
Japan	Fukushima Dai-ichi Unit 2	BWR 760 MWe	December 24, 1973 - March 11, 2011		
Japan	Fukushima Dai-ichi Unit 3	BWR 760 MWe	October 26, 1974 - March 11, 2011		
Japan	Fukushima Dai-ichi Unit 4	BWR 760 MWe	February 24, 1978 - March 11, 2011	Since March 11, 2011 Reactor defueled when tsunami hit Damage to spent fuel cooling-pool (INES 4)	
Japan	Fukushima Dai-ichi Unit 5	BWR 760 MWe	September 22, 1977 - March 11, 2011	Planned decommissioning Cold shutdown since March 11, 2011	
Japan	Fukushima Dai-ichi Unit 6	BWR 1067 MWe	May 4, 1979 - March 11, 2011	Planned decommissioning Cold shutdown since March 11, 2011	
Japan	Fukushima Daini Unit 1[79]	BWR 1067 MWe	July 31, 1981 - 11 March 2011	Planned decommissioning Cold shutdown since March 11, 2011 [80]	
Japan	Fugen [81]	Advanced thermal reactor (MOX fuel core, heavy water-BWR) 165 MWe	1979 – 2003	Cold shutdown [82] [83][84]	

Japan	Tokai Unit 1	Magnox (GCR) 160 MWe	1966 – 1998	Safstore: 10 years[85][86] then decon until 2018	¥93 billion[87] (€660 million of 2003)
North Korea	Yongbyon	Magnox-type (reactor for the production of nuclear weapons through PUREX treatment)	20 years (1985–2005) Deactivated after a treaty[88][89]	SAFSTOR: cooling tower dismantled	
Netherlands	Dodewaard	BWR Westinghouse 58 MWe[90]	28 years (1969–1997)	Defuelling completed SAFSTOR: 40 years	
Russia	Mayak[91] (Chelyabinsk-65)	PUREX plant for uranium enrichment	Several severe incidents (1946–1956)		
Russia	Seversk[92] (Tomsk-7)	Three plutonium reactors Plant for uranium enrichment	Two fast-breeder reactors closed (of three), after disarmaments agreements with USA in 2003.[93]		
Slovakia	Jaslovské Bohunice Units 1, 2[94][95]	VVER 440/230 2 X 440 MWe	(1978–2006) (1980–2008)		
Spain [96]	José Cabrera	PWR 1 x 160 MWe (Westinghouse)	38 years (1968-2006)	Defueled Dismantling [97] Objective: green field in 2018[98]	€217.8 million[99]
Spain	Santa María de Garoña (Burgos)	BWR/3 1 x 466 MWe (by Dutch RDM)	1966 - 2013 (possible restart, since reactor vessel is in good conditions)	Defueled Asked for renewal of license, until 2031 [100]	
Spain	Vandellós Unit 1	UNGG 480 MWe (gas-graphite)	18 years Incident: fire in a turbogenerator (1989)	SAFSTOR: 30 years (internal demolition)	Phases 1 and 2: €93 million

Sweden	Barsebäck Units 1, 2	BWR 2 x 615 MW	Reactor 1: 24 years 1975 – 1999 Reactor 2: 28 years 1977 – 2005	SAFSTOR: demolition will begin in 2020	The Swedish Radiation Safety Authority has assessed that the costs for decommissioning and final disposal for the Swedish nuclear power industry may be underestimated by SKB by at least 11 billion Swedish crowns ($1.63 billion)[101]
Switzerland[102]	DIORIT	MWe Gas-graphite (experimental)		SAFSTOR (internal demolition)	
Switzerland	LUCENS	8,3 MWe CO_2-heavy water (experimental)	(1962–1969) Incident: fire in 1969	Entombment for ? years SAFSTOR and Decon: 24 years (internal demolition)	
Switzerland	SAPHIR	0,01–0,1 MWe (Light water pool)	39 years (1955–1994) (Experimental demonstrator)	In public display since inauguration[*citation needed*]	
Ukraine	Chernobyl-4 (110 km from Kiev)	RBMK-1000 1000 MWe	hydrogen explosion, then graphite fire (1986) (INES 7)	ENTOMBMENT (armed concrete "sarcophagus")	Past: ? Future: riding sarcophagus in steel[103]
United Kingdom[104]	Berkeley	Magnox (2 x 138 MWe)	27 years (1962–1989)	SAFSTOR: 30 years (internal demolition)	around $2600/kWe
United Kingdom	Bradwell	Magnox 2 x 121 MWe	1962–2002	SAFSTOR: 30 years (internal demolition)	around $2600/kWe
United Kingdom	Dounreay (PFR was a pool-type fast breeder reactor, cooled by liquid sodium, fueled with MOX).	PFR 250 MWe.[105] (Research facility of UKAEA)	1974 – 1994 (with average 26.9% load)[106] Delays and reliability problems before reaching full power.[107]	Remotely operated robot 'Reactorsaurus' will be sent in to decontaminate equipment as too dangerous a task for a human.[108] Control panel has been earmarked for an exhibition at London Science Museum (2016). [109]	

United Kingdom	Sellafield-Calderhall	Magnox 4 x 60 MWe first nuclear power station.	August 27, 1956 – March 31, 2003 (World's first nuclear power station to generate electrical power on an industrial scale [110]) The first reactor had been in use for 47 years.[111]	SAFSTOR: 30 years (internal demolition).[112]	around $2600/kWe
United Kingdom	Chapelcross	Magnox 4 x 60 MWe ("sister reactor" to Calderhall)	1959 – 2004	SAFSTOR: 30 years (internal demolition)	around $2600/kWe
United Kingdom	Windscale Pile 1 Pile 2	Air-cooled, graphite-moderated reactor for weapons-grade plutonium	Windscale fire of October 1957 was the worst nuclear accident in Great Britain's history, ranked in severity at level 5 out of 7 on the International Nuclear Event Scale.[113] Giant towers reduced contamination[114]	In 1990, U.K. Atomic Energy Authority started plans to decommission, disassemble and clean up both piles. In 2004 Pile 1 contained about 15 tonnes (14.76 L/T) of uranium fuel, and final completion of the decommissioning is not expected until 2037.[115]	
United Kingdom	Winfrith-Dorset Research area of the UKAEA	SGHWR 100 MWe	Operated from 1958 to 1990.	All nine reactors mostly dismantled[116] [117][118]	
United States	Crystal River 3 (Florida)	PWR 860 MWe	33 years (1976–2009)[119] Plant scheduled to restart in April 2011, but the project encountered a	From 2015 to 2019 in defueling. expected SAFSTOR 2019–2067 Decommissioning Periods (Start – End); Duration (years)	~$1,2 billion[122]

				number of delays.[120] After repairs, additional delamination began to occur in adjacent bays. Duke Energy announced in Feb-2013 that the Crystal River NPP would be permanently shut down.[121]	Period 1: Planning and Preparations (Jun 2013 – Jul 2015) 2.08 y. P. 2a: Dormancy w/Wet Fuel Storage (Jul 2015 – Aug 2019) 4.12 y. 2b: Dormancy w/Dry Fuel Storage (Aug 2019 – Dec 2036) 17.39 y. 2c: Dormancy w/No Fuel Storage (Dec 2036 – May 2067) 30.39 y. P. 3a: Site Reactivation & D. Prep (May 2067 – Nov 2068) 1.50 y. P. 4a: Large Component Removal (Nov 2068 – May 2070) 1.45 y. 4b & 4c: Systems Removal & Building Remediation(2070–2072) 2 y. Period 4f: License Termination (May 2072 – Feb 2073) 0.75y. Period 5b: Site Restoration (Feb 2073 – Aug 2074) 1.50 y. [26]	
United States	Dresden Unit (Illinois)	1	BWR 207 MWe	18 years (1960–1978)	Defueled in safety in 1998 now in SAFSTOR[123] Fuel in on-site dry-casks.[124]	
United States	Fort St. Vrain GS (Colorado)		HTGR (helium-graphite) 380 MWe	12 years (1977–1989)	Immediate Decon	$195 million
United States	Rancho Seco NGS[125] (California)		PWR 913 MWe	12 years (Closed after a	SAFSTOR: 5–10 years	$538.1 million [127] ($200–500/kWe)[128]

			referendum in 1989)	completed in 2009 [126] Fuel in insite long-term dry-cask storage	
United States	Three Mile Island Unit 2 (Pennsylvania)	PWR 913 MWe	1978-1979 Core fusion incident	Post-Defuelling Phase 2 (1979)	$805 million (estimated)[129]
United States	Shippingport (Pennsylvania)	BWR 60 MWe	25 years (closed in 1989)	Decon completed dismantled in 5 years (first small experimental reactor)	$98.4 million[130]
United States	San Onofre NGS Unit 1 (California)	PWR 436 MWe[131] Westinghouse Electric Corporation	25 years (1967–1992)	Reactor dismantled and used as a storage site for spent fuel.[132]	
United States	San Onofre NGS Units 2, 3 (California)[133]	2 x PWR 1,075 MWe[131]	Unit 2: 1983 – 2013 Unit 3: 1984 – 2013 In 2011, Edison finished replacing the steam generators in both reactors with improved Mitsubishi ones, but the new design had several problems, cracked, causing leaks and vibrations.[134]	Permanent shutdown – DECON soon defueling[135]	2014 cost forecast: $3.926 billion[136] to $4.4 billion[137]
United States	Piqua NGS (Ohio)	OCM (Organically Cooled/Moderated) reactor 46 MWe[138]	2 years (closed in 1966)	ENTOMB (coolant design inadequate for neutron flux)	

United States	Trojan (Oregon)	PWR 1,180 MWe	16 years (Closed in 1993 because of nearby to seismic fault)	SAFSTOR (cooling tower demolished in 2006) [139]	
United States	Yankee Rowe (Massachusetts)	PWR 185 MW	31 years (1960–1991)	Decon completed – Demolished (greenfield open to visitors) [140]	$608 million with $8 million per year upkeep
United States	Maine Yankee	PWR 860 MWe	24 years (closed in 1996)	Decon completed – Demolished in 2004 (greenfield open to visitors) [141][142]	$635 million[143]
United States	Vermont Yankee	BWR 620 MWe (General Electric)	42 years (1972–2014)	Defueling (2015–2021)	~$1.24 billion
United States	Exelon – Zion Units 1, 2 (Illinois)	2 x PWR 1040 MWe (Westinghouse)	25 years (1973–1998)	SAFSTOR-EnergySolutions[*clarification needed*] (opening of the site to visitors for 2018) [144]	$900–1,100 million (2007 dollars)[145]
United States	Pacific Gas & Electric – Humboldt Bay Unit 3	BWR 63 MWe	13 years (1963–1976) (Shut down per seismic retrofit)	On July 2, 1976, Humboldt Bay Power Plant (HBPP) Unit 3 was shut down for annual refueling and to conduct seismic modifications. In 1983, updated economic analyses indicated that restarting Unit 3 would probably not be cost-effective, and in June 1983, PG&E announced its intention to decommission the unit. On July 16, 1985, the U.S. Nuclear Regulatory Commission (NRC) issued Amendment No. 19 to the HBPP Unit 3 Operating License to change	Unknown – Closure date: December 31, 2015[146]

				the status to possess-but-not-operate, and the plant was placed into a SAFSTOR status.	

Ships, mobile reactors, military reactors[edit]

Many warships and a few civil ships have used nuclear reactors for propulsion. Former Soviet and American warships have been taken out of service and their power plants removed or scuttled. Dismantling of Russian submarines and ships and American submarines and ships is ongoing. Marine power plants are generally smaller than land-based electrical generating stations.

The biggest American military nuclear facility for the production of weapons-grade plutonium was Hanford site (in the State of Washington), now defueled, but in a slow and problematic process of decontamination, decommissioning, and demolition. There is "the canyon" a giant structure for the chemical extraction of plutonium with the PUREX process. There are also many big containers and underground tanks with a solution of water, hydrocarbons and uranium-plutonium-neptunium-cesium-strontium (all highly radioactive). With all reactors now defueled, some were put in SAFSTOR (with their cooling towers demolished). Several reactors have been declared National Historic Landmarks.

See also



Wikimedia Commons has media related to ***Nuclear decommissioning***.

- Hanford Site
- Lists of nuclear disasters and radioactive incidents
- Nuclear Decommissioning Authority
- Ship-Submarine recycling program
- Nuclear entombment
- Marcoule (French nuclear site)
- D&D KM-IT (Deactivation and Decommissioning Knowledge Management Information Tool)

L No.1:LONG- MMLG OFB DWGSAND STEMS

It has been proposed that the dismantling of nuclear installations be delayed for periods ranging from several decades to about a hundred years. Thereupon, the radioactivity having largely died away, dismantling would be easier and the radiation exposure of the dismantling personnel would be less. The objective of this area is to determine the measures required for maintaining shut- down plants in a safe condition and to assess the radiological consequences of costs.

B. R **h performed under the previous programme (1979-**

19f) The research work has been focused on the

following main subjects:

inspection of selected nuclear power plants and examination of materials as they exist therein, in order to determine the mode and pace of degradation;

methodology studies of the measures necessary for maintaining plants in safe condition and for keeping the necessary ancillary equipment operable.

C. 1989-1993 Programme

Research in this area should be pursued with a constant moderate effort, enlarging the data base and exploiting the growing experience, in order to establish confidence in long-term forecasts. This involves in particular:

collection of additional experimental data, e.g. repetition of past examinations after a time interval of about five years, in order to determine the rate of degradation and derive or check forecasting rules;

comparison of confinement methods applied at specific shut-down nuclear installations in Member States;

- assessment of the merits of the Safe Storage option in the decommissioning of nuclear installations other than reactors.

D. Programme implementation

At thc end of 1990, one research contract relating to Area No. 1 was at the stage of negotiation.

- 1 -

2. AREA No. 2: **DECONTAMINATION FOR DECOMMISSIONING PURPOSES**

The objective of this research is to develop and assess techniques for decontaminating surfaces of components and structures of nuclear installations that are past use. The main purpose of decontamination would be reduction of the occupational radiation exposure during dismantling of the contaminated item and/or reduction of the volume of radioactive waste.

B. R h **performed under the previous** programmes (1979-1iXI8)

The following decontamination techniques have been developed and assessed: techniques using aggressive agents in liquid and gel-like form;

- electrochemical techniques using various electrolytes; hydromechanical techniques (high-pressure water lance, ultrasound); decontamination of concrete surfaces by flame jetting.

C. 1989-1993 Programme

Research in Area N° 2 should be pursued with a reduced effort focused on selected techniques. As a new subject, the use of liquid chemical agents carried by a large volume of air, in the form of foam or fog, should be developed with a view to decontaminating large-volume systems. Thermal techniques for removal of concrete surface layers should be investigated from a more general and fundamental view than in the past.

D. Programme implementation

At the end of 1990, three research contracts relating to Area No. 2 were at the stage.of execution and three contracts were at the stage ol‘ negotiation.

- 2-

II. **ON-LINE DECONTAMINATION** OF COMPLEX COMPONENTS FOR **UNRESTRICTED RELHASH. USING ULTRASONIC WAVES IN A FLOWING AGGRESSIVE CHEMICAL AGENT**

Contractor: ENEL, Milano
Contract No.: FI2D-0016
Work Period: July 1990 - June 1993
Prolect Manager: F BREGANI
Phone: 39/2/88 47 30 **46** **Fax: 39/2/88** 47 39 15 or 88 47 34 96

W **OBJECTIVE AND SCOPE**

Previous experiments made by ENEL on small valves, using aggressive chemicals, showed that zones with residual contamination remain inside the components.

The present work aims at solving this problem by enhancing the decontamination effectiveness with the action of focused ultrasonic waves. The main objective of the project is to set up and test in real conditions a new decontamination process based on the simultaneous use of ultrasonic waves and aggressive chemicals, with ultrasonic transducers applied outside the components.

This decontamination process, if its expected performances are confirmed, could become a useful tool in decommissioning activities. It should allow to increase the amount of decontaminable parts without having to spend many man-hours and man-rem (thus, without dismantling before decontamination).

The project is based on experimental investigations, mainly at laboratory scale but also in plant scale. It is the continuation of work performed by ENEL in the framework of previous EC programmes on decommissioning (contract DE-B-005, report EUR 9303; contract FI1D-0002, report EUR 12878).

B. WORK PROGRAMME

B.1. **Evaluation, selection and acquisition of special ultrasonic** transducers to be applied to complex components from outside.

B.2. Decontamination tests on specimens and componcnts in the DECO loop.

B.2.1. Preparation of the DECO loop for testing; selection and characterisation of test spccimcns and componcnts from Garigliano BWR.

B.2.2. Decontamination tests on contaminated spccimens.

B.2.3. Decontamination tests on valves: radioactivity measurements, decontamination factor evaluation and secondary waste assessment.

B.2.4. Data analysis.

BE. Decontamination and dismantling of a part of a real system of a nuclcar **power station**

B.3.1. Preparation of the system part to be decontaminated.

B.3.2. Initial radioactivity characterisation.

B.3.3. Process design and configuration.

B.3.4. Decontamination.

B.3.5. Dismantling and final radioactivity measurcments.

B.3.6. Evaluation of secondary wastes.

C. PROGRESS OF WORK AND OBTAINED RESULTS

Summary of main issues

The development of a new type of transducers which can be applied on the external surface of components of various geometry and thickness (e.g. valves, piping, fittings, etc.) has been started.

The type of transducers and wave generators to be used have been identified and their main design parameters have been defined. The executive design and the construction phases are in progress.

Progress and Results

1. Evaluation, selection and acquisition of special ultrasonic transducers (B.1.)

The ultrasonic transducers to be developed should basically meet these requirements:

- they should be applied on the external surfaces of components such piping of various diameters and thickness, fittings, valves etc.;
- they should be able to supply an high intensity ultrasound field inside the components above indicated; therefore the frequency and power of the ultrasound field should be varied as a function of the different operating parameters (e.g. component geometry and thickness).

Specifically for starting the present study, the following design parameters are considered:

- the transducers should be coupled to piping with a diameter ranging between 35 and 105 mm;
- the tubing thickness ranges between 5 to 20 mm;
- the power supply from the transducer inside the piping should be 300 W as a minimum and can be varied in a wide range;
- the ultrasound frequency should be between 20 to 40 kHz.

A market research, however, has evidenced that the transducers currently available do not meet contemporary all the requirements above indicated. As an example, high power commercial transducers are extensively used for metal surface working; however, in this application, the ultrasound transmission beyond the material surface is unimportant. Therefore key issues such as the determination of the characteristic resonance frequencies of the material in various working conditions are not commonly addressed.

Consequently the development of this new type of transducers requires a preliminary design study that has been committed to an ultrasonic laboratory which has developed a valuable experience in this field.

Specifically the design phase will address the following:

- simulation and design of the transducer and its coupler;
- simulation and design of the wave generator;
- coupling and calibration of the wave generator and the transducer.

The transducer will be of the Langevine type (e.g. precompressed) it basically consists (Fig. 1) of a piezoelectric ceramic material disc forced between two metallic blocks, it employs a conic wave guide to focus wave beam. The coupling to the piping surface will be made with an epossidic resin.

The optimum design configuration of the transducer will be defined by a computer study. Specifically the analysis of the equivalent loop of a piezoelectric transducer will be performed in order to define the working frequency which determines the highest coupling efficiency.

Similarly the design of the wave generator requires a computer modelling study (PS

pice programme). This program allows to evaluate the transducer impedance changes as a t'unction of the different operating conditions. Moreover it simulates a coupling transformer which minimizes the impedance changes.

As a basis for the computer study the electric loop of a generator able to supply 3500 W either at 23 or at 40 kHz will be used.

An example of the study performed is shown in Fig. 2 where the calculated voltages as a function of the resonance frequencies in various transducer points are plotted. It can be noted that the lower voltages, e.g. the maximum coupling efficiencies, are obtained at a frequency of 22 kHz approximately.

Based on the finding of the computer simulation, the prototype transducer and generator will be then designed and built.

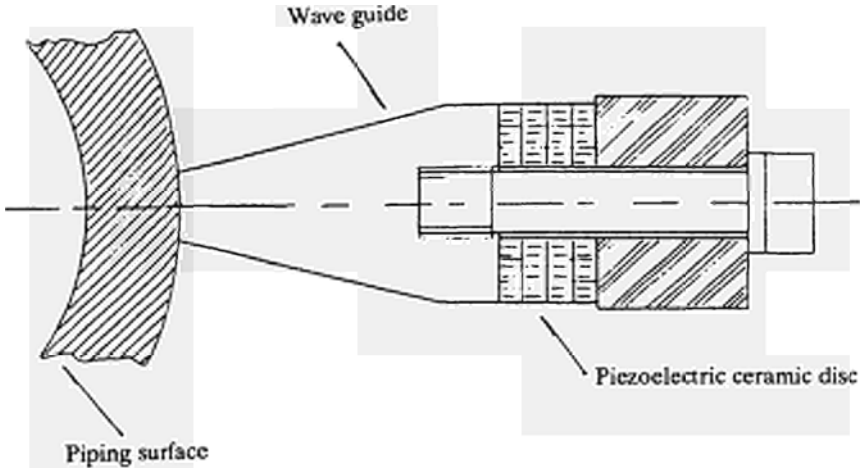


Figure 1 - Schemes of a piezoelectric transducers u'ith a conic wave guide.

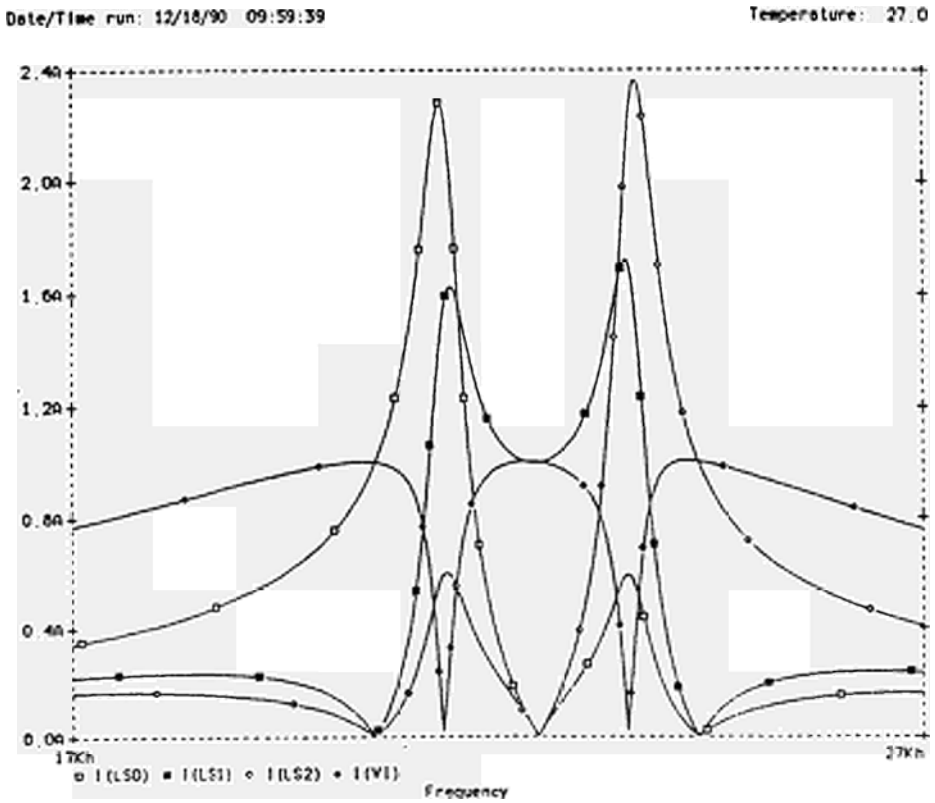


Figure 2 - simula t ion st udies. The calc ulatcd voltages x's. the

2.A DEVELOPMENT AHD OPTIMISATION OF AN EASY-TO-PROCESS **HLECTROLYTH F'OR ELECTROCHEMICAL DECONTAMINATION OF**

Contractor: KA, Heidelberg
Contract No.: **Fl2D-0ti20**
Work Period: July 1990 - June 1992 A STERINGER
Project Manager: Phone: 49/6221/39 42 50 **Fax: 49/6221/39** 47 07

A. OBJECTIVE AND SCOPE

This work aims at optimising an acetyl-acetone base electrolyte so that it can be used for electrochemical decontamination of stainless steels. Kraftanlagen Heidelberg developed the electrolyte under the preceding EC programme from 1984 to 1988, (contract No. FI1D-0004, report EUR 12383).

With regard to waste management and disposal, the obtained electrolyte came up to all expectations. An advantage of the organic electrolyte as compared to the phosphoricJsulphuric acid electrolyte is its long radiological service life (the activity settles out continuously). It is easy to convert the crystalline by-product (sediment) by high-pressure compaction into a form that is suitable for disposal. As only little residues of acetyl-acetonates are dissolved in the electrolyte, it is possible to considerably reduce the electrolyte volume by evaporation.

In tests with radioactive samples of carbon steel, the obtained results concerning removal effects, duration of treatment, surface quality, and decontamination factors, were satisfactory or good. However, pitting was stated in the tests with samples of stainless steel. As a consequence, the surface was not uniformly removed. Parts of the original surface were visible for a long time. This resulted in poor decontamination factors or long treatment times, respectively. In addition, larger volumes of secondary wastes were produced than with a uniformly removed surface. It is therefore required to optimise this electrolyte, if it is to be used for the treatment of stainless steel.

B.WORKPROGRAMME

B.1. Quantitative iavestigafions concerning the ‹lisso{ution mechanism

B.R Optimisation of the aqueous electrolyte through replacinii the potassium bromide by other conductive salts.

B.3. Invests a tterin d its eff t on abrasio g, surface quali d decontamination factor.

B.4. Development of a water-free electrolyte.

BE. Decontaminafion tmts with contaminated samples.

B.6. Pmcmsinz of spent electrolyte.

- 7 -

C. PROGRESSOFWORK OBT D ULES

S< W

Essentially, thc analytical testing and practical expcriments to develop a new electrolytc occur simultaneously. Only when the tests ot' dissolution mechanisms have bccn concluded, can the work of substituting the potassium bromide through other conductive salts, the examination of the scatter behaviour and the influence on removal efficiency, surface quality, decontamination effect and the development of a non-aqueous electrolyte be assessed.

There were many conductive salts that showed positive results. Satisfactory removal rates along with a good anode current yield could be achieved. It should be possible to improve the results through optimizing various parameters. A modified viscosity did not affect the electrolyte scattering, and the removal efficiency.

The investigations aiming at the development of a non-aqueous electrolyte are not to be restarted before completing positive tests with the aqueous electrolyte.

Progrms and Rmults

In the course of this project, an electrolyte on the basis of acetylacetone is to be optimized, for use in the electrochemical decontamination of stainless steels. Figure 1 shows the lists of the process parameters and the desirable process features of the easy-to-process electrolyte.

1. Quanntative invmtiga0on concerning the dissolunon

In order to exclude selective dissolution mechanisms phases, it is necessary to determine the quantitative dissolution of the alloying constituents, dependent on the time of treatment. To review local corrosion, the corrosion current is measured. The investigations of the dissolution mechanism are supported by galvanostatic and potentiostatic measuring methods.

1.1. Rmults to date

First investigations of the dissolution mechanisms showed that the metalion concentration corresponds at any point of time to the percentage of the stainless steel alloying constituents. The concentration of Cr, Ni and Fe, throughout the test time and at various strengths of the electrical current, is specified in Fig. 2.

Despite pitting, there were no signs of a selective dissolution of the various alloying constituents.

There are certain indications that, in the presence of inhibitor anions, the anodes are dissolved by halides, without any pitting.

IN Perspective

The investigations of the selective dissolution mechanism should be continued.

Further investigations to analyse the influence of inhibitors on the pitting behaviour of specific anions at the anode.

The results obtained in the tests are to be compared to the tests described in the relevant technical literature.

R **Optimisanon of aqueous electrolyte through replacing the potassium bromide by** other conductive salts

This step is to investigate various measures that are likely to reduce or entirely eliminate the aqueous electrolyte's tendency to pitting. To this end new conductive salts are being investigated as a KBr replacement.

In addition, it is aimed at finding inhibitors which prevent pitting, and with the high removal rate remaining unchanged.

Al. Rmults to date

Out of a great number of possible conductive salts and mixtures thereof used to replace KBr, satisfactory and even very good results were obtained in the test below.

The results are shown in Table 1.

- 8-

zz **Perspectives**

The positive effect of the various conductivc salts and mixtures thereof remains to be analysed. The results obtained were checked for a possible solid separation in the form of the Mc" (acac), which depends on the pH value. Moreover, the electrolyte service life must be investigated in more detail.

Thc results obtained during the investigation of the dissolution mechanism and the relevant factors will greatly influence any further steps in the development of an electrolyte where KBr is replaced by other conductive salts. The first results are expected by about mid-1991.

3. Invmtigatioos of scattering behaviour and the effects on removal efficiency, surface quality

and decontamination factors

This step is to investigate the effect of viscosity on the scattering power and removal efficiency of the new aqueous and non-aqueous electrolytcs. The respective tests are to accompany electrolyte development.

3.1. Results to date

To the electrolytes on the basis of acetylacetone containing KBr, CaCl and FeCl„ gelatin and polyglycol was added in order to increase the viscosity. No effect on the scattering power and removal behaviour was determinable.

3.2. Perspectives

The tests will be continued only when the other work packets promise no success.

4. Development of a **non-aqueous** electrolyte

An electrolyte is to be developed in which the water is entirely replaced by an organic solvent, in order to preclude pitting.

4.1. Results to date

In this test series, the water was replaced by methanol. During the tests, the anode current yield lay from 89 to 94 to, whereas the thickness losses were between 50 and 75 He with removal rates of 1.5 - 3.4 micron min '. Methanol must be added from time to time, to make up for the evaporation losses. The service life of the electrolyte based on MeOH is extremely short.

4.2. Perspectives

For the time being, the investigations aiming at the development of a non-aqueous electrolyte have been stopped, because the dissolution mechanism in aqueous electrolytes must be defined. The tests will be made in parallel as long as this is possible. First results are expected in the second half of 1991.

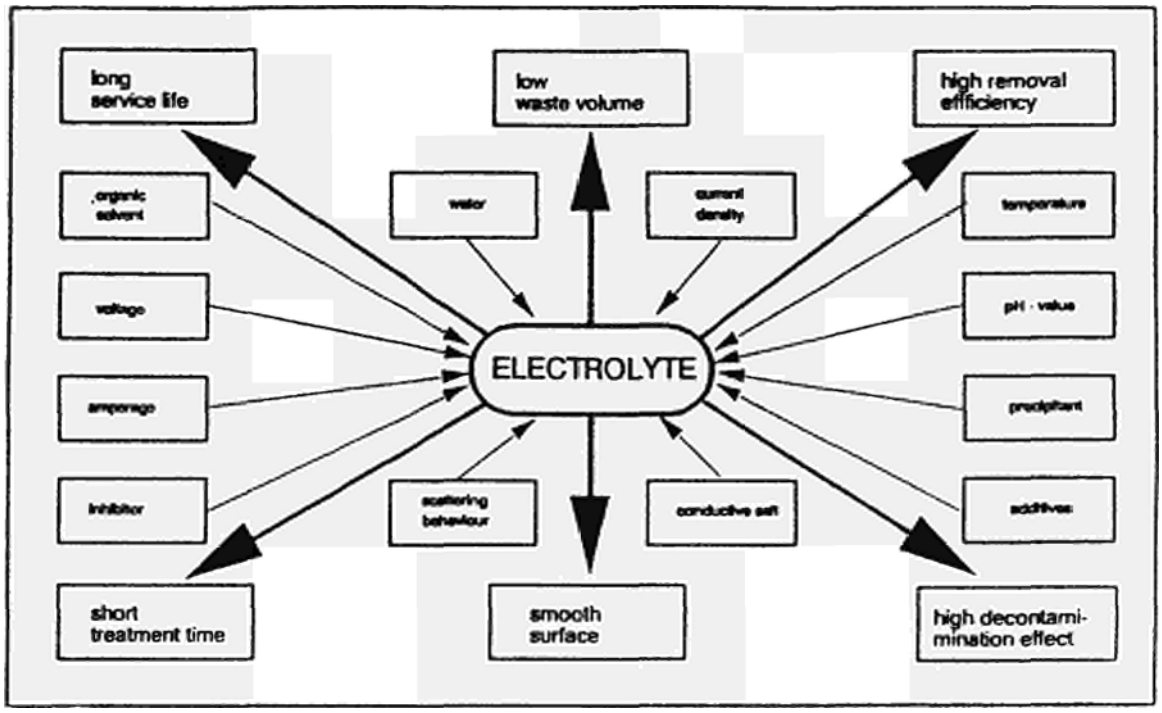
- 9 -

Tab. 1

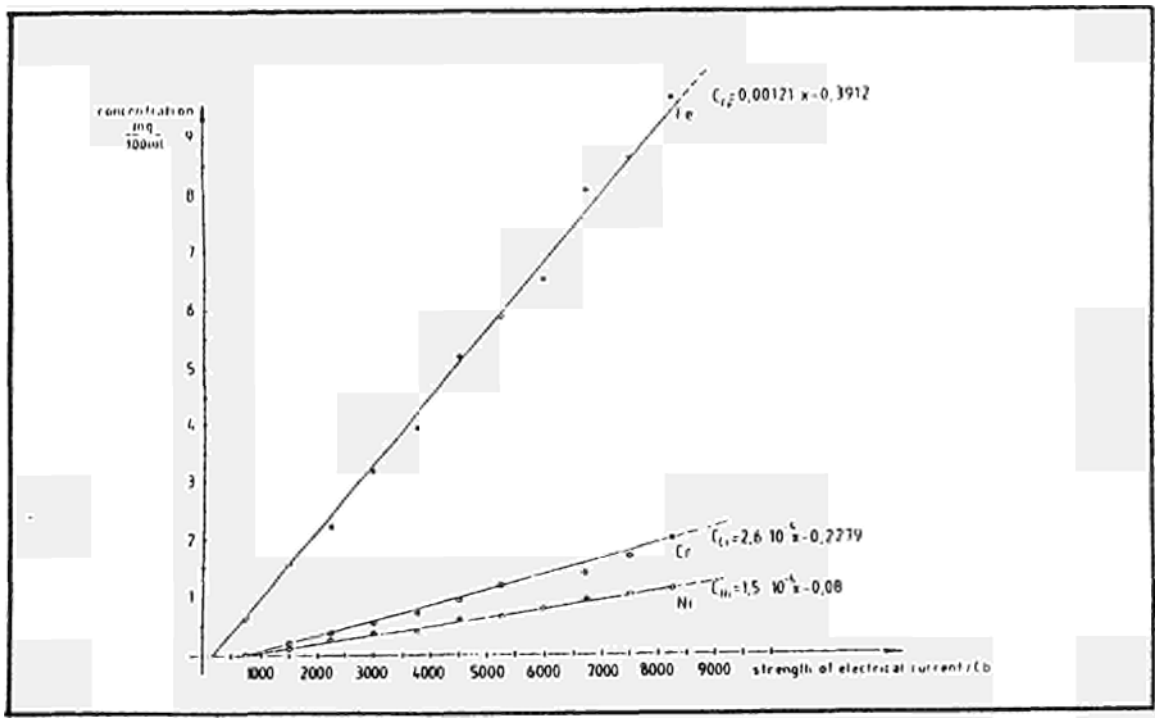
Resu1ts of the different conductive sa1ts used to rep1ace KBr

conductive salt	anode current y1eld g	removal rate jJ• a1ri-1	retxark
Nay S04	40	1,6 - 2,59	s•ooth surface
* 2	96,5	2, l3	snooth surface w1th sha11ou dimples
FeCl3 +	108	2,86	•aooth surface w1th a cav1ty
CrCl3 + TBA-Br	< 90	11,S	short service 11fe remova1 rate decreased cont1nua11y
NagSO,g + Ethano1am1n	5]- 100	0,09-0,97	good - very good
KHyPOg + NaySog	97 -59	0,17-0,33	very good
NagS0,g + KHyPOZt + Ethy1end1am1n	66	0,38	very good
Na$S0,g Ethano1an1n KBr	67 - 73	0, 28 - 0, 48	good

- 9 b s -



F1g. 1: The process paraaetezs and Lhe desirable process fmsturem otthe optinstmd cl•ctrolyte



F1g. 2.

D1str1but1on of the Fe , Cr and 81 concentration over the tinestvenousstrengthsoftheelectrical current

-
9
t
e
r
-

2-3. DECONTAMINATION OF LARGE-VOLUME NUCLEAR COMPONENTS USD'IG FOAMS

Contractors:	CEA-Cad, AEA	
C‹intract No.:	Winf FI2D-fJtl.35	
Work Pcricid:	October 1990 - March 1993	
Coordinator:	J P GAUCHON, CEA-Cad Phone: 33/42 25 61 93	Fax: 33/42 25 35 45

AOBI€CMVEANDSCOPE

There are only a few methods for in-situ decontamination of very large components usually in complex forms, such as large valves, reservoirs, heat exchangcrs, turbines, vessels, boilers.

The foam application processes have the major advantage of using only small quantities of liquid and being able to forcefully penetrate everywhere. Suitable chemical reagents are added to the foam, which acts a dynamic carrier.

In this contract, a technique of permanent foam circulation will be sought, so that decontamination can last for several hours in order to be as effective as possible and to use only a minimum amount of liquid. Decontamination factors of over 100 are expected.

The objectives of the programme are to:

develop and demonstrate an effective in-situ decontamination technique for large-volume components using chemical foams containing decontamination reagents;

minimise the volume of secondary wastes produced and demonstrate a treatment and disposal route, e.g. electrolytic processes, wet oxidation.

B. WORK PROGRAMME

B.1. Chemical foam formulation containing decontamination reagents (AEA and CEA)

B.1 Foam production and development o(a circulation sYstem (AEA and CHA)

BB. **Small pilot** tmts to qualify the decontamination method (CEA)

B.4. **Secondary waste treatment (AEA)**

B.l Dmign. construction and operation of a prototype foam production and circulation rig; non- radioactive demomtration (AEA and CEA)

B.6. Industrial application W radioactive tots on a 25 **m° contaminated vessel from Winfrith Steam Generating Heavy Water Reactor (AEA)**

C. PROGRESSOFWORK7UM]OBT7UNHDRHStfIL7S

No significant work was performed in this just starting contract.

- 10 -

3. **AREA No. 3: DISMANTLING TECHNIQUES**

AOb Ae

The objective of this research is the development of the special techniques needed for dismantling the large steel components (e.g. reactor pressure vessel) and reinforced-concrete structures (e.g. reactor shielding) of redundant nuclear installations, account being taken of the particular requirements due to radioactivity.

B. Subjects of the rmearch performed under the previous programmes (1979-88)

The following main dismantling techniques were developed and tested:
thermal techniques such as plasma-arc and oxygen cutting and cutting by laser beam; mechanical techniques such as abrasive water jet cutting;
explosive techniques for the dismantling of concrete structures.

C. Programme 1989 to 1993

Research in this Area should be pursued vigorously with particular respect to the:
development of the arc-saw technique for cutting thick-walled steel components; further development of the electrolytic technique for segmenting thick steel sections;
comparative assessment of various segmenting techniques with reference to standard cutting tasks;
full-scale testing of controlled explosive techniques for dismantling of concrete and metal structures.

D. Programme implementation

At the end of 1990, nine research contracts relating to Area No. 3 were at the stage of execution and two contracts were at the stage of negotiation.

- 11 -

3.1. EFFECTIVENESS AND LONG-THRM BEHAVIOUR OF CLEANABLE HIGH **EFFICIENCY AEROSOL FILTERS**

C‹intractor: TfIV Bayern
Contract No.: FI2D-(J007
Work Period: July 1990 - June 1992
Prolect Manager: P BOEHM, TEV Bayern.
Phone: 49/89/519 01 65 **Fax:** 49/89/519 02 80

K OBJECTIVE AND SCOPE

Because of the high quantity of dust generated by various cutting/dismantling processes, frequent replacement of high-efficiency sub-micron particulate air filters is necessary. If such filters could be cleaned during service, costs for the replacement of the filters, radiation exposures and the amount of secondary waste could be reduced.

The effectiveness in long-term operation (approx. one year) of high-efficiency submicron particle air filters will be investigated in the framework of the dismantling of the Niederaichbach nuclear power station (KKN) in Germany.

A high-efficiency submicron particle air filter system will be exposed to heavy dust generation during the remote-controlled dismantling of KKN primary circuit pressure tubes, and therefore must be dedusted periodically. The dust is radioactively charged (essentially Co-60 and Fe-55). The radioactivity could amount to approx. 1.10.' Bq/g (pressure tubes and moderator tank) and the dose rate to 0.1 Sv/h. There is at present no experience on the effectiveness and the long- term behaviour of high-efficiency submicron particle air filters that are dedustable during operation.

B. WORK PROGRAMME

B.1. Installation of the filters

B.R **Determination of the main parameters of the** clean filter station

B.3. Continuous measurements for-ure pickups. air humidiy and temper during cutting of KKN primary ‹exiling circuit (activated ‹xxilipg channel tubm inside the reactor vessel)

B.4. U-inal evaluation including radiation pureof workers. secondary waste arisings, specific costs. effectiven and lone-term behaviour of the filter svstem

C. Progress of Work and ObtainedResults

Summary

Putting the filter plant with cleaning equipment into operation was completed in November 1990. The measuring instruments formeasuringthe pressure differences of the high efficiency aerosol filters (S-filters) were installed in December 1990. Remote-controlled dismantling in the KKN commenced in January 1991. Measuring instruments for measuring relative air humidity and the temperature of clean air are currently beinginstalled.

Progress and Results

The room ventilation plant in the Niederaichbach nuclear power plant consists of a supply air plant and various exhaust air plants.

In order to retain radioactive dust particles, the exhaust air is conducted through a filter plant with two filter stages (HFA). Both filter stages contain high efficiency aerosol filters. The filtered exhaust air is discharged into the environment through an outgoing air flue. The maximum exhaust air flow rate is 110,000 m'/h.

During remote controlled dismantling the exhaust air flow contains a high percentage of dust particles. This exhaud air flow is additionally sent through a filter plant with cleanable filters. This filter plant contains a filter stage with high efficiency aerosol filters.

Thismeansthatduringremotecontrolled dismantling, the exhaust air volume flow, with its high dust particle content, isconducted firstthrough the filter plant with the cleanable filters (ARFA), then through the filter plant with the two aerosol filter stages.

The maximum exhaust air volume flow through the ARFA i s 3 o , 00 0 n' /h .

The ARFA consists of six filter bank housings,each containing five filter bank units. Each filter bank unit has shut-off valves on the dust air side and on the clean air side. The shut-off valves on the clean air side are closed automatically when the ARFA is notrunning.

In each of the thirty filter bank units is a filter box with a high efficiency aerosolfilter.

The flow circulation of the exhaust air being filtered is shown in the schematic representation of the plants (figures 1, 2 and3).

The aerosol filters are cleaned with compressed air. Blast air supports moved by compressed air cylinders are moved back and forth along the entire width and length of the aerosol filters.

The compressed air emitted from the blast jets ofthe supportblowsthedust particles accumulated in the aerosol filters into dust boxes. The compressed air requires a maximum operating pressure of 6 bar.

The aerosolfilters and blast jet supports can be inspected through windows in the filter bank housings.

An operating unit monitors the pressuredifferences

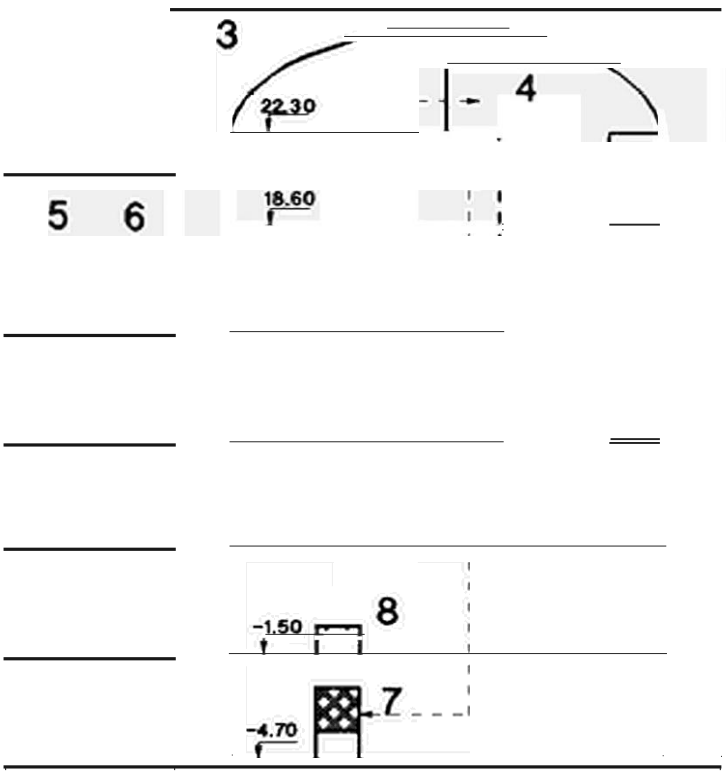
of the aerosol filters, using the pressure difference to control cleaning.

Only two aerosol filters are cleaned at any time. The shut-off valves on the clean air side are closed automatically during this process.

The starting period of the ARFA involved the following measurements and tests:

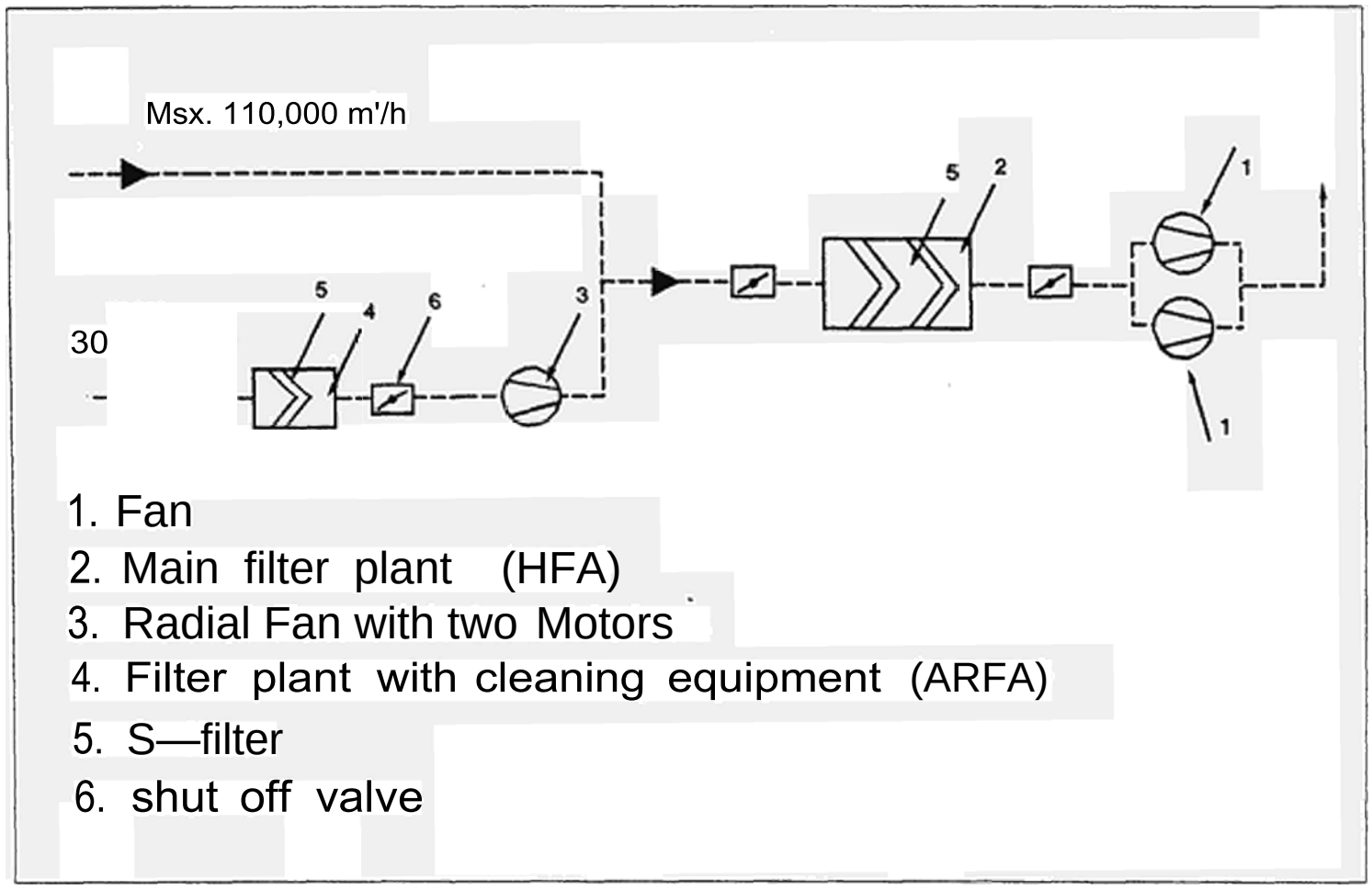
- Measurement of the supply and exhaust air flow rates.
- Measurement of the pressure differences at the clean aerosol filters.
- Measurement of the pressure in the reactor building and in the dismantling house.
- Measurement of the static pressures on the suction and pressure sides of the ventilators.
- Measurement of the temperatures and relative humidity of the supply and exhaust airflows.
- Leakage test on the filter bank housing.
- Leakage test on the shut-off valves on the clean air side.
- Leakage test of the sealing band of the filter boxes on the dust airside.
- Visual check of the function of the blast jet supports for cleaning the aerosol filters.
- **Measurement of ventilator speed.**
- **Test of electrical locking functions.**
- **Test of fault indication.**

There has been no automatic cleaning of the S-filters so far. Due to the dismantling schedule of KKN, increased dust in the waste air is not expected until mid-1991 (the beginning of the dismantling of the Moderator-Tank by grinding).



1 Reactor Plant Building
2 Auxiliary Plant Building
3 Ring Room
4 Dismantling House
5 Supply Air Plant
6 Exhaust Air Plant
7 ARFA
8 Measuring Equipment

Figure 1: Reactor and auxiliary plant building



grafical symbols DIN 1946

Figure 2: Diagram of the air flow circulation

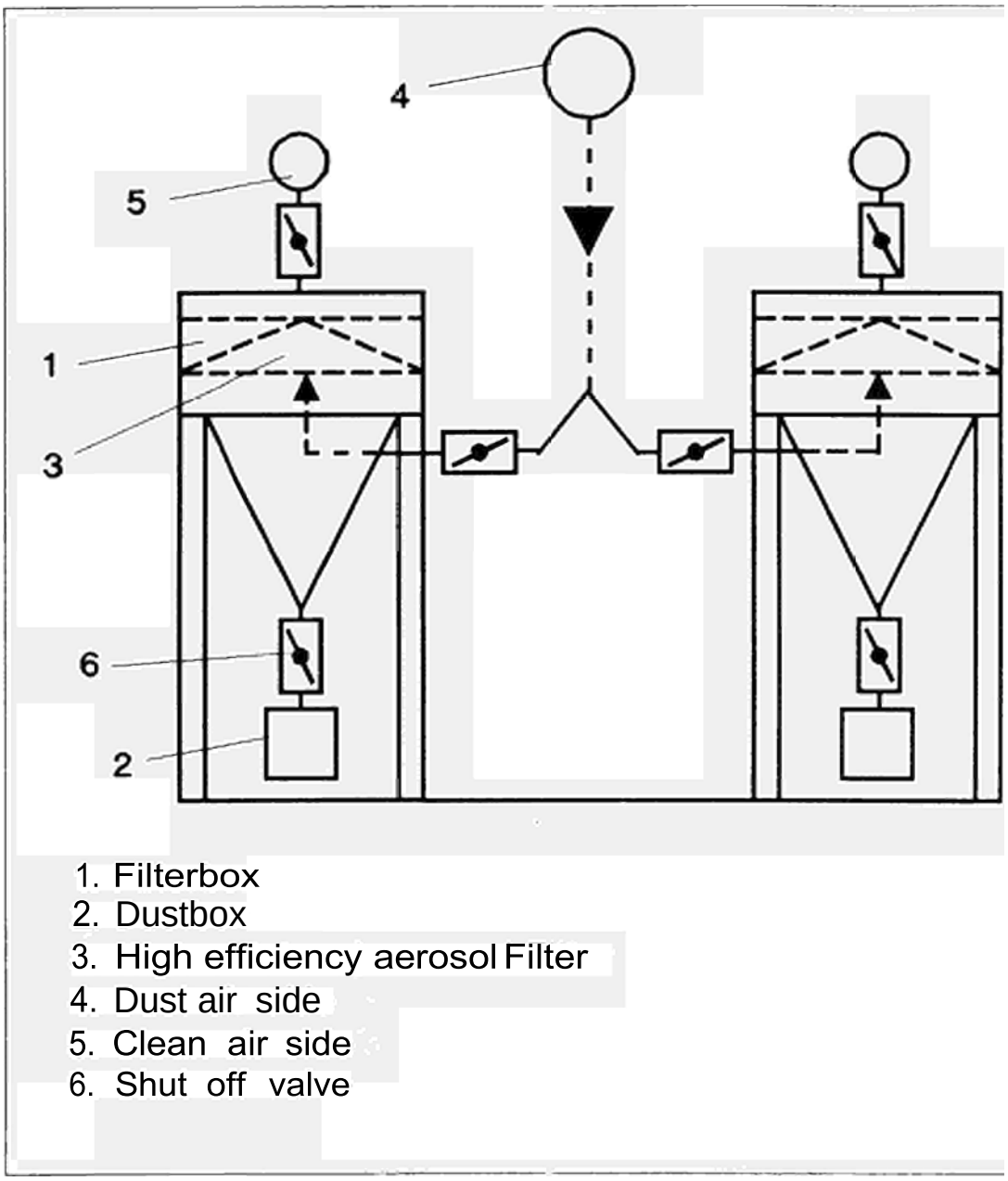


Figure 3: Diagram of the air flow circulation

3.1AB IVEWAN CUTMNGTE€IDdQ FROM TPH PAGE OF
ORATORYINTDREALAPPMCAWON

Contractors: UH-IW, CEA-
Contract No.: Sac FI2D-0009
Work Period: July 1990 - June 1992 H LOUIS, UH-IW,
Coordinator: Phone: 49/511/762 4320 Fax: 49/511/762 3456

W OBJECTIVE AND SCOPE

In order to qualify the cutting by abrasive water jets for application in **contaminated** or activated environment, the cutting techniques developed for laboratory application (CEC contracts FI1D-0069 **and FI1D-0067) are to** be adapted for remote-controlled application. Secondly, concepts for the handling of the secondary waste are to be developed and proved.

First, the existing abrasive cutting head is to be adapted to remote-controlled work under a water shield up to 15 m, in an inaccessible environment. For this application, methods have to be implemented and proved to control the cutting operation, for instance the state of wear and the cutting results (e.g. depth of the kerf, cutting through). Additionally, parts showing wear are to be remotely replaced so as to allow long-term reproducible operation.

The second step concerns investigations on the secondary waste. Besides a calculation of the composition and amount of secondary waste **depending on cutting parameters,** strategics will be developed and tested to catch the waste as close as possible at the place of production. **Filtration techniques** to **separate abrasives and cut material** from water and air will be adapted from other cutting techniques and will be tested.

All tests will be **carried out under non-radioactive** conditions, but at real scale in special water basins. **The aim** of this research work is to set up a tool which is suitable for work under realistic conditions. A control system and the remote replacement of worn parts are further important aims of this research work.

B. WORK PROGRAMME

Definition **of cutting parameters for decommissioning purposm (UH-IW)**

BE Development of ‹xintrollinz wstems for processes parameters and the cutting result (UH-

B.2.1. Preparation of a two-dimensional feeding mechanism for underwater cutting tests.
B.2.2. Development of an on-line controlling system to detect the state of wear inside the cutting head.
B.2.3. Development and adaptation of controlling methods to verify the cutting result during or just after cutting.
B.2.4. Design of a cutting head which includes controlling systems, cutting tests to qualify the sensor systems.

BE. Develope gent of replace worn parts of the **cuttin head der water**

B.4. Character ation and handling of secondary waste

B.4.1. Preparation of test facilities for measuring aerosols and suspended particles when cutting in air and under water (UH-IW).

B.4.2. Measurement and characterisation of the secondary emissions when cutting or kerfing in air or under water (CEA).

B.4.3. Development of methods to lower the spreading out of emissions in air or under water (UH-IW).

B.4.4. Cutting tests to determine the efficiency of measures to lower the emissions and to determine the filtration systems (UH-IW, CEA).

C . PROGRESS OF Yf0RK AND OBTAI NED RESULTS

Summary of maln Issues

I n the f i rst pe riod parane ters have been f ixed f o r ab ras ive wa t er jet cut t ing f or dec omit ssioning purposes . Spec ia 1 demands on the cut t i ng technique 1ike unde mate r app1i c ab i li t y because of rad rat ion p rot ec t ion and rim niniisat ton of was te must be not iced . To reach an op t iioa1 cut t ing ef f ic ie ncy regarding eat er and abras ive consuinp t ion it is use fu1 to mo rk on a h1gh pressure leve1 with a sma11 noz z1e d ianie t er .

Fo r d lsniant ling j obs a renio te-cont ro lted ope rat ion is necessary , the re f o re sensor sys tems are requi red to supe rvi se the too1 t unc t ion and the cutt ing result . A water basin was butlt to test sensor equiprent . A method was found to c ont ro1 the d iamet er of the f oc us ing no z z1e (i nc rea s- Ing by near) by nieasur ing the sucked-in at r f low.

Furthe r tests or11 be c arrled out t o opt iniise the set hod of no i se ana lys is f or c ont rod1ing the cut t ing resu1t .

Prog ress and resul ts

1. Def init ion of cut tiny paraniete rs (B.1 .)

For the app lic at ion of abrasive eat er jet s in contaminated envi ron- sent the reduc t ion of sec ondary was te i s very iinpo rt ant . So cu t t ing paran- ete rs are use f u1 which are qui te di f fe rent f rom ”no rna1" i nd ust r:ia1 app1 i - c at ions . Add it i ona11 y al so t he use of the t oo1 unde r rate r c reat es spec i a1 demands on the cut t ing technique reg a rd ing t he sens i t ivenes s aga ins t chang ina the no rking d ist ance , f or examp1e .

Results f rom contract Fl1D-0069 /ref . 1/ have shown that there is an opt imal nozz1e stze to reach the best cutting ef f iciency regard ing the used amount of water . This ef f ie ienc y i nc reases or th inc reas i ng ma t e r pressure . F ig . 1 shows t he opt ical noz z 1e d i amet e r f or a wate r pressure of 2400 bar. The optimal nozzle si z e is 0.2 rain. increasing the diameter ef fee ts a dec rease :in cut t ing perf o rmance re lat ed t o the used rate r f 1ow rat e / ref . 2/.

A simi lar ef f ec t i s g:iven f or the ab rasive f 1ow rate . I nc reasi ng the f low rate e f fec ts an i nc rease in cut t rna depth. But when t his cut t i ng depth is re lat ed on the used abras ive f low rate , there is an opt rna1 f 1oir rate at very low rates (f iz . 2) . Us ing f or examp1e on1 y 2 g/s f or a ce r— t ain cut means the losest produc t ion of ab rasive wast e , but the cut 1ant s 1onge r than usi ng a highe r ab ras:ive f 1or rate .

For the app1icat ion in containinated environnient i t is necessary to cut unde r the prot ec t ion of a rate r shle1d . I n that case the ab ras ive water jet is sens it ive against the var:rat ion of the wo rk ing d is tance . F ig .

3 g:ives the resul ts of cut t ing tes ts conparing app1 i cat ion in at r and under eat er . The riioment um loss unde r water is on1 y sna11 when us:Ing a short noz z ie-samp ie distance . For dist ances about 23 Ham t here is on1 y ha1f t he cut t ing perf o rnanc e than us ing 2 - S nun dist ance . This ef fee t resu1t s in high demands on the hand1i ng sys tent and the senso r sys tern to keep and

cont ro1 the work i ng d1s tance .

2. Deve1opment of contro11ing systeas (B. 2.)

2 . 1 . Pre pa rat ton of a two-d mens to iia1 f ee di ng mec han lsm

An exis t ing feeding Meehan lsn had to be mod1 f i ed to ca i ry ou t two-dimensiona1 cuttina tests with abrasive vater jets under water. So a water basin was mod i f red which a11ows the tes t ing o l senso r s ys tems t o det ec t the cutting resii1t (cutt i ng through or kerf ing). to-dinenslona1 cuttinc t est s are necessary t o check t he ef fee t of chang rna t he cut t i ng d i rec t i on on the senso r signa1s.

Add i t iona1ly this equi pinent a1 loss to f i 1te r t he wat er and t o ana-l yse the suspended par tic les . Tes ts vi 11 be c arr ied out t oge t he r ui th C EA-S ac1ay to quant if y the amount of wast e (B. 4.).

2.2 Deve lopinent of an on-line cont ro11i ng system to detect the s tate of near inside t he cut t ing he ad

Uhen ope rat i ng in i nac c ess ib1e envi ronmen t i t is necessary to c on-t ro1 the s tat e of the too1. I n the case she re undue wo rn part s have t o be removed wate r jet no z z1e and f ocus i ng no z z le espec i a11 y have to be c on- tro11ed to reach a suf f ie ient cutting ef f ie ienc y at eve r y time.

The near of the wate r jet no z z1e can be supe rvi sed by me asu ri ng t he wate r f low rate . I n case of near or chi pp ing the vat e r f low rate Inc rease s when the p ressure is cons tant.

The near of the Iocusing nozzle can be calcu1ated by contro11inc the ai r f 1ow rate sucked-in by the in jec t i on cut t ing head . F i g . 4 shows the ef fec t of the I ocus i ng d iame t er on the at r f low sue ked-in . To measure t his ai r f low ra te a f low mete r is necessary i n the t rans po rt a t i on tube of the ab rasi ves . So the abrasives have to p ass the f low mete r toge ther wi t h t he ai r where i t vi 11 be c aus ing wear.

Othe rux se the a bras1 ves can be st o red in a c1osed vesse1 and t he at r sucked-in in this vesse1 c an be me asure d .

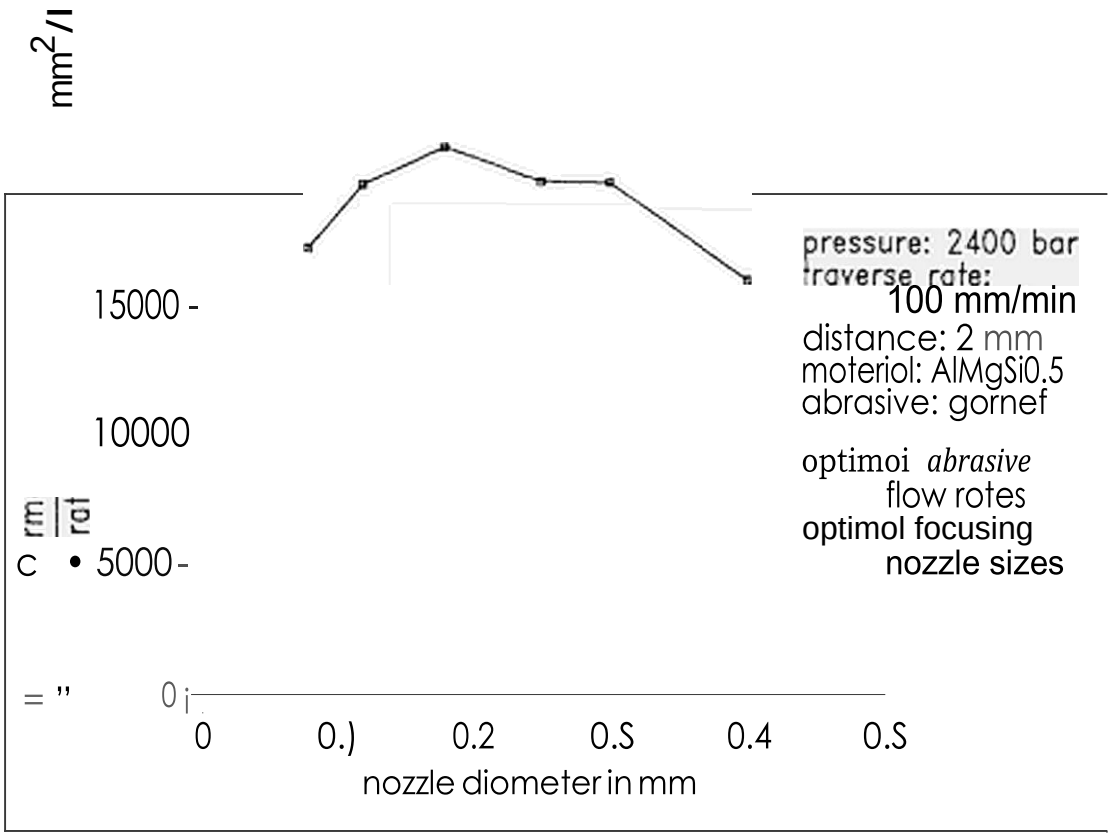
On the o the r hand the f 1or rate and so the d x ame t er of the no z z 1e can be ca lcu lated by ineasuri ng the p ressure drop in the transport atxon tube . This me thod is very easy to rea li se: to p re ssu re senso rs are adap t-ed in di f ferent posi t ions of the t ranspor t at ion tube , the p ressure d rop 1s p ropo rtiona1 to the f 1ow rate .

Re f e renc es

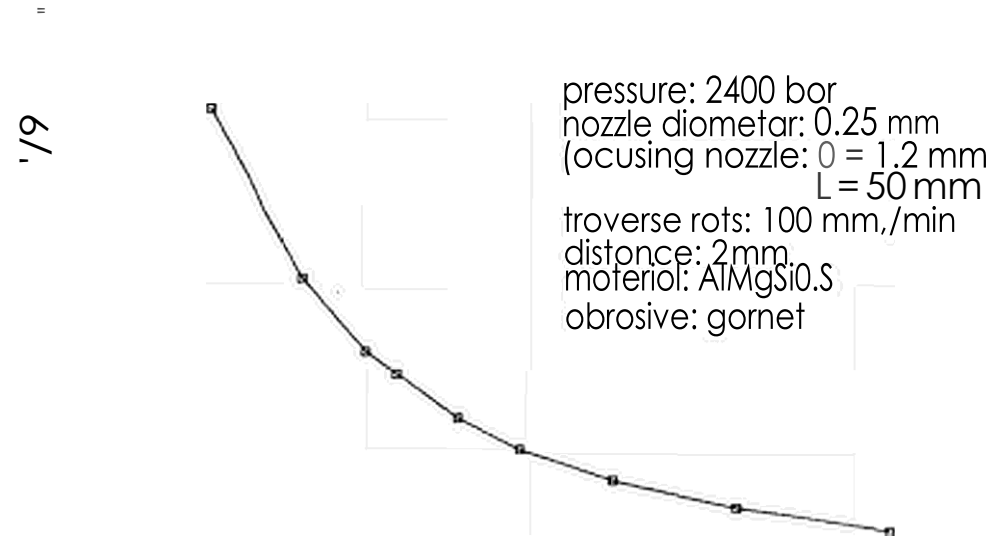
/1 / Hafe rkainp , H. , Louis , H. and He ie r , G . :

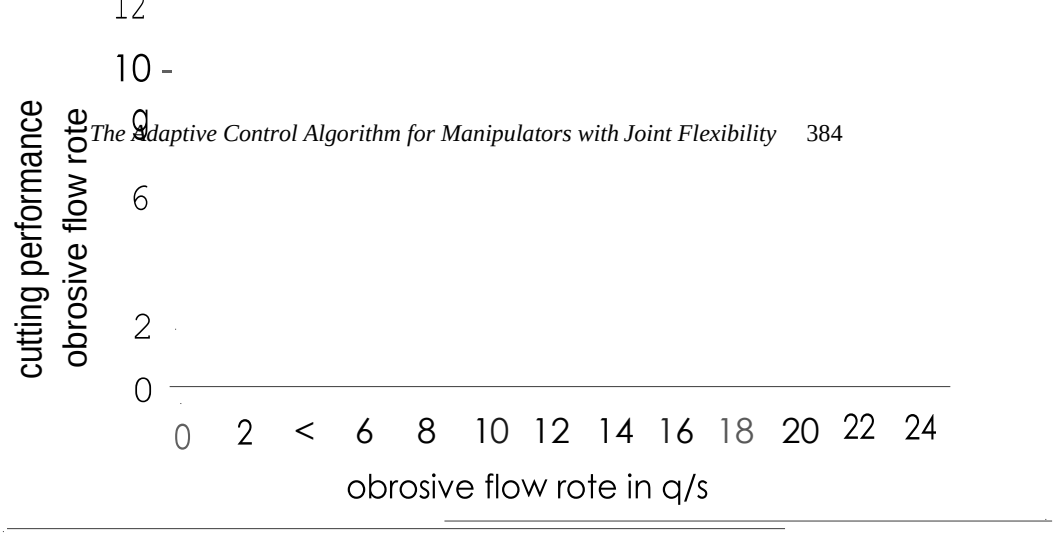
”Ptei te rentwick luna des Abrasi vstrah1-Schnei dverfahrens zum T rennen fe rri tischer und austenttischer Stah1e unte r Uasser”, EUR 12684 DE

/2/ Haf erkamp, H. ; Louis, H. and Heie r, G.:
”Submerged Cu t t ing of 5t ee1 by Ab raslve flat er le t s"
Proc. of the 1989 Inte rn. Conf. on Decomissi oni rig of Nuc1ear Insta1-lat ions , CEC , EUR 1 2690



F18ure I E£fect of uater l'1ou rate on cut ting eI f 1 c1 ency





Fiaure 2 Ef feet of abrasive I low rate on cut t ing ef I ie ienc y

21

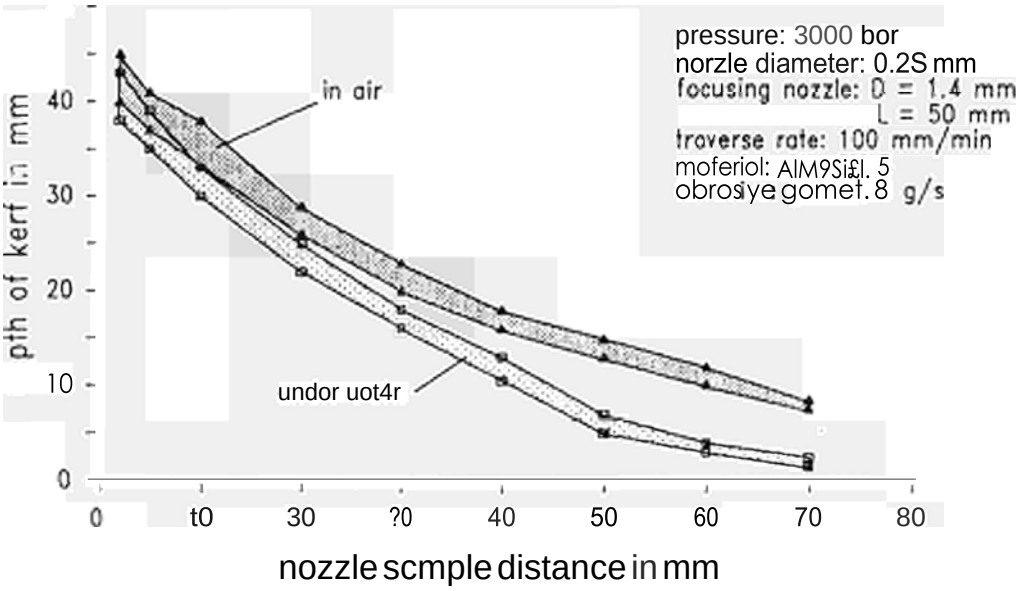


Figure 3 Ef fee l of noz z le-sanp1e d i.s t anc e on dep t h of ke rf

1 I.2 t.t \.6 1.8 2

diameter of the focusing nozzle in mm



Flgure 6 Ef feet o I diameter of t he i ocus i ng noz z l e on t he 11or ra t e o I the sucked-xn atr

3N. STHHL CUTTING USING LINHAR-SHAPHD CHARGES

Contractor: OTO MELARA
Contract No.: Fl2D-fD10
Work Period: July 1990 - June 1993
Prolect Manager: G PEZZICA,
Phone: 39/187/40 91 28 Fax: 39/187/42 10 26

A OBJECTIVE AND SCOPE

Various types of cutting charges already exist, but mainly for cutting of few millimetres thick material.

The research work will therefore focus on the development of a high performance cutting charge minimising the damages to surrounding structures for the dismantling of thick-walled steel components (ranging between 10 to 250 mm thickness), e.g. pipes, reactor pressure vessels. The work will include studies and experiments at small and large scale, as well as a study to possibly eliminate or minimise undesired secondary effects caused by the projection of splinters at high

-

Specific data will be produced on costs, work time and secondan• waste arisings from the application of this steel cutting technique.

It is expected that the project will result in an economical and dose-rate tolerant cutting technique particularly suitable for dismantling work in inaccessible places.

B. WORK PROGRAMME

Determination of basic charge parameters

Theoretical assessment to characterise high performance cutting charges.

Manufacture of charges and execution of tests.

B.I.3. Analyses of the experimental data compared with the theoretical results, conclusions on first phase.

BE Optimisation c arg es

B.2.1. Theoretical assessment to further optimise important parameters.

B.2.2. Manufacture of charges and execution of tests with measurements of blast effects in the air, of ground vibrations, photographs from an ultra-rapid framing camera and of flash X- ray tubes.

B.2.3. Analyses of the experimental data with a view to specify high-performance charges.

BE. High-performance cutting charam specifications and tmts.

B.3.1. Theoretical assessment of the final configuration of high-performance cutting charges and specification of 8 tests (in order to determine the scaling law).

B.3.2. Manufacture of charges and execution of large-scale tests in special areas allowing large amounts of expiosives.

B.4. Final evaluation including specific data on sts.work **time and secondary waste arisings.**

C. Progr ess of f4gv k and Ob'ta1ned B_esu 1't s
Summar y

The esear- ch wo r- k s t ar C ed z n No vembe›- 14VI , • of 4 months with respect to the contractual starting (01.07.1990), due to the delayed contract signature.

The preliminary theoretical study, (B.1.1.), has been z Cl a de l «, completed. By means of tke nor; lincai finitw-diff'r.-en'-s o niput er cocJe PI SCES ID i ›. cJ i l l e i- e‹a t Fcz nd ams ri l o i configurations of cutting char-ges nave ln»estigatec!. A detailed study has performed by using the same hydrodynamic computer code PISCES 2D but linked with the analytical code OTOSC1 which was "ad hoc" developed for studies on shaped charges. Dur ing this second study eight 'lifferont con$ igu<ations have been investigated anO &›qNt cutting *charges* defiincd by us ing loth the p'uk‹*: l>r•cl Uo to d!'‹1 the osui t• of the co.mputer , i n o l at i ores .

The mariu7actu‹-e of the two Fi-st bat‹.b.w= ot fcu• :.na' . f›as been sta'tz'd. Leer? cha'-oe co:-=c'=uor‹')='•o ›-efmrence conf,Qu‹ atiur. The best of two c::to•- t +r›anufact -linq proc.u=sses w. 11 sc room:nt.T+ :l. Tl'.is c' i'= iucludeo * B.I.S. of the w›o:' ;3+ ‹wgian«nw, •s p›o‹gre=-.

Progress and Results

1. Determination of basic charge parameters (B.1.1.

The basic parameters characterising the reference cutting charge have been defined:

- base width 50 mm, charge depth 50 mm;
- copper liner: thickness 1.5 mm, angle 100 degree;
- high explosive: Octol;
- aluminium confinement;

-cer.ti-al initration.

A sketch of the charge is shown in fig.1.

By means of the Eulerian processor of the hydrodynamic computer code PISCES 2D /1/, the processes of collapse and jet formation have been simulated for six different configurations of the cutting charge. The charges studied differ from the reference one in: detonation wave and lateral initiation (wave shaping); liner thickness; liner angle; charge depth. In fig.2 three contour plots of pressure and density at three different times are reported (reference T. I'.ci7e+-ical tiwu-c)imeinslui‹a) etoc)i

The higher jet velocities have been obtained in the case of wave shaping and in the case of a thin liner.

3. Studies with an hybrid technique

To obtain more detailed information on the characteristics of the formed laminar jet, the PISCES 2D hyd‹ ocodewas also used, lwVed with tDe ana]ytwa r-oo•'

DTOSC1, following the procedure described in /2/ and /3/. The configurations analysed differ from the reference one (X0) in: liner thickness 1.0 mm (X1A) and 2.0 mm (X1B) [X0=1.5mm]; charge depth 30 mm and 50 mm (X2B)

-24-

liner angle 80 degree (X3A) and 120 degree (X3B)
IXO=10JOdegcee3; 1atei-al iriitiatioia i•iasu stupirigi
IXG=centia1initiatiori3.

He uu1ts:

srna11ec 1inoi'tftickriesu: *I iQ e•riet* velc›cily. bo11owe:' :c-l

*)arge*rchar e depth: hIghe': Jtzl and mass, but hiqbei umdesideced uide ellecto;

— urna11ec 1*iver oinq*1e: hiqDec a-at velocity, bint lc••ec ;•

eave st apinqgive= an inc›-ease of both jet ass a:!n

manufacturing processes.

velocity, but requires very high precision our,.g

In order to avoid as far as possible ambiguities arising

4. Definition of test conf*qn-at*ons

from superimposition of different effects, it is plan ed to test charges which differ from the reference called C0, in a parameter only: liner thickness 1.0 (C1A) and 2.0 mm (C1B); liner angle 80 degree (C2A) and 120 degree (C2B); charge depth 40 mm (C3); wave shaper (C4); multiple detonators (C5).

fi. Manufacture of iefer unce c!aiqes US.1.5.i

The manufacture of two batches of four r efer ence' crai qes each has been s tar tod. 'thc fo1 losing manufuc tu- i mg p+ ocesses are under investigation:

a) the aluminium con†inwment is macl›i,ed tc a fi al t1,icf.e:-s

b) the confinement is obtained by cold forging of a 1.5mm-thick aluminium sheet.

Th1s wark 1s p*resent)y* li‹p-oqress.

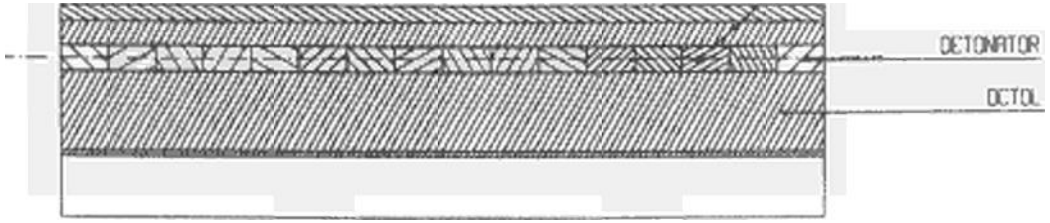
References

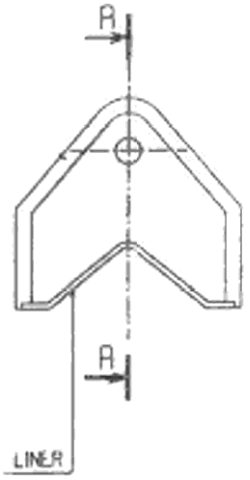
/1/ M. Trigg, S. Hancock and H. Hancock, "PISCES 2D ELK User's Manual", (version 4), Physics International Company, San Leandro, California, USA, October 1985.

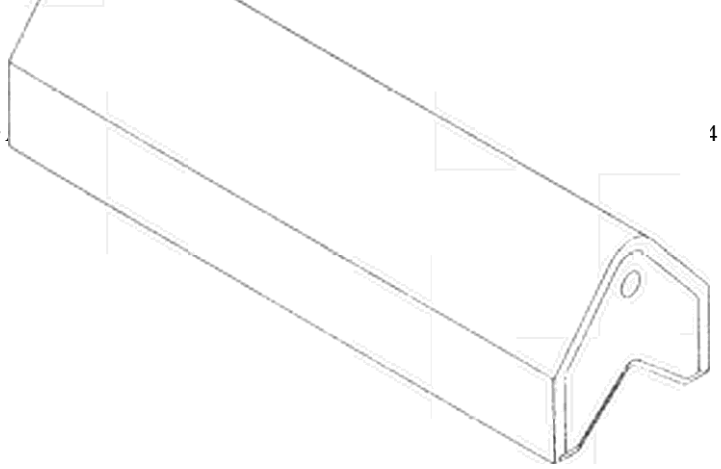
/E/ G. Pc zzloa, lS. Paz eiaza amd l=.l*l. *•'lcgi›aira, " £dL‹mei1<a1Nodc) ng 0f Shaped *hUarqe ss* l•l1ll-› Na ve — Sh ap ei-s, l›th l'-it.S,m.on Ba11 1st1c s, San D1ego . C*ali7or*n1a, fi7— E'-Y Oc+.nber l '20x.

/3/ Li. F'ezzzca and G. f°uzien za, "Sh ap od LF› •‹: es•: D 1•..c uss c› n

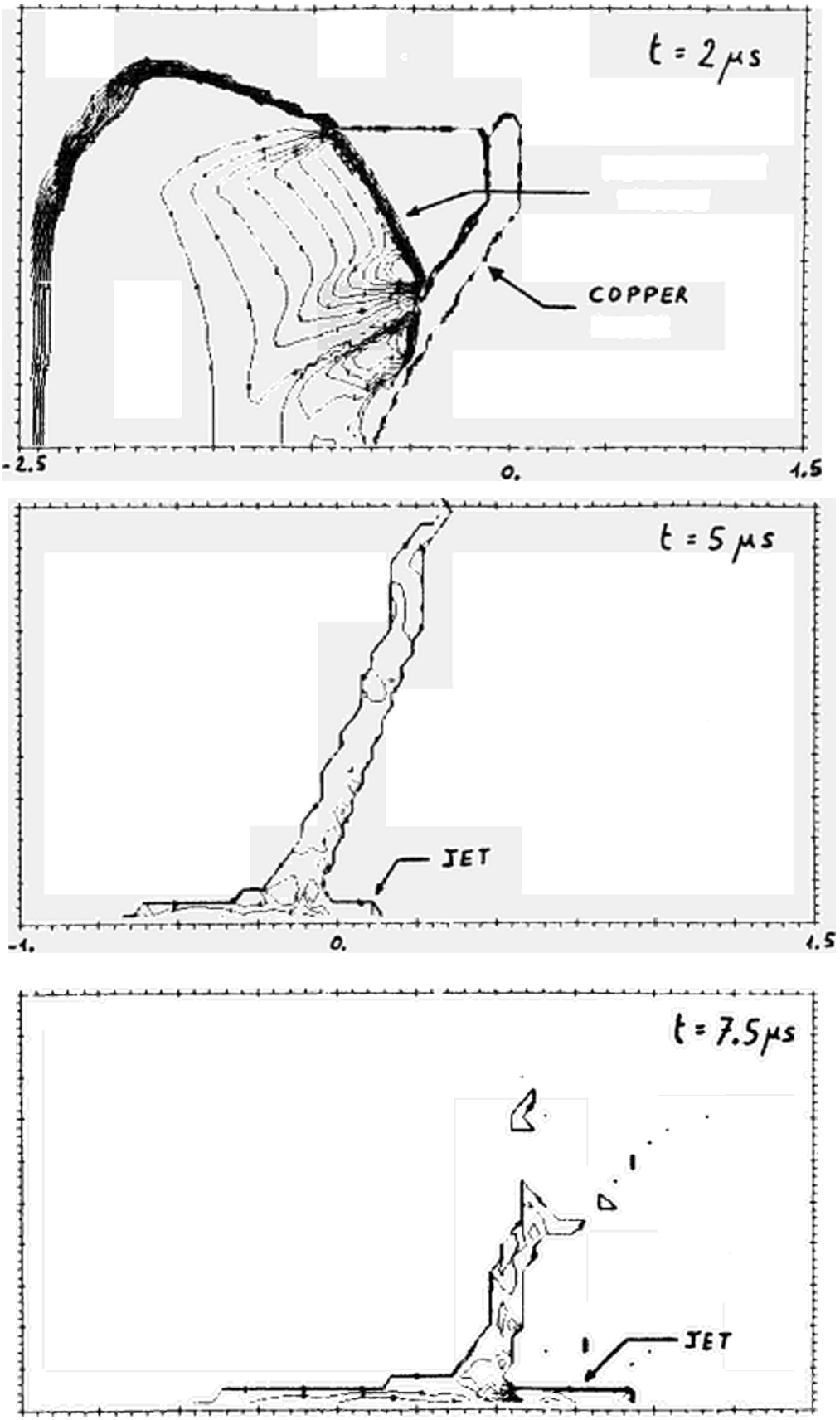
ᗅ Set For rat ior Grid Jet Peseta a l ioi i UiiDc•c S to l ic Gi'ici Dynom ic load i t i oris", 11 th lia l . Gym . on Ha 1 1 i+ t ic n, Bi o xc l ie+ . Be*lq* iom, 9—11 Play 19B9.


DETONATOR
OCTOL


A
A
LINER



F1gure 1: re torence cut.t Inq charge



J• 5

-1. 0.

F1gure 2: re lerenco con11qurat lon, con tour pl o ta o I pressure and den s1 t y (PISCES 2D code)

3.4. EVALUATION OFTHESEGMENTATION BYVARIOUS CUTTING TECHNIQUES (PLASMA TORCH, ARC SAW, CIRCULAR DISC, ETC.)

Contractors: CEA Valrho, CEA-
C‹intract No.: Sac FI2D-fJ013
Work Period: October 1990 - June 1992
Coordinator: Ch LORIN, CEA/DCC/UDIN
Phone: 33/66 79 63 04 **Fax:** 33/66 79 64 32

K OBJECTIVE AND SCOPE

The project relates to industrial-scale testing in air of various relevant cutting tools. Its originality is a comparison between tools in the same normalised conditions of use.

The main purpose of this work is a comparison of different cutting techniques for the same working conditions in order to determine the real cutting time, to improve the knowledge of the cutting tools, and to evaluate the generated secondary wastes, cost aspects and the radiological impact.

The work requires an inactive testing cell, as well as appropriate materials and tools: the cell, located in an inactive testing station at CEA/Fontenay-aux-Roses, is an airtight room in which it is possible to work in a controlled atmosphere. Carbon and stainless steel plates with thicknesses of 10, 30 and 50 (or 60) mm with exactly known composition of the radioelements will be cut; the cutting tools which will be used are arc air, plasma torch, arc saw, circular disc and alternative saw. Meetings will be arranged with partners after each tool test in order to improve their execution; therefore, the tests are carried out one after another. It is envisaged to cooperate in specific areas with the Universitat Hannover and with the French industry.

The potential benefits of these tests are the protection and security of workers, a decrease of the volume of waste effluents and a better use of the tools themselves for future decommissioning work.

B. WORK PROGRAMME

T.1. Preparation of the tmting_ceJJ (CEA-Sac)
B.1 Cutting under inactive condition with selected tm_ls and materials (CEA-Valrhé›) BE. Cutting under simulated radioactive condition (CEA-Valrhé›)
B.4. Secondary waste analysis after each specific cut (CHA-Sac)
B.S. U•ina1 evaluation of the cutting technique assessed. including the cost of the basis tool, the associated logistic. the **comumable part, the radiation** exposure **to workers and march of relevant radionuclide in the** cell (AII).

C. Progress of work and obtained results

The facility where the cuts teke place, the analytical techniQues emd the test specifications are described. In the first tests, made by automated mode, mild and stainlesssteelplateswiththicknessof10and30 mm were cut by grinder mnd reciprocating saw.

The first results show that the sedimented dross is the major part of the secondary emissions (up to 99.9 X for alternative saw), the wear of the tool is not negligible (grinder disc), the cutting speed end the tool driving are very influent parameters in the production of secondary
emissions snd mainly on aerosolone.

Progress and Results

(BI)

The test takes place in a 32 m' cell composed of modular stainless steel panels. A cutting rig, motorized in XY, on which the tool and the workpiece csn be adjusted, is located inside this cell (figure 1).

The workpiece is weighed before and after cutting. The sedimented dross is collected under the workpiece (figure 2) and weighed.

The attached slag is broken off memually or machined off and weighed.

The mass of particles on the walls of the cell is deduced from sample surfaces (figure 1) on which swabbing is carried out and weighed. The eventual wear of the tool is determined by weighing.

Nozzles are installed in the exhaust pipe connected to the cell to allow isokinetic sampling into (figure 3):

- filters of 130 mm diameter end filters of #7•m diameter upstream snd downstream of the electrostatic filter.
- sn inertial mnd diffusional spectrometer (SDI 2001).

Total aerosol mass concentrations are measured by filtration emd weighing. The fiberglass filters used are 130 mm end #7•m diameters and have a collection efficiency of more than 99.99] for particles of size superior to 0.3 micron.

The SDI 2001 is sn apparatus which combines an Andersen impactor with a diffusion battery containing beds of spheres of specified sizes. It allows determination of the size distribution of particles between 0.075 and 15 mi crons .

The flowrate in the exhaust duct, that can be adjusted by a valve located downstream the fan, is determined from the indication of a calibrated orifice plate.

The different steps of the tests (preparation of the sampling filters, of the cell snd of the exhaust duct, cutting ventilation, sampling, swabbing, collection of secondary wastes, weighing) are repetitive and carried out with great care.

2. Results for cutting under inactive conditions (B.2)

Grinder - Stainless steel

The sedimented dross represents the major part of the solid secondary emissions, about 9#] for e (thickness) = 10 mm and 97] for e - 30 mm.

The msss loss of the workpiece is in relation with the ratio of the thickness but the disk is worn more rapidly for e = 30 than for e = 10 mm (§o6 g/m for $\frac{mm}{e}$ = 30 mm and §4 g/m for e = 10 mm).

- 29 -

When the thickness is multiplied by 3. the aerosol mass is multiplied by 2 (6.4 g/m and 12.6 g/m) but the cutting speed is a very inFluent parameter on aerosol production end need a special study.

The size distribution of aerosols is bimodal with the main mode around 7 microns.

The sedimented dross represents the major part of solid secondary emissions, up to 99.9 X. There is no attached slag. In one test, we have emphasized that the particles mass on the walls of the cell, the aerosols and the wear of the blade were more important than in similar tests, because the blade was blocked with sn angle of 0' with the workpiece and thus resulted in a local raise of temperature.

- 30-

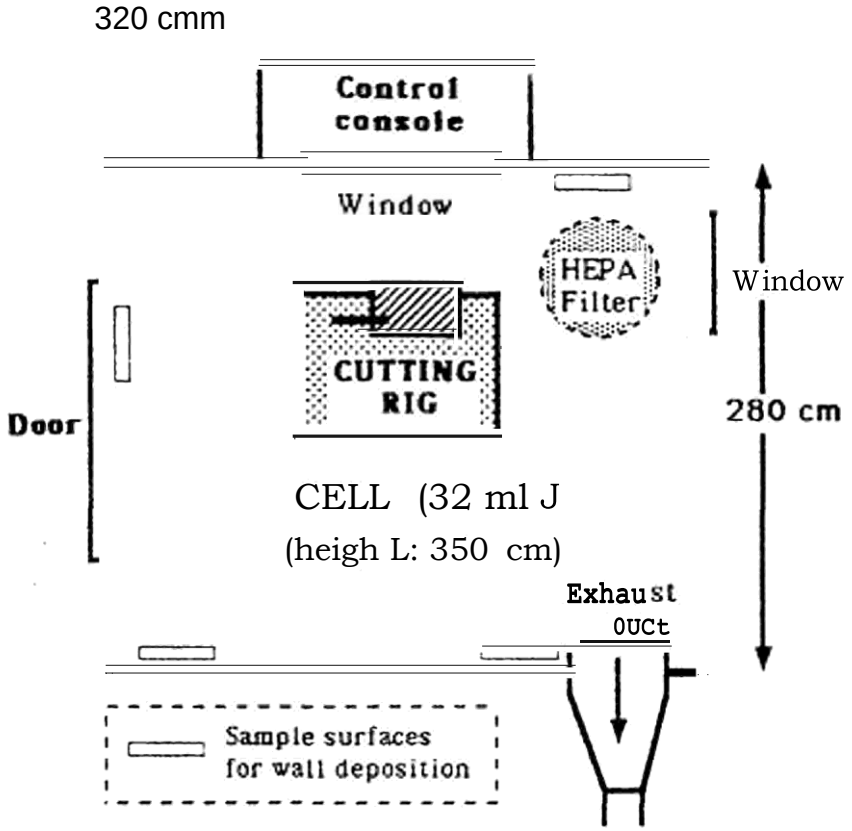
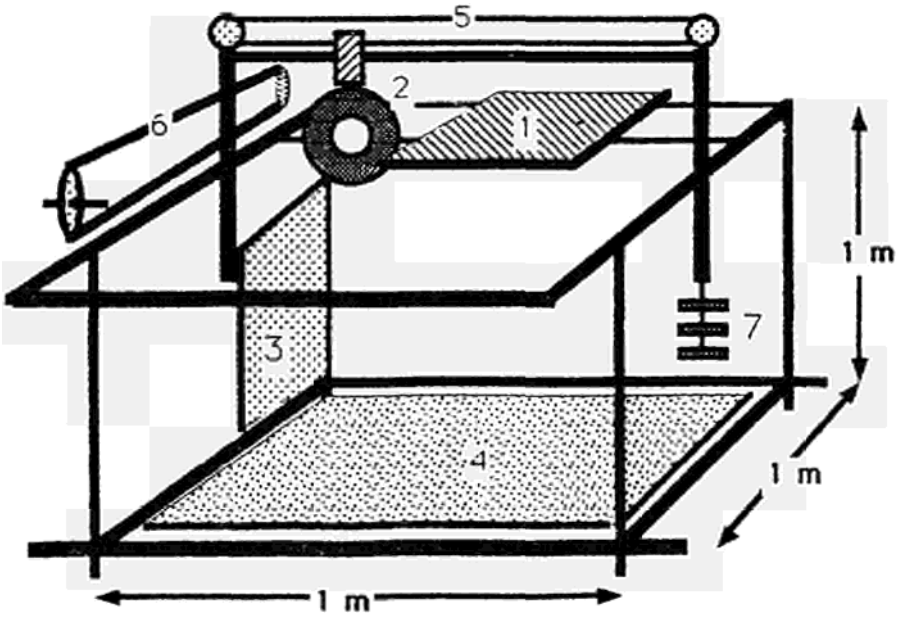


Figure 1 : Schematic via of c utting eel1



I - \x/orkpiece
?— Too
.s- ProLecL!cn olate
4- Dress tray"
5- Xdi=plucement
6- Ydi-placement '-
'Counterweight

FlgOfO Schematic view of c uttingrig

31 -

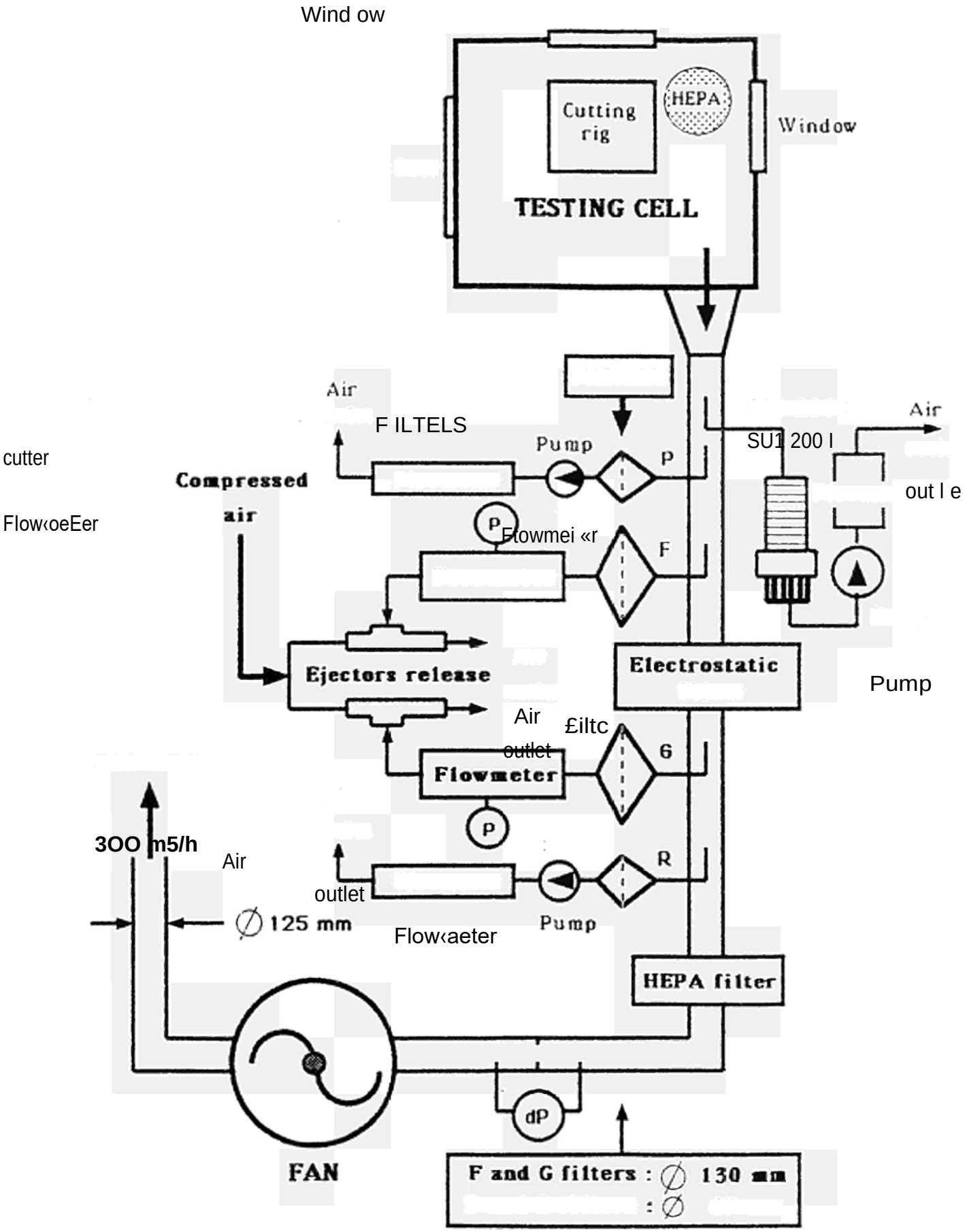

Wind ow
Cutting rig
HEPA
Window
TESTING CELL
Air
F ILTELS
Pump
P
Air
SU1 200 l
out l e
cutter
Flow‹oEEer
Compressed air
P
Flowmei «r
F
Ejectors release
Electrostatic
Pump
Air
£iltc
outlet
Flowmeter
G
P
3OO m5/h
Air
R
outlet
∅ 125 mm
Flow‹aeter
Pump
HEPA filter
dP
FAN
F and G filters : ∅ 130 mm
: ∅

Figure 3 • Schematic view of the ventilation system and associated sung1ings - 32

3A. UNDi RWATHR THERMAL CUTTING TECHNIQUES AND ASSOCIATED REMOTH-CONTROLLED MANIPULATOR SYSTEMS

Contractors: CPA-Cad, UH-IW, RWTHA, CEA-
Contract No.: Sae FI2D-fD19
Work Period: July 19Rl - December 1993
Coordinator: R LEAUTIER, CPA Cad, SST/SMP/GP
Phone: 33/42 25 **73 08** **Fax: 33/42 25 32** 62

W OBfECTfVE AUD SCOPE

This project aims at improving underwater thermal cutting techniques and their remote control. The main objectives are to cut greater thicknesses and improve the safety of operation,
e.g. assess harmful by-products, protect workers, assist the operator during operations.

So far, underwater thermal cutting of steel has been achieved up to 70 mm thickness. This project has the objective of **achieving cutting** up to 2fD mm. Sensors and associated systems studied in laboratory will be applied in a semi-industrial installation.

The work involves an experimental investigation in the laboratory of each contractor followed by real-case applications under non-radioactive and radioactive conditions in the former Pegase reactor in Cadarache.

The project is a follow-up of work performed in the 1984-88 EC programme (contracts FI1D-fD37, -tXD7 and **-(D39).**

B. WORK PROGRAMME

B.I. Preliminary tasLs (CEA-Cad)

B.1.1. Detailed requirements and objectives of the project
B.1.2. List of parameters and ranges to be studied
B.1.3. Specifications of sub-systems

BE Deveiopment of the plasma torch and adaptation of the movin ce (CEA-Cad)

B.2.1. Improvement of the performances of the plasma torch
B.2.2. Adaptation of the moving device
B.2.3. Integration of the sensors into the torch handling system
B.2.4. Cutting tests with measurement of effluents

BE. Development of other t‹x›is (UH-IW)

B.3.1. Optimisation of cutting parameters of plasma saw and consumable electrode
B.3.2. Control systems usable with the manipulator of CEA-Cad
B.3.3. Cutting tests with measurement of effluents

B.4. Development of control systems for sensor-controlled nilotine of the handling system for the tens and the procms parameters (RWTHA)

B.4.1. Improvement and application of inductive sensors
B.4.2. Process control and piloting of the tool handling system
B.4.3. Interfacing between the sensor system and the handling control system
B.4.4. Function testing in the laboratory

BE. Preparation of radioactive sampim taken from nuclear imtallatiom (all)

B.6. Final tmts in Cadarache (all)

B.6.1. Transport of the systems to Cadarache and installation on the manipulator
B.6.2. Cutting tests on non-radioactive representative models
B.6.3. Tests with samples prepared under B.S.

B.7. Final evaluation and recommendation (all)

C . PROGRESS OF WORK AJ'ID OBTAINED RESULTS

Summary of main issues

The work carried out in 1990, was connected with four main aims, in relation to the topic of work programme packages B.1, B.2, B.3, B.4, B.S.

. Firstly the d istribution of functions between the different partners involved in the contract, the definition of the models for i”lnal tests, the specifications and main features of the necessary equipment were d rawn up.

. Secondly the following working steps have begun

Development of the plasma torch, adaptation of the moving device and test tank.
Development of the plasma saw, the consumable electrode tool and the cont rol systems.
Development of control systems for sensor-controlled piloting of the handling system *for* the tools and the process parameters.
Preparation of radioactive samples.

Progress and results

1 . Prelimarv tasks (B.1)

With regards to the technical annex of the CEC contract, the dist ribu tion of functions and tasks was defined in close cooperation with CEA Cadarache, lW Hanover, RWTH Aachen, CEA Saclay, in order to specify the main features of the necessary equipment.

The models to cut at Cadarache during final tests come from the Rapsod ie reactor, which is in its decommissioning phase.

These models represent the least accessible points encountered in the reactor and some of them are shown in Figures 1 to 3.

As regards each model and the conformity to the cutting capability, we h ave made a selection of adapted tools for each model to cut.

Also associated to the above, the control of the motor system was defined wit h a selection of manual, semi -automatic or automatic control for each displacement ax is and rotational movement.

The distribution of the control system is given in Figure 4.

Regarding the requirements for final tests, specii”lcations of the sensor system fo r measurement and d istance guidance, detection of holes in the work-piece, recogn it ion of edges, were drawn u p.

Concerning the generated cutting effluents, specifi cations for ventilatio n a nd filtration, measurements of aerosols, suspended particles, sed imented d ross, at t ached slag. gas, were defined.

2 . Development of the plasma torch, adaptation of the moving device and test tan k (B.2)

As regards the accuracies required to position and move the tools in these thickness conditions, we have to design a new manipulator and motor system.

This design phase has begun.

Furthermore the dimensions and shape chosen for final tests have led to the realization of a tank greater than our current test tank ; its designing has also begun.

A i”lrst investigation concerning the improvement of the capabi'ity of the nuclearized torch has been made.

3 . Development of the plasma saw, the consumable electrode tool and’ the cont ro { systems (B.3)

The i”lrst cutting tests will take place in a water basin with a volume of 18 m" and a working area of 4 m x 2 m x 1.5 m (1 x b x h). To qualify the tools and con t rol systems

for cutting in 5 m water depth tests will then be done in a basin which is 5 m in diameter and 5.25 m in height.

- 34 -

The consumable electrode tool :

Stainless steel tubes **(88.9** x 1.5 mm) were successfully cut with the consumable electrode torch in a water depth of 5 m with a cutting speed of **400** mml min check and a current of **900** A using a stainless steel consumable wire with a diameter of 3.2 mm. The equipment for these cuts **was a 100 kW welding rectifier** which supplies a max. current of **2500** A at 40 v.

With the same power source **100** mm thick stainless plates could be cut with a cutting speed of **135 mm/min** and a current of **2500 A** using a mild steel consumable wire of **4mm in diameter. Refuting to these** results it may be necessary to operate two **rectifiers in parallel in order to reach greater sectile thicknesses.**

A sketch of the consumable electrode tool is shown in figure 5.

The plasma saw-

A sketch of the working principle of the plasma saw torch is shown in figure 6. Its **main characteristic** is the slim rod with the nozzle **positioned rectangular at the tip.** This rod immerses into the kerf during the cutting process as shown in figure 6. To **obtain a kerf** wide enough for it to dip in, the torch is rotated by approximately 60° around its **vertical axis at the top and the bottom dead center** of the up and down motion. The motoring device required for the plasma torch is be g designed.

The equipment for the plasma saw is a 30 kW power source. A **mixture** of argon and **nitrogen is** used as plasma gas.

The control systems

Promising results were achieved using a small CCD-Camera (12V DC) during **preliminary cutting tests with a plasma torch** and the consumable electrode tool. The dimensions of this camera are 50 mm x 60 mm x 60 mm (1 x b x h) and it is equipped with a selfadjusting iris. For underwater use it is mounted in a special water- **resistant housing.**

As **there** occurred some difficulties in positioning the tool to the workpiece in all **three dimensions with the camera** in a fixed position in relation to the torch holder it seems to be advisable to use a second camera. This **camera may either be fixed** to the torch holder or be manually movable around the torch.

4 . Development of control systems for sensor-controlled piloting of the handling system for the tools and the process parameters (B.4)

Inductive sensor :

Based upon tests made in the former Decommissioning project an inductive sensor for distance measurement was selected and proved the function of the device in the new **application.**

Investigations about the possibility of hole detection beared some problems because the diameter of the used sensor was too ereat. Therefore a sensor with a smaller diameter vi I I be t es ted.

Process control

The cutting process can be divided into several parts of automatic, semi-**automatic** and manual tasks under control of the operator. These tasks are Location of the **torch to the starting point** of the cutting trajectory by manual or semi-**automatic operation,** definition of cutting direction or ending point :
Select all power source parameters such as cutting current and gas flow by manual operation ;
Select manipulator parameters such as distance between torch and workpiece (respectively between sensor and workpiece) and **travel speed** (manual operation) ; Detection of the edge of the workpiece (automatic operation of manipulator control unit and inductive sensor) ;
Automatic teach-in operation for recognition of workpiece exact position, workpiece orientation and workpiece thickness along the **cutting trajectory ;**
Automatic return of the torch to **the starting** edge of the workpiece in correct

cutting distance ;
Switch on plasma gas, cooling water and pilot arc (manual operation) ;

- 35 -

Start the cutting arc at the workpiece, wait until workpiece thlckiiess has been bitriir‹l th rough and start motion (manual).
Motion will be cont rolled automatically, the operator has the possibilit y of an on -line correction of process parameters and of in term pt Ion of t he process in case of malfunction or reaching the end of the t rajectory ;
Turn off all systems, i.e. gas fiow and plasma power source (manual o per at ion)

Interfacing :

For the purposes of controlling the complete unit a microcompu ter systern w'ill be used. Figure 7 shows the schematic structure of the control system and interfaces.

The followlng interfaces wlll be developpe‹1 fo r the cont rol of t he d ifferent subsystems :
Interface for control of motors
Analog interface for the inductive sensor
Analog or d igltal interface for the lW ultrasonic sensor
User interface for control of the iv hole s3'stem

5 . Preparation of radioactive samples (B.5)

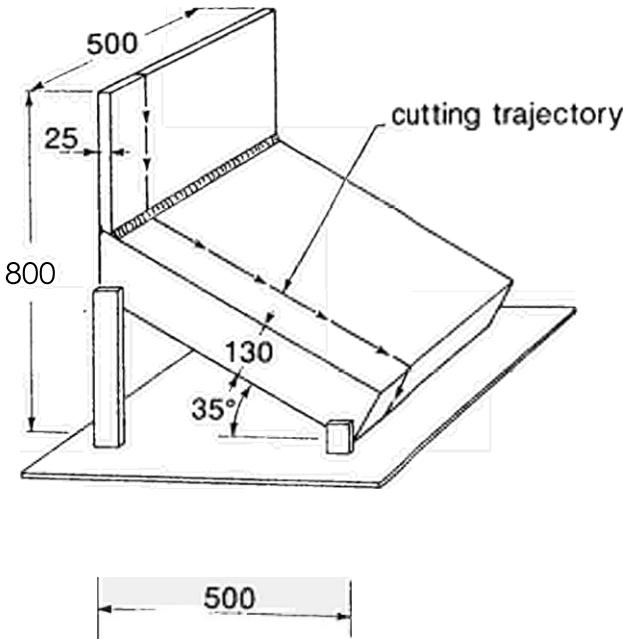
Radioactive samples that come front d isinant ling of nuclear installations a re we l come .

These radioactive samples hax'e to be : Free of in **emitters** :
If possible, with no loose contamination :
Within a radioactive range i.e. not too cont aminated (or irrad ia ted) in ord er to hav'e n o rad ioprotection problems and no liquid waste t reatment but su fficien tly con tarn in ed (or irradiated) in order to get significative radioactive measu remen ts fo r the d i fferen t secondary emissions.

Thus, for example, according to pres'ious experiments within t he seco nd programme of the CEC about decommissioning of nuclear installations, it wc›u l‹l be necessary to have a surface contamination between 10^2 and 10' Bq. cm‘“ fo r $^{1')7}$ c s.

054
Q 1 10

500



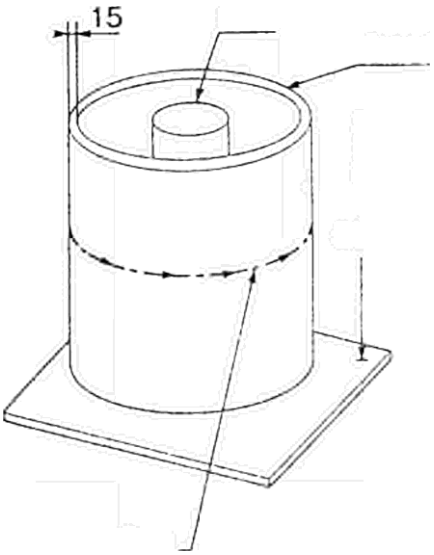


Figure 1: Vessel bottom head

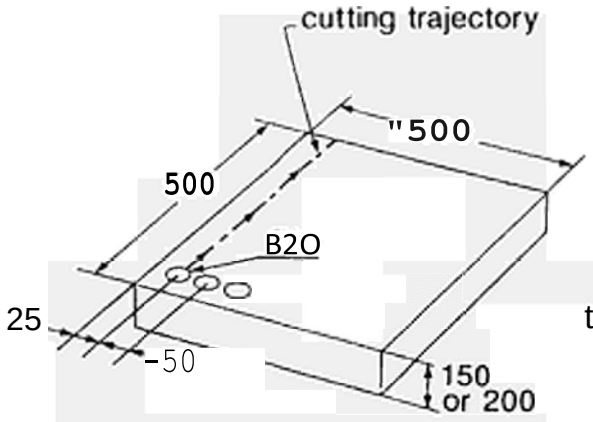
which is with variable thickness and requires change

of tool orientation during cutting

cutting trajectory

36

Figure 2: Stud and spaces to cut to separate the diagrid from the vessel bot tom heacl



!! gure 3: Diagrid

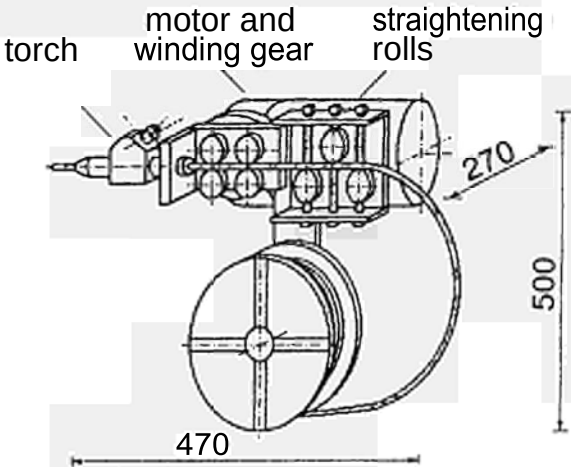


Figure 5: Sketch of the prototype consumable electrode

CEA Cad

tool

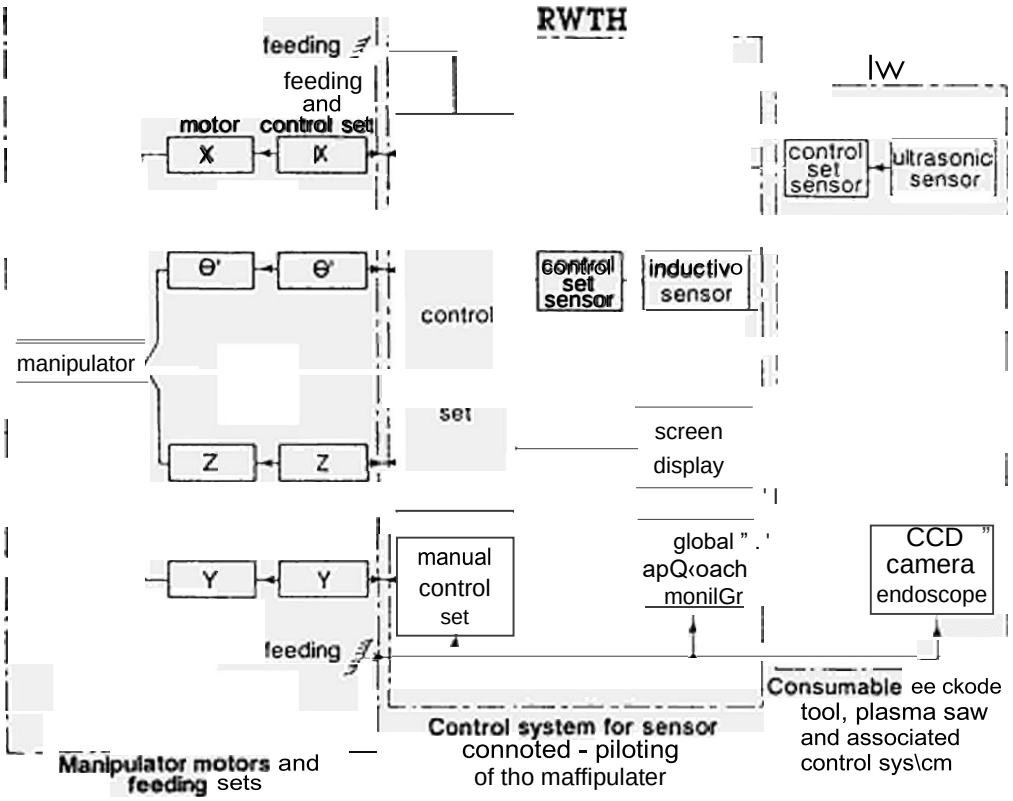


Figure 4: Distribution of tne control s;'siem

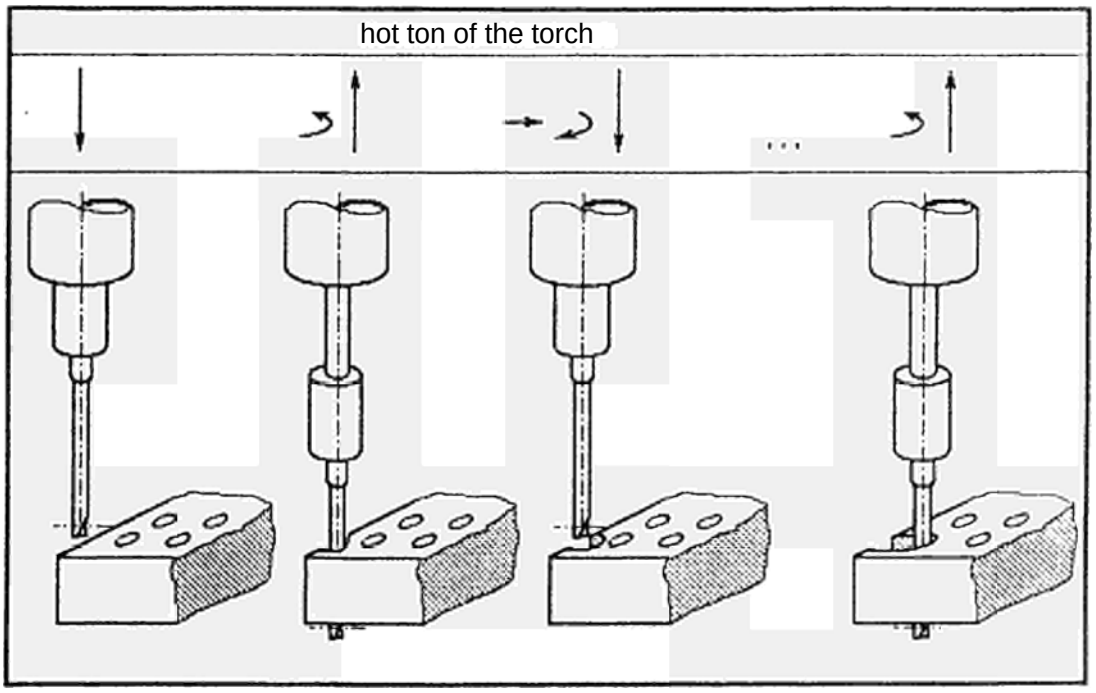


Figure 6: Working principle of the plasma saw

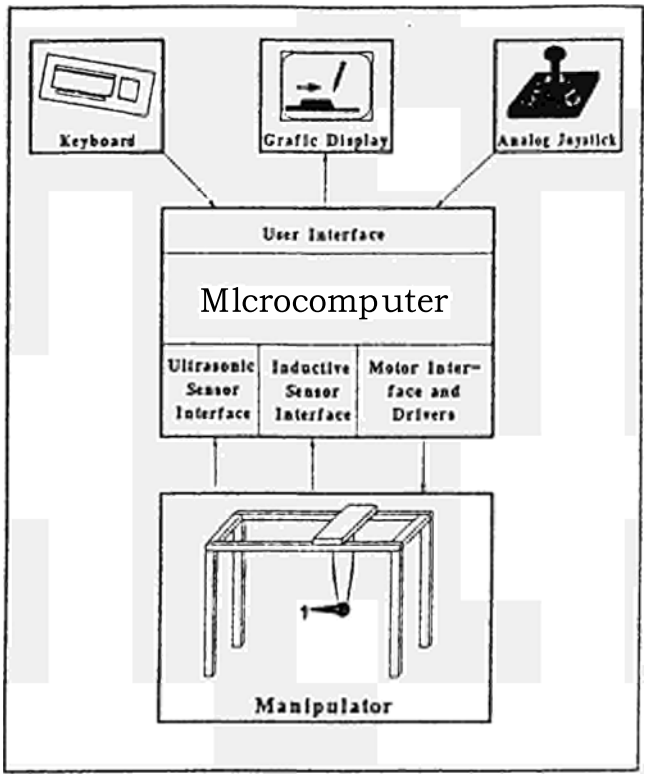


Figure 7: Structure o/ the control systems and inter faces

3.6. DEVELOPMENT OF A...PLASMA ARC TORCJ4 AND CONTRO ONITORING TECHNIOUE FOR THE INTERNAL CUTTING OF SMALL BORE PIPEWORK

Contractors: AEA Wind
Contract No.: FI2D-1D26
Work Period: July 199() - June **1993**
Protect Manager: M T CROSS, AEA Wind.
Phone: **44/9467/72432 Fax:** 44f9467/28023

K OBJECTIVE AND SCOPE

During decommissioning of nuclear facilities, small bore pipework needs to be cut remotely up to distances of 10m with access through the top of the pile cap. Often, due to the close packing of the pipework, the cutting operation must be performed internally through the bore of the tube. In the absence of direct viewing and manual access, there is a requirement to develop techniques for the cutting process and methods for monitoring and remotely controlling its operation and ensuring its effectiveness. The plasma torch process has been selected as the cutting method based on economic considerations and on its reliability and effectiveness in remote and manual operations.

The objective of the project is to develop:

- techniques based on non-contact sensors which can monitor and remotely control the progress and effectiveness of the cutting process;
- a small plasma torch capable of being inserted in the bore of < 50 mm internal diameter pipework with remote deployment (up to 10 m distance) under automatic control;
- the deployment system which can be located on the pile cap, positioned above each pipe in turn and lowered to a predetermined depth to perform a complete circumferential severance of the tube in one pass.

The work will include cutting trials of the complete system in a full-size mock-up of a reactor gas manifold.

The AEA Northern Research Laboratories will take into account the experience gained elsewhere and particularly at the "Institut fur Werkstoffkunde der Universitat Hannover" on plasma arc torch cutting and its control/monitoring.

B. WORK PROGRAMME

B.1. Literature sdue t be **plasma cuttin bina on fo** this application. BE Torch adaptanon for remote denlovment and automatically controlled rotation

BE. Examination of the cutting parameters on **reormentative pipework**

B.4. Control svstem developments: monitoring technique and feedback sYstem will be designed, develomd and interfaced for automatic controL

BE. Preliminaw tmtine of the deployment wstem in **small-size mock-up**

B.5.1. To test the workability of the remote deployment system.

B.5.2. To check the feedback control system under remote operation conditions.

B.5.3. To optimise the equipment to commercial standards.

B.6. To of e p t up to evaluate the optimised ip a representative ‹Jeco**mmissioning environment.**

B.7. final evaluanon including specific data **on sts and radiological impact on** work force and **working area. worline time and secondaw waste arise**

- 39 -

C. ProRress of Work and ObtainedResults

Summary of main issues

Significant progress has been attained in the early phases of this contract following finalisation during September 1990. The Literature Review part of the work(Task j has now been completed and has suggested a range of sensors which could be adapted for control of the cutting process. An air plasma torch is considered to be the most suitable technology for a compact torch to be deployed in a small bore tube geometry. Work has now started on the development of an acoustic sensing monitor for controlling the progress of cutting and, of allthe sensing technologies reviewed, we consider this technique to offer the best prospect for future development (Task B4j.

Some preliminary testing has now been carried out using a prototype compact plasma torch to sever a range of mock-up tube sections. These tests have been encouraging and, on this basis, a multi-axis deployment rig has been designed for placement of the torch at distances up to 10 m. Tenders have now been invited for construction of therig.

Progress and Results

1. Literature survey (TaskB1.)

The Literature Survey has included a systematic search through an Engineering Indexes Computer Database, containing details of Journal Articles published worldwide. Reference to Plasma Arc Cutting were found 172 times, going back to 1976 and the titles and synopses of these articles were obtained. From this information, a number were selected as being relevant to the task in hand and copies of the full article obtained. These have been grouped into the following areas.

(a) Articles discussing the general principles and merits of Plasma Arc Cutting. [ifteen articles of this nature have been collected.

(b) Articles which discuss the use of Plasma Arc Cutting in Decommissioning Projects. Plasma Arc Cutting has been used at Three Mile Island and on the Japanese JPDfl. A total of nine articles come into this category, which together with the proceedings of the CEC Conference on the Decommissioning of Nuclear Installations in October 1989 and our own experience at Windscale have provided valuable background information.

(c) Articles which focus on a particular aspect of the Plasma Arc Cutting process which could form the basis of a control mechanism. These include such topics as voltage calibration, kerf formation etc. Of particular interest has been a series of articles by scientists at several Russian Research Institutes. Their research seems to have concentrated on the physical processes taking place during cutting, particularly in the arc forming chamber. Eighteen such articles have beencollected.

A Patent Survey has also been undertaken. In a similar exercise to the Literature Survey, a search of Patent Indexes was performed, covering worldwide patents going back to 1963. A total of458 references to Plasma Arc Cutting were found. The search field was then restricted to the Control and Monitoring of the Plasma Arc Cutting process. A total of 110 references were found and a list of these obtained. This list is quite extensive and a good indication of previous work in this area.

Reports produced by RWTH Aachen and the “Institut fu- Werkstoffkunde” at ”Universitét Hannover" under previous CEC contracts have been received.

Part of the purpose of the Literature Survey has been to determine the types of

Plasma Sets and Torches which are commercially available, to

-40 -

enable selection of a Plasma Set suitable for this application. Considering the need to adapt a torch for operation within a small bore pipe, an air plasma torch has been identified as the most suitable for modification and has now been purchased and preliminary tests performed (see Section 2).

The Literature and Patent surveys have suggested that the following parameters are available for monitoring and control purposes: current, voltage, gas flow, stand-off distance, cutting speed, material thickness. The output current and voltage of the plasma set can be monitored by circuitry connected within the set. Similarly the Gas Flow rate can be measured by a flowmeter adjacent to the plasma set. Types of sensors which have previously been employed for the parameters measured external to the set and adjacent to the cut are inductive, ultrasonic, tactile and optical. Restrictions on the type of external sensors that may be employed are determined by the nature of the environment, particularly the excessive heat generated by the plasma arc, and the physical space available for sensors to be positioned internally within the pipework being cut.

However, it has been realised that there is a distinct difference in audible sound emitted by the cutting process when penetration of the material is achieved. It is intended to investigate this effect further as a possible parameter that could be monitored and incorporated into a control system (see Section *4).* It is necessary to ensure that the commercial plasma set purchased will be suitable for adaptation for the incorporation of control equipment. It is envisaged that the standard parameters of plasma set output current and voltage will be monitored and so there should be sufficient space within the control unit for the insertion of extra component boards.

2. TorchAdaptationDesi Study (TaskB2)

A design study has been undertaken to determine the method for attaching, rotating, suspending and positioning the torch for accurate location inside the small bore pipework. Initially, different types of plasma cutting systems were assessed to determine a suitable plasma unit with a torch head capable ofmodification.

The survey of equipment has shown that gas plasma torches are too bulky to fit down the inside of pipes of bore less than 50 mm. This is because they require a higher operating current than air plasma torches to cut material of the same thickness which means their torches need to be larger. As an example, a typical air plasma set requires 30 Amps to cut through 6 mm mild steel, whilst a gas plasma set requires 100 Amps. An air plasma unit has therefore been selected as being suitable for cutting through small bore pipework. A specific torch has been chosen for its simplicity and compact design and has been modified in order to permit access to small bore pipework.

The design study has revealed that the position of the torch head will have to be made adjustable in order to maintain a fixed distance between the nozzle tip and the pipe surface and also to allow the same torch to be used for different bore pipework.

A solution to this problem is being examined based on the use of a spring loaded coupling between the torch head and the rest of the deployment system which forces the torch nozzle to make contact with the inside wall of the tube during the cutting operation thus ensuring a constant stand-off distance.

Following a detailed analysis of the requirements for a remote deployment systen, a plasma More h dep loyment r ig capable of four degrees of freedom in pos i £ ion ing the torch (x, y, z , 8) has been des igned . The r ig cons is is of a supporting f ramework cons mucked in conj unct ion wi th l inear

slides which will be used to support and position a suspended plasma torch over the WAGR 'hot box' (hot gas manifold). Prior to active deployment, a series of optimisation trials to prove the workability/remote handling of this equipment is planned (Tasks 85 Bb.). Tenders have now been issued for construction of this deployment rig.

3. Rxamioation of Cutting Parameters (Task)

The plasma set which has been selected is manufactured by Econocut and has a fixed output current of 30 Amps. Initial cutting tests have been carried out on single lengths of tube, both insulated and non-insulated. A rotary stepping motor has been used to vary the cutting speed, and an optimum cutting speed of three quarters of a revolution per second selected. It was discovered that increasing the speed beyond this point meant that full penetration of the insulated type of tube was not achieved at the point where the insulation overlapped.

Beyond this, no further investigation has yet been done on the tolerance of the system to variations in the cutting parameters, or an assessment made of nozzle wear and damage. This is scheduled forlater on in the programme.

4. Control System (Task B4j

The requirements of the control system have been identified. These inc lude : -

(a) optimising the operation of the plasma cutter, by monitoring and controllin B the cutting parameters, so as to reduce dross production, fume and spatter
(b) ensuring the effectiveness of cut
(c) detectin B nozzle obstruction or damage

In addition to the monitoring techniques considered by RWTH Aachen under contract FIID-0039, some investigation using acoustic monitoring and non-contact sensors has been made. This has been carried out on a Plasma Arc Cutting facility at AEA Springfields.

The results so far appear encouraging and frequency spectrum analysis of the monitored signals suggest specific frequencies exist when satisfactory penetration of the metal is achieved with severe attenuation of these frequencies when penetration is lost.

5. Prelimina testing of the deployment system in a small-size mock-up (Task j

An experimental prototype of a small section of the WAGR hot box (Bas manifold) containin B tubing for test purposes has been designed. No deployment t r ials have yefi been conducted.

DEVELOPMENT OF A STEEL CABLE TO CUT HIGHLY RHINFORCHD CONCRETE WITH MINIMISED WATERCONSUMPTION

Contractor: Diamond Service
Contract No.: *n2c›-0027*
Work Period: September 1990 - May 1992
Proiect Manager: A BOSELLI
Phone: 39/523/822 447 Fax: 39/523/822 630

W **OBJECTIVE** AND SCOPE

The project is aimed at the development of a steel cable charged with diamond pearls with particular cutting qualities, considerable mechanical resistance and minimum consumption of water or other cooling mixtures. The cable should be particularly suitable for cutting highly reinforced concrete structures of nuclear installations. The main objective is the control of secondary waste generation (cooling and severed concrete) during the cutting operations. The cuts can be carried out at various distances from operator to structure and therefore offer considerable security and protection of work force. The cutting time and the derived radiation exposure to operators will be evaluated on a uncontaminated concrete structure.

The contractor will carry out cuts on concrete structures of a USSR nuclear plant; the obtained results will be compared with those obtained within the framework of this project.

B. WORK PROGRAMME

Development of a **is d ond pearl**

BE Development of suitable materials for the cable vulcanisation

BE. Preparation of the tmt mmk-up and of a reprmentative concrete block

B.4. Selection and improvement of a suitable steel cable

BE. Assemblinr of cable comfxinents (light steel cahle. diamond tx:arls, sprin and spacers)

B.6. Cutting tmts on non-contaminated concrete structure

B.7. final evaluation. taking into account cable consumption, sts of the technique. c‹xiling water consumption. secondaw waste arisines. radiation extiosure, and a comparison with the cuttina work carried out in the USSGL

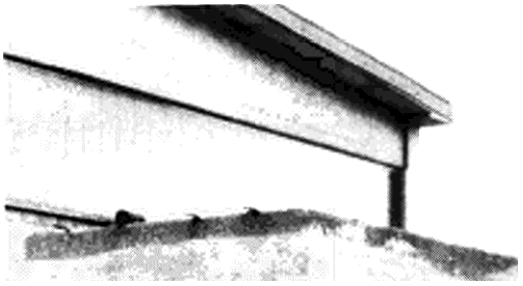
$$- \; 4S \; -$$

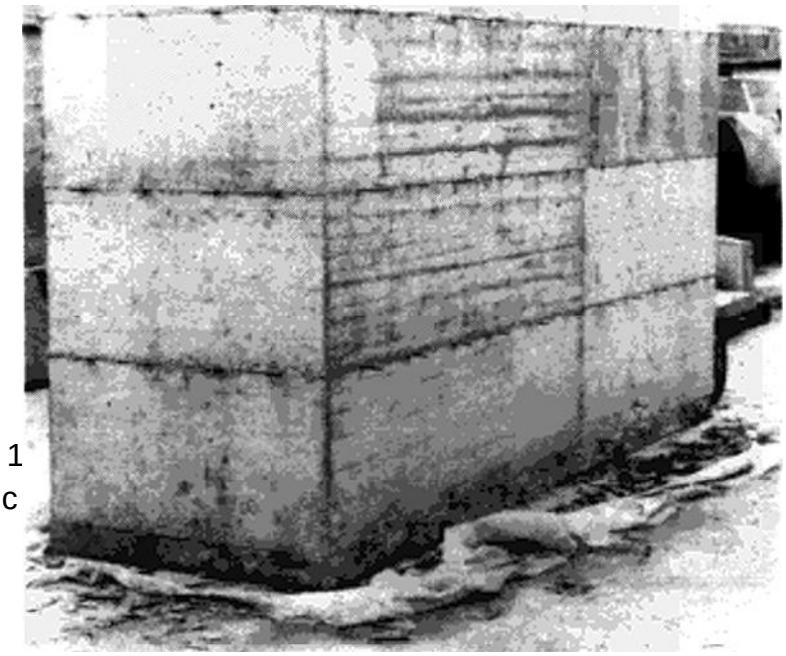
c rRocnnssor wonxaxooeraemonnsuzvs

Summary of main resu

During the period from September 90 to December RI, some Diamond pearls with various physical and mechanical features were manufactured. Furthermore, a highly reinforced concrete structure on which the cutting tests will be carried out has been built. During this first period, no considerable problems were encounterecL

1. Development of a hinbdr is a ond pearl (B.1.)
   Before starting this programme, the diamond pearls for cutting concrete were made of synthetic diamond 50/60 Mesh or 40/50 Mesh grading. For this new project, a synthetic **diamond 30/40** Mesh type SDA lfD S was used. It has the advantage over the previous one of a very high resistance both to mechanical impact and thermal shock, thus allowing the increase of the cutting speed.
   The **diamond** powder has been mixed with particular bonds **having** the twofold function of being anti-abrasive and resistant to possible rise of the temperature due to poor water cooling during the cutting operations.
2. Preparation of the test mock-up and of a representative concrete block (B.3.)
   For the cutting tests, a highly reinforced concrete structure with appropriate grading and strength (RBK 350) was built up (figure 1). The iron-cement ratio is Kg. 1850/c.m. Information about the cutting results will be given in the next progress report.





F gu r e 1
z e s t oc c

3fL **ASSESSMENT** OF STATE-OF-THE-ART CO LASER TECHNOLOGY AS AH **IMPROVED DISMANTLING TOOL**

Contractors: AEA Culh., DLR
Contract No.: Stuttgart FI2D-0028
Work Period: September 1990 - August **1992**
Coordinator: J H MEGAW, AEA Culham
Phone: **44/235/46 42 15** **Fax: 44/235/46 41** 38

W OBJECTIVE AND SCOPE

The main objective of this project is to carry out a laboratory-scale experimental investigation of the capabilities and potential advantages of carbon monoxide (CO) lasers, compared with carbon dioxide (CO_2) lasers. Previous studies on CO_2 lasers for decommissioning indicate that they can operate as elegant and flexible tools, but there are limitations with regard to cutting performance, and a need for articulated mirror-based beam delivery systems. The present project is motivated by: reported Japanese results indicating CO laser cutting performance significantly superior to that of CO_2; and the potential for use of optical fibre beam delivery at the shorter wavelength (5 qm cf 10.6 ptm).

The partner organisations (which are currently engaged in developing CO lasers in the power range up to approximately 1 kW) will carry out complementary investigations, using CO and C_2 beams, on steels, concrete and graphite concerning: the nature of the beam-workpiece interaction and how it differs at the two wavelengths; assessment of the respective cutting capabilities. It is expected that the work will: provide the sole European source of such information; enable quantification of possible technical and economic advantages of CO lasers for decommissioning; provide information on the parallel Japanese programme (where it is reported that CO lasers of > 20 kW are under development); make recommendations on a strategy regarding possible future use of CO lasers for decommissioning and commercial exploitation thereof.

The responsible partner for work on structural stccl and graphite and for work on stainless steel and concrete will be AEA and DLR, respectively.

B. WORK PROGRAMME

B.1. Assmsment of beam-workpiece interaction for CO laser and comparisons with CO, laser

BE Assmsment **of CO laser cutting capabilitim and comparisons with CO, laser (AII)**

BE. final evaluationshowineeuantifieddifferencm in materials-prix:msinzcapabilitim of the two lasers. specific **data on sts. secondary waste produced and radiological impact on workforce and working** area (AII) °

- 45 -

C. PROGRESS OF WORK

SummaryofmalnIssues

The opening four months of the project has been a pertod of schedulmg and preparation. m whlch there has been as yet a very low commitment of resources. but whtch nevertheless contained the flrst joint meeting of the collaborators where the experimental programme has been dlscussed In detall, agreed and planned. Notwithstanding a somewhat delayed start to experimentation. progress 1s stlll fully consistent with the planned overall tlmespan of lis months for Task B.1.

Piannlng

Beam-workpiece mteractlon for CO laser, and compartsons with CO laser

The followlng conclusloris and plans emerged from the first Project Meetmg at DLI InlHal experiments wtll concentrate on the role of the couplmg of the CO and CO beams to the kerf wall, and on the role of plasma formation. As regards the former, analysts of laeer-processed samples wlll feature careful characterisation of the kerf walls and In particular the mclmatlon of Its leading face as determined In a suddenly-stopped cut. A small amount of theoretical work wlll be carried out with the aim of modelling the energy deposltlon in the kerf as a function of depth, since thls should enable predlctlon of the cut shape. The calculation wlll be based on esttmation of Fresnel abeorptlon for the relevant local angle of mcldence, where thls wtll vary due to beam divergence and kerf mchnatlon. As regards the role of plasma In the couphng of beam energy. the methodology wlll employ what 1s expected to be a sensltlve method for quantlflcation of plasma effects (and thelr variation at the two laser wavelengthsl vtz: use of an ambient gas mlxture of helium and argon. These reepectlvely reelst and promote plasma formation (lonlsatlon potentials 24.6 eV and liS.8 eVJ so that variation of the relative proportions will provide a controlled method to study plasma inltlatlon and plasma absorption.

3.9. CUTTING OF CO, PRIMARY CIRCUIT PIPES OF GJG3 REACTORS USING EXPLOSIVE CHARGES

Contractors:	CEA Valrho, COMEX, EPC
Contract No.: Work Period:	**Fl2D-llfl36** September 1990 - April 1992
Coordinator:	Ch **LORIN, CEA/DCC/UDIN** Phone: **33/66 79 63 04** **Fax: 33/66 79** 64 32

A OBJECTIVE AND SCOPE

The projcct is part of the dismantling of thc primary cooling circuit **(CO,)** of the G2/G3 gas-graphite reactors, composed of valves, blowers and tubes (diameters 800, 1200 and 1600 mm with respective thicknesses of 10, *15* and 20 mm), using explosive charges. It includes technical studies, experimental investigations and tests at industrial scale, carried out under real radioactive conditions.

The innovation of this project is the use of shock waves, produced by the explosive charges, to remove the inside contaminated oxide layer of the tubes.

The use of explosive charges seems beneficial because allowing to cut remotely large activated or contaminated items under improved protection and safety conditions for workers and with a minimum of secondary waste arisings.

The data output will mainly be related **to:**

- thc necessary time to carry out dismantling operations using explosive charges and their respective costs,
- the safety and radiation exposure of personnel involved in the operations,
- the effectiveness of shock waves for decontamination purposes.

B. WORK PROGRAMME

Assmsment of basic cutting parameters

Definition of cutting power of dihedral-shaped charges (EPC)

Establishment of the agreement files (AII)

Preliminary test series on flat steel plates (EPC)

Calculation of the minimum quantity of explosive for each thickness (EPC) **BE Pre-test series with bounded** steel same! . **(sim atin t tio (EPC) BE.**

Definition of pwotechnic devicm (HPC, COMEX)

B.4. Detailed **engineering studv of validation tmts**

B.4.1. General assessment of the test conditions (COMEX, EPC).

B.4.2. Definition and design of auxiliary equipment required during cutting operations (COMEX, EPC)

B.4.3. Selection of representative items to be cut (AII)

BE. Validation tests on G2/G3 tubm

B.5.1. Definition of test procedure as needed for agreement by authority (CEA)

B.5.2. Preparation of the test area (AII)

B.5.3. Validation tests: 27 cutting operations on 800, 1200 and 1600 diameter tubes) (AII)

B.6. **-inal evaluation of all relevant data collected, e.g. specific** data on costs radioactive joJj dosm. working **time and secondary waste arisings** (AII).

- 47 -

The three partners, C2A/UDIN, C0M2X mnd NITROBICKFORD have already met three times since early November. The main directive lines of work have been defined. Three types of pipes have been chosen to be treated in the zone number 4 oF G2 reactor, at the level of the C02 turbo-pump nl. This area has to be isolated before beginning the operations, but it will be possible only during 1992. The contamination end irradiation levels in the involved pipes end in the working area are known. The confining will be supplied by a depression inside the pipes. It is expected to be reinforced at the time oF the external explosion.

An appropriate cutting device exploding around the pipe has been designed for each size.

Decontsminating end cutting tests will continue in 1991. They should allow to record stresses during en explosion and to evaluate the efficiency of decontsminating by explosive means. The study of the environment of pipes, mnd the elaboration of saFety files have been initiated.

1. (B. 1, B. 2,B.)

1.1.

The cutting device is a plastic ring supporting a circular hollow-shaped charge. The ring is divided into sectors which are filled up with an explosive (NITROROC). The internal side is made of a dihedral concave metallic part.

Three tests series of 27,9 and l§ shots have been pursued to define :

- the metal, englemndthickness of the dihedral part,
- the most efficient kind of NITROROC: liquid or gel,
- the width, height and "stand-off" of the ring section.

1.2 (for a thickness of steel of l§ mm)

Dihedral part :	metal	Copper (Cu)
	sngle	90’
	thickness	1.§mm
Section of the ring:	width	20 mm
	height	2é mm
	“steadoff"	10mm

Minimal charges for flat steel plates :

thickness 10mm needs 310 g/m of Nitroroc “ 20 mm needs §2O g/m of Nitroroc “ 2§ mm needs 1100 g/m of Nitroroc

The liquid Nitroroc gives slightly better results than the gel. Although copper is more efficient for the dihedral part, steel will probably be used. Indeed copper is a poison for the re-melting of cut **steel. See figures** 1 end 2.

2. (B.8.)

2.1. 3elertlRD

An experimental area has been specified in the zone number 4 of G2 reactor, at the level of the C02 turbo-pump number 1.

- 48 -

This area contains samples of the following primary pipes, which have been chosen for the tests.

Diaineter (oia)	Thickness (mm)
1600	2§
1200	19
80o	13

There are both aspiration and exhaust pipes, hanging at different heights.

2.2.

This zone isclassified in the category "2B“ (0.75 to 2.§ mrad/h i.e. 7 5 to 2§ qGy/h, with risk of contamination) end will become "2C“ during the trials (effective contamination). The zone is easily accessible for preliminary studies.

The confining system will be based on a dynamic depression inside the pipes : i.e. aspirationsndfiltration(electrostaticfiltersandveryhigh efficiency filters).

2.3.

Here contamination consists in a graphite layer on the lower part inside the pipes. It can be oily in the exhaust pipes. Contamination is due to Co6O(9b]) end Cs137(hX) end is valued at 100 to 2000 Bq/cm2. The irradiation in contact is valued at 0.§ to 10 mrad/h (§ to 100 pGy/h) with hot points at 10 to §0 mrad/h (100 to TOO pGy/h). The irradiation at a distance of 1 meter is below 1 mrad/h (10 qGy/h).

Contamination will be measured before end after cutting so as to value the efficiency of the method for decontaminating. It will be particularly paid attention to the scattering of aerosols at the time of explosions.

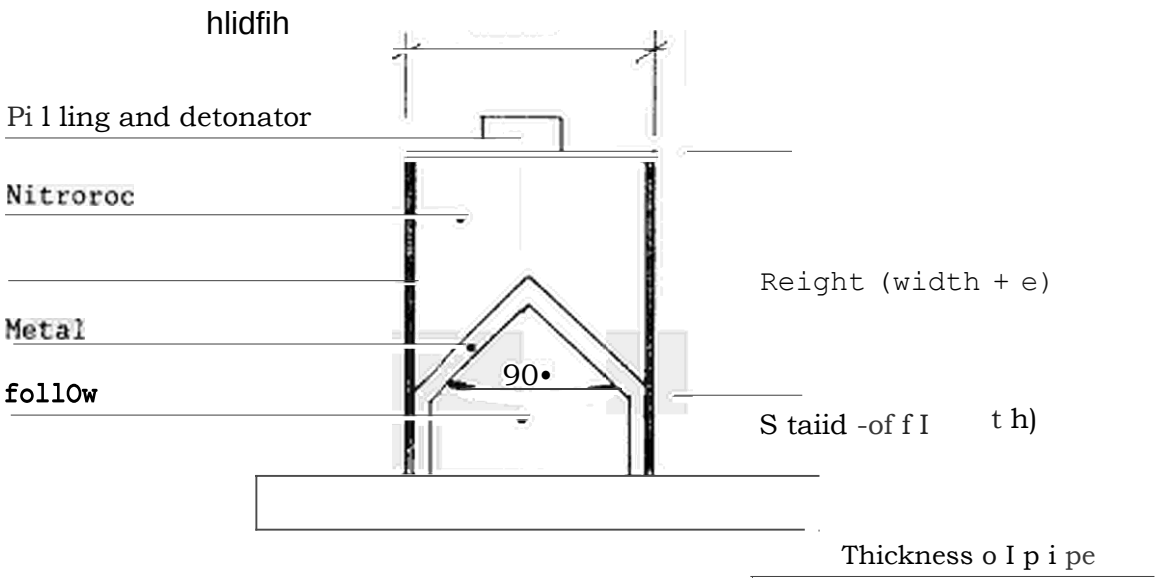
Pre-tests will be pursued at Saint-Martin-de-Crau toobserve several parameters.

3

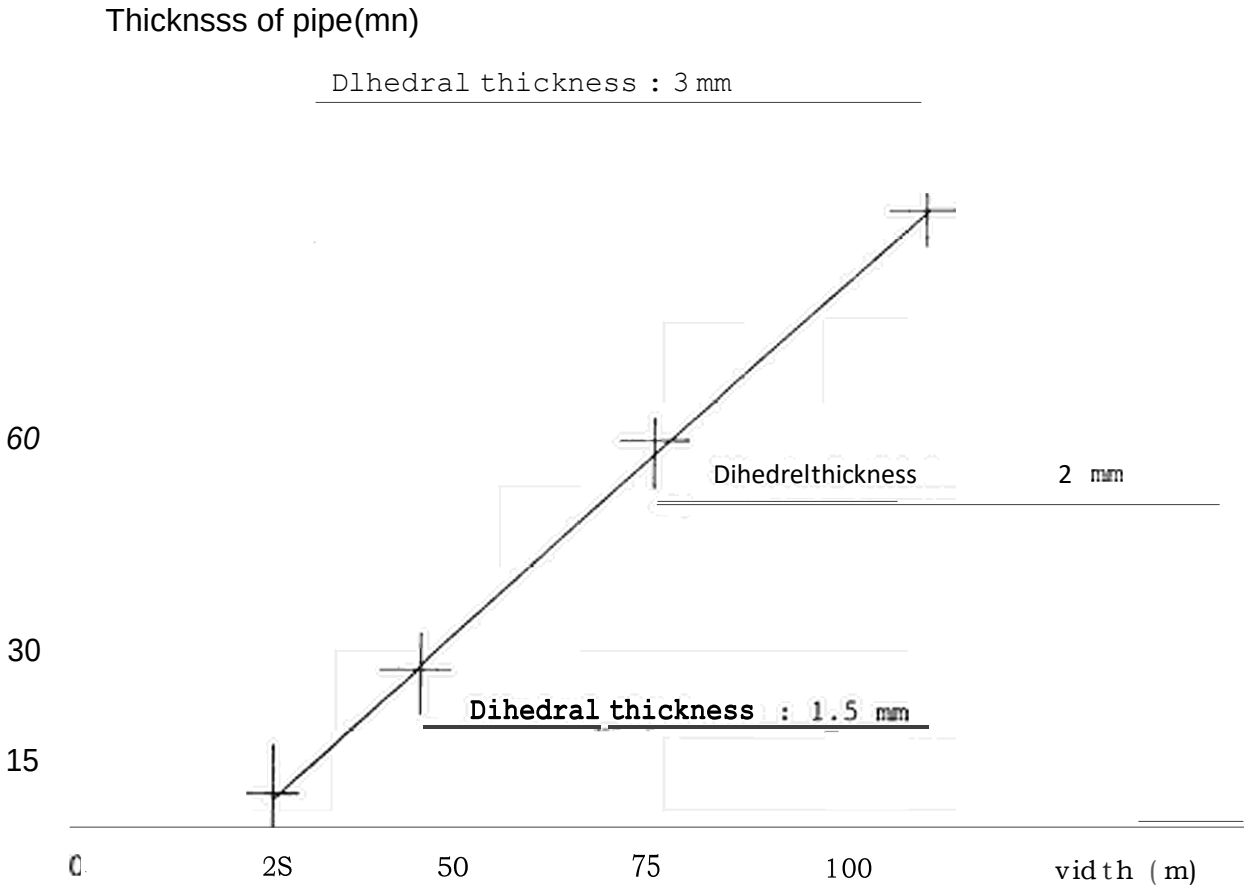
At the end oF 1990, the zone and the conditions for the industrial phase have been specified. A cutting device using explosives hasbeen designed. Theworkcontinueswith thestudyoftheenvironmental pipesand their supports. Tests will also be pursued to value the stresses end pressures during en explosion.

The First test in radioactive zone will take place in March 191 on an isolated pipe with contamination. The partners end especially COMEX and CEA, will soon have to elaborate the safety Files.

The industria1 phase is expected to begin in 1992, after the dismantling oF surroundingzones.



F lgure 1 : RING SECTIOtl



P1gure 2 : £XTRAPOLATTON

- 5O

4. AREA No. 4: TMENT OF SPEGFIC **WASTE MATERIALS: STEEL, CONCRETE AND GRAPHITE**

In the dismantling of nuclear installations, large amounts of radioactive metal, concrete and - in the case of gas-cooled reactors - graphite will arise. This waste must be suitably conditioned for disposal or recycling. The area has been strictly delimited to preclude overlapping with the Community research programme on radioactive waste management.

B. Subjects of the **rmearch performed under the previous programmes (1979-&I)**

Research work performed mainly related to:

the treatment of dismantled material such as steel, copper and brass by melting with a view tti its ptissiblc recycling/reuse; the reduction tel‘ its vtilumc; its dcctintaminatitin (c.g. eliminati‹›n ‹›l‘ uctinidcs);

dcvelopment and assessment of techniques mm coating mctal and concrete parts in order to

immobilisc surface contamination; asscssmcnt of treatment tcchniqucs for radioactive

concrete;

comparative assessment of various modcs of treatment and disposal of radioactive graphite; development of a conditioning technique for radioactive graphite bricks for shallow land disposal.

In all these investigations, due attention has been paid to the necessity of adapting treatment techniques to final waste destinations.

C. Programme 1989 to 1993

Melting of very low-level radioactive steel scrap from Light Water Reactor components, to produce new nuclear components, is already becoming industrial practice and is not expected to need further research. Further work is required, however, in relation to steel scrap originating from other types of nuclear installation, e.g. alpha-contaminated material, and non-ferrous scrap.

Further development is also needed for concrete and graphite waste,

i.e.: volume reduction of contaminated/activated concrete;

metallic coating of graphite parts by ionic deposition to fix radionuclides;

- recycling of the reinforcement steel in concrete.

D. Programme implementaBon

At the end of 1990, four research contracts relating to Area No. 4 were at the stage of execution and one contract was at the stage of negotiation.

- 51 -

4.1. DEVELOPMENT OF A PROCESS FOR VOLUME REDUCTION OF **CONTAMINATED/ACTIVATED CONCRETE WASTE INCLUDING PILOT-SCALE TESTING WITH ACTIVE WASTE**

Contractors:	KEMA, Taywood
Contract **No.:**	FI2D-0015
Work Period:	July 1990 - December 1993
Coordinator:	H A W CORNELISSEN, KEMA, Arnhem
	Phone: 31/85/56 61 04 Fax: 31/85/51 54 56

A. OBJECTIVE AND SCOPE

This work concerns the development of a semi-technical scale test installation for separation of concrete constituents. As only a relatively thin layer of concrete structures will be contaminated or activated, the proposed process consists in a further volume reduction of the material to dispose off by separation of the radioactive constituents (cementstone) from the supposed non-radioactive part (aggregates) of this removed concrete cover.

The material that will be conditioned originates from decommissioning activities at the Kahl nuclear power plant.

The research programme could be useful for developing an industrial-scale manufacturing process. Furthermore, the experience gained in this field by Taywood (CEC contract FI1D-0042) will be applied to solidification.

B. WORK PROGRAMME

B.1. Selection of a separation **technique: determined by the importance** of the activation/
contamination of the concrete constituents. (KEMA)

B.R Determination of procms **variable for** the conceptual design of the test installation.

BE. Dmi of a s all scale **tr portable tmt installation. (KHMA)**

B.4. Construction of the tmt **installation. (KHMA)**

BE. Testing and optimisation of the **installation with non—radioactive** concrete. (KEMA)

B.6. Verification with radioactive concrete. (KEMA)

B.7. Immobilisation and **solidifica0on of concrete debris. (Taywood)**

B.8. Evaluation of the results with rmpect to equipment. costs. released **activity** etc. (KEMA)

- 52 -

C. Progress of work and obtained results Summarv of main issues

In order to develop a test installation for volume re- duction of contaminated/activated concrete, first the basic decision was made with respect to the separation technique.
Based on laboratory tests it was concluded that separation by heating followed by milling was most favourable. This finding was supported by a feasibility study for the design of in- stallations. More information can be found in Ref./1/.

Progress and results

1. SeDaration bv cooling versus separation bvheating (B.1)

From laboratory tests at KEMA it was concluded that heating of concrete followed by milling results in separation of concrete in cementstone and aggregates (> 1 mm). By TNO a research programme was executed with respect to separation by cooling of concrete in liquid nitrogen.

An important step for the development of a testinstal- lation is the decision whether it will be based on cooling or on heating. Therefore verification tests were performedwith respect to separation by a thermal shock in liquidnitrogen. The results were compared with results obtained after a thermal treatment at 650 °C. In both cases the thermalshock was followed by milling for 4 hours. The results areexpres- sed as the separation efficiency (Ed):

Ed = **As/Ao**

in which As is amount of separated material (i 1 n) in a given grain size range, and Ao the corresponding original amount of fine material in the concrete.

In table I the results are presented for crushed port- land cement concretes with maximum grain size of 31.5 mm (OPC 31.5).

It can be seen that separation (of material < 1 mm) is much more effective after heating than after cooling.

Table I: Heating versus cooling for OPC 31.5concretes

thermal treatment	**separation efficiency (%)**
heating (4h, 650°C	
test 1	82
test 2	84
test 3	74
cooling (liquid Np/ test 1 (5 min,5.1*)	
test 2 (12 min,5.1)	34
test 3 (12 min,0.8)	45
	37

* concrete humidity (%)

Tests were also performed with portland cement concretes with maximum grain size of 4 mm (OPC 4). In order to improve milling, in some cases 16-25 mm aggregate particles were added to the mill, followed by another 1 hour milling. The results are expressed in table II.

Table II: Heating versus cooling for OPC 4 concretes

thermal treatment	**separation efficiency**	
additional	4h milling	after 1 h
heating (4h, 650 °C)	61	71
cooling (12 min, 5.1*)	36	36

* concrete humidity (%)

It can be seen that also for low maximum grain size concrete separation by heating gives better results. The addition of aggregate particles to the mill is only effective after heating.

From the laboratory tests it could be concluded that a pre-treatment of heating before milling has to be preferred to a thermal shock in liquid nitrogen.

2. Determination of process variables (B.2)

Based on separation by heating various important varia- bles were studied.

2.1. Effect of heating temperature

Two concrete cubes were heated for four hours, one at 750 °C the other at 650 °C, and then milled for 8 hours. The results are given in table III. As shown, no significant differences were found.

Table III: The effect of oven temperature

cement type	temperature	separation efficiency
OPC 31.5	**750**	93
PBC 31.5	**650**	88

2.2. Effect of heating period

Three concrete cubes were heated at 750 °C. One for 8 hours, one for 4 hours and one for 2 hours and subsequently milled for 8 hours. The results are given in table IV. No significant differences could be observed.

Table IV: The effect of heating period

cement type	period (h)	separation efficiency (%)
OPC 31.5	**8**	79
OPC 31.5	**4**	93
PBC 31.5	**2**	91

2.3. Effect of milling period

The effect of the milling period was investigated by milling for 2, 4, 6 and 8 hours respectively. Every 2 hours the sieve curve of the specimen was determined.

It was found that there are only minor effects.Additi- onal tests wereperformed with PBC 31.5 concretes heated for
4 hours at 650 °C and then milled for 5, 10, 20, 30, 60,120 and 180 minutes. After each time step the separation effi- ciency was calculated for the sieveresults.

Nilling for 1-2 hours proved to give good resultsunder the given test conditions.

2.4. Effect of dust on milling

Two cubes of OPC 31.5 were treated according to the same procedure as described before (heated at 750 °C for 8 hours). One specimen was milled for 8 hours without dust removal, whereas in the case of the other specimen the dust was removed every 2 hours followed by chargesieving.

The results indicate that dust removal leads to a slightly improved milling efficiency. Noreover inthecase of milling without dust, a raise of efficiency as afunction of milling period was observed.

3. Conceptual design (B.2)

Besides the physical aspects of separation and the resulting separation efficiencies, the consequences for the design of an installation have to be considered. Therefore global conceptual designs were made based on cooling as well as on heating. Basically four set-ups wereanalyzed:

- **heating followed by water cooling**
- **heating followed by natural cooling in air**
- **cooling in liquid nitrogen**
- **parallel system of heating and cooling.**

For economical and technical reasons the option based on heating followed by natural cooling in air was selected. This installation contains the following process steps:

- **crushing**
- **sieving over 1 mm**
- **heating in an electrical furnace**
- **cooling in air**
- **milling**
- **sieving over 1 mm**
- **conditioning of dust, reuse of sand and gravel.**

A schematic view of the set-up for the installation is shown in Figure 1.

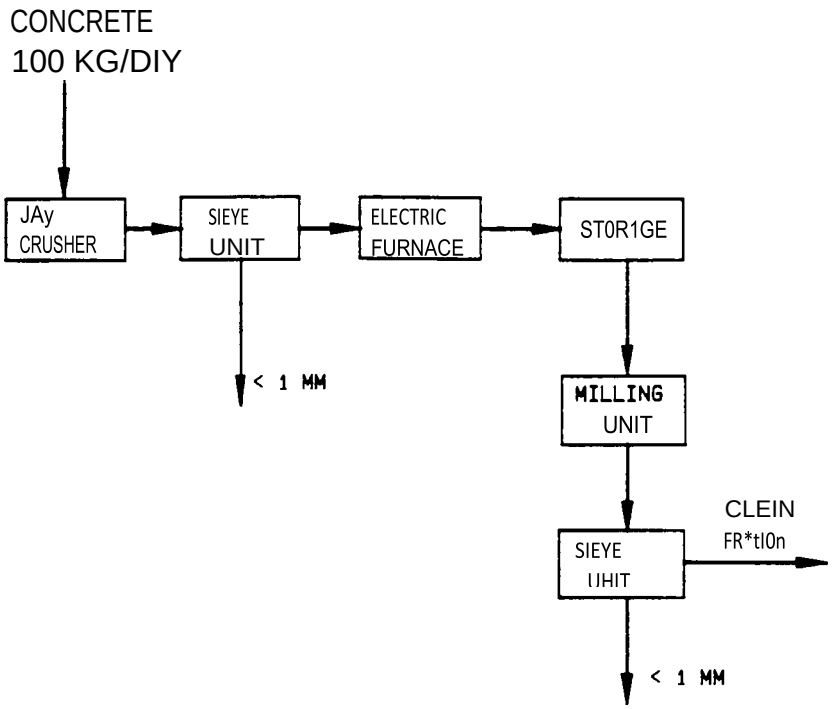


Figure 1: Set-up of the test-installation for separation of concrete

References

/l/ Cornelissen, H A W, Test-installation for separation of contaminated/activated concrete; progress report 1 (period 900701-901231) - selection of separation techni- que - determination of process variables for the design. KEMA-report 10140-CBP 91-6, January 4,1991.

k INVESTIGATIONS ON RECYCLING OF RADIOACTIVE NON-FERROUS ALUMINIUM AND COPPER BY MELTING PROCESS

Contractors: Siemens-KWU,
Contract No.: SG FI2D-fD37
Work Period: December 199fl - December 1993
Coordinator: K.H. GI IENER, Siemens-KWU
Phone: 49/69/807 36 45 Fax: 49/69/807 20 66

AOBIECMVE7UW]S€OPE

The research work aims principally at developing a method to refine contaminated Al and Cu scrap to a product that enables unrestricted reuse in conventional industrial process.

Parameters such as heating rate, temperature, slag former, surrounding atmosphere will be varied to get optimum conditions for decontamination by melting.

The behaviour of the most relevant isotopes will be investigated and the possibility of melt decontamination on Al and Cu will be examined. For the treatment of Al, co-operation with CIEMAT, Madrid, will be established (contract No. FI2D-tXl23).

The organic coatings on various Cu items represent a special handicap. Investigations will be made on how the radioactivity is distributed between metal and coatings, whcther the separation prior to melting is necessary or not and how harmful gaseous effluents can be managed.

In preceding works, the melting technique was already assessed for steel (contracts Nos.
FI1D-0144 and **FI1D-OJ16).**

B.WORKPROG

B.1. Arran e en T ad e e G **to co-operate in aluminium melting.**
B.A Installation of an **inductivelv** heated furnace with exhaust item. (SG)
BE. Prix:urement of representative contaminated Al and Cu samples. (Siemens)
B.4. Trcatmcni or Cu. (SG)
B.4. l. Invcstigati‹ins on mctal coating scparati‹in and gamma-nuclidc distribution.
B.4.2. Basic melting experiments with obscrvation of radiation and contamination of workers and working area.
B.4.3. Supplementary melting expcrimcnts with varying mclting conditions.
B.4.4. Determination of radionuclide distribution in slag, metal, dust and coating. BE. Laboratory-scale melting experiments with AT (Siemens)
B.5.1. Optimisation of melting conditions.
B.5.2. Determination of radionuclide distribution.
B.5.3. Investigations on recycling of the salt melts.
B.6. Meltin of Al in an industrial furnace. (SG)
B.7. Derivation of specific **data on sts. radioactive job** dc cs, **working time and secondary** waste **arising from** the above itenm (all)

- 57 -

C. Progress of Work and Obtained Results

Summary

The work was started in Dec. 1990 with a program arrage- ment between CIEMAT/Spain and Siemens-SG /Germany to co-0pe- rate in aluminium melting

The following conclusions have been adopted:

- Task B.5 of SIEMENS proposal and task B.3 of CIEMAT proposal have the same aim.
- Go ahead with co-operation on laboratory melting experiments with Al scraps, to avoid duplication of tests.
- SIEMENS and CIEMAT will receive information from one to another about the characteristics, composition and radionuclides content of the aluminium scraps to be melted.
- Referring to the timetables of the proposals subtasks, B.5.1 and B.5.2 of SIEMENS will be finished before 1992 and subtasks B.3.2, B.3.3 and B.3.4 of CIEMAT wi 11 start in 1992.
- As to the preceding, the activities of SIEMENS will be complemented by CIEMAT to avoid duplication of tests.
- There will be mutual information between SIEMENS and CIEMAT.
- There will be regular meetings between SIEMENS and CIEMAT to discuss the different aspects of co-operation.
- Each one of the participants will have to take over costs of their activities.

4N. RECYCMNG OF ACTIVATED/CONT"AMINATED R klNFORCEMENv servr IN CONCRETE

t '‹ ›iiti act I·I2I›-0021
No›.: Work September l99tl - Fcliru.try 1'nf2
Pcri‹xl: H H KOOLEN, Bureau A+
Cc›ordinator: Phone: 31/47/50 17 4tJtl rux: 31/47/50 33 264

A OBJECTIVE AND SCOPE

A large part of activated or contaminated steel and copper arising from decommissioning ol' nuclear installations could be recycled, as aggregate or reinforcement in concrete for new nuclear installations. The object of the study is:

1) choosing the type, amount and form of the meta!s to be used;
2) analysing the possible process to transform the metal into smaller particles and producing high grade concrete;
3) finding out the possible applications of different concrete qualities within the field of nuclear applications.

The first part will be a literature review, the second part will consist in laboratory expcriments with non-radioactive metals, and the third part will be a desk study.

During the study, specific data about the process costs will be estimated. This research programme has a strong relationship with thc melting technique devcloped by SGR (FI1D-0016 and (JO59) and could have interactions with the scparation technique studies by TNO/KEMA (FllD—tX)GR).

B. WORK PROGRAMME

B.1. Literatures on e q iti d o **contamination** levels in order to **select potential prix:msm for waste transformahom**

BE Conduction of a specific txt programme on **combinations** of different metals and metal forms with **concrete and mortam.**

BE. Evaluation of the rmults and survey of possible applications.

C. Progress of work and obtained results Summary of main issues

In this first part of our program we have started with the desk-top study about the quality and amounts of the conta- minated steel set free during nuclear plant decommissioning.

From several sources (mainly Progress Reports from the Euro- pean Community, 1987 International Decommissioning Symposium, Pittsburgh and the 1988 symposium Decommissioning of Nuclear facilities in London) the information on qualities and quanti- ties from different decommissioning projects were sampled.

Besides these sources there are some other sources from which information can be expected, but which are not available for the moment. We hope that within the next 6 months we will be able to gather all relevant public sources according to this subject. In order to become the necessary information, diffe- rent companies and research institutes have been contacted. As soon as the different types of steel are known, we start the organisation for getting samples of these types of metal in 3 different shapes: fibres, granules and curls. The fibres will be produced according to our specification. For both, granules and curls , we are in contact with potential suppliers which might be able to produce the wanted quantity and quality.

Progress and results (B.1, B.2)

1. The quantity and quality of the contaminated metal scrap

From the literature /l/, /2/, /3/, /4/ it can be seen that the main types of metal are stainless steel and mild steel. There are some other types of non-ferrous metal like Copper. But these are, as far as the information in our literature sources confirms, only small in quantity compared with stain- less and mild steel.

In table I some specific data about steel quantities and qualities are given, though it must be stated that we are still waiting for some reports. But from the different sources we already studied (/l/, /2/, /3/), there was no big differen- ce in quantities and qualities.

It should be clear that the figures given in the table are genera] infnrmatinns nn]y. The amnuntn fnr rarh individual uucteai iunlnllatiou will depend ‹n the time between nhut down and start of the decommissioning, type of reactor, duration of operation, etc. Nevertheless, they are permitting to choose the types of metal for our research program:

- Stainless steel3O4
- Stainless steel316
- Mild steel (18% Cr, 8-10% Ni)

For reason of low quantities non-ferrous metal is excluded from the research program.

About the amount of metal scrap

that will be released in the nearest future we are still waiting for further information.

Research on metal-concrete composites(B.2.)

Based on the results of the literature study we are preparing the metal-concretetests by first doing some preli- minary tests about the exact mixture of metal and concrete. Concerning fibres we found a company willing to produce these fibres according to our specifications. The application of steel fibres in concrete is well known, but investigations with different steel qualities have not yet been undertaken. Both steel granulesand curls are new applications for which not only the mechanical properties but also the workability- aspects have to be looked at in the next step.

References

/l/ CHAPUIS, A, Commission of the European Communities report EUR 10058 EN (1985).

/2/ BOORMAN, T, International Seminar on Decommissioning of Nuclear Facilities, Proceedings Planning and Progress of the WAGR Decommissioning Project (1988).

/3/ LOURME, etal, 1987 International Decommissioning Sympo- sium, Pittsburgh, 4-8 october 1987, Proceedings p.p. V-34 V-55.

/4/ ASHCROFT, et a1, 1987 International Decommissioning Sympo sium, Pittsburgh, 4-8 october 1987, Proceedings p.p. VI- 29-VI-47.

Table I: Amounts and activity of contaminated steel from several types of nuclear installations.

Steel type	**Steel mass (t)**	**surface activity Bq/cm^2**	**total activity (Bq)**
1 miscellaneous	**800**	**37-370**	8 * 10'
1 miscellaneous	**1600**	**3.7-37**	1.6 * 10^9
1 miscellaneous	**3200**	**0.37-3.7**	0.3 * 10'
2 stainless steel	90		2.2 * 10'
2 mildsteel	760		**0.5 * 109**
3 mild steel	2500	20	
4 mild steel	420		85-1200*10^9
4 stainless steel	20		1200-1700*10'

1 Results given for a PWR Reactor 1/

2 Results given for decommissioning of Windscale 2/
Advanced Gascooled Reactor 7 years after shutdown

down

3 Results given for decommissioning G2-reactor 3/

4 Results given for decommissioning of Windscale Advanded Gascooled Reactor of the principal active steel arisings (both activated and contaminated steel) 4/

4.4. TREATMENT AND CONDITIONING OF RADIOACTIVE GRAPHITE FROM NUCLEAR INSTALLATIONS

Contractors: CIEMAT, UDA
Guntract FI2D-0017
No.: W‹irk July 1990 - December 1993
Pericd: A ESTEBAN DUOUE, CIEMAT, Madrid
Guordinator: Phone: **34/1/346** 62 19 Fax: 34/1/346 60 05

AOEM3€XTM3ANDSCDPE

The objective of the laboratory-scale investigations is the development of chemical processes for the treatment of radioactive graphite for its safe storage. lt consists **in:**

- previous extraction of radionuclides (mainly tritium) to decrease the radioactivity of graphite; fixation of radionuclides (mainly C-14) to avoid their leaching during the storage of graphite; impermeabilisation of graphite by metal coating for its transport and storage.

Extraction of the radionuclides with chemical agents will be done before the metallising process for fixation, in order to minimise leaching of radioactive products during storage, followed by standard leaching tests. The radioactive graphite will be procured from the experimental reactor **JEN-1** and the gas-cooled reactor Vandellos-I.

B. WORK PROGRAMME

B.1. Removal an‹j/or fixation of radionuclide

B.1.1. Investigations on radioactive and inactive sample structure and texture using different analysing techniques. (all)
B.1.2. Testing of appropriate chemical agents on samples with regard to their possible decontamination and/or immobilisation features. (UDA)
B.1.3. Study of radionuclide removal, mainly titium.
B.l.4. Study of radionuclide fixation.
B.1.5. Characterisation of treated samples using methods from subtask B.1.1.

B.R Metal coating of graphite by ionic deposition

B.2.1. Characterisation of samples similar to B.1.1. (all)
B.2.2. Performance of process parameter studies for metal coating applications on inactive samples. (all)
B.2.3. Chemical modification of radioactive surfaces. (CIEMAT)
B.2.4. Metallisation of inactive samples. (all)
B.2.5. Metallisation of radioactive samples. (CIEMAT)
B.2.6. Characterisation of the treated samples concerning chemical properties and thickness of the metal layer, porosity of the surface etc. (all)

BE. Leachin experiments with the **metallised specimen (CIEMAT)**

B.4. Assmsment of results and conclusions.

- 63 -

C. PROGRESS OF WORK AND OBTAINED RESULTS

Summary of main issue

This period of the time has becn devoted to the implementation of thc project and the **adjustement** of laboratories, equipments and characterisation techniques. Samples of inactive and **active graphite** from experimental reactor JEN—1 and gas-cooled reactor Vandellos-I have been obtained.

The following characterisation studies have been achieved using **inactive graphite** samples:

X—ray diffraction

nitrogen adsorption

- mercury porosity
- water and carbon analysis.

Progr and results

1. Investigations on radioactive and inactive sample structure and texture using various analysing techniques (B.1.1., B.2.1.)

   The inactive graphite samples originate from the reflector of JEN-1 experimental reactor (R-samples) and from the fuel shirts of Vandellos—I gas—cooled reactor (C-samples). The graphite dust samples had a grain size between 6-12 qm and 60—100 qm.

   Analysis of the graphite structure

   X-ray diffraction technique was applied to study the structurc of graphite with a SEFER J50 equipment. The graphitisation grade is less on C-samples than on R—samples, where the graphitisation is non-homogeneous (Table I).

   StudY of the graphite surface

   The active surface has been studied by adsorption isotherms of nitrogen with a COULTER OMNISORP 100 CX equipment. An example of these results is given on Figure 1. Very high specific surfaces 13-15 m'/g were obtained on C—samples and less 6-8 m /g on R—samplcs. These values agree with the results obtained with X-ray diffraction study. The SBET paramcter is similar on R and C-samples, therefore the interaction between N, and both graphites will be similar.

   The porosity has been studied with a CARLO ERBA 2000 porosimeter. Thc results are given on Table II and an example of these results is depicted on Figure 2. The mesopores volume on dust and grain samples were 0.014 cm^3/g and 0.021 cm /g respectively for R—graphite and 0.040 cm^3/g and 0.083 cm'/g for C—graphite. The macroporosity was 0.083 cm^3/g on R—graphite and 0.040 cm'/g on C-graphite.

2. Testinoff appropriate chemical aoewns sa ples with re ard to their possiblc decontamination and/or immobilisation features (B.1.2.)

   The analysis of water and carbon content (Figure 3) have shown the presence of water and hydrocarbons on the surface as well as hydrocarbons inside thc graphitc structure. They wcre extracted at a temperature of about 400°C.

   The adsorption and desorption of water and hydrogen have been studied. The obtained results show the adsorbed water on samples C is desorbed completely but on R-samples, part of it is retained.

3. Performance of process parameter studies for metal coating applications on inactive samples (B.2.2.)

   A bibliographic study on the matter has been realised.

- 64 -

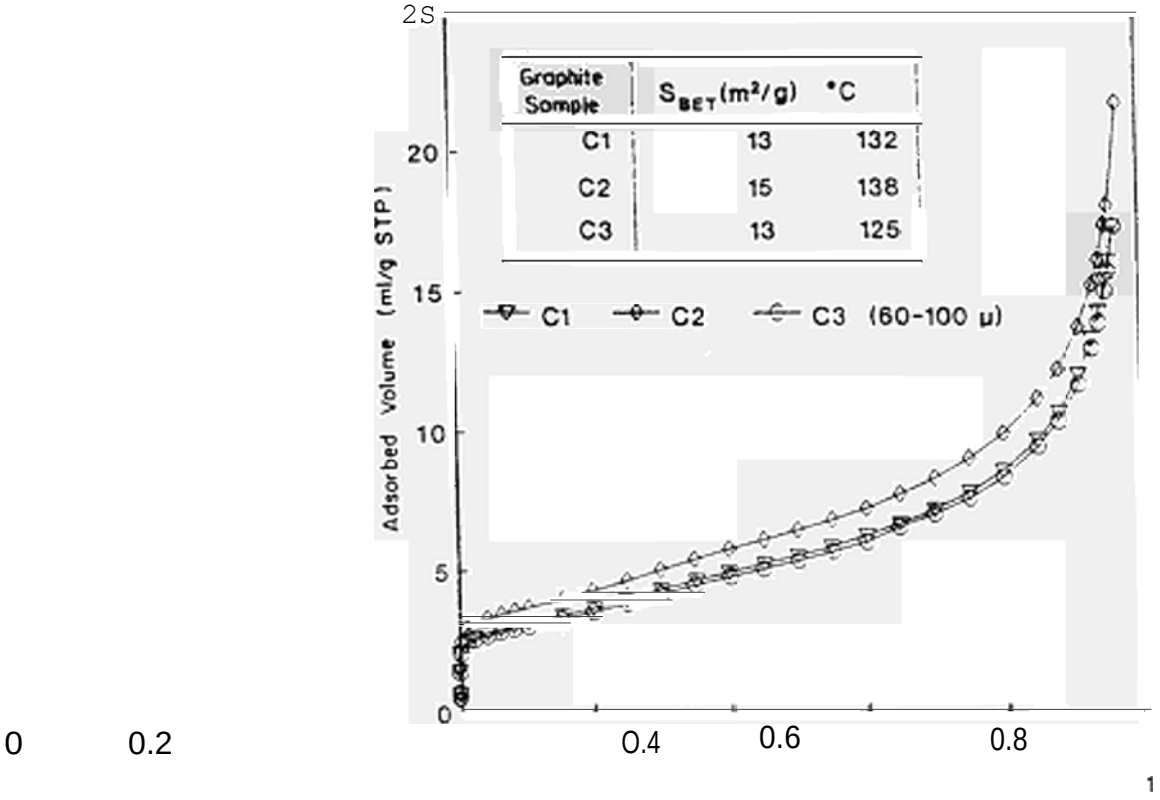
Tab1e I : X Hay D i f f rac t i on of Graph i te Samp l es R an C

Graphite Sample	28	D(A)	Irel	Imax	Graphite Sample	28	D(A)	Irel	Imax
R1	23.8 26.4 27.2 42.5 44.3 54.4 77.4	3.74 3.37 3.27 2.13 2.04 1.68 1.23	G. 7 100.0 1.5 1.0 1.6 4.2 1.0	'/0 1041 6 160 107 171 442 105	C1	23.8 26.4 27.2 42.5 44.1 54.4 77.4	3.74 3.38 3.28 2.13 2.05 1.69 1.23	1.8 100.0 3.1 1.2 1.6 4.1 1.2	1"// 962 8 300 118 156 393 115
R2	23.9 26.5 27.3 42.5 44.4 54.5 77.5	3.73 3.36 3.26 2.13 2.04 1.68 1.23	1.0 100.0 1.6 0.8 1.3 4.0 0.9	111 11314 178 85 150 452 102	C2	23.8 26.4 27.2 42.4 44.4 54.3 77.4	3.74 3.38 3.28 2.13 2.05 1.69 1.23	1.3 100.0 2.2 1.0 1.4 4.3 0.9	11 2 8823 195 92 125 376) 8 3
R3	23.8 26.4 27.2 42.4 44.3 54.4 77.4	3.74 3.37 3.27 2.13 2.04 1.69 1.23	1.2 100.0 1.9 1.1 1.8 4.1 1.0	122 10332 195 114 189 428 10	C3	23.8 26.4 27.2 42.5 44.2 54.4 77.5	3.74 3.37 3.27 2.13 2.05 1.69 1.23	1.3 100.0 2.2 0.8 1.1 4.2 0.8	12 2 9612 212 79 110 408 72

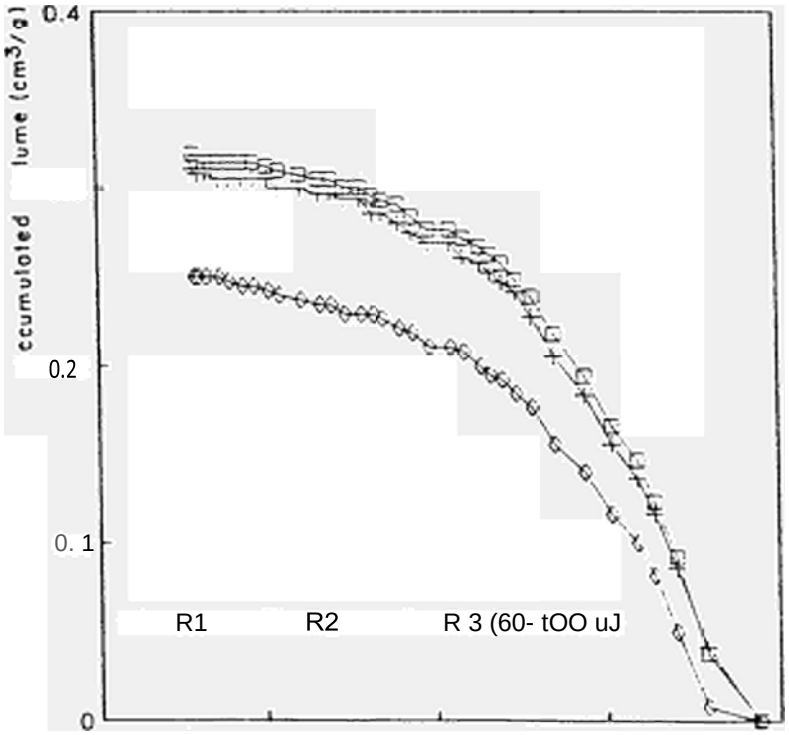
Table II: Volume of Pores by Mercury Porosimetry

Graphite Sample	Volume of Mesopores (cm^3/g)		Volume of Macropores (cm^3/g)
	Dust (60-100 p)	Grain (1-3 mm) R < 25 nm	Grain (1-3 mm) R > 25nm
RI	0.014	0. 021	0. 079
R 2	0.014		
R3	0.016		
C 1	0.018	0. 030	0.040
C 2	0.018		
C3	0.023		

- 65

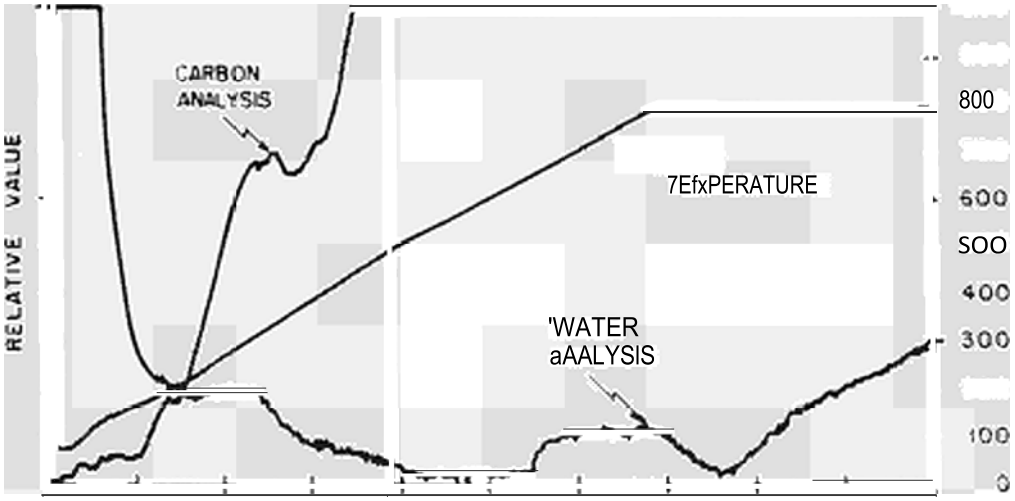


rig 1- N¿Adso‹b!ion IsothsnnsIT7• K 1



2 3

Fig. 2 Mercury Porosimetry



0 If 5&4 792 990 1t88 $88 \ 584 t7B2 1980
3gg

7IUE *iH* SEC.

Fig. 3 - Cor bon ond Woter An0lygic

s. ntmnno.s:quumcnviou nuo»oz+•raviou oF nzuovc<o1neouno
SEMt-AUTONOMOUS MANIPULATOR SYSTEMS

W Objective

Because of radiation fields, some decommissioning tasks must be performed with remote control, in order to minimise occupational exposure. This requirement forms a major technical challenge in decommissioning.

The objective of this research is to qualify and adapt remote-controlled semi-autonomous systems for manipulation of decommissioning tools and instruments.

B. Subjects of the rmearch performed under the previous programmes (1979-88)

Rcmote-controlled manipulation systems did not form the subject of a Project Area of its own, so far, but limited activities in this field were pcrtormed under Projects No. 2 (Decontamination) and No. 3 (Dismantling techniques).

C. Programme 1989 to 1993

Remote-controlled semi-autonomous manipulators should be adapted and tested, in order to qualify and improve their performances with typical decommissioning tasks and tools. For this purpose, existing components and sub-systems should be used and adapted as far as feasible. This concerns in particular sensing systems and computer programmes for semi-autonomous process control, which form important aspects of the research. Special attention should be paid to highly repetitive time-consuming operations, e.g. decontamination and clearance measurements of large surface areas of premises.

D. Programme implementation

At the end of 1990, six research contracts relating to Area No. 5 were at the stage of execution.

5.I. ROBOTIC SYSTEM FOR DISMANTLING OF THE PROCESS CELL OF A REPROCESSING PLANT

Contractor: ENEA, CRE
Contract No.: Trisaia FI2D-0036
Work Period: October 1990 - December 1993
Project Manager: P MATALONI
Phone: 39/835/97 43 94 Fax: 39/835/97 42 50

K OBJECTIVE AND SCOPE

Most reproccssing plants, at the cnd of their lifctime, consist of small shielded cclls, inside which the process equipment is installed. The plant philosophy required the operator to cnter the cells for any maintenance interventions; the cells are usually accessible from a top corridor through openings closed by shielded plugs.

The present research projects aims at testing a robotic system that can dismantle the equipment of a small cell of this type and remove cut parts from thc cell without any direct intervention of the operator. The envisaged robotic system consists in a servomanipulator (MASCOT IV) and a hoist installed inside a containment box; the box has the purpose of avoiding the dispersal of contamination both during the cutting operations and during the transfer of the cut parts to the conditioning cell.

The robotic system will be tested using a mock-up of the dissolution cell of the EUREX plant, built according to the criteria of small shicldcd cells.

B. WORK PROGRAMME

B.1. Dmign and construction of a mock-up of the dissolution cell of the EUREX plan{

B.1 I3csign and construction of a **containment box and installation of the MASCOT** IV **servomanipulator**

BE. Non-radioactive testing of the robotic sYstem with dismantling operations, using the cell

B.4. Non-radioactive testiml of **the robotic sYstem with simulated cell decontamination** operations, including simulated smear tests.

BE. Specific data on costs of the **wstem and its radiolORlCal impact on work force and workiiw** area.

- 69 -

C. Progress of Work and Obtained Results Summary of main issues

The activity concerning the research has a commencement date of 1st December 1990. The contract between European Community and E.N.E.A. was signed at the beginning of 1991.

The activity has been centred on the design of the robotic system (Task B.2). The design criteria of the containment box have been fixed.

Progress and Results

1. Wording of the first title (B.2)

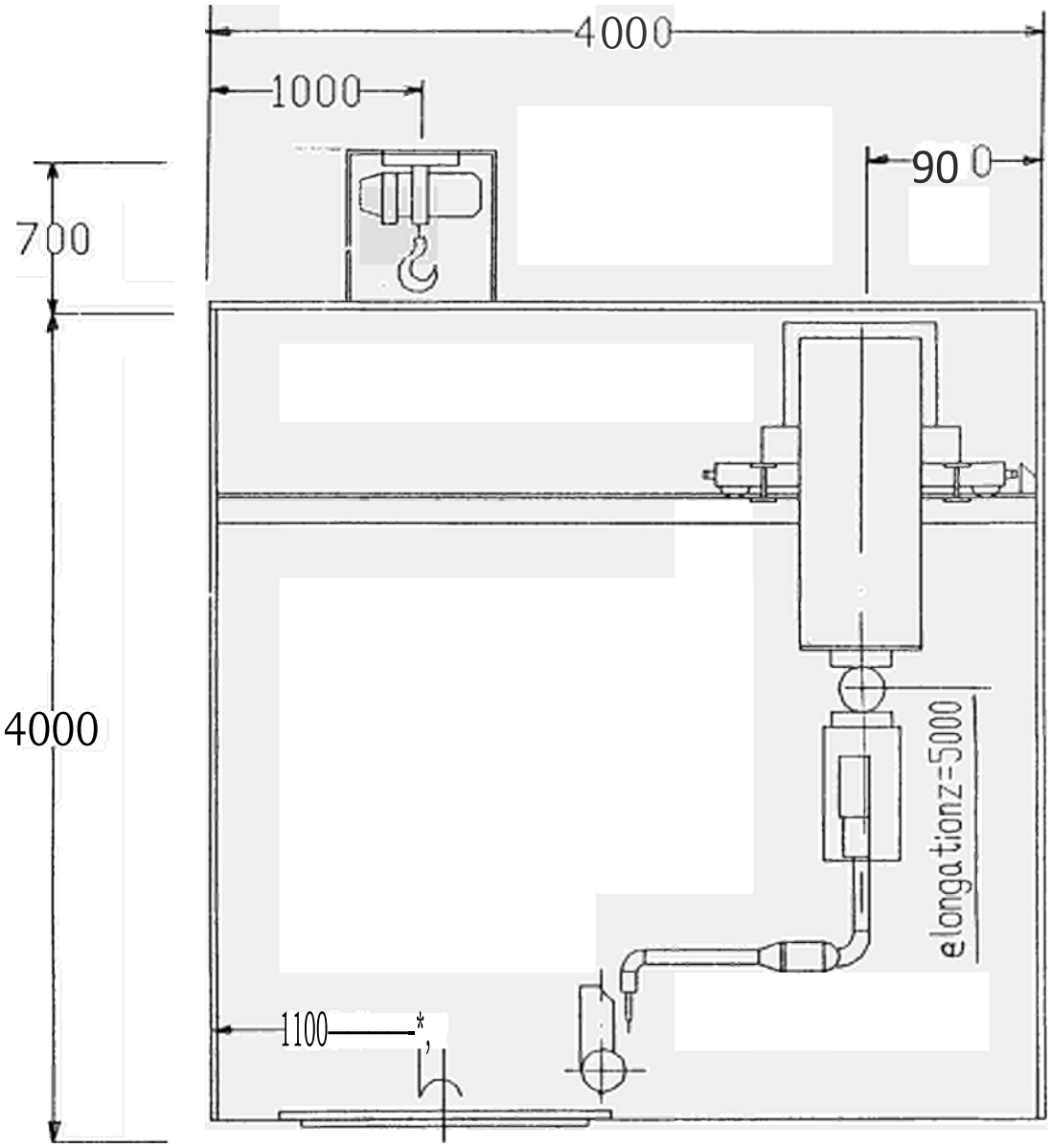
The robotic system consists of a servomanipulator (MASCOT IV) installed inside a containment box. The box communicates with the cell by means of a hole closed by a double lid system. A telescopic tube, mounted on a carriage, supports the MASCOT, its elongation is about 5 metres.

The box dimensions have been chosen according to the MASCOT dimensions, the height also according to the telescoping tube length.

The box preliminary design (Figure 1) is 4 metres long, 2.2 metres wide and 4 metres high, the possibility of reducing the dimensions is under consideration now (smaller dimensions simplify the box positioning).

A hole is present at the bottom of the box; it is square so as to allow box different orientations, it is about 1.2 metres wide.

The box dimensions allow the extraction of most of the appliances from the process cells: the bigger ones (e.g. the dissolver in the case of the dissolution cell) are cut inside the cell before they are extracted.



/[.) 0)0(i£S}S(Ph-FPlihi20F/)9S\2

- 71 -

DESIGN, CONSTRUCTION AND TESTINGOFAMANIPULATORFOR RHMOVINQ SLAG.MF GTHMPERATURE ANDTAKINGSAMPLESDURINGMELTING OF RADIOACTIVE METAL

Contractors : ANSALDO, Siempelkamp FI2D-0008
No.: Work Period: July 1990 - March 1993
Coordinator : M CIARAVOLO, DNU/RTC, ANSALDO S.p.A
Phone: 39/10/550 27 90 Fax: 39/10/550 20 32

K OBJECTIVE AND SCOPE

The work consists essentially in the improvement of an existing melting procedure for radioactive materials and mainly relates **to:**

- a system specification including a preliminary study to identify the most appropriate manipulator system,
  the components design and manufacturing,
- modifications of the existing melting plant for components housing,
- installation of the components and testing of the system.

The expected benefits relate mainly to a reduction of the radiation dose to the melting staff and a reduction of the contamination in the area surrounding the furnace - operations such as slag removing, temperature measuring and samples taking being nowadays carried out completely manually. The manipulator should also increase the efficiency of the melting technique.

The manipulator developed here has thus **to:**

- keep people away from the furnace while it is open, in order to avoid their radiation/contamination by the melt, in particular through inhalation of radionuclides leaving the melt;
- reduce the contamination of the surroundings of the furnace (nuclides like the volatile caesium leave the open furnace);
- remove dust during melting of zinc-plated metal.

The work is a follow-up of previous EC contracts (FI1D-0016, -0047 and -0059) under which Siempelkamp and KGB Gundremmingen developed the melting facilities TAURUS I, II and CARLA

B. WORK PROGRAMME

B.1. System **uirements such as basic operations environmental conditions interface will be specified (Siempelkamp)**

B- System definition (Ansaldo)

B.2.1. Selection of the basic concept, performing the three operations required, and comparison with a single-purpose device.

B.2.2. Definition of main manipulator operations required, i.e. scumming, sampling, and temperature measurements of the furnace melt bath.

BE. Dm of **fined tern ponents (Ansaldo)**

B.4. Manufacturing and shop tmtine o(components (Amaldo)

BE. btodiDcation of the **existing facility (Siempelkamp)**

B.6. Swtem imtallation and tmtine in the Siempelkamp melt shop CARLA (AII)

B.6.1. Gold tests, e.g. tool changing, manipulator working autonomy, at ambient temperature.

B.6.2. Tests at operational thermal conditions.

B.6.3. Tests with radioactive material < 74 Bq/g, i.e. carbon steel, stainless steel, steel plates covered with zinc, brass, copper and aluminium.

B.7. Fiiuilevaluation with re melt time, safe **occupational radiation pure and radioactive emission to the environment** (AII)

C. Progress of work and obtained results summary of main issues

During the 1990 basic concepts of the system have been developed considering the main operations.

The lay0ut of the manipulator and of the insulation system have been defined considering the Carla Plant interface dimensions.

Procedures for the process have been studied considering the main operations (Scumming, sampling and temperature measurements).

Progress and results.

1. System requirements such as basic operations, environmental conditions, interfaces will be specified (Siempelkamp) B.1.

System requirements and basic operations (Scumming, Sampling and temperature measurements) have been defined in the Spc. 915-000-000 index 0 issued by Siempelkamp.

In the specification, the environmental conditions as temperature radiations and pressure and the interface dimensions of the plant are considered. Other main interfaces such ag banret dimensions have been fixed.

The whole process has been examinated identifying auxiliary operations (e.g. scumming tool, grab coating and cleaning), necessary for the melting process but not originally described.

TMse auxiliary operations have been introduced to permit the complete process and the insulation between the furnace and the Carla Plant.

2. System definition (Ansaldo) B.2.

2.1 Selection of the basic concept, performing the three operations required, and comparison with a single-purpose device. B.2.l.

Considering the three operations (scumming,sampling, and temperature measurements) a comparison between a multi-purpose manipulator and single-purpose devices has been performed. Due to the necessity of enclosing all the

facilities in an insulating box (to avoid decontamination speed in the plant environment) and to the space constraints of the existing plants a multi-purpose manipulator has been preferred.

2.2 Definition of main manipulator operations required, i.e. scumming, sampling, and temperature measurements of the furnace melt bath. B.2.2

The manipulator is foreseen installed inside an insulation room to prevent contamination of the dust from the furnace in the Carla hall.

In the ANSALDO specification n. DEC SIE S00l Rev. 0 the manipulator is described. A telescopic mast has been chosen to permit a great stroke of the end effector.

The mast can rotate and translate to reach the furnace and the tools expositions inside the insulation room.

A particular slag grab has been studied to remove the slag from the edge of the crucible. The grab has two hemispherical jaws and an helical blade fixed at its periphery. The temperature measurement will be obtained using thermocouples automatically connected to the mast.

An optional pyrometer could be used to obtain a fast knowledge of the temperature.

The insulation room will be provided will auxiliary devices to change the slag barrel and tools, to clean and paint the grab and to take slag-samples.

Sensors will be installed to control the operations.

A TV camera will be placed for supervisors control during the process.

SP. TELEROBOTIC MONITORING, DECONTAMINATION AND SIZE REDUCTION **SYSTEM** - TMDSRS

Contractors: AEA Harw.,
Contract SCK/CEN FI2D-0012
No.: Work July 1990 - December
Period: 1993 M H BROWN, AEA
Coordinator: Harwell
Phone: 44/235/434 691 Fax. 44/235/436 **135**

K **OBJECTIVE** AND SCOPE

The objective of this work is to use existing equipment developed under the Harwell Nuclear Robotics Programme to investigate and demonstrate thc feasibility of telerobotic monitoring, decontamination and size-reduction systems (TMDSRS). The work will include experimental investigations at industrial scale, and use sample workpicces of an appropriate size and configuration similar to their active counterparts.

The work will proceed in two distinct stages. The first stage will involve the continued development of thc Harwell Telerobotic Controller and its interface to NEATER, a Nuclear Engineered Advanced Telerobot, and ancillary cquipment and mechanisms. This devclopment will allow in-active trials of a TMDSRS system on each of the three sets of target workpieces (B.3., B.4. and B.S.). The work will be carried out in the Harwell Robotics Demonstration laboratory. The second stage of the work (B.6.) will involve active trials of one of the areas demonstrated in the first stage. The selection of the appropriate application will ensure that a safe, useful and representative active trial can be accomplished.

This development will reduce man-Sv and costs of decommissioning projects. Greater efficiencies in placing or deploying decontamination tools and in cutting and packing waste will improve waste disposal strategies, and reduce waste arisings. Data on cost benefits will be produced in submissions made to justify the selection of a suitable project for the active trials (phase 2). Cooperation on sensors with SCK/CEN Mol is included in the work programme.

B. WORK PROGRAMME

Control system extension to work effectively with each of thc three non-active applications.

B.Z. E tro h n head unit development and irradiation tests (AEA)

B.2.1. Requirements analysis for the electropolishing head unit (AEA)

B.2.2. Rcquirements analysis for the sensor functions (SCK/CEN)

B.2.3. Selcction of sensors to meet the requiremcnts analyses of B.2.1. and B.2.2. (SCK/CEN)

B.2.4. Design and construction of the integrated head unit (AEA)

B.2.5. Irradiation tests of the integrated head unit (SCK/CEN)

B.3. Decontamination of diffcrent surface; radiation monitoring. elcctrojxilishing and registration sriftwarc (AEA)

B.4. Clearance monitoring dcvelopmcnts (AEA)

B.S. Glovchox size reduction devclopments

B.5.l. Analysis of subsystcms susceptible to radiation damage (SCK/CEN)

B.5.2. Tests on subsystem components in the gamma irradiation test facility at the BR2 rcactor (SCK/CEN)

B.5.3. Tool and operational softwarc dcvclopmcnt (AEA)

i3.5.4. Tool change adaptation and cutting tasLs demonstration jointly with a rangc of tt›ols (AEA)

B fi. Active dccnmmi.vsioning trials in the appropriate active area

B.6.l. Prc-trial analysis of the radiation cnvironmcnl (AEA)

i3.6›.2. Activc trials including the NEATER carrying out of a task or set of tasks (AEA)

i3.l›.3. Support for active trials to reducc thc probability of failures (SCK/CEN)

B.7. Ec‹inomic analysL$ Of TDMSRS and iLs radiological impact on work force and working area

B.7.l. Pre-activc trial cost-benefit analysis to establi.sh economic advantages of telerobotic opcrations (AEA)

B.7.2. Post-active trials analysis on ccsts, incurred dose burdens, working and exposurc times of ancillary opcrators, and estimatcs of scctindary waste arisings (AEA).

- 75 -

C Progress of Work and Obtained Results Summary of main issues

An analysis of the Electropolishing Head Unit [EHU] requirements has started late because of the delay in issuing the contract amendment to incorporate **CEN/SCK** into the project. To compensate the Glovebox Size Reduction, work programme has been brought forward. The telerobotic control system software has been extended to host force control algorithms for bilateral [force reflecting] teleoperation and automatic drill bit alignment.

Radiation monitoring and registration software to facilitate the detection and decontamination of radiation hot spots has been specified. To improve the cost effectiveness of the telerobotic size reduction of gloveboxes, compliant mounts for aggressive cutting tools have been developed and their performance evaluated.

Progress and Results

1. Background

The key elements of the TMDSRS are the Nuclear Engineered Advanced TeleRobot [NEATER], a TeleRobotic Controller [TRC] and a six degree-of-freedom input device to provide man-in-the-loop operation.

NEATER is based on Stiiubli Animation's clean room industrial robot, the PUMA 762 CR. To provide a cheap and reliable alternative to complex force reflecting manipulators, designed especially for the nuclear industry, deviations from the standard product have been kept to a minimum. It is modular for ease of maintenance, fully sealed for prevent- ion of contamination and radiation tolerant to lMGy. A prototype was delivered to Harwell in December 1989 on completion of an eighteen month development programme. Since then it has accumulated over 1500 hours of operation 111 gu re ?) .

The TRC has been designed to provide effective unilateral or bilateral teleoperation and a host for sensor-based control algorithms such as those required for decontamination and tool alignment. It runs on an IBM compatible 80486 based PC and is connected to Unimation's VAL II controller via a standard communications interface. A menu Even touchscreen provides a user-friendly operator interfacc.

A six degree-of-freedom Cartesian Master Arm [CARMA] has also been developed, under separate funding, to provide, via the TRC, unilateral control of NEATER. Bilateral operation will be available in April 1991.

2. Control system extension (B1)

Recent extensions to the software provide the option to communicate with the robot controller via its SLAVE software. SLAVE facilitates robot control through singularities, telerobotic configuration changes and interfacing to other servomanipulators. Work has started on a high speed version of SLAVE to provide effective force control for bilateral teleoperation and telerobotic tool deployment. The new version, scheduled for completion in September 1991, will reduce control system cycle times from 2SmS to 3.6mS. A proto- type Ethernet link has been developed to support the faster data rates required for Enhanced SLAVE. The TRC will host the application specific software necessary to meet the requirements of the three TMDSRS applications.

To provide a more effective man machine interface than the standard two unilateral three degree-of-freedom joysncks the six degree-of-freedom CARMA has been interfaced to the TRC. The interface includes ADC hardware and scaling software to input canesian

position data from CARMA and motor drive amplifiers to power the force reflecting motors. Bilateral force control algorithms are implemented in the TRC. A six degree-of-freedom force/torque sensor has also been interfaced to the TRC. This sensor provides robot end point force/torque data for a range of force control algorithms including bilateral operation.

tele-

3. Electropolishing head unit (B2)

A list of candidate EHU materials requiring an assessment for chemical stability in the presence of nitric acid and ionising radiation has been produced. EHU sensor requirements have also been identified.

4. Surface decontamination (B3)

The robotic decontamination of flat surfaces using the electropolishing head unit will be controlled by radiation monitoring and registration software. A requirements analysis for this task has been completed and a software specification issued. The software is required to scan the EHU over a specified flat surface on a pre—programmed grid, pausing at each monitoring point for twenty seconds. Position and radiation measurements will be recorded at each monitoring point to enable the generation of a radiation map of the scanned area. The system must provide a graphical display at a monitor and a hard copy via a commercial spreadsheet. Position data storage will enable the robot to return to radiation hot spots with the EHU. The application software will be fully integrated with the TRC software and accessible through the touchscreen. Application and EHU specific parameters will be selectable to enable other decontamination heads to be deployed in this way.

5. Glovebox size reduction (B5)

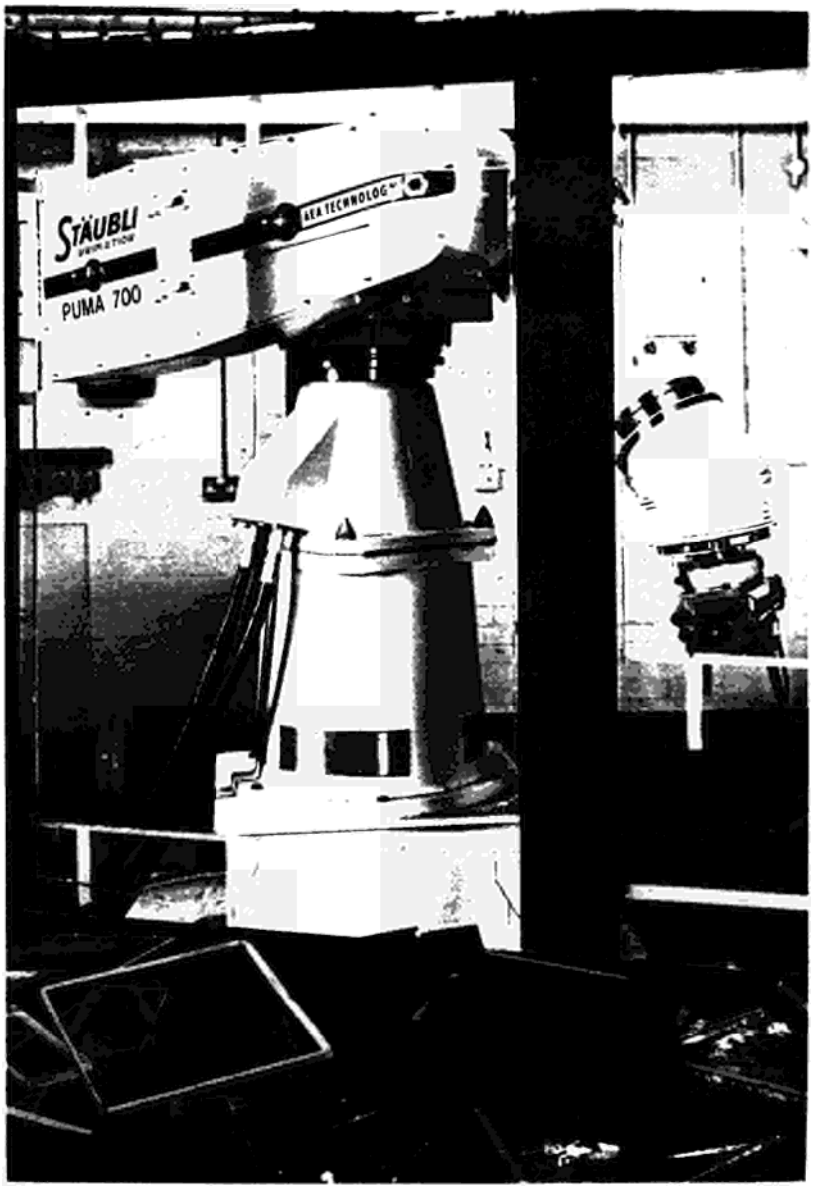
Telerobotic cutting trials have been carried out on a wide range of tools. The main objective was to define a tool kit before the commencement of size reduction operations on typical gloveboxes to confirm or otherwise predicted decommissioning times. New tools have been tested and deployment techniques for existing tools developed. Passive compliant mounts have been designed to meet the specific telerobotic deployment require- ments of a nibbler, bandsaw and reciprocating saw. The aim is to eliminate robot stalling by minimising the tool misalignment forces applied to the robot end effector.

Rotary drills are required to provide access holes for jigsaws and reciprocating saws. Trials have shown that it can take as long as five minutes to align the drill bit telerobotic- cally. To reduce this time an algorithm has been developed to align a drill bit orthogonal to a surface. Maximum alignment time is 20 seconds and occurs when the approach angle is greater than 45° from the vertical. If an operator is able to align telerobotically the drill bit closer to the desired orthogonal position, then the execution time is reduced to ten seconds. These times are much faster than the typical manual alignment times. Automatic alignment is also much more accurate than manual methods and consequently cutting efficiency is improved. During the execution of the alignment algorithm the drill bit touches the surface and the force/torque vector is read from the sensor. The required position of the robot is then computed to ensure that there is a single force along the drill bit axis, other forces and torques being set to zero. To provide a robust algorithm, a dynamic model of the VAL 0 controller was obtained from Unimation.

Trials with proprietary pneumatic jaw grippers from Cleveland Guest showed that they were able to lift waste arising from glovebox decommissioning trials. Vacuum grippers were, however, much more effective at lifting flat plates. Prototype vacuum gripper trials

revealed the difficulty of aligning the pads with waste metal that was not resting in the horizontal plane. To overcome this problem the gripped mount was modified to provide compliance. The new mount accommodates over 45 degrees of misalignment between the component to be lifted and the wrist mounting face. Further trials have demonstrated that the nsodified system allows quick and easy pick and place of sawn-off plates.

To permit size mduction tools to be changed remotely, a tool change system has been purchased from Stiiubli Unimation. A prototype tool change rack has been designed to meet glovebox decommissioning requirements/and manufacture is underway. Supporting tix›l change software has been specified; a prototype version is schedules to coded by March 1991.



F1gure 1: Adapted ndus t r1 a L robot .

78

5.4. ADAPTATION AND TESTING OF A REMOTELY CONTROLLED UNDERWATER VEHICLE

Contractor: AEA Winfi
Contract No.: **FI2D-1025**
Work Period: July 19Rl - June 1993
Protect Manager: P W WORTHINGTON, AEA Windscale
Phone: 44/9467f72414 Fax: 44f9467/28989

A. OBJECTIVE AND SCOPE

Preparatory work to **decommission** the Windscale piles is being carried out. As part of this work, fuel **debris and contaminated silt is** to be recovered from two water-filled, ltO m long,
2.7 m x 2.1 m section fuel transfer ducts which **connect the piles** to the fuel storage pon‹:L

As no commercial equipment exists which has been purpose-designed for generic nuclear **applications, the main** object of this work is to adapt and test a remotely controlled underwater vehicle **provided with manipulators, on-board television systems and** remote sensors for surveillance purposes. This includes the development of an underwater remotely controlled vehicle for use in nuclear applications, the development of techniques for fuel **handling and silt** recovery, and the assessment of **equipment durability, radiation** tolerance and of decontamination problems,
e.g. removal of concrete surfaces, etc.

The potential benefits of this work programme will be reduced doses to workers, decontamination and inspections, reduced secondary waste and reduced decommissioning costs due to lower labour inpuL

Information on costs, occupational exposure, work time and secondary waste arisings will
be made available.

The work will include non-active trials in a full-size mock-up.

B. WORK PR£K1RAMME

B.1. SpeciBcation of the uiiderwater vehicle to allow manufacturers to tender.
BE Vehicle manufiictuie. at the tenderer's work
BE. Preparation of the full-size that mx:k-up of the entrance area to the waii;t ducL
B.4. Adaptation and atine in the mock-up of the vehicItem on its ability to perform the

B.4.1. Dry **testing** of the complete system.
B.4.2. Wet testing of the complete system.
BE. Develonment in the active **environment of WuxIscale Pile No. 1.**
B.6. Final evaluation will include specific data on ‹x Is. worh time. occupational ezix ure and

C . Progress of work and obtained results

Summary of main issues

The main issues undertaken in this first year of the work programme are the preparation of the specification for the underwater vehicle, the manufacture of the vehicle and the preparation of a mock-up for vehicle development.

Progress and results

1. Specification of the underwater vehicle to allow manufacturers to tender (B.1)

The detailed specification for the vehicle has been written and completed in accordance with the programme. The specification is divided into two main parts:

(i) General contract conditions for all work carried out on behalf of AEA Technology;

(ii) Technical requirements of the vehicle. This details minimum reach, minimum lift capacity and access restrictions.

This specification was used as the basis for suitable manufacturers to tender against. These tenders have been received and analysed.

2. Vehicle manufacture at the tenderer's works (B.2)

The manufacture of the vehicle has been delayed because of changes in the financial sanctioning arrangements within AEA Technology. It is now forecast that vehicle manufacture will commence in March 1991.

3. Preparation of the test mock-up (B.3.)

The facility is under construction at Windscale Site and will be completed to programme.

4. Adaption and testing of the vehicle on its ability to perform the various decommissioning tasks (B.4.)

B.4.1. work schedules are being produced for fuel retrieval and operator training, and assessment programmes for vehicle and manipulator assessment are in preparation.

- 80-

5]. OF LONG-AGE OPERA ILUW]IJNG„EQLTF 7MTH DDTBRENI TJDIE FOR ODNOWWE DIS G AND IAWOH PROTECMOHMONMX)IUNG

Contractors: KfK, KA, AEA Harw., BAI
Contract No.: FI2D-fD32
Work Period: October 1990 - December 1992 K
Coordinator: MULLER, PHDR/HT, KfK
Phone: 49/7247/824343 Fax: 49/7247/823718

A oamcnvc AxoscoPs

An existing advanced handling system (EMIR) will be used as a carrier system for various devices for concrete dismantling and radiation protection monitoring. It combines the advantages of long reach and high payload with highly dexterous kinematics.

This system will be enhanced mechanically to allow the use of different tools. Tool attachment devices for automatic tool exchange will be investigated as well as interfaces (electric, hydraulic, compressed air, cooling water and signals).

The control system will be improved with regard to accuracy and sensor data processing. Programmable logic controller (PLC) functions for tool control will be incorporated. The free field of the EMIR will be used to build a mock-up that allows close simulation of that scenario without radioactive inventory. Aged concrete will be provided for the integration tests.

Finally, the economical and technical effectiveness of the different methods will be assessed/evaluated.

B. WORK PROGRAMME

Basic concept iirvmtiggjj n

Interface specification between tools and EMIR (KfK)

Investigation of tool attachment devices for an automatic tool exchange system (KfK)

Setting up of test parameters (AII)

Literature review concerning tool holders, adapters and tool replacement (KA)

B.l.5. Selection of the tool replacement system (KA)

B.1.6. Microwave equipment; design concept and interface specification (AEA)

B.1.7. Literature review on automation and measuring (BAI)

B.1.8. Selection of the type of radiation detector (BAI)

B.l.9. Definition of contaminants (BAI)

B.1.10 Design of the mechanics involved (BAI)

B.1.11 Electronics design for a noisy and dirty environment (BAI)

B.1.12 Conception of the hardware requirements for the computing system (BAI). BE

Development of tmls

B.2.1. Development of a tool positioning sensor (KfK)

B.2.2. Design and manufacture of a sensor equipment (KfK)

B.2.3. Examination of Cinematic requirements (KfK)

B.2.4. Enhancement of control system (KfK)

B.2.5. EMIR hardware enhancement (mechanical and non-mechanical interfaces) (KfK)

B.2.6. Setting up and optimisation of test parameters (KfK)

B.2.7. Adaptation of a commercial tool replacement system or development of an appropriate system (KA).

B.2.8. Development of a tool replacement adapter system suited to EMIR requirements (KA)

B.2.9. Installation of radiation measuring instrument plug connectors in the adapter (KA, BAI)

B.2.10 Tool holder rack design and development (KA)

B.2.11 Tool adapter plates, tool store and tool replacement equipment manufacturing (KA)

B.2.12 Assessment of treatment of specific cutting effluents (KA)

B.2.13 Provision of representative microwave equipment (AEA)

B.2.14 Manufacturing of measuring system for representative alpha-beta isotopes; software

development adapted to detectors (BAI).

B.3. Adaptation of t‹x›ls and experiments
B.3.1. Setting up of a representative test mock-up (KfK)
B.3.2. Tool integration and testing (AII)
B.4. Data evaluation
B.4.1. Evaluation of test results concerning EMIR (KfK)
B.4.2. Evaluation of test results concerning mechanical tmls (KA)
B.4.3. Microwave data evaluation (AEA)
B.4.4. Measuring system qualification (BAI)
B.4.5. Final evaluation and recommendations including specific data on costs, work time and occupational exposure and estimates of secondary waste arisings (AII).

G PROGRESS **OF WORK AHD OBTAINED RJ SULTS**

Summary

Within **1990,** the basic concept **investigation B.1.1.** - **B.1.12. started and** the integration parameters of all partners to the EMIR system were defined. The discussed basic concept was agreed at the first milestone meeting, end of **February 1991.**

Progrms and rmults

KfK activities: EMIR has been equipped with a wrist, which replaces the arm 5. This wrist carries a flange plate to allow the attachment of tools and sensors. For the decommissioning work, it was agreed to construct a tool exchange system of two plates A and B; the A-plate attached to the EMIR wrist, the B-plates carrying the various tools and measuring devices (B.1.1., B.1.2.). Figure 1 shows the overall working capacity of EMIR.

KA will construct the plates and take care of the couplings beside their tool development. Various tools have been taken into account but core drill, chisel and hydraulic cutter are considered to be installed (B.1.4., B.1.5.).

AEA-microwave system was defined and introduced with its needs for demonstration in the free field (B.1.6.).

The microwave device consists of a large box (16IXi x 900 x 800 mm) containing the magnetron, the circulator and the necessary electronic equipment. Attached to this box is a z-shape waveguide with a shroud that directs the microwave at the concrete (see Figure 2).

The input power of the microwave device will be 80 kW. The output power is adjustable from 5 to 60 kW.

BAI contamination measurement device will consist of an array of six detectors. Existing detector technology will be used for that purpose. Developments of new detectors are under way. If they are finished in time, they will be integrated into the system. This detector array is protected by a frame against contact with surface (B.1.7., B.1.8., B.1.10., B.1.11., B.1.12.).

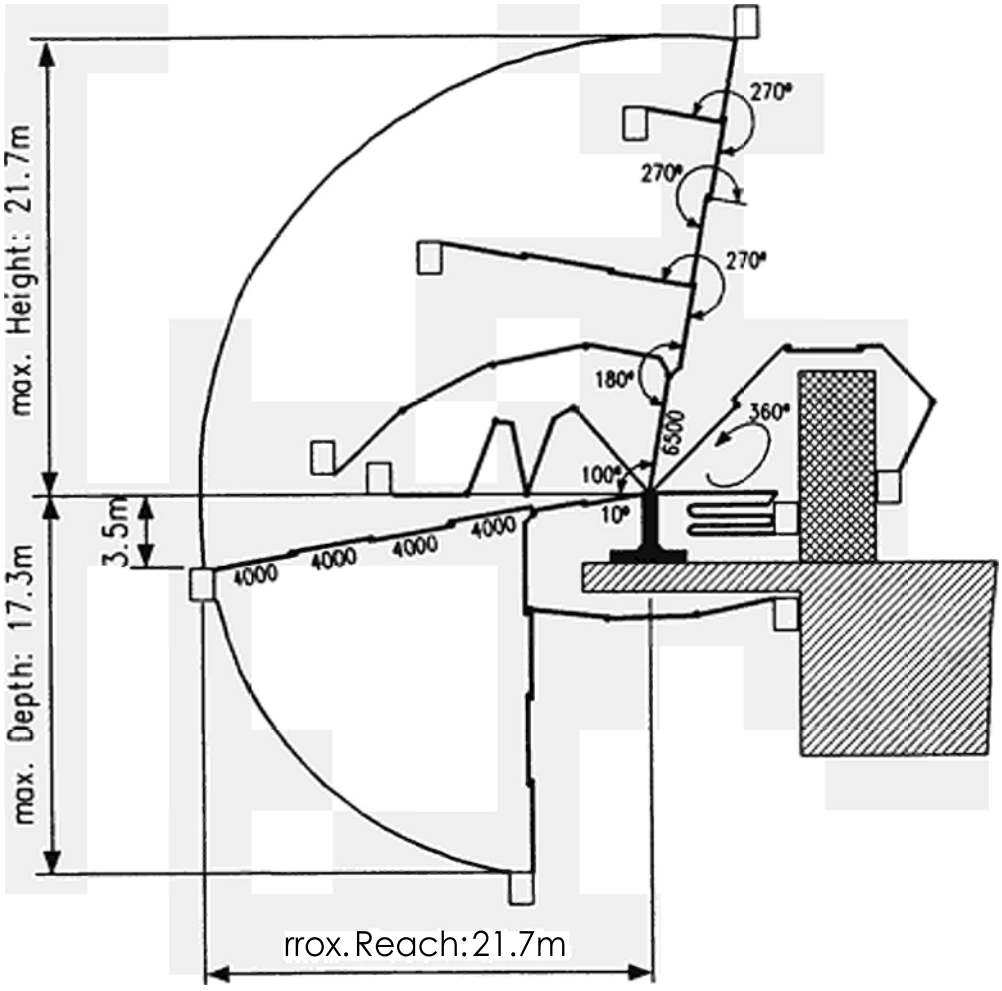
Definition of contaminants is still open (B.1.9.).

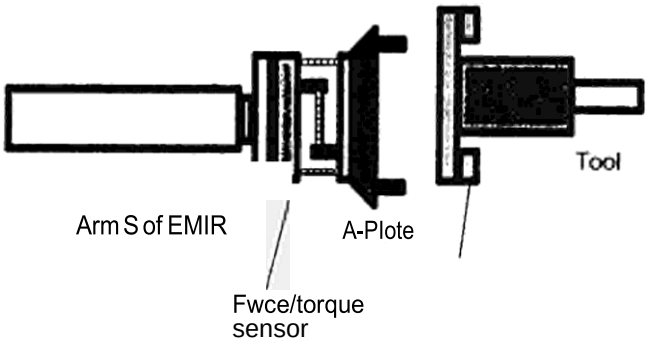
Test layout: A rough estimate of test parameters was discussed and agreed to demonstrate the teleoperability of tools separately from the **maneuvering capabilities of EMIR (B.1.3.).**

Problems: The licensing procedure for microwave **health impact and atmosphere disturbances by leakage has** to be started as well as the licensing to use **tracers in** free field conditions.

An extensive microwave monitoring seems to **be necessary for personnel protection.**

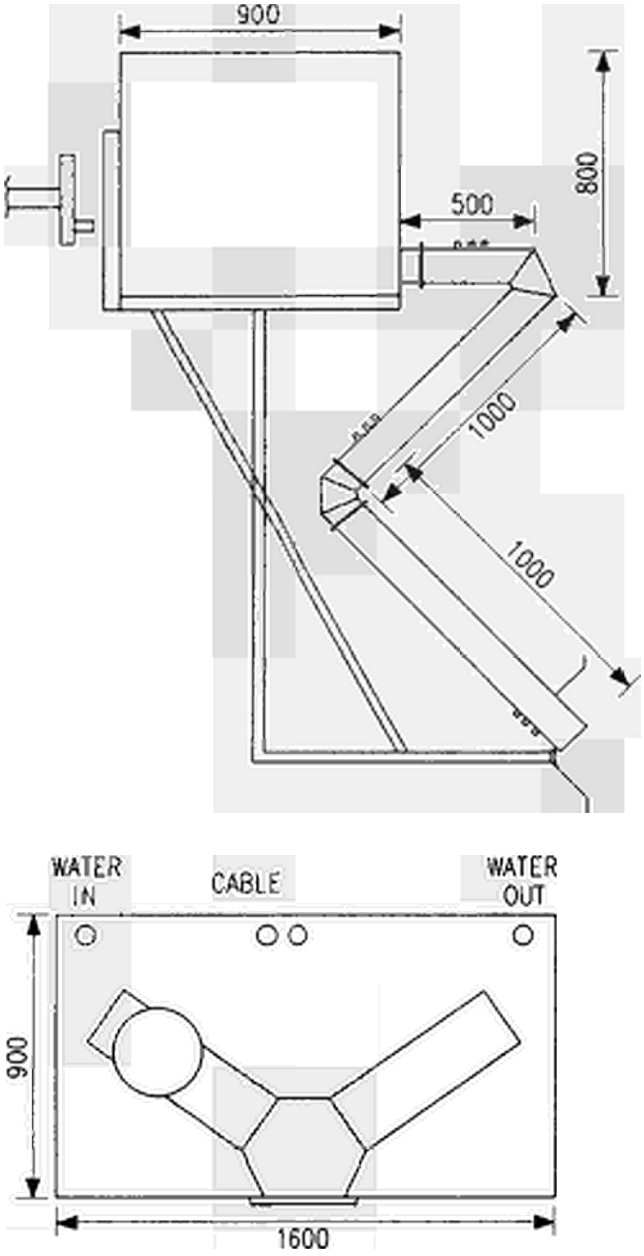
- 82 -





F \ gu re 1 :

Overall size of BMIR and tool plate design



F i gure Z:ABh N1c o -wave dev1ce

- 84 -

e unoERWATHR QUALIFICAcon or no xsix.sna•ULATOR

Contractors CEA FAR, Framatome, TNO
: Contract Delft FI2D-tD4l
No.: Work October I9RI - January 1993
Period: **G CLEMENT, CEA/DTA/UR, CEN/FAR**
Coordinator: Phone: **33/1/46 54 91 16 Fax: 33/1/46 54 02 36**

W OBJECTIVE AUD SCOPE

The work concerns industrial-scale underwater experimentation in non-radioactive conditions of the RD 500 prototype telemanipulation system, which has been already extensively tested **in air with** various tools. The typical nuclear dismantling **environment concerned** is a LWR vessel and fuel storage pool.

The objectives are:

- Adaptation of the **existing** RD 5fD manipulator for underwater **dismantling tasks;**
- Assessment of the capability of the RD 5fD manipulator to operate under water with various tools;
- Underwater qualiEcation and performance assessment of a new ultrasonic imaging system;
- Oualification of the complete system by an in-field application and definition of an industrial underwater RD 500 system.

The research work will assess the feasibility of underwater dismantling operations, the performance of the computer-assisted modes of control and the assumption that the RD 5fD system can be more elective than hands-on work in relevant decommissioning **environment.**

The CEA will coordinate the research work Subsidiary companies of the CEA and Framatome (SNE La Calhéne and ATEA) will perform specific technical adaptations on the RD 500 systems and the underwater qualification tests.

B. WORR PROGRAMME

B.1. Identification of underwater requirements and speciBcation to be done on the RD 5fD and the vision sYstem

B.1.1. IdentiEcation of relevant underwater tasks (CEA).
B.l.2. Selection of appropriate tooling systems (plasma arc, abrasive disc, electro-erosion) (CEA)-
B.l.3. Definition of test mock-ups on which the tooling will be operated (Framatome, CEA).
B.l.4. Specification of the auxiliary test equipment (Framatome).
B.l.5. Specification of RD 500 adaptations, with particular view to its water-tightness (CEA).
B.l.6. **Specification** of the optical vision systems (TNO, CEA).
B.l.7. Drafting of a qualification procedure document based on relevant cutting operations **(cEA).**

BE Preparation of the preliminary tpsts in air and under water-. the basic hardware and software will be developed/adapted. manufi :tured and assembled

B.2.1. Study, manufacturing and shop test of adaptation of tooling selected in B.l.2. (Fr. + CEA)
B.2.2. Design and manufacturing of RD 5fD adaptations; preliminary underwater tests (CEA).
B.2.3. Vision systems acquisition, adaptations and developments (TNO, CEA).
B.2.4. Manufacturing of the auxiliary test equipment (Framatome).

BE. Preliminary atine of the complete wstem

B.3.1. Individual air and underwater testing at each partner's laboratory (AII).
B.3.2. Installation of sirqplified test mock-ups for main sub-system testing in air (Fr. + CEA).
B.3.3. Main sub-systems testing (Framatome, CEA).
B.3.4. Implementation of improvements (AII).

B.4. Underwater eualifimtion tiats

B.4.l. Installation of the various equipments in a water p‹x›l at ATEA/Framatome (Framatome).
B.4.2. Operational verifications of the complete system (AII).

B.4.3. Performance of the qualification tests as defined in B.I.7. (Framatome)

BE. U•uial evaluation and specification **with rmpect to ‹x›nditiom in** real **dismantling projects;** evaluation of the sts **of an industrial RD 5tD system and of its r»dioloeical imoact on work force and working area** (AII).

- 8S -

C. PROGRESS **OF WORK AND OBTAINED RESULTS Summary** of main issum

The period was devoted to the review of the **possible dismantling** task and to the **identification** and analysis of the tasks which would best demonstrate and evaluate the **capabilities** of the *RD*500 manipulator system.

Progrms and rmults

1. **Identification** of underwater requirements and specifications to be done on the *RD* 500 and the wition svstem (B.1.)

FRAMATOME company has selected the electroerosion process in the context of the removal of a welded key securing the bolts **that maintain heavy plates constituting PWR** boiler internals. In this framework, the RD5tXl manipulator **will demonstrate its ability to carry and** position the tool in front of the welded key. Master-slave as well as **automatic modes of** controlling the arm will be evaluated in order to identify the most effective and fast combination to achieve the task. The operations will be performed with the help of video and ultrasonic feedbacks.

The electroerosion process requires to **very accurately position and** hold the tool **head during** operation. This constraint cannot be fulfilled when the tool **is directly handled** by the manipulator. This is due to the flexibility of the arm supports **(amplifying vibrations) and the** actual accuracy **positioning** limit of this type of manipulator. Consequently, a particular technique will be developed to render the process locally independent from the manipulator (the tool will be pressed by the manipulator on the support plate in order to bypass the vibrations). This technique may become generic and will be applicable to operate **similar** toolings.

CEA has selected two other underwater processes which ccirrespond to the type of tools which are of common use in the decommissioning activities. These are the plasma torch and the disk grinding tool. The operation of these tools will address the evaluation of some other capabilities of the RD5tXl manipulator.

The first tixil is a plasma torch underwater cutting head. The interests to consider plasma are numerous:

- the direct handling by the operator - in manual “master-slave" mode - of a plasma torch is very difficult. The operator is unable to perform acceptable work mainly because the accuracy and the regularity of the manually generated movements are poor, one needs some assistance in order to stabilize the motion and the speed of the torch, especially when segmenting thick metallic plates. The programme will consequently implement and evaluate the effectiveness of the computer-assisted teleoperation mode available in the control system of the RD5tXl manipulator;
- the **visual** control of the plasma **segmentation process is difficult** because of the arc **illumination (blinding** the cameras) and the production of gas bubbles. The computer assistance is one approach to overcome the problem (automatic movement generation and control), however the visual aid is still not available. To overcome this **difficulty** the programme will evaluate the help that can be provided by ultrasonic **imaging** techniques.

The second tml selected by CEA is a disk grinding machine which underwater test will address the field of geometric assistance (in order not to jam the disk) and the operation of heavy and **strongly vibrating t‹xils.**

TNO has started the analysis of the task envisaged by **CEA and FRAMATOME and** their surrounding environment in order to define the required characteristics of the ultrasonic system. The nature of the work scene is different from past experience in the field of offshore **applications, an adaptation study** is necessary.

FRAMATOME has started with CEA the analysis of the implementation of the whole system on an experimental work site in the pool of ATEA company in Nantes.

6. No.6:ESMMAWONOF QUO OF IOACMVE WMDT SING OMDECO SlO GOFNU H4 WONS D4 CONBMflWTY

The low-level radioactive waste **produced in the dismantling** of nuclear **installations will ultimately** constitute a substantial part of the overall volume of radioactive waste generated by nuclear industry. The objective of this area is to estimate the quantities of **various** categories of radioactive waste that will arise from the **decommissioning** of nuclear installations in the Community. This involves the **definition** of reference strategies for **decommissioning and is** therefore to be regarded as a long-term task

B. SA ofMe omxduekx usp (l)

Research has been performed in the **following main** areas:

- estimate of the quantities of radioactive waste arising from the decommissioning of typical nuclear installations, based on analysis of **radioactive** metal and concrete samples;
- study of strategies for the **decommissioning** of typical nuclear installations and for the **conditioning/management** of the radioactive waste arising therefrom;
- characterisation of the radioactivity associated with components and structures of **various** nuclear installations, with emphasis on long-lived radionuclides; in situ measurement techniques for the localisation **and identification of radionuclides, including** the case of mixtures of alpha, beta and gamma emitters;
  assessment of residual activity levels below which activated and/or contaminated parts could
  be reused and corresponding measurement methods.

C. Programme 1989 to 1993

Radioactivity measuring techniques should be improved/developed with particular regard to clearance procedures for materials, **buildings** and sites, **including** the case of mixtures of alpha, beta and gamma emitters. The quality assurance of clearance procedures should also be considered.
Strategies for the decommissioning of **typical** nuclear **installations** should be further studied, account being taken of the waste **disposal facilities existing** or planned in various member countries. Safety being one of the aspects to be considered, a methodology for evaluating the risk of **decommissioning** operations should be developed.
The evaluation of residual activity levels below which materials from **decommissioning** could be reused should be pursued, including consideration of statistical aspects.

D. Programme implementation

At the end of 199fJ, six research contracts relating to Area No. 6 were at the stage of execution and three contracts were at the stage of negotiation.

QICK GDflUMODS OFRADIONUCLIDES zn xnnmlws **AND**
WASTES DURING DECOMMISSIONINGOF HUCLHAR znsz»imnvions

Contractors: TUV-SWD,FHGF
Contract No.: **FI2D-0033**
Work Period: September 199(l - December 1993
Coordinator: L DIERKES, TffV, Mannheim
Phone: 49/621/395 530 Fax: 49/621/395 299

AOHM3€XTM3ANDSCOPE

Under the ALARA guidelines of the German Radiological Protection Ordinance, it is necessary to know the exact amount of radioactivity and the radiological potential of the materials of installations to be decommissioned.

The objective of this work programme is to determine a correlation between the gamma and beta emitters (electron capture nuclides) by analysing the activation products and contaminants in reactor materials and in waste products. These informations are essential for determining the radioactivity released to the environment and for radiological protection of the public and the personnel.

The extracted material (e.g. iron) will be submitted to beta-activity measurements, followed by a gamma-activity determination. The correlation of both measuring methods should make it possible to reduce the determination of the total radioactive material quantity to gamma- spectroscopic analyses.

The work programme will be performed in contact with the Chemistry **Division, Harwell** Laboratory UKAEA, especially concerning the exchange of measuring methods.

B.WORKPROGRAMME

B.1. Acquisidon of instrumenta0on (TOV-SWD)
BE Choice and pr‹xnaement of re tative **samples from the reactors FR2, KNK andor xwo(ruvxwo)**
BE. Laboratory activines. reference measurements and correlanon calculations for nuclear

B.4. Evaluation and documentation of the **cults (TEV-SWD)**

GPROGRESSOFWORKvUM]OBT RES TS

1. **Acquisition** of instrumentation (B.l.)
   A coaxial Ge-detector with high resolution spectrometer and a low-level proportional counter are installed and are now working.

2. Choice and procurement of representative samples (B.2.)
   Calibration procedures of photo-emitting nuclides and efficiency measurements are carried out. The low-level proportional counter is calibrated with Beta-emitting sources.

3. **Laboratory activities (B.3.)**
   For **the identification and** separation of radionuclides (especially electron capture nuclides), a wet chemical separation procedure will be develop‹xL

6R RADIOLOGICAL ASPECTS OF RECYCLING CONCRETE DEBRIS FROM DISMANTLING OF NUCLEAR INSTALLATIONS

Contractors: T()V-Bay., RWE
Contract No.: **FI2D-0339**
Work Periodi November 19Rl - December **1993**
Coordinator: F I SCHMID, TiiV-Bay.
Phone: 49/89/5791 1470 Fax: 49/89J5791 1551

AOBE8CMVE/dW]SODPE

Limiting values for the release of concrete with low-level residual **radioactivity** for the selective undangerous utilisation (e.g. for noise barriers, earth fill, earth bank or substitute for foundation material) are presently not defined. The research programme will examine whether it is possible to define limiting values for **radioactively** contaminated concrete in the range of the limiting values for steel. The effect of radioactively contaminated concrete on the soil (leach out of radionuclides) **and on man** (radiation exposure) will be determined.

The results of these studies will have an effect on the decommissioning activities as far as buildings of the controlled area and the **kind** and quantity of the radioactively contaminated concrete are concerned.

The advantage of the studies lies in an economic and safe recycling of large amounts of concrete with a low-level artificial residual radioactivity. Thereby, valuable ground storage space would be saved and natural gravel deposits would be preserved.

The research work will provide data concerning cost saving by recycling concrete from controlled areas, **radiation** exposure of the decommissioning workers and of the general public.

The research programme is performed in co-operation with CEA-IPSN, which has a research programme with a **similar objective** (see § 6.4.).

B.WOWKPROGRAMME

B.1. Leach tmts
B.1.1. Design of the test facility and determination of concrete test specimen. (all)
B.1.2. Construction and operation of the test facility. (T(IV-Bay.)
B.1.3. Literature survey on leaching out problems of radionuclides in concrete. (TOV-Bay.)
B.1.4. Radiological measurements on concrete rubble before, **during and after** leach out tests.

(TÜV-Bay.)

BE Natural radioactivity in concrete
B.2.1. Procurement of samples kom recently produced and aged concrete. (RWE)
B.2.2. Measurement of alpha, beta and **gamma radiation. (Ti)V-Bay.)**
B.2.3. Literature survey concerning the natural radioactivity of concrete.
BE. Development of me for
B.3.1. Examination of concrete **recycling possibilities** by a literature study. (RWE)
B.4. Calc••tinr of r+d‹atier mute==<Sn• ination of the artificial rmidual radioactivity
B.4.1. Determination of **radiation exposure scenarios. (T€fV-Bay.)**
B.4.2. Calculation of **radiation exposure** for man due to natural and artificial radioactivity. (T IV-Bay.)

- 90 -

G PROGRESS OF WORK AND OBTAINEDRESULTS

Summary of main inns

Due to the late transfer of the research contract, the work programme started not earlier than November 9fi.

In November/December, the following activities were carried out:

- planning of the test facility for the leach tests;
- procurement of approximately 15 (out of 50) samples of aged concrete from conventional **buildings and** approximately 15 (out of 50) samples of recently produced concrete;
- preparation of the measurement of alpha, beta and gamma radiation.

1. Design of the test facility and determination of concrete test specimen (B.1.1.)
   The layout of the six containers for the concrete test specimen and of the sprinkler system for the tests were planned (Figure 1). The amount of water for imitating the rain was defined as a precipitation of 1,000 mm per year. Using a time-lapse effect, the time for affecting the concrete by rain is reduced from 20 years to 20 months. 5 test specimen will be sprayed with 1,1100 mm of water every montk The sixth test specimen is constantly under water.
   The test facility is under construction at the moment. It will be installed in the turbine hall of the shut down nuclear power plant of Gundremmingen, unit K

2. Procurement of samples from recently produced and aged concrete (B.2.1.)
   In 1990, approximately 15 samples of recently produced concrete and aged concrete were collected in the state of Bavaria (FRG). At the moment, the remaining samples are being collected in various states of the Federal Republic of Germany.

3. Measurement of alpha, beta and gamma radiation (B.2.2.)
   The preparations for the measurement of alpha, beta and gamma radiation will be carried out. The measurements will start early in 1991.

The research programme proceeds according to the schedule.

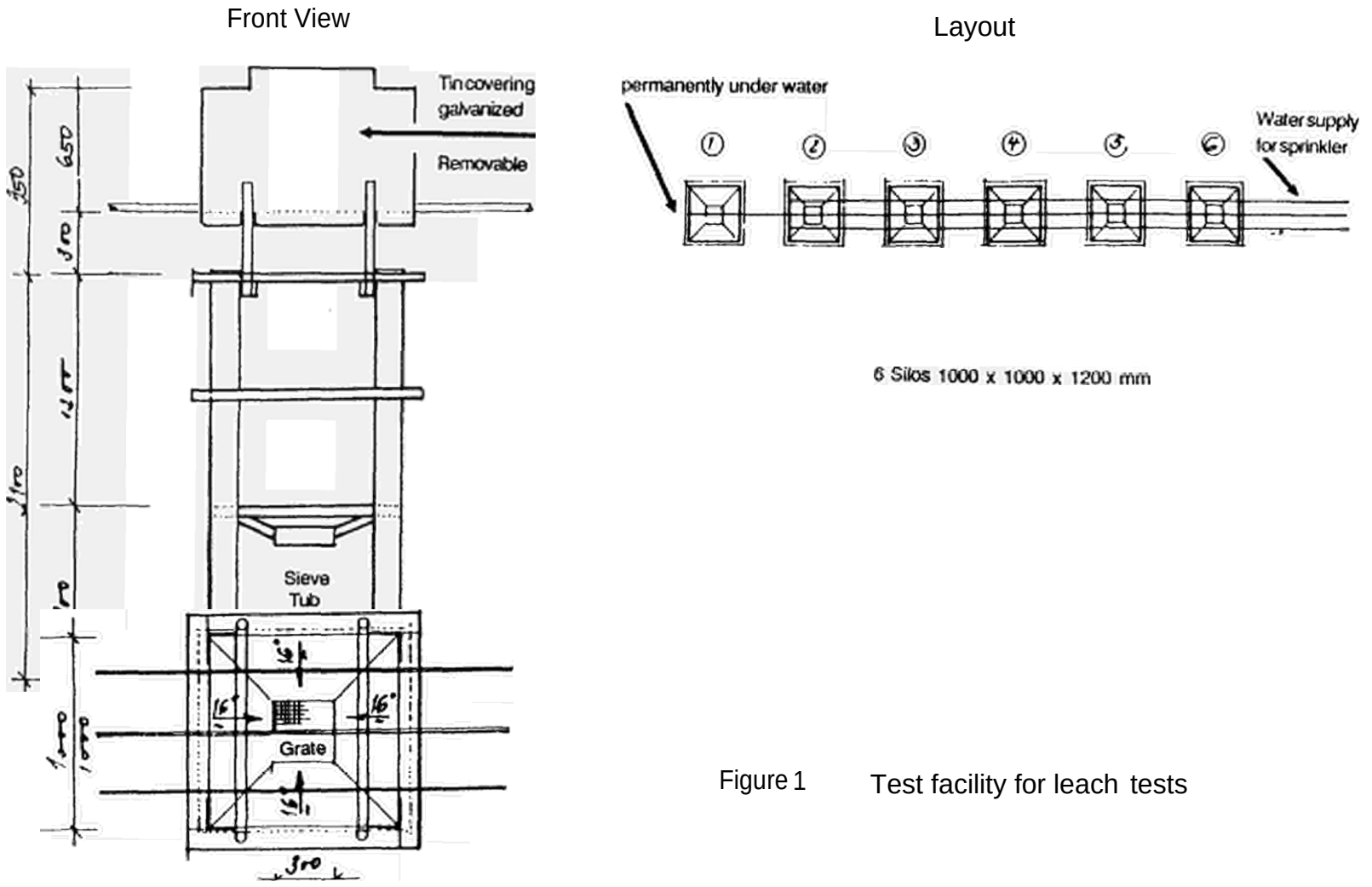


Figure 1 Test facility for leach tests

6.3. METHODOLOGY TO EVALUATE THE RISKS OF DECOMMISSIONING OPERATIONS ON NUCLEAR PLANTS

Contractors: AEA-Culch., NRPB, AEA-Win‹L
Contract No.: **Fl2D-tlfi30**
Work Period: October 199fi - September 1992 G
Coordinator: **C MEGGITT,** AEA-Culch.
Phone: 44/925/2542 24 Fax: 44/925/25 45 44

A OBJECTIVE AND SCOPE

The theoretical work is composed of two distinct but complementary **studies:**

a) Waste management options: The theoretical study continues to develop an **existing** methodology **to aid decommissioning** waste management decisions, and to demonstrate the improved methodology by applying it to the prototype AGR Windscale reactor decommissioning waste for which the final management option has not yet been chosen. The **main extension to the existing** methodology (see **final** report on contract FI1D-fD51 is to enable the incorporation of risks and uncertainties, rather than simply doses and environmental impact parameters. The improved **methodolgy, like the existing** one, will be applicable to decisions concerning the decommissioning of all types of nuclear reactors and could lead to reductions in radiation risks and financial costs, as well as promoting consistency between the approaches in various countries;

b) Decommissioning strateRles: The work **will aim at developing** a comprehensive methodology to evaluate radiological risks to the public and workers from decommissioning of non-reactor nuclear plants. Such a methodology will allow the comparison of different decommissioning strategies from a risk point of view so that the benefits associated with, for example, delay in decommissioning to more advanced stages could be assessed.

B. WORK PROGRAMME

B.1.a. Development of a radiologji3ij_;j§Y_evaluation methodology (NRPB)

Bra. Selection of the waste stream for an emmole annlication of the meth‹xkik›gy (A£IA) BE.a. Definition of the radionuclide inventory and their distribution in the se)ected waste

B.4.a. **Definition of waste manaeianent ootiom (AEA)**
BE.a. Estima0on of financial ‹x ts for each of the **management op0oos. (AHA)**
B.6.a. Calcula0on of drum and risks for individuals and the nublic. (NRPB)
B.7.a. bment of **social and environmental impacts of waste management optiom. (NRPB)**
B&a. **Demoiatration** of the metlxaloloeY iw **identifying the optimal management option (NRPB)**
B.9.a. Revi o e of a o r**‹lecommissionine deciaiom**

B.1.b. Definition of demmmissio hi m **of non-reactor. nuclear plants. (AEA-Culc for the**

Bob. Identibcation of techniaum for carrsine out demmmissioninz operation and their risk-bearing elements.

BE.b. Identification of risk men 1 ptixxxlurm taking into account normal and t ethic

B.4.b. Evaluation of pnxxxlurm for *•.••••'*•>'* <th lea"inr p!•si

BE.b. Examination of methods for the aji g tion of rms ass‹x:rated with

B. lb. Demomtration of the identified methodoloeim to a **non-reactor faciliy.**

B.7.b. Fma1 evaluation on the siiitabilitY and limita0om of the identified methcalolo

- 93 -

C. Progress of Work and Obtained Results

Summary of mainissues

The contract was issued in November 1990 and the work undertaken by AEA in the calendaryearwasrestrictedtothepreliminarydefinitionofrelevant stages and factors.

TheotherContractorswerenotprogrammedtostartuntilfirstQuarter 1991.

Progress and Results

1. Definition of decommissioning phases(B.lb)

Thethreedecommissioningstagesdefined byIAEAhavebeentakenasthe basisfor the project. They are, as defined for land-based reactors: storage with surveillance, restricted site release and unrestricted site use. It has become apparent that these categories are rather broad for the practical purposes of the project and Stage 1 has therefore been subdivided into a further 3 stages:

lA - Removal of active working material
lB - Decontamination to levels suitable for surveillance
lC -Decontaminationtolevels suitable for alternative active use

It is recognised that the lCtosome extent overlaps with Stage 2.
It has been found important to make distinctions between: Operations
whichareextensions ofnormaloperations.
Operations which have been conducted as maintenance operations. Operations which are not normally conducted.

Risks associated with the intended operations.
Risks associated with the plant not being in the expected state.

- The second of these is particularly importantin decommissioning where information may be incorrect orincomplete andareasof plant are entered which may have been unmonitored for a long period.

Plant which has been shut-down after normal operation. Plant whichhasbeenshut-down afteranaccident.

Accidental hazards.
Routine radiological hazards.

Hazards associated with hardwarefailures.
Hazards associated with faulty management procedures.

Operations which must be performed promptly. Operations which can be delayed.

These preliminary classifications willbe elaborated as a range of non- reactor plant decommissioning is considered.

6.4 DIONOF CB FOR EXRMFMON OF CDMA (X)]ANGFROMDN G

Contractors: **CEA-FAR**
Contract No.: **FDDOOW**
Work Period: October 199fi - September 1992
Coordinator: Mr D. **HARISTOY, CEA/IPSN/DPEI/SERGD, Fontenay-aux-Roses**
Phone: 33J1/46 5471 **56** **Fax: 33/1/47 35** 14 23

AOBRKXTM3ANDSODPE

The objective of the study **is to propose activity** limits below which very **slightly radioactive** concrete arising from nuclear facility dismantling could be treated in conventional industry, or slightly contaminated buildings could be reused or decommissioned.

The study is based on the evaluation of concerned concrete quantities and allows the identification of groups of people exposed to radiation hazards. From the evaluation of **individual** radiological risk, the **derived limits** for exemption of concrete will be deduced. The study is also meant to participate in the harmonisation of criteria and rules between countries of the European Community. Potential benefits **in determining** such limits are:

limitation of the decontamination time and operations, i.e. decontamination and disposal costs;
- recycling of valuable material to preserve natural resources;

The research programme is performed in co-operation with TfIV Bayern and RWE go (contract n2D-0039), into which CEA-IPSN will bring in the following information: natural radioactivity in concrete; work programme and results of each period; results of other French experiments connected with the subject.

B. WORKPROGRAMME

B.1. Data ‹x›llection
B.1.l. **Estimation** of contaminated and activated concrete quantities.
B.1.2. Identification of radionuclides spectra and activity levels.
B.1.3. Estimation of concrete **quantity** which is recycled or disposed off.
B.1.4. Determination of the state of the art to identify the critical group of workers and public.
B.1.5. **Investigations on the possibilities** of exposure of the public to different concrete by- products.
B.1.6. Dust measurements **and analysis in different** crushing stations.

BE Treatment of information and mi Jellinp.
B.2.1. Collection and evaluation of parameters for the different by-product pathways.
B.2.2. Modelling of the different realistic exposure situations for critical groups.

BE. Calculation of the naliological i0ipf :t i trip the ‹xillected parameters durinp the inquirim
i£4. I3etermination of the activity limits for each radionuclide on classm of them

C.PROGRESSOFWORK OBTvUNED PLTS

Progress and results

Data Collection (B.1.)

1) Determination of the state of the art to identify the critical group of workers and public (B.1.4.)

Our inquiries into the civil engineering workers in France, shows that there are two kinds of concrete crushing installations.

The big one, with a capacity greater than 200,0tD metric tons, is constituted by two crushers, several riddles and produces different qualities of aggregates.

The second one, with a capacity of 120,0tD metric tons or more, could move from site to site. From the economical point of view, the transfer is made if there is a crushing capacity allowing three month of work.

2) Investigations on the possibilities of exposure of the public to different concrete by-products (B.1.5.)

In France, at the present time, concrete by-products are essentially used **in civil** engineering works, as aggregates mixed with cement in road basements or landing-strips, or without additive in lanes or carriage drives.

In the construction industry, the quality of the aggregates limits their use to by-products for manufacturing of building blocks.

US. OOSES DUE TO THE RHUSE OF VERY SLIGHTLY RADIOALIIv . HMI-i

Contractors: CEA-FAR, BS, **SIEMENS** BEW
Contract No.: **FI2D-tO31**
Work Period: September 19Rl - February **1993**
Coordinator: Mrs H GARBAY, CEA-IPSN, Fontenay-aux-Roses Phone: **33/1/46 54 73 41 Fax: 33/1/47 35 14 23**

AOBE3€XTM3ANDSODPE

The scope of the study is the **determination** of doses due to the reuse or recycling of very slightly contaminated radioactive steel in case of mechanical and thermo-mechanical treatments applied to scrap when exempted from regulations.

The study will mainly be based on already available data both in the nuclear field and in the conventional scrap industry. Experimental **investigations will** be performed, as far as possible, on radioattive samples coming from nuclear installations being dismantled. The different treatments applied to scrap before its melting have not yet been studied and are of great interest. In **particular,** techniques used in scrapyards should be studied in the view of inhalation and external exposure **injuries.**

This study applies to a large quantity of steel arising from dismantling of nuclear installations (EUR 1tO52).

Benefits are expected as regards management and cost of radioactive waste **arisings,** protection still being secured. The results concerning contamination dispersion during cutting of scrap will be useful for the evaluation of future large-scale decommissioning operations.

B.WORKPROGRAMME

B.1. Oiscussion and **documentation of the prment regulatory situation. (BS-CEA)**
BE Performance of steel cutting and Tier ol samnli g **experiments obse dustrial conditioim (CEA-Siemens)**
BE. Evaluation of inhalation risk in realistic situations- (all)
B.4. determination of the radiological imnact **based either on bibliographic data or on**
BE. Develonment of a **stochastic programme to obtain the individ»J dccc distribution. (BS)**

C. PROGRESS OF WORK AND OBTAINED RESULTS

This progress report applies to the work done from september 1990 to december 1990.

The work performed by CEA was mainly bibliographic studies and collection of information on scrap recovery plants. Bibliographic studies were focused on the study of scrap market and on dust emission during cutting processes. Results were mainly obtained on oxygen cutting, dust concentration ranges from 4 mg.m^{-3} to 28 mg.m^{-3}. experiments have been made on different types of steel (special steel, painted or not, various scraps of carbon steel and stainless steel, thick ingot). The average dust concentration for each type of steel is ranging from 8 mg.m^{-3} to 15 mg.m^{-3} (B1).

A scrap recovery plant has been visited, which uses a 900 tonnes scrap shearing in an open air area. It operates the cutting of concrete reinforcement bars and of metal girders. The cutting of concrete reinforcement bars is dusty, this dust comes mainly from remaining concrete; the cutting of metal girders is less dusty, this dust comes mainly from the rust. An agreement has been established for a measurement campaign in this plant (Bl-B2).

The work performed by Brenk Systemplanung started with a survey of industrial exposure conditions for the cutting of slightly contaminated steel scrap. For alpha-emitters inhalation of aerosols produced by the cutting operations is the dominant pathway. The survey, therefore, was primarily directed to an assessment of the important parameters for the various cutting techniques employed in industry (B1).

In the lung models of ICRP the particle size of incorporated aerosols is considered as an important parameter. In order to deal with this factor of influence a formalism was developped that is capable introducing the particle sizes into the dose calculations (B3).

On the basis of this work first steps for the modeling of the radiation exposure have been taken.

The work performed by Siemens applied to characterization and treatment of scrap from the uranium processing division of the Siemens nuclear fuel fabrication facility in Hanau. By experience the following average scrap composition is known: ferritic steel 859» ; austenitic steel : 159». The applied reduction techniques are the following: mechanical methods are sawing with a hacksaw and compass-saw, reduction using plate shears, compacting using hydraulic presses; the thermal method is oxy-acetylene cutting.

According to the work program, it is intended to divide the tasks into the following steps:

Preparation of metallic scrap items with an alpha-activity in the range of about 0.05 10 Bq/cm^{2}. For the determination of the alpha-activity, the surfaces have to be as smooth as possible.

- Determination of the surface alpha-activity.

  Characterization of the material in terms of composition and surface roughness.

  Determination of the smearable proportion of the activity.
- Performance of the reduction operations with simultaneous sampling of alpha-aerosols for the determination of the released total quantity of alpha-active aerosols as well as the determination of relation between aerosol alpha-activity and the average particle size.
- Determination of the alpha-activity of aerosol samples using a suitable proportional counter (Bl-B2).

6.6. QUA1'ITIFICATIOi'I OF ACTIVITY LEVELS AND OPTIMISATION OF DOSE RATE MA1'IAGEMH1'IT TO PREPARE STAGE 3 DECOMMISSIONING OF GAS-COOLED REACTORS

Contractors : Contract No.: Work Period: Coordinator :

CEA-VALRH&, Radia
FI2D-tOl4
October **1990** - **September 1993**
J R **COSTES, CEA/DCC/UDIN, Bagnols-sur-Céze Phone: 33/66 79 13 Fax: 33/66** 79 64 32

AOBEEGMVE SOOPE

As part of the preparatory work for Stage 3 decommissioning of the G2/G3 gas-cooled reactors at Marcoule, the project involves:

quantifying the activity levels of complex core structures based on theoretical analysis and on a large number of dose rate measurements;

design of a software package to optimise the dismantling and related **operations and** best minimising of the dose rates incurred by the personnel.

It is **important** to determine the dose rates and time necessary on each manual dismantling operation, and to assess the material activity levels for optimum waste conditioning and disposal.

The development of suitable software tools and thorough examination of all the possible scenarios are very time-consuming undertakings requiring aid beyond national boundaries.

B.WORKPROGIUU4ME

B.1. £k›se rate measurements and anfee plc after a literature review (CHA).

B.k Analvsm of geometric. phwical anil radiological day (Radia)

BE. Development of a mmputer programme to calculate gamma-activity levels in the ensure core (Radia)

B.4. Development of a **computer programme to minimise dv rate during human interventions**

BE. Comparison of calculated and measured rmults (CEA).

B.6. Examination of **dismantling scenarios (CEA).**

B.7. Revision of expert software considering demmmissioninz time and dosm (CEA).

B.8. Evaluation of ‹x **ts, radioactive rob dosm, working time and secondary waste arising (AII).**

C . P ROGRPSSOFWORK7UM]OKEAMED ULB

No significant work was performed in this just starting contract.

4. Research Overview

13

Robust Adaptive Nonlinear Control for Robotic Manipulators withFlexible Joints

P. Krishnamurthy,[1] *F. Khorrami*[1,*] and *Z. Wang*[2]

ABSTRACT

The robust adaptive control problem for a multi-link robotic manipulator with flexible joints is considered in this chapter. A general uncertain dynamic model of a robotic manipulator with joint flexibility is considered including uncertainties in joint stiffness, Coriolis and centrifugal terms, friction, gravity, load torques and disturbances, and actuator inertia. Only the inertia matrix of the rigid links of the robotic manipulator is assumed to be known. A robust adaptive dynamic controller is designed through vector backstepping with adaptations for the joint stiffness matrix, actuator inertia matrix, and a lumped uncertain constant representing the other uncertainties in the system. It is shown that the designed dynamic controller provides global stabilization and practical tracking of reference trajectories specified for each of the joint variables. The

efficacy of the designed dynamic controller is demonstrated through simulation studies on a two-link manipulator with joint flexibility.

Keywords: Flexible joint, robotic manipulator, robust adaptive control

1 Control/Robotics Research Laboratory (CRRL), Dept. of Elec. and Comp. Engg., NYU Polytechnic School of Engineering, Six Metrotech Center, Brooklyn, NY 11201, USA.

2 Toshiba America Electronic Components, Inc., San Jose, CA, USA.

* Corresponding author

INTRODUCTION

Joint flexibility frequently occurs in robotic manipulators due to underlying effects such as elasticity in the gears, shaft wind-up, and bearing deformations. Hence, the dynamic modeling and control of manipulators with flexible joints has been studied in the literature through a variety of approaches (Khorasani and Kokotovic 1985, Luca et al. 1985, Spong 1987, Spong et al. 1987, Spong 1989, Dawson et al. 1991, Lozano and Brogliato 1992, Nicosia and Tomei 1992, Jankowski and Brussel 1993, Readman 1994, Qu 1995, Jain and Khorrami 1998, Wang and Khorrami 2000, Park and Cho 2003, Chien and Huang 2007). In parallel with the specific application to robotic manipulators with flexible joints, the development of nonlinear control designs for various classes of nonlinear systems has been heavily studied in the literature over the last few decades (e.g., (Krstic et al. 1995, Khalil 1996, Sepulchre et al. 1997, Isidori 1999, Khorrami et al. 2003, Krishnamurthy and Khorrami 2003, Krishnamurthy and Khorrami 2008)) to provide a rich toolbox of control design methodologies applicable to various practically relevant nonlinear dynamic systems.

Drawing from the literature on various control design methodologies, several control approaches have been developed for flexible joint manipulators as briefly summarized below. A dynamic feedback linearization method was proposed in (Luca et al. 1985). Singular perturbation based control designs were developed in (Khorasani and Kokotovic 1985, Spong et al. 1987, Spong 1989, Readman 1994). An adaptive controller based on passivity properties was presented in (Lozano and Brogliato 1992) and an integrator backstepping based methodology was proposed in (Nicosia and Tomei 1992). While approaches such as (Lozano and Brogliato 1992, Nicosia and Tomei 1992) required the nonlinearities multiplying the unknown parameters in the manipulator dynamics to be known, robust controllers were developed in (Dawson et al. 1991, Qu 1995) to alleviate the difficulty in explicitly modeling the manipulator dynamics and to reject possibly unknown disturbances. An inverse

dynamics based controller was developed in (Jankowski and Brussel 1993). A robust adaptive backstepping based control design was proposed in (Jain and Khorrami 1998) and extended in (Wang and Khorrami 2000) reducing overparametrization and allowing more general nonlinear uncertainties and disturbances. A fuzzy model reference based controller was proposed in (Park and Cho 2003) and a function approximation based adaptive controller for electrically driven flexible joint manipulators was developed in (Chien and Huang 2007). A general uncertain dynamic model of a multi-link robotic manipulator with flexible joints is considered in this paper and a robust adaptive backstepping based controller is developed. The uncertain dynamic model is allowed to include both parametric and functional uncertainties (as general nonlinear function bounds) and disturbance inputs. The designed dynamic controller is robust to uncertainties in joint stiffness, Coriolis and centrifugal terms, friction, gravity, load torques and disturbances, and actuator inertia. Only the inertia matrix corresponding to the rigid links of the robotic manipulator is assumed to be known. The designed controller achieves practical tracking of reference trajectories specified for each of the joint variables, i.e., the tracking errors can be made arbitrarily small through appropriate choice of the control parameters. The controller includes adaptations for the joint stiffness matrix and actuator inertia matrix as well as an additional scalar adaptation for a lumped uncertain constant representing all other uncertainties in the dynamic system resulting in a dynamic controller of order $(2n + 1)$ for an n-link manipulator. While the basic design approach is similar to our prior work in

(Jain and Khorrami 1998, Wang and Khorrami 2000), the control design here addresses a more general model of the uncertain terms in the system dynamics. While (Jain and Khorrami 1998) considered polynomial bounds on uncertain terms and required the actuator inertia matrix to be known, the design here addresses general nonlinear bounds and allows uncertainty in the actuator inertia matrix. Also, the design here addresses uncertain state-dependent disturbance torques on both the robot link side and actuator side in a more general structure than (Jain and Khorrami 1998, Wang and Khorrami 2000). Furthermore, the proposed adaptive control design results in a lower dynamic order ($2n + 1$) than in (Wang and Khorrami 2000) where a dynamic controller of order ($4n + 1$) was proposed. The considered dynamic model of a multi-link manipulator and the control design problem addressed here are described in Section **Problem Formulation**. The proposed robust adaptive control design is presented in Section **Control Design**. Simulation studies for a two-link flexible joint manipulator are given in Section **Simulation Studies**.

PROBLEM FORMULATION

The notations utilized throughout this paper are summarized below before describing the specific control design problem considered here.

Notations: $\Re$, $\Re^+$, and $\Re^k$ denote the set of real numbers, the set of non-negative real numbers, and the set of real k-dimensional column vectors, respectively. The notation $\max(a_1, \ldots, a_n)$ indicates the largest value among the numbers $a_1, \ldots, a_n$; the notation $\min(a_1, \ldots, a_n)$ similarly indicates the smallest value among the given arguments. With k being an integer, I_k denotes an identity matrix of dimension $k \times k$. With $\eta_1, \ldots, \eta_k$ being real numbers, $\mathrm{diag}(\eta_1, \ldots, \eta_k)$ denotes the $k \times k$ diagonal matrix with the i^{th} diagonal element being η_i. $|a|$ denotes the Euclidean norm of a vector a. If a is a scalar, $|a|$ denotes its absolute value. If a is a matrix, $|a|$ denotes the Euclidean norm of the vector obtained by

vertically stacking all the columns of a (i.e., Frobenius norm). If P is a symmetric positive-definite matrix, then $\lambda_{max}(P)$ denotes its maximum eigenvalue and $\lambda_{min}(P)$ denotes its minimum eigenvalue. A continuous function $\alpha : [0, a) \rightarrow [0, \infty)$ is said to belong to class K if it is strictly increasing and $\alpha(0) = 0$. It is said to belong to class K_∞ if furthermore $a = \infty$ and $\alpha(r) \rightarrow \infty$ as $r \rightarrow \infty$.

The model of a flexible joint manipulator under the assumption that the actuator motions can be modeled as torsion springs (Spong 1987) can be written as:

$$\ddot{q}_1 = -D^{-1}(q_1)\{C(q_1, \dot{q}_1)\dot{q}_1 + g(q_1) + \tau_1 + K(q_1 - q_2)\}$$

$$\ddot{q}_2 = J^{-1}\{K(q_1 - q_2) + \tau_2 + u\} \quad (1)$$

where q_1 and q_2 are the $n \times 1$ vectors of the link and actuator angles, respectively. $D(q_1)$ is the $n \times n$ symmetric positive definite inertia matrix corresponding to the rigid links of the manipulator. $J = \text{diag}\{J_1, \ldots, J_n\}$ is an $n \times n$ constant diagonal matrix modeling the actuator inertia. $C(q_1, \dot{q}_1)$ is an $n \times n$ matrix that models Coriolis and centrifugal terms. $g(q_1)$ represents the gravity terms. $K = \text{diag}\{K_1, \ldots, K_n\}$ is an $n \times n$ diagonal matrix of spring constants. τ_1 and τ_2 are $n \times 1$ time-varying and state-dependent vectors that include various uncertain torques (e.g., friction, disturbances, etc.) acting on the manipulator links side and actuators side, respectively. In general, the friction torques can be modeled through static or dynamic characterizations such as in (Sankaranarayanan

and Khorrami 1997). Only the link inertia matrix $D(q_1)$ is assumed to be known. $C(q_1, \dot{q}_1)\dot{q}_1$, $g(q_1)$, K, J, τ_1, and τ_{l1} are allowed to be uncertain. u is the $n \times 1$ vector of τ_{l2} applied input torques.

Defining

$$\tau_{n1} = C(q_1, \dot{q}_1)\dot{q}_1 + g(q_1) + \tau_{l1}, \tag{2}$$

the dynamics of q_1 can be written as

$$\ddot{q}_1 = -D_1^{-1}(q_1)\{\tau_{n1} + K(q_1 - q_2)\}. \tag{3}$$

Based on physical considerations (e.g., characterizations of friction and disturbance effects, physical manipulator limits, etc.), the uncertain torque vectors τ_{n1} and τ_{l2} can be bounded as summarized in the assumption below.

Assumption A1. τ_{n1} and τ_{l2} can be bounded as

$$|\tau_{n1}|^2 \leq \theta_1[\psi_{11}(|q_{11}|^2)\psi_{12}(|\dot{q}_1|^2) + \psi_{13}(|\dot{q}_1|^2) + \psi_{14}] \tag{4}$$

$$|\tau_{l2}|^2 \leq \theta_2[\psi_{21}(|q_{21} - q_{22}|^2) + \psi_{22}(|\dot{q}_2|^2)\psi_{23}(|\dot{q}_1|^2) + \psi_{24}(|\dot{q}_2|^2) + \psi_{25}(|q_2|^2) + \psi_{26}] \tag{5}$$

where θ_1, θ_2, ψ_1, and ψ_2 are unknown non-negative constants and ψ_{11}, ψ_{12}, ψ_{21}, ψ_{22}, ψ_{23}, and ψ_{24} are known class $\mathcal{K}_\infty$ functions.

Remark 1. Given any class $\mathcal{K}$ function $\Phi(s)$, it is possible to find a class $\mathcal{K}_\infty$ function $\tilde{\Phi}(s) = O[s]$ as $s \rightarrow 0^+$, and a positive constant, σ, to satisfy $\Phi(s) \leq \tilde{\Phi}(s) + \sigma$ for all $s \geq 0$. This can be easily seen by defining, for example, $\sigma = \sup_{s \leq 1} \Phi(s)$ and

$$\tilde{\Phi}(s) = \begin{cases} \Phi(1)s & \text{for } s \leq 1 \\ \Phi(s) + (s - 1) & \text{for } s > 1. \end{cases} \tag{6}$$

Hence, without loss of generality, the Assumption A1 can be replaced with the equivalent Assumption A1' given below.

Assumption A1'. τ_{n1} and τ_{l2} can be bounded as

$$|\tau_{n1}|^2 \leq \theta_1[\rho_{11}(|q_1|^2)|q_1|^2 + \rho_{12}(|\dot{q}_1|^2)|\dot{q}_1|^2 + \kappa_1] \tag{7}$$

$$|\tau_{l2}|^2 \leq \theta_2[\rho_{21}(|q_2 - q_1|^2)|q_2 - q_1|^2 + \rho_{22}(|\dot{q}_2|^2)|\dot{q}_2|^2 +$$

$$\rho_{23}(|\dot{q}_1|^2)|\dot{q}_1|^2$$

$$+ \rho_{24}(|q_2|^2)|q_2|^2 + \kappa_2] \quad (8)$$

where θ_1, θ_2, κ_1, and κ_2 are unknown non-negative constants and ρ_{11}, ρ_{12}, ρ_{21}, ρ_{22}, ρ_{23}, and ρ_{24} are known class $\square_\infty$ functions.

Defining

$$x_1 = q_1, x_2 = \dot{q}_1, x_3 = q_2, x_4 = \dot{q}_2, \quad (9)$$

the dynamics (1) can be written as

$$\begin{aligned}
\dot{x}_1 &= x_2 \\
\dot{x}_2 &= -D^{-1}(x_1)\{\tau_{n1} + K(x_1 - x_3)\} \\
\dot{x}_3 &= x_4 \\
\dot{x}_4 &= J^{-1}\{K(x_1 - x_3) + \tau_{l2} + u\}.
\end{aligned} \quad (10)$$

The control objective is defined as practical tracking of a reference trajectory q_r specified for q_1, i.e., we seek to design a dynamic control law for u utilizing measurement of x_1, x_2, x_3, and x_4 to make the tracking error $|x_1 - q_r|$ converge to $[-\delta_e, \delta_e]$ for any arbitrary prespecified δ_e while keeping all closed-loop signals bounded. $q_r(t)$ is assumed to be a given thrice-differentiable bounded reference signal with bounded derivatives up to order three. The i^{th} time derivative of q is denoted as $q^{(i)}$, i.e., $q^{(0)} = q$, $q^{(1)} = \dot{q}$, etc.

CONTROL DESIGN

The backstepping design proceeds by considering lower-dimensional subsystems and designing *virtual* control inputs (or equivalently, state transformations). The virtual control inputs in the first, second, and third steps are x_2, x_3, and x_4, respectively. In the fourth step, the control input u appears and can be designed.

Step 1: Defining the tracking error

$$z_1 = x_1 - q_r, \tag{11}$$

we get

$$\dot{z}_1 = x_2 - \dot{q}_r. \tag{12}$$

Defining the virtual control law x_2^* for x_2 as

$$x_2^* = -G_1 z_1 + \dot{q}_r \tag{13}$$

with G_1 being an $n \times n$ matrix and defining the Lyapunov function

$$V_1 = z_1^T P_1 z_1 \tag{14}$$

with P_1 being any $n \times n$ symmetric positive definite matrix, we get

$$\dot{V}_1 = -z_1^T [P_1 G_1 + G_1^T P_1] z_1 + 2 z_1^T P_1 z_2 \tag{15}$$

where

$$z_2 = x_2 - x_2^* = x_2 + G_1 z_1 - \dot{q}_r. \tag{16}$$

Picking G_1 such that

$$\begin{bmatrix} P_1 + G^T \geq \\ G_1 P \quad v_1 I \\ n \end{bmatrix} \tag{17}$$

with v_1 being a positive constant, (15) reduces to

$$\dot{V}_1 \leq -v_1 |z_1|^2 + 2z_1^T P_1 z_2 . \tag{18}$$

Step 2: Defining the Lyapunov function

$$V_2 = V_1 + z_2^T P_2 z_2 \tag{19}$$

with P_2 being any $n \times n$ symmetric positive definite matrix, we get

$$\dot{V}_2 \leq -v_1 |z_1|^2 + 2z_1^T P_1 z_2 + 2z_2^T D^{-1}(x_1) r - D^{-1}(x_1) K_1 (x_1 - x_2)$$

$$+ 2z_2^T P_2 G_2 [z_1 - G_1 z_2] - 2z_2^T P_2 \ddot{q}_r \tag{20}$$

Since $x = z - G z + q$, we have $x^2 \le 3(|z|^2 + |G z|^2 + |q|^2)$. Since $\rho(|x|^2)|x|^2$ is a class function of $|x|^2$, we can write

$$\rho(|x|^2)|x|^2 \le 9|z|^2\rho(9|z|^2) + 9|G z|^2\rho(9|G z|^2) + 9|q|^2\rho(9|q|^2). \quad (21)$$

Hence, using (7) and (21),

$$|2z^T P D^{-1}(x)\tau| \le \nu|z|^2 + c|z|^2 + \theta\mu(x, q_r, z)z^T P D^{-2}(x)P z + d \quad (22)$$

where c_2 is any positive constant and

$$\mu(x, q_r, z) = \frac{1}{2\nu}\left[\rho(|x|^2) + 9|G|^2\rho\left(9|z|^2\right)\right]^2 + c_2 \quad (23)$$

$$d = \nu|q|^2 + (9|q|^2). \quad (24)$$

Note that $\mu_1(x_1, q_r, z_2)$ is a known function of its arguments and d_1 is a time-varying signal that is upper bounded by an unknown non-negative constant.

Using (20) and (22), we get

$$\dot{V} \le -\frac{1}{2}|z|^2 + 2z^T P z + (x)K(x) + 2z^T P G[z - G z] - 2z^T P\ddot{q} + c|z|^2 + \theta\mu(x, q_r, z)z^T P D^{-2}(x)P z + d. \quad (25)$$

$$1 \qquad 2 \quad 2 \quad 1$$

The virtual control law for x_3 is defined as

$$x_3^* = x_2 - \hat{K} D(x_1)\alpha_1(z_1, z_2, \ddot{q}_r) - \hat{\beta}\mu(x_1, q_1, z_1)\hat{K} D^{-1}(x_1)P_2 z_2 \tag{26}$$

$$3 \quad 1 \qquad 1\ 1\ 1\ 2\ r \qquad 2 \qquad 1\ 1\ r\ 2 \qquad\qquad 1\ 2\ 2$$

where

$$\alpha_1(z_1, z_2, \ddot{q}_r) = \frac{1}{2}z_1^T P_1 z_1 + \frac{1}{2}z_2^T P_2 z_2 + \frac{8}{v_1}\|P_2 G\|^4 \|z_2\|^2 - \ddot{q}_r, \tag{27}$$

$$1\ 1\ 2\ r \qquad 2 \quad 2 \quad 2 \quad 2 \quad 2 \quad 2 \quad 1 \quad 1 \quad 2 \quad 1 \quad 2 \quad 2 \quad r$$

G is an $n \times n$ matrix, $\hat{K}$ is an $n \times n$ diagonal matrix, and $\hat{\beta}$ is a scalar. The matrix $\hat{K} = \mathrm{diag}\{\hat{K}_1, \ldots, \hat{K}_n\}$ is an adaptation estimate for the uncertain diagonal matrix K^{-1}. The scalar $\hat{\beta}$ is an adaptation estimate for a lumped uncertain non-negative constant β^* that will be defined further below.

G_2 is picked such that

$$P_2 G + G^T P_2 \geq v_2 I \tag{28}$$

$$2 \quad 2\ 2 \quad 2 \qquad 2\ n$$

with v_2 being a positive constant.

Defining

$$z_3 = x_3 - x_3^* \tag{29}$$

and using (25) and (26), we get

$$\dot{V} \le -\frac{13}{16}v\|z\|^2 - v\|z\|^2 + 2z^T P D^{-1}(x)K z_2 - (\hat{\beta}\theta_1)\tau_2 - 2z^T P D^{-1}(x)K(\hat{K}_1 - K_1^{-1})\{D(x)\alpha(z_1, z_2, \ddot{q}_r) + \frac{1}{2}\hat{\beta}\mu(x, q, z)D^{-1}(x)P z\} + d \quad (30)$$

where τ_1 denotes

$$\tau_1 = \mu_1(x, q_r, z)z^T P D^{-2}(x)P z. \quad (31)$$

Since K and $\hat{K}$ are diagonal matrices, (30) can be rewritten as

$$\dot{V} \le -\frac{13}{16}v\|z\|^2 - v\|z\|^2 + 2z^T P D^{-1}(x)Kz_2 + K_1(\hat{\beta}\theta_1)\tau_1 - \sum_{i=1}^{n} K_i\left(\hat{K}_i^{-1} - \frac{1}{K_i}\right)\gamma_i + d_1 \quad (32)$$

where γ_i, $i = 1, \ldots, n$, denote

$$\gamma_i = e_i^T \tilde{\gamma} e_i, \; i = 1, \ldots, n \quad (33)$$

where $e_i \in \mathbb{R}^n$ is the i^{th} unit vector, i.e., with i^{th} element being 1 and zeros elsewhere, and $\tilde{\gamma}$ denotes

$$\tilde{\gamma} = 2\{D(x_1)\alpha_1(z_1, z_2, \ddot{q}_r) + \frac{1}{2}\hat{\beta}\mu(x, q, z)D^{-1}(x)P z\}z^T P D^{-1}(x). \quad (34)$$

Designing the adaptation dynamics for $\hat{K}_i$, $i = 1, \ldots, n$, as

$$\dot{\hat{K}}_i = -\sigma_K\hat{K}_i + \frac{1}{c}K_i$$

$$\gamma_i, \quad i = 1, \ldots, n \tag{35}$$

with σ_{K_i}, $i = 1, \ldots, n$, and c_{K_i}, $i = 1, \ldots, n$, being any positive constants, and defining the Lyapunov function

$$V = \frac{1}{2a} V_2^2 + \frac{1}{2} \sum_{i=1}^{n} c_{K_i} \left(\hat{K}_i - K_i \right)^2, \tag{36}$$

we get

$$\dot{V} \le -\frac{13}{16} v |z|_2^2 + v |z|_2^2 + 2 z^T P D^{-1}(x) K z + \frac{1}{2} \sigma_0 (\beta - \theta)^2 - \frac{1}{2} \sum_{i=1}^{n} \sigma_{K_i} (K_i - K_i)^2 + d_1 + \frac{1}{2} \sum_{i=1}^{n} \frac{\sigma_{K_i} c_{K_i}}{c_{K_i}}. \tag{37}$$

[1] For notational convenience, we drop the arguments of functions when no confusion will result.

Step 3: Define the Lyapunov function

$$V = V_0 + z^T P z \tag{38}$$

with P being any $n \times n$ symmetric positive definite matrix. From (11), (16), and (26), we note that x^* can be considered a function of $(x, \hat{\beta}, \hat{K}, q, \dot{q}, \ddot{q})$. Hence, from (29) and (38), we can write

$$\dot{V} \le -\frac{1}{2} v_0 |z|^2 + 2 z^T P D^{-1}(x) K z$$

$$+ 2 z^T P \left[\frac{\partial x^*}{\partial x} \dot{x} + \frac{\partial x^*}{\partial \hat{\beta}} \dot{\hat{\beta}} + \frac{\partial x^*}{\partial \hat{K}} \dot{\hat{K}} + \frac{\partial x^*}{\partial q} \dot{q} + \frac{\partial x^*}{\partial \dot{q}} \ddot{q} \right]$$

$$- \frac{1}{2} \sum_{i=1}^{n} \frac{\sigma_{K_i} K_i}{K_i} (K_i - K_i^0)^2 + \frac{1}{2} \sum_{i=1}^{n} \frac{\sigma_{K_i} K_i}{K_i} (K_i - K_i^0)^2 + d_0 + \frac{1}{2} \sum_{i=1}^{n} \frac{\sigma_{c_i} c_i}{c_i} (\beta_i - \theta_i)^2 \tag{39}$$

Using (26), (27), and (29), the term $(x_1 - x_3)$ can be written in the form

$$\dot{x}_1 - \dot{x}_3 = \zeta_1(x, \hat{K}) z_2 + \zeta_2(x, \dot{x}, q, \dot{q}, \ddot{q}, \hat{\beta}, \hat{K}) z - z - \hat{K} D(x) \ddot{q} \tag{40}$$

where ζ_1 and ζ_2 denote

$$\zeta_1(x, \hat{K}) = \hat{K} D(x) \tag{41}$$

$$\zeta(x_1, x_2, q_r, \dot{q}_r, \hat{\beta}, \hat{K}) = \hat{K} D(x_1) G_2 + \frac{1}{2} G_2 + \frac{1}{2} c_2 P_{21} + G_1 + v_1 + \frac{1}{2} G_1 P_{12}$$

$$+ \frac{1}{2} \hat{\beta} \mu(x_1, q_r, x_2 + G_1 q_r - \dot{q}_r) \hat{K} D^{-1}(x_1) P_{12}. \quad (42)$$

Defining $\theta^* = \max\{\theta, \|K\|^2\}$, we have

$$2 z_2^T P_{12} [D^{-1}(x_1) \hat{K}(x_2 - x_1)] \le \frac{3}{2} v_1 \|z_1\|^2 + \frac{1}{2} v_1 \|z_1\|^2 + c_3 \|z_2\|^2$$

$$+ \frac{3}{2} \left\| \frac{\partial x_2^*}{\partial x_1} \right\|^2 \frac{1}{2} v_1 \|z_1\|^2 + \frac{n-1}{2} \left\| \frac{\partial x_2^*}{\partial x_1} \right\|^2 \frac{1}{2} v_1 \|z_1\|^2 + \frac{1}{16} v_1 \|z_1\|^2$$

$$+ \frac{1}{16} v_1 \|q_r\|^2 + \|\dot{q}_r\|^2 + c_q \|\ddot{q}_r\|^2 + \kappa$$

$$+ \theta^* \mu \left\| z_2^T P_{12} \left(\frac{\partial x_2^*}{\partial x_1} \right) D^{-2}(x_1) P_{12} z_2 \right\| \quad (43)$$

where c_3 and c_q are any positive constants and μ_2 denotes the function of $(x_1, x_2, q_r, \dot{q}_r, \hat{\beta}, \hat{K})$ given by

$$\mu_2 = \frac{32}{\rho} \|x_2\|^2 \left(\|x_2\|^2 \right) \left[\frac{8}{\rho} + \frac{16}{\rho} \|G_1\|^2 + \frac{16}{\rho} \|\zeta(x_1, \hat{K})\|^2 \right]$$

$$\times \left[1 + \frac{1}{\rho} + \frac{1}{\rho} \right]^2 \frac{v_1}{8} \left[\frac{11}{\rho} + \frac{12}{\rho} + \frac{2}{\rho} \frac{v_2}{v_1} + \frac{v_1}{\rho} \right]^{1+\frac{1}{\rho}}$$

$$+ \|\zeta(x_1, x_2, q_r, \dot{q}_r, \hat{\beta}, \hat{K})\|^2 + \frac{1}{\rho} + \|\hat{K} D(x_1)\|^2. \quad (44)$$

$$\frac{v_2}{2} \|z_1\|^2 + \frac{1}{2} \|z_2\|^2 \le \frac{1}{2} \|D^{-1}(x_1) P_{12} z_2\|^2 + \frac{8}{3} \theta^* \|P_{12} D^{-1}(x_1)\|^2 \|z_2\|^2. \quad (45)$$

$$8 \quad 2 \quad 2 \quad v_2 \quad 2 \quad 1 \quad 3$$

The virtual control law for x_4 is picked as

$$x_4^* = -\bar{G}^{-1}(x)\left[c_\beta P_3 z_3 - \hat{\beta}\left|P_3 D^{-1}(x)\right|^2 P_3 z_3 - \frac{\partial x_3^*}{\partial x_2}\left(x_3 - \frac{\partial x_2^*}{\partial x_1}x_2\right) - \frac{1}{2}\hat{\beta}\mu\frac{\partial x_3^*}{\partial x_2}D^{-2}(x)\left(\frac{\partial x_3^*}{\partial x_2}\right)^T P_3 z_3 + \frac{\partial x_3^*}{\partial \hat{\beta}}\left[-\sigma_\beta\hat{\beta} + \frac{c_\beta}{2}\left|P_3 D^{-1}(x)\right|^2 z_3^T z_3\right] + \sum_{i=1}^{3}\frac{\partial x_3^*}{\partial K_i}\dot{\hat{K}}_i + \sum_{i=0}^{3}\frac{\partial x_3^*}{\partial q^{(i)}_r}q^{(i+1)}_r\right] \quad (46)$$

where c_β and σ_β are any positive constants, G_3 is an $n \times n$ matrix, and τ_2 denotes

$$\tau_2 = \left(\frac{\partial x_3^*}{\partial x_2}\right)^T P_3 z_3 + \mu\left(\frac{\partial x_3^*}{\partial x_2}\right)^T P_3 z_3 D^{-2}(x)\left(x_3 - \frac{\partial x_2^*}{\partial x_1}x_2 - \frac{\partial x_3^*}{\partial x_2}\cdot x_3\right) + \frac{\partial x_3^*}{\partial \hat{\beta}}\frac{1}{2}\left|P_3 D^{-1}(x)\right|^2 z_3^T z_3 . \quad (47)$$

In (46), $\dot{\hat{K}}_i$ denotes the right hand side (i.e., the designed dynamics for $\hat{K}_i$) of (35).

G_3 is picked such that

$$P_3 + G_3^T P_3 \geq v_3 I_n \quad (48)$$

with v_3 being a positive constant.

Defining

$$z_4 = x_4 - x_4^* \quad (49)$$

and using (39), (43), (45), and (46), we get

$$\dot{V} \leq -\frac{10}{2}|z_2|^2 - \frac{5}{2}v_2|z_2|^2 - v_3|z_3|^2 - c_\beta|z_3|^2 + 2z_3^T P_3 z_3$$

$$\frac{3}{1}\frac{16}{}\frac{1}{}\frac{8}{2}\frac{2}{}\frac{3}{}\frac{3\,3\,3}{}\frac{3\,3\,4}{}$$

$$\hat{}\quad\tilde{}\qquad\frac{n}{2}\qquad\frac{1}{}\qquad\frac{2}{}\quad\frac{1}{}\quad\frac{1}{}\qquad\frac{}{}\qquad\frac{n\,\sigma\,c}{\kappa K}$$

$$\frac{}{}\qquad\frac{}{}$$

$$i=1\quad\overline{K}_i\left(\beta-\theta_1\right)\tau_2-2\sum\sigma_{Ki}c_{Ki}+d_2+\frac{}{i=1}\sum_{K}$$

$$\hat{}\quad\frac{1}{}\quad\cdot$$

$$+\xi_1\left[-\sigma_\beta\,\beta+\frac{}{\beta}\,c\;\tau_2-\hat{\beta}\right] \tag{50}$$

where $\theta = \max\{\theta, \theta^*\}$ and

$$\xi_1 = 2z_3\frac{1}{}\frac{T\partial x^*}{\partial\hat{\beta}}\frac{3}{}\frac{1}{}\frac{1}{} \tag{51}$$

$$d = d_2 + \frac{1}{16}\frac{1}{}\frac{1}{}\frac{}{}\frac{}{}\frac{

$$\dot{V} \le -\frac{10}{2}|z|^2 - \frac{5}{2}v|z|^2 - v|z|^2 - c|z|^2 + 2z^T P z$$

$$\frac{4}{1}\frac{16}{2}\frac{1}{2}\frac{8}{2}\frac{2}{3}\frac{3}{3}\frac{3}{3}\frac{3}{3}\frac{3}{4}\frac{4}{n}\sigma_{K_i}\frac{c_i}{K_i}$$

$$\hat{c}\,(\beta - \hat{\theta})\sum_{i=1}^{n}\frac{1}{2}\sigma_{K_i}K_i\dot{K}_i + d + \sum_{i=1}^{n}\frac{1}{2}\sigma_{K_i}K_i^2$$

$$+\xi\left[-\frac{1}{\beta}\sigma_\beta\hat{\beta} + c_\beta\|\tau - \hat{\beta}\|\right]$$

$$+ 2z^T P\left[J^{-1}\{K(x_1 - x_3) + u\} - \frac{\partial x_4^*}{\partial x_1}x_2 - \frac{\partial x_4^*}{\partial x_2}x_3 - \frac{\partial x_4^*}{\partial x_3}x_4 - \frac{\partial x_4^*}{\partial \hat{K}}\dot{\hat{K}} - \sum_{i=1}^{n-1}\frac{\partial x_4^*}{\partial \hat{\beta}_i}\dot{\hat{\beta}}_i - \sum_{i=0}^{n-1}\frac{\partial x_4^*}{\partial q^{(i)}}q^{(i+1)}\right]. \tag{54}$$

From (46) and (49), an upper bound on x_4 can be written as

$$|x_4| \le |z_1| + \chi_1|z_2| + \chi_2|z_3| + \chi_3|z_4| + \chi_4|\hat{\beta}| + \sum_{i=1}^{n}\chi_{K_i}|\hat{K}_i| + \sum_{i=1}^{n}\chi_{q,i}|q^{(i)}| \tag{55}$$

where

$$\chi_1 = \left|\frac{\partial x_3^*}{\partial x_1}\right| G \tag{56}$$

$$\chi_2 = \left\|\frac{\partial x_3^*}{\partial x_1}\right\| G + \left\|\frac{\partial x_3^*}{\partial x_2}\right\| G^2 + \left\|\frac{\partial x_3^*}{\partial x_1}\right\| G^2$$

$$\chi_3 = \left\|\frac{\partial x_3^*}{\partial x_2}\right\| G + \left\|\frac{\partial x_3^*}{\partial x_1}\right\| G^2 + \left\|\frac{\partial x_3^*}{\partial x_3}\right\| G^2$$

$$\chi_4 = \left\|\frac{\partial x_3^*}{\partial x_3}\right\| G + \left\|\frac{\partial x_3^*}{\partial x_2}\right\| G^2 + \left\|\frac{\partial x_3^*}{\partial x_1}\right\| G^2$$

$$\chi_{K_i} = \left\|\frac{\partial x_3^*}{\partial \hat{K}_i}\right\| G + \left\|\frac{\partial x_3^*}{\partial x_3}\right\| G^2 + \left\|\frac{\partial x_3^*}{\partial x_2}\right\| G^2 + \left\|\frac{\partial x_3^*}{\partial x_1}\right\| G^2$$

$$\chi_{q,i} = \left\|\frac{\partial x_3^*}{\partial q^{(i)}}\right\| G + \left\|\frac{\partial x_3^*}{\partial x_3}\right\| G^2 + \left\|\frac{\partial x_3^*}{\partial x_2}\right\| G^2 + \left\|\frac{\partial x_3^*}{\partial x_1}\right\| G^2$$

$$D^{-1}(x)P\,\mu\,(x, q, z)z^T P + \frac{\partial x_3^*}{\partial x_1}$$

$$\dot{\hat{\beta}} = \frac{c_\beta}{2}\left(\frac{\partial x_2^*}{\partial x_1}\right)^2 \|z_2\|^2 + \frac{1}{2}\left(\frac{\partial x_2^*}{\partial x_1}\right)^2 \|z_2\|^2 + \frac{1}{2}\left(\frac{\partial x_2^*}{\partial x_1}\right)^2 \|z_2\|^2 + \sum_{i=1}^{n} \frac{1}{2}\left(\frac{\partial x_2^*}{\partial \hat{K}_i}\right)^2 \|z_2\|^2 \alpha_i(z_1, z_2, q) + \frac{1}{2}\hat{\beta}\mu \|z_2\|^2 \|P_2 D^{-1}(x_1)\|^2 \|P_2 D^{-1}(x_1)e_i\|^2 \quad (57)$$

$$\dot{V} = -\frac{1}{2}z^T Q z + z^T P \begin{bmatrix} 0 \\ 0 \\ \left(\frac{\partial x_3^*}{\partial x_2}\right)^T \left(\frac{\partial x_3^*}{\partial x_2}\right)^T \end{bmatrix} \left[\frac{1}{2}\mu D^{-2}(x_1) + \frac{8}{\mu}\|P_2 D^{-1}(x_1)\|^2 z_2^T\right] \quad (58)$$

$$\dot{\hat{\beta}} = \sigma_\beta \left|\frac{\partial x_3^*}{\partial \hat{\beta}}\right| \quad (59)$$

$$\dot{\hat{K}}_i = \sigma_{K_i} \left|\frac{\partial x_3^*}{\partial \hat{K}_i}\right|, \; i = 1, \ldots, n \quad (60)$$

$$\frac{\partial x_3^*}{\partial x_r^*} = \left[\frac{\partial x_3^*}{\partial q}, \frac{\partial x_3^*}{\partial \dot{q}}, \frac{\partial x_3^*}{\partial \ddot{q}}\right]_{q,1} \cdot \qquad (61)$$

Hence, using (8) and (55),

$$2z^T P J^{-1} \left[\frac{3}{16} I_{11}\right] \le \frac{3}{16} v_{22} |z|^2 + \frac{1}{4} v |z|^2 + \frac{3}{4} v |z|^2 + c |z|^2 + 2c \sum_{i=1}^{n} |q(i)|^2 + \frac{3}{4} r_q I_1 + \frac{1}{2} c_\beta \sigma_\beta |\hat{\beta}|^2 + \sum_{i=1}^{n} \sigma_{K_i} |\hat{K}_i|^2 + \tilde{\theta} \mu z^T P Z \qquad (62)$$

where c is any positive constant, $\tilde{\theta}$ is defined as the uncertain non-negative constant

$$\tilde{\theta} = \theta_2 \max\{1, |J^{-1}|^2\} \min\{1, |J^{-1}|^2, K_1, \ldots, K_n\}, \qquad (63)$$

and μ_3 denotes

$$\mu_3 = \frac{16}{5} |G^{-1}| \rho(|x|^2) + 2\rho(|x - x^*|^2)|\zeta|^2 + \rho(|x|^2)\chi^2 + \frac{1}{2} v_{22} + \frac{1}{4} v_{11} + \frac{1}{4} v_{22} + \frac{1}{4} + \frac{1}{2} v_{11} + \frac{1}{2

$$v_3 \quad 21\ 3\ 1 \qquad 24 \qquad 3 \qquad 22 \qquad 4\ 3$$

$$+ 1 + \frac{1}{c}\left[\rho\ (|x|^2) + \rho\ (|x|^2)\sum \chi^2\right.$$

$$q \qquad 23 \qquad 22 \qquad q,i$$

$$+ \frac{2}{}\left[\rho\ (|x\right. \qquad i = 1 \qquad \left.\right]$$

$$\left. - x^{12}) + \rho\ (|x|^2)\right] K\hat{} D(x)^2$$

$$\text{e}q \quad 21 \quad 1 \quad 24 \quad 3 \quad 1 \qquad n \quad 8$$

$$1 \qquad 8 \qquad \rho\ (|x|^2) \quad \rho\ (|x|^2)\ \chi^2 \frac{}{c\ \sigma}\ \rho\ (|x|^2)\chi^2 \ . \qquad (64)$$

$$\ddagger \quad \rho\ (|x|^2) \qquad + \sum$$

$$c4 \quad 22 \quad c\beta \quad \sigma\beta \quad \beta \qquad i=1\ K_i\ K_i$$

$$4 \qquad 22\ 4$$

Using (7) and (40), we have

$$|2z^T P \quad \partial x^*4 \quad + \quad 3 \quad 1 \quad 1 \quad 1$$

$$D^{-1}(x)[\tau \quad K(x \quad - x)] \leq v\ |z|^2 + \quad v\ |z|^2 + c\ |z|^2$$

$$4 \quad 4 \quad 1 \quad n1 \quad 1 \quad 16\ 1 \quad 4 \quad 2 \quad 2 \quad 3\ 3$$

$$\partial x_2 \qquad 3 \qquad 1$$

$$1$$

$$+ v\ |q|^2 + |q^{\cdot}|^2 + c\ |q^{\cdot\cdot}|^2 + \kappa$$

$$16\ 1\ r \qquad r \quad q\ r \quad 1$$

$$+ \theta^* \mu\ z^T P \quad \partial x^*4 \quad D^{-2}(x \qquad (65)$$

$$\partial x^*4 \quad T \quad P\ z$$

$$)\left(\right.$$

$$1\ 2\ 4 \qquad 4 \qquad 1 \quad \partial x_2 \quad 4\ 4$$

$$\partial x$$

$$2$$

where μ_2 is as given in (44). Also, using (40),

$$|2z^T{}_4 P\ J^{-1} K(x \quad \frac{1}{16}{}^1 v\ |z \quad \frac{1}{8}\ v \quad |z \quad \frac{1}{4}\ v\ |z|^2{}_{q^{\cdot}} + c\ |q^{\cdot\cdot}|^2$$

$$- x)| \leq \qquad |^2 + \qquad |^2 +$$

$$+ \theta^* \mu\ z^T P^2 z \qquad (66)$$

2 4 4 4 4

where $\theta^* = \|J^{-1}K\|^2$ and μ denotes

$$\mu = \frac{1}{6\nu}\|\zeta\|^2 + \frac{8}{\nu^2}\|\zeta\|^2 + \frac{4}{\nu} + \frac{1}{c_q}\|\hat{K}_1 D(x)\|^2. \tag{67}$$

Using (62), (65), and (66), (54) can be rewritten as

$$\begin{aligned}\dot{V} \le {} & \frac{3}{4}\|z_1\|^2 - \frac{1}{16}\|z_2\|^2 - \frac{1}{16}\|z_3\|^2 - \frac{1}{2}\nu\|z_3\|^2 + 2z^T P z \\ & - \frac{1}{2}\sum_{i=1}^{n}\frac{\sigma_{K_i}}{K_i}\tilde{K}_i\dot{\hat{K}}_i + d_1 + \sum_{i=1}^{n}\frac{\sigma_{K_i}}{2K_i} \\ & - \frac{c_\beta\sigma_\beta}{2}\|\tilde{\beta}\|^2 + \frac{1}{2}c_{K_i}\|\hat{K}\|^2 + \xi\left(-\frac{1}{2}\tau - \hat{\beta}\right)\sum_{i=1}^{n}\sigma_{K_i}\hat{K}_i \\ & + \frac{c_\beta}{2}\|\beta\|^2 \\ & + 2z^T P\left(J^{-1}u - \frac{\partial x_4^*}{\partial x_3}x_4\right) \\ & - \frac{\partial x_4^*}{\partial \hat{\beta}}\dot{\hat{\beta}} - \sum_{i=1}^{n}\frac{\partial x_4^*}{\partial \hat{K}_i}\dot{\hat{K}} - \sum_{i=0}^{r}\frac{\partial x_4^*}{\partial q^{(i)}}q^{(i+1)} + c_4\|z\|^2 \\ & + \tilde{\beta}^*\left(\mu + \frac{1}{2}z_2^T P_2 z_2 + \mu + z_3^T P_3 z_3 + \beta^*\mu - \frac{\partial x_4^*}{\partial x_3}D(x) - \left(\frac{\partial x_4^*}{\partial x_2}\right)^T P_2 z_2\right)\end{aligned} \tag{68}$$

where $\beta^* = \max\{\tilde{\theta}, \tilde{\theta}, \theta^*\}$ and

$$d = d_1 + \frac{1}{16} v \|q\|^2 + \|\dot{q}\|^2 + 2c \|\ddot{q}\|^2 + \kappa + 2c \sum_{i=1}^{r} |q^{(i)}|^2 + \kappa . \quad (69)$$

From (68), the control input u is designed as

$$u = -\hat{J}\alpha - \beta \hat{J} \quad (70)$$

where

$$\dot{x}^* = G \begin{bmatrix} z_1 \\ z_2 \end{bmatrix} + \begin{bmatrix} 0 \\ \frac{1}{c} P_2 z_2 - \frac{1}{\xi} P_2 z_2 \frac{\partial x_4^*}{\partial x_4} \end{bmatrix}$$

$$- \frac{\partial x_4^*}{\partial x_4} \begin{bmatrix} 0 \\ \frac{1}{c} P_2 z_2 - \frac{1}{\xi} P_2 z_2 \frac{\partial x_4^*}{\partial x_4} \end{bmatrix} - \frac{\partial x_4^*}{\partial \hat{\beta}} \dot{\hat{\beta}} - \sum_{i=1}^{r} \frac{\partial x_4^*}{\partial \hat{K}_i} \dot{\hat{K}}_i - \sum_{i=0}^{r} \frac{\partial x_4^*}{\partial q^{(i)}} q^{(i+1)} \quad (71)$$

$$\chi = (\mu + \mu \frac{\partial x_4^*}{\partial x_4}) \left(\frac{\partial x_4^*}{\partial x_4} \right)^T D^{-2} (x_2 - \frac{\partial x_4^*}{\partial x_1}) \quad (72)$$

G_3 is an $n \times n$ matrix, and $\hat{J}$ is an $n \times n$ diagonal matrix. The matrix $\hat{J} = \text{diag}\{\hat{J}_1, \ldots, \hat{J}_n\}$ is an adaptation estimate for the uncertain diagonal matrix J. In (71), $\dot{\hat{\beta}}$ denotes the right hand side of (76) (i.e., the designed dynamics of $\hat{\beta}$) and $\dot{\hat{K}}_i$ denotes the right hand side of (35) (i.e., the designed dynamics of $\hat{K}_i$).

G_4 is picked such that

$$P_4 G_4 + G_4^T P_4 \geq \quad (73)$$

with v_4 being a positive constant.

Defining

$$\tau = \tau + z^T P \chi \tag{74}$$

and using (70), (71), and (72), (68) reduces to

$$\dot{V} \le -\frac{3}{4}|z|^2 - |z|^2 + \frac{1}{16}v|z|^2 + \frac{1}{16}v|z|^2 - v|z|^2 + \frac{1}{4}|z|^2 + \frac{2}{3}\|P\|^2\|\chi\|^2 + \frac{3}{4}\|P\|^2\|\chi\|^2 + \frac{1}{4}\|P\|^2\|\chi\|^2 + \frac{1}{4}\|P\|^2\|\chi\|^2 + \frac{1

element being 1 and zeros elsewhere. $\tilde{\varpi}$ denotes

$$\tilde{\varpi} = 2\left[\alpha_2 + \frac{1}{A_2}\hat{\beta}\chi_2 P z_2\right] z_2^T P . \tag{79}$$

Designing the adaptation dynamics for $\hat{J}_i$, $i = 1, \ldots, n$, as

$$\dot{\hat{J}}_i = -\sigma_{J_i}\left(\frac{1}{c_{J_i}}\varpi_i + \hat{J}_i\right), \quad i = 1, \ldots, n \tag{80}$$

with σ_{J_i}, $i = 1, \ldots, n$ and c_{J_i}, $i = 1, \ldots, n$, being any positive constants, and defining the Lyapunov function

$$V = \frac{1}{2}\sum_{i=1}^{n} c_{J_i}\left(\hat{J}_i - J_i\right)^2 + \frac{1}{2\beta} c_\beta (\hat{\beta} - \beta^*)^2, \tag{81}$$

(75) yields

$$\dot{V} \le -\frac{3}{16}\|z_1\|_2^2 - \frac{1}{16}\|z_2\|_2^2 - \frac{1}{4}\|z_2\|_2^2\|z_2\|_2^2 - v_{\sigma_\beta} c_\beta (\hat{\beta} - \beta^*)^2$$

$$-\sum_{i=1}^{n}\frac{c_J\,\sigma_{J_i}}{2J_i}(\hat{J}_i-J_i)^2-\frac{1}{4}\sum_{i=1}^{n}\frac{1}{K_i}\sigma_{K_i}c_{K_i}(\hat{K}_i-K_i)+d \tag{82}$$

where

$$d=d_4+\frac{3}{4}\sum_{i=1}^{n}\frac{\sigma_{K_i}}{K_i}+\frac{3}{4}\sum_{i=1}^{n}\frac{\sigma_{J_i}}{J_i}+\frac{3c_\beta\,\sigma_\beta}{4}(\beta^*)^2. \tag{83}$$

From (82), we see that

$$\dot{V}\le-\Upsilon(\chi)+d \tag{84}$$

where $\chi=(z_1,z_2,z_3,z_4,\tilde{K}_1,\ldots,\tilde{K}_n,\tilde{J}_1,\ldots,\tilde{J}_n,\hat{\beta}-\beta^*)$, and

$$\Upsilon(\chi)\le\frac{v_1}{16}|z_2|^2+\frac{v_1}{16}|z_2|^2+\frac{v_2}{2}|z_3|^2+v_3|z_4|^2+\frac{c_\beta\,\sigma_\beta}{4}(\hat{\beta}-\beta^*)^2$$

$$+\sum_{i=1}^{n}\frac{c_J\,\sigma_{J_i}}{2J_i}(\hat{J}_i-J_i)^2+\frac{1}{4}\sum_{i=1}^{n}\frac{1}{K_i}\sigma_{K_i}c_{K_i}(\hat{K}_i-K_i). \tag{85}$$

From (14), (19), (36), (38), (53), and (81), it follows that $\Upsilon(\chi)\ge\Pi V$ where

$$\Pi=\min\left\{\frac{3v_1}{16\lambda_{max}(P_1)},\frac{v_2}{16\lambda_{max}(P_2)},\frac{v_3}{2\lambda_{max}(P_3)},\frac{v_4}{\lambda_{max}(P_4)},\right.$$

$$\left.\frac{\sigma_{K_1}}{2},\ldots,\frac{\sigma_{K_n}}{2},\sigma_1,\ldots,\sigma_n,\frac{\sigma_\beta}{2}\right\}. \tag{86}$$

Thus,

$$2 \quad J_1 \qquad J_n \; 2$$

$$V \leq -\Pi V + d_4. \tag{87}$$

Applying the Comparison Lemma (Khalil 1996),

$$V(t) \leq V(0)e^{\Pi t} + \int_0^t e^{-\Pi(t-s)} d(s)ds. \tag{88}$$

Since the reference signal $\theta_{ref}(t)$ and its first three derivatives are bounded, $d_4(t)$ is a bounded time-varying signal. V is a smooth, positive definite, and radially unbounded function of χ. Thus, from (88), V and hence χ are bounded along the trajectories of the system. By routine signal chasing, it is seen that boundedness of χ implies boundedness of all closed-loop signals. Furthermore, the bound in (88) implies that solutions tend to the compact set in which

$$V \leq \Pi^{-1} d_4 \tag{89}$$

where $d_4 = \lim \sup_{t\to\infty} d_4(t)$ is a finite positive constant since the signal $d_4(t)$ is uniformly bounded. In the set defined by (89), the tracking error $z_1 = (q_1 - q_r)$ satisfies the inequality

$$z_1^T P z \leq \Pi^{-1} d_4. \tag{90}$$

From (90), it is seen that for any given constant $\varepsilon_e > 0$, the controller parameter P_1 can be picked large enough to regulate $|z_1|$ to $[-\varepsilon_e, \varepsilon_e]$. Hence, the designed dynamic

controller achieves practical trajectory tracking of the joint angles q_1 to a reference trajectory q_r.

SIMULATION STUDIES

The dynamic controller designed in Section **Control Design** is simulated here for a two-link manipulator with flexibility in both joints. The manipulator parameters are specified as:

- Masses: 1.1 kg for link 1 and 0.7 kg for link 2
- Link lengths: 0.7 m for link 1 and 0.65 m for link 2; center of gravity for each link at the center of the corresponding link
- Joint stiffness: 80 Nm/rad for joint 1 and 150 Nm/rad for joint 2
- Motor inertias: 1 kg.m^2 for each actuator
- $\tau = [0.1(q + \frac{\pi}{2}) + 0.2\sin(0.05t), 0.2q_3 + 0.3]^T$; $\tau = -0.6x$ where $q = [q_{1,1}, q_{1,2}, q_{2,1}, q_{2,2}]^T$
- Orientation of the links relative to gravity specified $[\frac{\pi}{2}, 0]^T$ such that $q_1 = [-$ corresponds to the downward position of the links.

The controller parameters are picked as

- G_1 = diag(7, 7); G_2 = diag(1, 1); G_3 = diag(30, 30); G_4 = diag(75, 75)
- P_1 = diag(40, 40); P_2 = diag(0.3, 0.3); P_3 = diag(1, 1); P_4 = diag(1, 1)
- $c_2 = 0.5$; $c_3 = 0.5$; $c_4 = 1$; $c_q = 1$
- $\sigma_\beta = 2$; $c_\beta = 50$; $\sigma_{K_1} = \sigma_{K_2} = 0.1$; $c_{K_1} = c_{K_2} = 10$; $\sigma_{J_1} = \sigma_{J_2} = 0.1$; $c_{J_1} = c_{J_2} = 1$.

The reference trajectories are specified to be smooth-start sinusoids given by $-\frac{\pi}{2}$ + 0.5(1 − $e^{-0.25t^2}$) sin(0.5t) for the first joint and 0.2(1 − $e^{-0.25t^2}$) sin(0.3t) for the second joint. The robotic manipulator is initially in the downward position given by $q_1 = [-\frac{\pi}{2}, 0]^T$ and $\dot{q} = [0, 0]^T$. The initial conditions for the controller adaptation $\hat{q} = \hat{\dot{q}}$ = $[0, 0]^T$. The initial conditions for the state variables are specified as $\beta = 0.001$, $K_1 = 0.01$, $K_2 = 0.005$, J

$J_1 = 1.5$, and $J_2 = 1.5$.

The simulation results are shown in Figs. 1 and 2. The joint angles $q = [q_{1,1} \; q_{1,2}]^T$, joint velocities $\dot{q} = [\dot{q}_{1,1} \; \dot{q}_{1,2}]^T$, actuator angles $\bar{q} = [\bar{q}_{2,1} \; \bar{q}_{2,2}]^T$, and actuator velocities $\dot{\bar{q}} = [\dot{\bar{q}}_{2,1} \; \dot{\bar{q}}_{2,2}]^T$ are shown in Fig. 1. The tracking errors ($e = [e_{(1,1)} \; e_{(1,2)} \; \dot{e}_{(1,1)} \; \dot{e}_{(1,2)}]^T$), the adaptation state variables ($\hat{\beta}_1, \hat{K}_1, \hat{K}_2, \hat{J}_1, \hat{J}_2$), and the control inputs ($u = [u_1 \; u_2]^T$) are shown in Fig. 2. It is seen that the designed dynamic controller achieves tracking of the specified reference trajectories with tracking errors regulated to around a degree. The tracking errors can be further reduced by increasing the controller gains. Note that the controller only requires the knowledge of $D(x_1)$, and hence therefore of the corresponding combination of link masses and link lengths that determines the inertia matrix $D(x_1)$, but does not require any knowledge of other parameters such as joint stiffness, motor inertias, load torques, etc. To illustrate the robustness of the controller, the joint stiffness parameters were changed to 60 Nm/rad for joint 1 and 170 Nm/rad for joint 2, and the motor inertia parameters were changed to 0.8 kg.m^2 for the actuator on joint 1 and 1.2 kg.m^2 for the actuator on joint 2. Keeping the controller parameters as given above, the simulations with these perturbed system parameters are shown in Figs. 3 and 4. It is seen that the trajectory tracking performance is very similar to the

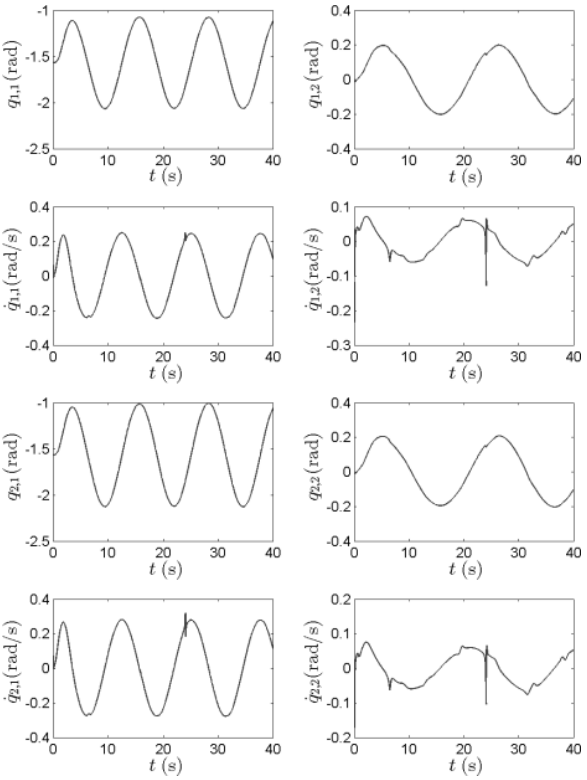


Figure 1. Simulation results for a two-link flexible joint manipulator. Joint angles $q = [q_1, q_2]^T$, joint velocities $\dot{q}_1 = [\dot{q}_{1,1}, \dot{q}_{1,2}]^T$, actuator angles $q_2 = [q_{2,1}, q_{2,2}]^T$, and actuator velocities $\dot{q}_2 = [\dot{q}_{2,1}, \dot{q}_{2,2}]^T$.

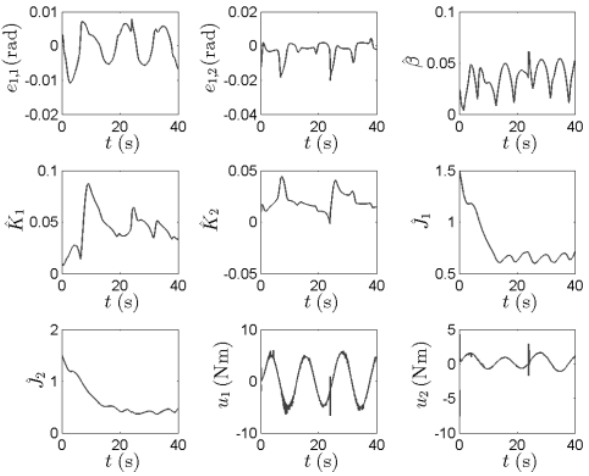


Figure 2. Simulation results for a two-link flexible joint manipulator. Tracking errors ($q_1 - q_r = [e_{(1,1)}, e_{(1,2)}]^T$), adaptation state variables ($\hat{\beta}, \hat{K}_1, \hat{K}_2, \hat{J}_1, \hat{J}_2$), and control inputs ($u = [u_1, u_2]^T$).

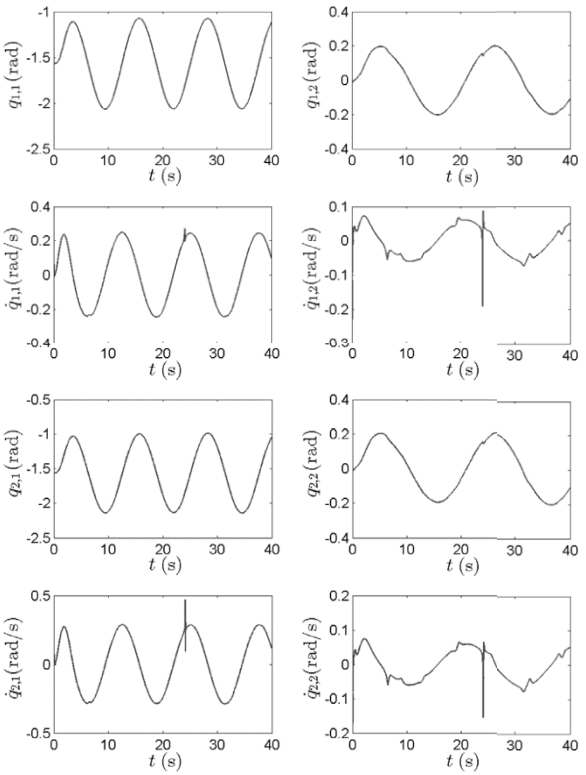


Figure 3. Simulation results for a two-link flexible joint manipulator with perturbations in system parameters K and J. Joint angles $q_1 = [q_{1,1}, q_{1,2}]^T$, joint velocities $\dot{q}_1 = [\dot{q}_{1,1}, \dot{q}_{1,2}]^T$, actuator angles $q_2 = [q_{2,1}, q_{2,2}]^T$ and actuator velocities $\dot{q}_2 = [\dot{q}_{2,1}, \dot{q}_{2,2}]^T$.

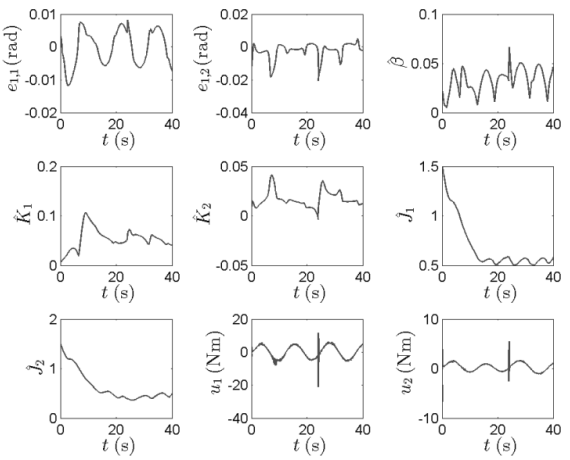


Figure 4. Simulation results for a two-link flexible joint manipulator with perturbations in system parameters K and J. Tracking errors ($q_d - q = [e_{1,1}, e_{1,2}]^T$), adaptation state variables ($\hat{\beta}$, $\hat{K}_1$, $\hat{K}_2$, $\hat{J}_1$,

Ĵ), and control inputs (u = $\begin{pmatrix} 1 & 2 \\ 1 & 2 \end{pmatrix}$, 1 2 1 $[u , u]^T$).

2 1 2

simulations in Figs. 1 and 2, i.e., the designed controller provides significant robustness to variations in the motor parameters. To further illustrate the robustness of the controller to time-varying system parameters, the joint stiffness parameters were changed to (80
−20 sin(*t*)) Nm/rad for joint 1 and (150 + 20 cos(0.9*t*)) Nm/rad for joint 2, and the motor inertia parameters were changed to (1− 0.2 sin(0.8*t*)) kg.m^2 for the actuator on joint 1 and (1 + 0.2 cos(0.7*t*)) kg.m^2 for the actuator on joint 2. Keeping the controller parameters as given above, the simulations with these perturbed system parameters are shown in Figs. 5 and 6 and it is seen that the designed dynamic controller still provides similar trajectory tracking performance even with the time-varying perturbations in the system parameters.

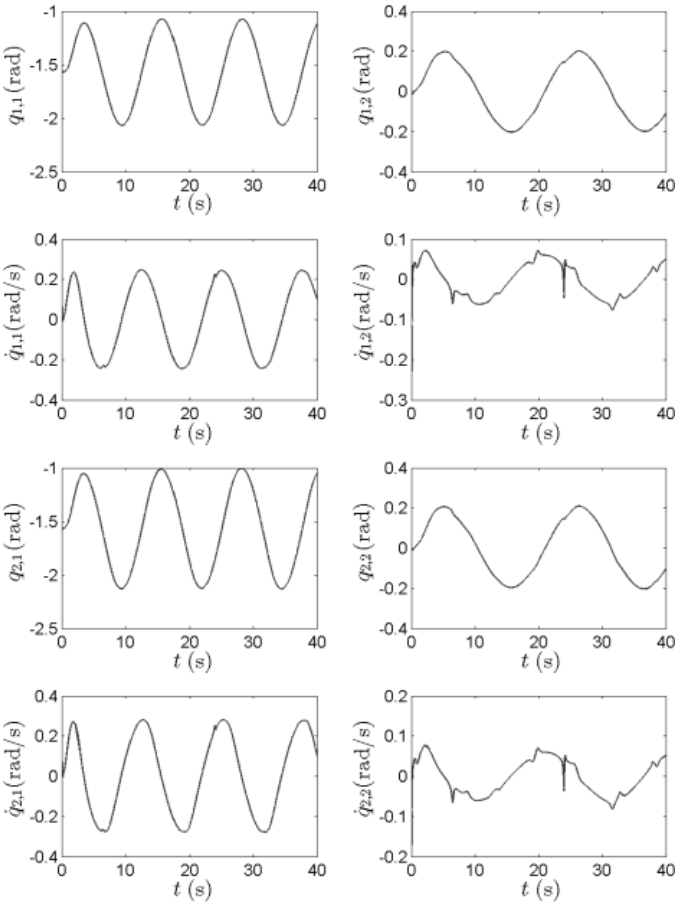


Figure 5. Simulation results for a two-link flexible joint manipulator with time-varying perturbations in system parameters K and J. Joint angles: $q_1 = [q_{1,1}, q_{1,2}]^T$, joint velocities $\dot{q}_1 = [\dot{q}_{1,1}, \dot{q}_{1,2}]^T$, actuator angles $q_2 = [q_{2,1}, q_{2,2}]^T$, and actuator velocities $\dot{q}_2 = [\dot{q}_{2,1}, \dot{q}_{2,2}]^T$.

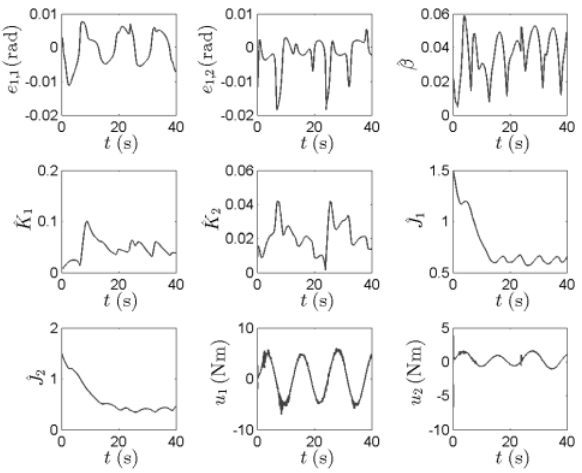


Figure 6. Simulation results for a two-link flexible joint manipulator with time-varying perturbations in system parameters K and J. Tracking errors ($q - q_d = [e_{1,1}, e_{1,2}]^T$), adaptation state variables ($\hat{\beta}, \hat{K}_1, \hat{K}_2, \hat{J}_1, \hat{J}_2$), and control inputs ($u = [u_1, u_2]^T$).

CONCLUSION

A robust adaptive backstepping based controller was developed considering a general uncertain dynamic model of a multi-link robotic manipulator. The designed dynamic controller only requires knowledge of the inertia matrix of the rigid links of the manipulator and is robust to uncertainties in joint stiffness, Coriolis and centrifugal terms, friction, gravity, load torques and disturbances, and actuator inertia. The controller achieves global stabilization and practical tracking of reference trajectories specified for the joint variables. The efficacy of the designed dynamic controller was demonstrated through simulation studies for a two-link manipulator with flexible joints.

REFERENCES

Chien, M. -C. and A. -C. Huang. 2007. Adaptive control for flexible-joint electrically driven robot with time-varying uncertainties. IEEE Transactions on Industrial Electronics, 54: 1032–1038, April 2007.

Dawson, D. M., Z. Qu, M. M. Bridges and J. J. Carrol. 1991. Robust tracking of rigid-link flexible- joint electrically-driven robots. pp. 1409–1412. *In*: Proceedings of the 30th Conference on Decision and Control (Brighton, England), Dec. 1991.

Isidori, A. 1999. Nonlinear Control Systems II. London, UK: Springer, 1999.

Jain, S. and F. Khorrami. 1998. Robust adaptive control of flexible joint manipulators. Automatica, 34: 609–615, May 1998.

Jankowski, K. P. and H. V. Brussel. 1993. Inverse dynamics task control of flexible joint robots i: Continuous-time approach. Mechanism and Machine Theory, 28(6): 741–749, Nov. 1993.

Khalil, H. 1996. Nonlinear Systems. Upper Saddle River, New Jersey: Prentice Hall Inc., Second ed., 1996.

Khorasani, K. and P. V. Kokotović. 1985. Feedback linearization for a flexible manipulator near its rigid body manifold. Systems and Control Letters, 6: 187–192, Aug. 1985.

Khorrami, F., P. Krishnamurthy and H. Melkote. 2003. Modeling and Adaptive Nonlinear Control of Electric Motors. New York, USA: Springer, 2003.

Krishnamurthy, P. and F. Khorrami. 2003. Robust adaptive control for non-linear systems in generalized output-feedback canonical form. International Journal of Adaptive Control and Signal Processing, 17: 285–311, May 2003.

Krishnamurthy, P. and F. Khorrami. 2008. Dual high-gain-based adaptive output-feedback control for a class of nonlinear systems. International Journal of Adaptive Control and Signal Processing, 22(1): 23–42, Feb. 2008.

Krstić, M., I. Kanellakopoulos and P. V. Kokotović. 1995. Nonlinear and adaptive control design. New York, USA: John Wiley and Sons, 1995.

Lozano, R. and B. Brogliato. 1992. Adaptive control of robot manipulators with flexible joints. IEEE Transactions on Automatic Control, 37: 174–181, Feb. 1992.

Luca, A. D., A. Isidori and F. Nicol`o. 1985. Control of a robot arm with elastic joints via nonlinear dynamic feedback. pp. 1671–1679. *In*: Proceedings of the 24th IEEE Conference on Decision and Control (Ft. Lauderdale), Dec. 1985.

Nicosia, S. and P. Tomé i. 1992. A method to design adaptive controllers for flexible joint robots. pp. 701–706. *In*: Proceedings of the 1992 International Conference on Robotics and Automation (Nice, France), May 1992.

Park, C. -W. and Y. -W. Cho. 2003. Adaptive tracking control of flexible joint manipulator based on fuzzy model reference approach. IEE Proceedings on Control Theory and Applications, 150: 198–204, March 2003.

Qu, Z. H. 1995. Input-output robust tracking control design for flexible joint robots. IEEE Transactions on Automatic Control, 40: 78–83, Jan. 1995.

Readman, M. C. 1994. Flexible Joint Robots. Boca Raton, FL, USA: CRC Press, 1994.

Sankaranarayanan, S. and F. Khorrami. 1997. Friction compensation via variable structure control:
regulation and low-velocity tracking. pp. 645–650. *In*: Proceedings of the IEEE International Conference on Control Applications (Hartford, CT), Oct. 1997.

Sepulchre, R., M. Janković and P. Kokotović. 1997. Constructive Nonlinear Control. London, UK: Springer, 1997.

Spong, M. W. 1987. Modeling and control of elastic joint robots. Transactions of the ASME: Journal of Dynamical Systems, Measurement and Control, 109: 310–319, Dec. 1987.

Spong, M. W. 1989. Adaptive control of flexible joint manipulators. Systems and Control Letters, 13: 15–21, July 1989.

Spong, M. W., K. Khorasani and P. V. Kokotović. 1987. An integral manifold approach to the feedback control of flexible joint robots. IEEE Journal of Robotics and Automation, Vol. RA–3, pp. 291– 300, Aug. 1987.

Wang, Z. and F. Khorrami. 2000. Robust trajectory tracking for manipulators with joint flexibility via backstepping. pp. 2849–2853. *In*: Proceedings of the American Control Conference (Chicago, IL), June 2000.

7. SECTION C: TESTING OF NEW TECHNIQUES IN PRACTICE

The objective of this research is the assesment of new decommissioning techniques under real conditions of radioactivity, configuration, size, accessibility and state of components aner long- term **operation.** Section C is focused on four outstanding pilot dismantling projects (WAGR in Windscale, BR-3 PWR in Mol, **KRB-A BWR in**

Gundremmingen, AT-1 FBR fuel reprocessing facility in La Hague), but **also includes alternative** large-scale tests in nuclear installations other than the pilot projects.
Occupational radiation exposure and specific costs for **typical unit operations, are important**
aspects to be considered besides technical assessment.
Work in the pilot projects should be **complemented by large-scale testing** of appropriate techniques proposed by other contractors from Member States.

B. Subjects of the rmearch performed under the previous programme (1979-&l)

Large-scale **investigations on various decommissioning** techniques (such as decontamination, **cutting, activity** measurements) were performed in the **1984-88 decommissioning programme.** These **investigations** concerned the **dismantling** of five reactors, three fuel fabrication facilities and one high-level waste vitrification facility.

C. Programme 1989 to 1993

Section C should include:
- the execution of four pilot dismantling projects
- alternative large-scale tests to be performed in nuclear installations other than the pilot dismantling projects.
  Here are included other nuclear reactors and other installations of the nuclear fuel cycle **having representative value for important upcoming decommissioning tasks in** the EC, such as for fuel fabrication facilities, for fuel reprocessing plants and waste **treatment facilities.**
- secondment of **scientific staff** from Member States to the pilot dismantling projects.
  The owners of pilot projects will receive staff from Member States for **active cooperation**
  within the framework of the project.
- large scale testing **within** the framework of the pilot dismantling projects of appropriate new techniques and procedures developed elsewhere in the Member States.
  The possibility of accepting such demomtration tests on the components of the dismantling
  site is provided in the contracts concluded with the owners of pilot projects.

At the end of 199fl, thirteen research contracts relating to Section C were at the stage of execution and two contracts were at the stage of **negotiation.**

7.1. PILOT **DISMANTLING OF THE WAGiL PHASE 1. DISMANTLING OF TOP BIOSHIELD REFUELLING STANDPIPES VESSEL TOP DOME: TRIALS OF REMOTE DISMANTLING SYSTEM**

Contractors: AEA-Wind.
Contract No.: FI2D-fED1
Work Period: October 1989 - September 1992
Coordinator: T BOORMAN, AEA

Phone: 44/9467/72410 **Fm:44/9467 9**

AOHfl3CMVE SOOPE

The Windscale Advanced Gas-cooled Reactor (WAGR) had a capacity of 33 MWe and was operated from 1962 to 1981. Dismantling of the plant has started and is planned to be completed in 1996.

Considering that the experience to be gained from the dismantling of the first large-scale nuclear installations in the Community should be made available to all Member States, the Commission selected WAGR as a pilot dismantling project for the 1989-93 R&D programme on the decommissioning of nuclear installations. The Commission, through shared-cost participation in specific parts of the project, is promoting the use of advanced techniques and the performance of collateral investigation, in order to enhance the production of useful knowledge and experience to serve in subsequent decommissioning tasks. In particular, the generation of specific data on costs, working hours and job doses as well as on the amount of created secondary waste is an important objective of this project.

As a gas-cooled reactor, WAGR provides opportunities for testing decommissioning techniques against the specific requirements of such reactors, which represent the majority of the first-generation nuclear power reactors to be decommissioned in the Community in the near future. The present contract involves in particular the dismantling of the top biological shield, of refuelling standpipes and of the reactor pressure vessel top dome as well as inactive trials of the remote dismantling machine.

The estimated radioactive inventory is in the order of lP Ci; estimated dose rates are in the range of 0,1 to 1,5 mSv/h.

B.WORKPROGRAMME

B.1. Dismantlin of the top biolo eld (TBS), a **6tl** t disc-shaped steel and concrete structure, by thermic lancing after its moving into a ventilated containment placed on the refuelling 0‹x›r.

B.R Cutting and handling of the **refuelling standpi i.e. 253 pipm of 6d** m length penetrating the upper **part of the reactor bl‹x:k,** by four cuts, with an internally rotating plasma arc

BE. Cutting and dismanoff e ptmsure vmsel top jji2igg, a complex steel structure of 6J m **diameter and iXl mm maximum thickn‹ae, by in-situ segmentation in two parta uaing** a semi-**remote operated ozy-gas cutter placed on a tractor followed by jxst-segmenting in a** temJxnaiy mntainment **placed on the rehmllipg fkmr.**

B.4. Inactive triab of the remote dismantling ssstem, comprising a rotating fkmr shiekl, an extendable **mast carrying a telemanipulainr arm, and a remotely operated conveying system,** in a **tmt facility reprmenting a 3tP sector of the reactor prmsure JL**

BE. Gemration of specific data on cuts, **radioactive job deem, working time and secondary**

C. Progress of Work aod Results Obtained

Summary of main issues

The reactor top biological shield was successfully removed from its recess in the refuelling floor by using hydraulic jacks attached to the gantry of the refuelling machine which had been retained for this purpose and was size-reduced for disposal as low-level waste using the thermic lancing process.

Refuelling standpipes (247) have been cut in three locations, using a family of internal plasma torch tools, to permit removal of the top bioshield and as part of the operation to release the reactor pressure vessel top dome. These operations will continue until all sections of the standpipe are removed.

The top dome of the reactor pressure vessel has been freed of all attachments and a circumferential cut has been made around the crown section using a tracked oxy-propane torch. Heavy duty flexible membranes have been attached to maintain containment when it is separated from the reactor.

A facility has been designed, to be constructed inside the reactor containment building, in which the remote dismantling system can be tested and the operations team trained in its use. Construction of the facility had to be postponed because of the methodology adopted for top dome dismantling.

Progress and Results

1. Disaaotling of the top biological shield (TBS)

When this operation was planned initially the intention was to cut the structure, in-situ over the reactor, into six pieces which would then be light enough to be lifted by the building 25 tonne crane and small enough to negotiate the route out of the building. A fundamental objection to this approach was that debris from cutting would fall onto the reactor and possibly into the refuelling branches. Whilst the refuelling machine was being dismantled its gantry section was identified as a suitable platform from which to lift out the TBS whole. A specialist lifting contractor was engaged for this operation. Dour synchronised 20 tonne hydro-mechanical jacks were fitted on beams running transversely across the gantry from which tie-bars were passed through four of the shutter tubes in the TBS. Supported in this manner the TBS was lifted as shown in Figure l and removed to an area prepared for the size-reduction operation.

Diamond cutting techniques, core drilling and wire sawing were the obvious choices for size reduction but the composition of the TBS, 50/50 steel to concrete by weight, resulted in a high degree of uncertainty regarding the time required. Thermic lancing was considered for size reduction as the high content worked to the advantage of the process. The disadvantage of this process is that it produces large amounts of fume. For this reason a temporary containment was built around the TBS to prevent the spread of any small amounts of contamination but more particularly to contain the fume generated when cutting, shown in Figure 2. Extract ventilation was provided by two 0.5 m'.s-'HEPA filters using Electrostatic Precipitators as pre-filters. A l m'.s-' air mover with a bag filter was used in a recirculating leg to improve working conditions.

The cutting process lasted fifteen working days with cutting occupying only three hours of each day. A total of 280 seven metre long lances were consumed to cut a cross sectional area of approximately 5.6 m'. The total mass of waste produced was 52 tonnes which was disposed of as low-level waste, dose uptake to operators was not raised above that for general operations.

The adopfi ion of thi s methodo logy has proved very success fu1 both in terms of minimising dose uptake, maintaining project timescales and demonstrating the use of standard industrial techniques in reactor dismantling.

2. Cutting and handling of the refuellinjg standpipes

The reactor was served by 247 refuelling standpipes which are being progressively cut and removed. Four vertical locations for cutting have currently been identified, just below the top biological shield, directly above the top dome, just inside the top dome and directly above the hot box of the reactor. An industrial water -cooled plasma arc cutting torch was adapted to use gas cooling and optimised to for minimum fume generation using a plasma gas of Argon with 5X Hydrogen. This torch is incorporated into a family of tools for internally cutting the standpipes. In all cases the tool is lowered from above the reactor into the standpipe.

The standpipes have an internal diameter of 143 mm and a wall thickness of 7 mm. Contamination on their inner surfaces results in a radiation dose of 20 pSv.h-'. Background dose from the reactor pressure vessel varied as the operations progressed. Prior to Top Bio-shield removal radiation levels in the general work area were very low at pSv.hr-',following its removal radiation level rose to 5 qSv.hr-1 but planning estimates for standpipes cutting operations after removal of the top dome assume the value then to be 150 pSv.hr-'. Three phases of standpipe cutting have now been completed. Phase one using the plasma torch on an extension tube with a motor driven panning motion cut just below the Top Biological shield to enable its removal. Phase two used a modification to the original tool producing a cut above the Top Dome. For this operation the tool was deployed from a scaffolding platform erected across top top of the reactor vault. During this phase a combined torch and pipe grab was tested which will be used for later operations. Following phase two a temporary floor was erected across the top of the reactor vault and from this phase three cutting detached the standpipes from the inside of the Top Dome. The plasma torch tool for this operation incorporated a mechanical sensor to located the correct position of the cut, shown in Figure 3, and this operation was followed by a video inspection of the cut tube.

Dose upta#e and waste arising for these operations is given below.

'able 1: Sui aazy oC dose tzptake

Phase	l	2	3
Dose man msv	3.6	7. 4	7.1

The average actlvi£y on each s£andp ipe was 0 . 14 GBq with a spec i f ie act iv ity of 1. 46 GBq. ee '.

Table 2: Suasary of wsste quxotities

Phase	l	2	3
number of cuts	247	247	247
weight of waste item	22 kg	75 kg	0
Total weight			0

The standpipe cutting technique has been developed and shown to be very successful during these early low dose operation. The future standpipecutting operationsfollowingremovalofthepressurevesseltop dome will be planned with much tighter estimation and control of dose uptake.

3. Disnaotliog tbepressurevesseltopdome

The Top Dome is the upper hemispherical end of the steel reactor pressure vessel, approximately 70 mm thick. Six independent pressure loop tubes and the 247 standpipes pass through the crown section which is thickened to 98 Am. The weight of this structure is approximately 45 tonnes. It is not activated but is contaminated to 370 Bq/cm' and radiation levels at its inside surface from other reactor components are estimated to be in the order of 4 mSv.hr-'. The original method of removal proposed was to cut it into sections small enough to remove through 1 m' openings in the temporary floor. Dose budgets showed this method to be impractical as operators would spend a large proportion of their time in the high radiator zone created as each section was removed. An alternative strategy has been formulated, this is to remove the top dome in two large pieces, the crown and the remaining plain section using a bulk posting technique to maintain the containment of the reactor and vault. Table 3 below summarised the results from the dose estimates for the two methods.

TabTe 3: S ry of esC1maCes for dose uptake

Dos e	Hethod 1	l4ethod 2
Total man(mSv)	178	58
Highest individual (msv)	32	5. 4

This operation has begun with a tracked oxy-propane cutter being used to cut around the six loop tubes and completely around the crown section as shown in Figure 4. A series of studs have been welded adjacent to the cut edge and also along the lip of the vault to provide attachment points for the sealing membrane which is sufficiently baggy to permit the top dome to be lifted clear of the vault. The specially designed heavy duty plastic membrane has been attached between the edge of the crown section and the edge of the reactor vault. As this section is removed from the reactor vault the membrane can be tied off thus ensuring that containment of the reactor will be maintained.

A test lift of this part of the structure using the building crane has indicated a weight of 28.5 tonnes. Dose uptake for the cutting operations was 0.94 man.mSv compared with 0.87 man.mSv estimated for this part of the operation which gives confidence in the values calculated for the subsequent operations.

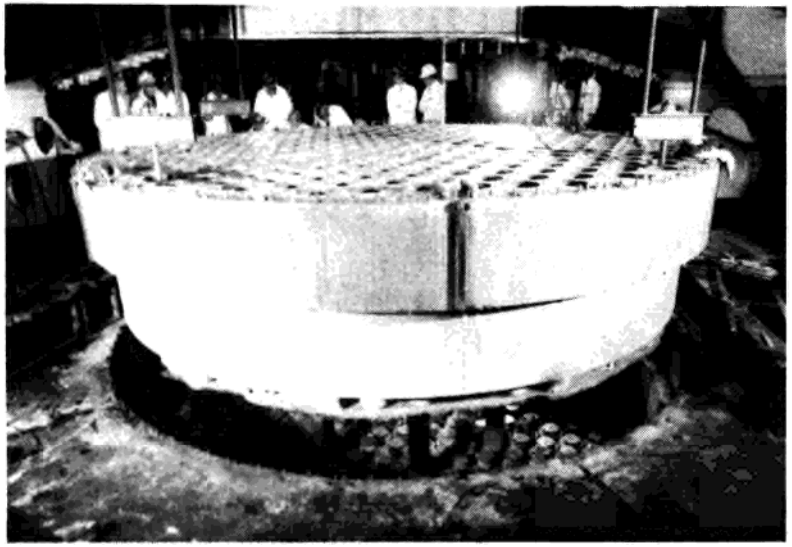
4. InactivetrialsoftbereMotedisMaotliogzachioe

Inactive trials of the WAGR remote dismantling system are to be carried out in a test facility to be constructed adjacent to the reactor bioshield. The position of the test facility has been chosen such that the Remote Dismantling Machine can be lifted out whole and positioned over the reactor on completion of the trials. With the design of the test facility for the remote dismantling system now complete, negotiations are currently in progress with selected contractors for its construction.

A change to the programme this task had been necessary as discussed

below. The methodology developed for the removal of the pressure vessel top dome requires a large area, at refuelling floor level, in the range of the overhead crane. The only suitable area is that to be occupied by the test facility. To meet this requirement construction of the test facility has been delayed.

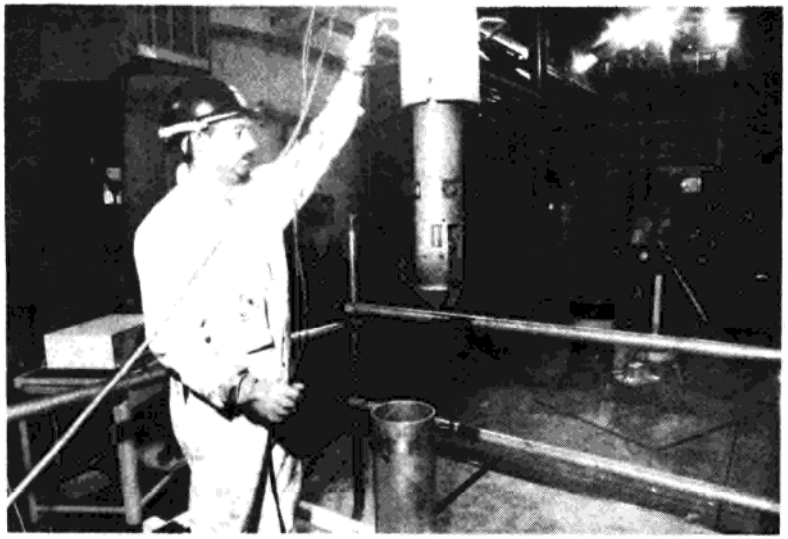
The revised programme for the test facility resulted in a contract placed on 19 November 1990 for work to commence on site on 12 June 1991. To prevent delay to the WAGR decommissioning programme shortened contract programme has been agreed with the contractors to completed construction of the Facility in September 1991, the remote dismantling machine will be installed at that time. A testing and training schedule for the facility is be ing devi sed .



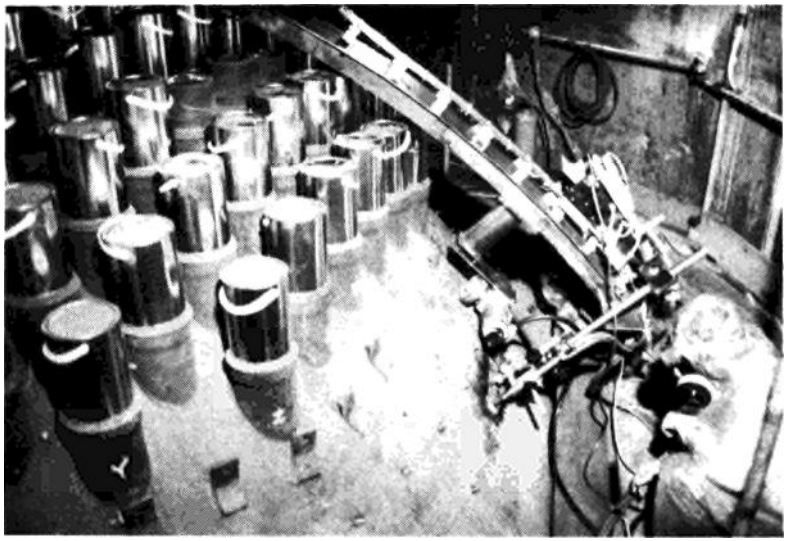
Flgure 1: L1f£1ng the Top Bioshield



Figure 2: Top Bioshield Gut.I.£ng



Pigure3:Phase3standpipecutting tool



Pigure4.Cutting around the topdose

the

OPERATION AND SEGMENTING TECHNIQUES FOR REACTOR VESSEL IHTHRNALS OF KRB-A

Contractors: **KRB**
Contract No.: Work FI2D-IOJ2
Period: October 1989 - September 199fl W STANG, KRB
Coordinator: **Phone: 49/8224/783 730** **Fax:** 49/8224/782 900

AOHMKIMFBvUfl]S PE

The Boiling Water Reactor plant Gundremmingen A (KRB-A) is one of the four pilot dismantling projects of the EC programme (see also § 7.5.).

The present contract is concerned by a **preliminary design and** assessment study of alternative remote operation and segmenting techniques for underwater dismantling of the pressure vessel internals of KRB-A Occupational radiation exposure, costs, and the conditioning and minimization of the radioactive waste will be considered in particular.

In the course of its implementation this study was extended to the case of the VAK BWR of

B.WOWKPROG

B.1. Inventory of KRB-A condition, e.g. materials and geometric of components, local dv ratm and radioactivities, acixasibility.

BE Literature struts on the state-of-the-arL

BE. Analysisofunderwaterseginentin qum including thermal, mechanical, electrical aiid chemical techniq

B.4. Invmtieationofremote-onerationtechnioumcomideringaltemative manipulator dmigns and various degrees of automatisation.

BE. Comparative evaluation of the alternative technique ilrvmtigate‹i, considering all relevant aspects; selection of the optimum technique(s); identification of experimental investigations needed, if any.

C. Progyq3.3 9 fpy pyk gn iJ f in.gd r .ti)J

Summarv of main issues

It was the aim of the study to prepare a concept for the dismantling of the internals of the reactor pressure vessel and the vessel itself of KRB-A. This concept should base on the state of the art and should be feasible in consideration of the local ‹:ircumstancez Therefore a work group was organize‹t This group consists of represen- tatives of contracted companies, specialists in nuclear topics and technical staff of the nuclear power plant of Gundremmingen (KRB—A) and of the nuclear power plant of Kahl (VAK). The participation of VAK guarantees that the results will be not too specific but generally valid. On the basis of all important data, drawings etc. of KRB—A and VAK, the contracted companies worked out different decommissioning concepts for the RPVs and their internals. Then a group of experts from KRB—A and VAK and some independent spe- :ialists evaluated the different concepts and made proposals for the further proceedings (definition of the dismantling strategy, planning of inactive tests, etc.).

At the same time a literature study on possible and generally used decommissioning techniques was accomplished and evaluated.

PrOg$fifi5 IP.del.s.U).t8.

l. Inventors of kRB-A con4itio»s IB I I

On the basis of drawings, calculations and other dossiers available component lists of the RPVs and their internals w•_re ıirepared. For each component cr part cf a component, weight, wall thickness, volume, dimensions, material, activation and con- tamination were noted. Furthermore handling and transportation facilities, storage aereas, filtering and cleaning devices etc. were listed. These data were given to the contracted companies of the work group as basis for the planning

In KRB-A, there is enough space at the operating platform (31,5 mJc‹ritrarity to the conditions in VAK. Furthermore the separate storage pool for fuel elements gives a significant advantage to decommissioning purposes This pool can be used for a separate segmenting station or as storage aerea

2. D 4

In order to compare and to check the planned decommissioning proposals a literature study on the decommissioning of nuclear facilities and the applied techniques was accomplished. The literature sources can be decided into three main groups:

- reports about decommissioning work in nuclear facilities;
- reports about reparation work in nuclear facilities;
- reports about developments of special techniques in laboratory scale.

The big wall thicknesses, complex structures, often narrow space conditions and the high radioactivity require special cutting techniques. It must be possible to use them in atmos- phere and /or under water as well as to operate them remotely conrolled and in all cutting positions Furthermore the primary and secondary cutting waste has to be captured safely. Mechanical and thermal cutting techniques are options for the application in decommissioning

Mechanical techniques require heavy machines to handle the high restoring forces. Size and weight of the applied tools depend on the dimensions of the component to be cut Application of mechanical cutting techniques is limited by complicated structures and narrow environment. Thermal cutting techniques cause smaller restoring forces, the handling equipment can be smaller. Therefore thermal cutting devices are generally more flexible in use. On the other hand much more secondary waste. and aerosols are produced and extensive filtering and water purifying systems are necessary.

Only very few literature was found about handling aner cr5pplneq techn) s for ‹decommissioning purposes. This problem seems to be neg l e c ted in case of handling pieces of scrap, so that there is no special development beside the normal handling instruments for nuclear facilities.

'the development of remote handling techniques shows, that nowadays electrical master- 'ilave manipulators arepreferred ro mechanically controlled manipulators. Obviously electrical controlled systems have been developed in the past and are reliable ‹•ven in under water application. Electrical master-slave manipulators are quite expensive tools, but they are very flexible in their application.
For the control of the manipulators various systems are suggested in the literature. New concepts use sensors to follow the cutting path. They are mostly supported by teach—in- techniques.

3. Re3plt5 of the study (B,5)

'iVhen working out the decommissioning concepts, some contracted companies of the working group had to respect not only the conditions given in the facility of KRB—A or VAK, but also spe c i l i c op t i eras :

- a concept using minimal automation;
- a concept using maximal automation;
- a concept using the fuel element storage pool with a segmenting station.

'the other cont.‹actors had to develop in their point of view an optima! decommissioning ‹concept

'there were five studies related to the KRB—A decommissioning project. The main results of these studies (A to E) are listed ia table I. Study A had to respect a minimal application of automated techniques, study B should concentrate on the use of the 'fuel element pool for a segmenting station. The studies C, D and E represent "optimal" decommissioning strategies.

All five concepts estimated about the same time requirement for the complete ‹decommissioning of the RPV and its internals:

- preparation time (development, planning etc.) 1.3—2.Syears
- execution time 2.2—3.0years.

In general the **decommissioning** work would be done with approximately 12 **workers, but** the **resulting** job dose was estimated very divergently. The minimum value is 270 msv and the maximum is **3OXi** msv! The costs were estimated between 12 and **26 million DM** in total, excluded the costs for the waste disposal.
All five **concepts distinguish dismounting** and segmenting works; the free fuel element storage pool is always used with a **separate segmenting station. Because of** the different **structures** of the RPV and **its internals in most concepts different decommissioning** methods are proposed.

According to the notion of all contracted companies, the RPV internals should be dismounted and segmented under water. J"he plasma arc cutting technique is mostly found to be the preferable cutting technique, because only minor restoring forces will be ccuring Therefore it would be possible, to cut the RPV internals without heavy guidance and fixing machinery. Furthermore the use of master—slave-technology was estimated to offer enough flexibility to handle even complex geometries of the internals

Table 1: Main data of the decommissioning concepts

A		CONCEPT B	c	D	E
total job dose [msv]	412	30fD	275	870	1000
number of workers	12	15	5-8	i 1	8-28
time required [y]					
preparation	1.3	1.75	2.0	2.5-3	2.3
execution	2.8	3.0	0.75	3.0	2.2
total	4.1	4.7.5	2.75	5.5-6	4.5
costs [Mio DM)					
hardware	4.8	6.5	2.0	13.0	14.8
personnel	7.5	13.5	0.8	13.0	6.9
total	12.3	20.0	2.8	26.0	21.7
waste [m^d]					
primary	140	-	191	233	225
se.rondary	7.g		936	113	-
total	**147.8**		1127	346	225

(e.g the core support). Contrarily, concept D proposed a completed echanical segmen- ting technique. Therefore a universal cutting unit was designe‹1. This machine is able to segment not only the RPV internals but also the RPV itself.

The segmentation of the RPV wall is suggested to be done in atmosphere. consequently most concepts propose the use of mechanical cutting (sawing) to avoid production of aerosols. The guiding of the tools is mainly done by special machines, which fit into the RPV and themselves r« to the wall by hydraulic plungers. These machites are transported by the crane and carry not only the cutting tool, but also serve as gri in9 crevice for the piece to be cut The wall of the RPV is either segmented into rings and then transported into the fuel element storage pool for further segmentation, or it is cut into rectangular pieces in situ and then directly packe‹1.

A proposal to maintain under water cutting of the RPV wall by installing a shirt around the RPV is being discusse‹1. Because there is only litUe space between the RPV and the biological shield, all the pipes and its connection pieces have to be cut very closely to the RPV walL The shirt has to be welded to the lower part of the RPV.

In order to find out the optimal techniques for the actual decommissioning of the RPV and its internals completeness, depth and diligent working up to the decommissioning concepts are valuated. Positive ideas and ‹letails of every concept are collected. The comparison of all proposed techniques and as well the information recieved by the literature study will give a good id.•a about the state of the art in decommissioning techniques. This will be the base to work out a feasible concept for KRB-A Further— more a lack of information wilt show up clearly and necessary inactive experiments can be defined.

7N. PILOT DISMANTLING OF THE BR-3 PWR PHASE 1: DECONTAMINATION OF A PRIMARY CIRCUIT, REALISATION OF CUTTING EQUIPMENT, SEGMENTATION OF FIRST REACTOR INTERNALS

Contractors : Contract No.: Work Period: Coordinator : **SCK/CEN, Siemens-KWU, Framatome FI2D-tOl3 October 1989 - September 1991 F MOTTE, SCK/CEN**

Phone: 32/14/33 21 11 Fax: 32/14/31 19 93

AOHH3(XPM3ANDSODPE

The BR-3 Pressurised Water Reactor had a capacity of 11 MWe and had been operated from 1962 to 1987. CEN/SCK has started the dismantling and decontamination of certain parts of the plant and is examining the possibility of its complete dismantling.

Considering that the experience to be gained from the dismantling of the first representative nuclear installations in the Community should be made available to all Member States, the Commission selected BR-3 as a pilot dismantling project for the 1989-93 R&D programme on the decommissioning of nuclear installations. The Commission, through shared-cost participation in specific parts of the project, intends promoting the use of advanced techniques and the performance of collateral investigations, in order to enhance the generation of useful knowledge and experience to serve in subsequent decommissioning tasks. In particular, the generation of specific data on costs, working hours and job doses as well as on the amount of created secondary waste is considered as an important objective of this project.

The assessment of techniques and procedures will be performed in collaboration with Kernkraftwerk RWE-Bayernwerk GmbH (Gundremmingen), which is decommissioning the Boiling Water Reactor KRB-A (see § 7.5) and with VAK GmbH which is decommissioning the VAK BWR (see § 7.10).

As a Pressurised Water Reactor, the BR-3 is representative of the reactor type most frequently used in the Community. In Phase 1, the contract involves the decontamination of the primary circuit of the reactor and the dismantling of the thermal shield, a highly radiating steel component (specific activity lW - 10' Bq/g, estimated contact dose rates lfF - IN Sv/h, estimated radioactive inventory 10' - IN Ci (at plant shut-down).

The contract is implemented in close cooperation between SCK/CEN as main contractor and Siemens-KWU (FRG) and Framatome (F) as associated contractors, with an agreement for cooperation with Belgatome.

B.WORKPRO€)IUW4ME

B.1. Chemical decontamination of the primary lmp
B.1.1. Cost benefit analysis and selection of a procedure
B.1.2. Decontamination operation
B.1.3. Treatment and removal of decontamination waste
B.R Seegig jj;in f the reactor internals
B.2.1. Concept and design of the segmenting and remote operation equipment
B.2.2. Manufacturing and procurement of the segmenting and remote-operating equipment
B.2.3. Inactive testing and commissioning of the segmenting and remote operating equipment
B.2.4. Segmenting of activated components
B.2.5. Waste treatment and packaging

BE. Generation of specific data on ‹x ts, radioactive job ‹knm, working time and secondary waste arisings, derived from the execution of iteim B.1. and B.R

- 111 -

G. Progress ofwork and obtained results

Summary of main issues

Chemical Decootsmioatioo of PrimaryLoop

Soft decon processes allowing to remove the activity by ion exchange were analysed and compared, the CORD process developed by SIEMENS was selected and tested on samples taken from the reactor system; it was concluded that a three-cycle application of the CORD process would allow a Decontamination Factor between 10 and lOO to be achieved, together with a minimization of the volume of ion exchange active resins. Preparation of the decon operation was undertaken, trying to minimize the modifications to be brought to the plant equipment.

Segmeotiog of Reactor loteroals

The BR3 pilot dismantling project is centered on the under-water segmenting of the highly activated reactor internals with the objective of a high density packaging, evacuation andstorage.

During the Work Period, it is foreseen to design and construct equipment allowing to utilize three cutting methods (mechanical sawing, plasma arc torch cutting and electro-discharge machining) and to demonstrate this equipment at the occasion of the segmenting of a first reactor internal, the reactor vessel thermal shield.

An important objective is a coat-benefit comparative analysis of these techniques, mainly mechanical sawing and plasma cutting, applied in the same conditions in a highly radioactive environment, radioprotection being an important aspect of this comparison.

During the reporting period, the cutting installations have been designed and constructed and the very first cold tests of this equipment were done on a mock-up of the BRL thermal shield; in parallel, the optimization of the reactor refueling pool space occupation inwhich the reactor internals will be unloaded and the cutting equipment installed has been carried out together with the preparation of auxiliary devices, mainly for the evacuation of the segmented piecesi the radiological optimization of the thermal shield segmentation was also in preparation.

Progress and results

1. Chemical decoot&mimetiooof the primary loop (B.l.)

The main objective of the chemical decontamination of the BR3 primary loop is to reduce the radiation dose rate in the vicinity of the low- or non-activated components of the primary loop (pipes, pumps, steam generator, etc.) and the dissemination of the surface contaminants during their dismantling.

The dismantling of the plant primary loop is not a subject of this pilot dismantling project but is intended to be executed in the framework of later BR3 plant dismantling activities. However, it is not wise to postpone for too long this decontamination operation as it implies that the primary loop in its entirety as well as its active components, the primary pumps in particular, are in a fully satisfactory operational condition.

It was decided to use a soft decontamination process using low chemical concentrations allowing to fulfil the following requirements :

- to reach a mean Decontamination Factor at least of the order of 10
- to minimize the radiation dose associated with the decon operation itself
- to concentrate the displaced contamination in a single form, active ion exchange resins with a minimum volume, not exceeding, if possible, the plant ion exchange normal capacity
- to use the plant as it is, without expensive additional equipment or modification.

From the comparative study of the decontamination processes on the market today, it was concluded that the CORD decon process (Fig. 1), developed by Siemens-KWU, was most satisfactorily fulfilling the previous requirements. As all the decon processes for PWR, CORD is first treating the surface oxide layers by oxidation, converting chromium from the insoluble CR(III) to soluble Cr(VI) state; in a second step, the surface layers are then removed by the decontamination solution, the displaced contaminants being trapped on the ion exchange resins; a third step, called the cleaning step, is devoted to the complete removal of the chemicals in solution before starting a new cyclus.

On the basis of laboratory decon tests, performed on small pieces removed from the reactor system, it was decided to apply the CORD process to the primary loop during three successive decon cycles : a three-step three-cycle process. The decon tests were performed on two types of samples taken from the reactor system; the first sample was a stainless steel internal piece of a few dm' located in the upper region of the reactor pressure vessel; the second set of samples were SS tubes which were situated during service close to the RPV; the specific surface contamination on these test samples was of the order of 1 E5 Bq/cm', after decon test no activity removable by smear test was possible to detect.

The plant was prepared for this decon operation, the main important tasks being closing of the primary loop and maintenance of the active components, mostly pumps and valves.

The working parameters of the primary loop and of the purification system were defined :

- the primary loop will be operated at a pressure of 20 kg/cm'eff and at a temperature of (952S)°C
- the purification system will operate at lower pressure, 5 to 6 kg/cm', and temperature (6S°G).

The temperature of the primary loop will be raised to 95°C by the heat generated by running the two primary pumps and stabilized at (95i5)°C by circulating water on the secondary side of the plant steam generator, the excess calories being evacuated by exchange with tertiary external cold source water.

The total inner surface of the systems to be submitted to the decon- tamination process is of the order of 1000 m'; the water inventory in the primary loop and purification system is approximately lS m .

The purification system will comprise the three BR3 operation ion exchange columns of 212 1 capacity each, plus three additional SIEMENS mobile ion exchange columns of 100 1 capacity : it is expected that this total capacity will allow to trap all the displaced activity.

- 113 -

Emptying the BR3 ion exchange columns still containing radioactive resins from the plant operation period relies since recently on a specialized evacuation container, the TN2l, the availability of this container is the mejor cause for delaying the decontamination operation up to the beginning of 1991.

2. Segmentation of Reactor Intervals (B.2.)

As it does appear that the so-called RPV-NST package method used at Shippingport, the first PWR reactor to be dismantled in the world, for the decommissioning of the reactor internals and reactor vessel is neither applicable to large commercial plants nor acceptable in Western Europe, the BR3 pilot project is dealing with the segmentation of the reactor internals with the objective of a high density packaging, evacuation and storage, trying to answer the question : 'How much does it cost to carry out this job safely, with an acceptable radiation dose intake 7'

The first BR3 internal to be dismantled will be the reactor vessel Thermal Shield, a stainless steel cylinder of 76.2 mn (3 inches) wall thickness with a total height of 2432 Rm; the thermal shield is the thickest and the heaviest (5.5 tons) of the reactor vessel internals. It will be segmented into forty pieces with an approximate size of (0.5 x 0.5)m and an individual weight of 150 kg.

Fig. 2 shows schematically how the three selected cutting methods (mechani ca1 s awing , e lec Pro-di scharge machining (EDlt) and pla sma arc torch cutting] will be applied in order to be compared; the segmentation will be done partly in-situ. it means inside the reactor vessel, as far as mechanical cutting and EDH are concerned; arc torch cutting will be performed inside a cutting chamber flooded into the plant refuelling pool, to cut into angular segments the rings separated from the thermal
shield by the two first techniques.

The cutting equipment and the cutting procedure will be experi- mented in a highly radioactive environment, in preparation for the cutting of the other reactor internals and, later, of the reactor vessel itself.

At the end of 1990, 3.5 years after finat p(ant shu own, the total activity of the gamma-emitter (Co-60 mainly, Mn-54) in the whole thermal shield reaches approximately 1 E14 Bq (2600 Ci), which represents approximately half a curie per kg of stainless steel; the gamme radiation dose rate under water at the surface of the thermal shield was estimated to reach a maximum of 1 E4 r/h or 100 Sv/h.

The equipment designed and manufactured for mechanical cutting and for EDM is schematically shown on Fig. 3 in cutting position, lowered into the reactor vessel, inside the thermal shield, this equipment is composed of two main parts : - the lower part or cutting device

- the upper part or lifting device

The cutting device consists mainly of a ring which is, after centering, clamped inside the thermal shield by means of radial hydraulic pistons. Vertical positioning of this ring is accomplished by vertically ad juscable tie rods . A cable mounted on I.his ring is rotated at low s peed by an elect.ric motor / gear uni t.; this I.able is provided by a tool suppor t for carrying the saw head which is moved in che radial di rec tion by an hydraul ie 1 inear dr ive .

- 114 -

The design provides for remote disassembly of the saw head and for lifting of the saw head for changing the saw blade under water. Chips produced during cutting are drawn off by suction equipment and collec- ted; the cutting operation is monitored by a TV-camera.
The electro-erosion head is designed to fit onto the support tool of the mechanical cutting saw head, both heads being therefore easily inter-changeabl.e .
The liftiog device has two main tasks : the first one is to eliminate the own weight of the thermal shield ring to be cut to avoid the saw blade being jammed during cutting; the second one is to remove a cut ring from the reactor pressure vessel and to transfer it into the plasma **arc torch cutting chamber.**

This equipment has been submitted to first cutting tests on a full scale partial mock-up of the reactor pressure vessel and of the thermal shield, all the diameters and tolerances of the thermal shield mock-up are scaled 1:1, only the height is reduced to approximately 50Z. The material is stainless steel identical to the composition and character- istics of the original mterial AISI 304. Analysis of the neutron irradiation of the thermal shield has shown that no considerable changes of the material mechanical properties are to be expected, at least not considerably affecting the cutting parameters.

The equipment designed and being manufactured for arc torch cutting of the annular rings separated from the Thermal Shield is shown on Fig. 4; this chamber flooded into the refueling pool has been specially designed to extract and collect the secondary wastes generated in the form of gas, aerosols, suspended particles, sedimented dross, etc. during arc torch cutting.

A ring separated from the thermal shield is deposited into the chamber on a table fitted with holding devices maintaining the angular segments in position after cutting; the water level in the refueling pool is about $.5 meters above the ring. The conical cover of the cutting chamber is topped by an axial vertical chimney in which the torch displacement mechanism and the torch feedings are located.

The water level in the cutting chamber is kept low above thering at the top of the cover of the cutting chamber, where pipes, check valves and suction fans allow to circulate an air flow carrying away the
ga (H$_2$ NO, ...)**and the aerosols formed during cutting; the aerosols trapped**
s on absobute fi 1te rs whiie the di1uted ga s es are re jec ted
ar
e

into the plant container ventilation system.

During and after cutting, the water of the chamber is circulated by pumps into two filtering units made of coarse and fine filters and ion exchange columns, until the water quality in the chamber allows to reopen the chamber for unloading the cut segments. The larger sedi- venting particles are collected by a cyclone effect into the lower part of the system where they form a cake to be evacuated as well.

In parallel with the design and construction of the arc torch cutting chamber, the optimization of the cutting parameters with the plasma torch (plasma current, torch stand-off, torch linear displacement speed, nature of the primary gas and of the secondary fluid) has been undertaken and organized in two successive series of tests :

- type 1 tests were dealing with cutting horizontal 75 mx thick stain- less steel plates under a few centimeters of water. Besides the

- 115 -

optimization of the cutting parameters, different characterization measurements of the secondary waste produced by the process have been carried out; these measurements, in conjunction with data from the literature, have been used for dimensioning the water purification and filtration systems to be connected to the flooded chamber.

- type 2 tests are dealing with thermal shield cutting in realistic conditions : vertical thick SS plate, water depth between 0.3 and l m, automatic drive mechanism for the torch; this second series of tests required the construction of a special installation including a large stainless steel vessel which was installed in the machine hall of the BR3 plant; this installation will be used later in 1991 for cold te s l.ing of che couplet.e cue ting chamber which will be f looded int.o this ve s se1 ; a ring separat.ed f rom I.he The rmal Shi eld mock-up wi11 be segment.ed in these condi tions , rich full - s ca le tes cing of the wa ter purification system and of the air (gas and aerosols) venti1at.ion sys cem .

CORD PROCESS for BR3 DE CONTAMINATION

(CORD: Chemic at Oxidizing Reducing Decontamination)

3 cycles (3 steps in each cycle)

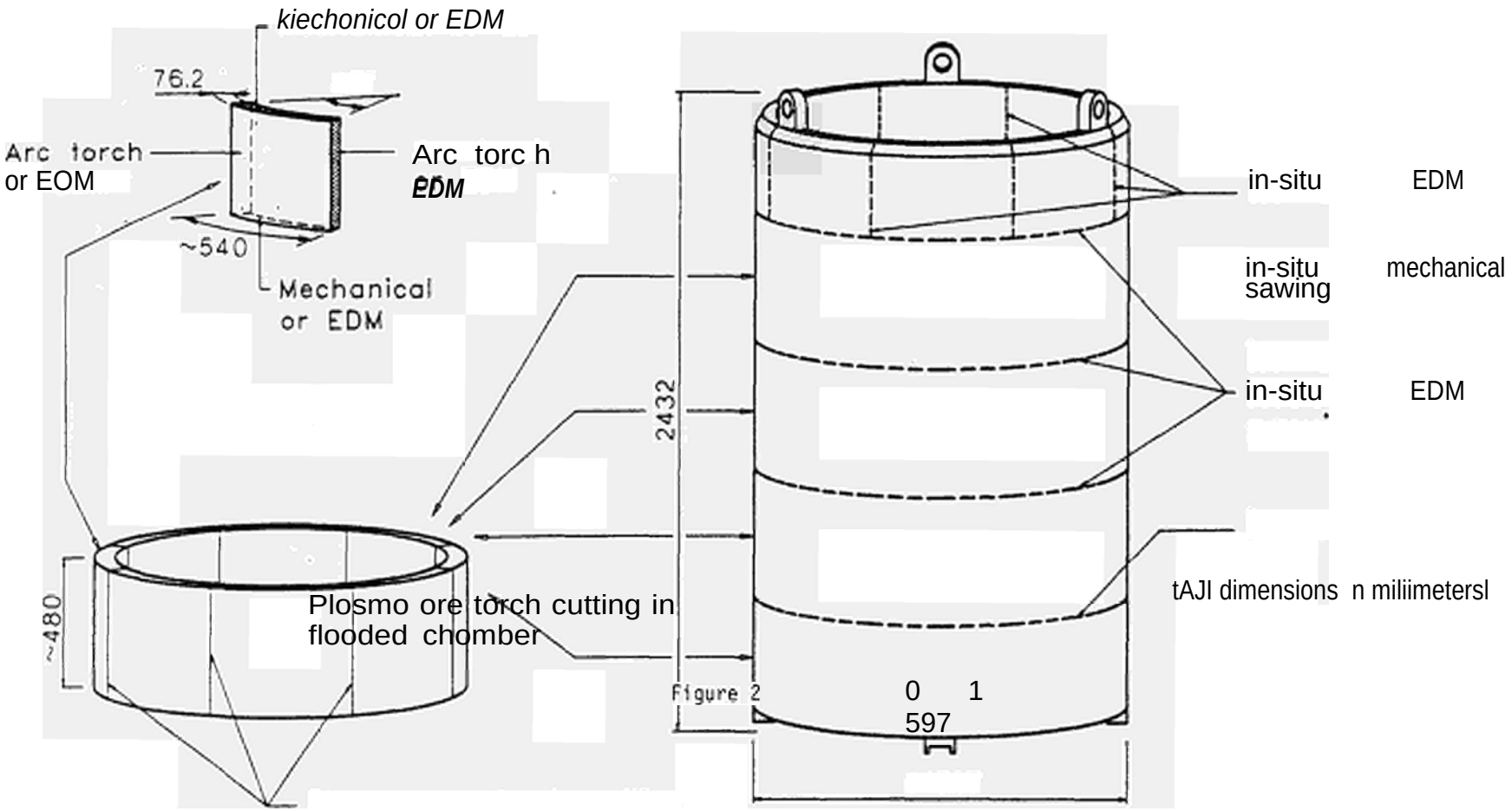
1. O XIDATION STEP (Cr ‴ -- Cr^{6})	: $HMnO_4$ (permanganic acid) 10,3 9/l)
2. DE CONTA MINATION STEP (dissolution of hematite)	: $H_2C_2O_4$ (oxalic acid) (3 g/l)
3. CLEANING STEP	:Destruction of the excess of oxalic acid by oxidation

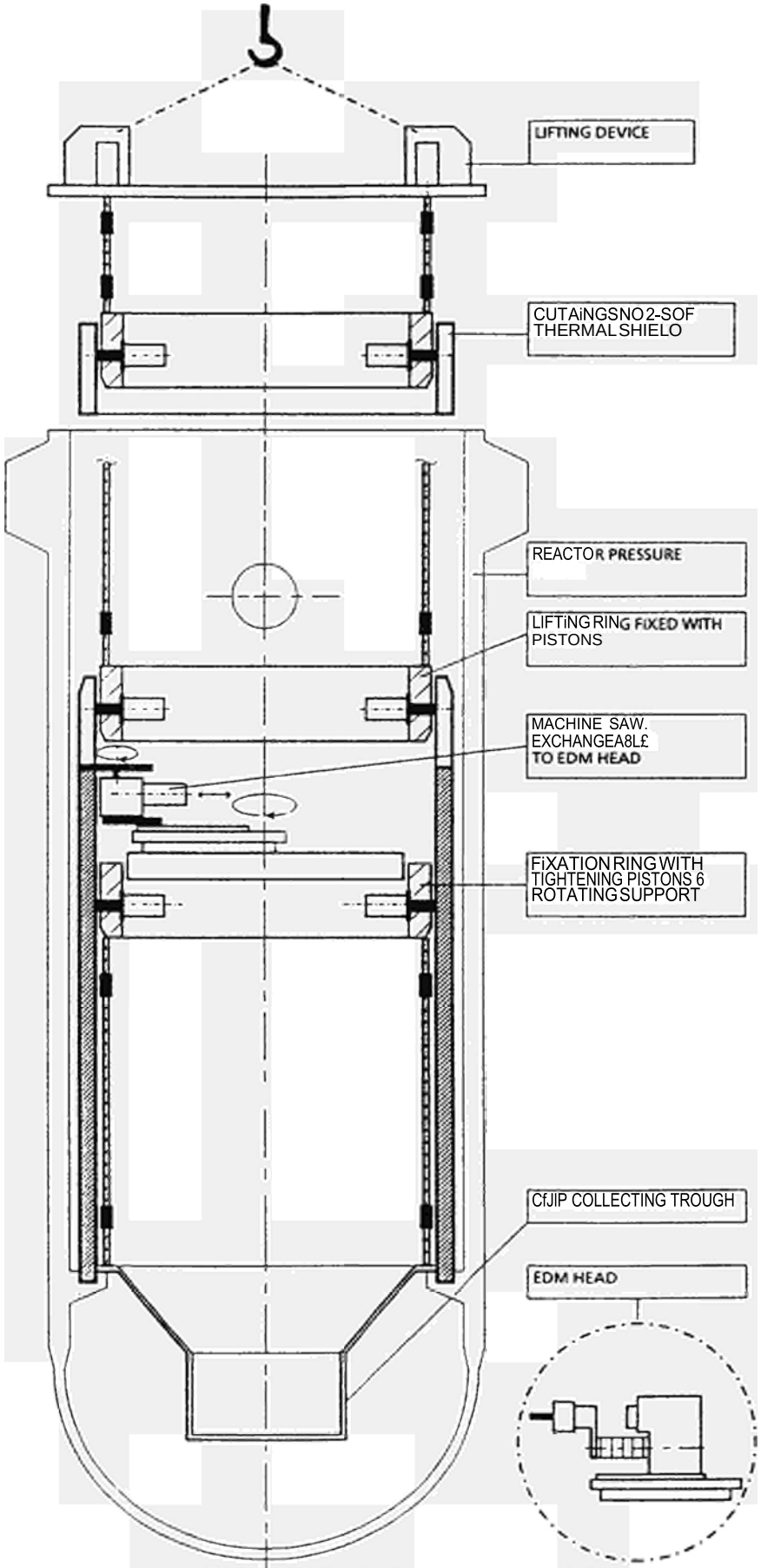
Low chemical concentrations Low temperature (95•)

Contamination fixed on ion exchange beds

Figure I

BR3 Yhermal Ohleld Segmentation





F I qure J : He chan I ca ± cu t. t I nq and £ oK

11 9 -

Yent:) 1a clon And £ il ce **ring untt**

Ch*«kvalve

CAeck valve



i 7orchlift

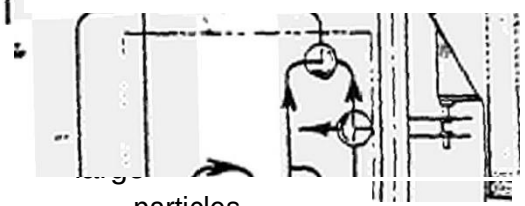


ater level in the
cue clog chamber

Cutting chamber

Thermal shield rin

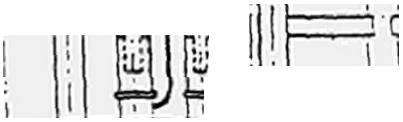
," F'x **lte rin g** *unLt* nr . 2 io1n t



, particles

1 **Sed Lie n.t ed** - a





"]9O C **E/9B**

7 i qu re 4 : Arc to rch cu Lt i ng

1 20 -

7.4. PILOT DISMANTLING OF THE FBR-FUEL REPROCESSING FACILITY AT-J PHASE 1: DISMANTLING OF DISSOLUTION AI'ID EXTRACTION SYST£IMS AHD OF FISSIONPRODUCT STORAGE TANKS

Contractors:	CEA-Valrhfi
Contract	FI2D-OX14
No.: Work	October 1989 - September 1992
Period:	F CORNU, COGEMA, La Hague
Coordinator:	Phone: 33/33 03 66 71 **Fax: 33/33 03 60** 14

AOBIEGMVE S€OPE

The pilot facility AT-1 for the reprocessing of FBR-fuel had a capacity of 2 kg/day and had been operated from **1969** to **1979.** Dismantling of the plant has started and is planned to be completed by 1992.

Considering that the experience to be gained kom the dismantling of the first representative nuclear installations in the Community should be made available to all Member States, the Commission selected AT-1 as a pilot dismantling project for the 1989-93 R&D programme on the decommissioningof nuclear installations. The Commission, through shared-cost participation in specific parts of the project, intends promoting the use of advanced techniques and the performance of collateral investigations, in order to enhance the generation of useful knowledge and experience to serve in subsequent decommissioning tasks. In particular, the generation of specific data on costs, working hours and job doses as well as on the amount of created secondary waste is considered as an important objective of this project.

The dismantling of the AT-1 facility is concerned by specific problems associated to the reprocessing of irradiated fuel, namely the presence of a mixture of alpha, beta and gamma emitters. This necessitates the use of remotely operated and controlled equipment for the dismantling and decontamination, partly due to the specific conception of the cells, without direct viewing. For this, the carrier ATENA is used (telescope + polyarticulated arm) supporting the telemanipulators MA 23 or RD 500.

Specific problems are also encountered with radioactive measurements needed for the sorting and preconditioning of the arising dismantling waste.

Estimated maximal values for the specific contamination and for dose rates are in the order of 10,000 Bq/cm' and 1 Gy/h, respectively.

B. WORK PROGRAMME

Remote-operated iijsman feqjjjpment out of **the strongJy contaminated cell iXi3 (used** for dissolution), and of cells OX14 and i i5 (used for extraction).

BE Measurement of **the radioactivity and mndiBoning of** the waste arising from B.1.

BE. Dismantling of tanks for the storage of fission puxh

B.4. Generation of specific data on cents, **radioactive job deem, working time and secondary waste arise derived from the execution of items B.1., BE and BE.**

C - WORK PROGRESS AND RESULTS

Summary of main issues

After test.irig t.he diemantl ing machine ATENA and its auxi l iaries were installed. . Then dismntlirig operations started me expected in rell 905. However, as i rradiat ion t.p s ery low in t.his eel l i t has been dcci ‹led , aft.er a short use, to transfer ATEft§ tO ‹tell 504 and I.o finish the di smant l ing of 905 in di reet intement ion.

Delay in t:h+• de1 iveririg of RD500 reniot.e-mriijnilator h" 2, ex- pe ied to be mount.ed on ATENA ‹4uring the necond half of 1990, resul- t.eel in a axxii fieat. ion in the UDIN schedule. On one hand, the ATENA reach me equipped sit.h the tIA23H getting go‹xi results i n the on-going operat ions , on the other hand, a romp) ementar,v operation I.o ‹ r›uple HD500 wi th ATLUA eras neer•ssary. I t wee I.hen dv icled l o os oicl ATENA to be iinevai l at) e for 2 or S nxinths, not. t.o use RD300 eoupl erl with ATENA b:st I.o i nt.egrate it in che n'aeta treatment system to put *'i t.* i n rev1 ccli s•• cr›ndi l ions.

The prepara l i on of the vast e t reatment ce I l, i ntegrat ing the R0500 dev i ce vas a Inos t coup Iet ed t90 XI at the end of last year.

8t.orage tnnks for I ission (›r‹xlunt.s haste bc•en dtenant.led itsing **ten pr esses**:

- plasim tor‹:h Brae useri t.o out. the Ienks in I.he exterior on Inti l ding (er• 1 520) with high centri nat i on btit no i ri-ad i a- ti r›n,
- 1 Inear-shapect explosi e ‹•haogc•s we. «sed tn r'eJ l s 90tt and fi09 in I.hr: nvztn bu:i 1‹t1ng her•wuse r›f' onnt 1nat1or› anrt I i•- radiation.

Progress and results

1. Renx›he - operated drum ntl ing of equitx»ent. out of highly contaminated cells (BI)

The First e.xt.ract1nn c¿c• Le i.s foe.ated i i› ‹•ell 9f)•\ . ‹Tel 1 d1r‹ens1ons arr• : 7 m. he1nht., .t ni. i•›dth, ti m. 1ength. Rad1c›aot.1x e m*:anurementn don thro**ghpen*tratiwnmessesafiershutds.nof the r:et1 and f) unhing I in 19ei i shoed °hot• j»in1s of 0,112 to 0, lGy/h ther an nmbi nt dose rate oF 0,03 to 0,04 thy/h . i taore pror.ise mnpy›i ng was ‹•erried out. in July 1985 sft.er reax›vino the ‹ ei1ing slahs ‹ f the r'e11 , aixl resul t.ed in val ues eoaipr i en lmtiror•ii 0,f10l and O ,050y/h .

Thus, i t ixppeured necessary to ident i t'y es <xn.itl.. us (›css i ble t.h•• "hot points usrng t.he phot.ographir• gnieui niat›ping s1‘s.t.eat. Two r›pertit.i‹ino wr•re planned, t.he fi i• t. one in fiox‹-ther 1'ltl9 throitgli the t.op .if the m) 1 and the second rune i n Febru.try lSiIO I.hrougli an ‹ peni ng made i n I.he l aterel e‹›rri‹4or tl02 as t.he tmt.tmm of the ‹:w1 1.

piq took g pt. ‹ rehn 13 weehs wr•• dex'‹tecl to sh‹•otirig l .

Seiei•:1 'hot" points »ere identified eu:'rrnpondirug tr. tne pi•a-cited ;'sl*ies.

fn m8Uitlnn, thewhowo2the every our:ippeared tr,heare ‹. l est contamiriat.erl anoordirig to the di fferent areas. As cont.wina- t i on i n 1 argel; spread, total act ivi t y is high ni id t iie rna., ›r part r›l' t.l«• anih.• ent. dr›ne rate r‹xaen frcim t.he f l‹x›r.

The second and third extraction cycles are located in cell 905. Dimensions are : 7 m. height, 3 m. width, 9 m. length. Radioactive mapping carried out in July 1989, in the same conditions as in cell 904, showed values lower than 1 mGy/h.

'1'he \l'F'N\ ‹3isrriant.Iirig ah ine mas de•sigri‹fi l'›r reiiiot.e dismn—41in o(Ihe A7'l high—3e•x•e1 ce IIs lxisecl on I.he PIADD. maniaine heart I‹o himnartle FSC fT R. it comprises a carrier and an electi'ioa4ly actua- ted them:wipufatnr.

the ‹arrlrr inclines a containment housing, a transfer lorry and a support arm with provisions for vertical and articula- ted pc›rti›n an snpporti the telemanipuiator.

The carrier in designed to ac.commodate either a 20diN MA 23 H talenmni later ora5()‹ RU 500 telemanipu4ator.

The A'£ENA machine is located in room 800 abc.ve delis 904-906, with vider› control and monitoring equipment auld ronsotes in moms

The lower biological shielding installed above cells 904-905 includes openings through which the carrier arm and telemanipulator can be introduced into the cell without breaking the containment integrity. Leaktightness is ensured by an obturator device set up at the selected work station. An other one provides for containment of ATENA at the maintenance station located at the South end of room 800.

Beneath the lower biological shielding, a twin-beam carriage with two hoists is used sling heavy parts and remove waste materials. Collision prevention systems are provided on the articulated ATENA arm and on the carriage to avoid damaging them and the equipment being dismantled.

The First three months nf contractual program loctober - nerember l989+ wr•re taken upb,y procurement., setup and test act4vi- l1a•a. lesLing of the ATENA machine with the MA 23' manipulator was r'ompleted. Auxillar.›-equipment,(carriage and ohtura:ors) were revived ririJ et up nn the site. The system was ?.est.ed, tor›)iri fixtures were i nst.a l l eel i n t.he i r g 1 ov‘o lx›xes and the' ATEkA mci nt.enanr::r s tnt.ion was

'I he l'ii t oritt.in.=qs l.or›k pIwo i n Jantaary aner February i. i tfi l.he T A machine equipped with the remote manipulator MA23M. The purpose as to clear the 1‹y‹froll 905 then to finish it tn dirert intrr•.en-

4'fiN.l was installed in ce!19t)4 in Marrh. fJismantling lasted !rrn thnn 6 mouths, broke off hy a shnrL intervention in cell 906 for ‹Jiamantl ing the mixer-setttnr lotteries.

During l.h‹' ccii l.t.iri,g operar.ions wi th ATEhA thr wash es were di op-J›rxl on I he f lr›or r›f' l.he eel.I except. f‹ r hear y J› rts which we pp r ego ved mast.es frm oe1 1 905 were rem rxi dur i ng the cli rat i nt.ci en-dl‹›n. Those f rc›m 90 l i‹ i 11 be rc•moved a ft.er Ohr n l:ar l.-up of' the i‹r‹s I e' l '•a t.ment eel l !s‹r fi' 2) .

Shears vcrre used for l.he f i rst. matt i nos . 'fire i mjx›r†.ant. we i gis t. '›f t,h i s i.oo1 1 1 S kp) rompare‹3 ivi l.h l.he span›i l.y l.he NA "2i1 1 eel I c i he motan t i nq= ‹› f a we i ght.-bnlari‹ae nys†.em on l.he kair-up t he pr

.+r
‹:ul›1o l.r› re1) w o l.hr st r.ui n on the• s l a e-arm.

\l l.ht Hugh t,ho w‹irk an sat 1 sfac tory, l.he tier i ›f o : non1ar s: iv n'as l.hen esserit. ial f‹or i ts grea†.er tisoab i l i ty (7 kz) cr›ns i dering †.he ci i ff*.run I t. access to l.he re 1 l arid l.he shape c› 2 nome the p◌rt,°. l..«

- 123 -

The most ale 1 i rate step of the d ismant l ing operat.ion was the 1 n t rodu c t i on of the NA23 i nto the cell , i•here the mach a rie had to cl ear i t.s «'ay i mo a '.ji irig1 e ot' pipes" ‹'hoos irig l he r ight tr›ol . Risks of col) is iron Set.seen the pol y-an i oulat.ed arm out of i l.s sheath and its env i rr›nment had to be co ns i de red especi al ly in ‹:e11 904 . Di ff icul4y was dr›ubbl ed because there i•ms no di reef x is i on of the operasion, every- th ing was oarri e‹1 out t.hrough a video-system. Co11i s ion however o‹ ourecl proc ing t.he eff ic iencyof the project i on s.vstein of the po) y -art.i cu lated arm .

The carrier was perfectly rel table . A pnre fr‹xn a fai lure of t.he comput.er , w‹auri rig fore• the a c t i ue ope ra t i on - there were on l y• a few oi l l eahu of no i mpr›rtance . After 6 months of operat i on the car ri er was swi tchcx) for pres ent.i ve• maim.enanri- .

The r i r‹cular saw was mph used by the remote-man ipulator NA23 . The rnnin fai lures rworded were breaks of tape and felt s and gear i•ear . The dev i we i•r'nt baclr ewh t tme t.o t.he ma intenanre shad ion .

To shor t.en l.he immobi 11zat i run peri od , a s ond slnve arra was twit. in operat ion in June , r›ne o‹ uld l.hen be repa i rrH whit e the second was work ing .

'the result s in days of the ATENA manh ine operat.ion for the di nmant. l ing ct' cel 1. 90?o and 904 are as follows :

	905	**904**
- Duration	39	95
- Actin-e stepn :		
. aoesnand cutting	16	\5
. equipment development end adjustment	3	6
- Silent steps :		
. leivU 1 mainte ce (failures of little importsrr:e)	b	11
. levy 2 nminte ce (f lures involving re ir)	12	24
. other causes		9

During theconsidered **m f tim the accumulated dose rateis as fo l lows :

- .4TENA and au.xi l iaries mountinsi and test ing I mSV
- ganina phr›tographio napping : 2 msV
- 905-903 d remarry1ing with .\TENA : 11 mS\
- dint. disrriarrtl ing :1t›" m.8V

The d*nmnntling ofcell 905 resulted in about 6tonsof Dante in ‹:ondi t.ionn vinyl protected parels. Ge are presently carrying ‹sit rW ioact i x-e measurements of thene Jmwe) s and are skor irig l.hem i n rc›nt ai ners .

- 124 -

2. Measurement of the rsdiosctivity snd conditioning of the waste (B2)

The high leve•1 «cede treat.ment ce3 I, also cal led "workshop ‹ e) 1", is lc›ca4ec1 on I.he northern side or' building 500, whr•re the JTENA machi rie operat es .

ft ismmdeofconcretewallsandstainless-steelmodular pan- nels coming fromtheATIworksite.Apartofthinworkshop well in located abnvecell905allowingcommunicationthroughremovableslabs. In the workshopcell,twoarticulatedbeamsstuchinthewall, support.15K hoist.s allowing t.n reach outol1 partn ofthecell.

The teleoperationtoolsinr]iWetwoM8remntemanipulatorsand I.wn- RD500 rolxat .

TooJingincludesacircularsn omd hydraulic shears hung abnve a mnhiLa w°°*1<an hy t.ke-i1p reels.

Wastr: la removedbyatransfercarthrough a hatch equipped with a hnint.

Waste fromrrlls904or903areputinabinthen removed with » twin beam carriage tn cell 905. The bin is then lifted by the lST(N hc›ist of I.lie .or1‹shop ee11 and ti pped i n I he remote-mini pu lators aren . A select.i on wi th an II' 104 probe is carr red out ac wording I.o †he i r racti at ion I ex rel cut each wasI.e . The wastes are cut again i I neeessar y anr) platen in c•on Lai ners with x ar i our Chi chness according €o thai r eat.egor3 .

The nont.amere are removed through the was†e exit hat‹zh aric(I r:‹nsjx›r†ec1 4 o the measuring s†ntl on .

At, I.he end of 1990, the workshop cell was comp1e€el.v instatted except for the exit-hatch which is in the process of being finished.

3. Dismantling of tenks forthestorage of fission products B3 Cell920 lextension building storage)

Th‹r tanks of eel 1 920 had been ins4al led €‹o i nrrease the ini - t.rat nt.enrage wapueiIy of fissi on prrxlur4s soluti ons .

In 198fi, the oe11 pipes were d1snmnt.1ed end the connect ionn plugged by welding.

Inside remained t.wo 30 m3 tanks (diameter : %800, height: 3600 and thickness:5:xm)includingsrinternalcoolings1'stem,&n homo- genizatinn pulsator,plimger-pipesfortesting,inputanddrainingof solutions.

,Although this cell has never been put into operation, it was inc(dentlx contaminated during ATl operation. The radioactive mapping carried out in 1986 showed a contamination of 100 to 4000 cps.

DernnLminstion oftherecovery-pen andofthetsnkswestemp- ted «Cththe hopeofeasing thedismantlingandeventuallyof decom- missioning the whole or pert of the stainless steel. Inspite the effort, itturnedouttoheimpossibleto lower certain cont ination pnintsunder500cpsalphaontherecovery-pen then inside the tsn4s.

Dismantling of thetanksendther.er.overy-pantnok place]n the above-cJted radiological situation with plasma torch cut.ting.

- 125 -

After cutting, a **decontamination** testwith electro-polishing ion carried outon a1m2semple. Thistest proud tnbe satisfactory and itwasthend.ecidedtoapplythe treatment Tnallthecut parts. Cons‹rquent) j- 80 P of the meLa1 sheet.s rould has e h en dwomni ss i on- ne‹1.

Cells908-909 (main building storage)

The purpose ofthese cells was to stnre fission products solu- tions coming fromthefirstextract.ioncvcle(hatedincellR0.t).

In bothcells, therewnsa15m3tsnkwithRnhorizontal exis (diameter: 2100 mm, length: 1R00 mm)and itnassociated pJpes.

Each tankhadawatercoolingloop,ant.irringringwithpres- nurize‹4 air and avent-hOleconnectedtmRWashcolumn located in smother'cm.

JIringshutdownoperations,thefissionprodutssolutionswere remmed from the tanks to the UP2 facility. The tanks were then strongly rinsed and emptied.

Access to celln 908 and 909 is made from building 803 through two openings blocks by bargebricks.

Irradiation measurements carried out in April 1989 showed ambient dose ates of about of 0,25 mGy/h with hot points of 10
t.o 100 mGy/h .

Linear shaped explosive charges were made of lead urapper f) I Ied with exjplonives.

Thisshouldbecompletedwithausuatcuttingtechniquewith nhears for small diameterpipen.

Fach tnnh vns cut in six nteps totalizi 7O shooti with 4000 goFeijplosives. Theopeatinnhasbeen fromDecem€ier 5th tn December 19th For bnth tans and was very satisfactory. Frior tn this, thepipesoutt3ng took plRceduring themonth ofUctoher.

The integrated dosefnrallthe908and90Poperations until **December 31a.** was 10,2 mBV.

4. Ueneratioh ofspecific dots(B4)

Results cited above for items Rl, B2 end B3 are incomplete. A detailed analxsinisunderway.Moreinformationwillbegiveninthe next reports.

7J. PILOT DISMANTLING OF THE KRB-A BWR PHASE 1: DISMANTLING OF CONTAMINATED COMPO OF REACTOR BUILDING AND OF ACTIVATED INTERNALS OF THE REACTOR PRESSURE VESSEL

Contractors: KRB
Contract No.: FI2D-0tXl5
Work Period: May 1990 - January 1993
Coordinator: W STANG, KRB
Phone: 49/8224/783 730 **Fax:** 49/8224/782 9IXl

W OBJECTIVE AND SCOPE

The prototype Boiling Water Reactor Gundremmingen A (KRB-A BWR) of the Kernkraftwerk RWE-Bayernwerk GmbH (KRB) had a capacity of 250 MWe and was operated from 1966 to 1977. Dismantling work has been started for some time (especially the turbine hall has been dismantled), and complete removal of the power station is foreseen to be completed by 2000. The two foregoing EC programmes have been involved by four R&D contracts in the past dismantling work on KRB-A KRB-A dismantling is a European undertaking according to the definition of the Euratom Treaty.

Considering that the experience to be gained from the dismantling of the first representative nuclear installations in the Community should be made available to all Member States, the Commission selected KRB-A as a pilot dismantling project for the 1989-93 R&D programme on the decommissioningof nuclear installations. The Commission, through shared-cost participation in specific parts of the project, intends promoting the use of advanced techniques and the performance of collateral investigations, in order to enhance the generation of useful knowledge and experience to serve in subsequent decommissioning tasks. In particular, the generation of specific data on costs, working hours and job doses as well as on the amount of created secondary waste is considered as an important objective of this project.

The assessment of techniques and procedures will be performed in collaboration with CEN/SCK Mol and VAK-GmbH, which are decommissioning the Pressurised Water Reactor BR- 3 and the VAK BWR, respectively (see § 7.3. and 7.10). The results and conclusions of the assessment work undertaken in contract FI2D-tD02 (see § 7.2.) will be considered for the implementation of work in this contract.

As a BWR, KRB-A is representative for such reactors, existing elsewhere in the Community. The present contract involves the dismantling and segmenting of contaminated components of the reactor building in air (partly with subsequent decontamination), and of activated internals of the reactor pressure vessel (RPV) in remotely controlled underwater operation. Estimations of maximal values for speciEc contamination or activation are in the order of 4.10’ and 10‘ Bq/cm', respectively.

B. WORKPROGRAMMP

B.1. Dismantling in air of contaminated and low-activated components of the **reactor buikling,** partly with subsequent dec ntaminating/melting.

B.1.1. Dismantling of a secondary steam generator with various tools (band saw, flame cutting)
B.1.2. Dismantling of a primary circulation pump by band saw.
B.1.3. Dismantling of a primary clean-up cooler with various tools (band saw, diamond-tipped wire saw)
B.1.4. Dismantling of a shutdown cooler with various tools (band saw, shears, flame

cutting)

B.1.5. Dismantling of the RPV-cover by flame cutting

B.1.6. Decontamination of segmented components by dipping technique and meltling for recycling and disposal.

- 127 -

BE Underwater disman o and higJjjy_contaminated jxim;xioents of the RPV

B.2.1. Segmenting of the steam-dryer by various t‹x›ls (shears, plasma-arc torch, consumable electric electrode torch)

B.2.2. Segmenting of the water-steam separator with the core head by various t‹x›ls (saw, shears, plasma arc torch with special gripping system)

~~B-3~~. Generation of speciBc data on ‹x tc, radioactive Job iknm, rking tins ainl aecc idary ate arias derived from th ezm:ation of item B.1. and BE

C. Proper..of work an4 obtained results

Summ_arv of main issues

The aim of the work in this project is to test dismantling, cutting and decontami— nation techniques on contaminated and activated components of KRB-A.

The selected contaminated parts for the application of well known and new techniques are a secondary steam generator, a primary cooling pump, a primary cleanup cooler, a shut down cooler and the RPY cover. They will be dismantled and cut in air. A new cutting technique was developed for the dismantling of heat exchangers. The cutting is done with a good success under frozen conditions with a large band saw.

Highly contaminated and activated components of the RPV like steam dryer and water separator will be segmented by **thermal cutting techniques (plasma** arc and consumable electrode) under water by **using remote controlled tools.**

Progr_$_@rk

1. Dismantling in. ir f n(2misaindo eAtm zctiyayxaj_gqmpgnrs1OBI.3

1.1 Dismantline of a secondarv steam eenerator IB 1 1.: B.l.4.)

Three secondary steam generators have to be dismantled in—situ, inside of the loop rooms, because a transport of the complete components out of their installation places is not possible. It was decided to apply a new cutting technique for the in—situ segmenting of such a large component

Following the strategy of KRB to apply in air only cutting techniques with low aerosol production, it was recommended to execute the segmenting of these components under frozen conditions by using a large mobile band saw (max. cutting diameter 2.2 m, weight appr. 8OXi kg). For this purpose the heat exchanger ui ll be fi lted uith uater and ccoted down.

There are some significant advantages by using this cutting technique:

- the dose rate in the loop room will be reduced at least by a factor of four
- the tube bundles and other internals will be fixed for the subsequent sawing
- the saw blade will be cooled without the necessity of using other cooling fluids.

At first, a **preliminary test with an inactive test model** was carried out in order to prove the feasibility of this technique. For the test, a large shell with a diameter of 1.5 m and a **wall thickness of 40 mm** enc l os i ng a heat exchanger bundle was filled with water to simulate the conditions in a scale **nearly 1** : 1. Afterwards an insulating casing was used to cover the test model. By blowing cold air, produced by a **commercial refrigerator,** under the **insulating casing the water in** the test model began to freeze from the outside **to the inside. After nearly four weeks, the temperature in** the center of the model comes to - 14 C and the cutting test could be **starte‹t** The changing of the temperature during cooling is **shown in figure 1.**

Then the cooling and **insulating system** was removed The **horizontally operating** band saw was fixed to the model in order to cut off slices of the shel(Three blocks have been cut **without any problems.**

Important parameters such as **cutting velocity** and feed rate have been investigated and optimized. The first cut could be done **within** 80 minutes. By increasing the feed rate, it was possible to cut the **third block within 50 minutes.**

Figure 2 indicates the increase of the temperature during sawing Furthermore the pro- blems of lifting the parts and the displacement of the saw could be studied This tecIs—

nique will be applied also to the shut down cooler in the beginning of 1991. This cooler is relativly small (diameter of 1.1 m) and has a dose rate up to 4(Ol csv/h at the surface.

1.2 Der

The planning for the segmenting of the RPV-cover (figure 3) is now finished. It was decided to dismantle the cover partially at first by thermal cutting techniques inside the reactor building into three pieces to allow a transport through the narrow lock gate to the turbine halL There the cutting into small pieces will take place in a special cell with a venting and aerosol filtration system.
Borings at the RPV cover indicated that the ferritic base material is not activate‹t Subsequent radioactivity investigations had to find out whether the austenitic cladding is contaminated or activated.

Further dismantling by applying different cutting techniques will make it possible to compare the cutting methods concerning costs, aerosol release and man dose.
It is intended to test flame cutting, plasma cutting, oxy-arc cutting and sawing

2. n n f

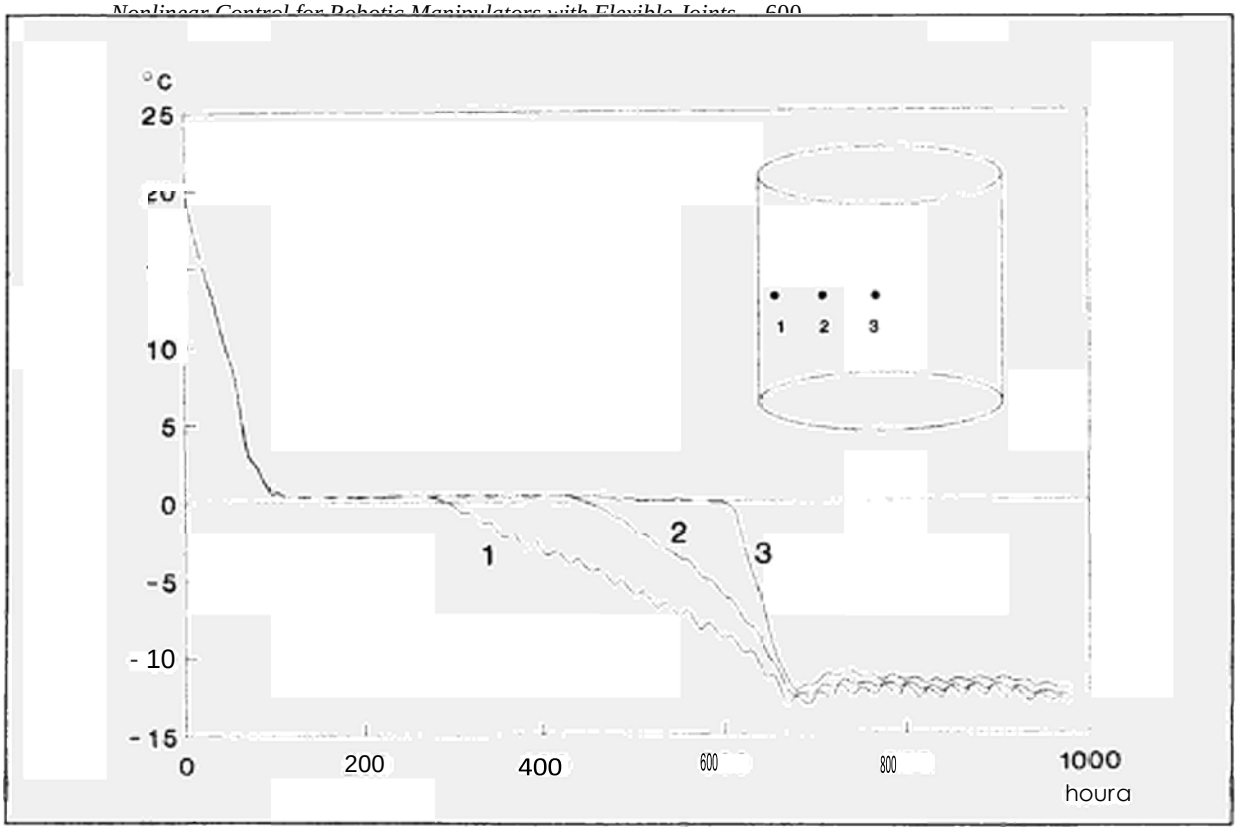
V

It is forseen in the frame of the research contract to dismantle the steam dryer and the water separator as examples for activated components. The steam dryer is already discounted and placed in its storage pool, where it was placed in former times during the changing of the nuclear fueL The position of the steam dryer inside the reactor pressure vessel is shown in figure 4. It is situated on top of the water separator, which will be dismantled in the next stage of the worL

Figure 5 gives some details about the des1 gn of the steam dryer. This component has a diameter of about 3.4 m and a total hight of nearly 4 m. The outer shielding is made out of a 5 mm material The vertical tubes at the inside of the dryer are placed on a ring, so that they are quite close together. This fact causes a dismantling from the outside to the inside of the steam dryer.
The tubes have various sizes between a diameter of 88 mm with a wall thickness of 2 mm and a diameter of 40 mm with a wall thickness of 4 mm.

For the cutting of this component an inactive model was constructed and)nstatted at the University of Hannover. The cutting concept includes the cutting of the shielding with plasma arc under water. The tubes will be cut with consumable electrode with water jec This technique allows the cutting of tubes from one side.

Figure 6 gives a side view of the cutting system, as it will be used in the storage pool of the steam dryer. The cutting will be done with a special equipment which is placed on a platform The guiding of the tool carrier is adapted to the diameter of the dryer, so that it is simple to cut windows in the shell of the steam dryer in order to cut the tubes afterwards.
At the moment, this cutting system is under construction and testing at Hannover. The correct function will be checked there. After the permission of the authority and after a training of the KRB staff at the equipment, the transport to Gundremmingen will take place.



Figur« I : changing uf the temperature during cn‹›ling

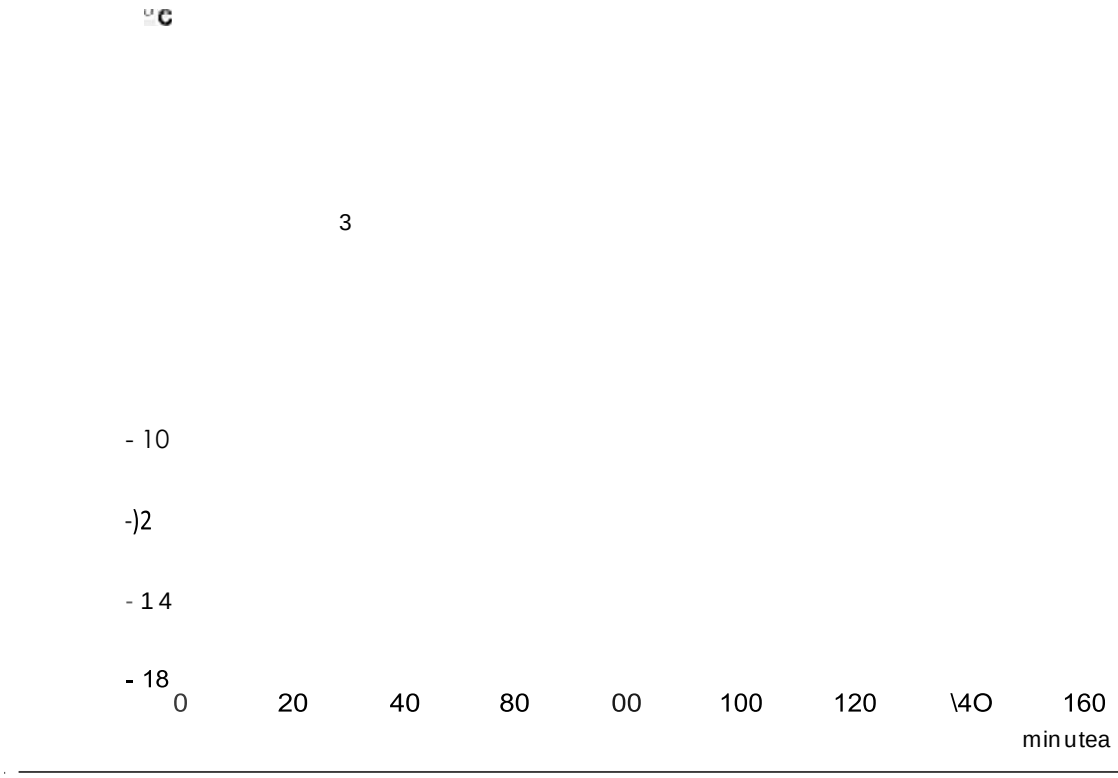


Figure ?: in«rcasc• ur ‹he temperature during sawing

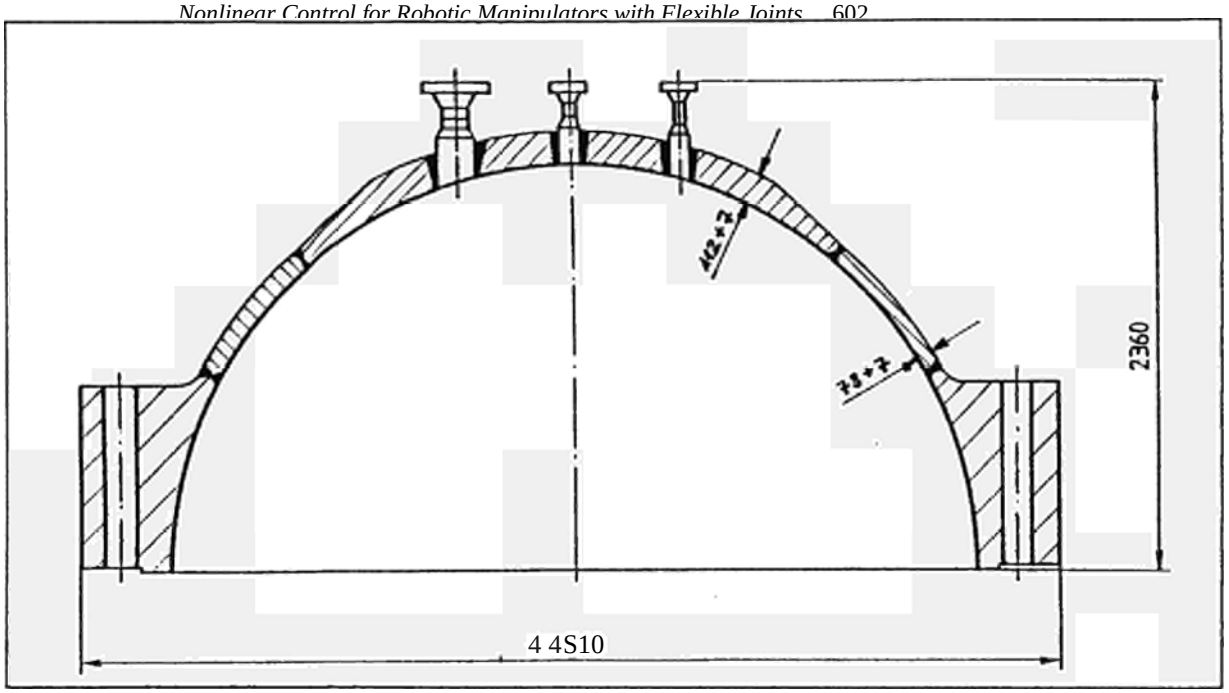


Figure 3: dimensions of the RPV-cover

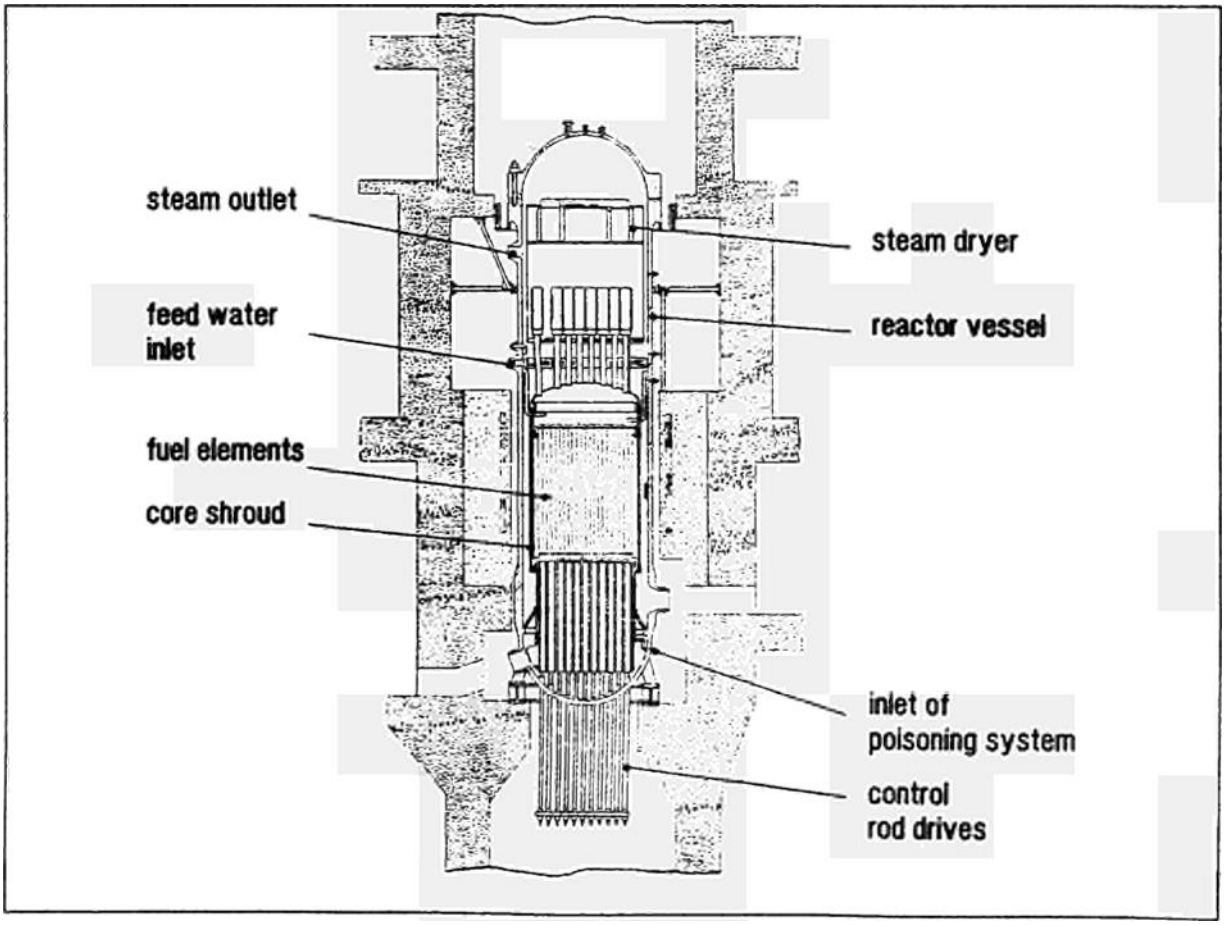


Figure 4: position of tbe steam dryer in the reactor pressure vwsel

13? -

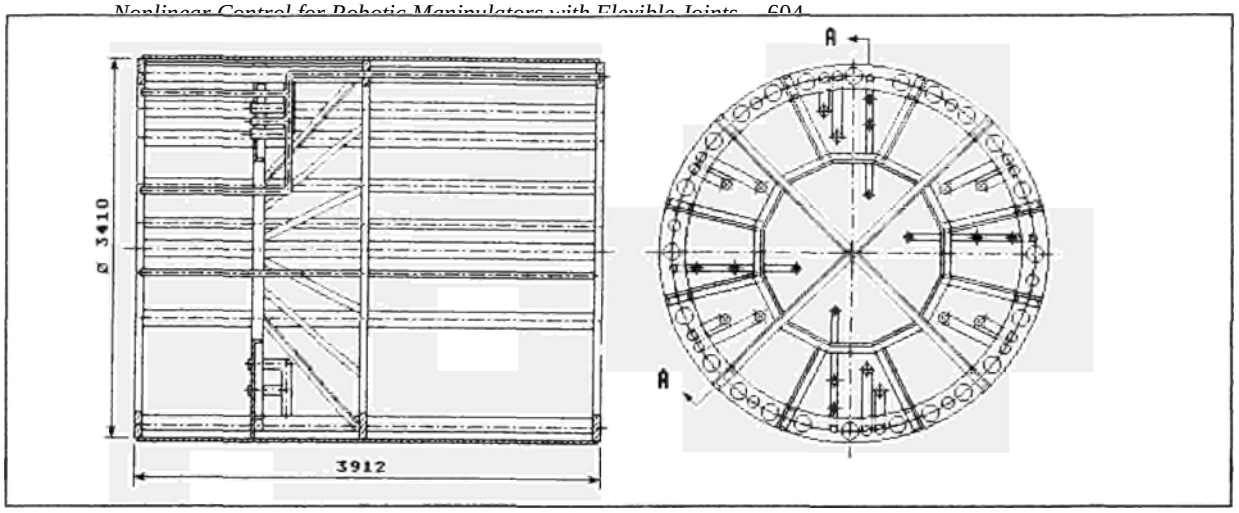


Figure 3: des i re of the steam dryer

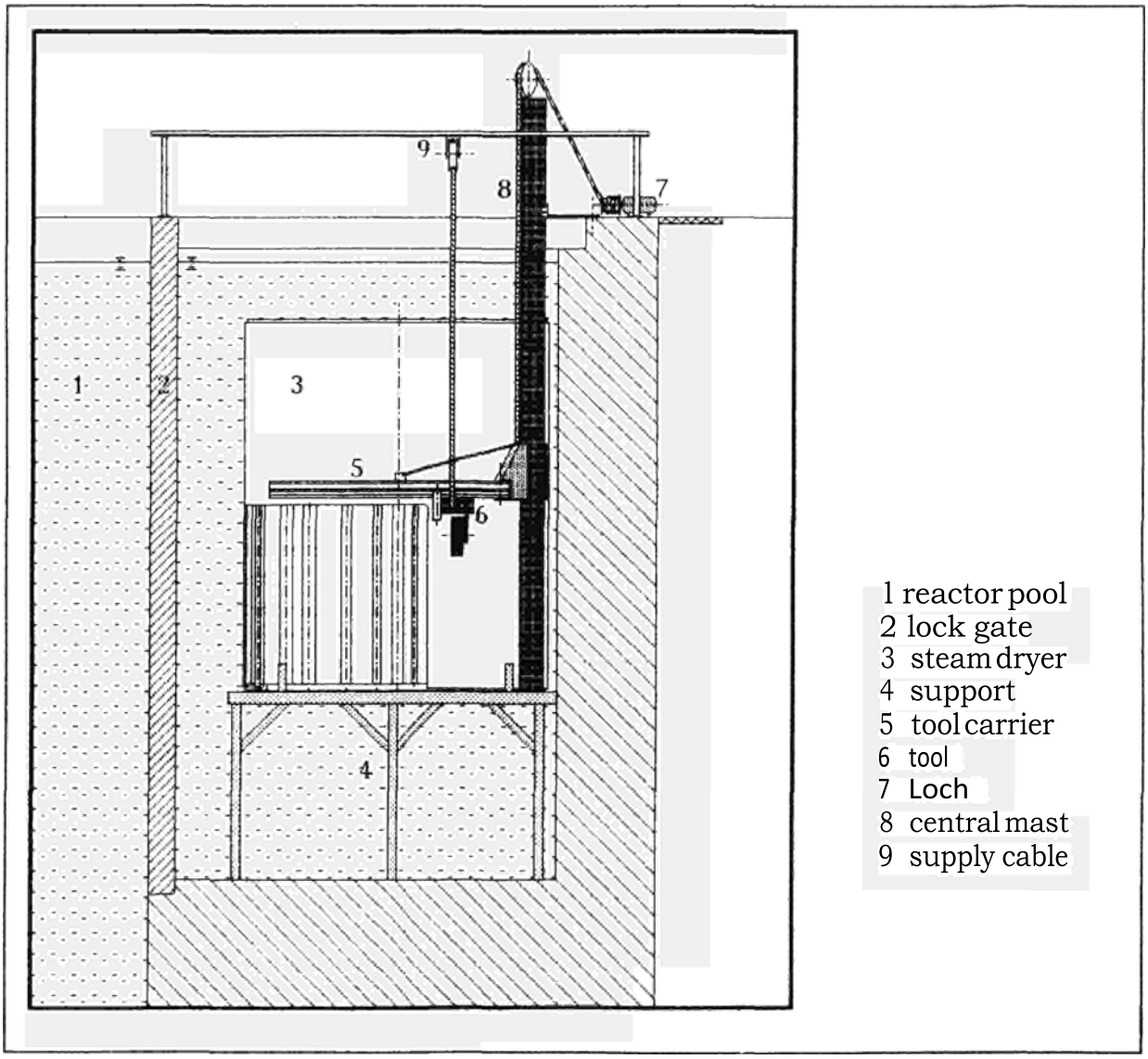


Figure 6: side view of the cutting system

7 DEO3MMISSIOHIHG OF THH RISQ HOT CHLL FACILITY

Contractors: **RNL**
Contract **FI2D-0011**
No.: Work Period: July 199fJ - December 1993 H CARLSEN, RNL
Coordinator: Phone: 45/423f712 12 **Fax: 45/423/511 73**

AOBMKXTM3ANDSODPE

The Rise Hot Cell Facility, which was in operation for 26 years (1964-199f1), comprises six concrete cells, lead cells, glove boxes, a shielded unit for temporary storage of waste **until** shipment, a frogman area, decontamination areas, workshops, various installations of importance for safe operation of the plant, offices, etc. The facility presented was used for physical and chemical **post-irradiation investigations** of various types of fuel pins (LWR, **HTGR), including Pu-** enriched pt

The general objective of the **decommissioning programme** for the Hot Cell facility is to **obtain** a safe **condition** for the whole **building** that does not **require** the special safety **provisions** which were necessary for operation of the hot cell plant. As a result, **the Hot Cell building will** be usable for the other purposes.

Work includes the removal of all **irradiated fuel items,** of other **radioactive items and** of contaminated equipment, and decontamination of all cells and rooms. The project is expected to produce specific data on manpower, waste **arisings and radiation exposures** for the decommissioning of a total hot cell line.

The contractual work will lead to the **identification** of an assessed procedure appropriate for the **decontamination** and the dismantling of equipment of a hot cell line used for post- **irradiation** tests on nuclear fuel **pins of different types.**

The contractor will execute the work programme in co-operation with BNFL plc, Sellafield (UK), which is decommissioning the B **205 Fuel Reprocessing** Pilot Plant, by using, to any **suitable** extent, common techniques, procedures and instrumentation.

The latest dose rate measurements determined aner a former partial decontamination of a concrete cell were in the order of magnitude of 1-2 mGy/h.

B.WOWKPROGRAMMM

B.1. Removal of fissile material in **the form of uranium oxidm and uraniumfplutonium mixed**

BE Oismantlinp, tramfer and ‹lemntamination of large cell internal including the power manipulator, the cell **crane and all experimental equipment.**

BE. Removal and demntamination of lareeeouinaient, including all lead-shiekkxlsteelixizmand **glove bozm, the .shieirte›ri_ storage facility, the ‹xinve er, the microscope cell.**

B.4. Decontaminanon of concrete celh by **various pnxxxluixa, with pnxxxling aml sutneqi** nt **radiation urements**

B.4.1. Initial mapping of radiation levels **in remote operation**

B.4.2. Goarse cleaning by vacuum **cleaning, conventional washing** and possibly by special techniques

B.4.3. Final cleaning with conventional methods

B.4.4. Hot spot removal by special techniques.

BE. Decontamination and radiology iiJ me urements of cell ventilators and ventilation ducts

B.6. Demntamination of ixxim **surfiuxa**

B.7. Removal **of active draim fremvariotn facilitim**

B.& Geoeratkin of smcific data on ‹x **ts, radioactive** job deem, working time and secondary

waste arise derived from the execution of iteim JIC to B.7.

- 134-

C. Progress of Work and Obtained Results

Summary of main issues

Most of the work performed has been of an initiating and conventional character, consisting mainly in removal of fissile and contaminated material.

Coarse cleaning of the lead shielded steel boxes and the glove boxes was initiated.

Some not contaminated equipment was removed from the facility, and areas not in use any more were allocated to other non-nuclear activities, where possible.

One experience has been gained. When planning to shut down on a nuclear site the only facility able to handle highly aclive material, it is most important to include all possible sources for such scrap material. Obviously, any voluminous scrap material must be delivered and processed in due time. We did not at the very starting point of our planning include all potential scrap material from the reactor site at Rise. An extra work effort on this task, however, resulted in acceptable remnants at the reactor site.

Progress and Results

1. Removal of fissile material (B.1.)

Packing of fissile fuel material in stainless steel containers h2S progressed well. Except for some acid solutions of fuel from burnup determinations, which will require chemical processing before being packed, all fuel has been packed, and most of it has been transferred to the Rise Waste Treatment facility for temporary storage.

2. Dismantling, transfer and decontamination of large cell internals (B.2.)

Packing of contaminated scrap material has progressed well. The material in the Hot Cell facility consists of various experimental and shop equipment, most of which is contaminated only at a lower level. Its form and surfaces is, however, of such a nature that decontamin2tion is impossible. Besides the material in the Hot Gell facility we have processed large amounts of rigs etc. from the DR3 re2ctor at Rise, all of which was of a similar nature. Depending on size and the degree of radiation the material is packed in different types of containers; common to these containers is that they provide only little — if any — shielding; only their volume differ. Before being packed the material is cut into pieces that fit the form of the container as well as the position among other pieces in the container; further, any smaller items are put into larger, hollow items where possible. In this way an optimal degree of packing in each container is obtained, and similarly a minimum storage volume is required. The amount of material from outside the Hot Gell facility was underestimated at the very first step of the planning. All the packed material has been or will be transferred to the Rise Waste Treatment facility for temporary storage.

3. Removal and decontamination of large equipment (B.3.)

Coarse cleaning of the lead shielded steel boxes and the glove boxes was initiated. A delay in manpower employment caused limited progress on this task. Our plan is to put together he2vily contaminated equipment from all of the glove boxes into one box and then consider this box as one heavily contaminated unit, which will be stored without further labour and dose commitments. The emptied boxes will be decontaminated.

4. Decontamination of concrete cells (B.4.)

Techniques for decontamination have been examined, in part by a study tour to the United Kingdom:

— High pressure water jetting equipment already purchased was tested in clean environ- ments.

– Sand blasting techniques was purchased and tested in clean environments.
– Foam cleaning technique was studied.

All the above mentioned techniques were technically found suitable for the foreseen jobs. BNFL at Sellafield was visited in order to survey any pos•'b1e cooperation on techniques, procedures and instrumentation as prescribed in the contract. F!o specific area ofco-operation
was identified at this occasion.

7.7. FINAL CUBAN-UP OF THE PIVER PROTOTYPE VITRIFICATION FACILITY: DECONTAMINATION OF THE HOT CBLL

Contractors: CEA-
Contract Valrho
No.: Work FI2D-0018
Period: July 1990 - June **1991**
Coordinator: A JOUAN, CEA-Vakhfi
Phonei **33/66 79 60 00**

Fax: 33/66 90 14 *35*

AOBEBGMVE SCOPE

The PIVER pilot vitrification facility at Marcoule was operated between 1969 and 1980, first using a batch process to vitrify Gas-Gooled Reactor fuel element reprocessing waste, and then to develop a continuous process to vitrify Fast Breeder Reactor (FBR) fuel reprocessing waste. A total of 12 t of glass was treated. It was then decided to remove the equipment and clean up the cell in order to install new equipment for continuous **vitrification** of waste generated by reprocessing FBR fuel (PIVER II).

PIVER is the first vitrification cell for fission product solutions to be decommissioned. Under a previous contract (FI1D-fD57), all process equipment items of the main cell were removed, followed by preliminary decontamination carried out in remote operation. So, the internal radiation level was reduced from several Gy/h to less than 10 mGy/h. The remaining radioactivity inventory is estimated at about 1.1.E 13 Bq (30) Ci). At this level, access to the cell is now possible for durations not exceeding about one minute; the cell remains highly contaminated and requires the use of ventilated protective clothing under severe working conditions.

The work to be carried out under this contract is aimed at continuing decontamination and dismantling work enabling further dismantling of in-cell equipment with hands-on techniques and finally to reach a radiation level allowing the installation of new equipment with standard working conditions for controlled zones. In particular, the generation of specific data on costs, working hours and job doses as well as on the amount of created secondary waste is considered as an important objective of this project.

The contractual work will result in assessed decontamination procedures for **highly** contaminated cells.

B. WORR PROGRAMME

B.1. Oismanfee e **anipulators in the PIVER cell including two MT 2tD master-slave** manipulators, a **robot manipulate (CAROLINE)** nod a **pantograph manipulator**

B.R Further decon » **‹nanon** of the **PIVFR** cell **with various decontaminanon technique** (chemicals wing liquids, foams and Els, electrojxilishing, and cryogenics), acmmpanied by **radiological measurements.**

B.2.1. First stage decontamination by short time in-cell work, aimed at strongly reducing the dose rates.

B.2.2. Second stage decontamination by long time in-cell operators'work

B.2.3. Final decontamination aimed **at obtaining standard working** conditions for controlled areas in the cell (dose rate < 0.1 mGy/h).

BE. Disman OOPOS not needed for the future use of the celh.

B.4. IdentiBcationofthe temab by photoprammetry for **fin:ilitating deaign worh** for the reuse of the celE

BE. Generation of specific data on ixnts, job **drum, working time azal secondary waste arisings, derived from the execution of items B.1. to B-3.**

- 137 -

C. PROGRESS OP WORK AND OBTAINED RESULTS Summary of Main Issues

The irradiation level in the cell at the end of 1989 was less than 10 zGy-h-*, and the cell has therefore been accessible to human operators since the beginning of 1990: first for only brief periods, then for up to one or two hours per operator beginning in Hay. This situation made it much easier to dismantle the remaining equipment and cut up the process lines.

Major accomplishments during 1990 included:

- dismant1ing of now unnecessary remote manipulators;
- installation of biological shielding on remaining irradiation sources;
- c1eaning up the recovery pan, drain channel and walls;
- identification and cutting of pipes.

These operations further reduced the in-cell irradiation level to less than 0.2 mGy-h-1 by the end of the year. The activity removed from the cell totaled 7.11 x $10^{1,}$ Bq (192 Ci), including 3.15 X 10^{12} Bq (85 Ci) of solid waste and 3.96 x $10^{1,}$ Bq (107 Ci) of liquid waste.

P o ess nd Results

1. Dismantling the telemanipulators (B.1)

Remote manipulation devices in the cell included:

- a heavy telemanipulator (Caroline),
- a pantograph handling device (Ancoine),
- two La Calhéne MT 200 master-slave manipulators.

The master-slave units were removed and the penetrations were sealed with lead plugs.

Caroline and An€olne were moved to utility room 712 where they were cut up and conditioned in ANDRA waste containers.

2. Decontaminatinp the cell (B.2.1 - B.2.2)

Several decontamination operations were completed in cell 74 using very high pressure (400 bar) and high pressure (150 bar) sprayers. At the beginning of the year, the recovery pan and drain channel were decontaminated from the cell entry door to reduce the in-cell irradiation level. Throughout the year, the cell walls were cleaned from scaffolding erected inside the cell, and the recovery pan and drain channel were cleaned at regular intervals.

3. Dismantling the pipes (B.3)

3.1 Installation of biological shielding

Despite the low irradiation level in the cell, several major irradiation sources remained: the filter casings (2 Gy-h-1), the hopper connecting the cell to room 075, the drain channels, the vessel pulse chambers, etc.

In order to prevent delays in decommissioning, biological shielding was provided around the irradiation sources: barited brick walls around the filter casing, lead wool and sand on the connecting hopper, and other shielding as necessary.

3.2 Identification and cutting of pipes

Some process equipment and pipes must be retained to allow continued operation of the fission product liquid storage unit in an adjacent cell beneath the PIVER cell. The pipes were first identified in 1989 using a 3D imaging system based on photos taken through the cell viewing ports were compared with cell layout drawings for precise equipment identification. Pipes provided for cutting were selected and discriminated from those that had to remain in place.

This preliminary identification was used in 1990 to mark all the process vessels and pipes that had to be retained, in order to avoid any errors during the cutup phase, and to label all equipment items that were to remain in the cell. All cut pipes were sealed with welded end-caps; the weld seams were inspected by dye-penetrant examination.

4. Irradiation sources

The drain channel contained a major irradiation source even after several high-pressure spray cleaning operations. The source was located in the drain outlet leading to a tank in cell 075; the measured irradiation level appeared to be due to diffusion of 7 radiation from inside the pipe. When the pipe was filled with water up to the shutoff valve and a lead plug was installed, the irradiation diminished, confirming this assumption.

Irradiation in the hopper appeared to be attributable to diffusion of 7 radiation inside the pipes, since the level remained stable after repeated decontamination.

The shielding set up at the beginning of 1990 may therefore be considered permanent.

5. Results obtained

At the beginning of 1990, the activity in cell 74 was estimated at 1.11×10^{1}, Bq (300 Ci).

5.1 Decontamination wastes

Cell cleaning operations conducted throughout the year resulted in the removal of 4×10^{2} Bq (108 Ci) and generated 22 m^2 of liquid waste that was transferred to the Liquid Waste Treatment Station at Marcoule.

5.2 Solid Waste Removal

Thirteen ANDRA waste packages (casings and shells) comprising 3.15×10^{12} Bq (85 Ci) were removed during 1990. They contained 27 drums of miscellaneous waste (tube scraps, vacuum cleaner wastes, cleaning swabs, etc.) and dismantled telemanipulator components.

At the end of the year, some wastes that were non irradiating and only slightly contaminated were transferred to the Radioactive Decontamination Section in double or triple vinyl wrapped packages without cement grout.

5.3 Occupational Doses

The collective doses sustained by the personnel are shown in Table I for each month of 1990.

It should be noted that the pipes were cut up during June and July: this operation required more personnel because of the difficult access and working conditions (ventilated protective clothing). Moreover, as the year went by, the work advanced farther into the cell where the strongest irradiation sources were found.

5.4 In-Cell Irradiation

A radiation sensor was installed in the cell in July 1990 to allow continuous monitoring of the in-cell irradiation level, which is displayed outside the cell. The measured irradiation diminished during the year, as indicated in Table II.

Outlook

The decontamination program will be completed in 1991. This will include accurate

measurements of the effectiveness of the decontamination techniques implemented.

- 139 -

Table I :

Occupational dose log for 1991

140

Month **(1990)**	Collec L:(ve Dose	
	ms v	**mRem**
January	4.25	**425**
February	5. 07	**507**
March	8.69	869
April	8.21	821
May	**10.07**	**1007**
June	28.7 5	2875
July	40.37	4037
August	18 . 41	1841
S epLembe r	16. 27	1627
October	11.17	1117
Novemb er	**10.58**	1058
De c emb er	**6.10**	610

Table I I :
Cell irradiation levels in 1991

Measurement Date	**Irradiation mGy-h"**
January 1990	< 10
September1990	< 0.6
December 1990	< 0.2

7 DESTRUCTION OF CONTAMINATED SODIUM OF THE PRIMARY CIRCUIT OF EXPERIMENTAL RAPSODIE REACTOR

Contractors:	CEA-
Contract No.:	Cadarache
Work Period:	FI2D-0022
Coordinator:	July 1990 - June 1993
	P ANTOINE, CEA-Cadarache
	Phone: 33/42 25 43 95 **Fax:** 33/42 25 48 68

AOEM3GNVE7UM]SCOPE

French regulations prohibit, for safety reasons, the disposal of sodium with other low-level radwaste in shallow land burial. The development of an industrial-scale procedure for the transformation of sodium into an acceptable product is thus a useful target generally for all LMFBRs.

The CEA has developed, at laboratory-scale, the so-called NOAH procedure transforming sodium by controlled addition of water into aqueous sodium hydroxide.

The objective of the present contract is to conceive and manufacture an industrial-scale facility (600 Kg/d), based on the NOAH process and its application to 13 t (out of a total of 37 t) of contaminated sodium (specific activity 4.1 KBq/g, mainly Cs-137) from the RAPSODIE pilot FBR. The facility will be conceived thus (mobile system, limited dimensions, easy adaptation), that it can be used on other FBR-sites.

The facility will be installed at the containment building of RAPSODIE (DESORA programme). Contractual work will be implemented in cooperation between two departments of the CEA-UDIN (Unite de Démantélement des Installations Nucléaires) and LEPE (Laboratoire d'Etudes, de Procédés et d'Expertises).

In particular, the generation of specific data on costs, working hours and job doses as well as on the amount of created secondary waste is considered as an important objective of this project.

B. WORK PROGRAMME

Goncepfional studies

Studies for the industrial application of NOAH (LEPE)

Studies for the installation of NOAH into the RAPSODIE containment building, including the needed auxiliary equipment (UDIN)

B.2. Manufacturing. installafion and tm of equipment

B.2.1. Manufacturing and installation of equipment (UDIN)

B.2.2. Commissioning, testing of equipment and operator training with non-radioactive sodium (UDIN)

BE. Main operafion for the transformafion of sodium (UDIN)

B.4. Gonditioninz and disposal of generated liquid waste

B.4.1. Investigations into possible ways for utilisation or treatment of waste including associated costs (LEPE)

B.4.2. Temporary storage of liquid waste (UDIN)

BE. Technical and economical balance on the feasibility for an industrial application of NOAH

B.5.1. Preliminary balance before main operation

B.5.2. Final balance after main operation, including generation of specific data on costs, radioactive job doses, working time and secondary waste arisings, derived from the execution of items B.3. and B.4.

- PROGRESS OF WORK AND OBTAINED RESULTS

Sunznar\- of ma i n issues

7'hree studi as have been started :

– for the industrialisation ofthe NOAH process in the nuclear f'ie1 d. '!'h*L* s st v l.akes into account Ihe r‹rsii1€s from the tesr i ng per i ocl , the new work i ng condi t.i ‹ans necess i t y and the ‹liFfi‹ulty of\OAH's impl tation in the RAPSODIE containment building. .I specific nt**dx' for the denhumidlfication of the gazeous i.an1‹ was ordered.

– fni' the installation of the machine in Eapnodie's confinement building. Technical data-nheets for sub-contractors pm- posaln nnd a draught of the safety report have been pre-

- for I*re.at* ment arid remova) of the I iquid waste Ic›r

Progress and results

B. 1. 1. Studies for the industrial application of I4OAH

és the NOAH proto€j • n next satisfact.ory f'or the I iE.SCvRA moral i on, so I.o meet the new operas ing requ i cements and for a e•t ter re4 iabi li I v arid safety a new machine was rlesigned — see dia—

The same general operating principles were considered to gain from past experience. Technological improvements integrating information from test-periods were applied. They took into account the amount of' contaminated sodium to treat new safety conditions related to the industrial application of the machine in a nuclear installation. These improvements are related' to the design and the building of the machine

gram 1.

.as›='l1 run il+ +m.ntenince and its tiir?inna1 operation.

'home r›t' t hem improx e Ihe instn11air on'n snfet j :

- setxar:iti›ti ‹il sodium/sc›citrim—fi,vdr-oxicio/‹ ‹›nt.ro1 w1 l.h a minimiim of' sc›rl1 um ne3 gh our ing sodium-h; droxide .
- maintr-nanrenfsodiumtemperaturetoaminimalvaluereqar- ding= I.he rJemand of emh st.ep I Iranster - st.oragr - dust i i«-- t i on l . ma1 ou lab ion and des ign pri net ples t'or I he srd ium l.rarisJx›rtii— r 5 run equi June•n† ident.ill to Ihe saii1e •q • r• ent. of' a man iea
- rim ‹Jesliumldifieation ‹›I †.he gaseous revel.e ightrh is lijc1rr›geri resuI i ing in a 3-step ptir'ill r'at.ion (I'igiire 2; :
  - de.asi‹:uInt ion ilt I.he int.erna1 rlouble f'i I I.er I.A)
  - oon‹)enso! i on i ri l.he fr-oz.en—not er—con‹tens•=r (Fi)
  - m st-rw.*lrscenrerum neparatinn in the twin-partition Fil- tri (('). £hese studies hn e been carried out 'ith the Fr*vnstomefi‹oiat* m*:

- 142 -

R.1.2. Studiesfortheintallation ofMOAHintotheRAPSODIEcontain-mentbuilding including theneededauxiliary'equipment

Novatome, in charge of the studies, wrote the technical specifications necessary for the design and development of the equipment and its installation by the contractors. A draught of the Safety Report has been issued.

The DESORA installation will be entirely set up in the Rapsodie

‹nntainmrnt huifding. It is mRinlv made nf

- Ihe ‹odinil ctest.rim t.ion ii.st.a1lat.1‹in O›\II, .s presr'nt.rd above in chapter B.1.1.
- the "upline-equipment" transporting sodium
- the "downline-equipment" receiving the liquid sodium hydroxide on one hand and transporting hydrogen from the reset i on tank on the rather henrl.
- linei1iary l'li ide oi rati! t.s
- ari e‹tiiy.ped prograrriraablr ront.rollet fc› r l ae inst.al 1at on.

F1gore ' nhoi s the i ns4a11 at, i on iii l.h i l x l stirig a:rri ! i ar j

B.4. Conditioning disposal of generated liquidwaste

II.4.1. 1 nv•es l i gat i on i nt.o nose i bL e wav s fr›r i .t .i i st.t.i ‹›n ‹ r t.realm rit. of waste including associated costs

Rr•fer lo '9gurr•4 ford:I.aids]presertati n ‹f' iuvest:Rat‹d possibilities.

Liquid soda will be recycled instead of being treated as a waste, this because of its low level of residual contamination (figure 4). But in case of a higher contamination, this choice is reversible. Several ways were investigated.

Apart from the case where sodium could be treated in a waste treatment installation the solutions are as follows (figure 5) :

- cesium is neutralized and indissolvable with PPFNI, with double-decantation through phase separation and dehydration of the waste treated with Lea Flash.
- same as above but then with phase separation through tangential filtration.
- cesium is neutralized then fixed on ban-copper columns and i a=.l e s s dehydratrxl w i t,h) sea Fl ash .

d ‹otal . ‹'sl inc)ndlrig reagent.s, inve'.t.nie•nt. an‹J i.aste is of about 5000 l'l• . 'l'he ce•u rum f i:‹at i on soma t. i on apjmarc•d to be l.he

The study was partly conducted by the Waste Disposal Department (Département de Stockage des Déchets) of CEA (DCC - DSD - CEA).
trios t f'easab1 e ‹ n‹•.

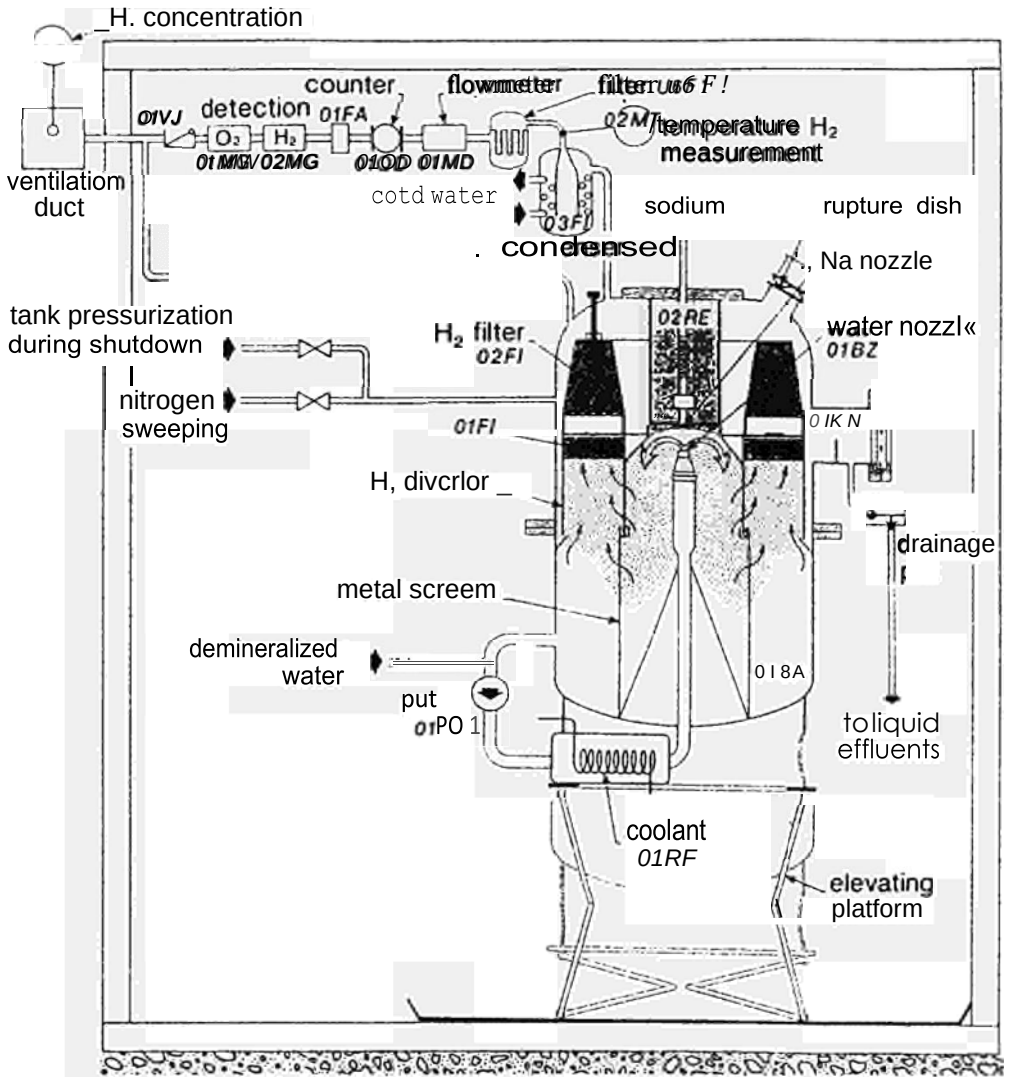


Figure 1 : NOAH sodium destruction facility
Reactor tank

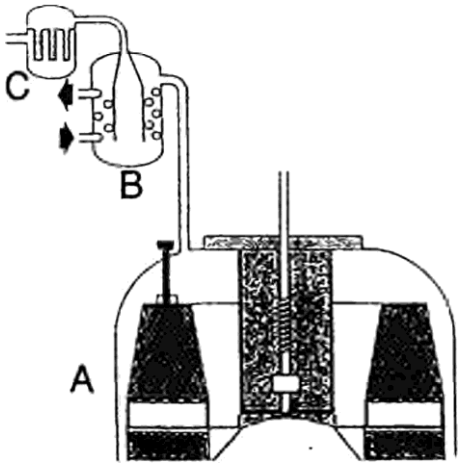


Figure 2 : Purification circuit of gaseous effluents

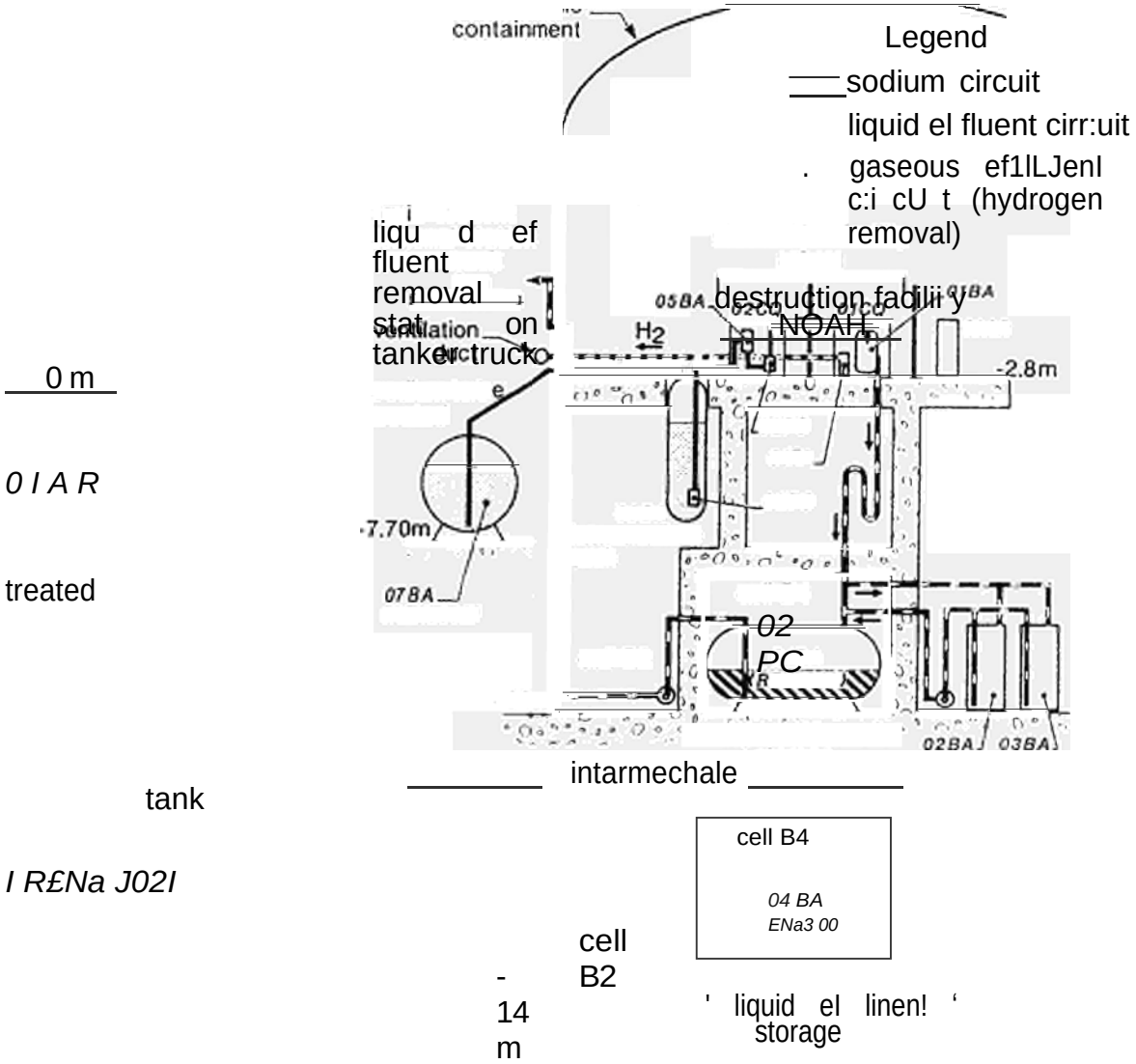
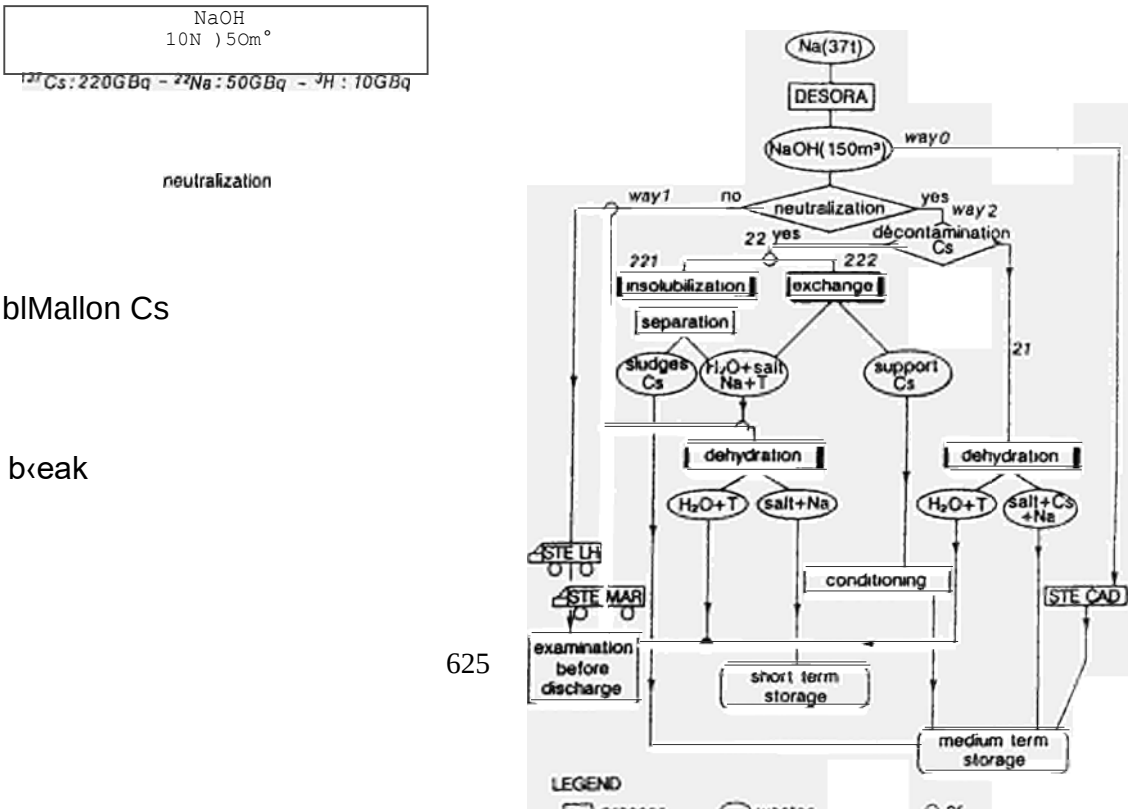


Figure 3 : Installation of DESORA in Rapsodie



SLUOCES
4 Ic 15m*

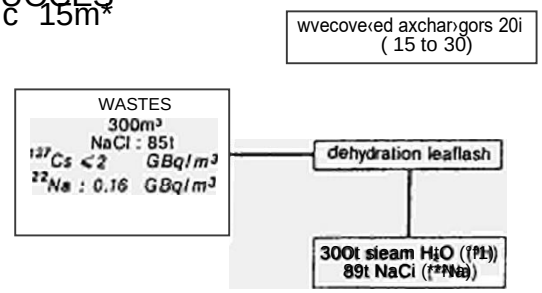


Figure 4 : Soda treatment

Figure 5 : Process selection

- 14 S

7.9. DECOMMISSIONING OF THE JEN-1 EXPERIMENTAL REACTOR

Contractors: CIEMAT, ENRESA, ENSA, LAINSA, UH-IW
Contract No.: FI2D-OJ23
Work Period: July 199(I - December **1993**
Coordinator: L SAS, CIEMAT

Phone: **34/1/346** 60 (D **Fax: 34/1/346 60** 05

AOBISCMVE SOOPE

JEN-1 is an experimental reactor of the swimming-pool type, moderated and c‹xi1ed by light water, with a power of 3 MWt. It was operated from 1958 till 1984 with a total generated energy of 2,7tXJ MWd. The radioactive inventory is estimated in the order of 3.5.E.11 Bq (9.5 Ci), the dose rates are estimated in the range of 20 to **150** mGy/h.

The main aim of this project is the study and development of decontamination, cutting and melting techniques on contaminated or neutron-activated aluminium components of JEN-1.

Underwater segmenting of **aluminium components** still represents some problems to be solved, which consist especially in the limited visibility of the cutting environment, due to an important amount of very small suspended articles (10a», compared to steel loo) and in the difficult filtration of these particles. An important aspect relevant to safety is the high H generation rate due to a rather long lasting reaction of molten aluminium particles with the surrounding water.

Industrial-scale melting of aluminium components still needs development work for appropriate foundry techniques, especially concerning crucible material and slag formation.

Results obtained in this contract will be useful in the future for the dismantling of numerous research reactors with aluminium components.

The project is expected to produce specific data on costs, working time, waste arisings and radiation exposures to operators for the dismantling of the JEN-1 reactor.

The work programme will be implemented in co-operation between following Spanish organisations: CIEMAT, ENRESA, ENSA and LAINSA, and with Institut fur Werkstoffkunde of Universitat Hannover (UH/IW), CIEMAT being the c‹xirdinator. A close co-operation on aluminium melting will be installed with Siemens AG KWU Group and Siempelkamp Gesserei Krefeld (SG).

B. WORKPROGRAMME

B.1. Radioiogic 1 characterisation of ‹ximpon and o(meliirig prix1ucts

B.1.1. Radiological characterisation of the grid and support **grid.**
B.1.2. Radiological characterisation of the control blade housings.
B.1.3. Radiological characterisation of the melting products.

BE Development. manuf ctuhng. tmnnr and subsequent imtallation in the JEN-1 reactor of an

B.2.1. Development and manufacturing of prototypes of plasma arc torch and consumable electrode torch (UH-IW)
B.2.2. Cutting tests with both t‹x›ls on representative aluminium sheets, **aiming** at defining optimal working parameters, cutting effluents and appropriate air and

water filters (UH- **IW, CIEMAT)**

B.2.3. Comparison of both tests with respect to cutting performance, generation and type of cutting effluents and tool handling abilities with subsequent selection of the most appropriate tool (CIEMAT + UH-IW)

B.2.4. Design and manufacturing of a cutting facility, including the selected cutting tool, handling and sensor systems and the cutting cell (UH-IW)

B.2.5. Testing at UH-IW and optimisation of the whole system in water depths of 5 m (UH-IW,
CIEMAT)

B.2.6. Training of the CIEMAT staff at UH-IW (UH-IW + CIEMAT)

B.2.7. Transport and assistance for the installation of the cutting facility in the JEN-1 reactor
(UH-IW)

BE. Underwater dismanour after pnxxxling dismounting ark (CIHMAT

B.3.1. Dismantling of the grid and grid support

B.3.2. Dismantling of the control blade housings

B.4. Decontamina0on of reactor internals (HNSA, LAINSA).

B.4.1. Selection of suitable procedures with respect to decontamination efficiency, amount and type of arising secondary wastes, reprocessing abilities and radiological impact

B.4.2. Decontamination of the grid and grid support

B.4.3. Decontamination of the control blade housings.

BE. Melting of aluminium waste (CIIIMAT, ENRESA)

B.5.l. Selection, manufacturing and adaptation of a melting furnace and implementation of cold melting tests.

B.5.2. Main melting programme, including generation of data on volume reduction and decontamination effects.

B.6. Assmsment of radia0on protection including both the personal and the ambient radiological impact (CIEMAT, UH-IW)

B.6.1. Assessment of radiological impact during dismantling operations (CIEMAT, UH-IW)

B.6.2. Assessment of radiological impact during decontamination operations (CIEMAT)

B.6.3. Assessment of radiological impact during melting operations (CIEMAT)

B.7. Genera0on of specific data on sts, radioactive job dosm, working time and secondary waste arisings, derived from the execu0on of items BE., B.4., BE. and B.6.

- 147 -

C. Progress of Stork and Obta i ned Resul is

The di smount ing act i v i t i es of the reac tor core have not been started , due to the de lay in the trans fer of fue l e lements out of the swi mm i ng pool of JEN-1 .

°or cutting operations, CIEMAT has received a ntasma arc cutting facitity, PAK4S, 80 KVA of pwer and a maximum of . Cutting operations with this unit have been started, mainly as training for the operators.

Design and development cutting activities are being performed by IN (Hannover University) about handling control of cutting operations, bassin cutting and exhaust air system for aerosols control.

Concerning melting, as a recycling material method, design of melting installation and building, where the furnace is to be placed, has been ach i eved .

Progre ss and resul is

1. Charac teri zati on of components (B . 1.)

Several analyses have been done on the same mater ials from wh i ch the reac tor core was made up , i n order to know the di f ferent i mpuri t i es of the— se al umi n i um al loys. On Table I are g1ven the results of Ches e analyses.

2. Development and manufacturing of prototypes of plasma arc torch and consumable electrode torch (B.2.l.)

In order to protect personal against dose exposure, IW has designed a torch with a plug-in consumable part (nozzle and electrode mounted to- gether) which can be exchanged all in one by a manipulator under water. A prototype of this torch has been already tested successfully at IN.

A sketch of the consumable electrode tool is shown in Fig. 1, which is composed of the torch body with a connection for the water hose, the mo tor and winding gear and wire strainghtening device.

3. Cutting tests (B.2.2.)

Cutting tests have been undertaken by IU on aluminium materials with the goal to obtain the optimal working parameters (speed and power cutting) using a mixture of argon and nitrogen as plasma gas and compressed air as secondary gas. In the same way cutting effluents and appropriate air and water filters are being studied. On the other hand, CIEMAT has started plasma arc cutting tests in a pool l md volune with a maximun water cutting depth of 1 m, as a training of people involved with plasma arc cutting operations.

4. Design and manufacturing of a cutting facility (B.2.4.)

IU is designing a handling control device for three axis to adapt body torches, which will be manufactured by CIEMAT, and a bassin cutting where the above device will be placed. Concerning control of cutting, IW is investigating into ultrasonic sensors for the determination of the d s I ance bet ueen ton L and uorkp ece as ue L L as the mate r a L t \ ckness .

5. Melting of aluminium waste (B.5.1.)

Design is being carried out about the settlement of the building where the melting furnace will be placed.

An ir.Auction melting furnace has been acquired which main characteris- tics are the following: Type: induction hea:ing; Nominal capacity: 50 Kg; Fower: 6S KVA; Frequency: 3000 Hz.

The aim of this activity is the melting of aluminium scrap coming from cutting operations in order to study distribution of activity among ingots and slag, as a recycling material method.

- 148 -

6. Assessment of radiation protection (B.6.)

Radiological measurements have been made on different components of the reactor core, in order to get the first dose rate estimations. These measurements have been carried out at different levels of:he JEN-1 reactor core,and the results are given on TableII.

Table I: Impurities Content of Aluminium (JEN-1 Reactor)

Elements (%)	Blade Control Housings (Al-99,5)	Grid and Support (Al-Mg)
Bi	0, 003	0 , 002
Cr	0, 0024	0 , 20
Cu	0, 0085	0 , 024
Fe	0, 38	0 ,34
Mn	0, 043	0 ,09
Ni	1 0, 002	0 ,003
Pb	0, 0051	0 ,005
Si	0, 12	0 ,36
Sn	0, 003	1 0 , 03
Ti	0, 0077	0 ,012
V	4 0, 002	0 ,003
Zn	0, 028	0 ,030
Mg		2, 5

Table II: Dose Rates at Reactor CoreJEN-1

Level	Dose Rate mSv/h
1.- Core grid	1 50
2.- Middle plane of the core	20
3.- Top of the blade housings	20
4.- Top of the thermal column	6
5. — Di f fuser of cool ant system	5

notorand

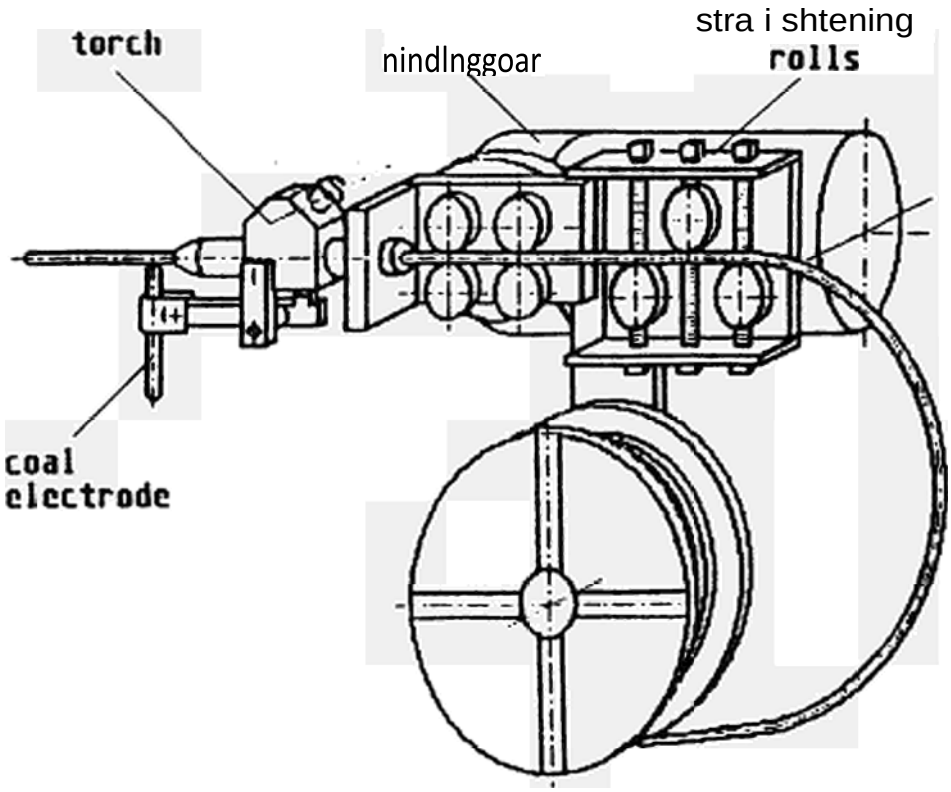


Fig. I - Sketch o£ the consumable electrode Loot

7.10. DEVELOPMENT OF SEGMENTING TOOLS AND RHMOTE HANDLING SYSTEMS AND APPLICATION TO THE DISMANTLING OF VAK BWR REACTOR PRESSURE VESSHL INTERNALS

Contractors: VAK GmbH
Contract No.: FI2D-0029
Work Period: July 1990 - December 1993
Coordinator: L PACHL, VAK
Phone: 49/61/882 081 Fax: 49/61/883 861

AORH3C7TM3ARDSODPE

The experimental Boiling Water Reactor Kahl (VAK-BWR) of 16 MWe has been shut down after 25 years of operation. Dismantling has been started for some time. The present estimation of the radioactive inventory of the reactor is in the order of 1.35.IN Ci.

The aim of the present contract is the development, qualification and practical application of different underwater (UW) segmenting and remote handling techniques on a series of internal components out of the reactor pressure vessel (RPV). Important targets are: minimisation of operators' dose uptake and of primary and secondary waste generation and economics of the procedure. Specific radioactivity of such components is in the order of magnitude of IN - IN Bq/g (activation) and of 10' - IN Bq/g (contamination). Due to its long-term operation, VAK dismantling can be considered to a large extent (dose rates, activation, contamination, material ageing) as representative for the future decommissioning of LWRs. In particular, the generation of specific data on costs, working hours and job doses as well as on the amount of created secondary waste is considered as an important objective of this project.

Work will be implemented in close co-operation with the pilot dismantling projects BR- 3/Mol (§ 7.3.) and KRB-A (§ 7.5.). The results of the comparative assessment study made by KRB (§ 7.2.) will be considered in the implementation of the contract.

B.WORKPROG

B.1. Concep on s **di d truction of a** e f fo UW **tmting of cutting t‹xil** and **devicm** for remote operation

BE Preliminary tmts on non-radioactivecomix›nents. including devicm for segmentation, remote operation technique, definifion of generated secondary wuste and studio of dismantling scenarios

BE. Qualification of dismantlin pnxxxlurm for an **application to radioactive components**

B.4. Oismantline of a serie **of RPV internals (upper grid plate, chimney above the core, control**

BE. Generation of specific data on ix **ts, radioactive job deem, working time** and secondary **waste arisings, derived from** the execution of item BE, BE. and B.4.

CPROGRESSOFWORK7UM]OWEADmD ULB

Summary of main issum

An additional evaluation of 7 firm offers for the decommissioning of VAK and KRB-A performed by NIS and NUKEM, resulted in a modified dismantling concept. Contrarily to the hardware configuration followed since, **main attention is given** now to such technologies, producing a minimum of aerosols. Reasons therefore are the matching of secondary waste and the consequent costs.

Thus plasma melt cutting for core internals was replaced by mechanical **cutting techniques.**

Though the means of a double arm EMSM (Electric Master 3lave Manipulator) in the dismantling concept is still taken into consideration, it will no longer serve for **handling** of **cutting** tech. The new tasks for it are: **handing** of the video system, place sucking nozzles, change tools etc.

RPV wall and rotation symmetric components shall be cut with a circumferential support for mechanical tooh.

For dismantling of core internals with complex geometries, special tools shall be used which allow their handling inside fuel elements and absorber shafts.

RPV as well as internals shall be cut to package size on site, the EMSM shall support this undertaking.

---

1. Gonceptional studies and construction of a **1:1** scale facility for UW testing of cuttin tel and devices for remote operation (B.1.)

For planning the test installation it is necessary to examine, which cutting technology (mechanical or thermal) in close connection with the cutting support technology (for instance electrical master-salve-manipulator, telescope mast, circumferential tool support etc.) and which handling technology for cut pieces, tools, **containers** etc. will probably be used.

The choice of the cutting- and handling technology was performed in two steps:

1.1. Performance of proposed concepts for **decommissioning** of VAK and KRB-A

The evaluation of 7 firm offers (2 for VAK and 5 for KRB-A) was performed without consideration of the specific differences between VAK and KRB-A such as plant dimensions, fuel pool availability for additional **dismantling,** and was performed without consideration of different specific features **like** level of automatization, use of an outer "sleeve" for **underwater dismantling** of the RPV-wall, use of simple, well-known tools etc.

An independent evaluation team analysed all received offers for completeness by means of an assessment matr

Following criteria are considered as principal: technology, safety and costs. In Table I, the considered subcriteria for each main criterium are presented. The evaluation of considered subcriteria was made with a **rating** scale of 1 = worst mark and 6 = best mark, and with a **weighing** scale for their **relative importance going** from 1 = low to 3 = high. In figure 1, the mean results of the numerical evaluation are presented for the 7 proposed dismantling concepts; proposals A and B are concerned **with the VAK-BWR dismantling** proposal C to G with the KRB-A dismantling. As can be stated, **the evaluation did not result in an outstanding** or peak rating. Among the various proposed concepts, common approaches could be found or agreement on significant features. Gommon features for an optimized approach are summarized in Table H.

1.2. Evaluation of supplementary criteria

In a second approach, we have evaluated supplementary criteria which were

insufficiently or not at all considered in the received offers, like local dose up-take **during handling, secondary** waste volume production, use of mechanical or thermal cutting tools, spreading of dust and aerosols into the containment, components of decommissioning equipment, especially air and water cleaning, crane communication, measurement of mass- **and activity inventory, needed man-** power and personal dose up-take, waste container logistics and detailed costs.

- 152 -

Based on the results of the additional evaluation performed by NIS and NUKEM we got a new optimized dismantling equipment (Table OI), which is characterized mainly by a predominance of mechanic segmenting tools.

The test installation to be installed shall demonstrate the appropriateness of this equipment, consisting of a circumferential tool support for various but mainly mechanical tools and including an EMSM dedicated to specific tasks including the handling technology for the cut internals and RPV wall pieces, filter technique, TV-technique, container logistics, tool exchange, radiation protection etc.

This test installation shall be used for the assessment of the appropriate interaction between
circumferential tool support or special tools and EMSM and will also be applied for training of the decommissioning team under cold conditions.

Tab. I: Considered main and sub-criteria for the evaluation

Main criteria	Sub-criteria
Technology	Completeness Reliability Maintainance and repair friendliness Universality Project relevance of preliminary tests Minimization of primary waste Minimization of secondary waste
SMeq	Minimization of man dose (msv) Design basis accident control Accident prevention
Costs	Hardware R&D and Personnel Dismantling time

153

Tab. **II: Optimized** dismantling equipment and tasks (1st step)

Equipment	Tasks
Circumferential tool support	- mechanical segmenting of rotation- symmetric - internals (thermal shield, core casing) - RPV-wall
EMSM	- support for the underwater plasma arc cutting of internals (core grids, chimney, rods and pipes), - positioning of TV-cameras, - construction of crane communication exchange of tools

Tab. **III:**

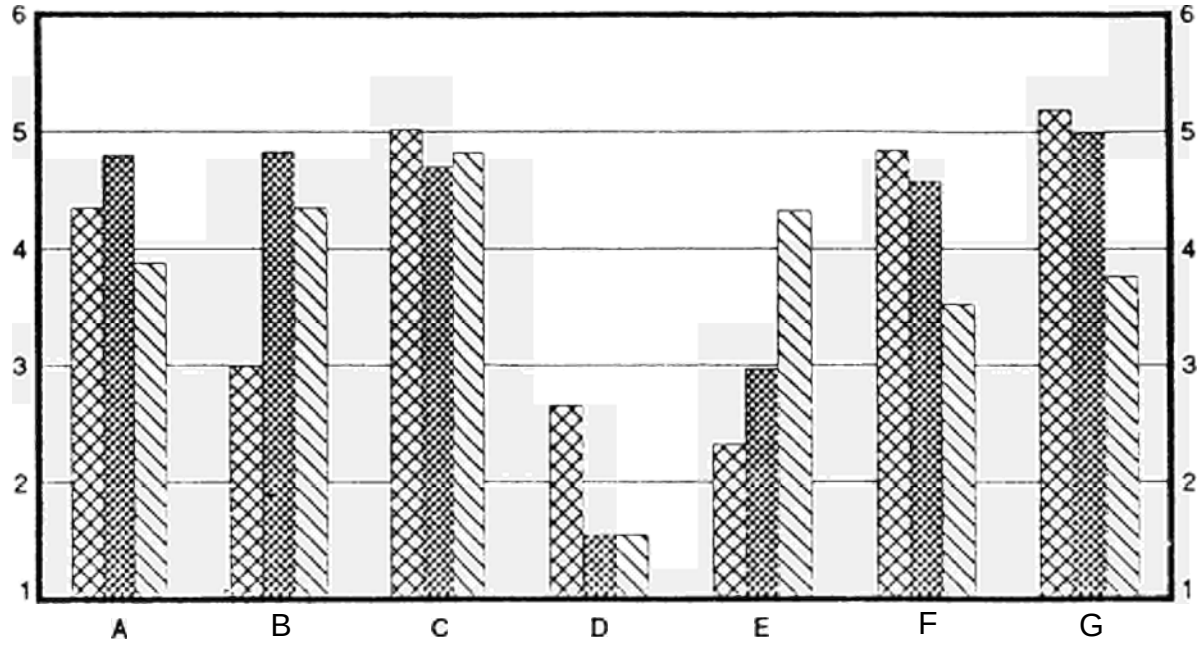
Optimized dismantling equipment and tasks (2nd step)

Equipment	**TwM**
Circumferential tool support	- mechanical segmenting of - rotation-symmetric internals (thermal shield, core casing) - RPV-wall
Special tool	mechanical segmenting of - internals (core plates, chimney, rods,

EMSM	positioning of - special t‹x›ls, - TV-cameras, - aerosol captation devices - construction of crane communication, - exchange of t‹x›ls, support container handling

154

E valuation mark



firm offer

V1 \t echnology aspec tJ V2 (s afety' asj:ect V3 Eco st aspect

Fig. 1! Mean re sults of evaluation

- 155 -

7.11. MELTING OF FERRITIC STEEL ARISING FROM THE DISMANTLING OF THE 3 G2/G REACTORS AT MARCOULE IN A FURNACE INSTALLED AT THH DISMANTLING SITE

Contractors: CEA-Valrho
Contract No.: FI2D-Ihl34
Work Period: September **1990** - December **1991**
Coordinator: I L DECITRE, CEA-Valrhfi

Phone: 33/66 79 63 03 **Fax: 33/66 79 64 32**

AOHM3€9TM3ANDSOOPE

In two foregoing EC R&D **decommissioning programmes,** a series of research contracts had been devoted to melting of metallic radwaste, **mainly** steel, **going from** laboratory scale to applications in adapted **foundries, treating** waste transported from the **dismantling** site to the melting facility.

The objective of the present contract is to conceive, manufacture and install a 15 t electric arc heated melting furnace on the dismantling site of **the G2/G3 graphite/gas** reactors at Marcoule, and to condition by melting 7(D t (out of a total of 4,030 t) of ferritic steel having a specific **contamination in** the order of 20 - 40 Bq/cm'.

The **innovation lies mainly in** the on-site installation of the furnace, **avoiding packaging** and transportation on public roads and in the large dimensions of the furnace (2 **m), enabling** feeding of pieces up to 1.7 m and reducing segmenting work. This should lead to economics by reducing the number of operations and by an optimised management of waste streams, enabling to a large extent unlimited recycling of steel.

In particular, the generation of specific data on costs, working hours and job doses as well as on the amount of created secondary waste is considered as an important objective of this project.

B.MOWKPROGRAMMP

B.1. GoncepBonal studies and cate risation of waste

B.1.1. **5tudies** for the installation of the melting furnace in the reactor building.

B.1.2. Investigation into the management of waste streams before and after melting.

BE **Manufacturing. installation and tmting** of equipment

B.2.1. Manufacturing and installation of equipment including auxiliary and control systems.

B.2.2. Commissioning testing of the melting facility.

BE. Main operation for the melting of 7fD t of dismantled steel

B.4. Generation of specific data on ccists, **radioactive job doses, working** time and secondary **waste arising, derived from the execuHon of items B.1.,** BE and BE.

- 156 -

C. PROGRESS OF WORK AND OBTAINED RESULTS

Process and installation studies for the melting facility havc been completed (B.1.1.).

Studies related to the deEnition and management of waste, before and after melting are nearly completed (up to 80 to). Studies of steel quantification methods before and after melting are almost totally done (up to 70 to). Preparatory works for the auxiliary equipment are finished. Civil works have been started (external buildings and structure strengthening for the melting facility).

Large equipment (furnace, power transformer, ingot-maker and travelling crane) is being developed with the manufacturers. It is expected that the furnace will be delivered to the site on May 1st, 1991. Apart from a slight delay at the start-up of the manufacturing and procurement of equipment, work is now on schedule.

Dismantling work of the pipes is completed, followed by the construction supplies for the melting facility representing several weeks of operation.

Fine quantification measurements of waste are satisfactory and show that 90 to of the steel to be melted has an activity of less than 1 Bq/g.

- 157 -

7. IN MHLTINGOFALPHA-CONTAMINATHDSTHHLSCRAPATINDUSTRIALSCALH

Contractors: Siemens-KWU,
Contract No.: SG FI2D-0038
Work Period: October 199t) - December **1993**
Coordinator: K H G ENER, Siemens-KWU
Phone: 49/69/807 **36 45 Fax: 49/69/807 20 66**

AOBM3€XFM3ANDSCDPE

The underlying large-scale investigation into melting of alpha-contaminated steel from nuclear facilities aims at demonstrating the feasibility of the unrestricted reuse of such radwaste within legal limits.

The work programme will be based on the results and experience obtained on melting of radwaste in former research contracts within the second EC programme on Decommissioning (1984-88), especially contract FI1D-0044 with Siemens AG and **contract FI1D-(016 with** Siempelkamp Giesserei GmbH.

Starting with laboratory-scale melts aimed at identifying the most suitable crucible material and slag former will be followed by large-scale melts with subsequent detailed analysis of the prevailing alpha-distribution in and between steel, slag and filter dust.

Based on the foregoing results, large-scale melts with about 1(O t of uranium and Pu- contaminated material from Siemens fuel fabrication will be carried out and finally, by two large- scale melts of Pu- and Th-contaminated steel waste (5 t), will be assessed how these alpha- emitters will behave.

It is anticipated that extensive testing and radiological measurements will enable the assessment that alpha-contaminated steel can be conditioned by melting for safe unrestricted reuse and that the melting plant can be operated safely also with respect to radiation protection of workers and the environment of the foundry, with special consideration of the arising slag and filter dust. In particular, the generation of specific data on costs, working hours and job doses as well as on the amount of created secondary waste is considered as an important objective of this project.

The specific contamination of the treated radwaste is estimated to be in the range of < 2(D Bq/g (alpha/beta) and the anticipated fission product inventory for large-scale melting is estimated at about 2fD g of **U-235** and 1 g of Pu. Expected dose rates in the controlled melting area are in the order of magnitude of < 0.1 mGy/h.

Work will be executed in close co-operation between Siemens AG, KWU Erlangen (Siemens) acting as coordinator and Siempelkamp Giesserei (SG).

B.WORKPROGRAMME

B.1. B.7.
B.8.
BI B.9.

B3.

B.4.

Bb.

B.6.

Identification of appropriate material for crucible and slag formers and procurement of U, Th and Pu containing rad waste samples (SG) Installation of an induct

ion-heated latmrato furnace and execution of referees:e tmts with non-radioactive materials (Siemem)

Laboratory-scale melting tmts with U, Th and fin-contaminated **steel (selection of material**
for crumble lining and **slag formers) (Siemens)**

Procurement of U aad Pu-contaminated material (Siemem) and Th-contaminated material

Pilot melting tmts aimed at determining the U (alpha)-content in ingot, slag and filter system (so, so)

Main melting programme of alxiut ltD t of U and Pu-contaminated radwaste with subsequent alpha-content determination in each t, slag and filter dust (SG)

munn or ia«•=•aa meia «ia ni a»d u•-«•nta›ninat‹xl steei (sn)

Determination of the **alpha-distribution** in the crucible material (Siemem)

Generation of smx:ific data on cents, radioactive job deem, working time and secondary **waste arisings, derived from** the execution of items BE and B.G.

- 158 -

C. PROGRESS OF WORK AND OBTAINED RESULTS

No significant work was completed in this just starting contract.

7.13. DEMONSTRATION OF EXPLOSIVE DISMANTLING TECHNIOUES OF THE BIOLOGICAL SHIELD OFTHE NIEDERAICHBACH NUCLEAR POWER PLANT" (KKN)

Contractors	BE, Noell, Siemens-KWU
: Contract	**FI2D-0346**
No.: Work Period:	November 1990 - **October 1993**
Coordinator:	U FREUND, BE **Phone: 49/69/79 08 23 46 Fax: 49/69/790 880**

AOBEBGMVEvUW]SODPE

This project aims at demonstrating explosive dismantling techniques on the biological shield of the nuclear power plant Niederaichbach (KKN), which was operated from 1972 to 1974 and is foreseen to be completely removed. The radioactive inventory of the shield is estimated in the order of 3.7.10' Bq (0.1 Ci). The level of **activation is estimated to be** in the order of 10 Bq/g, and the associated dose rates in the order of **10 pSv/h. Within this contract, blast peeling** of the activated concrete from a 30 sector of the biological shield will be performed.

This technique will be applied as one of **two main techniques (hydraulic hammer besides** blast peeling) for the dismantling of the whole biological shield of KKN; for this, the licensing authorities have already given their agreement. This demonstration project will be conducted according to the guidelines of the ongoing total dismantling of KKN.

In particular, the generation of specific data on **costs, working hours and** job doses as well as on the amount of created secondary waste is considered as an important objective of this project. This will facilitate the application of this technology and acceptance from the safety point of view in future large-scale decommissioning operations.

The project is a follow-up of small-scale work **on inactive samples performed jointly under contracts FI1D-0011** and FI1D-0012.

The work programme will be **implemented jointly by three main contractors: Battelle** Europe e.V./Frankfurt (BE), acting as coordinator, Noell/Wurzburg (Noell) and Siemens/KWU (Siemens), as well as Stangenberg, Schnellenbach & Partner (SSP) as sub-contractor.

Further cooperation is **foreseen with TUV Bayern for the assessment of air filter systems.**

B.WOR]CPROCIUUdME

B.1. Preparatory pdcadi rk for on-site equipment and regulatory requirements a (BE, Noell)

B.1.1. Layout of blasting patterns and of **bore holes charging, according to the area** of application (BE)

B.1.2. **Design** of blasting schemes according to the area of application (BE)

B.1.3. Definition of blasting area • **Oce::t°•r. :_•r.tr** ter t!•.e **r_•ier"==.** =f *•••t, •= l»di=g »••w»ted **filter systems (Noell, BE)**

B.1 Demonstration blasting on the KKN shield by manual handling (BE, Noell)

B.2.1. Site preparation for the installation of tools and measuring devices (BE, Noell)

B.2.2. Assessment and **implementation of auxiliary techniques** such as bore hole drilling, cutting of **the reinforcement by hydraulic shears,** use of a hydraulic ram (Noell)

B.2.3. Main operation and concrete removal, consisting of a sequence of about 10 individual blasts, including pre- and post-blast working (BE, Noell)

B.2.4. Assessment of blasting performance, **with respect to predetermined criteria such** as concrete **removal rate, safety aspects, integrated doses and generation** of secondary waste (BE, Noell)

BE. Assmsment of dust retention bv industrial filter system with rmpect to efficiency and safety of handling (Noell, BE)

B.4. Assmsinent of **structural** safeN (BE, Noell)

- 160 -

B.4.1. Modelling of shield response to the blast transient loading (BE)

B.4.2. Modelling of building response by simple models and comparison to pre-evaluations at selected safety-relevant locations (BE)

B.4.3. Safety control for compliance with limiting values by test accompanying measuremcnts (BE, Noell)

B.S. Final assmsment of the blasting procedure (BH, Nell)

B.S.1. Technical feasibility and reliability (BE, Noell)

B.5.2. Compliance with safety regulations concerning radiation protection, radioactivity release, contamination/decontamination and structural safety (BE, Noell)

B.5.3. Comparison with other concrete dismantling techniques, such as sawing by diamond or wire saw, core drilling, possibly combined with sawing, high pressure water jet with abrasives (Noell, BE)

B.5.4. Setting up of guidelines and rules for general application of the bore hole blasting technique to other shield structure, and of cost estimates (BE, Noell)

B.6. Related investi atio of ener 1 appi bi to various typm of nuclear power plants (BH, Siemens-KWU, SSP).

B.6.1. Building response by advanced modelling for the reactor building (BE, SSP)

B.6.2. Local damage, prediction of cracks and material failure (BE, Siemens)

B.6.3. Blast loading limits with regard to the integrity of light structures in close vicinity to the charge location (BE)

B.7. Generation of specific data on costs, radioactive job dosm, working time and secondary waste arisings, derived from the execution of items B.k and B.6.

C. PROGRESS OF WORK AND OBTAINED RESULTS

No significant work was completed in this just starting contract.

ANNHX I

LIST OF PUBLICATIONS RELATING TO THE RESULTS OF THE **1979-83** PROGRAMME ON THE DECOMMISSIONING OF NUCLEAR INSTALLATIONS

A. Annual Progress Reports

"The Community's Research and Development Programme on Decommissioning of Nuclear Power Plants - First Annual Progress Report (year 1980)", EUR **7440,** 1981.

"The Community's Research and Development Programme on Decommissioning of Nuclear Power Plants - Second Annual Progress Report (year 1981)", **EUR 83d3, 1983.**

"The Community's Research and Development Programme on Decommissioning of Nuclear Power Plants - Third Annual Progress Report (year 1982)", EUR **8Ri3,** 1984.

"The Community's Research and Development Programme on Decommissioning of Nuclear Power Plants - Fourth Annual Progress Report (year 1983)", HUR 9677, 1985.

B. 1989 European Conference

Schaller, K.H., Huber, B. (ed). Decommissioning of nuclear power plants. Proceedings of a European Conference held in Luxembourg, 22-24 May 1984. Graham & Trotman Ltd, London. EUR 8655.

c. Final Contract Reports

Boothby, R M, William, T M **(1983).** The control of cobalt content in reactor grade steels. European Appl. Res. Rept., **Nucl. Sci.** Technol., Vol. 5, No 2, Harwood Academic Publishers. EUR *8 SS.*

Ltircher, G, Pie1, W (1983). Dekontamination von Komponenten stillgelegter Kemkraftwerke fur die freie Beseitigung. EUR 8704.

Kloj, G, Tittel, G (1984). Thermische und mechanische Trennverfahren fiir Beton und Stahl. **EURM83.**

Harbecke, W, et al. (1984). Die Aktivierung des biologischen Schilds inn stillgelegten Kernkraftwerk Lingen. EUR **&I01.**

Verral, S, Fitzpatrick, I (1985). Design concepts to minimise the activation of the biological shield of light-water reactors. **EUR &Ri4.**

Eickelpasch, W, et al. (1984). Die Aktivierung des biologischen Schilds inn stillgelegten Kernkraftwerk Gundremmingen Block A EDR 8950.

Verry, P, Lecoffre, Y (1984). Décontamination de surfaces par erosion de cavitation. EUR

- 162 -

Allibert, M, Delabbaye, F (1984). Extraction du cobalt des aciers inoxydables. EUR **8966.**

Ebeling, W, et al. (1984). Dekontamination von Betonoberflachen durch Flammstrahlen.
EUR 8iXi9.

Boulitrop, D, Rouet, D (1984). Etude de la décontamination au moyen de supports gélifiés.
EUR 910Z

Peselli, M (1984). Individuazione quantitativa delle impurezze del contenitore a pressione del reattore del Garigliano. EUR **9167.**

Avanzini, P G, et al. (1984). Valutazione delle caratteristiche di progetto che facilitano lo smantellamento delle centrali nucleari PWR. **EUR 9191.**

Regan, J D, et a1. (1984). Design features facilitating the decommissioning of Advanced Gas- Cooled Reactors. EUR **9207.**

May, S, Piccot, D (1984). Determination analytique d'é1éments traces dans des échantillons de bétons utilises dans les réacteurs nucléaires de la Communauté européenne. EUR 920&

White, I F, et al. (1984). Assessment of management modes for graphite from reactor decommissioning. EUR **923a**

Goddard, A J H, et al. (1984). Trace element assessment of low-alloy and stainless steels with reference to gamma activity. EUR **9264.**

Bregani, F, et al. (1984). Chemical decontamination for decommissioning purposes. EUR

Larcombe, M H E, Halsall, D R (1984). Robotics in nuclear engineering. Graham & Trotman Ltd., London. EUR **9312.**

Glock, H -J, et al. (1984). Dokumentationssystem fur den Abbau von Kernkraftwerken.

Ahlfanger, W (1984). Zusammensetzung von Kontaminationsschichten und Wirksamkeit der Dekontamination. EUR *93SL*

Brambilla, G, et al. (1984). Vernici per la fissazione della contaminazione superficiale dei materiali. EUR *93S&*

Paton, A A, et al. (1984). Civil engineering design for decommissioning of nuclear installations. Graham & Trotman Ltd, London. EUR **9399.**

Bittner, A, et al. (1985). Konzepte zur Minimierung der Aktivierung des biologischen Schilds. EUR 944R

Brambilla, G, Beaulardi, L (1985). Rivestimenti rimovibili per la protezione di superfici in calcestruzzo dalla contaminazione. **EUR 9463.**

Arndt, K -D, et al. (1984). Thermisches Trennen von plattierten Komponenten des Primarkreises von Kernkraftwerken. EUR 9479.

Rawlings, G W (1985). Development of large diamond-tipped saws and their application to
cutting large radioactive reinforced concrete structures. EUR 9499.

Barody, I I, et al. (1985). Treatment of active concrete waste arising from dismantling of nuclear facilities. EUR 956&

Bernard, A, Gerland, H **(1985).** Recherche et caractérisation de revétements pour la protection des structures en **béton. EUR 9595.**

De Tassigny, C (1985). Misc au point et essais d'une méthode pour le revétement de déchets métalliques contaminés, par des résines thermodurcissables. HUR I i6

Migliorati, B, et al. (1985). Smantellamento di componenti metallici e di strutture in calcestruzzo mediante raggio laser. HUR **9715.**

Fleischer, C C (1985). A study of explosive demolition techniques for heavy reinforced and prestressed concrete structures. EUR IXI6R

Wieling, N, Hofmann, P I (1985). Erosionskorrosionsversuche mit kobaltfreien Werkstoffen.

Antoine, P, et al. (1985). Intégrité ii long terme des b3timents et des systémes. HUR **992a**

Lewis, G NH (1985). Degradation of building materials over a lifespan of 30-1(D years. EUR 1IXt I

Hasselhoff, H, Seidler, M (1985). Anlage zum Einschmelzen von radioaktiven metallischen Abfallen aus der Stillegung. EDR **1OJ21.**

Chavand, J, et al. (1985). Découpage de composants métalliques par fissuration intergranulaire. **EUR 1Oi37.**

Gauchon, J P, et al. (1986). Décontamination par des méthodes chimiques, électrochimiques et au jet d'eau. EUR **1tD43.**

Smith, G M, et al. (1985). Methodology for evaluating radiological consequences of the management of very low-level solid waste arising from decommissioning of nuclear power plants. EUR **1OJ5&**

Gomer, C R, Lambley, J T (1985). Melting of contaminated steel scrap arising in the dismantling of nuclear power plants. HUR **101ilil**

Da Gosta, L, et al. (1985). Systems for remotely-controlled decommissioning operations. Graham & Trotman Ltd, London. **EUR 10197.**

Price, M S T, Lafontaine, I **(1985).** System of large transport containers for waste from dismantling light water and gas-cooled nuclear reactors. **EUR 1023a**

Bargagliotti, A, et al. **(1986).** Plasma arc and thermal lance techniques for cutting concrete and steel. HUR **1O8i**

Lasch, M (1986). Entwicklung von wirtschaftlichen Dekontaminationsverfahren. EUR **10519.**

Hulot, M, et al. (1986). State-of-the-art review on technology for measuring and controlling very low-level radioactivity in relation to the decommissioning of nuclear power plants. EUR **1Oi43.**

- 164 -

LIST OF PUBLICATIONS RELATING TO THE RESULTS OF THE **19 84-88** PROGRAMME ON THE DECOMMISSIONING OF NUCLEAR INSTALLATIONS

A. Annual Progress Reports

"The Community's Research and Development Programme on Decommissioning of Nuclear Installations - First Annual Progress Report (year 1985)", EUR 10740, 1986.

"The Community's Research and Development Programme on Decommissioning of Nuclear Installations - Second Annual Progress Report (year 1986)", EUR 11112, 1987.

"The Community's Research and Development Programme on Decommissioning of Nuclear Installations - Third Annual Progress Report (year 1987)", EUR 11715, 1987.

B. 1989 European Conference

Pflugrad, K., et al (ed). Decommissioning of nuclear installations. Proceedings of an international conference held in Brussels, 24-27 October 1989, Elsevier, London, UKEUR 12690.

C. Final Contract Reports

Janberg, K. (1987). Economic comparison of management modes for contaminated metal scrap. EUR 11149.

Allibert, M. et al. (1987). Separation par transport en phase vapeur des constituants d'aciers inoxydables. EUR 11296.

Ahlfanger, W. (1988). Vollstandige Dekontamination einer Primardampfleitung des Kernkraftwerks Lingen. EUR 11435.

Ebeling, W. et al. (1989). Untersuchung und Optimierung von Filtersystemen zur Abscheidung von Stauben und Aerosolen bet der Dekontamination von Betonoberflachen. EUR 11995.

Gray, P W C (1989). The assessment of low-level contamination from gamma-emitting radionuclides. **EUR 12183.**

Hills, D L (1989). The removal of concrete layers from biological shields by microwaves. **EUR 12185.**

Lewis, C J A, Vibert, C J T (1989). Adaptation of a robot and tools for dismantling of a gas- cooled reactor. **EUR 12186.**

- 165 -

Hermanns, B (1989). Entwicklung von Mess-Systemen fur Kontaminationsmessungen an raumlich schwer zuganglichen Stellen. HUR **1223a**

Bishop, A (1989). Ventilation and filtration techniques for handling aerosols produced by thermal cutting operations. EUR **12321.**

Steringer, A, Moser, T (1989). Auswahl und Entwicklung eines leicht zu verarbeitenden Elektrolyten fur die Dekontamination durch Elektropolieren. HUR **12383.**

Morillon, C, Pilot, G (1989). Décontamination du béton par fusion superficielle a l'aide d'un nouveau briileur associé a un plasma (étude de faisabilité). HUR 12489.

Rouviére, R, et al. (1989). Adaptation des jets d'eau haute pression avec **abrasif** au démantélement des installations nucléaires. **HUR 124R**

Dawson, P, et al. (1989). Pre-stressed concrete reactor vessel with built-in planes of weakness. EUR 1251&

Alary, C, et al. (1990). Inventaire des composants activés d'un réacteur a neutrons rapides de puissance. EUR **12539.**

Bakiewicz, J L, Reymer, A P S (1990). Separation of contaminated concrete. HUR **1256k**

Jaouen, C (1990). Etude de conteneurs fibro-ciment de grandes dimensions pour déchets solides de démantélement. HUR **12563.**

Gasc, B (1990). Extension ii la téléopération d'un atelier modulaire étanche pour le démantélement de composants radioactifs. **EUR 12fDt.**

Harvey, D S (1990). Research into the melting/refining of contaminated steel scrap arising in the dismantling of nuclear **installations. EUR 126ti5.**

Haferkamp, H, et al. (1990). Weiterentwicklung des Abrasivstrahl-Schneidverfahrens zum Trennen ferritischer und austenitischer Stahle unter Wasser. HUR 12684.

Davis, J P, et al. (1990). Methodology for assessing suitable systems for management of reactor decommissioning wastes. **EUR 12701.**

Pocock, D C, et al. (1990). Long-term performance of structures comprising nuclear power plants. **EUR 1275&**

Deipenau, H, Seidler, M (19RJ). Cast-iron containers out of low radioactive steel. EUR

Costes, J R, et al. (19R)). Gonditionnement pour le stockage définitif des briques de graphite radioactif provenant du déclassement des réacteurs. **EDR 12815.**

Drews, P, Fuchs, K (1990). Development of **measuring** and control systems for underwater cutting of radioactive components. EUR 12869.

de Tassigny, C, Signoret, C **(199fl). Immobilisation de** la contamination par revétement de polyméres sur des déchets radioactifs de grandes dimensions en vue de leur stockage. **EUR 12874.**

- 166 -

Schuster, E, Haas, E W (1990). Behaviour of actinides and other radionuclides that are difficult to measure in the melting of contaminated steel. EUR **12875.**

Bregani, F, Borroni, P A (1990). Aggressive chemical decontamination tests on small valves from the Garigliano BWR. HUR **1287&**

Thorne, P (1990). Méthode de coupage de tubes par l'intérieur par scie a l'arc électrique.
EUR 12883.

Migliorati, B, et al. (1990). Investigation of specific applications of laser cutting for dismantling of nuclear power plants. HUR **12947.**

Fournié, J L, et al. (1990). Influence des caractéristiques de conception des installations sur le déclassement des Réacteurs a Neutrons Rapides. EUR UI.

Pellecchia, V, et al. **(1990).** Trattamento "in situ" di superfici in calcestruzzo mediante impregnazione e polimerizzazione con resine organiche. EUR **13O&**

Buck, S, Golquhoun, A (1990). Decommissioning of a mixed-oxide fuel fabrication facility.
EUR 13057.

McMahon, T D, et al. (1990). Monitoring gamma radioactivity over large land areas using portable equipment. HUR **13071.**

5.Methodology

14

Adaptive Switching Iterative Learning Control of Robot Manipulator

P. R. Ouyang[1,*] and *W. J. Zhang*[2]

ABSTRACT

In this chapter, a new adaptive switching learning control approach, called adaptive switching learning PD control (ASL-PD), is proposed for trajectory tracking of robot manipulators in an iterative operation mode. The ASL-PD control method is a combination of the feedback PD control law with a gain switching technique and the feedforward learning control law with the input torque profile from the previous iteration. The ASL-PD method achieves the asymptotical convergence based on the Lyapunov's method, and it possesses both adaptive and learning capabilities with a simple control structure. Also, a new ILC called switching gain PD-PD (SPD-PD) type ILC is presented for trajectory tracking control of time-varying nonlinear systems with uncertainty and disturbance. In the SPD- PD ILC, a PD feedback control with switching gains in the iteration

domain and a PD-type ILC based on the previous iteration combine together into one updating law. The proposed SPD-PD ILC can be viewed as online-offline ILC. It is theoretically proven that the boundednesses of the state error and the final tracking error are guaranteed in the presence of uncertainty, disturbance, and initialization error of the nonlinear systems. Simulation and experiments are conducted for trajectory tracking control of robot manipulators.

1 Department of Aerospace Engineering, Ryerson University, 350 Victoria St. Toronto, ON M5B 2K3, Canada.
E-mail: pouyang@ryerson.ca
2 Department of Mechanical Engineering, University of Saskatchewan, 57 Campus Drive, Saskatoon, SK S7N 5A9, Canada.
E-mail: wjz485@mail.usask.ca
* Corresponding author

Keywords: Adaptive control, iterative learning, switching gain control, PD control, trajectory tracking, robot manipulator, online-offline learning

INTRODUCTION

Trajectory tracking control of robot manipulators has attracted many attentions due to its wide applications in industrial systems. Basically, the control methods can be classified into the following three types. The first type is the traditional feedback control (proportional-integral-derivative (PID) control or proportional-derivative (PD) control (Chen et al. 2001, Craig 1986, Kerry 1997, Qu 1995) where the errors between the desired and the actual performance are treated in certain ways (proportional, derivative, and integral), multiplied by control gains, and fed back as the "correct" input torque. The second type is the adaptive control (Choi and Lee 2000, Craig 1988, Li et al. 1996, Li et al. 1998, Slotine and Li 1987, Tomei 1991) where the controller modifies its behaviour in response to the changes in the dynamics of the robot manipulator and the characteristics of the disturbances received by the manipulator system. The third type is the iterative learning control (ILC) (Arimoto et al. 1984, Chen and Moore 2002, Kawamura et al. 1988, Kue et al. 1991, Tayebi 2003, Yan et al. 2001) where the previous torque profile is added to the current torque in a certain manner. Some other control methods, including the robust control, model based control, switching control, and sliding mode control can be in one or another way reviewed either as specialization and/ or combination of the three basic types, or are simply different names due to different emphases when the basic types are examined.

The use of traditional PD/PID control is very popular not only because of its simple structure and easy implementation but also its acceptable performance for industrial applications. It is known that the PD control can be used for trajectory tracking with the asymptotic stability if the control gains are carefully selected (Chen et al. 2001, Kerry 1997, Qu 1995). However, the PD control is not satisfactory for applications which require high tracking accuracy. This limitation with the

PD control is simply due to the inherent “mismatch” between the nonlinear dynamics behaviour of a robot manipulator and the linear regulating behaviour of the PD controller. Such a limitation is also true for PID control.

The adaptive control can cope with parameter uncertainties, such as the link length, mass, inertia, and frictional nonlinearity, with a self-organizing capability. Having such a capability, however, requires extensive computation and thus compromises its application for real-time control problems (especially in high-speed operations). In addition, since the adaptive control generally does not guarantee that the estimated parameters of robot manipulators converge to their true values (Sun and Mills 1999), the tracking errors would repeatedly be brought into the system as the manipulators repeat their tasks.

Another active area of research in the control theory is the switching control (Fu and Barmish 1986, Martensson 1985, Middleton et al. 1988, Nussbaum 1983). In the switching control technique, the control of a given plant can be switched among several controllers, and each controller is designed for a specific “nominal model” of the plant. A switching control scheme usually consists of an inner loop (where a candidate controller is connected in closed-loop with the system) and an outer loop (where a supervisor decides which controller to be used and when to switch to a different one).

As such, the switching of controllers is taken place in the time domain. This underlying philosophy may be modified to perform such a switching with respect to the iteration of learning.

Robot manipulators are usually used for repetitive tasks. In this case, the reference trajectory is repeated over a given operation time. This repetitive nature makes it possible to apply ILC for improving tracking performance from iteration to iteration. It should be noted that ILC can be further classified into two kinds: off-line learning and on-line learning. In the case of off-line learning control, information in the controlled torque in the current iteration does not come from the current iteration but from the previous one. Philosophically, the learning in this case is shifted to the off-line mode. This then releases a part of the control workload at real-time, which implies the improvement of real-time trajectory tracking performance. In the case of the on-line learning control, the feedback control decision incorporates ILC at real-time.

ILC (Arimoto et al. 1984) based on the system's repetitive operations has drawn increasing attention because of its simple control structure and good tracking performances. The basic principle behind ILC is to use information collected from previous executions of the same task repetitively to form the control action for the current operation in order to improve tracking performances from iteration to iteration. Examples of systems that operate in a repetitive manner include robot manipulators, assembly line tasks, chemical batch processes, reliability testing rigs, and so on. In each of these tasks the system is required to perform the same action over and over again with high precision. In general, ILC improves the tracking performance by a self-tuning process without using a system model. The key purpose of using ILC is to achieve high performance after a few iterations. One advantage of ILC is that there is no requirement for dynamic model of the controlled system.

The classic type of ILC algorithms is a feed forward control system that is theoretically capable of reducing the tracking error to zero as the number of iterations increases towards infinity (Ahn et al. 2007, Bristow et al. 2006, Moore et al.

1992). According to the learning action type, ILC can be classified as P-type (Longman 2000, Xu et al. 2004), D-type (Arimoto et al. 1984, Yan et al. 2001, Song et al. 2005), PD-type (Chen and Moore 2002, Zhang et al. 2006), and PID-type (Madady 2008, Park et al. 1999). A PD-type averaged iterative learning control is proposed for linear systems in (Park 2005). Some detailed surveys for ILC can be found in (Ahn et al. 2007, Bristow et al. 2006, Moore et al. 1992).

Another direction in the development of ILC is using the current iteration tracking errors to form the control signal that can be viewed as online ILC (Amann et al. 1995, Cai et al. 2008, Ouyang et al. 2006, Ouyang et al. 2007, Owens and Munde 1998, Qu et al. 1991, Sun and Wang 2002, Xu et al. 1995). P-type online ILC systems based on the use of current tracking errors were proposed (Owens and Munde 1998, Sun and Wang 2002, Xu et al. 1995). A similar control algorithm was used for discrete time systems (Amann et al. 1995). D-type online ILC (Sun and Wang 2002, Yan et al. 2001), PD-type online ILC (Park 2005, Ouyang et al. 2006, Ouyang et al. 2007, Xu et al. 1995), and PID-type online ILC (Cai et al. 2008, Qu et al. 1991) were developed and applied into different systems control. As demonstrated in these papers, the iterative learning control with current tracking error signal can achieve fast convergence rates by selecting high feedback control gains.

It is well known that PD/PID feedback control is widely used in industrial applications such as robot systems and process control systems to achieve good performance. But PD/PID feedback control cannot achieve exactly the desired tracking performance because a non-zero error signal is required to activate the feedback control. Therefore, PD/PID control alone is not adequate for achieving a perfect trajectory tracking performance, especially when the system has nonlinearities and uncertainties. The combination of feedback control and iterative learning control is a promising technique to achieve good tracking performance and speed up the convergence process. P-type feedback plus P-type ILC control algorithms (P-P type) for continuous and discrete time-varying systems were proposed (Doh et al. 1999, Norrlöf and Gunnarsson 2005, Pi et al. 2000). A P-P ILC algorithm was developed for kinematic path-tracking of mobile robots in (Kang et al. 2005). High order D-D ILCs (Chen et al. 1996a, Xu et al. 2004) and PD-PD ILCs (Chen et al. 1996b, Ouyang 2009) were developed. A P-D ILC was proposed in (Yu et al. 2002) for discrete linear time-invariant systems.

In this chapter, we present two new control methods. The basic concept of these new control methods is to combine several control methods by taking advantage of each of them into a hybrid one. The architecture of this hybrid control method is as follows:
(1) the control is a learning process through several iterations of off-line operations of a manipulator, (2) the control structure consists of two parts: a PD feedback part and a feedforward learning part using the torque profile obtained from the previous iteration, and (3) the gains in the PD feedback law are adapted according to the gain switching strategy with respect to the iteration. The first new control method is called the adaptive switching learning PD (ASL-PD) control method (Ouyang et al. 2006), and the second one is called switching gain PD-PD (SPD-PD) iterative learning control method (Ouyang et al. 2011).

The remainder of this chapter is organized as follows. In Section **Adaptive Switching Iterative Learning PD Control**, the ASL-PD control method is described, and its features are

discussed, followed by the analysis of the asymptotic convergence of the ASL-PD control method using the Lyapunov's method. In Section **Switching Gain PD-PD Iterative Learning Control**, the SPD-PD ILC is introduced to control a general nonlinear system, and the convergence analysis is conducted. In Section **Simulation Study**, simulation studies are conducted for trajectory tracking control of robot manipulators where comparison studies are presented. Section **Experimental Verifications of ASL-PD Control** presents some experimental verification results to demonstrate the effectiveness of the proposed adaptive switching learning control methods. Conclusions are given in Section **Conclusion**.

ADAPTIVE SWITCHING ITERATIVE LEARNING PD CONTROL

Dynamic Model of A Robot Manipulator

Consider a robot manipulator with *n* joints running in repetitive operations. Its dynamics can be described by a set of nonlinear differential equations in the following form (Craig 1986)

$$D(q^j(t))\ddot{q}^j(t) + C(q^j(t), \dot{q}^j(t))\dot{q}^j(t) + G(q^j(t), \dot{q}^j(t)) + T_\ell(t) = T^j(t) \quad (1)$$

where $t \in [0, t_f]$ denotes the time and $j \in \mathbb{Z}$ denotes the operation or iteration number. $q^j(t) \in \mathbb{R}^n$, $\dot{q}^j(t) \in \mathbb{R}^n$, and $\ddot{q}^j(t) \in \mathbb{R}^n$ are the joint position, joint velocity, and joint acceleration vectors, respectively. $D(q^j(t)) \in \mathbb{R}^{n \times n}$ is the inertia matrix, $C(q^j(t), \dot{q}^j(t)) \dot{q}^j(t) \in \mathbb{R}^n$ denotes the vector containing the Coriolis and centrifugal terms, $G(q^j(t), q_d(t)) \in \mathbb{R}$ is the gravitational plus frictional force, $T_d(t) \in \mathbb{R}$ is the repetitive unknown disturbance, and $T^j(t) \in \mathbb{R}^n$ is the input torque vector.

It is common knowledge that robot manipulators have the following properties (Craig 1986):

P1) $D(q^j(t))$ is a symmetric, bounded, and positive definite matrix;

P2) The matrix $\dot{D}(q^j(t)) - 2C(q^j(t), \dot{q}^j(t))$ is skew symmetric. Therefore,

$$x^T (\dot{D}(q^j(t)) - 2C(q^j(t), \dot{q}^j(t))) x = 0, \forall x \in \mathbb{R}^n$$

Assume that all parameters of the robot are unknown and that:

A1) The desired trajectory $q_d(t)$ is of the third-order continuity *for* $t \in [0, t_f]$. A2) For each iteration, the same initial conditions are satisfied, which are $q^j(0) = q_d(0)$, $\dot{q}^j(0) = \dot{q}_d(0)$, $\forall j \in \mathbb{Z}$.

ASL-PD Controller Design

The ASL-PD control method has two operational modes: the single operational mode and the iterative operational mode. In the single operational mode, the PD control feedback with the gain switching is used, where information from the present operation is utilized. In the iterative operational mode, a simple iterative learning control is applied as feedforward where information from previous operations is used. Together with these two operational modes, all information from the current and previous operations is utilized. Specially, the ASL-PD control method can be described as follows:

Consider the jth iterative operation for system in Eq. (1) with properties (P1 and P2) and assumptions (A1 and A2) under the following control law

$$T^{j}(t) = K_p^{j} e^{j}(t) + K_d^{j} \dot{e}^{j}(t) \quad j = 0,1,\ldots,N \tag{2}$$

$$T^{j+1}(t) = T^{j}(t) + \underbrace{K_p^{j} e^{j}(t) + K_d^{j} \dot{e}^{j}(t)}_{feedback} + \underbrace{K_p^{j+1} e^{j+1}(t) + K_d^{j+1} \dot{e}^{j+1}(t)}_{feedforward}$$

with the following gain switching rule

$$\begin{cases} K_p^{j} = \beta(j) K_p^{0} \\ K_d^{j} = \beta(j) K_d^{0} \end{cases} \quad \begin{cases} j = 1, \\ j = 2,\ldots,N \end{cases} \tag{3}$$

$$\beta(j) \begin{cases} > 1 & \text{if } e^{j}(t) \cdot e^{j-1}(t) > 0 \\ \le 1 & \text{if } e^{j}(t) \cdot e^{j-1}(t) \le 0 \end{cases}$$

where $T^{j}(t) = 0$, $e^{j}(t) = q_d(t) - q^{j}(t)$, $\dot{e}^{j}(t) = \dot{q}_d(t) - \dot{q}^{j}(t)$ and K_p and K_d are the initial PD control gain matrices that are diagonal positive definite. The matrices K_p^{0} and K_d^{0} are called the initial proportional and derivative control gains, while matrices K_p^{j} and K_d^{j} are the control gains of the jth iteration. $\beta(j)$ is the gain switching factor where $\beta(j) > 1$ *for* $j = 1, 2,\cdots, N$, and it is a function of the iteration number.

The gain switching law in Eq. (3) is used to adjust the PD gains from iteration to iteration. Such a switching in the ASL-PD control method acts not in the time domain but in the iteration domain. This is the main difference between the ASL-PD control method and the traditional switching control method (where switching occurs in the time domain). Therefore, the transient process of the switched system, which must be carefully treated in the case of the traditional switching control method, does not occur in the ASL-PD control method.

From Eqs. (2) and (3) it can be seen that the ASL-PD control law is a combination of feedback (with the switching gain in each iteration) and feedforward (with the learning scheme). The ASL-PD control method possesses an adaptive ability, which is demonstrated by the adoption of different control gains in different iterations; see Eq. (3). Such a switching takes place at the beginning of each iteration. Therefore, a rapid convergence speed for the trajectory tracking can be expected.

Furthermore, in the ASL-PD control law, the learning occurs due to the memorization of the torque profiles generated by the previous iterations that include information about the dynamics of a controlled system. It should be noted that such learning is direct in the sense that it generates the controlled torque profile directly from the existing torque profile in the previous iteration without any modification.

Because of the introduction of the learning strategy in the iteration, the state of the controlled object changes from iteration to iteration. This requires an adaptive control to deal with those changes, and the ASL-PD has such an adaptive capability.

In the next section, the proof of the asymptotic convergence of the ASL-PD control method for both position tracking and velocity tracking will be given.

Asymptotic Convergence Analysis of ASL-PD Method

Equation (1) can be linearized along the desired trajectory $(q_d(t), \dot{q}_d(t), \ddot{q}_d(t))$ in the following way

$$D(t)\ddot{e}^{j}(t)+[C(t)+C_1(t)]\dot{e}^{j}(t)+F(t)e^{j}(t)+n(e^{j},\dot{e}^{j},e^{j},t)-T_a(t)=H(t)-T_1(t) \quad (4)$$

where $D(t) = D(q_d(t))$

$$C(t) \equiv C(q_d(t),\dot{q}_d(t))$$

$$C_1(t) \equiv \left.\frac{\partial C}{\partial \dot{q}_d}\right|_{(q_d(t),\dot{q}_d(t))} \dot{q}_d(t) + \left.\frac{\partial G}{\partial q_d}\right|_{(q_d(t),\dot{q}_d(t))}$$

$$F(t) \equiv \left.\frac{\partial D}{\partial q_d}\right|_{(t)} \ddot{q}_d(t) + \left.\frac{\partial C}{\partial q_d}\right|_{(q_d(t),\dot{q}_d(t))} \dot{q}_d(t) + \left.\frac{\partial G}{\partial q_d}\right|_{(q_d(t),\dot{q}_d(t))}$$

$$H(t) \equiv D(q_d(t))\ddot{q}_d(t) + C(q_d(t),\dot{q}_d(t))\dot{q}_d(t) + G(q_d(t))$$

The term $n(e^j, \dot{e}^j, \ddot{e}^j, t)$ contains the higher order terms $e^j(t)$, $\dot{e}^j(t)$, and $\ddot{e}^j(t)$, and it can be negligible. Therefore, for the jth and $j+1$th iterations, Eq. (4) can be rewritten, respectively, as follows

$$D(t)\ddot{e}^{j}(t)+[C(t)+C_1(t)]\dot{e}^{j}(t)+F(t)e^{j}(t)+T_a(t)=H(t)+T_1^{j}(t) \quad (5)$$

$$D(t)\ddot{e}^{j+1}(t)+[C(t)+C_1(t)]\dot{e}^{j+1}(t)+F(t)e^{j+1}(t)+T_a(t)=H(t)+T_1^{j+1}(t) \quad (6)$$

For the simplicity of analysis, let $K_p^0 = \Lambda K_d^0$ for the initial iteration, and define the following parameter

$$y_i^j(t) = \dot{e}_i^j(t) + \Lambda e_i^j(t) \tag{7}$$

The following theorem can be proved.

Theorem 1. *Suppose robot system Eq. (1) satisfies properties (P1, P2) and assumptions (A1, A2). Consider the robot manipulator performing repetitive tasks under the ASL- PD control method Eq. (2) with the gain switching rule Eq. (3). The following should hold for all* $t \in [0, t_f]$

$$q_i^j(t) \to q_{di}(t)$$

$$\dot{q}_i^j(t) \to \dot{q}_{di}(t)$$

provided that the control gains are selected so that the following relationships hold

$$\lambda_{\min}(K_d^0 + 2C_1 D) > 0 \tag{8}$$

$$\lambda_{\min}(K_p^0 + 2C_1 F/\lambda + 2C_1/\lambda) > 0 \tag{9}$$

$$\lambda_{\min}(\Lambda D) > \|F/\lambda + C_1\|_{\max} \tag{10}$$

where $\lambda_{min}(A)$ is the minimum eigenvalue of matrix A, and $\|M\|_{\max} = \max \|M(t)\|$ for $0 \le t \le t_f$. Here, $\|M\|$ represents the Euclidean norm of M.

Proof. Define a Lyapunov function candidate as

$$V^j = \int_0^t e^{-\rho t} y_i^{jT} K_d^0 y_i^j dt \ge 0 \tag{11}$$

where $K_d^0 > 0$ is the initial derivative gain of PD control, and ρ is a

positive constant.

Also, define $\delta y^j = y^{j+1} - y^j$ and $\delta e^j = e^{j+1} - e^j$. Then, from Eq. (7)

$$\delta \dot{y}^j = \delta \dot{e}^j + \Lambda \delta e^j \tag{12}$$

and from Eq. (10.2)

$$T^{j+1}(t) = K^{j+1} e^{j+1}(t) + K^{j+1} \dot{e}^{j+1}(t) + T^j(t) \tag{13}$$

From Eqs. (5–7, 12–13), one can obtain the following equation

$$D\delta \dot{y}^j + (C + C_d + \Lambda D + K^{j+1})\delta y^j + (F - \Lambda(C + C_d - \Lambda D))\delta e^j = -K^{j+1}\delta y^j \tag{14}$$

From the definition of V^j, for the $j+1$th iteration, one can get

$$V^{j+1} = \int_0^t e^{-rt} \left[\dot{y}_d^{j+1} \right]^T K \left[y^{j+1} \right] dt$$

Define $\Delta V^j = V^{j+1} - V^j$. Then from Eqs. (11–12) and (14), we obtain

$$\Delta V^{j} = \int_0^t e^{-\rho t}\left(\dot{\delta y}^{jT} K_0 \dot{\delta y}^{j} + 2\delta y^{jT} K_0 y^{j}\right)dt$$

$$= \frac{1}{\beta(j+1)}\int_0^t e^{-\rho t}\left(\dot{\delta y}^{jT} K^{j+1}\dot{\delta y}^{j} + 2\delta y^{jT} K^{j+1} y^{j}\right)dt$$

$$= \frac{1}{\beta(j+1)}\left\{\int_0^t e^{-\rho t}\dot{\delta y}^{jT} K^{j+1}\dot{\delta y}^{j}dt - 2\int_0^t e^{-\rho t}\dot{\delta y}^{jT} D\dot{\delta y}^{j}dt\right.$$

$$\left. -2\int_0^t e^{-\rho t}\dot{\delta y}^{jT}\left((C + C_d - LD + K^{j+1})\dot{\delta y}^{j} + (F - L(C + C_d - LD))\delta e^{j}\right)dt\right\}$$

Applying the partial integration and from (A2), we have

$$\int_0^t e^{-\rho\tau}\dot{\delta y}^{jT} D\dot{\delta y}^{j} d\tau = e^{-\rho\tau}\delta y^{jT} D\delta y^{j}\Big|_0^t - \int_0^t (e^{-\rho\tau}\delta y^{jT} D)'\delta y^{j} d\tau$$

$$= e^{-\rho\tau}\delta y^{jT}(t) D(t)\delta y^{j}(t) + \rho\int_0^t e^{-\rho\tau}\delta y^{jT} D\delta y^{j} d\tau - \int_0^t e^{-\rho\tau}\delta y^{jT}\dot{D}\delta y^{j} d\tau$$

From (P1), one can get

$$\int_0^t \dot{\delta y}^{jT} D\dot{\delta y}^{j}dt = 2\int_0^t \dot{\delta y}^{jT} C\dot{\delta y}^{j}dt$$

Then

$$\Delta V^{j} = \frac{1}{\beta(j+1)}\left\{-e^{-\rho t}\delta y^{jT}(t)D(t)\delta y^{j}(t) - \rho\int_0^t e^{-\rho\tau}\delta y^{jT} D\delta y^{j}d\tau\right.$$

$$-2\int_0^t e^{-\rho t}\dot{\delta y}^{jT}(F - L(C + C_d - LD))\delta e^{j}dt$$

$$\left. -\int_0^t e^{-\rho t}\dot{\delta y}^{jT}(K^{j+1} + 2C - 2L(C_d - LD))\dot{\delta y}^{j}dt\right\} \quad (15)$$

From Eq. (3), we have

$$\int_0^t e^{-rt}\delta y^{jT}K^{j+1}\delta\dot{y}^j dt = \int_0^t e^{-rt}\delta y^{jT}K^{(j+1)}\delta\dot{y}^j dt \tag{16}$$

$$\int_0^t e^{-rt}\delta y^{jT}K^{j}\delta\dot{y}^j dt$$

Substituting Eq. (12) into Eq. (15) and noticing Eq. (16), we obtain

$$\Delta V^j \le \frac{1}{\beta(j+1)}\Big\{-e^{-\rho t}\,\delta y^{jT}(t)D(t)\delta y^j(t) - \rho\int_0^t e^{-\rho\tau}\delta y^{jT}D\delta y^j d\tau$$

$$-\int_0^t e^{-rt}d\dot{e}^{jT}(K^0+2C_1-2LD)d\dot{e}^j dt - 2L\int_0^t e^{-rt}de^{jT}(K^0+2C_1-2LD)d\dot{e}^j dt$$

$$-2\int_0^t e^{-rt}d\dot{e}^{jT}(F-L(C+C_1-LD))de^j dt - L^2\int_0^t e^{-rt}de^{jT}(K^0+2C_1-2LD)de^j dt$$

$$-2L\int_0^t e^{-rt}de^{jT}(F-L(C+C_1-LD))de^j dt\Big\}$$

Applying the partial integration again gives

$$\int_0^t e^{-\rho\tau}\delta y^{jT}(K_0+2C-2\Lambda D)\delta e^j d\tau$$
$$= e^{-\rho t}\delta y^{jT}(K_0+2C-2\Lambda D)\delta e^j - \int_0^t e^{-\rho\tau}\delta y^{jT}(K_0+2C-2\Lambda D)\delta e^j d\tau + 2\int_0^t e^{-\rho\tau}\delta y^{jT}(\Lambda D-C)\delta e^j d\tau$$

Therefore,

$$\Delta V^j \le \frac{1}{\beta(j+1)}\Big\{-e^{-\rho t}\delta y^{jT}D\delta y^j - \rho\int_0^t e^{-\rho\tau}\delta y^{jT}D\delta y^j d\tau - \Lambda e^{-\rho t}\delta e^{jT}(K_0+2C-2\Lambda D)\delta e^j$$
$$-\rho\Lambda\int_0^t e^{-\rho\tau}\delta e^{jT}(K_0+2C-2\Lambda D)\delta e^j d\tau - \rho\int_0^t e^{-\rho\tau}w d\tau\Big\} \quad (17)$$
$$\le \frac{1}{\beta(j+1)}\Big\{-e^{-\rho t}\delta y^{jT}D\delta y^j - \Lambda e^{-\rho t}\delta e^{jT}I_p\delta e^j - \rho\int_0^t e^{-\rho\tau}\delta y^{jT}D\delta y^j d\tau$$
$$-\rho\Lambda\int_0^t e^{-\rho\tau}\delta e^{jT}I_p\delta e^j d\tau - \rho\int_0^t e^{-\rho\tau}w d\tau\Big\}$$

where $w = e^{jT}(K_0 + 2C + 2D)e^j + 2e^{jT}(F/\Lambda + (C + C_1 - \Lambda D)e^j + e^{jT}(K_0 + 2C_1 + 2F/\Lambda + 2C_1/\Lambda)e^j$

Let $Q = F/\Lambda - (C + C_1 - \Lambda D)$. Then from Eqs. (8–9), we obtain

$$w \le \lambda_p\|\delta e\|^2 + 2\Lambda\,\delta e^T Q\delta e + \Lambda^2\lambda_r\|\delta e\|^2$$

Applying the Cauchy-Schwartz inequality gives

$$\delta e^T Q\delta e \le \|\delta e\|\,\|Q\|_{\max}\|\delta e\|$$

From Eqs. (8–10)

$$w \le \lambda_p\|\delta e\|^2 + 2\Lambda\,\|\delta e\|\,\|Q\|_{\max}\|\delta e\| + \Lambda^2\lambda_r\|\delta e\|^2 \quad (18)$$

$= l_p(\|\delta e\|_l - \|Q\|_{\max} \|\delta e\|) + \Lambda (l_r - \|Q\|_p \|\delta e\|) \leq 0$

From (P1) and Eq. (8), based on Eq. (17), it can be ensured that $\Delta V^j \leq 0$. Therefore,

$$V^{j+1} \leq V^j \tag{19}$$

From the definition, K^0 is a positive definite matrix. From the definition of V^j, $V^j > 0$, and V^j is bounded. As a result, $y_d - y^j(t) \to 0$ when $j \to \infty$. Because $e^j(t)$ and $\dot{e}^j(t)$ are two independent variables, and Λ is a positive constant. Thus, if $j \to \infty$, then $e^j(t) \to 0$ and $\dot{e}^j(t) \to 0$ for $t \in [0, t_f]$.

Finally, the following conclusions hold

$$\begin{cases} q^j(t) \to q_d(t) \text{ for } t \in [0, t_f] \\ \dot{q}^j(t) \to \dot{q}_d(t) \end{cases} \tag{20}$$

From the above analysis it can be seen that the ASL-PD control method can guarantee that the tracking errors converge arbitrarily close to zero as the number of iterations increases. The following case studies based on simulation will demonstrate this conclusion.

SWITCHING GAIN PD-PD ITERATIVE LEARNING CONTROL

Dynamic Model and SPD-PD Control Law

In this Section, the considered problem is a nonlinear time-varying system with non- repetitive uncertainty and disturbance as follows:

$$\begin{cases} \dot{x}_k(t) = f(x_k(t),t) + B(t)u_k(t) + h_k(t) \\ y_k(t) = C(t)x_k(t) + x_k(t) \end{cases} \tag{21}$$

where k denotes the iteration index. $x \in R^n$, $u \in R^r$, and $y \in R^m$ are the state, control input and output of the system, respectively. $f(x(t),t) \in R^n$ is the system function, $B(t) \in R^{n\times r}$ the input matrix, $C(t) \in R^{m\times n}$ the output matrix, $\eta_k(t) \in R^n$ the uncertainty of the system, and $\xi_k(t) \in R^m$ the disturbance, respectively.

In this section, to evaluate tracking convergence, the following notational conventions for norms are adopted:

$$\|f\| = \max_{1\le i\le n} |f_i|$$

$$\|M(t)\| = \max_{1\le i\le m} \sum_{j=1}^{n} |m_{ij}|$$

$$\|h(t)\|_\lambda = \sup_{t\in[0,T]} \|h(t)\| e^{-\lambda t}, \quad \lambda > 0$$

where $f = [f_1,..., f_n]^T$ is a vector, $M = [m_{ij}] \in R^{m\times n}$ is a matrix, and $h(t)$ ($t \in [0, T]$) is a real function where T is the time period of a repetitive task.

To restrict the discussion, the following assumptions are made for the system.

A3) The desired trajectory $y_d(t)$ is first-order

continuous for $t \in [0, T]$. A4) The control input matrix $C(t)$ is first-order continuous for $t \in [0, T]$.

A5) The function $f(x(t), t)$ is globally, uniformly Lipschitz in x for $t \in [0, T]$. That means $\|f(x_{k+1}(t), t) - f(x_k(t), t)\| \le c\|x_{k+1}(t) - x_k(t)\|$ where k is the iteration index and c_f (> 0) is the Lipschitz constant.

A6) Uncertainty and disturbance terms $\eta(t)$ and $\xi(t)$ are bounded as follows: $\forall t \in [0, T]$ and $\forall k$, we have $\|\eta(t)\| \le b_\eta$ and $\|\xi(t)\| \le b_\xi$, and $\|\xi_i(t)\| \le \xi_{ik}$.

To control the nonlinear system stated in Eq. (21), we propose the following SPD-PD ILC law

$$u_{k+1}(t) = u_k(t) + K_{p1}(k+1)e_{k+1}(t) + K_{d1}(k+1)\dot{e}_{k+1}(t) + K_{p2}(t)e_k(t) + K_{d2}(t)\dot{e}_k(t) \quad (22)$$

with the feedback control gains given by:

$$\begin{cases} K_{p1}(k) = s(k)K_{p1}(0) \\ K_{d1}(k) = s(k)K_{d1}(0) \end{cases} \quad \text{with } s(k+1) > s(k) \tag{23}$$

where $e_{k+1}(t) = y_d(t) - y_{k+1}(t)$, $e_k(t) = y_d(t) - y_k(t)$, $e_{k+1}(t) = y_d(t) - y_{k+1}(t)$ and $e_k(t) = y_d(t) - y_k(t)$ are position errors and velocity errors of the output vector for the $k+1$ iteration and the k^{th} iteration, respectively. $K_{di} \in R^{m\times r}$ and $K_{pi} \in R^{m\times r}$ are the proportional and derivative gain matrices, respectively. Equation (23) represents the switching gains of the feedback control, and $s(k) > 1$ is a monotonically increasing function of the iteration index.

From Eq. (22), we can see that the proposed SPD-PD ILC law consists of two control loops. The first loop includes a PD feedback controller with switching gains in the iteration domain, and the second loop is a standard PD-type ILC. Therefore, SPD-PD ILC is effectively a hybrid control that aims to take the advantages offered by both feedback control and ILC. The key purpose of introducing switching gains in the feedback loop is to expedite the convergence of the iterative operations and avoid vibration of systems. Also, one can see that the proposed control algorithm is an extension of the ASL-PD in (Ouyang et al. 2006).

We assume that, in each iteration, the repeatability of the initial state setting is satisfied within the following admissible deviation level:

$$\|x_k(0) - x_0(0)\| \le \varepsilon \quad \text{for } k = 1, 2,... \tag{24}$$

where ε_x is a small positive constant that represents the acceptable accuracy of the designed state vector and $x_0(0)$ represents the desired initial state value.

For briefness of the convergence analysis, some notations are introduced first and used in the following sections:

$$B_{d1} \triangleq \max_{t\in[0,T]} \|K_{d1}\| \quad B_{d2} \triangleq \max_{t\in[0,T]} \|K_{d2}C(t)(0)C(t)\|$$

$$B_{pd1} \triangleq \max_{t\in[0,T]} \|K_{p1}(0)C + K_{d1}(0)C\dot{}\|, \quad B_{pd2} \triangleq \max_{t\in[0,T]} \|K_{p2}C + K_{d2}C\dot{}\|$$

$$B_{Kp1} \triangleq \max_{t\in[0,T]} \|K_{p1}(0)\|, \quad B_{Kp2} \triangleq \max_{t\in[0,T]} \|K_{p2}\|$$

$$B_{Kd1} \triangleq \max_{t\in[0,T]} \|K_{d1}(0)\|, \quad B_{Kd2} \triangleq \max_{t\in[0,T]} \|K_{d2}\|$$

$$B_B \triangleq \max_{t\in[0,T]} \|B(t)\|, \quad B_C \triangleq \max_{t\in[0,T]} \|C(t)\|, \quad B_s \triangleq \max s(k)$$

$$K_{B1} \triangleq \frac{B_{d1} + c_f B_{pd1}}{1 - c_f}, \quad K_{B2} \triangleq \frac{B_{d2} + c_f B_{pd2}}{1 - c_f}$$

$$K \triangleq \max\left\{\max_{t\in[0,T]} \|I - K_{d1}(0)CB\|, \max_{t\in[0,T]} \|K_{d2}CB\|\right\}$$

$$\rho \triangleq 1 - \frac{1}{B_B K_{B2}}, \quad \gamma \triangleq B_B K_{B2}$$

$$1 \quad s \quad B \quad B1$$

SPD-PD ILC Law and Convergence Analysis

Theorem 2. For the nonlinear time-varying system Eq. (21), if the SPD-PD type iterative learning control law Eq. (22) is applied and the switching gain algorithm Eq. (23) is adopted, then the final state error and the output tracking error are bounded and the boundednesses are given by

$$\lim_{k\to\infty} \|dx_k(t)\| \le \frac{1}{1-rb}\left(\frac{rF}{1-c}+Tb+e\right)$$

$$\lim_{k\to\infty} \|e_k(t)\| \le \frac{B}{1-rb}\left(\frac{rFC}{1-c}+Tb+e\right)+b \tag{25}$$

where $F=(B_1K_{d2}+B_1B_2+B_1)b+(B_1B_2+B_1)b+(B_1B_2)b+K_{p1}x_{d1}+K_{d1}x_{d1}+(B_1K_{s1}+K_{s1})e_x$.

Provided the control gain $k_{d1}(0)$ and the learning gain $K_{d2}(t)$ are selected such that

$I_m + k_{d1}(0)\,B(t)C(t)$ is non-singular, and

$$\max_{t\in[0,T]} \|(I_m + K_{d1}(0)B(t)C(t))^{-1}\| = r_1 < 1$$

$$\max_{t\in[0,T]} \|I - K_{d2}(t)B(t)C(t)\| = r_2 < 1 \tag{26}$$

Also we propose the following initial state learning algorithm:

$$x_{k+1}(0) = (1 + B(0)K_{d1}^{-1}(0)C(0))\{x_k(0) + B(0)K_{d1}(0) y_d(0) + B(0)K_{d2}(0)(y_d(0) - y_k(0))\} \quad (27)$$

In this Section, the λ–norm is used to examine the convergence of the tracking error for the proposed SPD-PD ILC algorithm. First of all, a relation between norm and λ–norm is represented by Lemma 1.

Lemma 1. Suppose that $x(t) = [x_1(t), x_2(t), \ldots, x_n(t)]^T$ is defined in $t \in [0, T]$. Then

$$\int_0^t \|x(t)\| dt \cdot e^{-\lambda t} \le \frac{1}{\lambda} \|x(t)\|_\lambda \quad \text{for } \lambda > 0 \quad (28)$$

Proof.

$$\int_0^t \|x(t)\| dt \cdot e^{-\lambda t} = \int_0^t \|x(t)\, e^{-\lambda t} e^{-\lambda(t-t)}\| dt$$

$$\le \sup_{t \in [0,T]} \{\|x(t)\, e^{-\lambda t}\|\} \int_0^t e^{-\lambda(t-t)} dt$$

$$\le \sup_{t \in [0,T]} \{\|x(t)\, e^{-\lambda t}\|\} \frac{1 - e^{-\lambda t}}{\lambda}$$

$$\le \frac{1}{\lambda} \|x(t)\|_\lambda$$

[End of proof].

We define the following four variables. $dx_k = x_d - x_k$, $e_k = y_d - y_k$, $du_k = u_d - u_k$ and $\delta f_k = f_d - f(x_k)$.

From Eq. (21), we can calculate the tracking errors as:

$$\begin{cases} e_k = C\,\Delta x_k + \delta_k \\ e_{k+1} = C\,\Delta x_{k+1} + \delta_{k+1} \end{cases} \tag{29}$$

The derivative of the tracking errors can be represented as

$$\begin{cases} \dot{e}_k = C\,\Delta\dot{x}_k + \dot{C}\,\Delta x_k + \dot{\delta}_k \\ \dot{e}_{k+1} = C\,\Delta\dot{x}_{k+1} + \dot{C}\,\Delta x_{k+1} + \dot{\delta}_{k+1} \end{cases} \tag{30}$$

From Eq. (22) we have:

$$du_{k+1} = du_k - s(k+1)K_{p1}(0)e_{k+1}(t) - s(k+1)K_{d1}(0)\dot{e}_{k+1}(t) - K_{p2}(t)e_k(t) - K_{d2}(t)\dot{e}_k(t) \tag{31}$$

Submitting Eqs. (29) and (30) into Eq. (31) gets:

$$\begin{aligned} du_{k+1} = {} & du_k - K_{p2}\{C\,dx_k - x_k\} - K_{d2}\{C\,d\dot{x}_k + \dot{C}\,dx_k - \dot{x}\} - \\ & s(k+1)K_{p1}(0)\{C\,dx_{k+1} - x_{k+1}\} \\ & - s(k+1)K_{d1}(0)\{C\,d\dot{x}_{k+1} + \dot{C}\,dx_{k+1} \\ & - \dot{x}_{k+1}\} \end{aligned} \tag{32}$$

Also from Eq. (21), we can get the following equations: (33)

$$\begin{cases} \Delta\dot{x}_k = \Delta f_k + B\,u_k + \delta_k \\ \dot{x}_{k+1} = f_k + B\,u_{k+1} \end{cases}$$

$\Box\Box_k \Box 1$

Submitting Eq. (32) into Eq. (33) and reorganizing gets:

$$\begin{aligned}(I + s(k+1)K_{d1}(0)CB)du_{k+1} &= (I - K_{d2}CB)du_k - s(k+1)(K_{p1}(0)C + K_{d1}(0)C\Box)dx_{k+1} \\ &\quad -(K_{p2}C + K_{d2}C\Box)dx_k - s(k+1)K_{d1_k}(0)(Cdf_k \\ &\quad +1 - Ch_{k+1} - x\Box_{+1}) \\ &\quad -K_{d2}(Cdf_{k_k} - Ch_k - x\Box) + s(k \\ &\quad +1)K_{p1}(0)x_{k+1} + K_{p2}x_k\end{aligned} \tag{34}$$

From A5 we have $||\delta f_k|| \le c_f ||\delta x_k||$, and $||\delta f_{k+1}|| \le c_f ||\delta x_{k+1}||$. As $s(k+1) > 1$, to choose a proper control gain $K_{p1}(0)$ and from Eq. (26) we can ensure:

$$\left\| \Box I \Box s\Box k_{d1}\Box 0\Box C \Box \Box I \Box 0\Box C \right\|_{\Box \Box} \tag{35}$$
$$\Box 1\Box K \quad B\Box \Box 1 \Box K \quad B\Box \Box 1 \Box 1$$
$$\| \| \quad d1 \quad 1$$

Applying Eq. (35), Eq. (34) can be rewritten in the λ-norm and simplified as:

$$\begin{aligned}du_{k+1} &= \Box r_1\{r_2 du_k + B_s(B_{pd1} + B_{d1}c_f)dx_{k+1} \\ &+(B_{pd2} + B_{d2}c_f)dx_k + (B_s B_{d1} + B_{d2})b_h \\ &\quad +(B_s B_{Kp1} + B_{Kp2})b_x \\ &\quad +(B_s B_{Kd1} + B_{Kd2})b_{x\Box}\}\end{aligned} \tag{36}$$

For the k^{th} iteration, the state vector can be written as:

$$x_k(t) = x_k(0) + \int_0^t \left(f\left(x_k(t), t\right) + B(t)u_k(t) \right) dt \tag{37}$$

From Eq. (21), we also have:

$$x_d(t) = x_d(0) + \int_0^t \left(f\left(x_d(t), t\right) + B(t)u_d(t) \right) dt \tag{38}$$

From Eqs. (37) and (38), we get:

$$dx_k = dx_k(0) + \int_0^t \left(f\left(x_d(t), t\right) - f\left(x(t), t\right) \right) dt + \int_0^t \left(B(t)du_k - h_k \right) dt \tag{39}$$

Applying A5 to Eq. (39), we get

$$\|dx_k\| \le c_f \int_0^t \|dx_k\| dt + \int_0^t \|B(t)du_k - h_k\| dt + \|dx_k(0)\| \tag{40}$$

Equation (40) can be written in the norm form as:

$$\|dx_k\| \le c_f \int_0^t \|dx_k\| dt + \int_0^t \left(\|B(t)du_k\| + \|h_k\| \right) dt + \|dx_k(0)\| \tag{41}$$

According to the definition of λ-norm, for $\lambda > c_f$, applying Lemma 1 to Eq. (41) obtains:

$$\|dx_k\| \le \frac{T}{e^{\lambda T} - c_f} \left(\|du_k\| + b \right) + \tag{42}$$

$$\| k \| \frac{B_B}{1-c_f} \| k \| \; / - c^h \; / - c$$

$f \qquad f$

For the $k + 1^{th}$ iteration, we can get a very similar result:

$$\| dx \| \pounds \quad du \quad \frac{T}{e_x} b \quad + \qquad (43)$$

$$\| k \; \frac{B_B}{1-c_f} \| \; k \; / - c \; / - c$$

$$+1 \quad + \quad h$$

$$/ \quad 1 \; / \; \|$$

$f \qquad f$

Submitting Eqs. (42–43) into Eq. (36) and simplifying it gets:

$$(1 - r_1 B_S \; B \| B \; K \| B1 \;) \; du_{k+1} \; / \| \pounds \| r_1 \; (r_2 \; + B_B K_{B2} \;) \; du_k \; / \; + r_1 \digamma \qquad (44)$$

Equation (44) can be simplified as

$$\| du_k \| +1 \; / \| \pounds \| rb \; du_k \; / \; + r \digamma \qquad (45)$$

From Eq. (26) we have $\rho_1 \rho_2 < 1$. If we choose:

$$/ > \frac{r_1 B_B \; (c_f \; (B_S B_{pd1} + B_{pd2}) + B_S B_{d1} + B_{d2})}{1 - r_1 r_2} + c_f$$

Then we can guarantee $\rho\beta < 1$. From Eq. (45) we can get:

$$\lim_{k\to\infty} \| du_k(t) \| = \frac{r\Gamma}{1-rb} \tag{46}$$

From Eq. (46), we can see that the control input is bounded and is close to the desired control input.

Submitting Eq. (46) into Eq. (42), we can get:

$$\lim_{k\to\infty} \| dx_k(t) \| \leq \left(1 - \frac{r\Gamma}{1-rb}\right) Tb + e \tag{47}$$

Equation (47) proves that the state error is bounded. Finally, from Eq. (29) we can get:

$$\lim_{k\to\infty} \| e_k(t) \| \leq \left(BC \left(1 - \frac{r\Gamma}{1-rb}\right) + b \right) Tb + e \tag{48}$$

Equation (48) demonstrates that the output error is bounded.

Remark 1. If the initial state updating law Eq. (27) is used, we will ensure $\lim_{k\to\infty} x_k(0) = x(0)$. In this manner, we can get $\lim_{k\to\infty} \varepsilon = 0$. Therefore,

$$\lim_{k\to\infty} \| e_k(t) \| = \frac{BC}{1-rb} \left(1 - \frac{r\Gamma}{1-rb}\right) Tb \tag{49}$$

Remark 2. If there is no uncertainty and disturbance in Eq. (21), then the final tracking error bound becomes:

$$\lim_{k\to\infty} \|e(t)\| = \frac{B_C}{e_X - c_f} \tag{50}$$

Remark 3. If the initial state updating law Eq. (27) is applied, and there is no uncertainty and disturbance, then the final tracking error is $\lim_{k\to\infty} \|e_k(t)\| = 0$. Such a conclusion can be derived directly from Remark 1 and Remark 2.

Remark 4. The convergence condition Eq. (26) doesn't include the proportional gains. Therefore, it provides some extra freedom for the choices of K_{p1} and K_{p2} in the proposed control law Eq. (22).

SIMULATION STUDY

ASL-PD Results

In order to have some idea about how effective the proposed ASL-PD control method would be, we conducted a simulation study; specifically we simulated two robot manipulators. The first one was a serial robot manipulator with parameters taken directly from (Choi and Lee 2000) for the purpose of comparing the ASL-PD method with the method proposed in Ref. (Choi and Lee 2000) called the adaptive ILC. It is noted that the result for the serial manipulator may not be applicable to the parallel

manipulator. Therefore, the second one is a parallel robot manipulator for which we show the effectiveness of the ASL-PD control method both in the trajectory tracking error and the required torque in the motor.

A. Trajectory Tracking of a Serial Robot Manipulator

A two degrees of freedom (DOF) serial robot is shown in Fig. 1, which was discussed in (Choi and Lee 2000) with an adaptive ILC method.

The physical parameters and desired trajectories are the same as in (Choi and Lee 2000) and listed as follows.

Physical parameters:

$m_1 = 10$ kg, $m_2 = 5$ kg, $l_1 = 1$ m, $l_2 = 0.5$ m, $lc_1 = 0.5$ m, $lc_2 = 0.25$ m, $I_1 = 0.83$ kgm^2 and $I_2 = 0.3$ kgm^2.

Desired trajectories and the repetitive disturbances:

$$q_1 = \sin 3t, \quad q_2 = \cos 3t \quad \text{for } t \in [0,5]$$

$$d_1(t) = 0.3a \sin t, \quad d_2(t) = 0.1a(1 - e^{-t}) \quad \text{for } t \in [0,5]$$

where a is a constant used to examine the capability of the ASL-PD control to deal with the repetitive disturbances.

The control gains were also set to be the same as in (Choi and Lee 2000).

$$K_p^0 = K_d^0 = \text{diag}\{20,10\}$$

In the ASL-PD control method, the control gains were switched from iteration to iteration based on the following rule

$$K_p^j = 2jK_p^0, \; K_d^j = 2jK_d^0 \quad j = 1, 2, \cdots, N$$

First, consider $a = 1$. In that way, the repetitive disturbances were the same as in (Choi and Lee 2000). Figure 2a shows the tracking performance for the initial iteration, where only the PD control with small control gains was used, and no feedforward is

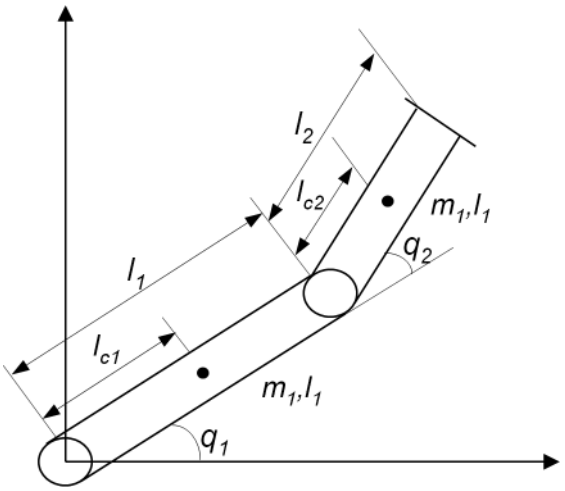
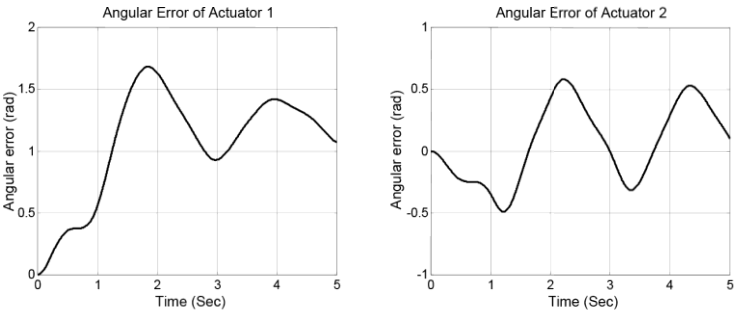


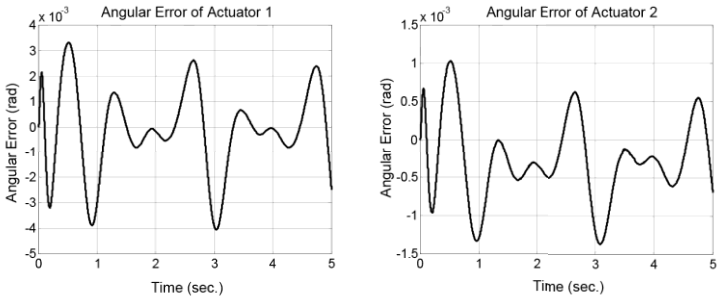
Figure 1. Configuration of a serial robot manipulator.

used. It can be seen that the tracking performance was not acceptable because the errors were too large for both joints. However, at the sixth iteration where the ASL-PD control method was applied, the tracking performance was improved dramatically as shown in Fig. 2b. At the eighth iteration, the performance was very good (Fig. 2c).

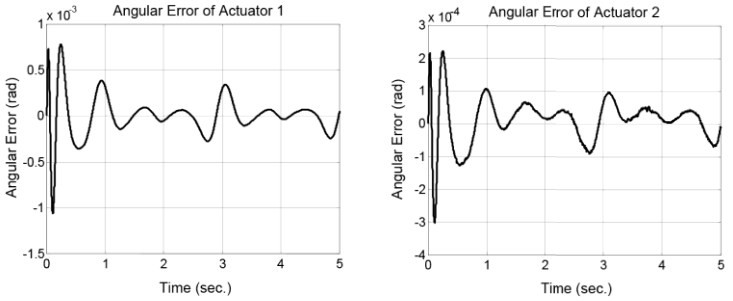
The velocity tracking performance is shown in Fig. 3. From it one can see that the velocity errors reduced from 1.96 (rad/s) at the initial iteration to 0.0657 (rad/s) at the sixth iteration, and further to 0.0385 (rad/s) at the eighth iteration for joint 1. The similar decreasing trend can be found for joint 2. From Figs. 2 and 3 it can be seen that the tracking performances were improved incrementally with the increase of the iteration number.



(a) Angular errors for two joints in the initial iteration.

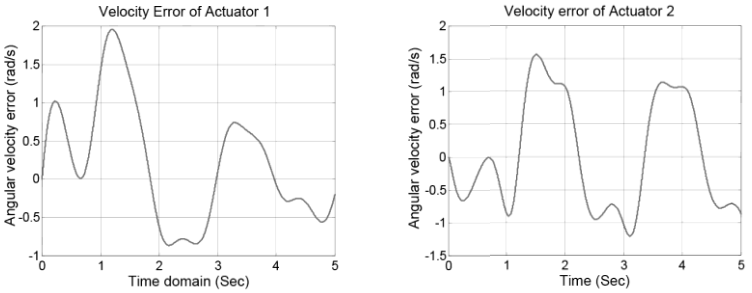


(b) Angular errors for two joints at the 6th iteration.

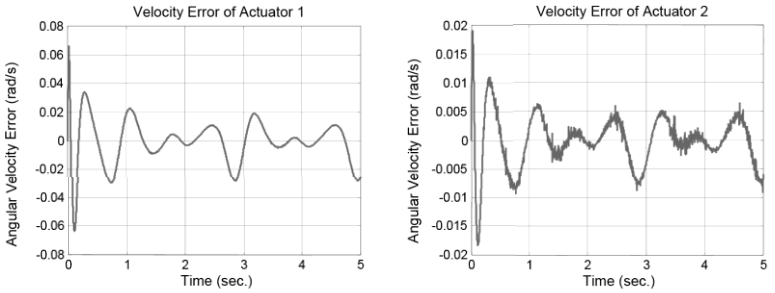


(c) Angular errors for two joints at the 8th iteration.

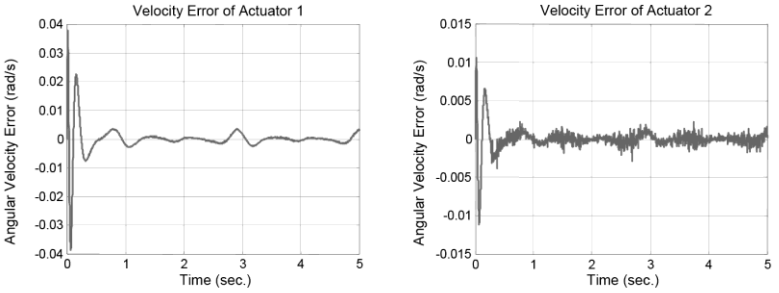
Figure 2. Position tracking errors for different iterations under ALS-PD control.



(a) Velocity errors for two joints in the initial iteration.



(b) Velocity errors for two joints at the 6th iteration.



(c) Velocity errors for two joints at the 8th iteration.

Figure 3. Velocity tracking errors for different iterations under ASL-PD control.

As the gain switching rule was introduced at each iteration, the convergence rate increased greatly compared with the control method developed in (Choi and Lee 2000). Table 1 shows the trajectory tracking errors from the initial iteration to the eighth iteration. From Table 1 it can be seen that the tracking performance was considerably improved at the sixth iteration. The maximum position errors for joints 1 and 2 were

0.0041 rads and 0.0014 rads, respectively, while the similar results were achieved after thirty iterations using the adaptive ILC in Choi and Lee 2000 (The maximum position errors for joints 1 and 2 were 0.0041 and 0.0046 (rad), respectively). Therefore, the comparison of their method and our method demonstrates a fast convergence rate with the ASL-PD control method. It should be noted that the comparison of the velocity errors was not done as such information was not presented in Ref. Choi and Lee 2000.

Table 1. Trajectory tracking errors from iteration to iteration.

Iteration	0	2	4	6	8
max|e^{j}| (rad)	1.6837	0.4493	0.0433	0.0041	0.0011
max|e^{j}| (rad)	0.5833	0.1075	0.0122	0.0014	0.0003
max|$\dot{e}^{j}$| (rad/s)	1.9596	0.7835	0.1902	0.0657	0.0385
max|$\dot{e}^{j}$| (rad/s)	1.5646	0.2534	0.0523	0.0191	0.0111

1

2

1

2

It is further noted that there were repetitive disturbances at each iteration in the simulation. To examine the capacity of the ASL-PD under the repetitive disturbance condition, different levels of the repetitive disturbances were applied in the simulation. Figure 4 shows the maximum tracking errors from iteration to iteration for different repetitive disturbances which are expressed by a constant *a*. A larger constant *a* means a more disturbance. It should be noted that in Fig. 4 *a* = 0 means there is no repetitive disturbance in the simulation, and *a* = 100 means a large repetitive disturbance included in the simulation (specifically, the disturbance acted in joint 1 was about 20% of the required torque and the disturbance acted in joint 2 was about 40% of the required torque). From this figure, one can see that although the tracking errors for the initial iteration increased with the increase of the disturbance level, the final tracking errors of both the position and the velocity were the same for the different repetitive disturbance levels at the final 2 iterations. Therefore, we conclude that the ASL-PD control method has an excellent capability in terms of both rejecting the repetitive disturbance and robustness with respect to the disturbance level.

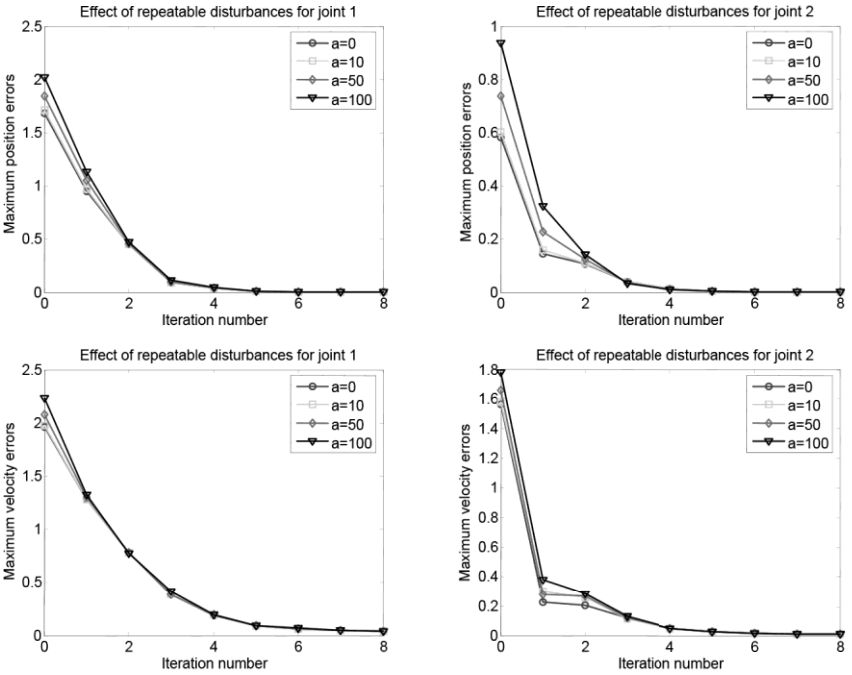


Figure 4. Effect of the repetitive disturbance on tracking errors.

B. Trajectory Tracking of a Parallel Robot Manipulator

A two DOFs parallel robot manipulator is shown in Fig. 5. Table 2 lists its physical parameters. The robot system can be viewed as two serial robotic systems with some constraints; that is, the two end-effectors of these two serial robotic systems reach the same position. Because of this constraint, the dynamics is more complex than that of its serial counterpart. The details about the dynamics of the parallel robot manipulator can be founded in Ouyang et al. 2004.

The end-effector of the robot was required to move from point A (0.7, 0.3), to point B (0.6, 0.4), and to point C(0.5,0.5). The time duration between two nearby points was 0.25 seconds. The control was carried out at the joint level where the inverse kinematics was used to calculate the joint position and velocity associated with the specific path of the end-effector. The path was designed to pass through these three points with the objective of meeting the positions, velocities, and accelerations at these three points using the motion planning method by Ouyang and Zhang 2005.

In this example, the control gains were selected as follows $K_p^0 = \text{diag}\{20, 20\}$, $K_d^0 = \text{diag}\{12, 12\}$

The gain switching rule was set to be $K_p^j = 2^j K_p^0$, $K_d^j = 2^j K_d^0$ for $j = 1, 2, \cdots, N$

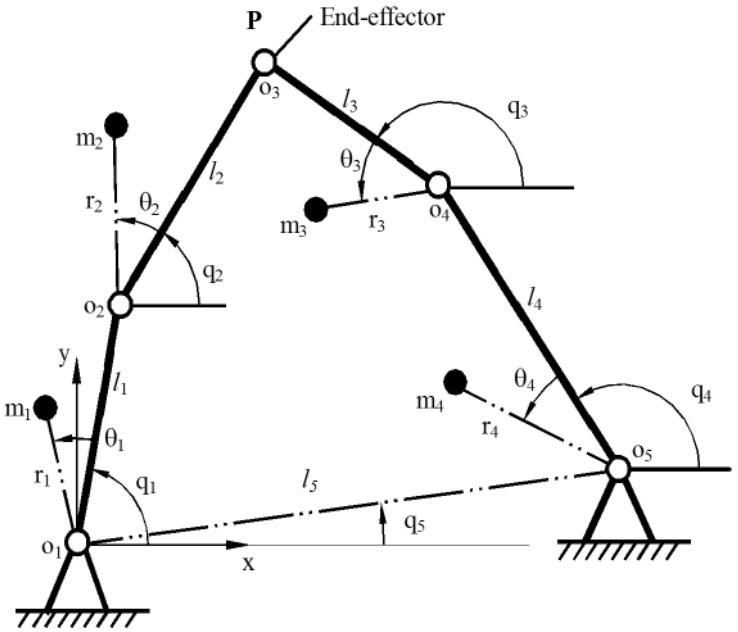


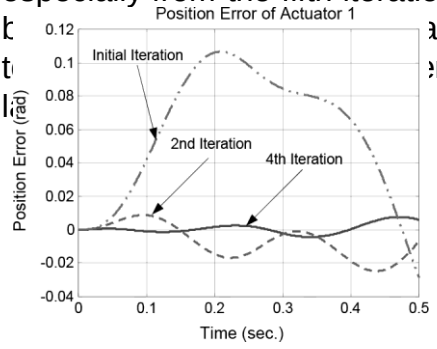
Figure 5. Scheme of a two DOFs parallel robot manipulator.

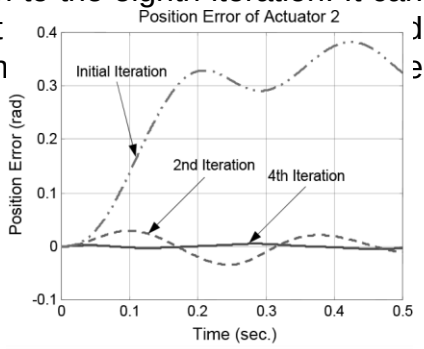
Table 2. Physical parameters of the parallel robotic manipulator.

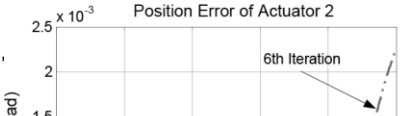
Link	m_i(kg)	l_i(m)	r_i(m)	I_i(N·m·s²)	θ_i(rad)
1	1	0.4	0.2	0.5	0
2	1.2	0.6	0.3	1	0
3	1.5	0.8	0.3	1	0
4	1	0.6	0.2	0.5	0
5	–	0.6	–	–	–

Figure 6 shows the position tracking performance improvement for the two actuators from iteration to iteration. From it one can see that, at the initial iteration, the maximum position errors were about 0.11 and 0.38 rad; only after four iterations, the maximum position errors were reduced to 0.08 and 0.05 rad. Finally, after eight iterations, the maximum errors were reduced to 0.0003 and 0.0008 rad. Figure 7 shows the velocity tracking performance improvement for the two actuators. At the initial iteration, the maximum velocity errors were about 1.17 and 2.68 rad/s in the two actuators, respectively. But after four iterations, the maximum values were reduced to 0.15 and 0.14 rad/s. After eight iterations, the maximum errors in the two actuators became 0.0046 and 0.0102 rad/s for velocity, respectively.

It should be noted that, while the tracking performance was improved from iteration to iteration, the torques required to drive the two actuators were nearly the same from iteration to iteration after a few iterations. This can be seen from Fig. 8, especially from the fifth iteration to the eighth iteration. It can b at d t en e l







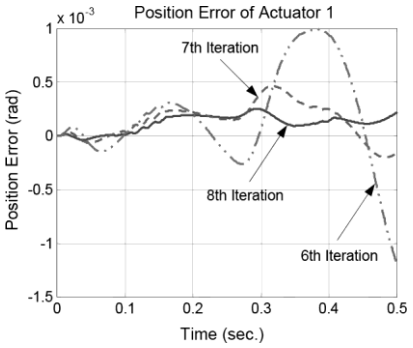


Figure 6. Position tracking performance improvement from iteration to iteration.

the iteration number is increased. Such a property is very useful for the safe use of the actuators and the attenuation of vibration of the controlled plant. It is noted that this property was missed in the switching technique in the time domain.

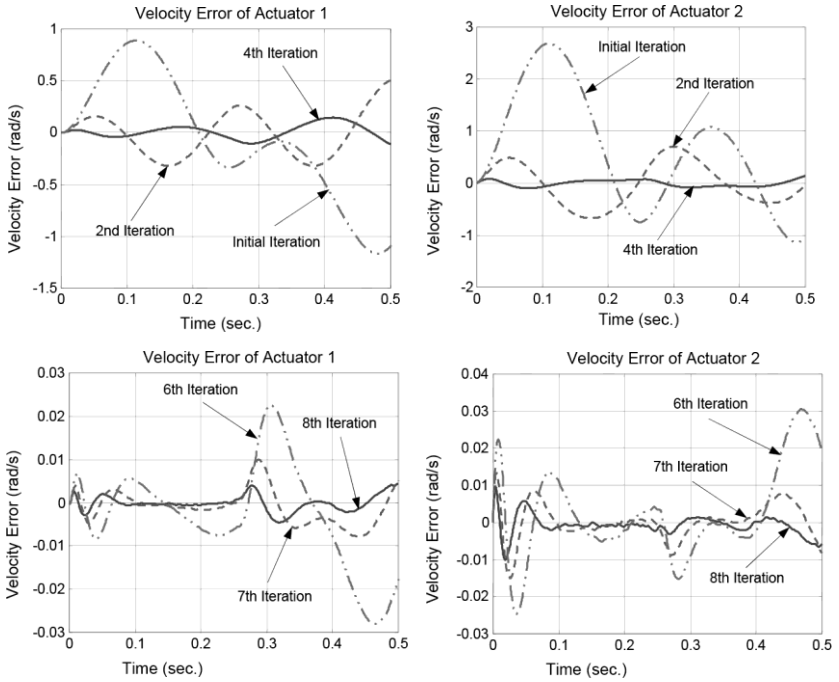


Figure 7. Velocity tracking performance improvement from iteration to iteration.

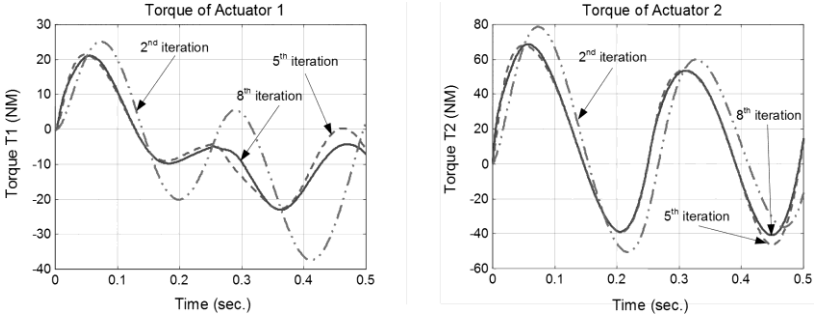


Figure 8. The required torque profiles for iteration j = 2,5,8.

SPD-PD Results

A. Simulation of Nonlinear System

In this section, we apply the proposed SPD-PD ILC algorithm for trajectory tracking control of a nonlinear system to improve its tracking performance through repetitive

operations. The simulation example used in (Chen et al. 1996b) is adopted for the purpose of comparison. The nonlinear system is described by

$$\begin{bmatrix} \dot{x}_{1k}(t) \\ \dot{x}_{2k}(t) \end{bmatrix} = \begin{bmatrix} 1 & 0 \\ 0 & 2 \end{bmatrix} \begin{bmatrix} u_{1k}(t) \\ u_{2k}(t) \end{bmatrix} + \begin{bmatrix} \sin(x_{2k}(t)) & 1+\sin(x_{1k}(t)) \\ 2-5t & \cos(2\pi f_0 t) \end{bmatrix} \begin{bmatrix} x_{1k}(t) \\ x_{2k}(t) \end{bmatrix} + (0.5+k\alpha_0) \begin{bmatrix} 3-2t & 0 \\ 4 & \cos(2\pi f_0 t) \end{bmatrix} \begin{bmatrix} x_{1k}(t) \\ x_{2k}(t) \end{bmatrix} + (0.5+k\alpha_0) \begin{bmatrix} 0 & \sin(2\pi f_0 t) \\ 1 & 2\sin(4\pi f_0 t) \end{bmatrix}$$

$$\begin{bmatrix} y_{1k}(t) \\ y_{2k}(t) \end{bmatrix} = \begin{bmatrix} 1 & 0 \\ 0 & 1 \end{bmatrix} \begin{bmatrix} x_{1k}(t) \\ x_{2k}(t) \end{bmatrix}$$

With f = 5 Hz. The desired tracking trajectories are set as

$$y_d(t) = \begin{bmatrix} y_{1d}(t) \\ y_{2d}(t) \end{bmatrix} = \begin{bmatrix} t^2 \\ 1-t \end{bmatrix} \quad \text{for } t \in [0,1]$$

To test the robustness of the proposed SPD-PD ILC algorithm, several simulation experiments are conducted using different control gains and learning gains. For all the cases, the initial states are set as $x_1(0) = 0.3$, and $x_2(0) = -0.3$. That means there are some initial state errors. Also, we assume the matrix B in the initial state learning schedule Eq. (27) is not accurate (The estimated value is 0.4B). In the following sections, the classic PD ILC is obtained from control law Eq. (22) by setting $K_{p1}(0) = K_{d1}(0) = 0$.

Example 1. *Repetitive Uncertainty and Disturbance*

In the first simulation experiment, we set $\alpha_0 = 0$ which means that the uncertainty and disturbance is repetitive from iteration to iteration. The following feedback control gains and learning control gains are chosen:

For classic PD ILC: $K_{p2} = diag\{1,1\}$, $K_{d2} = diag\{0.25, 0.5\}$.

For SPD-PD ILC: $K_{p1}(0) = diag\{0.5, 2.5\}$, $K_{d1}(0) = diag\{1.5\}$, $s(k) = k$ $K_{p2} = 0.6 * diag\{1,1\}$, $K_{d2} = 0.6 * diag\{0.25, 0.5\}$.

Referring to Eq. (21), we have $BC = diag\{4, 2\}$ for this nonlinear system. Therefore, the perfect learning gain is $K_{d2} = diag\{0.25, 0.5\}$ according to Eq. (26) that is used in the classic PD ILC. According to the chosen gains, from Eq. (26) we have $\rho_2 = 0$ for the classic ILC, and $\rho_1 = 0.2$ and $\rho_2 = 0.4$ for the SPD-PD ILC. That means inaccurate knowledge of matrices B and C are considered in the learning control gain design for

the SPD-PD ILC.

Figure 9 shows the maximum tracking error bounds for the proposed SPD-PD ILC and the classic PD ILC from iteration to iteration. From this figure, we can see that the SPD-PD ILC algorithm can obtain a very fast convergence rate (7 iterations) and very small and monotonic decreased tracking errors. But for the classic PD ILC case, although the best learning gain K_{d2} is used (as $\rho_2 = 0$), the tracking error bounds were still in a good-bad-good mode before reaching a stable boundedness, and more iterations (18 iterations) were needed in order to obtain a relatively acceptable tracking performance. We can see that the tracking errors using PD ILC are still relatively large compared with those using the SPD-PD ILC. Similar results were shown in (Chen et al. 1996b) where more than 20 iterations are needed to achieve a stable tracking performance. This example results demonstrate that the SPD-PD ILC is more powerful in terms of reducing the tracking error and facilitating the convergence.

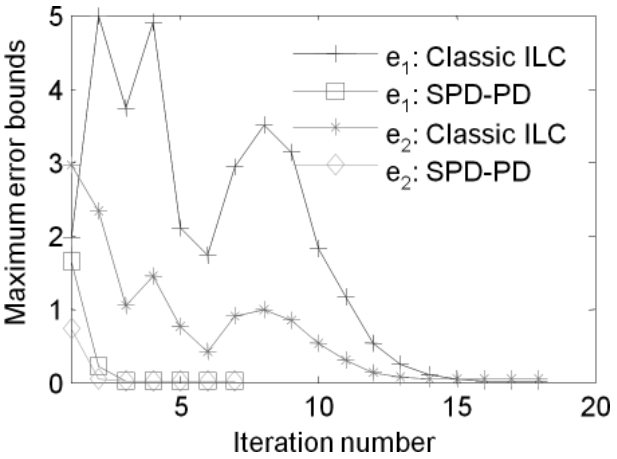


Figure 9. Maximum error bounds for Example 1.

Example 2. *Varying Uncertainty and Disturbance*

In this example, we consider a more general situation where the uncertainty and disturbance are increased from iteration to iteration by set $\alpha_0 = 0.05$. All the feedback control gains and iterative learning gains are set the same as in Example 1. Figure 10 shows the simulation results.

From Fig. 10 we can see that a good tracking performance can be achieved using the SPD-PD ILC algorithm, even in the situations where the uncertainty and disturbance are varied from iteration to iteration. Such a feature can be attributed to the switching gain feedback control which can compensate the disturbance by increasing the control gains from iteration to iteration. But for the classic PD ILC algorithm, there are large stable tracking error bounds (around 0.1 for e_1 and 0.2 for e_2). That is because the classic PD ILC cannot compensate the current iteration disturbance due to the limitation of the offline learning strategy.

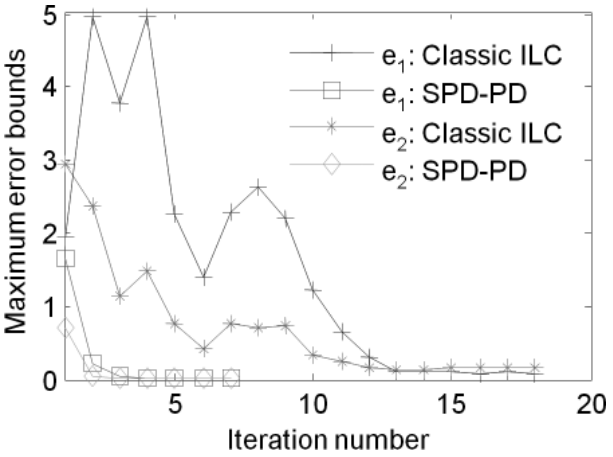


Figure 10. Maximum error bounds for Example 2.

Comparison on Different Feedback Control Gains

To adjust the final tracking error bounds, different feedback control gains are used for the SPD-PD ILC algorithm. In this example, the iterative learning control gains are set the same as the previous two examples. The following feedback control gains are used in the simulation experiments. For all three different gain cases, the switching function is set as $s(k) = k$. The middle gains are chosen the same as in Example 1.

High gains: $K_{p1}(0) = 1.5diag\{0.5,2.5\}$, $K_{d1}(0) = 1.5diag\{1,5\}$ Middle gains: $K_{p1}(0) = diag\{0.5,2.5\}$, $K_{d1}(0) = diag\{1,5\}$ Low gains: $K_{p1}(0) = 0.5diag\{0.5,2.5\}$, $K_{d1}(0) = 0.5diag\{1,5\}$

Table 3 lists the maximum final tracking error bounds under different feedback control gains in the SPD-PD ILC. From this table, we can see that, with the increase of the feedback control gains, the final tracking errors become smaller, and the convergence rate becomes faster. It demonstrates that the control parameter ρ_1 has significant effect
to the convergence rate.

Table 4 shows the final tracking error bounds (stable boundary) for SPD-PD ILC compared to a fixed gain PD-PD ILC ($s(k) = 1$) using the same learning gains. From this table, it is clearly shown that the SPD-PD ILC can obtain much better tracking performance (at least 5 times) even with the existence of the non-repetitive uncertainty and disturbance (Example 2). Figure 11 shows the tracking error bound results from iteration to iteration based on SPD-PD ILC and the fixed gain PD-PD ILC.

From Table 4 and Fig. 11 we can see that the tracking performances can be improved if high feedback control gains are used in the developed SPD-PD ILC algorithm. It also clearly shows that the tracking error bounds monotonically decrease from iteration to iteration.

The Effect of Proportional Gains

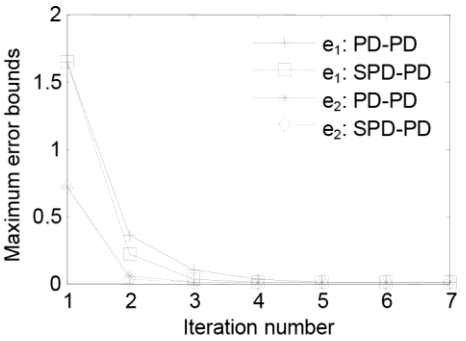
From the convergence analysis conducted in the previous section, we can see that the proportional feedback gain K_{p1} and iterative learning gain K_{p2} are not factors for guaranteeing convergence as they are not included in the convergence condition

Table 3. Comparison of maximum error bounds under different control gains.

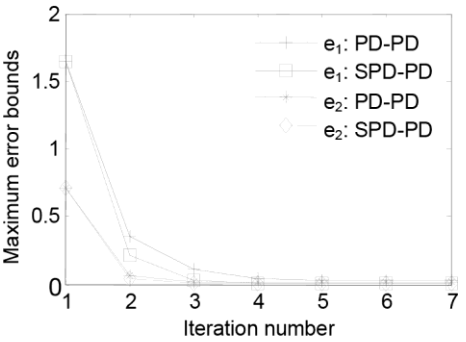
Control	**Example 1**			**Example 2**		
	Iteration	max|e_1|	max|e_2|	Iteration	max|e_1|	max|e_2|
Low gains	9	0.0005	0.0007	10	0.0058	0.0034
Mid. gains	7	0.0003	0.0007	7	0.0039	0.0022
High gains	6	0.0003	0.0006	6	0.0032	0.0017

Table 4. Comparison maximum error bounds for SPD-PD and PD-PD learning control.

Control	**Example 1**			**Example 2**		
	Iteration	max|e_1|	max|e_2|	Iteration	max|e_1|	max|e_2|
PD-PD	7	0.0023	0.0038	7	0.0241	0.0125
SPD-PD	7	0.0003	0.0007	7	0.0039	0.0022



(a) Tracking error bounds for Example 1.



(b) Tracking error bounds for Example 2.

Figure 11. Comparison of SPD-PD and PD-PD learning control.

Eq. (26). Therefore, it is a good point to examine the effect of proportional gains on the tracking performance improvement. Figure 12 shows one simulation result of the tracking error bounds from iteration to iteration using SPD-PD ILC, SD-PD ILC (K_{p1} = 0), SPD-D ILC (K_{p2} = 0), and SD-D ILC (K_{p1} = K_{p2} = 0), respectively. It is clearly shown that K_p gains have effect only on the first few (3 in this simulation) iterations. After that, K_p gains make little contribution to the convergence rate of the system. The simulation results show that the final tracking error bounds using these four learning control laws are almost the same.

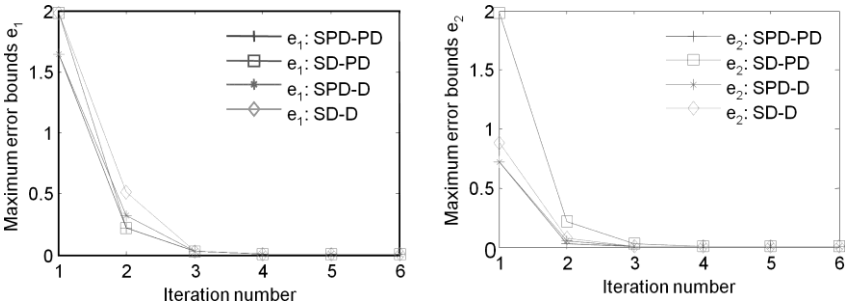


Figure 12. Effect of proportional control gains on convergence rate.

B. Simulation of Trajectory Tracking for a Planar Robotic System

It's well known that the dynamic model of a robotic system can be expressed as a second-order differential equation. If we introduce some state variables, the second-order differential equation can be easily transformed to a first-order nonlinear system expressed in (1). Therefore, the proposed SPD-PD ILC can be applied to tracking control of the robotic system. In this chapter, a 2-DOFs revolute planar robot discussed in (Choi and Lee 2001) is simulated for the trajectory tracking control, and the structural parameters of the robotic system can be found in Table 1.

The desired trajectories and the disturbances for both links are chosen as:

$$\begin{bmatrix} q_{1d} \\ q_{2d} \end{bmatrix} = a \begin{bmatrix} \sin 3t + 1 \\ \cos 3t + 2 \end{bmatrix} \quad \begin{bmatrix} 0.3\sin t \\ 0.1(1-e^{-t}) \end{bmatrix} \quad t \in [0,5]$$

Tracking Performance Improvement from Iteration to Iteration

In this simulation experiment, the feedback control gains and iterative learning gains are set as:

$K_{p1}(0) = K_{d1}(0) = diag\{20,10\}$ and $K_{p2} = K_{d2} = diag\{10,5\}$.

The switching function is set as $s(k) = 2k$, and the disturbance factor is $\alpha = 10$.

Figures 13 and 14 show the trajectory tracking performance improvements and the required control torques from iteration to iteration for joint 1 and joint 2, respectively. At the first iteration, there are very large tracking errors for both joints, and the required control torques are irregular. After 3 iterations, the tracking performances improved dramatically. After 5 iterations, we can see that the controlled joint motions are very close to the desired ones, while the required torques show the desired periodic features. Figure 15 shows the maximum tracking error bounds from iteration to iteration. From Fig. 15 we can see that the tracking errors decrease monotonically

from iteration to iteration. Simulation results show that only 14 iterations are needed to achieve a very good tracking performance (maximum errors are 1.75E-4 and 4.75E-5 for joints 1 and 2 from Table 5, respectively), while the maximum error bounds are 0.0041 and 0.0046 for joints 1 and 2 after 30 iterations using the control law developed in Choi and Lee 2000. Therefore, the SPD-PD ILC has a fast convergence rate, small tracking error bounds, and no vibration in the actuators. These figures demonstrate the effectiveness of the SPD-PD ILC for the trajectory tracking control of robotic systems.

Robustness for Rejecting Disturbance

To verify the effectiveness and robustness of the SPD-PD algorithm for the rejection of disturbances, different levels of disturbances are introduced in the dynamic model by adjusting the parameter α. Table 5 lists the maximum tracking error bounds for three different levels of disturbances. It shows that all the finally tracking error bounds after a few iterations (9 iterations in this example) are almost the same. From this table, we can conclude that the proposed SPD-PD ILC algorithm is robust to the disturbances.

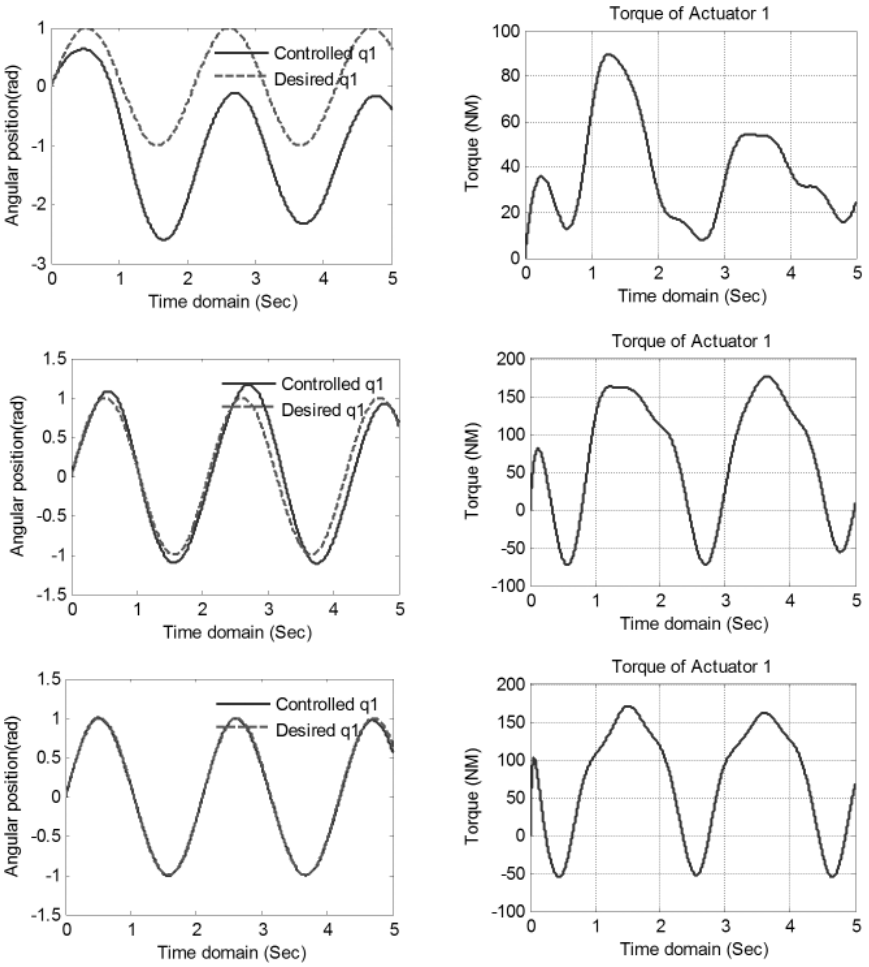


Figure 13. Tracking performance and controlled torque for joint 1 (the first, third and fifth iteration).

Table 5. Maximum tracking errors for two joints.

Iteration	**Maximum tracking error for joint 1**			**Maximum tracking error for joint 2**		
	$\alpha = 0$	$\alpha = 10$	$\alpha = 50$	$\alpha = 0$	$\alpha = 10$	$\alpha = 50$
1	1.6807	1.7112	1.8404	0.5812	0.6026	0.7363
3	0.3579	0.3578	0.3565	0.1096	0.1122	0.1213
6	0.0137	0.0136	0.013	0.0034	0.0033	0.0034

			5			
9	0.001	0.001	0.001	2.93E-4	2.92E-4	2.93E-4
12	3.13E-4	3.14E-4	3.04E-4	8.81E-5	8.90E-5	8.68E-5
14	1.76E-4	1.74E-4	1.82E-4	4.75E-5	4.75E-5	5.17E-5

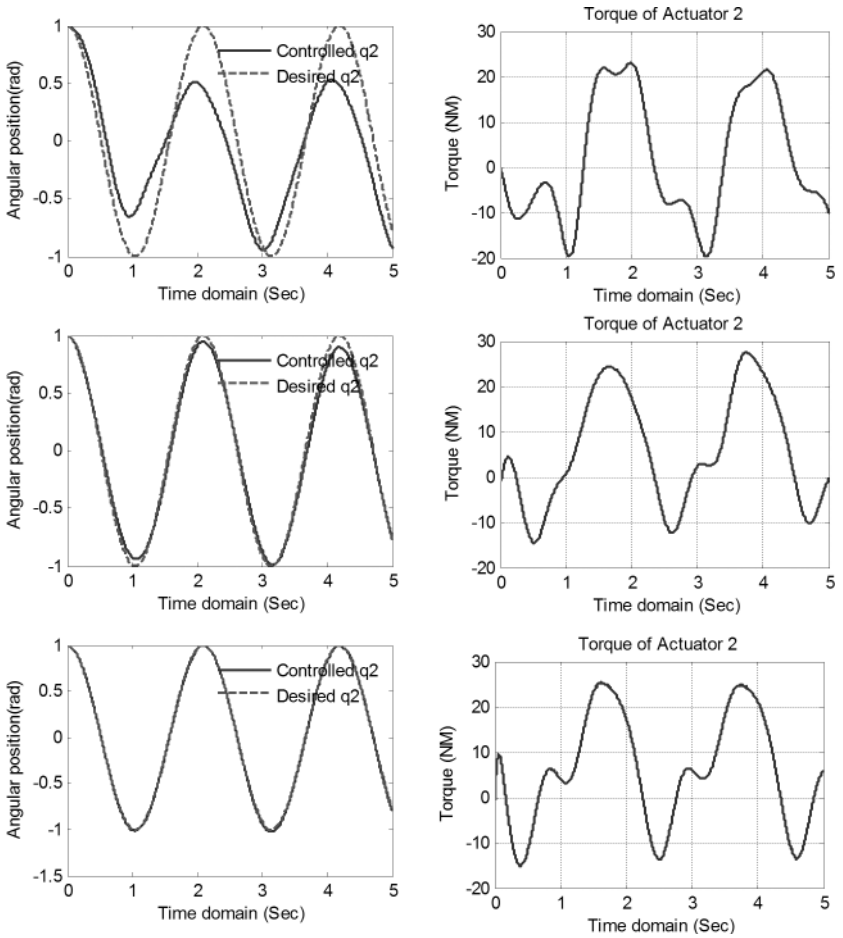


Figure 14. Tracking performance and controlled torque for joint 2 (the first, third and fifth iteration).

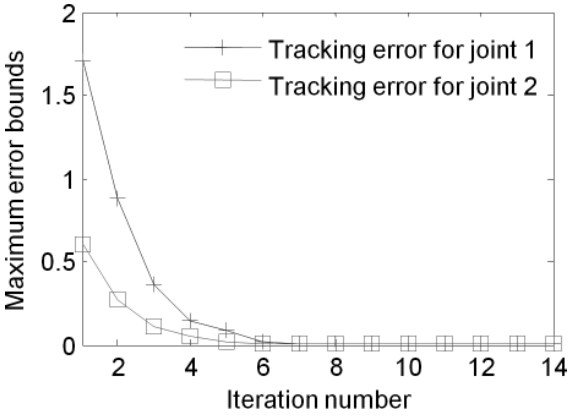


Figure 15. Tracking error bounds from iteration to iteration.

EXPERIMENTAL VERIFICATIONS OF ASL-PD CONTROL

In this section, some experiments are conducted to verify the effectiveness of the proposed ASL-PD for trajectory tracking control of a parallel robot manipulator, and comparison results are presented under different operation conditions.

Experimental Setup

A 2 DOF parallel robot manipulator shown in Fig. 16 was used to test the effectiveness of the ASL-PD control for the trajectory tracking where two servomotors drive the two input links directly. Table 6 lists the mechanical properties of the parallel robot manipulator.

The distance between the axes of servomotors 1 and 2, denoted by Link 5, is adjustable. In this study, it length is set to be 0.211 *m* in order to ensure the full rotatability of the robot manipulator. The sensors used to measure the rotation angles of the servomotors are incremental encoders with a resolution of 8000 pulses per revolution. The measured angular position is fed back and compared to the desired input. The difference between the desired position and the measured one is termed the position error. The velocity information is obtained from the measured positions by using the backwards finite-difference method. Based on the position error and the velocity information, the computer generates a voltage signal by using a given control law. This voltage signal is in turn sent to the Galil^{TM} motion analyzer, the servo amplifiers, and then to the servomotors to generate the required torques.

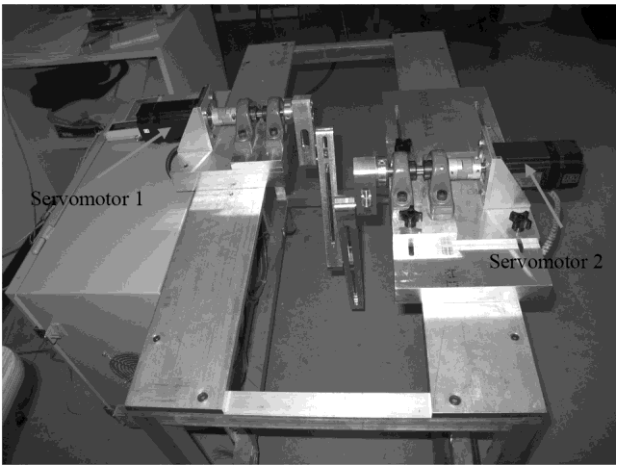


Figure 16. Parallel robot manipulator test bed.

Table 6. Parameters of the 2 DOF parallel robot manipulator.

	m_i(m)	r_i(m)	L_i(m)	4(m⁴)	
Link 1	0.2258	0.0342	0.0894	2.17	× 10–4
Link 2	0.2623	0.0351	0.0943	3.14	× 10–4
Link 3	0.4651	0.1243	0.2552	3.11	× 10–3
Link 4	0.7931	0.2454	0.2352	1.67	× 10–2
Link 5	0.2110	0	0	0	

Trajectory Planning for Servomotors

The trajectory tracking of a robot manipulator can be performed in either Cartesian space (i.e., trajectory of the end-effector) or joint space (i.e., trajectory of the motors). However, regardless of the trajectory tracking approach, since the control of a robot is performed at the joint level, the conversion of the end-effector coordinates to joint coordinates is essentially required. This section is concerned with the joint or actuator trajectory tracking. For the purposes of this study, the desired trajectories of the two servomotors are planed as functions of time. In particular, this function is a Hermite polynomial of the fifth degree with continuous bounded conditions for position, velocity, and acceleration, which is adopted from (Ouyang 2005). The mathematical expression of the trajectories for two servomotors are given by, respectively,

$$q_1^d(t) = q_{10}^d + (6\left(\frac{t}{t_f}\right)^5 - 15\left(\frac{t}{t_f}\right)^4 + 10\left(\frac{t}{t_f}\right)^3)(q_{1f}^d - q_{10}^d)$$

$$q_2^d(t) = q_{20}^d + (6\left(\frac{t}{t_f}\right)^5 - 15\left(\frac{t}{t_f}\right)^4 + 10\left(\frac{t}{t_f}\right)^3)(q_{2f}^d - q_{20}^d)$$

where $q_1^d(t)$ and $q_2^d(t)$ are the desired trajectories of the two servomotors, q_{10}^d, q_{1f}^d, q_{20}^d, and q_{2f}^d are the desired initial and final positions of the servomotors, respectively, and t_f represents the time period required for the servomotors to reach the desired final position. In this study, the initial positions for the two servomotors is set $q_{10}^d = 0$ and $q_{20}^d = 0$ for simplification; and two cases with different operating speeds are investigated experimentally. In the first case, the robot manipulator is operated at a lower speed with

$$t_f = 4\text{sec} \quad \text{and} \quad q_{1f}^d = \frac{p}{2}, \quad q_{1f}^d = p$$

Thus, the motor speed is $\omega = 60/(4 \times 4) = 3.75$ rpm for this case. In the second case, the robot manipulator is operated at a higher speed with

$t_f = 2\text{sec}$ $q_{1f}^d = \pi$, and $q_{2f}^d = \pi$

Thus, the motor speed is $\omega = 60/(2 \times 2) = 15$ rpm for this case. For convenience, the first case is referred to as the low speed case and the second one as the high speed case in the rest of this section.

ASL-PD Control Law Results

In the experiments for the ASL-PD control, the initial PD control gains and the switching factor β are selected as follows:

For the low speed case:

Servomotor 1: $K_{p1} = 0.000022$, $K_{d1} = 0.000002$, $\beta = 2.5$
Servomotor 2: $K_{p1} = 0.000036$, $K_{d1} = 0.000004$, $\beta = 2.5$

For the high speed case:

Servomotor 1: $K_{p1} = 0.000052$, $K_{d1} = 0.0000052$, $\beta = 2$
Servomotor 2: $K_{p1} = 0.000048$, $K_{d1} = 0.0000062$, $\beta = 2$

It can be seen that the initial PD control gains of the ASL-PD control are selected to be the same as that of the adaptive NPD-LC control. The reason for this is to be able to compare the performance improvement and the convergence rate of different ILC control techniques. Figure 17 shows the tracking errors from iteration to iteration for the low speed case. From this figure, one can see that the tracking performances are improved from iteration to iteration under the ASL-PD control. Tables 7 and 8 show the experimental results for the maximum absolute tracking errors and required torques at low and high speed cases from iteration to iteration.

From these results it is clear how the position tracking errors are reduced from one iteration to the next. At low speeds, for the first iteration, the maximum tracking errors were 0.324 rad and 0.278rad for servomotors 1 and 2, respectively. After 6 iterations, the maximum tracking error was about 0.009 rad for both servomotors. The tests at

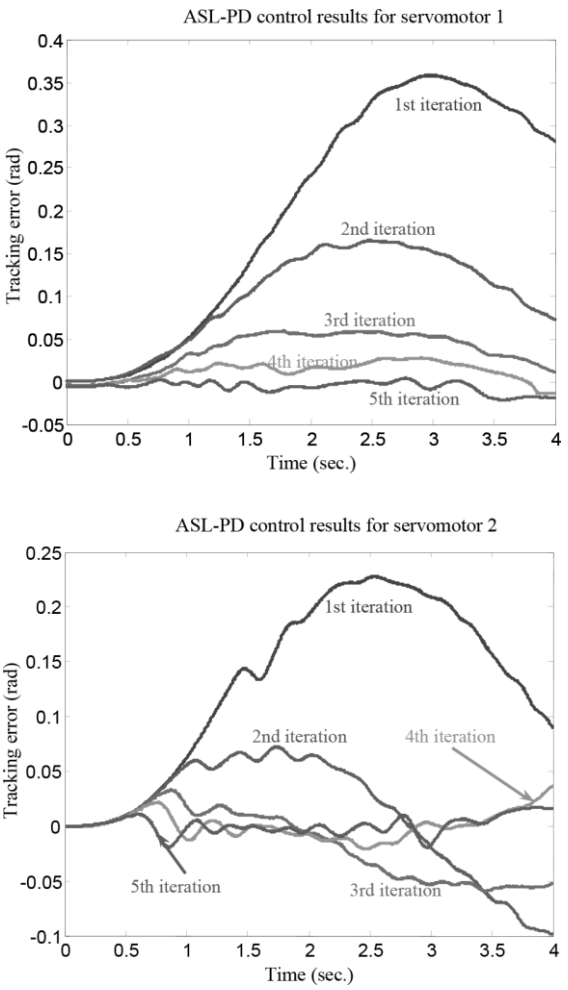


Figure 17. ASL-PD control results from iteration to iteration for low-speed case.

high speeds also demonstrated similar conclusions regarding the reduction in errors using the ASL-PD control method. In this case, for the first iteration, the maximum tracking errors were 0.135 rad and 0.110 rad for actuators 1 and 2, respectively. After 4 iterations, the maximum tracking errors were 0.017 rad and 0.016 rad for joints 1 and 2, respectively. The above figures and discussion provide a clear presentation of the effectiveness of the ASL-PD control law at both high and low speeds.

Table 7. Performance improvement with the ASL-PD control at low-speed case.

Generation	max abs(e_1)	max abs(e_2)	max abs(T_1)	max abs(T_2)
Iteration 1	0.324	0.278	0.023	0.027
Iteration 2	0.107	0.076	0.021	0.025
Iteration 3	0.045	0.055	0.022	0.022
Iteration 4	0.029	0.012	0.020	0.019
Iteration 5	0.019	0.010	0.021	0.020
Iteration 6	0.009	0.009	0.022	0.020

Table 8. Performance improvement with the ASL-PD control at high-speed case.

Generation	max abs(e_1)	max abs(e_2)	max abs(T_1)	max abs(T_2)
Iteration 1	0.135	0.110	0.054	0.051
Iteration 2	0.034	0.047	0.052	0.052
Iteration 3	0.020	0.032	0.049	0.048
Iteration 4	0.017	0.016	0.050	0.051

Comparison of the ASL-PD and the Adaptive NPD-LC

As shown in Ouyang 2005, the adaptive NPD-LC and the ASL-PD control could be used to improve the tracking performance of the parallel robotic manipulator. It should be

noted that the convergence rate was different for these two learning control laws. Generally speaking, the ASL-PD control has a faster convergence rate than the adaptive NPD-LC. Figure 18 shows the comparison results obtained from the experiments. From this figure, one can see that the tracking errors after 5 iterations using the ASL-PD control were smaller than the tracking errors after 7 iterations using the adaptive NPD- LC. Such a conclusion agrees with the theoretical analysis and the simulation results as presented in Ouyang 2005. Therefore, through experiment studies for a parallel robot manipulator, the effectiveness of the ASL-PD control is demonstrated for trajectory tracking control under different operation conditions.

CONCLUSIONS

In this chapter, a new adaptive switching learning PD (ASL-PD) control method is proposed. This control method is a simple combination of a traditional PD control with a gain-switching strategy as feedback and an iterative learning control using the input torque profile obtained from the previous iteration as feedforward. The ASL-PD control incorporates both adaptive and learning capabilities; therefore, it can provide an incrementally improved tracking performance with the increase of the iteration number. The ASL-PD control method achieves the asymptotic convergence based on the Lyapunov's method. The position and velocity tracking errors monotonically decrease with the increase of the iteration number. The concept of integrating the switching

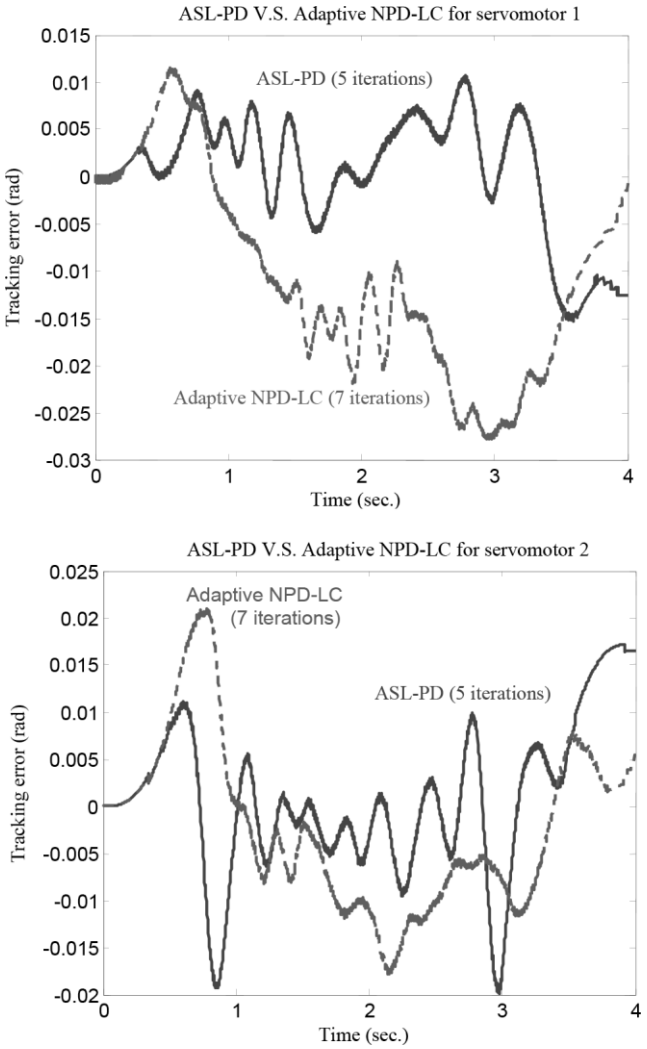


Figure 18. Comparing results of the adaptive NPD-LC and the ASL-PD.

technique and the iterative learning scheme works very well. The simulation study has demonstrated the effectiveness of the ASL-PD control method. Its distinct features are the simple structure, easy implementation, fast convergence, and excellent performance.

In addition, a new iterative learning control called SPD-PD ILC is also proposed that is a combination of a PD feedback

control with switching control gains in the iteration domain and a PD-type ILC based on the previous iteration information in the updating control law. The proposed SPD-PD ILC takes the advantages offered by feedback control and iterative learning control. The proposed control law uses the current and previous system information to enhance the stability characteristics and quickly drive the tracking trajectories to the desired ones within bounds. The new SPD-PD ILC achieves tracking accuracy with very fast convergence rate and is robust against

unpredictable disturbances and uncertainties by adjusting the feedback control gains. In addition, the SPD-PD ILC can provide extra degrees of freedom for the choices of the learning gains. The final tracking error bounds and the convergence rate can be adjusted by the switching gain of the PD feedback control that makes this control scheme more promising from a practical viewpoint. Nonlinear systems and a planar robotic system are used as examples to test the effectiveness of the proposed SPD-PD ILC.

Finally, the control strategies have been implemented and tested on an experimental environment of a 2 DOF parallel robot manipulator. The performances of the developed control strategies have been evaluated in terms of tracking performances. The experimental results show that the ASL-PD control results in the best performance in terms of tracking errors and iteration generations.

ACKNOWLEDGMENT

This work was supported by the Natural Sciences and Engineering Research Council of Canada (NSERC) to the authors.

REFERENCES

Ahn, H. S., Y. Q. Chen and K. L. Moore. 2007. Iterative learning control: brief survey and categorization. IEEE Transactions on Systems, Man and Cybernetics Part C: Applications and Reviews, 37(6): 1099–1121.

Amann, N., D. H. Owens and E. Rogers. 1995. Iterative learning control for discrete time systems using optimal feedback and feedforward actions. Proc. of the 34th Conference on Decision & Control, pp. 1696–1701.

Arimoto, S., S. Kawamura and F. Miyasaki. 1984. Bettering operation of robots by learning. Journal of Robotic Systems, 1(2): 123–140.

Bristow, D. A., M. Tharayil and A. G. Alleyne. 2006. A survey of iterative learning control: a learning- based method for high-performance tracking control. IEEE Control Systems Magazine, 26(3): 96–114.

Cai, Z., C. T. Freeman, P. L. Lewin and E. Rogers. 2008. Experimental comparison of stochastic iterative learning control. Proceedings of the American Control Conference, pp. 4548–4553.

Chen, Q. J., H. T. Chen, Y. J. Wang and P. Y. Woo. 2001. Global stability analysis for some trajectory tracking control schemes of robotic manipulators. Journal of Robotic Systems, 18(2): 69–75.

Chen, Y. Q. and K. L. Moore. 2002. An optimal design of PD-type iterative learning control with monotonic convergence. Proceedings of IEEE International Symposium on Intelligent Control, pp. 55–60.

Chen, Y. Q. and K. L. Moore. 2002. PI-type iterative learning control revisited. pp. 2138–2143. *In*: Proceedings of the American Control Conference, Anchorage, AK, USA.

Chen, Y. Q., J. X. Xu and T. H. Lee. 1996a. Current iterative tracking error assisted iterative learning control of uncertain discrete-time systems. Proceedings of the IEEE Conference on Decision and Control, pp. 2355–3592.

Chen, Y. Q., J. X. Xu and T. H. Lee. 1996b. An iterative learning controller using current iteration tracking error information and initial state learning. Proc. of 35th IEEE Conf. Decision and Control, pp. 3064–3069.

Choi, J. Y. and J. S. Lee. 2000. Adaptive iterative learning control of uncertain robotic systems. IEE Proc. Control Theory Application, 147(2): 217–223.

Craig, J. J. 1986. Introduction to robotics: mechanics and control. Reading, Addison-Wesley, MA. Craig, J. J. 1988. Adaptive control of mechanical manipulators, Addison-Wesley.

Doh, T. Y., J. H. Moon, K. B. Jin and M. J. Chung. 1999. Robust iterative learning control with current feedback for uncertain linear systems. International Journal of Systems Science, 30(1): 39–47.

Fu, M. and B. R. Barmish. 1986. Adaptive stabilization of linear systems via switching control. IEEE Trans. on Automatic Control, 31(6): 1097–1103.

Kang, M. K., J. S. Lee and K. L. Han. 2005. Kinematic path-tracking of mobile robot using iterative learning control. Journal of Robotic Systems, 22(2): 111–121.

Kawamura, S., F. Miyazaki and S. Arimoto. 1988. Realization of robot motion based on a learning method. IEEE Trans. on Systems, Man, and Cybernetics, 18(1): 126–123.

Kerry, R. 1997. PD control with desired gravity compensation of robotic manipulators: a review. The International Journal of Robotics Research, 16(5): 660–672.

Kuc, T. Y., K. Nam and J. S. Lee. 1991. An iterative learning control of robot manipulators. IEEE Trans. on Robotics and Automation, 7(6): 835–842.

Li, Q., A. N. Poo, C. L. Teo and C. M. Lim. 1996. Developing a neuro-compensator for the adaptive control of robots. IEE Proc. Cont. Theory and Appl., 142(6): 562–568.

Li, Q., S. K. Tso and W. J. Zhang. 1998. Trajectory tracking control of robot manipulators using a neural-network-based torque-compensator. Proceedings of I. Mech. E, Part I, J. of System and Control, 212(5): 361–372.

Longman, R. W. 2000. Iterative learning control and repetitive control for engineering practice.
International Journal of Control, 73(10): 930–954.

Madady, A. 2008. PID type iterative learning control with optimal gains. International Journal of Control, Automation, and Systems, 6(2): 194–203.

Martensson, B. 1985. The order of any stabilizing regulator is sufficient a priori information for adaptive stabilizing. Systems & Control Letters, 6(2): 87–91.

Middleton, R. H., G. C. Goodwin, D. J. Hill and D. Q. Mayne. 1988. Design issues in adaptive control.
IEEE Trans. on Automatic Control, 33(1): 50–58.

Moore, K. L., M. Dahleh and S. P. Bhattacharyya. 1992. Iterative learning control: a survey and new results. Journal of Robotic Systems, 9(5): 563–594.

Norrlöf, M. and S. Gunnarsson. 2005. A note on causal and CITE iterative learning control algorithms.
Automatica, 41(2): 345–350.

Nussbaum, R. D. 1983. Some remarks on a conjecture in parameter adaptive control. Systems & Control Letters, 3:

243–246.
Ouyang, P. R. 2005. Integrated design, modeling, and control of hybrid systems, Ph.D. Dissertation, University of Saskatchewan, Saskatoon, Canada.
Ouyang, P. R. 2009. PD-PD type learning control for uncertain nonlinear systems. The 2009 ASME International Design Engineering Technical Conferences and Computers and Information in Engineering Conference, pp. 699–707.
Ouyang, P. R., Q. Li, W. J. Zhang and L. S. Guo. 2004. Design, modelling and control of a hybrid machine system. Mechatronics, 14(10): 1197–1217.
Ouyang, P. R., B. A. Petz and F. F. Xi. 2011. Iterative learning control with switching gain feedback for nonlinear systems. ASME Journal of Computational and Nonlinear Dynamics, 6(1): 011020–7. Ouyang, P. R. and P. Pipatpaibul. 2010. Iterative learning control: a comparison study. ASME 2010 International Mechanical Engineering Congress and Exposition, 8: 939–945.
Ouyang, P. R. and W. J. Zhang. 2005. Force balancing of robotic mechanisms based on adjustment of kinematic parameters. ASME Journal of Mechanical Design, 127(3): 433–440.
Ouyang, P. R., W. J. Zhang and M. M. Gupta. 2006. An adaptive switching learning control method for trajectory tracking of robot manipulators. Mechatronics, 16(1): 51–61.
Ouyang, P. R., W. J. Zhang and M. M. Gupta. 2007. PD-type on-line learning control for nonlinear system with uncertainty and disturbance. Control and Intelligent Systems, 35(6): 351–358.
Owens, D. H. and G. S. Munde. 1998. Universal adaptive iterative learning control. Proc. of the 37th IEEE Conference on Decision & Control, pp. 181–185.
Park, K. H. 2005. An average operator-based PD-type iterative learning control for variable initial state error. IEEE Trans. on Automatic Control, 50(6): 865–869.
Park, K. H., Z. Bien and D. H. Hwang. 1999. A study on the robustness of a PID-type iterative learning controller against initial state error. International Journal of Systems Science, 30(1): 49–59.
Pi, D. Y., S. Seborg, J. Shou, Y. Sun and Q. Lin. 2000. Analysis

of current cycle error assisted iterative learning control for discrete nonlinear time-varying systems. IEEE International Conference on Systems, Man, and Cybernetics, 5: 3508–3513.

Qu, Z. H. 1995. Global stability of trajectory tracking of robot under PD control. Dynamics and Control, 5(1): 59–71.

Qu, Z. H., J. Dorsey, M. Dawson and R. W. Johnson. 1991. A new learning control scheme for robots.

Proceedings of the 1991 IEEE ICRA, pp. 1463–1468.

Slotine, J. J. and W. Li. 1987. On the adaptive control of robot manipulators. The International Journal of Robotics Research, 6(3): 49–59.

Song, Z. Q., J. Q. Mao and S. W. Dai. 2005. First-order D-type iterative learning control for nonlinear systems with unknown relative degree. ACTA Automatica Sinca, 31(4): 555–561.

Sun, D. and J. K. Mills. 1999. Performance improvement of industrial robot trajectory tracking using adaptive-learning scheme. Trans. of the ASME, Journal of Dynamic Systems, Measurement and Control, 121(2): 285–292.

Sun, M. and D. Wang. 2002. Closed-loop iterative learning control for nonlinear systems with initial shifts. International Journal of Adaptive Control and Signal Processing, 16(7): 515–538.

Tayebi, A. 2003. Adaptive iterative learning control for robot manipulators. pp. 4518–4523. *In*: Proceedings of the American Control Conference, Denver, CO, USA.

Tomei, P. 1991. Adaptive PD controller for robot manipulators. IEEE Trans. on Robot and Automation, 7(4): 565–570.

Xu, J. X., T. H. Lee and H. W. Zhang. 2004. Analysis and comparison of iterative learning control schemes. Engineering Applications of Artificial Intelligence, 17(6): 675–686.

Xu, J. X., X. W. Wang and L. T. Heng. 1995. Analysis of continuous iterative learning control systems using current cycle feedback. Proceedings of the American Control Conference, pp. 4221–4225.

Xu, J. X., L. Sun, T. Chai and D. Tan. 2004. High-order open and closed loop iterative learning control scheme with initial state learning. 8th International Conference on Control, Automation, Robotics and Vision, pp. 637–641.

Yan, X. G., I. M. Chen and J. Lam. 2001. D-type learning control for nonlinear time-varying systems with unknown initial states and inputs. Trans. of the Institute of Measurement and Control, 23(2): 69–82.

Yu, S. J., J. H. Wu and X. W. Yan. 2002. A PD-type open-closed-loop iterative learning control and its convergence for discrete systems. Proceedings of the First International

Conference on Machine Learning and Cybernetics, pp. 659–662.

Zhang, B., G. Tang and S. Zheng. 2006. PD-type iterative learning control for nonlinear time-delay system with external disturbance. Journal of Systems Engineering and Electronics, 17(3): 600–605.

15

Adaptive Robust Control Design for Robot Manipulators Based on Online Estimation of the Lumped Time-Varying Model Uncertainties

Meysar Zeinali[1,*] and *Ebrahim Esmailzadeh*[2]

ABSTRACT

This chapter presents a systematic method to design an adaptive robust control based on online estimation of the lumped time-varying model uncertainties for tracking control of the robot manipulators. The proposed adaptive robust control methodology is based on approaches developed in recent publications, which allows eliminating the chattering while retaining the system robustness in the presence of bounded time-varying uncertainties. By online estimation of the lumped model uncertainties, main drawbacks of conventional robust sliding mode control, and adaptive control of manipulators namely: the chattering phenomenon; the requirement for a priori knowledge of the bounds of the uncertainties, and the requirement for linearly parameterized dynamic model of the manipulator with known constant bound of the parameters are addressed. The global stability and robustness of the proposed controller are established in the presence of time-varying uncertainties using

Lyapunov's approach and

1 School of Engineering, Mechanical and Mchatronics Program, Laurentian University, Sudbury,
Ontario, P3E 2C6, Canada.
E-mail: mzeinali@laurentian.ca
2 Department of Automotive, Mechanical and Manufacturing Engineering, Faculty of Engineering and Applied Science.
E-mail: Ebrahim.Esmailzadeh@uoit.ca
* Corresponding author

fundamentals of sliding mode theory. Based on the simulations and experimental results, the proposed controller performs remarkably well in comparison to adaptive control in terms of the tracking error convergence and robustness against un-modeled dynamics, external disturbances, and time-varying parameters and its high performance and simplicity makes this method attractive for industrial applications.

Keywords: Adaptive robust control, chattering-free sliding mode control, robot manipulator, nonlinear uncertain system, estimation of uncertainties

INTRODUCTION

Many dynamic systems such as robot manipulators to be controlled have unknown or time-varying uncertain parameters. For instance, it is impossible or very difficult to obtain an exact dynamic model of the robot manipulator, due to the presence of large flexibility, Coulomb friction, backlash, unknown disturbances, large dynamic coupling between different links, and time-varying parameters such as parameters relating to the robot age (tear and wear) which are all uncertain to some extent, or robot manipulators may carry large payload with unknown inertial parameters or joint friction dependent on the operating condition or various adjustment (Slotine and Li 1991). To deal with uncertainties, in the last few decades, much research effort has been devoted to the design or improvement of the controller of uncertain systems (Gutman 1979, Chandrasekharan 1996, Zhou et al. 1996). Some of the main components of nonlinear robust control methods are sliding mode control (SMC), (Utkin 1977), adaptive control (AC) (Slotine and Li 1991), and adaptive sliding mode control (ASMC), (Zeinali and Notash 2010, Zeinali 2015). Generally, the basic objective of adaptive control is to maintain performance and stability of the closed-loop system in the presence of structured uncertainties (i.e., parametric uncertainties), and unstructured uncertainties (i.e., un-modeled dynamic and external disturbances). The traditional

approach to achieve above objective is on-line estimation of the uncertain parameters or equivalently, the corresponding controller parameters, based on the system performance, and measured system signals and then using the estimated parameters to compute the control input (Slotine and Li 1991). This approach requires linearly parameterized model of the robot manipulator or controller, which may lead to a large number of parameters.

The adaptive control strategies proposed in Craig et al. 1987, Sadegh and Horowitz's 1987, Slotine and Li 1991, mainly addressing the difficulties arising from parametric uncertainty, and the controller proposed in (Seraji 1987) requires linearized model of the manipulator for each operating point and it is based on model reference adaptive control (MRAC). The work by Craig et al. and Sadegh and Horowitz are based on the generalization of the computed torque (inverse dynamic) approach and the objective of the adaptive controller of this class is to render the closed-loop system linear and decupled even though the parameters are unknown. The adaptive controller of Slotine and Li is conceptually different from the adaptive inverse dynamic approach in the sense that the controller does not feedback linearize the closed-loop system, while the proposed controller has the advantages of both approaches. As will be shown perfect linearization can be achieved in the presence of slowly time-varying uncertainties, and approximately linearized closed-loop can be obtained in the presence of time-varying uncertainties.

The adaptive robust controller presented in this chapter is designed using the theory of the sliding mode controller, since SMC have widely been used in many applications due to their capability to deal with uncertainties, good transient performance and their simplicity (Utkin 1977). One of the underlying assumptions in the SMC is that the control input can be switched from one value to another infinitely fast. In practice switching is not instantaneous, because finite delays are inherent in all physical actuators (Young et al. 1999). The uncertainties, imperfections in switching devices or delays, lead to high-frequency oscillations called chattering, which can cause a fast breakdown of mechanical elements in actuators, e.g., high wear. It may also excite un-modelled high-frequency dynamics, which may lead to instability. The performance of a SMC is therefore measured by its robustness and severity of chattering. Thus, it is of primary importance to reduce or eliminate the chattering, in order to make SMC to be practical. To reduce or eliminate the chattering, various approaches have been proposed by many researchers which are summarized in (Young et al. 1999, Plestan et al. 2010, Utkin and Poznyak 2013). The first and most commonly cited approach to eliminate the chattering has been the boundary layer method (Slotine and Li 1991), which requires a trade-off between performance and chattering and it is also very difficult to determine the thickness of boundary layer correctly in most cases. In (Boiko et al. 2007) it is proven that the chattering-free property associated with the continuous SMC algorithms proposed in references (Man et al. 1994) and (Yu 1998) is a misconception, and the algorithms can lead to a periodic motions (chattering).

Another issue limiting the application of the sliding mode control is that, a priori knowledge of the upper and lower bounds of the uncertainties (i.e., worst case scenario) is required to obtain robustness and convergence. This issue recently tackled in (Lee and Utkin 2007, Plestan et al. 2010) by proposing online gain adaptation algorithm. However, in both of these approaches tuning of parameter ε is a hard task and controller is discontinuous. According to Young et al. 1999, if uncertainties are sufficiently compensated there is no

need to use discontinuous control law to achieve sliding mode, thus the chattering can be reduced or eliminated if the online estimation of the uncertainties is properly designed. Therefore, an alternative method to reduce or eliminate the chattering and to overcome the drawbacks of using the bounds of uncertainties is to use estimated uncertainties. The above approach has been studied and discussed in Elmali and Olgac 1992, Kim et al. 1998, Curk and Jezernik 2001, Saengdeejing and Qu 2002, Lee and Utkin 2007, Dong et al. 2006, Li and Xu 2010. However, an adaptive and chattering-free SMC based on estimated uncertainties for robot manipulators are not fully developed and due to a lack of a unified systematic approach is remained mainly unsolved.

In uncertainty estimation-based approach, the control law consists of a continuous model-based component and a component constructed based on the estimated uncertainties for compensation of the uncertainties. In this chapter an adaptive robust controller is systematically constructed based on an effective on-line estimation of the lumped time-varying uncertainties using the dynamic behaviour of a sliding function which is defined later. The formulation of the proposed uncertainty estimation is derived from the systematic stability analysis of the closed-loop system using Lyapunov stability method in Section **The Proposed Adaptive Robust Controller Design Methodology** and **Stability Analysis of Closed-Loop System in the Presence of Time-Varying Uncertainties**. The estimated uncertainty term is used to replace the discontinuous component, also called the switching component, of the standard sliding mode control.

This, in turn, eliminates the chattering and the requirements for the bounds of the uncertainties. In this method, trajectories are forced to converge to sliding surface in finite time by suitably adjusting the estimated uncertainty term of the controller.

The remainder of this chapter is organized as follows. Section **Problem Formulation and Definition** presents the system description and problem formulation. Section **The Proposed Adaptive Robust Controller Design Methodology** describes the adaptive robust control design methodology. Stability of the closed-loop system in the presence of the time-varying uncertainties is proven in Section **Stability Analysis of Closed-Loop System in the Presence of Time-Varying Uncertainties**. The Simulation results are presented in Section **Simulation Results**. Section **Experimental Results and Application to a Two-DOF Flexible Link Robot** describes the experimental results and application of the proposed method to a two-DOF Flexible Link robot. Section **Conclusion** concludes the chapter.

PROBLEM FORMULATION AND DEFINITION

Robot Manipulator Dynamics

The dynamic model (equation of motion) of a rigid robot manipulator can generally be described by the following second-order differential equation, in active joint space Codourey 1998, Angeles 2003.

$$\tau = M(q)\ddot{q} + C(q, \dot{q})\dot{q} + F_v(\dot{q}) + g(q) + d(t) \quad (1)$$

where $\tau = [\tau_1, \tau_2, ..., \tau_n]^T$ is the vector of joints generalized forces (torques/forces), n denotes the number of generalized coordinates of a robot manipulator, for instance, the number of DOF for serial robot manipulators or the number of actuated joints (active joints) for parallel robot manipulator. The generalized coordinates of a mechanical system (e.g., a robot manipulator) are all those displacement variables, whether rotational or translational, that determines uniquely a configuration of the system.

Vectors $q = [q_1, q_2, ..., q_n]^T$, $\dot{q} = [\dot{q}_1, \dot{q}_2, ..., \dot{q}_n]^T$ and $\ddot{q} = [\ddot{q}_1, \ddot{q}_2, ..., \ddot{q}_n]^T$ denote the vectors

of joints displacements, velocities and accelerations respectively, $M(q)$ is an $n \times n$ robot manipulator inertia matrix (which is symmetric positive definite), $C(q, \dot{q})$ is an $n \times n$ matrix of centripetal and Coriolis terms, $g(q)$ is an $n \times 1$ vector of gravity terms, F_f is an $n \times 1$ vector denoting the torque due to viscous and Coulomb friction, and $d(t)$ is an $n \times 1$ vector denoting the un-modeled dynamics and external disturbances.

For parallel robot manipulators, because of the closed-loop kinematic chains and existence of passive joints (not all joints of closed-loop kinematic chains are actuated) a set of constraint equations derived from kinematics of a robot manipulator is required to derive the equations of motion. Based on the literature Ghorbel et al. 2000, to derive the dynamic model for general n-DOF parallel robot manipulator, first the equations of motion are formulated in terms of, for instance $n'(n' > n)$, dependent generalized coordinates. Following this $n' - n$ holonomic (i.e., geometric) constraints are eliminated to end up with n independent differential equations with n independent generalized coordinates corresponding to the number of the *actuated joints* of the parallel robot manipulator. According to Angeles (Angeles 2003, page 473), by proper definition of the inertia matrix and quadratic terms of inertia force (matrix of centripetal and Coriolis terms), the dynamic model of a parallel robot manipulator also can be expressed in the form of Eq. (1). For detailed information the reader is referred to Angeles 2003.

Properties of Robot Manipulator Dynamics

The dynamic model presented in Eq. (1) contains two important structural properties, which are useful for developing control laws as well as for the identification of the parameters of the dynamic model (e.g., link mass and moment of inertia). The two important properties are reviewed in order to clarify the discussions in the following sections and use them for design and analysis purposes of the proposed controller throughout this chapter. The properties are as follows.

***Skew-symmetry property*:** this property refers to an important relationship between the inertia matrix $M(q)$ and the matrix $C(q, \dot{q})$ appearing in Eq. (1). The property states that matrix $N(q, \dot{q}) = \dot{M}(q) - 2C(q, \dot{q})$ is a skew-symmetric matrix, i.e., the components satisfy $n_{ij} = -n_{ji}$. The proof of this property for serial, parallel and redundantly actuated parallel robot manipulators can be found in Ghorbel et al. 2000. The skew-symmetry property is employed in the stability and robustness analysis of the proposed control methodology in Section **The Proposed Adaptive Robust Controller Design Methodology** of this chapter.

***Linearity-in-the-parameters property*:** the dynamic model presented in Eq. (1) can be defined in terms of certain parameters, such as the link mass and moment of inertia, friction coefficient, etc. Usually a priori knowledge about these parameters is not complete and therefore, they must be determined in order to modify the dynamic model or tune a model-based controller. Fortunately, it can be shown that the nonlinear dynamic model presented in Eq. (1) is linear in terms of above mentioned parameters in the following sense (Slotine and Li 1991). There exists an $n \times p$ matrix function $Y(q, \dot{q}, \ddot{q})$, which is called the regressor, and a $p \times 1$ vector Φ such that the dynamic model can be written as

$$\tau = M(q)\ddot{q} + C(q, \dot{q})\dot{q} + F_f(\dot{q}) + g(q) = Y(q, \dot{q}, \ddot{q})\,\Phi \qquad (2)$$
$$\tau = Y(q, \dot{q}, \ddot{q})\,\Phi$$

where Φ is a $p \times 1$ vector of dynamic parameters and p is the

number of parameters. The linearity in the dynamic parameters property is a base for the traditional adaptive control design and on-line parameter estimation method. This property is only used to explain the existing control methodologies and clarify the discussions, and it is not used for the design and analysis of the proposed controller in this chapter.

After discussing the dynamic model of the manipulator and its properties, it should be noted that the dynamic model of the system is an approximation of the real system, due to the presence of complex phenomena such as large flexibility, Coulomb friction, backlash, payload variation, external disturbances and time-varying parameters, which are all uncertain to some extent and cannot be modeled mathematically. Therefore, in the presence of uncertainties, the components of the dynamic model are of the form

$$\begin{aligned} M(q) &= \hat{M}(q) + \Delta M(q) \\ C(q, \dot{q}) &= \hat{C}(q, \dot{q}) + \Delta C(q, \dot{q}) \\ g(q) &= \hat{g}(q) + \Delta g(q) \end{aligned} \tag{3}$$

where $\hat{M}(q)$, $\hat{C}(q, \dot{q})$ and $\hat{g}(q)$ are the known (estimated) parts and $\Delta M(q)$, $\Delta C(q, \dot{q})$ and $\Delta g(q)$ are the unknown parts. In this work, without loss of generality, it is assumed that the term denoting the viscous and Coulomb friction effects is completely unknown. Therefore, in the presence of the parameter uncertainty, un-modelled dynamics and external disturbances, Eq. (1) can be written as follows

$$\tau = \hat{M}\ddot{q} + \hat{C}(q, \dot{q}, t)\dot{q} + \hat{g}(q) + \delta(q, \dot{q}, \ddot{q}, t) \quad (4)$$

$$\delta(q, \dot{q}, \ddot{q}, t) = \Delta M\ddot{q} + \Delta C\dot{q} + \Delta g + F_f(\dot{q}, \ddot{q}) + d(t) \quad (5)$$

where $\delta(q, \dot{q}, \ddot{q}, t)$ is an unknown bounded function that *lumps together various uncertain terms* (i.e., un-modelled dynamics, parameter uncertainty, external disturbances). It is worth noting that inclusion of the complexities in the vector of the lumped uncertainty has two advantages:

1. It reduces the order of the dynamic model in the sense that higher order un-modelled dynamics terms can be included in uncertainty term (i.e., additive representation) and also the number of unknown parameters, which are needed to be estimated and identified.
2. As a consequence of reducing the number of unknown parameters, the computation burden is also reduced in real-time estimation. Since, only one uncertain parameter per joint needs to be estimated this, in turn, simplifies the controller design to some extent in the sense that only one adaptation gain per joint is required to be tunned.

Along this line, it should be noted that the potential vibration modes of flexible link robots and cables in the cable-based parallel robot manipulators and other types of uncertainties might be lumped into the uncertainty vector and the additive representation of uncertainties is selected to describe the nonlinear uncertain system (i.e., Eq. (4)). According to Zhou and Doyle 1996 and Sanchez-Pena and Sznaier 1998, the above additive representations of uncertainty is well suited to represent the modelling errors caused by flexibility, by neglected high-frequency dynamics

such as measurement noise, and by parametric uncertainties, if they are not included in the dynamic model. Therefore, in order to develop the controller and analyze the stability of closed-loop system, the "nominal" dynamic model of the system—that is, the system without uncertainty ($\delta(q, \dot{q}, \ddot{q}, t) = 0$)-is built based on the rigid body mode and all uncertain terms lumped into one uncertainty term which results in the general Euler-Lagrange dynamic model of the robot manipulators, Eq. (4), and is used throughout this chapter.

At this point, the following assumption is made in order to design the controller and analyze the stability of the closed loop system.

Assumption 1. The uncertainty $\delta(q, \dot{q}, \ddot{q}, t)$ is bounded in Euclidian norm and so are its partial derivatives:

$$\|\delta(q, \dot{q}, \ddot{q}, t)\| \leq \dot{\rho}(q, \dot{q}, \ddot{q}, t)$$

where $\rho(q, \dot{q}, \ddot{q}, t)$ is the unknown bounding function of the uncertainties, $\| \|$ is Euclidian norm.

THE PROPOSED ADAPTIVE ROBUST CONTROLLER DESIGN METHODOLOGY

The standard robust sliding mode control law for a nonlinear uncertain system described by Eqs. (4) and (5), which guarantees the stability and convergence is a discontinuous and has the following form:

$$u(t) = u_{eq}(t) - K_b\, sgn(S) \tag{6}$$

where K_b is the bounds of uncertainty vector which have to be known a priori, and $sgn(S)$ is a signum function, $u(t)$ is the control input and can be divided into two components, $u_{eq}(t)$ which is the model-based component, and $u_{SW} = -K_b sgn(S)$ which is the discontinuous term, and $S(q, t)$ is the sliding variable which is defined as (Slotine and Li 1991):

$$S(q, t) = \left(\frac{d}{dt} + \Lambda\right)^2 \int e\,dt = \dot{e} + 2\Lambda e + \Lambda^2 \int e\,dt \tag{7}$$

where Λ is an $n \times n$ symmetric positive definite diagonal constant matrix and $e = q - q_d$, $\dot{e} = \dot{q} - \dot{q}_d$, $e = q - q_d$ are the tracking error and the rate of error respectively. q_d and q are the desired and measured joint variables respectively. The integral of error is included to ensure zero offset error.

The control objective is to force the system state trajectory to reach sliding surface $S(q, t) = 0$ in finite time and stay on the sliding surface $S(q, t) = 0$ for all subsequent time. To clarify the subject, the ideal and real sliding mode is defined as follows.

Definition 1 (Levant 1993). The motion that takes place strictly on $S(q, t) = 0$ is called

"ideal" sliding mode and described by (Utkin 1977, 2013)

$$\lim_{s_i \to 0^+} \dot{s}_i \leq 0 \quad \text{and} \quad \lim_{s_i \to 0^-} \dot{s}_i \geq 0$$

In real world applications such as robot manipulator, due to uncertainties the "ideal"

sliding mode concept as defined above, cannot be stablished. Therefore, it is required to introduce the concept of "real" sliding mode.

Definition 2 (Levant 1993). Given the sliding variable $S(q, t)$, the **"real" sliding mode** is called the motion that takes place in a small neighbourhood of the sliding surface $S(q, t) = 0$, with $\varepsilon > 0$ and is defined as:

$$|S(t)| < \varepsilon, \lim_{\varepsilon \to 0} |S(t)| = 0,$$

However, the application of control law given in Eq. (6) can be limited mainly due to chattering and unknown bounds of the uncertainties. The discontinuous term $u_{SW} = K_b \mathrm{sgn}(S)$ is the fundamental cause of chattering and also is designed conservatively based on the bounds of uncertainties. In this study, to eliminate the chattering the discontinuous term will be replaced by an adaptive continuous term which is obtained through systematic Lyapunov design procedure. The task of the continuous sliding mode control design with the above mentioned characteristics and without knowing the bounds of uncertainties consists of two phases as follows.

- For the first phase of the design, an exponentially stable error dynamic is chosen as a desired sliding surface (i.e., $S(q, t) = \dot{e} + 2\Lambda e + \Lambda^2 \int e dt = 0$) to guarantee the convergence of tracking error to a small neighbourhood of sliding surface.
- The second phase is to design a control law with variable parameters such that it guaranties the existence of real sliding mode, or makes the associated Lyapunov function a decreasing function of time in the presence of time-varying uncertainties.

Unlike the traditional SMC, and AC of robot manipulators, the proposed control law that guarantees achieving the control objectives is continuous and consist of two components:

1. Model-based component which is constructed based on approximately known dynamic model of the system and desired acceleration not the measured acceleration and is derive in Section **Control Design for Nominal System**, that is:

$$u_{eq}(t) = \hat{\tau}_n = \hat{M}\ddot{q}_r + \hat{C}(\hat{q}, \dot{q}, t)\dot{q}_r + \hat{g}(q) - KS \quad (8)$$

where $\ddot{q}_r$, $\dot{q}_r$ are the *reference acceleration* and *reference velocity*, respectively, and are defined in the sequel.

2. The second component is a continuous component constructed based on estimated uncertainty and state feedback control which replaces the discontinuous component u_{SW} in Eq. (6) and is derived in section as:

$$\tau_c = \hat{\delta}_{est} \quad (9)$$

where $\hat{\delta}_{est}$ is estimate of the lumped uncertainty term $\delta(q, \dot{q}, \ddot{q}, t)$ and is obtained from systematic Lyapunov design procedure in the next subsection, and $-KS$ is the term to improve the transient performance and enhance the closed-loop stability. Diagonal matrix K is positive definite constant and is a design parameter. Based on the above discussion the proposed ARC is designed as follows.

Control Design for Nominal System

In the first step, the controller design for the "nominal" system—that is, the system without uncertainty ($\delta(q, \dot{q}, \ddot{q}, t) = 0$)—is considered. The nominal dynamic of the robot manipulator is described by

$$\tau = \hat{M}\ddot{q} + \hat{C}(q, \dot{q}, t)\dot{q} + g(q) \tag{10}$$

In this case the control law is designed such that it satisfies a sufficient condition for the existence and reachability of the trajectories to the small neighbourhood of sliding surface for the nominal system. This control law derives the system trajectories to the small neighbourhood of the sliding surface in a finite time, if $q(t_0)$ is actually off $q_d(t_0)$ (i.e., desired value of $q(t)$). One method to design a control law that derives the system trajectories to the sliding surface from any initial condition is the Lyapunov direct method.

Theorem 1. *Given the nominal system described by (10), with the sliding variable described by (7), and the following Lyapunov function, the asymptotic stability of closed- loop system is guaranteed, and there exist a finite time t_F such that a real sliding mode*

is stablished for (i.e., *all system trajectories converge to small all* $t \geq t_r$ *of sliding neighborhood surface*).

$$V = \frac{1}{2}(S^T \hat{M} S) \tag{11}$$

For the sake of simplicity, the arguments of sliding variable $S(q, t)$ are eliminated.

Now, taking the derivative of Lyapunov function (11) results in

$$\dot{V} = \frac{1}{2} S^T \dot{\hat{M}} S + S^T \hat{M} \dot{S} \tag{12}$$

From Eq. (7) the derivative of $S(t)$ is determined as

$$\dot{S} = \ddot{e} + 2\lambda \dot{e} + \lambda^2 e$$
$$= (\ddot{q} - \ddot{q}_d) + 2\lambda(\dot{q} - \dot{q}_d) + \lambda^2(q - q_d)) \tag{13}$$

where $\ddot{q}_d - 2\lambda \dot{e} - \lambda^2 e$ in Eq. (13) is called the *reference acceleration* and denoted by $\ddot{q}_r$. Thus, the derivative of the sliding variable can be determined as

$$\dot{S} = \ddot{q} - \ddot{q}_r \tag{14}$$

Substituting (11) into (12) and using equation (10) yields

$$\dot{V} = \frac{1}{2} S^T \dot{\hat{M}} S + S^T \hat{M}(\ddot{q} - \ddot{q}_r) \tag{15}$$

$$\dot{V} = \frac{1}{2} S^T \dot{\hat{M}} S + S^T (\tau - C\dot{q} - g) - S^T \hat{M} \ddot{q}_r) \tag{16}$$

From equation (7) i.e., $S = \dot{e} + \lambda e$, one has the following

$$\dot{S} = \ddot{q} - \ddot{q}_r \tag{17}$$

where $\dot{q} = \dot{q} - 2\lambda e - \lambda^2 \int e dt$, using equation (17) and replacing for $\dot{q}$

in equation (16), $r = \dot{q}_d$ yields

$$V = \frac{1}{2} S^T \hat{M} S \qquad (18)$$

$$\dot{V} = \frac{1}{2} S^T (\dot{\hat{M}} - 2\hat{C}) S + S^T (\hat{M}\dot{q}_r + \hat{C}\dot{q}_r + \hat{g}) \qquad (19)$$

Considering the skew symmetry property of matrix $(\dot{M} - 2C)$, which is one of the structural properties of the robot manipulators dynamic model, the following holds

$$S^T (\dot{\hat{M}} - 2\hat{C}) S = 0 \qquad (20)$$

Therefore, the skew symmetry property can be used to eliminate the term $\frac{1}{2} S^T (\dot{\hat{M}} - 2\hat{C}) S$ in Eq. (19) and $\dot{V}$ is as:

$$\dot{V} = S^T (\hat{M}\dot{q}_r + \hat{C}\dot{q}_r + \hat{g}) \qquad (21)$$

In order to guarantee the stability of the system, derivative of Lyapunov function needs to be a negative definite function. Therefore, $\dot{V}$ can be chosen as follows:

$$\dot{V} = -S^T K S \leq 0 \qquad (22)$$

$$\dot{V} = -S^T KS = S^T (\tau - \hat{C}\dot{q}_r - \hat{g} - \hat{M}\ddot{q}_r) \quad (23)$$

$$S^T(\tau - \hat{C}\dot{q}_r - \hat{g} - \hat{M}\ddot{q}_r) + S^T KS = 0 \quad (24)$$

$$S^T(\tau - \hat{C}\dot{q}_r - \hat{g} - \hat{M}\ddot{q}_r + KS) = 0 \quad (25)$$

By solving the above equation for the control input (i.e., τ), the following expression is obtained for τ, which is called nominal control and denoted with τ_n in this study, that is

$$\tau_n = \hat{M}\ddot{q}_r + \hat{C}\dot{q}_r + g - KS \quad (26)$$

The above control input τ_n makes $\dot{V} \leq 0$ for nominal system, which guarantees that the nominal closed-loop system is uniformly asymptotically stable. Using Barbalat's lemma, it can be shown that the semi negative derivative of Lyapunov function guarantees the reachability of the system trajectories to small neighborhood of sliding surface in a finite time, which means real sliding mode (i.e., Definition 2) can be stablished in finite time, if $q(t_0)$ is actually off $q_d(t_0)$ (i.e., desired value of $q(t)$).

Remark 1. The proportional term KS in equation (26), is in agreement with practical consideration which dictates that the control input should be reduced as the state trajectory converge to the sliding surface. But, if the control law is designed based on the bound of uncertainties a high control input is imposed for all $t \approx t_0$.

Compensation of Time-Varying Uncertainties

In the second step, it is assumed that the lumped time-varying uncertainty present (i.e., $\delta(q, \dot{q}, \ddot{q}, t) \neq 0$). As it is described in Section **Problem Formulation and Definition** (Assumption 1), the uncertainties are bounded, but this bound is not known, and system dynamic described by Eq. (4). To compensate for the effect of uncertainties an additional adaptive control component is required. This additional component which is denoted by τ_a in this manuscript, should be designed such that the overall control $\tau = \tau_n + \tau_a$

satisfies a sufficient condition for existence and reachability of sliding mode for the dynamic (4). Since it is assumed that the matching condition is satisfied therefore, the uncertain term $\delta(q, \dot{q}, \ddot{q}, t)$ appears in the same channel the control input. For the sake of brevity, the arguments of the functions are dropped. Therefore, if δ were known, then including the term $\tau_a = \delta$ in the control law would compensate for the effects of all the uncertainties. Since δ is not known, the control component τ_a can be designed based on the estimate of the lumped uncertainty term δ, which is denoted by δ_{est}, hereafter. Based on the above discussion, including $\tau_a = \delta_{est}$ in the control law could compensate for the effects of the uncertainties, provided that the estimated uncertainty, δ_{est}, approaches δ as time tends to infinity. Therefore, τ_a is a variable (adaptive) term which is constructed based on online estimation of the uncertainties and defined as follows

$$\tau_a = \delta_{est} \tag{27}$$

By combining the components derived in the above steps the proposed robust adaptive control law is obtained as:

$$\tau = \tau_n + \delta_{est}$$

$$\tau = \hat{M}\ddot{q}_r + \hat{C}(q, \dot{q}, t)\dot{q}_r + \hat{g}(q) - KS + \delta_{est} \tag{28}$$

In the following section stability of the closed-loop system with the above proposed control law is analyzed and proved and an appropriate estimation mechanism also called update law is derived systematically through Lyapunov redesign method to estimate δ_{est} (Khalil, page 579). It will also be shown that real sliding mode can be reached in finite time.

STABILITY ANALYSIS OF CLOSED-LOOP SYSTEM IN THE PRESENCE OF TIME-VARYING UNCERTAINTIES

Theorem 2. *Given the MIMO nonlinear uncertain system* (*the multi-link robot manipulator*) *described by Eqs.* (*4*), (*5*), *with the sliding variable* (7) *and the robust control law of* (28), *and the adaptive law that will be derived later in this section, the stability of closed-loop system in the presence of model uncertainties and disturbances is guaranteed, and there exist a finite time* t_r *such that a real sliding mode is stablished for all* $t > t_r$.

***Proof*:** To prove the robust stability of the proposed controller, the following Lyapunov function is considered.

$$V = \frac{1}{2}(S^T MS + \tilde{\delta}^T \Gamma^{-1}\tilde{\delta}) \tag{29}$$

where Γ is a symmetric positive definite diagonal constant, and

$$\tilde{\delta} = \delta_{est} - \delta \tag{30}$$

Taking the derivative of Lyapunov function (29) results in

$$\dot{V} = \frac{1}{2} S^T \dot{M} S + S^T M\dot{S} + \tilde{\delta}^T \Gamma^{-1}\dot{\tilde{\delta}} \tag{31}$$

From Eq. (14) the derivative of $S(t)$ is as

$$\dot{S} = \ddot{q} - \ddot{q}_r \tag{32}$$

Substituting (32) into (31) yields

$$\dot{V} = \frac{1}{2} S^T \dot{M} S + S^T M(\ddot{q} - \ddot{q}_r) + \tilde{\delta}^T \Gamma^{-1}\dot{\tilde{\delta}} \tag{33}$$

Substituting Mq from Eq. (1), Eq. (29) can be written as

$$\dot{V} = -\frac{1}{2} S^T \dot{M} S + S^T (\tau - \tau_f - (Cq + F + g + \tau_r) + M\ddot{q}_d(t)) = S^T \tau - S^T \tilde{\delta}^T \Phi^{-1} \tilde{\delta} \quad (34)$$

Similar to the reference acceleration, another term, called the reference velocity, can be derived from the definition of sliding surface as follows

$$S = \dot{e} + 2\Lambda e + \Lambda^2 \int e dt \quad (35)$$

Replacing $\dot{e} = \dot{q} - \dot{q}_d$ in Eq. (35) yields

$$S = \dot{q} - (\dot{q}_d - 2\Lambda e - \Lambda^2 \int e dt) \quad (36)$$

Substituting $\dot{q}_r = \dot{q}_d - 2\Lambda e - \Lambda^2 \int e dt$ in Eq. (36) leads to

$$S = \dot{q} - \dot{q}_r \tag{37}$$

Replacing q in terms of q_r and S in Eq. (34), yields

$$V(t) = \frac{1}{2} S^T M S + S^T [\tau - (C(S + \dot{q}_r) + F + g + d(t))] + \tilde{\delta}^T \Gamma^{-1} \dot{\tilde{\delta}} \tag{38}$$

Rearranging Eq. (34) yields

$$V(t) = \frac{1}{2} S^T \dot{M} S + S^T [\tau - (M \ddot{q}_r + C\dot{q}_r + F + g + d(t))] + \tilde{\delta}^T \Gamma^{-1} \dot{\tilde{\delta}} \tag{39}$$

As mentioned earlier in Eq. (20), using skew-symmetry property of robot matrix $(M - 2C)$, the term $0.5 S^T (M - 2C) S$ in Eq. (39) is equal to zero, and thus Eq. (39) can be written as

$$V = S^T [\tau - (M \ddot{q}_r + C\dot{q}_r + F + g + d(t))] + \tilde{\delta}^T \Gamma^{-1} \dot{\tilde{\delta}} \tag{40}$$

Substituting for control input from Eq. (28) into (40) yields

$$V = S^T [(\hat{M} \ddot{q}_r + \hat{C} \dot{q}_r + \hat{g}(q)) - (M \ddot{q}_r + C\dot{q}_r + F + g(q) + d(t))] + \tilde{\delta}^T \Gamma^{-1} \dot{\tilde{\delta}} - KS + \delta_{est}$$

$$V = S^T [\hat{M} \ddot{q}_r + \hat{C} \dot{q}_r + \hat{g}(q) - (M \ddot{q}_r + C\dot{q}_r + F + g(q) + d(t))] + \tilde{\delta}^T \Gamma^{-1} \dot{\tilde{\delta}} - KS + \delta_{est} \tag{41}$$

$$V = S^T [((\hat{M} - M)\ddot{q}_r + (\hat{C} - C)\dot{q}_r + (\hat{g} - g) - F(q, t) - d(t)) - KS + \delta_{est}]$$

$$V = S^T [-\tilde{\delta} - KS + \delta_{est}] + \tilde{\delta}^T \Gamma^{-1} \dot{\tilde{\delta}} \tag{42}$$

$$V = -S^T KS + S^T \tilde{\delta} + \tilde{\delta}^T \Gamma^{-1} \dot{\tilde{\delta}}$$

From equation (30) $\dot{\tilde{\delta}} = -\dot{\delta}_{est}$, substituting this into equation (42) yields

$$V = -S^T KS + S^T \tilde{\delta} - \delta) + \tilde{\delta}^T \Gamma^{-1} (\delta_{est}) \quad (43)$$

The above equation implies that if the adaptive law is chosen as

$$\dot{\delta}_{est} = -\Gamma S \quad (44)$$

Equation (43) can be written as

$$\dot{V} = -S^T KS + S^T \tilde{\delta} - S^T \Gamma\Gamma^{-1} \tilde{\delta} - \tilde{\delta}^T \Gamma^{-1} \dot{\delta} \quad (45)$$

Equating $\Gamma\Gamma^{-1} = I$ (I is identity matrix of appropriate size), using the symmetric property of matrix Γ, results in

$$\dot{V} = -S^T KS - \tilde{\delta}^T \Gamma^{-1} \dot{\delta} \quad (46)$$

The second term of Eq. (46), i.e., $\tilde{\delta}^T \Gamma^{-1} \dot{\delta}$ shows the combined effects of the estimation error, estimation gain and the rate of change of the uncertainties with respect to time on V. Since the complete knowledge of the above term is not available, the best possible way is worse case analysis, when $\tilde{\delta}^T \Gamma^{-1} \dot{\delta} \neq 0$. Therefore, Eq. (46) can be written as follows:

$$\dot{V} \leq -S^T KS - \tilde{\delta}^T \Gamma^{-1} \dot{\delta} \leq -S^T KS + \|\tilde{\delta}^T \Gamma^{-1} \dot{\delta}\| \quad (47)$$

As mentioned earlier K and Γ symmetric positive definite diagonal matrices and the following relationship hold

$$\lambda_{min}(K)\|S\|^2 \leq S^T K S \leq \lambda_{max}(K)\|S\|^2 \tag{48}$$

where $\lambda_{min}(K)$, and $\lambda_{max}(K)$ denote the minimum and maximum eigenvalues of the matrix K, respectively. Thus, Eq. (48) can be written as

$$\dot{V} \leq -\lambda_{min}(K)\|S\|^2 + \|\tilde{\delta}^T S\| + \|\tilde{\delta}^T \dot{\delta}\| \|\Gamma^{-1}\| \tag{49}$$

$$\dot{V} \leq -\lambda_{min}(K)\|S\|^2 + \|\tilde{\delta}^T \dot{\delta}\| \left[\frac{1}{\lambda_{min}(\Gamma^{-1})}\right]$$

From Eq. (45), $\dot{V} < 0$ if

$$\lambda_{min}(K)\|S\|^2 > \frac{\|\tilde{\delta}^T \dot{\delta}\|}{\lambda_{min}(\Gamma)} \tag{50}$$

or, equivalently

$$\dot{V} < 0 \quad if \quad \|S\| > \left(\frac{\|\tilde{\delta}^T \dot{\delta}\|}{\lambda_{min}(K)\,\lambda_{min}(\Gamma)}\right)^{\frac{1}{2}} > \varepsilon \tag{51}$$

where ε is a positive scalar value and as can be seen from (51) its magnitude depends on the choice of K and Γ. The designer of the controller can make it arbitrarily small by using the design parameters, e.g., large K and Γ, and hence, the magnitude of $S(t)$ for which $\dot{V}$ is negative definite, can be reduced arbitrarily using the design parameters K and Γ in the presence of time-varying uncertainties. Equation (51) also implies that:

Case 1. If initially $\|S\| > \varepsilon$, all trajectories will converge to the ε-vicinity of the sliding surface $S(t) = 0$ in finite time, because,

V is negative definite for all $||S|| > \varepsilon$ and real sliding mode is stablished. Therefore, the finite time convergence of all solutions to a domain $||S|| \leq \varepsilon$ is guaranteed from any initial condition $||S(0)|| > \varepsilon$.

Case 2. If initially $||S|| < \varepsilon$, then $\dot{V}$ is sign indefinite and $||S||$ can increase over ε. Once $||S|| > \varepsilon$ situation will return to the Case 1 and V become negative definite. Therefore, closed-loop system is stable and all solutions of the closed-loop system are uniformly ultimately bounded.

The above behavior of the proposed controller is illustrated using the simulation results for two links robot, Fig. 1. As can be seen the system trajectory is converged to small vicinity of the $S(t) = 0$ and real sliding mode is stablished in finite time.

Case 3. Equation (46) implies that, for the slowly time-varying uncertainties (i.e., the variation of uncertainty with respect to time $\dot{\delta} \approx 0$), one can achieve asymptotic stability with the proposed controller and Eq. (46) can be written as:

$$\dot{V} \leq -S^T K S \leq 0 \tag{52}$$

Condition (52) implies that the system trajectories can reach small neighborhood of sliding surface in finite time and the real sliding mode is stablished. Furthermore, the system trajectories will reach the surface $S = 0$ as time tends to infinity. The only concern is that the system cannot get "stuck" at a stage where $\dot{V} = 0$, while q does not equal q_d. This problem can be solved readily using Barbalat's lemma. The reader is referred to Slotine and Li 1991 for more detail.

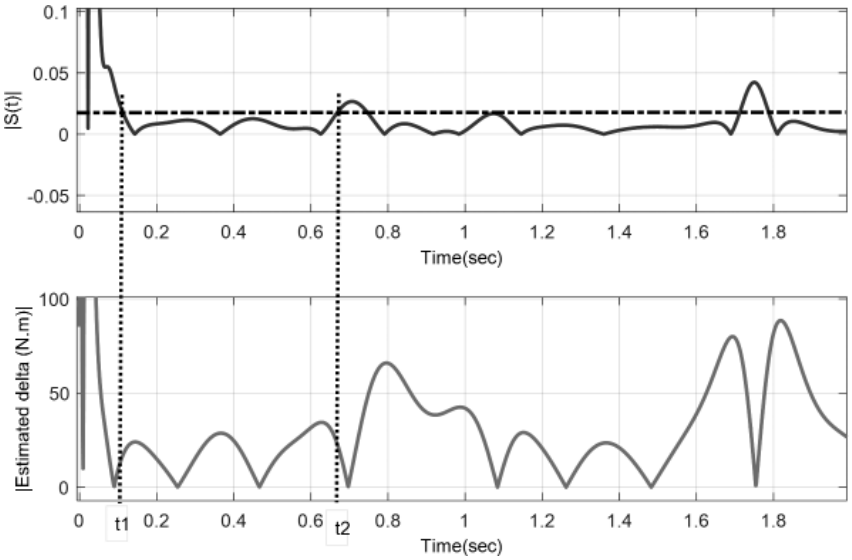


Figure 1. Behavior of sliding variable $S(t)$, and estimated uncertainty δ_{est} vs. time around ε-vicinity.

Discussion. The proposed adaptive robust control law of (28) along with adaptive law of (44), that is:

$$\begin{cases} \tau = \tau_n + \delta_{est} \\ \tau = \hat{M}\dot{q}_r + \hat{C}(q, \hat{q}, t)q_r + g(q) \\ \quad - KS + \delta_{est} \end{cases} \tag{53}$$

$$\dot{\delta}_{est} = -\Gamma S$$

Works as follows:

- As can be seen from Fig. 1, there exist a time instant t_1 such that $|S(t_1)| < \varepsilon$, which means the sliding variable reached to the ε-domain of sliding surface and a real sliding mode is stablished. This implies that the estimated uncertainty term plus proportional term $\delta_{est} + KS$ is large enough to compensate for the bounded uncertainty and estimated uncertainty term will increase due to adaptive law of
(44) until the sliding variable converges to $S(t) = 0$, although proportional term decreases as S(t) tends to zero.

- At this point $S(t)$ crosses the sliding surface and its sign changes. The sign change causes δ_{est} to decrease and $S(t)$ starts increasing as well as the proportional term KS, when $||S|| > \varepsilon$, situation will return to Case 1 explained above.
- However, if the time-varying uncertainty exceeds some values that makes $|S(t_2)| > \varepsilon$ at time t_2 (see Fig. 1), then δ_{est} and KS will increase up to the value that can counteract the uncertainty and makes it converge to ε-domain again, and this is the next reaching time.

To complete the derivation of the proposed control law, the estimated lumped uncertainty can be obtained simply by integrating Eq. (44), as follows

$$\delta_{est} = -\Gamma \int S dt \tag{54}$$

Substituting from Eq. (55) into Eq. (28), the following adaptive robust control law is obtained

$$\tau = \hat{M}\ddot{q}_r + \hat{C}\dot{q}_r + g - KS - \Gamma \int S dt \quad (55)$$

Equation (54) shows that control torque consists of two main components: (i) a model-based component, i.e., $\tau_M = \hat{M}\ddot{q}_r + \hat{C}\dot{q}_r + g$, which can be constructed based on the available knowledge of the dynamic model of the robot manipulator, without knowing the model parameters; and (ii) a sliding function-based proportional-integral component $\tau_{PI} = -KS - \Gamma \int S dt$, which is constructed based on dynamic behavior of sliding function. Equation (54) also shows that the proposed control law can be implemented using approximately known inertia matrix, centripetal matrix and gravity terms and PI component accounts for the parametric uncertainties and non-parametric uncertainties such as external disturbances.

Remark 2. The main features of the proposed adaptive robust control is that the control law is continuous, thus chattering is eliminated, and there is no need to find a boundary layer thickness, which is very difficult to be obtained properly. In this approach the uncertainty is estimated on-line with a proper choice of the adaptation gain and using adaptation law given in Eq. (40). Therefore, a priori knowledge of the uncertainty bounds is not needed.

SIMULATION RESULTS

In this section, the performance of the proposed controller is evaluated by simulation study using analytical dynamic model of a 2-DOF serial manipulator, Fig. 2. The dynamic model of the manipulator is given below (Slotine and Li 1991, page 396). This is because a 2-DOF planar serial robot manipulator is widely used in the literature for illustration of the performance of the developed controller Slotine and Li 1991, Seraji 1987, Craig et al. 1987, and therefore, simulation results can be compared with the existing results.

The inverse dynamic model of a 2-DOF robot manipulator is given as

$$\tau_1 \quad M_{11} \quad M_{12} \quad \ddot{q}_1 \quad C \quad \dot{q}_2 \quad -C(\cdot \dot{q}_2) \cdot \dot{q}_1 \quad F_{fr1} \quad g(\quad)_1$$

$$\quad M_{22} \quad \ddot{q}_2 \quad \dot{q}_1 \quad 771\dot{q}_2 \quad F_{fr2} \quad 2 \quad 2$$

$$\begin{bmatrix} \tau_1 \\ \tau_2 \end{bmatrix} = \begin{bmatrix} M_{11} & M_{12} \\ M_{21} & M_{22} \end{bmatrix} \begin{bmatrix} \ddot{q}_1 \\ \ddot{q}_2 \end{bmatrix} + \begin{bmatrix} C\dot{q}_2 & C(\dot{q}_1 + \dot{q}_2) \\ -C\dot{q}_1 & 0 \end{bmatrix} \begin{bmatrix} \dot{q}_1 \\ \dot{q}_2 \end{bmatrix} + \begin{bmatrix} F_{fr1} \\ F_{fr2} \end{bmatrix} + \begin{bmatrix} g_1(t) \\ g_2(t) \end{bmatrix} + \begin{bmatrix} d_1(t) \\ d_2(t) \end{bmatrix} \quad (56)$$

where

$$\begin{cases} M_{11} = a_1 + 2a_3\cos(q_2) - 2a_4\sin(q_2) \\ M_{12} = M_{21} = a_2 + a_3\cos(q_2) + a_4\sin(q_2) \\ M_{22} = a_2 \\ \begin{bmatrix} F_{fr1} \\ F_{fr2} \end{bmatrix} = \begin{bmatrix} f_{c1} & 0 \\ 0 & f_{c2} \end{bmatrix} \begin{bmatrix} \mathrm{sgn}(\dot{q}_1) \\ \mathrm{sgn}(\dot{q}_2) \end{bmatrix} + \begin{bmatrix} v_1 & 0 \\ 0 & v_2 \end{bmatrix} \begin{bmatrix} \dot{q}_1 \\ \dot{q}_2 \end{bmatrix} \end{cases} \quad (57)$$

$$C = a_3\sin(q_2) - a_4\cos(q_2)$$

$$g_1 = a_5\cos(q_1) + a_6\cos(\delta_e + q_1 + q_2)$$

$$g_2 = a_6\cos(\delta_e + q_1 + q_2)$$

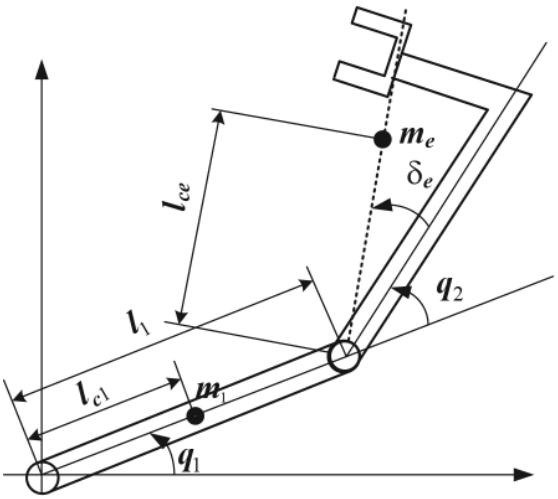


Figure 2. 2-DOF serial manipulator (Zeinali and Notash 2010).

with

$$\begin{cases} a_1 = I_1 + m_1 l_{c1}^2 + I_e + m_e l_{ce}^2 + m_e l_1^2 \\ a_2 = I_e + m_e l_{ce} \\ a_3 = m_e l_{ce} l_1 \cos\delta_e \\ a_4 = m_e l_{ce} l_1 \sin\delta_e \\ a_5 = (m_1 l_{c1} + m_e l_1) g \\ a_6 = m_e l_{ce} g \end{cases} \tag{58}$$

where $[\delta_e \; v_1 \; v_2 \; F_{c1} \; F_{c2}]^T = [30^0 \; 5.5 \; 2.7 \; 5 \; 5]^T$, and the robot is modelled as two rigid links with the following parameters:

$$\begin{cases} m_1 = 1\ [\text{kg}]\ I_1 = 0.12[\text{kg.m}^2]\ l_1 = 1.0\ [\text{m}]\ l_{c1} = 0.5[\text{m}] \\ m_e = 2\ [\text{kg}]\ I_e = 0.25[\text{kg.m}^2]\ l_{ce} = 0.25[\text{m}] \end{cases} \tag{59}$$

where m_1 and m_e are respectively the masses of links one and two concentrated at the center of mass of the corresponding links as shown in Fig. 5.3 (link two and end effector are considered as one rigid body), I_1 and I_e are the moments of inertia relative to the centers of mass of the corresponding link, l_1 is the length of link one, and l_{c1} and l_{ce} are the distance of centre of mass of the two links from the respective joint axes, as indicated in Fig. 2. The viscous friction coefficients $\square$ and Coulomb friction forces F_{ci} are included at the two joints.

In the first part of the simulation, the performance of the controller in terms of trajectory tracking capability and eliminating the chattering is investigated using the following trajectories.

$$q_d^T = [\pi/6(1 - \cos(2\pi t) + \sin(4\pi t))\ \pi/4(1 - \cos(2\pi t) + \cos(1.5\pi t))]^T \quad (60)$$

The results are illustrated in Fig. 3(a) and 3(b), and 4. As shown in Fig. 3, the tracking a desired trajectory described by Eq. (60) from non-zero initial condition is successfully performed using the proposed controller. The associated sliding function (i.e., $S(t)$) of joint one is illustrated in Fig. 4 (Top Row). As can be seen the chattering phenomenon which is the most important issue that limiting the practical application of the standard SMC is eliminated while the performance and robustness of the proposed controller is preserved.

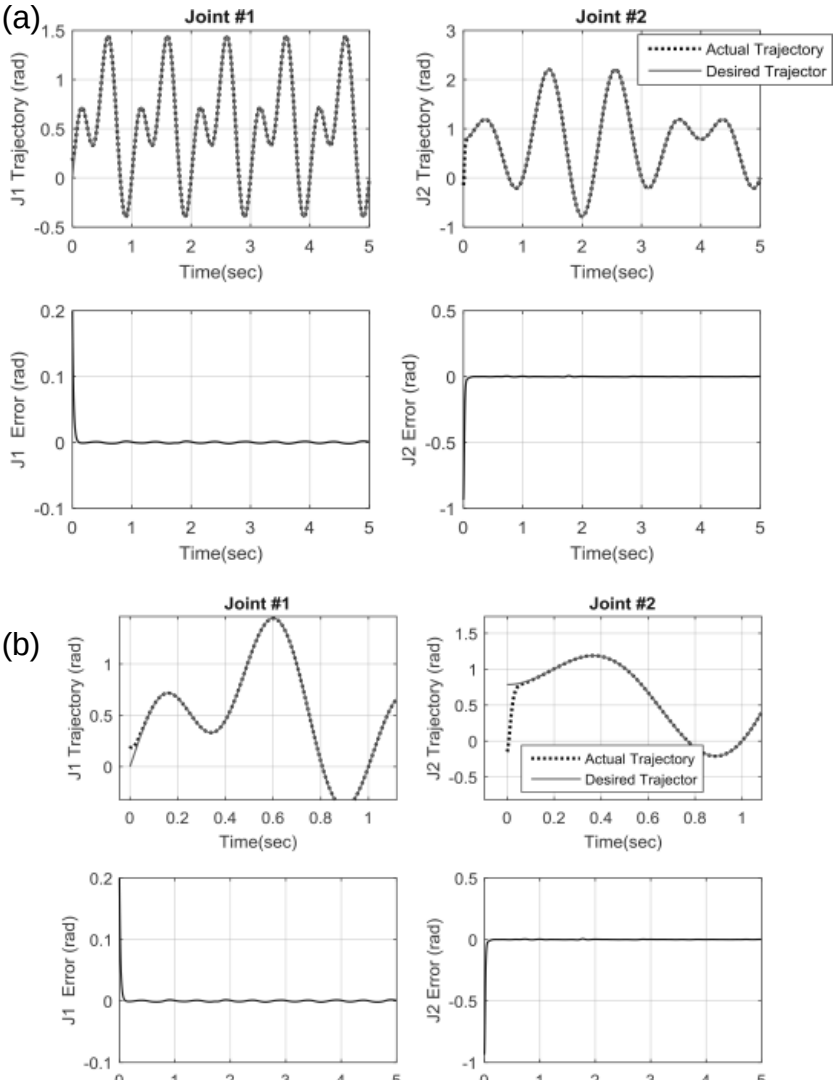


Figure 3. Trajectory tracking performance of the proposed controller from non-zero initial condition.

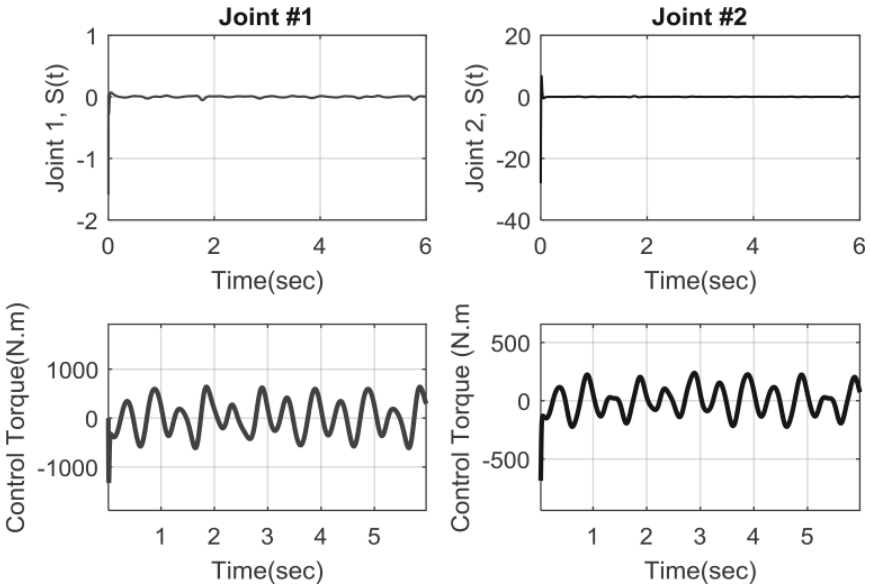


Figure 4. Convergence of system trajectories to $S(t) = 0$ (sliding surface) in finite time: (top Row) Sliding function behavior in time domain; (bottom Row) Control input in time domain.

At this point it is aimed to demonstrate the performance, adaptive capability, and robustness of the proposed controller, in the presence of the following external disturbances.

$$\begin{bmatrix} d_1(t) \\ d_2(t) \end{bmatrix} = \begin{bmatrix} 200 + 20\sin(2\pi t) \\ 100 + 15\sin(3\pi t) \end{bmatrix} \tag{61}$$

As shown in Fig. 5, the manipulator is disturbed by the external disturbance $d(t)$, at $t = 2.5$ seconds, to evaluate the stability and robustness of the closed-loop system. As can be seen from Fig. 5(a) and (b), large model uncertainties, and external disturbances are tolerated by the closed-loop system. The results also show how tracking error rapidly converges to zero after the manipulator is disturbed by the external disturbance $d(t)$, at $t = 2.5$, which is an indication of the adaptive capability of the proposed controller. Figure 6 shows a comparison of the estimated uncertainty with the model

uncertainty. As can be seen, the proposed uncertainty estimator, i.e., $\delta_{est} = -\Gamma \int S dt$, can successfully track the time-varying complex disturbances. This implies that at the steady state, the uncertainty estimation is only subjected to a small estimation error, which can
be compensated for by the proportional term, i.e., term KS in Eq. (28) of the control law. In the second part of the simulation, trajectory tracking performance and disturbance attenuation capability of the proposed controller is compared with Slotine and Li
adaptive control.

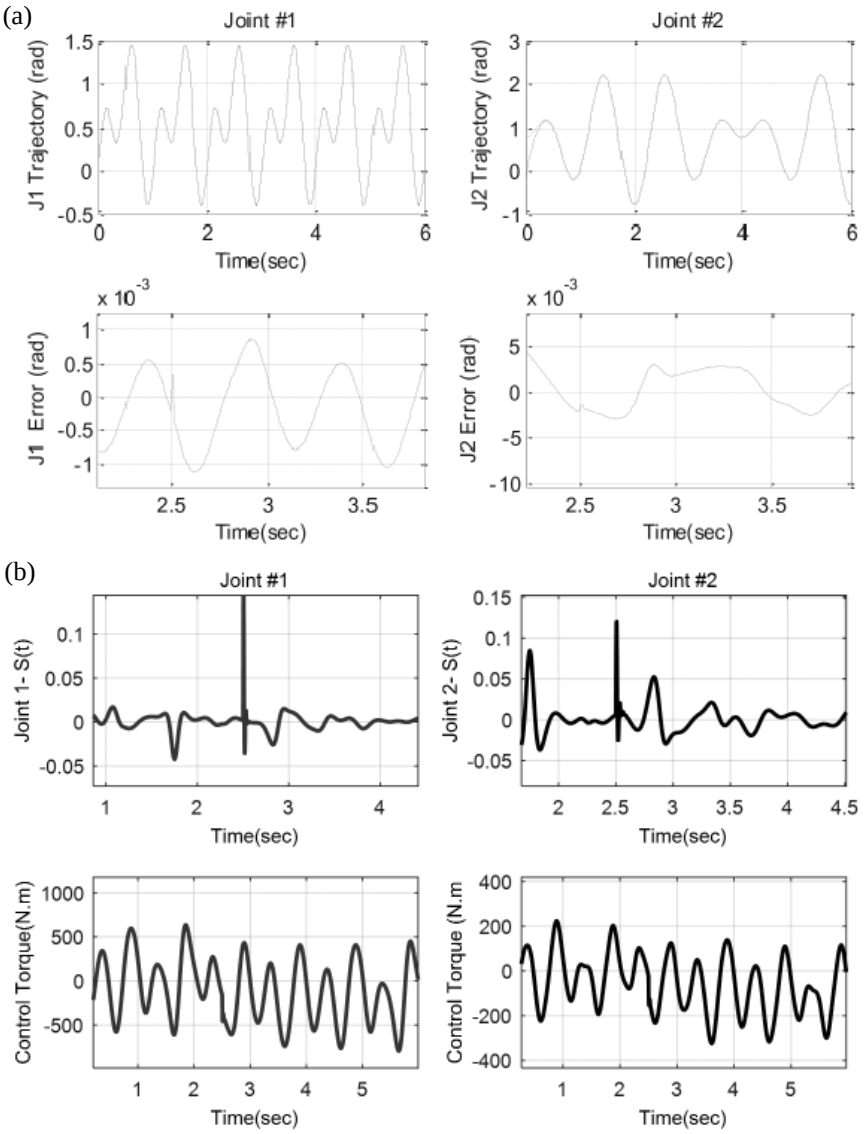


Figure 5. Trajectory tracking performance of the proposed controller in the presence of large external disturbances.

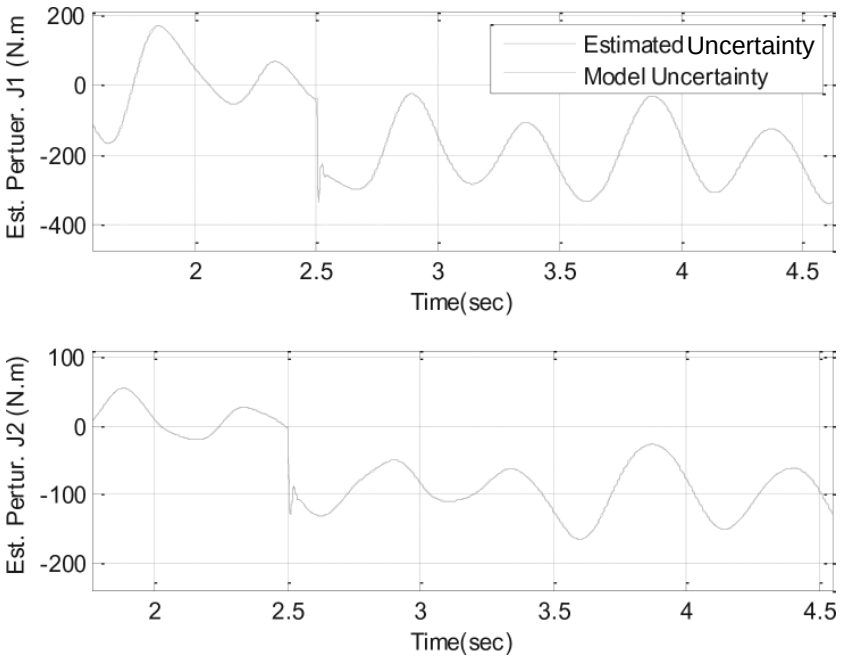


Figure 6. Comparison of model uncertainty and estimated uncertainties for joints one and two.

Comparison of the Proposed Control and Slotine and Li Adaptive Control

The control law of the SLAC method introduced by (Slotine and Li 1988) is as follows:

$$\tau = Y(q, \dot{q}, \dot{q}_r, \ddot{q}_r)\,\hat{\Phi} - KS \qquad (62)$$

where matrix function $Y(q, \dot{q}, \dot{q}_r, \ddot{q}_r)$ is called the regressor, and $\hat{\Phi}$ is the estimated vector of the dynamic model parameters Φ which was defined in Eq. (2). In Slotine and Li 1991, for the 2-DOF example robot manipulator, the following parameters, which are
defined in Eq. (58), are considered as the unknown parameters to be estimated.

$$\hat{\Phi} = [a_1\ a_2\ a_3\ a_4]^T \text{ with } \hat{\Phi}(0) = 0 \qquad (63)$$

The parameter update law of SLAC method is:

$$\dot{\hat{\Phi}} = -\Gamma Y(q, \dot{q}, \dot{q}_r, \ddot{q}_r)S \qquad (64)$$

where Γ_{SL} is a symmetric positive definite matrix, and q_r, $\dot{q}_r$ and S are defined as:

$$S = \begin{bmatrix} e_1 \\ \dot{e}_1 + \lambda_1 e_1 \\ e_2 \\ \dot{e}_2 + \lambda_2 e_2 \end{bmatrix}, \dot{q}_r = \begin{bmatrix} \dot{q}_{d1} - \lambda_1 e_1 \\ \dot{q}_{d2} - \lambda_2 e_2 \end{bmatrix} \text{ and } \ddot{q}_r = \begin{bmatrix} \ddot{q}_{d1} + \lambda_1 \dot{e}_1 \\ \ddot{q}_{d2} + \lambda_2 \dot{e}_2 \end{bmatrix} \tag{65}$$

where $\lambda_1 = 50$; $\lambda_2 = 15$. In order to have the same basis for comparison of SLAC and the controller proposed in Eq. (28), the sliding function defined in Eq. (7) are used for both controller without the integral term of the sliding function. Furthermore, the same gain matrix K are chosen for both controllers as:

$$K = \begin{bmatrix} 300 & 0 \\ 0 & 200 \end{bmatrix} \tag{66}$$

The adaptation gains for SLAC controller are extracted from Slotine and Li (1991), and for the proposed controller are chosen as:

$$\Gamma_{SLAC} = \begin{bmatrix} 0.2 & 0 & 0 & 0 \\ 0 & 0.15 & 0 & 0 \\ 0 & 0 & 0.1 & 0 \\ 0 & 0 & 0 & 0.2 \end{bmatrix} \text{ and } \Gamma_{ARC} = \begin{bmatrix} 25000 & 0 \\ 0 & 25000 \end{bmatrix} \tag{67}$$

In this comparison study, the goal is to show that SLAC controller results in an offset error in the case of the consistent disturbances (undamped), while the adaptive capability of adaptive robust controller compensates for the effects of the consistent disturbances. For both control laws the simulation is conducted ***without disturbances*** and ***with disturbances*** as shown in Figs. 7 and 8. The disturbance vector defined in Eq.
(64) applied at t = 2.5 second.

As can be seen from Fig. 7, before applying disturbance the performance of both methods in terms of the tracking errors are almost the same. But in the presence of consistent disturbance SLAC controller has considerable tracking error which depends on the amplitude of disturbance and parameter adaptation, while the tracking performance of the proposed method remains unchanged. The comparison of the two methods with disturbance is illustrated in Fig. 8.

The comparison of the two methods with disturbance is illustrated in Figure 8.

$$\mathbf{d}(t) = \begin{bmatrix} d_1(t) \\ d_2(t) \end{bmatrix} = \begin{bmatrix} 0 \\ 0 \end{bmatrix} \qquad t < 2.5$$

$$\mathbf{d}(t) = \begin{bmatrix} d_1(t) \\ d_2(t) \end{bmatrix} = \begin{bmatrix} 200 + 20\sin(2\pi t) \\ 100 + 15\sin(3\pi t) \end{bmatrix} \qquad t > 2.5 \tag{68}$$

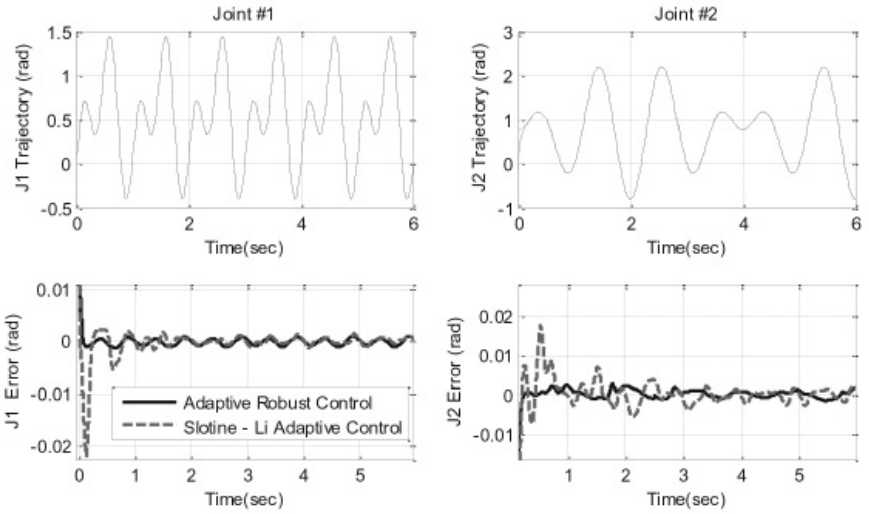


Figure 7. Comparison of the proposed Adaptive Robust Control with SLAC before applying a disturbance.

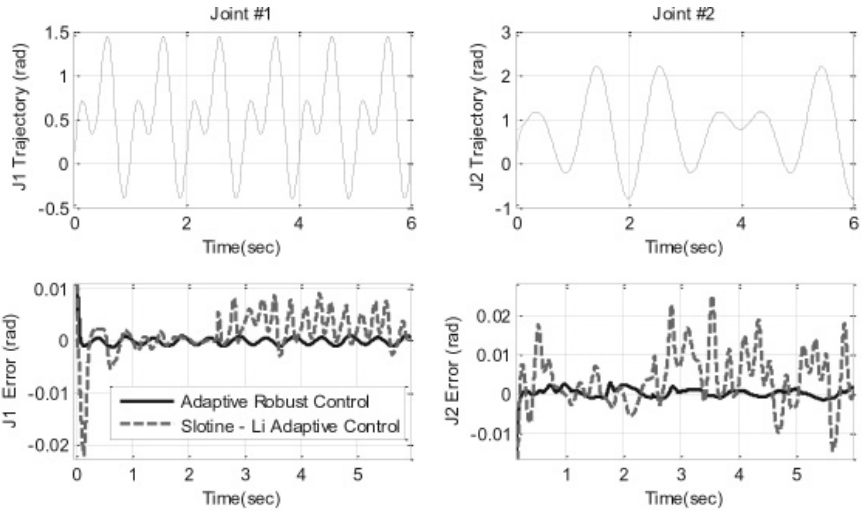


Figure 8. Comparison of proposed ARC with SLAC Adaptive Control after applying disturbance.

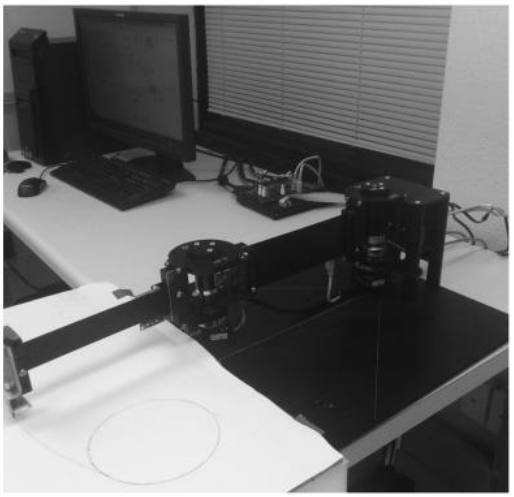


Figure 9. The 2-DOF serial flexible link (COURTESY OF QANSER Inc.).

EXPERIMENTAL RESULTS AND APPLICATION TO A TWO-DOF FLEXIBLE LINK ROBOT

The experimental test-bed used to validate the controller is an open-architecture 2-DOF serial flexible link robot (2D-SFLR), which has been designed and built by QUANSER Company.

Figure 9 shows the general configuration of the 2-DOF SFLR. This experimental system consists of two DC motors each driving harmonic gearboxes (zero backlash), and two serial flexible linkages. As a result of link flexibility, vibration in the manipulator appears during the control, which in turn, makes the control more complex than rigid-link robots.

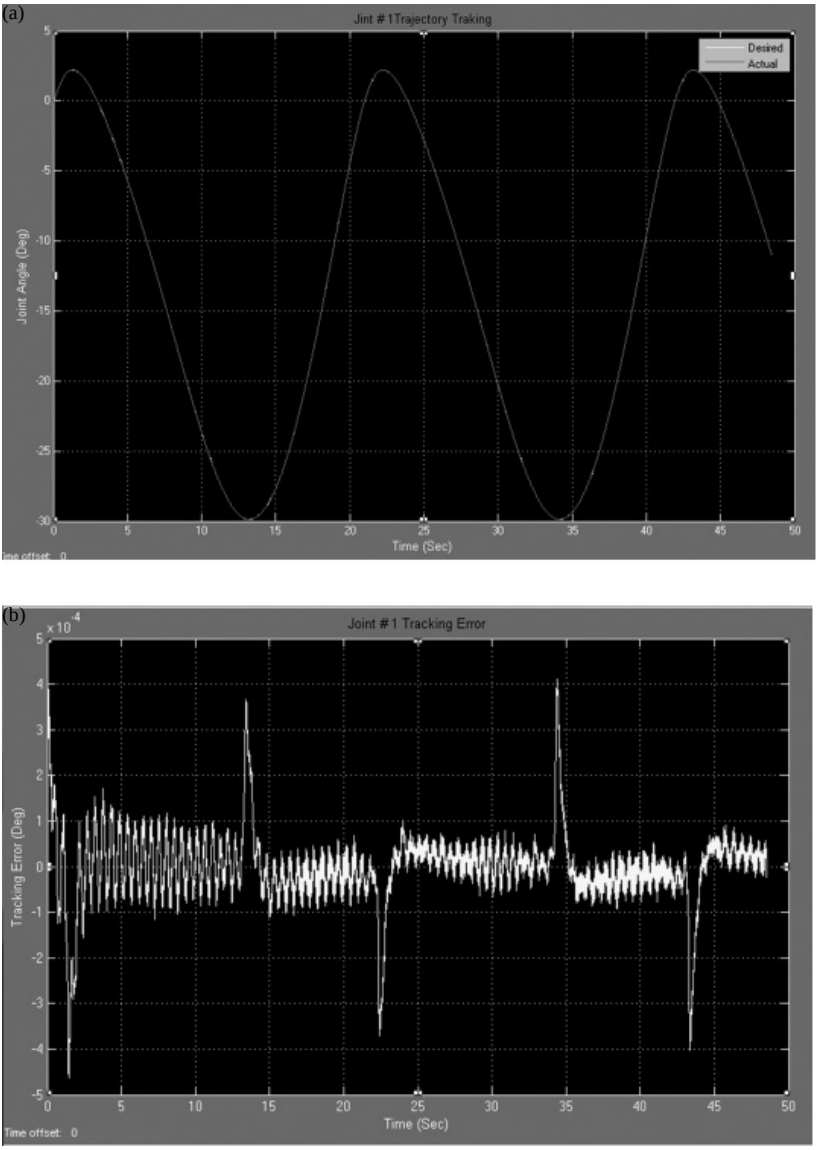


Figure 10. Trajectory Tracking Performance of the Proposed Controller: (a) Joint one angle; and (b) Joint one tracking error.

To demonstrate the performance, adaptive capability and robustness of the developed controller extensive experimental studies were performed using 2-DOF robot. In all experiments it is assumed that there exists very large parametric uncertainty

(90% error in robot dynamic parameters) and an external disturbance in the form of external torque which is equal to joint torque. Figures 10(a), and (b), illustrate the tracking performance of the proposed controllers for a sinusoidal trajectory for both joint one and joint two in the presence of the model uncertainty. Figure 11 show the trajectory

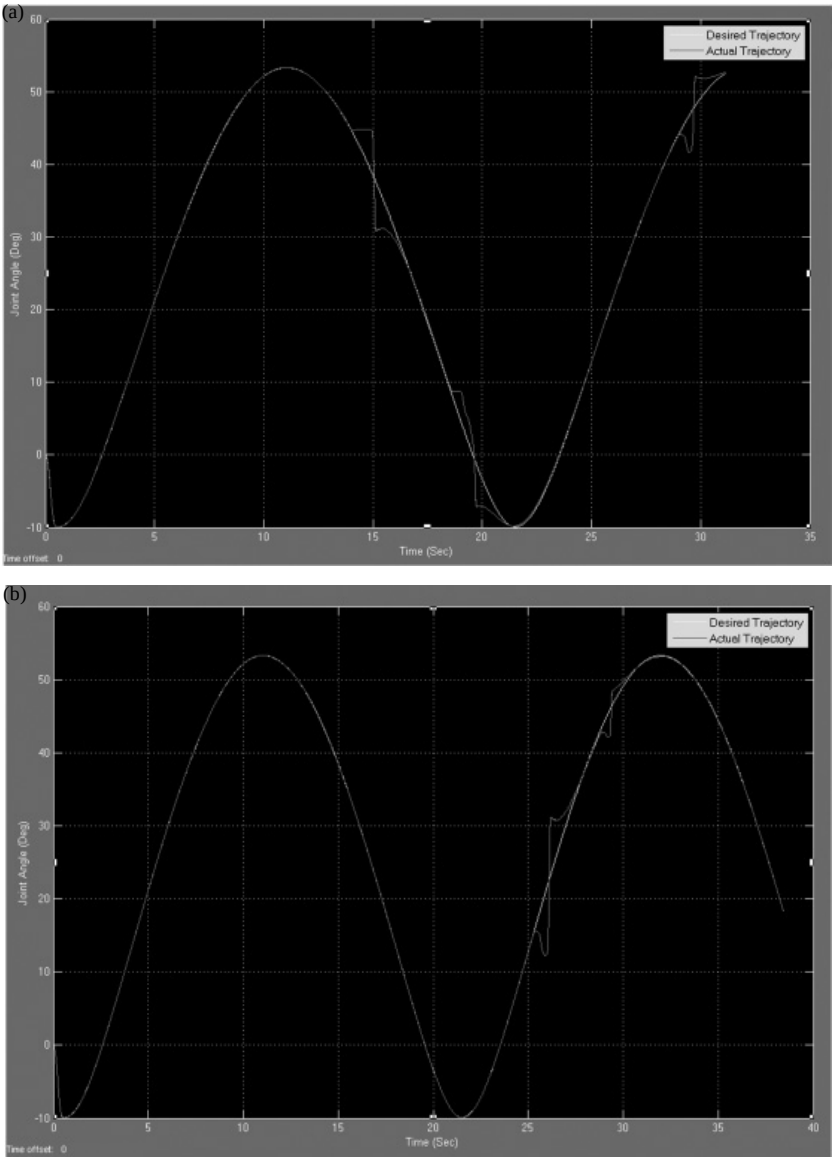


Figure 11. The Trajectory tracking performance of the proposed controller in the presence of severe external disturbances: (a) joint one; (b) Joint two.

tracking performance, and robustness of the proposed controller in the presence of the external disturbances. The

results also confirmed that the proposed ARC completely eliminates the chattering, which is illustrated in Fig. 12. Unlike to the boundary layer method, in this method chattering eliminated while accuracy and performance were not compromised.

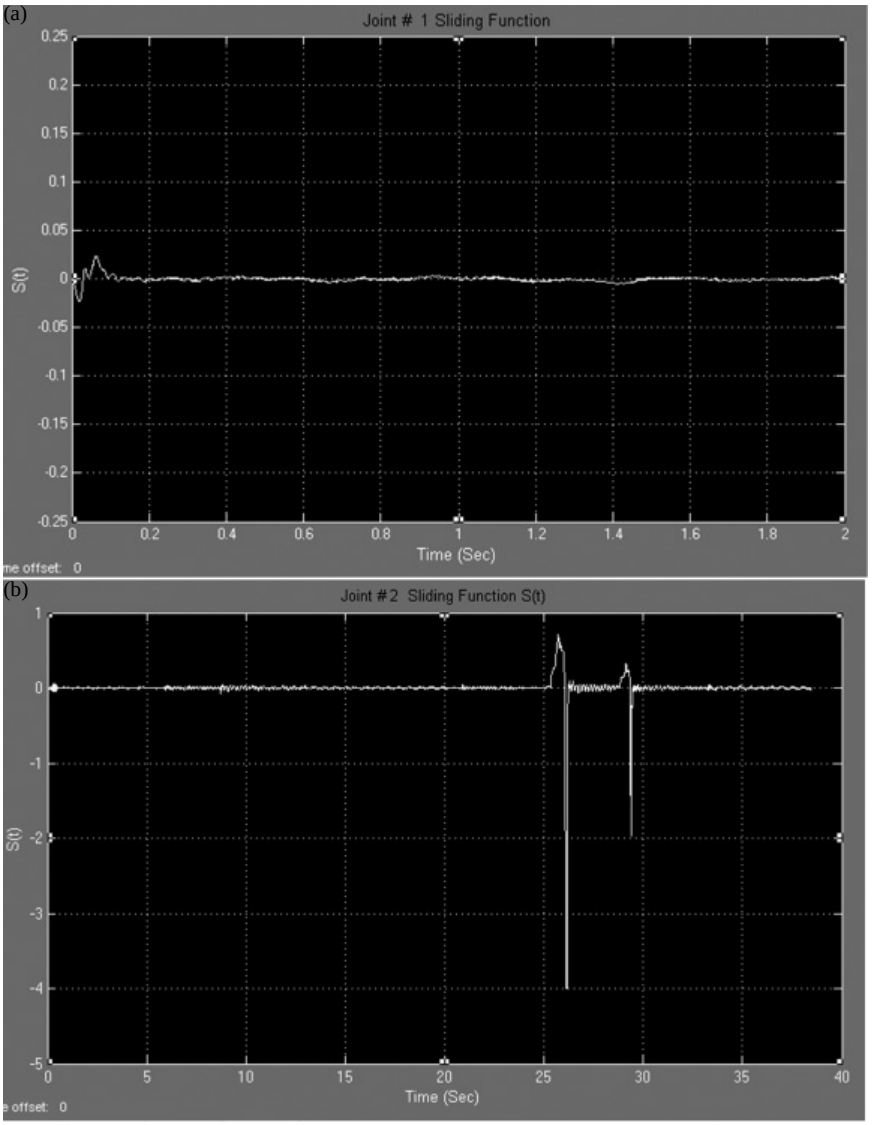


Figure 12: Convergence of sliding function $S(t)$ to zero, and staying in small neighborhood of $S(t) = 0$, also there is no chattering: (a) Joint one sliding function convergence; (b) Joint two sliding function convergence after applying disturbance two times at about $t = 26$ sec and $t = 29$ sec.

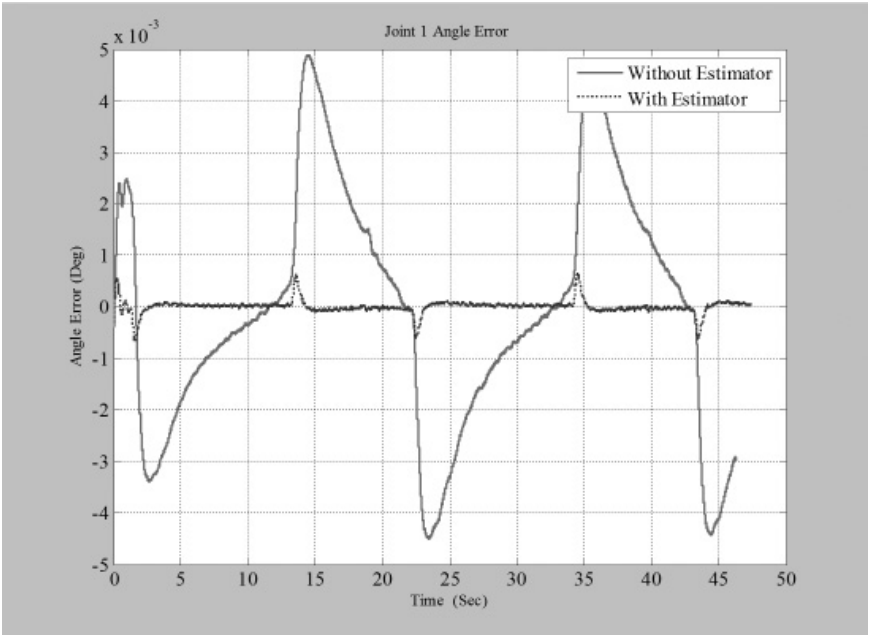


Figure 13. Comparison of tracking error with and without online estimation of the uncertainties.

CONCLUSION

In this work a systematic methodology to design an adaptive robust control using fundamentals of sliding mode control, adaptive control and Lyapunov redesign method for real-time applications of multi-link robot manipulator is developed and tested. The proposed method uses the advantages of sliding mode, adaptive control and PID techniques, while the disadvantages attributed to these methods are remedied by each other. The main contributions of the proposed approach are as follows. (1) It is proven that in the presence of fast time-varying uncertainties all trajectories will approaches the ε vicinity of the sliding surface $S(t) = 0$, because, $\dot{V}$ is negative definite for all $||S|| > \varepsilon$, i.e., Eq. (51). (2) The controller is suitable for real-time applications due to simplicity in terms of implementation and computation burden. The proposed controller can be implemented with or without any knowledge of the manipulator dynamics and the size of the uncertainties. (3) The developed

continuous adaptive robust control law can effectively eliminate the chattering. Simulation and experimental results confirmed that the proposed controller performs remarkably well in terms of the robustness, tracking error convergence and disturbance attenuation.

ACKNOWLEDGMENT

The author would like to acknowledge the financial support of Research, Development & Creativity Office (RDC Office) of Laurentian University.

REFERENCES

Angeles, J. 2003. Fundamental of robotic mechanical systems, theory, methods, and algorithms, 2nd Edition, Springer.

Boiko, I., L. Fridman, A. Pisano and E. Usai. 2007. Analysis of chattering in systems with second- order sliding modes. Automatic Control, IEEE Transactions on, 52(11): 2085–2102.

Chandrasekharan, P. C. 1996. Robust Control of Linear Dynamical Systems. Academic Press Limited, London.

Codourey, A. 1998. Dynamic modeling of parallel robots for computed-torque control implementation.
Int. J. of Robotics Research, 17(2): 1325–1336.

Craig, J. J., P. Hsu and S. S. Sastry. 1987. Adaptive control of mechanical manipulators. Int. J. of Robotics Research, 6(2): 16–28.

Curk, B. and K. Jezernik. 2001. Sliding mode control with perturbation estimation: application on DD robot mechanism. Robotica, 19: 641–648.

Elmali, H. and N. Olgac. 1992. Theory and implementation of sliding mode control with perturbation estimation. IEEE, Int. Conf. on Robotics and Automation, 3: 2114–2119.

Ghorbel, F. H., O. Chételat, R. Gunawardana and R. Longchamp. 2000. Modeling and set point control of closed-chain mechanisms: Theory and experiment. IEEE Trans. Contr. Syst. Technol., 8(5): 801–815.

Gutman, S. 1979. Uncertain dynamical systems: a Lyapunov min-max approach. IEEE, Trans.
Automatic Control AC-24, Issue 3, pp. 437–443.

Khalil, K. H. 2002. Nonlinear Systems (3rd Edition), Prentice Hall.

Kim, N., C. W. Lee and P. H. Chang. 1998. Sliding mode control with perturbation estimation: application to motion control of parallel manipulators. Control Engineering Practice, 6(11): 1321–1330.

Lee, H. and V. I. Utkin. 2007. Chattering suppression methods in sliding mode control systems.
Annual Reviews in Control, 31: 179–188.

Levant, A. 1993. Sliding order and sliding accuracy in sliding mode control. Int. J. Control, 58: 1247– 1263.

Man, Z., A. P. Poplinsky and H. R. Wu. 1994. A robust terminal sliding-mode control scheme for rigid robot manipulators. IEEE Trans. Autom. Control, 39(12): 2465–2469.

Sadeghn, N. and R. Horowitz. 1987. Stability analysis of an adaptive controller for robotic manipulators. Proc. IEEE Int. Conf. on Robotics and Automation, 3: 1223–1229.

Saengdeejing, A. and Z. Qu. 2002. Recursive estimation of unstructured uncertainty and robust control design. Proc. IEEE Conf. on Decision and Control, pp. 2220–2225.

Sanchez-Pena, R. and M. Sznaier. 1998. Robust systems theory and applications, John Wiley and Sons Inc.

Seraji, H. 1987. A new approach to adaptive control of manipulators. ASME, J. of

Dynamic Systems, Measurement and Control, 109(3): 193–202.
Slotine, J. J. E. and W. Li. 1991. Applied Nonlinear Control, Prentice-Hall Inc.
Utkin, V. 1977. Variable structure systems with sliding modes. IEEE, Trans. Auto. Control, AC-22, No. 2, pp. 212–222.
Young, K. D., V. I. Utkin and U. Ozguner. 1999. A control engineer's guide to sliding mode control.
IEEE Trans. on Cont. Systems Technology, 7(3): 328–342.
Yu, T. 1998. Terminal sliding-mode control for rigid robots. Automatica, 34(1): 51–56.
Zeinali, M. and L. Notash. 2010. Adaptive sliding mode control with uncertainty estimator for robot manipulators. Journal of Mechanism and Machine Theory, 45(1): 80–90.
Zeinali, M. 2015, Adaptive chattering-free sliding mode control design for robot manipulators based on online estimation of uncertainties and its experimental verification. Journal of Mechatronics, 3(2): 85–97.
Zhou, K., C. J. Doyle and K. Glover. 1996. Robust and Optimal Control, Prentice-Hall Inc., New Jersey.
Zhou, K., C. J. Doyle and K. Glover. 1996. Robust Optimal Control, Prentice-Hall, Inc.

6. Related Work and Discussion

Chapter 5

Robust Control of Robotic Manipulators

In this chapter we discuss the control of robots when their dynamical model is uncertain. This may arise because the robot is carrying an unknown load or because the exact evaluation of the robot's dynamics is too costly. The robust controllers in this chapter are obtained from modifications to the controllers designed in Chapter 4.

5.1 Introduction

The control of uncertain systems is usually accomplished using either an adaptive control or a robust control philosophy. In the adaptive approach, one designs a controller that attempts to "learn" the uncertain parameters of the system and, if properly designed, will eventually be a "best" controller for the system in question. In the robust approach, the controller has a fixed structure that yields "acceptable" performance for a class of plants which include the plant in question. In general, the adaptive approach is applicable to a wider range of uncertainties, but robust controller are simpler to implement and no time is required to "tune" the controller to the particular plant. In this chapter we review different robust control designs used in controlling the motion of robots. The adaptive control approach is discussed in Chapter 6. The robust control methods presented in this chapter may be used to analyze the performance of the simple controllers used by robot manufacturers which were discussed in Chapter 4, and to suggest improvements and modifications. In fact, we are able to determine the range

263

of applicability of the simple PID controllers of Chapter 4, as a function of the inherent lack of knowledge of the robot's dynamics.

The controllers designed in this chapter may be analyzed using input- output stability tools or state-space tools. In the input-output approach, the stability of the controlled robot is shown using the small-gain theorem or the passivity theorem. In the state-space approach, most designs are shown to be stable using Lyapunov-based arguments. See Chapter 2 for an overview of both approaches.

Consider the robot dynamics given in Chapter 3:

$$M(q)\ddot{q} + V_m(q,\dot{q})\dot{q} + F(\dot{q}) + G(q) = M(q)\ddot{q} + N(q,\dot{q}) = \tau - \tau_d \tag{5.1.1}$$

and assume that a desired trajectory in joint space is specified by the time function $x_d^T(t) = [q_d^T(t) \quad \dot{q}_d^T(t)]$. We will suppress the time dependence if no ambiguity results. Let q_d, $\dot{q}_d$, $\ddot{q}_d$ and v_d be bounded functions of time. In a fashion similar to Chapter 4, we assume the trajectory error e to have two components:

$$e = q_d - q, \qquad \dot{e} = \dot{q}_d - \dot{q} \tag{5.1.2}$$

The controllers of this chapter assume that measurements of q and $\dot{q}$ are available. As described in Section 3.5, variables other than q and $\dot{q}$ may be measured. The Cartesian computed-torque controllers of Section 4.7 provide a setting where Cartesian trajectory is to be followed directly. We limit our discussion to the case of joint measurements with the understanding that a desired trajectory in another coordinate system may be followed by first obtaining the corresponding joint trajectory then applying the methods of this chapter.

We may, however, assume that the measurements p and p of q and p are corrupted by a bounded noise, that is,

$$p = q + w; \qquad \dot{p} = \dot{q} + w + 2 \tag{5.1.3}$$

where $||w_i|| \square c_i$.

In Section 5.2 we discuss the computed-torque-like controllers of Section 4.4 and study their robustness properties. The section is divided into controllers whose robustness is deduced using Lyapunov stability and others whose robustness relies on input-output stability. Nonlinear controllers which are not necessarily derived from the computed-torque controllers are presented in Section 5.3. These include controllers that exploit the passivity of the robot dynamics and others which are variable-structure methods and saturation controllers without particular emphasis on the special properties of the robot. Finally, in Section 5.4 we review approaches that attempt to

robustify the controllers by modifying the robot dynamics either explicitly or implicitly.

5.2 Feedback-Linearization Controllers

The controllers designed in this section may be obtained as modification of the feedback-linearization (or computed-torque) controllers of Chapter 3. They are basically the computed-torque-like controllers of Section 4.4. We study both static and dynamic feedback designs and compare different controllers found in the literature. Note that such a study was started in Section 4.4 and some of the controllers introduced there will reappear in this chapter. The emphasis will be here on relating many of the controllers scattered through the literature and to give them a common theoretical justification.

We assume for simplicity that $v_d = 0$ in (5.1.1) and that $w_i=0$ in (5.1.3), although the effects of bounded v_d and w_i can be easily accounted for and will be considered in most examples. In a fashion similar to Chapter 4, the dynamics of the robot are transformed into the linear system

$$\begin{bmatrix} \dot{e} \\ \ddot{e} \end{bmatrix} = \begin{bmatrix} 0 & I \\ 0 & 0 \end{bmatrix} \begin{bmatrix} e \\ \dot{e} \end{bmatrix} + \begin{bmatrix} 0 \\ I \end{bmatrix} u$$

and

$$u = M(q)^{-1}[N(q,\dot{q}) - \tau] + \ddot{q}_d \tag{5.2.1}$$

leading to the nonlinear computed-torque controller

$$\tau_d = M(q)[\ddot{q}_d - u] + N(q,\dot{q}) \tag{5.2.2}$$

which, due to the invertibility of $M(q)$, gives the following closed-loop system:

$$\ddot{e}=u \tag{5.2.3}$$

which is described by the transfer function

$$E(s) = \frac{I}{s^2}U(s). \tag{5.2.4}$$

The problem is then reduced to finding a linear control u that will achieve a desired closed-loop performance; that is, find F, G, H, and J in

$$\dot{z} = Fz + Ge$$
$$u = Hz + Je,$$

or

(5.2.5) $$u(t) = [H(sI - F)^{-1}G + J]e(t) \equiv C(s)e(t)$$

Not that the notion above indicates that *u(t)* is the output of a system *C(s)* when an input *e(t)* is applied. Note also from (5.2.4) that the different joints or the robot are decoupled so that at this level, *n* SISO separate controllers may be designed to control the *n* joints of the robot. Unfortunately, the control law (5.2.2) cannot usually be implemented due to its complexity or to uncertainties present in *M(q)* and *N*(*q, $\dot{q}$*) and to the presence of v_d and w_i. Instead, one applies *v* in (5.2.6) below where $\hat{M}$ and $\hat{N}$ are estimates of *M* and *N,*

(5.2.6) $$\tau = \hat{M}[\ddot{q}_d - u] + \hat{N}$$

This in turn will reintroduce some coupling in the linear model and leads to (Fig. 5.5.1)

(5.2.7)
$$\begin{aligned} \dot{\mathbf{e}} &= A\mathbf{e} + B(u + \eta) \\ \eta &= \Delta(u - \ddot{q}_d) + M^{-1}\delta \\ \Delta &= M^{-1}\hat{M} - I_n, \qquad \delta = N - \hat{N}. \end{aligned}$$

Note *fir*st that A, 6, and therefore μ are zero if $\hat{M} = M$ and $\hat{N} = N$. In general, however, the vector μ is a nonlinear function of both *e* and *u* and cannot be treated as an external disturbance. It represents an internal disturbance of the globally linearized error dynamics caused by modelling uncertainties,
parameter variations, external disturbances, friction terms, and maybe even noise measurements [Spong and Vidyasagar 1987]. Most commercial robots are in fact controlled with the controller given in (5.2.6) with choices of $\hat{M} = I$ and $\hat{N} = 0$ See, for example, [Luh 1983] and Section 4.4. The choice of $\hat{M}$ is validated by the powerful motors used to drive the robot links, and the gearing mechanisms used to torque the motor output to an acceptable level, while showing its speed down. The choice of is validated by keeping the different motors from driving their links too fast, thus limiting the Coriolis and centripetal torques. Such commercial controllers are known as “non- model-based controllers” and have been used since the early days of robotics.

The quest for more performance is, however, leading researchers and manufacturers to use direct-drive robots and to attempt moving them at higher speeds with less powerful but more efficient motors [Asada and Youcef- Toumi 1987]. This new direction is increasing the need for more robust controllers such as the ones described next.

The approaches of this section revolve around the design of linear controllers *C(s)* such that the complete closed-loop system in Figure 5.5.1 is stable in some suitable sense (e.g., uniformly ultimately bounded, globally asymptotically stable, $p\mathcal{L}$ stable etc.) for a given class of nonlinear perturbation *μ.* In other words choose *C(s)* in (5.2.5) such that the error *e(t)* in (5.2.8) is stable in some desired sense.

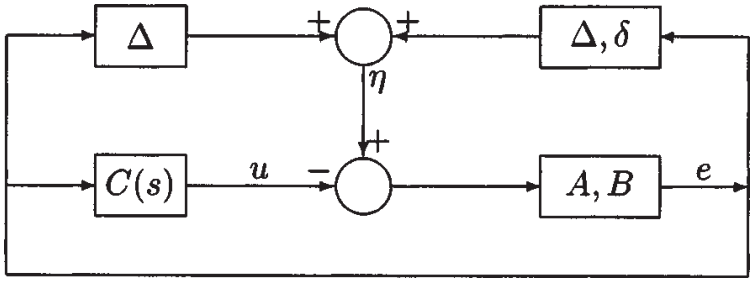


Figure 5.2.1: Feedback-linearization; uncertain structure.

The reasonable assumptions (5.2.9)–(5.2.11) below are often made for revolute-joint robots when using this approach [Spong and Vidyasagar 1987]. In the following, μ_1, μ_2, *a*, b_0, b_1, and b_2 are nonnegative finite constants which depend on the size of the uncertainties.

$$\frac{1}{\mu_2} \leq ||M^{-1}|| \leq \frac{1}{\mu_1}, \qquad \mu_1 \neq 0 \tag{5.2.8}$$

$$||\Delta|| \leq \alpha \leq 1 \tag{5.2.9}$$

$$||\delta|| \leq \beta_0 + \beta_1||\mathbf{e}|| + \beta_2||\mathbf{e}||^2 \tag{5.2.10}$$

$$||\ddot{q}_d|| \leq c. \tag{5.2.11}$$

Recall that inequality (5.2.8) was introduced in Section 3.3, and note that the norms used in the inequalities above can be, depending on the application, either □ or $\mathcal{L}_2$ norms. Also note that the bounds μ_i and b_i are scalar functions

of q for robots with prismatic joints, and that (5.2.10) is satisfied by $\hat{M} = 0.5(\mu_1 + \mu_2)I$, so that $\alpha = (\mu_2 - \mu_1)/(\mu_2 + \mu_1))$ so that $a=(\mu_2-\mu_1)/(\mu_2+\mu_1))$ [Spong and Vidyasagar 1987]. Finally, (5.2.10) is a result of the properties of the Coriolis and centripetal terms discussed in Section 3.3.

We will give different representative designs of the feedback-linearization approach, starting with controllers whose behavior is studied using Lyapunov stability theory.

Lyapunov Designs

Static feedback compensators have been extensively used starting with the works of [Freund 1982] and [Tarn et al. 1984]. Consider the controller introduced in (4.4.13):

$$u = C(s)\mathbf{e} = -K\mathbf{e} \tag{5.2.12}$$

such that

$$\dot{\mathbf{e}} = A\mathbf{e} + B(u + \eta) = (A - Bk)\mathbf{e} + B\eta = A_c\mathbf{e} + B\eta. \tag{5.2.13}$$

It can be seen that by placing the poles of A_C sufficiently far in the left half- plane, the robust stability of the closed- loop system in the presence of μ is guaranteed. This was shown true in [Arimoto and Miyazaki 1985] for the case where $\dot{q}_d = 0$ and $\tau_d = 0$ as described in Theorem 4.4.1 and Example 4.4.3. It was also shown true for the trajectory-following problem assuming that $e(0) = \dot{e}(0) = 0$ in [Dawson et al. 1990] as described in Theorem 4.4.2. There are as many robust controllers designed using Lyapunov stability concepts as there are ways of choosing Lyapunov function candidates, and of designing the gain K to guarantee that the Lyapunov function candidate is decreasing along the trajectories of (5.2.13). To decrease the asymptotic trajectory error, however, excessively large gains may be required (see Example 4.4.3). We therefore choose to use the passivity theorem and a choice of the gain matrix K that renders the linear part of the closed-loop system SPR. As described in Section 2.11, an output may be chosen to make the closed-loop system SPR; therefore allowing large passive uncertainties in the knowledge of $M(q)$. In fact, the state-feedback controller may be used to define an appropriate output Ke such that the input-output closed-loop linear systems $K(sI-A+BK)^{-1}B$ is strictly positive real (SPR). Consider the following closed- loop linear system:

$$\dot{\mathbf{e}} = \begin{bmatrix} 0 & I \\ -K_p & -K_v \end{bmatrix} \mathbf{e} + \begin{bmatrix} 0 \\ I \end{bmatrix} u$$

$$y = [K_p \quad K_v] \begin{bmatrix} e \\ \dot{e} \end{bmatrix} = K\mathbf{e}. \tag{5.2.14}$$

It may then be shown using Theorem 2.11.5 that this system is SPR if

$$K_v^2 > K_p \tag{5.2.15}$$

with the choice of

$$Q = \begin{bmatrix} 2K_p^2 & 0 \\ 0 & 2K_v^2 - 2K_p \end{bmatrix} \tag{5.2.16}$$

such that

$$P = \begin{bmatrix} 2K_pK_v & K_p \\ K_p & K_v \end{bmatrix} \tag{5.2.17}$$

is the positive-definite solution to the Lyapunov equation

$$A_c^T P + PA_c = -Q \tag{5.2.18}$$

and

$$K = B^T P = [K_v^2/a \quad K_v], \qquad a > 1. \tag{5.2.19}$$

The next theorem presents sufficient conditions for the uniform boundedness of the trajectory error.

THEOREM 5.2–1: *The closed-loop system given by (5.2.13) will be uniformly bounded if*

$$e(0) = \dot{e}(0)$$

and

$$a > 1 + \frac{1}{\mu_1}[\beta_1 + 2(\beta_2\beta_0 + \beta_2(\mu_1 + \mu_2)c)^{\frac{1}{2}}],$$

where K_V=2*aI* *and* K_P=4*aI*.

Proof:

Consider the closed-loop system given by (5.2.8), with the controller (5.2.12), and choose the following Lyapunov function candidate:

$$V = \frac{1}{2}\mathbf{e}^T P\mathbf{e} + \int_0^t y^T(\sigma)\Delta y(\sigma)d\sigma \tag{1}$$

where $\frac{1}{2}\mathbf{e}^T P\mathbf{e}$ *is the Lyapunov function corresponding to the SPR system (5.2.14). Then if* A□0, *we have that V*>0. *This condition is satisfied for* $\hat{M}$□*μ2I. Then differentiate to find*

$$\dot{V} = -\frac{1}{2}\mathbf{e}^T P\mathbf{e} + \mathbf{e}K(M^{-1}\delta - \Delta\ddot{q}_d). \tag{2}$$

To guarantee that V < 0 recall the bounds (5.2.8)–(5.2.11), and write

$$\dot{V} \leq \frac{-q_1}{2}||\mathbf{e}||^2 + \frac{k}{\mu_1}[\beta_2||\mathbf{e}||^3 + \beta_1||\mathbf{e}||^2 + (\beta_0 + (\mu_2 + \mu_1)c)||\mathbf{e}||], \tag{3}$$

where $q_1 = \lambda_{min}(Q) = 2(a-1)k$, $(a-1)I < K_p = kI$. *Let* $K_v = 2aI < K_p = 4aI < K_v^2$. *Note that* ||e|| *may be factored out of (3) without affecting the sign definiteness of the equation. The uniform boundedness of the error is then guaranteed using Lemma 2.10.3 and Theorem 2.10.3 if*

$$k\beta_2||\mathbf{e}||^2 + \left(k\beta_1 - \mu_1\frac{q_1}{2}\right)||\mathbf{e}|| + k[\beta_0 + (\mu_1 + \mu_2)c] < 0, \tag{4}$$

which is guaranteed if

$$q_1 > 2\frac{k}{\mu_1}[\beta_1 + 2(\beta_2\beta_0 + \beta_2(\mu_1 + \mu_2)c)^{1/2}] \tag{5}$$

or

$$a > 1 + \frac{1}{\mu_1}[\beta_1 + 2(\beta_2\beta_0 + \beta_2(\mu_1 + \mu_2)c)^{1/2}] \tag{6}$$

■

The error will be bounded by a term that goes to zero as *a* increases (see Theorem 2.10.3 and its proof in [Dawson et al. 1990] for details). This analysis then allows A to be arbitrarily large as long as $\hat{M}$□*μ2I,* as shown in the next example. In fact, if *N* were known, global asymptotic stability is assured from the passivity theorem since in that case 6=0. The controller is summarized in Table 5.2.1.

It is instructive to study (6) and try to understand the contribution of each of its terms. The following choices will help satisfy (6).

1. Large gains K_p and K_V which correspond to a large *a*.

2. A good knowledge of N which translates into small p_i's.
3. A large μ_1 or a large inertia matrix $M(q)$.
4. A trajectory with a small c, this a small desired acceleration $\ddot{q}_d$.

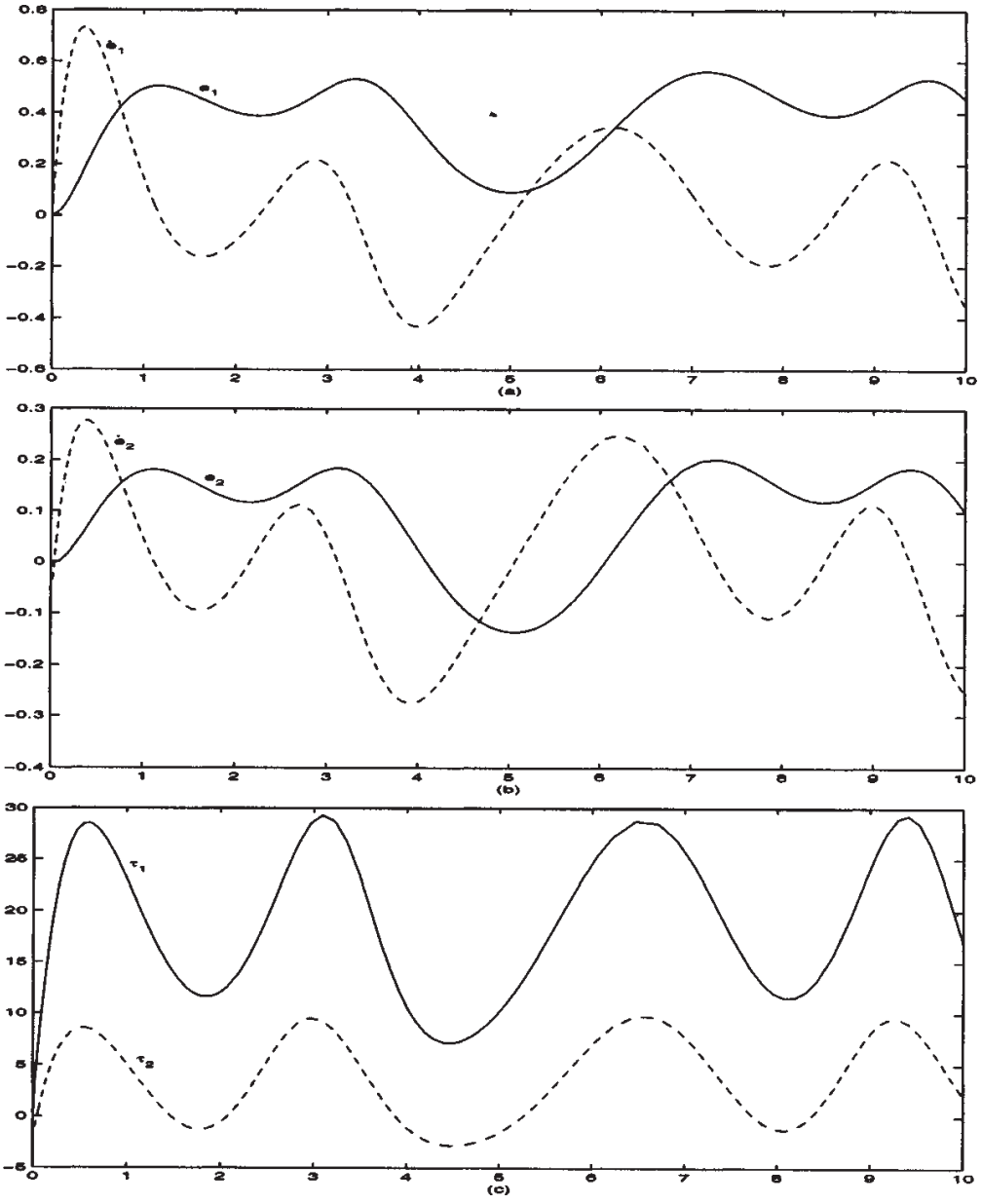


Figure 5.2.2: K_p=50, K_V=25 (a) errors of joint 1; (b) errors of joint 2; (c) torques of joints 1 and 2.

The following example illustrates the sufficiency of condition (6) and of the effects of larger gains K_p and K_V.

EXAMPLE 5.2–1: Static Controller (Lyapunov Design)

In all our examples in this chapter we use the two-link revolute-joint robot first described in Chapter 3, Example 3.2.2, whose dynamics are repeated here:

$$\begin{bmatrix} M_{11}(q) & M_{12}(q) \\ M_{12}(q) & M_{22}(q) \end{bmatrix} \begin{bmatrix} \ddot{q}_1 \\ \ddot{q}_2 \end{bmatrix} + \begin{bmatrix} m_1(q,\dot{q}) \\ m_2(q,\dot{q}) \end{bmatrix} = \begin{bmatrix} \tau_1 \\ \tau_2 \end{bmatrix} \tag{1}$$

where

$$\begin{aligned} M_{11}(q) &= (m_1+m_2)a_1^2 + m_2a_2^2 + 2m_2a_1a_2\cos(q_2) \\ M_{12}(q) &= m_2a_2^2 + m_2a_1a_2\cos(q_2) \\ M_{22}(q) &= m_2a_2^2 \\ m_1(q,\dot{q}) &= -m_2a_1a_2(2\dot{q}_1\dot{q}_2 + \dot{q}_2^2)\sin(q_2) + (m_1+m_2)ga_1\cos(q_1) \\ &\quad + m_2ga_2\cos(q_1+q_2) \\ m_2(q,\dot{q}) &= m_2a_1a_2\dot{q}_1^2\sin(q_2) + m_2gq_2\cos(q_1+q_2) \end{aligned} \tag{2}$$

The parameters m_1=1kg, m_2=1kg, a_1=1m, a_2=1m, and g=9.8 m/s^2 are given. Let the desired trajectory used in all examples throughout this chapter be described by

$$q_d = \begin{bmatrix} \sin t \\ \sin t \end{bmatrix}, \qquad \dot{q}_d = \begin{bmatrix} \cos t \\ \cos t \end{bmatrix}$$

Then $||q_d||_\infty = 1$ rad, $||\dot{q}_d||_\infty = 1 rad/s^2$. It may then be shown that

$$\mu_1 = 0.1, \qquad \mu_2 = 6$$

Let $\hat{N}$=0 then

$$||\delta|| \le \sqrt{10}||\mathbf{e}||^2 + 2\sqrt{10}||\mathbf{e}|| + \sqrt{10}$$

or that

$$\beta_0 = \sqrt{10}, \qquad \beta_1 = 2\sqrt{10}, \qquad \beta_2 = \sqrt{10}$$

Then use $\hat{M}$=6I and a=172 to satisfy (6). In fact, these values will lead to a larger controller gains than are actually needed. Suppose instead that we let $6\hat{I}$, $\hat{N}$=0, and that

(3)
$$u = -\frac{50}{6}e - \frac{25}{6}\dot{e}$$
$$\tau = 6(\ddot{q}_d - u).$$

Note that this is basically a computed-torque-like PD controller. A simulation of the robot's trajectory is shown in Figure 5.2.2. We also start our simulation at $e(0) = \dot{e}(0)$=0. The effect of increasing the gains is shown in Figure 5.2.3, which corresponds to the controller

(4)
$$u = -\frac{225}{6}e - \frac{30}{6}\dot{e}$$
$$\tau = 6(\ddot{q}_d - u).$$

Note that at least initially, more torque is required for the higher-gains case (compare Figs. 5.2.2c and 5.2.3c) but that the errors magnitude is greatly reduced by expanding more effort.

■

There are other proofs of the uniform boundedness of these static controllers. In particular, the results in [Dawson et al. 1990] provide an explicit expression for the bound on e in terms of the controller gains. In the interest of brevity and to present different designs, we choose to limit our development to one controller in this section.

As discussed in Section 4.4, a residual stead-state error may be present even when using an exact computed-torque controller if disturbances are present. A common cure for this problem (and one that will eliminate constant disturbances) is to introduce integral feedback as done in Section 4.4. Such a controller may again be used within a robust controller framework and will lead to similar improvements if the integrator windup problem is avoided (see Section 4.4).

In the next section we show the stability of static controllers similar to the ones designed here and use input-output stability methods to design more general dynamic compensators.

Input-Output Designs

In this section we group designs that show the stability of the trajectory error using input-output methods. In particular, we present controllers that show $\mathcal{L}_\infty$ and $\mathcal{L}_2$ stability of the error. We divide this section into a subsection that deals with static controllers such as the ones described previously,

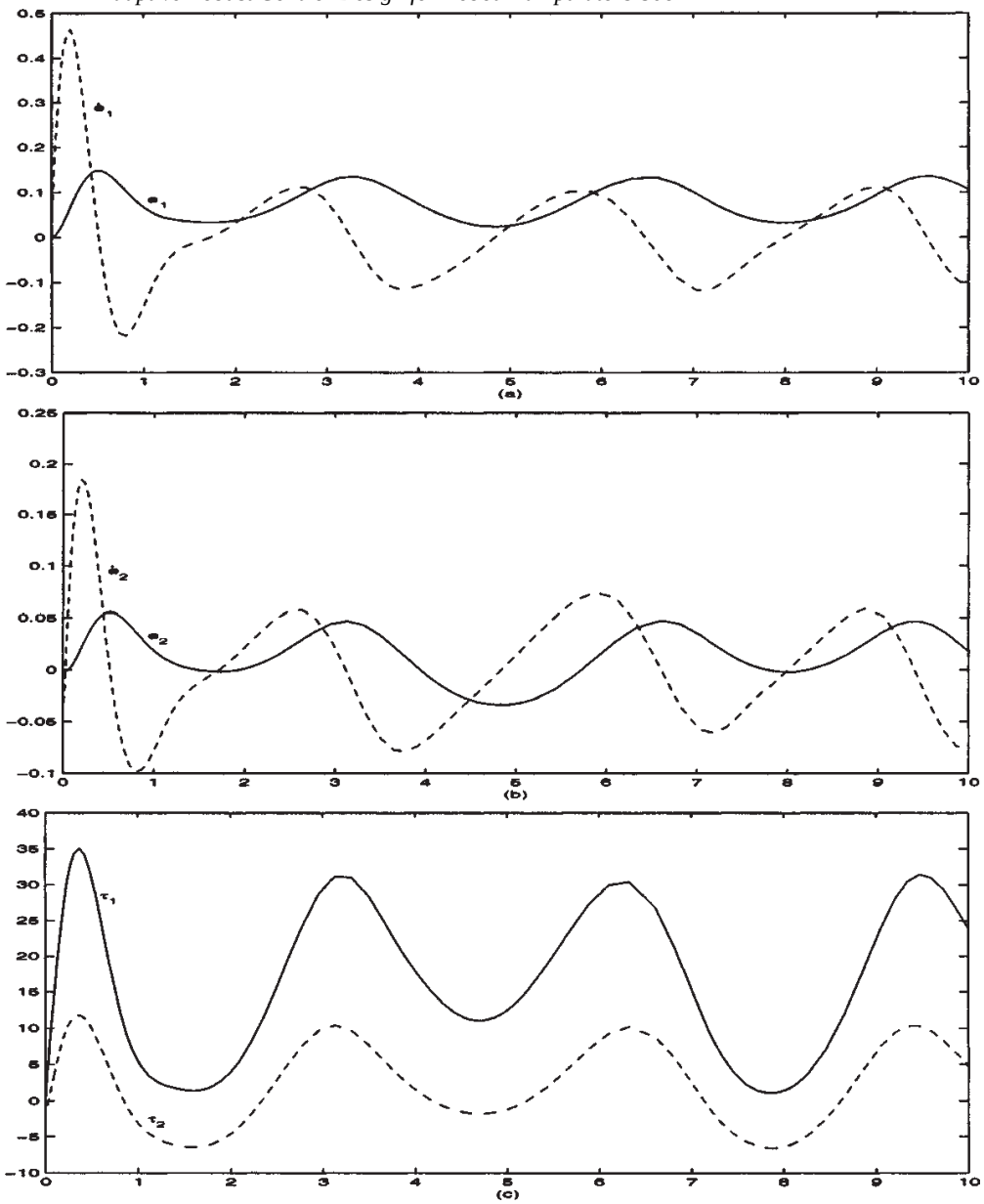


Figure 5.2.3: K_p=225, K_v=30 (a) errors of joint 1; (b) errors of joint 2; (c) torques of joints 1 and 2.

and a subsection dealing with the more general dynamic controllers, which have similar gains in general.

Static Controllers

These controllers have the same structure as the ones described in Section 4.4 and in the preceding section. The difference is that here we show the stability of the error using input-output concepts rather that the state-space methods implied by Lyapunov theory. In [Craig 1988] the boundedness of

Table 5.2.1: Static Controller, Lyapunov Design

Assumptions:

$$\begin{aligned} \frac{1}{\mu_2} &\leq ||M^{-1}|| \leq \frac{1}{\mu_1}, \quad \mu_i \neq 0 \\ ||\Delta|| &\leq a \leq 1 \\ ||\delta|| &\leq \beta_0 + \beta_1||\mathbf{e}|| + \beta_2||\mathbf{e}||^2 \\ ||\ddot{q}_d|| &\leq c \\ e(0) &= \dot{e}(0) = 0 \end{aligned}$$

Controller:

$$\begin{aligned} \tau &= \hat{M}(\ddot{q}_d + 2a\dot{e} + 4ae) + \hat{N} \\ \hat{M} &> \mu_2 I \\ a &> 1 + \frac{1}{\mu_1}[\beta_1 + (2\beta_2\beta_0 + \beta_2(\mu_1 + \mu_2)c)^{\frac{1}{2}}] \end{aligned}$$

Performance:
Guaranteed Lyapunov stability of e and $\dot{e}$. The errors go to zero as a is increased.

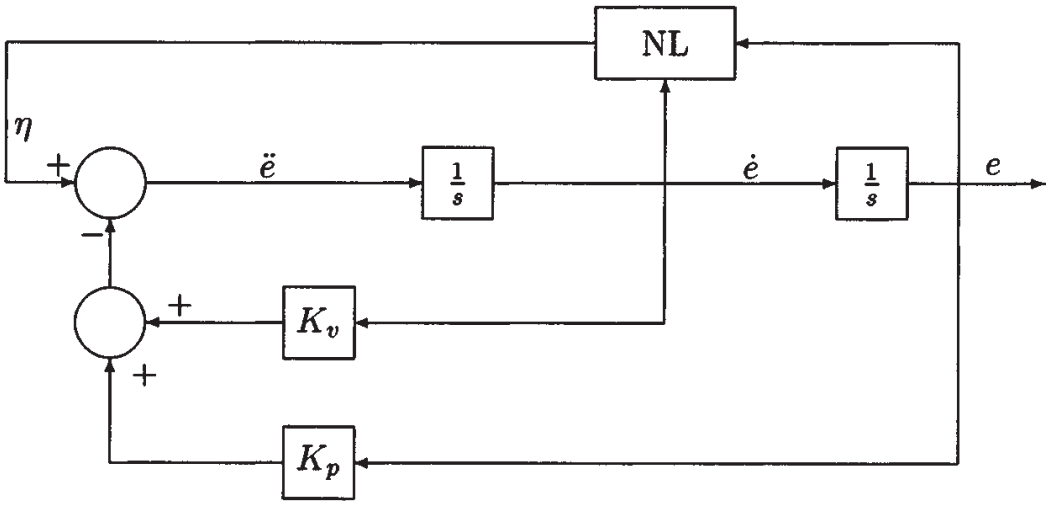


Figure 5.2.4: Block Diagram for second-order differential equation.

the error signals was shown using a static controller. The norms used in (5.2.8)–(5.2.10) are then $\mathcal{L}$ norms. The development of this controller starts with assumptions (5.2.8), (5.2.9), and a modification of (5.2.10) to

(5.2.20) $$||\delta|| \leq \beta_0 + \beta_1||\dot{e}|| + \beta_2||\dot{e}||^2$$

This assumption is justified by the fact that *N* is composed of gravity and velocity-dependent terms which may be bounded independent from the position error *e* [see (5.1.1)]. We shall also assume that $e(0) = \dot{e}(0)$=0. Let us then choose the state-feedback controller (5.2.12) repeated here for convenience:

$$u = -K_p e - K_v \dot{e} \tag{5.2.21}$$

The corresponding input-output differential equation

(5.2.22) $$\ddot{e} + K_v\dot{e} + K_p e = \eta$$

A block diagram description of this equation is given in Figure 5.2.4. Consider now the transfer function from η (taken as an independent input) to e:

$$\begin{bmatrix} E(s) \\ sE(s) \end{bmatrix} = \begin{bmatrix} (s^2 + sK_v + K_p)^{-1} \\ s(s^2 + sK_v + K_p)^{-1} \end{bmatrix} \eta(s) = \begin{bmatrix} P_{11}(s) \\ P_{12}(s) \end{bmatrix} \tag{5.2.23}$$

or

(5.2.24) $$\mathbf{E}(s) = P_1(s)\eta(s)$$

It can be seen that K_V and K_P are both diagonal, with $K_v^2 = 4K_p$, a critically damped response it achieved at every joint [see (4.4.22), (4.4.30), and (3.3.32)]. The infinity operator gains of $P_{11}(s)$ and $P_{12}(s)$ are (see Lemma 2.5.2 and Example 2.5.8)

$$\gamma_\infty(P_{11}) \equiv \gamma_{11} = \frac{1}{k_p}, \qquad \gamma_\infty(P_{12}) \equiv \gamma_{12} = \frac{4}{ek_v} \tag{5.2.25}$$

where

$$k_p = \max\{K_{pi}\}, \qquad k_v = \max\{K_{vi}\}, \qquad e = 2.71828 \tag{5.2.26}$$

Consider then the following inequalities:

$$\begin{aligned} ||e||_{T\infty} &\leq \gamma_{11}||\eta||_{T\infty} \\ ||\dot{e}||_{T\infty} &\leq \gamma_{12}||\eta||_{T\infty} \end{aligned}$$

and using (5.2.8)–(5.2.11), we have that

$$||r||_{T\infty} \leq ac + ak_p||e||_{T\infty} + ak_v||\dot{e}||_{T\infty} + \frac{\beta_0}{\mu_1} + \frac{\beta_1}{\mu_1}||\dot{e}||_{T\infty} + \frac{\beta_2}{\mu_1}||\dot{e}||^2_{T\infty} \tag{5.2.27}$$

The following theorem presents sufficient conditions for the boundedness of the error that parallel those of Theorem 5.2.1.

THEOREM 5.2–2: *Suppose that*

$$e(0) = \dot{e}(0) = 0$$

and

$$\gamma_{12}\left(ak_v + \frac{\beta_1}{\mu_1}\right) = \frac{4a}{e} + \frac{4\beta_1}{e\mu_1 k_v} < 1 \tag{1}$$

Then the $\mathcal{L}_\infty$ stability of the error is guaranteed if

$$1 - \gamma_{11}ak_p - \gamma_{12}\left(ak_v + \frac{\beta_1}{\mu_1}\right) - 2\gamma_{12}\left[\left(a||\ddot{q}_d|| + \frac{\beta_0}{\mu_1}\right)\frac{\beta_2}{\mu_1}\right]^{\frac{1}{2}} > 0 \tag{2}$$

Proof:

The condition above results from applying the small-gain theorem to the closed-loop system, under the assumption that e(0)=0 *so that the quadratic term* ||e||^2 *is small. See [Craig 1988] for details.*

Note that (2) reduces to

$$1 - a\left(1 + \frac{4}{e}\right) - \frac{4\beta_1}{\mu_1 e k_v} - 2\frac{4}{ek_v}\left[\left(a||\ddot{q}_d|| + \frac{\beta_0}{\mu_1}\right)\frac{\beta_2}{\mu_1}\right]^{\frac{1}{2}} > 0$$

and further to

$$k_v = \frac{4\beta_1 - 8[(a\mu_1 c + \beta_0)\beta_2]^{\frac{1}{2}}}{\mu_1 e[1 - a(1 + \frac{4}{e})]}. \tag{5.2.28}$$

Let us study the inequality above to determine the effect of each term. The following observations are made to help satisfy (5.2.28).

1. A large k_V will help satisfy the stability condition. Note: That will also imply a large k_P.

2. A good knowledge of *N,* which will translate into small p_i's.

3. A large μ_1 or a large inertia matrix *M(q)*.

4. A trajectory with a small $\ddot{q}_d$.

5. Robots whose inertia matrix *M(q)* does not vary greatly throughout its workspace (i.e. $\mu_1 \square \mu_2$)), so that *a* is small. Note that a small a is needed to guarantee that at least $a(1+\frac{4}{e})<1$ in (5.2.28). This will translate into the severe requirement that the matrix *M* should be close to the inertia matrix *M(q)* in all configurations of the robot.

The controller is summarized in Table 5.2.2.

These observations are similar to those made after inequality (6) and are illustrated in the next example.

EXAMPLE 5.2–2: Static Controller (Input-Output Design)

Consider the nonlinear controller (5.2.6), where

$$\hat{M} = \frac{M(q)}{4}, \qquad \hat{N} = 0 \tag{1}$$

Therefore,

$$a = \frac{1}{4} \tag{2}$$

Condition (1) is then satisfied if k_V>720. This of course is a large bound that can be improved by choosing a better $\hat{N}$. A simulation of the closed-loop behavior for k_P=225 and k_V=30 is shown in Figure 5.2.5. The errors magnitudes are much smaller than those achieved with the PD controllers of Example 5.2.1 with a comparable control effort. This improvement came with the expense of knowing the inertia matrix *M(q)* as seen in (1).

■

Dynamic Controllers

The controllers discussed so far are static controllers in that they do not have a mechanism of storing previous state information. In Chapter 4 and in this chapter, these controllers could operate only on the current position and velocity errors. In this section we present three approaches to show the robustness of dynamic controllers based on the feedback-linearization

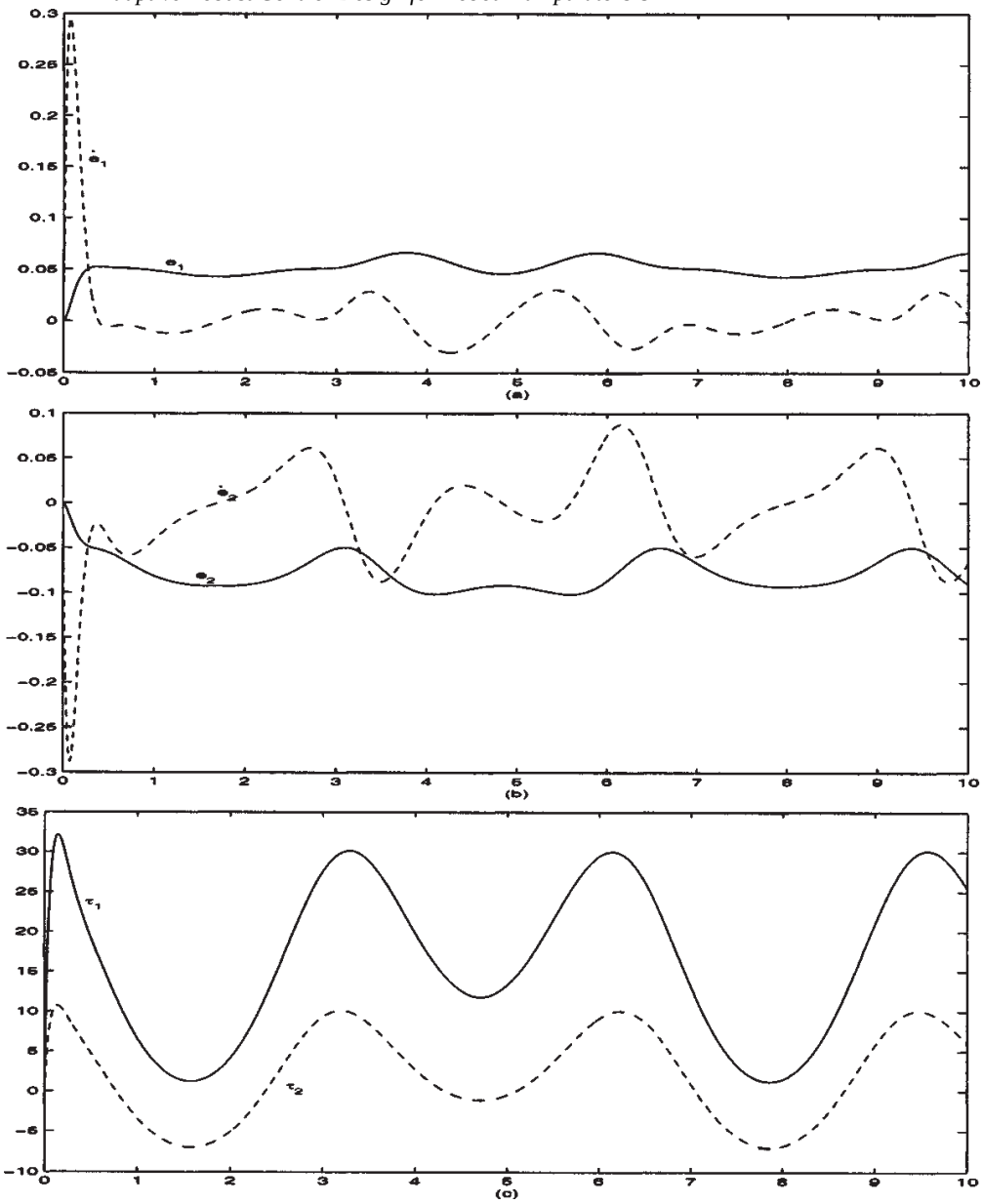


Figure 5.2.5: K_p=225, K_V=30 (a) errors of joint 1; (b) errors of joint 2; (c) torques of joints 1 and 2.

method. The first two approaches are one-degree-of-freedom (DOF) feedback compensators, while the last one is a two-DOF compensator.

One-Degree-of-Freedom Designs.

The first class of dynamic controllers are called one-degree-of-freedom controllers because they can only operate on the measured output of the robot. In other words, these are controllers that will take the measured signals and filter them through a dynamical system before feeding the signal back to the input. They should be contrasted with the static controllers,

Table 5.2.2: Static Controller, Input-Output Design

Assumptions:

$$\begin{aligned} \frac{1}{\mu_2} &\leq ||M^{-1}|| \leq \frac{1}{\mu_1}, \quad \mu_i \neq 0 \\ ||\Delta|| &\leq a \leq 1 \\ ||\delta|| &\leq \beta_0 + \beta_1||\mathbf{e}|| + \beta_2||\mathbf{e}||^2 \\ ||\ddot{q}_d|| &\leq c \\ e(0) &= \dot{e}(0) = 0 \end{aligned}$$

Controller:

$$\tau = \hat{M}(\ddot{q}_d + k_v\dot{e} + \frac{k_v^2}{4}e) + \hat{N}$$

$$1 - a\left(1 + \frac{4}{e}\right) - \frac{4\beta_1}{\mu_1 e k_v} - 2\frac{4}{e k_v}\left[\left(a||\ddot{q}_d|| + \frac{\beta_0}{\mu_1}\right)\frac{\beta_2}{\mu_1}\right]^{\frac{1}{2}} > 0 \quad (5.2.29)$$

Performance:

Guaranteed boundedness of e and $\dot{e}$. The errors go to zero as k_v is increased.

which did not used dynamical feedback, and with the two-degree-of-freedom controllers considered next.

In [Spong and Vidyasagar 1987] the factorization approach was used to design a class of dynamic linear compensators *C(s),* parameterized by a stable transfer matrix *Q(s),* which guarantee that the solution *e(t)* to the linear system (5.2.9) is bounded. The actual factorization approach design is beyond the scope of this book, but fairly general representative of the methodology as it applies to robotics is given in Example 5.2.3. In [Spong and Vidyasagar 1987] it was actually assumed that the bound on *6* is linear [i.e., p_2=0 in 5.2.10)] before the family of all □ stabilizing compensators of the nominal plant was found. Although the case of noisy measurements was treated in [Spong and Vidyasagar 1987], we limit ourselves to the noiseless case for simplicity. Let us first recall the system (5.2.16), while suppressing the *s* dependence,

$$\mathbf{e} = G(I - CG)^{-1}\eta \equiv P_1\eta \quad (5.2.30)$$

and define

$$u = CG(I - CG)^{-1}\eta \equiv P_2\eta \tag{5.2.31}$$

and let the operator gains of P_i, i=1,2, be given by

$$\gamma_\infty(P_i) = \gamma_i, \qquad i = 1, 2. \tag{5.2.32}$$

Note that μ_1=max μ_{11}, μ_{12}. See Lemma 2.5.2 and Example 2.5.8. Consider then

$$\begin{aligned} ||\mathbf{e}||_{T\infty} &\leq \gamma_1||\eta||_{T\infty} \\ ||u||_{T\infty} &\leq \gamma_2||\eta||_{T\infty} \\ ||\eta||_{T\infty} &\leq a||\ddot{q}_d||_{T\infty} + a||u||_{T\infty} + \frac{\beta_0}{\mu_1} + \frac{\beta_1}{\mu_1}||\mathbf{e}||_{T\infty}. \end{aligned} \tag{5.2.33}$$

The next theorem gives sufficient conditions for the BIBO stability of the trajectory error.

THEOREM 5.2–3: *The BIBO stability of the closed-loop system (5.2.30) will be guaranteed if*

$$1 - \frac{\beta_1\gamma_1}{\mu_1} - a\gamma_2 > 0 \tag{1}$$

In fact, the trajectory error is bounded by

$$\begin{aligned} ||\mathbf{e}||_\infty &\leq \frac{\gamma_1 b}{1 - \beta_1\gamma_1/\mu_1 - a\gamma_2} \\ b &= a||\ddot{q}_d||_{T\infty} + \frac{\beta_0}{\mu_1} \end{aligned} \tag{2}$$

Proof:

By the small-gain theorem. See [Spong and Vidyasagar 1987] for details. ■

If we study (1) carefully we note that it will be satisfied if

1. μ_1 is large or $M(q)$ is large.
2. Good knowledge of N, resulting in a small β_1.
3. Small μ_1 due to a large gain of the compensator C.

4. μ_2 close to 1, which may also be obtained with a large-gain compensator *C.*

Note that in the limit, and as the gain of *C(s)* becomes infinitely large, μ_1 goes to zero. This will then transform condition (1) to

$$a < \frac{1}{\gamma_2} \tag{5.2.34}$$

It is also seen from (5.2.33)–(5.2.34) that increasing the gain *k* of *C(s)* will decrease μ_1, therefore decreasing $\|\mathbf{e}\|$. A particular compensator may now be obtained by choosing the parameter *Q(s)* to satisfy other design criteria, such as suppressing the effects of *μ*. One can, for example, recover Graig's compensator, by choosing *C(s)=-K* so that the control effort is given by

$$u=K\mathrm{e}. \tag{5.2.35}$$

Then note that conditions (5.2.28) and (1) are identical if $p_2=0$ and $\mu_2=\mu_{11}k_p+\mu_{12}k_v$. Also note from (2) that a smaller $\ddot{q}_d$ results in a smaller tracking error. In fact, if $\ddot{q}_e=0$ and $p_0=0$, the asymptotic stability of the error may be shown. Finally, note that the presence of bounded disturbance will make the bound on the error e larger but will not affect the stability condition (1). This controller is summarized in Table 5.2.3.

The factorization approach gives the family of all one-degree-of-freedom stabilizing compensators *C(s).* The design methodology is illustrated for the two-link robot in the next example.

EXAMPLE 5.2–3: Dynamic Controller (Input-Output Design)

Let $G_v(s)$ of Example 4.2.1 be factored as

(1)
$$G_v(s) = [\tilde{D}(s)]^{-1}\tilde{N}(s) = N(s)D(s)$$

where *N(s), D(s), N(s)*, and *D(s)* are matrices of stable rational functions. We can then find

(2)
$$\begin{aligned} N(s) &= \tilde{N}(s) = \frac{1}{(s+1)^2}\begin{bmatrix} I \\ sI \end{bmatrix} \\ D(s) &= \frac{s^2}{(s+1)^2}I \\ \tilde{D}(s) &= \frac{1}{(s+1)^2}\begin{bmatrix} (s^2+2s)I & -2I \\ -sI & (s^2+1)I \end{bmatrix}. \end{aligned}$$

Table 5.2.3: Dynamic One-DOF Controller: Design 1

Assumptions:

$$\begin{aligned} \frac{1}{\mu_2} &\leq ||M^{-1}|| \leq \frac{1}{\mu_1}, \quad \mu_i \neq 0 \\ ||\Delta|| &\leq a \leq 1 \\ ||\delta|| &\leq \beta_0 + \beta_1||\mathbf{e}|| + \beta_2||\mathbf{e}||^2 \\ ||\ddot{q}_d|| &\leq c \\ e(0) &= \dot{e}(0) = 0 \end{aligned}$$

Controller:

$$\tau = \hat{M}(\ddot{q}_d + C(s)\mathbf{e}) + \hat{N}$$

with

$$\begin{aligned} ||\mathbf{e}||_{T\infty} &\leq \gamma_1||\eta||_{T\infty} \\ ||u||_{T\infty} &\leq \gamma_2||\eta||_{T\infty} \\ ||\eta||_{T\infty} &\leq a||\ddot{q}_d||_{T\infty} + a||u||_{T\infty} + \frac{\beta_0}{\mu_1} + \frac{\beta_1}{\mu_1}||\mathbf{e}||_{T\infty} \\ 1 - \frac{\beta_1\gamma_1}{\mu_1} - a\gamma_2 &> 0 \end{aligned}$$

Performance:

$$\begin{aligned} ||\mathbf{e}||_\infty &\leq \frac{\gamma_1 b}{1 - \beta_1\gamma_1/\mu_1 - a\gamma_2} \\ b &= a||\ddot{q}_d||_{T\infty} + \frac{\beta_0}{\mu_1} \end{aligned}$$

Next we solve the Bezout indentity [Vidyasagar 1985] for *X(s)* and *Y(s),* which are also stable rational functions,

Y(s)D(s)+X(s)N(s)=I

to get

$$X(s) = \frac{1}{(s+1)^2}[(1+2s)I \quad (2+4s)I], \qquad Y(s) = \frac{s^2+4s+2}{(s+1)^2}I. \tag{3}$$

Then all the stabilizing controllers are given by

$$C(s) = -[Y(s) - Q(s)\tilde{N}(s)]^{-1}[X(s) + Q(s)\tilde{D}(s)], \tag{4}$$

where *Q(s)* is a stable rational function which is otherwise arbitrary. One choice, of course, is to let *Q(s)*=0, which leads to the "central solution" [Vidyasagar 1985]

$$C(s) = \frac{2s+1}{s^2+4s+2}[I \quad 2I]. \tag{5}$$

One can also choose *Q(s)* to satisfy the required performance. In particular, the following choice of *Q(s)* is presented in [Spong and Vidyasagar 1987]:

$$Q(s) = \left[2I \quad \frac{4k+(k+2)s}{s+k}I\right], \qquad k = 1, 2, 3, \ldots, \tag{6}$$

which leads to the following controller:

$$C(s) = [C_1(s) \quad C_2(s)],$$

where

$$C_1(s) = \frac{-[2s^3+(k+4)s^2+(2k+1)s+k]}{s^2(s+2)}I$$

$$C_2(s) = \frac{-[(k+2)s^3+4(k+1)s^2+5ks+2k]}{s^2(s+2)}I$$

and

$$u = C_1(s)e + C_2(s)\dot{e}. \tag{7}$$

As *k* increases, the disturbance rejection property of the controller is enhanced at the expense of higher gains as seen from the expression of *C(s).* A simulation

of this controller for k=225 is shown in Figure 5.2.6. The following observations are in order: The trajectory errors are smaller than any of the previous controllers while the torque efforts are comparable. In addition, the complexity of the controller is acceptable since the dynamics of the robot are not used in implementing the control.

■

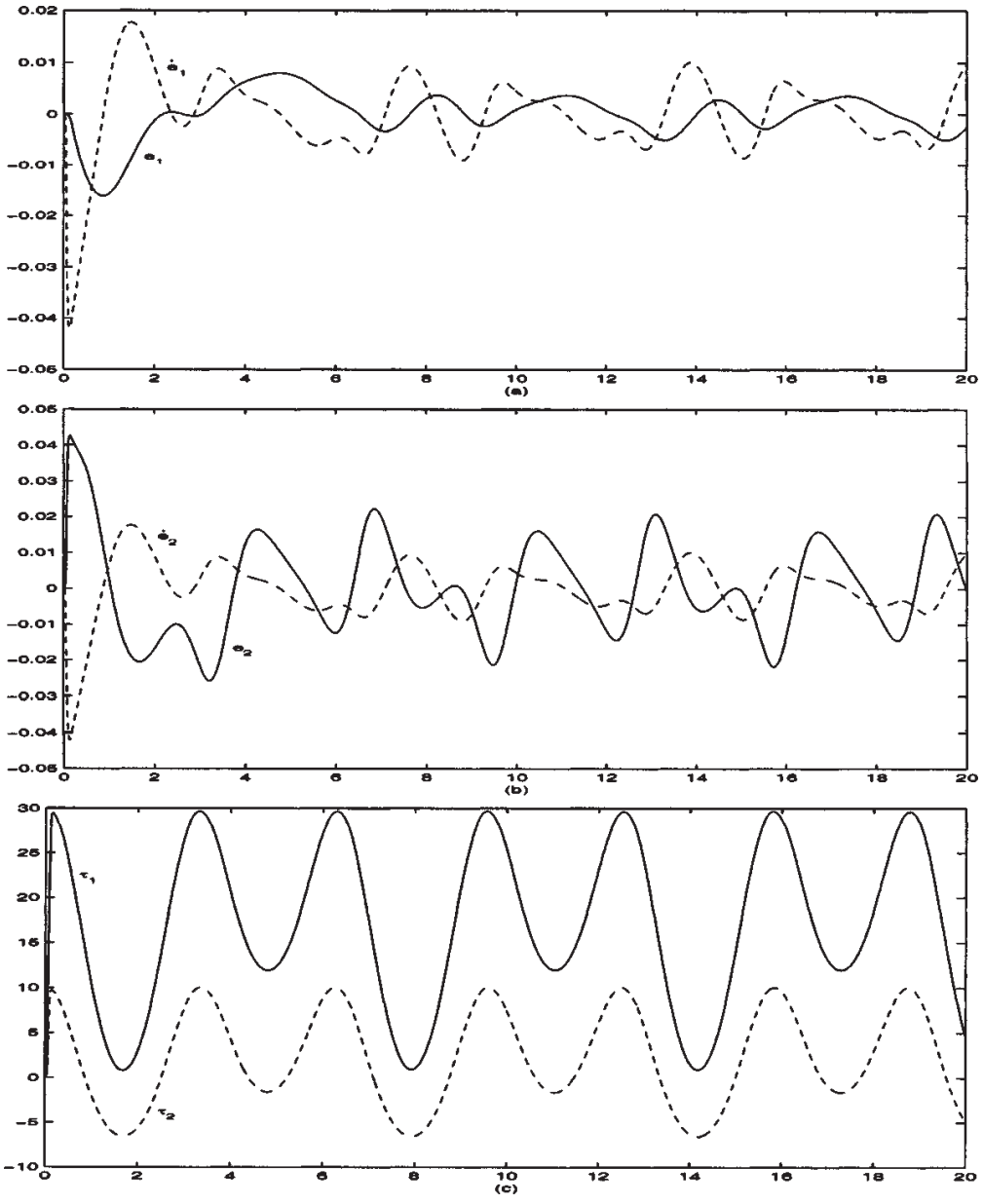


Figure 5.2.6: (a) errors of joint 1; (b) errors of joint 2; (c) torques of joints 1 and 2.

As it was discussed in [Craig 1988] and presented in Theorem 5.2.2, including the more reasonable quadratic bound will not destroy the L

□

stability result of [Spong and Vidyasagar 1987]. It was shown in [Becker and Grimm 1988], however, that the $\mathcal{L}$ stability of the error cannot be guaranteed unless the problem is reformulated and more assumptions are made. It effect, the error will be bounded, but it may or may not have a finite energy. In particular, noisy measurements are no longer tolerated for $\mathcal{L}$ stability to hold. We next present an extension of the $\mathcal{L}$ stability result that applies to dynamical compensators similar to the one described in Theorem 5.2.3 but without the requirement that p_2=0.

THEOREM 5.2–4: *The error system of (5.2.30) is $\mathcal{L}$ bounded if*

$$e(0) = \dot{e}(0)=0$$

and

(1)
$$1 - \gamma_2 ak - \gamma_1 \frac{\beta_1}{\mu_1} - 2\gamma_1 \left[\left(ac + \frac{\beta_0}{\mu_1} \right) \frac{\beta_2}{\mu_1} \right]^{\frac{1}{2}} > 0$$

Proof:

An extension of the small-gain theorem. See [Becker and Grimm 1988] for details. ■

A study of (1) reveals that the following desired characteristics will help satisfy the inequality:

1. A large μ_1 due to a large $M(q)$.
2. A small μ_1 and a μ_2 close to 1, which will result from a large-gain compensator C.
3. Small p_i's, which will result from a good knowledge of N.
4. A small c due to a small $\ddot{q}_d$.

Note that Craig's conditions in Theorem 5.2.2 are recovered if μ_1=max μ_{11}, μ_{12} and $\mu_2 k$=$\mu_{11} k_p$+$\mu_{12} k_v$.

On the other hand, assuming that $\ddot{q}_d$=0 and p_2=0, the $\mathcal{L}$ stability of e was shown in [Becker and Grimm 1988] if

$$1 - \gamma_2 ak - \gamma_1 \frac{\beta_1}{\mu_1} > 0 \qquad (5.2.36)$$

where $\gamma_i = \gamma_2(P_i) = \max_{\omega \in \Re} ||P_i(j\omega)||$ as given in Lemma 2.5.2. This controller is summarized in Table 5.2.4.

Table 5.2.4: Dynamic One DOF Controller: Design 2

Assumptions:

$$\begin{aligned} \frac{1}{\mu_2} &\leq ||M^{-1}|| \leq \frac{1}{\mu_1}, \quad \mu_i \neq 0 \\ ||\Delta|| &\leq a \leq 1 \\ ||\delta|| &\leq \beta_0 + \beta_1||\mathbf{e}|| + \beta_2||\mathbf{e}||^2 \\ ||\ddot{q}_d|| &\leq c \end{aligned}$$

Controller:

$$\tau = \hat{M}(\ddot{q}_d + C(s)\mathbf{e}) + \hat{N}$$

For $\mathcal{L}_\infty$ stability

$$1 - \gamma_2 ak - \gamma_1 \frac{\beta_1}{\mu_1} - 2\gamma_1 \left[\left(ac + \frac{\beta_0}{\mu_1}\right)\frac{\beta_2}{\mu_1}\right]^{\frac{1}{2}} > 0$$

For $\mathcal{L}_2$ stability

$$\ddot{q}_d = 0; \quad \beta_2 = 0 \quad [\text{i.e., } \hat{N} = V_m(q,\dot{q})\dot{q}]$$

$$1 - \gamma_2 ak - \gamma_1 \frac{\beta_1}{\mu_1} > 0$$

Performance:
Guaranteed boundedness of e and $\dot{e}$. The errors go to zero as the gain k of $C(s)$ is increased.

EXAMPLE 5.2–4: Dynamic One DOF Design

Use the same linear controller as that of Example 5.2.3, but assume that the quadratic velocity terms in *N* are known so that p_2=0; that is

$$\tau = \hat{M}(\ddot{q}_d - u) + V_m(q,\dot{q})\dot{q}.$$

The results are shown in Figure 5.2.7 for the parameter *k*=150. They do not look remarkably different from those of Example 5.2.3 in Figure 5.2.6. This

is due to the fact that the velocity terms are truly negligent in this particular application. Such terms will, however, make a more vital contribution in faster trajectories.

■

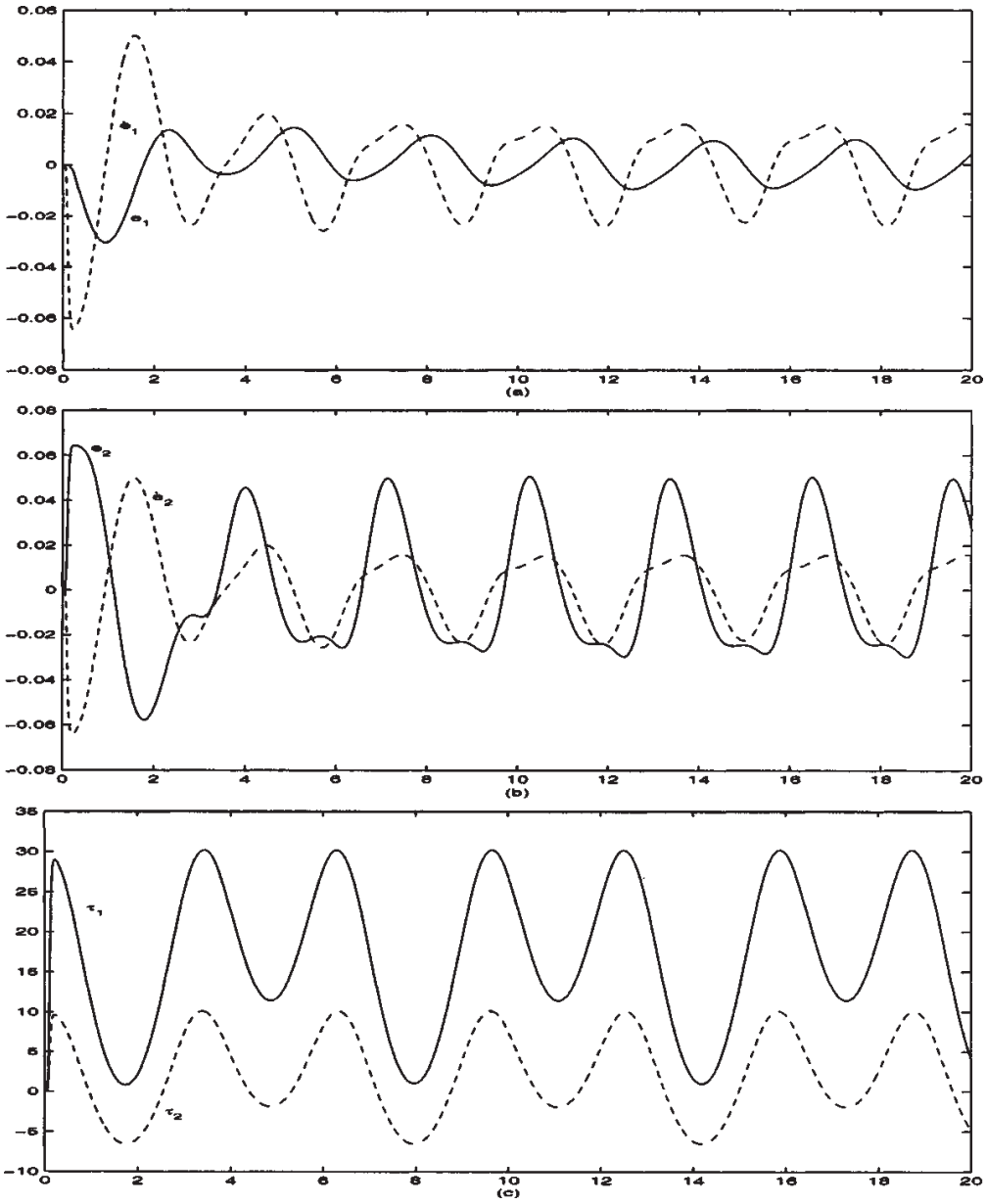


Figure 5.2.7: (a) errors of joint 1; (b) errors of joint 2; (c) torques of joints 1 and 2.

Two-Degree-of-Freedom Design.

It is well known that the two-DOF structure is the most general linear controller structure. The two-DOF design allows us simultaneously to specify the desired response to a command input and guarantee the robustness of

the closed-loop system. This design was briefly discussed in Chapter 2, Example 2.11.4. It is in a different spirit from the other design of this chapter, because it relies on classical frequency-domain SISO concepts. The general structure is shown in Figure 5.2.8. A two-DOF robust controller was designed and simulated in [Sugie et al. 1988] and will be presented next. Let the plant be given by (5.2.5) and consider the following factorization:

$$G(s)=N(s)D^{-1}(s),$$

where

$$D(s)=s^2,\ N(s)=I. \tag{5.2.37}$$

The following result presents a two-DOF compensator which will robustly stabilize (in the $\mathcal{L}$ sense) the error system.

THEOREM 5.2–5: *Consider the two-DOF structure of Figure 5.2.8. Let $K_1(S)$ be a stable system and $K_2(s)$ be a compensator to stabilize $G(s)$. Then the controller*

$$u=s^2K_1v+K_2(K_1v-q) \tag{1}$$

will lead to the closed-loop system

$$q=K1v \tag{2}$$

and the closed-loop error system (5.2.13) will be $\mathcal{L}$

stable. Proof:

With simple block-diagram manipulations, it may be shown that the closed-loop system is

$$q=K_1v.$$

The actual robustness analysis is involved and will be omitted, but a particular design and its robustness are discussed in the next example. ■

Note from (2) that $K_1(s)$ is used to obtain the desired closed-loop transfer function. It should then be stable, and to guarantee a zero steady-state error, we choose $v=qd$ and make sure that the dc gain $K_1(0)=1$. Finally, we would like $K_1(S)$ to be exactly proper (i.e., zero relative degree). $K_2(s)$, on the other hand, will assure the robustness of the closed-loop system. Therefore, $K_2(s)$ should stabilize $G(s)$ and provide suitable stability margins. It should contain

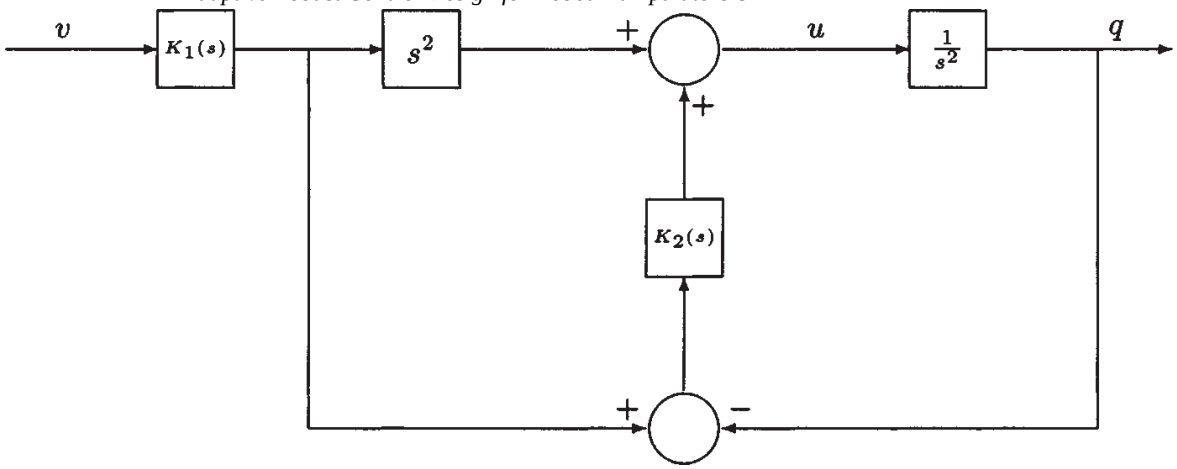


Figure 5.2.8: Two-degree-of-freedom controller structure.

an integral term to achieve static accuracy. Its relative degree may be -1 since both q and $\dot{q}$ are available.

EXAMPLE 5.2–5: Dynamic Two DOF Design

Consider the two-DOF structure of Figure 5.2.8, where

$$\begin{aligned} G(s) &= \frac{1}{s^2} I \\ v &= q_d. \end{aligned} \tag{1}$$

Then a two-DOF regulator is described by

$$\begin{aligned} K_1(s) &= \frac{w_1^2}{s^2 + a_1 w_1 s + w_1^2} I \\ K_2(s) &= \left[b_2 w_2 s + b_1 w_2^2 + \frac{w_2^3}{s} \right] I, \end{aligned} \tag{2}$$

where $s^3+b_2s^2+b_1s+1$ is a stable polynomial, and w_1, w_2, a_1, b_1, and b_2 are design parameters. Note that $K_2(s)$ is a PID controller and that the closed-loop system given by $K_1(S)$ is a second-order system with natural frequency w_1 and damping ration $\zeta = \frac{a_1}{2}$. Note also that the input to the robot becomes

$$\tau - K_2(K_1 q_d - q) s^2 K_1 q_d$$

or

(3) $$\tau = K_2 q + (K_2 + s^2) K_1 q_d.$$

We can immediately see that the joint position vector q is filtered through the PID controller K_2. Therefore, the differentiation of q is required unless the measurement of is $\dot{q}$ available. The behavior of the nonlinear closed-loop system is shown in Figure 5.2.9, when $\hat{M}$=1 and $\hat{N}$=0, a_1=2, b_1=b_2=10, w_1=8, and w_2=12. It is seen that initially, the torque effort and the trajectory errors are too large. To understand the behavior of this controller, consider the controller □ in the limit (i.e., as time goes to infinity). The output of $K_1 q_d$ has settled down to its final value q_d and therefore the controller (3) becomes equivalent to a PID compensator [see Chapter 4, equation (4.4.35)]. It seems that a different structure for k_1 and K_2 is warranted because in the meantime, the two-DOF controller preforms rather poorly. This is a characteristic of the example rather than an inherent flow in the twoDOF methodology. As a matter of fact, this structure has shown better performance than the one- DOF PID compensator in [Sugie et al. 1988] for a set-tracking case. The reader is encouraged to work the problems at the end of the chapter related to this design in order to compare the performance of one- and two-DOF designs.

■

We have this presented a large sample of controllers that are more or less computed-torque based. We have shown using different stability arguments that the computed-torque structure is inherently robust and that by increasing the gains on the outer-loop linear compensator, the position and velocity errors tend to decrease in the norm. This class of compensators constitutes by far the most common structure used by robotics manufacturers and is the simplest to implement and study. There are more compensators that would fit into this structure while appealing to some classical control applications. The PD and PID compensators may be replaced with the lead-lag compensators. These are especially appealing when only position measurements are available. Such designs are discussed in [Chen 1989] in the discrete-time case. There is also some work being done in the nonlinear observer area which is directly relevant to this problem [Canudas de Wit and Fixot 1991]. We refer the reader to the observability discussion in Section 2.11. We also suggest some of the problems at the end of this chapter, which discuss further modification of the feedback-linearization designs.

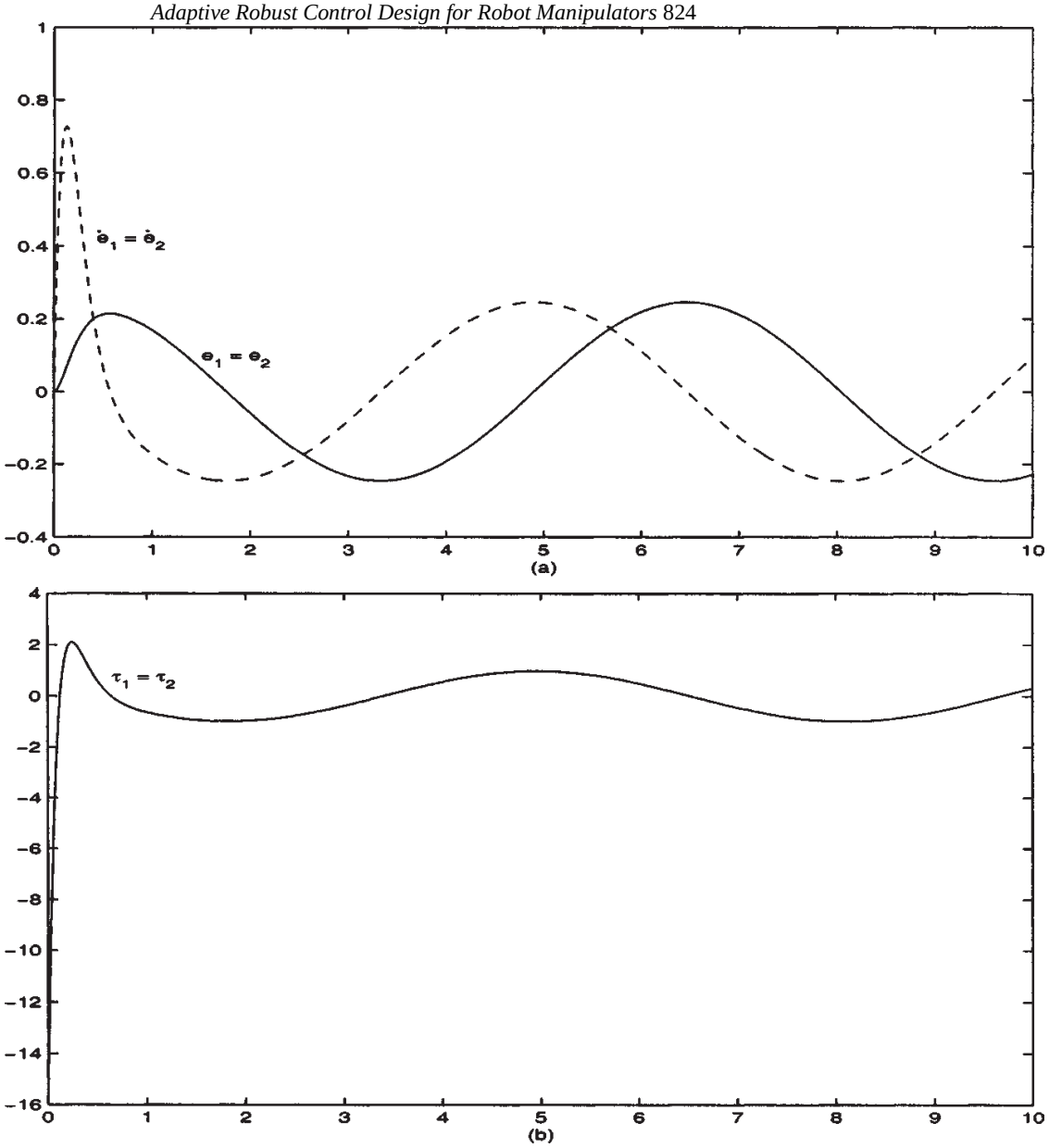


Figure 5.2.9: (a) errors of joints 1 and 2; (b) torques of joints 1 and 2.

On the other hand, there exists other types of controllers, which although less prevalent, still constitute a very important class of robot compensators. These are nonlinear controllers which do not rely directly on the feedback linearizability of the robot. Instead, the may be obtained from the passivity of its dynamics or may even bypass any special structural properties of the robot. These controllers are discussed next.

5.3 Nonlinear Controllers

There is a class of robot controllers that are not computed-torque-like controllers. These controllers are obtained directly from the robot equations without using the feedback-linearization procedure. Instead, these controller may rely on other properties of the robot (such as the passivity of its Lagrange- Euler description) or may be obtained without even considering the physics of the robot. In general, these controllers may be written as a computed- torque controller with an auxiliary, nonlinear controller added to it. The nonlinear control term introduces coupling between the different joints independently from the computed-torque term. In other words, even if the computed-torque controller is a simple PID, the nonlinear term couples all joints together as will be seen in Theorems 5.3.4 and 5.3.5, for example.

Direct Passive Controllers

First, we present controllers that rely directly on the passive structure of rigid robots as described in equations (5.1.1), where $\dot{M}(q)$-$2V_m(q, \dot{q})$ is skew symmetric by an appropriate choice of $V_m(q, \dot{q})$ as described in Section 3.3.

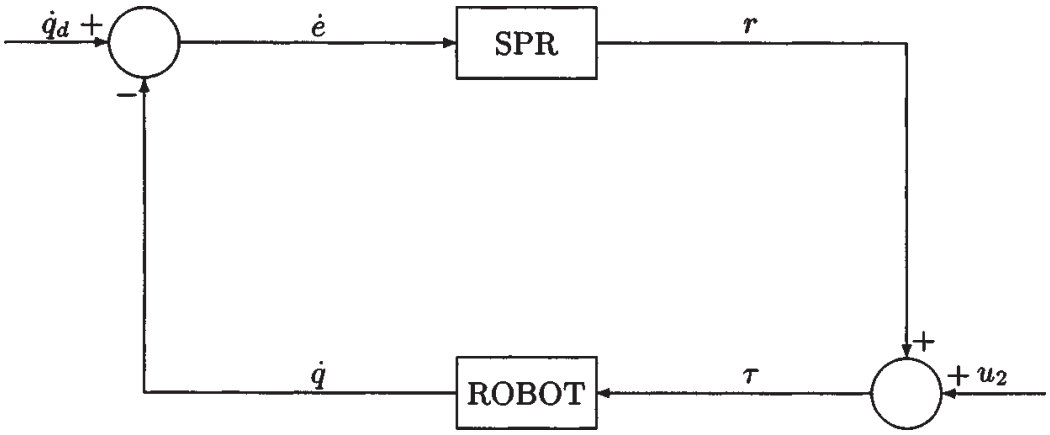


Figure 5.3.1: Passive-control structure.

Based on the passivity property, if one can close the loop from $\dot{q}$ to v with a passive system (along with $\mathcal{L}$ bounded inputs) as in Figure 5.3.1, the closed- loop system will be asymptotically stable using the passivity theorem. Note that the input u_2 gives an extra degree of freedom to satisfy some performance criteria. In other words, by choosing different $\mathcal{L}$ bounded u_2 we may be able to obtain better trajectory tracking or noise immunity. This structure will show the asymptotic stability of e but only the Lyapunov stability of $\dot{e}$. On

the other hand, if one can show the passivity of the system, which maps *v* to a new vector *r* which is a filtered version of e, a controller that closes the loop between -*r* and *v* will guarantee the asymptotic stability of both *e* and $\dot{e}$. This indirect use of the passivity property was illustrated in [Ortega and Spong 1988] and will be discussed first.

Let the controller be given by (5.3.1), where *F(s)* is a strictly proper, stable, rational function, and K_r is a positive-definite matrix,

$$\tau = M(q)[\ddot{q}_d + C(s)e] + V_m(q,\dot{q})(\dot{q} + r) + G(q) + K_r r$$
$$r = \left[sI + \frac{C(s)}{s}\right] e = F(s)^{-1} e. \tag{5.3.1}$$

Substituting (5.3.1) into (5.1.1) and assuming no friction [i.e., $F(\dot{q})$=0], we obtain

$$M(q)\dot{r} + V_m(q,\dot{q})r + K_r r = 0. \tag{5.3.2}$$

Then it may be shown that both *e* and $\dot{e}$ are asymptotically stable. In fact, choose the following Lyapunov function:

$$V = \frac{1}{2} r^T M(q) r.$$

Then

$$\dot{V} = r^T M(q)\dot{r} + \frac{1}{2} r^T \dot{M}(q) r.$$

Substituting for $M(q)\ \dot{r}$ from (5.3.2), we obtain

$$\dot{V} = -r^T K_r r < 0.$$

Therefore, *r* is asymptotically stable, which can be used to show that both *e* and *e* are asymptotically stable [Slotine 1988]. This approach was used in the adaptive control literature to design passive controllers [Ortega and Spong 1988], but its modification in the design of robust controllers when *M,* V_m and *G* are not exactly known is not immediately obvious. Such modifications will be given in the variable-structure designs, but first, we present a simple controller to illustrate the robustness of passive compensators.

THEOREM 5.3–1: *Consider the control law (1)*

(1) $$\tau = \Lambda(s)\dot{e} + u_2,$$

where K(s) *is an SPR transfer function, to be chosen by the designer, and the external input* u_2 *is bounded in the* $\mathcal{L}$ *norm. Then* $\dot{e}$ *is asymptotically stable, and e is Lyapunov stable.*

Proof:

Using the control law above, one gets from Figure 5.3.1,

(2) $$r = \Lambda(s)\dot{e}.$$

By an appropriate choice of K(s) *and* u_2*, one can apply the passivity theorem and deduce that* $\dot{e}$ *and r are bounded in the* $\mathcal{L}$ *norm, and since* $K(s)^{-1}$ *is SPR (being inverse of an SPR function), one deduces that is asymptotically stable because* $\dot{e}$

(3) $$\dot{e} = \Lambda(s)^{-1} r.$$

This will imply that the position error e is bounded but not its asymptotic stability in the case of time-varying trajectories $[q_d^T \quad \dot{q}_d^T]^T$*. In the set-point tracking case, however (i.e.,* $\dot{q}_d$*=0), and with gravity precompensation, the asymptotic stability of e may be deduced using LaSalle's theorem. The robustness of the closed-loop system is guaranteed as long as* K*(s) is SPR and that* u_2 *is* $\mathcal{L}$ *bounded, regardless of the exact values of the robot's parameters.* ■

The controller is summarized in Table 5.3.1.

Table 5.3.1: Passive Controller

Assumptions:
$\Lambda(s)$ is an SPR transfer function. u_2 is a finite energy signal.
Controller:

$$\tau = \Lambda(s)\dot{e} + u_2$$

Performance:
Guaranteed Lyapunov stability of e, asymptotic stability of $\dot{e}$. In the case where $\dot{q}_d = 0$, asymptotic stability of e is also guaranteed.

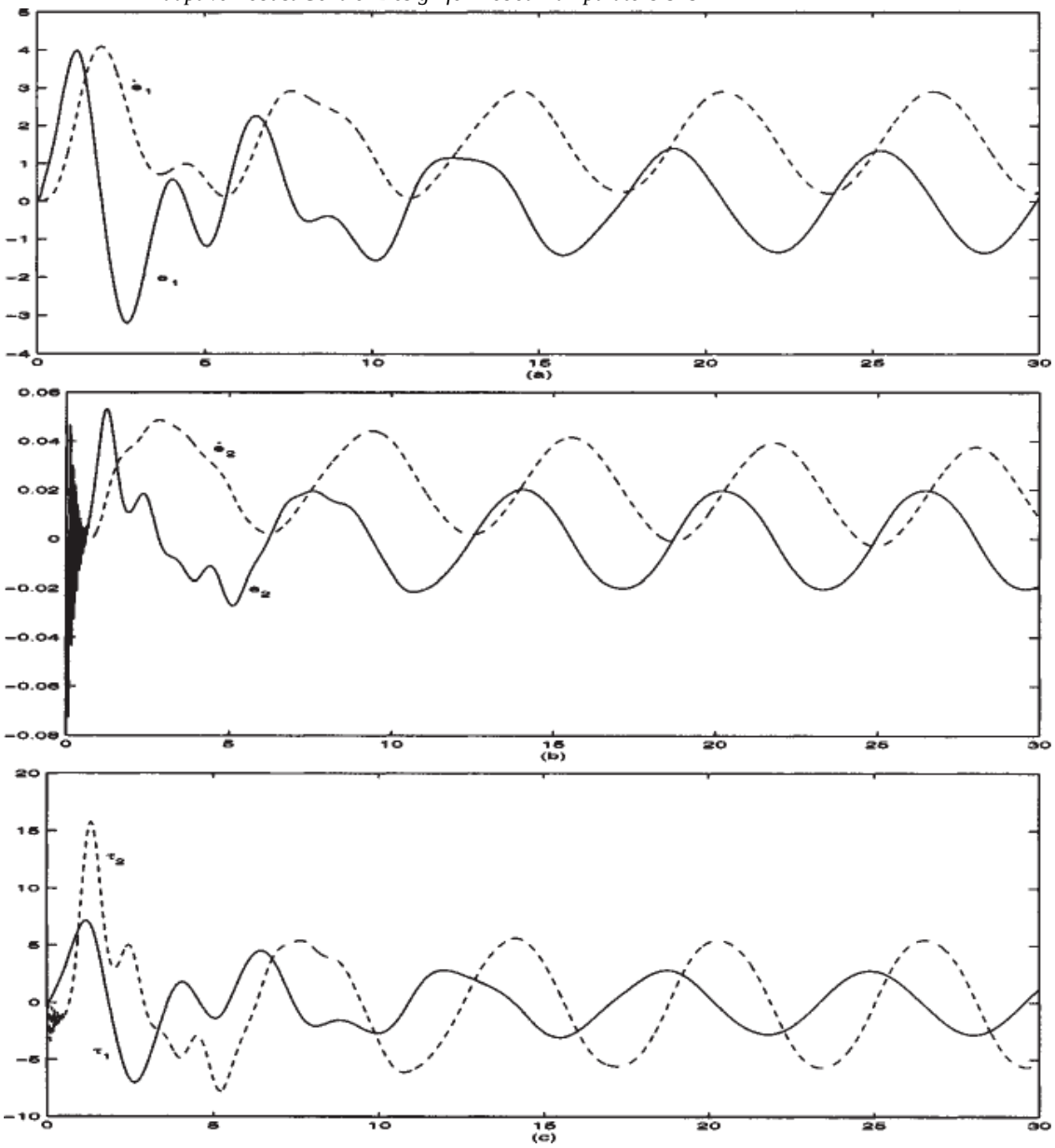


Figure 5.3.2: (a) errors of joints 1; (b) errors of joint 2; (c) torques of joints 1 and 2.

EXAMPLE 5.3–1: Passive Controllers

We choose an SPR transfer function

(1) $$\Lambda(s) = \begin{bmatrix} \frac{s+450}{s+225} & 0 \\ 0 & \frac{s+3300}{s+10} \end{bmatrix}$$

and we let $u_2 = \ddot{q}_d$. Note that the desired trajectory used so far violates the assumption that u_2 should be $\mathcal{L}2$ stable. Nevertheless, the trajectories of

Figure 5.3.2 show that his controller, when started at $e(0)= (0)=0$, performs rather well for the sinusoidal trajectory. Of course, since the passivity theorem provides sufficient conditions for stability, this example is not contradicting the previous theorem but merely pointing out its conservatism.

■

Note that the compensator of Theorem 5.3.1 is a generalization of the PD compensators of Chapter 4 and of the preceding section. In [Anderson 1989] it was demonstrated, using network-theoretic concepts, that even in the absence of the contact forces, a computed-torque-like controller is not passive and may therefore cause instabilities in the presence of uncertainties. His solution to the problem consisted of using proportionalderivative (PD) controllers with variable gains $K_1(q)$ and $K_2(q)$ which depend on the inertia matrix $M(q)$, that is,

(5.3.3) $$\tau = K_p(q)e + K_v(q)\dot{e}_2 + G(q)$$

Even though $M(q)$ is not exactly known, the stability of the closed-loop error is guaranteed by the passivity of the robot and the feedback law. The advantage of this approach is that contact forces and larger uncertainties may now be accommodated. Its main disadvantage is that although robust stability is guaranteed, the closed-loop performance depends on the knowledge of $M(q)$, whose singular values are needed in order to find K_p and K_V. We will not discuss this particular design and refer the interested reader to [Anderson 1989].

Variable-Structure Controllers

In this section we group designs that use variable-structure (VSS) controllers. The VSS theory has been applied to the control of many nonlinear processes [DeCarlo et al. 1988]. One of the main features of this approach is that one only needs to drive the error to a “switching surface,” after which the system is in “sliding mode” and will not be affected by any modelling uncertainties and/or disturbances.

There are two main criticisms of these controllers as they apply to robots. The first is that by ignoring the physics or the robot, these controllers will necessarily perform no better (if not worse) that controllers which exploit the structure of the Lagrange-Euler equations. The other criticism relates to the “chattering” problem commonly associated with variable-structure controllers. We shall address the second issue later in this section, and answer the first by admitting that although initial applications of variable-structure theory did indeed gloss over the physics of robots, later designs (such as the

ones discussed here) by [Slotine 1985] and [Chen et al. 1990] remedied the problem.

The first application of this theory to robot control seems to be in [Young 1978], where the set-point regulation problem ($\dot{q}_d$=0)was solved using the following controller:

$$\tau_i = \begin{cases} \tau_i^+ & \text{if } r_i(e_{1i}, \dot{q}_i) > 0 \\ \tau_i^- & \text{if } r_i(e_{1i}, \dot{q}_i) < 0 \end{cases} \tag{5.3.4}$$

where i=1,…, n for an n-link robot, and r_i are the switching planes,

$$r_i(e_{1i}, \dot{q}_i) = \lambda_i e_i + \dot{q}_i, \quad \lambda_i > 0. \tag{5.3.5}$$

It is then shown, using the hierarchy of the sliding surfaces $r_1, r_2, \ldots, r_n$ and given bounds on the uncertainties in the manipulators model, that one can find v^+ and v^- in order to drive the error signal to the intersection of the sliding surfaces, after which the error will "slide" to zero. This controller eliminates the nonlinear coupling of the joints by forcing the system into the sliding mode. Other VSS robot controllers have since been designed. Unfortunately, for most of these schemes, the control effort as seen from (5.3.4) is discontinuous along r_i=0 and will therefore create chattering, which may excite unmodelled high-frequency dynamics. In addition, these controllers do not exploit the physics of the robot and are therefore less effective than controllers that do.

To address this problem, the original VSS controllers were modified in [Slotine 1985] as described in the next theorem. Let us first define a few variables to simplify the statement of the theorem. Let

$$\begin{aligned} r &= \Lambda e + \dot{e}, \quad \Lambda = \text{diag}[\lambda_1, \lambda_2, \ldots, \lambda_n], \quad \lambda_i > 0 \\ \dot{q}_r &= \Lambda e + \dot{q}_d \\ \text{sgn}(r_i) &= [\text{sgn}(r_1), \text{sgn}(r_2), \ldots, \text{sgn}(r_n)]^T \end{aligned} \tag{5.3.6}$$

where

$$\text{sgn}(r_i) = +1 \quad \text{if } r_i > 0, \qquad \text{sgn}(r_i) = -1 \quad \text{if } r_i < 0.$$

THEOREM 5.3–2: *Consider the controller*

$$\tau = \hat{M}\ddot{q}_r + \hat{V}_m \dot{q}_r + \hat{G} + K\,sgn(r),$$

where

$$K = diag[k_1, k_2, \ldots, k_n], \quad k_i > 0.$$

Then the error reaches the surface

$$r = \Lambda e + \dot{e}$$

in a finite time. In addition, once on the surface, q(t) will go to $q_d(t)$ exponentially fast.

Proof:

Consider the Lyapunov function candidate

$$V(r) = \frac{1}{2} r^T M(q) r.$$

Then

$$\dot{V}(r) = r^T M \dot{r} + \frac{1}{2} \dot{M}(q) r.$$

Substituting for $\dot{r}$ and using the skew-symmetric property of $\dot{M}(q)$-2$V_m(q, \dot{q})$ we obtain

$$\dot{V}(r) = r^T [M \ddot{q}_r + V_m \dot{q}_r + G - \tau].$$

Then, if we use the controller given by

$$\tau = \hat{M} \ddot{q}_r + \hat{V}_m \dot{q}_r + \hat{G} + K sgn(r),$$

we obtain

$$\dot{V}(r) = r^T [\tilde{M} \ddot{q}_r + \tilde{V}_m \dot{q}_r + \tilde{G}] - \sum_{i=1}^{n} k_i |r_i|,$$

where

$$\tilde{M} = M - \hat{M}, \quad \tilde{V}_m = V_m - \hat{V}_m, \quad \tilde{G} = G - \hat{G}.$$

Then it is sufficient to choose

$$k_i \geq |[\tilde{M}\ddot{q}_r + \tilde{V}_m\dot{q}_r + \tilde{G}]_i| + \eta_i,$$

where μ_i>0. *Therefore,*

$$\dot{V}(r) \leq -\sum_{i=1}^{n} \eta_i |r_i|,$$

which implies that r=0 *is reached in a finite time*. *In addition, once in sliding mode, e converges exponentially fast to zero.* ■

The controller is summarized in Table 5.3.2.

EXAMPLE 5.3–2: VSS Controller 1

Consider the two-link robot and choose *K*=10*I* and K=5*I*. The trajectory errors for joint 1 are given in Figure 5.3.3. Note that the chattering behavior due to the infinitely fast switching of the controller is becoming apparent. A common remedy of the problem is to sacrifice asymptotic stability by using sat(s/c), c > 0 instead of sgn*(s)* in the torque calculation. The saturation function is depicted in Figure 5.3.4a and will result in the errors being uniformly ultimately bounded. The behavior of such a controller is shown in Figure 5.3.5, where K=5*I, K*=75*I,* and c = 0.001. Note that we were able to greatly increase the gains in this case, which results in a smaller error trajectories.

■

More recently, in [Chen et al. 1990], another VSS controller was introduced. We describe this controller in detail to give a flavor of a different VSS approach, which will exploit the dynamics of the robot. The assumptions required by this controller are listed below.

$$\begin{aligned} |(M - \hat{M})_{ij}| &< \bar{M}_{ij}(q) \\ |\dot{M}_{ij}| &< \bar{m}_{ij}(q, \dot{q}) \\ |[(M - \hat{M})\ddot{q}_d]_i| &< \bar{c}_i(t) \\ |(N - \hat{N})_i| &< \bar{n}_i(q, \dot{q}) \end{aligned} \tag{5.3.7}$$

Note that these bounds are different in spirit that those given in (5.2.8)– (5.2.11). The current bounds are often more useful since they depend on the uncertainty of each element of the inertia matrix *M* and the velocity-dependent torques *N*.

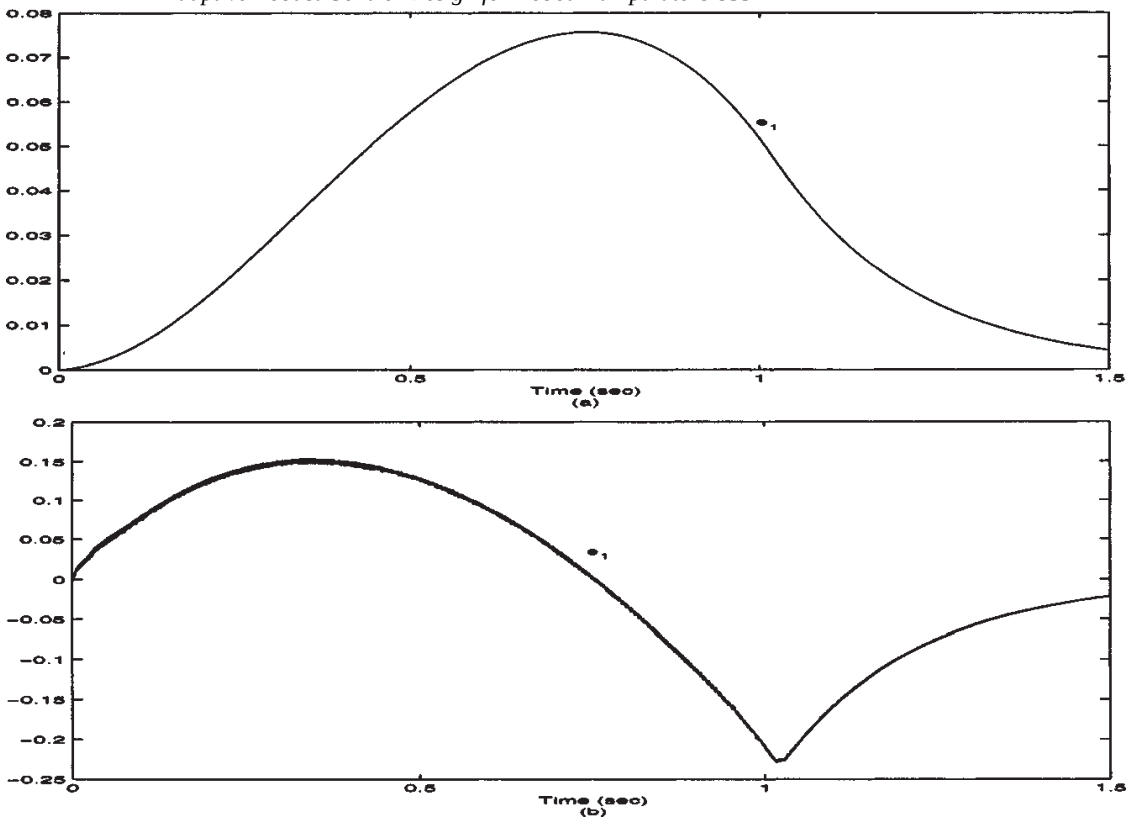


Figure 5.3.3: errors of joint 1: (a) e_1; (b) $\dot{e}_1$

THEOREM 5.3–3: *The errors e and $\dot{e}$ are asymptotically stable if the input torque is given by*

$$\tau = \hat{M}\ddot{q}_r + \hat{N} + P(t)r(t) + Q(t)sgn(r), \tag{1}$$

where

$$\begin{aligned} P(t) &= diag[p_1(t), p_2(t), \ldots, p_n(t)], \\ Q(t) &= diag[q_1(t), q_2(t), \ldots, q_n(t)] \\ p_i(t) &= \frac{1}{2}\sum_{i=1}^{n} \bar{m}_{ij} + k_i, \quad k_i > 0 \\ q_i(t) &= \sum_{i=1}^{n} \bar{M}\Lambda_{ij}|\dot{e}_j| + \bar{n}_i + \bar{c}_i. \end{aligned}$$

Proof:

Choose the same Lyapunov function as in Theore

(2)

(3)

(4)

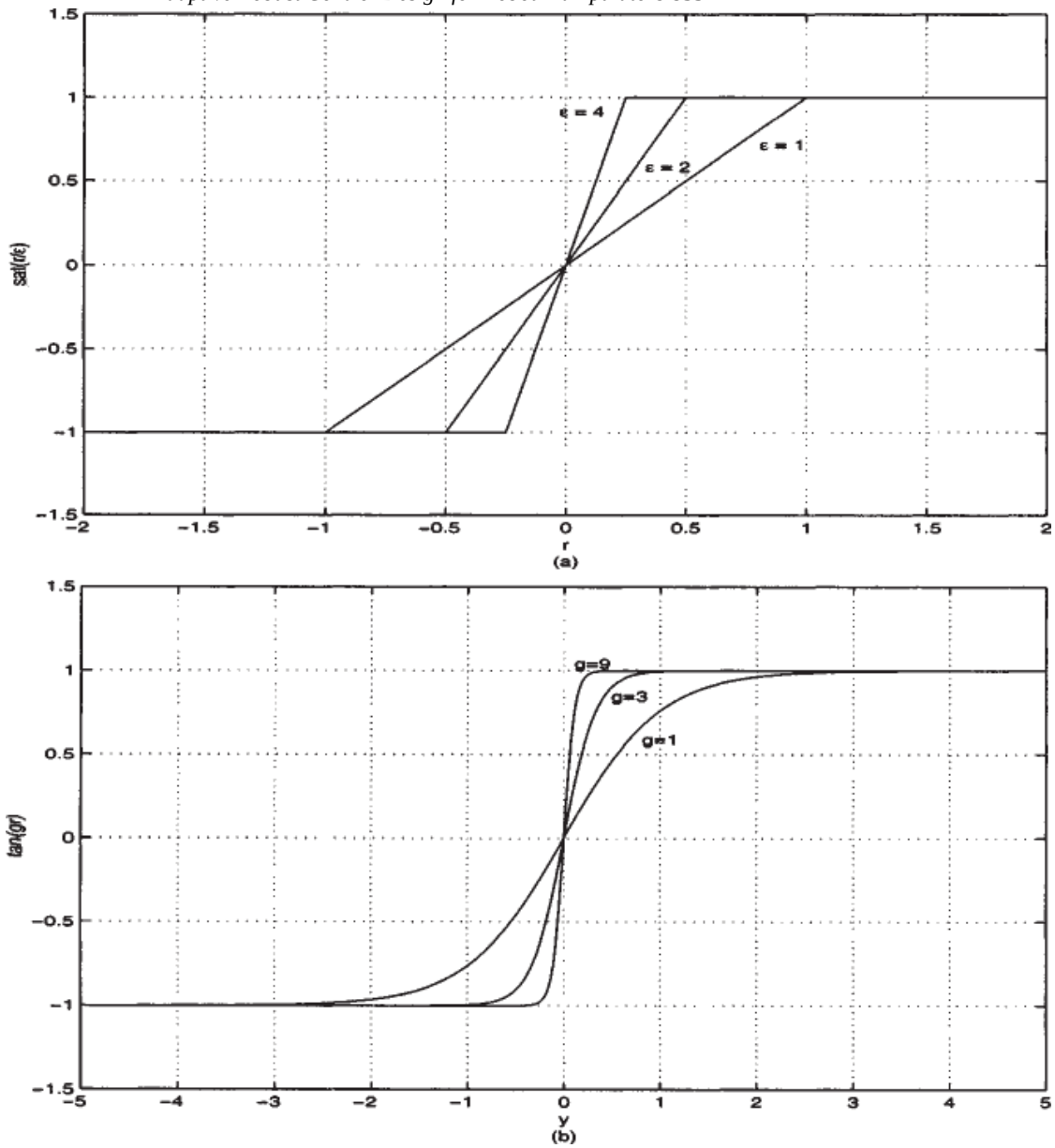


Figure 5.3.4: (a) plot of *sat*(*r*/c); (b) plot of *tanh*(*gr*)

$$V(r) = \frac{1}{2} r^T M(q) r.$$

Then, differentiating and substituting for v, we obtain

$$\dot{V} = -t^T \left[P - \frac{\dot{M}}{2} \right] r + r^T [-Q sgn(r) + \tilde{M} \Lambda \dot{e} + \tilde{N} + \tilde{M} \ddot{q}_d],$$

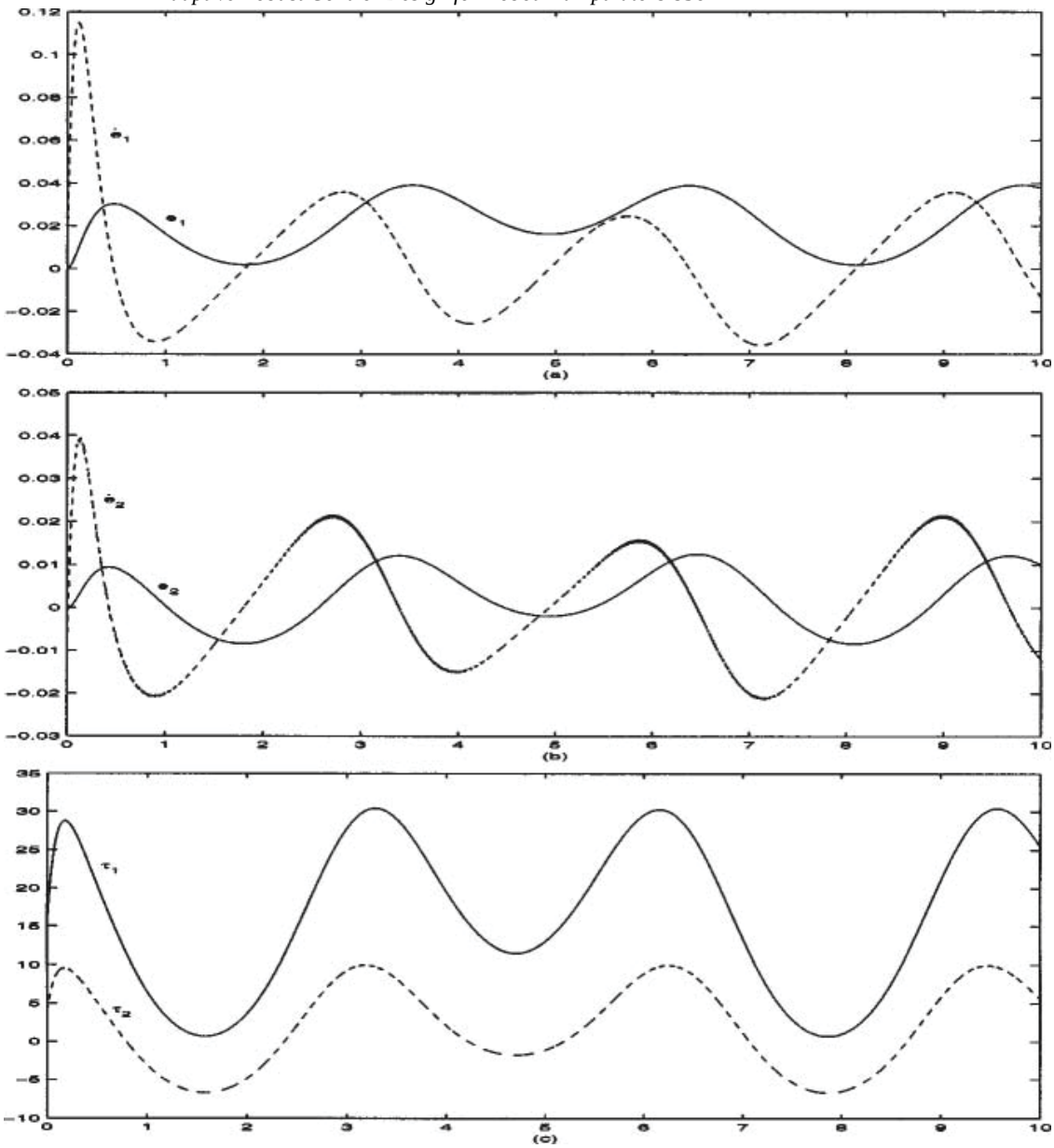


Figure 5.3.5: (a) errors of joint 1; (b) errors of joint 2; (c) torques of joints 1 and 2

which using (4)–(5.3.8) may be shown to be

$$\dot{V} \leq -r^T K r \leq 0.$$

Therefore, the surface r(t)=0 *is reached in a finite time, after which the exponential stability of the error results as discussed in Theorem 5.3.2*.

■

This controller is summarized in Table 5.3.3.

Table 5.3.2: Variable Structure Controller 1

Assumptions:
None
Controller:

$$
\begin{aligned}
r &= \Lambda e + \dot{e}, \quad \Lambda = \mathrm{diag}[\lambda_1, \lambda_2, \ldots, \lambda_n], \quad \lambda_i > 0 \\
\dot{q}_r &= \Lambda e + \dot{q}_d \\
\mathrm{sgn}(r_i) &= [\mathrm{sgn}(r_1), \mathrm{sgn}(r_2), \ldots, \mathrm{sgn}(r_n)]^T \\
\mathrm{sgn}(r_i) &= +1 \quad \text{if } r_i > 0, \qquad \mathrm{sgn}(r_i) = -1 \quad \text{if } r_i < 0. \\
\tau &= \hat{M}\ddot{q}_r + \hat{V}_m \dot{q}_r + \hat{G} + K\,\mathrm{sgn}(r), \\
K &= \mathrm{diag}[k_1, k_2, \ldots, k_n], \quad k_i > 0.
\end{aligned}
$$

Performance:
Guaranteed uniform ultimate boundedness of e and $\dot{e}$.
Guaranteed uniform boundedness if $e(0) = \dot{e}(0) = 0$.

EXAMPLE 5.3–3: VSS Controller 2 (Saturation)

The two-link robot was controlled using this controller with the following design parameters:

$$
\begin{aligned}
\hat{M} &= \begin{bmatrix} 3 & 1 \\ 1 & 1 \end{bmatrix}, \qquad \bar{M} = \begin{bmatrix} 2 & 1 \\ 1 & 0 \end{bmatrix} \\
\hat{N} &= 0, \qquad \bar{N} = \begin{bmatrix} 2\dot{q}_1\dot{q}_2 + \dot{q}_2^2 + 3(9.8) \\ \dot{q}_1^2 + 9.8 \end{bmatrix} \\
\bar{c} &= \begin{bmatrix} 3 \\ 1 \end{bmatrix}, \qquad \Lambda = \begin{bmatrix} 3 & 0 \\ 0 & 1 \end{bmatrix}, \qquad K = \begin{bmatrix} 10 \\ 10 \end{bmatrix}
\end{aligned}
$$

The resulting errors for joint 1 are shown in Figure 5.3.5. Due to the same chattering problems encountered in Example 5.3.2, we choose instead a controller with a saturation function and parameters identical to those in Example 5.3.2. The resulting behavior is plotted in Figure 5.3.7.

■

As seen in Figures 5.3.3 and 5.3.5, the algorithms of Theorems 5.3.2 and 5.3.3, although using the physics of the robot, suffer from the chattering

Table 5.3.3: Variable Structure Controller 2

Assumptions:

$$\begin{aligned} |(M-\hat{M})_{ij}| &< \bar{M}_{ij}(q) \\ |\dot{M}_{ij}| &< \bar{m}_{ij}(q,\dot{q}) \\ |[(M-\hat{M})\ddot{q}_d]_i| &< \bar{c}_i(t) \\ |(N-\hat{N})_i| &< \bar{n}_i(q,\dot{q}) \end{aligned}$$

Controller:

$$\tau = \hat{M}\ddot{q}_r + \hat{N} + P(t)r(t) + Q(t)\text{sgn}(r)$$

where

$$\begin{aligned} P(t) &= \text{diag}[p_1(t), p_2(t), \ldots, p_n(t)], \\ Q(t) &= \text{diag}[q_1(t), q_2(t), \ldots, q_n(t)] \\ p_i(t) &= \frac{1}{2}\sum_{i=1}^{n} \bar{m}_{ij} + k_i, \quad k_i > 0 \\ q_i(t) &= \sum_{i=1}^{n} \bar{M}\Lambda_{ij}|\dot{e}_j| + \bar{n}_i + \bar{c}_i \end{aligned}$$

Performance:
Guaranteed uniform ultimate boundedness of e and $\dot{e}$.
Guaranteed uniform boundedness if $e(0) = \dot{e}(0) = 0$.

commonly encountered in VSS control because of the presence of the sgn*(r)* term. A common remedy of the problem is to sacrifice asymptotic stability by using *sat*(*r*/c), c > 0, instead of sgn*(r)* in the torque calculation as done in both Examples 5.3.2 and 5.3.3. We propose instead to use a term tanh*(gr),* where tanh is the hyperbolic tangent and *g* is a gain parameter that adjusts the slope of tanh around the origin as shown in Figure 5.3.7b. This term is continuously differentiable, and a good approximation of sgn*(r)* for large *s,* will result in uniformly ultimately bounded errors, and by adjusting *g* we are able to get similar performance to the sgn*(r)* controller without the chattering behavior. The next example illustrates this controller and compares it to the usual saturation controller.

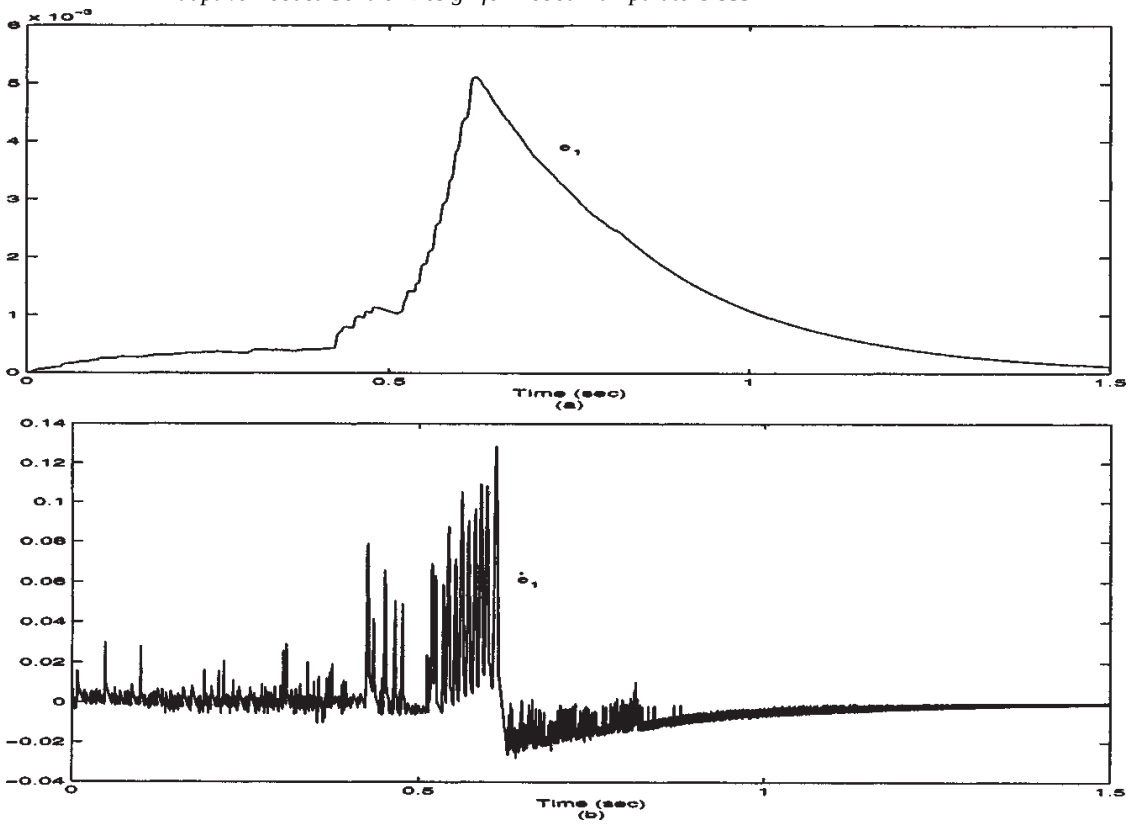


Figure 5.3.6: errors of joint 1(a) $e1$; (b) $e1$

EXAMPLE 5.3–4: VSS Controller 2 (Hyperbolic Tangent)

Contrast the saturation controller behavior of Example 5.3.2 with the hyperbolic tangent modification with g=3 in Figure 5.3.8. Similar comparisons should be made between Example 5.3.3 and the behavior shown in Figure 5.3.9, where g=3 is also used.

■

Saturation-Type Controllers

In this section we present controllers that utilize an auxiliary saturating signal to compensate for the uncertainty present in the robot dynamics as given by (5.2.1), where $V_m(q,\dot{q})$ is defined in Chapter 3.

$$M(q)\ddot{q} + V_m(q,\dot{q})\dot{q} + F(\dot{q}) + G(q) - \tau_d = \tau \tag{5.3.8}$$

or

$$M(q)\ddot{q} + V_m(q,\dot{q})\dot{q} + Z(q,\dot{q}) = M(q)\ddot{q} + N(q,\dot{q}) = \tau \tag{5.3.9}$$

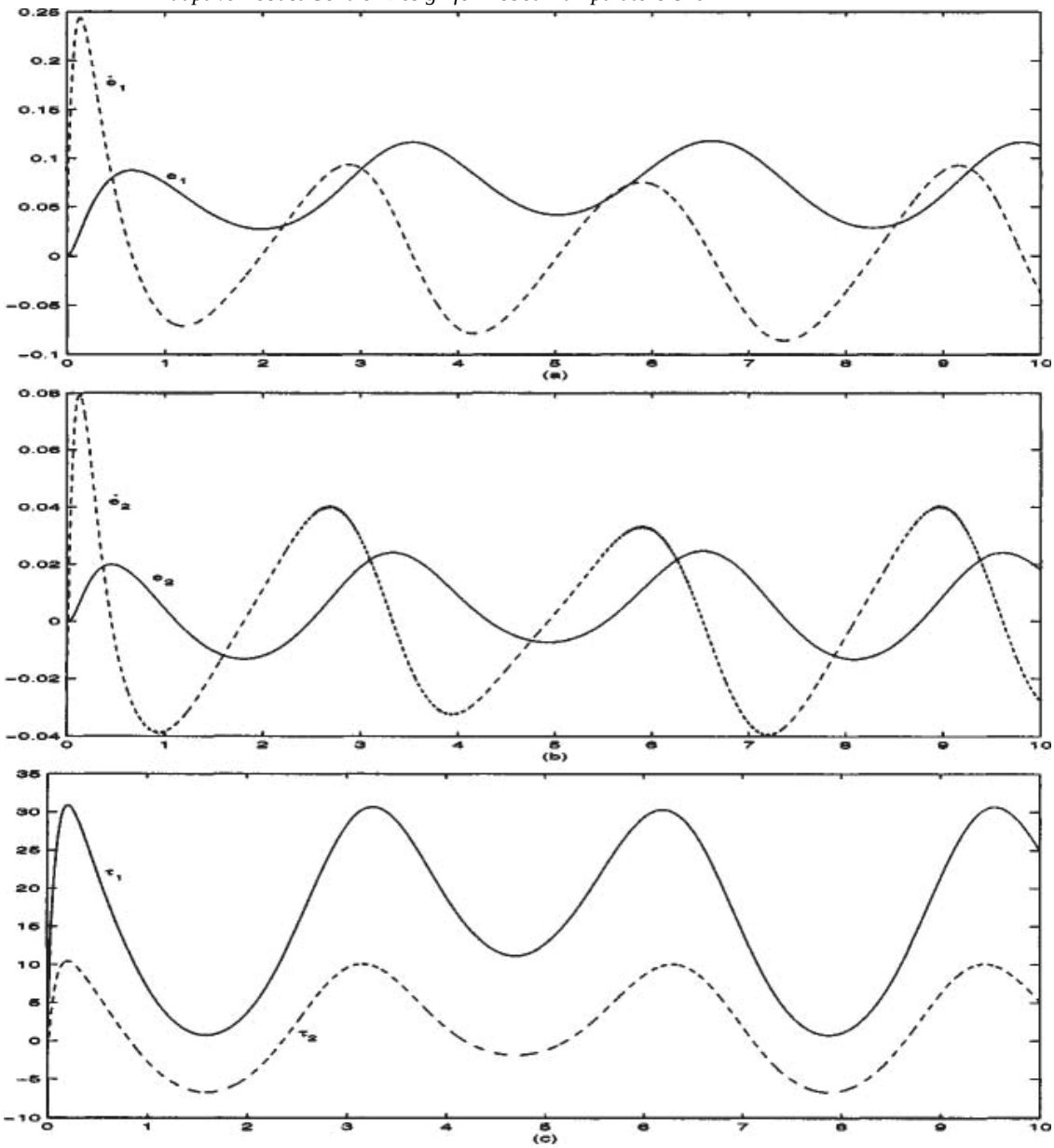


Figure 5.3.7: (a) errors of joint 1; (b) errors of joint 1; (c) torques of joints 1 and 2

Therefore, *Z(q,q)* is an *n*-vector representing friction, gravity and bounded torque disturbances. The controllers introduced in this section are robust due to the fact that they are designed based on uncertainty bounds rather than on the actual values of the parameters. The following bounds are needed and may be physically justified. The $*i*'s in (5.3.11) are positive scalar constants and the trajectory error **e** is defined before.

(5.3.10)
$$\mu_1 I \leq M(q) \leq \mu_2 I$$

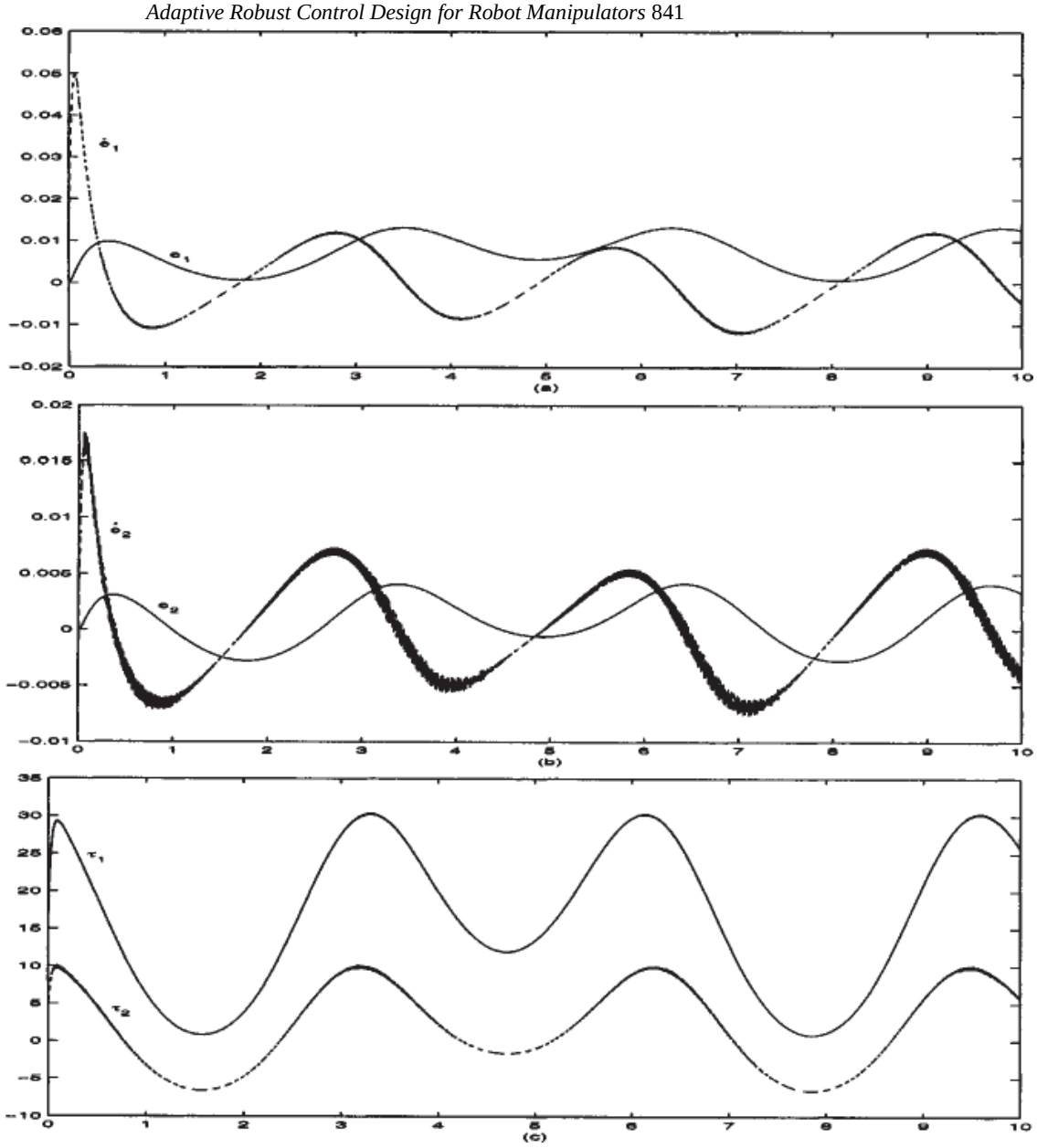


Figure 5.3.8: (a) errors of joint 1; (b) errors of joint 1; (c) torques of joints 1 and 2

$$\|N(q,\dot{q})\| = \|V_m(q,\dot{q})\dot{q} + Z(q,\dot{q})\| \le \zeta_0 + \zeta_1\|e\| + \zeta_2\|\mathbf{e}\|^2 \tag{5.3.11}$$

A representative of this class was developed in [Spong et al. 1987] and is given as follows.

THEOREM 5.3–4: *The trajectory error* **e** *is uniformly ultimately bounded (UUB) with the controller*

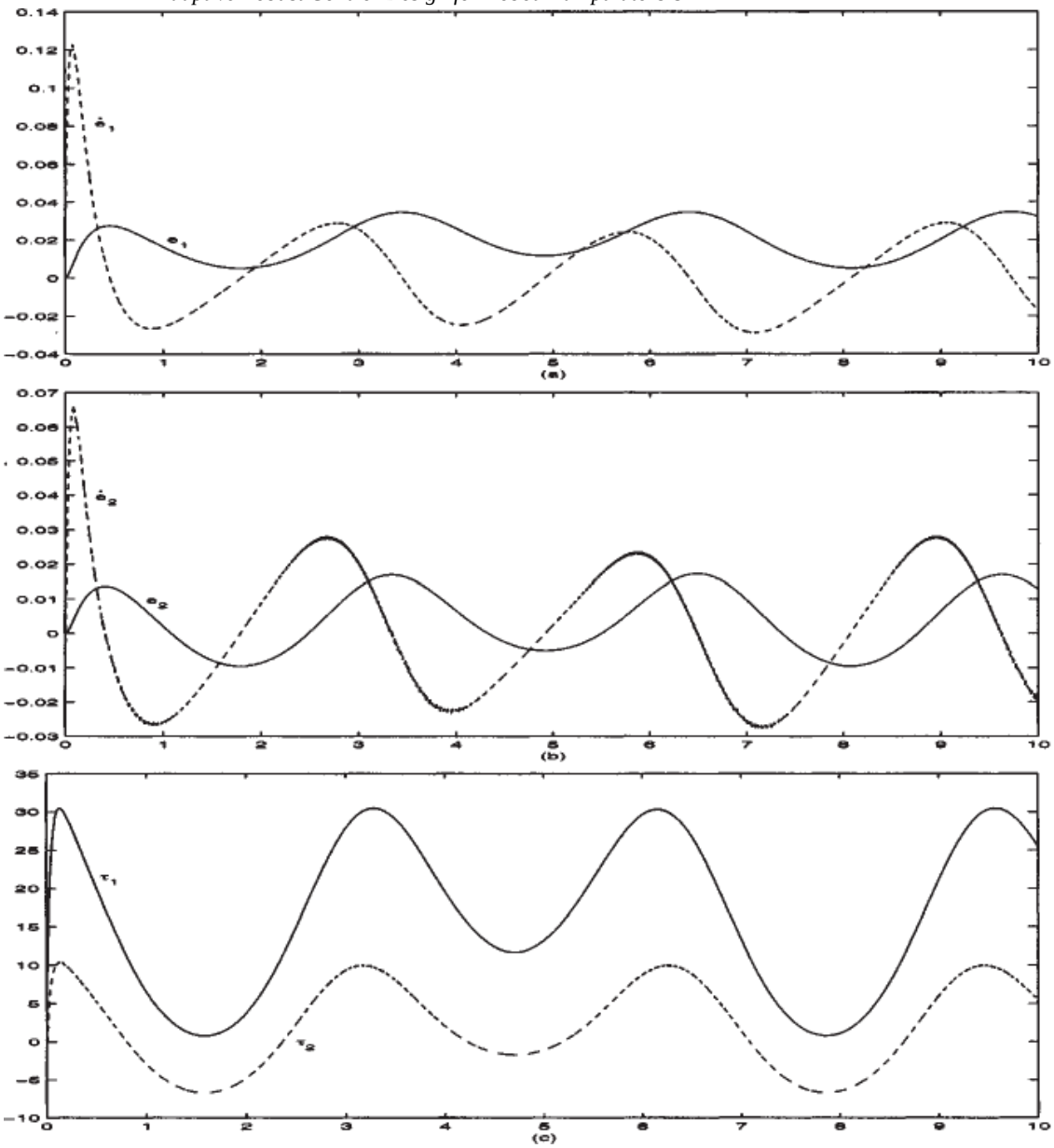


Figure 5.3.9: (a) errors of joint 1; (b) errors of joint 1; (c) torques of joints 1 and 2

(1) $$\tau = \frac{2\mu_1\mu_2}{\mu_1+\mu_2}[\ddot{q}_d + K_v\dot{e} + K_p e + v_r] + \hat{N}(q,\dot{q}),$$

where

$$K_v = k_v I, \quad K_p = k_p I$$

(2) $$v_r = \begin{cases} (B^T P e)p(||B^T P e||)^{-1} & if\ ||B^T P e|| > \epsilon \\ (B^T P e)p/\epsilon & if\ ||B^T P e|| \le \epsilon \end{cases}$$

and

$$p = \frac{1}{1-a}\left[a||\ddot{q}_d|| + k_p||e|| + k_v||\dot{e}|| + \frac{1}{\mu_1}\phi\right] \tag{3}$$

$$\phi = \beta_0 + \beta_1||e|| + \beta_2||e||^2 \tag{4}$$

$$a = \frac{\mu_2 - \mu_1}{\mu_1 + \mu_2} \tag{5}$$

Proof:

Choose the Lyapunov function

$$V(\mathbf{e}) = \mathbf{e}^T P \mathbf{e}$$

and proceed as in Theorem 2.10.4. See [Spong et al. 1987] for details. ■

Note that in the equations above, the matrix B is defined as in (5.2.3), the β_i's are defined as in (5.2.10), and the matrix P is the symmetric, positive- definite solution of the lyapunov equation (5.3.12), where Q is symmetric and positive-definite matrix and A_C is given in (5.2.14).

$$A_c^T P + P A_c = -Q \tag{5.3.12}$$

In particular, the choice of Q

$$Q = \begin{bmatrix} K_p & 0 \\ 0 & 2K_v - I \end{bmatrix}, \qquad K_v > I \tag{5.3.13}$$

leads to the following P:

$$P = \begin{bmatrix} K_p + 0.5K_v & 0.5I \\ 0.5I & I \end{bmatrix}. \tag{5.3.14}$$

The expression of P in (5.3.14) may therefore be used in the expression of v_r in (2). This design is summarized in Table 5.3.4.

Table 5.3.4: Saturation Controller 1

Assumptions:

$$\begin{aligned} \mu_1 I_n \leq M(q) &\leq \mu_2 I_n \\ ||N(q,\dot{q})|| &\leq \zeta_0 + \zeta_1||e|| + \zeta_2||\mathbf{e}||^2 \end{aligned}$$

Controller:

$$\tau = \frac{2\mu_1\mu_2}{\mu_1+\mu_2}[\ddot{q}_d + K_v\dot{e} + K_p e + v_r] + \hat{N}(q,\dot{q})$$

where

$$\begin{aligned} v_r &= \begin{cases} (B^T P e)p(||B^T P e||)^{-1} & \text{if } ||B^T P e|| > \epsilon \\ (B^T P e)p/\epsilon & \text{if } ||B^T P e|| \leq \epsilon \end{cases} \\ p &= \frac{1}{1-a}\left[a||\ddot{q}_d|| + k_p||e|| + k_v||\dot{e}|| + \frac{1}{\mu_1}\phi\right] \\ \phi &= \beta_0 + \beta_1||e|| + \beta_2||e||^2 \\ a &= \frac{\mu_2-\mu_1}{\mu_1+\mu_2} \end{aligned}$$

Performance:
Guaranteed uniform ultimate boundedness of e and $\dot{e}$.
Guaranteed uniform boundedness if $e(0) = \dot{e}(0) = 0$.

EXAMPLE 5.3–5: Saturation Controller 1

The following design parameters were chosen in simulating this controller:

$$\begin{array}{cccc} K_p = 15I, & K_v = 30I, & \mu_1 = 0.15, & \mu_2 = 6.5 \\ \beta_0 = 50, & \beta_1 = 10, & \beta_2 = 10, & \epsilon = 5 \\ & \hat{C} = 0, & \hat{Z} = 0, & \end{array}$$

and

e (0)=0 $e(0)=$

The same trajectory is followed by the two-link robot as shown in Figure 5.3.10. Note that although the trajectory errors seem to be diverging, they are indeed ultimately bounded and may be shown to be so by running the simulation for a long time.

■

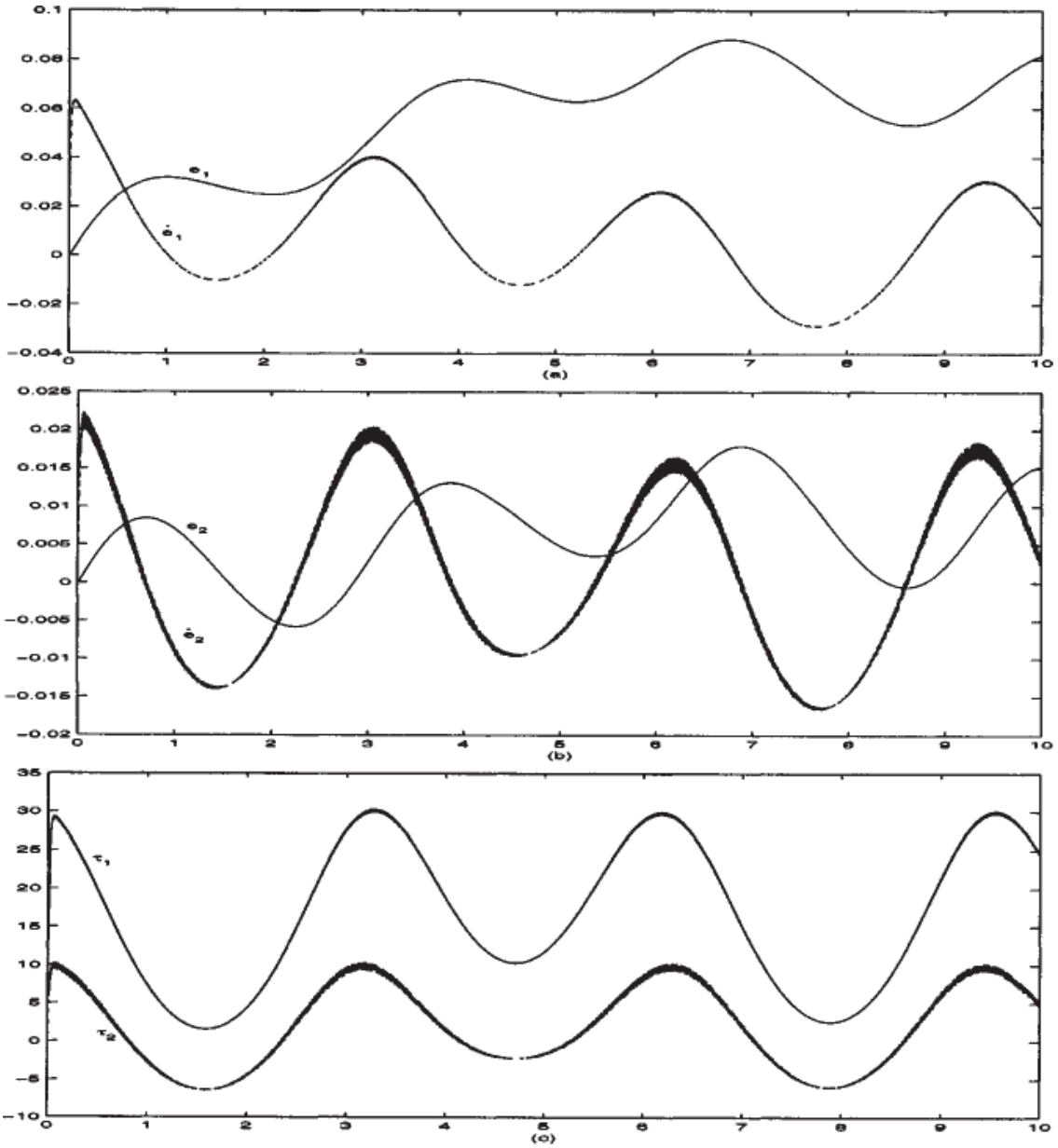


Figure 5.3.10: (a) errors of joint 1; (b) errors of joint 1; (c) torques of joints 1 and 2

Upon closer examination of Spong's controller in Theorem 5.3.4, it becomes clear that v_r depends on the servo gains K_p and K_v through p. This might obscure the effect of adjusting the servo gains and may be avoided

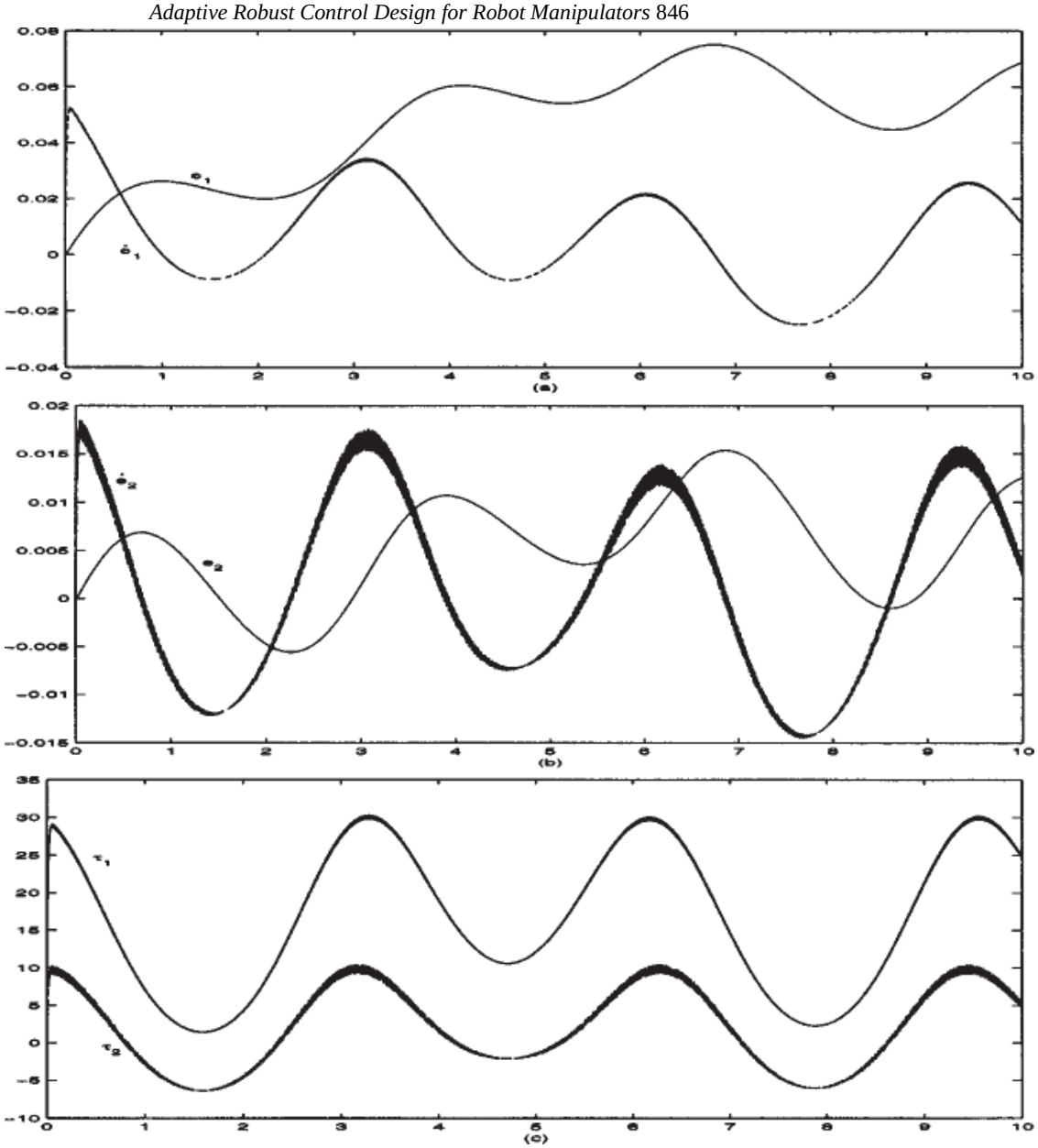


Figure 5.3.11: (a) errors of joint 1; (b) errors of joint 1; (c) torques of joints 1 and 2

as described in [Dawson et al. 1990].

THEOREM 5.3–5: *The trajectory error* **e** *is uniformly ultimately bounded (UUB) with the controller*

$$\tau = K_v \dot{e} + v_r(p, e, \dot{e}, \epsilon), \tag{1}$$

where

$$v_r = \begin{cases} (\frac{e}{2} + \dot{e})p(||\frac{e}{2} + \dot{e}||)^{-1} & \text{if } ||\frac{e}{2} + \dot{e}|| > \epsilon \\ (\frac{e}{2} + \dot{e})p/\epsilon & \text{if } ||\frac{e}{2} + \dot{e}|| \leq \epsilon \end{cases}$$

and

$$p = \delta_0 + \delta_1||e|| + \delta_2||\dot{e}||^2 \tag{2}$$

where μ_i*'s are positive scalars*.

Proof:

We again choose

$$V(\mathbf{e}) = \mathbf{e}^T P \mathbf{e}$$

and

$$Q = \begin{bmatrix} 0.5K_p & 0 \\ 0 & K_v \end{bmatrix}$$

and proceed as in Theorem 2.10.4. See [Dawson et al. 1990] for details. ■

Note that *p* no longer contains the servo gains and, as such, one may adjust K_P and K_V without tampering with the auxiliary control v_r. As was also shown in [Dawson et al. 1990], if the initial error *e*(0)=0 and by choosing $K_V=2K_P=k_V I$, the tracking error may be bounded by the following, which shows the direct effect of the control parameters on the tracking error:

$$||\mathbf{e}|| \leq \left[\frac{(8k_v + 6\mu_2)\epsilon}{k_v}\right]^{\frac{1}{2}}. \tag{5.3.15}$$

Finally, note that if *e*(0)=$\dot{e}$(0)=0, the uniform boundedness of e*(t)* may be deduced. This controller is given in Table 5.3.5.

EXAMPLE 5.3–6: Saturation Controller 2

In this example, let

$$K_p = 15I, \quad K_v = 30I,$$
$$\delta_0 = 50, \quad \delta_1 = 10, \quad \delta_2 = 10, \quad \epsilon = 0.1.$$

Table 5.3.5: Saturation Controller 2

Assumptions:

$$\mu_1 I_n \leq M(q) \leq \mu_2 I_n$$

Controller:

$$\tau = K_v \dot{e} + v_r(p, e, \dot{e}, \epsilon)$$

where

$$v_r = \begin{cases} (\frac{e}{2} + \dot{e}) p (||\frac{e}{2} + \dot{e}||)^{-1} & \text{if } ||\frac{e}{2} + \dot{e}|| > \epsilon \\ (\frac{e}{2} + \dot{e}) p / \epsilon & \text{if } ||\frac{e}{2} + \dot{e}|| \leq \epsilon \end{cases}$$

$$p = \delta_0 + \delta_1 ||e|| + \delta_2 ||\dot{e}||^2$$

Performance:
Guaranteed uniform ultimate boundedness of e and $\dot{e}$.
Guaranteed uniform boundedness if $e(0) = \dot{e}(0) = 0$.

The results of this simulation are presented in Figure 5.3.11. The errors are ultimately bounded as may be seen after a long simulation run.

■

Note that the last two controllers, although using a continuous term v_r, may be modified using the hyperbolic tangent term introduced in Example 5.3.4. In fact, there are many extensions to these types of controllers. A particularly simple one that uses linearity of the dynamics with respect to the unknown physical parameters of the robot 3.3.59 was given in (3.3.62), where p=||W||0$_m$*ax*. In this formulation, W is a matrix containing time-varying but known terms, while O is a vector of unknown but constant terms in the dynamic formulation (3.3.59) repeated here:

$$\tau = W(q, \dot{q}, \ddot{q})\Phi. \tag{5.3.16}$$

More on this formulation and its usage is presented in Chapter 6.

5.4 Dynamics Redesign

In this section we present two other approaches to design robust controllers. The first starts with the mechanical design of the robot and proposes to design robots such that their dynamics are simple and decoupled. It then solves the robust controller problem by eliminating its causes. The second approach may be recast into one of the approaches discussed previously, but it presents such a novel way to looking at the problem that we decided to include it separately.

Decoupled Designs

It was shown throughout the previous chapters that the controller complexity is directly dependent on that of the robot dynamics. Thus it would make sense to design robots such that they have simple dynamics making their control much easier. This approach is advocated in [Asada and Youcef-Toumi 1987]. In fact, it is shown that certain robotic structures will have a decoupled dynamical structures resulting in a decoupled set of *n* SISO nonlinear systems which are easier controlled than the one MIMO nonlinear system. The decoupling is achieved by modifying the dimensions and mass properties of the arm to cancel out the velocity-dependent terms and decouple the inertia matrix. An illustrative example of such robots is given in the next example.

EXAMPLE 5.4–1: Decoupled Design

Consider the robot described in Figure 5.4.1. This mechanism is known as the five-bar linkage and its dynamics are described when the following condition holds:

$$\frac{m_4 g_4}{m_3 g_3} = \frac{l_2}{l_1}$$

by

$$\tau = \begin{bmatrix} I_1 + I_3 + m_1 g_1^2 + m_4 l_1^2 \left(1 + \frac{g_3 g_4}{l_1 l_2}\right) & 0 \\ 0 & I_2 + I_4 + m_3 l_2^2 + m_4 g_4^2 \left(1 + \frac{l_1 l_2}{g_3 g_4}\right) \end{bmatrix} \ddot{q}.$$

Note that the inertia matrix is decoupled and position independent. The controller given by

$$\tau = M(\ddot{q}_d + K_v \dot{e} + K_p e)$$

with positive-definite K_p and K_v is enough to achieve any desired level of performance. In particular, consider the following case:

$$I_1 = I_2 = I_3 = I_4 = 1$$

$$\begin{array}{llll} m_1 = 5, & m_2 = \frac{1}{2}, & m_3 = 2, & m_4 = 1, \\ l_1 = 1, & l_2 = \frac{1}{2}, & l_3 = \frac{3}{4}, & l_4 = 1, \\ g_1 = \frac{1}{2}, & g_2 = \frac{1}{4}, & g_3 = \frac{1}{2}, & g_4 = \frac{1}{2}. \end{array}$$

The closed-loop error system is a linear second-order system which will be stable with positive-definite gains.

■

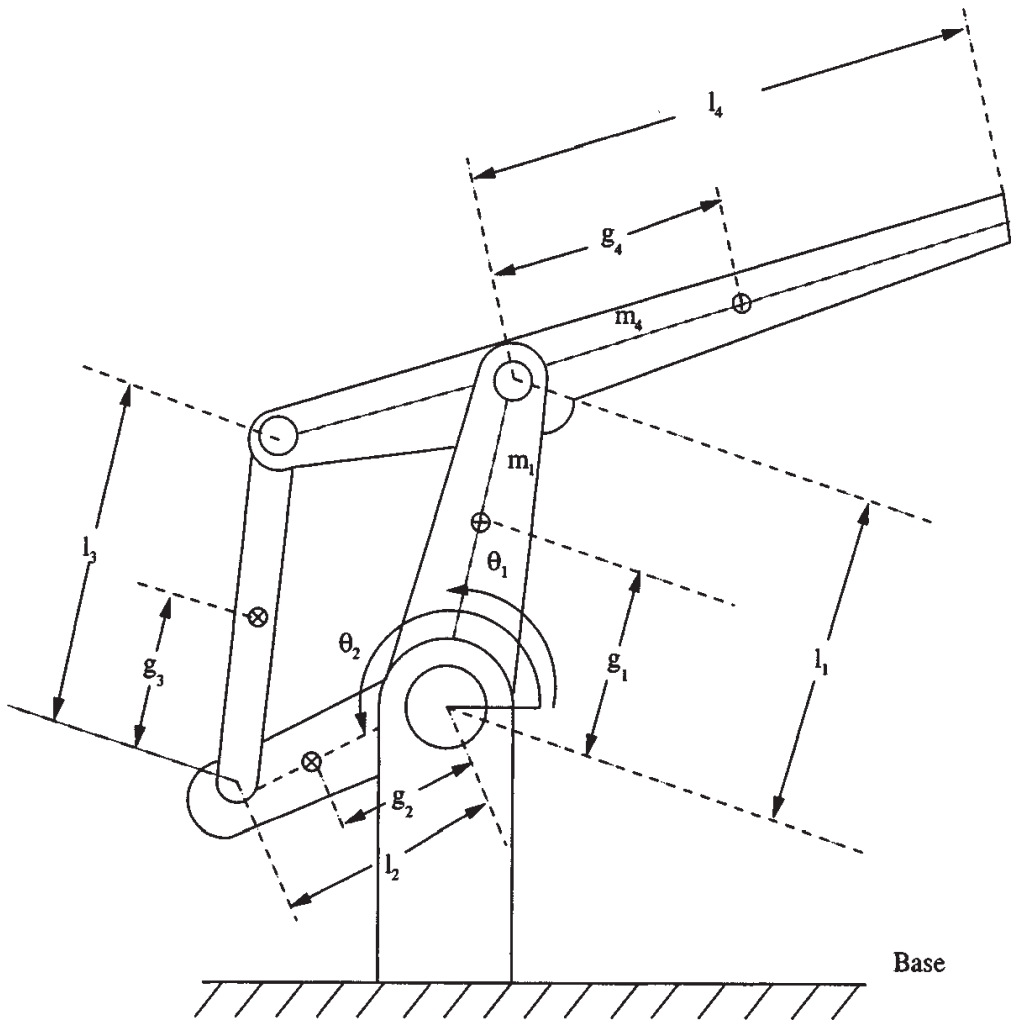


Figure 5.4.1: Five-bar linkage.

Some standard robotic structures may also be decoupled by design. Studies have been carried out to partially or totally decouple robots up to six links. The interested reader is referred to [Yang and Tzeng 1986], [Asada and Youcef-Toumi 1987], and [Kazerooni 1989] for good discussions of this topic.

Imaginary Robot Concept

The decoupled design alternative is very useful if the control engineer has access to, or can modify, the robot design at an early stage. It is more reasonable, however, to assume that the robot has already been constructed to satisfy may mechanical requirements before the control law is actually implemented. Thus a dynamics redesign is difficult if not impossible. The *imaginary robot* concept is presented as an alternative robust design methodology [Gu and Loh 1988]. The development of this approach is described next. Consider an output function of the robot given by

$$y = h(q), \tag{5.4.1}$$

so that

$$\dot{y} = \left(\frac{\partial h}{\partial q}\right)^T \dot{q} = J\dot{q} \tag{5.4.2}$$

and

$$\ddot{y} = J\ddot{q} + \dot{J}\dot{q}. \tag{5.4.3}$$

The generalized output *y* may denote the coordinates of the end effector of the robot or the trajectory joint error q_d-q. The imaginary robot concept attempts to simplify the design of the control law for the physical robot, by controlling an "imaginary" robot that is close to the actual robot. This choice of the controller is shown to achieve the global stability of an imaginary robot whose joint positions are described by the components of the vector *y*.

The methodology starts by decomposing *M(q)* as follows:

$$M(q) = J^T(q)J(q) + \tilde{M}(q) \tag{5.4.4}$$

and then using the controller

$$\tau = J^T\ddot{y} + (\hat{M} - J^T J)\ddot{q} \tag{5.4.5}$$

$$\ddot{y} = \ddot{y}_d + K_p(y_d - y) + K_v(\dot{y}_d - \dot{y}). \tag{5.4.6}$$

Since $M(q)$ is unknown, however, the actual $\tilde{M}$ is not available. The resulting controller is then simpler and may be applied to the physical robot to lead acceptable, if not optimal behavior.

The following theorem illustrates a controller to guarantee the boundedness of the error.

THEOREM 5.4–1: *Let*

$$\tau = J^T \ddot{y} + (\hat{M} - J^T J)\ddot{q} \tag{1}$$

$$\ddot{y} = \ddot{y}_d + K_p(y_d - y) + K_v(\dot{y}_d - \dot{y}). \tag{2}$$

The $\mathcal{L}$ stability of the closed-loop system is guaranteed if (3)

$$||JM^{-1}(\tilde{M} - \hat{M} + J^T J)J^{-1}|| = ||J(I - M^{-1}\hat{M})J^{-1}|| < \frac{1}{2}.$$

Proof:

This is an immediate result of Theorem 5.2.2. See [Gu and Loh 1988] for more detail and for illustrative examples. ■

The controller is shown in Table 5.4.1.

Table 5.4.1: Computed-Torque-Like Robot Controllers.

Assumptions:

$$y = h(q)$$

$$\dot{y} = \left(\frac{\partial h}{\partial q}\right)^T \dot{q} = J\dot{q}$$

$$M(q) = J^T(q)J(q) + \tilde{M}(q)$$

$$||JM^{-1}(\tilde{M} - \hat{M} + J^T J)J^{-1}|| = ||J(I - M^{-1}\hat{M})J^{-1}|| < \tfrac{1}{2}$$

Controller:

$$\tau = J^T \ddot{y} + (\hat{M} - J^T J)\ddot{q}$$
$$\ddot{y} = \ddot{y}_d + K_p(y_d - y) + K_v(\dot{y}_d - \dot{y})$$

Performance:

The errors e and $\dot{e}$ are bounded in the $\mathcal{L}_\infty$ norm. Larger gains K_p and K_v will decrease the bounds on e and $\dot{e}$.

5.5 Summary

The design of robust motion controllers of rigid robots was reviewed. There main designs were identified and explained. All controllers were robust with respect to a range of uncertain parameters and will guarantee the boundedness of the position-tracking error. In the presence of disturbance torques, a bounded error is best achievable outcome. The question of which robust control method to choose is difficult to answer analytically, but the following guidelines are suggested. The linear-multivariable approach is useful when linear performance specifications (percent overshoot, damping ratio, etc.) are available. The one-DOF dynamic compensators performed rather well, with little or no knowledge of the robot dynamics. They may, however, result in high-gain control laws in the attempt to achieve robustness. The passive controllers are easy to implement but do not provide easily quantifiable performance measures. The modified variable- structure controllers seem to preform well when using the physics of the robot without excessive torque effort. The saturation controllers are most useful when a short transient error can be tolerated, but ultimately, the error will have to be bounded.

A common thread throughout this chapter has been the fact that a high- gain controller will guarantee the robustness of the closed-loop system. The challenge is, however, to guarantee the robust stability of the robot without requiring excessive torques. The robustness of the motion controllers when nonzero initial errors or disturbances are present was also verified through some of the examples and is discussed in the problems at the end of the chapter. It is useful to note that although the robot's dynamics are highly nonlinear, most successful controllers have exploited their physics and their very special structure. In the next chapter we describe the design of adaptive controllers in the case of uncertain dynamical description of the robots.

REFERENCES

[Abdallah et al. 1991] C.T.Abdallah and D.Dawson and P.Dorato and M. Jamshidi. “Survey of Robust Control for Rigid Robots”. *IEEE Control Syst. Mag.,* vol. 11, number 2, pp. 24–30, 1991.

[Anderson 1989] R.J.Anderson. “A Network Approach to Force Control in Robotics and Teleoperation”. Ph.D. Thesis, Departemnt of Electrical & Computer Engineering. *University of Illinois at Urbana-Champaign,* 1989.

[Arimoto and Miyazaki 1985] S.Arimoto and F.Miyazaki. “Stabiliy and Robustness of PID Feedback Control for Robot Manipulators of Sensory Capability”. *Proc. Third Int. Symp. Robot. Res.,* Gouvieux, France. July, 1985.

[Asada and Youcef-Toumi 1987] H.Asada and K.Youcef-Toumi. “Direct-Drive Robots: Theory and Practice”. *MIT Press,* Cambridge, MA, 1987.

[Becker and Grimm 1988] N.Becker and W.M.Grimm. “On L_2 and L_8 Stability Approaches for the Robust Control of Robot Manipulators”. *IEEE Trans. Autom. Control,* vol. 33, number 1, pp. 118–122, January, 1988.

[Canudas de Wit and Fixot 1991] C.Canudas de Wit and N.Fixot. “Robot Control via Robust Estimated State Feedback”. *IEEE Trans. Autom. Control,* vol. 36, number 12, pp. 1497–1501, December, 1991.

[Chen 1989] Y.Chen. “Replacing a PID Controller by a Lag-Lead Compensator for a Robot: A Frequency Response Approach”. *IEEE Trans. Robot. Autom.* vol. 5, number 2, pp. 174–182, April, 1989.

[Chen et al. 1990] Y-F Chen and T.Mita and S.Wahui. “A New and simple Algorithm for Sliding Mode Control of Robot Arms”. *IEEE Trans. Autom. Control,* vol. 35, number 7, pp. 828–829, 1990.

[Corless 1989] M.Corless. “Tracking Controllers for Uncertain Systems: Application to a Manutec R3 Robot”. *J. Dyn. Syst. Meas. Control* vol. 111, pp. 609–618, December, 1989.

[Craig 1988] J.J.Craig. “Adaptive Control of Mechanical Manipulators”. *Addis on- Wesley,* Reading, MA, 1988.

321

[Dawson et al. 1990] D.M.Dawson et. al. “Robust Control for the Tracking of Robot Motion”. *Int. J. Control,* vol. 52, number 3, pp. 581–595, 1990.

[DeCarlo et al. 1988] R.A.DeCarlo and S.H.Zak and G.P.Matthews. “Variable Structure Control of Nonlinear Multivariable Systems”. *IEEE Proc.* vol. 76, number 3, pp. 212–232, March, 1988.

[Freund 1982] E.Freund. “Fast Nonlinear Control with Arbitrary Pole-Placement for Industrial Robots and Manipulators”. *Int. J. Robot. Res.* vol. 1, number 1, pp. 65–78, 1982.

[Gu and Loh 1988] Y-L.Gu and N.K.Loh. “Dynamic Modeling and Control by Utilizing an Imaginary Robot Model”. *IEEE Trans. Rob. Aut.* vol. 4, number 5, 1988.

[Kazerooni 1989] H.Kazerooni. “Design and Analysis of a Statically Balanced Direct- Drive Manipulator”. *IEEE Control Syst. Mag.* vol. 9, number 2, pp. 30–34, February, 1989.

[Luh 1983] J.Y.S.Luh. “Conventional Controller Design for Industrial Robots: A Tutorial”. *IEEE Trans. Syst. Man Cybern.* vol. 13, pp. 298–316, May-June, 1983.

[Ortega and Spong 1988] R.Ortega and M.W.Spong. “Adaptive Motion Control of Rigid Robots: A Tutorial”. *Proc. IEEE Conf. Decision Control,* Austin, TX, December, 1988.

[Slotine 1985] J-J.E.Slotine. “The Robust Control of Robot Manipulators”. *Int. J. Rob. Res.* vol. 4, number 4, pp. 49–64, 1985.

[Slotine 1988] J-J.E.Slotine. “Putting Physics Back in Control: The Example of Robotics”. *IEEE Contr. Syst. Mag.* vol. 8, number 7, pp. 12–17, December, 1988.

[Spong and Vidyasagar 1987] M.W.Spong and M.Vidyasagar. “Robust Linear Compensator Design for Nonlinear Robotic Control”. *IEEE Trans. Robot. Autom.* vol. 3, number 4, pp. 345–351, August, 1987.

[Spong et al. 1987] M.W.Spong and J.S.Thorp and J.M.Kleinwaks. “Robust Microprocessor Control of Robot Manipulators”. *Automatica.* vol. 23, number 3, pp. 373–379, 1987.

[Sugie et al. 1988] T.Sugie et. al. “Robust Controller Design for Robot Manipulators”. *Trans. ASME Dyn. Syst. Meas. Control,* vol. 110, number 1, pp. 94–96, March, 1988.

[Tarn et al. 1984] T.J.Tarn and A.K.Bejczy and A.Isidori and Y.Chen. “Nonlinear Feedback in Robot Arm Control”. *Proc. IEEE Conf. Decision Control,* Las Vegas, NV. December, 1984.

[Utkin 1977] V.I. Utkin. “Variable Structure Systems with Sliding Modes”. *IEEE TRans. Autom. Control* vol. 22, pp. 212–222, April, 1977.

[Vidyasagar 1985] M.Vidyasagar. “Control Systems Synthesis: A Factorization Approach”. *MIT Press,* Cambridge, MA. 1985.

[Yang and Tzeng 1986] D.C-H.Yang and S.W.Tzeng. “Simplification and Linearization of Manipulator Dynamics by the Design of Inertia Distribution”. *Int. J. Rob. Res.* vol. 5, number 3, pp. 120–128, 1986.

[Yeung and Chen 1988] K.S.Yeung and Y.P.Chen. “A New Controller Design for Manipulators Using the Theory of Variable Structure Systems”. *IEEE Trans. Autom. Control,* vol. 33, number 2, pp. 200–206, February, 1988.

[Young 1978] K-K.D.Young. “Controller Design for a Manipulator Using theory of Variale Structure Systems”. *IEEE Trans. Syst. Man Cybern.* vol. 8, number 2, pp. 210–218, February, 1978.

Chapter 6

Adaptive Control of Robotic Manipulators

In this chapter adaptive controllers are formulated by separating unknown constant parameters from known functions in the robot dynamic equation. The type of stability for each adaptive control strategy is discussed at length to motivate the formulation of the controllers. Some issues regarding parameter error convergence, persistency of excitation, and robustness are also discussed.

6.1 Introduction

The problem of designing adaptive control laws for rigid-robot manipulators that ensure asymptotic trajectory tracking has interested researchers for many years. The development of effective adaptive controllers represents an important step toward high-speed/precision robotic applications. Even in a well-structured industrial facility, robots may face uncertainty regarding the parameters describing the dynamic properties of the grasp load (e.g., unknown moments of inertia). Since these parameters are difficult to compute or measure, they limit the potential for robots to manipulate accurately objects of considerable size and weight. It has recently been recognized that the accuracy of conventional approaches in high-speed applications is greatly affected by parametric uncertainties.

To compensate for this parametric uncertainty, many researchers have proposed adaptive strategies for the control of robotic manipulators. An advantage of the adaptive approach over the robust control strategies discussed in Chapter 5 is that the accuracy of a manipulator carrying unknown

329

loads improves with time because the adaptation mechanism continues extracting information from the tracking error. Therefore, adaptive controllers can give consistent performance in the face of load variations.

It is only recently that adaptive control results have included rigorous proofs for global convergence of the tracking error. Now that the existence of globally convergent adaptive control laws has been established, it is difficult to justify control schemes based on approximate models, local linearization techniques, or slowly time varying assumptions. In the control literature there also seems to be no general agreement as to what constitutes an adaptive control algorithm; therefore, in this chapter, the discussion will be limited to control schemes that explicitly incorporate parameter estimation in the control law.

6.2 Adaptive Control by a Computed-Torque Approach

In Chapter 3 we motivated the use of the computed-torque control law for controlling the robotic manipulator dynamics given by

$$\tau = M(q)\ddot{q} + V_m(q,\dot{q})\dot{q} + G(q) + F(\dot{q}). \tag{6.2.1}$$

This motivation was actually quite simple. Specifically, if there are some nonlinear dynamics which one does not wish to deal with, one can change the nonlinear control problem to a linear control problem by directly canceling the nonlinearities. There is a wealth of available knowledge for controlling linear systems; therefore, if exact knowledge of the robot model is available, there is not much need for sophisticated nonlinear control techniques.

Approximate Computed-Torque Controller

Of course, in reality, we never have exact knowledge of the robot model due to many problems associated with model formulation. Two common uncertainties that do not allow exact model cancellation in robotic applications are unknown link masses due to payload disturbances and unknown friction coefficients. One way of dealing with these types of *parametric* uncertainties would be to use the computed-torque controller given in Chapter 3 with some fixed estimate of the unknown parameters in place of the actual parameters. This approximate computed-torque controller would have the form

$$\tau = \hat{M}(q)(\ddot{q}_d + K_v\dot{e} + K_p e) + \hat{V}_m(q,\dot{q})\dot{q} + \hat{G}(q) + \hat{F}(\dot{q}). \tag{6.2.2}$$

where the superscript $\hat{}$ denotes the estimated dynamics with the unknown actual parameters replaced by the parameter estimates, K_V and K_P are control gain matrices, q_d is used to denote the desired trajectory, and the tracking error e is defined by

$$e=q_d-q.$$

We now illustrate the approximate computed-torque controller by examining an example.

EXAMPLE 6.2–1: Approximate Computed-Torque Controller

We wish to design and simulate an approximate computed-torque controller for the two-link arm given in Figure 6.2.1 (see Chapter 2 for the two-link revolute robot arm dynamics). Assuming that the friction is negligible, the link lengths are exactly known, and the masses m_1 and m_2 are known to be in the regions 0.8±0.05 kg and 2.3±0.1 kg, respectively, a possible approximated computed-torque controller can be written as

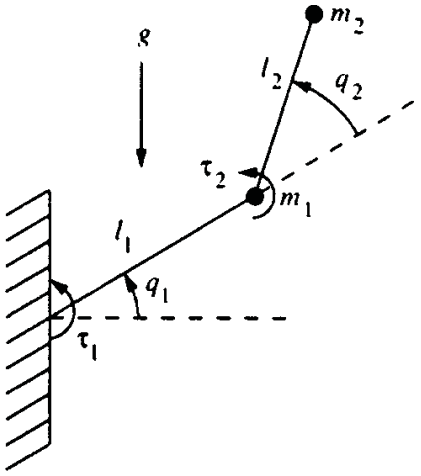


Figure 6.2.1: Two-link planar arm.

$$\begin{aligned}\tau_1 &= \left(2\hat{m}_2 l_1 l_2 c_2 + \hat{m}_2 l_2^2 + (\hat{m}_1+\hat{m}_2) l_1^2\right)(\ddot{q}_{d1} + k_{v1}\dot{e}_1 + k_{p1}e_1) \\ &\quad + \left(\hat{m}_2 l_1 l_2 c_2 + \hat{m}_2 l_2^2\right)(\ddot{q}_{d2} + k_{v2}\dot{e}_2 + k_{p2}e_2) - \hat{m}_2 l_1 l_2 s_2 \dot{q}_2^2 \\ &\quad - 2\hat{m}_2 l_1 l_2 s_2 \dot{q}_1 \dot{q}_2 + \hat{m}_2 l_2 g c_{12} + (\hat{m}_1+\hat{m}_2) l_1 g c_1 \end{aligned} \tag{1}$$

$$\begin{aligned}\tau_2 &= \left(\hat{m}_2 l_2^2 + \hat{m}_2 l_1 l_2 c_2\right)(\ddot{q}_{d1} + k_{v1}\dot{e}_1 + k_{p1}e_1) + \hat{m}_2 l_2 g c_{12} \\ &\quad + \hat{m}_2 l_2^2 (\ddot{q}_{d2} + k_{v2}\dot{e}_2 + k_{p2}e_2) + \hat{m}_2 l_1 l_2 s_2 \dot{q}_1^2, \end{aligned} \tag{2}$$

where $l_1=l_2=1$ m and g is the gravitational constant. We choose $\hat{m}_1=0.85$ kg and $\hat{m}_2=2.2$ kg since the actual values are assumed to be unknown. After substituting the control law above into the two-link robot dynamics, we can form the error system

$$\ddot{e} + K_v\dot{e} + K_p e = \hat{M}^{-1}(q)\, W(q, \dot{q}, \ddot{q})\, \tilde{\varphi}, \tag{3}$$

where $\hat{M}^{-1}(q)$ is the inverse of the inertia matrix $M(q)$ with m_1 and m_2 replaced by $\hat{m}_1$ and $\hat{m}_2$, respectively. The matrix $W(q, \dot{q}, \ddot{q})$, sometimes called the *regression* matrix [Craig 1985], is a 2×2 matrix given by

$$W(q, \dot{q}, \ddot{q}) = \begin{bmatrix} W_{11} & W_{12} \\ W_{21} & W_{22} \end{bmatrix}, \tag{4}$$

where

$$\begin{aligned}
W_{11} &= l_1^2\ddot{q}_1 + l_1 g c_1, \\
W_{12} &= l_2^2(\ddot{q}_1 + \ddot{q}_2) + l_1 l_2 c_2(2\ddot{q}_1 + \ddot{q}_2) + l_1^2\ddot{q}_1 - l_1 l_2 s_2 \dot{q}_2^2 \\
&\quad - 2l_1 l_2 s_2 \dot{q}_1 \dot{q}_2 + l_2 g c_{12} + l_1 g c_1, \\
W_{21} &= 0, \\
W_{22} &= l_1 l_2 c_2 \ddot{q}_1 + l_1 l_2 s_2 \dot{q}_1^2 + l_2 g c_{12} + l_2^2(\ddot{q}_1 + \ddot{q}_2).
\end{aligned}$$

The vector $\tilde{\varphi}$ called the parameter error vector, is a 2×1 vector given by

$$\tilde{\varphi} = \begin{bmatrix} \tilde{\varphi}_1 \\ \tilde{\varphi}_2 \end{bmatrix}, \tag{5}$$

where

$$\tilde{\varphi}_1 = m_1 - \hat{m}_1$$

and

$$\tilde{\varphi}_2 = m_2 - \hat{m}_2.$$

The associated tracking error 2×1 vector and 2×2 gain matrices in (3) are given

by

$$e = \begin{bmatrix} e_1 \\ e_2 \end{bmatrix}, \quad K_v = \begin{bmatrix} k_{v1} & 0 \\ 0 & k_{v2} \end{bmatrix}, \quad \text{and} \quad K_p = \begin{bmatrix} k_{p1} & 0 \\ 0 & k_{p2} \end{bmatrix}.$$

We cannot use the error system (3) to select the values for K_V and K_P with standard linear control methods since the right-hand side of the error system is composed of nonlinear functions of q, $\dot{q}$, and $\ddot{q}$. For the approximate computed-torque controller, simulation can be used to select the appropriate values for K_V and K_P. A good starting point for selecting the values of K_P and K_V for the approximate computed-torque controller is to use the same values, as the computed-torque scheme would dictate, for a given desired damping ratio and natural frequency.

For m_1=0.8 kg and m_2=2.3 kg, the approximate computed torque controller (1)–(2) was simulated with $q(0)=\dot{q}(0)=0$, with the controller gains set at

$$K_p = K_v = \begin{bmatrix} 4 & 0 \\ 0 & 4 \end{bmatrix} \tag{6}$$

and with a desired trajectory of

$$q_{d1}=q_{d2}=\sin t. \tag{7}$$

The tracking error is depicted in Figure 6.2.2. As illustrated by these figures, the tracking error remains bounded rather than going to zero. The reason for this type of bounded tracking error performance is that the error system given by (3) is constantly being excited by the dynamics on the right-hand side of (3).

■

Adaptive Computed-Torque Controller

For unknown parametric quantities such as link masses or friction coefficients, the approximate computed-torque controller simply substitutes a fixed estimate $\hat{\varphi}$ for the unknown parametric quantities. From Equation (3) in Example 6.2.1, one can clearly see that if the parameter error vector $\tilde{\varphi}$ is equal to zero, the tracking error can be shown to be asymptotically stable. For many applications, we cannot assume that $\tilde{\varphi}$ is equal to zero. For example, in the case of an unknown payload mass attached to the end effector of a robot, there will always be an unknown parametric quantity related to the payload mass that would appear in the parameter error vector.

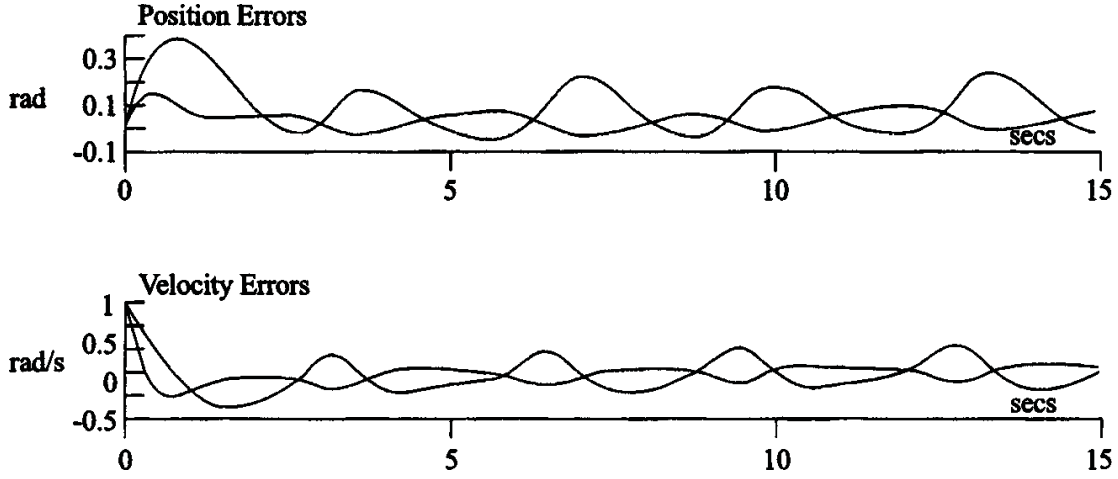


Figure 6.2.2: Simulation of approximate computed-torque controller.

The adaptive control strategy can, heuristically, be motivated by reasoning that one could expect better tracking performance if the parameter estimate was adjusted as the robot manipulator moves instead of always being a fixed quantity. That is, it seems reasonable to attempt to change our parameter estimates based on an adaptive update rule that would be a function of the robot configuration and the tracking error. The question then becomes: How do we formulate an adaptive control strategy, and how does this adaptive update rule affect the stability of the tracking error? The answer to both of these questions is that the adaptive update rule is formulated from the stability analysis of the tracking error system. That is, we ensure stability of the tracking error system by formulating the adaptive update rule and by analyzing the stability of the tracking error system at the same time.

The first adaptive control strategy that we will examine is the method outlined in [Craig 1985]. The adaptive computed-torque controller is the same as the approximate computed-torque controller (6.2.2) with the addition of an adaptive update rule for adjusting the parameter estimates. This adaptive controller is based on the fact that the parameters appear linearly in the robot model (see Chapter 2). That is, the robot dynamics (6.2.1) can be written in the form

$$W(q,\dot{q},\ddot{q})\,\varphi = M(q)\,\ddot{q} + V_m(q,\dot{q})\,\dot{q} + G(q) + F(\dot{q}), \tag{6.2.3}$$

where $W(q, \dot{q}, \ddot{q})$ is an $n \times r$ matrix of known time functions and is an $r \times 1$ vector of unknown constant parameters. This property is crucial for the type of adaptive control that Craig formulated in that it illustrates the separation of unknown parameters and the known time functions. The reason that the

robot dynamics can be separated in this form is that the robot dynamics are linear in the parameters expressed in the vector form φ. This separation of unknown parameters and known time functions will be used in the formulation of the adaptive update rule and also in the stability analysis of the tracking error system.

The first step in the study of the adaptive computed-torque controller is to form the tracking error system. Note that, by using (6.2.3), we may write the robot dynamic Equation given by (6.2.1) as

$$\tau = W(q, \dot{q}, \ddot{q})\,\varphi. \tag{6.2.4}$$

From [Craig 1985], the adaptive computed-torque controller is given by

$$\tau = \hat{M}(q)(\ddot{q}_d + K_v\dot{e} + K_p e) + \hat{V}_m(q, \dot{q})\,\dot{q} + \hat{G}(q) + \hat{F}(\dot{q}). \tag{6.2.5}$$

It is easy to see from our definition of the tracking error how (6.2.5) can be written as

$$\tau = \hat{M}(q)(\ddot{e} + K_v\dot{e} + K_p e) + \hat{M}(q)\,\ddot{q} + \hat{V}_m(q, \dot{q})\,\dot{q} + \hat{G}(q) + \hat{F}(\dot{q}). \tag{6.2.6}$$

By utilizing (6.2.3), (6.2.6) can be written as

$$\tau = \hat{M}(q)(\ddot{e} + K_v\dot{e} + K_p e) + W(q, \dot{q}, \ddot{q})\,\hat{\varphi}, \tag{6.2.7}$$

where $\hat{\varphi}$ is an $n\times 1$ vector used to represent a time-varying estimate of the unknown constant parameters. Substituting (6.2.7) into (6.2.4), we can form the *tracking error system*

$$\ddot{e} + K_v\dot{e} + K_p e = \hat{M}^{-1}(q)\,W(q, \dot{q}, \ddot{q})\,\tilde{\varphi}, \tag{6.2.8}$$

where the *parameter error* is

$$\tilde{\varphi} = \varphi - \hat{\varphi}. \tag{6.2.9}$$

Now for convenience, rewrite (6.2.8) in the state-space form

$$\dot{\mathbf{e}} = A\mathbf{e} + BM^{-1}(q)\,W(q, \dot{q}, \ddot{q})\,\tilde{\varphi}, \tag{6.2.10}$$

where the *tracking error vector* is

$$\mathbf{e} = \begin{bmatrix} e \\ \dot{e} \end{bmatrix}$$

and

$$B = \begin{bmatrix} O_n \\ I_n \end{bmatrix}, \quad A = \begin{bmatrix} O_n & I_n \\ -K_p & -K_v \end{bmatrix},$$

with I_n being the $n \times n$ identity matrix, and O_n being the $n \times n$ zero matrix.

Now that the tracking error system has been formed, we use Lyapunov stability analysis (see Chapter 1) to show that the tracking error vector **e** is asymptotically stable with the right choice of adaptive update law. We first select the positive-definite Lyapunov-like function

$$V = \mathbf{e}^T P \mathbf{e} + \tilde{\varphi}^T \Gamma^{-1} \tilde{\varphi}, \tag{6.2.11}$$

where P is a $2n \times 2n$ positive-definite, constant, symmetric matrix, and Γ is a diagonal, positive-definite $r \times r$ matrix. That is, Γ can be written as

$$\Gamma = diag\,(\gamma_1,\ \gamma_2,\ \ldots,\ \gamma_r)\,,$$

where the γ_i's are positive scalar constants.

Differentiating (6.2.11) with respect to time yields

$$\dot{V} = \mathbf{e}^T P \dot{\mathbf{e}} + \dot{\mathbf{e}}^T P \mathbf{e} + 2\tilde{\varphi}^T \Gamma^{-1} \dot{\tilde{\varphi}}. \tag{6.2.12}$$

It is important to note in (6.2.12) that we have used the fact that

$$\left[\tilde{\varphi}^T \Gamma^{-1} \tilde{\varphi}\right]^T = \tilde{\varphi}^T \Gamma^{-1} \dot{\tilde{\varphi}} \tag{6.2.13}$$

since $\Gamma = \Gamma^T$. (Note that a scalar quantity can always be transposed.) Now, substituting for e from (6.2.10) into (6.2.12) yields

$$\begin{aligned} \dot{V} =& \mathbf{e}^T P \left(A\mathbf{e} + B\hat{M}^{-1}(q)\, W(\cdot)\, \tilde{\varphi} \right) \\ &+ \left(A\mathbf{e} + B\hat{M}^{-1}(q)\, W(\cdot)\, \tilde{\varphi} \right)^T P\mathbf{e} + 2\tilde{\varphi}^T \Gamma^{-1} \dot{\tilde{\varphi}}. \end{aligned} \tag{6.2.14}$$

Combining terms in (6.2.14) and using the scalar transportation property gives

$$\dot{V} = -\mathbf{e}^T Q \mathbf{e} + 2\tilde{\varphi}^T \left(\Gamma^{-1} \dot{\tilde{\varphi}} + W^T(\cdot)\, \hat{M}^{-1}(q)\, B^T P \mathbf{e} \right), \tag{6.2.15}$$

where Q is a positive-definite, symmetric matrix that satisfies the Lyapunov equation

$$A^T P + PA = -Q. \tag{6.2.16}$$

From Chapter 1 we note that for stability, it is always desirable to have $\dot{V}$ at least negative semidefinite; therefore, the choice of adaptation update rule becomes obvious. Specifically, by substituting

$$\dot{\hat{\varphi}} = -\Gamma W^T(\cdot)\,\hat{M}^{-1}(q)\,B^T P\mathbf{e}, \tag{6.2.17}$$

(6.2.15) becomes

$$\dot{V} = -\mathbf{e}^T Q\mathbf{e}. \tag{6.2.18}$$

To determine explicitly the type of stability, we must do further analysis; however, note first that (6.2.17) gives the adaptive update rule for the parameter estimate vector $\hat{\varphi}$ since $\dot{\varphi}$ is equal to zero. That is, by recalling that the actual unknown parameters are *constant,* we can substitute (6.2.9) into (6.2.17) to obtain the *adaptive update rule:*

(6.2.19)
$$\dot{\hat{\varphi}} = \Gamma W^T(\cdot)\,\hat{M}^{-1}(q)\,B^T P\mathbf{e}$$

for the parameter estimate vector $\hat{\varphi}$.

Before examining the type of stability for the tracking error system, we note that Craig modified the adaptation update rule in (6.2.19) to prevent a circular argument in the stability analysis [Craig 1985]. Specifically, the parameter estimates are forced to remain within some known region. That is, if parameter estimates drift out of a known region, they are reset to within a known region. By resetting the parameter estimates in "software," we are guaranteed that the parameter estimates $\hat{\varphi}$ remain bounded.

We now detail the stability for the tracking error. Since $\dot{V}$ is negative semidefinite and *V* is lower bounded by zero, *V* remains upper bounded in the time interval [*O,* □); furthermore,

(6.2.20)
$$\lim_{t\to\infty} V = V_\infty,$$

where V_∞ is a positive scalar constant. Since *V* is upper bounded, it is obvious from the definition of *V* given in (6.2.11) that **e** and $\tilde{\varphi}$ are bounded, which also means that *q,* $\dot{q}$ and $\hat{\varphi}$ are bounded. Note that we have already assumed that $\hat{\varphi}$ is bounded, and we will always assume that the desired trajectory and its first two derivatives are bounded.

Now, from the robot Equation (6.2.1), it is clear that

(6.2.21)
$$\ddot{q} = M^{-1}(q)\left(\tau - V_m(q,\dot{q})\,\dot{q} - G(q) - F(\dot{q})\right);$$

therefore, $\ddot{q}$ is bounded since $M^{-1}(q)$ and $V_m(q,\dot{q})$ depend only on the bounded quantities *q*, $\dot{q}$, and $\hat{\varphi}$. If $\dot{q}$ is bounded, (6.2.10) shows that $\dot{r}$ is bounded. Since $\dot{r}$ is bounded, we can state from (6.2.18) that $\dot{V}$ is bounded. Therefore, since *V* is

lower bounded by zero, V is negative semidefinite, and $\ddot{V}$ is bounded, then by Barbalat's lemma (see Chapter 1),

$$\lim_{t\to\infty} \dot{V} = 0$$

which means that by the Rayleigh-Ritz Theorem (see Chapter 1)

$$\lim_{t\to\infty} \lambda_{\min}\{Q\}\,\|\mathbf{e}\|^2 = 0 \quad \text{which means that} \quad \lim_{t\to\infty} \mathbf{e} = 0. \tag{6.2.22}$$

Table 6.2.1: Adaptive Computed-Torque Controller

Torque Controller:

$$\tau = \hat{M}(q)\,(\ddot{q}_d + K_v\dot{e} + K_p e) + \hat{V}_m(q,\dot{q})\,\dot{q} + \hat{G}(q) + \hat{F}(\dot{q})$$

Update Rule:

$$\dot{\hat{\varphi}} = \Gamma W^T(q,\dot{q},\ddot{q})\,\hat{M}^{-1}(q)\,B^T P\mathbf{e}$$

where

$$\mathbf{e} = \begin{bmatrix} e \\ \dot{e} \end{bmatrix}, \quad B = \begin{bmatrix} O_n \\ I_n \end{bmatrix}, \quad A = \begin{bmatrix} O_n & I_n \\ -K_p & -K_v \end{bmatrix}$$

$$W(q,\dot{q},\ddot{q})\,\hat{\varphi} = \hat{M}(q)\,\ddot{q} + \hat{V}_m(q,\dot{q})\,\dot{q} + \hat{G}(q) + \hat{F}(\dot{q})$$

$$A^T P + PA = -Q$$

for some positive-definite, symmetric matrices P and Q.

Stability:

Tracking error vector $\mathbf{e}$ is asymptotically stable.

Restrictions:

Parameter resetting method is required. Measurement of $\ddot{q}$ is required.

The information given in (6.2.22) informs us that the tracking error vector e is asymptotically stable. But what of the parameter error $\tilde{\varphi}$? Does it also converge to zero? From our analysis, all we can say about the parameter error is that it remains bounded if $\hat{M}^{-1}(q)$ exists. Indeed, this places a restriction on the parameter update law given in (6.2.19). That is, we must use the parameter resetting method discussed earlier to ensure that poor parameter

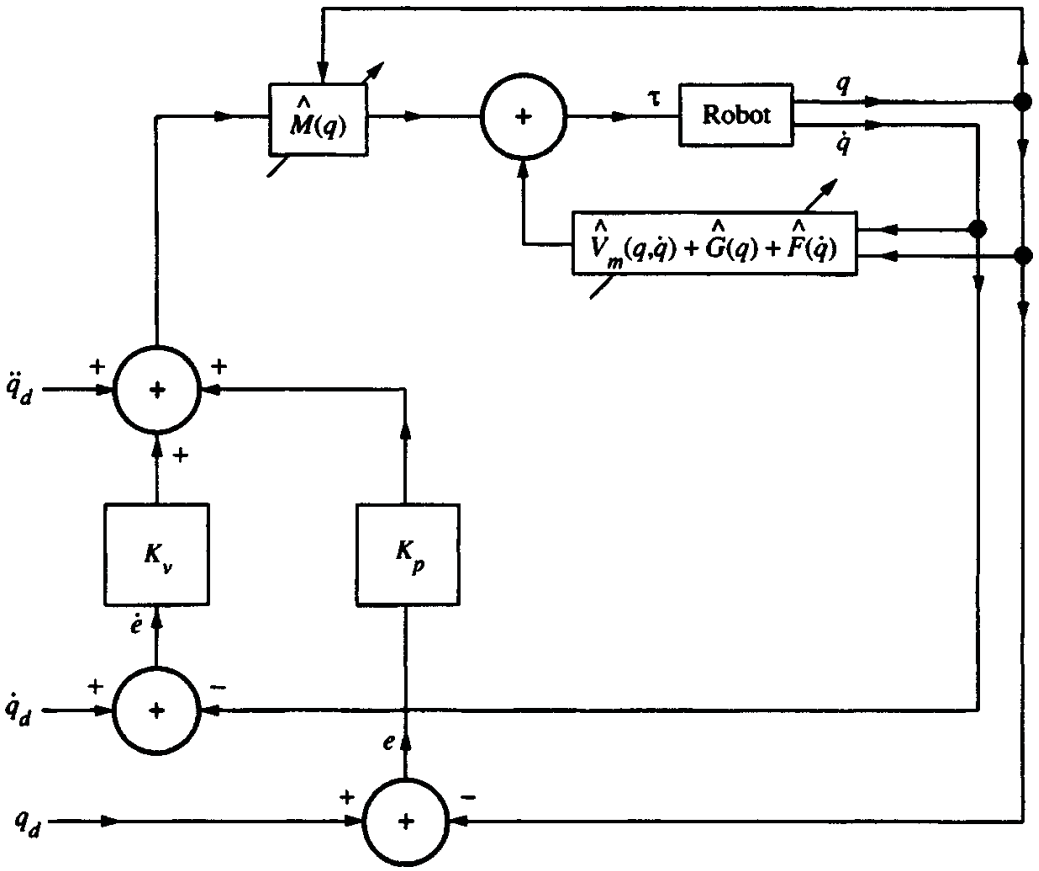


Figure 6.2.3: Block diagram of the adaptive computed-torque controller.

estimates do not cause the inverse of $\hat{M}$ (q) to explode. In [Craig 1985] a possible method for ensuring that the parameter estimates and $\hat{M}^{-1}(q)$ remain bounded is outlined; furthermore, he shows how this method does not interfere with the stability result delineated by (6.2.22). We will not discuss this parameter estimate resetting method and the resulting stability proof since we will show later in this chapter how Slotine and Li used a more judicious choice of Lyapunov function to remove the need for resetting the parameter estimates, and at the same time remove the need for acceleration measurements in the regression matrix $W(q, \dot{q}, \ddot{q})$! The adaptive computed-torque controller is summarized in Table 6.2.1 and depicted in Figure 6.2.3.

We now present an example to illustrate how Table 6.2.1 can be used to generate adaptive controllers for robotic manipulators.

EXAMPLE 6.2–2: Adaptive Computed-Torque Controller

It is desired to design and simulate the adaptive computed-torque controller given in Table 6.2.1 for the two-link arm given in Figure 6.2.1.

Assuming that the friction is negligible and that the link lengths are exactly known, the adaptive computed-torque controller can be written in the same form as that given in Example 6.2.1, with the exception that *we* must find the update rules for $\hat{m}_1$ and $\hat{m}_2$. That is, we use Equations (1) and (2) in Example 6.2.1 for the joint torque control and then formulate the update rule for m_1 and m_2 according to Table 6.2.1.

For simplicity, in this example we select the servo gains as

(1) $$K_v = k_v I_n \quad \text{and} \quad K_p = k_p I_n,$$

where k_V and k_P are positive, scalar constants and for this case I_n is the 2×2 identity matrix. We propose that the matrix P in Table 6.2.1 be selected as

$$P = \begin{bmatrix} P_1 I_n & P_2 I_n \\ P_2 I_n & P_3 I_n \end{bmatrix} = \tfrac{1}{2} \begin{bmatrix} (K_p + \tfrac{1}{2} k_v) I_n & \tfrac{1}{2} I_n \\ \tfrac{1}{2} I_n & I_n \end{bmatrix}. \tag{2}$$

Note that P is symmetric, and that it is positive definite if k_V is selected to be greater than 1 (see the Gerschgorin Theorem in Chapter 1). To see if our selection of P gives a positive-definite Q, perform the matrix operation

$$A^T P + PA = -Q \tag{3}$$

(4) $$Q = \begin{bmatrix} \tfrac{1}{2} k_p I_n & O_n \\ O_n & (K_v + \tfrac{1}{2}) I_n \end{bmatrix}.$$

Since we have already restricted k_V>1, it can be verified that Q is a positive definite, symmetric matrix. We note here that the process of finding a positive definite, symmetric P and Q for the general Lyapunov approach is not always an easy task.

Now that we have found an appropriate P, we can formulate the adaptive update rule given in Table 6.2.1. The associated parameter estimate vector is

$$\hat{\varphi} = \begin{bmatrix} \hat{m}_1 \\ \hat{m}_2 \end{bmatrix}$$

with update rules

$$\begin{aligned}\dot{\hat{m}}_1 =& \gamma_1[(W_{11}MI_{11} + W_{21}MI_{21})(P_2e_1 + P_3\dot{e}_1) \\ &+ (W_{11}MI_{21} + W_{21}MI_{22})(P_2e_2 + P_3\dot{e}_2)]\end{aligned} \tag{5}$$

and

$$\begin{aligned}\dot{\hat{m}}_2 =& \gamma_2[(W_{12}MI_{11} + W_{22}MI_{21})(P_2e_1 + P_3\dot{e}_1) \\ &+ (W_{12}MI_{21} + W_{22}MI_{22})(P_2e_2 + P_3\dot{e}_2)],\end{aligned} \tag{6}$$

where

$$MI_{11} = \frac{1}{\Delta}\left(\hat{m}_2 l_2^2\right),$$

$$MI_{21} = -\frac{1}{\Delta}\left(\hat{m}_2 l_1 l_2 c_2 + \hat{m}_2 l_2^2\right),$$

$$MI_{22} = \frac{1}{\Delta}\left(2\hat{m}_2 l_1 l_2 c_2 + \hat{m}_2 l_2^2 + (\hat{m}_1 + \hat{m}_2) l_1^2\right),$$

$$\Delta = \left(2\hat{m}_2 l_1 l_2 c_2 + \hat{m}_2 l_2^2 + (\hat{m}_1 + \hat{m}_2) l_1^2\right)\left(\hat{m}_2 l_2^2\right) - \left(\hat{m}_2 l_2^2 + \hat{m}_2 l_1 l_2 c_2\right)^2,$$

the P_i's are defined in (2), and the quantities forming the regression matrix W_{ij}'s are found in Example 6.2.1.

For m_1=0.8 kg and m_2=2.3 kg, this adaptive computed-torque controller was simulated with k_V=50, k_P=125, γ_1=500, γ_2=500, $\hat{m}_1(0)$=0.85, $\hat{m}_2(0)$=2.2, and with the same desired trajectory and initial joint conditions used in Example 6.2.1. The tracking error and mass estimates are depicted in Figure 6.2.4. As illustrated by this figure, the tracking error goes to zero, and the parameter estimates remain bounded as predicted by the theory. Note that we did not take any special precautions in this simulation to ensure the existence of $\hat{M}^{-1}(q)$. We could have developed some sort of procedure to guarantee that $\hat{M}^{-1}(q)$ existed; however, this is not really needed since we show in the next section how to eliminate this restriction.

■

6.3 Adaptive Control by an Inertia-Related Approach

In Section 6.2 we showed how adaptive control can be used to compensate for parametric uncertainties. This led Craig to develop the adaptive computed-torque controller. We also gave the two restrictions required for the

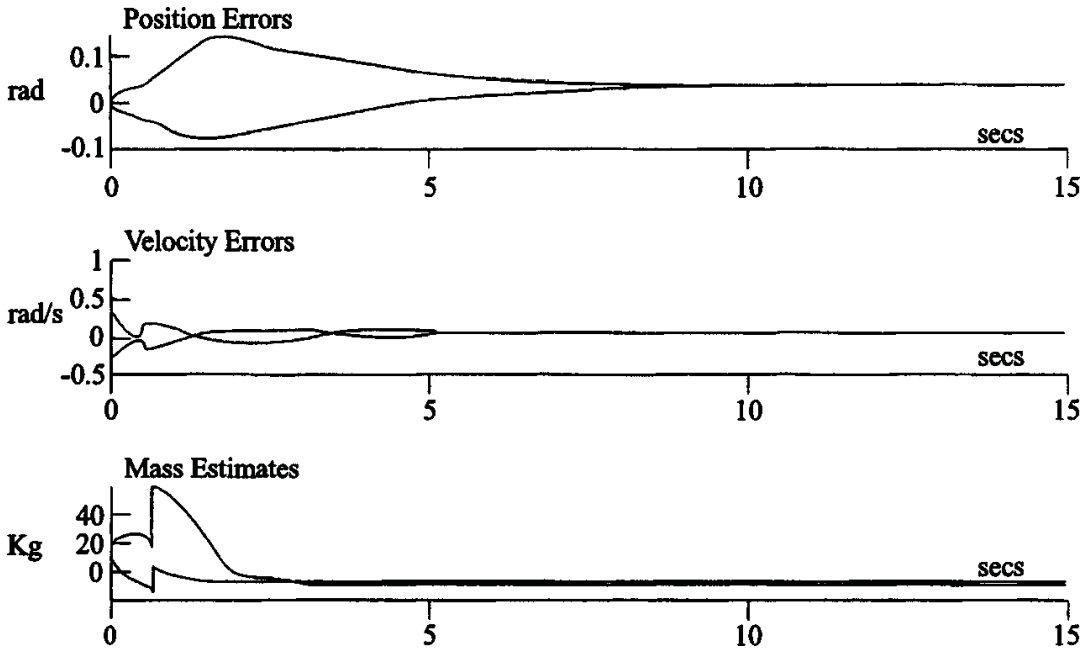


Figure 6.2.4: Simulation of the adaptive computed-torque controller.

implementation of the adaptive computed-torque controller [i.e., the need for measuring $\ddot{q}$ and ensuring that $\hat{M}^{-1}(q)$ exists]. Both of these restrictions can be quite cumbersome. For example, most industrial robots have only position and velocity sensors, and since differentiation of velocity is not desirable in general, we must add additional costly sensors for measuring $\ddot{q}$. Furthermore, if large, unknown payloads relative to the manipulator's weight are being lifted by the manipulator, it may be extremely difficult to ensure that $\hat{M}^{-1}(q)$ exists.

After researchers reexamined the structure of the adaptive computedtorque controller, they began to wonder if all the available information about the robot manipulator was being used in designing adaptive control schemes. That is, are all the properties inherent to a mechanical manipulator being exploited? In [Arimoto and Miyazaki 1986] a proportionalderivative (PD) feedback controller with gravity compensation is proposed. It should be noted that this controller is not a product of the feedback linearization approach. Rather, this controller employs an inertia-related Lyapunov function in the stability analysis which utilizes physical properties inherent to a mechanical manipulator. After reexamining the adaptive computed-torque controller, one can see that the Lyapunov function used in the stability analysis is not inertia-related but is somewhat arbitrary.

Examination of a PD Plus Gravity Controller

One method [Slotine 1988] of motivating a PD plus gravity controller [Arimoto and Miyazaki 1986] is to write the manipulator dynamics in the conservation- of-energy form

$$\frac{1}{2}\frac{d}{dt}\left[\dot{q}^T M(q)\dot{q}\right] = \dot{q}^T\left(\tau - G(q) - F(\dot{q})\right), \tag{6.3.1}$$

where the left-hand side of (6.3.1) is the derivative of the manipulator kinetic energy, and the right-hand side of (6.3.1) represents the power supplied from the actuators minus the power dissipated due to gravity and friction. Note that the Coriolis and centripetal terms are accounted for in (6.3.1) since these terms are related to the time derivative of the inertia matrix.

Suppose that we now want to design a constant set-point controller (i.e., $\dot{q}_d$=0) for the system given in the conservation of energy form (6.3.1). To begin, we select the inertia-related Lyapunov function

$$V = \tfrac{1}{2}\dot{q}^T M(q)\dot{q} + \tfrac{1}{2}e^T K_p e. \tag{6.3.2}$$

Since a Lyapunov function can be thought of heuristically as an energy function, this Lyapunov function seems quite reasonable. That is, the Lyapunov function is composed of the kinetic energy of the robotic manipulator system $\left(\frac{1}{2}\dot{q}^T M(q)\dot{q}\right)$ and an additional energy damping term $\left(\frac{1}{2}e^T K_p e\right)$. This energy damping term can be thought of as using physical springs so that the manipulator will be better behaved.

Differentiating (6.3.2) with respect to time yields

$$\dot{V} = \frac{1}{2}\frac{d}{dt}\left[\dot{q}^T M(q)\dot{q}\right] + e^T K_p \dot{e}. \tag{6.3.3}$$

Substituting (6.3.1) into (6.3.3), we have

$$\dot{V} = \dot{q}^T\left(\tau - G(q) - F(\dot{q}) - K_p e\right), \tag{6.3.4}$$

since we are solving the set-point control problem. Since it is desirable for $\dot{V}$ to be at least negative semidefinite, the control

$$\tau = G(q) + F(\dot{q}) + K_p e - K_v \dot{q} \tag{6.3.5}$$

is motivated by the form of (6.3.4). That is, substituting (6.3.5) into (6.3.4) yields

$$\dot{V} = -\dot{q}^T K_v \dot{q}. \tag{6.3.6}$$

The analysis above illustrates that V is decreasing for all time except for $\dot{q}$ equal to zero. We now use this information to illustrate that the desired set

point q_d is achieved. That is, if $\dot{V}=0$, then $\dot{q}=0$, and $\ddot{q}=0$; hence therefore, for $\dot{q}=\ddot{q}=0$, we can utilize (6.2.1) and (6.3.5) to write the closed-loop system in the form $K_p e=0$, which implies that $e=0$. From Chapter 1, LaSalle's Theorem can now be used to show that the tracking error e is asymptotically stable.

Adaptive Inertia-Related Controller

Although the controller given in (6.3.5) utilizes the conservation of energy property, it has two disadvantages. First, the controller merely ensures that the manipulator reaches a desired set point. In general, a robot control designer must ensure that the manipulator tracks a desired time-varying trajectory. Second, the controller requires exact knowledge of any parameters associated with the robot manipulator model since the gravity and friction terms are included in the control law (6.3.5).

In [Slotine and Li 1985 (a)] the conservation of energy formulation given in (6.3.1) is exploited to design an adaptive controller for the trajectory- following problem. This controller can be motivated in much the same way as our treatment of the PD plus gravity controller. In other words, we use the stability analysis to guide us in finding an adaptive controller. Since we are designing an adaptive trajectory-following controller, we should select a Lyapunov function that is a function of the tracking error and the parameter error. Slotine selected the inertia-related Lyapunov-like function

$$V = \tfrac{1}{2} r^T M(q)^r + \tfrac{1}{2}\tilde{\varphi}^T \Gamma^{-1}\tilde{\varphi}, \tag{6.3.7}$$

where

$$r = \Lambda e + \dot{e}, \tag{6.3.8}$$

with □ defined as in (6.2.11), □ defined as positive-definite, diagonal matrix such that

$$\Lambda = \operatorname{diag}(\lambda_1, \lambda_2, \ldots, \lambda_n),$$

and $\tilde{\varphi}$ defined as in (6.2.9). The auxiliary signal *r(t)* given in (6.3.8) may be considered as a filtered tracking error.

After differentiating (6.3.7) with respect to time, we have

(6.3.9) $$\dot{V} = r^T M(q)\dot{r} + \tfrac{1}{2} r^T \dot{M}(q) r + \tilde{\varphi}^T \Gamma^{-1}\dot{\tilde{\varphi}}.$$

From (6.3.9) it is clear that we must substitute for the variable ; therefore, we must write the robot equation in terms of the variable *r*. Using (6.2.1), the robot dynamics can be rewritten as

$$M(q)\dot{r} = Y(\cdot)\varphi - \tau - V_m(q,\dot{q})r, \tag{6.3.10}$$

where

$$Y(\cdot)\varphi = M(q)(\ddot{q}_d + \Lambda\dot{e}) + V_m(q,\dot{q})(\dot{q}_d + \Lambda e) + G(q) + F(\dot{q}), \tag{6.3.11}$$

and $Y(\cdot)$ is an $n \times r$ matrix of known time functions. This is the same type of parametric separation that was used in the formulation of the adaptive computed-torque controller; however, note that $Y(\cdot)$ is not a function of joint acceleration $\ddot{q}$!

Substituting (6.3.10) into (6.3.9) gives

$$\dot{V} = r^T(Y(\cdot)\varphi - \tau) + r^T\left(\tfrac{1}{2}\dot{M}(q) - V_m(q,\dot{q})\right)r + \tilde{\varphi}^T\Gamma^{-1}\dot{\tilde{\varphi}}. \tag{6.3.12}$$

Applying the skew-symmetric property (see Chapter 2), we can write (6.3.12) as

$$\dot{V} = r^T(Y(\cdot)\varphi - \tau) + \tilde{\varphi}^T\Gamma^{-1}\dot{\tilde{\varphi}}. \tag{6.3.13}$$

Again, the stability analysis has guided us to a choice of torque controller and adaptive update rule. That is, if we select the torque control to be

$$\tau = Y(\cdot)\hat{\varphi} + K_v r, \tag{6.3.14}$$

(6.3.13) becomes

$$\dot{V} = -r^T K_v r + \tilde{\varphi}^T\left(\Gamma^{-1}\dot{\tilde{\varphi}} + Y^T(\cdot)r\right). \tag{6.3.15}$$

By selecting the adaptive update rule as

$$\dot{\hat{\varphi}} = -\dot{\tilde{\varphi}} = \Gamma Y^T(\cdot)r, \tag{6.3.16}$$

(6.3.15) becomes

$$\dot{V} = -r^T K_v r. \tag{6.3.17}$$

We now detail the type of stability for the tracking error. First, since $\dot{V}$ in (6.3.17) is negative semidefinite, we can state that V in (6.3.7) is upper bounded. Using the facts that V is upper bounded and that $M(q)$ is a positive-definite matrix (see Chapter 2), we can state that r and $\tilde{\varphi}$ are bounded. From the definition of r given in (6.3.8), we can use standard linear control arguments to state that e and $\dot{e}$ (and hence q and $\dot{q}$) are bounded. Since e, $\dot{e}$, r, and are bounded, we can use (6.3.10) and (6.3.14) to show that $\dot{r}$ (and hence $\dot{\varphi}$ $\dot{V}$

obtained by differentiating (6.3.17)) is bounded. Second, note that since $M(q)$ is lower bounded, we can state that V given in (6.3.7) is lower bounded. Since $\dot{V}$ is lower bounded, V is negative semidefinite, and $\dot{V}$ is bounded, we can use Barbalat's lemma (see Chapter 1) to state that

$$\lim_{t\to\infty} \dot{V} = 0, \tag{6.3.18}$$

which means that by the Rayleigh-Ritz Theorem (see Chapter 1)

$$\lim_{t\to\infty} \lambda_{\min}\{K_v\}\|r\|^2 = 0 \quad \text{or} \quad \lim_{t\to\infty} r = 0. \tag{6.3.19}$$

Note that (6.3.8) is a stable first-order differential equation driven by the "input" r; therefore, by standard linear control arguments and (6.3.19), we can write

$$\lim_{t\to\infty} e = 0 \quad \text{and} \quad \lim_{t\to\infty} \dot{e} = 0. \tag{6.3.20}$$

This result informs us that the tracking errors e and $\dot{e}$ are asymptotically stable. Again, from the analysis above, all we can say about the parameter error is that it remains bounded. Later, we will show that the parameter error also converges to zero under certain conditions on the desired trajectory. The adaptive controller derived above is summarized in Table 6.3.1 and depicted in Figure 6.3.1.

After glancing through Table 6.3.1, we can see that the restrictions with regard to the adaptive computed-torque controller have been removed. Specifically, for the adaptive inertia-related controller, we do not require measurements of acceleration or any ad hoc adjustment of the parameter estimates to ensure $\hat{M}^{-1}(q)$ that exists.

We now present an example to illustrate how Table 6.3.1 can be used to design adaptive controllers for robotic manipulators.

EXAMPLE 6.3–1: Adaptive Inertia-Related Controller

We wish to design and simulate the adaptive inertia-related controller given in Table 6.3.1 for the two-link arm given in Figure 6.2.1. Assuming that the friction is negligible and the link lengths are exactly known, the adaptive inertia-related torque controller can be written as

$$\tau_1 = Y_{11}\hat{m}_1 + Y_{12}\hat{m}_2 + k_{v1}\dot{e}_1 + k_{v1}\lambda_1 e_1 \tag{1}$$

and

Table 6.3.1: Adaptive Inertia-Related Controller

Torque Controller:

$$\tau = Y(\cdot)\hat{\varphi} + K_v\dot{e} + K_v\Lambda e$$

Update Rule:

$$\dot{\hat{\varphi}} = \Gamma Y^T(\cdot)(\Lambda e + \dot{e})$$

where

$$Y(\cdot)\hat{\varphi} = \hat{M}(q)(\ddot{q}_d + \Lambda\dot{e}) + \hat{V}_m(q,\dot{q})(\dot{q}_d + \Lambda e) + \hat{G}(q) + \hat{F}(\dot{q})$$

Stability:

Tracking error e and $\dot{e}$ are asymptotically stable. Parameter estimate $\hat{\varphi}$ is bounded.

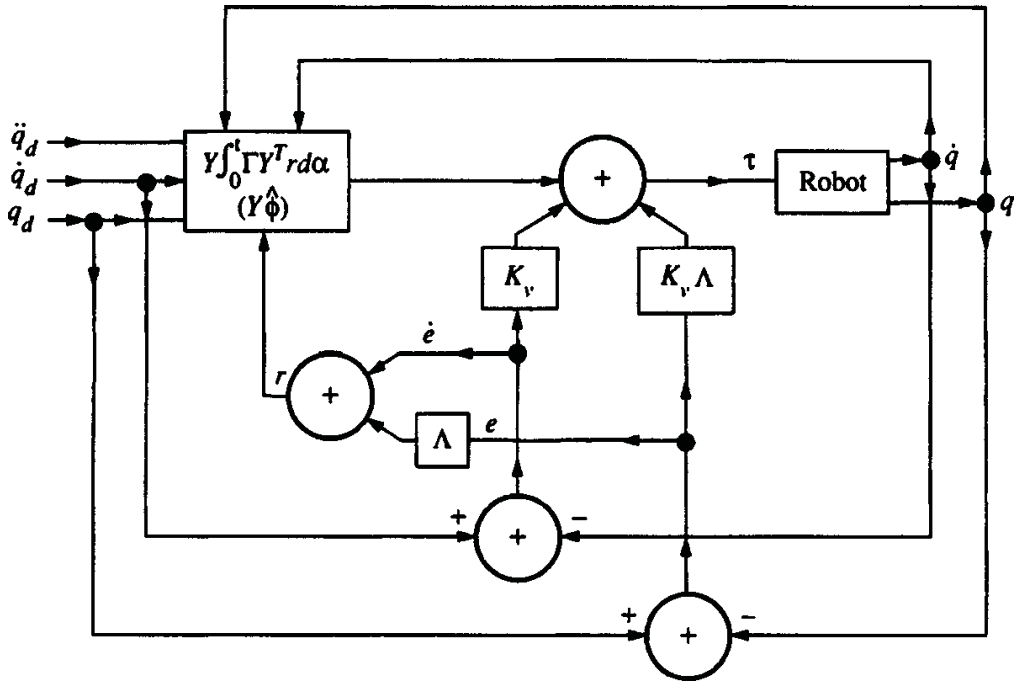


Figure 6.3.1: Block diagram of the adaptive inertia-related controller.

(2) $$\tau = Y(\cdot)\hat{\varphi} + K_v\dot{e} + K_v\Lambda e$$

In the expression for the control torques, the regression matrix $Y(\cdot)$ is given by

$$Y(\ddot{q}_d, \dot{q}_d, q_d, q, \dot{q}) = \begin{bmatrix} Y_{11} & Y_{12} \\ Y_{21} & Y_{22} \end{bmatrix}, \tag{3}$$

where

$$Y_{11} = l_1^2(\ddot{q}_{d1} + \lambda_1 \dot{e}_1) + l_1 g c_1, \tag{4}$$

$$\begin{aligned} Y_{12} = {} & (l_2^2 + 2l_1 l_2 c_2 + l_1^2)(\ddot{q}_{d1} + \lambda_1 \dot{e}_1) \\ & + (l_2^2 + l_1 l_2 c_2)(\ddot{q}_{d2} + \lambda_2 \dot{e}_2) - l_1 l_2 s_2 \dot{q}_2 (\dot{q}_{d1} + \lambda_1 e_1) \\ & - l_1 l_2 s_2 (\dot{q}_1 + \dot{q}_2)(\dot{q}_{d2} + \lambda_2 e_2) + l_2 g c_{12} + l_1 g c_1, \end{aligned} \tag{5}$$

$$Y_{21} = 0, \tag{6}$$

and

$$\begin{aligned} Y_{22} = {} & (l_1 l_2 c_2 + l_2^2)(\ddot{q}_{d1} + \lambda_1 \dot{e}_1) + l_2^2 (\ddot{q}_{d2} + \lambda_2 \dot{e}_2) \\ & - l_1 l_2 s_2 \dot{q}_1 (\dot{q}_{d1} + \lambda_1 e_1) + l_2 g c_{12}. \end{aligned}$$

Formulating the adaptive update rule as given in Table 6.3.1, the associated parameter estimate vector is

$$\hat{\varphi} = \begin{bmatrix} \hat{m}_1 \\ \hat{m}_2 \end{bmatrix}$$

with the adaptive update rules

$$\dot{\hat{m}}_1 = \gamma_1 [Y_{11}(\lambda_1 e_1 + \dot{e}_1) + Y_{21}(\lambda_2 e_2 + \dot{e}_2)] \tag{8}$$

and

$$\dot{\hat{m}}_2 = \gamma_2 [Y_{12}(\lambda_1 e_1 + \dot{e}_1) + Y_{22}(\lambda_2 e_2 + \dot{e}_2)]. \tag{9}$$

For m_1=0.8 kg and m_2=2.3 kg, the adaptive inertia-related controller was simulated with k_{V1}=k_{V2}=10, □1=□2=2.5, □1=□2=20, $\hat{m}_1(0)$=0, $\hat{m}_2(0)$=0, and with

the same desired trajectory and initial joint conditions as given in Example 6.2.1. The tracking error and mass estimates are depicted in Figure 6.3.2. As illustrated by the figure, the tracking error is asymptotically stable, and the parameter estimates remain bounded.

■

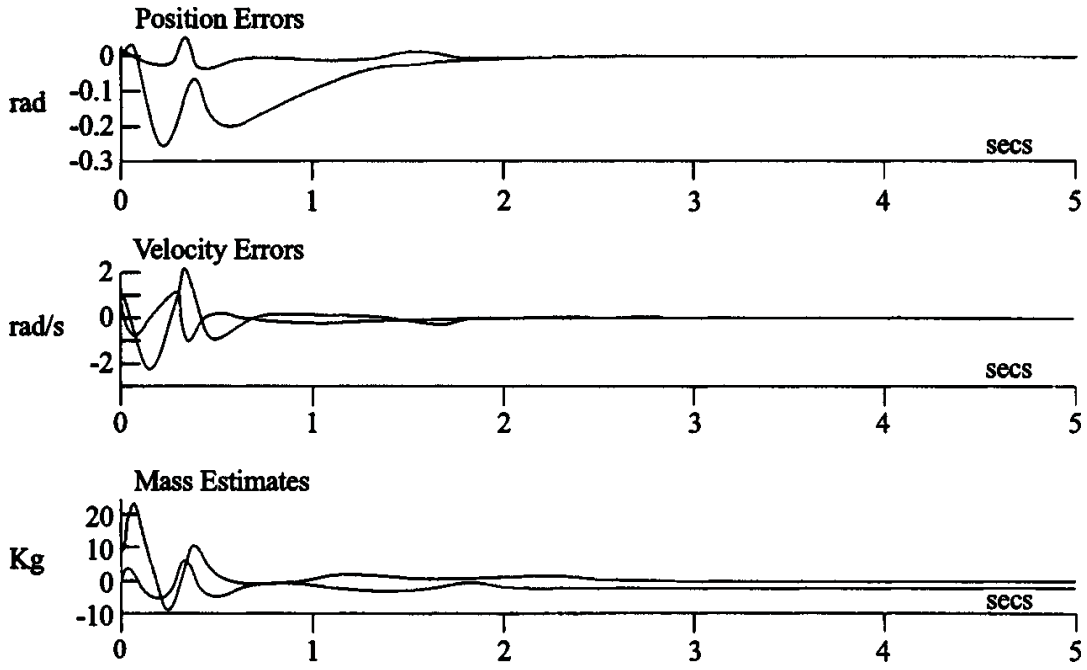


Figure 6.3.2: Simulation of the adaptive inertia-related controller.

6.4 Adaptive Controllers Based on Passivity

In recent years, many authors have developed adaptive control schemes that are different with regard to the torque control law or the adaptive update rule. To unify some of the approaches, general adaptive control strategies have been developed based on the passivity approach (see [Ortega and Spong 1988] and [Brogliato et al. 1990]). In this section we illustrate how the passivity approach can be used to develop a class of torque control laws and adaptive update rules for the control of robot manipulators.

Passive Adaptive Controller

First, we define an auxiliary filtered tracking error variable that is similar to that defined for the adaptive inertia-related controller. That is, we define

our tracking variable to be

$$r(s) = H^{-1}(s)\, e(s), \tag{6.4.1}$$

where

$$H^{-1}(s) = \left[sI_n + \frac{1}{s} K(s) \right] \tag{6.4.2}$$

and s is the Laplace transform variable. In (6.4.2), the $n \times n$ gain matrix $K(s)$ is chosen such that $H(s)$ is a strictly proper, stable transfer function matrix. The reason for this restriction on $H(s)$ will be clear after we analyze the stability of the adaptive controller that is presented later in this section.

As in the preceding sections, our adaptive control strategies have been centered around the ability to separate the known time functions from the unknown constant parameters. Therefore, we use the expressions given in (6.4.1) and (6.4.2) to define

$$\begin{aligned} Z(\cdot)\,\varphi = & M(q)\left(\ddot{q}_d + K(s)\, e\right) + V_m(q, \dot{q}) \left(\dot{q}_d + \frac{1}{s} K(s)\, e \right) \\ & + G(q) + F(\dot{q}), \end{aligned} \tag{6.4.3}$$

where in this control formulation, $Z(\cdot)$ is a known $n \times r$ regression matrix. [Note the standard abuse of notation in (6.4.3), where $K(s)e$ is used to represent the inverse Laplace transform of $K(s)$ convolved with $e(t)$.] It is important to note that $K(s)$ can be selected so that $Z(\cdot)$ and r do not depend on measurement of $\ddot{q}$. Indeed, if $K(s)$ is selected such that $H(s)$ has a relative degree of 1 [Kailath 1980], $Z(\cdot)$ and r will not depend on $\ddot{q}$.

The adaptive control formulation given in this section is called the *passivity approach* because the mapping of -r □ Z(·) $\tilde{\varphi}$ is constructed to be a passive mapping. That is, we construct an adaptive update rule such that

$$\int_0^t -r^T(\sigma)\, Z(\sigma)\, \tilde{\varphi}(\sigma)\, d\sigma \geq -\beta \tag{6.4.4}$$

is satisfied for all time and for some positive scalar constant ß. This passivity concept is used in analyzing the stability of the error system, as we shall show. However, for now let us illustrate the use of (6.4.4) in generating an adaptive update rule.

EXAMPLE 6.4–1: Adaptive Update Rule by Passivity

Let us show that the adaptive update rule

(1) $$\dot{\tilde{\varphi}} = -\dot{\hat{\varphi}} = -\Gamma Z^T(\cdot)\, r$$

satisfies the inequality given by (6.4.4). Note that G is defined as in (6.2.11).

First rewrite (1) in the form

(2) $$\dot{\tilde{\varphi}}^T \Gamma^{-1} = -r^T Z(\cdot),$$

where we have used the fact that G is a diagonal matrix. Substituting (2) into (6.4.4) gives

$$\int_0^t \dot{\tilde{\varphi}}^T(\sigma)\, \Gamma^{-1} \tilde{\varphi}(\sigma)\; d\sigma \geq -\beta. \tag{3}$$

Since □ is a constant matrix, we can use the product rule to rewrite (3) as

$$1/2 \int_0^t \frac{d}{d\sigma} \left(\tilde{\varphi}^T(\sigma)\, \Gamma^{-1} \tilde{\varphi}(\sigma) \right) d\sigma \geq -\beta \tag{4}$$

or

$$1/2 \tilde{\varphi}^T(t)\, \Gamma^{-1} \tilde{\varphi}(t) - 1/2 \tilde{\varphi}^T(0)\, \Gamma^{-1} \tilde{\varphi}(0) \geq -\beta. \tag{5}$$

From (5) it is now obvious that if ß is selected as

(6) $$\beta = 1/2 \tilde{\varphi}^T(0)\, \Gamma^{-1} \tilde{\varphi}(0),$$

then the passivity integral given in (6.4.4) is satisfied for the adaptive update rule given in (1).

■

Now that we have a feeling for how the passivity integral (6.4.4) can be used to generate adaptive update rules, we use the concept of passivity to analyze the stability of a class of adaptive controllers. For this class of adaptive controllers, the torque control is given by

(6.4.5) $$\tau = Z(\cdot)\, \hat{\varphi} + K_v r.$$

Note that many types of torque controllers can be generated from (6.4.5) by selecting different transfer function matrices for $K(s)$ in the definition of r. That is, for different $K(s)$, we have different types of feedback because the feedback term $K_V r$ will change accordingly.

To form the error system, rewrite the robot dynamics (6.2.1) in terms of the tracking error variable r and the regression matrix $Z(\cdot)$ as

$$M(q)\dot{r} = -\tau - V_m(q,\dot{q})\,r + Z(\cdot)\,\varphi. \tag{6.4.6}$$

Substituting (6.4.5) into (6.4.6) yields the tracking error system

$$M(q)\dot{r} = -K_v r - V_m(q,\dot{q})\,r + Z(\cdot)\,\hat{\varphi}. \tag{6.4.7}$$

For analyzing the stability of this system, we use the Lyapunov-like function

$$V = \tfrac{1}{2} r^T M(q)\,r + \beta - \int_0^t r^T(\sigma)\,Z(\sigma)\,\tilde{\varphi}(\sigma)\;d\sigma \tag{6.4.8}$$

[Ortega and Spong 1988]. Note that V is positive since the parameter estimate update rule is constructed to guarantee (6.4.4). That is, if (6.4.4) is satisfied, then

$$\beta - \int_0^t r^T(\sigma)\,Z(\sigma)\,\tilde{\varphi}(\sigma)\;d\sigma \geq 0; \tag{6.4.9}$$

therefore, V is a positive scalar function. Differentiating (6.4.8) with respect to time gives

$$\dot{V} = r^T M(q)\,\dot{r} + \tfrac{1}{2} r^T \dot{M}(q)\,r - r^T Z(\cdot)\,\hat{\varphi}. \tag{6.4.10}$$

Substituting (6.4.7) into (6.4.10) yields

$$\dot{V} = -r^T K_v r + r^T\left(\tfrac{1}{2}\dot{M}(q) - V_m(q,\dot{q})\right) r. \tag{6.4.11}$$

Utilizing the skew-symmetric property (see Chapter 2) allows one to write

$$\dot{V} = -r^T K_v r. \tag{6.4.12}$$

We now detail the type of stability for the tracking error. First note from (6.4.12) that we can place the new upper bound on $\dot{V}$:

$$\dot{V} \leq -\lambda_{\min}\{K_v\}\,\|r\|^2, \tag{6.4.13}$$

which can also be written as

$$\int_0^\infty \dot{V}(\sigma)\, d\sigma \leq -\lambda_{\min}\{K_v\} \int_0^\infty \|r(\sigma)\|^2 d\sigma. \tag{6.4.14}$$

Multiplying (6.4.14) by -1 and integrating the left-hand side of (6.4.14) yields

$$V(0) - V(\infty) \geq \lambda_{\min}\{K_v\} \int_0^\infty \|r(\sigma)\|^2 d\sigma. \tag{6.4.15}$$

Since $\dot{V}$ is negative semidefinite as delineated by (6.4.12), we can state that *V* is a nonincreasing function that is upper bounded by *V*(0). By recalling that *M(q)* is lower bounded, as delineated by the positive-definite property of the inertia matrix (see Chapter 2), we can state that *V* given in (6.4.8) is lower bounded by zero. Since *V* is nonincreasing, upper bounded by *V*(0), and lower bounded by zero, we can write (6.4.15) as

$$\lambda_{\min}\{K_v\} \int_0^\infty \|r(\sigma)\|^2 d\sigma < \infty \tag{6.4.16}$$

or

$$\sqrt{\int_0^\infty \|r(\sigma)\|^2 d\sigma} < \infty. \tag{6.4.17}$$

The bound delineated by (6.4.17) informs us that $r \in L_2^n$ (see Chapter 1), which means that the filtered tracking r is bounded in the "special" way given by (6.4.17).

To establish a stability result for the position tracking error *e,* we establish the transfer function relationship between the position tracking error and the filtered tracking error *r*. From (6.4.1) we can state that

$$e(s) = H(s)\, r(s), \tag{6.4.18}$$

where *H(s)* is as defined in (6.4.2). Since *H(s)* is a strictly proper, asymptotically stable transfer function matrix and $r \in L_2^n$, we can use Theorem 1.4.7 in Chapter 1 to state that

$$\lim_{t \to \infty} e = 0. \tag{6.4.19}$$

The result above informs us that the position tracking error is asymptotically stable. In accordance with the theoretical development above, all we can say about the velocity tracking error is that it is bounded.

The passivity-based controller is summarized in Table 6.4.1. From this table we can see that the passivity approach gives a general class of torque

control laws. We illustrate this concept with some examples that unify some of the research in adaptive control.

EXAMPLE 6.4–2: Passivity of the Adaptive Inertia-Related Controller

In this example we show how the adaptive inertia-related controller can be derived using passivity concepts. First, note that by defining

$$K(s) = \Lambda s \tag{1}$$

and

$$H(s) = (sI_n + \Lambda)^{-1} \tag{2}$$

in Table 6.4.1, we obtain the torque control law

$$\tau = Z(\cdot)\hat{\varphi} + K_v\dot{e} + K_v\Lambda e, \tag{3}$$

where

$$Z(\cdot)\hat{\varphi} = \hat{M}(q)(\ddot{q}_d + \Lambda\dot{e}) + \hat{V}_m(q,\dot{q})(\dot{q}_d + \Lambda e) + \hat{G}(q) + \hat{F}(\dot{q}). \tag{4}$$

This corresponds to the definition given in (6.3.11); therefore, using (2), we have obtained the adaptive inertia-related torque controller as given in Table 6.3.1.

The last item to check is whether the adaptive inertia-related update rule satisfies the passivity integral given in Table 6.4.1. From Table 6.3.1 the adaptive inertia-related update rule can be written as

$$\dot{\tilde{\varphi}} = -\Gamma Z^T(\cdot)(\dot{e} + \Lambda e) = -\dot{\hat{\varphi}} \tag{5}$$

for the choice of *K(s)* given in (1). After reexamining Example 6.4.1 it is now obvious that we have derived the adaptive inertia-related controller with the passivity approach.

■

Table 6.4.1: Passive Class of Adaptive Controllers

Torque Controller:

$$\tau = Z(\cdot)\hat{\varphi} + K_v r$$

where

$$Z(\cdot)\hat{\varphi} = \hat{M}(q)\left(\ddot{q}_d + K(s)e\right) + \hat{V}_m(q,\dot{q})\left(\dot{q}_d + \tfrac{1}{s}K(s)e\right) + \hat{G}(q) + \hat{F}(\dot{q}),$$

$$r(s) = H^{-1}(s)e(s), \quad H^{-1}(s) = \left[sI_n + \tfrac{1}{s}K(s)\right],$$

and the gain matrix $K(s)$ is chosen such that $H(s)$ is a strictly proper, stable transfer function matrix with relative degree 1.

Update Rule Must Satisfy:

$$\int_0^t -r^T(\sigma)Z(\sigma)\tilde{\varphi}(\sigma)\,d\sigma \geq -\beta$$

Stability:

Position tracking error e is asymptotically stable.

EXAMPLE 6.4-3: PID Torque Control Law

In Example 6.4.2 the torque control law was shown to be

(1) $$\tau = Z(\cdot)\hat{\varphi} + K_v\dot{e} + K_v\Lambda e.$$

This torque controller is a proportional-derivative (PD) feedback controller since we are using *e* and in the feedback portion of the control. It is now desired to find the choice of *K(s)* in Table 6.4.1 to give a proportional-integral- derivative (PID) type of torque controller of the form

$$\tau = Z(\cdot)\hat{\varphi} + K_v\dot{e} + K_p e + K_I\int e\,dt. \qquad (2)$$

Using Table 6.4.1, we can select

(3) $$K(s) = \Lambda s + \Psi,$$

where

$$\Lambda = \text{diag } \{\lambda_1, \lambda_2, \ldots, \lambda_r\},$$
$$\Psi = \text{diag } \{\Psi_1, \Psi_2, \ldots, \Psi_r\},$$

h_i's are positive scalar constants, $\dagger_i$'s are positive scalar constants, $K_P = K_V K$, and $K_I = K_V T$. Now we must check to verify that *H(s)* is indeed a strictly proper, stable transfer function matrix. For this choice of *K(s)* in Table 6.4.1, we can write

(4) $$H(s) = \left(sI_n + \Lambda + \frac{1}{s}\Psi \right)^{-1}.$$

Note that since K and T have been selected to be diagonal positive-definite matrices, *H(s)* is a decoupled transfer function matrix. That is, the transfer function for the *i*th system is

$$h_i(s) = \frac{s}{s^2 + \lambda_i s + \Psi_i}. \tag{5}$$

Since the h_i's and $\dagger$'s are positive, *H(s)* is a strictly proper, stable transfer function matrix.

■

General Adaptive Update Rule

As mentioned earlier, the adaptive control scheme outlined in Table 6.4.1 allows one to formulate different adaptive update laws by ensuring that the proposed update satisfies the passivity integral given in (6.4.4). Landau proposed the general update rule (which satisfies the passivity integral)

$$\hat{\varphi} = \int_0^t F_I(t-\sigma) Z^T(\sigma) r(\sigma) \, d\sigma + F_p Z^T(\cdot) r, \tag{6.4.20}$$

where F_P is an $r \times r$ positive definite, constant matrix, and $F_I(t)$ is an $r \times r$ positive definite matrix kernel whose Laplace transform is a positive real transfer function matrix with a pole at $s=0$ [Landau 1979].

By utilizing this general update law, many types of adaptation may be designed. All we need to keep in mind is that the conditions on $F_I(t)$ and F_P must be met. One possible adaptive scheme that comes directly from (6.4.20) is the proportional + integral (PI) adaptation scheme. The PI update law is the same as that given by (6.4.20), with

$$\Gamma(t)=K_1, \tag{6.4.21}$$

where K_1 is a diagonal, constant positive-definite matrix. It has been pointed out in [Landau 1979] that with regard to adaptive model following, PI adaptation has shown a significant improvement over integral adaptation. Therefore, this type of adaptation might be beneficial for the tracking control of robot manipulators.

6.5 Persistency of Excitation

For the adaptive controllers presented in the previous sections the tracking error has been shown to be asymptotically stable; however, all that could be said about the parameter error was that it was bounded. In general, parameter identification will occur in adaptive control systems only if certain conditions on the regression matrix can be established. Specifically, several researchers [Morgan and Narendra 1977], [Anderson 1977] have studied the asymptotic stability of adaptive control systems similar to the ones we have presented in this chapter. For example, parameter error convergence can be established for the adaptive inertia-related controller if the regression matrix $Y(\cdot)$ satisfies

$$aI_r \leq \int_{t_0}^{t_0+\rho} Y^T(q,\dot{q},q_d,\dot{q}_d,\ddot{q}_d)\, Y(q,\dot{q},q_d,\dot{q}_d,\ddot{q}_d)\, dt \leq \beta I_r \tag{6.5.1}$$

for all t_0, where □, ß, and □ are all positive scalars. Furthermore, since the tracking error is asymptotically stable, we can rewrite (6.5.1) as

$$aI_r \leq \int_{t_0}^{t_0+\rho} Y^T(q_d,\dot{q}_d,\ddot{q}_d)\, Y(q_d,\dot{q}_d,\ddot{q}_d)\, dt \leq \beta I_r, \tag{6.5.2}$$

where the arguments q and q have been replaced by q_d and $\dot{q}_d$, respectively. The condition given in (6.5.2) informs us that if $Y(\cdot)$ varies sufficiently over the interval given by □ so that the entire r-dimensional parameter space is spanned, we know the parameter error converges to zero. This amounts to a condition on the desired trajectory such that all parameters will be identified after a sufficient learning interval. This condition can be helpful in formulating desired trajectories to ensure that parameters such as friction coefficients or payload masses are identified. We now illustrate the meaning of a persistently exciting trajectory with some examples.

EXAMPLE 6.5–1: Lack of Persistency of Excitation for a One-Link Robot Arm

We wish to investigate the persistency of excitation conditions for the one-link robot arm given in Figure 6.5.1. The dynamics of this robot arm will be taken to be

(1) $$\tau = m\ddot{q} + b\dot{q},$$

$$\tau = m\ddot{q} + b\dot{q},$$

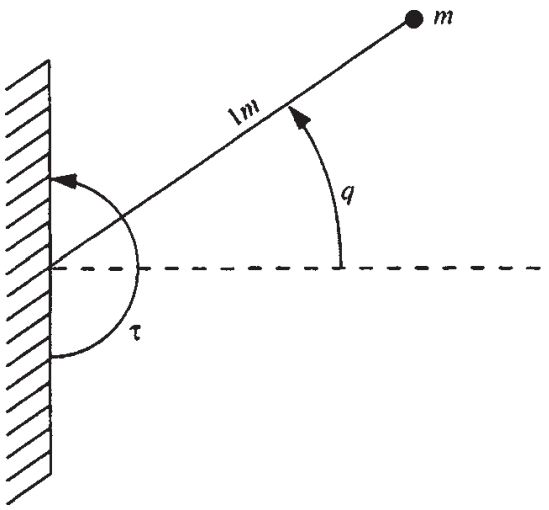


Figure 6.5.1: One-link revolute arm.

where the term *b* is used to denote the positive scalar representing the dynamic coefficient of friction. We assume that this robot arm is in the plane not affected by the gravitational force and that *m* and *b* are unknown positive constants.

a. Adaptive Controller

By using Table 6.3.1, the adaptive inertia-related controller for the dynamics (1) can be shown to be given by

(2) $$\tau = Y_{11}\hat{m} + Y_{12}\hat{b} + k_v\dot{e} + k_v\lambda e.$$

In the expression above for the control torque, the regression matrix $Y(\cdot)$ is given by

$$Y(q_d, \dot{q}_d, \ddot{q}_d, q, \dot{q}) = \begin{bmatrix} Y_{11} & Y_{12} \end{bmatrix} \tag{3}$$

where

$$Y_{11} = (\ddot{q}_d + \lambda \dot{e}) \quad \text{and} \quad Y_{12} = \dot{q}.$$

The corresponding parameter estimate vector is given by

$$\hat{\varphi} = \begin{bmatrix} \hat{m} \\ \hat{b} \end{bmatrix}.$$

We can formulate the adaptive update rule given in Table 6.3.1 as

$$\dot{\hat{m}} = \gamma_1 Y_{11} (\lambda e + \dot{e}) \tag{4}$$

and

$$\dot{\hat{b}} = \gamma_2 Y_{12} (\lambda e + \dot{e}). \tag{5}$$

b. Persistency of Excitation

With this adaptive controller it is desired to show analytically that $q_d = 1 - e^{-2t}$ is not persistently exciting. From (6.5.2), the integrand of the persistently exciting condition for this example is given by

$$Y^T(q_d, \dot{q}_d, \ddot{q}_d) Y(q_d, \dot{q}_d, \ddot{q}_d) = \begin{bmatrix} \ddot{q}_d^2 & \dot{q}_d \ddot{q}_d \\ \dot{q}_d \ddot{q}_d & \dot{q}_d^2 \end{bmatrix}$$

or

$$Y^T(\cdot) Y(\cdot) = \begin{bmatrix} 16e^{-4t} & -8e^{-4t} \\ -8e^{-4t} & 4e^{-4t} \end{bmatrix}. \tag{6}$$

Multiplying the first column of $Y^T(\cdot)Y(\cdot)$ by $\frac{1}{2}$ and adding it to the second column of $Y^T(\cdot)Y(\cdot)$ gives

$$R_{YY} = \begin{bmatrix} 16e^{-4t} & 0 \\ -8e^{-4t} & 0 \end{bmatrix}. \tag{7}$$

Since the matrix R_{YY} has the same range space as the matrix $Y^T(\cdot)Y(\cdot)$, we can see from (7) that the range space of the matrix $Y^T(\cdot)Y(\cdot)$ will always be one-dimensional; therefore, the persistent excitation condition does not hold for

$q_d=1-e^{-2t}$.

■

EXAMPLE 6.5–2: Persistency of Excitation for a One-Link Arm

a. Desired Trajectory with Single Frequency

With the adaptive controller in Example 6.5.1, we would like to show by simulation that $q_d=\sin t$ is not persistently exciting. For m=1 kg and b=1 N-m- s, the adaptive inertia-related controller was simulated with

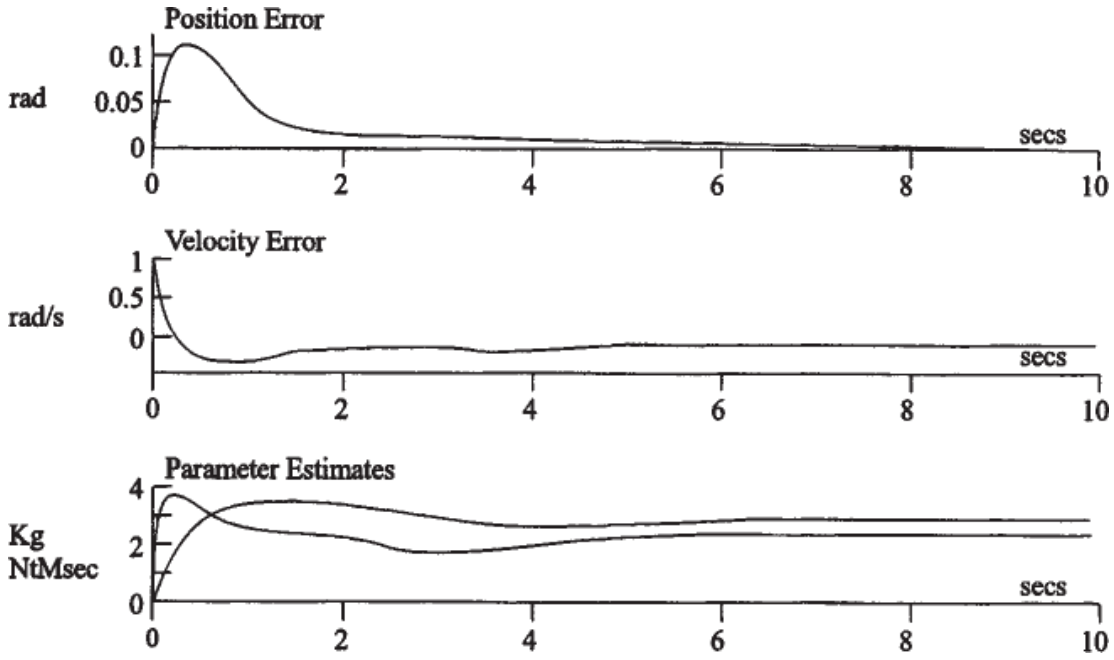


Figure 6.5.2: Lack of persistency of excitation.

$$k_v = 10, \quad \lambda = 2.5, \quad \gamma_1 = \gamma_2 = 20, \tag{1}$$

with initial conditions of

$$q(0) = \dot{q}(0) = \hat{m}_1(0) = \hat{m}_2(0) = 0. \tag{2}$$

The tracking error and the parameter estimates are depicted in Figure 6.5.2. As anticipated, the tracking error is asymptotically stable, and the parameter estimates remain bounded. Note that $\tilde{b}$ and $\hat{m}$ do not go to zero since the desired trajectory is not persistently exciting.

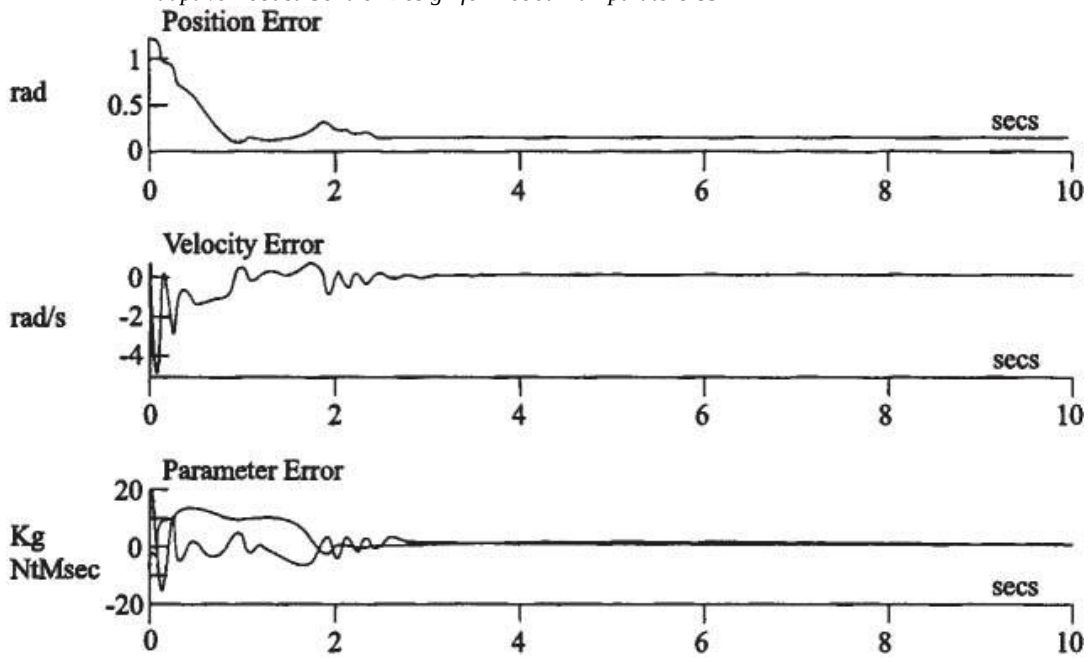


Figure 6.5.3: Persistency of excitation.

b. Desired Trajectory with Multiple Frequencies

With the adaptive controller in Example 6.5.1, we desire to show by simulation that q_d=sin t+cos 3t is persistently exciting. The adaptive controller given in Example 6.5.1 should be simulated under the same conditions as those given in part (a) of this example except for the change in the desired trajectory. The tracking error and the parameter error are depicted in Figure 6.5.3. As illustrated by the figure, the tracking error is asymptotically stable, and the parameter estimates remain bounded. Note that $\tilde{b}$ and converge to the exact values of b and m, respectively. This is because the desired trajectory is persistently exciting. $\hat{m}$

■

6.6 Composite Adaptive Controller

In both the adaptive computed-torque and the adaptive inertia-related control strategies, we have shown that the tracking error is asymptotically stable and the parameter error is bounded. It was then illustrated that if a persistency of excitation condition holds, the parameter error $\tilde{\varphi}$ converges to zero. In some robotic applications it may not be practical to utilize a persistently exciting

trajectory; therefore, we are motivated to redesign the adaptive control strategy to achieve parameter identification.

In this section we show how the adaptive controller given in Section 6.3 can be modified to ensure asymptotic convergence of both the tracking error and the parameter error [Slotine and Li 1985(b)]. The asymptotic convergence of the parameter error is shown to hold if a condition on the filtered regression matrix holds. This condition, often called the *infinite integral condition,* is less restrictive than the persistency of excitation condition.

The procedure for designing the new adaptive controller can be out-lined as follows. First, a filtered regression matrix is formed from torque measurements. Second, it is shown how this filtered regression matrix can be used to formulate a least-squares estimator for estimating the unknown parameters. Finally, the adaptive update rule in Table 6.3.1 is modified to include an additional least-squares estimator term.

Torque Filtering

We now show how the regression matrix that is formed from a torque measurement can be filtered to eliminate the need for acceleration measurements. From Section 6.2 we can write the robot Equation (6.2.1) in the following form:

$$\tau = M(q)\ddot{q} + V_m(q,\dot{q})\dot{q} + G(q) + F(\dot{q}) = W(q,\dot{q},\ddot{q})\varphi. \tag{6.6.1}$$

The middle expression in (6.6.1) is written in the form

$$\tau = \dot{h} + g, \tag{6.6.2}$$

where

$$(6\dot{h} = \frac{d}{dt}(M(q)\dot{q})$$

and

$$g = -\dot{M}(q)\dot{q} + V_m(q,\dot{q})\dot{q} + G(q) + F(\dot{q}). \tag{6.6.4}$$

The reason for writing the robot equation in the form given by (6.6.2) is that this equation has now been separated in a way that allows $\ddot{q}$ to be filtered out or removed. That is, by filtering (6.6.2), we have

$$\tau_f = f * \tau = f * \dot{h} + f * g, \tag{6.6.5}$$

where *f* is the impulse response of a linear stable, strictly proper filter, and the * is used to denote the convolution operation. For example, we could use the first-order filter given by

$$f(s) = \frac{a}{s+a}, \tag{6.6.6}$$

where *a* is a positive scalar constant. By using the property of convolution

$$f * \dot{h} = \dot{f} * h + f(0)\, h - f h(0), \tag{6.6.7}$$

we can rewrite (6.6.5) as

$$\tau_f = f * \tau = \dot{f} * h + f(0)\, h - f h(0) + f * g. \tag{6.6.8}$$

After substituting the expressions for *h* and *g,* note that $\ddot{q}$ has been filtered out. That is, the explicit expression for if is given by

$$\begin{aligned} \tau_f =& \dot{f} * (M(q)\dot{q}) + f(0)\, M(q)\dot{q} - f M(q(0))\dot{q}(0) \\ &+ f * \left(-\dot{M}(q)\dot{q} + V_m(q,\dot{q})\dot{q} + G(q) + F(\dot{q})\right), \end{aligned} \tag{6.6.9}$$

where $\dot{f}$ is the impulse response of a proper, stable filter; for example,

$$sf(s) = \frac{as}{s+a}. \tag{6.6.10}$$

By linearity, the unknown parameters can still be separated out with regard to (6.6.9). That is, (6.6.9) can be rewritten as

$$\tau_f = W_f(q,\dot{q})\,\varphi, \tag{6.6.11}$$

where $W_f(\cdot)$ is an $n \times r$ filtered regression matrix, and φ is an $r \times 1$ vector of unknown parameters. We now use an example to show how torque filtering can be used to eliminate the need for acceleration measurements.

EXAMPLE 6.6–1: Torque Filtering of a One-Link Robot Arm

Using the dynamics of the one-link robot arm given in Example 6.5.1, it is desired to find the filter regression matrix $W_f(q, \dot{q})$ given in (6.6.11), where the linear filter is given by

$$f(s) = \frac{1}{s+1}, \tag{1}$$

or, in the time domain,

$$f(t)=e^{-t}. \tag{2}$$

Using (6.6.9), the filtered torque expression for the one-link arm is given by

$$\tau_f = \dot{f} * m\dot{q} + m\dot{q} - fm\dot{q}(0) + f * b\dot{q}, \tag{3}$$

where

$$\dot{f}(s) = \frac{s}{s+1}. \tag{4}$$

The expression in (3) is used to separate the known functions from the unknown constants into the form

$$\tau_f = W_f(q,\dot{q})\,\varphi, \tag{5}$$

where the filtered regression matrix and parameter vector are given by

$$W_f(q,\dot{q}) = \left[\left(\dot{f} * \dot{q}\right) + \dot{q} - f\dot{q}(0) \quad \dot{f} * \dot{q}\right] \tag{6}$$

and

$$\varphi = \begin{bmatrix} m & b \end{bmatrix}^T. \tag{7}$$

■

The important concept to realize in the regression matrix formulation given by (6.6.11) is that the quantities τ_f and $W_f(q, \dot{q})$ are known or assumed to be measurable; however, φ is unknown. To estimate φ, we define the estimate of the filtered torque based on the estimate of the unknown parameters, that is,

$$\hat{\tau}_f = W_f(\cdot)\,\hat{\varphi}. \tag{6.6.12}$$

We can now define the measurable quantity

$$\tilde{\tau}_f = W_f(\cdot)\,\tilde{\varphi}, \tag{6.6.13}$$

where

$$\tilde{\tau}_f = \tau_f - \hat{\tau}_f. \tag{6.6.14}$$

The use of $\tilde{\tau}_f$ is crucial in the development of the least-squares estimator that is developed in the next section. We can easily see how τ_f is measurable by writing (6.6.14) in the form

$$\tilde{\tau}_f = \tau_f - W_f(\cdot)\hat{\varphi}. \tag{6.6.15}$$

As explained earlier, $\tilde{\tau}_f$ and $W_f(\cdot)$ are assumed to be known or measurable; therefore, all we need is the parameter estimate term [i.e., $\hat{\varphi}$ in (6.6.15)] for τ_f to be known. Later, we generate an adaptive update rule that will give us the parameter estimate term $\hat{\varphi}$ in (6.6.15). So for now we will assume that τ_f is known.

Least-Squares Estimation

Least-squares estimation methods have been used in many types of parameter identification schemes [Astrom and Wittenmark 1989]. It turns out that this type of estimation method extracts the maximum amount of parametric information even when the desired trajectory is not persistently exciting. This is an important fact to realize when designating adaptive control systems for robot manipulators because in many robot applications, the persistency of excitation condition will not be valid. Therefore, least-squares estimation offers an attractive solution to the design of adaptive controllers for robot manipulators.

We now show how the least-squares estimation method can be used to generate an adaptive update rule. First, define the least-squares update rule

$$\dot{\hat{\varphi}} = PW_f^T(\cdot)\tilde{\tau}_f, \tag{6.6.16}$$

where

$$\dot{P} = -PW_f^T(\cdot)W_f(\cdot)P \tag{6.6.17}$$

and P is an $r \times r$ time-varying symmetric matrix.

With this least-squares estimation method, if an "infinite integral" condition holds, the parameter error converges to zero. Specifically, if

$$\lim_{t\to\infty} \lambda_{\min}\left\{\int_0^t W_f^T(\sigma)W_f(\sigma)\,d\sigma\right\} = \infty \tag{6.6.18}$$

holds, then

$$\lim_{t\to\infty} \tilde{\varphi} = 0. \tag{6.6.19}$$

As pointed out in [Slotine and Li 1985(b)], this infinite integral condition is a weaker condition than the persistency of excitation condition. That is, in practical robot applications, (6.6.18) can often be validated.

EXAMPLE 6.6–2: Least-Squares Estimator for a One-Link Robot Arm

Using the dynamics of the one-link robot arm given in Example 6.5.1, it is desired to find the least-squares estimator given by (6.6.16) and (6.6.17). Since the number of unknown parameters is two, define the matrix P to be

$$P = \begin{bmatrix} P_1 & P_2 \\ P_2 & P_3 \end{bmatrix}. \tag{1}$$

Utilizing the filtered regression matrix from Example 6.6.1, we have

$$W_f(q, \dot{q}) = \begin{bmatrix} W_{f11} & W_{f12} \end{bmatrix}, \tag{2}$$

where

$$W_{f11} = \left(\dot{f} * \dot{q}\right) + \dot{q} - f\dot{q}(0) \quad \text{and} \quad W_{f12} = \dot{f} * \dot{q}.$$

Using (6.6.17), it is easy to see that the matrix P should be updated in the following manner:

$$\dot{P}_1 = -\left(W_{f11}P_1 + W_{f12}P_2\right)^2 \tag{3}$$

$$\dot{P}_2 = -W_{f11}^2 P_1 P_2 - W_{f12}^2 P_2 P_3 - W_{f11}W_{f12}\left(P_1 P_3 + P_2^2\right),$$

and

and

$$\dot{P}_3 = -\left(W_{f11}P_2 + W_{f12}P_3\right)^2.$$

Now using (6.6.16), the parameter update rules are

$$\dot{\hat{m}} = \left(P_1 W_{f11} + P_2 W_{f12}\right)\tilde{\tau}_f$$

(5)

(6)

$$\dot{\hat{b}} = (P_2 W_{f11} + P_3 W_{f12})\, \tilde{\tau}_f, \tag{7}$$

where, from (6.6.16), v_f is given by

$$\tilde{\tau}_f = \tau_f - W_{f11}\hat{m} - W_{f12}\hat{b}. \tag{8}$$

■

For insight into how the least-squares estimation method extracts parameter information, we now show how (6.6.18) is obtained. Utilizing (6.6.13) and the fact that the parameters are constant, we write (6.6.16) as

$$\dot{\tilde{\varphi}} = -PW_f^T(\cdot)\, W_f(\cdot)\, \tilde{\varphi}. \tag{6.6.20}$$

Using the matrix identity $\dot{P} = -P\dot{P}^{-1}P$ we can write (6.6.17) as

$$\dot{P}^{-1} = W_f^T(\cdot)\, W_f(\cdot). \tag{6.6.21}$$

Substituting (6.6.21) into (6.6.20) yields the differential equation

$$\dot{\tilde{\varphi}} = -P\dot{P}^{-1}\tilde{\varphi}. \tag{6.6.22}$$

We claim that

$$\tilde{\varphi} = -PP^{-1}(0)\, \tilde{\varphi}(0) \tag{6.6.23}$$

is the solution to (6.6.22). This fact can be verified by substituting (6.6.23) into the right-hand and left-hand sides of (6.6.22). That is, we obtain

$$-\dot{P}P^{-1}(0)\, \tilde{\varphi}(0) = P\dot{P}^{-1}PP^{-1}(0)\, \tilde{\varphi}(0); \tag{6.6.24}$$

therefore, (6.6.23) is the solution. Now from (6.6.21) it is easy to see that the solution for P is given by

$$P = \left\{ P^{-1}(0) + \int_0^t W_f^T(\sigma)\, W_f(\sigma)\, d\sigma \right\}^{-1}. \tag{6.6.25}$$

After examining (6.6.25), we can intuitively see that if the infinite integral condition is satisfied, then

$$\lim_{t\to\infty} \lambda_{\max}\{P\} = 0 \tag{6.6.26}$$

and

$$(6 \lim_{t\to\infty} \lambda_{\min}\{P^{-1}\} = \infty.$$

Now if (6.6.26) holds, we can see from (6.6.23) that the parameter error converges to zero. This proof is detailed in [Li and Slotine 1987].

Composite Adaptive Controller

The composite adaptive controller is the same as the controller given in Table 6.3.1, with the exception of a modification to the adaptive update rule. This modification is given by

$$\dot{\hat{\varphi}} = -\dot{\tilde{\varphi}} = PY^T(\cdot)\, r + PW_f^T(\cdot)\,\tilde{\tau}_f. \tag{6.6.28}$$

To prove that the tracking error and the parameter error both converge to zero, start with the Lyapunov-like function,

$$V = {}^1\!/_2 r^T M(q)\, r + {}^1\!/_2 \tilde{\varphi}^T P^{-1} \tilde{\varphi}. \tag{6.6.29}$$

Differentiating (6.6.29) with respect to time yields

$$\dot{V} = r^T M(q)\,\dot{r} + {}^1\!/_2 r^T \dot{M}(q)\, r + \tilde{\varphi}^T P^{-1} \dot{\tilde{\varphi}} + {}^1\!/_2 \tilde{\varphi}^T \dot{P}^{-1} \tilde{\varphi}. \tag{6.6.30}$$

From the control law given in Table 6.3.1 and the development in Section 6.3, we can form the tracking error system

$$M(q)\,\dot{r} = Y(\cdot)\,\tilde{\varphi} - K_v r - V_m(q, \dot{q})\, r. \tag{6.6.31}$$

Substituting (6.6.31) into (6.6.30) yields

$$\dot{V} = -r^T K_v r + \tilde{\varphi}^T \left(P^{-1} \dot{\tilde{\varphi}} + Y^T(\cdot)\, r \right) + {}^1\!/_2 \tilde{\varphi}^T \dot{P}^{-1} \tilde{\varphi}. \tag{6.6.32}$$

After substituting $\dot{\tilde{\varphi}}$ in (6.6.28), $\dot{P}^{-1}$ in (6.6.21), and $\tilde{\tau}_f$ in (6.6.13) into (6.6.32), we have

$$\dot{V} = -r^T K_v r - {}^1\!/_2 \tilde{\varphi}^T W_f^T(\cdot)\, W_f(\cdot)\, \tilde{\varphi}. \tag{6.6.33}$$

We now detail the type of stability for the tracking error and the parameter error. First, since $\dot{V}$ in (6.6.33) is at least negative semidefinite in the form

$$\dot{V} \leq -\lambda_{\min}\{K_v\}\, \|r\|^2, \tag{6.6.34}$$

we can state that V in (6.6.29) is bounded. Since V is bounded, $M(q)$ is a positive-definite matrix, and P^{-1} satisfies the condition given by (6.6.27), we can state that r and $\tilde{\varphi}$ are bounded. Furthermore, from the definition of r given in (6.3.8), we can use standard linear control arguments to state that e

and e (and $\dot{e}$ hence q and $\dot{q}$) are bounded. We can now use the same arguments presented in Section 6.4 to show that $r \in L_2^n$. Given that $r \in L_2^n$, we can determine a stability result for the position tracking error by establishing the transfer function relationship between the position tracking error and the filtered tracking error r. From (6.3.8), we can state that

$$e(s) = G(s)\, r(s), \tag{6.6.35}$$

where s is the Laplace transform variable,

(6.6.36)

I is the $n \times n$ identity matrix, and K is an $n \times n$ positive-definite matrix. Since $G(s)$ is a strictly proper, asymptotically stable transfer function and $r \in L_2^n$ we can use Theorem 1.4.7 in Chapter 1 to state that

$$\lim_{t \to \infty} e = 0. \tag{6.6.37}$$

Second, since $\dot{V}$ is at least negative semidefinite, we know that V must be nonincreasing, and hence $\dot{V}$ is upper bounded by $V(0)$. Furthermore, by the infinite integral assumption, we have concluded in (6.6.27) that

$$\lim_{t \to \infty} \lambda_{\min} \left\{ P^{-1} \right\} = \infty. \tag{6.6.38}$$

Since the term

(6.6.39) $$1/2 \tilde{\varphi}^T P^{-1} \tilde{\varphi}$$

in V given in (6.6.29) is upper bounded by $V(0)$, we can see that for (6.6.38) to hold, we must have

$$\lim_{t \to \infty} \tilde{\varphi} = 0.$$

Therefore, from the argument above, the position tracking error and the parameter error are asymptotically stable for the composite adaptive controller outlined in Table 6.6.1. In accordance with the theoretical development above, all we can say about the velocity tracking error is that it is bounded; however, Barbalat's lemma can be invoked to illustrate that the velocity tracking error is also asymptotically stable (see Problem 6.6–3). We now use an example to illustrate how the composite adaptive controller is formulated.

Table 6.6.1: Composite Adaptive Controller

Controller:

$$\tau = Y(\cdot)\hat{\varphi} + K_v\dot{e} + K_v\Lambda e$$

Update Rule:

$$\dot{\hat{\varphi}} = PY^T(\cdot)(\dot{e} + \Lambda e) + PW_f^T(\cdot)(f * \tau - W_f(\cdot)\hat{\varphi})$$

where

$$Y(\cdot)\hat{\varphi} = \hat{M}(q)(\ddot{q}_d + \Lambda\dot{e}) + \hat{V}_m(q,\dot{q})(\dot{q}_d + \Lambda e) + \hat{G}(q) + \hat{F}(\dot{q})$$

$$\dot{P} = -PW_f^T(\cdot)W_f(\cdot)P$$

$$W_f(\cdot)\hat{\varphi} = f * \left[\hat{M}(q)\ddot{q} + \hat{V}_m(q,\dot{q})\dot{q} + \hat{G}(q) + \hat{F}(\dot{q})\right]$$

f is the impulse response of a strictly proper stable filter.

Stability:

Tracking error e is asymptotically stable. Parameter error $\tilde{\varphi}$ is asymptotically stable if the infinite integral condition is satisfied.

EXAMPLE 6.6–3: Composite Adaptive Controller for a One-Link Robot Arm

It is desired to formulate the composite adaptive controller for the one-link robot arm given in Figure 6.5.1. The torque control law is the same as that given by Equation (2) in Example 6.5.1; therefore, all that need be done is the formulation of the composite adaptive update rule. From Table 6.6.1, the composite parameter update rules are

$$\dot{\hat{m}} = (P_1Y_{11} + P_2Y_{12})r + (P_1W_{f11} + P_2W_{f12})\tilde{\tau}_f \tag{1}$$

and

$$\dot{\hat{b}} = (P_2Y_{11} + P_3Y_{12})r + (P_2W_{f11} + P_3W_{f12})\tilde{\tau}_f, \tag{2}$$

where r is defined in (6.5.8), Y_{11}, Y_{12} are defined in Example 6.5.1, and P_1, P_2, P_3, W_{f11}, W_{f12}, f are defined in Example 6.6.2.

■

6.7 Robustness of AdaptiveControllers

All of the adaptive control schemes discussed ensure asymptotic tracking of a desired reference trajectory for the robot manipulator dynamics; however, in reality we know that there will always be disturbances in any electromechanical system. A simplistic way to take into account some sort of disturbance effect is to add a bounded disturbance term to the manipulator dynamic equation. With this additive disturbance term the robot equation becomes

$$\tau = M(q)\ddot{q} + V_m(q,\dot{q})\dot{q} + G(q) + F(\dot{q}) + T_d, \tag{6.7.1}$$

where T_d is an $n\times 1$ vector that represents an additive disturbance.

Applying the adaptive inertia-related control strategy and ignoring the term T_d in (6.7.1) gives the adaptive control scheme of Table 6.3.1. However, if we reexamine the stability analysis given in Section 6.3 for the adaptive inertia-related controller, we can see that a bounded disturbance term gives us a different type of stability result for the tracking error. Specifically, with the addition of the bounded disturbance term in (6.7.1), the derivative of the Lyapunov function in (6.3.7) becomes

$$\dot{V} = -r^T K_v r + r^T T_d. \tag{6.7.2}$$

From (6.7.2) it is obvious that $\dot{V}$ can no longer be taken to be negative semidefinite. From our previous experience with Lyapunov stability theory, it was desired to have $\dot{V}$ be "negative"; therefore, it stands to reason that it would be advantageous to find the region where $\dot{V}$ is negative in (6.7.2). By the use of the Rayleigh-Ritz Theorem (see Chapter 1), we can write (6.7.2) as

$$\dot{V} \le -\lambda_{\min}\{K_v\}\|r\|^2 + \|r\|\,\|T_d\|. \tag{6.7.3}$$

From (6.7.3), a sufficient condition on the negativity of $\dot{V}$ can be obtained. That is, $\dot{V}$ will be negative if

$$\|r\| > \frac{\|T_d\|}{\lambda_{\min}\{K_v\}}. \tag{6.7.4}$$

If (6.7.4) is satisfied, $\dot{V}$ is negative and V will decrease. If V decreases, then by our definition of the Lyapunov function given in (6.3.7), r must eventually decrease. However, if r decreases such that

(6.7.5) *Adaptive Robust Control Di* $\|r\| \leq \dfrac{\|T_d\|}{\lambda_{\min}\{K_v\}}$. *s* 903

then $\dot{V}$ may become positive, which means that V will start to increase. If V starts to increase, we gain insight into the problem by examining two possibilities. One, the increase in V causes r to increase such that (6.7.4) is satisfied. This means that V will start to decrease and hence r will eventually decrease. If r increased and decreased in this fashion continually, then r and $\tilde{\varphi}$ both remain bounded. The other possibility is that the increase in V causes $\tilde{\varphi}$ to increase while r stays small enough such that (6.7.5) is satisfied. For this case, V remains positive; therefore, $\tilde{\varphi}$ could continue to increase. If V continues to increase in this fashion, r is bounded; however, $\tilde{\varphi}$ and hence $\hat{\varphi}$ both become unbounded.

The argument above reveals that the parameter estimate in the adaptive inertia-related control law *may* go unstable in the presence of a bounded disturbance. That is, the parameter estimate may diverge under the assumption that the robot model is given by (6.7.1). If the parameter estimate becomes too large, we can see from Table 6.3.1 that the input torque will start to grow and possibly saturate the joint motors; therefore, it would be desirable to modify the adaptive controller to eliminate the possibility of torque saturation.

EXAMPLE 6.7–1: Effects of Disturbance on Adaptive Control

In this example we simulate the same adaptive controller given in Example 6.3.1 with the same control parameters, initial conditions, and desired trajectory; however, we have added the disturbance term

(1) $$T_d = \begin{bmatrix} 2\sin(10t) \\ 2\sin(10t) \end{bmatrix}$$

to the two-link manipulator dynamics. The tracking error and parameter estimates are illustrated in Figure 6.7.1. From the figure, note that for the disturbance given by (1), the parameter estimates do not become unbounded; however, the tracking error is no longer asymptotically stable.

■

Torque-Based Disturbance Rejection Method

To reject an additive disturbance term in the robot model, we illustrate how the parameter estimates remain bounded if the torque control is modified to be

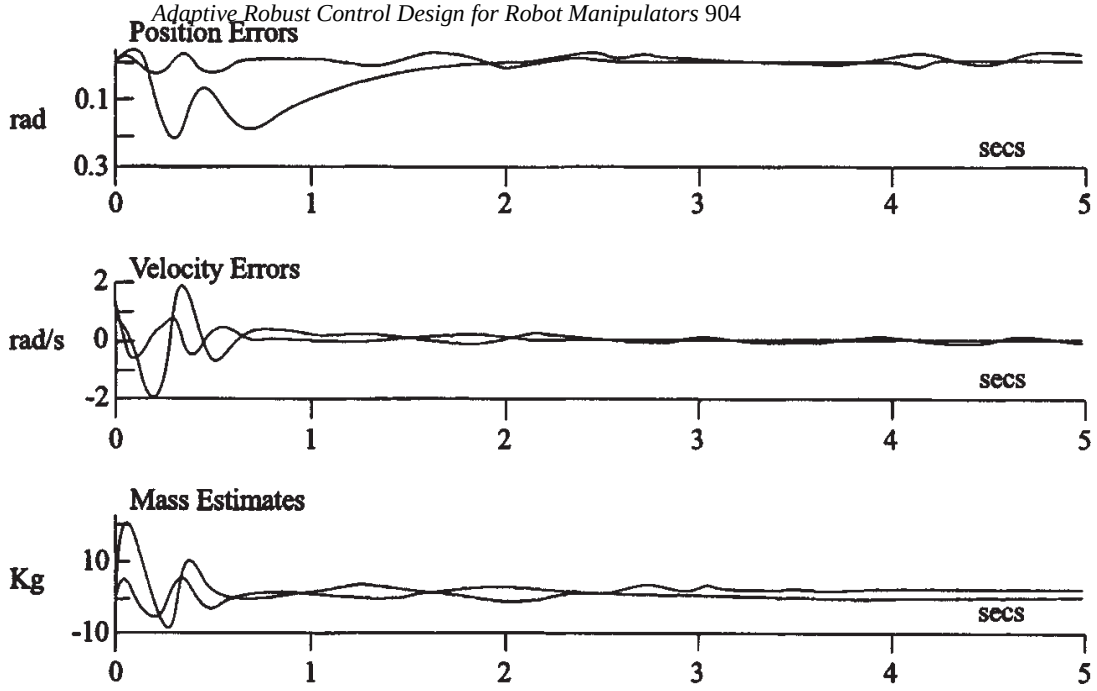


Figure 6.7.1: Simulation of adaptive controller in the pressence of disturbance.

$$\tau = \tau_a + k_d \, \mathrm{sgn}\,(r) \tag{6.7.6}$$

where v_d is the torque control given in Table 6.3.1,

$$\mathrm{sgn}\,(r) = [\mathrm{sgn}\,(r_1)\,, \mathrm{sgn}\,(r_2)\,, \ldots, \mathrm{sgn}\,(r_n)]^T\,, \tag{6.7.7}$$

sgn(·) is used to denote the signum function, and k_d is a scalar constant that satisfies

$$k_d > \max\{|T_{di}|\} \tag{6.7.8}$$

with $T_{di;}$ representing the ith component of the n×1 vector T_d [Slotine and Li 1985(c)].

Applying the disturbance rejection controller given in (6.7.6), the derivative of the Lyapunov function in (6.3.7) becomes

$$\dot{V} = -r^T K_v r + r^T T_d - k_d r^T \mathrm{sgn}\,(r)\,. \tag{6.7.9}$$

By noting that

$$|r_i| = r_i \mathrm{sgn}\,(r_i)\,, \tag{6.7.10}$$

(6.7.9) can be written as

$$\dot{V} \leq -r^T K_v r + \sum_{i=1}^{n} |r_i| \left(|T_{di}| - k_d \right) . \tag{6.7.11}$$

By utilizing (6.7.8), we can write (6.7.11) as

$$\dot{V} \leq -r^T K_v r. \tag{6.7.12}$$

The same arguments as in Section 6.6 can be used to show that the position tracking error is asymptotically stable while the velocity tracking error and the parameter estimate are bounded.

EXAMPLE 6.7–2: Disturbance Rejection for a Two-Link Robot Arm

In this example we simulate the modified adaptive controller given in (6.7.6) with the same control parameters, initial conditions, and desired trajectory as in Example 6.3.1 and also with the disturbance given in Example 6.7.1. The modified torque controller is given by

$$\tau_1 = \tau_{a1} + k_d \text{sgn} \left(\lambda_1 e_1 + \dot{e}_1 \right) \tag{1}$$

and

$$\tau_2 = \tau_{a2} + k_d \text{sgn} \left(\lambda_2 e_2 + \dot{e}_2 \right) , \tag{2}$$

where v_{a1}, and v_{a2} are the same adaptive torque controllers given in Example 6.3.1, h_1, and h_2 are the same scalar constants defined in Example 6.3.1, and

$$k_d = 2.2. \tag{3}$$

Note that k_d has been chosen to satisfy the condition given in (6.7.8) and that the update laws are the same as those given in Example 6.3.1. The tracking error and parameter estimates are illustrated in Figure 6.7.2. From the figure we note that the parameter estimates remain bounded; furthermore, the tracking error is now asymptotically stable even in the presence of a disturbance. It is important to note that for the theoretical development given for the torque-based disturbance rejection method above, we only guaranteed the velocity tracking error to be bounded.

■

Estimator-Based Disturbance Rejection Method

In [Reed and Ioannou 1988] a modified version of the o-modification [Ioannou and Tsakalis 1985] to the adaptive inertia-related control algorithm [Slotine and Li 1985(a)] was introduced to compensate for unmodeled dynamics and bounded disturbances in the robot model. In this method the torque control is the same as that given by Table 6.3.1; however, the adaptive update rule is modified to be

$$\dot{\hat{\varphi}} = \Gamma Y^T(\cdot) r - \sigma_s \hat{\varphi}, \tag{6.7.13}$$

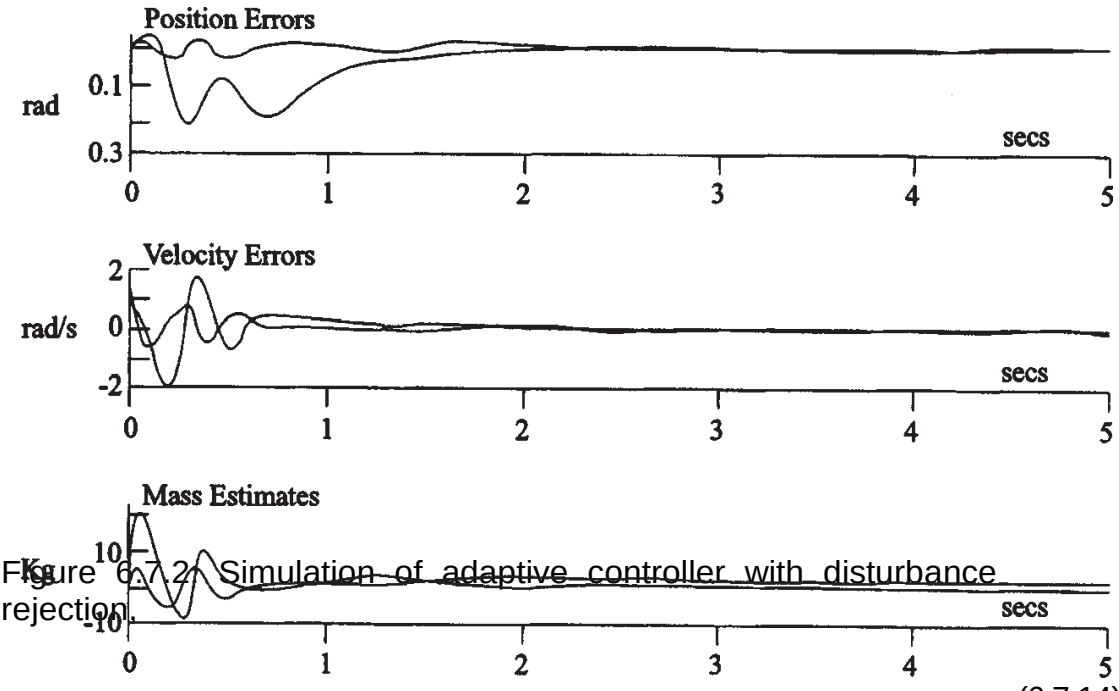


Figure 6.7.2: Simulation of adaptive controller with disturbance rejection.

where

$$\sigma_s = \begin{cases} 0 & \text{if } \|\hat{\varphi}\| < \varphi_0 \\ \frac{\|\hat{\varphi}\|}{\varphi_0} - 1 & \text{if } \varphi_0 \le \|\hat{\varphi}\| \le 2\varphi_0 \\ 1 & \text{if } \|\hat{\varphi}\| > 2\varphi_0 \end{cases} \tag{6.7.14}$$

(6.7.15)

and

$$\varphi_0 > \|\varphi\| .$$

With the update rule (6.7.13), Reed showed that the tracking error could be confined to a residual set and that all closed-loop signals are bounded.

As we have shown, a bounded disturbance can cause the parameter estimates to go unstable. The update rule given by (6.7.13) is intended to remedy this

problem by regulating on-line the size of the parameter estimates. This is done by the scalar design constant 0. That is, by checking the size of the parameter estimates against 0, the parameter estimates are forced to remain bounded by using this new update rule. One can see clearly that if "$\hat{\varphi}$"< 0, the update rule is the same as that given by Table 6.3.1. In other words, if the parameter estimates do not get too large, the controller is the same as the adaptive inertia-related controller. On the other hand, if parameter estimates get too large, the adaptive update rule is modified to ensure that the parameter estimates remain bounded. How this □*-modification* accomplishes this task is now discussed.

To motivate how the update rule given in (6.7.13) was formulated, examine the case when " $\hat{\varphi}$"> 0. This is the stabilizing part of the update rule. That is, if the parameter estimates become too large, the update rule switches to

$$\dot{\hat{\varphi}} = \Gamma Y^T(\cdot) r - \hat{\varphi}, \tag{6.7.16}$$

or in terms of the parameter error,

$$\dot{\tilde{\varphi}} = -\Gamma Y^T(\cdot) r - \tilde{\varphi} + \varphi. \tag{6.7.17}$$

We now reexamine the stability analysis given in Section 6.3 for the adaptive inertia-related controller with the parameter update rule given by (6.7.16). Specifically, with the addition of the bounded disturbance term in (6.7.1), the derivative of the Lyapunov function in (6.3.7) becomes

$$\dot{V} = -r^T K_v r - \tilde{\varphi}^T \Gamma^{-1} \tilde{\varphi} + r^T T_d + \tilde{\varphi}^T \Gamma^{-1} \varphi \tag{6.7.18}$$

or

$$\dot{V} = -x^T K^* x + x^T T_d^*, \tag{6.7.19}$$

where

$$x = \begin{bmatrix} r \\ \tilde{\varphi} \end{bmatrix}, \quad K^* = \begin{bmatrix} K_v & 0 \\ 0 & \Gamma^{-1} \end{bmatrix}, \quad \text{and} \quad T_d^* = \begin{bmatrix} T_d \\ \Gamma^{-1}\varphi \end{bmatrix}. \tag{6.7.2}$$

By the use of the Rayleigh-Ritz Theorem (see Chapter 1), we can write (6.7.19) as

$$\dot{V} \leq -\lambda_{\min}\{K^*\} \|x\|^2 + \|x\| \|T_d^*\|. \tag{6.7.21}$$

From (6.7.21), $\dot{V}$ will be negative if

(6.7.22) $$\|x\| > \frac{\|T_d^*\|}{\lambda_{\min}\{K^*\}}.$$

It is important to note that the right-hand side of (6.7.22) is a constant; therefore, if (6.7.22) is satisfied, $\dot{V}$ is negative, which causes *V* to decrease. If *V* decreases, then by our definition of the Lyapunov function given in (6.3.7), *x* must eventually decrease. However, if *x* decreases such that

$$\|x\| \leq \frac{\|T_d^*\|}{\lambda_{\min}\{K^*\}}, \tag{6.7.23}$$

then $\dot{V}$ may be positive, which means that *V* will start to increase. The increase in *V* causes *x* to increase such that (6.7.22) is satisfied. This means that *V* now starts to decrease again and hence *x* eventually decreases. This argument illustrates how *x* is bounded. If *x* is bounded, then from (6.7.20), *r* and $\tilde{\varphi}$ are bounded. Since *r* is bounded, standard linear control arguments can be used to show that *e* and $\dot{e}$ are bounded.

One last point is now discussed regarding the region 0Š"$\tilde{\varphi}$"Š2 0. for the adaptive update rule given in (6.7.13). This part of the adaptive update rule is used to ensure that there is a smooth transition between the adaptive inertia-related update rule and the stabilizing portion of the update rule given by (6.7.16). That is, this ensures that we do not obtain any discontinuities in the parameter estimates, which could cause a large discontinuity in the input torque. A large discontinuity is undesirable in the input torque signal since this type of signal could cause the robot manipulator to jerk violently.

6.8 Summary

In this chapter an account of several of the most recent adaptive control results for rigid robots has been given. The intent has been to lend some perspective to the growing list of adaptive control results for robot manipulators. Some research areas, such as transient behavior, digital implementation, and robustness to unmodeled dynamics, will no doubt be addressed in the future. An issue that remains to be investigated is the comparison of the advantages and disadvantages of the different servo and adaptive laws.

Some excellent adaptive control work with regard to robot manipulators by other researchers is outlined in [Ortega and Spong 1988]. Since this is such a well-studied field and there is limited space available in this chapter, we apologize to anyone who has been left out.

REFERENCES

[Anderson 1977] Anderson, B., "Exponential stability of linear equations arising in adaptive identification," *IEEE Trans. Autom. Control,* Feb. 1977, pp. 83–88.g

[Arimoto and Miyazaki 1986] Arimoto, S., and F.Miyazaki, "Stability and robustness of PD feedback control with gravity compensation for robot manipulators," *Robot. Theory Pract.,* DSC Vol. 3, pp. 67–72, *ASME Winter Annual Meeting,* Dec. 1986.

[Åström and Wittenmark 1989] K.Åström and B.Wittenmark, *Adaptive Control.* Reading, MA: Addison-Wesley, 1989.

[Brogliato et al. 1990] Brogliato, B., I.Landau, and R.Lozano-Leal, "Adaptive motion control of robot manipulators: a unified approach based on passitivity," *Proc. IEEE Am. Controls Conf,* pp. 2259–2264, San Diego, CA, May 1990.

[Craig 1985] Craig, J., *Adaptive Control of Mechanical Manipulators.* Reading, MA.: Addison Wesley, 1985.

[Ioannou and Tsakalis 1985] Ioannou, P., and K.Tsakalis, "A robust direct adaptive controller," *IEEE Trans. Autom. Control,* vol. AC-31, no. 11, pp. 1033–1043, 1985.

[Kailath 1980] Kailath, T, *Linear Systems.* Englewood Cliffs, NJ: Prentice Hall, 1980.

[Landau 1979] Landau, Y., *Adaptive Control: The Model Reference Approach.* New York: Marcel Dekker, 1979.

[Li and Slotine 1987] Li, W., and J.Slotine, "Parameter estimation strategies for robotic applications," *ASME Winter Annual Meeting,* Boston, 1987.

[Morgan and Narendra 1977] Morgan, A., and K.Narendra, "On the uniform asymptotic stability of certain linear nonautonomous differential equations," *SIAM J. Control Optim.,* 1977, p. 15.

379

[Ortega and Spong 1988] Ortega, R., and M.Spong, “Adaptive motion control of rigid robots: a tutorial,” *Proc. IEEE Conf Decision Control,* Austin, TX, 1988.

[Reed and Ioannou 1988] Reed, J., and P.Ioannou, “Instability analysis and robust adaptive control of robotic manipulators,” *Proc. IEEE Conf Decision Control,* Austin, TX, 1988.

[Slotine 1988] Slotine, J., (1988), “Putting physics in control: the example of robotics,” *Control Syst. Mag.,* Dec. 1988, Vol. 8, pp 12–15.

[Slotine and Li 1985(a)] Slotine, J., and W.Li, “Theoretical issues in adaptive control,” *5th Yale Workshop on Applications of Adaptive Systems Theory,* Yale University, New Haven, CT, 1985(a).

[Slotine and Li 1985(b)] Slotine, J., and W.Li, “Adaptive robot control: a new perspective,” *Proc. IEEE Conf Decision Control,* Los Angeles, 1985(b).

[Slotine and Li 1985(c)] Slotine, J., and W.Li, “Adaptive strategies in constrained manipulation,” *Proc. IEEE Int. Conf Robot. Autom.,* Raleigh, NC, Mar. 1985(c), pp. 595–601.

[Vidyasagar 1978] Vidyasagar, M., *Nonlinear Systems Analysis.* Englewood Cliffs, NJ: Prentice Hall, 1978.

Chapter 8

Neural Network Control of Robots

A framework is given for controller design using neural networks. These structures possess a universal approximation property that allows them to be used in feedback control of unknown systems without requirements for linearity in the system parameters or finding a regression matrix. Feedback control topologies and weight tuning algorithms are given here that guarantee closed-loop stability and bounded weights.

8.1 Introduction

In recent years, there has been a great deal of effort to design feedback control systems that mimic the functions of living biological systems [White and Sofge

1992], [Miller et al. 1991]. There has been great interest recently in ‘universal model-free controllers’ that do not need a mathematical model of the controlled plant, but mimic the functions of biological processes to learn about the systems they are controlling on-line, so that performance improves automatically. Techniques include fuzzy logic control, which mimics linguistic and reasoning functions, and artificial neural networks, which are based on biological neuronal structures of interconnected nodes. Neural networks (NNs) have achieved great success in classification, pattern recognition, and other open-loop applications in digital signal processing and elsewhere. Rigorous analyses have shown how to select NN topologies and weights, for instance, to discriminate between specified exemplar patterns. By now, the theory and applications of NN in open-loop applications are well understood, so that

431

NN have become an important tool in the repertoire of the signal processor and computer scientist.

There is a large literature on NN for feedback control of unknown plants. Until the 1990's, design and analysis techniques were ad hoc, with no repeatable design algorithms or proofs of stability and guaranteed performance. In spite of this, simulation results appearing in the literature showed good performance. Most of the early approaches used standard backpropagation weight tuning [Werbos 1992] since rigorous derivations of tuning algorithms suitable for closed-loop control purposes were not available. Many NN design techniques mimicked adaptive control approaches, where rigorous analysis results were available [Åström and Wittenmark 1989], [Landau 1979], [Goodwin et al. 1984], proposing NN feedback control topologies such as indirect identification-based control, inverse dynamics control, series-parallel techniques, etc.

In keeping with the philosophy of those working in control system theory since Maxwell, Lyapunov, A.N.Whitehead, von Bertalanffy, and others, to address such issues it is necessary to begin with the knowledge available about the system being controlled. Narendra [Narendra 1991], [Narendra and Parthasarathy 1991] and others [Miller et al. 1991], [White and Sofge 1992], [Werbos 1992] pioneered rigorous NN controls applications by studying the dynamical behavior of NN in closed-loop systems, including computation of the gradients needed for backprop tuning. Other groups providing rigorous analysis and design techniques for closed-loop NN controllers included [Sanner and Slotine 1991] who showed how to use radial basis function NN in feedback control, [Chen and Khalil 1992], [Chen and Liu 1994] who provided NN tuning algorithms based on dead-zone methods, [Polycarpou and Ioannou 1991], [Polycarpou 1996] who used projection methods, [Lewis et al. 1993], [Lewis et al. 1995] who used an e-mod approach, [Sadegh 1993] who provided NN controllers for discrete-time systems, and [Rovithakis and Christodoulou 1994] who used dynamic NN for feedback control.

In this chapter is given an approach to the design and analysis of *neural network* controllers based on several PhD dissertations and a body of published work, including [Lewis et al. 1999], [Kim and Lewis 1998]. The control structures discussed here are *multiloop controllers* with NN in some of the loops and an outer tracking unity-gain PD loop. There are repeatable design algorithms and guarantees of system performance including both small tracking errors and bounded NN weights. It is shown that as uncertainty about the controlled system increases or performance requirements increase, the NN controllers require more and more structure. An exposition of this material in greater depth appears in [Lewis 1999], which also shows relationships with Fuzzy Logic Systems.

8.2 Background in Neural Networks

In this section is provided the background in neural network structures required for feedback control. For more details see [Haykin 1994], [Lewis et al. 1999], [Lewis and Kim 1998]. Two key features that make NN useful for feedback control are their *universal approximation property* and their *learning capability,* which arises due to the fact that their weights are tunable parameters that can be updated to improve controller performance. The universal approximation property is the main feature that makes non-linear network structures more suitable for robot control than adaptive robot controllers, which have generally relied upon the determination of a regression matrix, which in turn requires linearity in the tunable parameters (LIP).

Multilayer Neural Networks

A multilayer neural network is shown in Figure 8.2.1. This NN has two layers of adjustable weights, and is called here a 'two-layer' net. This NN has no internal feedback connections and so is termed *feedforward,* and no internal dynamics and so is said to be *static*. The NN output y is a vector with m components that are determined in terms of the n components of the input vector x by the recall equation

$$y_i = \sum_{j=1}^{L} \left[w_{ij} \sigma \left(\sum_{k=1}^{n} v_{jk} x_k + \theta_{v_j} \right) + \theta_{w_i} \right]; \quad i = 1, \ldots, m \tag{8.2.1}$$

where $\sigma(\cdot)$ are the *activation functions* and L is the number of *hidden-layer neurons*. The first-layer interconnections weights are denoted v_{jk} and the second-layer interconnection weights by w_{ij}. The threshold offsets are denoted by θ_{vj}, θ_{wi}.

Many different activation functions $\sigma(\cdot)$ are in common use. For feed-back control using multilayer NN it is required that $\sigma(\cdot)$ be smooth enough so that at least its first derivative exists. Suitable choices include the sigmoid

$$\sigma(x) = \frac{1}{1 + e^{-x}}, \tag{8.2.2}$$

the hyperbolic tangent

$$\sigma(x) = \frac{e^{x} - e^{-x}}{e^{x} + e^{-x}}, \tag{8.2.3}$$

and other logistic-curve-type functions, as well as the gaussian and an assortment of other functions.

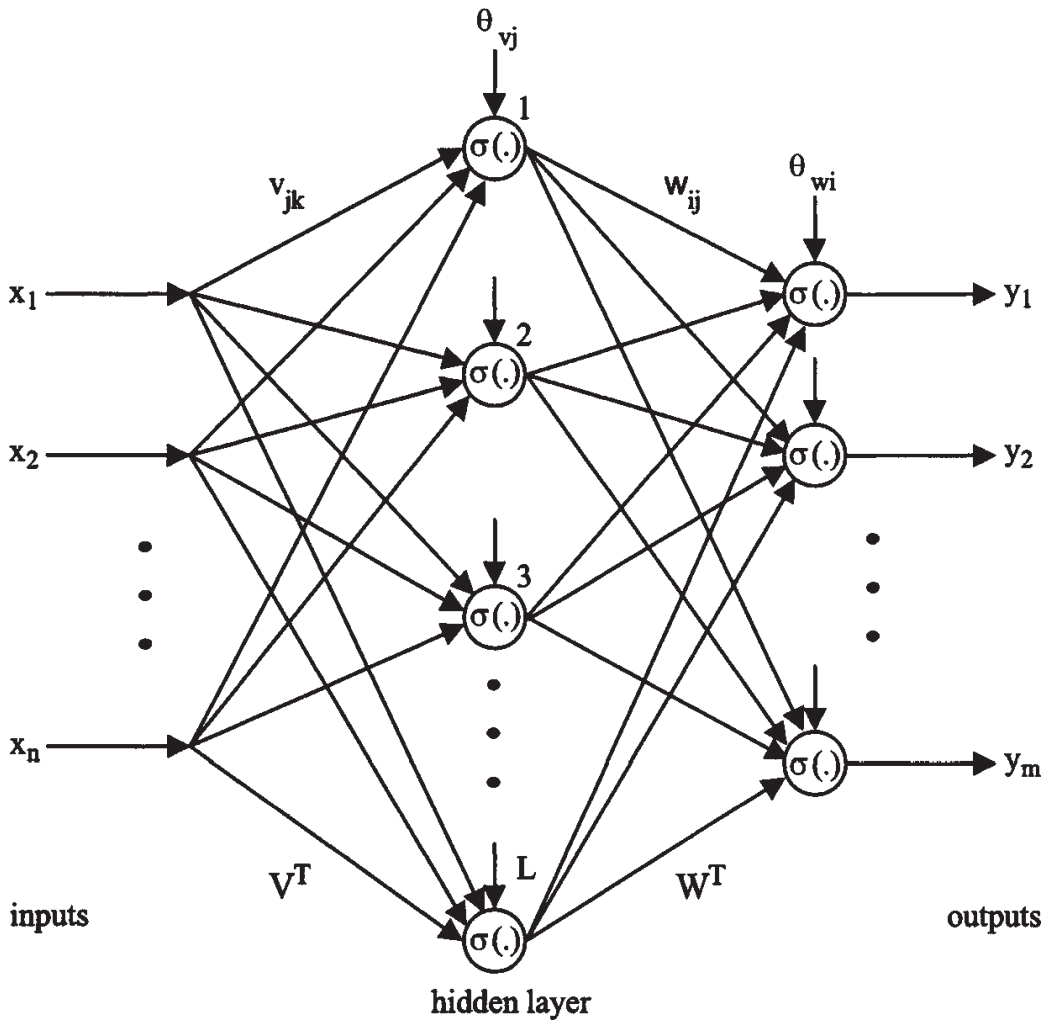


Figure 8.2.1: Two-layer feedforward neural network.

By collecting all the NN weights v_{jk}, w_{ij} into matrices of weights V^T, W^T, the NN recall equation may be written in terms of vectors as

(8.2.4) $$y = W^T \sigma(V^T x).$$

The thresholds are included as the first columns of the weight matrices W^T, V^T; to accommodate this, the vectors x and $o(\cdot)$ need to be augmented by placing a '1' as their first element (e.g. $x=[1\ x_1\ x_2 \ldots x_n]^T$). In this equation, to represent (8.2.1) one has sufficient generality if $o(\cdot)$ is taken as a diagonal function from R^L to R^L that is $o(z)=diag\{o(z_j)\}$ for a vector $z=[z_1\ z_2\ \ldots z_L]^T \in R^L$.

Note that the recall equation is *nonlinear* in the first-layer weights and thresholds V.

Universal Function Approximation Property. NN satisfy many important properties. A main one of concern for feedback control purposes is the *universal function approximation property* [Hornik and Stinchombe 1989]. Let *f*(x) be a general smooth function from R^n to R^m. Then, it can be shown that, as long as *x* is restricted to a compact set *S* of R^n, there exist weights and thresholds such that one has

(8.2.5) $$f(x) = W^T \sigma(V^T x) + \epsilon$$

for some number of hidden-layer neurons *L*. This holds for a large class of activation functions, including those just mentioned. The value *c* is called the *NN functional approximation error,* and it generally decreases as the net size *L* increases. In fact, for any choice of a positive number c_N, one can find a feedforward NN such that

(8.2.6) $$\|\epsilon\| < \epsilon_N$$

for all *x* in *S.* The selection of the net size *L* for a prescribed accuracy c_N is an open question for general unstructured fully-connected NN. This problem can be solved for CMAC, FL nets, and other structured nonlinear nets as subsequently described.

The ideal NN weights in matrices *W, V* that are needed to best approximate a given nonlinear function *f(x)* are difficult to determine. In fact, they may not even be unique. However, all one needs to know for controls purposes is that, for a specified value of c_N *some ideal approximating NN weights exist*. Then, an *estimate* of *f(x)* can be given by

(8.2.7) $$\hat{f}(x) = \hat{W}^T \sigma(\hat{V}^T x)$$

where W, V are estimates of the ideal NN weights that are provided by some on-line weight tuning algorithms subsequently to be detailed. Note that all 'hat' quantities are known, since they may be computed using measurable signals and current NN weight estimates.

The assumption that there exist ideal weights such that the approximation property holds is very much like various similar assumptions in adaptive control [Åström and Wittenmark 1989], [Landau 1979], including *Erzberger's assumptions* and *linearity in the parameters*. The very important difference is that in the NN case, *the universal approximation property always holds,* while in adaptive control such assumptions often do not hold in practice, and so they imply restrictions on the form of the systems that can be controlled. **Overcoming the NLIP Problem.** Multilayer NN are nonlinear in the weights

V and so weight tuning algorithms that yield guaranteed stability and bounded weights in closed-loop feedback systems have been difficult to discover until a few years ago. The NLIP problem is easily overcome if a correct and rigorous approach is taken. One approach is the following appropriate use of the Taylor series [Lewis et al. 1996].

Define the functional estimation error

$$\tilde{f} = f - \hat{f}, \tag{8.2.8}$$

the weight estimation errors

$$\tilde{W} = W - \hat{W}, \quad \tilde{V} = V - \hat{V}, \tag{8.2.9}$$

and the hidden-layer output error

$$\tilde{\sigma} = \sigma - \hat{\sigma} \equiv \sigma(V^T x) - \sigma(\hat{V}^T x). \tag{8.2.10}$$

For any *z* one may write the Taylor series

$$\sigma(z) = \sigma(\hat{z}) + \sigma'(\hat{z})\tilde{z} + O(\tilde{z})^2, \tag{8.2.11}$$

where o' is the jacobian and the last term means terms of order z^2.Therefore,

$$\tilde{\sigma} = \sigma'(\hat{V}^T x)\tilde{V}^T x + O(\tilde{V}^T x)^2 \equiv \hat{\sigma}'\tilde{V}^T x + O(\tilde{V}^T x)^2. \tag{8.2.12}$$

This key equation allows one to write the functional estimation error as

$$\begin{aligned}
\tilde{f} = f - \hat{f} &= W^T \sigma\left(V^T x\right) - \hat{W}^T \sigma\left(\hat{V}^T x\right) + \varepsilon \\
&= \tilde{W}^T \sigma(\hat{V}^T x) + W^T[\sigma(V^T x) - \sigma(\hat{V}^T x)] + \epsilon \\
&= \tilde{W}^T \hat{\sigma} + W^T[\hat{\sigma}'\tilde{V}^T x + O(\tilde{V}^T x)^2] + \epsilon \\
&= \tilde{W}^T[\hat{\sigma} - \hat{\sigma}'\hat{V}^T x] + \hat{W}^T\hat{\sigma}'\tilde{V}^T x + \tilde{W}^T\hat{\sigma}'V^T x \\
&\quad + W^T O(\tilde{V}^T x)^2 + \epsilon.
\end{aligned} \tag{8.2.13}$$

The first term has *W* multiplied by a known quantity (in square braces), and the second term has *V* multipled by a known quantity. When used subsequently in the closed-loop error dynamics, this form allows one to derive tuning laws for *V* and *W* that guarantee closed-loop stability.

Linear-in-the-parameter neural nets

If the first-layer weights and thresholds *V* in (8.2.4) are fixed and only the second-layer weights and thresholds *W* are tuned, then the NN has only one layer of tunable weights. One may then define the fixed function $\phi(x) = \sigma(V^T x)$ so that such a 1-layer NN has the recall equation

(8.2.14) $$y = W^T \phi(x),$$

where $x \in \Re^n, y \in \Re^m, \phi(\cdot) : \Re^n \to \Re^L$ and *L* is the number of hidden-layer neurons. This NN is linear in the tunable parameters *W,* so that it is far easier to tune. In fact, standard adaptive control proofs can be used to derive suitable tuning algorithms.

Though LIP, these NN still offer an enormous advantage over standard adaptive control approaches that require the determination of a regression matrix since they satisfy a universal approximation property if the functions *$(·)* are correctly chosen. Note that adaptive controllers are linear in the *system* parameters, while 1-layer NN are linear in the *NN weights*. An advantage of 1-layer NN over 2-layer NN is that firm results exist for the former on the selection of the number of hidden layer neurons *L* for a specified approximation accuracy. A disadvantage of LIP networks is that Barron [Barron 1993] has shown a lower bound on the approximation accuracy.

Functional-Link Basis Neural Networks. More generality is gained if *o*(·) is not diagonal, but *$(·)* is allowed to be a general function from R^n to R^L. This is called a *functional-link neural net (FLNN)* [Sadegh 1993]. For LIP NN, the functional approximation property does not generally hold. However, a 1- layer NN can still approximate functions as long as the activation functions *$(·)* are selected as a *basis,* which must satisfy the following two requirements on a compact simply-connected set of *S* of R^n:

1. A constant function on *S* can be expressed as (8.2.14) for a finite number *L* of hidden-layer neurons.
2. The functional range of (8.2.14) is dense in the space of continuous functions from *S* to R^m for countable *L*.

If *$(·)* provides a basis, then a smooth function *f(x)* from R^n to R^m can be approximated on a compact set *S* of R^n, by

(8.2.15) $$f(x) = W^T \phi(x) + \epsilon.$$

for some ideal weights and thresholds *W* and some number of hidden layer neurons *L*. In fact, for any choice of a positive number c_N, one can find a feedforward NN such that $\|\epsilon\| < \epsilon_N$ for all *x* in *S.*

The approximation for *f(x)* is given by

(8.2.16) $$\hat{f}(x) = \hat{W}^T \phi(x),$$

where *W* are the NN weight and threshold estimates given by the tuning algorithm. For LIP NN, the functional estimation error is given by

(8.2.17) $$\begin{aligned} \tilde{f} &= f - \hat{f} = W^T \phi(x) - \hat{W}^T \phi(x) + \epsilon \\ &= \tilde{W}^T \phi(x) + \epsilon, \end{aligned}$$

which, when used subsequently in the error dynamics, directly yields tuning algorithms for *W* that guarantee closed-loop stability.

Barron [Barron 1993] has shown that for all LIP approximators there is a fundamental lower bound, so that *c* is bounded below by terms on the order of $1/L^{2/n}$. Thus, as the number of NN inputs *n* increases, increasing *L* to improve the approximation accuracy becomes less effective. As shown subsequently, this is not a major limitation on adaptive controllers designed using 1-layer NN. This lower bound problem does not occur in the NLIP multilayer nonlinear nets.

A special FLNN is now discussed. We often use *o*(·) in place of *$*(·), with the understanding that, for LIP nets, this activation function vector is not diagonal, but is a general function from R^L to R^L.

Gaussian or Radial Basis Function (RBF) Networks. The selection of a basis set of activation functions is considerably simplified in various sorts of *structured nonlinear networks,* including radial basis function, CMAC, and fuzzy logic nets. It will be shown here that the key to the design of such structured nonlinear nets lies in a *more general set of NN thresholds* than allowed in the standard equation (8.2.1), and in their appropriate selection.

A NN activation function often used is the gaussian or radial basis function (RBF) [Sanner and Slotine 1991] given when *x* is a scalar as

(8.2.18) $$\sigma(x) = e^{-(x-\bar{x})^2/2p},$$

where *x* is the mean and *p* the variance. RBF NN can be written as (8.2.4), but have an advantage over the usual sigmoid NN in that the *n*-dimensional gaussian function is well understood from probability theory, Kalman filtering, and elsewhere, so that *n*-dimensional RBF are easy to conceptualize.

The *j*-th activation function can be written as

$$\sigma_j(x) = e^{-\frac{1}{2}(x-\bar{x}_j)^T P_j^{-1}(x-\bar{x}_j)} \tag{8.2.19}$$

with $x, \bar{x}_j \in \Re^n$. Define the vector of activation functions as $o(x) \div [o_1(x)\ o_2(x) \ldots o_L(x)]^T$. If the covariance matrix is diagonal so that $P_j = diag\{p_{jk}\}$, then (8.2.19) becomes *separable* and may be decomposed into components as

$$\sigma_j(x) = e^{-\frac{1}{2}\sum_{k=1}^{n} -(x_k-\bar{x}_{jk})^2/p_{jk}} = \prod_{k=1}^{n} e^{-\frac{1}{2}(x_k-\bar{x}_{jk})^2/p_{jk}}, \tag{8.2.20}$$

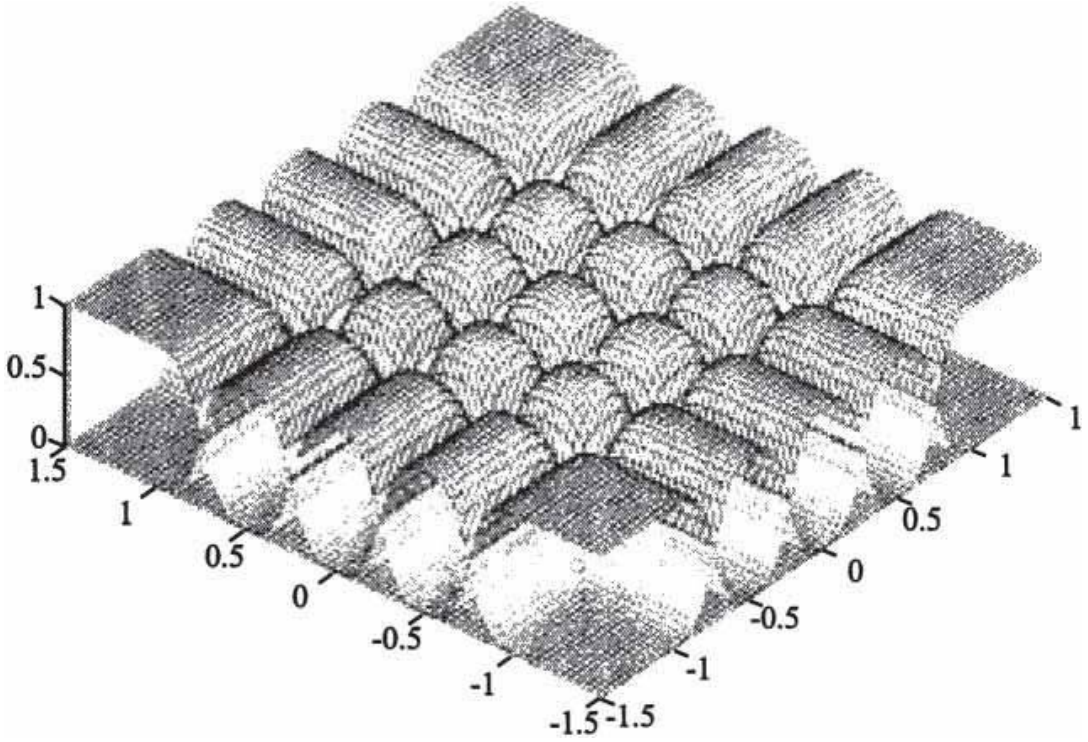


Figure 8.2.2:2-dimensional separable gaussian functions for an RBF NN.

where $x_k, \bar{x}_{jk}$ are the *k*-th components of $x, \bar{x}_j$. Thus, the *n*-dimensional activation functions are the product of *n* scalar functions. Note that this equation is of the form of the activation functions in (8.2.1), but with *more general thresholds,* as a threshold is required for each different component of *x* at each hidden layer neuron *j;* that is, the threshold at each hidden-layer neuron in Figure 8.2.1 is a *vector*. The RBF variances p_{jk} and offsets x_{jk} are usually selected in designing the RBF NN and left fixed; only the output-layer weights W^T are generally tuned. Therefore, the RBF NN is a special sort of FLNN (8.2.14) (where *$(x)=a(x)*).

Figure 8.2.2 shows separable gaussians for the case $x \mathrm{CR}^2$. In this figure, all the variances p_{jk} are identical, and the mean values x_{jk} are chosen in a special way that spaces the activation functions at the node points of a 2-D grid. To form an RBF NN that approximates functions over the region $\{-1<x_1 Š 1, -1<x_2 Š 1\}$ one has here selected $L=5\times5=25$ hidden-layer neurons, corresponding to 5 cells along x_1 and 5 along x_2. Nine of these neurons have 2-D gaussian activation functions, while those along the boundary require the illustrated 'one-sided' activation functions.

8.3 Tracking Control Using Static Neural Networks

In this section is discussed feedback tracking control design using nonlinear nets and assuming full state-variable feedback. For more details see [Lewis et al. 1999] and other listed references. If full state feedback is available, then a static feedforward NN suffices for control. A control topology and net tuning algorithms are provided here that guarantee closed-loop stability and bounded weights. The techniques to be discussed apply for general nonlinear nets including both neural networks and fuzzy logic systems [Wang 1997], [Lewis et al. 1997], so that the abbreviation NN might henceforth be construed as meaning 'nonlinear network'. The resulting multiloop control topology has an *outer PD tracking loop* and an inner NN feedback linearization or *action generating loop*. It is found that backprop tuning does not generally suffice, but modified tuning algorithms are needed for guaranteed closed-loop performance.

Many industrial mechanical systems, as well as automobiles, aircraft, and spacecraft, have dynamics in the *Lagrangian form,* which are exemplified by the class of rigid robot systems. Therefore, the Lagrangian robot dynamics will be considered [Lewis et al. 1993], [Lewis et al. 1996]. The NN control techniques presented may also be applied to other unknown systems including certain important classes of nonlinear systems [Lewis et al. 1999].

Robot Arm Dynamics and Error System

The dynamics of rigid Lagrangian systems, including robot arms, have some important physical, structural, and passivity properties [Craig 1988], [Lewis et al. 1993], [Slotine 1988], [Spong and Vidyasagar 1989] that make it very natural to use NN in their control. These properties should be taken into account in the design of any controller—in fact, they provide the foundation for rigorous design algorithms for NN controllers.

The dynamics of an *n*-link rigid (i.e. no flexible links or high-frequency

joint/motor dynamics) robot manipulator may be expressed in the Lagrange form

(8.3.1) $$M(q)\ddot{q} + V_m(q,\dot{q})\dot{q} + G(q) + F(\dot{q}) + \tau_d = \tau$$

with $q(t) \in R^n$ the joint variable vector, whose entries are the robot arm joint angles or link extensions. $M(q)$ is the inertia matrix, $Vm(q,q)$ the coriolis/ centripetal matrix, $G(q)$ the gravity vector, and $F(q)$ the friction. Bounded unknown disturbances (including e.g. unstructured unmodelled dynamics) are denoted by v_d, and the control input torque is $v(t)$ The robot dynamics have the following standard properties:

Property 1: $M(q)$ is a positive definite symmetric matrix bounded by $m_1 I < M(q) < m_2 I$, with m_1, m_2 positive constants.

Property 2: The norm of the matrix $Vm(q, q)$ is bounded by $v_b(q)\|q\|$, for some function $v_b(q)$.

Property 3: The matrix $M–2Vm$ is skew-symmetric. This is equivalent to the fact that the internal forces do no work.

Property 4: The unknown disturbance satisfies $\|\tau_d\| < d_B$ with b_D a positive constant.

Given a desired arm trajectory $q_d(t) \in R^n$ the tracking error is

$$e(t) = q_d(t) - q(t) \tag{8.3.2}$$

and the filtered tracking error is

(8.3.3) $$r = \dot{e} + \Lambda e$$

where K is a symmetric positive definite design parameter matrix, usually selected diagonal. If a controller is found such that $r(t)$ is bounded, then $e(t)$ is also bounded; in fact $\|e\| \leq \|r\|/\lambda_{min}(\Lambda)$ and $\|\dot{e}\| \leq \|r\|$, with $\lambda_{min}(\Lambda)$ the minimum singular value of K.

Differentiating $r(t)$ and using (8.3.1), the arm dynamics may be written in terms of the filtered tracking error as

$$M\dot{r} = -V_m r - \tau + f + \tau_d \tag{8.3.4}$$

where the nonlinear robot function is

(8.3.5) $$f(x) = M(q)(\ddot{q}_d + \Lambda\dot{e}) + V_m(q,\dot{q})(\dot{q}_d + \Lambda e) + G(q) + F(\dot{q}).$$

The vector *x* required to compute *f(x)* can be defined, for instance, as

(8.3.6) $$x \equiv [e^T \ \dot{e}^T \ q_d^T \ \dot{q}_d^T \ \ddot{q}_d^T]^T,$$

which can be measured. Function *f(x)* contains potentially unknown robot parameters including pay load mass and complex forms of friction.

A suitable control input for trajectory following is given by the computed-torque-like control

(8.3.7) $$\tau = \hat{f} + K_v r - v$$

with $K_v = K_v^T > 0$ a gain matrix, generally chosen diagonal, and *f(x)* an estimate of the robot function *f(x)* that is provided by some means. The robustifying signal *v(t)* is needed to compensate for unmodelled unstructured disturbances. Using this control, the closed-loop error dynamics is

(8.3.8) $$M\dot{r} = -(K_v + V_m)r + \tilde{f} + \tau_d + v.$$

In computing the control signal, the estimate *f* can be provided by several techniques, including adaptive control or neural or fuzzy networks. The auxiliary control signal *v(t)* can be selected by several techniques, including sliding-mode methods and others under the general aegis of robust control methods.

The desired trajectory is assumed bounded so that

$$\left\| \begin{array}{c} q_d(t) \\ \dot{q}_d(t) \\ \ddot{q}_d(t) \end{array} \right\| \leq q_B, \tag{8.3.9}$$

with q_B a known scalar bound. It is easy to show that for each time *t, x(t)* is bounded by

(8.3.10) $$\|x\| \leq c_1 + c_2\|r\| \leq q_B + c_0\|r(0)\| + c_2\|r\|$$

for computable positive constants c_0, c_1, c_2.

Adaptive Control

Standard adaptive control techniques in robotics [Craig 1988], [Slotine 1988], [Spong and Vidyasagar 1989], [Lewis et al. 1993] use the assumption that the nonlinear robot function is linear in the tunable parameters so that

(8.3.11) $$f(x) = \Theta(x)p + \epsilon$$

where *p* is a vector of unknown parameters and ©*(x)* is a known *regression matrix*. The control is selected as

(8.3.12) $$\tau = K_v r + \Theta(x)\hat{p}$$

and tuning algorithms are determined for the parameter estimates *P.* This is facilitated by the LIP assumption. If the approximation error *c* is non-zero, then the tuning algorithm must be modified in order to guarantee bounded parameter estimates. Various robustifying techniques may be used for this including the *o*-mod [Ioannou and Kokotovic 1984], the *e*-modification [Narendra and Annaswamy 1987], or the dead-zone techniques [Kreisselmeier and Anderson 1986]. There are adaptive control techniques by now that do not require LIP or the determination of a regression matrix [Colbaugh and Seraji 1994]. It is interesting to compare the complexity of these to the NN controllers to be discussed herein.

Neural Net Feedback Tracking Controller

A NN will be used in the control *v(t)* in (8.3.7) to provide the estimate *f* for the unknown robot function *f(x)*. The NN approximation property assures us that there always exists a NN that can accomplish this within a given accuracy c_N. For 2-layer NLIP NN the approximation is

$$\hat{f}(x) = \hat{W}^T \sigma(\hat{V}^T x), \tag{8.3.13}$$

while for 1-layer LIP NN it is

$$\hat{f}(x) = \hat{W}^T \phi(x), \tag{8.3.14}$$

with *$(·)* selected as a basis.

The structure of the NN controller appears in Figure 8.3.1, where $e \div [e^T \quad \dot{e}^T]^T$, $\underline{q} \equiv [q^T \quad \dot{q}^T]^T$. The neural network that provides the estimate for *f(x)* appears in an *inner control loop,* and there is an *outer tracking loop* provided by the PD term $K_V r$. In control theory terminology, the inner loop is a *feedback linearization* controller [Slotine and Li 1991], while in computer science terms it is the *action generating loop* [Werbos 1992], [Miller et al. 1991], [White and Sofge 1992]. This *multiloop intelligent control structure* is derived naturally from robot control notions, and is not ad hoc. As such, it is immune to philosophical deliberations concerning suitable NN control topologies including the common discussions on feed-forward vs. feedback, direct vs. indirect, and so on. It is to be noted that the static feedforward NN in this diagram is turned into a *dynamic NN* by closing a feedback loop around it (c.f. [Narendra 1991]).

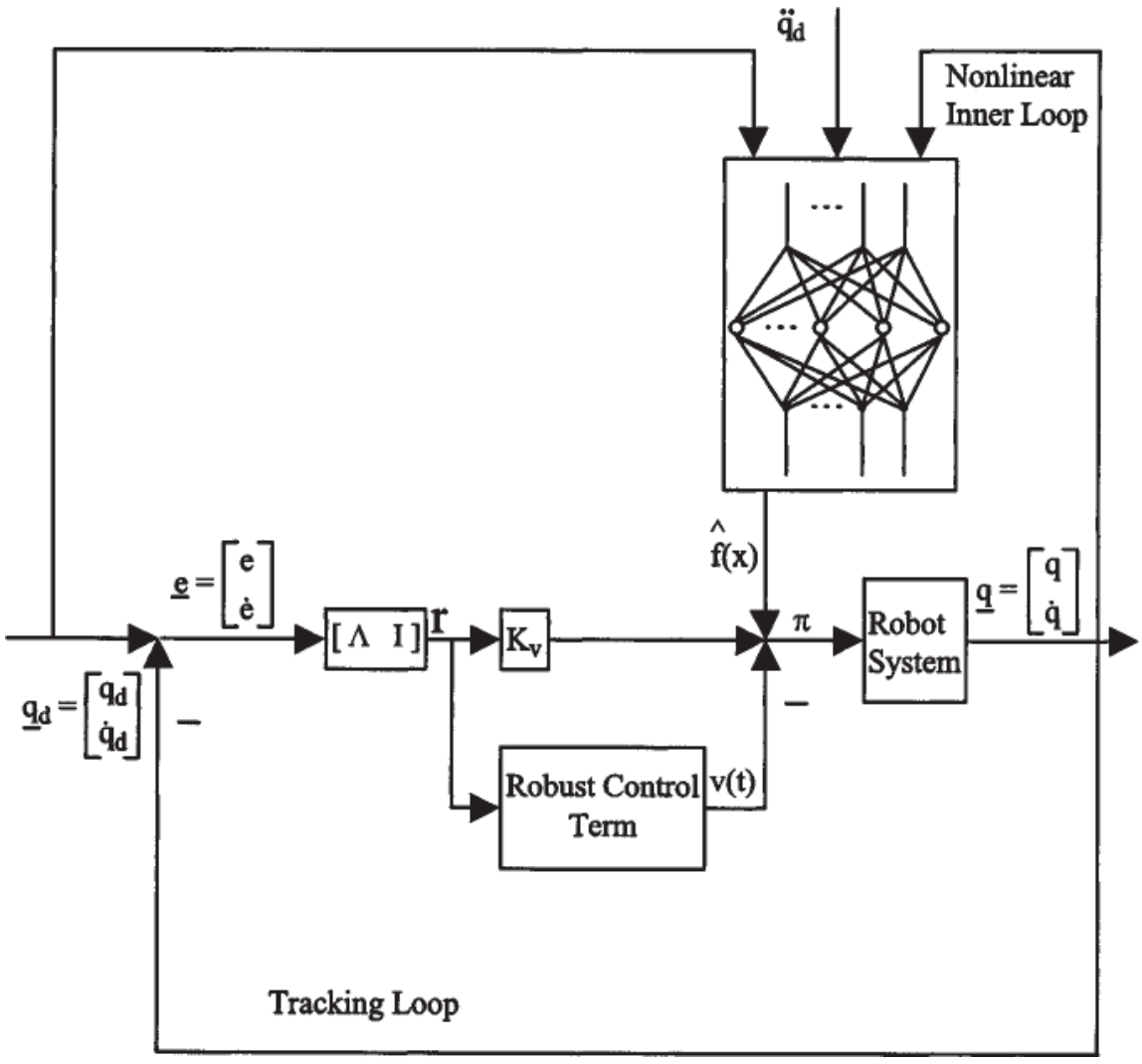


Figure 8.3.1: Neural net robot controller, showing nonlinear neural network loop and outer tracking loop.

Advantage of NN over LIP Adaptive Control. Each robotic system has its own regression matrix, so that a different ©*(x)* must be determined for each system. This regression matrix is often complicated and determining it can be time consuming. One notes that the regression matrix effectively provides a basis for function approximation for a *specific* given system. On the other hand, the universal approximation property of non-linear networks shows that NN provide a basis for *all* sufficiently smooth systems. Therefore, NN can be used to approximate smooth *f(x)* for *all rigid robotic systems,* effectively allowing the design of a single tunable controller for a class of systems. No regression matrix need be determined, for the same NN activation functions suffice for the whole class of plants.

Even the 1-layer NN, which is LIP, has this advantage. Note that the 1-layer NN is linear not in the *system parameters,* but in the NN weights. Even the LIP NN has a universal approximation property so that no regression matrix is needed.

Initial Tracking Errors and Initial NN Weights. It is now required to determine how to tune the NN weights to yield guaranteed closed-loop stability. Several cases are considered for NN controller design in this section. All of them need the following construction.

Since the NN approximation property holds on a compact set, one must define an *allowable initial condition set* as follows. Let the NN approximation property hold for the function *f(x)* given in (8.3.5) with a given accuracy c_N in (8.2.6) for all x inside the ball of radius $b_x > q_B$. Define the set of allowable initial tracking errors as

$$S_r = \{r \mid \|r\| < (b_x - q_B)/(c_0 + c_2)\}. \tag{8.3.15}$$

Note that the approximation accuracy of the NN determines size of S_r. For a larger NN (i.e. more hidden-layer units), c_N is small for a larger radius b_x. Thus, the allowed initial condition set S_r is larger. On the other hand, a more active desired trajectory (e.g. containing higher frequency components) results in a larger acceleration $q_d(t)$, which yields a larger bound q_B, thereby decreasing S_r. It is important to note the dependence of S_r on the PD design ratio K—both c_0 and c_2 depend on K.

A key feature of our the Initial Condition Requirement is its *independence of the NN initial weights*. This is in stark contrast to other techniques in the literature where the proofs of stability depend on selecting some initial stabilizing NN weights, which is very difficult to do.

8.4 Tuning Algorithms for Linear-in-the-Parameters NN

Suppose now that a LIP FLNN is used to approximate the nonlinear robot function (8.3.5) according to (8.2.15) with $\|\epsilon\| \leq \epsilon_N$ on a compact set, the ideal approximating weights W constant, and $\phi(x)$ selected as a basis. An estimate of *f(x)* is given by (8.3.14). Then the control law (8.3.7) becomes

$$\tau = \hat{W}^T \phi(x) + K_v r - v \tag{8.4.1}$$

and the closed-loop filtered error dynamics (8.3.8) are

$$M\dot{r} = -(K_v + V_m)r + \tilde{W}^T \phi(x) + (\epsilon + \tau_d) + v. \tag{8.4.2}$$

The next theorem derives the tuning law for a NN controller that is augmented by an *e*-mod term as in [Narendra and Annaswamy 1987].

It must now be assumed that the ideal weights *W* are constant and *bounded* so that

$$\|W\|_F \leq W_B, \tag{8.4.3}$$

with the bound W_B known. In [Polycarpou 1996] it is shown how to use standard adaptive robust techniques to avoid the assumption that the bound W_B is known.

THEOREM 8.4–1: *(NN Weight Tuning Algorithm).*

Let the desired trajectory $q_d(t)$ be bounded by q_B and the initial tracking error r(0) *be in S_r. Let the NN reconstruction error bound c_N and the disturbance bound dB be constants. Assume the ideal NN target weights are bounded by W_B as in (8.4.3). Let the control input for the robot arm be given by (8.4–1) with v(t)*=0 *and gain*

$$K_{v_{min}} > \frac{(\kappa W_B^2/4 + \varepsilon_N + d_B)(c_0 + c_2)}{b_x - q_B}. \tag{1}$$

Let the weight tuning be

$$\dot{\hat{W}} = F\phi r^T - \kappa F\|r\|\hat{W}, \tag{2}$$

with $F=F^T>0$ and n>0 a small design parameter. Then the filtered tracking error r(t) and the NN weight estimates W(t) are UUB with practical bounds given respectively by the right-hand sides of (8), (9). Moreover, the tracking error may be made as small as desired by increasing the tracking gain K_V.

Proof:

Let the NN approximation property (8.2.15) hold for the function f(x) given in (8.3.5) with a given accuracy c_N for all x in the compact set $S_x \equiv \{x \mid \|x\| < b_x\}$ with $b_X>q_B$. Let r(0)CSr. Then the approximation property holds at time 0.

Define the Lyapunov function candidate

$$L = \frac{1}{2}r^T M r^T + \frac{1}{2}tr\{\tilde{W}^T F^{-1}\tilde{W}\} \tag{3}$$

Differentiating yields

$$\dot{L} = r^T M\dot{r} + \frac{1}{2}r^T\dot{M}r + tr\{\tilde{W}^T F^{-1}\dot{\tilde{W}}\} \tag{4}$$

whence substitution from (8.4.2) yields

(5)

$$\dot{L} = -r^T K_v r + \frac{1}{2} r^T (\dot{M} - 2V_m) r + tr\{\tilde{W}^T (F^{-1}\dot{\tilde{W}} + \phi r^T)\} + r^T(\epsilon + \tau_d).$$

Then, using tuning rule (2) yields

$$\dot{L} = -r^T K_v r + \kappa \|r\| tr\{\tilde{W}^T (W - \tilde{W})\} + r^T(\varepsilon + \tau_d). \tag{6}$$

Since

$$tr\{\tilde{W}^T (W - \tilde{W})\} = < \tilde{W}, W >_F - \|\tilde{W}\|_F^2 \leq \|\tilde{W}\|_F \|W\|_F - \|\tilde{W}\|_F^2,$$

there results

$$\begin{aligned} \dot{L} &\leq - K_{v_{min}} \|r\|^2 + \kappa \|r\| \cdot \|\tilde{W}\|_F (W_B - \|\tilde{W}\|_F) + (\varepsilon_N + d_B)\|r\| \\ &= - \|r\| [K_{v_{min}} \|r\| + \kappa \|\tilde{W}\|_F (\|\tilde{W}\|_F - W_B) - (\varepsilon_N + d_B)], \end{aligned} \tag{7}$$

which is negative as long as the term in braces is positive. Completing the square yields

$$\begin{aligned} & K_{v_{min}} \|r\| + \kappa \|\tilde{W}\|_F (\|\tilde{W}\|_F - W_B) - (\varepsilon_N + d_B) \\ =& \kappa (\|\tilde{W}\|_F - W_B/2)^2 - \kappa W_B^2/4 + K_{v_{min}} \|r\| - (\varepsilon_N + d_B) \end{aligned}$$

which is guaranteed positive as long as

$$\|r\| > \frac{\kappa W_B^2/4 + (\varepsilon_N + d_B)}{K_{v_{min}}} \equiv b_r \tag{8}$$

or

$$\|\tilde{W}\|_F > W_B/2 + \sqrt{\kappa W_B^2/4 + (\varepsilon_N + d_B)/\kappa} \equiv b_W. \tag{9}$$

Thus, L is negative outside a compact set. Selecting the gain according to (1) ensures that the compact set defined by ||r||Šb$_r$ is contained in S$_r$, so that the approximation property holds throughout. This demonstrates the UUB of both ||r|| and ||W||F. ■

This proof is similar to [Narendra and Annaswamy 1987] but is modified to reflect the fact that the NN approximates only on a compact set. In this result one now requires the bound W_B on the ideal weights *W,* which appears in the PD

gain condition (1). Now, bounds are discovered both for the

tracking error *r(t)* and the weights *W(t)*. Note that no persistence of exictation condition is needed to establish the bounds on *W* with the modified weight tuning algorithm.

The NN weight tuning algorithm (2) consists of a backpropagation through time term plus a new second term. The importance of the *n,* term, called the e-modification, is that it adds a quadratric term in $\|\tilde{W}\|_F$ in (7), so that it is possible to establish that *L* is negative outside a compact set in the $(\|r\|, \|\tilde{W}\|_F)$ plane [Narendra and Annaswamy 1987]. The *e*-mod term makes the tuning law *robust* to unmodelled dynamics so that the PE condition is not needed. In [Polycarpou and Ioannou 1991] a projection algorithm is used to keep the NN weights bounded. In [Chen and Khalil 1992], [Chen and Liu 1994] a deadzone technique is employed.

Weight Initialization and On-Line Tuning. In the NN control schemes derived in this paper there is *no preliminary off-line learning phase*. The weights are simply initialized at zero, for then Figure 8.3.1 shows that the controller is just a PD controller. Standard results in the robotics literature [Dawson et al. 1990] show that a PD controller gives bounded errors if K_V is large enough. Therefore, the closed-loop system remains stable until the NN begins to learn. The weights are tuned *on-line in real-time* as the system tracks the desired trajectory. As the NN learns *f(x),* the tracking performance improves. This is a significant improvement over other NN control techniques where one must find some *initial stabilizing weights,* generally an impossible feat for complex nonlinear systems.

Bounds on the Tracking Error and NN Weight Estimation Errors. The right-hand side of (8) can be taken as a *practical bound on the tracking error* in the sense that *r(t)* will never stray far above it. It is important to note from this equation that the tracking error increases with the NN reconstruction error c_N and robot disturbances d_B, yet *arbitrarily small tracking errors may be achieved* by selecting large gains K_V. This is in spite of Barron's lower bound on *c*.

Note that the NN weights *W* are not guaranteed to approach the ideal unknown weights *W* that give good approximation of *f(x)*. However, this is of no concern as long as *W*–*W* is bounded, as the proof guarantees. This guarantees bounded control inputs so that the tracking objective can be achieved.

8.5 Tuning Algorithms for Nonlinear-in-the-Parameters NN

Now suppose that a 2-layer NN is used to approximate the robot function according to (8.2.5) with $||c||\check{S}c_N$ on a compact set, and the ideal approximating weights *W, V* constant. Then the control law (8.3.7) becomes

(8.5.1) $$\tau = \hat{W}^T\sigma(\hat{V}^T x) + K_v r - v.$$

The proposed NN control structure is shown in Figure 8.3.1.

The NLIP NN controller is far more powerful than the 1-layer FLNN as it is not necessary to select a basis of activation functions. In effect, the weights *V* are adjusted on-line to automatically provide a suitable basis. The control is nonlinear in the first-layer weights *V,* which presents complications in deriving suitable weight tuning laws. Auxiliary signal *v(t)* is a function to be detailed subsequently that provides robustness in the face of higher-order terms in the Taylor series arising from the NLIP problem.

Using the result (8.2.13) to properly address the NLIP problem, the closed- loop error dynamics (8.3.8) can be written as

$$M\dot{r} = -(K_v + V_m)r + \tilde{W}^T(\hat{\sigma} - \hat{\sigma}'\hat{V}^T x) + \hat{W}^T\hat{\sigma}'\tilde{V}^T x + w + v \qquad (8.5.2)$$

where the disturbance terms are

$$w(t) = \tilde{W}^T\hat{\sigma}'V^T x + W^T O(\tilde{V}^T x)^2 + \varepsilon + \tau_d \qquad (8.5.3)$$

Define

(8.5.4) $$Z \equiv \begin{bmatrix} W & 0 \\ 0 & V \end{bmatrix}$$

and Z, Z equivalently. It is not difficult to show that

$$\|w(t)\| \leq C_0 + C_1\|\tilde{Z}\|_F + C_2\|\tilde{Z}\|_F\|r\| \qquad (8.5.5)$$

with C_i known positive constants.

It is assumed that the ideal weights are bounded so that

$$\|Z\|_F \leq Z_B \qquad (8.5.6)$$

with Z_B known. (Standard adaptive robust control techniques can be used to lift the assumption that Z_B is known [Polycarpou 1996].)

The next theorem presents the most powerful NN controller in this chapter.

THEOREM 8.5–1: *(Augmented Backprop Weight Tuning for Multi-layer NN Controller).*

Let the desired trajectory $q_d(t)$ be bounded by q_B and the initial tracking error $r(0)$ be in S_r. Let the ideal target NN weights be bounded by known Z_B. Take the control input for the robot dynamics (8.3.1) as (8.5.1) with PD gain satisfying

(1)
$$K_{v_{min}} > \frac{(C_0 + \kappa C_3^2/4)(c_0 + c_2)}{b_x - q_B},$$

where C_3 is defined in the proof. Let the robustifying term be

(2)
$$v(t) = -K_z(\|\hat{Z}\|_F + Z_B)r$$

with gain

(3)
$$K_z > C_2.$$

Let NN weight tuning be provided by

(4)
$$\dot{\hat{W}} = F\hat{\sigma}r^T - F\hat{\sigma}'\hat{V}^T x r^T - \kappa F\|r\|\hat{W}$$
$$\dot{\hat{V}} = Gx(\hat{\sigma}'^T\hat{W}r)^T - \kappa G\|r\|\hat{V} \quad (5)$$

with any constant matrices $F=F^T>0$, $G=G^T>0$, and $n>0$ a small scalar design parameter. Then the filtered tracking error $r(t)$ and NN weight estimates V, W are UUB, with the bounds given specifically by (10) and (11). Moreover, the tracking error may be kept as small as desired by increasing the gains K_V in (8.5.1).

Proof:

Let the NN approximation property (8.2.5) hold for the function $f(x)$ given in (8.3.5) with a given accuracy ε_N for all x in the compact set $S_x \equiv \{x \mid \|x\| < b_x\}$ with $b_x>q_B$. Let $r(0)\subset S_r$. Then the approximation property holds at time 0.

Define the Lyapunov function candidate

(6)
$$L = \frac{1}{2}r^T M(q)r + \frac{1}{2}tr\left\{\tilde{W}^T F^{-1}\tilde{W}\right\} + \frac{1}{2}tr\left\{\tilde{V}^T G^{-1}\tilde{V}\right\}$$

Differentiate (7)
$$\dot{L} = r^T M\dot{r} + \frac{1}{2}r^T\dot{M}r + tr\{\tilde{W}^T F^{-1}\dot{\tilde{W}}\} + tr\{\tilde{V}^T G^{-1}\dot{\tilde{V}}\}.$$

Substituting now from the error system (8.5.2) yields

$$\begin{aligned}\dot{L} = &- r^T K_v r + \frac{1}{2} r^T (\dot{M} - 2V_m) r \\ &+ tr\{\tilde{W}^T (F^{-1}\dot{\tilde{W}} + \hat{\sigma} r^T - \sigma' \hat{V}^T x r^T)\} \\ &+ tr\{\tilde{V}^T (G^{-1}\dot{\tilde{V}} + x r^T \hat{W}^T \hat{\sigma}')\}\end{aligned} \tag{8}$$

The tuning rules give

$$\begin{aligned}\dot{L} &= - r^T K_v r + \kappa \|r\| tr\{\tilde{W}^T (W - \tilde{W})\} \\ &\quad + \kappa \|r\| tr\{\tilde{V}^T (V - \tilde{V})\} + r^T (w + v) \\ &= - r^T K_v r + \kappa \|r\| tr\{\tilde{Z}^T (Z - \tilde{Z})\} + r^T (w + v).\end{aligned}$$

Since

$$tr\{\tilde{Z}^T (Z - \tilde{Z})\} = < \tilde{Z}, Z > - \|\tilde{Z}\|_F^2 \leq \|\tilde{Z}\|_F \|Z\|_F - \|\tilde{Z}\|_F^2,$$

there results

$$\begin{aligned}\dot{L} \leq &- r^T K_v r + \kappa \|r\| \cdot \|\tilde{Z}\|_F (Z_B - \|\tilde{Z}\|_F) \\ &- K_Z (\|\hat{Z}\|_F + Z_B) \|r\|^2 + \|r\| \cdot \|w\| \\ \leq &- K_{v_{min}} \|r\|^2 + \kappa \|r\| \cdot \|\tilde{Z}\|_F (Z_B - \|\tilde{Z}\|_F) \\ &- K_Z (\|\hat{Z}\|_F + Z_B) \|r\|^2 \\ &+ \|r\| \left[C_0 + C_1 \|\tilde{Z}\|_F + C_2 \|r\| \cdot \|\tilde{Z}\|_F \right] \\ \leq &- \|r\| \left\{ K_{v_{min}} \|r\| - \kappa \cdot \|\tilde{Z}\|_F (Z_B - \|\tilde{Z}\|_F) - C_0 - C_1 \|\tilde{Z}\|_F \right\}\end{aligned}$$

where Kv_{min} is the minimum singular value of K_V, and the last inequality holds due to (3).

L is negative as long as the term in braces is positive. Defining $C_3 = Z_B + C_1/n$ and completing the square yields

$$\begin{aligned}&K_{v_{min}} \|r\| - \kappa \cdot \|\tilde{Z}\|_F (Z_B - \|\tilde{Z}\|_F) - C_0 - C_1 \|\tilde{Z}\|_F \\ &= \kappa (\|\tilde{Z}\|_F - C_3/2)^2 + K_{v_{min}} \|r\| - C_0 - \kappa C_3^2/4\end{aligned} \tag{9}$$

which is guaranteed positive as long as either

$$\|r\| > \frac{C_0 + \kappa C_3^2/4}{K_{v_{min}}} \equiv b_r \tag{10}$$

or

$$\|\tilde{Z}\|_F > C_3/2 + \sqrt{C_0/\kappa + C_3^2/4} \equiv b_Z. \tag{11}$$

Thus, L is negative outside a compact set. According to the LaSalle extension [Lewis et al. 1993] this demonstrates the UUB of both ||r|| and $||Z||_F$ as long as the control remains valid within this set. However, the PD gain condition (1) shows that the compact set defined by ||r||Šb$_r$ is contained in S_r, so that the approximation property holds throughout. ■

The first terms in the tuning algorithms (4), (5) are nothing but backpropagation of the tracking error through time. The last terms are the Narendra *e*-mod, and the second term in (4) is a novel second-order term needed due to the NLIP of the NN. The robustifying term *v(t)* is required also due to the NLIP problem.

The comments appearing after Theorem 8.4.1 are germane here. Specifically, there is no preliminary off-line tuning phase and NN weight tuning occurs on-line in real-time simultaneously with control action. Weight initialization is not an issue in the proof and it is not necessary to provide initial stabilizing weights; the weights are simply initialized so that the NN output is equal to zero, for then the PD loop keeps the system stable until the NN begins to learn. However, practical experiments [Gutierrez and Lewis 1998] show that it is important to initialize the weights suitably. A good choice is to select *V(0)* randomly and *W(0)* equal to zero.

In practice it is not necessary to compute the constants c_0, c_1, c_2, C_0, C_1, C_2, Z_B nor determine S_r. The size *L* of the NN and the PD gains K_V are simply selected large and a simulation is performed. The simulation is then repeated with a different *L* and K_V. Based on the difference in behavior between the two simulations, *L* and K_V can be modified.

Straight Backpropagation Weight Tuning. The backprop algorithm (usually in discrete-time form) has been proposed innumerable times in the literature for closed-loop control. It can be shown that if the NN approximation error *c* is zero, the disturbances are $v_d(t)$ zero, and there are no higher-order terms in the Taylor series (8.2.12), then the straight backprop algorithm

$$\begin{aligned} \dot{\hat{W}} &= F\hat{\sigma}r^T \\ \dot{\hat{V}} &= Gx(\hat{\sigma}'^T\hat{W}r)^T \end{aligned} \tag{8.5.7}$$

may be used for closed-loop control instead of (4), (5). PE is required to show that the NN weights are bounded using straight backprop. The conditions mentioned are very restrictive and do not occur in practice; they essentially require the robot arm to be linear (e.g. 1=link). Moreover, PE conditions are not easy to guarantee in NN.

Passivity Properties of NN Controllers

The NN used in this paper are static feedforward nets, but since they appear in a closed feedback loop and are tuned using differential equations, they are dynamical systems. Therefore, one can discuss the *passivity* of these NN. In general a NN cannot be guaranteed to be passive. However, the NN controllers in this paper have some important passivity properties that result in robust closed-loop performance.

The system *x=f (x, u),y=h(x, u)* is said to be *passive* if it verifies an equality of the so-called *power form* [Slotine and Li 1991]

$$\dot{L}(t) = y^T u - g(t) \tag{8.5.8}$$

for some lower-bounded *L(t)* and some *g(t)*Š0. That is,

$$\int_0^T y^T(\tau)u(\tau)d\tau \geq \int_0^T g(\tau)d\tau - \gamma^2 \tag{8.5.9}$$

for all *T*Š0 and some γŠ0. The system is *dissipative* if it is passive and in addition

$$\int_0^\infty y^T(\tau)u(\tau)d\tau \neq 0 \ \text{ implies } \ \int_0^\infty g(\tau)d\tau > 0. \tag{8.5.10}$$

A special sort of dissipativity occurs if *g(t)* is a quadratic function of ||*x*|| with bounded coefficients. We call this *state strict passivity (SSP);* then, the norm of the internal states is bounded in terms of the power delivered to the system. Somewhat surprisingly, the concept of SSP has not been extensively used in the literature [Lewis et al. 1993], [Seron et al. 1994], though see [Goodwin et al. 1984] where input and output strict pasivity are defined. SSP turns out to be pivotal in studying the passivity properties of NN controllers, and allows one to conclude some internal boundedness properties without any assumptions of persistence of excitation.

Passivity of the Robot Tracking Error Dynamics

The error dynamics in this paper (e.g. (8.5.2)) appear in Figure 8.5.1 and have the form

$$M\dot{r} = -(K_v + V_m)r + \xi_0 \tag{8.5.11}$$

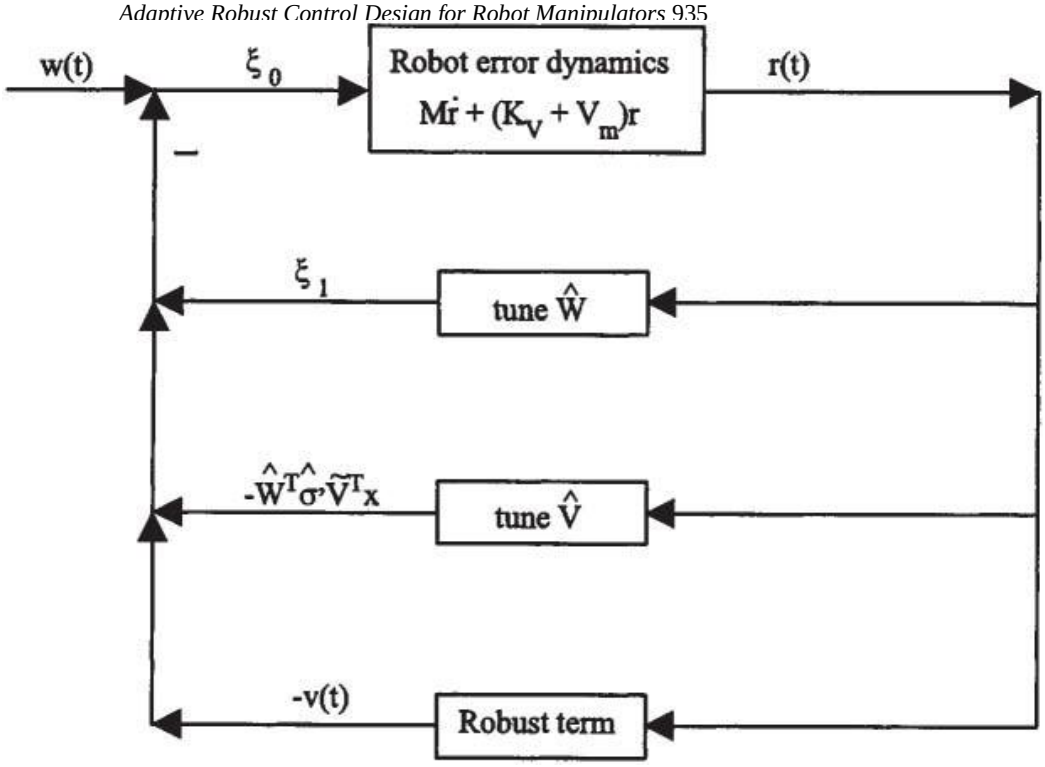


Figure 8.5.1: Two-layer neural net closed-loop error system.

where *r(t)* is the filtered tracking error and *$0(t)* is appropriately defined. This system satisfies the following strong passivity property.

THEOREM 8.5–2: *(SSP of Robot Error Dynamics).*

The dynamics (8.5.11) from $0(t) to r(t) are a state strict passive system.

Proof:

Take the nonnegative function

$$L = \frac{1}{2} r^T M(q) r$$

so that, using (8.5.11), one obtains

$$\dot{L} = r^T M \dot{r} + \frac{1}{2} r^T \dot{M} r = -r^T K_v r + \frac{1}{2} r^T (\dot{M} - 2V_m) r + r^T \xi_0$$

whence, the skew-symmetry property yields the power form

$$\dot{L} = r^T \xi_0 - r^T K_v r.$$

This is the power delivered to the system minus a quadratic term in ||r||, verifying state strict passivity. ■

Passivity Properties of 2-layer NN Controllers

The closed-loop system is in Figure 8.3.1, where the NN appears in an inner feedback linearization loop. The error dynamics for the 2-layer NN controller are given by (8.5.2). The closed-loop error system appears in Figure 8.5.1, with the signal $\$_1$ defined as

$$\xi_1(t) = -\tilde{W}^T(\hat{\sigma} - \hat{\sigma}'\hat{V}^T x) \tag{8.5.12}$$

Note the role of the NN in the error dynamics, where it is decomposed into two effective blocks appearing in a typical feedback configuration.

We now reveal the passivity properties engendered by straight back-propagation tuning (8.5.7). To prove this algorithm, one uses the error dynaqmics in a different form than (8.5.2), so that in Figure 8.5.1 one has $\xi_1(t) = -\tilde{W}^T\hat{\sigma}$.

THEOREM 8.5–3: *(Passivity of Backprop NN Tuning Algorithm).*

The simple backprop weight tuning algorithm (8.5.7) makes the map from $r(t)$ *to* $-\tilde{W}^T\hat{\sigma}$*, and the map from r(t)* *to* $-\hat{W}^T\hat{\sigma}'\tilde{V}^T x$*, both passive maps.*

Proof:

The dynamics with respect W, V are

$$\dot{\tilde{W}} = -F\hat{\sigma}r^T \tag{1}$$

$$\dot{\tilde{V}} = -Gx(\hat{\sigma}'^T\hat{W}r)^T \tag{2}$$

1. Selecting the nonnegative function

$$L = \frac{1}{2}tr\{\tilde{W}^T F^{-1}\tilde{W}\}$$

and evaluating L along the trajectories of (1) yields

$$\dot{L} = tr\{\tilde{W}^T F^{-1}\dot{\tilde{W}}\} = -tr\{\tilde{W}^T\hat{\sigma}r^T\} = r^T(-\tilde{W}^T\hat{\sigma}),$$

which is in power form (8.5.8).

2. Selecting the nonnegative function

$$L = \frac{1}{2}tr\{\tilde{V}^T G^{-1}\tilde{V}\}$$

and evaluating along the trajectories of (2) yields

$$\dot{L} = tr\{\tilde{V}^T G^{-1} \dot{\tilde{V}}\} = -tr\{\tilde{V}^T x(\hat{\sigma}'^T \hat{W} r)^T\} = r^T(-\hat{W}^T \hat{\sigma}' \tilde{V}^T x).$$

which is in power form. ■

Thus, the robot error system in Figure 8.5.1 is state strict passive (SSP) and the weight error blocks are passive; this guarantees the passivity of the closed- loop system. Using the passivity theorem [Slotine and Li 1991] one may now conclude that the input/output signals of each block are bounded as long as the external inputs are bounded.

Unfortunately, though passive, the closed-loop system cannot be guaranteed to be SSP, so that when disturbances are nonzero, this does not yield boundedness of the internal states of the weight blocks (i.e. *W, V*) unless those blocks are *observable,* that is persistently exciting (PE).

The next result shows why a PE condition is not needed with the modified weight update algorithm given in Theorem 8.5.1.

THEOREM 8.5–4: *(SSP of Augmented Backprop NN Tuning Algorithm). The modified weight tuning algorithms in Theorem 8.5.1 make the map from* $r(t)$ *to* $-\tilde{W}^T(\hat{\sigma} - \hat{\sigma}'\hat{V}^T x)$*, and the map from* $r(t)$ *to* $-\hat{W}^T\hat{\sigma}'\tilde{V}^T x$*, both state strict passive (SSP) maps.*

Proof:

The dynamics relative to W, V using the tuning algorithms in Theorem 8.5.1 are given by

$$\dot{\tilde{W}} = -F\hat{\sigma}r^T + F\hat{\sigma}'\hat{V}^T x r^T + \kappa F\|r\|\hat{W}$$

$$\dot{\tilde{V}} = -Gx(\hat{\sigma}'^T\hat{W}r)^T + \kappa G\|r\|\hat{V}.$$

1. Selecting the nonnegative function

$$L = \frac{1}{2}tr\{\tilde{W}^T F^{-1}\tilde{W}\}$$

and evaluating L yields

$$\begin{aligned}\dot{L} =& tr\{\tilde{W}^T F^{-1}\dot{\tilde{W}}\} \\ =& tr\left\{\left[-\tilde{W}^T(\hat{\sigma} - \hat{\sigma}'^T\hat{V}^T x)\right] r^T + \kappa\|r\|\tilde{W}^T\hat{W}\right\}\end{aligned}$$

Since

$$tr\{\tilde{W}^T(W-\tilde{W}) = <\tilde{W},\ W>_F - \|\tilde{W}\|_F^2$$
$$\leq \|\tilde{W}\ \|_F \cdot \|W\|_F - \|\tilde{W}\|_F^2,$$

there results

$$\dot{L} \leq r^T\left[-\tilde{W}^T(\hat{\sigma}-\hat{\sigma}'\hat{V}^T x)\right] - \kappa\|r\|\cdot(\|\tilde{W}\|_F^2 - \|\tilde{W}\|_F\|W\|_F)$$
$$\leq r^T\left[-\tilde{W}^T(\hat{\sigma}-\hat{\sigma}'\hat{V}^T x)\right] - \kappa\|r\|\cdot(\|\tilde{W}\|_F^2 - W_B\|\tilde{W}\|_F)$$

which is in power form with the last function quadratic in

2. Selecting the nonnegative function

$$L = \frac{1}{2}tr\{\tilde{V}^T G^{-1}\tilde{V}\}$$

and evaluating L yields

$$\dot{L} = tr\{\tilde{V}^T G^{-1}\dot{\tilde{V}}\}$$
$$= r^T(-\hat{W}^T\hat{\sigma}'\tilde{V}^T x) - \kappa\|r\|(\|\tilde{V}\|_F^2 - <\tilde{V},\ V>_F)$$
$$\leq r^T(-\hat{W}^T\hat{\sigma}'\tilde{V}^T x) - \kappa\|r\|(\|\tilde{V}\|_F^2 - V_B\|\tilde{V}\|)$$

which is in power form with the last function quadratic in $\|V\|_F$. ■

The SSP of both the robot dynamics and the weight tuning blocks does guarantee SSP of the closed-loop system, so that *the norms of the internal states are bounded in terms of the power delivered to each block*. Then, boundedness of input/output signals assures state boundedness without any sort of observability or PE requirement.

Definition of Passive NN and Robust NN. We define a dynamically tuned NN as *passive* if, in the error formulation, the tuning guarantees the passivity of the weight tuning subsystems. Then, an extra PE condition is needed to guarantee boundedness of the weights. This PE condition is generally in terms of the outputs of the hidden layers of the NN. We define a dynamically tuned NN as *robust* if, in the error formulation, the tuning guarantees the SSP of the weight tuning subsystem. Then, no extra PE condition is needed for boundedness of the weights. Note that (1) SSP of the open-loop plant error system is needed in addition for tracking stability, and (2) the NN passivity properties are dependent on the weight tuning algorithm used.

Passivity Properties of 1-Layer NN Controllers

In a similar fashion, it is shown that the FLNN controller tuning algorithm makes the system passive, so that an additional PE condition is needed to verify internal stability of the NN weights. On the other hand, the augmented tuning algorithm in Theorem 8.4.1 yields SSP, so that no PE is needed.

8.6 Summary

Neural network controller design algorithms were given for a general class of industrial Lagrangian motion systems characterized by the rigid robot arms. The design procedures are based on rigorous nonlinear derivations and stability proofs, and yield a *multiloop intelligent control structure* with NN in some of the loops. NN weight tuning algorithms were given that do not require complicated initialization procedures or any off-line learning phase, work on-line in real-time, and offer guaranteed tracking and bounded NN weights and control signals. The NN controllers given here are *model-free controllers* in that they work for any system in a prescribed class without the need for extensive modeling and preliminary analysis to find a 'regression matrix'. Unlike standard robot adaptive controllers, they do not require linearity in the parameters (see also [Colbaugh and Seraji 1994] which does not need LIP). Proper design allows the NN controllers to avoid requirements such as persistence of excitation and certainty equivalence. NN passivity and robustness properties are defined and studied here.

REFERENCES

[Åström and Wittenmark 1989] K.J.Åström and B.Wittenmark, *Adaptive Control,* Addision Wesley, Reading, MA, 1989.

[Barron 1993] Barren, A.R., "Universal approximation bounds for superpositions of a sigmoidal function," *IEEE Trans. Info. Theory,* vol. 39, no. 3, pp. 930–945, May 1993.

[Chen and Khalil 1992] F.-C.Chen and H.K.Khalil, "Adaptive control of nonlinear systems using neural networks," *Int. J. Control,* vol. 55, no. 6, pp. 1299–1317, 1992.

[Chen and Liu 1994] F.-C.Chen and C.-C.Liu, "Adaptively controlling nonlinear continuous-time systems using multilayer neural networks," *IEEE Trans. Automat. Control,* vol. 39, no. 6, pp. 1306–1310, June 1994.

[Colbaugh and Seraji 1994] R.Colbaugh, H.Seraji, and K.Glass, "A new class of adaptive controllers for robot trajectory tracking," *J. Robotic Systems,* vol. 11, no. 8, pp. 761–772, 1994.

[Craig 1988] Craig, J.J., *Adaptive Control of Mechanical Manipulators,* Reading, MA: Addison-Wesley, 1988.

[Dawson et al. 1990] Dawson, D.M., Z.Qu, F.L.Lewis, and J.F.Dorsey, "Robust control for the tracking of robot motion," *Int. J. Control,* vol. 52, no. 3, pp. 581–595, 1990.

[Goodwin et al. 1984] Goodwin, C.G., and K.S.Sin, *Adaptive Filtering, Prediction, and Control,* Prentice-Hall, New Jersey, 1984.

[Gorinevsky 1995] D.Gorinevsky, "On the persistency of excitation in radial basis function network identificaiton of nonlinear systems," *IEEE Trans. Neural Networks,* vol. 6, no. 5, pp. 1237–1244, Sept. 1995.

[Gutierrez and Lewis 1998] L.B.Gutierrez and F.L.Lewis, "Implementation of a neural net tracking controller for a single flexible link: comparison

459

with PD and PID controllers," *IEEE Trans. Industrial Electronics,* to appear, April 1998.

[Haykin 1994] S.Haykin, *Neural Networks,* IEEE Press, New York, 1994. [Hornik and Stinchombe 1989] K.Hornik, M.Stinchombe, and H.White, "Multilayer feedforward networks are universal approximators," *Neural Networks,* vol. 2, pp. 359–366, 1989.

[Ioannou and Kokotovic 1984] P.A.Ioannou and P.V.Kokotovic, "Instability analysis and improvement of robustness of adaptive control," *Automatica,* vol. 20, no. 5, pp. 583–594, 1984.

[Kim and Lewis 1998] Y.H.Kim and F.L.Lewis, *High-Level Feedback Control with Neural Networks,* World Scientific, Singapore, 1998.

[Kreisselmeier and Anderson 1986] Kreisselmeier, G., and B.Anderson, "Robust model reference adaptive control," *IEEE Trans. Automat. Control,* vol. AC-31, no. 2, pp. 127–133, Feb. 1986.

[Landau 1979] Y.D.Landau, *Adaptive Control,* Marcel Dekker, Basel, 1979.

[Lewis 1999] F.L.Lewis, "Nonlinear Network Structures for Feedback Control", *Asian Journal of Control,* vol. 1, no. 4, pp.205–228, December 1999.

[Lewis et al. 1993] F.L.Lewis, C.T.Abdallah, and D.M.Dawson, *Control of Robot Manipulators,* New York: Macmillam, 1993.

[Lewis et al. 1999] F.L.Lewis, S.Jagannathan, and A.Yesildirek, *Neural Network Control of Robot Manipulators and Nonlinear Systems,* Taylor and Francis, London, 1999.

[Lewis and Kim 1998] F.L.Lewis and Y.H.Kim, "Neural Networks for Feedback Control," Encyclopedia of Electrical and Electronics Engineering, ed. J.G.Webster, New York: Wiley, 1998. To appear.

[Lewis et al. 1993] Lewis, F.L., K.Liu, and A.Yesildirek, "Neural net robot controller with guaranteed tracking performance," *Proc. Int. Symp. Intelligent Control,* pp. 225–231, Chicago., Aug. 1993.

[Lewis et al. 1995] Lewis, F.L., K.Liu, and A.Yesildirek, "Neural net robot controller with guaranteed tracking performance," *IEEE Trans. Neural Networks,* vol. 6, no. 3, pp. 703–715, 1995.

[Lewis et al. 1997] F.L.Lewis, K.Liu, and S.Commuri, "Neural networks and fuzzy logic systems for robot control," in *Fuzzy Logic and Neural Network Applications,* ed. F.Wang, World Scientific Pub., to appear, 1997.

[Lewis et al. 1996] F.L.Lewis, A.Yesildirek, and K.Liu, "Multilayer neural net robot controller: structure and stability proofs," *IEEE Trans. Neural Networks,* vol. 7, no. 2, pp. 1–12, Mar. 1996.

[Miller et al. 1991] W.T.Miller, R.S.Sutton, P.J.Werbos, ed., *Neural Networks for Control,* Cambridge: MIT Press, 1991.

[Narendra 1991] K.S.Narendra, “Adaptive Control Using Neural Networks,” *Neural Networks for Control,* pp 115–142. ed. W.T.Miller, R.S.Sutton, P.J.Werbos, Cambridge: MIT Press, 1991.

[Narendra and Annaswamy 1987] K.S.Narendra and A.M.Annaswamy, “A new adaptive law for robust adaptive control without persistent excitation,” *IEEE Trans. Automat. Control,* vol. 32, pp. 134–145, Feb., 1987.

[Narendra and Parthasarathy 1991] Narendra, K.S., and K. Parthasarathy, “Gradient methods for the optimization of dynamical systems containing neural networks,” *IEEE Trans. Neural Networks,* vol. 2, no. 2, pp. 252–262, Mar. 1991.

[Polycarpou 1996] M.M.Polycarpou, “Stable adaptive neural control scheme for nonlinear systems,” *IEEE Trans. Automat. Control,* vol. 41, no. 3, pp. 447–451, Mar. 1996.

[Polycarpou and Ioannou 1991] M.M.Polycarpou and P.A.Ioannou, “Identification and control using neural network models: design and stability analysis,” *Tech. Report 91–09–01,* Dept. Elect. Eng. Sys., Univ. S. Cal., Sept. 1991.

[Rovithakis and Christodoulou 1994] G.A.Rovithakis and M.A. Christodoulou, “Adaptive control of unknown plants using dynamical neural networks,” *IEEE Trans. Systems, Man, and Cybernetics,* vol. 24, no. 3, pp. 400–412, Mar. 1994.

[Sadegh 1993] N.Sadegh, “A perceptron network for functional identification and control of nonlinear systems,” *IEEE Trans. Neural Networks,* vol. 4, no. 6, pp. 982–988, Nov. 1993.

[Sanner and Slotine 1991] R.M.Sanner and J.-J.E.Slotine, “Stable adaptive control and recursive identification using radial gaussian networks,” *Proc. IEEE Conf. Decision and Control,* Brighton, 1991.

[Seron et al. 1994] Seron, M.M., D.J.Hill, and A.L.Fradkov, “Adaptive passification of nonlinear systems,” *Proc. IEEE Conf. Decision and Control,* pp. 190–195, Dec. 1994.

[Slotine 1988] Slotine, J.-J.E., “Putting physics in control the example of robotics,” *IEEE Control Systems Magazine,* pp. 12–17, Dec. 1988.

[Slotine and Li 1991] J.-J.Slotine and W.Li, *Applied Nonlinear Control,* Prentice Hall, New Jersey, 1991.

[Spong and Vidyasagar 1989] Spong, M.W., and M.Vidyasagar, *Robot Dynamics and Control,* New York: Wiley, 1989.

[Wang 1997] L.-X.Wang, *A course in fuzzy systems and control,* Prentice-Hall, New Jersey, 1997.

[Werbos 1989] P.J.Werbos, “Back propagation: past and future,” *Proc. 1988 Int. Conf. Neural Nets,* vol. 1, pp. I343-I353, 1989.

[Werbos 1992] P.J.Werbos, “Neurocontrol and supervised learning: an overview and evaluation,” in *Handbook of Intelligent Control,* ed. D.A. White and D.A.Sofge, New York: Van Nostrand Reinhold, 1992.

[White and Sofge 1992] D.A.White and D.A.Sofge, ed. *Handbook of Intelligent Control,* New York: Van Nostrand Reinhold, 1992.

Chapter 10

Robot Control Implementation and Software

The diversity of robot manipulator research along with the complex requirements of the associated hardware/software systems has always presented a challenge for software developers. As a result, many of the previously developed software control platforms were complex, expensive, and not very user friendly. Even though several of the previous platforms were designed to provide an open architecture-based system, very few of the previous platforms have been reused. To address previous disadvantages, this chapter describes the design and implementation of a software control platform called the Robotic Platform. The Robotic Platform is an open software development platform for robot manipulator applications. It includes hardware interfacing, servo control, trajectory generation, 3D simulation, a graphical user interface, and a math library. As opposed to distributed solutions, the Robotic Platform implements all of these components on a single hardware platform, with a single programming language (C++), and on a single operating system while guaranteeing hard real-time performance. This design leads to an open architecture that is less complex, easier to use, and easier to extend, and hence, builds on the following state-of-the-art technologies and general purpose components to further increase simplicity and reliability: i) PC technology, ii) the QNX Real-Time Operating System, iii) the Open Inventor and STL libraries, iv) object-oriented design, and v) an easy-to-use, previously-developed, low-level control environment.

517

10.1 Introduction

Since the construction of a software control platform requires building blocks that cover a wide range of disciplines (see Figure 10.1.1), it would be desirable to create a common generic platform that can be reused by researchers for different applications. Considering the variety of robotic applications and research areas, this task is made even more challenging due to the fact that robot manipulator vendors often supply the user with proprietary robot control languages that run on proprietary hardware components. Due to the lack of flexibility and performance of proprietary robot control languages, some of the previous work has focused on building robot control libraries on top of a commonly used programming language (RCCL [Lloyd et al. 1988] and ARCL [Corke] are examples of such libraries). While many of the previous software approaches achieved new levels of flexibility and performance by using a common programming language, many software control platforms developed in the 80's and early 90's were inherently complex due to the limitations of the operating systems and the hardware components of that time. That is, most operating systems did not support real-time programming, and hence, fostered the development of projects such as RCI [Lloyd 1990] and Chimera [Stewart 1989]. In addition, procedural programming languages, such as "C", tend to reach their limits with regard to reusability for complex projects. In addition, the limited performance of hardware components of that era forced system developers to utilize distributed architectures (see [Miller 1991], [Kapoor 1996], and [Pelich 1996]) that integrated a mix of proprietary hardware and software. Besides the obvious advantages of distributed systems (e.g., greater extensibility and more computational power), there are several disadvantages. Specifically, a distributed architecture increases the complexity of the software significantly. Additionally, hard real-time behavior over network connections often requires expensive proprietary hardware. Generally, the overall hardware cost is also higher; furthermore, users have to familiarize themselves with different hardware architectures and operating systems. Even though many software control platforms have attempted to be flexible, reconfigurable, and open, these platforms are seldom reused (compared to non-robotic platforms like Open Inventor or Corba). Apparently, engineers consider it faster and easier to develop their applications from scratch. Indeed, as many researchers have noted, the learning curve of installing, learning, and modifying previously developed software control platforms of the past is extremely steep.

Over the last ten years, many innovations in the computing area have occurred. Specifically, the advent of object-oriented software design [Stroustrup 1991] facilitated the management of more complex projects

while also fostering code reuse and flexibility. For example, robot control libraries like RIPE [Miller 1991], MMROC+ [Zielinski 1997], OSCAR [Kapoor 1996], and ZERO++ [Pelich 1996] utilized object-oriented techniques in robot programming. The engineering community has also witnessed the proliferation of real-time Unix-like operating systems for the PC [QSSL], which facilitates the replacement of proprietary hardware components for real-time control [Costescu 1999]. Likewise, in the hardware sector, the engineering community has witnessed the advent of high-speed, low-cost PCs, fast 3D graphics video boards, and inexpensive motion control cards. Consequently, the PC platform now provides versatile functionality, and hence, makes complex software architectures and proprietary hardware components superfluous. As a result of these technological advances, the QMotor Robotic Toolkit (QMotor RTK) [Loffler 2001] was developed. The QMotor RTK was one of the first software control platforms to integrate real-time manipulator control and the graphical user interface (GUI) all on a single PC. Despite, the many advantages of the QMotor RTK, it lacked some capabilities due to the limitations of the real-time operating system (i.e., QNX4) on which it was based. For example, it lacked a 3D simulation capability, and it did not support the use of threads.

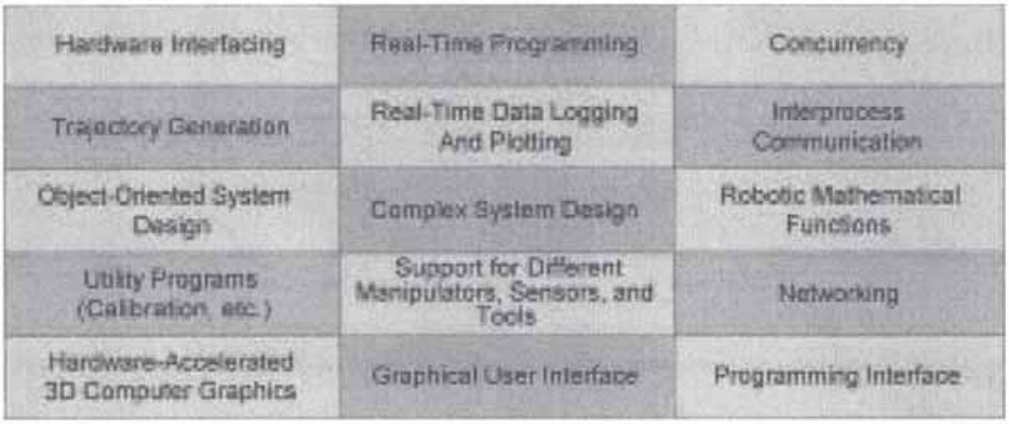


Figure 10.1.1: Building Blocks of a Robotic Software Control Platform

In the late 1990's, QSSL, one of the leading real-time software development houses, substantially upgraded QNX4 with the release of QNX6 [QSSL] (i.e., QNX6/Neutrino operating system). This microkernel-based operating system is probably the most advanced real-time operating system currently available; furthermore, it has additional components for software development and multimedia applications. Indeed, the new attributes of QNX6 greatly facilitated the potential capabilities of an upgrade of the QMotor RTK, in fact so much so, QMotor RTK was completely transformed into a new software control platform call the Robotic Platform [Bhargava

2001]. The rest of this chapter provides a broad overview of the Robotic Platform by examining its advantages, its design, and its operation. The word “broad” needs to be emphasized because it is really impossible to give a detailed explanation of how a software control platform should be developed for robot manipulators in one chapter of a book. With that being said, it is hope that this chapter will give the reader a better understanding of the associated complexities.

10.2 Tools and Technologies

Given recent technological advances, it now seems almost obvious that new software control platforms should integrate servo control loops, trajectory generation, task level programs, GUI programs, and 3D simulation in a homogeneous software architecture. That is, next-generation software control platforms should utilize one hardware platform (e.g., the PC), only one operating system (e.g., the QNX6 Real-Time Operating System [QSSL]), and only one programming language (e.g., C++ [Stroustrup 1998]). The advantages of this next-generation software control platform are as follows:

Simplicity. A homogeneous non-distributed architecture is much smaller and simpler than a distributed inhomogeneous architecture. It is easier to install, easier to understand, and easier to extend. Simplicity is critical with regard to motivating code reuse of the platform for different applications.

Performance. The homogeneous, non-distributed architecture also ensures high performance and hard real-time behavior, since overhead due to interprocess communication is minimal.

Flexibility at all Levels. Every component of the platform is open for extensions and modifications. Many past platforms have utilized an open architecture at some levels, but other levels had been implemented on proprietary hardware such that they could not be modified.

Cost. The Robotic Platform requires fewer hardware components than a distributed platform. Basically, a single PC with one or more input/output (I/O) boards is sufficient. Additionally, PC hardware is very cost effective as compared to other hardware platforms.

To explain the advantages in more detail and delineate how the Robotic Platform reduces software development and complexity, the general purpose tools and technologies that are used to develop the Robotic Platform are

now examined. It seems logical to begin this discussion with the hardware engine, namely the standard desktop PC. Due to its popularity in the consumer market, the standard desktop PC has evolved dramatically over the past 20 years. While in the past, only expensive UNIX workstations provided the processing power necessary to control robotic systems, the PC has caught up or even exceeded the performance of workstations [Costescu 1999]. Compared to UNIX workstations, a PC based system allows for a greater variety of hardware and software components. Additionally, these components and the PC itself are usually cheaper than their UNIX counterparts; furthermore, the PC is a well-known platform that is comfortable for most software developers.

The second most important part of any software control platform is the operating systems. Indeed since reliability is extremely important for robot manipulation, the QNX6 Real-Time Operating Systems by QSSL [QSSL] was selected. The programming interface of QNX6 is compliant with the POSIX standards and is the first platform that combines the following features:

Hard Real-Time. QNX6 provides hard real-time response (e.g., it can execute a control loop at a certain frequency without falling behind). The real- time functionality is integrated in the microkernel.

Self-Hosted Development. The development and the execution of software are performed in the same environment and on the same PC.

Fast 3D Graphics. QNX6 provides support for hardware-accelerated 3D, as required for the graphical simulation of a robotic work cell.

Threads. QNX6 supports the concurrent execution of processes, known as threads.

Device Driver Architecture. It is very easy to develop device drivers under QNX6, as is required for integrating different robotic hardware.

Cost. QNX6 is also very cost-effective as it is free for non-commercial use and runs on low-cost standard PCs.

The third most important part or design aspect of any software control platform is the programming philosophy. With regard to developing robot manipulator control software, object-oriented programming has three main benefits over procedural programming. First, it provides language constructs that allow for a much easier programming interface. For example, a matrix multiplication can be expressed by a simple “*”, similar to MATLAB programming. Second, object-oriented programming allows

for a system architecture that is very flexible but yet very simple. That is, the components (classes) of a system can have a built-in default behavior and default settings. The use of this default behavior and/or default settings allows the programmer to reduce the code size. The programmer, however, can still override the default behavior for specific applications. Finally, object-oriented programming supports generic programming by facilitating the development of components that are independent from a specific implementation (e.g., a generic class “Manipulator” will work with different manipulator types). All of the above benefits are based on the general concepts of object-oriented programming, such as abstraction, encapsulation, polymorphism, and inheritance [Stroustrup 1991]. As will be shown later in this chapter, these object-oriented design concepts lead to an intuitive system architecture. As one might expect, the language of choice is C++, as it provides the whole spectrum of object-oriented concepts while maintaining high performance [Stroustrup 1998] (e.g., templates and inline functions can be used to create highly versatile and optimized code in the Robotic Platform). The power of C++ and object-oriented programming can be further increased when using strong object-oriented libraries such as STL [Musser 1996]. STL provides standard data structures (e.g., lists, vectors, etc.) and algorithms. These standard data structures and algorithms simplify programming effort since these tools are often required in common programming tasks. The data structures of the STL are very universal since they can be used with different data types (i.e., template programming).

The last design aspect of a software control platform has do with how the roboticist interacts with the system. Specifically, how does the roboticist animate objects for simulation purposes and how does the roboticist implement and tune control algorithms. For purposes of simulation animation, Open Inventor [Wernecke] was utilized. Open Inventor, developed by Silicon Graphics, is an object-oriented C++ library for creating 3D graphics and animation. Open Inventor minimizes development effort, as it is able to load 3D models that were created in the Virtual Reality Modeling Language (VRML) format [Hartman 1996]. A variety of software packages are available that facilitate the construction of 3D VRML models. These packages can be utilized to quickly create a graphical representation of robotic components. The Robotic Platform utilizes the built-in functionality of Open Inventor to animate these components. Open Inventor also provides advanced features like object picking, which is very useful in the programming of operator interfaces. For purposes of control implementation, QMotor [Loffler 2002] was utilized because it allows users to establish a real-time control loop, to log data, to tune control parameters, and to plot signals. QMotor control programs can be directly integrated in the class design of the Robotic Platform since QMotor supports object- oriented programming.

10.3 Design of the Robotic Platform

Overview

Each component of the Robotic Platform (e.g., the teachpendant, the trajectory generator, etc.) is modeled by a C++ class. A C++ class definition combines the data and the functions related to that component. For example, the class "Puma560" contains the data related to the Puma 560 robot (e.g., the current joint position) as well as functions related to the Puma 560 robot (e.g., enabling of the arm power). Hence, the design of the Robotic Platform results from grouping data and functions in a number of classes in a meaningful and intuitive way. A class can also use parts of the functionality and the data of another class (called the base class) by deriving this class from the base class. The classes of the Robotic Platform include GUI components and a 3D model for graphical simulation. These types of components are traditionally found in separate programs (e.g., see the RCCL robot simulator [Lloyd et al. 1988]). However, by including them in the same class, one can achieve tight integration of the user interface, 3D modeling, and other functional parts.

To provide new capabilities for different applications, the user creates new classes. Usually, new classes are derived from one of the already existing classes to minimize coding effort. This process is called inheritance, and it greatly facilitates code reuse and eliminates redundancy. To illustrate how classes are derived from each other, class hierarchy diagrams are used. The main class hierarchy diagram of the Robotic Platform is shown in Figure 10.3.1. Each arrow is drawn from the derived class to the parent class. The further to the right a class is listed, the more specific it must become. The further to the left a class is listed, the more generic it must become. The classes of the Robotic Platform can be separated into the following categories (note that some of the classes discussed below are not shown in Figure 10.3.1 since their class hierarchies will be discussed later):

The Core Classes. The classes RoboticObject, FunctionalObject, and PhysicalObject build the core of the Robotic Platform by defining the overall behavior of all robotic objects. These classes by themselves can be the basis for any robotic system.

Generic Robotic Classes. Derived from the core classes are a number of generic robotic classes. These classes (e.g., ServoControl, Manipulator, and Gripper) cannot be instantiated. Rather, these classes serve as base classes that implement common functionality while also presenting a generic interface to the programmer (i.e., these classes can be used to

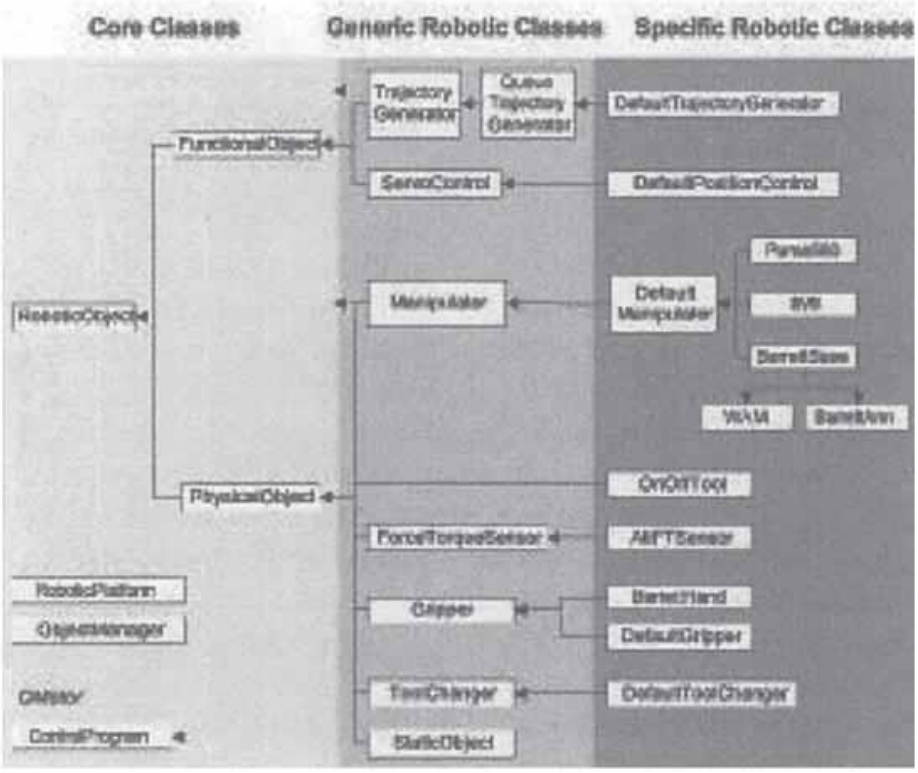


Figure 10.3.1: Class Hierarchy of the Robotic Platform.

create programs that are independent from the specific hardware or the specific algorithm).

Specific Robotic Classes. Derived from the generic robotic classes are classes that implement a specific piece of hardware (e.g., the class Puma560 implements the Puma 560 robot) or a specific functional component (e.g., the class DefaultPositionControl implements a proportional integral derivative (PID) position controller).

The ControlProgram Class. This class is the basis for all real-time control loops.

Utility Classes. The utility classes manage common tasks (e.g., managing configuration files).

The Object Manager. The object manager supervises all objects and classes existing in the system.

The Math Library. The math library consists of classes for using matrices, vectors, transformations, filters, differentiators, and integrators.

The Manipulator Model Library. The manipulator model library consists of classes that model the kinematic and dynamic behavior of manipulators.

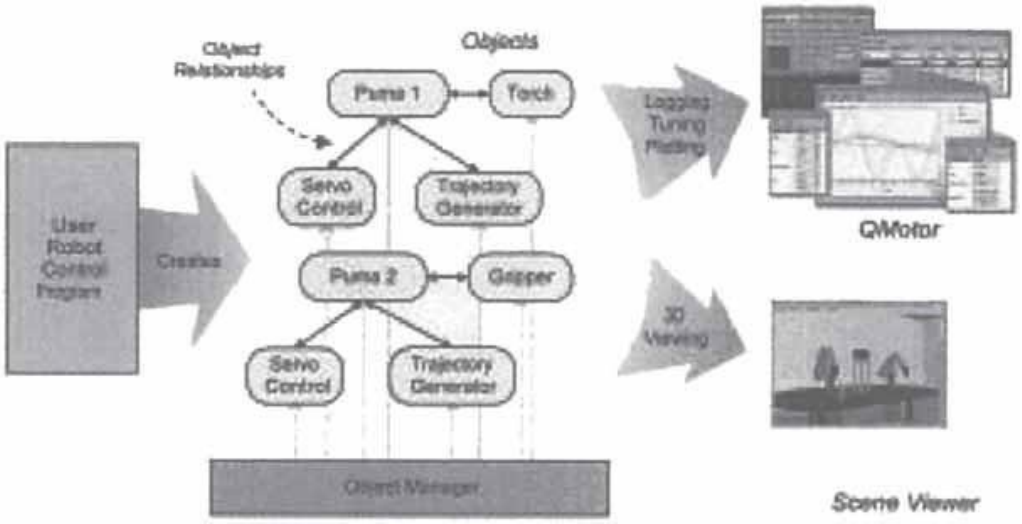


Figure 10.3.2: Run-Time Architecture of the Robotic Platform.

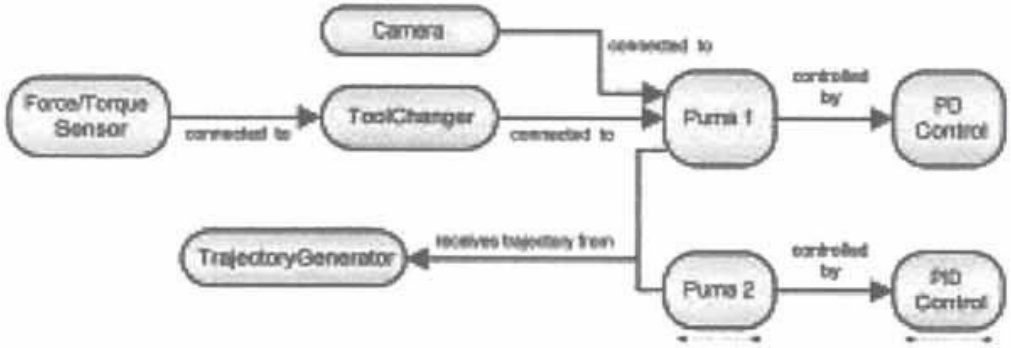


Figure 10.3.3: Object Relationships in an Example Scenario.

In a robot control program, the user instantiates objects from classes. When instantiating an object, memory for the object is reserved, and the object initializes itself. The user can create as many objects as desired from the same class. For example, two Puma robots can be operated by simply creating two objects of the class Puma560. As soon as objects are created, the user can employ their functionality. The object manager maintains a list of all currently existing objects. With the object manager, it is possible to initiate functionality on multiple objects (e.g., shutdown all objects). The Scene Viewer is the default GUI of the Robotic Platform. It contains windows

to view the 3D scene of the robotic work cell and to list all objects. The overall run-time architecture is shown in Figure 10.3.2.

In a robotic system, different components are related to each other. To reflect this fact, object relationships are established between objects. For example, objects can specify their physical connection to each other. Object relationships are implemented by C++ pointers to the related object. The object relationships in an example scenario are shown in Figure 10.3.3.

Core Classes

The class RoboticObject is the base class for all classes. It defines a generic interface (i.e., a set of functions that can be used with all classes of the Robotic Platform). For example, a program can use the startShutdown( ) function to instruct an object of either the class Puma560 or the class Gripper to shutdown. Specifically, the following generic functionality is defined in the class RoboticObject (see also Figure 10.3.4):

Error Handling. Every object must indicate its error status.

Interactive Commands. Each object can define a set of interactive commands (e.g., “Open Gripper”) that will show up in the object pop-up menu of the Scene Viewer.

Configuration Management. Each object can use the global configuration file to set itself up. Additionally, each object can also have a local object configuration file.

Shutdown Behavior. Each object is able to shutdown itself.

GUI Control Panel. Each object is able to create a control panel.

Message Handler. Each object has a message handler that can interpret custom messages.

Thread Management. Each object indicates if additional threads are required for its operation and also provides functions that execute those additional threads.

Note that the actual functionality is usually implemented in the derived class. However, the class RoboticObject also implements simple default functionality. This feature supports code reuse and simplicity by giving all classes derived from the class RoboticObject the ability to take over this default functionality if necessary. Table 10.3.1 shows all functions and their default behavior.

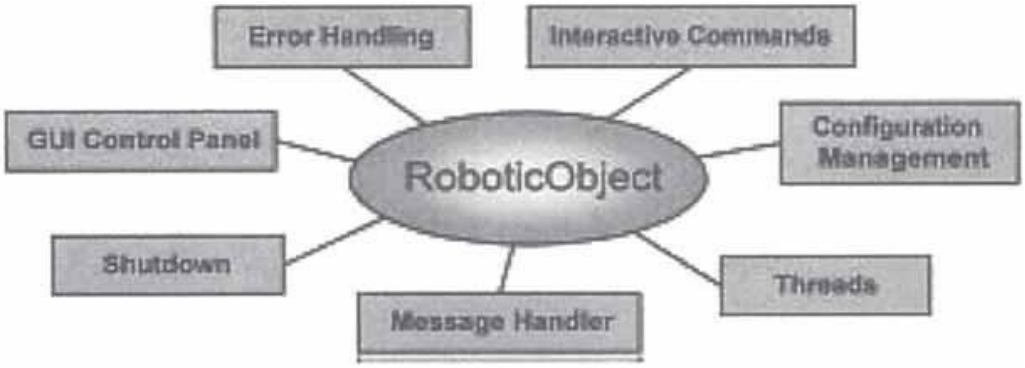


Figure 10.3.4: The Class Robotic Object.

The class PhysicalObject is derived from the class RoboticObject. It is the base class for all classes that represent physical objects (e.g., manipulators, sensors, grippers, etc.). It defines a generic interface for these classes as illustrated in Figure 10.3.5 and Table 10.3.2. Specifically, the following generic functionality is defined in PhysicalObject:

3D Visualization. Every physical object can create its Open Inventor 3D model. The Scene Viewer loops through all physical objects to create the entire 3D scene.

Object Connections. A physical object can specify another object as a mounting location. By using this object relationship, the Scene Viewer draws objects at the right location (e.g., the gripper being mounted on the end-effector of the manipulator).

Position and Orientation. The position/orientation information specifies the absolute location of the object in the scene (or the mounting location, if an object connection is specified).

Simulation Mode. Every physical object can be locked into simulation mode. That is, the object does not perform any hardware I/O (i.e., its behavior is only simulated).

The class FunctionalObject does not contain any functionality; however, it is use to build other classes. For example, functional classes, such as the class TrajectoryGenerator, are derived from the class FunctionalObject.

Robot Control Classes

The central components of any robotic work cell are manipulators. The class Manipulator is a generic class that defines common functionality of

Function	Description	Default Behavior
startShutdown()	Starts shutdown of the object	No action
isShutdownComplete()	Indicates when the shutdown is complete	Indicates shutdown is complete immediately
getStatus()	Returns the objects status (ok/error, including error message)	Returns ok
getCommandName()	Returns the name of one of the interactive commands.	No interactive commands are defined
doCommand()	Performs one of the interactive commands	No action
SetGlobalConfiguration()	Passes the global configuration to the object	No action
SetObjectConfiguration()	Passes the local object configuration to the object	No action
createControlPanel()	Creates the GUI of the object's control panel	No action
updateGUI()	This function is called continuously from the main GUI to allow the object to update its GUI windows (e.g., update the control panel)	No action
getNumAdditionalThreads()	Indicates how many additional threads are required	Indicates no additional threads are required
thread()	This function is executed as an additional thread	Runs control program if existing
handleMessage()	This function is called to interpret a message	No action

Table 10.3.1: The Interface of the Class RoboticObject and its Default Behavior.

manipulators with any number of joints. Derived from the class Manipulator is the class DefaultManipulator, which contains the defaultimplementation of a manipulator. The class DefaultManipulator is a template class (i.e., it is parameterized with the number of joints). The generic programming

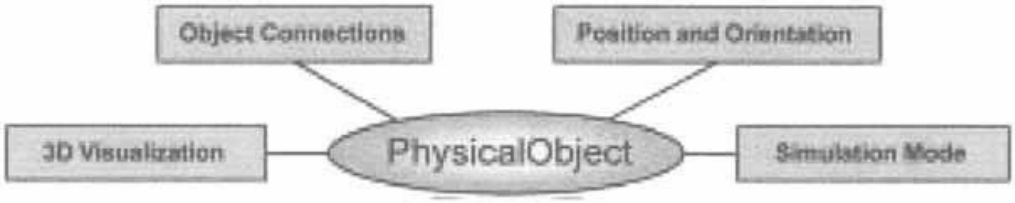


Figure 10.3.5: The Class Physical Object.

Function	Description	Default Behavior
get3DModel()	Returns the Open Inventor 3D model	Loads the VRML file <ClassName>.wrl
update3DModel()	Updates the Open Inventor 3D model with the current state of the object	No action
setConnection()	Specifies another object on which the object is mounted.	Sets an internal pointer
removeConnection()	Removes the connection	Sets the internal pointer to zero
setTransform() getTransform()	Sets/gets the position and orientation of the object or the mounting location	Sets/gets the root transform of the Open Inventor object tree
setDisplayOff() setDisplaySolid() setDisplayWireframe()	Disables the display of the object or selects wire frame or solid display	Sets the properties of the Open Inventor tree accordingly
setSimulationModeOn() setSimulationModeOff()	Enables/disables the simulation mode	Sets an internal variable to 1/0

Table 10.3.2: The Interface of the Class PhysicalObject and its Default Behavior.

interface and the default implementation are illustrated in Table 10.3.3. Derived from the class DefaultManipulator are the classes that implement specific manipulator types. Currently, three manipulators are supported: the Puma 560 robot, the IMI robot [Berkeley 1992], and the Barrett Whole Arm Manipulator (WAM) [Barrett] in both the 4 link and 7 link configuration. More information about the specific control implementation of these robot manipulators can be found in [Loffler 2001] and [Costescu et al. 1999]. For simulation of the manipulators, their dynamic model is required. Additionally, for Cartesian control, forward/ inverse kinematics and the calculation of the Jacobian matrix are needed. All of these functions are located in the ManipulatorModel classes. The

class hierarchy and the generic interface of the ManipulatorModel classes are displayed in Figure 10.3.6.

Interface (class Manipulator)	Default Implementation (class DefaultManipulator)
Determine the current manipulator joint position	Reads the motor position from the encoders of an I/O board and converts it to the joint space
Set the current manipulator joint position (position calibration)	Converts the position to the motor space, and sets the encoders of an I/O board to the motor position
Output a control torque/force to the joints	Converts the torque/force to motor space, sets the D/A channels to the control output
Convert position/torques between joint and motor space	Linear relationship, no coupling
Enable/disable the arm power	Sets/resets a digital output of the I/O board

Table 10.3.3: Functionality defined in the Classes Manipulator and Default-Manipulator.

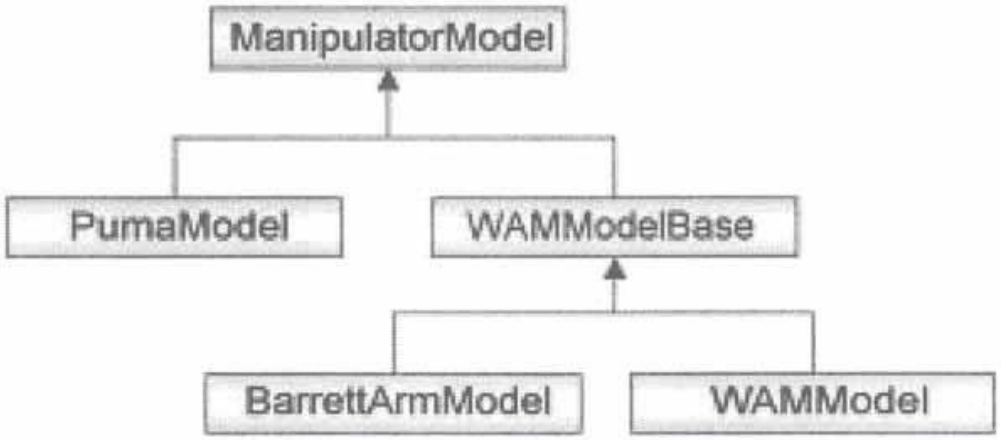


Figure 10.3.6: The ManipulatorModel Classes.

The class DefaultManipulator creates a real-time control loop, but it does not include the servo control algorithm. The servo control algorithm is contained in a separate object of the class ServoControl or of a derived class. The class ServoControl is a generic class that defines common properties and functionality of a ServoControl. That is, a servo control obtains the

current position from the manipulator object and calculates the required output control signal to achieve the control task (e.g., servo the manipulator to a desired setpoint). Derived from the class ServoControl is the class DefaultPositionControl, which contains a PID position control with friction compensation in joint and Cartesian space. The control loop in the class DefaultManipulator first determines the current position of the manipulator and then calls the calculate() function of the class ServoControl. The advantage of the servo control being a separate object is that the user can switch between multiple servo control algorithms, even while the manipulator is moving.

The trajectory generation is also performed in a separate class. The class TrajectoryGenerator defines the interface of a generic trajectory generator. A trajectory generator is any object that creates a continuous stream of setpoints and forwards this stream to a servo control object. A trajectory generator must implement its own loop such that the trajectory generator can run independently and at a different frequency than the frequency used in the servo control. The servo control calls the getCurrentSetpoint () function of the trajectory generator to determine the current desired position. It is also possible to define multiple trajectory generators and switch between them while the manipulator is moving. The class QueueTrajectoryGenerator is derived from the class TrajectoryGenerator to implement the generic interface and common functionality of a trajectory generator that creates the trajectory along via points and target points (i.e., motion queue management functions are implemented). Derived from the class QueueTrajectoryGenerator is the class DefaultTrajectoryGenerator. This class is the specific implementation of a trajectory generator that can interpolate both in joint space and Cartesian space, including path blending between two motion segments at the via points. Table 10.3.4 shows the interface of the default trajectory generator.



Figure 10.3.7: Object Setup for the Servo Control and the Trajectory Generation of a Manipulator.

Classes, such as Puma560 or WAM, automatically create a default trajectory generator and a default servo control for the convenience of the user. However, the user can switch to a different trajectory generator or servo control if desired. Figure 10.3.7 illustrates in a typical scenario how

Function	Description
setJointInterpolation()	Sets the joint interpolation mode
setCartesianInterpolation()	Sets the Cartesian interpolation mode
setVelocity()	Sets the velocity
move()	Queues a new target point or via point
stop()	Stops the manipulator for a certain time
setBlockingMovesOn() setBlockingMovesOff()	Specifies if move/stop commands block until they return
waitForAllMovesCompleted()	Returns after all moves have been completed
getNumRequestsInQueue()	Returns the number of via/target points that are currently in the motion queue

Table 10.3.4: Interface of the class DefaultTrajectoryGenerator.

the manipulator object, the servo control object, and the trajectory generator object work together.

External Device Classes

Besides the classes related to specific manipulators, there are a several other classes that can be used for robotic applications. Specifically, these classes give the robot manipulator the ability to interface with other physical objects by means of grippers, robotic hands, and/or tools. These external device classes are given below:

Gripper. The class Gripper is the generic interface for a gripper. Basically, it defines the functions open(), close(), and relax().

DefaultGripper. The class DefaultGripper assumes that two digital output lines control the gripper, one digital line to open the gripper, and one to close it.

BarrettHand. This is a class to operate the BarrettHand [Barrett]. This class allows the user to move each of the three fingers to certain positions and also control the spread motion.

ForceTorqueSensor. This class defines the generic interface for a force/ torque sensor. That is, it defines functions to read the forces and the torques.

AtiFTSensor. This class is the specific implementation of the ATI Industrial Automation Gamma 30/100 Force/Torque sensor.

ToolChanger. The class ToolChanger is the generic interface of a tool changer. Basically, it defines the functions lock(), unlock(), and relax().

DefaultToolChanger. The class Def aultToolChanger assumes that one digital output line controls the lock function of the toolchanger and another line the unlock function.

StaticObject. An object of the class StaticObject has no functionality other than specifying its 3D model. It can be used to add objects such as a table or work pieces to the 3D scene.

Utility Classes

As with any complex software system, utility programs are needed for communication purposes and for providing the user with system related information. To this end, several separate, general-purpose utility classes are used throughout the Robotic Platform. These utility classes are given below:

Status. The class Status provides functionality to stack status messages. It returns detailed status reports to the user. Each class has a data member of class Status that indicates the status of the object.

Client. The class Client simplifies the sending of messages to a separate task or thread.

Server. The class Server, the counterpart to the class Client, simplifies receiving of messages and replying to messages.

Config. The class Conf ig handles configuration files in ASCII format.

IOBoardClient. The class IOBoardClient allows communication with an I/ O board (e.g., providing encoders readings, writing D/A values, reading A/D values, setting and reading digital inputs/outputs).

Lock. The class Lock provides mutual exclusion between two threads.

Configuration Management

The Robotic Platform utilizes a global configuration file, which is parsed by the object manager and the objects to determine the system's configuration. This file is called rp.cfg by default. The object manager searches for this file

in the path specified by the shell variable RP_CONFIG_PATH. By starting a Robotic Platform program with the option -config <filename>, a different filename and path for the configuration file can be specified. The format of the configuration file is now discussed. For each object, the configuration file lists the object name in brackets, the class name of the object, and some additional settings (see Figure 10.3.8). Table 10.3.5 lists possible object settings and their related member functions defined by the classes RoboticObject and PhysicalObject. Derived classes can be used to define additional settings.

```
[leader]
class Puma560
config leader.cfg
position 0 0 0

[secondrobot]
class WAM
position 300 0 0
simulationMode 0
display solid

[follower]
class WAM
config /root/config/follower.cfg
position 600 0 100

[gripper]
class BarrettHand
port /dev/ser1
```

Figure 10.3–8: An Example Global Configuration File.

Object Manager

The object manager, implemented as the class ObjectManager, handles all objects in the system. Every time a new object is created, it registers itself with the object manager. Similarly, every time an object is destroyed, it is removed from the object list that is maintained by the object manager. The object manager contains the necessary functionality to loop through this list, and hence, allows one to perform operations on multiple objects. For example, the Scene Viewer retrieves a list of all objects that are derived from the class PhysicalObject. This list retrieval operation allows the Scene Viewer to render each of the objects, and thereby, render the entire 3D scene.

The object manager also maintains a list of all the classes used in the Robotic Platform. This feature is essential for fostering generic programming. The advantages of generic programming for this application are obvious.

Specifically, generic code utilizes only components that provide a generic interface; hence, generic code does not need to be changed when a component with a different implementation is used. That is, the same code can be used for a number of specific implementations, and hence, attributes to code reuse (e.g., a generic trajectory generator can be used with different manipulator types). Fortunately, C++ utilizes class inheritance and virtual functions to facilitate generic programming. To illustrate this concept, consider a section of the class hierarchy as shown in Figure 10.3.9. The following snippet of generic code demonstrates how to write a manipulator independent program that works with either the Puma robot, the WAM, the IMI, or any robot that might be added in the future:

```
Manipulator     *manipulator;
ObjectManager om;

manipulator  =  om.createDerivedObject<Manipulator>("leader");
// Creates either a Puma, an IMI or a WAM object, depending on
// what is specified in the global configuration file under the
name "leader"

// Now, we can do generic operations
manipulator->enableArmPower();
Transform t = manipulator->getCurrentCartesianPosition();}
```

To utilize generic programming in C++, the above code creates an object of the derived class (e.g., an object of the class Puma or the class WAM), and operates the object via a pointer to the generic base class (i.e., Manipulator *manipulator). The function createDerivedObject() of the object manager is utilized to create an object of either the class Puma560, Barrett Arm, WAM or IMI. To create the correct object, the createDerivedObject() function looks for the object name in the global configuration file (see Figure 10.3.8). Then, the createDerivedObject() function reads the class name of the object from the configuration file and creates an object of this class. Hence, to switch to a different manipulator type, only the class name in the global configuration file has to be changed when utilizing an existing generic program.

Name of Setting	Description	Equivalent Member Functions
class <className>	Specifies the class name of the object	-
config <configFileName>	Specifies an additional configuration file for this object. This is usually a QMotor configuration file.	RoboticObject:: setObjectConfiguration()
position <x,y,z> orientation <r,p,y>	Specifies the position and orientation of the object	PhysicalObject::setTransform()
simulationMode on simulationMode off	If "on" is specified, use simulation mode for this object	PhysicalObject::setSimulationModeOn() PhysicalObject::setSimulationModeOff()
display off display solid display wireframe	Specifies if and how the object is displayed in the Scene Viewer	PhysicalObject::setDisplayOff() PhysicalObject::setDisplaySolid() PhysicalObject::setDisplayWireframe()

Table 10.3.5: Object Settings of the Configuration File.

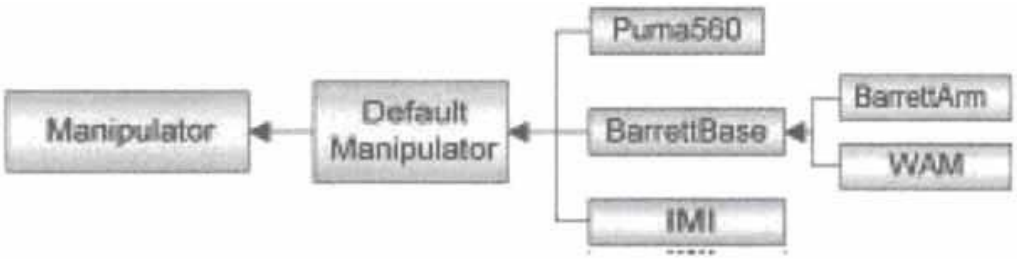


Figure 10.3.9: The Generic Class Manipulator and its Derived Classes.

Concurrency/Communication Model

An inherent complication associated with the development of a software control platform for robot manipulator systems is the issue of concurrency. That is, while it is often sufficient for many engineering systems to run as a single task, robotic systems require components, such as the servo control, to be executed concurrently with other components (e.g., the trajectory generator). The Robotic Platform addresses this issue by running all concurrent tasks on the same PC. It should be noted that since QNX6 supports symmetric multiprocessing, it is possible to distribute the tasks over multiple processors.

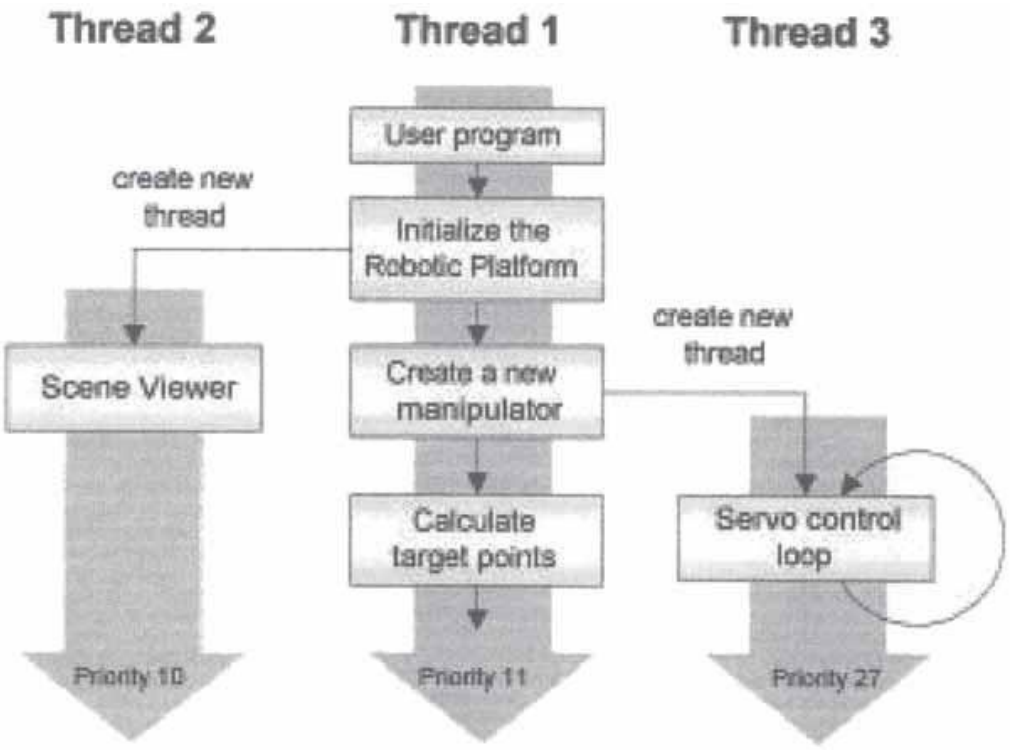


Figure 10.3.10: Creating New Threads for Concurrency.

The predecessor of the Robotic Platform, the QMotor RTK [Loffler 2001], executed multiple programs to achieve concurrency on a single processor. While this concept fosters modularity, it is inconvenient to manage the startup and termination of multiple programs. In contrast, an application that uses the Robotic Platform is compiled and linked to a single program instead. This program spawns threads if concurrent execution is required. Once the program terminates; all threads terminate automatically. Figure 10.3.10 illustrates an example of how a user program spawns multiple threads. At program start, only thread 1 is executing. At the initialization of the Robotic Platform library, a new thread is created that executes the 3D Scene Viewer.

Then, the user utilizes a new object of a manipulator class. The creation of this manipulator object automatically spawns a third thread for the servo control loop. Hence, the first thread can go ahead and calculate target points for the manipulator, while the servo control loop and the Scene Viewer run in the background. To ensure real-time behavior of time critical tasks, the threads run at different priorities (e.g., the servo control loop runs at the high priority 27).

Since threads access the same address space, communication between threads can easily be performed by using this address space. However, it is important to synchronize this access to avoid corruption of the data structures. Synchronization is achieved by using the class Lock to provide mutual exclusion for accessing the data that is shared between multiple threads.

Plotting and Control Tuning Capabilities

The issue of tuning and debugging the low-level controller and trajectory planning algorithms has usually not addressed in many of the previously developed software control platforms. However, this is an extremely important issue given the level of complexity associated with accurately positioning a multi-degree of freedom system such as robot manipulator. To address this issue, the Robotic Platform utilizes QMotor for low-level algorithm development. QMotor [Loffler 2002] is a comprehensive environment for implementing and tuning control strategies. QMotor consists of: i) a client/server architecture for hardware access, ii) a C++ library to create control programs, and iii) custom GUI for control parameter tuning, data logging, and plotting.

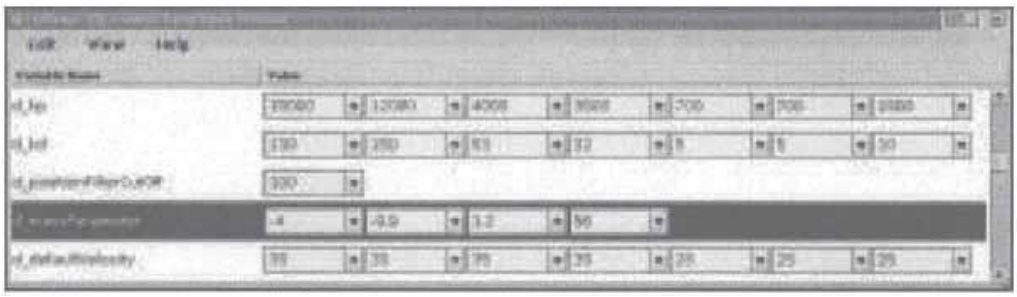


Figure 10.3.11: The QMotor Control Parameter Window.

To communicate with hardware, QMotor uses hardware servers that run in the background and perform hardware I/O at a fixed rate. Servers for different I/O boards are available (e.g., the ServoToGo board, the Quanser MultiQ board, and the ATI force/torque sensor interface board). The use of hardware servers provides an abstract client/server communication

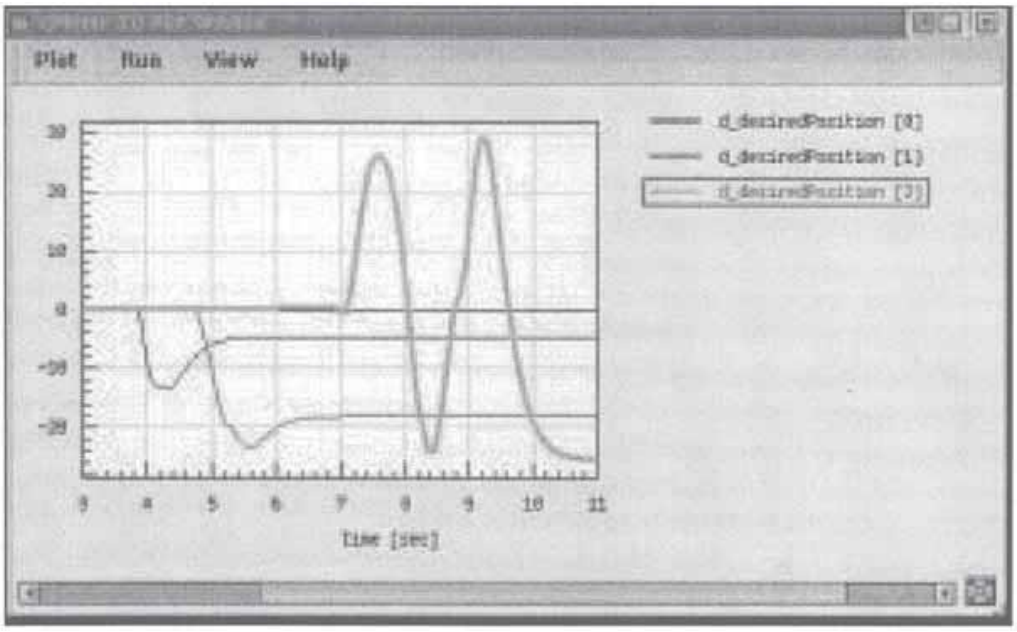


Figure 10.3.12: The QMotor Plot Window.

interface such that clients can perform the same generic operations with different servers. Hence, one can quickly reconfigure the system to use different I/O boards by simply starting different servers. For writing control programs, QMotor provides a library, which defines the class ControlProgram. To implement a real-time control loop, the user derives a specific class from the class ControlProgram and defines several functions that perform the control calculation and the necessary housekeeping. Once a control program is implemented and compiled, the user can start up the QMotor GUI, load the control program, start it, and tune the control strategy from the control parameter window (see Figure 10.3.11). Furthermore, the user can open multiple plot windows (see Figure 10.3.12) and set the logging parameters.

To utilize QMotor for the Robotic Platform, classes such as the class Def aultManipulator are derived from the class ControlProgram. Hence, these classes inherit the functionality of a control program (i.e., real-time execution, data logging, and communication with the GUI). If a class is derived from the class ControlProgram, the base class RoboticObject automatically creates a new thread of execution that runs the control loop in the background. QMotor was originally designed to load and tune one control program at a time. That is, to switch to a different control program, the current control program had to be stopped and unloaded. The Robotic Platform is designed to start and run multiple control loops at the same time; hence, it became necessary to upgrade QMotor. Specifically, QMotor can now attach itself to an executing control program instead of loading and starting the control program. This QMotor modification now allows the

following operational scenario in the Robotic Platform. The user first starts the control program. This control program creates several threads that execute real-time control loops. The user can then start the QMotor GUI and attach it to any of the control programs. Once the QMotor GUI is attached to a control program, control parameters can be changed and data can be plotted.

Math Library

Past robot control libraries often introduced their own specific robotic data types. Most of these data types are based on vectors or matrices (e.g., a homogeneous transformation is a 4x4 matrix). Hence, it is more feasible to use a general C++ matrix library and define robotic types on top of it. Most of the matrix libraries available for C++ use dynamic memory allocation, which risks the loss of deterministic real-time response [Loffler 2001]. Hence, the big disadvantage of libraries that use dynamic memory allocation is that they can not be used in large sections of the Robotic Platform. To overcome this problem, special real-time matrix classes were developed for the Robotic Platform that use templates for the matrix size. This means that the matrix size is known at compile time and dynamic memory allocation is not required. Besides being feasible for real-time applications, this solution also produces highly optimized code. That is, due to the use of templates and inline functions, the matrix classes can be as fast as direct programming. Specifically, with optimized implementation, the multiplication of two 2x2 matrices C=A * B is as fast as writing

```
c11=a11 * b11 + a12 * b21;
c12=a11 * b12 + a12 * b22; etc.
```

An additional advantage is that the compiler can check for the correct matrix sizes at compile time (e.g., a matrix multiplication of two matrices with incompatible size is detected during compilation). Figure 10.3.13, Table 10.3.6, and Table 10.3.7. Functions of the Matrix, Vector, and Transformation Classes illustrates the class hierarchy, the types classes, and the data types. The classes MatrixBase, VectorBase, Matrix, Column Vector, and RowVector are parameterized with the data type of the elements. The default element data type is double, which is the standard floating-point data type of the Robotic Platform. The classes MatrixBase and VectorBase are pure virtual base classes that allow for manipulation of matrices and vectors of an unknown size (matrices and vectors of an unknown size are required during generic manipulator programming). Figure 10.4.1 shows an example program that uses the math library to calculate a position equation.

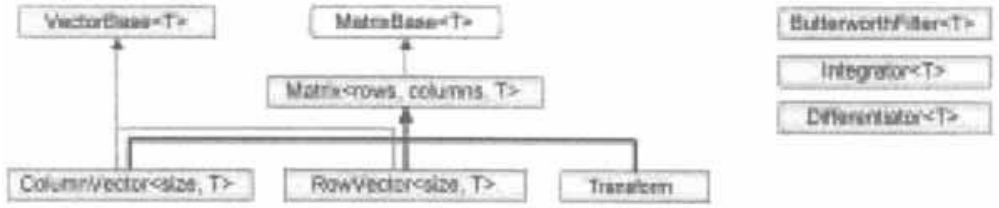


Figure 10.3.13: Class Hierarchy of the Matrix Classes.

MatrixBase<T>	Base class of all matrix and vector classes of data type <T> (e.g., T = int, float, etc.)
VectorBase<T>	Base class of all vector classes of data type <T> (e.g., T = int, float, etc.)
Matrix<row,columns,T>	Matrix of data type <T> and size <rows*columns>
ColumnVector<size,T>	Column Vector of data type <T> and <size> elements
RowVector<size,T>	Row Vector of data type <T> and <size> elements
Transform	Homogeneous transformation (4 x 4 Matrix of type double)
ButterworthFilter<T>	Low-pass 2nd order filter of data type <T>
Differentiator<T>	Numerical differentiation of data type <T>
Integrator<T>	Numerical integration of data type <T>

Table 10.3.6: Classes of the Math Library.

Matrix Functions	Vector Functions	Transformation Functions
Multiplication/division Addition/difference Transpose Getting/setting elements Getting/setting sub-matrices Inverse Unit/Zero matrix Input/output from/to streams	Length (2-norm) Cross-product Dot-product Element-by-element multiplication	Translation matrix Rotation matrix about x, y, or z axis Rotation matrix about an arbitrary vector Conversion from/to Euler angles Conversion from/to RPY angles

Table 10.3.7: Functions of the Matrix, Vector, and Transformation Classes.



```
Transform Z, T6, E, P, W;

Z = translation(0, 0, 75);
E = translation(0, 0, 20);
W = translation(100, -50,50) * xRotation(180);
P = translation(20, 0, 0);

// Solve Z*T6*E == W*P
T6 = inverse(Z) * W * P * inverse(E);
cout << "T6 of target: " << T6 << endl;
```

Figure 10.3.14: Example Program for the Matrix classes.

In addition to the matrix, vector, and transformation classes, the classes ButterworthFilter, Differentiator and Integrator are part of the math library. The class ButterworthFilter is used for low-pass filtering. The class Differentiator implements numerical differentiation via the backwards difference method plus low-pass filtering. Finally, the class Integrator utilizes the trapezoidal method for numerical integration. The user can derive a specific class from the class Integrator to implement more advanced integration methods. Both classes are parameterized with the data type (i.e., they work with scalars, vectors, and matrices).

Error Management and the Front-End GUI

Each object is responsible for maintaining the appropriate error status. If a fatal error occurs, any object can request the object manager to shut down the system. For example, this could be the case when a control torque exceeds its limit. For such a system shutdown, the object manager loops through all objects in the system and calls their start Shut down () function. Then, the object manager waits until all objects have completed their shutdown. The completion of the object shutdown is indicated by the is ShutdownComplete() function.

The front-end GUI components for the Robotic Platform were developed with the C++ GUI class library QWidgets++. QWidgets++ allows for object-oriented techniques in GUI programs. The GUI consists of three parts:

- The Scene Viewer is the default supervising GUI, which is opened automatically at startup of every Robotic Platform program.

- Each class can have its own control panel. The control panels are opened from the Scene Viewer.

- Several utility programs (e.g., the Manual Move program and the Teachpendant program) have a GUI.

Operation of the front-end GUI for the Robotic Platform is further explained in the next section.

10.4 Operation of the Robotic Platform

Scene Viewer and Control Panels

When a program running inside the Robotic Platform is executed, the Scene Viewer window opens up. The Scene Viewer window displays the entire 3D scene and also allows the user to open a window that displays a list of currently running objects (see Figure 10.4.2). To create a 3D scene, the Scene Viewer loops through all objects that are derived from the class PhysicalObject and calls the get3DModel() function to obtain the Open Inventor 3D data of that object. Then, the Scene Viewer uses the object connection relationships (specified by the function setConnection() of the class PhysicalObject) to display the 3D objects at the right position (e.g., to display a gripper being mounted at the end-effector of a robot manipulator). Furthermore, the Scene Viewer continuously updates the 3D scene with the current state of all objects (e.g., it uses the current joint position of a robot manipulator to display the robot joints in the correct position). Hence, the 3D scene rendered in the Scene Viewer window always represents the current state of the actual hardware (in simulation mode, the simulated state of the hardware is represented). To select the best viewing position, the user navigates in the 3D scene using a mouse. The user can rotate the view, move forward and backward, and also store/restore desired viewing positions. Additionally, the user can hide objects in the scene to increase the frame rate. Many different Scene Viewer windows can be opened to view the 3D scene from different viewing positions at the same time. The user can also open the Object Viewer window to display the list of all objects that are currently being instantiated.

Each object also has an individual pop-up menu (See Figure 10.4.3. The Object Pop-Up Menu). This pop-menu appears if the user either: i) right clicks on the object in the Scene Viewer rendering area, or ii) right clicks on an entry in the Object Viewer window. Options associated with pop-up menu can be used to hide the object in the rendering area and to select between a wire frame or a solid display. In addition, the pop-up menu displays interactive commands that are defined in the specific class of the object. For example, a gripper object has additional menu items to open, close, and relax the gripper. Finally, the user can open the control panel from the object pop-up menu. Figure 10.4.5 shows the control panel of the Barrett WAM as an example. Each control panel appears in a new window.

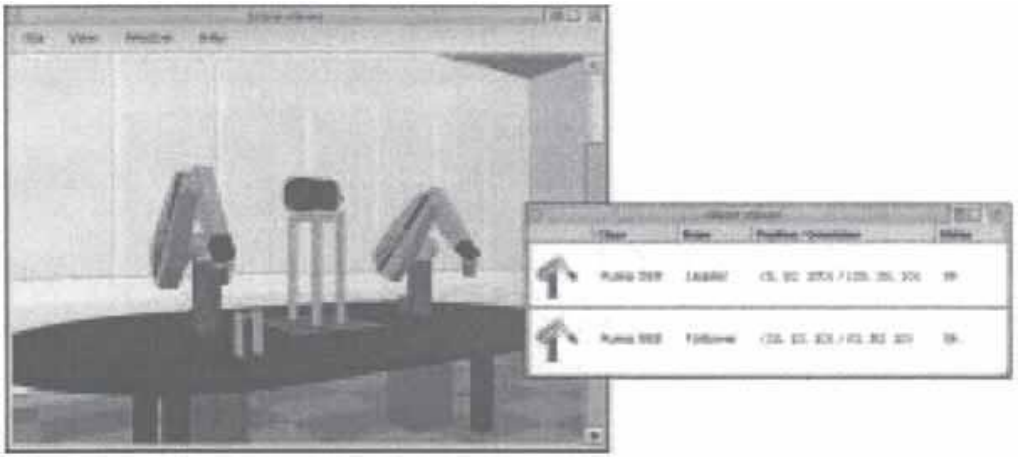


Figure 10.4.1: The Scene Viewer and Object List Windows.

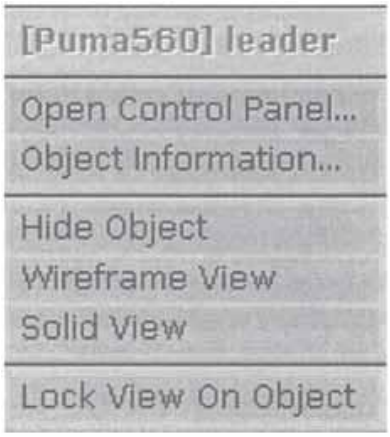


Figure 10.4.2: The Object Pop-Up Menu.

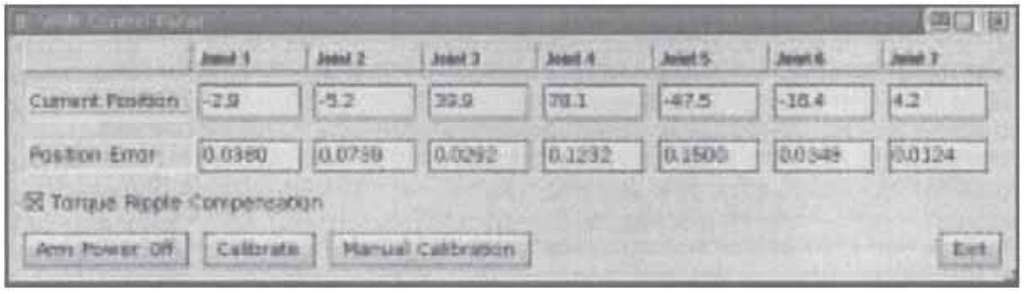


Figure 10.4.3: The Control Panel of the WAM Class.

Utility Programs for Moving the Robot To facilitate low-level algorithm development, utility programs for moving the robot must be created. For example, the Manual Move utility (see Figure 10.4.6) is a

program that gives the user the ability to test the low-level servo control of a robot manipulator. Specifically, the Manual Move utility contains a slider for each joint. As, the user can move the sliders with the mouse, the selected robot manipulator joint immediately follows the commanded user input.

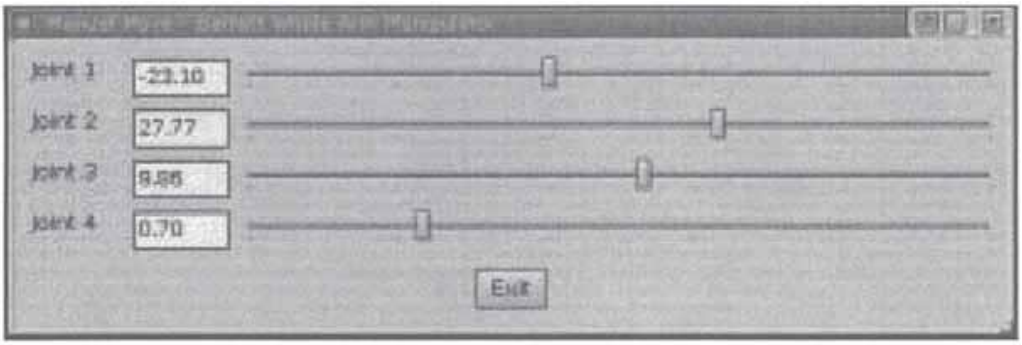


Figure 10.4.4: The Manual Move Utility.

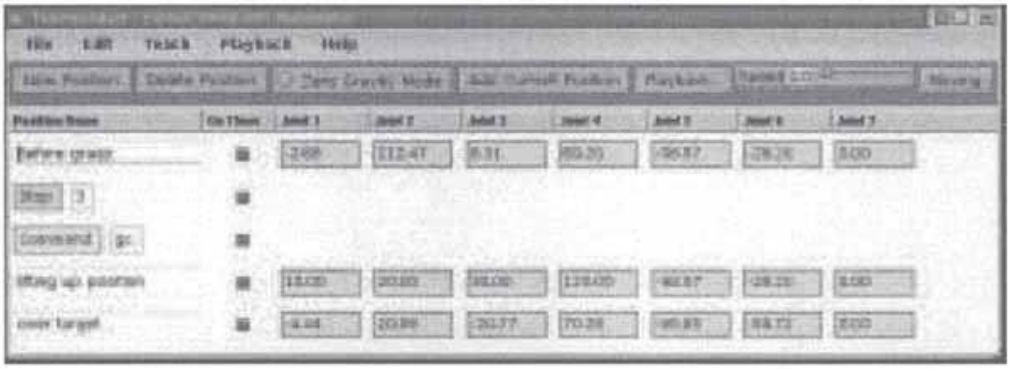


Figure 10.4.5: The Teachpendant.

The Teachpendant (see Figure 10.5.1) implements a low-level zero gravity controller that allows the user to physically position the robot manipulator joints in any location. Once the user has moved the robot manipulator joints to a desired target position, this position can be stored as in list of robot manipulator positions. The Teachpendant utilizes the Robotic Platform's trajectory generator to move the robot manipulator to the stored positions. In this way, the user can cycle the robot manipulator through all or some of the stored positions.

Writing, Compiling, Linking, and Starting Control Programs

A control program is first compiled and then linked to the Robotic Platform library. The entire Robotic Platform (i.e., all classes and the Scene Viewer) is contained in one library. As explained earlier, the Robotic Platform can easily be extended by adding new classes. If the extension is specific to a certain control program, the classes can be added to the code of the associated control program. If an extension is used in different control programs, it would probably be more convenient to add this new functionality to the Robotic Platform library. To reflect the extensions in preexisting compiled and linked programs, the Robotic Platform library is constructed to be a dynamic library (i.e., a program loads the library whenever it is started). Therefore, after the library is extended with new functionality, programs such as the Teachpendant will take advantage of the new functionality (e.g., the teachpendant will be able to operate new manipulator types).

Figure 10.4.6 shows the listing of an example control program for a simple pick and place operation. Every Robotic Platform control program must first call RoboticPlatform::init(). This function initializes the Robotic Platform and starts up the Scene Viewer. The command line arguments are passed to RoboticPlatform:: init () such that any Robotic Platform program can be started with certain default command line options (see Table 10.4.1). Additionally, these options can be controlled from C++ code as well by using the functions listed in the third column of Table 10.4.1. After RoboticPlatform::init() is called, the user's program creates all objects that are required for the associated robotic task (i.e., a gripper object, a Puma 560 object, and a trajectory generator object are created). If the option -wait was specified in the command line, no control loops are started until the user's program executes the RoboticPlatf orm:: start () function. This function waits for the user to hit the start button. This feature is necessary since this function gives the user the ability to start the QMotor GUI, set control parameters, and select logging modes before the control loops are started. The last part of the example program utilizes the trajectory generator object and the gripper object to move the robot to the workpiece, close the gripper, pick up the workpiece, and drop it at the target position.

```
// Simple pick and place operation
#include "RoboticPlatform.hpp"

void main(int argc, char *argv[])
{
   RoboticPlatform::init(argc, argv);

   Puma560 puma;              // Create Puma560 object
   DefaultGripper gripper;    // Create gripper object

   DefaultTrajectoryGenerator tragen;
```

Command Line Switch	Description	Equivalent in C++
-sim -nosim	Enables/disables simulation mode for all objects	RoboticPlatform::setSimulationModeOn() RoboticPlatform::setSimulationModeOff()
-gui -nogui	Enables/disables automatic start of the Scene Viewer	RoboticPlatform::setGuiOn() RoboticPlatform::setGuiOff()
-config <filename>	Specifies the name of the global configuration file	RoboticPlatform::setConfigurationFileName()
-wait -nowait	If wait is specified, holds the program until the START button is pressed.	RoboticPlatform::setUseStartButtonOn() RoboticPlatform::setUseStartButtonOff()

Table 10.4.1: Default Command Line Options of Robotic Platform Programs.

```
  puma.setTrajectoryGenerator(tragen);

  RoboticPlatform::start();

  tragen.moveToParkPosition();
  gripper.open();
  tragen.moveTo(0, 0, 0);   // Position specified by x,y,z
  tragen.stop(1);
  gripper.close();
  tragen.stop(1);
  tragen.moveTo(50, 50, 300);
  tragen.moveTo(100, 100, 0);
  tragen.stop(1);
  gripper.open();
  tragen.stop(1);
  tragen.moveTo(50, 50, 300);
}
```

Figure 10.4–6: A Simple Pick and Place Program

10.5 Programming Examples

Comparison of Simulation and Implementation

A very interesting option is to forward the setpoints created by a trajectory generator to two manipulators. In this way, the motion of two manipulators with the same kinematics can be compared, or the behavior of a real manipulator can be compared with a dynamic simulation. The latter application is implemented in the program in Figure 10.5.1. First, two objects of the class Puma 560 are created, and one of the objects is configured into simulation mode. Then, both objects are connected to the same trajectory generator to receive the same setpoints.

```
#include "RoboticPlatform.hpp"

void main(int argc, char *argv[])
{
  RoboticPlatform::init(argc, argv);

  // Create the robot objects
  Puma560 puma;
  Puma560 pumaSimulated;
  pumaSimulated.setSimulationModeOn();

  // Connect both to the same trajectory generator
  DefaultTrajectoryGenerator tragen;
  puma.setTrajectoryGenerator(tragen);
  pumaSimulated.setTrajectoryGenerator(tragen);

  RoboticPlatform::start();

  tragen.move(0, 45, -90, 0, 0, 0);
  tragen.move(-50, 0, -70, 50, -80, 0);
}
```

Figure 10.5–1: Example to Forward the Same Trajectory to two Robots.

Virtual Walls

This is a good example on how to create a custom servo control. It also demonstrates the use of the manipulator model functions and the math library. Virtual walls are virtual planes in the manipulator's workspace that generate a reaction force once the manipulator is moved into the wall. Given a plane with the plane equation (using homogeneous coordinates):

$$\underline{w}\underline{x} = 0; \quad \underline{w} = \begin{bmatrix} \underline{n} \\ d_0 \end{bmatrix}$$

where n is the normal vector of the plane, and d_0 is the distance from the origin. If *xEndEf fector* is the current end-effector position, then

$$d = \underline{wx}_{EndEffector} = \begin{cases} < 0 \text{ end} - \text{effector is outside the wall} \\ > 0 \text{ end} - \text{effector is inside the wall} \end{cases}$$

Using the control law

$$\tau = \begin{cases} 0 & d < 0 \text{ end} - \text{effector is outside the wall} \\ \underline{J}^T (k_f d\underline{n}) & d > 0 \text{ end} - \text{effector is inside the wall} \end{cases},$$

creates a joint torque that resists moving the robot into the wall.

To implement a new servo control algorithm, a class is derived from the class ServoControl (See line (1) of Figure 10.5.2). The above virtual wall functions are implemented in the function calculate(), which calculates the control output. In the function main(), the robot object is created as usual. In addition, an object of the virtual wall servo control class is created (See line (2) of Figure 10.5.2). Finally, the robot object is instructed to utilize the new servo control instead of the default position control, and the gravity compensation is enabled to allow the robot to be pushed around (See line (3) of Figure 10.5.2).

```
#include "RoboticPlatform.hpp"

// ----- Create a new servo control class -----

template <int numJoints>
class VirtualWallServoControl : public ServoControl
{
 public:
  virtual void calculate()
{
    // What is the distance of the end-effector to the wall?
    Transform t = d_manipulator->getEndEffectorPosition();
    double distance =
      dotProduct(d_wallCoefficients, t.getColumn(4));

    if (distance > 0)   // No control output
      return;

    // We are inside the wall. Generate reacting force
    Vector<3> force = distance * d_wallCoefficients * d_kf;

    // Convert to joint torque
    Vector<numJoints> pos = d_manipulator->getJointPositon();
    Vector<numJoints> torque;
    d_manipulator->endEffectorForceToJointTorque(pos, force, torque);

    // Do the control output
```

```
    d_manipulator->setControlOutput(torque);
  }

  Vector<4> d_wallCoefficients;
  double d_kf;
};

// ----- Use the virtual walls servo control -----

void main(int argc, char *argv[])
{
  RoboticPlatform::init(argc, argv);

  Puma560 puma;    // Create the robot object

  // Virtual wall control for 6 joints
  VirtualWallServoControl<6> wallControl;
  wallControl.d_kf = 0.01;
  wallControl.d_wallCoefficients = 0, 0, -1, 3;

  puma.setGravityCompensationOn();
  puma.setServoControl(wallControl);

  RoboticPlatform::start();
}
```

Figure 10.5–2: Virtual Walls Example.

10.6 Summary

The Robotic Platform is a software framework to support the implementation of a wide range of robotic applications. As opposed to past distributed architecture-based software control platforms, the Robotic Platform presents a homogeneous, non-distributed object-oriented architecture. That is, based on PC technology and the real-time operating system QNX6, all non real- time and real-time components are integrated in a single C++ library. The architecture of the Robotic Platform provides efficient integration and extensibility of devices, control strategies, trajectory generation, and GUI components. In addition, software-based control systems implemented with the Robotic Platform are inexpensive and offer high performance. The Robotic Platform is also built on the QMotor control environment for data logging, control parameter tuning, and real-time plotting. A real-time math library simplifies operations and provides an easy-to-use programming interface. Built-in GUI components like the Scene Viewer and the control panels provide for easy operation of the Robotic Platform and a quick ramp- up-time for users that are inexperienced in C++ programming.

REFERENCES

[Lloyd et al. 1988] J. Lloyd, M.Parker and R.McClain, “Extending the RCCL Programming Environment to Multiple Robots and Processors”, Proc. IEEE International Conference on Robotics & Automation, 1988, pp. 465–469.

[Corke] P.Corke and R.Kirkham, “The ARCL Robot Programming System”, Proc. of the International Conference on Robots for Competitive Industries, Brisbane, Australia, pp. 484–493.

[Lloyd 1990] J.Lloyd, M.Parker and G.Holder, “Real Time Control Under UNIX for RCCL”, Proceedings of the 3rd International Symposium on Robotics and Manufacturing (ISRAM ‘90).

[Stewart 1989] D.B.Stewart, D.E.Schmitz, and P.K.Khosla, “CHIMERA II: A Real-Time UNIX-Compatible Multiprocessor Operating System for Sensor-based Control Applications”, Technical Report CMU-RI-TR-89–24, Robotics Institute, Carnegie Mellon University, September, 1989.

[Stroustrup 1991] B.Stroustrup, “What is ‘Object-Oriented Programming’?”, Proc. 1st European Software Festival. February, 1991.

[Miller 1991] D.J.Miller and R.C.Lennox, “An Object-Oriented Environment for Robot System Architectures”, IEEE Control Systems Magazine, Feb. 1991, pp. 14–23.

[Zielinski 1997] C.Zielinski, “Object-Oriented Robot Programming”, Robotica, Vol.15, 1997, pp. 41–48.

[Kapoor 1996] Chetan Kapoor, “A Reusable Operational Software Architecture for Advanced Robotics”, Ph.D. thesis, University of Texas at Austin, December 1996.

551

[Pelich 1996] C.Pelich & F.M.Wahl, “A Programming Environment for a Multiprocessor-Net Based Robot Control Unit”, Proc. 10th International Conference on High Performance Computing, Ottawa, Canada, 1996.

[QSSL] QSSL, Corporate Headquarters, 175 Terence Matthews Crescent, Kanata, Ontario K2M 1W8 Canada, Tel: +1 800–676–0566 or +1 613–591–0931, Fax: +1 613–591–3579, Email:info@qnx.com, http://qnx.com.

[Costescu 1999] N.Costescu, D.M.Dawson, and M.Loffler, “QMotor 2.0—A PC Based Real-Time Multitasking Graphical Control Environment”, IEEE Control Systems Magazine, Vol. 19 Number 3, Jun., 1999, pp. 68–76.

[Loffler 2001] M.Loffler, D.Dawson, E.Zergeroglu, and N.Costescu, “Object-Oriented Techniques in Robot Manipulator Control Software Development”, Proc. of the American Control Conference, Arlington, VA, June 2001, pp. 4520–4525.

[Bhargava 2001] M.Loffler, A.Bhargava, V.Chitrakaran, and D.Dawson, “Design and Implementation of the Robotic Platform”, Proc. of the IEEE Conference on Control Applications, Mexico City, Mexico, Sept., 2001, pp. 357–362.

[Stroustrup 1998] B.Stroustrup, “An Overview of the C++ Programming Language”, Handbook of Object Technology, CRC Press. 1998. ISBN 0–8493–3135–8.

[Musser 1996] D.R.Musser, A.Saini, “STL Tutorial and Reference Guide”, Addison-Wesley, 1996. ISBN 0–201–63398–1.

[Wernecke] Josie Wernecke, “The Inventor Mentor”, Addison-Wesley, ISBN 0–201–62495–8.

[Hartman 1996] Hartman, Jed and Josie Wernecke, “The VRML 2.0 Handbook”, Addison-Wesley, Reading Massachusetts, 1996.

[Loffler 2002] M.Loffler, N.Costescu, and D.Dawson, “QMotor 3.0 and the QMotor Robotic Toolkit—An Advanced PC-Based Real-Time Control Platform”, IEEE Control Systems Magazine, Vol. 22, No. 3, pp. 12–26, June, 2002

[Berkeley 1992] “Direct Drive Manipulator Research and Development Package, Operations Manual”, Integrated Motion Inc., Berkeley, CA, 1992.

[Barrett] Barrett Technologies, 139 Main St, Kendall Square, Cambridge, MA 02142, http://www.barretttechnology.com/robot.

[Costescu et al. 1999] N.Costescu, M.Loffler, E.Zergeroglu, and D.M. Dawson, "QRobot—A Multitasking PC Based Robot Control System", Microcomputer Applications Journal Special Issue on Robotics, Vol. 18, No. 1, pp.13–22, 1999.

16

Evaluation of Microgenetic and Microimmune Algorithms for Solving Inverse Kinematics of Hyper-redundant Robotic Manipulators On-line

D. Dužanec,[1] *S. Glumac*,[2] *Z. Kovačić*[3,*] and *M. Pavčević*[4]

ABSTRACT

This chapter concerns with evaluation of the micro-genetic and micro-immune optimization algorithms for solving inverse kinematics of a redundant robotic arm as a prerequisite for adaptive trajectory planning in various manipulation tasks. To make sure the quickest search of the optimal solution, the structure and parameters of genetic algorithms might be optimized. The advantage of the micro-genetic algorithms is that they work with smaller genetic populations than standard genetic algorithms. Describe the method of

determining the optimal (best possible) mutation interval for micro-genetic algorithms based on the analysis of their behaviour. Then define a multi-objective criterion to compare performances of micro-immune and micro-genetic algorithms. Use multi-objective optimization to determine a set of best algorithms, and the micro-immune algorithm proved superior in solving a selected optimization

1 S Tempera d.o.o., Construction and Development Department, Zagreb, Croatia.

2 AVL d.o.o., Zagreb, Croatia.

3 University of Zagreb, Faculty of EE&C, Department of Control and Computer Engineering, Zagreb, Croatia.

4 University of Zagreb, Faculty of EE&C, Department of Applied Mathematics, Zagreb, Croatia.

* Corresponding author: zdenko.kovacic@fer.hr

problem. The results obtained analytically and numerically for the chosen vector optimization problem (the search for the inverse kinematics solution of a hyper-redundant robot) demonstrate the practical value of these methods. Make assessment of the time needed for algorithms to solve the inverse kinematics problem on-line based on the tests carried out on a low-cost micro-controller.

Keywords: Optimization algorithm, microgenetic algorithm, microimmune algorithm, inverse kinematics, hyper-redundant robots, real time execution

INTRODUCTION

The construction of hyper-redundant robotic manipulators is characterized by a large number of links and joints which significantly exceed the minimum number of links and joints needed for executing tasks. Typical forms of hyper-redundant robots are the forms of snakes, tentacles and elephant trunks. It is a well known fact that even the simplest robot configurations like a two degrees of freedom (DOF) planar rotational robot can be kinematically redundant. In Fig. 1 we can see a 4 DOF planar robot executing a rectangular path. Addition of two DOF has increased the redundancy of the robot and allowed the execution of a given robot task in four possible ways. Further increasing the number of joints will eventually turn a simple two DOF robot into a hyper-redundant planar robot.

By definition, a kinematically redundant robot is one whose forward kinematics is a non-bijective function. According to this definition, robots with less than 6 degrees of freedom can be considered redundant as long as there are two or more joint configurations that give the same end effector pose. This definition also means that a unique inverse kinematics function for such robot does not exist. Instead, there is a set of possible inverse kinematic solutions which satisfy the given robot pose. Obviously,

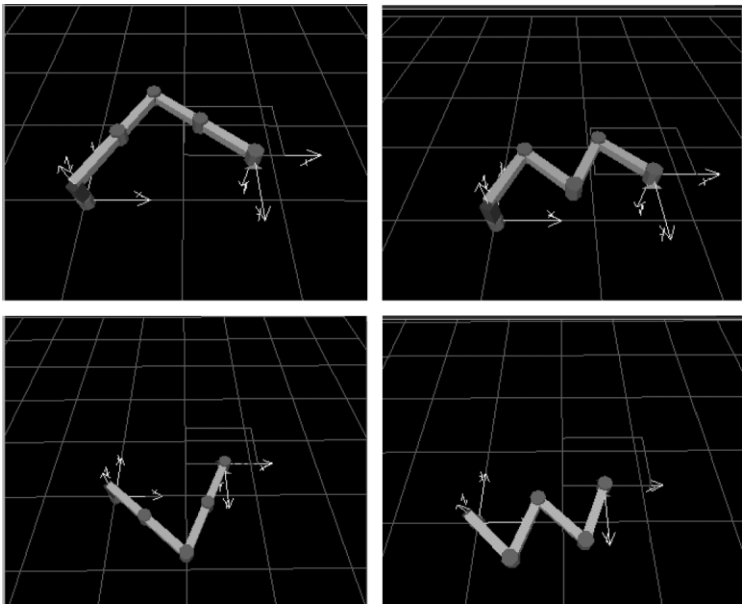


Figure 1. Four-way execution of a rectangular trajectory by a redundant 4 DOF planar robot.

such set for a 4 DOF redundant planar robot shown in Fig. 1 contains four concurrent candidate solutions.

The excessive number of redundant DOF becomes very beneficial in applications like inspection and maintenance in nuclear power plants, manufacturing and assembly in very confined spaces or medical diagnosis of the human intestine. Hyper-redundant robots are able to avoid obstacles in the workspace in much easier way than standard robots and also, they can adapt to variations of workspace if such changes occur during task execution.

Depending on the type of a hyper-redundant robot, different locomotion patterns can be targeted to resemble the locomotion patterns seen in nature (Chirikjian and Burdick 1995). This imposes a handful of design requirements, from solving the inverse kinematics problem to generating the trajectories which are both feasible and close to optimal. Real time trajectory planning for hyper-redundant robots designed to operate in industry-driven scenarios is a computationally demanding task. Usually complex mechanical constructions of hyper-redundant robots disallow easy assessment of robot's dynamical constraints affecting the trajectory planning.

Prompt adaptation of planned trajectories to static and dynamic changes in the workspace depends on the timeliness of an inverse kinematics solution for a new situation. This has become a driving force for research described herein—to find computationally effective ways of solving inverse kinematics in real-time or at least in the timeframe as close as possible to the real time.

The concept adopted here is that an inverse kinematics solution can be found using optimization algorithms (Davidor 1991, Aydin and Kocaoglan 1995, Huang et al. 2012, Wampler 1986). If the least square criterion is defined and the forward kinematics is a smooth function, gradient techniques can be employed. In the case of hyper-redundant robots, calculating a forward kinematics Jacobian matrix becomes computationally demanding and scales quadratically with the number of joints. This approach is also prone to singularity issues. In order to handle them even more computational effort is required. Providing this solution is computationally

tractable it can be difficult to deal with constraints such as workspace obstacles.

The ultimate goal is to develop a real time inverse kinematics algorithm capable of handling nonlinear constraints (Glumac and Kovačić 2013). Computational complexity of calculating the forward kinematics function scales linearly with the number of joints. Since genetic algorithms (GA) only require evaluation of candidate solutions, it is assumed that this algorithm tends to be faster than gradient-based algorithms (Goldberg 1989, Michlewicz 1992, Michlewicz 2005, Alvarez 2002, Mezura et al. 2006). This approach eliminates problems due to mechanical and algorithmic singularities. In order to avoid permanent attraction to local optima, GA use techniques such as crossover, mutation, rejection of the least fit and selection of the fittest (elitism) trying to imitate the natural process of evolution.

Bearing in mind the optimization problem, GA designs may vary depending on the type of structure, the GA operators and parameters (Kelly Senecal 2000, Tian et al. 2005, Simões and Costa 2003, Zamanifar and Koorangi 2007, Derigs et al. 1997, Elmihoub et al. 2004, Beaty et al. 1990). Understanding what happens to it when an operator changes or a parameter changes is a prerequisite for a successful GA design. Defining the Schema Theorem, Holland tried to make a theoretical analysis of GA performance (Holland 1975, Srivastava and Goldberg 2001). Liepins and Vose in

(1991) and (Vose 1993) have modeled the genetic search directly, instead of looking at the scheme. They considered infinite populations and observed them as a probability distribution, and then studied the way in which such distribution is changing under the influence of genetic operators. Prügel-Bennett and Shapiro analyzed GA using a statistical mechanics theory (Prügel-Benett and Shapiro 1974).

Although there is a number of contributions to a better understanding of the performance of GA (Alvarez 2002, Schmitt and Rothlauf 2001, Zhang and Mühlenbein 2004, Hartl 1990), some practical GA design criteria for determining the optimal GA parameters for a particular optimization problem are not still there. Usually, only simple GA structures are analyzed and parameters for the optimal behavior of the algorithm are obtained heuristically. In other words, the "optimal" GA parameters are regularly determined by practical experiments.

The so-called microgenetic algorithms (μGA) appear promising for use in online inverse kinematics solvers as they work with small populations (Tian et al. 2005, Krishnakumar 1989, Toscano and Coello 2001, Fuentes and Coello 2007). They use a mutation algorithm that periodically saves only the fittest solution in the population, while other solutions are replaced with new randomly selected entities (Kelly Senecal 2000, Tian et al. 2005). The rate of mutation affects the speed of convergence of μGA but useful criteria for selecting the optimal interval for a particular mutation optimization problem do not exist. Here we demonstrate a method for determining the "optimal" (best possible) μGA mutation interval based on a theoretical analysis of μGA. The theoretical analysis is based on the Markov chain theory (Stewart 2009, Ching et al. 2007), which has been used for analysis of GA by other authors (Poli et al. 2001). Further improvement can be searched through the consideration of other evolutionary computational approaches such as optimization using the clonal selection principle (Nunes de Castro and Von Zuben 2002), and microimmune algorithms (μIA). These algorithms do not use crossover operation, but also work with small

populations (Nunes de Castro and Timmis 2002, Dasgupta 2006, Wong and Lau 2009, Zhang 2007, Chen et al. 2010, Lin and Chen 2011). This makes them rational candidates for use in on-line inverse kinematics solvers.

ROBOT KINEMATICS

A hyper-redundant robot is represented as a rigid body serial chain composed of N joints represented by a joint variable vector $\mathbf{q} = [q_1 \; q_2 \; \ldots \; q_N]^T$. A kinematic model of such chain is described with homogeneous transformation matrices.

The robot model used for testing optimization algorithms is presented Fig. 2. Such robot has rotational joints which can be described with the following homogeneous matrices (Glumac and Kovačić 2013):

$$T_{2k-1}^{2k} = \begin{bmatrix} \cos(q_{2k}+1) & 0 & -\sin(q_{2k}+1) & 0 \\ \sin(q_{2k}+1) & 0 & \cos(q_{2k}+1) & 0 \\ 0 & -1 & 0 & 0 \\ 0 & 0 & 0 & 1 \end{bmatrix} \quad (1)$$

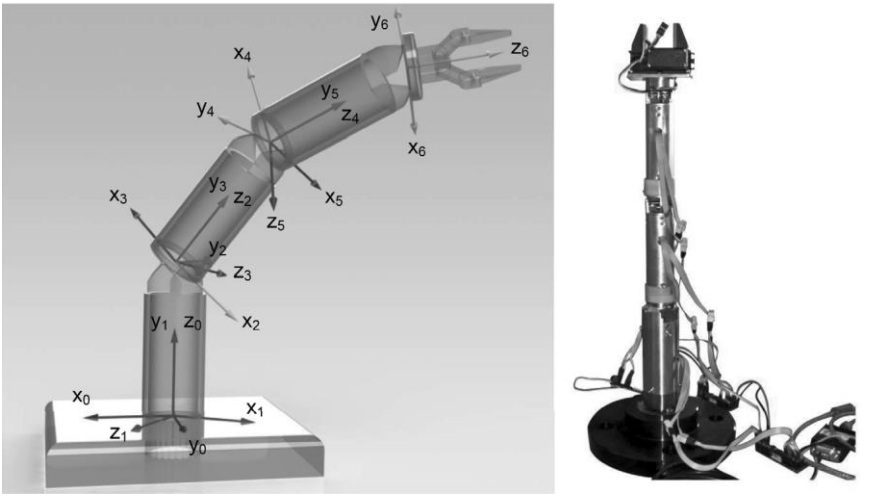


Figure 2. A kinematic model of a robotic arm with six revolute joints used for testing inverse kinematics algorithms presented in this chapter.

$$\mathbf{T}_{2k+1} = \begin{bmatrix} \cos(q_{2k+1}) & 0 & \sin(q_{2k+1}) & 0 \\ \sin(q_{2k+1}) & 0 & -\cos(q_{2k+1}) & 0 \\ 0 & 1 & 0 & l \\ 0 & 0 & 0 & 1 \end{bmatrix} \quad (2)$$

where l = 12.5 cm is a link length, $k \in \{0; 1; 2; \ldots\}$ is a link index and q_i is the angle of rotation for joint $i \in \{1; 2; \ldots; N\}$.

Robot configuration $\mathbf{q} \in S$ is influenced by mechanical limitations of each joint q_i; $q_{2k+1} \in [-\pi \text{ rad}, \pi \text{ rad}]$, $q_{2k+2} \in [-\pi/4 \text{ rad}, \pi/4 \text{ rad}]$. These limitations are due to mechanical construction and electrical wiring of the robot. From the algorithmic point of view, a set of possible robot configurations is a bounded box $S \subset \mathbb{R}^n$.

Homogeneous transformation which transforms the end effector coordinate system into the base coordinate system is presented with the following matrix:

$$\mathbf{T}_0^N = \mathbf{T}_0^1 \mathbf{T}_1^2 \ldots \mathbf{T}_{N-1}^N = \begin{bmatrix} x_1 & y_1 & z_1 & p_1 \\ x_2 & y_2 & z_2 & p_2 \\ x & y & z & p \end{bmatrix}$$

$$\begin{bmatrix} & & & \\ & & & \\ & & & \\ 0 & 0 & 0 & 1 \end{bmatrix} \tag{3}$$

Forward kinematics is the problem of determining the end effector pose **w** (position **p** and orientation ϕ) for a given joint configuration **q**. We assume that the end effector orientation is represented by an approach vector **a** = $[z_1 \; z_2 \; z_3]^T$. Such representation is good enough for many standard applications where robot grippers rotate around the approach vector. The main reason for using this representation is a simple way of calculating and visualizing an orientation error.

Let *W* denote a set of feasible end effector poses. Then a forward kinematics function $f : S \rightarrow W$ calculates the end effector pose **w** for given joint parameters **q**:

$$\mathbf{w} = f(\mathbf{q}) = [\mathbf{p}] = [p_3 \quad z_3] \tag{4}$$
$$[p \; p \qquad z_1$$
$$z_2$$

Solving inverse kinematics is a problem of finding some robot configuration $\mathbf{q}_{opt}$ in which the end effector pose is equal to the reference pose $\mathbf{w} = \mathbf{w}_{ref}$. It is desirable to find a closed form solution which would be extracted from a set of solution candidates after satisfying some additional criteria (spatial distribution of obstacles in robot's workspace, shortest displacement of all joints for a given pose change, etc.) Solutions for a large number of configurations can be found in (Crane and Duffy 1998). In this chapter we are focused on hyper-redundant robots with a large number of joints which prevent elegant formulation of a closed form solution. By increasing the number of joints and having finer resolutions of joint displacement measurements, the set of possible solutions increases dramatically, asking so for other ways of solving the inverse kinematics problem.

A frequently used way to solve the inverse kinematics problem is by using velocity based control. The relationship between the rate of change of the end effector's pose and the rate of change of *N* joint parameters is given with the following relation:

$$\dot{\mathbf{w}} = \mathbf{J}\dot{\mathbf{q}} \tag{5}$$

where $\mathbf{J} = \partial\mathbf{w}/\partial\mathbf{q}$ is the Fréchet derivative of (4). Dimensions of Jacobian $\mathbf{J}$ are $6 \times N$ and the solution of inverse kinematics problem using velocity control may attain the following form:

$$\dot{\mathbf{q}} = \mathbf{J}^{*}\dot{\mathbf{w}} \tag{6}$$

where $\mathbf{J}^{*}$ is the pseudo inverse of Jacobian $\mathbf{J}$. This approach is prone to singularity issues which may be solved by introducing regularization or by augmenting the end effector pose with energy or manipulability constraints (Galicki 2007, Brock et al. 2008).

This approach has an issue of large computational complexity with respect to the number of joints. The forward kinematics of the robot used for case study in this chapter can be calculated using (3). This calculation is linear $o(N)$ in the

number of joints as it requires multiplication of joint transformation matrices. The Jacobian matrix of (4) needs calculation of the rate of change of the end effector coordinate system with respect to the change of a robot joint displacement:

$$\frac{\partial \mathbf{T}_N^0}{\partial q_k} = \mathbf{T}_1^0 \mathbf{T}_2^1 \cdots \frac{\partial \mathbf{T}_k^{k-1}}{\partial q_k} \cdots \mathbf{T}_N^{N-1} \quad (7)$$

which makes that its calculation is quadratic $o(N^2)$ in the number of joints. After calculation of the Jacobian matrix **J** follows additional calculation of pseudoinverse $\mathbf{J}^*$ or its regularized form which further increases the computational complexity. For robots with a large number of joints this may be a serious limitation in using this approach for solving inverse kinematics.

Optimization Approach

When dealing with hyper-redundant robots different inverse kinematics solutions may need to be employed. In other words the inverse kinematics problem is determined as a problem of minimizing a suitable penalty function f_p:

$$\mathbf{q}_{opt} = \arg\min_{\mathbf{q} \in S} f_p(\mathbf{q}) \quad (8)$$

As stated in (8), the solution $\mathbf{q}_{opt}$ minimizes a penalty function $f_p : S \rightarrow R$ over the space of possible robot configurations S. A penalty function f_p needs to be defined so that its minima are robot configurations which achieve the reference end effector pose $\mathbf{w}_{ref}$. The penalty function is defined as follows (Glumac and Kovačić 2013):

$$f_p(\boldsymbol{q}) = \|\boldsymbol{p}_{ref_1} + l\|\boldsymbol{a}_{ref} - \boldsymbol{p}\| + \|\boldsymbol{a}\| \quad (9)$$

where $\|.\|_1$ is a vector norm defined as $\|\mathbf{x}\|_1 = \sum_{i=0}^{n} |x_i|$ and l is a parameter used to impacts of two deviation terms.

Graphical presentation of the terms used in this criterion is given in Fig. 3.

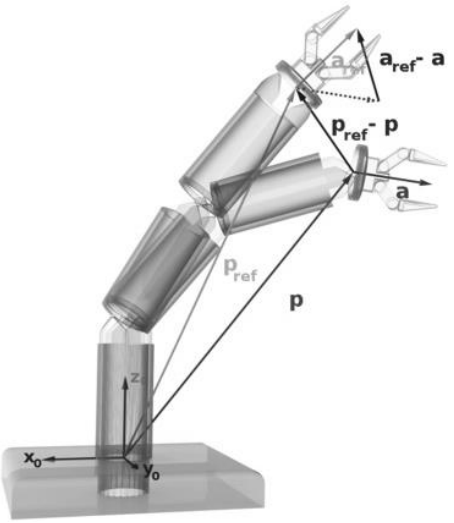


Figure 3. A reference position $\mathbf{p}_{ref}$ and approach vector $\mathbf{a}_{ref}$ are presented in light gray and a candidate solution (position **p** and approach vector **a**) are in black. Differences in respective vectors are colored black. © [2013] IEEE. Reprinted, with permission, from Glumac, S. and Z. Kovačić. 2013. Micro- immune algorithm for solving inverse kinematics of redundant robots. Proceedings of the 2013 IEEE International Conference on Systems, Man, and Cybernetics, pp. 201–207, Manchester, CPS (Conference Publishing Services), 2013.

COMPARISON OF MICROGENETIC AND MICROIMMUNE OPTIMIZATION ALGORITHMS

The μGA and μIA optimization algorithms presented in this section are used in solving the problem (8) over a bounded box $S \subset \square^n$. Without loss of generality it can be assumed that the search space S is the Cartesian product of n unit intervals $S = [0, 1]^n$. Any bounded box can be reduced to S using translation and scaling.

μGA and μIA considered in this analysis are described respectively in pseudocode blocks Algorithm 1 and Algorithm 2. μGA is taken from (Dužanec and Kovačić 2009) while μIA was developed as a simplification of μGA (Glumac and Kovačić 2013).

While searching for an optimal solution both algorithms use the contraction operator (Dužanec and Kovačić 2009). This operator contracts the search space around the latest best solution found. At the beginning of the search initial search space is set to $S^0 = S$. Let $\mathbf{q}^v = [q_1^v \; q_2^v \; \ldots \; q_n^v]^T$ denote a best solution found after v contractions of search space. Search space after the v-th contraction is given with the following expression:

$$S^v = \{\mathbf{q} \in \mathbb{R}^n : \mathbf{q}_i \in [q^v_i - \frac{\lambda^v}{2}, q^v_i + \frac{\lambda^v}{2}] \text{ and } \mathbf{q} \in S\} \quad (10)$$

$$\prod_{i=1}^{n}$$

where λ is a contraction factor $\lambda \in [0, 1)$ and Π is a Cartesian product of sets. In μGA contraction of search space is used after every i_S steps. A step is one iteration of algorithm's main loop. In μIA contraction operator is alternating with the mutation operator.

The value λ^V is named the diameter of the search space S^V. The set S^V has the form of a ball with the radius length defined with $||.||_\infty$ norm and λ as its diameter if the constraint on S in (10) is ignored. When the diameter of the search space becomes smaller than an arbitrary value $d^* \in [0, 1)$, it is assumed that the search space has become so small that no better solution can be found. This eventually leads to stopping condition used in the experimental evaluation of optimization algorithms.

Algorithm 1. Pseudocode of μGA[1]

initialize *Population* of *L* individuals
while $\lambda^V > d^*$ **do**
  select two *Parents* and *Bad individual* from *Population*
  create a *Child* using **crossover**
  from *Parents* remove *Bad* individual from *Population* insert *Child* into *Population*
  if i_m iterations have passed **then mutate** *Population* with elitism
  if i_S iterations have passed **then**
    contract *Search space*
  end if
 end if
end while

Algorithm 2. Pseudocode of μIA[2] **initialize** *Population* of *L* individuals
while $\lambda^{V} > d^{*}$ **do**
  mutate *Population* with elitism
  contract *Search space*
end while

In the case the minimum value of penalty function is known, the value of the penalty function can be used to terminate the search. Since the value of (9) is known to be 0 for the optimal solution, the algorithm can terminate the search when the best found solution assesses better than some threshold parameter f^{*}. Parameter f^{*} should be a small value close to 0. This stopping condition is used in the algorithm executed on the microcontroller platform.

Population initialization is generation of *L* candidate solutions. Candidate solutions are sampled from the uniform distribution over the initial search space *S*. This step is the same for μIA and μGA.

[1,2] © [2013] IEEE. Reprinted, with permission, from Glumac, S. and Z. Kovačić. 2013. Micro- immune algorithm for solving inverse kinematics of redundant robots. Proceedings of the 2013 IEEE International Conference on Systems, Man, and Cybernetics, pp. 201–207, Manchester, CPS (Conference Publishing Services), 2013.

Mutation reinitializes population with preserving elitism. This saves the best solution and samples new $L-1$ candidate solutions from the uniform distribution over the contracted search space S^v. μGA mutates population after every i crossovers, while μIA mutates population along with every search space contraction.

Another difference between μIA and μGA is the use of crossover. Like most genetic algorithms μGA uses crossover, while μIA does not. Since artificial immune system algorithms do not use crossover, the microimmune algorithm is named after this property. μGA uses a 3-tournament selection to select three individuals from the population. Of three selected individuals, two more fitting individuals are used as parents (the mother and the father) while the third is removed from the population. Let $\mathbf{q}_f = [q_{f1} \; q_{f2} \; \ldots \; q_{fn}]^T$ denote the father and $\mathbf{q}_m = [q_{m1} \; q_{m2} \; \ldots \; q_{mn}]^T$ denote the mother. The child $\mathbf{q}_c$ is generated using the uniform distribution in the set (bounded box determined by its parents):

$$q_{ci} = \mathrm{rand}_i[\min(q_{fi}, q_{mi}), \max(q_{fi}, q_{mi})] \quad (11)$$

$$\mathbf{q}_c \in S = \prod_{i=1}^{n} [\min(q_{fi}, q_{mi}), \max(q_{fi}, q_{mi})]$$

and inserted in the population.

The crossover operation employed here creates new children (solutions) that reside in the portion of S bounded by their parents. This creates the possibility that both parents possess the same genes at the same positions in their genetic codes, and crossover would not be able to change them. The effect is that only a part of S is searched and an algorithm can easily get stuck in a local optimum. In order to prevent that, the mutation operator is applied. The rate of mutation must be chosen carefully; take too large, the crossover effect will be weakened by predominantly stochastic nature of GA. Take too small, the rate of mutation would

increase the probability of missing the global optimum. Memory requirements of μIA are independent of its parameters. Amount of memory used by μIA depends only on the number of dimensions in the penalty function domain, i.e., the number of robot joints *N*. During search, μIA needs space to store the best solution and values of search space limits, generate a new candidate solution and calculate a penalty function. The algorithm adds almost no memory requirements than those required to calculate the penalty function. μGA is also a memory efficient algorithm, but as opposed to μIA it needs to store an entire population of candidate solutions. Since the property of μGA is that number of individuals are small, this is not
a big increase in memory requirements.

Both μIA and μGA algorithms are not guaranteed to find an optimal solution in search space *S*. A final solution of an algorithm run may not be even close to optimal. In order to accommodate for this, an algorithm parameters need to be tuned. When properly tuned, μIA and μGA are expected to produce high quality solutions.

Mutation optimization in μGA

Bearing in mind the task of solving inverse kinematics of a hyper-redundant robot with *N* DOF the optimal solution vector $\mathbf{q}_{opt}$ we are looking for lies in the space of all possible solutions *S*. In order to find $\mathbf{q}_{opt}$, we use the penalty function $f_p(\mathbf{q})$ defined in (9).

Theoretical analysis of mutation effects in μGA

Generally, the solution space S of the N-dimensional optimization problem is the N-dimensional solid. Let us divide each dimension of the solution space into three subgroups:

$$\begin{aligned} A &= \{x \mid x \in [x_1, x_{opt} - \Delta_{opt})\} \\ B &= \{x \mid x \in [x_{opt} - \Delta_{opt}, x_{opt} + \Delta_{opt}]\} \\ C &= \{x \mid x \in (x_{opt} + \Delta_{opt}, x_2]\} \end{aligned} \tag{12}$$

Then the N-dimensional solution space is divided into 3^N subgroups. Figure 4 shows the solution space subgroups for $N = 1$ and $N = 2$.

Subgroup B is the region around the optimal solution given by the required precision of optimization problem solution. In the case of the N-dimensional optimization problem the chromosomes that have all the vector elements in the subgroup B represent a global solution.

The idea of behavioral analysis of □GA is to calculate the probability that the optimization problem will be solved near the global optimum. To get a better insight

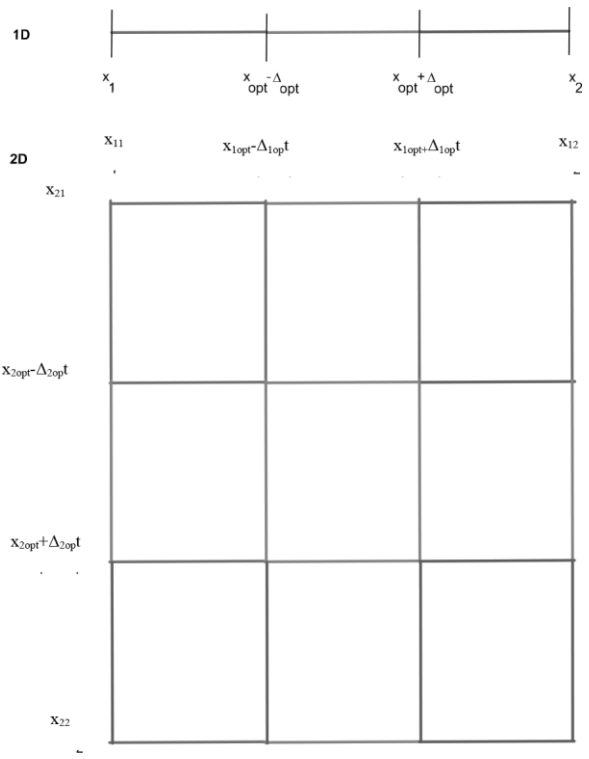


Figure 4. Subgroups for solution space dimensions N = 1, 2.

into the matter, first one-dimensional solution space is analyzed. Figure 5 shows an example of one-dimensional penalty function.

The probability of randomly generated number x from S to belong to subgroups A, B or C can be determined using geometric probability:

$$p_A = \frac{(x_{opt} - \varepsilon_{opt}) - x_1}{x_2 - x_1}, \quad p_B = \frac{2\varepsilon_{opt}}{x_2 - x_1}, \quad p_C = \frac{x_2 - (x_{opt} + \varepsilon_{opt})}{x_2 - x_1} \tag{13}$$

As described in (11), crossover operation results with a new chromosome (child) lying in the section of S bounded by both parents, which can be rewritten in the following way:

$$q_{id} = \min(q_{ip1}, q_{ip2}) + \text{rand}(|q_{ip1} - q_{ip2}|), \quad i = \overline{1, N} \tag{14}$$

where q_{id}, q_{ip1} and q_{ip2} represent the ith elements of the child and parent chromosomes (vectors), respectively.

In the one-dimensional optimization problem, this means that the crossover operation can generate a child in subgroup B (find a solution) if one parent is picked from the subgroup A, and the other from the subgroup B. To make sure that GA will find a solution, the chromosomes of the population should not be harvested from the same subgroup.

Let us index subgroups A, B and C as follows: 0 (A), 1 (B) and 2 (C). To determine all the possible states of the population, the *association matrix* must be defined, whose elements contain data that indicate whether the possible solutions are belonging to a subgroup A, B and C. Using the above introduced indexation the association matrix can be defined as follows:

$$\mathbf{Pr} = [pr_{ij}] = mod(floor(\frac{i}{3^j}), 3), \quad i \in [0, 3^N - 1], \quad j \in [0, N - 1] \tag{15}$$

Now, the probability of generating a chromosome in a

solution space subgroup must be defined. For a one-dimensional optimization problem the elements of the probability vector $\mathbf{d}_S$ are defined with (13):

$$\mathbf{d} = [p^{A\,B}\, p\ p\ ]^T \tag{16}$$

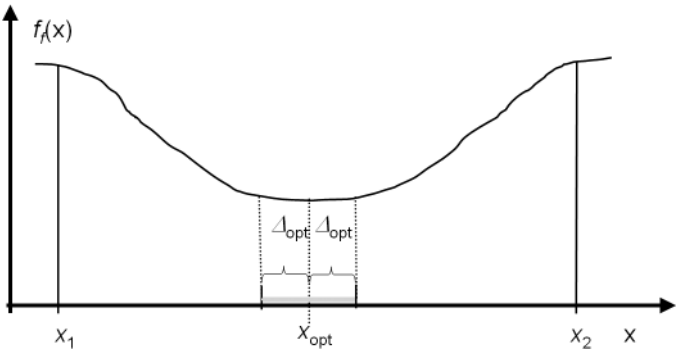


Figure 5. Example of a penalty function of a one-dimensional optimization problem.

The probability is actually proportional to the "size" of a subgroup in relation to the whole space of solutions, so the probability vector $\mathbf{d}_S$ can also be called the size vector. Using (15) and (16) the size vector for the *N*-dimensional space of solutions can be defined as follows:

$$\mathbf{d} = [d_{sv(i)}], \quad i \in [0, 3^N - 1]$$
$$d_{sv(i)} = \sum_{j=0}^{N-1} d_{js}(Pr_j), \quad i \in [0, 3^N] \tag{17}$$

In Eq. (17) we assume that the solution space of each vector element is the same. Generally, this is not true, however, the probabilities p_A, p_B and p_C really depend on the relations between ($x_2 - x_1$, x_{opt} and Δ_{opt}), and not actual values. Therefore, in order to simplify the calculation the reasonable assumption is that these probabilities are the same for each vector element.

L solutions of the population can be distributed to 3^N subgroups in $\bar{C}^{(L)}_{3^N}$ different ways. The *combination matrix* $\mathbf{T}_{vp}$ that contains all possible distributions of *L* chromosomes in 3^N subgroups is defined by the expression:

$$\mathbf{T}_{vp} = [\mathbf{t}^T_{vpi}] = [t_{vpij}], \quad 1 \le i \le \bar{C}^{(L)}_{3^N}, 1 \le j \le 3^N$$
$$\mathbf{t}^T_{vpi} = [t_{pi1} \cdots t_{piN}], \quad 0 \le t_{pij} \le L, \quad \sum_{j=1}^{3^N} t_{pij} = L, \quad \forall i \in [1, \bar{C}^{(L)}_{3^N}] \tag{18}$$

The probability of generating the initial population for each distribution of solutions as defined in the $\mathbf{T}_{vp}$ can be defined

using the size vector:

$$\mathbf{p} \quad \square \square p \quad \square, \; i \square \; \square 1, C^{3N} \quad \square$$
$$v0 \qquad \square\square L \; \square\square$$
$$v$$
$$0i$$

$$p = L! \prod_{v0} \frac{1}{t} \square \frac{3^N \square 1}{j \square 1} \frac{d_{vsj}}{vpij} \square \frac{t}{vp} \qquad (19)$$
$$t \quad \square (x \square x)^N \square$$
$$2\,1 \square$$

The next step of the genetic algorithm is selection. In our case, the three- chromosome tournament selection operator is used. Therefore, all possible distributions of three selected chromosomes in 3^N subgroups must be defined. Therefore the *selection state matrix* is defined as follows:

$$T \quad \square \mathbf{t} \quad \square t \square \quad \square, 1 \square i \square C^{(3)}, 1 \square j \square 3^N$$
$$vs \square \qquad \square \qquad 3N$$
$$vsi \square \quad vsij \qquad (20)$$
$$\square \qquad 3N$$
$$T$$
$$\mathbf{t} \square t \quad \square \quad \ldots t \quad \square t, \; 0 \quad \square 3, \quad t \quad \square 3, \square i \square \square 1, C^{(3)} \quad \square$$
$$\square \qquad \square \qquad \square$$
$$v \quad si \qquad si3 \qquad s \qquad sij \qquad \square\square 3^N \square\square$$
$$s \quad 1 \qquad N \square \qquad ij \qquad j \square 1$$
$$i$$

After selection and elimination of one chromosome, other two chromosomes become parents. All possible distributions of two parent chromosomes can be defined using the *parent matrix*:

$$T \; \mathbf{t}^T \; t \quad , 1 \le i \le C^{(2)} , 1 \le j \le 3^N$$

$$vc \quad \quad \overline{3^N} \qquad (21)$$
$$vci \quad vcij$$

$$\mathbf{t}^T t \quad \ldots t \quad t, \; 0 \le 2, \quad t \le 2, \; i \le 1, C^{(2)}$$

$$v \quad ci1 \quad ci3^N \quad c \quad cij \; j \quad 3^N$$
$$c \quad \quad \quad ij \quad 1$$
$$i$$

The *selection result matrix* $(C_L^{3^N} \times C^{3^N})$ defines the probability to jump from a state defined by the matrix $\mathbf{T}_{VP}$ to a state defined by the matrix $\mathbf{T}_{VS}$. Assuming that the selection probability for each chromosome is the same, regardless of position in the space of solutions, the elements of the selection result matrix **O** can be defined by:

$$o_{ij} = \frac{\sum_{k=1}^{3^N} C^{(3)}(t_{sjk}) \cdot C^{(3)}(t_{pik})}{t} \quad 1, t \; 3 \; N \qquad (22)$$

$$L^{(3)} \quad \overline{C} \quad pil \; sjl$$

$$0 \quad \text{else}$$

$$i \le 1, \text{rows}(\mathbf{T}_{VP}) \; , j \le 1, 1, \text{rows}(\mathbf{T}_{VS})$$

After selection, the worst chromosome is eliminated. This means that the algorithm jumps from the state defined by the matrix $\mathbf{T}_{VS}$ to the state of the matrix $\mathbf{T}_{VC}$. Because the worst chromosome is deleted, it is not possible to delete a global solution (chromosomes that have all the vector elements in the subgroup *B*). Under this assumption the elements of the *elimination matrix* **E** are defined as follows:

$$e = \begin{cases} \dfrac{\sum_{k=1}^{3^N} C^{(2)}(t_{cjk}) \cdot C(t_{sik})}{3} & t_{sib} \le t_{cjb} \\ v_{ij} & 3 \le t_{cjb} \end{cases}$$

$$1 \quad \begin{cases} t_{cj} \; b \; 3 \; t_{si} \; b \; 2 \\ 0 \quad \text{else} \end{cases} \tag{23}$$

$$\forall i \in [1, \text{rows}(\mathbf{T}_{vs})], \forall j \in [1, 1, \text{rows}(\mathbf{T}_{vc})]$$

where b is the column of the association matrix describing a global solution:

$$\text{Pr}_{bi} \leftarrow 1 \forall i \in [1, \text{rows}(\text{Pr})] \tag{24}$$

Selection and elimination are followed by a crossover operation defined in expression (14). Positions of children generated within the solution space depend on the positions of their parents. The probability of generating a child within a specific subgroup of S depends on two conditions: subgroups to which parents belong and parents' positions therein. However, the probabilities of these two conditions are unknown. Therefore, the crossover result probability is calculated using mathematical expected values within all subgroups of S:

$$x_{opt} \quad x \quad x$$

$$x_{opt} \quad x$$

$$x_p \quad \frac{dx}{x_{opt} \quad x_1} \quad \frac{opt}{opt} \quad \frac{1}{2} \tag{25}$$

$$x_p \quad \frac{x}{(x \quad) \quad (x \quad)} dx \quad x_{opt}$$

$$x_{opt} \quad opt \quad opt \quad opt \quad opt$$

$$opt$$

$$x_2 \quad x \quad x \quad x$$

$$x_p \quad \frac{}{x_2 \quad (x_{opt} \quad opt)} dx \quad \frac{2opt \quad opt}{2}$$

$$opt \quad opt$$

Let us define the affiliation matrix of a 2-dimensional problem in the following form:

$$\mathbf{Pr} \quad \begin{matrix} 0 & 1 & 2 & 0 & 1 & 2 \\ 0 & 0 & 0 & 1 & 1 & 1 & 2 & 2 & 2 \end{matrix} \quad \begin{matrix} | \\ 0 \quad 1 \quad 2 \end{matrix} \tag{26}$$

A crossover probability vector based on the expected values of parents and the affiliation matrix (26), is defined by the expression:

$$\quad \quad 1 \quad 0 \quad 0 \quad T \qquad , p_1 \quad 0 \quad p_2 \quad 0$$

$$x \quad x \quad T$$

$$\quad \frac{opt \quad p \quad opt}{opt} \quad 0 \qquad , p_1 \quad 0 \quad p_2 \quad 1$$

□ x_{opt} $x_{opt} \square x_p \square$ □□
□ T
□□ $x_p \square$
□

□□ x_{opt} □ 2□ $x_p \square$ □ x_{opt} , $p \square 0 \square p \square 2$
$x_p \square$ □□ $_{opt}$ $_{opt}$ □ □ $_{opt}$ □

□□ x $\frac{-x}{p\square}$ $\frac{\square x}{p\square}$ $\frac{x \square x}{opt\ p\square}$ □ 1 2 □□
$_{opt}$ $_{opt}$ $_{opt}$

□ $x \square x$ □ □ □ □ T
□ □ $_{opt}$ $p\square$ $_{opt}$, $p \square 1 \square p \square 0$
$_{opt}$ 0□
□ x_{opt} □ $x_p \square$ 1 2
□□ x_{opt} □ (27)
$x_p \square$ □□

x (□p , p) 0□ ^{T} 1 , $p \square 1 \square p \square 1$
□
ve 1 2 □
□ □

1 2 T
□ $x \square x \square \square$
□0 $_{opt\ p\square}$ $_{opt}$, $p \square 1 \square p \square 2$
$_{opt}$ □
□ x_{opt} $x_{opt} \square x_p \square$ □□ ^{1} ^{2}
□□ □
$x_p \square$
□ □ x □ x □ □ 2□ $x \square x \square \square$ ^{T}
□ □ $_{opt}$ $p\square$ $_{opt}$ $_{opt}$, $p \square 2 \square p \square 0$
$p\square$ $_{opt\ opt}$ □
|
□ □□ x_{opt} x_{opt} $x_{opt} \square x_p \square$ ^{1} ^{2} □□
$x_p \square$ $x_p \square$
□ □ □ $x \square x \square \square$ ^{T}
□ □0 $_{opt\ p\square}$ $_{opt}$, $p \square 2 \square p \square 1$
$_{opt}$ □
□ x_{opt} □ x_{opt} □ 1 2
| $x_p \square$ $x_p \square$
□□
□ □0
□ □□ , $p_1 \square 2 \square p_2 \square 2$

0 1□ ^{T}

The crossover probability vector defines the probability that an element of the child chromosome will belong to a specific subgroup of S, if affiliations of respective parent elements are known. To determine the affiliation of the whole solution all vector

elements must be taken into account. The total probability is the product of probabilities of all elements of the vector:

$$\mathbf{x}_{vt}(s_1, s_2) = \prod \mathbf{x}_{vti}(s_1, s_2)$$
$$\mathbf{x}_{vti}(s_1, s_2) = \mathbf{x}_{ve}(pr_{i,s}, pr_{i,s}), 1 \le i \le N \quad (28)$$

$$\mathbf{x}_v(s_1, s_2) = x_{vi}, 1 \le i \le 3^N$$
$$x_{vi} = \prod_{k=1}^{N} x_{vt}(k, pr_k, i)$$

A *crossover probability matrix* defines the probabilities that the child chromosome belongs to a subgroup of S for every possible distribution of parents' chromosomes. It is defined as follows:

$$\mathbf{B} = b_{ij}, 0 \le i \le C^{(2)}, 0 \le j \le C^{(2)}$$
$$\mathbf{v} = v_{ij} \quad 3^N \quad (29)$$
$$3^N$$

$$\mathbf{b}_{vi} = \mathbf{x}_v(t_{vci,par1}, t_{vci,par})^T$$

At this point all probabilities, starting from generating the initial population, selection, elimination and crossover are defined. The result is that the probability of generating a new child chromosome within defined subgroups of S can be determined. Now the analysis can be made to determine how this affects the complete population. By elimination of the worst chromosome and generating a new one by the crossover operator the algorithm actually changes from one state of the selection state matrix $\mathbf{T}_{VS}$ to another. The probabilities of jumping from one state of the selection state matrix to another are defined with the *transition probability matrix* **K**:

$$k_{i,g_s(\mathbf{T}, inc_{c(i)}(\mathbf{T}, j))} = b_{ij}$$
$$\forall i = 1, rows(\mathbf{B}), \forall j = 1, cols(\mathbf{B}) \quad (30)$$

where g is the function that returns the index of the matrix row

containing a set of values:

$$g(\mathbf{M}, \mathbf{x}) \rightarrow i \rightarrow \mathbf{M}_i \rightarrow \mathbf{x}^T \quad (31)$$

while inc is the function that increments the ith element of the vector:

$$\text{inc}(\mathbf{x}, i) \rightarrow x_i \rightarrow x_i + 1 \quad (32)$$

The objective of the analysis is to determine the expected state of the overall population. The probability of jumping from one state of the combination matrix $\mathbf{T}_{VP}$ to another state of the selection state matrix $\mathbf{T}_{VS}$ is defined with the selection result matrix (22). The product of the elimination matrix **E** and the transition probability matrix **K** defines the probability of jumping from one state of $\mathbf{T}_{VS}$ to another by using a crossover operator. All possible changes caused by the crossover operator can be determined by the *change matrix* $\mathbf{T}_d$, which is defined for a 1-dimensional optimization problem as follows:

$$\mathbf{T}_d = \begin{bmatrix} d & d & d \\ 0 & 0 & 0 \\ 1 & 1 & 0 \\ 1 & 0 & 1 \\ 1 & 0 & 1 \end{bmatrix} \qquad (33)$$

$$d = \begin{bmatrix} 0 & 1 & 1 \\ 1 & 1 & 1 \\ 1 & 1 & 0 \\ 0 & 0 & 1 \end{bmatrix}$$

The first row of $\mathbf{T}_d$ describes a state where no change in the population distribution has occurred. This means that elimination of the worst chromosome and generation of a new chromosome affected the same subgroup (*A*, *B* or *C*). The second row indicates that elimination took place in *A* and generation happened in *B*. For the *N*-dimensional problem the dimension of the change matrix $\mathbf{T}_d$ becomes $(3^N) \times \frac{(3^N)!}{2!(3^N - 2)!}$.

The *change probability matrix* **D** describes the probability of population distribution changes defined by $\mathbf{T}_d$:

$$d(\mathbf{K})_{ij} = \begin{cases} 1, & \text{if } \mathbf{E}_{ij}(\mathbf{K}) \neq 0 \\ 0 & \text{else} \end{cases}, \quad i, j = 1, \ldots, \text{rows}(\mathbf{E}(\mathbf{K})) \qquad (34)$$

where

$$\mathbf{E}_{ij} = g(\mathbf{T}_d, (\mathbf{T}_{sj} - \mathbf{T}_{si})^T) \qquad (35)$$

The probability of jumping from one state of the $\mathbf{T}_{vp}$ can now be defined with the

transition matrix **C**:

$$c_{ij} = \begin{cases} 1, & \text{if } (o_{ij} - d_{ij}) = 0 \\ 0, & \text{otherwise} \end{cases} \quad i, j = 1, \ldots, (\text{rows}(\mathbf{O}) \cdot \text{cols}(\mathbf{O})) \tag{36}$$

where

$$g_{ij} = (\mathbf{T}_{pi} - d_j)^T \tag{37}$$

The state of population in the ith iteration can now be determined as follows:

$$\mathbf{P}(i) = \mathbf{P}^T \cdot \mathbf{C}^i \tag{38}$$

The probability of finding the optimal solution is equal to the probability that the population has reached the state where all the affiliation matrix elements are equal to 1:

$$p_{vopt}(i) = \mathbf{p}_v(i)_k \quad pr_{l,k} = 1, \quad l = 1, N \tag{39}$$

, where

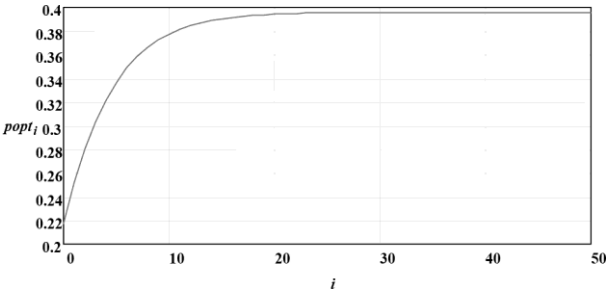


Figure 6. Probability of finding the optimal solution for a 2-dimensional optimization problem by using only the crossover operation for $x_1 = 0$, $x_2 = 255$, $x_{opt} = 127$, $\Box_{opt} = 1$ and $L = 5$.

The probability of finding the optimal solution by using only the crossover operation as defined in (36) is shown in Fig. 6. The whole process starts with a limited genetic material brought in by a randomly generated initial population, which does not guarantee that the optimal solution will be found. For example, the crossover of two chromosomes from the same subgroup of S will result with a new chromosome in the same subgroup, not necessarily the optimal one. Mutation operator inserts new genetic material into the population. In the microgenetic algorithms, mutation is performed periodically after every i_m iterations. All chromosomes except the best one are deleted
and replaced with new randomly generated chromosomes.

The problem is how to determine the number of iterations i_m for the optimal mutation interval. According to the graph shown in Fig. 6, the probability of finding the optimal solution saturates approximately after 33 crossovers (the whole genetic material becomes exhausted), which clearly indicates that this number of iterations
corresponds to the optimal mutation interval i_m.

To analyze the influence of mutation on the behavior of the genetic algorithm, the
mutation matrix, which contains all the possible combinations of generating L-1 new chromosomes, must be defined:

$$\mathbf{T}_{\mathbf{t}^T} \Box \quad \Box_t \Box \quad \Box, 1 \Box i \Box C^{(L\Box 1)}, 1 \Box j \Box 3^N$$

$$vm \Box \quad vmi \quad \Box \; vmij \Box \quad 3N$$

$$3^N \quad (40$$

$$vmi_{\square} \quad vmi3 \quad vmij \quad \square vmij \quad \square\square 3^N \square\square$$

$$vmi1 \quad {}_N \square \quad 3$$

$$\mathbf{t}^T \quad \square t \quad \square \quad \ldots t \quad \square t' \quad 0^N \quad \square (L \square 1 \quad t \quad \square L, \quad j \quad \square \quad 1 \quad \square L \square 1, \square i \square \square 1, C^{(L \square 1)} \square$$

Bearing in mind that only the best fitting chromosome will not be deleted during mutation, an assumption is made that all chromosomes except the one around x_{opt} have the same probability to survive. This can be described with the *best probabilities matrix* **U** defined as follows:

$$\square t_{ij}^{tmp} \quad t \quad \square 0$$

$$u_{ij} = \begin{cases} \square \overline{L} \; pi1 \\ 1 \quad j \; t \end{cases} \square 1 \square\square mpj1 \square\square 0 \qquad (41)$$

$$\square 0 \quad else$$

$$\square i \square \square 1, \text{rows}(\mathbf{T}_{mp}) \square , j \square \square 1, \text{cols}(\mathbf{T}_{mp}) \square$$

Now the probabilities of generating L-1 chromosomes in the subgroups of S must be defined:

$$\mathbf{p}_{vm} \;\; p_{vmi} \;\; C \;\; \beta^{N} \;\; 1 \;\; \left| \begin{array}{l} 1, \\ 3^{N} \;\; 1 \;\; \frac{1}{d} \end{array} \right. \;\; t_{ij}^{vm} \qquad (42)$$

$$p_{vmi} \;\; (L \;\; t_{vmij} \;\; \frac{vsj}{(x_2 \;\; x_1)^{N}} \;\; 1)! \;\; j \;\; 1$$

From the probabilities of generating new L-1 chromosomes and the probability of the best fitting chromosome, the probability of a new generated population state can be defined with the *mutation transfer matrix* **M**:

$$m_{i,g_p} \;\; \mathbf{T}_{vmj} \;\; \text{rows } p_{vMj} \;\; (\mathbf{T}_m) \;\; u_{i1} \;\; \text{,inc}(\mathbf{T} \;\;) \;\; \text{,} k \;\; \sum_{j \;\; 1} \qquad (43)$$

$$i \;\; 1, \text{rows}(\mathbf{T}_{vp}) \;\; , k \;\; 1, \text{rows}(\mathbf{T}_{vm})$$

The population state in the ith iteration can now be determined as follows:

$$\mathbf{P}(i) \;\; \mathbf{P} \;\; \mathbf{C}^{i_m} \;\; \mathbf{M} \;\; \left| \begin{array}{l} T_{round}(i) \\ \mathbf{C}^{mod(i,i_m)} \end{array} \right. \qquad (44)$$

Figure 7 shows the probability of finding the optimal solution for a 2-dimensional optimization problem by using crossover and mutation for $x_1 = 0$, $x_2 = 256$, $x_{opt} = 128$, $\Delta_{opt} = 1$, $L = 5$ and $i_m = 33$. It can be seen that every mutation gradually increases the

probability of finding the optimal solution and this probability finally settles in 1, thus
guaranteeing that the solution will be found after a given number of iterations.

μGA Optimization - Numerical Experiments

The described microgenetic algorithm was tested in the case of solving the inverse kinematics problem of a hyper-redundant robot arm shown in Fig. 2, which required

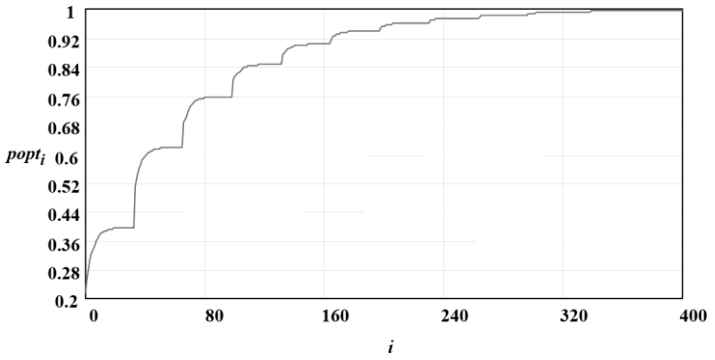


Figure 7. Probability of finding the optimal solution for a 2-dimensional optimization problem by using crossover and mutation for $x_1 = 0$, $x_2 = 256$, $x_{opt} = 128$, $\Delta_{opt} = 1$, $L = 5$ and $i_m = 33$.

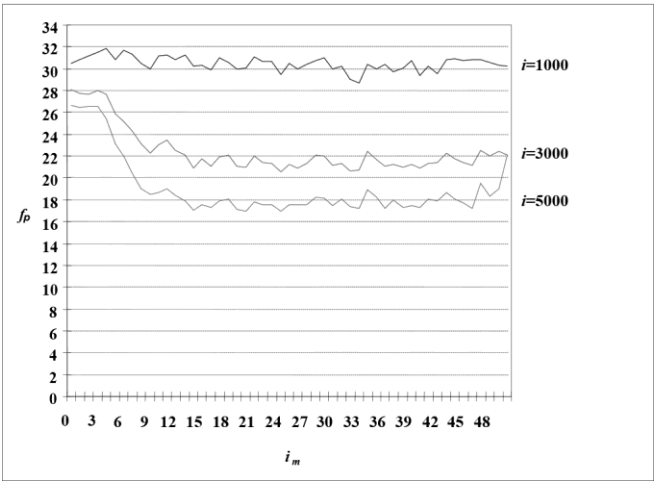


Figure 8. Penalty function vs. mutation interval after 1000, 3000 and 5000 GA iterations (Dužanec and Kovačić 2009).

solving a vector optimization problem (Dužanec and Kovačić 2009). To reduce the randomization effects in initial genetic populations, the algorithm was started 100 times with the same set of parameters, while the value of the mutation interval i_m was changed in the range of 1–50.

Results were used to calculate the average penalty function based on the best solutions found. Figure 8 shows the penalty function as a function of mutation interval after 1000, 3000 and 5000 iterations. We know that the optimal value of the mutation interval lies where the penalty function value is the lowest. As shown in Fig. 8, it can be seen that the numerically determined values of the best possible mutation intervals

lie in the wide range of $i_m \approx 15–40$, which is a good match with the behavior of μGA determined analytically ($i_m \approx 33$) (Dužanec and Kovačić 2009) and practically (Dužanec and Kovačić 2009).

MULTIOBJECTIVE OPTIMIZATION OF ALGORITHMS

Selection and crossover change the way an algorithm seeks an optimal solution. Depending on the choice of penalty function their use can slow down the convergence of an algorithm without increasing the quality of the final solution

(Glumac and Kovačić 2013). From the previous statement two criteria for evaluating the algorithm can be identified; the quality of solutions and the execution time. For inverse kinematics problem and algorithms being presented, these criteria are in conflict as experimentally shown in this section. There is no single fastest, most accurate algorithm and the trade-off between these two criteria is needed. Multiobjective optimization is used to determine which algorithms provide the best trade-off.

Let X denote a set of algorithms that are evaluated, $f_1 : X \rightarrow \mathrm{R}$ a criterion representing the quality of the final solutions and $f_2 : X \rightarrow \mathrm{N}$ the criterion representing the execution time. Algorithm $x \in X$ is dominated by algorithm $y \in X$ if y is strictly better than x by one criterion, and better than or equal by the other criterion. The goal

of multiobjective optimization is to find the Pareto frontier; the subset of algorithms such that no algorithm in this set is dominated by some other algorithm. An algorithm which is not in the Pareto frontier is strictly inferior in performance than at least one algorithm in the Pareto frontier.

In order to find the Pareto frontier of X, criteria f_1 and f_2 need to be defined. Let $\mathbf{q}_f$ denote the stochastic variable which models the final algorithm solution. In that case $f_p(\mathbf{q}_f)$ is the stochastic variable presenting the penalty function value. Since $f_p(\mathbf{q}_f)$ is a stochastic variable, its expected value is used as a criterion $f_1 : S \rightarrow \mathrm{R}$. In order to approximate the value of f_1 the arithmetic mean for a final number of optimization runs is used. Samples from the distribution of $f_p(\mathbf{q}_f)$ are generated in the manner described in Algorithm 3.

Algorithm 3. Generation of random criterion[3] uniformly sample a robot configuration $\mathbf{q} \in S$ calculate a pose $\mathbf{w}$ for the sampled configuration $\mathbf{q}$ generate a penalty function (9) using $\mathbf{w}_{ref} = \mathbf{w}$

The execution time must be measured in quantity which is independent of processor and implementation details. The number of penalty function calls m is a property of the algorithm itself and the penalty function calculation is considered computationally the most demanding task of one algorithm iteration. This makes m ideal for evaluating execution time. Since m is almost proportional to execution time measured in seconds, approximate time for algorithm run can be calculated using this property. The number of penalty function calls is a deterministic value and can be calculated for given parameters of μIA (Glumac and Kovačić 2013):

$$m = L + (L - 1)\log d^* \tag{45}$$

The multiobjective optimization is performed by brute force search using the experimental data described in the next section. A final result of this optimization is the comparison of Pareto frontiers of a μIA set and a μGA set presented in the next section.

NUMERICAL EXPERIMENTS WITH μGA AND μIA

Let $\mu IA_{(L,\lambda)}$ denote the instance of μIA with a population size L and a contraction factor λ. Let $\mu GA_{(L,\lambda,im,is)}$ denote the instance of μGA with a population size L, a contraction factor λ, a mutation step i_M and a contraction step i_S. Experiments are done on the set of $\mu IA_{(L,\lambda)}$ for each combination of $L \in \{3, 4, \ldots, 29\}$, $\lambda \in \{0.4, 0.41, \ldots, 0.99\}$ and the set of $\mu GA_{(L,\lambda,im,is)}$ for each combination of $\lambda \in \{0.55, 0.65, \ldots, 0.95\}$, $i_M \in \{1, 2, \ldots, 29\}$, $i_S \in \{i_M, 2\,i_M, \ldots\}$. In these experiments the minimal diameter of search space is set to be $d^* = 0.001$.

In order to evaluate the quality of the final solution each instance of algorithm is run 500 times. Samples of criterion $f_D(\mathbf{q}_f)$ are generated as in Algorithm 3 for each of those runs. The criterion f_1 is plotted in Fig. 9. Since the minimum value of this criterion is known to be 0, that plot can be used to assess how good solution can be reached using

3 © [2013] IEEE. Reprinted, with permission, from Glumac, S. and Z. Kovačić. 2013. Micro-immune algorithm for solving inverse kinematics of redundant robots. Proceedings of the 2013 IEEE International Conference on Systems, Man, and Cybernetics, pp. 201–207, Manchester, CPS (Conference Publishing Services), 2013.

μIA with some combination of parameters. It can be seen that both for bigger L and bigger λ the quality of the solution increases (Glumac and Kovačić 2013).

As described in the previous section, the execution time of each μIA instance is evaluated in algorithm with the number of penalty function calls (45). This criterion is plotted in Fig. 10. From the analysis of (45) it can be concluded that the number of penalty function calls increases as L or λ increases.

In order to perform multiobjective optimization both μIA set and μGA set need to be presented in the objective space. The set of μIA and the set of μGA are presented respectively in Fig. 11 and Fig. 12. The comparison of their Pareto frontiers is presented in Fig. 13. It can be observed that the Pareto frontier of the μIA set tends to dominate the Pareto frontier of the μGA set. The high percentage (88%) of algorithms in the Pareto frontier of μGA set have a small mutation step $i_M \in \{1, 2\}$. This can suggest that best algorithms in the set of μGA tend to decrease crossover frequency in favor of mutation (Glumac and Kovačić 2013).

To test how the quality of μIA solution scales with the number of robot joints, the quality of the solution and the execution time of μIA set was measured for the robot model with N = 12 joints. Results in the objective space are presented in Fig. 14 and the comparison of Pareto frontiers of this set and the μIA set for the robot model with 6 joints is presented in Fig. 15.

ALGORITHM PERFORMANCE TESTING ON THE MICROCONTROLLER PLATFORM

A modified μIA was tested on the Microchip dsPIC30F4011 microcontroller platform (Glumac and Kovačić 2013). This microcontroller has 32 kB of program memory and 4 kB of working memory. While performing experiments its instruction frequency

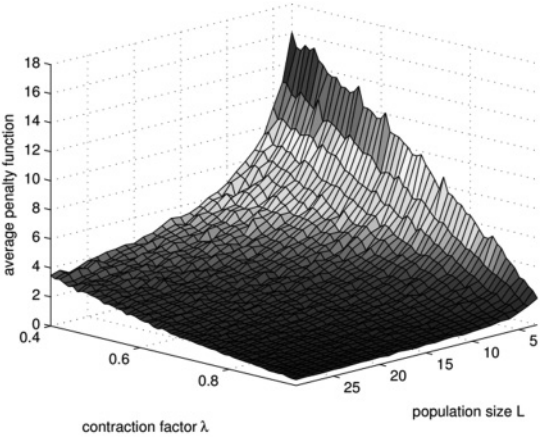


Figure 9. The mean value of μIA solution penalty function in μIA set for each combination of $L \in \{3, 4, \ldots, 29\}$, $\lambda \in \{0.4, 0.41, \ldots, 0.95\}$. © [2013] IEEE. Reprinted, with permission, from Glumac, S. and Z. Kovačić. 2013. Micro-immune algorithm for solving inverse kinematics of redundant robots. Proceedings of the 2013 IEEE International Conference on Systems, Man, and Cybernetics, pp. 201–207, Manchester, CPS (Conference Publishing Services), 2013.

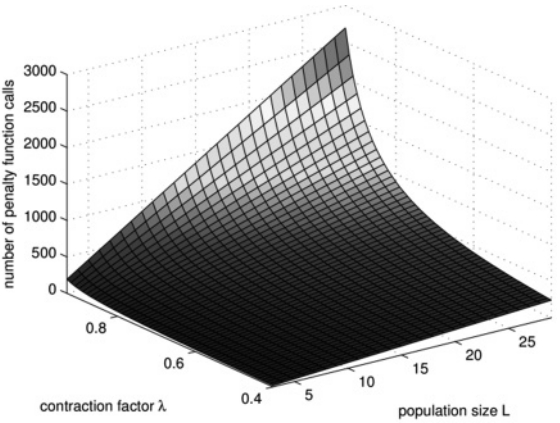


Figure 10. The number of penalty function calls in μIA set for each combination of $L \in \{3, 4, \ldots, 29\}$, $\lambda \in \{0.4, 0.41, \ldots, 0.93\}$. © [2013] IEEE. Reprinted, with permission, from Glumac, S. and Z. Kovačić. 2013. Micro-immune algorithm for solving inverse kinematics of redundant robots. Proceedings of the 2013 IEEE International Conference on Systems, Man, and Cybernetics, pp. 201–207, Manchester, CPS (Conference Publishing Services), 2013.

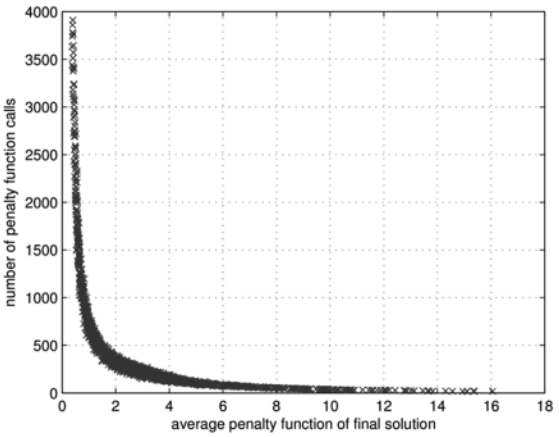


Figure 11. μIA set for each combination of $L \in \{3, 4, \ldots, 29\}$, $\lambda \in \{0.4, 0.41, \ldots, 0.99\}$ used in solving the inverse kinematics of a robot with $N = 6$ joints (presented in the objective space). © [2013] IEEE. Reprinted, with permission, from Glumac, S. and Z. Kovačić. 2013. Micro-immune algorithm for solving inverse kinematics of redundant robots. Proceedings of the

2013 IEEE International Conference on Systems, Man, and Cybernetics, pp. 201–207, Manchester, CPS (Conference Publishing Services), 2013.

was set to 29.49 MHz. Algorithm implementation was optimized using the fixed point arithmetic and lookup tables.

μIA implemented on the microcontroller is presented in the pseudocode block Algorithm 4. Two instances of μIA were tested; $\mu IA_{(7,0.93)}$ and $\mu IA_{(5,0.91)}$. Each instance was run 100 times on a randomly generated penalty function as in Algorithm 3. A reference
pose $\mathbf{w}_{ref}$ was generated on the personal computer and sent to the microcontroller over CAN bus. The microcontroller ran the algorithm and returned a final solution and a

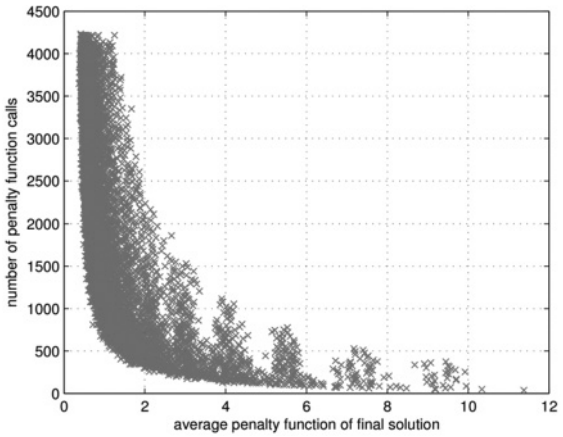


Figure 12. μGA set for each combination of $L = 5$, $\lambda \in \{0.55, 0.65, \ldots, 0.95\}$, $i_m \in \{1, 2, \ldots, 29\}$, $i_s \in \{i_m, 2\,i_m, \ldots\}$ used in solving the inverse kinematics of a robot with $N = 6$ joints (presented in the objective space). © [2013] IEEE. Reprinted, with permission, from Glumac, S. and Z. Kovačić. 2013. Micro-immune algorithm for solving inverse kinematics of redundant robots. Proceedings of the 2013 IEEE International Conference on Systems, Man, and Cybernetics, pp. 201–207, Manchester, CPS (Conference Publishing Services), 2013.

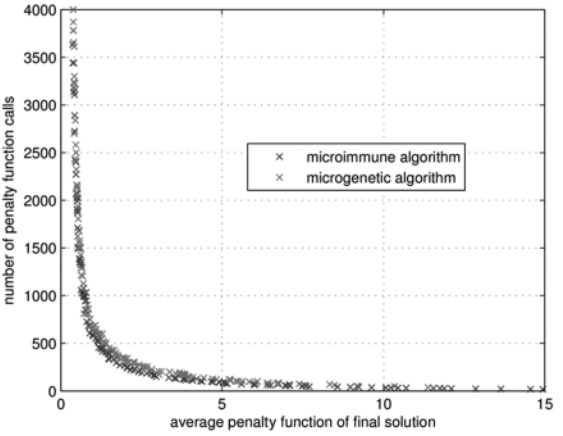


Figure 13. Pareto frontiers for the μIA set from Fig. 11 (black) and the μGA set from Fig. 12 gray.
© [2013] IEEE. Reprinted, with permission, from Glumac, S. and Z. Kovačić. 2013. Micro-immune algorithm for solving inverse kinematics of redundant robots. Proceedings of the 2013 IEEE International Conference on Systems, Man, and Cybernetics, pp. 201–207, Manchester, CPS (Conference Publishing Services), 2013.

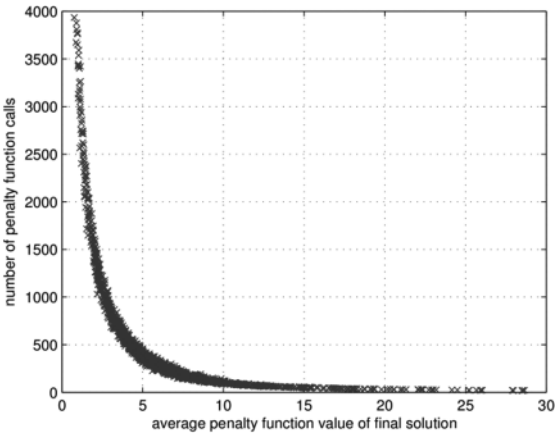


Figure 14. μIA set for each combination of $L \in \{3, 4, \ldots, 29\}$, $\lambda \in \{0.4, 0.41, \ldots, 0.99\}$ used in solving the inverse kinematics of a robot with $N = 12$ joints (presented in the objective space).
© [2013] IEEE. Reprinted, with permission, from Glumac, S. and Z. Kovačić. 2013. Micro-immune algorithm for solving inverse kinematics of redundant robots. Proceedings of the 2013 IEEE International Conference on Systems, Man, and Cybernetics, pp. 201–207, Manchester, CPS (Conference Publishing Services), 2013.

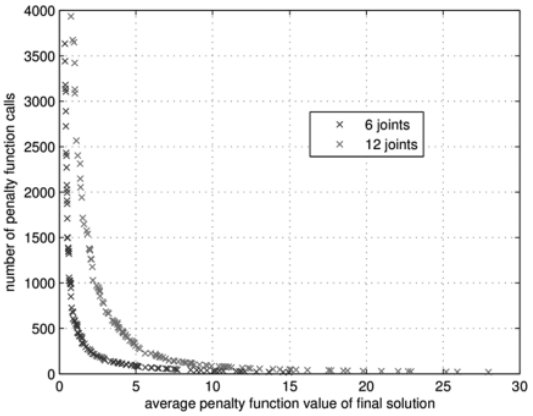


Figure 15. Pareto frontiers for the μIA set from Fig. 11 (black) and the μIA set from Fig. 14 (gray).
© [2013] IEEE. Reprinted, with permission, from Glumac, S. and Z. Kovačić. 2013. Micro-immune algorithm for solving inverse kinematics of redundant robots. Proceedings of the 2013 IEEE International Conference on Systems, Man, and

Cybernetics, pp. 201–207, Manchester, CPS (Conference Publishing Services), 2013.

measured execution time to the personal computer. Execution times for each algorithm run are presented in Fig. 16 and Fig. 17. The maximum execution times for $\mu IA_{(5,0.91)}$ and $\mu IA_{(7,0.93)}$ are respectively 55 ms and 98 ms. These execution times appear short enough for on-line inverse kinematics solvers in some robotic applications.

Algorithm 4 Pseudocode of μ1A^4
initialize *Population*
while J_W (**q**) > J^* **and** $d < d^*$ **do**
mutate *Population*
contract *Search space*
end while

Validity of using the number of penalty function calls as a measure for execution time relies on the assumption that the maximum execution time in seconds is proportional to the maximum number of penalty function calls. This assumption appears correct for algorithms tested in this section and allows the maximum execution time of any μIA on dsPIC4011 to be assessed.

Since algorithm used on the microcontroller is given a wanted penalty function value f^*, the percentage of algorithm runs able to achieve that value is presented in Fig. 18. This figure presents the fact that μIA offers no guarantee to find an optimal solution. Despite this fact, μIA can find high quality solutions (Glumac and Kovačić 2013). Since the value of (9) cannot be used to determine position and orientation errors of the algorithm's final solution, these quantities are presented respectively in Fig. 19 and Fig. 20. Figure 19 shows the Euclidean distance deviation of the final solution from a reference end-effector position $||\mathbf{p} - \mathbf{p}_{ref}||_2$. Likewise, Fig. 20 shows the angular deviation of the approach vector obtained from a reference approach vector of end-effector $\cos^{-1}(\mathbf{a}_{ref}^T \cdot \mathbf{a})$. The quality of these solutions needs to be evaluated in relation to the actual size of the robotic arm. The robot used for evaluation (see Fig. 2) is a three-link arm with each link of length equal to 12.5 cm. In the hard-home position the distance between the end effector and the arm base is 37.5 cm.

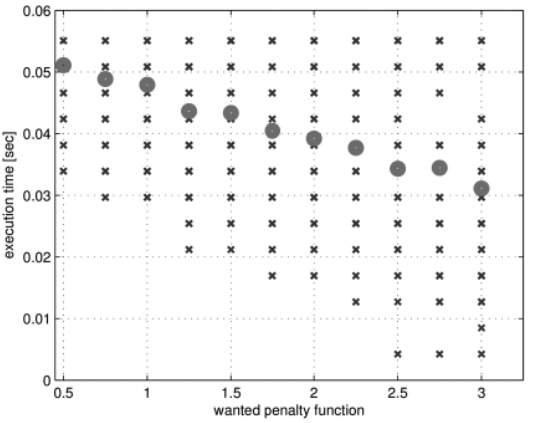


Figure 16. Run times in seconds for μIA(5,0.91) executed on PIC microcontroller, circles are the average case. © [2013] IEEE. Reprinted, with permission, from Glumac, S. and Z. Kovačić. 2013. Micro- immune algorithm for solving inverse kinematics of redundant robots. Proceedings of the 2013 IEEE International Conference on Systems, Man, and Cybernetics, pp. 201–207, Manchester, CPS (Conference Publishing Services), 2013.

4 © [2013] IEEE. Reprinted, with permission, from Glumac, S. and Z. Kovačić. 2013. Micro-immune algorithm for solving inverse kinematics of redundant robots. Proceedings of the 2013 IEEE International Conference on Systems, Man, and Cybernetics, pp. 201–207, Manchester, CPS (Conference Publishing Services), 2013.

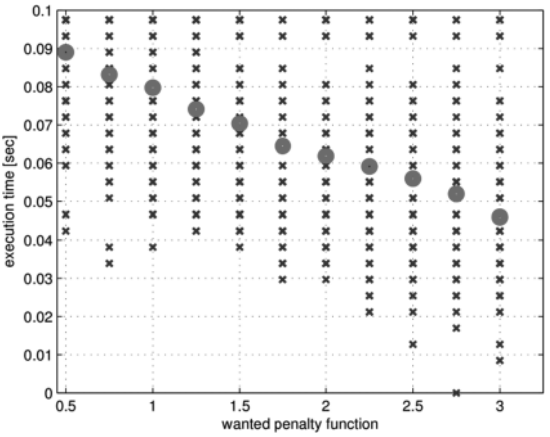


Figure 17. Run times in seconds for $\mu IA_{(7,0.93)}$ executed on PIC microcontroller with instruction, circles are the average case. © [2013] IEEE. Reprinted, with permission, from Glumac, S. and Z. Kovačić. 2013. Micro-immune algorithm for solving inverse kinematics of redundant robots. Proceedings of the 2013 IEEE International Conference on Systems, Man, and Cybernetics, pp. 201–207, Manchester, CPS (Conference Publishing Services), 2013.

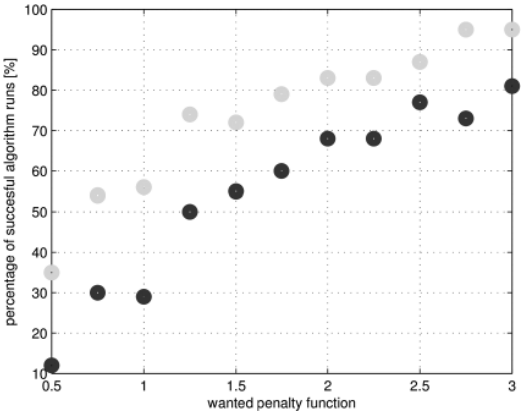


Figure 18. Ratio of runs for $\mu IA_{(5,0.91)}$ (black) and $\mu IA_{(7,0.93)}$ (light gray) that have found the solution with the wanted value of the penalty function. © [2013] IEEE. Reprinted, with permission, from Glumac,
S. and Z. Kovačić. 2013. Micro-immune algorithm for solving inverse kinematics of redundant robots. Proceedings of the 2013 IEEE International Conference on Systems, Man, and Cybernetics, pp. 201–207, Manchester, CPS (Conference

Publishing Services), 2013.

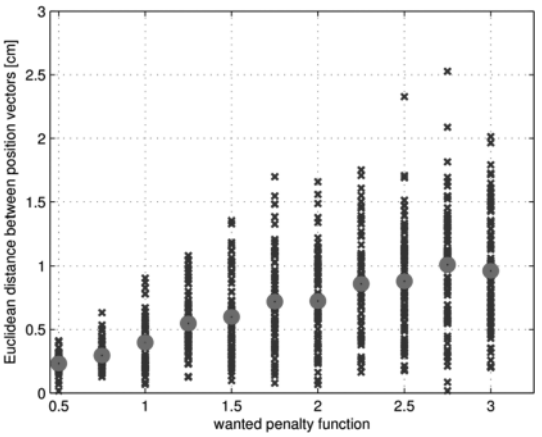


Figure 19. Position error for μIA$_{(7,0.93)}$ measured as the Euclidean distance between a reference and a calculated position of end-effector in cm. © [2013] IEEE. Reprinted, with permission, from Glumac,
S. and Z. Kovačić. 2013. Micro-immune algorithm for solving inverse kinematics of redundant robots. Proceedings of the 2013 IEEE International Conference on Systems, Man, and Cybernetics, pp. 201–207, Manchester, CPS (Conference Publishing Services), 2013.

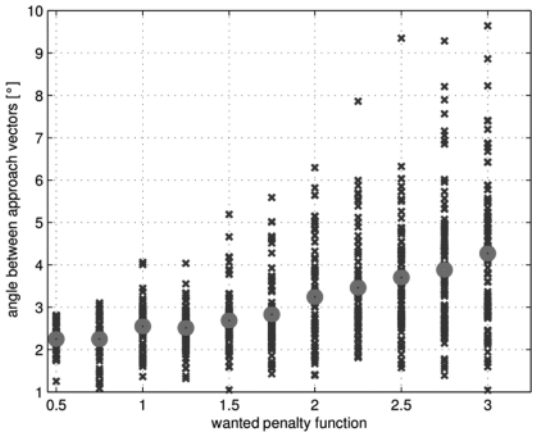


Figure 20. Orientation error for μIA$_{(7,0.93)}$ measured as the angle between a reference and a calculated approach vector of end-effector in degrees. © [2013] IEEE. Reprinted, with permission, from Glumac,
S. and Z. Kovačić. 2013. Micro-immune algorithm for solving

inverse kinematics of redundant robots. Proceedings of the 2013 IEEE International Conference on Systems, Man, and Cybernetics, pp. 201–207, Manchester, CPS (Conference Publishing Services), 2013.

CONCLUSIONS

This chapter is concerned with evaluation of microgenetic and microimmune optimization algorithms for solving inverse kinematics of a redundant robotic arm as a prerequisite for adaptive trajectory planning in various manipulation tasks. To ensure the quickest search of the optimal solution, it is desirable to have the structure and parameters of genetic algorithms optimized. The advantage of microgenetic algorithms is that they work with smaller genetic populations and thus allow for faster optimization runs.

The method of determining the optimal (best possible) mutation interval for microgenetic algorithms based on the analysis of their behavior is described. This provides a theoretical basis for the use of microgenetic algorithms in concrete optimization problems.

Since the theoretical analysis of algorithms is not always possible, multiobjective optimization of optimization algorithms is the approach being proposed and presented in this chapter. This kind of metaoptimization provides a straightforward way to determine a good optimization algorithm and its parameters without the need for making a deep theoretical analysis. Additional benefit of this procedure is that it provides the means to find out whether the considered type of optimization algorithm is a feasible candidate for solving a particular optimization problem.

As shown first by numerical experiments with μGA and μIA, and then by performance testing of μIA on a standard low-cost microcontroller platform, μIA enables the solution for inverse kinematics problem of a redundant robot with a small expected error. This shows that simplicity of μGA/μIA and low memory consumption are features that determine their very good potential for use in robust robotic systems trying to adapt their motion to slower and faster changes of their working environment.

REFERENCES

Alvarez, G. 2002. Can we make genetic algorithms work in

high–dimensionality problems? Stanford Exploration Project (SEP) report, 112, 2002.

Aydin, K. K. and E. Kocaoglan. 1995. Genetic algorithm based redundancy resolution of robot manipulators. 3rd International Symposium on Uncertainty Modelling and Analysis, p. 322.

Beaty, S., D. Whitley and G. Johnson. 1990. Motivation and framework for using genetic algorithms for microcode compaction. Proceedings of the 23rd Annual Workshop in Micro-programming and Micro-architecture (MICRO-23), pp. 117–124.

Brock, O., J. Kuffner and J. Xiao. 2008. Motion for manipulation tasks. Springer Handbook of Robotics, pp. 615–645, Springer, 2008.

Chen, J., Q. Lin and Z. Ji. 2010. A hybrid immune multiobjective optimization algorithm. European Journal of Operational Research (Elsevier), 204(2): 294–302. 16 July 2010.

Ching, W., S. Zhang and M. K. Ng. 2007. On multi-dimensional Markov chain models. Pacific Journal of Optimization, 3: 235–243.

Chirikjian, G. S. and J. W. Burdick. 1991. The kinematics of hyper-redundant robot locomotion. IEEE Transactions on Robotics and Automation, 11(6): 781–793, Dec. 1995.

Crane, C. D. and J. Duffy. 1998. Kinematic Analysis of Robot Manipulators, Cambridge University Press, 1998.

Dasgupta, D. 2006. Advances in artificial immune systems. Computational Intelligence Magazine, IEEE, 1(4): 40–49, Nov. 2006.

Davidor, Y. 1991. Genetic algorithms and robotics. World Scientific, 1991.

Derigs, U., M. Kabath and M. Zils. 1997. Adaptive genetic algorithms: A methodology for dynamic autoconfiguration of genetic search algorithms, MIC97, Sophia-Antipolis, France, pp. 231–248, 1997.

Dužanec, D. and Z. Kovačić. 2009. Performance analysis-based GA parameter selection and increase of μGA accuracy by gradual contraction of solution space. IEEE Conference on Industrial Technology ICIT 2009, 10–13 February 2009, Gippsland, Victoria, Australia.

Dužanec, D. and Z. Kovačić. 2009. Determination of optimal mutation interval for μGA based on the performance analysis of GA and μGA. Proceedings of the European Control Conference 2009, Budapest, pp. 3214–3220.

Elmihoub, T., A. A. Hopgood, L. Nolle and A. Battersby. 2004. Performance of hybrid genetic algorithms incorporating local search. Proceedings 18th European Simulation Multi-conference, Graham Horton (c) SCS Europe, pp. 154–160.

Fuentes, J. C. and C. A. Coello. 2007. Handling constraints in particle swarm optimization using a small population size. Lecture Notes in Computer Science, MICAI 2007: Advances in Artificial Intelligence, Vol. 4827, Springer, 2007.

Galicki, M. 2007. Generalized kinematic control of redundant manipulators. Lecture on Information Sciences, 2007, pp. 219–226.

Glumac, S. and Z. Kovačić. 2013. Micro-immune algorithm for solving inverse kinematics of redundant robots. Proceedings of the 2013 IEEE International Conference on Systems, Man, and Cybernetics, pp. 201–207, Manchester, CPS (Conference Publishing Services), 2013.

Goldberg, D. E. 1989. Genetic Algorithms in Search, Optimization and Machine Learning, Addison Wesley, Reading, MA, 1989.

Hartl, R. F. 1990. A Global Convergence Proof for a Class of Genetic Algorithms, Univ. of Technology, Vienna, 1990.

Holland, J. H. 1975. Adaptation in Natural and Artificial Systems, University of Michigan Press, 1975. Huang, H. C., C. P. Chen and P. R. Wang. 2012. Particle swarm optimization for solving the inverse kinematics of 7-DOF robotic manipulators. Systems, Man and Cybernetics (SMC), 2012 IEEE

International Conference on, 2012.

Kelly Senecal, P. 2000. Numerical optimization using then GEN4 micro-genetic algorithm code, Engine research center, University of Wisconsin-Madison, Draft Manuscript, August 2000.

Krishnakumar, K. 1989. Micro-genetic algorithms for stationary and non-stationary function optimization. pp. 289–296. *In*: SPIE Proceedings: Intelligent Control and Adaptive Systems, 1989.

Lin, Q. and J. Chen. 2011. A novel micro-population immune multiobjective optimization algorithm.
Computers & Operations Research (Elsevier), on-line, November 2011.

Mezura, E., J. Velázquez and C. A. Coello. 2006. A comparative study of differential evolution variants for global optimization. pp. 485–492. *In*: ACM, GECCO 2006.

Michlewicz, Z. 1992. Genetic Algorithms + Data Structures = Evolution Programs, Springer Verlag, 1992.

Michlewicz, Z. 2005. Evolutionary Computation for Modelling and Optimization, Springer, 2005.

Nunes de Castro, L. and F. J. Von Zuben. 2002. Learning and optimization using the clonal selection principle. IEEE Trans. Evol. Comput., 6(3): 239–251, June 2002.

Nunes de Castro, L. and J. Timmis. 2002. Artificial Immune Systems: A new Computational Intelligence Approach, Springer, 2002.

Poli, R., J. E. Rowe and N. F. McPhee. 2001. Markov chain models for GP and variable-length GAs with homologous crossover, Proceedings of the Genetic and Evolutionary Computation Conference GECCO-2001, pp. 112–119.

Prügel-Benett, A. and J. L. Shapiro. 1974. An analysis of genetic algorithms using statistical mechanics.
Phys. Rev. Lett., 72: 75–114.

Schmitt, F. and F. Rothlauf. 2001. On the mean of the second largest eigenvalue on the convergence rate of genetic algorithms. Working Paper 1/2001, Morgan Kaufmann Publishers, San Francisco, California.

Simões, A. and E. Costa. 2003. Improving the genetic algorithm's performance when using transformation, International Conference on Neural Networks and Genetic Algorithms (ICANNGA'03), pp. 175–181, Roanne, France,

23–25 April, Springer, 2003.

Srivastava, P. and David E. Goldberg. 2001. Verification of the Theory of Genetic and Evolutionary Continuation. IlliGAL Report No. 2001007, January, 2001.

Stewart, W. J. 2009. Probability, Markov chains, queues and simulation: the mathematical basis of performance modelling, Princeton University Press, 2009.

Tian, Y., J. Qian and F. Meng. 2005. Optimal design of matched load by immune micro genetic algorithm. Progress in Electromagnetics Research Symposium, Hangzhou, China, August 22– 26, pp. 101–104.

Toscano, G. and Carlos A. Coello. 2001. A micro-genetic algorithm for multiobjective optimization. *In*: First International Conference on Evolutionary Multi-criterion Optimization, Lecture Notes in Computer Science, Vol. 1993, Springer, 2001, pp. 126–140.

Vose, M. D. and G. E. Lipiens. 1991. Punctuated equilibria in genetic search. Complex Systems, 5: 31–44.

Vose, M. D. 1993. A Critical Examination of the Schema Theorem, Technical Report ut-cs-93-212, University of Tennessee, Knoxville, 1993.

Wampler, C. W. 1986. Manipulator inverse kinematic solutions based on vector formulations and damped least-squares methods. Systems, Man and Cybernetics, IEEE Transactions on, 1986.

Wong, E. Y. C. and H. Y. K. Lau. 2009. Advancement in the twentieth century in artificial immune systems for optimization: Review and future outlook. Systems, Man and Cybernetics, 2009. SMC 2009. IEEE International Conference on, 2009.

Zamanifar, K. and M. Koorangi. 2007. Designing optimal binary search tree using parallel genetic algorithms. IJCSNS International Journal of Computer Science and Network Security, 7(1): 138–146, January 2007.

Zhang, Q. and H. Mühlenbein. 2004. On the convergence of a class of estimation of distribution algorithms. IEEE Transactions on Evolutionary Computation, 8(2): 127–136, April 2004.

Zhang, Z. 2007. Immune optimization algorithm for constrained nonlinear multiobjective optimization problems. Applied Soft Computing (Elsevier), 7(3): 840–857, June 2007.

7. Conclusion and Future Work

Software for Controller Simulation

```
C     FILE DIGCTLF.FOR
C     PROGRAM TO FIND TIME HISTORY
C        USES NONADAPTIVE RUNGE-KUTTA
C     ALLOWS SIMULATION OF SYSTEMS WITH DELAY
C     NEEDS SUBROUTINES:
C        F(TIME,X,XP) FOR CONTINUOUS DYNAMICS
C        DIG(IK,T,X) FOR DISCRETE DYNAMICS
C        SYSINP(IT,X,TIME) FOR CONTINUOUS SYSTEM INPUT (OPTIONAL)

            PROGRAM TRESP
            PARAMETER (NN=20,MM=10)
            REAL Y(0:1024,0:NN+MM),X(NN),SX(NN),XP(NN)
            INTEGER IX(NN+MM),IZ(NN+MM)
            CHARACTER *20 FILNAM,ANS,ANSC
            COMMON/CONTROL/U(MM)
            COMMON/OUTPUT/Z(MM)
            COMMON/DELAY/IT,TS
            COMMON/PARAM/PAR(10)
C
10          WRITE(*,*)'HOW MANY STATES?'
            READ(*,*) NX
            DO 15 I= 1,NX
15          SX(I)= 0.
            WRITE(*,*)'ENTER INITIAL STATES (Def= 0):'
            READ(*,*) (SX(I), I= 1,NX)
C
            I= 0
20          I= I+1
            PAR(I)= -1111
            WRITE(*,*) 'Enter parameter (Def= continue):'
            READ(*,*) PAR(I)
            IF (PAR(I) .NE. -1111) GO TO 20
C
```

```
      WRITE(*,*)'DIGITAL CONTROLLER (C) OR FILTER (F)? (DEF=N)'
      READ(*,'(A)') ANS
      IF(ANS.EQ.'F' .OR. ANS.EQ.'f') ANS= 'F'
      IF(ANS.EQ.'C' .OR. ANS.EQ.'c') ANS= 'C'
      WRITE(*,*)'CONTIN. INPUT SUBROUTINE REQUIRED? (DEF=N)'
      READ(*,'(A)') ANSC
      IF(ANSC.EQ.'Y' .OR. ANSC.EQ.'y') ANSC=  'Y'
30    WRITE(*,*) 'HOW MANY STATES TO BE PLOTTED?'
      READ(*,*) MX
      IF(MX.EQ.0) GO TO 37
      DO 35 I= 1,MX
35    IX(I)= I
      WRITE(*,*)'WHICH ONES? (DEF = IN ORDER)'
      READ(*,*) (IX(I), I= 1,MX)
37    WRITE(*,*)'PLOT HOW MANY OUTPUTS?'
      READ(*,*) MZ
      IF(MZ.EQ.0) GO TO 50
      DO 36 I= 1,MZ
36    IZ(I)= I
      WRITE(*,*)'WHICH ONES? (DEF= IN ORDER)'
      READ(*,*) (IZ(I), I= 1,MZ)
C
50    WRITE(*,*) 'RUN TIME?'
      READ(*,*) TR
      WRITE(*,*)'PRINTING TIME INTERVAL ON SCREEN?'
      READ(*,*) TPR
      IF(ANS.EQ.'F' .OR. ANS.EQ.'C') THEN
         WRITE(*,*)'SAMPLE PERIOD?'
         READ(*,*) TD
      END IF
      WRITE(*,*)'PLOTTING TIME INTERVAL?'
      READ(*,*) TPL
      IF(ANS.NE.'F' .AND. ANS.NE.'C') TD= TPL
      WRITE(*,*)'RUNGE-KUTTA INTEGRATION PERIOD?'
      READ(*,*) TS
      NPR= NINT(TR/TPR)
      NPL= NINT(TPR/TD)
      NT = NINT(TD/TPL)
      NTD= NINT(TPL/TS)
C
      TIME= 0.
      IT= 0
      IP= 0
      IK=0
      DO 60 I= 1,NX
60    X(I)= SX(I)
      Y(0,0)= TIME
      DO 70 I= 1,MX
70    Y(0,I)= X(IX(I))
      IF(MZ.GT.0) THEN
         IF(ANS.EQ.'C') CALL DIG(IK,TD,X)
         IF(ANSC.EQ.'Y') CALL SYSINP(IT,X,TIME)
         CALL F(TIME,X,XP)
```

11.

```
            IF(ANS.EQ.'F') CALL DIG(IK,TD,X)
            DO 75 I= 1,MZ
75          Y(0,MX+I)= Z(IZ(I))
         END IF
C
         DO 110 I= 1,NPR
         DO 90 J= 1,NPL
         IF(ANS.EQ.'C') CALL DIG(IK,TD,X)
         DO 100 K= 1,NT
         DO 85 KID= 1,NTD
         IF(IT.EQ.0) THEN
            WRITE(*,*)
            WRITE(*,80) (IX(IND), IND= 1,MX)
80          FORMAT(35X,'STATES'/'     TIME',10(I12))
            WRITE(*,'(11(1PE12.3))') (Y(0,IND), IND= 0,MX+MZ)
         END IF
         IF(ANSC.EQ.'Y') CALL SYSINP(IT,X,TIME)
         CALL RUNKUT(TIME,TS,X,NX)
         IT= IT+1
85       TIME= FLOAT(IT)*TS
         IP= IP+1
         Y(IP,0)= TIME
         DO 101 Ir 1,MX
101      Y(IP,L)= X(IX(L))
         IF(MZ.LE.0) GO TO 100
         DO 105 L= 1,MZ
105      Y(IP,MX+L)= Z(IZ(L))
100      CONTINUE
         IK= IK+1
         IF(ANS.EQ.'F') CALL DIG(IK,TD,X)
90       CONTINUE
         WRITE(*,'(11(1PE12.3))') (Y(IP,L), L= 0,MX+MZ)
110      CONTINUE
C
120      WRITE(*,130)
130      FORMAT(//2X,'ENTER 0 TO FILE ANSWERS'/8X,'1 TO QUIT'
     &   /8X,'2 TO RESTART',/8X,'3 TO PICK NEW STATES',
     &   /8X,'4 TO CHANGE TIME SCALE')
         READ(*,*) I
         GO TO (150,10,30,50) 1
C
         WRITE(*,*)'OUTPUT FILE NAME?'
         READ(*,'(A)') FILNAM
         OPEN(20,FILE= FILNAM)
         REWIND 20
         WRITE(20,*) MX+MZ
         WRITE(20,*) IP+1
         DO 140 J= 1,MX+MZ
         DO 140 I= 0,IP
140      WRITE(20,'(8(1PE14.6))') Y(I,J)
         REWIND 20
         CLOSE (20)
         GO TO 120
```

```
C
150         STOP
            END
C
C
C     FOURTH-ORDER RUNGE-KUTTA INTEGRATION SUBROUTINE
C
C     REQUIRES SUBROUTINE F(TIME,X,XP) TO DESCRIBE PLANT DYNAMICS
C
            SUBROUTINE RUNKUT(TIME,TS,X,N)
C
C     TS    SAMPLE PERIOD
C     X     STATE VECTOR
C     N     NUMBER OF STATES
C     XP    DERIVATIVE OF STATE VECTOR
C
            PARAMETER (NDIM=32)
            REAL X(*), XP(NDIM), X1(NDIM), XP1(NDIM)
C
            CALL F(TIME,X,XP)
            DO 10 I= 1,N
10          X1(I)= X(I) + .5*TS*XP(I)
C
            TIME= TIME + .5*TS
            CALL F(TIME,XI,XP1)
            DO 20 I= 1,N
            XP(I)= XP(I) + 2.*XP1(I)
20          X1(I)= X(I) + .5*TS*XP1(I)
C
            CALL F(TIME,XI,XP1)
            DO 30 I= 1,N
            XP(I)= XP(I) + 2.*XP1(I)
30          X1(I)= X(I) + TS*XP1(I)
C
            TIME= TIME + .5*TS
            CALL F(TIME,XI,XP1)
            DO 40 I= 1,N
40          X(I)= X(I) + TS*( XP(I)+XP1(I) )/6.
C
            RETURN
            END
```

REFERENCE

18. [Press *et al.* 1986] Press, W.H., Flannery, B.P., Teukolsky, S.A., and Vetterling, W.T., *Numerical Recipes.* New York: Cambridge University Press, 1986.

8. References

References[edit]

1. Benjamin K. Sovacool. "A Critical Evaluation of Nuclear Power and Renewable Electricity in Asia", *Journal of Contemporary Asia*, Vol. 40, No. 3, August 2010, p. 373.
2. *Invernizzi, Diletta Colette; Locatelli, Giorgio; Brookes, Naomi J. (2017-08-01). "How benchmarking can support the selection, planning and delivery of nuclear decommissioning projects". Progress in Nuclear Energy. **99**: 155–164. doi:10.1016/j.pnucene.2017.05.002.*
3. *Invernizzi, Diletta Colette; Locatelli, Giorgio; Brookes, Naomi J. (2017-10-01). "Managing social challenges in the nuclear decommissioning industry: A responsible approach towards better performance". International Journal of Project Management. Social Responsibilities for the Management of Megaprojects. **35** (7): 1350–1364. doi:10.1016/j.ijproman.2016.12.002.*
4. https://www.nrc.gov/reading-rm/doc-collections/fact-sheets/decommissioning.html Quote: Before a nuclear power plant begins operations, the licensee must establish or obtain a financial mechanism – such as a trust fund or a guarantee from its parent company – to ensure there will be sufficient money to pay for the ultimate decommissioning of the facility.
5. Liability for Nuclear Damage
6. *"Fact Sheets: Decommissioning Of Nuclear Power Plants". National Energy Institute. Retrieved 2014-06-19.*
7. DECON: a method of decommissioning, in which structures, systems, and components that contain radioactive contamination are removed from a site and safely disposed at a commercially operated low-level waste disposal facility, or decontaminated to a level that permits the site to be released for unrestricted use shortly after it ceases operation.
8. SAFSTOR: a method of decommissioning in which a nuclear facility is placed and maintained in a condition that allows the facility to be safely stored and subsequently decontaminated (deferred decontamination) to levels that permit release for unrestricted use.
9. ENTOMB: a method of decommissioning, in which radioactive contaminants are encased in a structurally long-lived material, such as concrete. The entombed structure is maintained and surveillance is continued until the entombed radioactive waste decays to a level permitting termination of the license and unrestricted release of the property. During the entombment period, the licensee maintains the license previously issued by the NRC.
10. Heuel-Fabianek, B., Kümmerle, E., Möllmann-Coers, M., Lennartz, R. (2008): The relevance of Article 37 of the Euratom Treaty for the dismantling of nuclear

reactors. atw – International Journal for Nuclear Power 6/2008 Archived September 11, 2008, at the Wayback Machine.
11. NRC Factsheet Decomissoning Quote: Before a nuclear power plant begins operations, the licensee must establish or obtain a financial mechanism – such as a trust fund or a guarantee from its parent company – to ensure there will be sufficient money to pay for the ultimate decommissioning of the facility.
12. Repository delay reduces Swiss NPPs' decommissioning costs
13. Le Télégramme: Brennilis
14. Ouest-France: "Brennilis : EDF se fait taper sur les doigts" Archived May 1, 2011, at the Wayback Machine.
15. *House of Commons Committee of Public Accounts (February 4, 2013). "Nuclear Decommissioning Authority: Managing risk at Sellafield" (PDF). London: The Stationery Office Limited. Retrieved December 2, 2013.*
16. *"SRS P and R Reactor Basins ISD Final" (PDF). D&D KM-IT – Deactivation and Decommissioning Knowledge Management Information Tool.*
17. Status of Decommissioning of Nuclear Facilities around the World
18. ENDS: Nuclear decommissioning funds "require oversight"
19. *Christoph Steitz, Barbara Lewis (February 16, 2016). "EU short of 118 billion euros in nuclear decommissioning funds". Reuters. Retrieved February 17, 2016.*
20. *"NRC Requests Plans from 18 Nuclear Power Plants to Address Apparent Decommissioning Funding Assurance Shortfalls" (PDF). Nuclear Regulatory Commission. June 19, 2009. Retrieved 2014-12-30.*
21. *Locatelli, Giorgio; Mancini, Mauro (July 2, 2010). "Competitiveness of Small-Medium, New Generation Reactors: A Comparative Study on Decommissioning". Journal of Engineering for Gas Turbines and Power. **132** (10): 102906–102906. doi:10.1115/1.4000613. ISSN 0742-4795.*
22. ^ Jump up to: [a] [b] [c] World Nuclear Association Decommissioning Nuclear Facilities published by www.world-nuclear.org (Association of nuclear reactors builders), March 2017
23. Wolrd Nuclear Association: Decommissioning Nuclear Facilities
24. http://infcis.iaea.org/NFCIS/Facilities
25. *OECD Nuclear Energy Agency (May 2007). Management of recyclable fissile and fertile materials. OECD Publishing. p. 34. ISBN 978-92-64-03255-2. Retrieved 22 March 2011.*
26. Estimate of Decommissioning Periods and Cost for Crystal River 3 NPP
27. www.world-nuclear.org: Decommissioning nuclear facilities
28. ^ Jump up to: [a] [b] *"Nuclear Decommissioning: Decommission nuclear facilities". World-nuclear.org. Retrieved 2013-09-06.*
29. U.S. Nuclear Regulatory Commission:Sites Undergoing Decommissioning (by Location or Name)
30. ^ Jump up to: [a] [b] *"How old are U.S. nuclear power plants and when was the last one built? – FAQ –". U.S. Energy Information Administration (EIA). Retrieved 2013-09-06.*
31. *"NRC: Decommissioning of Nuclear Facilities". Nrc.gov. June 28, 2013. Retrieved 2013-09-06.*
32. http://www.world-nuclear.org/information-library/nuclear-fuel-cycle/nuclear-wastes/decommissioning-nuclear-facilities.aspx
33. NRC Locations of Power Reactor Sites Undergoing Decommissioning

34. Office of Scientific and Technical Information (OSTI)Appendix A – A Summary of the Shutdown and Decommissioning Experience for Nuclear Power Plants in the United States and the Russian Federation. Appendix B – A Summary of the Regulatory Environment for the Shutdown and Decommissioning of Nuclear Power Plants in the United States and the Russian Federation. Appendix C – Recommended Outlines for Decommissioning Documentation
35. NEA: Decommissioning in Austria
36. SUSTAINABILITY INSTITUTE: Zwentendorf, a Nuclear Plant That Will Never Be Turned On Archived May 11, 2011, at the Wayback Machine.
37. *"BR3". Eu-decom.be. Archived from the original on April 24, 2013. Retrieved September 6, 2013.*
38. *"Nuclear Power in Belgium | Belgian Nuclear Energy". World-nuclear.org. Retrieved 2013-09-06.*
39. EU-DECOM-belgium – From 1979 until now: five framework programmes Archived October 9, 2008, at the Wayback Machine.
40. The European Nuclear Decommissioning Training Facility – Mol, Belgium, 2002 Archived May 11, 2011, at the Wayback Machine.
41. World Nuclear Association: Nuclear Power in Bulgaria
42. IAEA: Taking Canada's Gentilly-1 to a "static state (by Balarko Gupta) Archived April 29, 2011, at the Wayback Machine.
43. ASCE: Gentilly-1 a study in nuclear decommission Archived April 27, 2011, at the Wayback Machine.
44. A Chernobyl in Québec? (correspondence on the dangers of Québec's only nuclear plant)
45. Ontario Power Generation: Pickering Nuclear Power
46. FAIREWINDS: Relicensing Pickering Nuclear Generating Station
47. IAEA: Decommissioning in China
48. Nuclear Power in France
49. Brennilis: Incendie À La Centrale Nucléaire, Le Plan D'urgence Déclenché
50. The global state of nuclear decommissioning: costs rising, funds shrinking, and industry looks to escape liability by decades of delay
51. BRENNILIS, LABORATOIRE DU DÉMANTÈLEMENT
52. MAMMOET: Nuclear decommissioning through a bottleneck.
53. WM2009 Conference, March 1–5, 2009 Phoenix, AZ – International Cooperation for the Dismantling of Chooz A Reactor Pressure Vessel – 9087
54. Segmentation of Reactor Vessel Internals
55. Decommissioning of LMRs in France
56. SCITECH CONNECT: Phenix Decommissioning Project – Overview
57. WISEINTERNATIONAL: Superphénix; still more problems ahead
58. http://www.ans.org/store/j_3608
59. Decommissioning of Fast Reactors after Sodium Draining
60. http://uk.areva.com/EN/home-824/news2013decommissioning-of-nuclear-installations-world-first-for-the-robot-charli.html
61. INDIA – CISED: Economics of Nuclear Power Heavy Water Reactors
62. Federation of American Scientists: Osiraq/Tammuz Nuclear Reactor
63. The IAEA Online Information Resource for Radioactive Waste Management: ITALY
64. Zona Nucleare – La centrale nucleare in fase di smantellamento ex-ENEL di Caorso (Piacenza)

65. Il Fiume Po: La Centrale Nucleare di Caorso Archived May 1, 2011, at the Wayback Machine.
66. *Renzo Guerzoni. "Il decommissioning della centrale nucleare di Caorso" (PDF). Sogin. p. 6. Archived from the original (PDF) on 2015-05-03.*
67. Via libera allo smantellamento della centrale di Caorso
68. Accordo tra la SOGIN e la Sudsvik svedese Archived March 28, 2012, at the Wayback Machine.
69. LA REPUBBLICA: Per Caorso un addio lungo mezzo secolo, piano ENEL per smantellare la centrale
70. Zona Nucleare – La centrale nucleare in fase di smantellamento ex-ENEL di Garigliano (Caserta)
71. Zona Nucleare – La centrale nucleare in fase di smantellamento ex-ENEL di Foce Verde (Latina)
72. Zona Nucleare – La centrale nucleare in fase di smantellamento ex-ENEL di Trino Vercellese (Vercelli)
73. Fukushima Nuclear Accident Update Log
74. *"3 nuclear reactors melted down after quake, Japan confirms". CNN. June 7, 2011. Retrieved July 13, 2011.*
75. *"'Melt-through' at Fukushima? / Govt report to IAEA suggests situation worse than meltdown". Yomiuri. June 8, 2011. Retrieved June 8, 2011.*
76. *"Japan to raise Fukushima crisis level to worst". Archived from the original on April 12, 2011. Retrieved April 12, 2011.*
77. *"Japan raises nuclear crisis to same level as Chernobyl". Reuters. April 12, 2011.*
78. The Japan Times: Whether Tepco fails or not, it's taxpayers' tab
79. The Other Fukushima Nuclear Power Plant
80. Fukushima Daini Nuclear Power Station all shutdown
81. Fugen NPP official website
82. Fugen Decommissioning Engineering Center Archived May 23, 2011, at the Wayback Machine.
83. Transcript of NHK TV special in Japanese
84. NHK video of Fugen NPP
85. Article in IAEA-TECDOC—1043: Permanent cessation of Tokai power plant's operation.
86. Science Links Japan: Progression of decommissioning of Tokai power plant. First case of power reactor in Japan Archived May 13, 2011, at the Wayback Machine..
87. Organisation for Economic Co-operation and Development/Nuclear Energy Agency, report 2003: *Strategy Selection for the Decommissioning of Nuclear Facilities* (page 118).
88. PRESS TV (Iranian News Agency): North Korea to decommission nuclear facility
89. THE GUARDIAN: Nuclear agreement: North Korea halts decommissioning
90. NEA: Decommissioning in the Netherlands
91. La storia dei ripetuti incidenti a Majak
92. UK-Russia Closed Nuclear Cities Partnership Archived August 14, 2009, at the Wayback Machine.
93. Russia shuts second plutonium-producing reactor at Seversk
94. BBC: Austria against restarting of nuclear reactor at Jaslovské Bohunice
95. YAHOO NEWS: Slovakia forced to restart nuclear reactors after Ukrainian gas crisis
96. Nuclear Power in Spain - February 2017

97. NUCLEAR ENGINEERING INTERNATIONAL: Decommissioning of José Cabrera NPP, 7 November 2013
98. *"José Cabrera moves into decommissioning". World Nuclear News. 2010-02-11. Retrieved 2010-02-14.*
99. Comparison of estimated and actual decommissioning cost of José Cabrera NPP
100. SPANISH STAKEHOLDER FOR THE NEA WORKSHOP ON STAKEHOLDER INVOLVEMENT IN NUCLEAR DECISION MAKING - Paris, January 2017
101. Sweden plans big rise in fees to nuclear decommissioning fund
102. Nuclear Energy Agency: Decommissioning in Switzerland
103. European Bank for Reconstruction and Development: Breakthrough for Chernobyl nuclear decommissioning efforts (Consortium Novarka to build New Safe Confinement Holtec International to complete Spent Fuel Storage) Archived August 21, 2008, at the Wayback Machine.
104. Radiological hazard on all Magnox nuclear sites across UK set to reduce by 99%
105. *"New nuclear reactor for Dounreay". BBC. February 9, 1966. Retrieved April 10, 2016.*
106. *"PRIS: Dounreay PFR". IAEA. Retrieved April 28, 2014.*
107. *Frank von Hippel; et al. (February 2010). Fast Breeder Reactor Programs: History and Status (PDF). International Panel on Fissile Materials. pp. 73–88. ISBN 978-0-9819275-6-5. Retrieved April 28, 2014.*
108. *"'Reactorsaurus' to rip up station". BBC. May 5, 2009. Retrieved May 5, 2009.*
109. *"BBC News – Plan to display parts of Dounreay at London museum". BBC Online. Retrieved April 24, 2014.*
110. *"Calder Hall Celebrates 40 Years of Operation – Press Release". BNFL. Archived from the original on February 22, 2004. Retrieved February 22, 2004.*
111. *Brown, Paul (March 21, 2003). "First nuclear power plant to close". The Guardian. London. Retrieved May 12, 2010.*
112. *NDA Calder Hall Nuclear Power Station Feasibility Study 2007*.
113. *Richard Black (March 18, 2011). "Fukushima – disaster or distraction?". BBC. Retrieved April 7, 2011.*
114. Windscale Piles: Cockcroft's Follies avoided nuclear disaster
115. *George Coupe (May 14, 2004). "Getting to the core issue". The Engineer. Archived from the original on September 5, 2008. Retrieved October 23, 2008.*
116. *"MP's vow to fight for Winfrith future (From Thisisdorset)". Thisisdorset.net. September 4, 2007. Retrieved 2013-09-06.*
117. *"Winfrith – Quarterly report for 1 July – 30 September 2011". Hse.gov.uk. Retrieved 2013-09-06.*
118. https://www.gov.uk/government/news/work-underway-to-remove-nuclear-reactor-core-in-dorset
119. *Duke Energy (October 12, 2010). "CRYSTAL RIVER NUCLEAR PLANT – SPECIAL INSPECTION REPORT 05000302/2009007" (PDF).*
120. *"Progress analyzing Crystal River repair proposals". World Nuclear News. January 11, 2012.*
121. *"Crystal River Nuclear Plant to be retired; company evaluating sites for potential new gas-fueled generation". February 5, 2013. Archived from the original on October 22, 2013.*

122. Shutting down Crystal River nuclear plant will cost $1.2 billion, take 60 years Tampabay news
123. U.S.NRC Dresden – Unit 1
124. UCSUSA: Dresden Nuclear Generating Station
125. OSTI: Energy Citations Database about Rancho Seco nuclear power plant
126. Rancho Seco nuclear power plant ends decommissioning 10-2009
127. SACRAMENTO MUNICIPAL AUTHORITY DISTRICT: RANCHO SECO REPORT ON DECOMMISSIONING FUNDING STATUS
128. US-NRC: Rancho Seco nuclear power plant
129. UNITED STATES NUCLEAR REGULATORY COMMISSION: Three Mile Island – Decommissioning Unit 2
130. OSTI, Office of Scientific and Technical Information – Shippingport station decommissioning project: start of physical decommissioning
131. ^ Jump up to: [a] [b] *"United States of America". Power Reactor Information System (PRIS). International Atomic Energy Agency (IAEA). Retrieved June 9, 2013.*
132. *Jim Shephard (March 29, 2012). "San Onofre – Unit 1". United States Nuclear Regulatory Commission. Retrieved September 4, 2012.*
133. Fission Stories #92: San Onofre's Allegators
134. Cracked Steam Generator Tubes at San Onofre
135. NRC Plans for Decommissioning of San Onofre Nuclear Generating Station Units 2 and 3 July 8, 2016
136. *Southern California Edison (September 23, 2014). "San Onofre Nuclear Generating Station Units 2 and 3 Irradiated Fuel Management Plan" (PDF). NRC. p. 14.*
137. *"Calif. nuclear plant to cost $4.4 billion to dismantle". CBS News. AP. Aug 2, 2014. Retrieved 3 August 2014.*
138. US NRC Information Digest 2008–2009
139. *Koberstein, Paul (March 9, 2005). "Trojan: PGE's Nuclear Gamble". Willamette Week. p. A1. Archived from the original on September 29, 2007. Retrieved June 15, 2007.*
140. Yankee Rowe Nuclear Reactor (third nuclear reactor in USA, totally dismantled)
141. Maine Yankee Nuclear Power Station, ME – Power Technology
142. Maine Yankee Decommissioning 80% Complete Archived May 1, 2011, at the Wayback Machine.
143. Maine Yankee Decommissioning Experience Report
144. With Exelon's Zion 1 and 2 reactors (2 x 1098 MWe) closed down in 1998 and in Safstor, a slightly different process is envisaged, considerably accelerating the decommissioning. Exelon has contracted with a specialist company – EnergySolutions, to remove the plant and return the site to greenfield status. To achieve this, the plant's licence and decommissioning funds will be transferred to EnergySolutions, which will then be owner and licensee, and the site will be returned to Exelon about 2018. Used fuel would remain on site until taken to the national repository.
145. WEBWIRE: Exelon Nuclear To Accelerate Decommissioning Of Zion Station
146. *"NRC: Humboldt Bay". Nrc.gov. Retrieved 2013-09-06.*

9. Appendices

A. Review of Robot Kinematics and Jacobians

We review here the basic information from a first course in robotics that is needed for this book. This includes robot kinematics, the arm Jacobian, and the issue of specifying the Cartesian position. The review is detailed since those with a background in system theory and controls may not yet have seen this material. Several examples are given which are used throughout the book for design and simulation purposes.

A.1 Basic ManipulatorGeometries

In this section we look at some basic arm geometries. A robot arm or manipulator is composed of a set of *joints* separated in space by the arm links. The joints are where the motion in the arm occurs (cf. our own wrist and elbow), while the links are of fixed construction (cf. our own forearm). Thus the links maintain a fixed relationship between the joints. [Although the links may be *flexible* (i.e., they may bend); we ignore flexibility effects here.] The joints may be actuated by motors or hydraulic actuators. There are two sorts of robot joints, involving two sorts of motion. A *revolute joint* (denoted R) is one that allows rotary motion about an axis of rotation. An example is the human elbow. A *prismatic joint* (denoted P) is one that allows extension or telescopic motion. An example is a telescoping automobile antenna. There is no anthropomorphous analogy to the prismatic link. The *joint variables* of a manipulator are the variable parameters of the joints. For

555

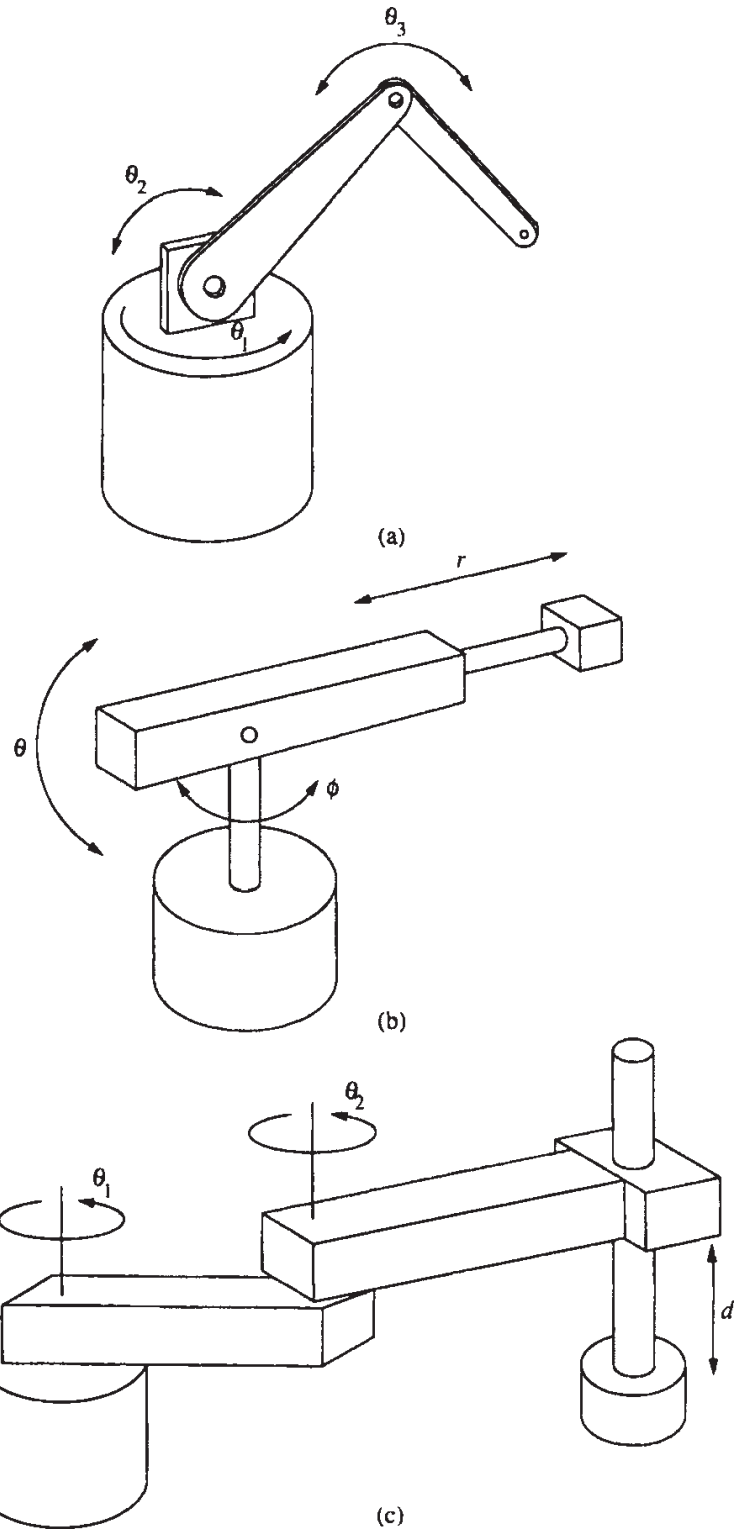


Figure A.1.1: Basic robot arm geometries: (a) articulated arm, revolute coordinates (RRR); (b) spherical coordinates (RRP); (c) SCARA arm (RRP).

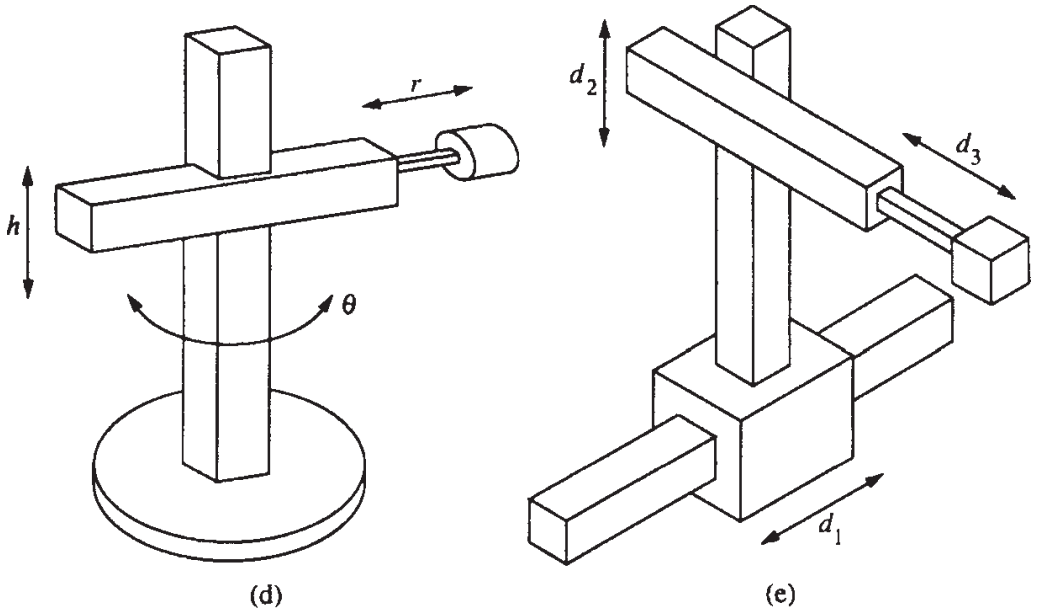


Figure A.1.1:(*C*ont.) (d) cylindrical coordinates (RPP); (e) Cartesian arm, rectangular coordinates (PPP).

a revolute joint the variable is an angle, denoted *0*. For a prismatic joint it is a length, denoted *d*.

Some basic arm geometries are shown in Figure A.1.1. The RRR *articulated arm* in Figure A.1.1a is like the human arm, while the PPP *Cartesian arm* in Figure A.1.1e is closely tied to the coordinates used in the manipulator *workspace,* where the Cartesian coordinates *(x, y, z)* are often used to describe tasks to be performed. The workspace is the total volume swept out by the end effector as the robot executes all possible motions.

The *joint axis* of a revolute joint is the axis about which the rotation *0* occurs. (The sense of rotation is determined using the right-handed screw rule: If the curled fingers of the right hand indicate the direction of rotation, the thumb indicates the direction of the axis of rotation.) For a prismatic joint, it is the axis along which the telescoping action *d* occurs. The relative orientations of the joint axes of an arm determine its fundamental properties. Figure A.1.1c shows a RRP manipulator known as the SCARA (selected compliant articulated robot for assembly) arm. It has quite a different structure than the RRP spherical arm shown in Figure A.1.1b, since its joint axes are all parallel. On the other hand, the joint axes of the spherical arm intersect at a point.

Industrial examples of the RRR arm are the PUMA and Cincinnati-Milacron T^3 735 manipulators. The Stanford manipulator is a spherical RRP arm; the AdeptOne is a SCARA RRP arm. An example of the RPP arm is the GMF M-100. The Cincinnati-Milacron T^3 gantry robot is a PPP arm.

Many industrial robots are *serial link* manipulators since they consist of a series of links connected together by actuated joints. The base is called link 0, and the last link is terminated by the tool or *end effector*. Many robots have six joints, corresponding to the *six degrees of freedom* needed to obtain arbitrary position and orientation of the end effector in three- dimensional space.

Arms like the PUMA 560 have six revolute joints. In such an arm, the joints may be grouped into two sets of three joints each. The first three joints may be used to place the end effector at an arbitrary position within the three-dimensional workspace. The last three joints may be used to obtain an arbitrary orientation of the end effector at that position. In the PUMA 560, the axes of joints 4, 5, and 6 intersect at a common point and are mutually orthogonal. This makes orienting the end-effector convenient. The last three joints are known as the *wrist mechanism* (see Example A.2.4).

A.2 Robot Kinematics

Here we review the kinematics of robot manipulators, including the arm A matrices, homogeneous transformations, the *T* matrix, forward and inverse kinematics, and joint-space and Cartesian coordinates. Several illustrative examples are given.

A Matrices

For given values of the joint variables, it is important to be able to specify the locations of the links with respect to each other. This is accomplished by using the manipulator *kinematic equations*.

We may associate with each link *i* a coordinate frame (x_i, y_i, z_i) fixed to that link. See Figure A.2.1. A standard and consistent paradigm for so doing is the *Denavit-Hartenberg (D-H)* representation [Paul 1981], [Spong and Vidyasagar 1989]. The frame attached to link 0 (i.e., the base of the manipulator) is called the *base frame* or *inertial frame.*

The relation between coordinate frame *i*-1 and coordinate frame *i* is given by the transformation matrix

$$A_i = \left[\begin{array}{ccc|c} \cos\theta_i & -\cos\alpha_i \sin\theta_i & \sin\alpha_i \sin\theta_i & a_i \cos\theta_i \\ \sin\theta_i & \cos\alpha_i \cos\theta_i & -\sin\alpha_i \cos\theta_i & a_i \sin\theta_i \\ 0 & \sin\alpha_i & \cos\alpha_i & d_i \\ \hline 0 & 0 & 0 & 1 \end{array}\right]. \quad \text{(A.2.1)}$$

Most of the parameters in this *A matrix for link i* are fixed. The *link parameters* are a_i, the twist of the link *i*, and a_i, the length of link *i*. These parameters are tabulated for each link in the arm manufacturer's specifications. The *joint parameters* are the joint angle 0_i and the joint offset d_i. If joint *i* is revolute, the joint variable is 0_i and d_i is a constant tabulated in the specs. On the other hand, if the link is prismatic, then d_i is the joint variable and 0_i is a constant provided in the specs. The parameter a_i for a prismatic joint is defined to be zero, since the link length is variable and described by d_i.

By the D-H convention, for a revolute joint, the rotation 0_i occurs about axis z_i-1. For a prismatic joint d_i occurs along axis z_i-1. Thus the link coordinate frame is considered to be attached to the *outer end* of the link. See the examples.

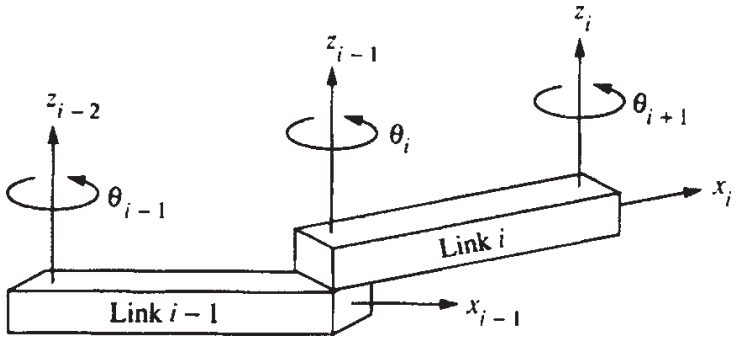


Figure A.2.1: Link kinematic relations in a manipulator.

The *A* matrix A_i is a function of only a single variable, namely the joint variable 0_i or d_i, since all the other parameters in A_i are fixed for a specific joint. If a manipulator has n links, *the joint-variable vector q* is an *n*-vector composed of the individual joint variables. Thus *q* is in general a combination of angles 0_i and lengths d_i. For instance, for an RRP arm,

$$q = \left[\begin{array}{ccc} \theta_1 & \theta_2 & d_3 \end{array}\right]^T.$$

The components of q are denoted by q_i; that is, the general joint variable q_i can represent either an angle 0_i or a length d_i as appropriate.

Homogeneous Transformations

The A matrix is a *homogeneous transformation* matrix of the form

$$A_i = \begin{bmatrix} R_i & P_i \\ 0 & 1 \end{bmatrix}, \tag{A.2.2}$$

where R_i is a *rotation matrix* and p_i is a *translation vector*. Thus if ${}^{i}r$ is a point described with respect to the coordinate frame of link i, the same point has coordinates ${}^{i-1}r$ with respect to the frame of link i-1 given by

$${}^{i-1}r = A_i {}^{i}r. \tag{A.2.3}$$

The homogeneous transformation is a 4×4 matrix, so that it can describe both rotations and translations; therefore, the vectors describing position in a given coordinate frame are 4-vectors. They are of the form

$${}^{i}r = \begin{bmatrix} {}^{i}x \\ {}^{i}y \\ {}^{i}z \\ 1 \end{bmatrix}, \tag{A.2.4}$$

where $({}^{i}x, {}^{i}y, {}^{i}z)$ are the coordinates of the point in frame i. Thus, according to (A.2.3) and (A.2.2),

$$\begin{bmatrix} {}^{i-1}x \\ {}^{i-1}y \\ {}^{i-1}z \end{bmatrix} = R_i \begin{bmatrix} {}^{i}x \\ {}^{i}y \\ {}^{i}z \end{bmatrix} + p_i, \tag{A.2.5}$$

which is just a rotation of R_i applied to the coordinates in frame i plus a translation of p_i.

We may interpret frame i-1 as the fixed (i.e., “original”) frame and frame i as the rotated and translated (i.e., “new”) frame due to the following considerations. According to (A.2.5), there is an easy way to find the rotation matrix R_i that rotates a given coordinate frame i-1 into another given frame i. Set p_i equal to zero and $({}^{i}x, {}^{i}y, {}^{i}z)$=(1,0,0). Then (A.2.5) is equal to the first column of R_i. That is, the first column of R_i is nothing but *the representation of the new x-axis* ${}^{i}x$ *in terms of the original coordinates* $({}^{i-1}x, {}^{i-1}y, {}^{i-1}z)$. Similarly, the second (respectively third) column of R_i is the representation of the rotated y-axis ${}^{i}y$ (respectively, z-axis and ${}^{i}z$) in the fixed frame i-1. We shall illustrate this in Example A.2.1.

Therefore, A_i may be interpreted from several points of view. It is the transformation that takes a representation ${}^{i}r$ of a vector in frame i to its

representation ^{i-1}r in frame *i*-1. On the other hand, it is the description of frame *i* in terms of frame *i*-1; in fact, R_i describes the orientation of the axes of frame *i* in terms of frame *i*-1, while p_i describes the origin of frame *i* in terms of the coordinates of frame *i*-1.

A rotation matrix *R* enjoys the property of *orthogonality,* that is, $R^T=R^{-1}$. It has one eigenvalue at h=1, whose eigenvector is the axis of rotation. A rotation of *0* about the *x* axis, for instance, looks like

$$R_{x,\theta} = \begin{bmatrix} 1 & 0 & 0 \\ 0 & \cos\theta & -\sin\theta \\ 0 & \sin\theta & \cos\theta \end{bmatrix}. \tag{A.2.6}$$

The last entry of "1" in (A.2.4) represents a *scaling factor* for the length of the vector. By using a homogeneous transformation whose (4, 4) entry is not unity, vectors may be scaled. By using entries in positions, (4, 1), (4, 2), (4, 3) of the transformation matrix, *perspective transformations* may be performed. These ideas are important, for instance, in camera-frame transformations but will not be useful in the transformations associated with the manipulator arm.

Arm T Matrix

To obtain the coordinates of a point in terms of the base (i.e., link 0) frame, we may use the matrices

$$T_i = A_1 A_2 \cdots A_i. \tag{A.2.7}$$

Then, given the coordinates ^ir of a point expressed in the frame attached to link *i,* the coordinates of the same point in the base frame are given by

$$^0r = T_i\,{}^ir. \tag{A.2.8}$$

We call T_i a *kinematic chain* of transformations.

We define the *arm T matrix* as

$$T \equiv T_n = A_1 \cdots A_n, \tag{A.2.9}$$

with *n* the number of links in the manipulator. Then, if ^nr are the coordinates of a point referred to the last link, the base coordinates of the point are

$$^0r = T^n r. \tag{A.2.10}$$

This is an important relation since ^nr, the coordinates of an object in the *n*th frame, can represent the location of the object *with respect to the tool or end effector*. It is thus important in specifying tasks to be accomplished. On the

other hand, ${}^0r$ represents the location of the object with respect to the base frame, which is the object's absolute position with respect to the manipulator base.

Forward Kinematics

The position and orientation of the end effector with respect to the manipulator base frame are given by evaluating the arm *T* matrix. It is conventional to symbolize this homogeneous transformation as

(A.2.11)
$$T = \begin{bmatrix} n & o & a & p \\ 0 & 0 & 0 & 1 \end{bmatrix} = \begin{bmatrix} R & P \\ 0 & 1 \end{bmatrix}.$$

Thus the orientations of the axes of the end-effector reference frame are described with respect to base coordinates by the rotation matrix *R=[n o a],* and the origin of the end-effector frame has a position of *p* in base coordinates.

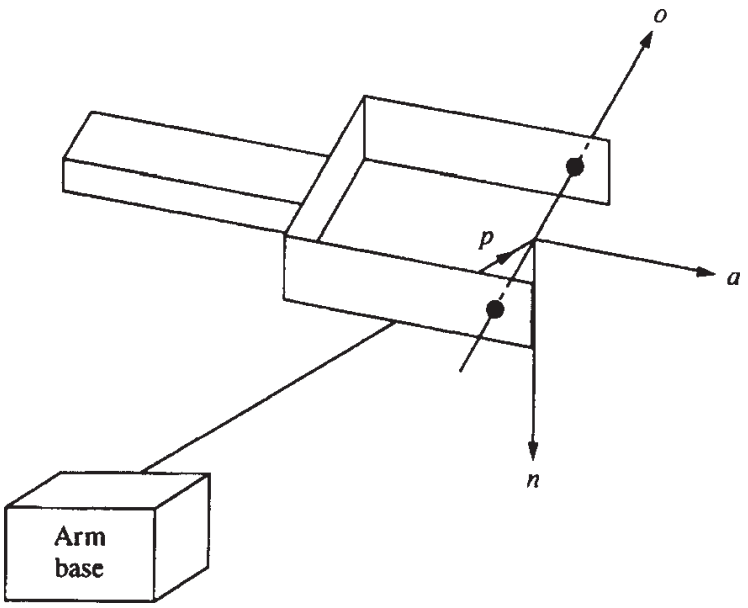


Figure A.2.2: Robot end effector, showing the definition of *(n, o, a, p)*.

The 3-vectors *n, o, a,* and *p* are defined as in Figure A.2.2. The *approach* vector of the end effector is *"a";* the *orientation vector "o"* is the direction specifying the orientation of the hand, from fingertip to fingertip. The *normal* vector *"n"* is chosen to complete the definition of a right-handed coordinate system using

$$n = o \times a.$$

Thus *(n, o, a)* are the base coordinates of an *(x, y, z)* Cartesian coordinate system attached to the end effector. The *position* vector *p* specifies the location of the origin of the *(n, o, a)* frame with respect to the base frame.

The representation *(n, o, a)* for the orientation of the end effector is inefficient. Note that *[n o a]* is a 3×3 matrix, so that it has nine entries. However, it does not take nine degrees of freedom to specify orientation. Indeed, *[n o a]* is a rotation matrix, so that its columns are orthogonal; this orthogonality requirement imposes extra constraints on the elements of *[n o a],* so that the nine entries of *[n o a]* are not independent. Alternative more efficient methods of specifying the orientation of the end effector in base coordinates are the roll-pitch-yaw, Euler angle, quaternion, and tool-configuration vector descriptions. We discuss some of these later. The reason we use *(n, o, a)* is that the arm *T* matrix is easily computed using the *A* matrices in terms of the arm parameters and join variables. Then *n, o, a,* and *p* are simply read off by examining the *T* matrix, as we shall see in the examples.

At this point we should like to distinguish between two sets of coordinates describing the end effector. The *joint variable* coordinates of the end effector are given by the *n*-vector.

$$q = \begin{bmatrix} q_1 & q_2 & \cdots & q_n \end{bmatrix}^T,$$

where q_i can represent angles or lengths, depending on whether the links are revolute or prismatic. Generally, n=6, so that the arm has six degrees of freedom. The end-effector *Cartesian coordinates* are the description of end effector orientation and position in terms of the arm base coordinates. According to (A.2.11), where *T* may be computed knowing *q,* the joint variable and Cartesian coordinates are equivalent, for both specify the location of the end effector.

We say that *q* is the *joint-space* description of the position and orientation of the end effector, while *(n, o, a, p)* is the *Cartesian* or *task space* description. This terminology derives from the fact that descriptions of tasks to be performed by an arm are generally given in Cartesian coordinates, not in joint coordinates.

The robot arm *kinematics problem* is as follows. Given the joint variables *q,* find the Cartesian position and orientation of the end of the manipulator. Thus the kinematics problem amounts to converting given joint variables into the Cartesian position and orientation of the end effector expressed in base coordinates. Let us illustrate the solution of this problem for several simple robot arms which we use as examples throughout the book. It amounts to computing *T*.

It should be mentioned that there are several software packages commercially available for computing the *A* matrices and the *T* matrix for a given robot arm. See, for instance, [MATMAN 1986].

EXAMPLE A.2–1: Kinematics for Three-Link Cylindrical Arm

A simple RPP manipulator is shown in Figure A.2.3a. It may be interpreted as the first three joints of an arm much as the GMF M-100. These are the joints used to position the end effector. A wrist mechanism consisting of three joints may be added to the end of the RPP arm to orient the end effector in space (see Example A.2.4). The joint variables of the three-link arm shown are *0, h, r,* which correspond to the coordinates of a cylindrical coordinate system, so that the joint-variable vector is

(1) $$q = \begin{bmatrix} \theta & h & r \end{bmatrix}^T.$$

a. *A* Matrices

Coordinate frames may be attached to links 1, 2, and 3 using any technique desired. The D-H frames, to which (A.2.1) corresponds, are shown in Figure A.2.3b. For this choice of frames, the *A* matrices may be determined as follows.

Frame 1 is related to the base frame 0 by a simple rotation of *0* degrees about the axis z_0. A *z*-axis rotation, $R_{z,\,0,}$ with no translation is described by

(2) $$A_1 = \left[\begin{array}{ccc|c} c\theta & -s\theta & 0 & 0 \\ s\theta & c\theta & 0 & 0 \\ 0 & 0 & 1 & 0 \\ \hline 0 & 0 & 0 & 1 \end{array}\right],$$

where *c0* represents cos *0* and *s0* represents sin *0*.

To find A_2 we may use (A.2.1). Since link 2 is prismatic with extension *h,* the length a_2 is zero. In this example the rotation 0_2 is also zero. The twist a_2 of link 2 is the angle of rotation about axis x_2 required to align z_1 with z_2–that is, -90°. Therefore,

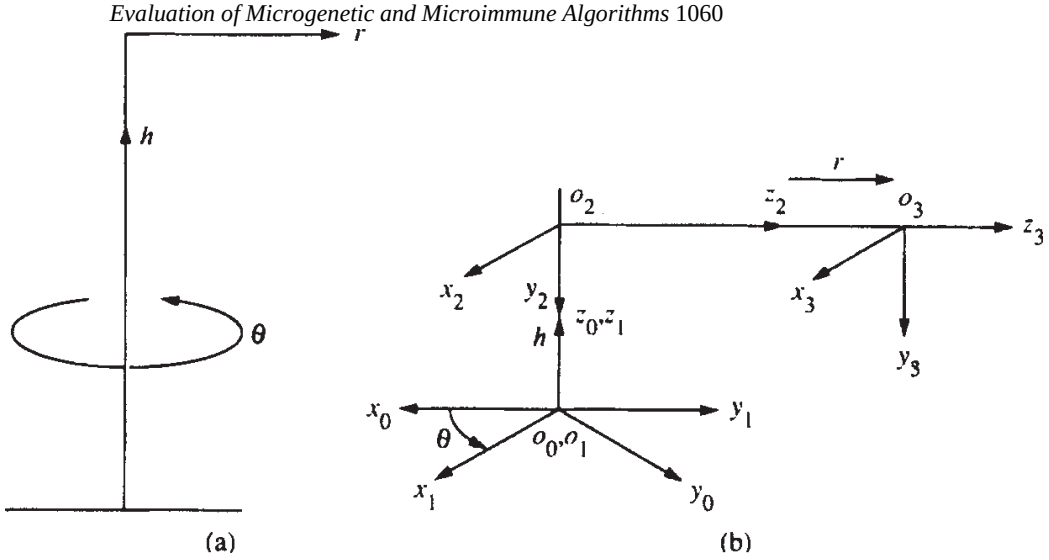


Figure A.2.3: Three-link cylindrical manipulator: (a) arm schematic; (b) D-H coordinate frames.

(3)
$$A_2 = \left[\begin{array}{ccc|c} 1 & 0 & 0 & 0 \\ 0 & 0 & 1 & 0 \\ 0 & -1 & 0 & h \\ \hline 0 & 0 & 0 & 1 \end{array}\right].$$

There is an attractive alternative to (A.2.1) for determining the link A matrix in simple cases. Recall that the first column of A_2 is the representation of x_2 in the coordinates (x_1, y_1, z_1). According to the figure, this is just $[1\ 0\ 0]^T$. The second column of A_2 is the representation of y_2 in the coordinates (x_1, y_1, z_1), which the figure shows is $[0\ 0\ -1]^T$. The third column of A_2 is the representation of 22 in frame o_1, which is just $[0\ 1\ 0]^T$. Thus (3) is obtained by inspection.

In similar fashion we obtain,

(4)
$$A_3 = \left[\begin{array}{ccc|c} 1 & 0 & 0 & 0 \\ 0 & 1 & 0 & 0 \\ 0 & 0 & 1 & r \\ \hline 0 & 0 & 0 & 1 \end{array}\right].$$

b. T Matrix and Arm Kinematics

The arm T matrix is now obtained as

(5)
$$T = A_1 A_2 A_3 = \left[\begin{array}{ccc|c} c\theta & 0 & -s\theta & -r\ s\theta \\ s\theta & 0 & c\theta & r\ c\theta \\ 0 & -1 & 0 & h \\ \hline 0 & 0 & 0 & 1 \end{array}\right].$$

To interpret the T matrix, examine (A.2.11). The position in base coordinates of the end of the manipulator, that is, the origin of frame 3, is

(6)
$$p = \left[\begin{array}{ccc} -r\ s\theta & r\ c\theta & h \end{array}\right]^T.$$

The orientation of frame 3 described in base coordinates is expressed in *(n, o, a)* form by giving the coordinates of the normal, orientation, and approach vectors in terms of the base frame. These are given by

(7)
$$\begin{aligned} n &= \left[\begin{array}{ccc} c\theta & s\theta & 0 \end{array}\right]^T \\ o &= \left[\begin{array}{ccc} 0 & 0 & -1 \end{array}\right]^T \\ a &= \left[\begin{array}{ccc} -s\theta & c\theta & 0 \end{array}\right]^T. \end{aligned}$$

A glance at Figure A.2.3b verifies these expressions.

■

EXAMPLE A.2-2: Kinematics for Two-Link Planar Elbow Arm

A two-link planar RR arm is shown in Figure A.2.4a where a_1 and a_2 are the fixed and known link length parameters. The link coordinate frames are shown in Figure A.2.4b. We have taken the *z*-axes perpendicular to the page to conform to the convention of specifying points in a plane by *(x, y)* coordinates. Therefore, the frames are not defined quite as in the D-H convention.

The arm *A* matrices may be written by inspection as

$$A_1 = \left[\begin{array}{ccc|c} c_1 & -s_1 & 0 & a_1 c_1 \\ s_1 & c_1 & 0 & a_1 s_1 \\ 0 & 0 & 1 & 0 \\ \hline 0 & 0 & 0 & 1 \end{array}\right]. \tag{1}$$

where c_1, s_1, represent respectively cos θ_1, sin θ_1 and

$$A_2 = \left[\begin{array}{ccc|c} c_2 & -s_2 & 0 & a_2 c_2 \\ s_2 & c_2 & 0 & a_2 s_2 \\ 0 & 0 & 1 & 0 \\ \hline 0 & 0 & 0 & 1 \end{array}\right]. \tag{2}$$

The arm *T* matrix is given by

$$T = A_1 A_2 = \left[\begin{array}{ccc|c} c_{12} & -s_{12} & 0 & a_1 c_1 + a_2 c_{12} \\ s_{12} & c_{12} & 0 & a_1 s_1 + a_2 s_{12} \\ 0 & 0 & 1 & 0 \\ \hline 0 & 0 & 0 & 1 \end{array}\right]. \tag{3}$$

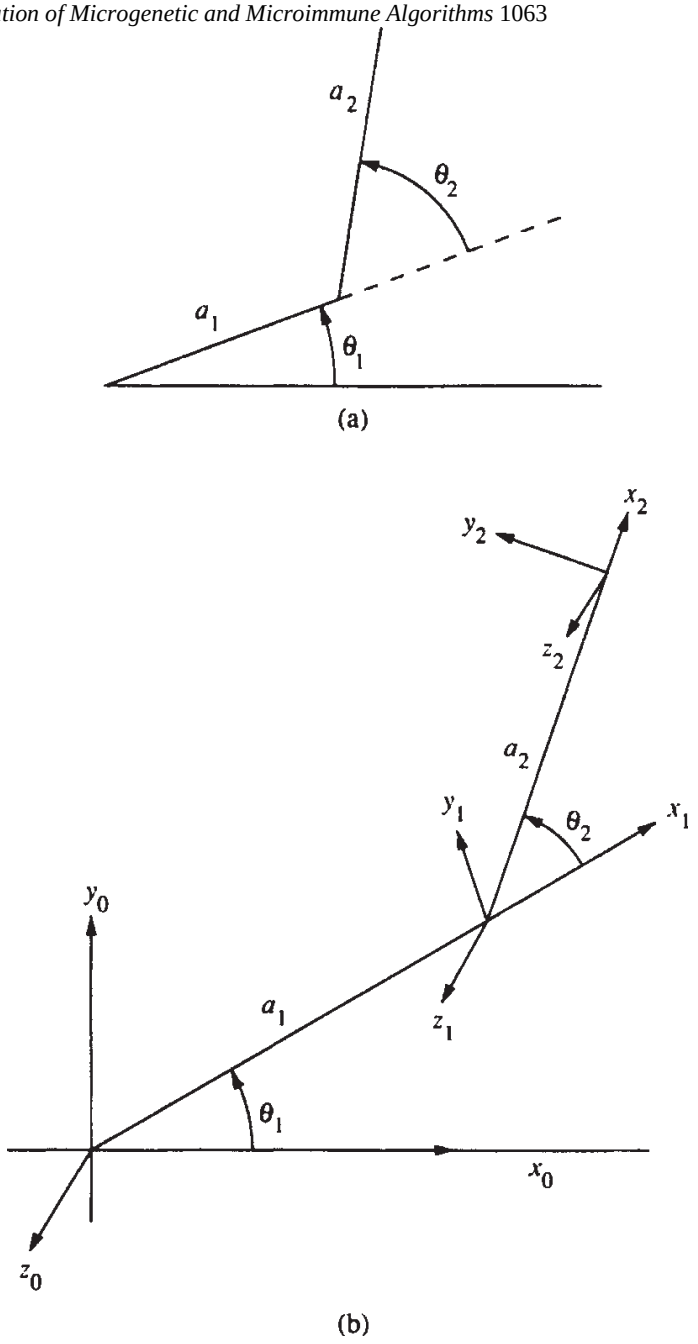


Figure A.2.4: Two-link planar RR arm: (a) arm schematic; (b) D-H coordinate frames.

where $c_{12} \equiv \cos(\theta_1 + \theta_2)$ and $s_{12} \equiv \sin(\theta_1 + \theta_2)$.

Therefore, the origin o_2 of frame 2 in terms of base coordinates is located at

$$p = \begin{bmatrix} a_1 c_1 + a_2 c_{12} & a_1 s_1 + a_2 s_{12} & 0 \end{bmatrix}^T. \tag{4}$$

This represents the kinematic solution, which converts the joint variable coordinates (θ_1, θ_2) into the base-frame Cartesian coordinates of the end of the arm. The reader should examine Figure A.2.4a to verify this expression.

■

EXAMPLE A.2–3: Kinematics for Two-Link Polar Arm

A two-link planar RP arm is shown in Figure A.2.5a where 9 is the fixed known length of the base link. The link frames, with the *z*-axes perpendicular to the page, are shown in Figure A.2.5b. The joint vector is

$$q = \begin{bmatrix} \theta & r \end{bmatrix}^T, \tag{1}$$

which corresponds to polar coordinates in the plane.

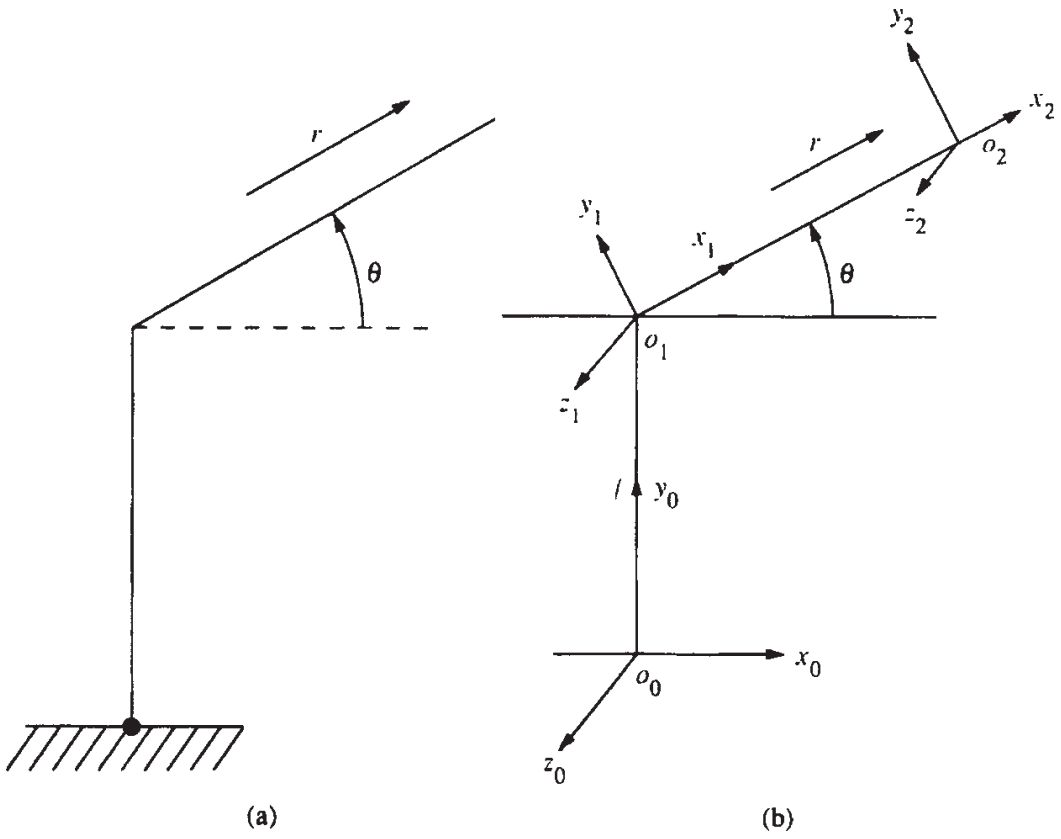


Figure A.2.5: Two-link planar RP arm: (a) arm schematic; (b) D-H coordinate frames.

By inspection, the *A* matrices are found to be

$$A_1 = \left[\begin{array}{ccc|c} c\theta & -s\theta & 0 & 0 \\ s\theta & c\theta & 0 & \ell \\ 0 & 0 & 1 & 0 \\ \hline 0 & 0 & 1 & 1 \end{array}\right]. \tag{2}$$

$$A_2 = \left[\begin{array}{ccc|c} 1 & 0 & 0 & r \\ 0 & 1 & 0 & 0 \\ 0 & 0 & 1 & 0 \\ \hline 0 & 0 & 0 & 1 \end{array}\right]. \tag{3}$$

The T matrix is

$$T = A_1 A_2 = \left[\begin{array}{ccc|c} c\theta & -s\theta & 0 & rc\theta \\ s\theta & c\theta & 0 & \ell + rs\theta \\ 0 & 0 & 1 & 0 \\ \hline 0 & 0 & 0 & 1 \end{array}\right]. \tag{4}$$

Therefore, the base coordinates of the end of the arm are

$$p = \left[\begin{array}{ccc} r\,c\theta & \ell + rs\theta & 0 \end{array}\right]^T, \tag{5}$$

which should be verified by examining Figure A.2.5a. This may be interpreted as the forward kinematics solution for the arm.

This example illustrates the freedom we have to select the base frame origin o_0. We could have selected o_0 coincident with o_1. However, we have chosen to include the length 9 of link 0 by placing o_0 at the bottom of the base link.

■

EXAMPLE A.2–4: Kinematics for Spherical Wrist

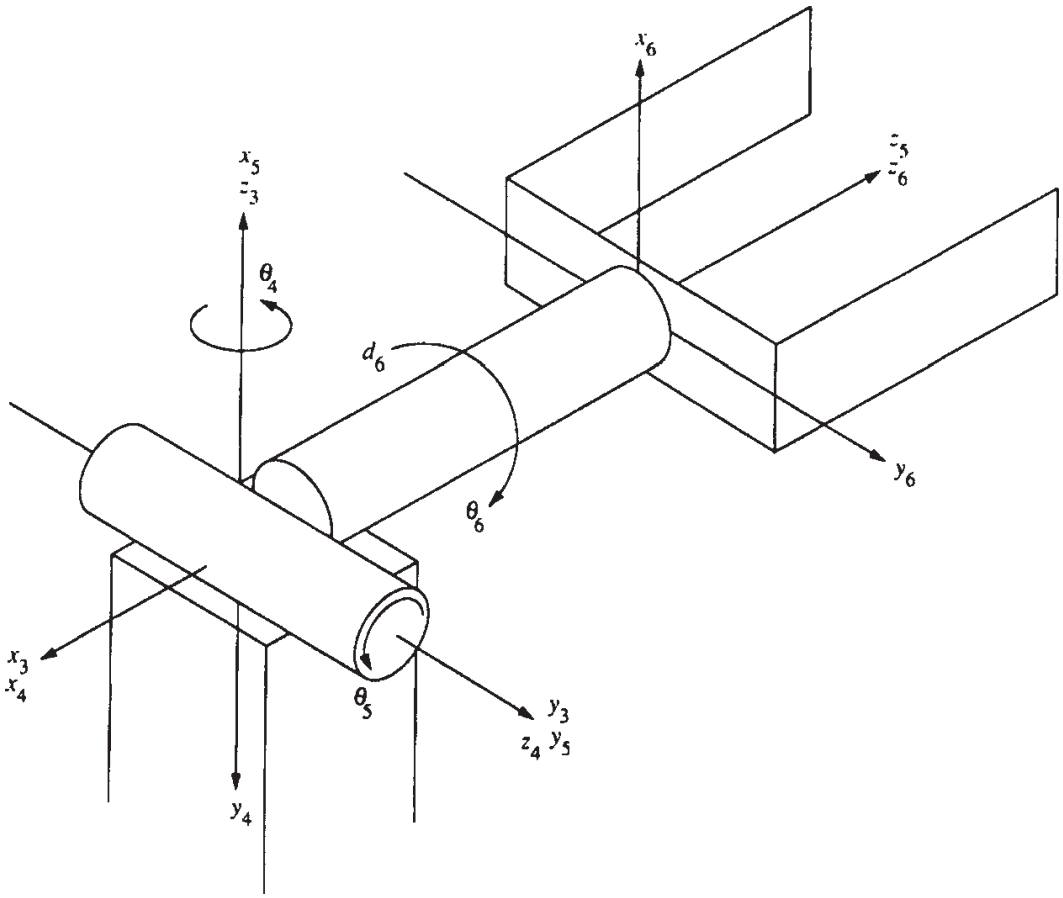


Figure A.2.6: Spherical wrist.

A spherical wrist mechanism is shown in Figure A.2.6. See [Paul 1981], [Spong and Vidyasagar 1989]. For convenient orientational control, all three joint axes intersect at a common point. Since many six-link industrial arms, including the Stanford arm, end in such a configuration, we have labeled the three joint variables 0_4, 0_5, 0_6. The D-H frames are also shown in the figure. Recall that the rotation 0_i occurs about axis z_{i-1} in the D-H convention. The origin of frame 6 has been chosen at the base of the fingered gripper. The length d_6 is a fixed known parameter.

By expressing the axes x_4, y_4, z_4 in terms of the coordinates (x_3, y_3, z_3), we are able to directly determine the columns of A4 to obtain

(1)
$$A_4 = \left[\begin{array}{ccc|c} c_4 & 0 & -s_4 & 0 \\ s_4 & 0 & c_4 & 0 \\ 0 & -1 & 0 & 0 \\ \hline 0 & 0 & 0 & 1 \end{array}\right].$$

Determining x_5, y_5, z_5 in terms of (x_4, y_4, z_4) yields

(2)
$$A_5 = \left[\begin{array}{ccc|c} c_5 & 0 & s_5 & 0 \\ s_5 & 0 & -c_5 & 0 \\ 0 & 1 & 0 & 0 \\ \hline 0 & 0 & 0 & 1 \end{array}\right].$$

In writing down A_5, it is important to note that θ_5 is defined to be zero when the end effector is in an upright position, that is, when the arm is fully extended. We have drawn the figure with θ_5=-90° to show more clearly the different coordinate systems.

In similar fashion, we obtain

(3)
$$A_6 = \left[\begin{array}{ccc|c} c_6 & -s_6 & 0 & 0 \\ s_6 & c_6 & 0 & 0 \\ 0 & 0 & 1 & d_6 \\ \hline 0 & 0 & 0 & 1 \end{array}\right].$$

The wrist T matrix is

$$T = A_4 A_5 A_6$$

$$= \left[\begin{array}{ccc|c} c_4c_5c_6 - s_4s_6 & -c_4c_5s_6 - s_4c_6 & c_4s_5 & c_4s_5d_6 \\ s_4c_5c_6 + c_4s_6 & -s_4c_5s_6 + c_4c_6 & s_4s_5 & s_4s_5d_6 \\ -s_5c_6 & s_5s_6 & c_5 & c_5d_6 \\ \hline 0 & 0 & 0 & 1 \end{array}\right], \quad (4)$$

where $c4 \square \cos 04$, and so on. It is quite interesting to note that the rotational part of this T matrix corresponds to the Euler angle transformation [Spong and Vidyasagar 1989]. Therefore, 04, 05, 06 may be interpreted as the Euler angles with respect to frame 3.

Suppose that we would like to determine the kinematic transformations of the 3-link cylindrical arm in Example A.2.1 terminated with a spherical wrist. Then it is only necessary to multiply the T matrix in Example A.2.1 and (4), in that order, to obtain the overall manipulator T matrix.

■

Inverse Kinematics

The location of the end effector is specified in base coordinates by the arm T matrix. On the other hand, the location of the end effector is specified in joint coordinates by giving the values of the joint variables q_i. We may compute the T matrix knowing the joint-variable vector q, as in the examples just shown. Finding T from q is the kinematics problem.

The *inverse-kinematics* problem is as follows. Given *(n, o, a, p)* for the end effector in base coordinates, determine the joint variables q_i in the T matrix

(A.2.12)
$$T = \begin{bmatrix} n & o & a & p \\ 0 & 0 & 0 & 1 \end{bmatrix}$$

that yield the specified *(n, o, a, p)*. This problem is important in manipulator control, for the desired Cartesian orientation and position of the end effector are specified by the task. Then the solution to the inverse kinematics problems gives the joint variables q_i required to achieve that orientation and position.

Due to the functions involved in the T matrix, the relations between q_i and *(n, o, a, p)* are highly nonlinear; these must be inverted to obtain the

inverse kinematic solution q. The solutions for q_i are generally not unique. If the last three arm axes intersect at a point (e.g., the wrist mechanism in Example A.2.4), it is common to split the inverse kinematics problem into two parts. In a six-link arm, for instance, one first determines q_1, q_2, and q_3 required to obtain the desired Cartesian position p. Then the wrist variables q_4, q_5, and q_6 that give the desired orientation *(n, o, a)* are determined. Some techniques for solving the inverse kinematics problem are given in [Paul 1981], [Craig 1989], [Spong and Vidyasagar 1989]. An example is now given.

EXAMPLE A.2–5: Inverse Kinematics for Two-Link Planar Elbow Arm

For the planar RR arm of Example A.2.2, the inverse kinematics problem amounts to finding the joint variable 0_1 and 0_2 given a desired Cartesian position *(x, y)* of the end of the arm. See Figure A.2.7.

The first thing that is evident is that, as long as $a_1^2+a_2^2 < r \equiv x^2+y^2$, there are two solutions. The one shown in Figure A.2.7 is the "elbow down" solution. Another solution may be determined for the "elbow up"configuration, where both links are above the vector $[x\ y]^T$. Thus *the inverse kinematics problem generally has a nonunique solution*. This may often be taken advantage of to obtain end-effector positioning with *collision avoidance*.

Given the T matrix from Example A.2.2, we see that 0_1 and 0_2 may be found by solving

$$a_1 c_1 + a_2 c_{12} = x \tag{1}$$

$$a_1 s_1 + a_2 s_{12} = y. \tag{2}$$

Determining 0_1 and 0_2 based on algebraic manipulations of such equations is called the *algebraic* inverse kinematics solution technique [Paul 1981]. Let us show a *geometric technique* here.

Referring to Figure A.2.7, define

$$r^2 = x^2 + y^2 \tag{3}$$

and use the law of cosines to obtain

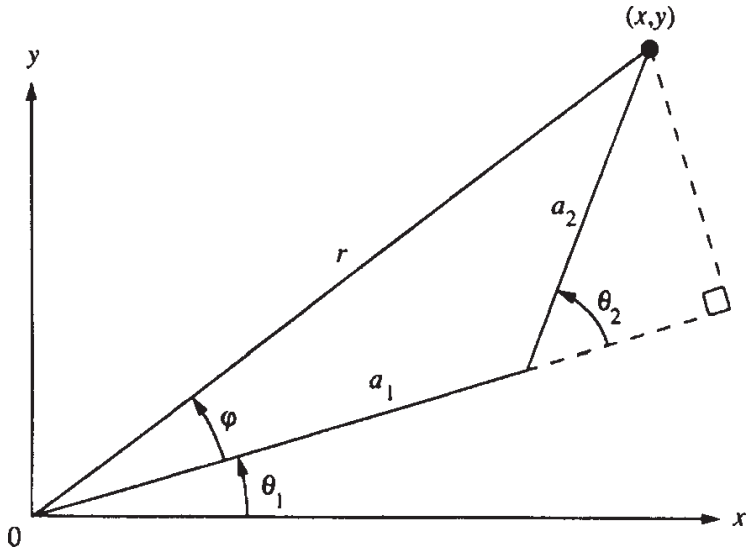


Figure A.2.7: Inverse kinematics for two-link planar RR arm.

$$\begin{aligned} r^2 &= a_1^2 + a_2^2 - 2a_1a_2\cos(\pi - \theta_2) \\ &= a_1^2 + a_2^2 + 2a_1a_2\cos\theta_2. \end{aligned} \tag{4}$$

We could now solve for θ_2 using the $\cos^{-1}$ function. However, it is better to use $\tan^{-1}$ for reasons of numerical accuracy. The FORTRAN function implementing $\tan^{-1}(b/c)$ is ATAN2(b, c). This function has a uniform accuracy over the range of its arguments, returns a unique value for the angle depending on the signs of *b* and *c,* and gives the correct solution if *b* and/or *c* is zero.

Therefore, we proceed by computing

$$\cos\theta_2 = \frac{r^2 - a_1^2 - a_2^2}{2a_1a_2} \equiv C \tag{5}$$

$$\sin\theta_2 = \pm\sqrt{1 - \cos^2\theta_2} = \pm\sqrt{1 - C^2} \equiv D \tag{6}$$

$$\theta_2 = \mathrm{ATAN2}(D, C). \tag{7}$$

An additional advantage of using the arctangent is that the multiple solutions of the inverse kinematics problem are explicitly revealed by the choice of negative or positive sign in (6).

To determine θ_1 define the auxiliary angle in the figure. By inspection of the right triangle shown,

$$\tan\varphi = \frac{a_2 \sin\theta_2}{a_1 + a_2 \cos\theta_2}. \tag{8}$$

Moreover,

$$\tan(\varphi + \theta_1) = \frac{y}{x}, \tag{9}$$

so that

$$\theta_1 = \mathrm{ATAN2}(y, x) - \mathrm{ATAN2}(a_2 \sin\theta_2,\ a_1 + a_2 \cos\theta_2). \tag{10}$$

Note that θ_1 depends on θ_2. ■

A.3 The Manipulator Jacobian

Given a generally nonlinear transformation from the joint variable $q(t) \in R^n$ to $y(t) \in R^p$,

$$y = h(q) \tag{A.3.1}$$

we define the Jacobian associated with $h(q)$ as

$$J(q) \equiv \frac{\partial h(q)}{\partial q}. \tag{A.3.2}$$

As we have just seen, the Jacobian is useful in feedback linearization, and therefore in robot manipulator control. It is also the means by which we transform velocity, acceleration, and force between coordinate frames.

Transformation of Velocity and Acceleration

Since

$$\dot{y} = \frac{\partial h}{\partial q}\dot{q} = J\dot{q}, \tag{A.3.3}$$

the Jacobian allows us to transform velocity from joint space to "y-space." Let us discuss the special case where $y(t)$ is the Cartesian velocity. Then $J(q)$ is called the *manipulator Jacobian*.

It is usual to define the generalized Cartesian velocity as

(A.3.4) $$\dot{y} = \begin{bmatrix} \nu \\ \omega \end{bmatrix},$$

with $v=[v_X\ v_Y\ v_Z]^T$ the linear velocity and $m=[m_X\ m_Y\ m_Z]^T$ the angular velocity. For instance, m_X represents angular velocity about the *x*-axis. Thus *y* has six components and the arm Jacobian *J* is a 6×*n* matrix, with *n* the number of joints in the manipulator. If *n*=6, the Jacobian is square. We shall soon show how to compute the manipulator Jacobian.

Using (A.3.3), we can obtain an expression for the transformation of *differential motion*. Let $dq=[dq_1 \ldots dq_n]^T$ be a differential motion in joint space, with dq_i a small rotation if joint *i* is revolute, and a small linear displacement if joint *i* is prismatic. Let

$$\mathrm{dy} = \begin{bmatrix} dx \\ dy \\ dz \\ \delta x \\ \delta y \\ \delta z \end{bmatrix} \tag{A.3.5}$$

describe the same differential motion in Cartesian coordinates, with $[d_X\ d_Y\ d_Z]^T$ the differential linear motion and $[6_X\ 6_Y\ 6_Z]^T$ representing the differential rotation. Here 6_X, for instance, means a small rotation about the *x*-axis. We have written the Cartesian differential motion vector **dy** in boldface to distinguish it from the small change *dy* in the second coordinate of Cartesian position.

According to (A.3.3), where $\dot{y} = dy/dt$ and $\dot{q} = dq/dt$, we see that

$$\mathrm{dy} = J\ dq, \tag{A.3.6}$$

with *J* the Jacobian relating joint space and Cartesian space.

The transformation of acceleration is found by differentiating (A.3.3) to be

(A.3.7) $$\ddot{y} = J\ddot{q} + \dot{J}\dot{q}.$$

Transformation of Force

To discover the transformation of static force between coordinate frames, consider the following.

The *virtual work* resulting from the application of a generalized force/ torque in joint space that results in a differential motion *dq* is

(A.3.8) $$\delta W = \tau^T dq,$$

with v the n-vector of arm control torques/forces, and $dq=[dq_1 \ldots dq_n]^T$ the differential change in the joint variable. If the description in another coordinate frame of the force is F and the description there of position is y, we must also have

$$\delta W = F^T \mathrm{d}y. \tag{A.3.9}$$

Now taking (A.3.6) into account, we may write

$$\delta W = \tau^T dq = F^T J dq,$$

so that the transformation from force to torque is given by

$$\tau = J^T(q) F. \tag{A.3.10}$$

In the case that $y(t)$ is Cartesian position, we define the Cartesian generalized force to be the 6-vector

$$F = \begin{bmatrix} f_c \\ \tau_c \end{bmatrix}, \tag{A.3.11}$$

with $\mathbf{f}_C=[f_X \ f_Y \ f_Z]^T$ a Cartesian force 3-vector, and $v_C=[v_X \ v_Y \ v_Z]^T$ a 3-vector representing Cartesian torques. For instance, v_X represents torque exerted about the x-axis.

If the arm has six links and the Jacobian is nonsingular, the transformation from generalized torque to generalized force is given by

$$F = J^{-T}(q) \tau. \tag{A.3.12}$$

The singularities in the Jacobian generally occur at the extremities of the manipulator workspace.

Specification of Cartesian Position

It is now necessary to confront an issue that is a source of confusion in robotics. Consider Equation (A.3.2). Unfortunately, when discussing the transformation $h(q)$ from joint space to Cartesian space, this equation may only be interpreted as a convenience of notation, not as a rigorous mathematical formula. The reason is that although the generalized Cartesian velocity (A.3.4) and acceleration, and the generalized Cartesian force (A.3.11) are bona fide 6- vectors, there is a problem with conveniently specifying the generalized Cartesian position $y(t)$. We now discuss several ways to specify the Cartesian position.

Representing Generalized Cartesian Position as (n, o, a, p). In our context, both the *location of the origin* of the end-effector frame as well as its orientation

must be specified in base coordinates. It is easy to specify the origin of the end-effector frame in base coordinates *(x, y, z)* using a 3-vector $p(t)=[p_X\ p_Y\ p_Z]^T$. However, specification of orientation is not so easy. This is because it takes more than three independent variables to specify uniquely the orientation of one frame with respect to another.

It should be mentioned that conventions such as the Euler angles and roll-pitch-yaw [Paul 1981], [Spong and Vidyasagar 1989] involve only three variables. However, they may not be used to uniquely specify the *absolute* orientation of one frame with respect to another, but only relative changes in orientation. We have already seen in (A.3.5) that only three variables are needed to describe *differential rotations*.

In our work we have specified the Cartesian position *y(t)* of the end effector in base coordinates by using the *(n, o, a, p)* approach (see Section A.2). There we define the generalized Cartesian position as

$$y(t) \equiv \begin{bmatrix} n(t) & o(t) & a(t) & p(t) \\ 0 & 0 & 0 & 1 \end{bmatrix} = T(t), \tag{A 3.13}$$

with *T(t)* the arm *T* matrix, (n, o, a) the vectors needed to describe the end-effector orientation, and $p=[p_X\ p_Y\ p_Z]^T$ the positional portion of the Cartesian description that specifies the origin of the end-effector frame.

It is clear that the selection of the transformation *h(q)* depends on how we wish to describe the Cartesian position *y(t)*. If we use (A.3.13), then *h(q)* is just the arm kinematics transformation discussed in Section A.2. However, then *y(t)* is not a 6-vector but a 4×4 matrix. Therefore, the definition of the arm Jacobian as $J(q)=\partial h/\partial q$ is a loose one purely for notational convenience. Therefore, we are faced with the problem of providing a suitable definition for *J(q)*. Before we do this, let us discuss some more techniques for representing the generalized Cartesian position.

Representing Cartesian Orientation Using Euler's Theorem. The positional portion of *y* is easy to specify; it is just the 3-vector $p= [p_X\ p_Y\ p_Z]^T$ found from the last column of the *T* matrix in (A.3.13). However, since *[n o a]* is a rotation matrix having nine elements, it does not afford an efficient representation of orientation. The orthogonality of the rotation matrix imposes some constraints among its elements, meaning that it actually has only four degrees of freedom.

The orientation of one coordinate frame (frame 1) with respect to another (frame 0) may be specified uniquely using a 3-vector *k* representing the axis of rotation of frame 1 with respect to frame 0, and an angle θ specifying the amount of rotation about that axis. We call *(k,)* the *Euler rotation parameters*. The *(k,)* convention involves four variables, which may be found as follows. Suppose that the rotation matrix

(A.3.14) $$R = \begin{bmatrix} n & o & a \end{bmatrix}$$

describes the orientation of frame 1 with respect to frame 0. Note that *R* is the upper left 3×3 submatrix of the arm *T* matrix, so that it may be computed given the joint vector *q*.

A rotation matrix is orthogonal, so that it has one eigenvalue equal to 1. Then the axis of rotation *k* is the eigenvector of the eigenvalue. That is,

(A.3.15) $$(R - I)\,k = 0.$$

This is known as *Euler's theorem*. It says that *Rk=k,* or that the rotation axis is not rotated by *R*. There are many good routines for computing eigenvectors (e.g., [IMSL]), which may be used to find *k* from *R*. See the problems to find an explicit formula for *k* in terms of *(n, o, a)* [Paul 1981].

The angle of rotation about the axis *k* may easily be found, for the trace of a rotation matrix is equal to 1+2 cos . Therefore,

(A.3.16) $$\cos\varphi = {}^1\!/_2\,(n_x + o_y + a_z - 1)\,,$$

where n_X, for instance, denotes the *x* component of the normal vector *n*.

Using Euler's rotation parameters we may specify the generalized Cartesian position as a 7-vector, with three components for position (i.e., the last column *p* of the *T* matrix) and four components (i.e., *k* and) for orientation.

Representing Cartesian Orientation Using Quaternions. The *quaternion* representation is a 4-vector which is often used to describe the end-effector frame orientation [Ickes 1970], [Sheppard 1978], [Yuan 1988], [Stevens and Lewis 1992].

The quaternions are four numbers represented as (q_0, q), with $q=[q_1\ q_2\ q_3]^T$ a 3-vector. They are given in terms of the Euler parameters *(k,)* by

(A.3.17) $$\begin{aligned} q_0 &= \cos(\varphi/2) \\ q &= k\sin(\varphi/2)\,. \end{aligned}$$

Using quaternions, the generalized Cartesian position may be represented as the 7-vector $y=[p_X\ p_Y\ p_Z\ q_0\ q_1\ q_2\ q_3\ ]^T$. An advantage of this representation is that no angles are involved.

Tool-Configuration Vector. A technique for specifying *y(t)* as a 6-vector is given in [Schilling 1990]. It depends on adopting a convention for encoding orientational information.

Consider the arm *T* matrix in (A.3.13) whose rotational portion is *R* in (A.3.14). Let us select the 3-vector *p* to represent Cartesian linear position. The approach vector *a* is a 3-vector specifying the direction in which the end effector points in terms of base coordinates. Recall from the discussion on kinematics in Section A.2 that this vector specifies in base coordinates the axis z_n of the frame attached to the end of link *n*. Since the rotation matrix *R* is orthogonal, the approach vector has a length of one.

The two vectors *p* and *a* almost completely specify the Cartesian position of the end effector. The only piece of information missing is the roll angle of the end effector. However, this angle is nothing by $q_n=0_n$, the last joint variable of the manipulator.

To capture the information q_n, let us propose scaling the approach vector by the exponential function $e^{qn/g}$ to define the *tool-configuration* vector as

$$w = \begin{bmatrix} p \\ a e^{q_n/\pi} \end{bmatrix}. \tag{A.3.18}$$

This is a 6-vector, which uniquely specifies the Cartesian position of the end effector in base coordinates.

Note that there is a unique mapping between *w* and *(p, a, q_n),* since, given *w* and the fact that ||*a*||=1, we may compute

$$q_n = \pi \ln \left(w_4^2 + w_5^2 + w_6^2\right)^{1/2} \tag{A.3.19}$$

$$a = \frac{1}{\left(w_4^2 + w_5^2 + w_6^2\right)^{1/2}} \begin{bmatrix} w_4 \\ w_5 \\ w_6 \end{bmatrix}, \tag{A.3.20}$$

with w_i the ith component of *w*.

Finding Cartesian Velocity from the Arm T Matrix. Note that using the definition (A.3.4), the Cartesian velocity *y* is a 6-vector that is not strictly speaking the derivative of *y(t)* in (A.3.13), which is a 4×4 matrix. To compute *y,* we may find the Jacobian *J(q)* and then use (A.3.3). Alternatively, the Cartesian velocity may be found directly from the arm *T* matrix (A.2.11) as follows.

Setting $\dot{y} = [\nu^T \quad \omega^T]^T$ with *v* the linear velocity and *m* the angular velocity, it is clear that

(A.3.21) $$\nu = \dot{p},$$

with *p* found from the last column of *T*.

To find *m,* proceed as follows. Since *R* in (A.2.11) is orthogonal, we have

$$RR^T = I, \tag{A.3.22}$$

which on differentiation yields

$$\dot{R}R^T + R\dot{R}^T = 0.$$

Therefore, the matrix defined as

$$\Omega \equiv \dot{R}R^T \tag{A.3.23}$$

satisfies $\Omega + \Omega^T = 0$, so it is skew symmetric. It may therefore be represented as

$$\Omega = \begin{bmatrix} 0 & -\omega_z & \omega_y \\ \omega_z & 0 & -\omega_x \\ -\omega_y & \omega_x & 0 \end{bmatrix}. \tag{A.3.24}$$

The relation between the *cross-product matrix* K and the angular velocity vector

$$\omega = \begin{bmatrix} \omega_x \\ \omega_y \\ \omega_z \end{bmatrix} \tag{A.3.25}$$

is an interesting one, for one may easily demonstrate that

(A.3.26) $$\omega \times w = \Omega w$$

for any 3-vector *w*. That is, the cross product may be replaced by a matrix multiplication in terms of the cross-product matrix. We denote by K*(w)* the cross-product matrix associated with a vector *m*.

The complete procedure for determining *y* from the *T* matrix is then as follows. First, compute *v* using the *p* vector as in (A.3.21). Then, compute K*(w)* from the rotation matrix *R* using (A.3.23), and hence find the last three components m of *y* from the definition of K*(w)*. Computing *y* from *q* thus requires a *computer subroutine*. Robot controllers generally have block diagrams in which some of the blocks are standard components like integrators, but some of the blocks are implemented in software.

Using (A.3.23), we may write the *strapdown equation*

(A.3.27) $$\dot{R} = \Omega R,$$

which is of fundamental importance in inertial navigation [Stevens and Lewis 1992].

Computing the Arm Jacobian

Let us now return to the problem of defining and computing the arm Jacobian *J(q)*. If the Cartesian position is defined by (A.3.13), then (A.3.2) does not afford an appropriate definition. Therefore, let us select (A.3.3) as the definition of *J(q)*. That is, define *J(q)* by

(A.3.28) $$\dot{y} = J(q)\,\dot{q},$$

so that it maps the joint velocity *q* to the Cartesian velocity *y* as defined by (A.3.4). Then *J(q)* is a 6×*n* matrix.

Let us consider a few examples showing how to compute the arm Jacobian to demonstrate that the procedure is not complicated. A methodical technique for computing *J(q)* will then be given.

EXAMPLE A.3–1: Arm Jacobian for Three-Link Cylindrical Arm

Let us use the kinematics derived in Example A.2.1 to compute the Jacobian for the three-link cylindrical arm. We shall call the joint variables *(0, z, r)* instead of *(0, h, r)* to avoid confusion with the nonlinear function *h(q)*.

Since there is no wrist on this three-link arm, the orientation of the last coordinate frame is fixed in terms of *(0, z, r)*, so that is not necessary to specify Cartesian orientation. This simplifies things for this example.

Denote the linear Cartesian position of the end effector in base co-ordinates (i.e., the first three components of *y*) as y_p. Then, according to Example A.2.1, y_p is the last column of the arm *T* matrix, so that

(1) $$y_p = \begin{bmatrix} -r\sin\theta \\ r\cos\theta \\ z \end{bmatrix} \equiv h_p(q)\,.$$

Omitting the orientational information has allowed us to define a (positional) transformation function $h_p(q)$ simply as the last column *p* of the *T* matrix.

Using (A.3.2) and the definition of $h_p(q)$ given in (1), the Jacobian is

(2) $$J(q) = \frac{\partial h_p}{\partial q} = \begin{bmatrix} \frac{\partial h_p}{\partial \theta} & \frac{\partial h_p}{\partial z} & \frac{\partial h_p}{\partial r} \end{bmatrix} = \begin{bmatrix} -r\cos\theta & 0 & -\sin\theta \\ -r\sin\theta & 0 & \cos\theta \\ 0 & 1 & 0 \end{bmatrix}.$$

Therefore, the velocities of the joints are converted into Cartesian velocities using

$$\frac{dy_p}{dt} = \begin{bmatrix} -r\cos\theta & 0 & -\sin\theta \\ -r\sin\theta & 0 & \cos\theta \\ 0 & 1 & 0 \end{bmatrix} \begin{bmatrix} \dot{\theta} \\ \dot{z} \\ \dot{r} \end{bmatrix}. \tag{3}$$

The determinant of J is $(r\cos^2 0 + r\sin^2 0) = r$, so that J is nonsingular as long as $r \neq 0$.

Note that the definition (1) of the positional function $h_p(q)$ means that the Jacobian is equal to $\partial h_p / \partial q$. This is a result of neglecting the orientation portion of y.

■

EXAMPLE A.3–2: Arm Jacobian for Two-Link Planar Elbow Arm

In Example A.2.2 the joint variable was $q = [\theta_1 \ \theta_2]^T$. As in Example A.3.1, the orientation of the last coordinate frame is fixed once q is given, so that we are not concerned with the orientational portion of y, but only its linear position portion y_p.

The linear Cartesian position of the end effector in the (x_1, x_2)-plane is given by the last column of the arm T matrix as

(1) $$y_p = \begin{bmatrix} a_1\cos\theta_1 + a_2\cos(\theta_1 + \theta_2) \\ a_1\sin\theta_1 + a_2\sin(\theta_1 + \theta_2) \end{bmatrix} \equiv h_p(q).$$

Since the motion is constrained to the plane, we have suppressed the x_3 component of y_p.

The Jacobian is

(2) $$J = \frac{\partial h_p}{\partial q} = \begin{bmatrix} -a_1\sin\theta_1 - a_2\sin(\theta_1 + \theta_2) & -a_2\sin(\theta_1 + \theta_2) \\ a_1\cos\theta_1 + a_2\cos(\theta_1 + \theta_2) & a_2\cos(\theta_1 + \theta_2) \end{bmatrix}.$$

Note that the definition of $h_p(q)$ in (1) means that the Jacobian is equal to $\partial h_p / \partial q$.

The determinant of J is (verify!) equal to $a_1 a_2 \sin\theta_2$, so that J is nonsingular unless $\theta_2 = 0$ or π; that is, unless the arm is fully extended or link 2 is folded back on top of link 1.

■

EXAMPLE A.3–3: Jacobian for Transformation to Camera Co-ordinates

Consider the three-link cylindrical arm of Examples A.2.1 and A.3.1 with a camera mounted vertically above the arm that measures only the position (x_1, x_2) of the end effector in the horizontal plane (in base coordinates). Call this position y. Then, according to those examples, the transformation from joint coordinates (θ, z, r) to camera coordinates (x_1, x_2) is

$$y = \begin{bmatrix} x_1 \\ x_2 \end{bmatrix} = \begin{bmatrix} -r\sin\theta \\ r\cos\theta \end{bmatrix} \equiv h(q) \tag{1}$$

and the associated Jacobian is

$$J = \begin{bmatrix} -r\cos\theta & 0 & -\sin\theta \\ -r\sin\theta & 0 & \cos\theta \end{bmatrix}. \tag{2}$$

The determinant of J with the second column deleted is equal to $-r$, so that J has full row rank as long as $r \neq 0$. The pseudo-inverse of J is

$$J^+ = \begin{bmatrix} -(\cos\theta)/r & -(\sin\theta)/r \\ 0 & 0 \\ -\sin\theta & \cos\theta \end{bmatrix}. \tag{3}$$

Since the camera cannot measure the distance x_3 perpendicular to the plane, that coordinate must be selected in any control scheme using an independent means that does not involve trajectory following control in the horizontal plane.

■

Algorithm for Computing the Arm Jacobian. We are finally in a position to show how to compute the arm Jacobian given the joint variables q_i. The procedure follows.

Given q_i, compute the matrices T_i defined in Section A.2 as

$$T_i = A_1 A_2 \cdots A_i \equiv \begin{bmatrix} R_i & p_i \\ 0 & 1 \end{bmatrix}, \tag{A.3.29}$$

whose corresponding rotation matrices will be denoted

$$R_i = \begin{bmatrix} x_i & y_i & z_i \end{bmatrix}. \tag{A.3.30}$$

Define $T_O=I$, $R_O=I$, and the arm T matrix

$$T = T_n = \begin{bmatrix} R_n & p_n \\ 0 & 1 \end{bmatrix} \equiv \begin{bmatrix} n & o & a & p \\ 0 & 0 & 0 & 1 \end{bmatrix}. \tag{A.3.31}$$

The vector z_i represents the z-axis of frame i in base coordinates. The vector p represents the location of the origin of link frame n (the end-effector frame) in terms of base coordinates. The Jacobian is computed using the vectors p and z_i as follows.

The generalized Cartesian velocity is $\dot{y} = [\nu^T \quad \omega^T]^T$. Therefore, we may partition the Jacobian matrix into a linear and an orientational part by writing

$$\begin{bmatrix} \nu \\ \omega \end{bmatrix} = J(q)\,\dot{q} = \begin{bmatrix} J_p(q) \\ J_o(q) \end{bmatrix} \dot{q}, \tag{A.3.32}$$

with $J_p(q)$ the first three rows of $J(q)$ and $J_O(q)$ its last three rows.

First, consider the computation of the linear position Jacobian $J_p(q)$. Given that the linear portion of the generalized Cartesian position y is just p, we may write

$$\nu = \sum_{i=1}^{n} \frac{\partial p}{\partial q_1}\dot{q}_i = \begin{bmatrix} \frac{\partial p}{\partial q_1} & \frac{\partial p}{\partial q_2} & \cdots & \frac{\partial p}{\partial q_n} \end{bmatrix} \dot{q}. \tag{A.3.33}$$

Therefore, $J_p(q)$ is given by

$$J_p(q) = \begin{bmatrix} \frac{\partial p}{\partial q_1} & \frac{\partial p}{\partial q_2} & \cdots & \frac{\partial p}{\partial q_n} \end{bmatrix}. \tag{A.3.34}$$

It should be clearly understood that this is exactly what we used in Examples A.3.1 and A.3.2.

Let us now turn to the orientational portion $J_O(q)$ of the Jacobian. Exactly as for linear velocities, one may add angular velocities as long as they are represented in the same coordinate frame. Let us therefore add the individual angular velocities of the links in the arm to obtain the angular velocity of the end effector. A prismatic joint does not contribute to the angular velocity of the end effector.

For a revolute joint, the joint rotation $q_i=0_i$ occurs about joint axis z_{i-1} (see Section A.2, especially Figure A.2.1). The angular velocity for joint variable i is therefore given by $z_{i-1}\dot{q}_i$. To add the effects of all the links, it is necessary to express z_{i-1} in a common frame; we select base coordinates. However, the last column of R_{i-1} is exactly z_{i-1} in base coordinates. Therefore, we may write

(A.3.35) $$\omega = \sum_{i=1}^{n} k_i z_{i-1} \dot{q}_i = \begin{bmatrix} k_1 z_0 & k_2 z_1 & \cdots & k_n z_{n-1} \end{bmatrix} \dot{q}.$$

where $z_0=[0\ 0\ 1]^T$ and the selection parameter n_i is zero if q_i is prismatic and 1 if q_i is revolute. Thus

(A.3.36) $$J_o(q) = \begin{bmatrix} k_1 z_0 & k_2 z_1 & \cdots & k_n z_{n-1} \end{bmatrix}.$$

The complete Jacobian is now given by stacking $J_i(q)$ on top of $J_O(q)$. It should now be clear that the arm Jacobian must be found from the joint vector q using a significant amount of computation. Therefore, whenever the Jacobian is required in a robot arm control scheme, it should be computed using a *computer subroutine*.

It is a good exercise to rework Examples A.3.1 and A.3.2 to determine the complete Jacobian, including the angular portion (see the problems).

EXAMPLE A.3–4: Jacobian for Spherical Wrist

In Example A.2.4 we derived the kinematics for a spherical wrist. Although the wrist would normally terminate an arm, for illustration let us take link 3 as the base link in this example. See Figure A.2.6. Thus we shall determine the Jacobian in the coordinates of the link 3 frame of reference.

To find the Jacobian, we compute the matrices

$$T_3 = I$$

$$T_4 = A_4 = \left[\begin{array}{ccc|c} c_4 & 0 & -s_4 & 0 \\ s_4 & 0 & c_4 & 0 \\ 0 & -1 & 0 & 0 \\ \hline 0 & 0 & 0 & 1 \end{array}\right]$$

$$T_5 = A_4 A_5 = \left[\begin{array}{ccc|c} c_4c_5 & -s_4 & c_4s_5 & 0 \\ s_4c_5 & c_4 & s_4s_5 & 0 \\ -s_5 & 0 & c_5 & 0 \\ \hline 0 & 0 & 0 & 1 \end{array}\right]$$

$$T = T_6 = A_4 A_5 A_6$$

$$= \left[\begin{array}{ccc|c} c_4c_5c_6 - s_4s_6 & -c_4c_5s_6 - s_4c_6 & c_4s_5 & c_4s_5d_6 \\ s_4c_5c_6 - c_4s_6 & -s_4c_5s_6 - c_4c_6 & s_4s_5 & s_4s_5d_6 \\ -s_5c_6 & s_5s_6 & c_5 & c_5d_6 \\ \hline 0 & 0 & 0 & 1 \end{array}\right].$$

Using the approach just derived, we compute directly that

$$J_p = \left[\begin{array}{ccc} \frac{\partial p}{\partial \theta_4} & \frac{\partial p}{\partial \theta_5} & \frac{\partial p}{\partial \theta_6} \end{array}\right] = \left[\begin{array}{ccc} -s_4s_5d_6 & c_4c_5d_6 & 0 \\ c_4s_5d_6 & s_4c_5d_6 & 0 \\ 0 & -s_5d_6 & 0 \end{array}\right]$$

$$J_o = \left[\begin{array}{ccc} z_3 & z_4 & z_5 \end{array}\right] = \left[\begin{array}{ccc} 0 & -s_4 & c_4s_5 \\ 0 & c_4 & s_4s_5 \\ 1 & 0 & c_5 \end{array}\right].$$

■

REFERENCES

[Craig 1989] Craig, J.J., *Introduction to Robotics.* Reading, MA: Addison-Wesley, 1989.

[Ickes 1970] Ickes, B.P., "A new method for performing digital control system altitude computations using quaternions," *AIAA J.,* vol. 8, no. 1, pp. 13–17, Jan. 1970.

[IMSL] IMSL, *Library Contents Document,* 8th ed. Houston, TX: International Mathematical and Statistical Libraries.

[MATMAN 1986] MATMAN, *Symbolic Matrix Manipulation,* M.R.Driels, Pembroke, MA: Kern International, 1986.

[Paul 1981] Paul, R.P., *Robot Manipulators,* Cambridge, MA: MIT Press, 1981.

[Schilling 1990] Schilling, R.J., *Fundamentals of Robotics,* Englewood Cliffs, NJ: Prentice Hall, 1990.

[Sheppard 1978] Sheppard, S.W., "Quaternion from rotation matrix," *Eng. Notes,* pp. 223–224, May/June 1978.

[Spong and Vidyasagar 1989] Spong, M.W., and M.Vidyasagar, *Robot Dynamics and Control.* New York: Wiley, 1989.

[Stevens and Lewis 1992] Stevens, B.L., and F.L.Lewis, *Aircraft Modeling, Dynamics, and Control.* New York: Wiley, 1992.

[Yuan 1988] Yuan, J.S.-C., "Closed-loop manipulator control using quaternion feedback," *IEEE J. Robot. Autom.,* vol. 4, no. 4, pp. 434–440, Aug. 1988.

Appendix C

Dynamics of Some Common Robot Arms

In this appendix we give the dynamics of some common robot arms. We assume that the robot dynamics are given by

$$\tau = M(q)\ddot{q} + V_m(q,\dot{q})\dot{q} + G(q) = M(q)\ddot{q} + N(q,\dot{q}), \qquad \text{(C.1.1)}$$

where the matrix $M(q)$ is symmetric and positive definite with elements $m_{ij}(q)$, that is,

$$M(q) = [m_{ij}(q)]_{n\times n}, i, j = 1, \ldots, n$$
$$m_{ij}(q) = m_{ji}(q)$$

and $N(q, q)$ is an $n\times1$ vector with elements n_i, that is,

$$N(q,\dot{q}) = [n_i(q,\dot{q})]_{n\times 1}.$$

Note in particular that the gravity terms are indentified in the expressions of n_i by the gravity constant g=9.8 meters/s^2. We will also adopt the following notation:

Length of link i is L_i in meters
Mass of link i is m_i in kilograms
Mass moment of inertia of Link i about axis u is I_{uui} in kg-m-m
S_i=sin q_i and C_i=cos q_i
S_{ij}=sin(q_i+q_j) and
C_{ij}=cos(q_i+q_j)
S_{ijk}=sin$(q_i+q_j+q_k)$ and C_{ijk}=cos$(q_i+q_j+q_k)$
SS_i=sin^2 q_i, CC_i=cos^2 q_i, and CS_i=cos q_i sin q_i; SS_{ij}=sin$^2(q_i+q_j)$

Evaluation of Microgenetic and Microimmune Algorithms 1086

C.1 SCARA ARM

The first robot we consider is a general SCARA configuration robot shown in Figure C.1.1. These equations will apply to the AdeptOne and AdeptTwo robots. The dynamics include the first four degrees of freedom and are symbolically given by

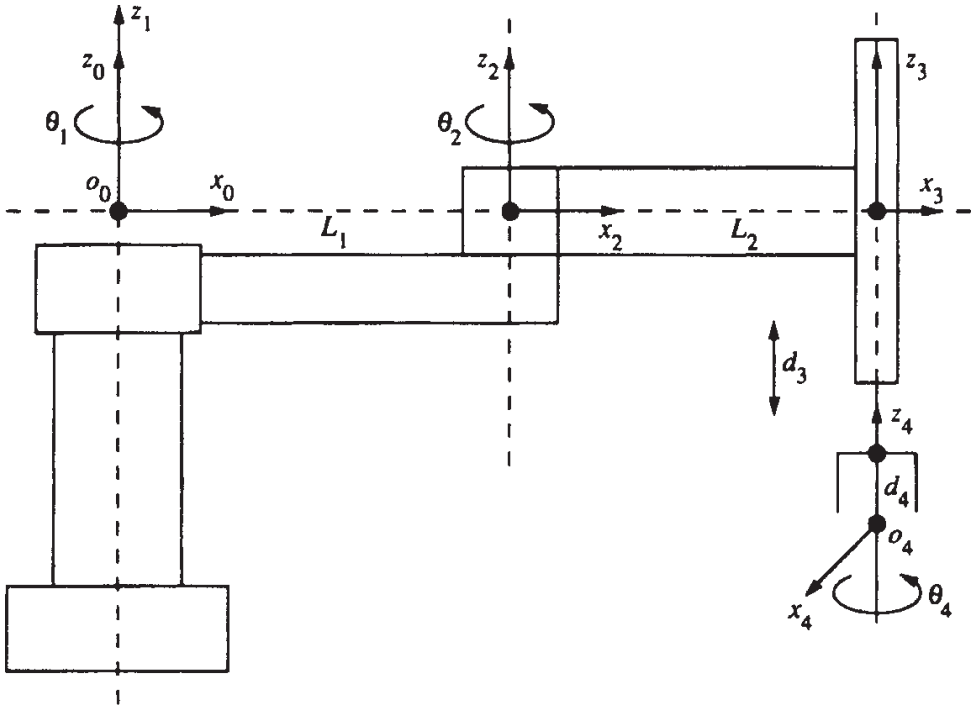


Figure C.1.1: SCARA manipulator.

$$
\begin{aligned}
m_{11} =& (I_{zz1} + I_{zz2} + I_{zz3} + I_{zz4}) + (\frac{m_1}{4} + 2m_3 + m_4)L_1^2 \\
&+ (\frac{m_2}{2} + 3m_3 + m_4)L_1 L_2 C_2 + (\frac{m_2}{4} + m_3 + m_4)L_2^2 \\
m_{12} =& (I_{zz2} + I_{zz3} + I_{zz4}) + (\frac{m_2}{4} + m_3 + m_4)L_2^2 \\
&+ (2m_3 + m_4)L_1 L_2 C_2 \\
m_{13} =& 0 \\
m_{14} =& I_{zz4} \\
m_{22} =& (I_{zz2} + I_{zz3} + I_{zz4}) + (\frac{m_2}{4} + m_3 + m_4)L_2^2 \\
m_{23} =& 0
\end{aligned}
$$

$$
\begin{aligned}
m_{24} &= I_{zz4} \\
m_{33} &= m_3 m_4 \\
m_{34} &= 0 \\
m_{44} &= I_{zz4}
\end{aligned}
$$

$$
\begin{aligned}
n_1 &= (\frac{m_2}{2} - m3) L_1 L_2 \dot{q}_1^2 - (4m_3 + 2m_4) L_1 L_2 \dot{q}_1 \dot{q}_2 \\
n_2 &= (\frac{m_2}{2} + m_3 + m_4) L_l L_2 S_2 \dot{q}_1^2 \\
n_3 &= (m_3 + m_4) g \\
n_4 &= 0.
\end{aligned}
$$

C.2 Stanford Manipulator

The Stanford manipulator shown in Figure C.2.1 has the following dynamics [Bejczy 1974], [Paul 1981]:

$$
\begin{aligned}
M_{11} &= 1.316 - 1.056108 d_2 + 11.48 d_2^2 + 2.51 S_2^2 \\
&\quad - 5.47995 S_2^2 d_3 + 6.47 S_2^2 d_3^2 + 0.23 S_2^2 d_3 C_5 \\
m_{12} &= -6.47 C_2 d_2 d_3 \\
m_{13} &= -6.47 S_2 d_2 \\
m_{14} &= 0 \\
m_{15} &= 0 \\
m_{16} &= 0 \\
m_{22} &= 4.721 - 5.47995 d_3 + 6.47 d_3^2 + 0.23 d_3 C_5 \\
m_{23} &= 0 \\
m_{24} &= 0 \\
m_{25} &= 0 \\
m_{26} &= 0 \\
m_{33} &= 7.252 \\
m_{34} &= 0 \\
m_{35} &= 0 \\
m_{36} &= 0
\end{aligned}
$$

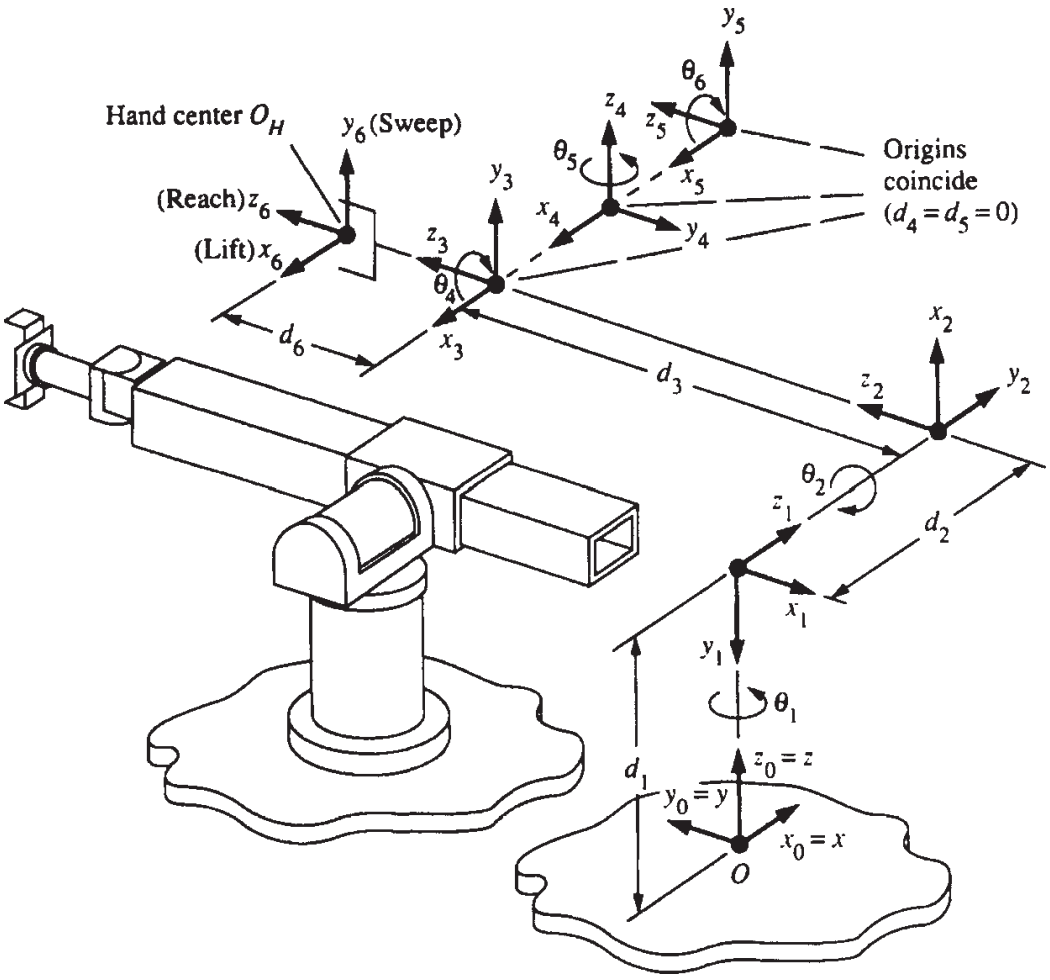


Figure C.2.1: Stanford manipulator.

$$
\begin{aligned}
m_{44} &= 0.107 + 0.203S_5^2 \\
m_{45} &= 0 \\
m_{46} &= 0 \\
m_{55} &= 0.113 \\
m_{56} &= 0 \\
m_{66} &= 0.0203
\end{aligned}
$$

$$
\begin{aligned}
n_1 &= 0 \\
n_2 &= -\left[2.734S_2 + 6.47S_2d_3 + 0.115(S_2C_5 + C_2C_4S_5)\right]g \\
n_3 &= 6.47C_2g \\
n_4 &= 0.115(S_2S_4S_5)g \\
n_5 &= 0.115(S_2C_4C_5 - C_2S_5)g \\
n_6 &= 0.
\end{aligned}
$$

C.3 PUMA 560 Manipulator

The PUMA 560 is shown in Figure C.3.1. Many simplifications can be made for this particular structure in order to obtain the following dynamics which appeared in [Armstrong *et al.* 1986].

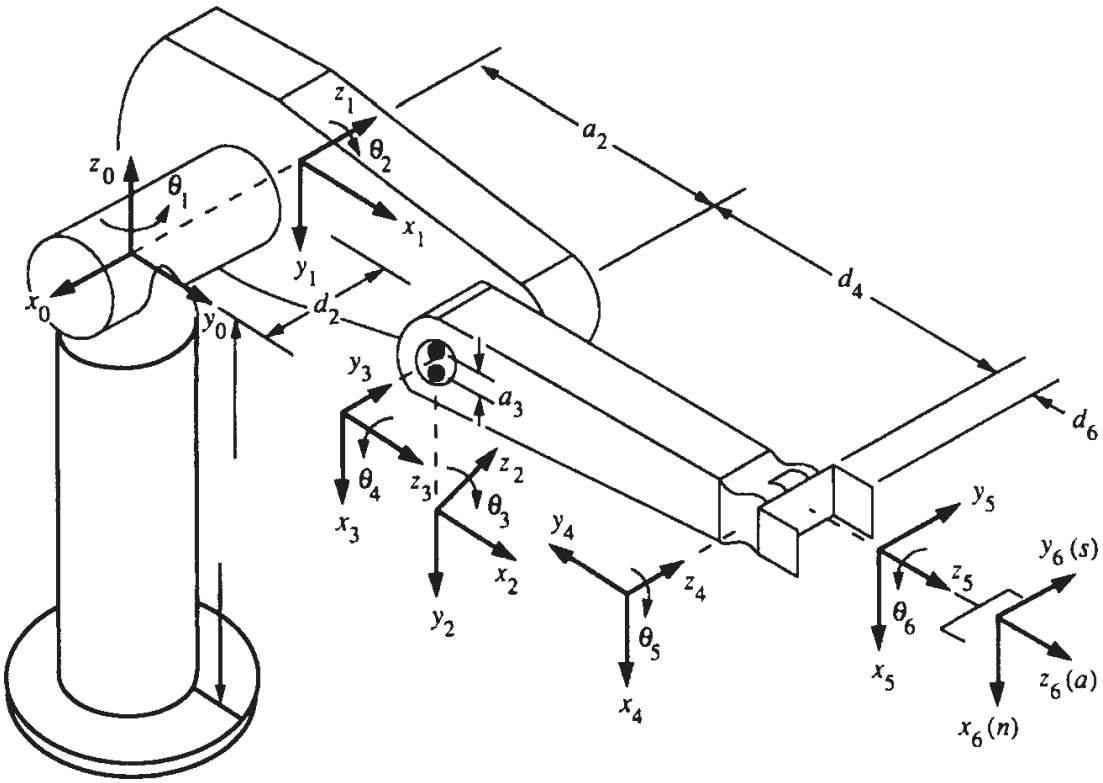


Figure C.3.1: PUMA 560 manipulator.

$$
\begin{aligned}
m_{11} =& 2.57 + 1.38CC_2 + 0.3SS_{23} + 0.744C_2S_{23} \\
m_{12} =& 0.69S_2 - 0.134C_{23} + 0.0238C_2 \\
m_{13} =& -0.134C_{23} - 0.00397S_{23} \\
m_{14} =& 0 \\
m_{15} =& 0 \\
m_{16} =& 0 \\
m_{22} =& 6.79 + 0.744S_3 \\
m_{23} =& 0.333 + 0.372S_3 - 0.011C_3 \\
m_{24} =& 0
\end{aligned}
$$

$$
\begin{aligned}
m_{25} &= 0 \\
m_{26} &= 0 \\
m_{33} &= 1.16 \\
m_{34} &= -0.00125 S_4 S_5 \\
m_{35} &= -0.00125 C_4 C_5 \\
m_{36} &= 0 \\
m_{44} &= 0.2 \\
m_{45} &= 0 \\
m_{46} &= 0 \\
m_{55} &= 0.18 \\
m_{56} &= 0 \\
m_{66} &= 0.19
\end{aligned}
$$

$$
\begin{aligned}
n_1 = & [0.69 C_2 + 0.134 S_{23} - 0.0238 S_2] \dot{q}_2^2 + [0.1335 S_{23} - 0.00379 C_{23}] \dot{q}_3^2 \\
& + [-2.76 S C_2 + 0.744 C_{223} + 0.6 S C_{23} - 0.0213 (1 - 2 S S_{23})] \dot{q}_1 \dot{q}_2 \\
& + [0.744 C_2 C_{23} + 0.6 S C_{23} + 0.022 C_2 S_{23} - 0.0213 (1 - 2 S S_{23})] \dot{q}_1 \dot{q}_3 \\
& + [-0.0025 S C_{23} S_4 S_5 + 0.00086 C_4 S_5 - 0.00248 C_2 C_{23} S_4 S_5] \dot{q}_1 \dot{q}_4 \\
& + [-0.0025 (S S_{23} S_5 - S C_{23} C_4 C_5) - 0.00248 C_2 (S_{23} S_5 - C_{23} C_4 C_5) \\
& + 0.000864 S_4 C_5] \dot{q}_1 \dot{q}_5 + [0.267 S_{23} - 0.00758 C_{23}] \dot{q}_2 \dot{q}_3
\end{aligned}
$$

$$
\begin{aligned}
n_2 = & -\frac{1}{2} [-2.76 S C_2 + 0.744 C_{223} + 0.6 S C_{23} - 0.0213 (1 - 2 S S_{23})] \dot{q}_1^2 \\
& + \frac{1}{2} [0.022 S_3 + 0.744 C_3] \dot{q}_3^2 \\
& + [0.00164 S_{23} - 0.0025 C_{23} C_4 S_5 + 0.00248 S_2 C_4 S_5 + 0.00003 S_{23} \\
& \quad (1 - 2 S S_4)] \dot{q}_1 \dot{q}_4 \\
& + [-0.00215 C_{23} S_4 C_5 + 0.00248 S_2 S_4 C_5 - 0.000642 C_{23} S_4] \dot{q}_1 \dot{q}_5 \\
& + [0.022 S_3 + 0.744 C_3] \dot{q}_2 \dot{q}_3 - [0.00248 C_3 S_4 S_5] \dot{q}_2 \dot{q}_4 \\
& + [-0.0025 S_5 + 0.00248 (C_3 C_4 C_5 - S_3 S_5)] \dot{q}_2 \dot{q}_5 \\
& - [0.00248 C_3 S_4 S_5] \dot{q}_3 \dot{q}_4 \\
& + [-0.0025 S_5 + 0.00248 (C_3 C_4 C_5 - S_3 S_5)] \dot{q}_3 \dot{q}_5 \\
& - 37.2 C_2 - 8.4 S_{23} + 1.02 S_2
\end{aligned}
$$

$$
\begin{aligned}
n_3 = &-\frac{1}{2}[-2.76SC_2 + 0.744C_{223} + 0.6SC_{23} - 0.0213(1 - 2SS_{23})]\dot{q}_1^2 \\
&-\frac{1}{2}[0.022S_3 + 0.744C_3]\dot{q}_2^2 - [0.00125C_4S_5]\dot{q}_5^2 - [0.00125C_4S_5]\dot{q}_4^2 \\
&+[-0.0025C_{23}C_4S_5 + 0.00164S_{23} + 0.0003S_{23}(1 - 2SS_4)]\dot{q}_1\dot{q}_4 \\
&-[0.0025C_{23}S_4C_5 + 0.000642C_{23}S_4]\dot{q}_1\dot{q}_5 - [0.0025S_5]\dot{q}_2\dot{q}_5 \\
&-[0.0025S_5]\dot{q}_3\dot{q}_5 - [0.0025S_4C_5]\dot{q}_4\dot{q}_5 - 8.4S_{23} + 0.25C_{23}
\end{aligned}
$$

$$
\begin{aligned}
n_4 = &\frac{1}{2}[0.0025SC_{23}S_4S_5 - O.0OO86C_4S_5 + 0.00248C_2C_{23}S_4S_5]\dot{q}_1^2 \\
&-\frac{1}{2}[0.00248C_3S_4S_5]\dot{q}_2^2 \\
&+[0.00164S_{23} - 0.0025C_{23}C_4S_5 + 0.00248S_2C_4S_5 \\
&+0.0003S_{23}(1 - 2SS_4)]\dot{q}_1\dot{q}_2 \\
&+[0.0025C_{23}C_4S_5 - 0.00164S_{23} - 0.003S_{23}(1 - 2SS_4)]\dot{q}_1\dot{q}_3 \\
&-[0.000642S_{23}C_4]\dot{q}_1\dot{q}_5 + [0.000642S_4]\dot{q}_2\dot{q}_5 \\
&+[0.000642S_4]\dot{q}_3\dot{q}_5 + 0.028S_{23}S4S5
\end{aligned}
$$

$$
\begin{aligned}
n_5 = &\frac{1}{2}[0.0025(SS_{23}S_5 - SC_{23}C_4C_5) + 0.00248C_2(S_{23}S_5 - C_{23}C_4C_5) \\
&-0.000864S_4C_5]\dot{q}_1^2 - \frac{1}{2}[0.0025S_5 - 0.00248(C_3C_4C_5 - S_3S_5)]\dot{q}_2^2 \\
&+[0.0026C_{23}S_4C_5 - 0.00248S_2S_4C_5 + 0.000642C_{23}S_4]\dot{q}_1\dot{q}_2 \\
&+[0.0025C_{23}S_4C_5 + 0.000642C_{23}S_4]\dot{q}_1\dot{q}_3 + [0.000642S_{23}C_4]\dot{q}_1\dot{q}_4 \\
&-[0.000642S_4]\dot{q}_2\dot{q}_4 - [0.000642S_4]\dot{q}_3\dot{q}_4 - 0.028(C_{23}S5 + S_{23}C4C5)
\end{aligned}
$$

$$n_6 = 0.$$

REFERENCES

[Armstrong *et al.* 1986] Armstrong, B., O.Khatib, and J.Burdick, "The explicit dynamic model and inertial parameters of the PUMA 560 arm," *Proc. 1986 IEEE Conf. Robot. Autom.,* pp. 510–518, San Francisco, Apr. 7– 10, 1986.

[Bejczy 1974] Bejczy, A.K., "Robot arm dynamics and control," *NASA-JPL Technical Memorandum 33–669,* 1974.

[Paul 1981] Paul, R.P., *Robot Manipulators: Mathematics*, *Programming and Control.* Cambridge, MA: MIT Press, 1981.